

050776

**Reinforced
Concrete
Structures**

R. PARK and T. PAULAY

TU37
P129

050776



E0051670

Reinforced Concrete Structures

R. PARK and T. PAULAY

*Department of Civil Engineering,
University of Canterbury, Christchurch,
New Zealand*

武汉水利电力学院
藏 书
图 书 馆

A WILEY-INTERSCIENCE PUBLICATION

JOHN WILEY & SONS

New York · London · Sydney · Toronto

Preface

We hope that the content and the treatment of the subject of reinforced concrete structures in this book will appeal to students, teachers, and practicing members of the structural engineering profession.

The book has grown from two editions of seminar notes entitled *Ultimate Strength Design of Reinforced Concrete Structures* (Vol. 1), printed by the University of Canterbury for extension study seminars conducted for practicing structural engineers in New Zealand. Those early editions of seminar notes have been considerably extended and updated. Many years of experience in teaching theory and design, and in design and research, have helped to form ideas and to provide background material for the book.

The text emphasizes the basic behavior of reinforced concrete elements and of structures—in particular, their strength and deformation characteristics up to ultimate load. It endeavors to give the reader a thorough knowledge of the fundamentals of reinforced concrete. Such a background is essential to a complete and proper understanding of building codes and design procedures. The design engineer may be disappointed that the text does not extend into a range of design charts, tables, and examples. Such information is available elsewhere. The main purpose of the text is to bring about a basic understanding of the background to such applied material.

The current building code of the American Concrete Institute (ACI 318-71) is one of the most widely accepted reinforced concrete codes. It has been adopted by some countries and has strongly influenced the codes of many others. For this reason extensive reference is made to the ACI provisions, but comparison with other building codes appears where necessary. The book is not heavily code oriented, however. The emphasis is on why certain engineering decisions should be made, rather than how they should be executed. It is our belief that engineers should be capable of rationally assessing design procedures and should not be blind followers of code provisions.

The strength and serviceability approach to design is emphasized throughout the book because we believe that it is the most realistic method.

The book commences with a discussion of basic design criteria and the

properties of concrete and steel. The strength and deformation of reinforced concrete structural members with flexure, flexure and axial load, shear, and torsion are then presented in some depth, followed by a discussion of bond and anchorage. The service load behavior of reinforced concrete members is then examined, with emphasis on deflection and crack control. This material is followed by a treatment of frames and shear walls. Because we believe that correct proportioning of components is insufficient to ensure a successful design, the book ends with a discussion on the detailing of structural components and joints.

We have not attempted to treat the design of specific types of structures. Thorough understanding of the behavior of reinforced concrete components and of structural analysis should enable a designer to undertake the design of the common range of structures and to find solutions to special problems.

An aspect of the book that distinguishes it from most other texts on reinforced concrete is the treatment of the effects of earthquake loading and means of achieving design procedures for seismic-resistant structures. Seismic design is assuming more importance with the realization that seismic zones may be more extensive than has heretofore been assumed. Seismic design involves more than a consideration of additional static lateral loads on the structure. Proper attention to details, and an understanding of possible failure mechanisms, are essential if structures capable of surviving major earthquakes are to be designed. Considerations of behavior under intense seismic loading involve an understanding of the deformation characteristics of members and structures in the inelastic range, as well as the development of strength, and these areas are given due regard in the text.

A detailed discussion of slabs has been omitted because a book-length treatment is in preparation.

We hope that the book will serve as a useful text to teachers preparing a syllabus for undergraduate courses in reinforced concrete. Each major topic has been treated in enough depth to permit the book to be used by graduate students in advanced courses in reinforced concrete. It is hoped that many practicing engineers, particularly those facing the formidable task of having to design earthquake-resistant structures, will also find this book a useful reference.

We would be grateful for any constructive comments or criticisms that readers may have and for notification of any errors that they will inevitably detect.

The authors have received a great deal of assistance, encouragement, and inspiration from numerous sources. Thanks are due to our many colleagues at the University of Canterbury, particularly to Prof. H. J. Hopkins, who initiated a strong interest in concrete at this University, to Dr. A. J. Carr, who read part of the manuscript, and to Mrs. Alice Watt, whose patience when

typing the manuscript is greatly appreciated. Also, the dedicated technicians of the Department of Civil Engineering of the University of Canterbury and our graduate students have carried the major burden of the testing reported, as well as the photographic and drafting work, and their efforts must be recorded with appreciation. To many professional engineering colleagues in New Zealand, including O. A. Glogau, G. F. McKenzie, and I. C. Armstrong of the New Zealand Ministry of Works, and consulting engineers A. L. Andrews, J. F. Hollings, R. J. P. Garden, and K. Williamson, we owe a great deal for constructive comment and discussions. To our many colleagues in North America, Europe, and Australia, including M. P. Collins, R. F. Furlong, W. L. Gamble, P. Lampert, J. MacGregor, and G. Base, who read part of the manuscript, and to V. V. Bertero, F. Leonhardt, and H. Rüsch, we are grateful. Also our thanks are due to our own University of Canterbury, the Portland Cement Association, the American Iron and Steel Institute, the American Society of Civil Engineers, and the American Concrete Institute.

Finally, this undertaking could never have been achieved without the patience, encouragement, and understanding of our wives.

R. PARK
T. PAULAY

*Christchurch, New Zealand
August 1974*

Contents

1 THE DESIGN APPROACH	1
1.1 Development of Working Stress and Ultimate Strength Design Procedures	1
1.2 Design for Strength and Serviceability	3
1.3 ACI Strength and Serviceability Design Method	4
1.3.1 Strength Provisions, 4	
1.3.2 Serviceability Provisions, 6	
1.3.3 Ductility Provisions, 7	
1.4 Considerations of Member Strength	7
1.4.1 Development of Member Strength, 7	
1.4.2 Ideal Strength, 8	
1.4.3 Dependable Strength, 8	
1.4.4 Probable Strength, 8	
1.4.5 Overstrength, 9	
1.4.6 Relationships Between Different Strengths, 9	
1.5 References	10
2 STRESS-STRAIN RELATIONSHIPS FOR CONCRETE AND STEEL	11
2.1 Concrete	11
2.1.1 Uniaxial Stress Behavior, 11	
2.1.2 Combined Stress Behavior, 17	
2.1.3 Concrete Confinement by Reinforcement, 21	
2.1.4 Creep of Concrete, 30	
2.1.5 Shrinkage of Concrete, 33	
2.2 Steel Reinforcement	36
2.2.1 Bar Shape and Sizes, 36	

2.2.2	Monotonic Stress Behavior, 37	
2.2.3	Repeated Stress Behavior, 40	
2.2.4	Reversed Stress Behavior, 40	
2.3.	References	45
3	BASIC ASSUMPTIONS OF THEORY FOR FLEXURAL STRENGTH	48
3.1	Basic Behavior Assumptions	48
3.2	Equivalent Rectangular Stress Block	52
3.3	Concrete Strain at the Flexural Strength	54
3.4	Nonrectangular Compressed Areas	56
3.5	Effects of Slow Rates of Loading and of Sustained Load	58
3.6	Summary of Recommendations for the Determination of the Strength of Sections with Flexure and Axial Load	58
3.7	References	59
4	STRENGTH OF MEMBERS WITH FLEXURE	61
4.1	Rectangular Sections	61
4.1.1	Analysis of Singly Reinforced Sections, 61	
4.1.2	Design of Singly Reinforced Sections, 69	
4.1.3	Analysis of Doubly Reinforced Sections, 79	
4.1.4	Design of Doubly Reinforced Sections, 83	
4.2	<i>T</i> and <i>I</i> Sections	92
4.2.1	Analysis of <i>T</i> and <i>I</i> Sections, 92	
4.2.2	Design of <i>T</i> and <i>I</i> Sections, 95	
4.2.3	Effective Width of <i>T</i> Beams, 99	
4.3	Sections Having Bars at Various Levels or Steel Lacking a Well-Defined Yield Strength	101
4.4	Biaxial Bending of Sections	106
4.5	Lateral Instability of Beams	113
4.6	References	116
5	STRENGTH OF MEMBERS WITH FLEXURE AND AXIAL LOAD	118
5.1	Introduction	118
5.2	Axially Loaded Short Columns	118
5.3	Eccentrically Loaded Short Columns with Uniaxial Bending	123
5.3.1	Introduction, 123	

5.3.2	Analysis of Rectangular Sections with Bars at One or Two Faces, 125	
5.3.3	Design of Rectangular Sections with Bars at One or Two Faces, 135	
5.3.4	Rectangular Sections with Bars at Four Faces, 143	
5.3.5	Sections with Bars in Circular Array, 148	
5.3.6	Design Charts and Tables, 152	
5.4	Eccentrically Loaded Short Columns with Biaxial Bending	154
5.4.1	General Theory, 154	
5.4.2	Approximate Methods of Analysis and Design for Biaxial Bending, 158	
5.4.3	Design Charts, 162	
5.5	Slender Columns	172
5.5.1	Behavior of Slender Columns, 172	
5.5.2	"Exact" Design Approach for Slender Columns, 179	
5.5.3	Approximate Design Approach for Slender Columns: The Moment Magnifier Method, 180	
5.6	References	192
6	ULTIMATE DEFORMATION AND DUCTILITY OF MEMBERS WITH FLEXURE	195
6.1	Introduction	195
6.2	Moment-Curvature Relationships	196
6.2.1	Curvature of a Member, 196	
6.2.2	Theoretical Moment-Curvature Determination, 199	
6.3	Ductility of Unconfined Beam Sections	203
6.3.1	Yield and Ultimate Moment and Curvature, 203	
6.3.2	Code-Specified Ductility Requirements for Beams, 216	
6.4	Ductility of Unconfined Column Sections	217
6.5	Members with Confined Concrete	221
6.5.1	Effect of Confining the Concrete, 221	
6.5.2	Compressive Stress Block Parameters for Concrete Confined by Rectangular Hoops, 224	
6.5.3	Theoretical Moment-Curvature Curves for Sections with Confined Concrete, 229	
6.6	Flexural Deformations of Members	236

6.6.1	Calculation of Deformations from Curvatures, 236	
6.6.2	Additional Effects on the Deformations of Members Calculated from Curvatures, 237	
6.6.3	Idealized Ultimate Deformations Calculated from Curvatures, 242	
6.6.4	Empirical Expressions for Ultimate Plastic Rotation Calculated from Curvatures, 245	
6.6.5	Alternative Approach to the Calculation of Deformations Based on the Summation of Discrete Rotations at Cracks, 250	
6.7	Deformations of Members With Cyclic Loading	254
6.7.1	Moment-Curvature Relationships, 254	
6.7.2	Load-Deformation Behavior, 264	
6.8	Application of Theory	268
6.9	References	268
7	STRENGTH AND DEFORMATION OF MEMBERS WITH SHEAR	270
7.1	Introduction	271
7.2	The Concept of Shear Stresses	271
7.3	The Mechanism of Shear Resistance in Reinforced Concrete Beams Without Shear Reinforcement	276
7.3.1	The Formation of Diagonal Cracks, 276	
7.3.2	Equilibrium in the Shear Span of a Beam, 276	
7.3.3	The Principal Mechanisms of Shear Resistance, 278	
7.3.4	Size Effects, 287	
7.3.5	Shear Failure Mechanisms, 288	
7.3.6	The Design for Shear of Beams Without Web Reinforcement, 291	
7.4	The Mechanism of Shear Resistance in Reinforced Concrete Beams with Web Reinforcement	293
7.4.1	The Role of Web Reinforcement, 293	
7.4.2	The Truss Mechanism, 294	
7.4.3	The Design for Shear of Beams with Web Reinforcement, 299	
7.5	The Interaction of Flexure and Shear	301
7.5.1	The Effect of Shear on Flexural Steel Requirements, 304	
7.5.2	Shear at Plastic Hinges, 307	
7.5.3	Interaction Effects in Deep Beams, 310	

Contents

xiii

7.6 The Interaction of Shear, Flexure, and Axial Forces	310
7.6.1 Shear and Axial Compression, 310	
7.6.2 Shear and Axial Tension, 312	
7.7 Shear Deformations	315
7.7.1 Uncracked Members, 315	
7.7.2 Shear Deformations in Cracked Members, 316	
7.8 Interface Shear	319
7.8.1 Shear Transfer Across Uncracked Concrete Interfaces, 320	
7.8.2 Shear Transfer Across Precracked Concrete Interfaces, 321	
7.8.3 Shear Transfer Across Construction Joints, 325	
7.9 The Effects of Repeated and Cyclic Loading on Shear Strength	332
7.9.1 Effects on the Web Reinforcement, 332	
7.9.2 Effects on Interface Shear Transfer, 335	
7.10 Special Members and Loadings	338
7.11 References	343
8 STRENGTH AND DEFORMATION OF MEMBERS WITH TORSION 346	
8.1 Introduction	346
8.2 Plain Concrete Subject to Torsion	348
8.2.1 Elastic Behavior, 348	
8.2.2 Plastic Behavior, 351	
8.2.3 Tubular Sections, 354	
8.3 Beams Without Web Reinforcement Subject to Flexure and Torsion	357
8.4 Torsion and Shear in Beams Without Web Reinforcement	359
8.5 Torsion Members Requiring Web Reinforcement	361
8.6 Combined Shear and Torsion in Beams with Web Reinforcement	370
8.7 Combined Flexure and Torsion	377
8.8 Torsional Stiffness	383
8.9 Torsion in Statically Indeterminate Structures	389
8.10 References	390
9 BOND AND ANCHORAGE 392	
9.1 Introduction	392
9.1.1 Basic Considerations, 392	

9.1.2	Anchorage or Development Bond, 393	
9.1.3	Flexural Bond, 394	
9.2	The Nature of Bond Resistance	394
9.2.1	Basic Features of Bond Resistance, 394	
9.2.2	The Position of Bars with Respect to the Placing of the Surrounding Concrete, 397	
9.2.3	Bar Profiles and Surface Conditions, 398	
9.2.4	The State of Stress in the Surrounding Concrete, 401	
9.2.5	The Splitting Failure, 403	
9.2.6	Confinement, 404	
9.2.7	Repeated and Cyclic Reversed Loading, 404	
9.3	The Determination of Usable Bond Strength	407
9.4	The Anchorage of Bars	410
9.4.1	Straight Anchorages for Bars with Tension, 410	
9.4.2	Hook Anchorages for Bars with Tension, 411	
9.4.3	Anchorage for Bars with Compression, 416	
9.5	Anchorage Requirements for Flexural Bond	417
9.6	Splices	418
9.6.1	Introduction, 418	
9.6.2	Tension Splices, 419	
9.6.3	Compression Splices, 421	
9.6.4	Mechanical or Contact Splices, 423	
9.7	References	424
10	SERVICE LOAD BEHAVIOR	426
10.1	Service Load Performance	426
10.2	Elastic Theory for Stresses in Members due to Flexure	427
10.2.1	Effective Modulus of Elasticity, 427	
10.2.2	Elastic Theory Assumptions, 428	
10.2.3	Analysis of Beams Using the Internal Couple Approach, 429	
10.2.4	Analysis of Beams Using the Transformed Section Approach, 436	
10.2.5	Design of Beams Using the Alternative (Elastic Theory) Method, 441	
10.2.6	Analysis of Short Columns, 450	
10.2.7	Shrinkage Stresses, 457	

Contents	xv
10.3 Control of Deflections	461
10.3.1 The Need for Deflection Control, 461	
10.3.2 Method of Deflection Control, 463	
10.3.3 Calculation of Deflections, 465	
10.3.4 More Accurate Methods for Calculating Deflections, 470	
10.4 Control of Cracking	476
10.4.1 The Need for Crack Control, 476	
10.4.2 Causes of Cracking, 477	
10.4.3 Mechanism of Flexural Cracking, 479	
10.4.4 Control of Flexural Cracks in Design, 490	
10.5 References	494
11 STRENGTH AND DUCTILITY OF FRAMES	496
11.1 Introduction	496
11.2 Moment Redistribution and Plastic Hinge Rotation	496
11.3 Complete Analysis of Frames	502
11.4 Methods for Determining Bending Moment, Shear Force, and Axial Force Distributions at the Ultimate Load for Use in Design	505
11.4.1 The Elastic Bending Moment Diagram, 505	
11.4.2 The Elastic Bending Moment Diagram Modified for Moment Redistribution, 507	
11.4.3 Limit Design, 512	
11.5 Limit Design Methods	515
11.5.1 ACI-ASCE Committee 428 Report, 515	
11.5.2 Available Limit Design Methods, 518	
11.5.3 General Method for Calculating Required Plastic Hinge Rotations, 521	
11.5.4 Calculation of Service Load Moments and Stresses, 529	
11.5.5 Comments on Limit Design, 544	
11.6 Design for Seismic Loading	545
11.6.1 Basic Concepts, 545	
11.6.2 Displacement Ductility Requirements, 547	
11.6.3 Curvature Ductility Requirements, 552	
11.6.4 Determining Curvature Ductility Demand of Multi-story Frames Using Static Collapse Mechanisms, 554	

11.6.5	Determining Curvature Ductility Demand of Multistory Frames Using Nonlinear Dynamic Analyses, 563
11.6.6	Additional Factors in Analysis for Ductility, 568
11.6.7	ACI Code Special Provisions for Seismic Design of Ductile Frames, 580
11.6.8	Discussion of ACI Code Special Provisions for Seismic Design of Ductile Frames, 584
11.6.9	An Alternative Procedure for Calculating Special Transverse Reinforcement for Confinement in the Plastic Hinge Zones of Columns, 591
11.6.10	Earthquake Energy Dissipation by Special Devices, 599
11.6.11	Capacity Design for Seismic Loading of Frames, 600
11.7	References 607
12 SHEAR WALLS OF MULTISTORY BUILDINGS 610	
12.1	Introduction 610
12.2	The Behavior of Cantilever Walls 611
12.2.1	Tall Walls Having Rectangular Cross Sections, 611
12.2.2	Squat Shear Walls Having Rectangular Cross Sections, 618
12.2.3	Flanged Cantilever Shear Walls, 627
12.2.4	Moment-Axial Load Interaction for Shear Wall Sections, 629
12.2.5	Interaction of Cantilever Shear Walls with Each Other, 631
12.3	Interaction of Shear Walls and Rigid Jointed Frames 633
12.4	Shear Walls With Openings 634
12.5	Coupled Shear Walls 637
12.5.1	Introduction, 637
12.5.2	The Laminar Analysis Used to Predict Linear Elastic Response, 638
12.5.3	Elastoplastic Behavior of Coupled Shear Walls, 641
12.5.4	Experiments with Coupled Shear Walls, 657
12.5.5	Summary of Design Principles, 658
12.6	References 660
13 THE ART OF DETAILING 663	
13.1	Introduction 663
13.2	The Purpose of Reinforcement 664

Contents	xvii
13.3 Directional Changes of Internal Forces	665
13.4 The Detailing of Beams	669
13.4.1 Localities for Anchorage, 669	
13.4.2 Interaction of Flexural and Shear Reinforcement, 675	
13.4.3 The Detailing of Support and Load Points, 680	
13.4.4 Cutting Off the Flexural Reinforcement, 685	
13.5 The Detailing of Compression Members	686
13.6 Brackets and Corbels	690
13.6.1 Behavior, 690	
13.6.2 Failure Mechanisms, 692	
13.6.3 Proportioning and Detailing of Corbels, 694	
13.6.4 Other Types of Bracket, 697	
13.7 Deep Beams	700
13.7.1 Introduction, 700	
13.7.2 Simply Supported Beams, 703	
13.7.3 Continuous Deep Beams, 705	
13.7.4 Web Reinforcement in Deep Beams, 707	
13.7.5 Introduction of Concentrated Loads, 714	
13.8 Beam-Column Joints	716
13.8.1 Introduction, 716	
13.8.2 Knee Joints, 717	
13.8.3 Exterior Joints of Multistory Plane Frames, 726	
13.8.4 Interior Joints of Multistory Plane Frames, 736	
13.8.5 Suggestions for the Detailing of Joints, 746	
13.8.6 Joints of Multistory Space Frames, 750	
13.9 Conclusions	758
13.10 References	758
INDEX	763

The Design Approach

1.1 DEVELOPMENT OF WORKING STRESS AND ULTIMATE STRENGTH DESIGN PROCEDURES

Several of the early studies of reinforced concrete members were based on ultimate strength theories, for example, Thullie's flexural theory of 1897 and the parabolic stress distribution theory of Ritter in 1899. However at about 1900 the straight-line (elastic) theory of Coignet and Tedesco became generally accepted, mainly because elastic theory was the conventional method of design for other materials and also because it was thought that the straight-line distribution of stress led to mathematical simplification. In addition, tests had shown that the use of elastic theory with carefully chosen values for the allowable working stresses led to a structure displaying satisfactory behavior at the service loads and having an adequate margin of safety against collapse. Thus elastic theory has been the basis of reinforced concrete design for many years.

Recently there has been renewed interest in ultimate strength theory as a basis of design. After more than half a century of practical experience and laboratory tests, the knowledge of the behavior of structural concrete has vastly increased and the deficiencies of the elastic theory (working stress) design method have become evident. This has resulted in periodic adjustment to the working stress design method, but it has become increasingly apparent that a design method should be based on the actual inelastic properties of the concrete and steel. Thus ultimate strength design became accepted as an alternative to working stress design in the building codes for reinforced concrete of the American Concrete Institute (ACI) in 1956 and of the United Kingdom in 1957. These two design approaches may be summarized as follows.

Working Stress Design (Elastic Theory)

The sections of the members of the structure are designed assuming straight-line stress-strain relationships ensuring that at service loads the stresses in

the steel and the concrete do not exceed the allowable working stresses. The allowable stresses are taken as fixed proportions of the ultimate or yield strength of the materials; for example, for compression in bending 0.45 of the cylinder strength of the concrete may be assumed. The bending moments and forces that act on statically indeterminate structures are calculated assuming linear-elastic behavior.

Ultimate Strength Design

The sections of the members of the structures are designed taking inelastic strains into account to reach ultimate (maximum) strength (i.e., the concrete at maximum strength and usually the steel yielding) when an ultimate load, equal to the sum of each service load multiplied by its respective load factor, is applied to the structure. Typical load factors used in practice are 1.4 for dead load and 1.7 for live load. The bending moments and forces that act on statically indeterminate structures at the ultimate load are calculated assuming linear-elastic behavior of the structure up to the ultimate load. Alternatively, the bending moments and forces are calculated taking some account of the redistribution of actions that may occur because of the non-linear relationships that exist between the actions and deformations in the members at high loads.

Some of the reasons for the trend towards ultimate strength design are as follows:

1. Reinforced concrete sections behave inelastically at high loads; hence elastic theory cannot give a reliable prediction of the ultimate strength of the members because inelastic strains are not taken into account. For structures designed by the working stress method, therefore, the exact load factor (ultimate load/service load) is unknown and varies from structure to structure.
2. Ultimate strength design allows a more rational selection of the load factors. For example, a low load factor may be used for loading known more exactly, such as dead load, and a higher load factor for less certain loads, such as live load.
3. The stress-strain curve for concrete is nonlinear and is time dependent. For example, the creep strains for concrete under constant sustained stress may be several times the initial elastic strain. Therefore, the value of the modular ratio (ratio of the elastic modulus of steel to that of concrete) used in working stress design is a crude approximation. Creep strains can cause a substantial redistribution of stress in reinforced concrete sections, and this means that the stresses that actually exist at the service loads often bear little relation to the design stresses. For example, the compression steel in columns may reach the yield strength during the sustained application of service

loads, although this occurrence is not evident from working stress analysis using a normally recommended value for the modular ratio. Ultimate strength design does not require a knowledge of the modular ratio.

4. Ultimate strength design utilizes reserves of strength resulting from a more efficient distribution of stresses allowed by inelastic strains, and at times it indicates the working stress method to be very conservative. For example, the compression steel in doubly reinforced beams usually reaches the yield strength at the ultimate load, but elastic theory may indicate a low stress in this steel.

5. Ultimate strength design makes more efficient use of high strength reinforcement, and smaller beam depths can be used without compression steel.

6. Ultimate strength design allows the designer to assess the ductility of the structure in the postelastic range. This is an important aspect when he considers the possible redistribution of bending moments in the design for gravity loads and in the design for earthquake or blast loading.

地震
爆破

1.2 DESIGN FOR STRENGTH AND SERVICEABILITY

More recently it has been recognized that the design approach for reinforced concrete ideally should combine the best features of ultimate strength and working stress design. This is desirable because if sections are proportioned by ultimate strength requirements alone, there is a danger that although the load factor is adequate, the cracking and the deflections at the service loads may be excessive. Cracking may be excessive if the steel stresses are high or if the bars are badly distributed. Deflections may be critical if the shallow sections, which are possible in ultimate strength design, are used and the stresses are high. Thus to ensure a satisfactory design, the crack widths and deflections at service loads must be checked to make certain that they lie within reasonable limiting values, dictated by functional requirements of the structure. This check requires the use of elastic theory.

In 1964 the European Concrete Committee produced its recommendations for an international code of practice for reinforced concrete.^{1.1} This document introduced the concept of limit state design, proposing that the structure be designed with reference to several limit states. The most important limit states were: strength at ultimate load, deflections at service load, and crack widths at service load. The approach is gaining acceptance in many countries. Thus ultimate strength theory is becoming the predominant approach for proportioning sections, with elastic theory used only for ensuring serviceability. It is also worth noting that ultimate strength theory has been used for proportioning sections in the USSR and in some other European countries for many years. It is likely that the trend toward the use of

ultimate strength design will continue, and it is apparent that it may not be many years before the example of the European Concrete Committee is followed and the working stress method disappears from building codes for reinforced concrete.

The 1956 and 1963 building codes of the American Concrete Institute allowed the use of either working stress or ultimate strength design. The 1971 ACI code^{1,2} emphasizes design based on strength with serviceability checks. However, the 1971 code also allows an alternative design method in which the working stress method is used to design beams for flexure and factored-down ultimate strength equations are used to design members for all other actions. It is evident that this alternative method has been retained only in an attempt to keep what has been the conventional design approach. Future ACI codes may omit this alternative procedure completely. It is also of interest to note a change in the terminology in the 1971 ACI code. The word "ultimate" rarely appears. For example, "strength" is written for "ultimate strength."

In this book the strength and serviceability approach of the 1971 ACI code is adopted because it is considered to emphasize the real behavior of reinforced concrete and to be the more logical approach to design. Whenever possible, the background to the ACI code provisions are outlined. Where necessary, the code provisions are supplemented in the light of new research evidence that has become available, and some comparison with other codes is given.

1.3 ACI STRENGTH AND SERVICEABILITY DESIGN METHOD

1.3.1 Strength Provisions

The 1971 ACI code^{1,2} separates the strength provisions for structural safety into two parts, load factors and capacity reduction factors.

Load Factors

Load factors are intended to ensure adequate safety against an increase in service loads beyond loads specified in design so that failure is extremely unlikely. Load factors also help to ensure that the deformations at the service load are not excessive. The load factors used for dead load, live load, lateral earth and fluid pressure, and wind and earthquake loading differ in magnitude. The load factors are different for various types of loading because, for instance, the dead load of a structure is less likely to be exceeded than the prescribed live load. The ultimate load of the structure should at least equal the sum of each service load multiplied by its respective load factor. The 1971 ACI code recommends that the required strength U provided to resist

dead load D and live load L be at least equal to

$$U = 1.4D + 1.7L \quad (1.1)$$

When wind load W is to be considered in the design the required strength U provided should also be at least equal to

$$U = 0.75(1.4D + 1.7L + 1.7W) \quad (1.2)$$

where the case of L having its full value or zero should be checked, and

$$U = 0.9D + 1.3W \quad (1.3)$$

when actions resulting from D and W are of opposite sign. If earthquake load E is to be included, Eqs. 1.2 and 1.3 should also comply, with $1.1E$ substituted for W . Strength requirements for other types of loading are given in the code.

The load factors as prescribed do not vary with the seriousness of the consequence of failure. For example, one might expect the load factor used for a hospital building to be higher than that for an industrial building. However, it is assumed that the prescribed service loads include the effect of the seriousness of the failure. Nevertheless, the load factors prescribed should be regarded as minimum values. Some increases may be appropriate if the consequences of failure are especially serious or if a reasonable estimate of the service load cannot be made.

Capacity Reduction Factors

Capacity reduction factors φ are provided to allow for approximations in the calculations and variations in the material strengths, workmanship, and dimensions. Each one of these may be within tolerable limits, but in combination they may result in undercapacity. The basic strength equation for a section may be said to give the ideal strength, assuming that the equation is scientifically correct, that the materials are as strong as specified, and that sizes are as shown on the drawings. The dependable or reliable strength of the section to be used in the design calculations is taken as the ideal strength multiplied by φ where the value for the capacity reduction factor φ depends on the importance of the variable quantities. Values recommended by the 1971 ACI code are:

flexure, with or without axial tension, or axial tension $\varphi = 0.90$

flexure with axial compression, or axial compression:

if spirally reinforced $\varphi = 0.75$

otherwise $\varphi = 0.70$

(φ may be increased linearly to 0.9 for sections

with small axial compression tending to zero)

shear and torsion $\varphi = 0.85$

Other values are given in the code.

Additional variables that have been considered in prescribing capacity reduction factors include the seriousness of the consequence of failure of the members with respect to the whole structure, and the degree of warning involved in the mode of failure. Beams have the highest φ value because they are designed to fail in a ductile manner with yielding of the tension steel. Warning of such a failure would normally be given by considerable cracking and large deflections, and since the variability of steel strength is less than that for concrete, the flexural strength can be accurately predicted. Columns have the lowest φ values because they can fail in a brittle way when the concrete strength is the critical factor. Also, failure of a column can mean collapse of the whole structure, and repair of columns is difficult to carry out. Spirally reinforced columns are more ductile than tied columns, hence they have been allocated a higher φ value. The φ value for shear and torsion is intermediate because the concrete contribution to strength is less critical than in the case of compression members, and the theory predicting the strength is less accurate than that for flexure.

In design the ultimate load is calculated on the basis of the dependable strength. On the basis of the ideal strength, the overall safety factor for a structure loaded by dead and live load is

$$\frac{1.4D + 1.7L}{D + L} \frac{1}{\varphi} \quad (1.4)$$

On this basis, the overall safety factor against the ideal strength of the section being reached (in the case of flexure, with or without axial tension) varies from 1.56 for $L/D = 0$ to 1.82 for $L/D = 4$, the higher value properly applying to the higher live load conditions. For members with flexure and axial compression, the overall safety factor varies between 2.00 and 2.34 for L/D between 0 and 4, thus giving greater overall safety to a more critical building element.

The ideal strength is calculated using the specified strengths of the concrete and the steel. Because these strength values are normally exceeded in a real structure, an additional reserve of strength is available.

1.3.2 Serviceability Provisions

The assessment of the performance of the structure at the service load is an extremely important consideration when members are proportioned on the basis of the required strength. This is because members with small sections, and sections with little compression steel, can satisfy the strength requirements but lead to high stresses and deformations at the service load. Therefore, it must be verified that deflections at service load are within acceptable limits. The control of cracking is also very important for the sake of appearance and durability. Therefore, the crack widths at the service load should

not exceed specified limits. The acceptable limits for deflections and crack widths are difficult to specify, but recommendations for these are given in the 1971 ACI code.^{1,2}

1.3.3 Ductility Provisions

A significant consideration that may have to be added to strength and serviceability is ductility. It is important to ensure that in the extreme event of a structure being loaded to failure, it will behave in a ductile manner. This means ensuring that the structure will not fail in a brittle fashion without warning but will be capable of large deformations at near-maximum load carrying capacity. The large deflections at near-maximum load give ample warning of failure, and by maintaining load carrying capacity, total collapse may be prevented and lives saved. Also, ductile behavior of members enables the use in design of distributions of bending moments that take into account the redistribution possible from the elastic bending moment pattern.

In areas requiring design for seismic loading, ductility becomes an extremely important consideration. This is because the present philosophy of codes for seismic loading (e.g., the Uniform Building code^{1,3}) is to design structures to resist only relatively moderate earthquakes elastically; in the case of a severe earthquake, reliance is placed on the availability of sufficient ductility after yielding to enable a structure to survive without collapse. Hence the recommendations for seismic loading can be justified only if the structure has sufficient ductility to absorb and dissipate energy by post-elastic deformations when subjected to several cycles of loading well into the yield range.

To ensure ductile behavior designers should give special attention to details such as longitudinal reinforcement contents, anchorage of reinforcement and confinement of compressed concrete, ensuring that all brittle types of failure (e.g., failure due to shear) are avoided. The 1971 ACI code^{1,2} makes recommendations for longitudinal steel contents that result in ductile sections, and it allows some redistribution of bending moments from the elastic moment diagram. Also, for the first time, the code includes an appendix giving special provisions for seismic design.

1.4 CONSIDERATIONS OF MEMBER STRENGTH

1.4.1 Development of Member Strength

In design it is often necessary to evaluate the possible upper and lower bounds of the likely strength of structural components. This is the case when a desired sequence of strength attainment in the members of a structure loaded

to failure is to be ensured. For example, at a beam-column joint in a continuous frame, if a column failure with its possible catastrophic consequences is to be avoided, it is always desirable to develop the strength of the beam before the strength of the column. The avoidance of all types of nonductile failure mode is a particular feature of seismic design. Thus it is important to know the possible variation of the likely strengths of structural members.

Real structures contain variations in the strengths of the concrete and steel from the specified values, and there are unavoidable deviations from the specified dimensions because of constructional tolerances. Also, assumptions have been made in the derivation of the strength equations. Hence it is difficult to calculate exactly the real strength of a structure; but it is possible to define levels of possible strength of members, which can be used in various types of design calculations. The levels of ideal strength, dependable strength, probable strength and overstrength will be defined in the following sections.

1.4.2 Ideal Strength S_i

The ideal or nominal strength of a section of a member S_i is obtained from theory predicting the failure behavior of the section and on assumed section geometry and specified material strengths. The major part of this book deals with the derivation of the ideal strength, to which other strength levels can be conveniently related.

1.4.3 Dependable Strength S_d

In the strength provisions described in Section 1.3.1 the purpose of the capacity reduction factor φ was outlined. The capacity reduction factor allows the dependable or reliable strength S_d to be related to the ideal strength by

$$S_d = \varphi S_i \quad (1.5)$$

where φ , the capacity reduction factor, is less than 1.

1.4.4 Probable Strength S_p

The probable strength S_p takes into account the fact that the materials strengths are generally greater than the specified strengths. For example, the yield strength of the steel may be as much as 20% higher than the specified strength and the concrete strength may be as much as 30% higher than the specified concrete strength, or even higher at a greater age or if the material is triaxially compressed. The probable strengths of the materials can be obtained from routine testing, normally conducted during construction of the structure. If the information is required at the design stage, it must be based on previous experience with the materials. The probable strength can

be related to the ideal strength by

$$S_p = \varphi_p S_i \quad (1.6)$$

where φ_p is the probable strength factor allowing for materials being stronger than specified and is greater than 1.

1.4.5 Overstrength S_o

The overstrength S_o takes into account all the possible factors that may cause a strength increase. These include a steel strength higher than the specified yield strength plus additional steel strength due to strain hardening at large deformations, a concrete strength higher than specified, section sizes larger than assumed, axial compression in flexural members due to lateral restraint, and additional reinforcement placed for construction purposes or unaccounted for in calculations. The overstrength can be related to the ideal strength by

$$S_o = \varphi_o S_i \quad (1.7)$$

where φ_o is the overstrength factor allowing for all sources of strength increase and is greater than 1.

1.4.6 Relationships Between Different Strengths

The highest level of protection to ensure that component A which receives load from component B does not fail before the strength of component B is developed is found when the dependable strength of component A exceeds the overstrength of component B , $S_{dA} \geq S_{oB}$. A lower level of protection is given by $S_{iA} \geq S_{oB}$, and an even lower level of protection is given by $S_{pA} \geq S_{oB}$. The degree of protection afforded by these cases may best be expressed by the ratio of probable strengths, S_{pA}/S_{pB} , of the two components. For the foregoing levels of protection, high to low, it will be found from Eqs. 1.5 to 1.7 that

$$\frac{S_{dA}}{S_{oB}} = \frac{\varphi_A S_{pA}/\varphi_{pA}}{\varphi_{oB} S_{pB}/\varphi_{pB}} \geq 1 \quad \therefore \quad \frac{S_{pA}}{S_{pB}} \geq \frac{\varphi_{pA} \varphi_{oB}}{\varphi_{pB} \varphi_A} \quad (1.8a)$$

$$\frac{S_{iA}}{S_{oB}} = \frac{S_{pA}/\varphi_{pA}}{\varphi_{oB} S_{pB}/\varphi_{pB}} \geq 1 \quad \therefore \quad \frac{S_{pA}}{S_{pB}} \geq \frac{\varphi_{pA} \varphi_{oB}}{\varphi_{pB}} \quad (1.8b)$$

$$\frac{S_{pA}}{S_{oB}} = \frac{S_{pA}}{\varphi_{oB} S_{pB}/\varphi_{pB}} \geq 1 \quad \therefore \quad \frac{S_{pA}}{S_{pB}} \geq \frac{\varphi_{oB}}{\varphi_{pB}} \quad (1.8c)$$

For example, if $\varphi_A = 0.9$, $\varphi_{pA} = \varphi_{pB} = 1.1$, and $\varphi_{oB} = 1.3$, the ratios of the probable strength of component A to the probable strength of

component *B* necessary to ensure that component *B* does not fail are $(1.1 \times 1.3)/(1.1 \times 0.9) = 1.44$, $1.1 \times 1.3/1.1 = 1.30$, and $1.3/1.1 = 1.18$, according to Eqs. 1.8a, 1.8b, and 1.8c, respectively, indicating the different levels of protection for component *B*.

1.5 REFERENCES

- 1.1 CEB, "Recommendations for an International Code of Practice for Reinforced Concrete," Comité Européen du Beton (CEB), Paris, 1964. (English translation available from Cement and Concrete Association, London, 156 pp.)
- 1.2 ACI Committee 318, "Building Code Requirements for Reinforced Concrete (ACI 318-74)," American Concrete Institute, Detroit, 1971, 78 pp.
- 1.3 ICBO, "Uniform Building Code," 1970 edition, Vol. 1, International Conference of Building Officials, Pasadena, Calif., 651 pp.

Stress-Strain Relationships for Concrete and Steel

2.1 CONCRETE

2.1.1 Uniaxial Stress Behavior

Under practical conditions concrete is seldom stressed in one direction only (uniaxial stress), since in most structural situations the concrete is stressed simultaneously in a number of directions. Nevertheless, an assumed uniaxial stress condition can be justified in many cases.

Compressive Stress Behavior

The compressive strength of concrete is usually obtained from cylinders with a height to diameter ratio of 2. The cylinders are loaded longitudinally at a slow strain rate to reach maximum stress in 2 or 3 minutes. The normal standard cylinder is 12 in (305 mm) high by 6 in (152 mm) diameter and the compressive strength attained at 28 days usually ranges between 2000 and 8000 psi (13.8 to 55.2 N/mm²). Smaller size cylinders, or cubes, are also used, particularly for production control, and the compressive strength of these units is higher. With appropriate conversion factors obtained from tests, the results from such specimens can be converted into equivalent standard cylinder strength values.

Figure 2.1 presents typical stress-strain curves obtained from concrete cylinders loaded in uniaxial compression in a test conducted over several minutes. The curves are almost linear up to about one-half the compressive strength. The peak of the curve for high-strength concrete is relatively sharp, but for low-strength concrete the curve has a flat top. The strain at the maximum stress is approximately 0.002. At higher strains, after the maximum stress is reached, stress can still be carried even though cracks parallel to the direction of the loading become visible in the concrete. Concrete tested in flexible testing machines sometimes fails explosively because the concrete

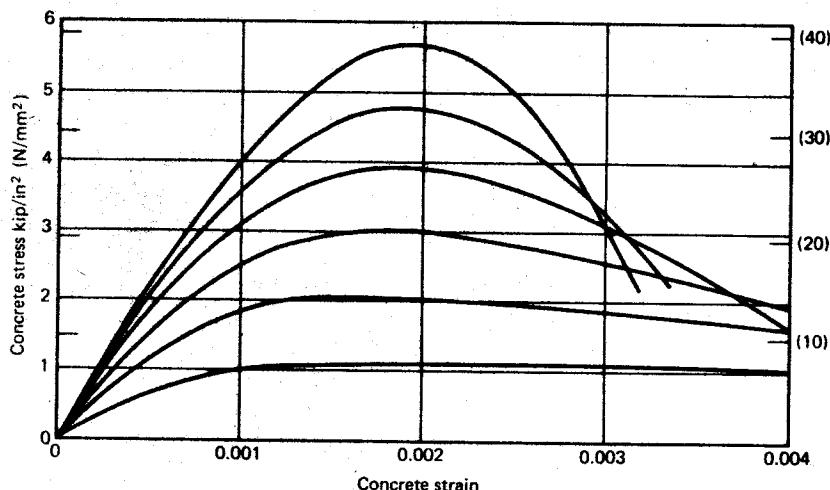


Fig. 2.1. Stress-strain curves for concrete cylinders loaded in uniaxial compression.

cannot absorb the release in strain energy from the testing machine when the load decreases after maximum stress. A stiff testing machine is necessary to trace the full extent of the descending branch of the stress-strain curve.

The modulus of elasticity for concrete E_c may be taken as^{2,1}

$$E_c = w^{1.5} 33\sqrt{f'_c} \text{ psi} \quad (2.1)$$

(1 psi = 0.00689 N/mm²), where w is the density of concrete in pounds per cubic foot (1 lb/ft³ = 16.02 kg/m³) and f'_c is the compressive cylinder strength in psi. Equation 2.1, which applies for values of w between 90 and 155 lb/ft³, was determined by Pauw^{2,2} from short-term loading tests; it gives the secant modulus at a stress of approximately $0.5f'_c$. For normal weight concrete, E_c may be considered to be $57,000\sqrt{f'_c}$ psi or $4730\sqrt{f'_c}$ N/mm².

Tests by Rüsch^{2,3} have indicated that the shape of the stress-strain curve before maximum stress depends on the strength of the concrete (see Fig. 2.2). However, a widely used approximation for the shape of the stress-strain curve before maximum stress is a second-degree parabola. For example, the often quoted stress-strain curve due to Hognestad^{2,4} is shown in Fig. 2.3, where f''_c is the maximum stress reached in the concrete. The extent of falling branch behavior adopted depends on the limit of useful concrete strain assumed. This aspect is further discussed in Chapters 3 and 6 with regard to calculations for the flexural strength and ultimate deformations of members. The maximum compressive stress reached in the concrete of a flexural member f''_c may differ from the cylinder strength f'_c because of the difference in size

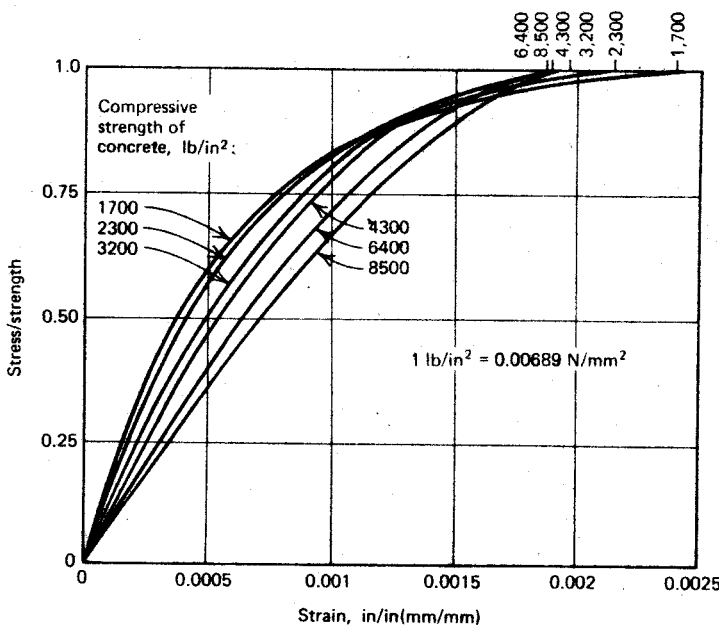


Fig. 2.2. Relationship between the stress to strength ratio and strain for concrete of different strengths.^{2,3}

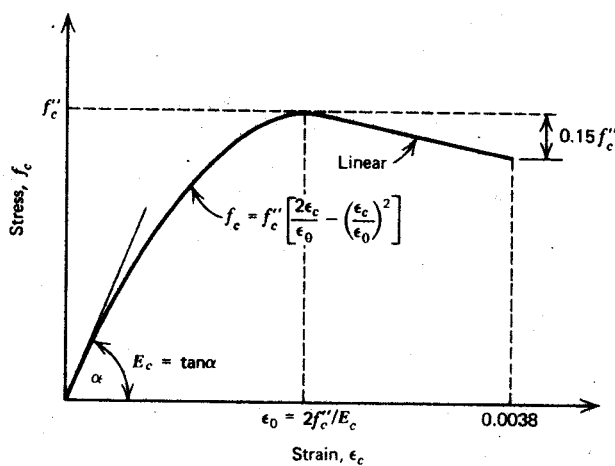


Fig. 2.3. Idealized stress-strain curve for concrete in uniaxial compression.^{2,4}

and shape of the compressed concrete. The strength of concrete in members with flexure is treated at greater length in Chapter 3.

When the load is applied at a fast strain rate, both the modulus of elasticity and the strength of the concrete increase. For example, it has been reported^{2,5} that for a strain rate of 0.01/sec the concrete strength may be increased as much as 17%.

Repeated high-intensity compressive loading produces a pronounced hysteresis effect in the stress-strain curve. Figure 2.4 gives test data obtained

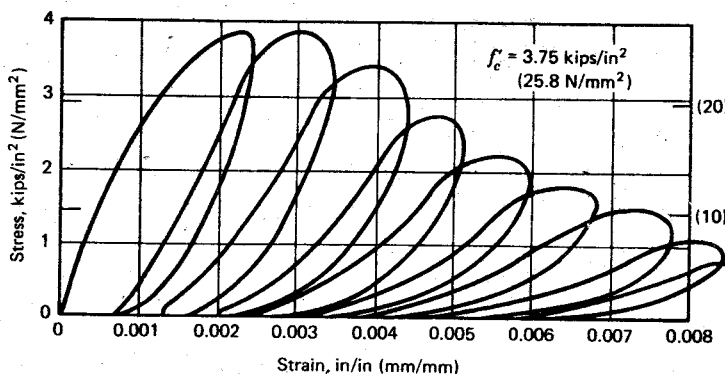


Fig. 2.4. Stress-strain curves for concrete cylinder with high-intensity repeated axial compressive cyclic loading.^{2,6}

by Sinha, Gerstle, and Tulin^{2,6} for slow strain rates. Their tests, and those of Karsan and Jirsa,^{2,7} indicated that the envelope curve was almost identical to the curve obtained from a single continuous load application.

Rüsch,^{2,8} who has conducted long-term loading tests on unconfined concrete, has found that the sustained load compressive strength is approximately 80% of the short-term strength, where the short-term strength is the strength of an identically old and identically cast specimen that is loaded to failure over a 10-minute period when the specimen under sustained load has collapsed. In practice, concrete strengths considered in the design of structures are usually based on the anticipated short-term strength at 28 days. The strength reduction due to long-term loading will be at least partly offset by the property of concrete to reach a higher strength at greater ages. Also, the capacity reduction factor φ is low when the compressive strength of concrete is critical. Creep strains due to long-term loading cause modification in the shape of the stress-strain curve. Some curves obtained by Rüsch^{2,8} for various rates of loading (Fig. 2.5) indicate that with a decreasing rate of strain, the

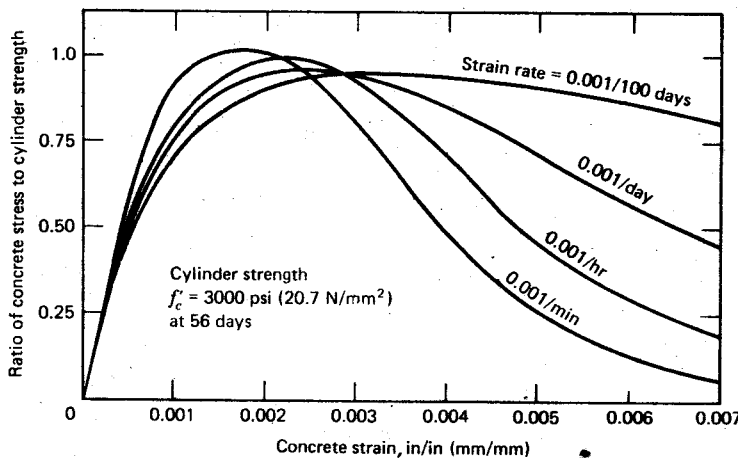


Fig. 2.5. Stress-strain curves for concrete with various rates of axial compressive loading.^{2.8}

value of maximum stress reached gradually decreases but the descending branch of the curve falls less quickly, the strain at which the maximum stress is reached is increased.

Tensile Stress Behavior

The tensile strength of concrete, generally less than 20% of the compressive strength, can be obtained directly from tension specimens. However, because of the difficulties of holding the specimens to achieve axial tension and the uncertainties of secondary stresses induced by the holding devices, the direct tension test is infrequently used, even for research purposes.

The tensile strength of concrete may be measured indirectly in terms of the computed tensile stress at which a cylinder placed horizontally in a testing machine and loaded along a diameter will split. The method of test and the stresses induced along the loaded diameter, as found from the theory of elasticity, are represented in Fig. 2.6. The tensile stress across the diameter at splitting is found from the relationship $2P/(\pi hd)$, where P is the applied load at splitting, h is the length of the cylinder, and d is the diameter of the cylinder.

The tensile strength of concrete can also be evaluated by means of bending tests conducted on plain concrete beams. The beams normally have a 6 in (150 mm) square cross section. The tensile strength in flexure, known as the modulus of rupture f_r , is computed from the flexural formula M/Z , where M is the bending moment at the failure of the specimen and Z is the

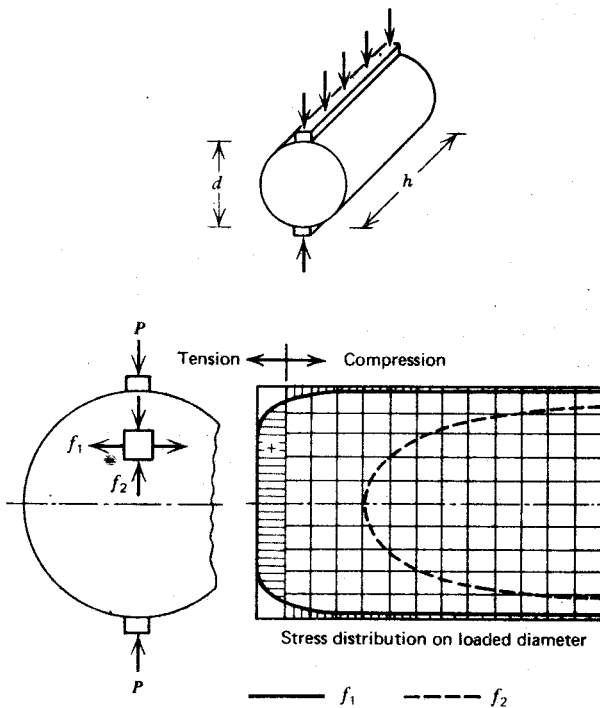


Fig. 2.6. Split-cylinder test for tensile strength.

section modulus of the cross section. The split cylinder tensile strength usually ranges from 50 to 75% of the modulus of rupture. The difference is mainly due to the stress distribution in the concrete of the flexural member being nonlinear when failure is imminent. An approximate relationship for the modulus of rupture is

$$f_r = K \sqrt{f'_c} \text{ psi} \quad (2.2)$$

where f'_c is the cylinder strength in psi ($1 \text{ psi} = 0.00689 \text{ N/mm}^2$). For sand and gravel concrete K can range between 7 and 13; a lower bound of $K = 7.5$ is often assumed. It is evident that an increase in compressive strength is not accompanied by a proportionate increase in the modulus of rupture.

Because of the low tensile strength of concrete, concrete in tension is usually ignored in strength calculations of reinforced concrete members. When it is taken into account, however, the stress-strain curve in tension may

be idealized as a straight line up to the tensile strength. Within this range the modulus of elasticity in tension may be assumed to be the same as in compression.

Poisson's Ratio

The ratio between the transverse strain and the strain in the direction of applied uniaxial loading, referred to as Poisson's ratio, is usually found to be in the range 0.15 to 0.20 for concrete. However, values between 0.10 and 0.30 have been determined. No reliable information appears to exist regarding the variation of Poisson's ratio with the concrete properties, but it is generally considered that Poisson's ratio is lower for high-strength concrete.

At high compressive stresses the transverse strains increase rapidly, owing to internal cracking parallel to the direction of loading within the specimen. Strains measured in a specimen tested to failure are plotted in Fig. 2.7. During most of the loading range the volume of the specimen decreases; but at high stresses near the compressive strength of the specimen, the transverse strains become so high that the volume of the specimen will actually commence to increase, indicating the breakdown of strength. The failure of a specimen loaded uniaxially in compression is generally accompanied by splitting in the direction parallel to the load and volume increase.

2.1.2 Combined Stress Behavior

In many structural situations concrete is subjected to direct and shear stresses acting in a number of directions. Considering the equilibrium of the forces

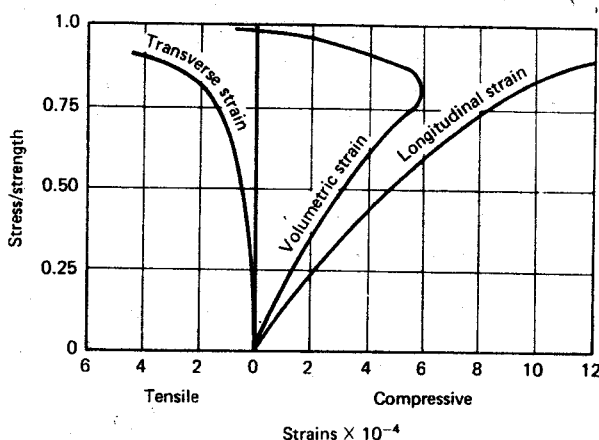


Fig. 2.7. Strains measured in a concrete specimen loaded uniaxially in compression.

acting on an element of the concrete, it can be shown (e.g., see Popov^{2,9}) that any combined stress situation can be reduced to three normal stresses acting on three mutually perpendicular planes. These three normal stresses are the principal stresses, and the shear stresses acting on these planes are zero.

In spite of extensive research, no reliable theory has yet been developed for the failure strength of concrete for the general case of complex three-dimensional states of stress. Modifications of the conventional theories of strength of materials have been attempted, but no single theory is accurately applicable to all cases. In many applications, however, one of the simpler theories of failure gives sufficient accuracy.

Biaxial Stress Behavior

A biaxial stress condition occurs if the principal stresses act only in two directions; that is, the stresses act in one plane and the third principal stress is zero. Figure 2.8 presents the combinations of direct stress in two directions which caused failure, as found by Kupfer, Hilsdorf, and Rüsch.^{2,10} These investigators concluded that the strength of concrete subjected to biaxial compression may be as much as 27% higher than the uniaxial strength. For equal biaxial compressive stresses, the strength increase is approximately 16%. The strength under biaxial tension is approximately equal to the uniaxial tensile strength. Note, however, that combined tension and compression loadings reduce both the tensile and the compressive stresses at failure.

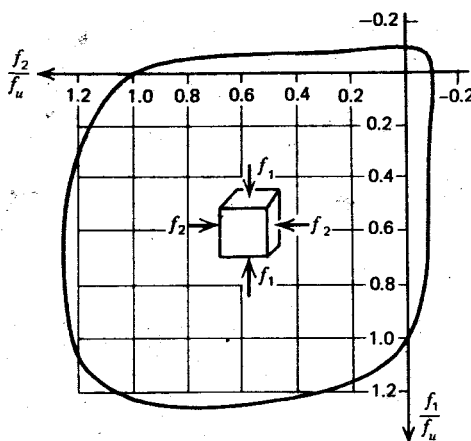


Fig. 2.8. Biaxial strength of concrete, f_u = uniaxial strength.^{2,10}

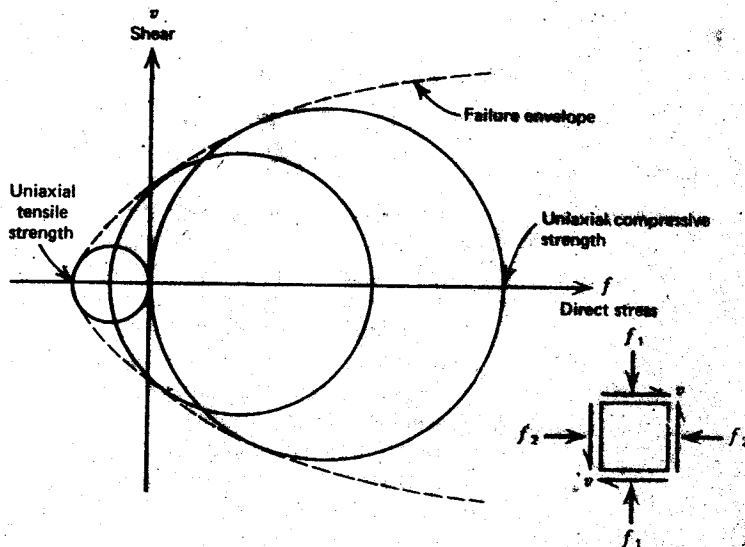


Fig. 2.9. Strength of concrete under general two-dimensional stress system.

On planes other than the principal planes, the direct stresses are accompanied by shear stresses. Mohr's theory of failure^{2,11} has been used to obtain a prediction of strength for this combined stress case. Figure 2.9 indicates how a family of Mohr's circles representing failure conditions in simple tension, simple compression, and other combinations, are enclosed by an envelope curve. Any combination of stresses having a Mohr's circle that is tangent to this envelope or intersects it can be regarded as a failure condition.

A failure curve for elements with direct stress in one direction combined with shear stress, as found by Bresler and Pister,^{2,12} appears in Fig. 2.10.

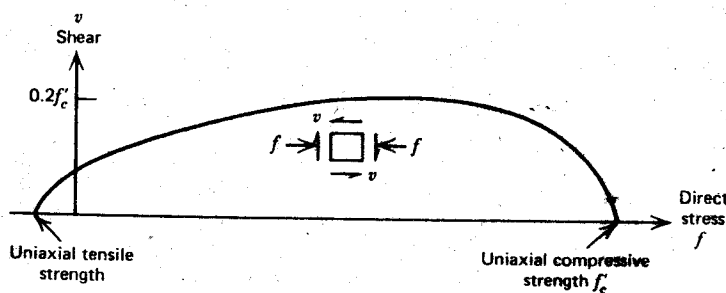


Fig. 2.10. Combinations of direct stress and shear causing failure of concrete.^{2,12}

The curve indicates that the compressive strength of concrete is reduced in the presence of shear stress. This action may, for example, influence the strength of concrete in the compression zone of beams and columns when shear is present.

Triaxial Compressive Stress Behavior

The strength and ductility of concrete are greatly increased under conditions of triaxial compression. Richart, Brandtzaeg, and Brown^{2,13} found the following relationship for the strength of concrete cylinders loaded axially to failure while subjected to confining fluid pressure

$$f'_{cc} = f'_c + 4.1f_l \quad (2.3)$$

where f'_{cc} = axial compressive strength of confined specimen

f'_c = uniaxial compressive strength of unconfined specimen

f_l = lateral confining pressure

Other tests by Balmer^{2,14} have given values for the lateral stress coefficient which range between 4.5 and 7.0 with an average value of 5.6, rather than the 4.1 found by Richart et al. The high values for the coefficient occurred at low lateral pressures.

Figure 2.11 gives the axial stress-strain curves obtained by Richart et al^{2,13} for triaxial compression tests conducted on concrete cylinders. The cylinders were confined laterally by fluid pressure. For each curve the fluid pressure

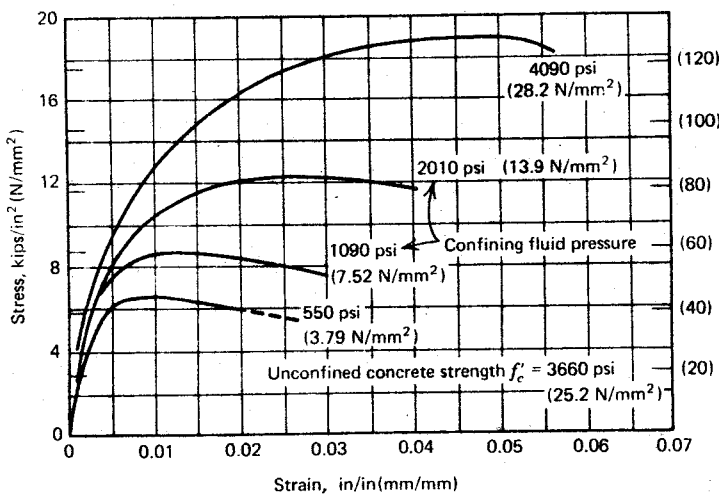


Fig. 2.11. Axial stress-strain curves from triaxial compression tests on concrete cylinders.^{2,13}

was held constant while the axial compressive stress was increased to failure and the axial strains measured. The tests were carried out over short-term periods. It is evident that an increase in lateral pressure brings very significant increases in ductility, as well as strength. This effect is due to the lateral pressure that confines the concrete and reduces the tendency for internal cracking and volume increase just prior to failure.

2.1.3 Concrete Confinement by Reinforcement

In practice, concrete may be confined by transverse reinforcement, commonly in the form of closely spaced steel spirals or hoops. In this case, at low levels of stress in the concrete, the transverse reinforcement is hardly stressed; hence the concrete is unconfined. The concrete becomes confined when at stresses approaching the uniaxial strength, the transverse strains become very high because of progressive internal cracking and the concrete bears out against the transverse reinforcement, which then applies a confining reaction to the concrete. Thus the transverse reinforcement provides passive confinement. Tests by many investigators have shown that confinement by transverse reinforcement can considerably improve the stress-strain characteristics of concrete at high strains. Richart et al^{2.15} found, for example, that Eq. 2.3, for the strength of concrete confined by fluid pressure, applies approximately to concrete confined by circular spirals. Figure 2.12 shows stress-strain curves obtained from three sets of concrete cylinders confined by circular spirals tested by Iyengar et al.^{2.16} Each set was for a different unconfined strength of concrete. The increase in strength and ductility with content of confining steel is very significant. Tests have demonstrated that circular spirals confine concrete much more effectively than rectangular or square hoops. In Fig. 2.13 we have load-strain curves from concrete prisms tested by Bertero and Felippa^{2.17} which contained various amounts of square ties. The effect of the different transverse steel contents on the ductility is quite appreciable, but the effect on strength is much smaller.

The reason for the considerable difference between the confinement by circular steel spirals and confinement by rectangular or square steel hoops is illustrated in Fig. 2.14. Circular spirals, because of their shape, are in axial hoop tension and provide a continuous confining pressure around the circumference, which at large transverse strains approximates fluid confinement. As a rule, however, square hoops can apply only confining reactions near the corners of the hoops because the pressure of the concrete against the sides of the hoops tends to bend the sides outwards, as in Fig. 2.14. Therefore a considerable portion of the concrete cross section may be unconfined. Because of internal arching between the corners, the concrete is confined effectively only in the corners and the central region of the section.

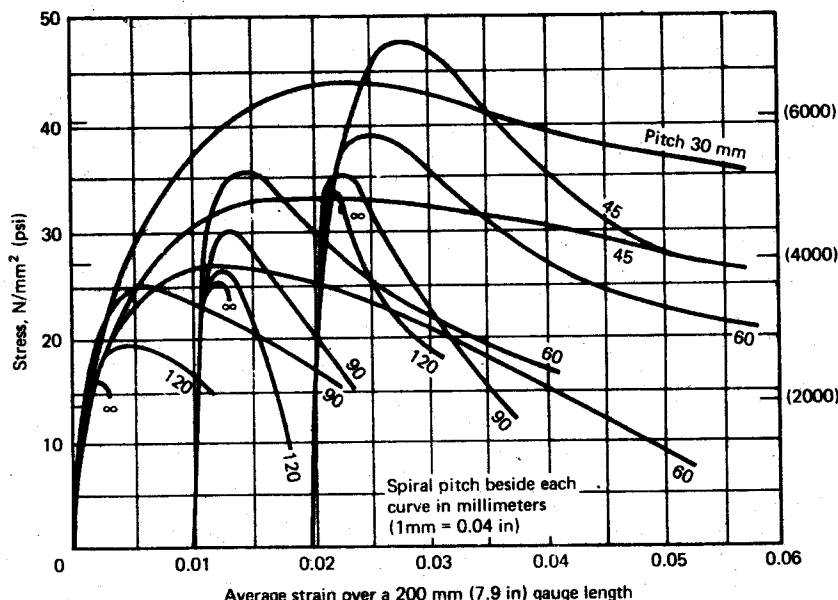


Fig. 2.12. Stress-strain curves for concrete cylinders 150 mm (5.9 in) diameter by 300 mm (11.8 in) high, confined by circular spirals from 6.5 mm (0.26 in) diameter mild steel bar.^{2,16}

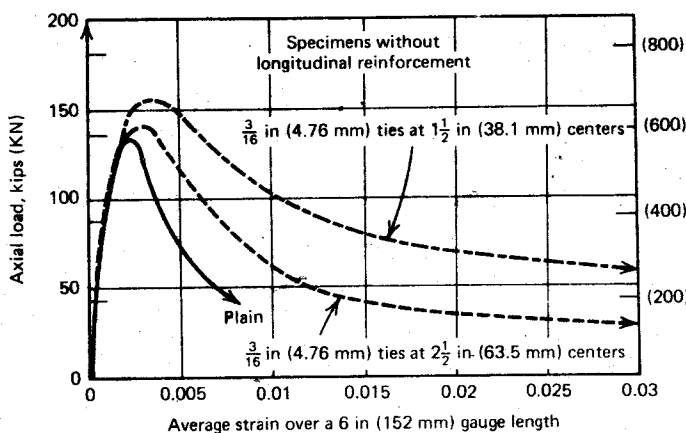


Fig. 2.13. Axial load-strain curves for $4\frac{1}{2}$ in (108 mm) square concrete prisms with various contents of square ties.^{2,17}

323/2

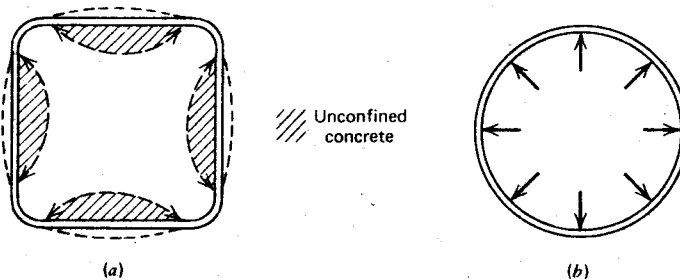


Fig. 2.14. Confinement by square hoops and circular spirals. (a) Square hoop, (b) Circular spiral.

Nevertheless, square confining steel does produce a significant increase in ductility, and some enhancement of strength has been observed by many investigators.

It is evident from Figs. 2.12 and 2.13 that confinement by transverse reinforcement has little effect on the stress-strain curve until the uniaxial strength of the concrete is approached. The shape of the stress-strain curve at high strains is a function of many variables, the major ones being the following:

1. ✓ The ratio of the volume of transverse steel to the volume of the concrete core, because a high transverse steel content will mean a high transverse confining pressure.
2. ✓ The yield strength of the transverse steel, because this gives an upper limit to the confining pressure.
3. The ratio of the spacing of the transverse steel to the dimensions of the concrete core, because a smaller spacing leads to more effective confinement, as illustrated in Fig. 2.15. The concrete is confined by arching of the concrete between the transverse bars and if the spacing is large it is evident that a large volume of the concrete cannot be confined and may spall away.
4. ✓ The ratio of the diameter of the transverse bar to the unsupported length of transverse bars in the case of rectangular stirrups or hoops, because a larger bar diameter leads to more effective confinement. This effect is illustrated in Fig. 2.14. Transverse bars of small diameter will act merely as ties between the corners because the flexural stiffness of the hoop bar is small and the hoops bow outward rather than effectively confining the concrete in the regions between the corners. With a larger transverse bar diameter to unsupported length ratio, the area of concrete effectively confined will be larger because of the greater flexural stiffness of the hoop side. In the case of a circular spiral this variable has no significance: given its shape, the

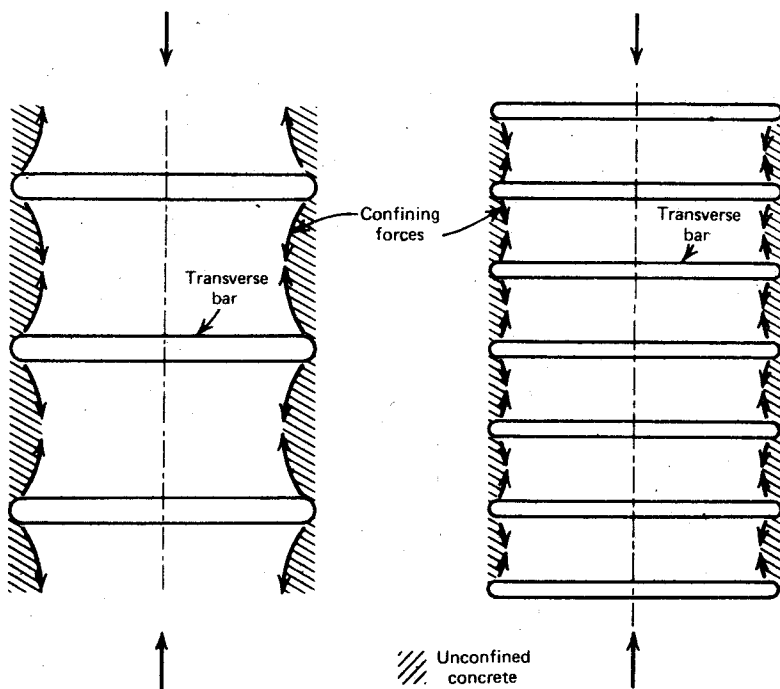


Fig. 2.15. Effect of spacing of transverse steel on efficiency of confinement.

spiral will be in axial tension and will apply a uniform radial pressure to the concrete.

5. The content and size of longitudinal reinforcement, because this steel will also confine the concrete. Longitudinal bars are usually of large diameter, and the ratio of bar diameter to unsupported length is generally such that the bars can effectively confine the concrete. However, the longitudinal bars must be placed tightly against the transverse steel because the transverse steel provides the confining reactions to the longitudinal bars, and if movement of the longitudinal bars is necessary to bring them into effective contact with the transverse steel, the efficiency of the confinement will be reduced.

6. The strength of the concrete, because low-strength concrete is rather more ductile than high-strength concrete (see Fig. 2.1).

7. The rate of loading, because the stress-strain characteristics of concrete are time dependent.

Outside the transverse steel the concrete is not confined, and this cover or shell concrete can be expected to have stress-strain characteristics different

from that of the concrete within the transverse steel. The cover concrete generally commences to spall when the unconfined strength is reached, particularly if the content of transverse steel is high, because the presence of a large number of transverse bars creates a plane or surface of weakness between the core and the cover concrete and precipitates spalling. Thus for high transverse steel contents the contribution of the cover concrete at high strains should be ignored. The cover concrete could be assumed to have the characteristics of unconfined concrete up to an assumed spalling strain and to make no contribution at higher strains. If the transverse steel content is low, the cover concrete will tend to spall less readily and will tend to act more with the confined core. Some account could be taken of the cover concrete at high strains in that case.

Some proposals for the strength and ductility of concrete confined by reinforcement are discussed below.

Concrete Confined by Circular Spirals

Assuming that the spirals are sufficiently close to apply a near-uniform pressure, the confining pressure may be calculated from the hoop tension developed by the spiral steel. Figure 2.16 shows a free body of half a spiral turn. The lateral pressure on the concrete f_l reaches a maximum when the spiral reinforcement reaches the yield strength f_y . If d_s is the diameter of the spiral, A_{sp} is the area of the spiral bar, and s is the pitch of the spiral, equilibrium of the forces acting on the half turn of spiral shown in Fig. 2.16 requires that

$$2f_y A_{sp} = d_s s f_l \quad \therefore \quad f_l = \frac{2f_y A_{sp}}{d_s s} \quad (2.4)$$

Substituting Eq. 2.4 into Eq. 2.3, we see that the axial compressive strength of concrete confined by a spiral is

$$f'_{cc} = f'_c + 8.2 \frac{f_y A_{sp}}{d_s s} \quad (2.5)$$

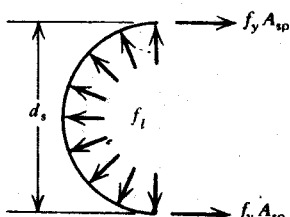


Fig. 2.16. Confinement of concrete by spiral reinforcement.

The increase in ductility of concrete confined by a spiral is also substantial. Iyengar et al^{2,16} and others, have proposed stress-strain relationships for concrete confined by circular spirals based on empirical data obtained from tests.

Concrete Confined by Rectangular Hoops

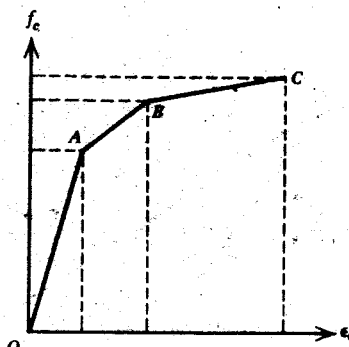
Various investigators have proposed stress-strain relationships for concrete confined by rectangular hoops. Some of the proposed curves appear in Fig. 2.17. In Chan's^{2,18} trilinear curve *OAB* approximated the curve for unconfined concrete and the shape of *BC* depended on the transverse reinforcement. Blume et al^{2,19} also adopted a trilinear curve in which *OA* approximated the curve for unconfined concrete up to $0.85f'_c$ and *ABC* (sometimes replaced by a single straight line) depended on the content and yield stress of the transverse confinement. Baker^{2,20} recommended a parabola up to a maximum stress dependent on the strain gradient across the section, then a horizontal branch to a strain dependent on the strain gradient and the transverse steel content. Roy and Sozen^{2,21} suggested replacing the failing branch with a straight line having a strain at $0.5f'_c$ which was linearly related to the transverse steel content. The curve of Soliman and Yu^{2,22} consisted of a parabola and two straight lines with stresses and strains at the critical points related to transverse steel content and spacing and the confined area. Sargin et al^{2,23} have proposed a general equation that gives a continuous stress-strain curve related to the content, spacing, and yield strength of the transverse steel, the strain gradient across the section, and concrete strength.

On the basis of the existing experimental evidence, Kent and Park^{2,24} have proposed the stress-strain curve in Fig. 2.18 for concrete confined by rectangular hoops. This suggested relationship combines many of the features of the previously proposed curves. The characteristics of the suggested curve are as follows:

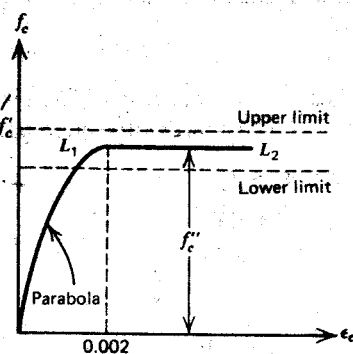
region *AB*: $\epsilon_c \leq 0.002$

$$f_c = f'_c \left[\frac{2\epsilon_c}{0.002} - \left(\frac{\epsilon_c}{0.002} \right)^2 \right] \quad (2.6)$$

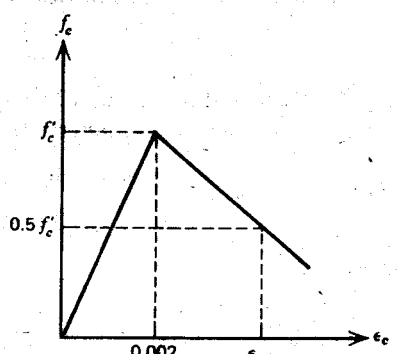
This ascending part of the curve is represented by a second-degree parabola and assumes that the confining steel has no effect on the shape of this part of the curve or the strain at maximum stress. It is also assumed that the maximum stress reached by the confined concrete is the cylinder strength f'_c . There is evidence that rectangular hoops will cause an increase in strength; see for example, Refs. 2.16, 2.17, 2.18, 2.22, and 2.23. However, this increase



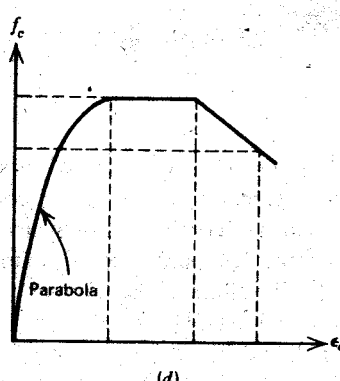
(a)



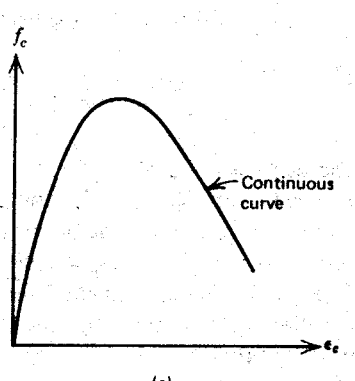
(b)



(c)



(d)



(e)

Fig. 2.17. Some proposed stress-strain curves for concrete confined by rectangular hoops.
 (a) Chan^{2,18} and Blume et al.^{2,19} (b) Baker,^{2,20} (c) Roy and Sozen^{2,21} (d) Soliman and Yu^{2,22}
 (e) Sargin et al.^{2,23}

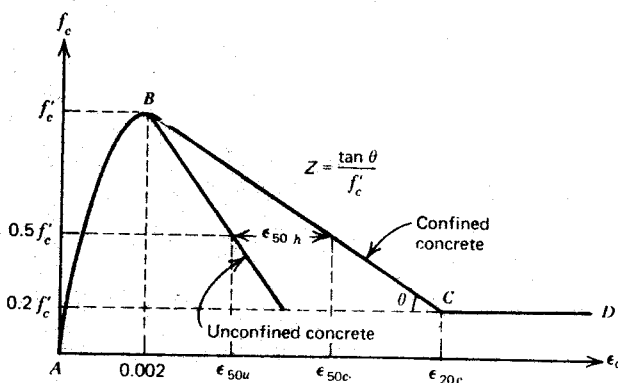


Fig. 2.18. Stress-strain curve for concrete confined by rectangular hoops, Kent and Park.^{2,24}

may be small, and in Roy and Sozen's tests^{2,21} no increase in strength was found. The assumed maximum stress of f'_c will be conservative in most cases.

$$\text{region } BC: 0.002 \leq \epsilon_c \leq \epsilon_{20c}$$

$$f_c' = f'_c [1 - Z(\epsilon_c - 0.002)] \quad (2.7)$$

where

$$Z = \frac{0.5}{\epsilon_{50u} + \epsilon_{50h} - 0.002} \quad (2.8)$$

$$\epsilon_{50u} = \frac{3 + 0.002f'_c}{f'_c - 1000} \quad (2.9)$$

$$\epsilon_{50h} = \frac{3}{4} \rho_s \sqrt{\frac{b''}{s_h}} \quad (2.10)$$

where f'_c = concrete cylinder strength in psi (1 psi = 0.00689 N/mm²), ρ_s = ratio of volume of transverse reinforcement to volume of concrete core measured to outside of hoops, b'' = width of confined core measured to outside of hoops, and s_h = spacing of hoops. The parameter Z defines the slope of the assumed linear falling branch. The slope of the falling branch is specified by the strain when the stress has fallen to $0.5f'_c$, as obtained^{2,24} from existing experimental evidence. Equation 2.9 for ϵ_{50u} takes into account the effect of concrete strength on the slope of the falling branch of unconfined concrete, high-strength concrete being more brittle than low-strength concrete. Equation 2.10 for ϵ_{50h} gives the additional ductility due to rectangular hoops and was derived from the experimental results of three

investigations.^{2.21, 2.22, 2.17} One study^{2.22} gave results including the effect of strain gradient across the section (eccentrically loaded specimens), but since the effect was not marked it does not appear in the equations. When analyzing the results of the three investigations it was assumed that the cover concrete had spalled away by the time the stress had fallen to 0.5 of the maximum stress. The confined core was assumed to be inside the center of the hoop sides, but it is evident that little error will occur if the confined core is taken as that volume of concrete within the outside of the hoops. This will make a small allowance for the presence of some cover concrete at high strains.

$$\text{region } CD: \varepsilon_c \geq \varepsilon_{20c} \quad (2.11)$$

$$f_c = 0.2f'_c$$

This equation accounts for the ability of concrete to sustain some stresses at very large strains.

Figure 2.19 shows the influence of rectangular steel hoops on the stress-strain curve given by Eqs. 2.6 to 2.11 when the concrete cylinder strength is

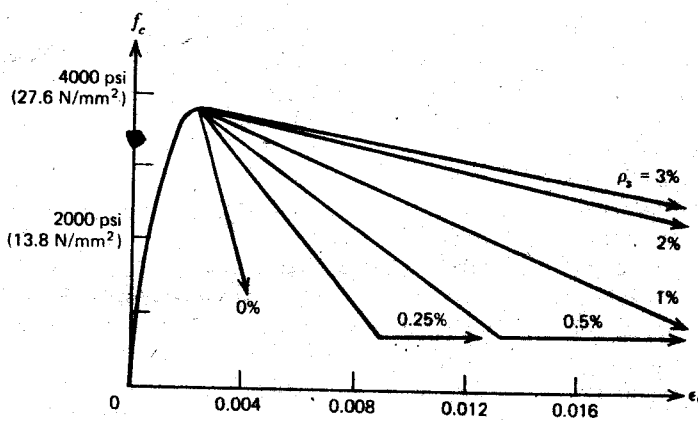


Fig. 2.19. Influence of quantity of hoops on stress-strain curve for concrete when $s_h/b'' = 0.5$ and $f'_c = 4000 \text{ psi (27.6 N/mm}^2\text{)}.$ ^{2.24}

4000 psi (27.6 N/mm²) and $s_h/b'' = 0.5$. Clearly there is a great improvement in the falling branch behavior for small contents of rectangular hoops, but the improvement becomes progressively less significant as more hoops are added.

Equations 2.7 to 2.10 were derived from results from specimens with the variables in the following ranges: $s_h/b = 0.35$ to 2.0, $\rho_s = 0.35$ to 2.4%, and f'_c

mainly in the range 3000 to 4000 psi (20.7 to 27.6 N/mm²), although some f'_c values were in the range 7800 to 8600 psi (53.8 to 59.3 N/mm²).

It is evident that more experimental work is required on confined concrete specimens to provide more data for statistical analysis and to enable the inclusion of more variables. In particular, tests on various arrangements of transverse steel including overlapping hoops, and hoops with supplementary cross ties, are badly needed. In the meantime the proposed equations for concrete confined by rectangular hoops can be regarded only as approximations, but it is believed that they will give reasonable results.

2.1.4 Creep of Concrete

Figure 2.5 indicates that the stress-strain relationship of concrete is a function of time. Concrete under stress undergoes a gradual increase of strain with time because of creep deformations of the concrete. The final creep strain may be several times as large as the initial elastic strain. Generally creep has little effect on the strength of a structure, but it will cause a redistribution of stress in reinforced concrete members at the service loads, and lead to an increase in the service load deflections. Creep deformations are beneficial in some cases. For example, concrete stresses due to differential settlement of structures are reduced by creep. Creep in tension also delays shrinkage cracking in concrete. The method of calculation of stresses and deformations due to creep is examined in Chapter 10.

The creep deformation of concrete under constant axial compressive stress is illustrated in Fig. 2.20. As the figure reveals, the creep proceeds at a

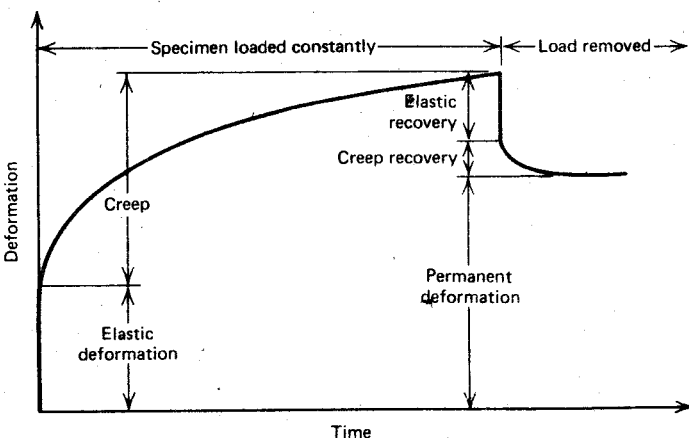


Fig. 2.20. Typical creep curve for concrete with constant axial compressive stress.

decreasing rate with time. If the load is removed, the elastic strain is immediately recovered. However, this recovered elastic strain is less than the initial elastic strain because the elastic modulus increases with age. The elastic recovery is followed by a creep recovery, which is a small proportion of the total creep strain.

Experimental evidence indicates that the creep strain occurring over a given period is proportional to the applied stress, provided the stress level is not high. Research evidence is conflicting with respect to the stress level at which the linearity between creep and applied stress ceases. Some research indicates loss of linearity at compressive stresses as low as $0.2f'_c$; other data suggest a value as high as $0.5f'_c$. However, the assumption of a linear relationship between creep strain and applied stress for the usual range of service load stresses used in structural design results in acceptable accuracy.

The magnitude of creep strain depends on the composition of the concrete, the environment, and the stress-time history.

The composition of concrete may be described in terms of aggregate type and proportions, cement type and content, water/cement ratio, and additives. Aggregate type can have a marked effect on creep because of different absorption and elastic properties of the aggregates. For example, use of sandstone aggregates may result in twice the creep strain than for a limestone aggregate.^{2,25} Aggregates are volumetrically more stable than the cement paste; therefore an increase in aggregate content leads to a decrease in creep strains. An increase in the water/cement ratio and an increase in the cement content, increases creep, as does high air entrainment.

The environment may be described in terms of humidity and member shape and size. The ambient relative humidity has a significant influence on creep. Creep strains are low when the relative humidity is high. Creep is reduced if water loss from the member is restricted, hence the size and shape of a member affect the amount of creep that occurs. In addition, since the outside regions of a large member restricts the water loss from the internal regions of the member, creep is reduced in large members. The influence of size and shape of concrete may be represented by the ratio of volume to surface area, or by an effective thickness.

The stress-time history may be described in terms of age at the stage of first loading and the time under loading. Loading at an early age causes high creep strains. With increase in age at first loading, there is a marked decrease in creep strain. The creep strains increase with duration of loading.

Several empirical methods exist for the calculation of creep strains. The most widely used methods are those of ACI Committee 209^{2,26} and of the CEB-FIP.^{2,27} The methods give the creep coefficient of the concrete C_t as a function of the dependent variables, where C_t is the ratio of creep strain to initial elastic strain. No allowance is made for the type of aggregate in either

method. The approach of ACI Committee 209 is described below. It must be borne in mind that although the approach is based on a comprehensive review of the literature, the problem is essentially a statistical one, since the scatter of test data and actual values may show significant variations from the mean values proposed.

According to ACI Committee 209,^{2,26} for normal weight, sand lightweight, and all lightweight concrete (using both moist and steam curing and types I and III cement), the creep coefficient C_t (defined as the ratio of creep strain to initial elastic strain) at any time may be written as

$$C_t = C_u K_t K_a K_h K_{th} K_s K_f K_e \quad (2.12)$$

The coefficients for Eq. 2.12 are defined below.

Ultimate creep coefficient, C_u

The value of C_u can vary widely. In the ACI Committee 209 review, C_u was found to be in the range 1.30 to 4.15, with an average value of 2.35. This average value should be assumed only in the absence of more exact data for the concrete to be used.

Time under load coefficient, K_t

$$K_t = \frac{t^{0.6}}{10 + t^{0.6}} \quad (2.13)$$

where t = time in days after application of load

(K_t = 0.44, 0.60, 0.69, 0.78, and 0.90 for t = 1 month, 3 months, 6 months, 1 year, and 5 years, respectively)

Age when loaded coefficient, K_a

$$K_a = 1.25t_i^{-0.118} \quad \text{for moist-cured concrete} \quad (2.14a)$$

or

$$K_a = 1.13t_i^{-0.095} \quad \text{for steam-cured concrete} \quad (2.14b)$$

where t_i = age of concrete in days when load is first applied (K_a = 1.00, 0.95, 0.83, and 0.74 for moist-cured concrete loaded at 7, 10, 30, and 90 days, respectively; K_a = 1.00, 0.90, 0.82, and 0.74 for steam-cured concrete loaded at 1 to 3, 10, 30, and 90 days, respectively)

Relative humidity coefficient, K_h

$$K_h = 1.27 - 0.0067H \quad \text{for } H > 40\% \quad (2.15)$$

where H = relative humidity in percent

(K_h = 1.00, 0.87, 0.73, and 0.60, for ≤ 40 , 60, 80, and 100% relative humidity)

Minimum thickness of member coefficient, K_{th}

$K_{th} = 1.00$ for 6 in or less, and 0.82 for 12 in (1 in = 25.4 mm)

Slump of concrete coefficient, K_s

$K_s = 0.95$ for 2 in, 1.00 for 2.7 in, 1.02 for 3 in, 1.09 for 4 in, and 1.16 for 5 in slump (1 in = 25.4 mm)

Fines coefficient, K_f

$K_f = 0.95$ for 30%, 1.00 for 50%, and 1.05 for 70% fines by weight

Air content coefficient, K_e

$K_e = 1.00$ up to 6%, 1.09 for 7%, and 1.17 for 8% air

The cement content need not be taken into account for concrete with cement contents between 470 and 750 lb/yd³ (1 lb/yd³ = 0.593 kg/m³).

Example 2.1

Estimate the creep strain that can be expected to occur in a 12 in (304 mm) thick concrete wall loaded at age 10 days for a 5-year period at a relative humidity of 60%. The concrete has a slump of 3 in (76 mm), a fines content of 34% by weight, an air content of 5%, and is moist cured.

Solution

From Eq. 2.12 we have

$$C_t = 2.35 \times 0.9 \times 0.95 \times 0.87 \times 0.91 \times 1.02 \times 0.96 \times 1.00 \\ = 1.56$$

Hence the probable creep strain is 1.56 times the initial elastic strain.

2.1.5 Shrinkage of Concrete

When concrete loses moisture by evaporation, it shrinks. Shrinkage strains are independent of the stress conditions in the concrete. If restrained, shrinkage strains can cause cracking of concrete and will generally cause the deflection of structural members to increase with time. The calculation of stress and deformations due to shrinkage is deferred until Chapter 10.

A curve showing the increase in shrinkage strain with time appears in Fig. 2.21. The shrinkage occurs at a decreasing rate with time. The final shrinkage strains vary greatly, being generally in the range 0.0002 to 0.0006 but sometimes as much as 0.0010.

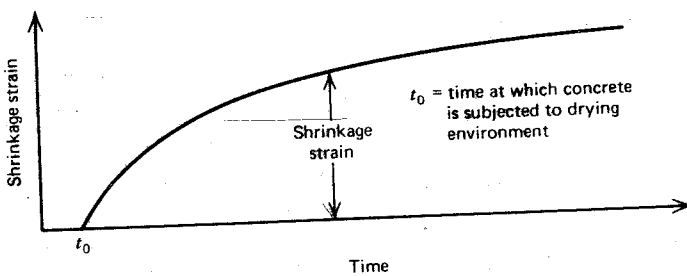


Fig. 2.21. Typical shrinkage curve for concrete.

Shrinkage is to a large extent a reversible phenomenon. If the concrete is saturated with water after it has shrunk, it will expand to almost its original volume. Thus alternating dry and wet conditions will cause alternating volume changes of concrete. This phenomenon is partly responsible for the fluctuating deflections of structures (e.g., concrete bridges) exposed to seasonal changes each year.

As a rule, concrete that exhibits a high creep also displays high shrinkage. Thus the magnitude of the shrinkage strain depends on the composition of the concrete and on the environment in much the same way as discussed previously for creep.

Both the ACI Committee 209^{2.26} and the CEB-FIP^{2.27} have proposed empirical methods for the estimation of shrinkage strains. The former approach is described below.

According to ACI Committee 209^{2.26} for normal weight, sand lightweight, and all lightweight concrete (using both moist and steam curing and types I and III cement), the unrestrained shrinkage strain at any time t is given by

$$\epsilon_{sh} = \epsilon_{shu} S_i S_h S_{th} S_s S_f S_e S_c \quad (2.16)$$

where the coefficients are given below.

Ultimate shrinkage strain, ϵ_{shu}

The value of ϵ_{shu} can vary widely. In the ACI Committee 209 review, ϵ_{shu} was found to be in the range 0.000415 to 0.00107, with mean values of 0.00080 for moist-cured concrete or 0.00073 for steam-cured concrete. These average values should be assumed only in the absence of more exact data for the concrete to be used.

Time of shrinkage coefficient, S_t

At any time after age 7 days, for moist-cured concrete,

$$S_t = \frac{t}{35 + t} \quad (2.17a)$$

where t = time in days from age 7 days

($S_t = 0.46, 0.72, 0.84, 0.91$, and 0.98 for $t = 1$ month, 3 months, 6 months, 1 year, and 5 years, respectively)

or, at any time after age 1 to 3 days for steam-cured concrete,

$$S_t = \frac{t}{55 + t} \quad (2.17b)$$

where t = time in days from age 1 to 3 days

($S_t = 0.35, 0.62, 0.77, 0.87$, and 0.97 for $t = 1$ month, 3 months, 6 months, 1 year, and 5 years, respectively)

For shrinkage considered from greater ages than given above, the difference may be determined using Eq. 2.17a or 2.17b for any period after that time. That is, shrinkage for moist-cured concrete between, say, 1 month and 1 year would be equal to the 7-day to 1-year shrinkage minus the 7-day to 1-month shrinkage. The foregoing procedure assumes that the moist-cured concrete has been cured for 3 to 7 days. For the shrinkage of moist-cured concrete from 1 day, the shrinkage needs to be multiplied by 1.2; a linear interpolation between 1.2 at 1 day and 1.0 at 7 days may be used.

Relative humidity coefficient, S_h

$$S_h = 1.4 - 0.01H \quad \text{for } 40 < H < 80\% \quad (2.18a)$$

or

$$S_h = 3.0 - 0.03H \quad \text{for } 80 < H < 100\% \quad (2.18b)$$

where H = relative humidity in percent

($S_h = 1.00, 0.80, 0.60, 0$, for $\leq 40, 60, 80$, and 100% relative humidity)

Minimum thickness of member coefficient, S_{th}

$$S_{th} = 1.00 \text{ for 6 in or less and } 0.84 \text{ for 9 in (1 in = 25.4 mm)}$$

Slump of concrete coefficient, S_s

$$S_s = 0.97 \text{ for 2 in, } 1.00 \text{ for 2.7 in, } 1.01 \text{ for 3 in, } 1.05 \text{ for 4 in, and } 1.09 \text{ for 5 in (1 in = 25.4 mm)}$$

Fines coefficient, S_f

$$S_f = 0.86 \text{ for } 40\%, 1.00 \text{ for } 50\%, \text{ and } 1.04 \text{ for } 70\% \text{ fines by weight}$$

Air content coefficient, S_e

$S_e = 0.98$ for 4%, 1.00 for 6%, and 1.03 for 10% air

Cement content factor, S_c

$S_c = 0.87$ for 376 lb/yd³, 0.95 for 564 lb/yd³, 1.00 for 705 lb/yd³, and 1.09 for 940 lb/yd³ (1 lb/yd³ = 0.593 kg/m³)

Example 2.2

Estimate the free shrinkage strain that can be expected to occur in a 9 in (230 mm) thick concrete wall from the age of 7 days during a 5-year period at a relative humidity of 60%. The concrete has a slump of 3 in (76 mm), a fines content of 34% by weight, a cement content of 600 lb/yd³ (356 kg/m³), an air content of 5%, and is moist cured for 5 days after being placed.

Solution

From Eq. 2.16 we have

$$\begin{aligned}\varepsilon_{sh} &= 0.0008 \times 0.98 \times 0.80 \times 0.84 \times 1.01 \times 0.78 \times 0.99 \times 0.96 \\ &= 0.000394\end{aligned}$$

2.2 STEEL REINFORCEMENT

2.2.1 Bar Shape and Sizes

Steel reinforcing bars are generally round in cross section. To restrict longitudinal movement of the bars relative to the surrounding concrete, lugs or protrusions called deformations are rolled on to the bar surface. Minimum requirements for the deformations (spacing, height, and circumferential coverage) have been established by experimental research and are indicated by steel specifications. ASTM specifications^{2,28} require the deformations to have an average spacing not exceeding 0.7 of the nominal bar diameter and a height at least 0.04 to 0.05 of the nominal bar diameter; also, they must be present around at least 75% of the nominal bar perimeter. The deformations are placed so that the angle to the axis of the bar is not less than 45°. Generally longitudinal ribs are present on the surface of the bar as well.

Deformed steel bars are produced in sizes ranging from Nos. 3 to 18, where the bar number is based on the number of eighths of an inch ($\frac{1}{8}$ in = 3.18 mm) included in the nominal diameter of the bar. The nominal dimensions

of a deformed bar are equivalent to those of a plain bar having the same weight per unit length as the deformed bar. Table 2.1 gives the range of deformed bar sizes produced to ASTM specifications.^{2.28}

according

Table 2.1 Steel Deformed Bar Sizes

Bar No.	Unit Weight		Nominal Dimensions		Cross-Sectional Area	
	lb/ft	(kg/m)	Diameter in (mm)		in ² (mm ²)	
3	0.376	(0.560)	0.375	(9.52)	0.11	(71)
4	0.668	(0.994)	0.500	(12.70)	0.20	(129)
5	1.043	(1.552)	0.625	(15.88)	0.31	(200)
6	1.502	(2.235)	0.750	(19.05)	0.44	(284)
7	2.044	(3.042)	0.875	(22.22)	0.60	(387)
8	2.670	(3.973)	1.000	(25.40)	0.79	(510)
9	3.400	(4.960)	1.128	(28.65)	1.00	(645)
10	4.303	(6.403)	1.270	(32.26)	1.27	(819)
11	5.313	(7.906)	1.410	(35.81)	1.56	(1006)
14	7.65	(11.384)	1.693	(43.00)	2.25	(1452)
18	13.60	(20.238)	2.257	(57.33)	4.00	(2581)

Welded wire fabric made from steel wires running in two directions at right angles and welded at their intersections, and other forms of wire reinforcement, are in common use for reinforcing slabs, shells, and pavements.

2.2.2 Monotonic Stress Behavior

Typical stress-strain curves for steel bars used in reinforced concrete construction (Fig. 2.22) were obtained from steel bars loaded monotonically in tension. The curves exhibit an initial linear elastic portion, a yield plateau (i.e., a yield point beyond which the strain increases with little or no increase in stress), a strain-hardening range in which stress again increases with strain, and finally a range in which the stress drops off until fracture occurs.

The modulus of elasticity of the steel is given by the slope of the linear elastic portion of the curve. The modulus of elasticity of steel reinforcement E_s is generally taken as 29×10^6 psi (0.2×10^6 N/mm²).^{2.1}

The stress at the yield point, referred to as the yield strength, is a very important property of steel reinforcement. Sometimes yielding is accompanied by an abrupt decrease in stress, and the stress-strain diagram has the

Stress-Strain Relationships for Concrete and Steel

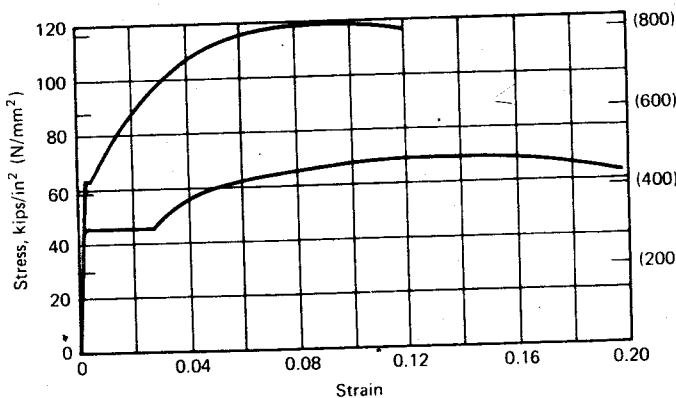


Fig. 2.22. Typical stress-strain curves for steel reinforcement.

shape appearing in Fig. 2.23. In such a case the stresses at *A* and *B* are referred to as the upper and lower yield strengths, respectively. The position of the upper yield point depends on the speed of testing, the shape of the section, and the form of the specimen. The lower yield strength is usually considered to be the true characteristic of the material and is referred to simply as the yield strength. For steels lacking a well-defined yield plateau, the yield strength is generally taken as the stress corresponding to a particular strain, as illustrated in Fig. 2.24.

The length of the yield plateau is generally a function of the strength of the steel. High-strength high-carbon steels generally have a much shorter yield plateau than lower strength low-carbon steels. Similarly, the cold working of steel can cause the shortening of the yield plateau to the extent that strain

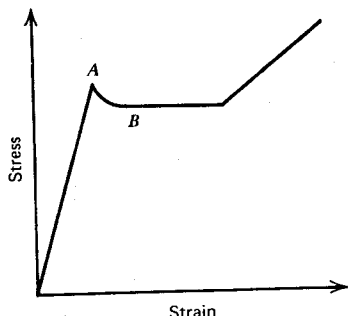


Fig. 2.23. Stress-strain curve illustrating upper and lower yield points.

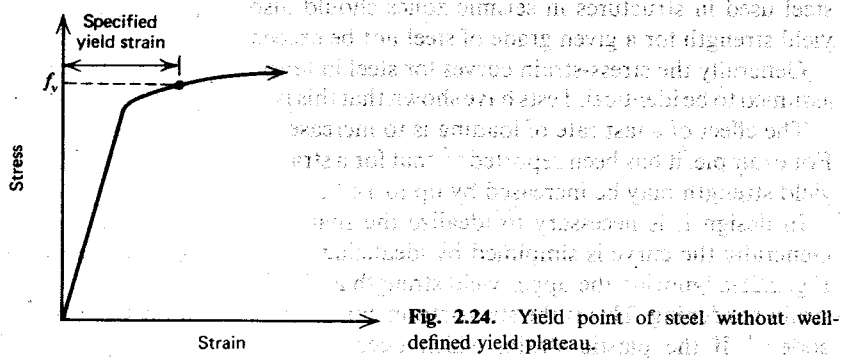


Fig. 2.24. Yield point of steel without well-defined yield plateau.

hardening commences immediately after the onset of yielding. High-strength steels also have a smaller elongation before fracture than low-strength steels.

Deformed steel bars produced to ASTM specifications^{2,28} have a specified (minimum) yield strength of either 40, 50, 60, or 75 ksi (276, 345, 414, or 517 N/mm²); they are referred to as Grades 40, 50, 60, and 75, respectively. For steels lacking a well-defined yield point, the yield strength is taken as the stress corresponding to a strain of 0.005 for Grades 40, 50, and 60,^{2,28} and 0.0035 for Grade 75.^{2,1} The ultimate strengths (tensile strengths) corresponding to Grades 40, 50, 60, and 75 steel are at least 70, 80, 90, and 100 ksi (483, 552, 621, and 690 N/mm²).^{2,28} Steel wires normally have yield and ultimate strengths in the upper part of the ranges just given. The minimum strain in the steel at fracture is also defined in steel specifications, since it is essential for the safety of the structure that the steel be ductile enough to undergo large deformations before fracture. ASTM specifications^{2,28} for deformed bars require an elongation, defined by the permanent extension of an 8 in (203 mm) gauge length at the fracture of the specimen, expressed as a percentage of the gauge length, which varies with the source, grade, and bar diameter of the steel and ranges from at least 4.5 to 12%.

The specified yield strength normally refers to a guaranteed minimum. The actual yield strength of the bars is usually somewhat higher than this specified value. In some cases (e.g., in the assessment of the seismic strength of members) it is undesirable to have a yield strength much higher than that considered in the design. This is because the increased flexural strength of a member, for example, will produce increased shear forces acting on the member at ultimate load, which could result in a brittle shear failure of the member rather than a ductile flexural failure. Therefore, specifications for

steel used in structures in seismic zones should also require that a certain yield strength for a given grade of steel not be exceeded.

Generally the stress-strain curves for steel in tension and compression are assumed to be identical. Tests have shown that this is a reasonable assumption.

The effect of a fast rate of loading is to increase the yield strength of steel. For example, it has been reported^{2,5} that for a strain rate of 0.01 sec the lower yield strength may be increased by up to 14%.

In design it is necessary to idealize the shape of the stress-strain curve. Generally the curve is simplified by idealizing it as two straight lines, as in Fig. 2.25a, ignoring the upper yield strength and the increase in stress due to strain hardening. This is the stress-strain curve for steel assumed by the ACI code.^{2,1} If the plastic strain, which occurs at near-constant stress after yielding, is much greater than the elastic extension at yield, this assumed curve gives a very good accuracy. This simplification is particularly accurate for steel having a low yield strength. If the steel strain hardens soon after the onset of yielding, this assumed curve will underestimate the steel stress at high strains. In some cases it may be necessary to evaluate the steel stress at strains higher than yield, to more accurately assess the strength of members at large deformations. This is particularly true in seismic design, where ductility requirements may mean considering the possibility of reaching strains many times the yield strain. More accurate idealizations usable for the stress-strain curve are given in Figs. 2.25b and 2.25c. Values for the stresses and strains at the onset of yield, strain hardening, and tensile strength are necessary for use of such idealizations. These points can be located from stress-strain curves obtained from tests.

2.2.3 Repeated Stress Behavior

Figure 2.22 is the stress-strain curve for a steel specimen loaded either in axial tension or in compression to failure in a single loading run. If the load is released before failure, the specimen will recover along a stress-strain path that is parallel to the original elastic portion of the curve. If loaded again, the specimen will follow the same path up to the original curve, as in Fig. 2.26, with perhaps a small hysteresis and/or strain-hardening effect. The virgin curve is then closely followed, as if unloading had not occurred. Hence the monotonic stress-strain curve gives a good idealization for the envelope curve for repeated loading of the same sign.

2.2.4 Reversed Stress Behavior

If reversed (tension-compression) axial loading is applied to a steel specimen in the yield range, a stress-strain curve of the type presented in Fig. 2.27a is obtained. The figure shows the Bauschinger effect, in which under reversed

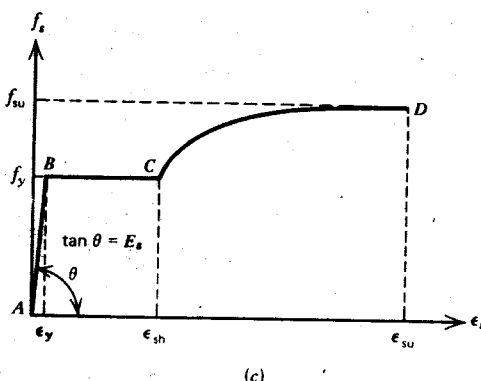
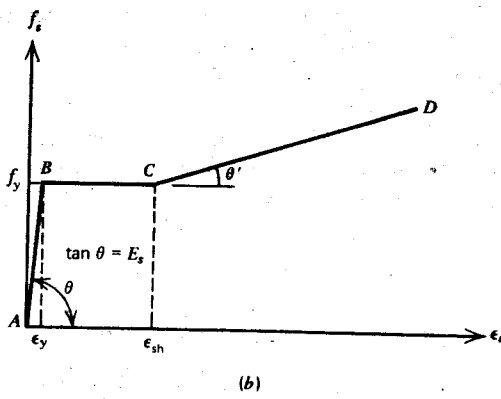
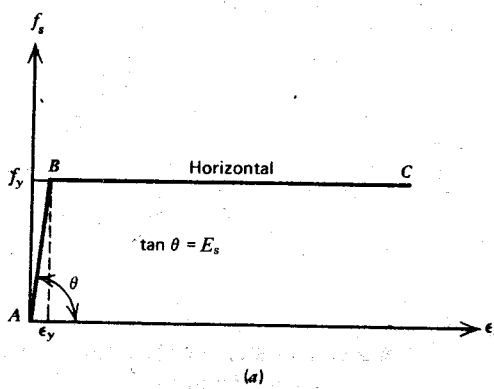


Fig. 2.25. Idealizations for the stress-strain curve for steel in tension or compression. (a) Elastic perfectly plastic approximation (b) Trilinear approximate (c) Complete curve.

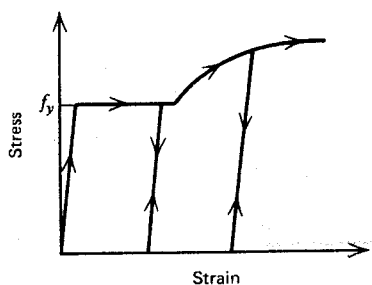


Fig. 2.26. Stress-strain curve for steel under repeated loading.

loading the stress-strain curve becomes nonlinear at a stress much lower than the initial yield strength. This steel behavior is strongly influenced by previous strain history; time and temperature also have an effect. The unloading path follows the initial elastic slope. The often-used elastic-perfectly plastic idealization for reversed loading (Fig. 2.27b) is only an approximation. Reversed loading curves are important when considering the effects of high-intensity seismic loading on members.

An idealization by Kato et al.,^{2,29} based on observation of experimental stress-strain data, obtains the stress-strain curve for reversed loading from the monotonic curves for tension and compression in the manner illustrated in Fig. 2.28. The reversed load diagram (Fig. 2.28a) is divided in curves

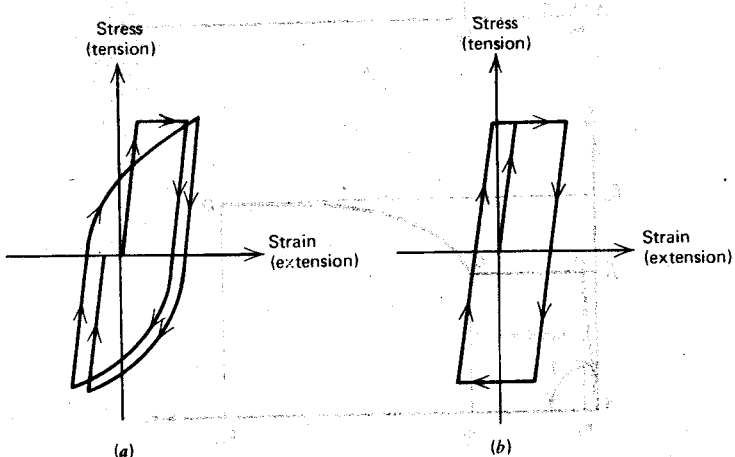


Fig. 2.27. (a) Bauschinger effect for steel under reversed loading. (b) Elastic-perfectly plastic idealization for steel under reversed loading.

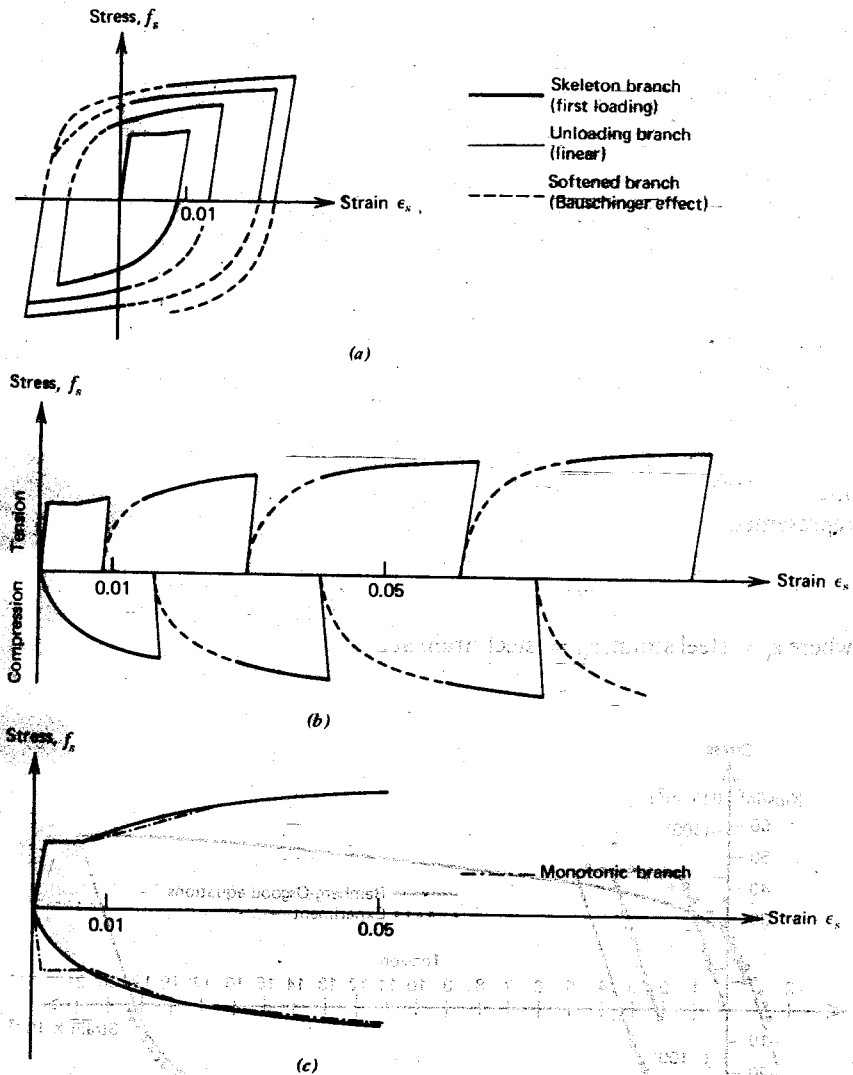


Fig. 2.28. Stress-strain curves for steel with reversed loading.^{2,29} (a) Reversed loading curve. (b) Expanded curves (c) Skeleton curves.

corresponding to loadings attained for the first time, unloading branches (straight lines), and loadings attained in previous cycles (softened curves due to the Bauschinger effect). The parts of the diagram of the same sign can be plotted in sequence, as in Fig. 2.28b. Connecting the segments of the first loading branches end for end (Fig. 2.28c) leads to a diagram similar to the monotonic curves. A difference exists at the initial part of the curve in compression, which is considerably curved, compared with the monotonic curve. Kato et al^{2,29} represented the softened curves, due to the Bauschinger effect, by hyperbolas commencing at zero stress. Using this idealization, the reversed load stress-strain curves can be obtained approximately from the monotonic curves.

Aktan et al^{2,30} and Kent and Park^{2,31} have used Ramberg-Osgood relationships^{2,32} to idealize the shape of the softened branches of the stress-strain curve. In the method of Kent and Park, the unloading branches of the curve for stresses of both signs are assumed to follow the initial elastic slope; after the first yield excursion, the loading parts of the stress-strain curve are represented by the following form of the Ramberg-Osgood relationship:

$$\varepsilon_s - \varepsilon_{si} = \frac{f_s}{E_s} \left(1 + \left| \frac{f_s}{f_{ch}} \right|^{r-1} \right) \quad (2.19)$$

where ε_s = steel strain, ε_{si} = steel strain at zero stress at beginning of loading

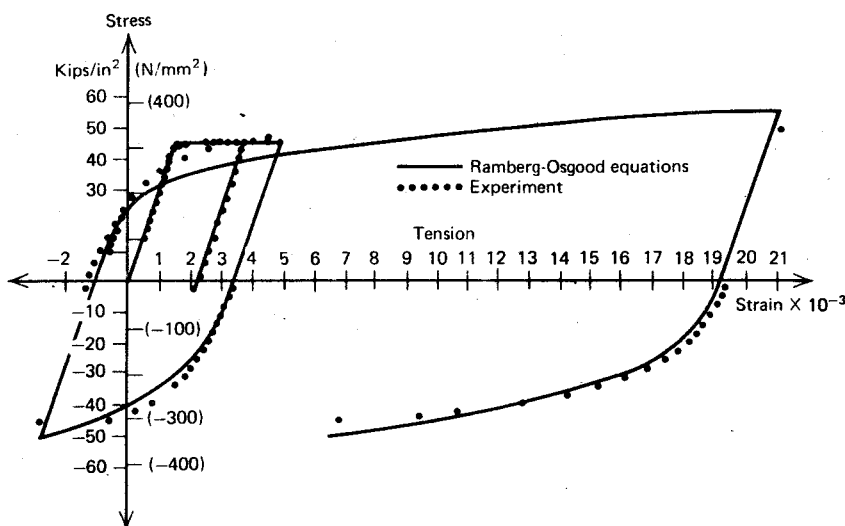


Fig. 2.29. Stress-strain curves for steel with reversed loading.^{2,31}

run, f_s = steel stress, E_s = modulus of elasticity of steel, f_{ch} = stress dependent on the yield strength and the plastic strain in the steel produced in the previous loading run, and r = parameter dependent on the loading run number. Figure 2.29 compares experimental stress-strain data with the curve given by Eq. 2.19, using empirical values for f_{ch} and r .^{2,31} Aktan et al^{2,30} used the Ramberg-Osgood equation to define both the loading and unloading branches of the curves and obtained good agreement with test results. They also devised an alternative idealization consisting of sets of straight lines parallel to the elastic slope and inclined to it.

It is evident that the degree of complexity of the idealization used depends on the needs of the particular application.

2.3 REFERENCES

- 2.1 ACI Committee 318, "Building Code Requirements for Reinforced Concrete (ACI 318-71)," American Concrete Institute, Detroit, 1971, 78 pp.
- 2.2 A. Pauw, "Static Modulus of Elasticity of Concrete as Affected by Density," *Journal ACI*, Vol. 57, No. 6, December 1960, pp. 679-687.
- 2.3 H. Rüsch, "Versuche zur Festigkeit der Biegendruckzone," Deutscher Ausschuss für Stahlbetonbau, Bulletin No. 120, Berlin, 1955, 94 pp.
- 2.4 E. Hognestad, "A Study of Combined Bending and Axial Load in Reinforced Concrete Members," University of Illinois Engineering Experimental Station, Bulletin Series No. 399, November 1951, 128 pp.
- 2.5 ACI Committee 439, "Effect of Steel Strength and Reinforcement Ratio on the Mode of Failure and Strain Energy Capacity of Reinforced Concrete Beams," *Journal ACI*, Vol. 66, No. 3, March 1969, pp. 165-173.
- 2.6 B. P. Sinha, K. H. Gerstle, and L. G. Tulin, "Stress-Strain Relationships for Concrete Under Cyclic Loading," *Journal ACI*, Vol. 61, No. 2, February 1964, pp. 195-211.
- 2.7 I. D. Karsan and J. O. Jirsa, "Behaviour of Concrete Under Compressive Loadings," *Journal of Structural Division, ASCE*, Vol. 95, ST12, December 1969, pp. 2543-2563.
- 2.8 H. Rüsch, "Researches Toward a General Flexural Theory for Structural Concrete," *Journal ACI*, Vol. 57, No. 1, July 1960, pp. 1-28.
- 2.9 E. P. Popov, *Introduction to Mechanics of Solids*, Prentice-Hall, Englewood Cliffs, N.J., 1968, 571 pp.
- 2.10 H. Kupfer, H. K. Hilsdorf, and H. Rüsch, "Behaviour of Concrete Under Biaxial Stress," *Journal ACI*, Vol. 66, No. 8, August 1969, pp. 656-666.
- 2.11 H. J. Cowan, "The Strength of Plain, Reinforced and Prestressed Concrete Under the Action of Combined Stresses, with Particular Reference to the Combined Bending and Torsion of Rectangular Sections," *Magazine of Concrete Research*, No. 14, December 1953, pp. 75-86.
- 2.12 B. Bresler and K. S. Pister, "Strength of Concrete Under Combined Stresses," *Journal ACI*, Vol. 55, No. 3, September 1958, pp. 321-345.
- 2.13 F. E. Richart, A. Brandtzaeg, and R. L. Brown, "A Study of the Failure of Concrete Under Combined Compressive Stresses," University of Illinois Engineering Experimental Station, Bulletin No. 185, 1928, 104 pp.

- 2.14 G. G. Balmer, "Shearing Strength of Concrete Under High Triaxial Stress—Computation of Mohr's Envelope as a Curve," Structural Research Laboratory Report No. SP-23, U.S. Bureau of Reclamation, 1949, 13 pp. plus tables and figures.
- 2.15 F. E. Richart, A. Brandtzaeg, and R. L. Brown, "The Failure of Plain and Spirally Reinforced Concrete in Compression," University of Illinois Engineering Experimental Station, Bulletin No. 190, 1929, 74 pp.
- 2.16 K. T. R. J. Iyengar, P. Desai, and K. N. Reddy, "Stress-Strain Characteristics of Concrete Confined in Steel Binders," *Magazine of Concrete Research*, Vol. 22, No. 72, September 1970, pp. 173-184.
- 2.17 V. V. Bertero and C. Felippa, Discussion of "Ductility of Concrete" by H. E. H. Roy and M. A. Sozen, *Proceedings of the International Symposium on Flexural Mechanics of Reinforced Concrete*, ASCE-ACI, Miami, November 1964, pp. 227-234.
- 2.18 W. L. Chan, "The Ultimate Strength and Deformation of Plastic Hinges in Reinforced Concrete Frameworks," *Magazine of Concrete Research*, Vol. 7, No. 21, November 1955, pp. 121-132.
- 2.19 J. A. Blume, N. M. Newmark, and L. H. Corning, "Design of Multistorey Reinforced Concrete Buildings for Earthquake Motions," Portland Cement Association, Chicago, 1961, 318 pp.
- 2.20 A. L. L. Baker and A. M. N. Amarakone, "Inelastic Hyperstatic Frames Analysis," *Proceedings of the International Symposium on the Flexural Mechanics of Reinforced Concrete*, ASCE-ACI, Miami, November 1964, pp. 85-142.
- 2.21 H. E. H. Roy and M. A. Sozen, "Ductility of Concrete," *Proceedings of the International Symposium on Flexural Mechanics of Reinforced Concrete*, ASCE-ACI, Miami, November 1964, pp. 213-224.
- 2.22 M. T. M. Soliman and C. W. Yu, "The Flexural Stress-Strain Relationship of Concrete Confined by Rectangular Transverse Reinforcement," *Magazine of Concrete Research*, Vol. 19, No. 61, December 1967, pp. 223-238.
- 2.23 M. Sargin, S. K. Ghosh, and V. K. Handa, "Effects of Lateral Reinforcement upon the Strength and Deformation Properties of Concrete," *Magazine of Concrete Research*, Vol. 23, No. 75-76, June-September, 1971, pp. 99-110.
- 2.24 D. C. Kent and R. Park, "Flexural Members with Confined Concrete," *Journal of the Structural Division, ASCE*, Vol. 97, ST7, July 1971, pp. 1969-1990.
- 2.25 A. M. Neville, "Properties of Concrete," Pitman, London, 1963, 532 pp.
- 2.26 ACI Committee 209, "Prediction of Creep, Shrinkage and Temperature Effects in Concrete Structures," *Designing for the Effects of Creep, Shrinkage and Temperature in Concrete Structures*, SP-27, American Concrete Institute, Detroit, 1971, pp. 51-93.
- 2.27 CEB-FIP, "International Recommendations for the Design and Construction of Concrete Structures," Comité Européen du Béton-Fédération Internationale de la Précontrainte, Paris, 1970. (English translation available from Cement and Concrete Association, London, 88 pp.)
- 2.28 ASTM, 1973 *Annual Book of ASTM Standards*, Part 4, American Society for Testing and Materials, Philadelphia, 1973. (Standards for deformed steel bar are A615-72, pp. 684-689; A616-72, pp. 690-694; A617-72, pp. 695-699.)
- 2.29 B. Kato, H. Akiyama, and Y. Yamanouchi, "Predictable Properties of Material Under Incremental Cyclic Loading," *Symposium on Resistance and Ultimate Deformability of Structures Acted on by Well-Defined Repeated Loads, Reports of Working Commissions*, Vol. 13, International Association for Bridge and Structural Engineering, Lisbon, 1973, pp. 119-124.

References

- 2.30 A. E. Aktan, B. I. Karlsson, and M. A. Sozen, "Stress-Strain Relationships of Reinforcing Bars Subjected to Large Strain Reversals," Civil Engineering Studies, Structural Research Series No. 397, University of Illinois, Urbana, June 1973.
- 2.31 D. C. Kent and R. Park, "Cyclic Load Behaviour of Reinforcing Steel," *Strain* (Journal of the British Society for Strain Measurement), Vol. 9, No. 3, July 1973, pp. 98-103.
- 2.32 W. Ramberg and W. R. Osgood, "Description of Stress-Strain Curves by Three Parameters," Technical Note 902, National Advisory Committee for Aeronautics, July 1943.

3

Basic Assumptions of Theory for Flexural Strength

3.1 BASIC BEHAVIOR ASSUMPTIONS

Four basic assumptions are made when deriving a general theory for the flexural strength of reinforced concrete sections:

1. Plane sections before bending remain plane after bending.
2. The stress-strain curve for the steel is known.
3. The tensile strength of the concrete may be neglected.
4. The stress-strain curve for concrete, defining the magnitude and distribution of compressive stress, is known.

The first assumption, Bernoulli's principle, implies that the longitudinal strain in the concrete and the steel at the various points across a section is proportional to the distance from the neutral axis. A large number of tests on reinforced concrete members have indicated that this assumption is very nearly correct at all stages of loading up to flexural failure, provided good bond exists between the concrete and steel. Certainly it is accurate in the compression zone of the concrete. A crack in the tension zone of the concrete implies that some slip has occurred between the steel reinforcement and the surrounding concrete, and this means that the assumption is not completely applicable to the concrete in the neighborhood of a crack. However, if the concrete strain is measured over a gauge length that includes several cracks, it is found that Bernoulli's principle applies to this average tensile strain. Figure 3.1 shows the strain distributions measured across sections of reinforced concrete columns near the failure regions at various loading increments. The column sections were either 10 in (254 mm) square or 12 in (305 mm) diameter round. The stains on the steel were measured over a 1 in (25 mm) gauge length and the strains on the concrete over a 6 in (150 mm) gauge length. Some deviation from linearity must be expected because of small inaccuracies in individual strain measurements and small errors in the

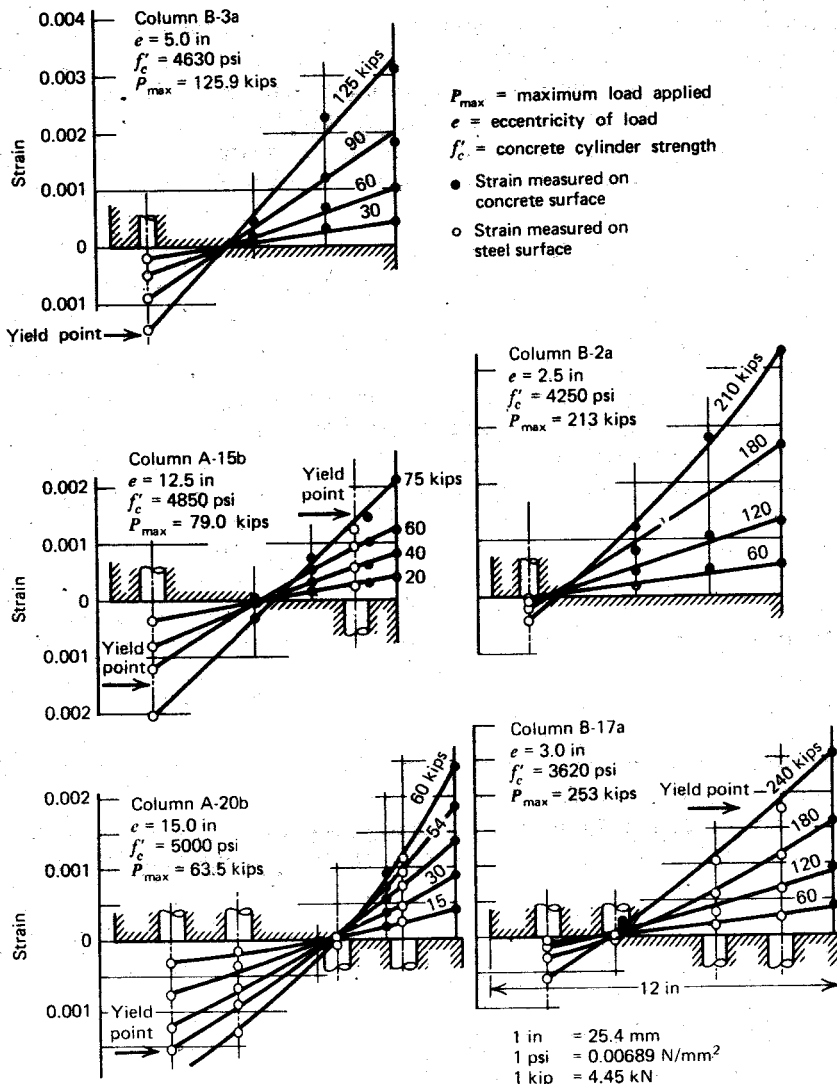


Fig. 3.1 Strain distribution across sections of reinforced concrete columns at various loading increments.^{3.1}

location of gauge lines. It is evident from Fig. 3.1 that the measured strain profiles are reasonably linear. Certainly the assumption of plane sections remaining plane is sufficiently accurate for design purposes. The assumption does not hold for deep beams or in regions of high shear.

The second assumption means that the stress-strain properties of the steel are well defined. Normally a bilinear stress-strain curve is assumed (see Fig. 2.25a); hence strain hardening is neglected. The point at which strain hardening begins is not stipulated in specifications for steel, and therefore it is difficult to include it. Normally it would be unwise to rely on any increase in strength due to strain hardening because this could be associated with very large ultimate deformations of the members. When an increase in strength could cause an unfavorable condition (e.g., resulting in a brittle shear failure rather than a ductile flexural failure in seismic design), the designer may take the additional strength due to strain hardening into account by referring to the actual stress-strain curve for the steel.

The third assumption is very nearly exact. Any tensile stress that exists in the concrete just below the neutral axis is small and has a small lever arm.

The fourth assumption is necessary to assess the true behavior of the section. Since the strains in the compressed concrete are proportional to the distance from the neutral axis, the shape of the stress-strain curves of Fig. 2.1 indicate the shape of the compressive stress block at various stages of loading. Figure 3.2 presents the changing shape of the stress block as the bending moment at a beam section is increased. The section reaches its flexural strength (maximum moment of resistance) when the total compressive force in the concrete multiplied by the internal lever arm jd is a maximum. The properties of the compressive stress block at the section of maximum moment may be defined by parameters k_1 , k_2 , and k_3 , as in Fig. 3.3a. For a rectangular section of width b and effective depth d , the total compressive force in the

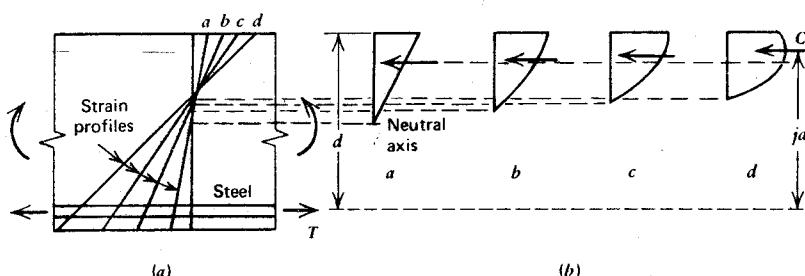


Fig. 3.2. Strain and stress distribution in the compressed concrete of a section as the bending moment is increased up to the flexural strength. (a) Beam element. (b) Compression stress distributions in concrete corresponding to strain profiles a , b , c , and d .

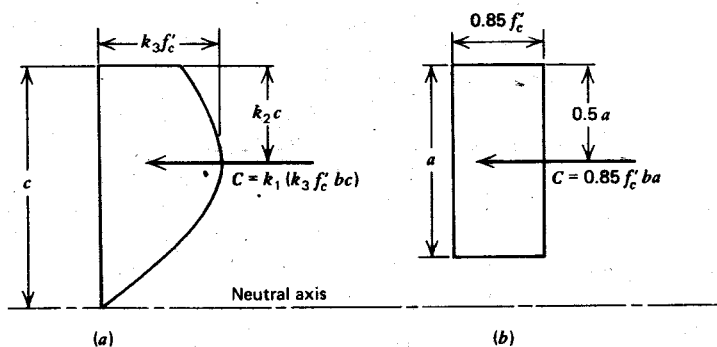


Fig. 3.3. Compressive stress distribution in the compression zone of a rectangular concrete section. (a) Actual distribution. (b) Equivalent rectangular distribution.

concrete becomes $k_1 k_3 f'_c b c$ and the internal level arm is $d - k_2 c$, where c is the neutral axis depth. A great deal of research has been conducted to determine the magnitude of these parameters for unconfined concrete. The most notable work has consisted of the short-term tests conducted by Hognestad et al at the Portland Cement Association (PCA)^{3,2} and by Rüsch.^{3,3} The specimens used in the PCA tests were like those appearing in Fig. 3.4. The test region of the specimen was loaded eccentrically by increasing the two thrusts P_1 and P_2 . The thrusts P_1 and P_2 were varied independently such that the neutral axis (i.e., fiber of zero strain) was maintained at the bottom face of the specimen throughout the test; therefore, the stress distribution in the compression zone of a member with flexure was simulated. By equating the internal and external forces and moments, it was possible to calculate the values of k_1 , k_2 , and k_3 directly, obtaining as well the stress-strain curve for the concrete in the specimen. Stress-strain curves for the

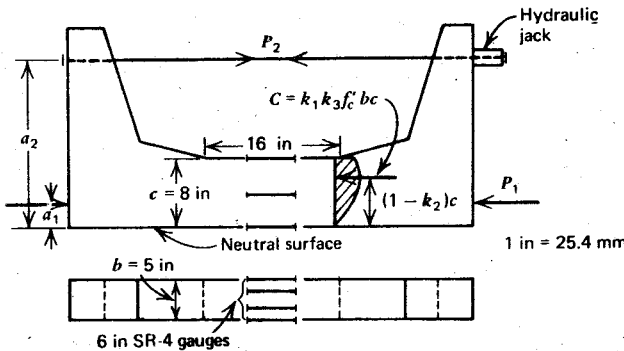


Fig. 3.4. Portland Cement Association test specimen.^{3,2}

concrete were also determined from axially loaded cylinders and were found to be similar to the stress-strain curves for the concrete in the specimens. For higher strength concrete, however, the maximum stress reached in the specimens at the flexural strength $k_3 f'_c$ was slightly less than the cylinder strength. The tests also determined the concrete strain ϵ_c at the extreme compression fiber at the flexural strength. The values found for the stress block parameters of concrete with sand-gravel aggregates varied with the cylinder strength f'_c and are given in Table 3.1. These quantities correspond to the maximum values of $k_1 k_3$ found in each test.

Table 3.1 Stress Block Parameters at the Flexural Strength of Rectangular Sections as Found by the PCA Tests on Unconfined Specimens^{3,2}

f'_c		k_1	k_2	k_3	ϵ_c
psi	N/mm ²				
2000	13.8	0.86	0.48	1.03	0.0037
3000	20.7	0.82	0.46	0.97	0.0035
4000	27.6	0.79	0.45	0.94	0.0034
5000	34.5	0.75	0.44	0.92	0.0032
6000	41.4	0.71	0.42	0.92	0.0031
7000	48.3	0.67	0.41	0.93	0.0029

The finding of the PCA tests—namely, that the stress-strain curve for concrete in axial compression has a striking similarity to that found from eccentrically loaded specimens—has been questioned from time to time. For example, Sturman, Shah, and Winter^{3,4} conducted tests on eccentrically and concentrically loaded specimens and concluded that the peak of the curve for the eccentric specimens occurred at a 20% higher stress and a 50% higher strain than for the concentric specimens. The presence of a strain gradient may not have a significant effect, but if anything it will result in an improvement in the properties of the compressive stress block. It is also worth noting that the presence of a strain gradient delays the appearance of longitudinal cracking in the compression zone.

3.2 EQUIVALENT RECTANGULAR STRESS BLOCK

A number of investigators (e.g., Whitney^{3,5}) have suggested the replacement of the actual shape of the concrete compressive stress block by an equivalent

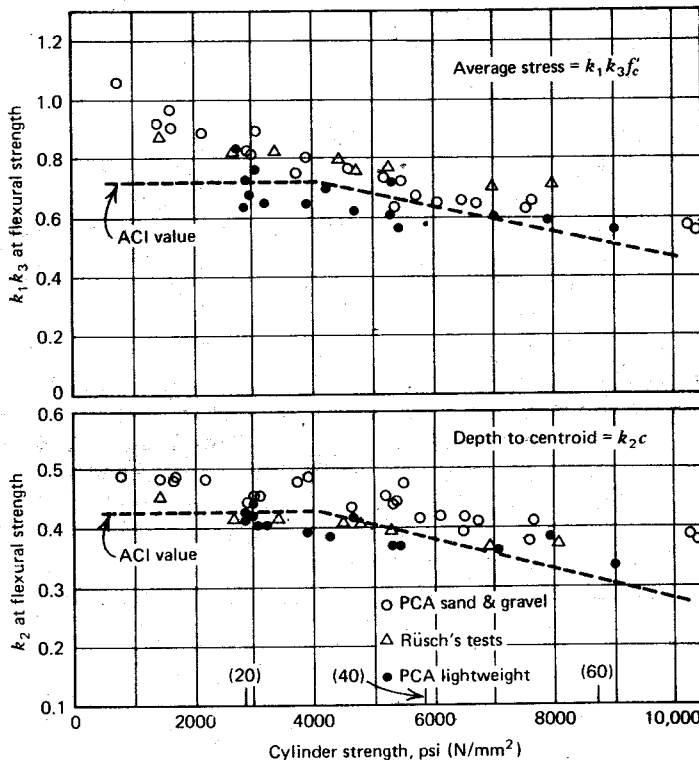


Fig. 3.5. Properties of concrete compressive stress distribution at the flexural strength of a rectangular section: comparison of ACI parameters with test results.^{3,7}

rectangle as a means of simplification. For deriving the flexural strength, only the magnitude ($k_1 k_3$) and the position (k_2) of the concrete compression force need be known. The equivalent rectangular stress block achieves this and greatly facilitates computations. American practice, as represented by the ACI code,^{3,6} has been to replace the actual stress block by the equivalent rectangle (Fig. 3.3b). The rectangle has a mean stress of $0.85 f'_c$ and a depth a , where $a/c = \beta_1 = 0.85$ for $f'_c \leq 4000$ psi (27.6 N/mm 2); β_1 is reduced continuously by 0.05 for each 1000 psi (6.89 N/mm 2) of strength in excess of 4000 psi (27.6 N/mm 2). The reduction in β_1 for high-strength concrete is mainly due to the less favourable shape of the stress-strain curve of that concrete (see Figs. 2.1 and 2.2).

For the resultant compressive forces of the actual and equivalent stress blocks of Fig. 3.3 to have the same magnitude and line of action, the values for

the parameters must be

$$C = k_1 k_3 f'_c bc = 0.85 f'_c ba \quad \therefore \quad k_1 k_3 = 0.85 \frac{a}{c} = 0.85 \beta_1 \quad (3.1)$$

and

$$k_2 c = 0.5a \quad \therefore \quad k_2 = 0.5 \frac{a}{c} = 0.5 \beta_1 \quad (3.2)$$

The values of $k_1 k_3$ and k_2 from Eqs. 3.1 and 3.2, with the recommended ACI values for β_1 substituted, are compared with the actual values found in the tests on unconfined specimens by the PCA^{3.2} and Rüsch^{3.3} in Fig. 3.5. This comparison is from a paper by Mattock, Kriz, and Hognestad.^{3.7} It is seen that the recommended values for the properties of the rectangular stress block agree fairly closely with the experimental values. The scatter of experimental results indicates clearly that the use of more complicated values for the parameters of the rectangular stress block is unwarranted. In addition, there are very few experimental results in Fig. 3.5 for cylinder strengths greater than 8000 psi (55.2 N/mm²). However it does appear from the trend of results in the figure that the ACI stress block parameters are conservative for cylinder strengths greater than 8000 psi. Indeed, it could be considered that the ACI parameters are unduly conservative at high concrete strengths.

3.3 CONCRETE STRAIN AT THE FLEXURAL STRENGTH

American practice (ACI 318-71^{3.6}) is to recommend a maximum usable strain of 0.003 at the extreme compression fiber of the concrete at the flexural strength of the section. The strain when $k_1 k_3$ or the moment of resistance of

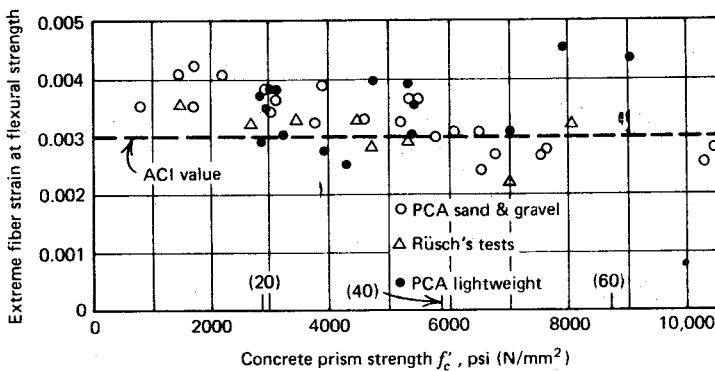


Fig. 3.6. Concrete strain at the extreme compression fiber at the flexural strength of a rectangular section: comparison of ACI value with test results.^{3.7}

the section is a maximum has been measured by many investigators. The values obtained by the PCA^{3,2} and by Rüsch^{3,3} on unconfined specimens are given in Fig. 3.6, which was taken from Reference 3.7. The figure indicates that 0.003 is a reasonably conservative value. At this strain, the compressed concrete in a flexural member will not normally show any visible cracking or spalling, even though the strain is greater than that corresponding to maximum stress. An axially loaded cylinder will usually crack considerably if strained beyond the maximum stress, but in flexural tests cracks are not visible until a greater strain is reached, probably because of the presence of the less strained material closer to the neutral axis.

The computed flexural strength of a reinforced concrete beam is usually relatively insensitive to the value of the assumed maximum concrete strain. Figure 3.7, taken from Blume, Newmark, and Corning,^{3,8} makes this point very clearly: for a singly reinforced concrete beam cross section and for two different tension steel contents, the ratio of resisting moment computed from a stress-strain curve for the concrete to the resisting moment computed according to the ACI code has been plotted against strain in the extreme compression fiber. The stress-strain curve used in the first computation was from cylinders having a strength of approximately 3600 psi (24.8 N/mm²).

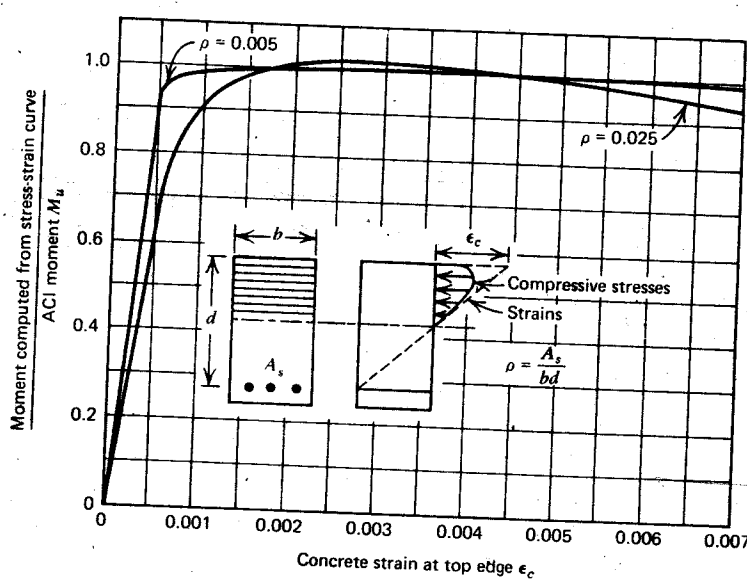


Fig. 3.7. Moment-strain curves for a singly reinforced concrete beam based on compression tests on cylinders.^{3,8}

The area under the stress-strain curve and its centroid were determined for various strains, thus establishing the $k_1 k_3$ and k_2 values for a range of extreme fiber strains, ϵ_c . Then the moment capacities of the section for the two steel contents were computed for various strains at the extreme fiber and compared with the flexural strength calculated according to the ACI code. At a compressive strain in the extreme fiber of 0.007, the decrease in the moment of resistance was less than 1% for $\rho = 0.005$ and less than 6% for $\rho = 0.025$. Thus the chosen value for the extreme fiber concrete strain has little influence on the flexural strength of beams within wide limits. However, for eccentrically loaded columns that fail in compression, the changes in the stress block parameters, which occur as the extreme fiber strain increases, will cause the change in flexural strength with strain to be larger.

In contrast, it is evident that the curvature at a section depends very much on the value taken for the extreme fiber strain. For the calculation of ultimate curvature, it would appear to be reasonable to take a value higher than 0.003. Blume, Newmark, and Corning^{3,8} recommend a value of 0.004 for ultimate curvature calculations involving unconfined concrete.

3.4 NONRECTANGULAR COMPRESSED AREAS

For members in which the compressed area of the concrete section is not rectangular, such as *T* and *L* beams with the neutral axis in the web, or beams and columns with biaxial bending moments, the parameters recommended for the equivalent rectangular stress block of rectangular compressed areas are not strictly applicable. This is because the mean stress and the depth of the equivalent rectangular stress block for various shapes of compressed area will be different; also the extreme fiber concrete strain at the maximum moment will be different. Figure 3.8 gives the extreme fiber compressive strain in the concrete at the maximum moment for several typical cross sections as computed by Rüsch.^{3,9} The curve represents the stress-strain curve for the concrete and the shape of the compressive stress block in the section. Two mathematically extreme cases of position of the neutral axis were considered. The solid circles represent the case of neutral axis at the centroid of the tension steel; the open circles denote the case of the neutral axis lying at the extreme compression fiber. The actual case of most members will lie between these two extremes. Figure 3.8 clearly reveals the effect of the shape of compressed area on the extreme fiber strain at the flexural strength of the member. For example, for a triangular compression zone, as occurs in biaxial flexure of columns, the strain at maximum moment may be twice that of a *T* section. This difference occurs because for the triangular zone the

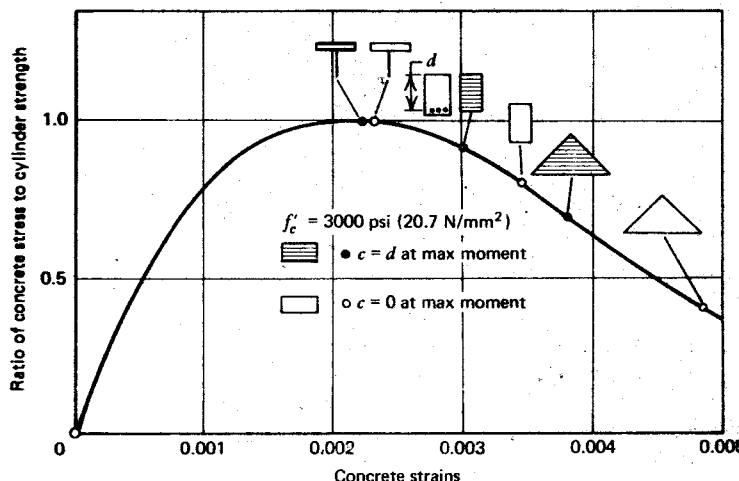


Fig. 3.8. Effect of section shape on the concrete strain at the extreme compression fiber at maximum moment.^{3,9}

major part of the compressed area is close to the neutral axis, hence the maximum moment occurs at a relatively large extreme fiber strain, whereas for the *T* section the reverse is the case.

Further work by Rüscher and Stöckl^{3,10} has produced stress block parameters for nonrectangular compressed areas. However, it is evident from this work and from that of Mattock and Kriz^{3,11} that, unless the section is heavily overreinforced, the flexural strength of beams with nonrectangular compressed areas can be estimated quite accurately using the stress block parameters and extreme fiber strain derived for rectangular compressed areas, because the lever arm and the internal forces are not affected significantly. For columns with nonrectangular compressed areas, the use of parameters based on rectangular compressed areas may not result in acceptable accuracy because the compressive forces are larger and the distribution of the concrete compressive stress has a more significant influence on the flexural strength of the section.¹ For column sections subjected to biaxial bending, for example, it may be necessary to use more exact parameters derived from first principles from the concrete stress-strain curve. Hence the parameters derived for rectangular compressed areas will yield sufficient accuracy in the design of beams but should be used with caution for columns having nonrectangular compressed areas.

3.5 EFFECTS OF SLOW RATES OF LOADING AND OF SUSTAINED LOAD

The stress block parameters reported by the PCA^{3,2} and Rüsch^{3,3} were found from short-term loading tests. The effects of slow rate of loading and of sustained loading are of interest. An indication of the shape of the stress-strain curves due to slow rates of loading is given in Fig. 2.5. However, these curves cannot be taken to represent the shape of the compressive stress blocks of flexural members, since each is for a constant strain rate, whereas in a member with slowly applied external load, the strain rate varies across the compression zone, being a maximum at the extreme compression fiber and zero at the neutral axis. However, compressive stress block parameters for slow rates of loading can be calculated from stress-strain curves for various strain rates. The biggest difference from the short-term load parameters will arise in the case of sustained loading. Rüsch^{3,9} has reported the results of tests on concrete prisms indicating the influence of sustained load on the compressive stress block parameters. Sustained load causes a reduction in the strength of the concrete and a higher compressive strain at the development of the flexural strength of the member. In the discussion to Rüsch's paper,^{3,9} Hognestad used Rüsch's sustained load stress block parameters to demonstrate that the strength of columns could be up to 10% less than that given using the short-term loading rectangular stress block parameters, although the influence of sustained loading on the strength of beams was not significant. Since it is not unreasonable to have a slightly smaller load factor for the case of a sustained overload, and because the capacity reduction factor φ used for column design is low, it is apparent that the stress block parameters found from short-term loading tests are satisfactory for design under all loading conditions.

3.6 SUMMARY OF RECOMMENDATIONS FOR THE DETERMINATION OF THE STRENGTH OF SECTIONS WITH FLEXURE AND AXIAL LOAD

The assumptions made for the determination of the strength of sections with flexure and axial load may be summarized as follows:

1. Plane sections before bending remain plane after bending.
2. The distribution of concrete stress may be taken to be a rectangle with a mean stress of $0.85f'_c$ and a depth from the compressed edge of $\beta_1 c$, where c is the neutral axis depth. The value of β_1 is 0.85 for $f'_c \leq 4000$ psi

(27.6 N/mm²) and is reduced continuously at a rate of 0.05 for each 1000 psi (6.89 N/mm²) of strength in excess of 4000 psi (27.6 N/mm²).

3. Tensile strength of concrete may be neglected.
4. The concrete strain at the extreme compression fiber at the flexural strength of the member may be taken as 0.003.
5. The stress in the steel at less than the yield strength may be taken as the steel strain multiplied by the modulus of elasticity of 29×10^6 psi (0.20×10^6 N/mm²). For strains higher than that at the yield strength, the steel stress may be considered to remain at the yield strength.
6. The above concrete compressive strain and stress distribution may be used for beams with nonrectangular compressed areas; for columns with nonrectangular compressed areas, however, the use of more accurate parameters based on the concrete stress-strain curve may be necessary.
7. The effect of sustained loading may be neglected.

The distribution of compressive stress in the concrete may also be taken as any shape that results in a reliable prediction of the flexural strength of the member. Some alternative relationships previously employed between concrete compressive stress and strain are bilinear, parabolic, and combined parabolic-linear curves. A curve consisting of a second-degree parabola up to a strain of 0.002 followed by a straight horizontal branch to a strain of 0.0035 is recommended by the CEB-FIP^{3,12} and is common in Europe. However the rectangular compressive stress distribution recommended by the ACI code^{3,6} (see assumption 2 above) makes allowance for the effect of concrete strength on the shape of stress block and leads to a simple derivation of the flexural strength equations.

Another difference between ACI and common European practice is in the maximum usable steel strain recommended. For example, the CEB-FIP recommendations^{3,12} limit the maximum tensile strain in the steel at the flexural strength of the member to 0.01, whereas the ACI code^{3,6} does not place any limitation on the magnitude of the tensile steel strain at the flexural strength (see assumption 5). This restriction of steel strain makes little difference to the magnitude of the calculated flexural strength but does limit the calculated available ultimate deformation of a member. Since the ultimate strain of steel reinforcement is much higher than 0.01, it is difficult to see the need for such a restriction.

3.7 REFERENCES

- 3.1 E. Hognestad, "A Study of Combined Bending and Axial Load in Reinforced Concrete Members," University of Illinois Engineering Experimental Station Bulletin No. 399, 1951, 128 pp.

- 3.2 E. Hognestad, N. W. Hanson, and D. McHenry, "Concrete Stress Distribution in Ultimate Strength Design," *Journal ACI*, Vol. 52, No. 6, December 1955, pp. 455-479.
- 3.3 H. Rüsch, "Versuche zur Festigkeit der Biegedruckzone," Bulletin No. 120, Deutscher Ausschuss für Stahlbeton, Berlin, 1955, 94 pp.
- 3.4 G. M. Sturman, S. P. Shah, and G. Winter, "Effect of Flexural Strain Gradients on Micro-cracking and Stress-Strain Behaviour of Concrete," *Journal ACI*, Vol. 62, No. 7, July 1965, pp. 805-822.
- 3.5 C. S. Whitney, "Plastic Theory of Reinforced Concrete Design," *Proceedings ASCE*, December 1940; *Transactions ASCE*, Vol. 107, 1942, pp. 251-326.
- 3.6 ACI Committee 318, "Building Code Requirements for Reinforced Concrete (ACI 318-71)," American Concrete Institute, Detroit, 1971, 78 pp.
- 3.7 A. H. Mattock, L. B. Kriz, and E. Hognestad, "Rectangular Concrete Stress Distribution in Ultimate Strength Design," *Journal ACI*, Vol. 57, No. 8, February 1961, pp. 875-926.
- 3.8 J. A. Blume, N. M. Newmark, and L. H. Corning, "Design of Multistorey Reinforced Concrete Buildings for Earthquake Motions," Portland Cement Association, Chicago 1961, 318 pp.
- 3.9 H. Rüsch, "Researches Toward a General Flexural Theory for Structural Concrete," *Journal ACI*, Vol. 57, No. 1, July 1960, pp. 1-28. Discussion in *Journal ACI*, Vol. 57, No. 9, March 1961, pp. 1147-1164.
- 3.10 H. Rüsch and S. Stöckl, "Versuche zur Festigkeit der Biegedruckzone Einflüsse der Querschnittsform," Bulletin No. 207, Deutscher Ausschuss für Stahlbeton, Berlin, 1969, pp. 27-68.
- 3.11 A. H. Mattock and L. B. Kriz, "Ultimate Strength of Nonrectangular Structural Concrete Members," *Journal ACI*, Vol. 57, No. 7, January 1961, pp. 737-766.
- 3.12 CEB-FIP, "International Recommendations for the Design and Construction of Concrete Structures," Comité Européen du Béton—Fédération Internationale de la Précontrainte, Paris, 1970. (English translation available from Cement and Concrete Association, London, 88 pp.)

4

Strength of Members with Flexure

Beams are structural elements carrying transverse external loads that cause bending moments and shear forces along their length. The flexural (bending) strength of sections of beams is considered in this chapter.

4.1 RECTANGULAR SECTIONS

4.1.1 Analysis of Singly Reinforced Sections

A singly reinforced concrete section when the flexural strength is reached at the section appears in Fig. 4.1. The resultant internal tensile force is

$$T = A_s f_s \quad (4.1)$$

where A_s = area of steel and f_s = steel stress.

Since the thickness of the steel is small compared with the depth of the section, the stress over the entire steel area is assumed to be uniform and to equal the stress at the centroid of the steel area.

The resultant internal compressive force is

$$C = 0.85 f'_c a b = f'_c a b \quad (4.2)$$

where a = depth of the equivalent rectangular stress block

b = width of section

f'_c = compressive cylinder strength of the concrete.

The distance between the resultant internal forces, known as the internal lever arm, is given by

$$jd = d - 0.5a \quad (4.3)$$

where d , the distance from the extreme compression fiber to the centroid of the steel area, is known as the effective depth.

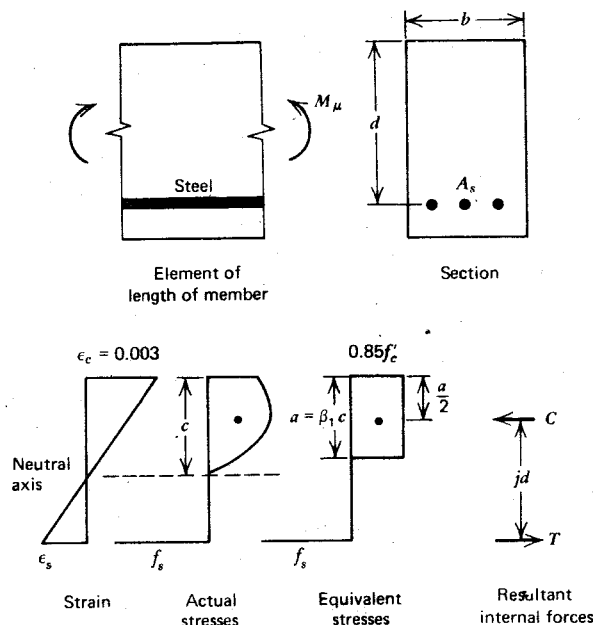


Fig. 4.1. Singly reinforced concrete section when the flexural strength is reached.

The moment of resistance is therefore

$$M_u = Tjd = Cjd \quad (4.4)$$

The types of flexural failure possible (tension, compression, and balanced) and the ideal flexural strength of the section are discussed next.

✓ Tension Failure

If the steel content of the section is small, the steel will reach the yield strength f_y before the concrete reaches its maximum capacity. The steel force remains constant at $A_s f_y$ with further loading. A slight additional load causes large plastic elongation of the steel across the flexural cracks, resulting in wide cracking and a large increase in the strain at the extreme compression fiber of the concrete. With this increase in strain, the distribution of compressive stress in the concrete becomes distinctly nonlinear, resulting in an increase in the mean stress in the compressive stress block and, because equilibrium of the internal forces must be maintained, a reduction in the neutral axis depth. The reduction in the neutral axis depth causes a slight increase in the



Fig. 4.2. Flexural failure of a reinforced concrete beam.

lever arm, hence in the moment of resistance. The flexural strength of the section (maximum moment of resistance) is reached when the strain in the extreme compression fiber of the concrete is approximately 0.003, as discussed in Section 3.3. With further increase in strain, the moment of resistance eventually reduces, and crushing commences in the compressed region of the concrete. Figure 3.2 showed the changes in shape of the concrete stress block during the loading up to the flexural strength; Figure 4.2 shows a beam at a beam-column joint after testing to failure. A flexural failure due to positive bending moment has occurred in the beam. (The studs on the sides of the beam enabled strain measurements to be made.) This type of failure could be referred to more properly as a "primary tension failure," since the failure is initiated by yielding of the tension steel. For the sake of brevity, however, the term "tension failure" is used. Note that the steel does not fracture at the flexural strength of the section unless the steel content is extremely small. The very high steel strains required to cause fracture are associated with extremely small neutral axis depths.

For a tension failure, $f_s = f_y$, where f_y is the yield strength of the steel; for equilibrium, $C = T$. Therefore from Eqs. 4.1 and 4.2 we have

$$0.85 f'_c ab = A_s f_y \quad a = \frac{A_s f_y}{0.85 f'_c b} \quad (4.5)$$

Hence from Eqs. 4.3 and 4.4 the following equations can be written

$$M_u = A_s f_y (d - 0.5a) \\ = A_s f_y \left(d - 0.59 \frac{A_s f_y}{f'_c b} \right) \quad (4.6a)$$

$$= \rho b d^2 f_y \left(1 - 0.59 \frac{\rho f_y}{f'_c} \right) \quad (4.6b)$$

$$= b d^2 f'_c \omega (1 - 0.59 \omega) \quad (4.6c)$$

where

$$\rho = \frac{A_s}{bd} \quad \text{and} \quad \omega = \frac{\rho f_y}{f'_c}$$

✓ Compression Failure

If the steel content of the section is large, the concrete may reach its maximum capacity before the steel yields. In such a case the neutral axis depth increases considerably, causing an increase in the compressive force. This is slightly offset by a reduction in the lever arm. Again the flexural strength of the section is reached when the strain in the extreme compression fiber of the concrete is approximately 0.003. The section then fails suddenly in a brittle fashion. There may be little visible warning of failure because the widths of the flexural cracks in the tension zone of the concrete at the failure section are small, owing to the low steel stress.

For a compression failure, $f_s < f_y$ as the steel remains in the elastic range. The steel stress may be determined in terms of the neutral axis depth considering the similar triangles of the strain diagram of Fig. 4.1.

$$\frac{\varepsilon_s}{0.003} = \frac{d - c}{c} \quad \therefore \quad \varepsilon_s = 0.003 \frac{d - c}{c} \quad (4.7)$$

$$\therefore \quad f_s = \varepsilon_s E_s = 0.003 \frac{d - c}{c} E_s \quad (4.8a)$$

Or, since $a = \beta_1 c$,

$$f_s = 0.003 \frac{\beta_1 d - a}{a} E_s \quad (4.8b)$$

For equilibrium, $C = T$, hence from Eqs. 4.1 and 4.2, we have

$$0.85 f'_c ab = A_s f_s = 0.003 \frac{\beta_1 d - a}{a} E_s A_s \\ \therefore \quad \left(\frac{0.85 f'_c}{0.003 E_s \rho} \right) a^2 + ad - \beta_1 d^2 = 0 \quad (4.9)$$

Rectangular Sections

Equation 4.9 may be solved to find a , and from Eqs. 4.3 and 4.4 we put

$$M_u = 0.85 f'_c ab(d - 0.5a) \quad (4.10)$$

Balanced Failure

At a particular steel content, the steel reaches the yield strength f_y and the concrete reaches the extreme fiber compression strain of 0.003, simultaneously.

Then $\epsilon_s = f_y/E_s$, and from the similar triangles of the strain diagram of Fig. 4.1 we can write

$$\frac{f_y/E_s}{0.003} = \frac{d - c_b}{c_b}$$

where c_b = neutral axis depth for a balanced failure

$$\therefore c_b = \frac{0.003E_s}{0.003E_s + f_y} d \quad (4.11)$$

or

$$a_b = \frac{0.003E_s}{0.003E_s + f_y} \beta_1 d \quad (4.12)$$

where a_b = depth of equivalent rectangular stress block for a balanced failure

For equilibrium, $C = T$; hence we have

$$0.85 f'_c a_b = A_s f_y = \rho_b b d f_y$$

where

$$\rho_b = \frac{A_s}{bd}$$

for a balanced failure

$$\therefore \rho_b = \frac{0.85 f'_c a_b}{f_y d} \quad (4.13)$$

Substituting Eq. 4.12 into Eq. 4.13 gives

$$\rho_b = \frac{0.85 f'_c \beta_1}{f_y} \frac{0.003E_s}{0.003E_s + f_y} \quad (4.14)$$

In the general case when ρ for the section is different from ρ_b , the type of failure that occurs will depend on whether ρ is less than or greater than ρ_b . Figure 4.3 shows the strain profiles at a section at the flexural strength for

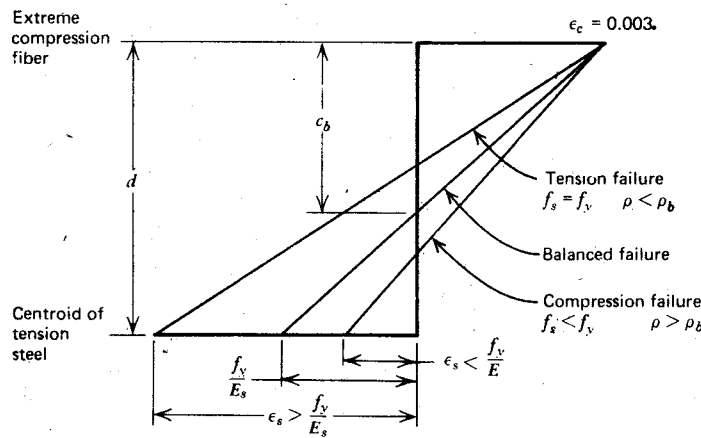


Fig. 4.3. Strain profiles at the flexural strength of a section.

three different steel contents. The neutral axis depth depends on the steel content, as indicated by Eqs. 4.5 and 4.9. Inspection of Fig. 4.3 reveals that if ρ for the section is less than ρ_b , then $c < c_b$ and $\epsilon_s > f_y/E_s$; hence a tension failure occurs. Similarly, if $\rho > \rho_b$ then $c > c_b$ and $\epsilon_s < f_y/E_s$, and a compression failure occurs.

∴ when $\rho < \rho_b$, a tension failure occurs

and

when $\rho > \rho_b$, a compression failure occurs

Note that these strength equations may be said to give the ideal flexural strength of the section, assuming that the equations are scientifically correct, that the materials are as strong as specified, and that the sizes are as assumed.

Example 4.1

A singly reinforced rectangular section has a width of 10 in (254 mm) and an effective depth of 18 in (457 mm). The concrete has a compressive cylinder strength of 3000 psi (20.7 N/mm²). The steel has a modulus of elasticity of 29×10^6 psi (0.20×10^6 N/mm²) and a yield strength of 40,000 psi (275.8 N/mm²). Calculate the ideal flexural strength for the following areas of the steel: (1) 4 in² (2581 mm²), (2) 8 in² (5161 mm²), and (3) the value at balanced failure.

Solution

From Eq. 4.14 we can put

$$\rho_b = \frac{0.85 \times 3000 \times 0.85}{40,000} = \frac{0.003 \times 29 \times 10^6}{0.003 \times 29 \times 10^6 + 40,000} = 0.0371$$

1. $A_s = 4 \text{ in}^2$

$$\therefore \rho = \frac{A_s}{bd} = \frac{4}{10 \times 18} = 0.0222 < \rho_b$$

Therefore, a tension failure occurs.

From Eq. 4.6a we have

$$M_u = 4 \times 40,000 \left(18 - 0.59 \frac{4 \times 40,000}{3000 \times 10} \right) = 2.37 \times 10^6 \text{ lb} \cdot \text{in} \quad (268 \text{ kN} \cdot \text{m})$$

2. $A_s = 8 \text{ in}^2$

$$\therefore \rho = \frac{8}{10 \times 18} = 0.0444 > \rho_b$$

Therefore, a compression failure occurs.

From Eq. 4.9 we have

$$\frac{0.85 \times 3000}{0.003 \times 29 \times 10^6 \times 0.0444} a^2 + 18a - 0.85 \times 18^2 = 0$$

$$\therefore a^2 + 27.27a - 417.3 = 0$$

Solution of the quadratic equation gives $a = 10.93 \text{ in}$ (278 mm) (the other root of the equation is negative).

From Eq. 4.10 we have

$$M_u = 0.85 \times 3000 \times 10.93 \times 10(18 - 0.5 \times 10.93) = 3.49 \times 10^6 \text{ lb} \cdot \text{in} \quad (394 \text{ kN} \cdot \text{m})$$

3. $\rho = \rho_b = 0.0371$

From Eq. 4.6b we write

$$M_u = 0.0371 \times 10 \times 18^2 \times 40,000 \left(1 - 0.59 \frac{0.0371 \times 40,000}{3000} \right) = 3.41 \times 10^6 \text{ lb} \cdot \text{in} \quad (385 \text{ kN} \cdot \text{m})$$

The curve in Fig. 4.4 illustrates the variation in the flexural strength with the steel area for the section of the example. The curve was determined using the equations as in Example 4.1 for a range of steel areas well into the compression failure region. It is evident that in the tension failure region the moment of resistance does not increase linearly with steel area. This is because although the steel force is increasing linearly, there is a reduction in the lever arm with increasing steel content. In the example, the lever arm coefficient j , see Eq. 4.3, reduces from 1.00 when the steel area is zero to 0.71 at balanced failure. In the compression failure region the increase in moment of resistance with steel area is extremely small because both the steel stress and the lever arm decrease with increase in steel area in this region. Hence there is little additional flexural strength to be gained by an increase in the steel area above that for a balanced failure.

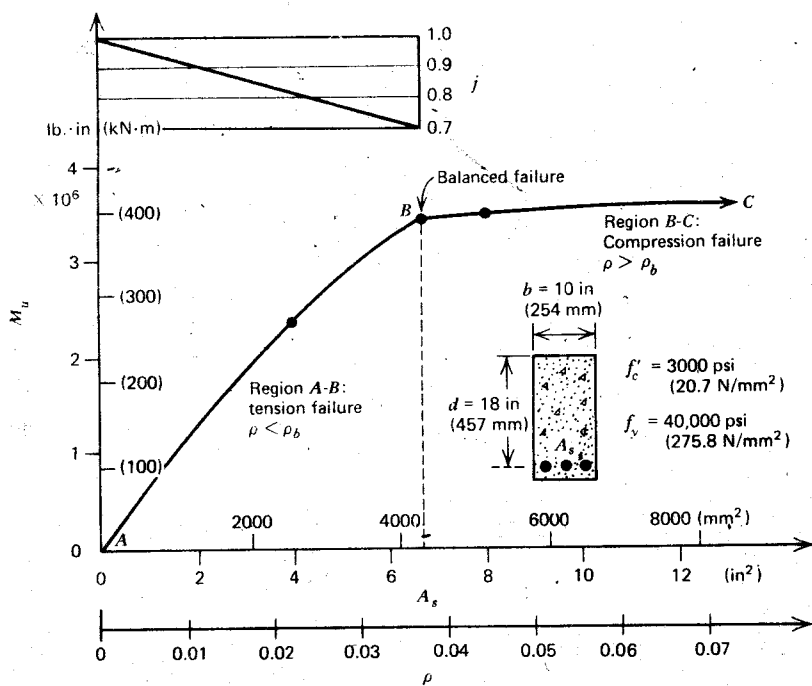


Fig. 4.4. Flexural strength of a singly reinforced concrete section with various steel contents.

arm with increasing steel content. In the example, the lever arm coefficient j , see Eq. 4.3, reduces from 1.00 when the steel area is zero to 0.71 at balanced failure. In the compression failure region the increase in moment of resistance with steel area is extremely small because both the steel stress and the lever arm decrease with increase in steel area in this region. Hence there is little additional flexural strength to be gained by an increase in the steel area above that for a balanced failure.

It is of interest to note that in 1937 Whitney^{4.1} proposed the following strength equations: if

$$\rho < \rho_b, \quad M_u = \rho bd^2 f_y \left(1 - 0.59 \frac{\rho f_y}{f'_c} \right) \quad (4.15)$$

or

$$\rho > \rho_b, \quad M_u = 0.333bd^2 f'_c \quad (4.16)$$

where

$$\rho_b = 0.456 \frac{f'_c}{f_y} \quad (4.17)$$

Whitney based these equations on a rectangular concrete stress block, derived by him, identical to that used today. Whitney's tension failure equation (Eq. 4.15) is the same as Eq. 4.6 used today. Whitney found his value for the balanced steel ratio by determining from tests on beams the steel ratio beyond which a further increase in steel resulted in no apparent increase in flexural strength. Equation 4.17 is this steel ratio, and Whitney's compression failure formula (Eq. 4.16) is this limiting moment of resistance. Although found empirically, Whitney's values for ρ_b and M_u when $\rho > \rho_b$ are reasonably accurate. Using Eqs. 4.9, 4.10, and 4.14, it can be shown that for f_y in the range 40,000 to 60,000 psi (276 to 414 N/mm²) and f'_c in the range 3000 to 6000 psi (20.7 to 41.4 N/mm²), the exact value for the coefficient in Whitney's expression for ρ_b (Eq. 4.17) varies between 0.377 and 0.495, and the coefficient in Eq. 4.16 for the moment of resistance for a compression failure varies between 0.294 and 0.351 at balanced failure.

4.1.2 Design of Singly Reinforced Sections

The use of strength equations in design with load factors and capacity reduction factors to ensure structural safety was discussed in Section 1.3.

Compression failures are dangerous in practice because they occur suddenly, giving little visible warning, and are brittle. Tension failures, however, are preceded by wide cracking of the concrete and have a ductile character. To ensure that all beams have the desirable characteristics of visible warning if failure is imminent, as well as reasonable ductility at failure, it is recommended^{4.2} that the area of tension steel in singly reinforced beams not exceed 0.75 of the area for a balanced failure. It is necessary to limit the steel area to a proportion of the balanced area because, as Eq. 4.14 indicates, if the yield strength of the steel is higher or the concrete strength is lower, a compression failure may occur in a beam that is loaded to the flexural strength.

Hence singly reinforced beams are designed so that $\rho \leq 0.75\rho_b$ where ρ_b is given by Eq. 4.14. Therefore the maximum allowable steel ratio ρ_{\max} is

$$\rho_{\max} = 0.75 \frac{0.85f'_c\beta_1}{f_y} \frac{0.003E_s}{0.003E_s + f_y} \quad (4.18)$$

which on substituting $E_s = 29 \times 10^6$ psi (0.20×10^6 N/mm 2) gives

$$\rho_{\max} = \frac{0.638f'_c\beta_1}{f_y} \frac{87,000}{87,000 + f_y} \quad (4.19a)$$

with stresses in psi, or

$$\rho_{\max} = \frac{0.638f'_c\beta_1}{f_y} \frac{600}{600 + f_y} \quad (4.19b)$$

with stresses in newtons per square millimeter.

Also, the maximum allowable value for ω is

$$\omega_{\max} = \frac{\rho_{\max}f_y}{f'_c} \quad (4.20)$$

The requirement that $\rho \leq 0.75\rho_b$ can be equally well specified as $a \leq 0.75a_b$, where the depth of the rectangular stress block for balanced failure a_b is given by Eq. 4.12. This means that the maximum allowable depth of the rectangular compressive stress block is

$$a_{\max} = 0.75a_b = 0.75 \frac{0.003E_s}{0.003E_s + f_y} \beta_1 d \quad (4.21)$$

In design, a dependable strength of $\varphi \times$ ideal strength is used, where φ is the capacity reduction factor. Therefore, from Eqs. 4.5 and 4.6, the ultimate design resisting moment is

$$M_u = \varphi A_s f_y \left(d - 0.59 \frac{A_s f_y}{f'_c b} \right) \quad (4.22a)$$

$$= \varphi \rho b d^2 f_y \left(1 - 0.59 \frac{\rho f_y}{f'_c} \right) \quad (4.22b)$$

$$= \varphi \omega b d^2 f'_c (1 - 0.59\omega) \quad (4.22c)$$

where

$$\rho = \frac{A_s}{bd} \quad \text{and} \quad \omega = \frac{\rho f_y}{f'_c}$$

In design, the variables in Eqs. 4.22 can be b , d , and A_s . It is evident that there is a range of satisfactory sections having the same strength, and before a solution can be obtained the designer must assume the value for one or more of these variables.

A number of design aids in the form of tables and charts may be devised, or found published. Table 4.1 gives values for ρ_{\max} , ω_{\max} , and a_{\max}/d from Eqs. 4.18, 4.20, and 4.21 for a range of commonly used steel yield and concrete strengths. If the value of ρ , ω , or a/d used in design is less than the maximum value listed in Table 4.1 for the given steel and concrete strength, the steel

Table 4.1 Coefficients for Singly Reinforced Concrete Sections

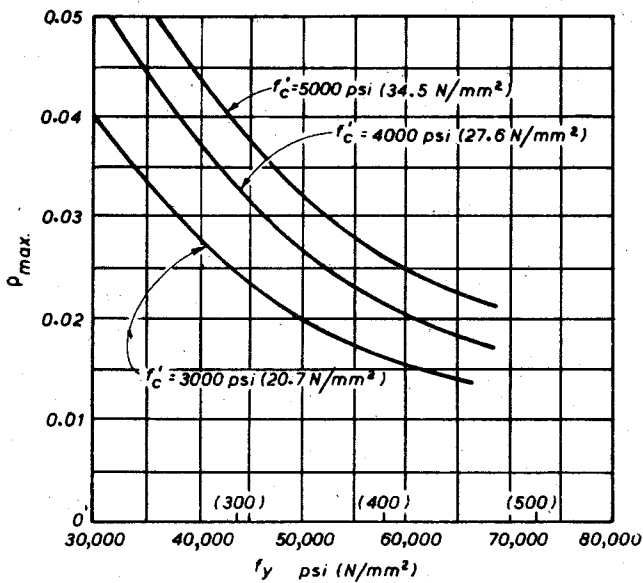
f'_c psi (N/mm ²)	f_y psi (N/mm ²)	ρ_{\max}	ω_{\max}	a_{\max}/d
3000 (20.7)	40,000 (276)	0.0278	0.371	0.437
3000 (20.7)	60,000 (414)	0.0160	0.322	0.377
4000 (27.6)	40,000 (276)	0.0371	0.371	0.437
4000 (27.6)	60,000 (414)	0.0214	0.321	0.377
5000 (34.5)	40,000 (276)	0.0437	0.350	0.411
5000 (34.5)	60,000 (414)	0.0252	0.302	0.355

content is satisfactory. In Figs. 4.5a and 4.5b, curves from Everard and Tanner^{4,3} for ρ_{\max} and ω_{\max} are plotted against the steel yield strength for various concrete strengths.

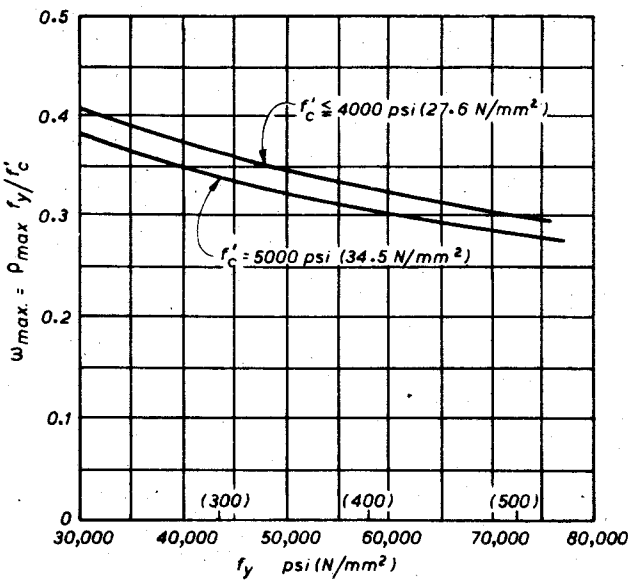
Table 4.2, also from Everard and Tanner,^{4,3} gives a solution of the following form of Eq. 4.6c:

$$\frac{M_u}{bd^2f'_c} = \omega(1 - 0.59\omega) \quad (4.23)$$

The first column in Table 4.2 gives the value of ω to two decimal places, and the first row gives the third decimal place of ω . The remainder of the table gives the corresponding values for $M_u/bd^2f'_c$. Using Table 4.2, the design of a rectangular section for a given flexural strength may be accomplished by assuming a value for ρ or ω and solving for b and d ; alternatively, b and d may be assumed and ρ and ω found. Table 4.2 is the solution for ideal strength, hence the M_u value must be modified by $\varphi = 0.9$.



(a)



(b)

Fig. 4.5. Design curves for a singly reinforced rectangular section.^{4.3} (a) ρ_{max} . (b) ω_{max} .

Table 4.2 Flexural Strength of a Singly Reinforced Rectangular Section^{a,b}

ω	.000	.001	.002	.003	.004	.005	.006	.007	.008	.009
$M_u/f'_c bd^2$										
.0	0	.0010	.0020	.0030	.0040	.0050	.0060	.0070	.0080	.0090
.01	.0099	.0109	.0119	.0129	.0139	.0149	.0159	.0168	.0178	.0188
.02	.0197	.0207	.0217	.0226	.0236	.0246	.0256	.0266	.0275	.0285
.03	.0295	.0304	.0314	.0324	.0333	.0343	.0352	.0362	.0372	.0381
.04	.0391	.0400	.0410	.0420	.0429	.0438	.0448	.0457	.0467	.0476
.05	.0485	.0495	.0504	.0513	.0523	.0532	.0541	.0551	.0560	.0569
.06	.0579	.0588	.0597	.0607	.0616	.0625	.0634	.0643	.0653	.0662
.07	.0671	.0680	.0689	.0699	.0708	.0717	.0726	.0735	.0744	.0753
.08	.0762	.0771	.0780	.0789	.0798	.0807	.0816	.0825	.0834	.0843
.09	.0852	.0861	.0870	.0879	.0888	.0897	.0906	.0915	.0923	.0932
.10	.0941	.0950	.0959	.0967	.0976	.0985	.0994	.1002	.1011	.1020
.11	.1029	.1037	.1046	.1055	.1063	.1072	.1081	.1089	.1098	.1106
.12	.1115	.1124	.1133	.1141	.1149	.1158	.1166	.1175	.1183	.1192
.13	.1200	.1209	.1217	.1226	.1234	.1243	.1251	.1259	.1268	.1276
.14	.1284	.1293	.1301	.1309	.1318	.1326	.1334	.1342	.1351	.1359
.15	.1367	.1375	.1384	.1392	.1400	.1408	.1416	.1425	.1433	.1441
.16	.1449	.1457	.1465	.1473	.1481	.1489	.1497	.1506	.1514	.1522
.17	.1529	.1537	.1545	.1553	.1561	.1569	.1577	.1585	.1593	.1601
.18	.1609	.1617	.1624	.1632	.1640	.1648	.1656	.1664	.1671	.1679
.19	.1687	.1695	.1703	.1710	.1718	.1726	.1733	.1741	.1749	.1756
.20	.1764	.1772	.1779	.1787	.1794	.1802	.1810	.1817	.1825	.1832
.21	.1840	.1847	.1855	.1862	.1870	.1877	.1885	.1892	.1900	.1907
.22	.1914	.1922	.1929	.1937	.1944	.1951	.1959	.1966	.1973	.1981
.23	.1988	.1995	.2002	.2010	.2017	.2024	.2031	.2039	.2046	.2053
.24	.2060	.2067	.2075	.2082	.2089	.2096	.2103	.2110	.2117	.2124
.25	.2131	.2138	.2145	.2152	.2159	.2166	.2173	.2180	.2187	.2194
.26	.2201	.2208	.2215	.2222	.2229	.2236	.2243	.2249	.2256	.2263
.27	.2270	.2277	.2284	.2290	.2297	.2304	.2311	.2317	.2324	.2331
.28	.2337	.2344	.2351	.2357	.2364	.2371	.2377	.2384	.2391	.2397
.29	.2404	.2410	.2417	.2423	.2430	.2437	.2443	.2450	.2456	.2463
.30	.2469	.2475	.2482	.2488	.2495	.2501	.2508	.2514	.2520	.2527
.31	.2533	.2539	.2546	.2552	.2558	.2565	.2571	.2577	.2583	.2590
.32	.2596	.2602	.2608	.2614	.2621	.2627	.2633	.2639	.2645	.2651
.33	.2657	.2664	.2670	.2676	.2682	.2688	.2694	.2700	.2706	.2712
.34	.2718	.2724	.2730	.2736	.2742	.2748	.2754	.2760	.2766	.2771
.35	.2777	.2783	.2789	.2795	.2801	.2807	.2812	.2818	.2824	.2830
.36	.2835	.2841	.2847	.2853	.2858	.2864	.2870	.2875	.2881	.2887
.37	.2892	.2898	.2904	.2909	.2915	.2920	.2926	.2931	.2937	.2943
.38	.2948	.2954	.2959	.2965	.2970	.2975	.2981	.2986	.2992	.2997
.39	.3003	.3008	.3013	.3019	.3024	.3029	.3035	.3040	.3045	.3051
.40	.3056									

^a From Reference 4.3.

^b The M_u value does not include the effect of φ .

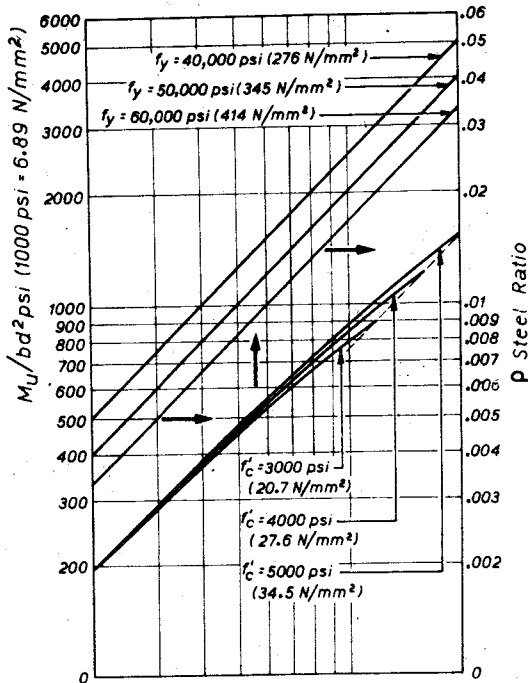


Fig. 4.6. Flexural strength of a singly reinforced rectangular section.^{4.4}

Figure 4.6, a chart originally published by Whitney and Cohen,^{4.4} also gives a solution for Eq. 4.23. The chart may be entered with the required value of M_u/bd^2 , traversed horizontally to the f'_c value, then vertically to the f_y value, and finally horizontally to the value of ρ to be used. If ρ is assumed, M_u/bd^2 may be found by reversing the procedure. Again, since Fig. 4.6 is the solution for the ideal strength, M_u must be modified by the capacity reduction factor.

A most comprehensive set of design aids has been published by the ACI.^{4.5} The publication contains a wide range of tables and charts for specified f'_c and f_y values, enabling one to obtain extremely quick solutions for sections.

It is also possible to use a trial-and-error method for the design of sections in which the internal lever arm, $jd = d - 0.5a$, is estimated. This method can be convenient because the internal lever arm is not very sensitive to variation of the steel content within practical limits, as Fig. 4.4 illustrates. Moreover, this procedure helps one to visualize the location of the resultant RP of the internal compressive force. Design by this trial-and-error method involves estimating jd , determining the resulting steel content, determining

the resulting depth of the rectangular stress block a for the steel area, and verifying that a is less than a_{\max} and that the initially assumed value for jd is correct or is at least conservative. *1/2*

In general, if a section is to be designed to have minimum depth, the steel content required will be the maximum allowable, ρ_{\max} . It is evident from Fig. 4.5 that such a design requires a very high steel content. Unless a very shallow depth is essential, use of ρ_{\max} is not economical and it is better to use a deeper section with less steel. Also, the deflections of a beam with the minimum possible depth may be excessive and may need to be checked. A good guide to reasonably proportioned members are the span/depth ratios listed in the ACI code^{4,2}, which if exceeded require the deflection of the member to be checked. *8/12*

It is possible to design much shallower singly reinforced beams when using the strength design method than when using the alternate design method involving elastic theory and allowable stresses. (The alternate design method is described in Section 10.2.5.) Suppose for instance, that $f'_c = 3000$ psi (20.7 N/mm^2) and $f_y = 40,000$ psi (276 N/mm^2). A beam designed by the alternative design method of ACI 318-71^{4,2} with allowable stresses of $0.45f'_c$ in the concrete and $0.5f_y$ in the steel reached simultaneously at the service load bending moment, requires a steel ratio $\rho = 0.0128$. However strength design results in $\rho_{\max} = 0.0278$ and therefore a much shallower section can be used. Thus a good deal of freedom exists when choosing the size of singly reinforced sections in strength design.

Note that although ρ_{\max} has been taken as $0.75\rho_b$, to avoid the possibility of compression failures, there is a danger in using "overstrong" steel. For example, a singly reinforced beam containing the maximum allowable content ρ_{\max} of steel with a design yield strength of 40,000 psi (276 N/mm^2) will fail in compression if the actual yield strength is greater than 49,600 psi (342 N/mm^2). Thus a yield strength higher than specified could lead to a brittle failure, although at a higher bending moment. Similarly, a concrete of lower strength than specified may lead to a compression failure at a lower bending moment. *8/12*

It is also reasonable to stipulate a minimum reinforcement ratio that should always be exceeded. This is necessary because if the reinforcement ratio is very small, the computed flexural strength as a reinforced concrete section becomes less than the bending moment required to crack the section, and on cracking, failure is sudden and brittle. To prevent this, it is recommended^{4,2} that ρ in beams be not less than $200/f_y$, where f_y is in psi, or $1.38/f_y$, where f_y is in N/mm^2 . This quantity was found by equating the cracking moment of the section, using the modulus of rupture of the plain concrete section, to the strength computed as a reinforced concrete section, and solving for the steel ratio.^{4,6}

Example 4.2

A 12 in (305 mm) wide, singly reinforced rectangular section is to carry service load bending moments of 0.75×10^6 lb·in (84.7 kN·m) from dead load and 1.07×10^6 lb·in (120.8 kN·m) from live load. Using $f'_c = 3000$ psi (20.7 N/mm^2) and $f_y = 60,000$ psi (414 N/mm^2), design the section for (1) minimum depth, (2) an effective depth of 27.4 in (696 mm), and (3) an overall depth of 30 in (762 mm) using a trial-and-error method.

Solution

The required strength U as given by Eq. 1.1 is $U = 1.4D + 1.7L$, where D and L are the dead and live service load moments, respectively. Therefore the flexural strength is to be

$$M_u = 1.4 \times 0.75 \times 10^6 + 1.7 \times 1.07 \times 10^6 \\ = 2.87 \times 10^6 \text{ lb} \cdot \text{in} (324 \text{ kN} \cdot \text{m})$$

1. Minimum depth

The depth will be a minimum if ρ is the maximum allowed. From Eq. 4.19 we have

$$\rho = \rho_{\max} = \frac{0.638 \times 3000 \times 0.85}{60,000} \frac{87,000}{87,000 + 60,000} = 0.0160$$

From Eq. 4.22b we have

$$2.87 \times 10^6 = 0.9 \times 0.0160 \times 12$$

$$\times 60,000 \left(1 - 0.59 \frac{0.0160 \times 60,000}{3000} \right) d^2$$

$$\therefore d = 18.5 \text{ in} (470 \text{ mm})$$

$$\therefore A_s = \rho b d = 0.160 \times 12 \times 18.5 = 3.55 \text{ in}^2 (2290 \text{ mm}^2)$$

Since $200/f_y = 200/60,000 = 0.0033 < \rho$, it is evident that the reinforcement area is satisfactory. An arrangement of bars making up this area would be used.

2. Effective depth of 27.4 in (696 mm)

From Eq. 4.22b we write

$$2.87 \times 10^6 = 0.9 \times 12 \times 27.4^2 \times 60,000 \rho \left(1 - 0.59 \frac{60,000}{3000} \rho \right)$$

$$\therefore 11.8\rho^2 - \rho + 0.0059 = 0$$

Solution of the quadratic equation gives $\rho = 0.00638$ as the required root.

$$\therefore A_s = \rho bd = 0.00638 \times 12 \times 27.4 = 2.10 \text{ in}^2 (1353 \text{ mm}^2)$$

It is evident that $\rho < \rho_{\max}$ and $\rho > 200/f_y$; hence the reinforcement area is satisfactory. An arrangement of bars making up this area would be used.

Overall depth of 30 in (762 mm)

The steel area will be determined by trial and error. Assume 2 in of concrete cover over the bars and one row of No. 8 (25.4 mm diameter) bars, giving preliminary $d = 30 - 2 - 0.5 = 27.5$ in. Assume $j = 0.87$ (i.e., $a/d = 0.26$). From Table 4.1, we find that $0.26 < 0.377 = a_{\max}/d$; hence the section is not overreinforced.

From $M_u = \phi A_s f_y jd$ with the assumed lever arm substituted, the approximate steel area is

$$A_s = \frac{2.87 \times 10^6}{0.9 \times 60,000 \times 0.87 \times 27.5} = 2.22 \text{ in}^2$$

This is easily accommodated in one layer of bars. The a/d resulting from this steel area may be calculated using Eq. 4.5:

$$\frac{a}{d} = \frac{2.22 \times 60,000}{0.85 \times 3000 \times 12 \times 27.5} = 0.158$$

Since this a/d value is less than the assumed value of 0.26, the assumed lever arm is smaller than the actual value, and the determined steel content will be less than $0.75\rho_b$. The selection of bars may now be made. The use of three No. 8 bars giving 2.35 in^2 will obviously be more than adequate.

Try two No. 7 (22.2 mm diameter) and two No. 6 (19.1 mm diameter) bars, giving $A_s = 2.08 \text{ in}^2 (1342 \text{ mm}^2)$. Then $a/d = 2.08 \times 0.158/2.22 = 0.148$, $j = 1 - 0.5 \times 0.148 = 0.926$, and the flexural strength of the section would be

$$M_u = \phi A_s f_y jd = 0.9 \times 2.08 \times 60,000 \times 0.926 \times 27.6 \\ = 2.87 \times 10^6 \text{ lb} \cdot \text{in}$$

which equals the required flexural strength. It may be demonstrated that for the strength properties used in the example, the limitations for steel content will always be satisfied when $0.1 < a/d < 0.35$. Such rounded off values are easily remembered by designers.

In item 1 of the foregoing example a quadratic equation had to be solved to determine the steel ratio (or area) for a section of given dimensions. The quadratic has two real roots, and the value to be taken in design is always the smaller root. The reason for this is illustrated in Fig. 4.7, a plot of M_u

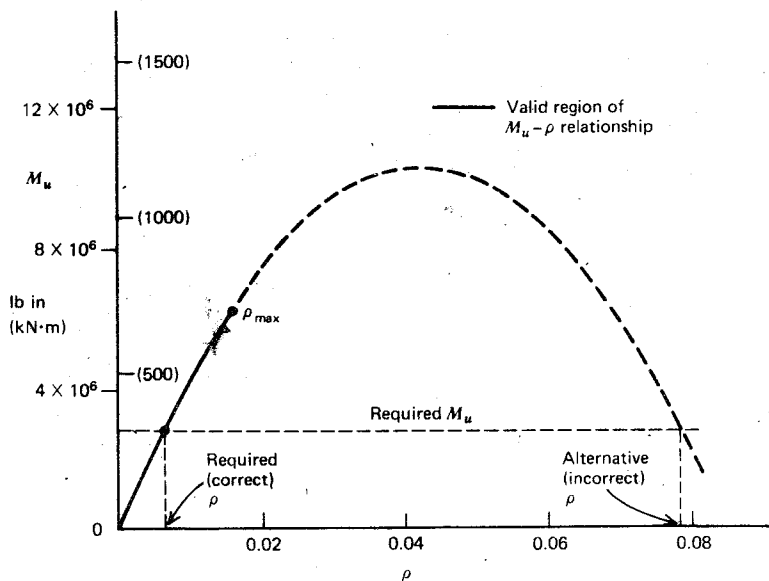


Fig. 4.7. Calculation of correct steel ratio for a given section and flexural strength.

versus ρ for a single reinforced section. The curve is only valid when $0 < \rho < \rho_{\max}$, but the solution of the quadratic gives as an alternative root the value of ρ for the point at which the falling branch of the curve reduces to the design moment.

The solution of the example is simplified by referring to Table 4.2 or Fig. 4.6. For example, in item 2 if $M_u/bd^2f'_c$ is calculated, the table will give the corresponding value of ω from which A_s can be determined.

It is of interest to compare the results of this design example with results obtained using the alternative design method of ACI 318-71^{4,2} described in Section 10.2.5. For the above-specified strengths of steel and concrete, the modular ratio would be 9 and the allowable stresses would be 24,000 psi (165 N/mm²) for the steel and 1350 psi (9.31 N/mm²) for the concrete. A design in which the allowable stresses in the steel and concrete are developed simultaneously at the service load requires $d = 27.4$ in (696 mm) and

- $A_s = 3.11 \text{ in}^2 (2006 \text{ mm}^2)$. This may be compared with the $2.10 \text{ in}^2 (1353 \text{ mm}^2)$ required for this effective depth by the strength design method in the example. The marked difference in steel content required by the two approaches in this example is due to the low allowable stress for the steel. For a smaller effective depth than 27.4 in (696 mm), a design by the alternative design method based on working stresses would require a doubly reinforced section and a great deal more steel than for the singly reinforced section possible by the strength design method.

4.1.3 Analysis of Doubly Reinforced Sections

Figure 4.8 shows a doubly reinforced section when the flexural strength is reached. Depending on the steel areas and positions, the tension and compression steel may or may not be at the yield strength when the maximum moment is reached. However, the analysis of such a section is best carried out by assuming first that all the steel is yielding, modifying the calculations later if it is found that some or all of the steel is not at the yield strength.

If all the steel is yielding, $f_s = f'_s = f_y$, where f_s is the stress in the tension steel, f'_s is the stress in the compression steel, and f_y is the yield strength of the steel. Then the resultant internal forces are

compression in the concrete

$$C_c = 0.85 f'_c ab \quad (4.24)$$

compression in the steel

$$C_s = A'_s f_y \quad (4.25)$$

where A'_s = area of compression steel

tension in the steel

$$T = A_s f_y \quad (4.26)$$

where A_s = area of tension steel.

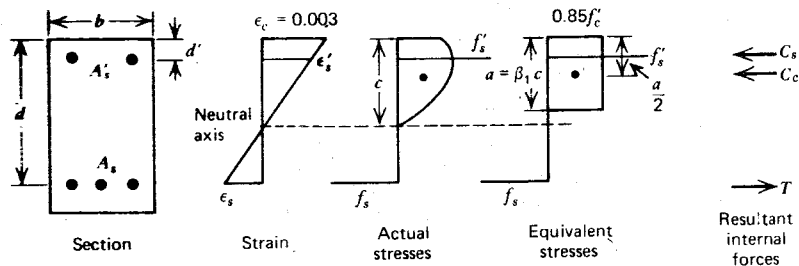


Fig. 4.8. Doubly reinforced concrete section when the flexural strength is reached.

For equilibrium, we write

$$C = C_c + C_s = T \quad \therefore \quad 0.85 f'_c ab + A'_s f_y = A_s f_y$$

$$\therefore a = \frac{(A_s - A'_s) f_y}{0.85 f'_c b} \quad (4.27)$$

The strain diagram may now be used to check whether the steel is yielding. The steel is at yield stress if its strain exceeds f_y/E_s . From the similar triangles of the strain diagram, we have

$$\epsilon'_s = 0.003 \frac{c - d'}{c} = 0.003 \frac{a - \beta_1 d'}{a} \quad (4.28)$$

$$\epsilon_s = 0.003 \frac{d - c}{c} = 0.003 \frac{\beta_1 d - a}{a} \quad (4.29)$$

$$\therefore f'_s = f_y \quad \text{if} \quad 0.003 \frac{a - \beta_1 d'}{a} \geq \frac{f_y}{E_s} \quad (4.30)$$

and

$$f_s = f_y \quad \text{if} \quad 0.003 \frac{\beta_1 d - a}{a} \geq \frac{f_y}{E_s} \quad (4.31)$$

If these conditions hold, the assumption of all steel yielding is correct and, by taking moments about the tension steel, the flexural strength is given by

$$M_u = 0.85 f'_c ab \left(d - \frac{a}{2} \right) + A'_s f_y (d - d') \quad (4.32)$$

where a is given by Eq. 4.27.

When checks by Eqs. 4.30 and 4.31 reveal that the steel is not yielding, the value of a calculated from Eq. 4.27 is incorrect, and the actual steel stress and a have to be calculated from the equilibrium equation and the strain diagram: thus, in general, from the equilibrium equation

$$a = \frac{A_s f_s - A'_s f'_s}{0.85 f'_c b} \quad (4.33)$$

where from the strain diagram

$$f'_s = \epsilon'_s E_s = 0.003 \frac{a - \beta_1 d'}{a} E_s \quad \text{or} \quad f_y \quad (4.34)$$

$$f_s = \epsilon_s E_s = 0.003 \frac{\beta_1 d - a}{a} E_s \quad \text{or} \quad f_y \quad (4.35)$$

and then

$$M_u = 0.85 f'_c ab \left(d - \frac{a}{2} \right) + A'_s f'_s (d - d') \quad (4.36)$$

Tension and compression failures can occur in doubly reinforced beams as well as in singly reinforced beams. In tension failures the tension steel yields, but in compression failures the tension steel remains in the elastic range; in both types of failure the compression steel may or may not be yielding. In practical beams the tension steel will always be yielding, and very often the strain at the level of the compression steel is great enough for that steel to be at yield strength as well. The greater the value of a , and the lower the values of d' and f_y , the more probable it is that the compression steel is yielding. Rather than develop general equations for all cases, it is better to work each case numerically from first principles. The general equations, if required, are given in a paper by Mattock, Kriz, and Hognestad.^{4,7} The following example illustrates the numerical approach.

Example 4.3

A doubly reinforced rectangular section has the following properties: $b = 11$ in (279 mm), $d = 20$ in (508 mm), $d' = 2$ in (51 mm), $A'_s = 1$ in 2 (645 mm 2), $A_s = 4$ in 2 (2581 mm 2), $E_s = 29 \times 10^6$ psi (0.2 \times 10 6 N/mm 2), and $f_y = 40,000$ psi (276 N/mm 2). Calculate the ideal flexural strength if (1) $f'_c = 3000$ psi (20.7 N/mm 2), and (2) $f' = 5000$ psi (34.5 N/mm 2).

Solution

1. If $f'_c = 3000$ psi (20.7 N/mm 2)

Assume that all steel is yielding.

$$C_c = 0.85 f'_c ab = 0.85 \times 3000 \times a \times 11 = 28,050a \text{ lb}$$

$$C_s = A'_s f_y = 1 \times 40,000 = 40,000 \text{ lb}$$

$$T = A_s f_y = 4 \times 40,000 = 160,000 \text{ lb}$$

But $C_c + C_s = T$.

$$\therefore a = \frac{160,000 - 40,000}{28,050} = 4.28 \text{ in}$$

And since $\beta_1 = 0.85$, $c = a/\beta_1 = 4.28/0.85 = 5.03$ in.

Now the yield strain is $f_y/E_s = 40,000/(29 \times 10^6) = 0.00138$. Check the steel stresses by referring to the strain diagram (see Fig. 4.8)

$$\epsilon'_s = 0.003 \frac{c - d'}{c} = 0.003 \frac{5.03 - 2}{5.03} = 0.00181 > \frac{f_y}{E_s}$$

$$\therefore f'_s = f_y$$

$$\epsilon_s = 0.003 \frac{d - c}{c} = 0.003 \frac{20 - 5.03}{5.03} = 0.00892 > \frac{f_y}{E_s}$$

$$\therefore f_s = f_y$$

Hence all the steel is yielding as assumed.

$$\begin{aligned}\therefore M_u &= C_c(d - 0.5a) + C_s(d - d') \\ &= 28,050 \times 4.28(20 - 2.14) + 40,000(20 - 2) \\ &= 2.86 \times 10^6 \text{ lb} \cdot \text{in} (323 \text{ kN} \cdot \text{m})\end{aligned}$$

2. If $f'_c = 5000 \text{ psi}$ (34.5 N/mm^2)

Assume that all steel is yielding.

$$C_c = 0.85 \times 5000 \times a \times 11 = 46,750a \text{ lb}$$

$$C_s = 1 \times 40,000 = 40,000 \text{ lb}$$

$$T = 4 \times 40,000 = 160,000 \text{ lb}$$

$$\therefore a = \frac{160,000 - 40,000}{46,750} = 2.57 \text{ in}$$

and since $\beta_1 = 0.8$, $c = 2.57/0.8 = 3.21 \text{ in}$.

The yield strain of the steel is 0.00138, and the steel stresses may be checked by referring to the strain diagram.

$$\epsilon'_s = 0.003 \frac{3.21 - 2}{3.21} = 0.00113 < \frac{f_y}{E_s} \quad \therefore f'_s < f_y$$

$$\epsilon_s = 0.003 \frac{20 - 3.21}{3.21} = 0.0157 > \frac{f_y}{E_s} \quad \therefore f_s = f_y$$

Therefore the compression steel is not yielding (although the tension steel is), and the foregoing values for C_s and a are incorrect. The actual value for ϵ'_s in terms of a may be determined from the strain diagram, and since the compression steel remains elastic, we have

$$\begin{aligned}f'_s &= \epsilon'_s E_s = 0.003 \frac{c - d'}{c} E_s = 0.003 \frac{a - \beta_1 d'}{a} E_s \\ \therefore C_s &= A'_s f'_s = 1 \times 0.003 \times \frac{a - 0.8 \times 2}{a} \times 29 \times 10^6 \\ &= 87,000 \frac{a - 1.6}{a} \text{ lb}\end{aligned}$$

But $C_c + C_s = T$.

$$\therefore 46,750a + 87,000 \frac{a - 1.6}{a} = 160,000$$

$$\therefore a^2 - 1.561a - 2.978 = 0$$

Solution of the quadratic equation gives $a = 2.68$ in.

$$\therefore C_s = 87,000 \frac{2.68 - 1.6}{2.68} = 34,960 \text{ lb}$$

$$\left(\therefore f'_s = \frac{C_s}{A'_s} = \frac{34,960}{1} = 34,960 \text{ psi} \right)$$

$$\therefore C_c = 46,750 \times 2.68 = 125,060 \text{ lb}$$

(Note that $C_c + C_s = 160,020 \text{ lb} = T$; therefore, equilibrium checks.)

$$\begin{aligned} \therefore M_u &= C_c(d - 0.5a) + C_s(d - d') \\ &= 125,060(20 - 1.34) + 34,960(20 - 2) \\ &= 2.96 \times 10^6 \text{ lb} \cdot \text{in} (334 \text{ kN} \cdot \text{m}) \end{aligned}$$

It is of interest to note that the increase of concrete strength from 3000 psi (20.7 N/mm²) to 5000 psi (34.5 N/mm²) in Example 4.3 has made little difference to the flexural strength, a characteristic of reinforced concrete beams which fail in tension. Moreover, if the compression steel had not been present in the section, both beams still would have failed in tension and the flexural strength would have been $2.74 \times 10^6 \text{ lb} \cdot \text{in}$ (309 kN · m) for $f'_c = 3000 \text{ psi}$ (20.7 N/mm²), and $2.93 \times 10^6 \text{ lb} \cdot \text{in}$ (331 kN · m) for $f'_c = 5000 \text{ psi}$ (34.5 N/mm²). Therefore, the presence of compression steel has not enhanced the ultimate strength of the sections as much as one perhaps expected—another characteristic of beams failing in tension, particularly when the steel ratio ρ is a good deal less than ρ_b .

4.1.4 Design of Doubly Reinforced Sections

Compression steel may be required in design for the following reasons:

1. When a beam of shallow depth is used, the flexural strength obtained using ρ_{\max} may be insufficient. The moment capacity may be increased by placing compression steel and additional tension steel. Such an occurrence is rare in design because the ρ_{\max} values allowed by the strength design method are much higher than the balanced ρ of beams designed by the alternative design method (working stress method). For instance, for beams with

$f'_c = 3000 \text{ psi (20.7 N/mm}^2)$ and $f_y = 40,000 \text{ psi (276 N/mm}^2)$, the strength design ρ_{\max} is 0.0278 and the working stress design balanced ρ is 0.0128. Thus although compression steel is frequently necessary in the working stress design method, it is seldom required in the strength design method to enhance the flexural strength.

2. Compression steel may be used in design to increase the ductility of the section at the flexural strength. It is evident that if compression steel is in a section, the neutral axis depth will be smaller because the internal compressive force is shared by the concrete and the compression steel. Hence the ultimate curvature (given by ε_c/c) of the section with compression steel will be greater (see Section 6.3.1).

3. Compression steel may be used to reduce deflection of beams at the service load. Singly reinforced beams containing ρ_{\max} have high stresses in the concrete at the service load. For instance, the singly reinforced beam designed for minimum depth in Example 4.2 with $f'_c = 3000 \text{ psi (20.7 N/mm}^2)$ has a maximum stress in the concrete of 2490 psi (17.2 N/mm^2), at service load, according to elastic theory ignoring creep, even though the stress in the steel is approximately one-half (54%) the yield strength. The actual stress in the concrete will be less due to the curved shape of the actual stress block, but clearly the concrete strain will be high and the deflections may be large. The deflections can be made smaller by reducing the stress carried by the concrete. This is achieved by placing compression steel in the section.

Compression steel also reduces the long-term deflections of beams at service loads because when the concrete commences to creep, the compressive force in the beam tends to be transferred from the concrete to the steel. Thus the concrete stress is lowered and the deflection due to creep is much reduced. Curvatures due to shrinkage of concrete are also reduced by compression steel.

4. Frequently considerations of possible combinations of external loading reveal that the bending moment can change sign. This is a common case for the beams of continuous frames under gravity and lateral loading. Such members require reinforcement near both faces to carry the possible tensile forces and therefore act as doubly reinforced members. In the evaluation of the flexural strength of sections, it is always conservative to ignore the presence of compression steel. In certain cases, however, an accurate assessment of the flexural strength of the section, including the effect of compression steel, may be required.

The design resisting moment of a doubly reinforced beam, assuming all the steel is yielding as given by Eq. 4.32, is

$$M_u = \varphi \left[0.85 f'_c ab \left(d - \frac{a}{2} \right) + A'_s f_y (d - d') \right] \quad (4.37)$$

where

$$a = \frac{(A_s - A'_s)f_y}{0.85f'_c b} \quad (4.38)$$

Since for equilibrium $0.85f'_c ab = (A_s - A'_s)f_y$, Eq. 4.37 may be written

$$M_u = \varphi \left[(A_s - A'_s)f_y \left(d - \frac{a}{2} \right) + A'_s f_y (d - d') \right] \quad (4.39)$$

where a is as given by Eq. 4.38.

Equations 4.37 to 4.39 assume that the compression steel is yielding, and this may be checked by considering the strain diagram of Fig. 4.8. From similar triangles of the strain diagram, for the compression steel to be yielding, we need

$$\varepsilon'_s = 0.003 \frac{c - d'}{c} = 0.003 \frac{a - \beta_1 d'}{a} \geq \frac{f_y}{\varepsilon_s}$$

This requires

$$a \geq \frac{0.003E_s}{0.003E_s - f_y} \beta_1 d' \quad (4.40)$$

Equating Eqs. 4.38 and 4.40 shows that for the compression steel to be yielding, we must have

$$\frac{(A_s - A'_s)f_y}{0.85f'_c b} \geq \frac{0.003E_s}{0.003E_s - f_y} \beta_1 d'$$

or

$$\rho - \rho' \geq \frac{0.85f'_c \beta_1 d'}{f_y d} \frac{0.003E_s}{0.003E_s - f_y} \quad (4.41)$$

If the compression steel is not yielding, the stress in it may be found in terms of a , using the strain diagram. This actual stress f'_s should then be used instead of f_y for the compression steel in the equation for the flexural strength. The stress to be substituted is

$$f'_s = \varepsilon'_s E_s = 0.003 \frac{a - \beta_1 d'}{a} E_s \quad (4.42)$$

The design equations become

$$M_u = \varphi \left[0.85f'_c ab \left(d - \frac{a}{2} \right) + A'_s f'_s (d - d') \right] \quad (4.43)$$

where

$$a = \frac{A_s f_y - A'_s f'_s}{0.85 f'_c b} \quad (4.44)$$

with f'_s as given by Eq. 4.42.

The design equations 4.37 to 4.44 also assume that the tension steel is yielding. Yield of the tension steel is essential to avoid brittle failures. For a balanced failure (tension steel reaching yield and concrete reaching an extreme fiber compression strain of 0.003 simultaneously), the similar triangles of the strain diagram of Fig. 4.8 show that

$$\begin{aligned} \varepsilon_s &= 0.003 \frac{d - c_b}{c_b} = 0.003 \frac{\beta_1 d - a_b}{a_b} = \frac{f_y}{E_s} \\ \therefore a_b &= \frac{0.003 E_s}{0.003 E_s + f_y} \beta_1 d \end{aligned} \quad (4.45)$$

and for equilibrium

$$\begin{aligned} 0.85 f'_c a_b b &= A_s f_y - A'_s f'_s \\ &= (\rho_b f_y - \rho' f'_s) b d \end{aligned}$$

where $\rho_b = A_s/bd$ for a balanced failure and $\rho' = A'_s/bd$.

$$\therefore a_b = \frac{(\rho_b f_y - \rho' f'_s) d}{0.85 f'_c} \quad (4.46)$$

Therefore, for a balanced failure, f'_s is given by Eq. 4.42 with $a = a_b$ from Eq. 4.45 substituted, or is equal to f_y , whichever is least.

$$\begin{aligned} \therefore f'_s &= 0.003 E_s \left(1 - \frac{\beta_1 d'}{a_b} \right) \\ &= 0.003 E_s \left[1 - \frac{d'}{d} \left(\frac{0.003 E_s + f_y}{0.003 E_s} \right) \right] \end{aligned} \quad (4.47)$$

or f_y , whichever is least.

Equating Eqs. 4.45 and 4.46 gives

$$\rho_b = \frac{0.85 f'_c \beta_1}{f_y} \frac{0.003 E_s}{0.003 E_s + f_y} + \frac{\rho' f'_s}{f_y} \quad (4.48)$$

where f'_s is given by Eq. 4.47 or f_y , whichever is least. The first term on the right-hand side of Eq. 4.48 is identical to ρ_b for a balanced failure of a single reinforced beam, Eq. 4.14. This is to be expected because the neutral axis depth, hence the concrete force, is the same in both cases. The second term on

the right-hand side of Eq. 4.48 is due to the compression steel. Thus for a doubly reinforced beam, to ensure that the tension steel yields, ρ must be less than ρ_b given by Eq. 4.48.

For design, to ensure that the tension steel is yielding and that the failure is not brittle, it is recommended^{4,2} that the reinforcement ratio ρ of the tension steel of a doubly reinforced beam not exceed $0.75\rho_b$. This requires

$$\rho \leq 0.75 \left(\frac{0.85f'_c\beta_1}{f_y} \frac{0.003E_s}{0.003E_s + f_y} + \frac{\rho'f'_s}{f_y} \right) \quad (4.49)$$

where f'_s is either as given by Eq. 4.47 or f_y , whichever is least. Stated another way, the requirement is that the force in the tension steel be limited to 0.75 of the total compressive force (concrete plus steel) at balanced failure.

Example 4.4

A rectangular section with $b = 11$ in (279 mm), $d = 20$ in (508 mm), $d' = 2.5$ in (64 mm), $f'_c = 3000$ psi (20.7 N/mm^2), $E_s = 29 \times 10^6$ psi ($0.2 \times 10^6 \text{ N/mm}^2$), $f_y = 40,000$ psi (276 N/mm^2) is to carry service load bending moments of 125 kip·ft (169 kN·m) due to dead load and 158.8 kip·ft (215 kN·m) due to live load. Calculate the steel areas required for the following two cases: (1) $\rho - \rho'$ is limited to 0.5 of ρ_b for a singly reinforced beam in order to reduce deflection and increase ductility, and (2) the area of compression steel is a minimum.

Solution

The flexural strength is required to be $U = 1.4D + 1.7L$

$$\begin{aligned} M_u &= 1.4 \times 1.25 + 1.7 \times 158.8 = 445 \text{ kip}\cdot\text{ft} \\ &= 5.34 \times 10^6 \text{ lb}\cdot\text{in} (603 \text{ kN}\cdot\text{m}) \end{aligned}$$

1. $\rho - \rho' = 0.5\rho_b$ for singly reinforced section

From Eq. 4.14 we have

$$\begin{aligned} \rho - \rho' &= 0.5 \frac{0.85 \times 3000 \times 0.85}{40,000} \frac{0.003 \times 29 \times 10^6}{0.003 \times 29 \times 10^6 + 40,000} \\ &= 0.0186 \end{aligned}$$

$$\therefore A_s - A'_s = (\rho - \rho')bd = 0.0186 \times 11 \times 20 = 4.09 \text{ in}^2$$

From Eq. 4.38, assuming that all steel is yielding, we have

$$a = \frac{4.09 \times 40,000}{0.85 \times 3000 \times 11} = 5.83 \text{ in}$$

From Eq. 4.39, assuming that all steel is yielding

$$5.34 \times 10^6 = 0.9[4.09 \times 40,000(20 - 2.92) + A'_s 40,000(20 - 2.5)]$$

$$\therefore A'_s = 4.48 \text{ in}^2 (2890 \text{ mm}^2)$$

and

$$A_s = 4.09 + 4.48 = 8.57 \text{ in}^2 (5529 \text{ mm}^2)$$

Check stress in the compression steel:

$$c = \frac{a}{\beta_1} = \frac{5.83}{0.85} = 6.86 \text{ in}$$

By similar triangles of strain diagram, we find

$$\varepsilon'_s = 0.003 \frac{c - d'}{c} = 0.003 \frac{6.86 - 2.5}{6.86} = 0.00191$$

But $f_y/E_s = 40,000/(29 \times 10^6) = 0.00138$; therefore, compression steel is yielding, $f'_s = f_y$, as assumed. (This could have been checked using Eq. 4.41.)

Also

$$\rho = \frac{8.57}{11 \times 20} = 0.0390$$

$$\rho' = \frac{4.48}{11 \times 20} = 0.0204$$

Substituting into the right-hand side of Eq. 4.49 to check total tension steel content, we have

$$0.75 \left(\frac{0.85 \times 3000 \times 0.85}{40,000} \frac{0.003 \times 29 \times 10^6}{0.003 \times 29 \times 10^6 + 40,000} + \frac{0.0204 \times 40,000}{40,000} \right)$$

$$= 0.0431 > 0.0390 \quad \text{as required}$$

2. Minimum compression steel

This design has the maximum possible contribution from the compressed concrete. Thus the first term within the bracket on the right-hand side of Eq. 4.49 is the maximum possible, and the limiting condition of Eq. 4.49 applies.

Substituting into the limiting condition of Eq. 4.49, and assuming that the compression steel is yielding, we write

$$\rho = 0.75 \left(\frac{0.85 \times 3000 \times 0.85}{40,000} \frac{0.003 \times 29 \times 10^6}{0.003 \times 29 \times 10^6 + 40,000} + \rho' \right)$$

$$\therefore \rho = 0.0278 + 0.75\rho'$$

or

$$\begin{aligned} A_s &= (0.0278 \times 11 \times 20) + 0.75A'_s \\ &= 6.12 + 0.75A'_s \end{aligned}$$

Substituting for A_s into Eq. 4.38 gives

$$\begin{aligned} a &= \frac{(6.12 + 0.75A'_s - A'_s)40,000}{0.85 \times 3000 \times 11} \\ &= 1.426(6.12 - 0.25A'_s) \end{aligned}$$

Substituting for A_s and a into Eq. 4.39 gives

$$\begin{aligned} 5.34 \times 10^6 &= 0.9 \{ (6.12 + 0.75A'_s - A'_s) \\ &\quad \times 40,000[20 - 0.713(6.12 - 0.25A'_s)] \\ &\quad + A'_s 40,000(20 - 2.5) \} \\ \therefore (A'_s)^2 - 329.9A'_s + 1184 &= 0 \end{aligned}$$

Solution of the quadratic equation gives $A'_s = 3.63 \text{ in}^2$ (2342 mm^2). Substituting A'_s back into the equation for A_s , we have

$$A_s = 6.12 + 0.75 \times 3.63 = 8.84 \text{ in}^2$$
 (5703 mm^2)

To check that the compression steel is yielding, substitute A'_s back into the equation for a :

$$a = 1.426(6.12 - 0.25 \times 3.63) = 7.43 \text{ in}$$

$$\therefore c = \frac{a}{\beta_1} = \frac{7.43}{0.85} = 8.74 \text{ in}$$

By similar triangles of the strain diagram, we have

$$\varepsilon'_s = 0.003 \frac{8.74 - 2.5}{8.74} = 0.00214$$

But $f_y/E_s = 40,000/(29 \times 10^6) = 0.00138$; therefore, compression steel is yielding, $f'_s = f_y$, as assumed.

(This could also have been checked using Eq. 4.41.)

Note that in this example the second design with minimum compression steel contains a little less steel (5%) than the first design, but the

first design is preferable from the point of view of deflection control and ductility.

The design equations for compression reinforcement do not take into account the small area of compressed concrete displaced by the compression steel. This means a loss of concrete force of $0.85f'_c A'_s$, and if this amount is significant, the area of compression steel should be increased by $0.85f'_c A'_s/f_y$ in compensation. For example, to be more exact, the area of compression steel in the second part of Example 4.4 should be increased from 3.63 in^2 (2342 mm^2) to

$$3.63 + \frac{0.85 \times 3000 \times 3.63}{40,000} = 3.86 \text{ in}^2 (2490 \text{ mm}^2)$$

Sometimes in design it is necessary to check the flexural strength of doubly reinforced sections. This can be performed accurately using the derived equations. Also available is an approximate method, which results in reasonable accuracy. The approximation is in the assumption made regarding the lever arm. In Fig. 4.8, the two internal compressive forces C_c and C_s are located close to each other. The total compressive force C will be located between these two forces. If the line of action of C were known, the flexural strength of the section could be derived in a single step; that is, $M_u = \varphi A_s f_y jd$, where jd is the distance between C and T . For a conservative approximation, the lever arm jd may be taken as the lesser of the two distances locating C_c and C_s from the centroid of the tension steel.

Example 4.5

The section of Fig. 4.9 is reinforced by steel with $f_y = 40,000 \text{ psi}$ (276 N/mm^2) and $E_s = 29 \times 10^6 \text{ psi}$ ($0.2 \times 10^6 \text{ N/mm}^2$). For the concrete, $f'_c = 3000 \text{ psi}$ (20.7 N/mm^2). Estimate the dependable flexural strength of the section for (1) positive bending moment, and (2) negative bending moment.

Solution

An approximate solution will be used.

1. For positive bending moment

$$A_s = 8.57 \text{ in}^2 \quad \text{and} \quad A'_s = 4.48 \text{ in}^2$$

The depth of the compressive stress block may be found from Eq. 4.38.

$$a = \frac{(8.57 - 4.48)40,000}{0.85 \times 3000 \times 11} = 5.83 \text{ in}$$

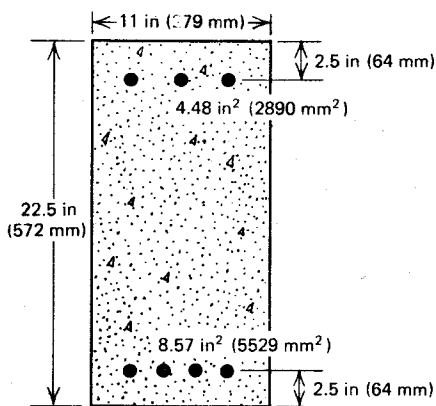


Fig. 4.9. Doubly reinforced concrete section for Example 4.5.

The yield strain of the steel is $40,000/(29 \times 10^6) = 0.00138$, and inspection of the strain diagram indicates that both the tension and compression steel are yielding, as assumed. Equation 4.49 can be used to check that the section is not overreinforced. The lever arm for the concrete compressive force is

$$d - 0.5a = 20 - 0.5 \times 5.83 = 17.08 \text{ in}$$

The lever arm for the steel compressive force is

$$d - d' = 20 - 2.5 = 17.50 \text{ in}$$

Hence the lever arm of the resultant compressive force is $17.08 < jd < 17.50$ in, and a conservative approximation is $jd = 17.08$ in, which gives

$$\begin{aligned} M_u &= \varphi A_s f_y jd \\ &= 0.9(8.57 \times 40,000 \times 17.08) \\ &= 5.27 \times 10^6 \text{ lb} \cdot \text{in} (595 \text{ kN} \cdot \text{m}) \end{aligned}$$

Exact analysis reveals that the design flexural strength is 1.0% greater than the approximate value calculated (see Example 4.4, part 1.)

2. For negative bending moment

$$A_s = 4.48 \text{ in}^2 \quad \text{and} \quad A'_s = 8.57 \text{ in}^2$$

Because the area of the compression steel is greater than the area of the tension steel, it is obvious that the compression steel cannot be yielding. Comparison of the two steel areas indicates that f'_s is

considerably less than f_y . Therefore, from an examination of the strain diagram, the depth of the rectangular stress block will not be large, and the lever arm of the concrete compressive force will be greater than the lever arm of the steel compressive force. Hence a conservative approximation is $jd = d - d' = 17.50$ in, which gives

$$M_u = 0.9(4.48 \times 40,000 \times 17.5) \\ = 2.82 \times 10^6 \text{ lb} \cdot \text{in} (318 \text{ kN} \cdot \text{m})$$

From exact analysis we learn that $f'_s = 12,770 \text{ psi}$ (88.1 N/mm^2) and the design flexural strength is 2.9 % greater than the approximate value calculated.

4.2 T AND I SECTIONS

4.2.1 Analysis of T and I Sections

Figure 4.10 shows a T-beam section when the flexural strength is reached. The depth to the neutral axis is generally small because of the large flange area. Therefore a tension failure generally occurs, and it is usually safe to assume in analysis that $f_s = f_y$; the validity of this assumption can be checked later when the neutral axis depth is found. The neutral axis may lie in either the flange or the web.

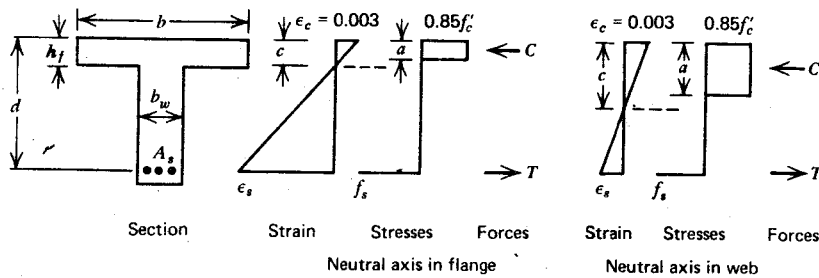


Fig. 4.10. Reinforced concrete T beam when the flexural strength is reached.

The analysis may be commenced by assuming that $c < h_f$ (i.e., that the neutral axis is in flange) where h_f = flange thickness. For equilibrium, $C = T$,

$$\therefore 0.85 f'_c ab = A_s f_y \\ \therefore a = \frac{A_s f_y}{0.85 f'_c b} = \frac{\rho f_y d}{0.85 f'_c} = \frac{\omega d}{0.85} \quad (4.50)$$

where $\rho = A_s/bd$ and $\omega = \rho f_y/f'_c$.

$$\therefore c = \frac{a}{\beta_1} = 1.18 \frac{\omega d}{\beta_1} \quad (4.51)$$

If $c < h_f$, the neutral axis lies in the flange as assumed, and

$$M_u = A_s f_y (d - 0.5a) \quad (4.52)$$

When the neutral axis lies in the flange, the section may be analyzed as for a rectangular section of width b . The balanced steel ratio ρ_b is given by Eq. 4.14, and if $\rho < \rho_b$, or $a < a_b$, the tension steel is yielding. In the large majority of practical situations, the neutral axis will lie in the flange and the tension steel will be yielding.

If $c = 1.18 \omega d / \beta_1 > h_f$, the neutral axis lies in the web. Then the calculated values for a and c from Eqs. 4.50 and 4.51 are incorrect. Rewriting the equilibrium equation $C = T$ for neutral axis in the web, we have

$$0.85f'_c [ab_w + h_f(b - b_w)] = A_s f_y \quad (4.53)$$

$$\therefore a = \frac{A_s f_y - 0.85f'_c h_f(b - b_w)}{0.85f'_c b_w}$$

where b_w is the width of the web. The resultant compressive force acts at the centroid of the T-shaped compressed area, which can be divided into the rectangle over the web and two side rectangles in the overhang of the flange. Taking moments of these rectangles about the tension steel gives

$$M_u = 0.85f'_c ab_w \left(d - \frac{a}{2} \right) + 0.85f'_c (b - b_w) h_f \left(d - \frac{h_f}{2} \right) \quad (4.54)$$

where a is given by Eq. 4.53.

The strain diagram can be checked to ensure that the tension steel is yielding. The tension steel is yielding if

$$\varepsilon_s = 0.003 \frac{d - c}{c} = 0.003 \frac{\beta_1 d - a}{a} \geq \frac{f_y}{E_s} \quad (4.55)$$

If the tension steel is not yielding, f_y in Eqs. 4.50 to 4.54 should be replaced by the following steel stress, found from the strain diagram:

$$f_s = \varepsilon_s E_s = 0.003 \frac{\beta_1 d - a}{a} E_s \quad (4.56)$$

and the calculations reworked.

Example 4.6

Calculate the ideal flexural strength of a *T*-beam section with $b = 32$ in (813 mm), $b_w = 8$ in (203 mm), $d = 12$ in (305 mm), $A_s = 3.00 \text{ in}^2$ (1935 mm 2), $E_s = 29 \times 10^6$ psi (0.20 $\times 10^6$ N/mm 2), $f_y = 60,000$ psi (414 N/mm 2), and $f'_c = 3000$ psi (20.7 N/mm 2) if (1) $h_f = 4$ in (102 mm), and (2) $h_f = 2$ in (50.8 mm).

Solution**1. Flange thickness of 4 in (102 mm)**

Assume that the tension steel yields $f_s = f_y$ and that the neutral axis lies in the flange.

From Eq. 4.50 we have

$$a = \frac{3 \times 60,000}{0.85 \times 3000 \times 32} = 2.21 \text{ in}$$

$$c = \frac{a}{\beta_1} = \frac{2.21}{0.85} = 2.60 \text{ in}$$

$\therefore c < h_f$ and neutral axis lies in the flange as assumed

From Eq. 4.52 we have

$$M_u = 3 \times 60,000 (12 - 0.5 \times 2.21) \\ = 1.96 \times 10^6 \text{ lb} \cdot \text{in} (221 \text{ kN} \cdot \text{m})$$

Check that tension steel is yielding:

From Eq. 4.55 we have

$$\varepsilon_s = 0.003 \frac{12 - 2.60}{2.60} = 0.0108$$

$$\frac{f_y}{E_s} = \frac{60,000}{29 \times 10^6} = 0.00207 < 0.0108$$

(Alternatively, $a/d = 2.21/12 = 0.18$, which is less than $a_{\max}/d = 0.377$ from Table 4.1). Therefore, tension steel yields as assumed.

2. Flange thickness of 2 in (51.8 mm)

Assume that the tension steel yields and that the neutral axis lies in the flange.

From Eq. 4.50, as before, $a = 2.21$ in and $c = 2.60$ in.

$\therefore c > h_f$ and the neutral axis lies in the web

Now $T = A_s f_y = 3 \times 60,000 = 180,000$ lb, and

$$0.85f'_c(b - b_w)h_f = 0.85 \times 3000(32 - 8)2 = 122,400 \text{ lb}$$

$$0.85f'_c ab_w = 0.85 \times 3000 \times 8a = 20,400a \text{ lb}$$

From Eq. 4.53 we write

$$a = \frac{180,000 - 122,400}{20,400} = 2.82 \text{ in}$$

and

$$c = \frac{a}{\beta_1} = \frac{2.82}{0.85} = 3.32 \text{ in}$$

From Eq. 4.54 we find

$$M_u = 20,400 \times 2.82(12 - 0.5 \times 2.82) + 122,400(12 - 0.5 \times 2) \\ = 1.95 \times 10^6 \text{ lb} \cdot \text{in} (220 \text{ kN} \cdot \text{m})$$

Check that the tension steel is yielding:

From Eq. 4.55

$$\epsilon_s = 0.003 \frac{12 - 3.32}{3.32} = 0.00784$$

$$\frac{f_y}{E_s} = \frac{60,000}{29 \times 10^6} = 0.00207 < 0.00784$$

(Alternatively, $a/d = 2.82/12 = 0.235$, which is less than $a_{\max}/d = 0.377$ from Table 4.1.) Therefore, tension steel yields as assumed.

Any compression steel that a section may contain in the flange can be taken into account by including $A'_s f'_s$ terms in the equations. The stress in this steel can be found using the strain diagram.

4.2.2 Design of T and I Sections

When the neutral axis depth is less than the flange thickness, according to Eq. 4.51 we have

$$1.18 \frac{\omega d}{\beta_1} \leq h_f \quad \text{where} \quad \omega = \frac{A_s f_y}{b d f'_c}$$

and the section may be designed as a rectangular section of width b using Eqs. 4.18 to 4.23.

When the neutral axis depth is greater than the flange thickness, $1.18\omega d/\beta_1 > h_f$. For this case the section may be designed using the equations

for a doubly reinforced beam, as follows. The tension steel may be considered to be divided into an area A_{sf} , which resists the compression in the concrete in the overhang of the flange, and an area $A_s - A_{sf}$, which resists the compression in the concrete over the web. Then, assuming that the tension steel is yielding, the equilibrium equations are

$$A_{sf} f_y = 0.85 f'_c h_f (b - b_w)$$

$$\therefore A_{sf} = \frac{0.85 f'_c h_f (b - b_w)}{f_y} \quad (4.57)$$

and

$$(A_s - A_{sf}) f_y = 0.85 f'_c a b_w$$

$$\therefore a = \frac{(A_s - A_{sf}) f_y}{0.85 f'_c b_w} \quad (4.58)$$

The design flexural strength may be written with reference to Eq. 4.54 as

$$M_u = \phi \left[(A_s - A_{sf}) f_y \left(d - \frac{a}{2} \right) + A_{sf} f_y \left(d - \frac{h_f}{2} \right) \right] \quad (4.59)$$

where A_{sf} and a are given by Eqs. 4.57 and 4.58.

Comparison of Eqs. 4.59 and 4.39 shows that the compressive force in the overhang of the concrete flange is equivalent to an area of compression steel A_{sf} at the yield strength at the middepth of the flange. This equivalence is illustrated in Fig. 4.11.

To ensure a ductile failure with the tension steel yielding, the same limiting steel ratio as for a doubly reinforced beam must be satisfied in design.^{4.2} The requirement is that the force in the tension steel be limited to 0.75 of the

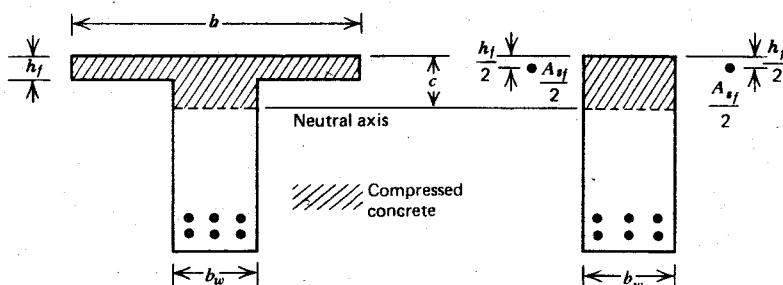


Fig. 4.11. *T* section and equivalent doubly reinforced rectangular section.

total compressive force at balanced failure. Equation 4.49 shows that this requires

$$\rho_w \leq 0.75 \left(\frac{0.85 f'_c \beta_1}{f_y} \frac{0.003 E_s}{0.003 E_s + f_y} + \rho_f \right) \quad (4.60)$$

where $\rho_w = A_s/b_w d$ and $\rho_f = A_{sf}/b_w d$.

The imaginary area of compression steel is always yielding, hence its stress need not be checked. The foregoing approach to limiting brittle failure does not result in a section with the same ductility as a real doubly reinforced section, however, because the compression flange is inevitably more brittle than compression steel.

It is also necessary to check that the steel area in the section is sufficient to ensure that the flexural strength of the cracked section exceeds the moment required to crack the section; otherwise the failure is sudden and brittle. To prevent such a failure, it is recommended^{4,2} that ρ_w should be not less than $200/f_y$, where f_y is in psi, or $1.38/f_y$, where f_y is in N/mm² units.

Example 4.7

A T-beam section with $b = 30$ in (762 mm), $b_w = 12$ in (305 mm), $d = 23$ in (584 mm), and $h_f = 4$ in (102 mm) is to have a design flexural strength of 7×10^6 lb·in (790 kN·m). Using $f'_c = 3000$ psi (20.7 N/mm²) and $f_y = 60,000$ psi (414 N/mm²), calculate the required steel area.

Solution

As an approximation, to determine whether the neutral axis lies in the flange or the web, assume $jd = d - 0.5h_f = 23 - 2 = 21$ in. Then we have approximately

$$A_s = \frac{M_u}{\varphi j d f_y} = \frac{7 \times 10^6}{0.9 \times 21 \times 60,000} = 6.17 \text{ in}^2$$

giving

$$\omega = \frac{\rho f_y}{f'_c} = \frac{6.17 \times 60,000}{30 \times 23 \times 3000} = 0.179$$

From Eq. 4.51 we have

$$c = 1.18 \frac{\omega d}{\beta_1} = 1.18 \frac{0.179 \times 23}{0.85} = 5.72 \text{ in} > h_f$$

Therefore, the neutral axis lies in the web.

Now from Eq. 4.57 we write

$$A_{sf} f_y = 0.85 f'_c h_f (b - b_w)$$

$$= 0.85 \times 3000 \times 4(30 - 12) = 183,600 \text{ lb}$$

And from Eq. 4.58 we put

$$(A_s - A_{sf}) f_y = 0.85 f'_c a b_w$$

$$= 0.85 \times 3000 \times 12a = 30,600a \text{ lb}$$

From Eq. 4.59 we have

$$7 \times 10^6 = 0.9[30,600a(23 - 0.5a) + 183,600(23 - 2)]$$

$$\therefore a^2 - 46.00a + 256.34 = 0$$

Solution of the quadratic equation gives $a = 6.49$ in.

$$\therefore (A_s - A_{sf}) f_y = 30,600 \times 6.49 = 198,600 \text{ lb}$$

Substituting $A_{sf} f_y$ from Eq. 4.57 gives

$$A_s = \frac{198,600 + 183,600}{60,000}$$

$$= 6.37 \text{ in}^2 (4110 \text{ mm}^2)$$

Check whether steel area is satisfactory:

$$\rho_w = \frac{6.37}{12 \times 23} = 0.0231$$

Check maximum allowable steel content, using Eq. 4.60:

$$0.75 \left(\frac{0.85 \times 3000 \times 0.85}{60,000} \frac{0.003 \times 29 \times 10^6}{0.003 \times 29 \times 10^6 + 60,000} \right. \\ \left. + \frac{183,600}{60,000 \times 12 \times 23} \right)$$

$$= 0.0244 > 0.0231$$

Therefore steel area does not exceed maximum allowable.
Check minimum allowable steel, using

$$\frac{200}{f_y} = \frac{200}{60,000}$$

$$= 0.0033 < 0.0231$$

Therefore, steel area is not less than minimum allowable.

4.2.3 Effective Width of T Beams

When reinforced concrete slab and beam floors are built monolithically, the beam and the slab will act integrally.

When the beam is subjected to positive bending moment, part of the slab will act as the flange of the beam resisting the longitudinal compression balancing the tensile force in the reinforcement in the web. When the spacing between the beams is large, it is evident that simple bending theory does not strictly apply because the longitudinal compressive stress in the flange will vary with distance from the beam web, the flange being more highly stressed over the web than in the extremities. This variation in flange compressive stress, illustrated in Fig. 4.12, occurs because of shear deformations in the

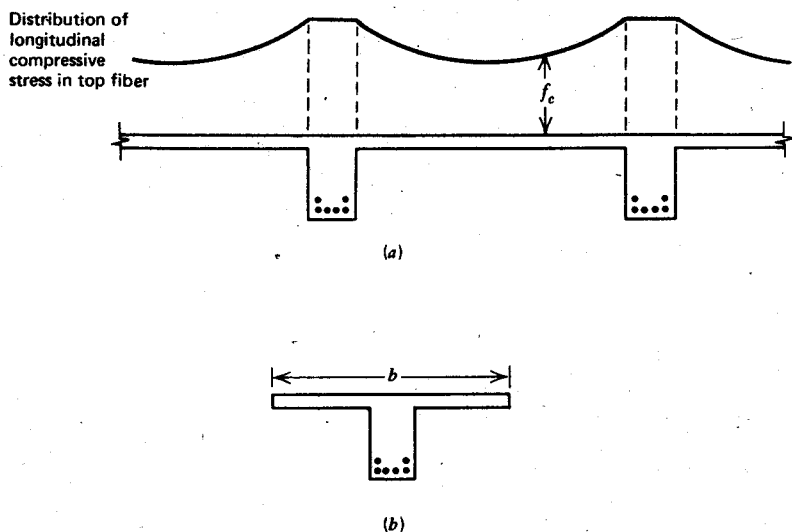


Fig. 4.12. Effective width of T beam for positive bending moment. (a) Section of slab and beam floor. (b) Effective width for positive bending moment.

flange (shear lag), which reduce the longitudinal compressive strain with distance from the web.

The actual distribution of compressive stress for the beam in the elastic range may be calculated using the theory of elasticity, and it depends on the relative dimensions of the cross section and the span, and on the type of loading. At the flexural strength of the member, the distribution of longitudinal compressive stress across the flange will be more uniform than indicated by the theory of elasticity because at near-maximum stress the

concrete stress-strain curve shows a smaller variation of stress with strain. In addition, however, the slab will usually be bending transversely because of the load supported between the beams, and this can cause cracking in the top of the flange parallel to the beam over the web-flange junction. Transverse reinforcement in the slab and shear-friction along the crack will allow longitudinal compression to be transferred out into the flange, but nevertheless there are grounds for using a conservatively low effective width.

In design, to take the variation of compressive stress across the flange into account, it is convenient to use an effective width of flange that may be smaller than the actual width but is considered to be uniformly stressed. The present code-specified effective widths are conservative estimates based on approximations to elastic theory. For symmetrical *T* beams, ACI 318-71^{4,2} recommends that the effective width used should not exceed one-quarter of the span length of the beam, and its overhanging width on each side of the web should not exceed 8 times the slab thickness, or one-half of the clear distance to the next beam. For beams having a flange on one side only, the effective overhanging flange width should not exceed $\frac{1}{12}$ of the span length of the beam, or 6 times the slab thickness, or half the clear distance to the next beam.

When the beam is subjected to negative bending moment, some of the longitudinal reinforcement in the flange clearly acts as tension steel with the main steel over the web (see Fig. 4.13). The tensile force is transferred

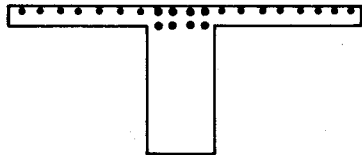


Fig. 4.13. Effective width of *T* beam for negative bending moment.

across the flange into the web by shear in flange, much as the compressive force in the case of positive bending is transferred. Codes do not specify effective widths over which slab steel may be considered to be acting as tension reinforcement, but it is evident that a realistic appraisal of the beam strength for negative bending moment would include the effect of the slab steel. As an approximation, the slab steel within a width of four times the slab thickness each side of the web could be included with the tension steel of the beam.

4.3 SECTIONS HAVING BARS AT VARIOUS LEVELS OR STEEL LACKING A WELL-DEFINED YIELD STRENGTH

When reinforcement bars are placed in the tension and/or compression regions in a beam, it is usual to consider only the stress at the centroids of the tension and the compression steel, even though the bars may be in several layers. However, it may be desired to perform more exact analysis when large differences may exist between the levels of stress in the various layers. Also, when the reinforcement does not have a well-defined yield strength, it may be desired to make an accurate assessment of the flexural strength of the section, including the effect of strain hardening of the steel.

For the general analysis of such sections, an iterative procedure involving the satisfaction of the requirements of equilibrium and compatibility of strains may be used. Consider the section shown in Fig. 4.14 when the flexural strength is reached. Let the stress-strain curve for the steel have a

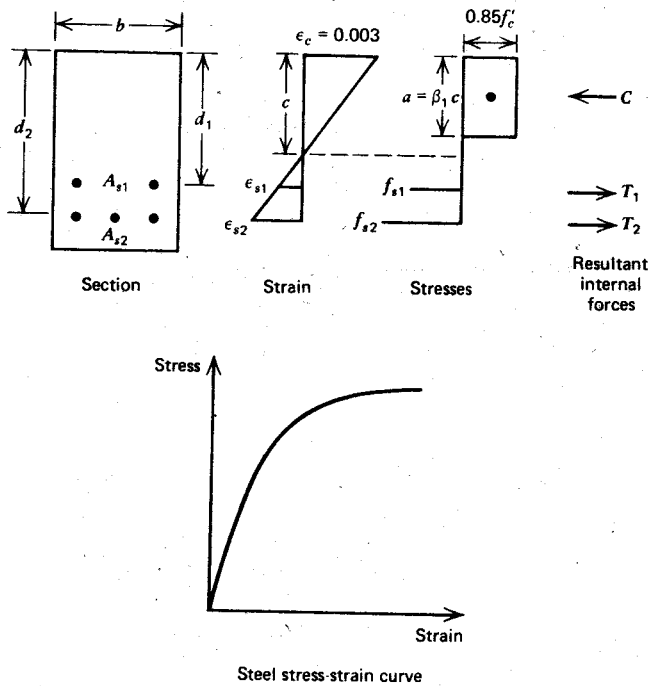


Fig. 4.14. Reinforced concrete section when the flexural strength is reached and general stress-strain curve for steel.

general shape. For the purpose of illustration, the tension steel in the section is considered to be in two layers. For strain compatibility, the strain diagram gives

$$\frac{0.003}{c} = \frac{\varepsilon_{s1}}{d_1 - c} = \frac{\varepsilon_{s2}}{d_2 - c}$$

$$\therefore \varepsilon_{s1} = 0.003 \frac{d_1 - c}{c} \quad (4.61a)$$

and

$$\varepsilon_{s2} = 0.003 \frac{d_2 - c}{c} \quad (4.61b)$$

For equilibrium, we have

$$C = T_1 + T_2$$

$$\therefore 0.85f'_c ab = A_{s1}f_{s1} + A_{s2}f_{s2} \quad (4.62)$$

The section may be analyzed by a trial and adjustment procedure as follows:

1. Choose a value for c .
2. Calculate ε_{s1} and ε_{s2} from Eqs. 4.61a and 4.61b and determine f_{s1} and f_{s2} from the stress-strain curve for the steel.
3. Check whether Eq. 4.62 is satisfied.
4. Repeat steps 1, 2, and 3 until a value for c is found that satisfies Eq. 4.62.

Then by taking moments about the centroid of compression, the flexural strength is given by

$$M_u = A_{s1}f_{s1}(d_1 - 0.5a) + A_{s2}f_{s2}(d_2 - 0.5a) \quad (4.63)$$

Example 4.8

A rectangular section of width 8 in (203 mm) is reinforced by two No. 6 (19 mm diameter) bars at an effective depth of 8 in (203 mm) and three No. 6 bars at an effective depth of 10 in (254 mm) (see Fig. 4.15a). The bars are of cold-worked steel, and the stress-strain curve appears in Fig. 4.15b. For the concrete $f'_c = 4000$ psi (27.6 N/mm²). Calculate the ideal flexural strength of the section.

Solution

$$A_{s1} = 2 \times 0.44 = 0.88 \text{ in}^2 \quad \text{and} \quad A_{s2} = 3 \times 0.44 = 1.32 \text{ in}^2$$

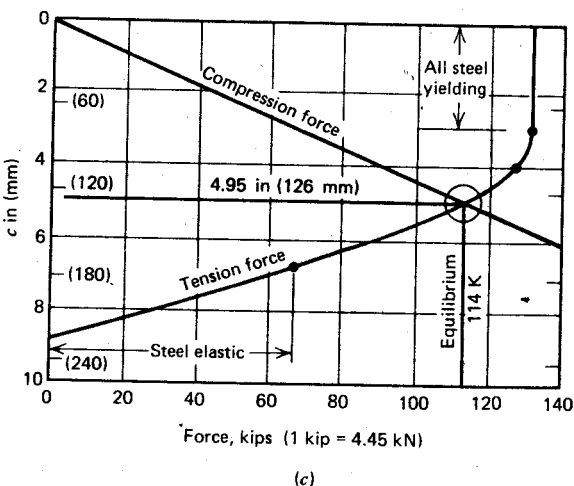
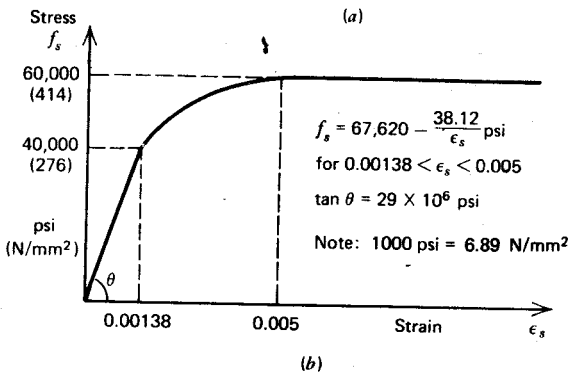
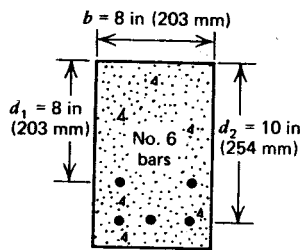


Fig. 4.15. Example 4.8. (a) Section. (b) Stress-strain curve for the steel. (c) Variation of internal forces with neutral axis depth.

First estimate

Let $c = 4$ in $\therefore a = \beta_1 c = 0.85 \times 4 = 3.40$ in

From Eqs. 4.61a and 4.61b we have

$$\epsilon_{s1} = 0.003 \frac{8 - 4}{4} = 0.003$$

$$\epsilon_{s2} = 0.003 \frac{10 - 4}{4} = 0.0045$$

Reference to the stress-strain curve shows that

$$f_{s1} = 67,620 - \frac{38.12}{0.003} = 54,910 \text{ psi}$$

$$f_{s2} = 67,620 - \frac{38.12}{0.0045} = 59,150 \text{ psi}$$

Check equilibrium using Eq. 4.62:

$$T_1 = 54,910 \times 0.88 = 48,300 \text{ lb}$$

$$T_2 = 59,150 \times 1.32 = 78,100 \text{ lb}$$

$$C = 0.85 \times 4000 \times 3.40 \times 8 = 92,500 \text{ lb}$$

and

$$C - T_1 - T_2 = -33,900 \text{ lb}$$

Therefore, equilibrium is not satisfied because the compressive force is too small and the steel forces are too large.

Therefore, shift the neutral axis down to increase the compressive force and reduce the steel forces.

Second estimate

Let $c = 5$ in $\therefore a = 4.25$ in

Then using the equations as before, write

$$\epsilon_{s1} = 0.0018 \quad \epsilon_{s2} = 0.003$$

$$f_{s1} = 46,440 \text{ psi} \quad f_{s2} = 54,910 \text{ psi}$$

$$T_1 = 40,900 \text{ lb} \quad T_2 = 72,500 \text{ lb}$$

$$C = 115,600 \text{ lb}$$

and

$$C - T_1 - T_2 = 2,200 \text{ lb}$$

Therefore, the neutral axis depth is slightly too large.
Therefore reduce c slightly.

Third estimate

The first and second estimates show that $4 \text{ in} < c < 5 \text{ in}$. Linearly interpolate, using the previous residual forces from the equilibrium equations

$$c = 4 + \frac{33,900}{33,900 + 2,200} = 4.94 \text{ in} \quad \therefore a = 4.20 \text{ in}$$

Then using the equations as before, write

$$\epsilon_{s1} = 0.00186 \quad \epsilon_{s2} = 0.00307$$

$$f_{s1} = 47,130 \text{ psi} \quad f_{s2} = 55,200 \text{ psi}$$

$$T_1 = 41,500 \text{ lb} \quad T_2 = 72,900 \text{ lb}$$

$$C = 114,220 \text{ lb}$$

and

$$C - T_1 - T_2 = -200 \text{ lb}$$

The equilibrium balance is satisfactory.

From Eq. 4.63 we have

$$M_u = 41,500(8 - 0.5 \times 4.20) + 72,900(10 - 0.5 \times 4.20) \\ = 820,800 \text{ lb} \cdot \text{in} (92.7 \text{ kN} \cdot \text{m})$$

A graphical construction can also be used for the determination of the neutral axis depth that gives equilibrium balance (see Fig. 4.15c for the section of Example 4.8). In a rectangular section the compression force increases linearly with the increase of the neutral axis depth. Hence the position of the straight line giving the value for the compressive force can be calculated readily. The tension force line is not linear over its whole length. A straight line applies when the tension steel is in the elastic range, and a constant force is obtained when both layers of steel reach the yield stress. The tension force line can be established by calculating the force corresponding to a number of neutral axis depths. The point of intersection of the two force lines gives the neutral axis depth for equilibrium balance. In fact, only the parts of the lines near the likely points of intersection need be plotted.

The foregoing trial and adjustment procedure, either analytical or graphical, can be used to analyze any section. Equations 4.61 and 4.62 can be generalized easily to include more groups of steel: $A_{s1}, A_{s2}, A_{s3}, A_{s4}, \dots$. Because of the number of possible cases of steel stress, it would not

be practical in problems of this type to write equations that would enable the neutral axis depth to be found directly by solving the equilibrium equation with c as an unknown.

If the neutral axis depth at the flexural strength is very small, the steel strains may be extremely large, and the designer should verify that these do not exceed the strain at which the steel is likely to fracture.

4.4 BIAXIAL BENDING OF SECTIONS

Reinforced concrete beams are sometimes subjected to loading that causes biaxial (unsymmetrical) bending. For example, an isolated beam carrying a wall exposed to wind pressure may receive both horizontal and vertical loading. A section with biaxial bending is shown in Fig. 4.16.

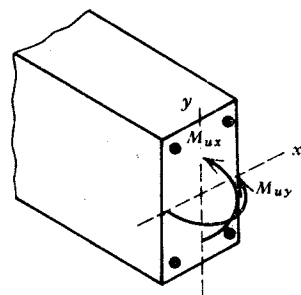


Fig. 4.16. Reinforced concrete beam section with biaxial bending moments.

The section when the flexural strength is reached appears in Fig. 4.17. The section will be assumed to be reinforced by the four bars numbered 1, 2, 3, and 4, as in Fig. 4.17. Sections having more bars could be analyzed using the equations to follow, by dividing the bars into four groups, of which points 1, 2, 3, and 4 are the centroids. Computer programs are available, or can be developed, using an extension to the equations of the following sections, to analyze sections with distributed steel along the four faces or to consider individual bars in any position.

In a section with biaxial bending, the neutral axis is inclined to the horizontal, the amount of inclination depending on the ratio of the bending moments in the two directions and the section properties. The equivalent stress block is assumed to have a depth of β_1 times the neutral axis depth, and a mean stress of $0.85f'_c$. This equivalent stress block is not quite equivalent to the actual stress block (see Section 3.4), but it is sufficiently accurate for design purposes.

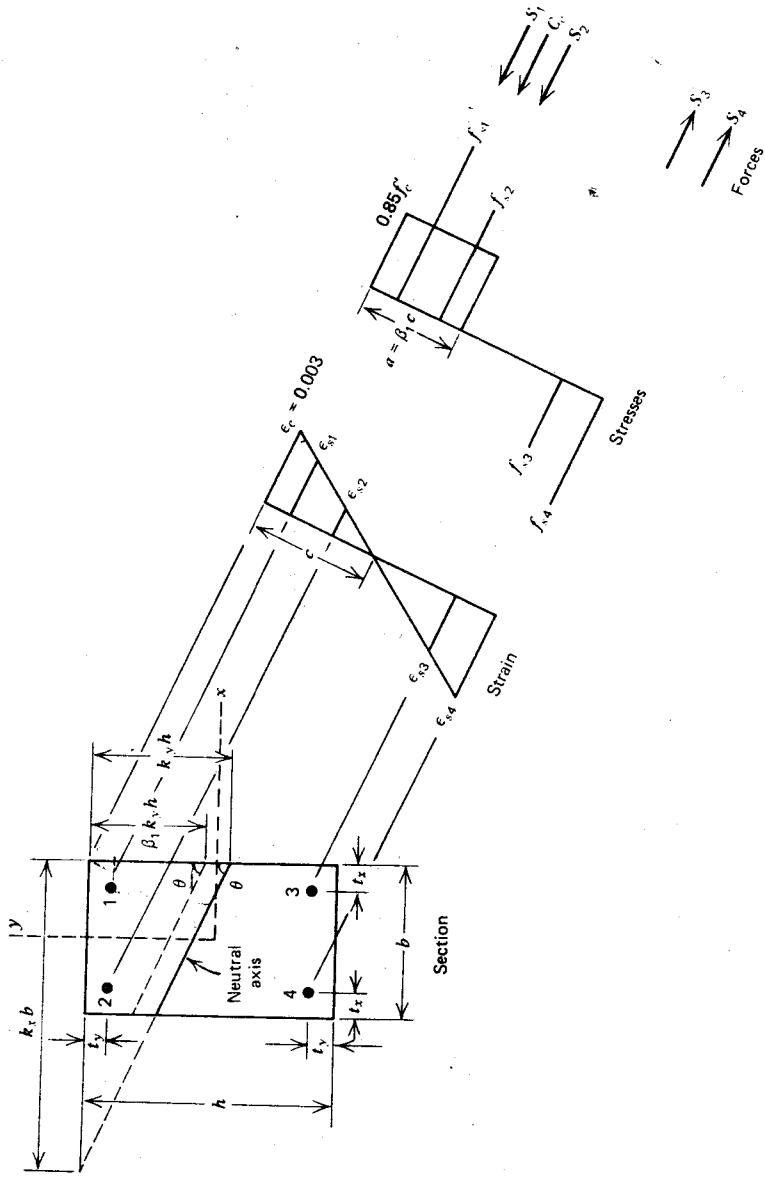


Fig. 4.17. Reinforced concrete section with biaxial bending moments when the flexural strength is reached.

For a given section the flexural strength may be found as follows:

1. The strains in the steel may be found by considering the similar triangles of the strain diagram of Fig. 4.17:

$$\frac{\varepsilon_{s1}}{k_y h - t_y - t_x \cot \theta} = \frac{0.003}{k_y h}$$

$$\frac{t_x \cot \theta}{k_y h} = \frac{t_y}{k_y h} \cdot K_x$$

$$\therefore \varepsilon_{s1} = 0.003 \left(1 - \frac{t_x}{k_x b} - \frac{t_y}{k_y h} \right) \quad (4.64)$$

Similarly, we have

$$\varepsilon_{s2} = 0.003 \left(1 - \frac{b - t_x}{k_x b} - \frac{t_y}{k_y h} \right) \quad (4.65)$$

$$\varepsilon_{s3} = 0.003 \left(1 - \frac{t_x}{k_x b} - \frac{h - t_y}{k_y h} \right) \quad (4.66)$$

$$\varepsilon_{s4} = 0.003 \left(1 - \frac{b - t_x}{k_x b} - \frac{h - t_y}{k_y h} \right) \quad (4.67)$$

where positive strain indicates compression.

2. The steel stresses and forces then follow from the stress-strain curve for the steel. For the usual case of a well-defined yield point, for bar 1 if

$$\varepsilon_{s1} \geq \frac{f_y}{E_s}, \quad f_{s1} = f_y$$

or if

$$\frac{f_y}{E_s} > \varepsilon_{s1} > -\frac{f_y}{E_s}, \quad f_{s1} = \varepsilon_{s1} E_s \quad (4.68)$$

or if

$$\varepsilon_{s1} \leq -\frac{f_y}{E_s}, \quad f_{s1} = -f_y$$

The stresses in bars 2, 3, and 4 are found similarly.

Then the steel forces are given by

$$S_1 = A_{s1} f_{s1} \quad (4.69)$$

$$S_2 = A_{s2} f_{s2} \quad (4.70)$$

$$S_3 = A_{s3} f_{s3} \quad (4.71)$$

$$S_4 = A_{s4} f_{s4} \quad (4.72)$$

3. The resultant compressive force in the concrete and its position will depend on the shape and area of the equivalent compressive stress block. The four possible shapes are presented in Fig. 4.18.

For case 1 we have

$$C_c = \frac{0.85 f'_c \beta_1 k_y h \beta_1 k_x b}{2} = 0.425 f'_c \beta_1^2 k_x k_y b h \quad (4.73)$$

$$\bar{x} = 0.333 \beta_1 k_x b \quad (4.74)$$

$$\bar{y} = 0.333 \beta_1 k_y h \quad (4.75)$$

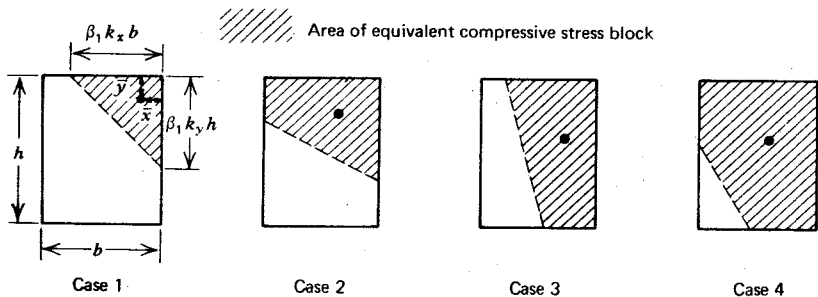


Fig. 4.18. Possible shapes of the area of the equivalent compressive stress block.

Similarly, expressions may be found for C_c , \bar{x} and \bar{y} for cases 2, 3, and 4, and are given by Mattock, Kriz, and Hognestad.^{4,7}

4. For equilibrium, the position of the neutral axis must be such that the sum of the longitudinal forces is zero.

$$C_c + S_1 + S_2 + S_3 + S_4 = 0 \quad (4.76)$$

5. The moments acting about the axes at the flexural strength may be found by taking the moments of the internal forces about an x -direction axis (say the bottom edge of the section) and a y -direction axis (say the left-hand edge of the section). Then we have

$$M_{ux} = C_c(h - \bar{y}) + (S_1 + S_2)(h - t_y) + (S_3 + S_4)t_y \quad (4.77)$$

$$M_{uy} = C_c(b - \bar{x}) + (S_1 + S_3)(b - t_x) + (S_2 + S_4)t_x \quad (4.78)$$

The appropriate signs (positive for compression, negative for tension) should be substituted into Eqs. 4.76 to 4.78 when these expressions are used.

Both the analysis and the design of sections with biaxial bending moments are difficult because trial and adjustment procedures are necessary to find the inclination and depth of the neutral axis.

Example 4.9

A concrete beam has a 10 in (254 mm) square section and is reinforced by four No. 9 (28.7 mm diameter) steel bars, one bar being placed in each corner of the section. The distance from the centroid of each bar to the adjacent sides of the section is 2 in (50.8 mm). The steel has a well-defined yield strength of 40,000 psi (276 N/mm²) and a modulus of elasticity of 29×10^6 psi (0.2 $\times 10^6$ N/mm²). The concrete has a cylinder strength of 4000 psi (27.6 N/mm²). Calculate the flexural strength of the section if it is subjected to biaxial bending moments of equal magnitude about axes parallel to the edges.

Solution

Since the section is square and the biaxial bending moments are equal, the compressed area of concrete has the shape of an isosceles triangle ($k_x = k_y = k$); hence the inclination of the neutral axis is known. Figure 4.19 shows the section. A trial and adjustment procedure will be used to find the neutral axis depth.

$$A_{s1} = A_{s2} = A_{s3} = A_{s4} = 1.00 \text{ in}^2$$

First estimate

For the neutral axis position in Fig. 4.19, let $k = 0.70$. From Eqs. 4.64 to 4.67, write

$$\varepsilon_{s1} = 0.003 \left(1 - \frac{2}{0.7 \times 10} - \frac{2}{0.7 \times 10} \right) = 0.001286$$

$$\varepsilon_{s2} = \varepsilon_{s3} = 0.003 \left(1 - \frac{10 - 2}{0.7 \times 10} - \frac{2}{0.7 \times 10} \right) = -0.001286$$

$$\varepsilon_{s4} = 0.003 \left(1 - \frac{8}{0.7 \times 10} - \frac{8}{0.7 \times 10} \right) = -0.00386$$

Also $f_y/E_s = 40,000/(29 \times 10^6) = 0.00138$. Therefore, Eq. 4.68 gives

$$f_{s1} = 0.001286 \times 29 \times 10^6 = 37,290 \text{ psi}$$

$$f_{s2} = f_{s3} = -0.001286 \times 29 \times 10^6 = -37,290 \text{ psi}$$

$$f_{s4} = -40,000 \text{ psi}$$

From Eqs. 4.69 to 4.72 we find

$$S_1 = 37,290 \text{ lb} \quad S_2 = S_3 = -37,290 \text{ lb} \quad S_4 = -40,000 \text{ lb}$$

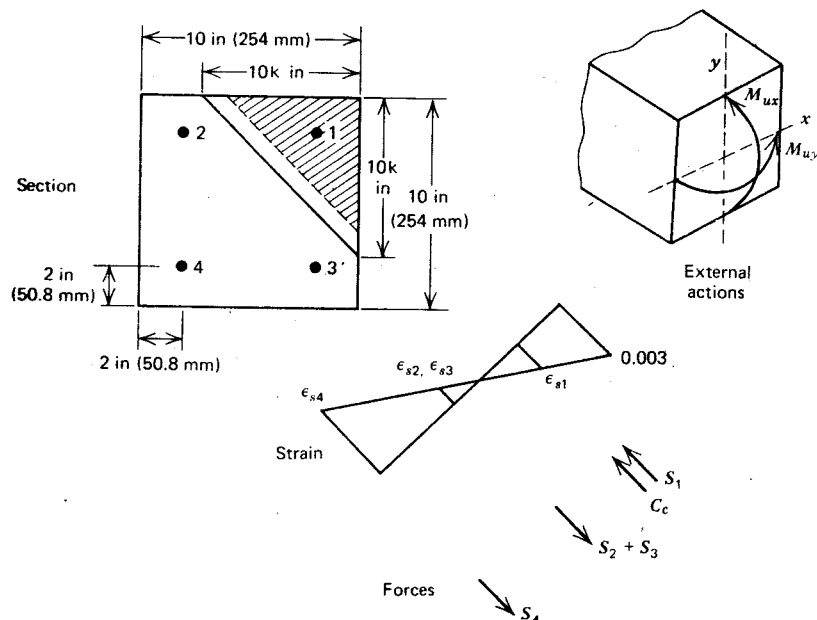


Fig. 4.19. Section and internal and external actions for Example 4.9.

And Eq. 4.73 gives

$$C_c = 0.425 \times 4000 \times 0.85^2 \times 0.7^2 \times 10^2 = 60,180 \text{ lb}$$

$$\therefore C_c + S_1 + S_2 + S_3 + S_4 = -17,110 \text{ lb}$$

Therefore, too much tension. Hence increase k .

Second estimate

Let $k = 0.8$. Then using the equations as before, write

$$\epsilon_{s1} = 0.0015 \quad \epsilon_{s2} = \epsilon_{s3} = -0.00075 \quad \epsilon_{s4} = -0.003$$

$$\therefore f_{s1} = 40,000 \text{ psi} \quad f_{s2} = f_{s3} = -21,750 \text{ psi}$$

$$f_{s4} = -40,000 \text{ psi}$$

$$\therefore S_1 = 40,000 \text{ lb} \quad S_2 = S_3 = -21,750 \text{ lb} \quad S_4 = -40,000 \text{ lb}$$

$$C_c = 78,610 \text{ lb}$$

$$\therefore C_c + S_1 + S_2 + S_3 + S_4 = 35,110 \text{ lb}$$

Therefore, too much compression. Hence reduce k .

Third estimate

Linearly interpolate, using the previous residual forces from the equilibrium equation

$$k = 0.7 + \frac{17,110}{52,220} \times 0.1 = 0.73$$

Using the equilibrium equations as before, put

$$\varepsilon_{s1} = 0.001356 \quad \varepsilon_{s2} = \varepsilon_{s3} = -0.001110 \quad \varepsilon_{s4} = -0.003575$$

$$\therefore f_{s1} = 39,320 \text{ psi} \quad f_{s2} = f_{s3} = -32,190 \text{ psi}$$

$$f_{s4} = -40,000 \text{ psi}$$

$$\therefore S_1 = 39,320 \text{ lb} \quad S_2 = S_3 = -32,190 \text{ lb} \quad S_4 = -40,000 \text{ lb}$$

$$C_c = 65,450 \text{ lb}$$

$$\therefore C_c + S_1 + S_2 + S_3 + S_4 = 390 \text{ lb}$$

Therefore, the equilibrium balance is satisfactory.

From Eqs. 4.74 and 4.75, we have

$$\bar{x} = \bar{y} = 0.333 \times 0.85 \times 0.73 \times 10 = 2.07 \text{ in}$$

From Eqs. 4.77 and 4.78 we have

$$M_{ux} = M_{uy} = 65,450(10 - 2.07) + (39,320 - 32,190)(10 - 2) \\ + (-32,190 - 40,000)2 \\ = 431,700 \text{ lb} \cdot \text{in} \quad (48.7 \text{ kN} \cdot \text{m})$$

or, the resultant bending moment acting about the diagonal is

$$\sqrt{M_{ux}^2 + M_{uy}^2} = \sqrt{2} \times 431,700 = 610,500 \text{ lb} \cdot \text{in} \quad (68.9 \text{ kN} \cdot \text{m})$$

It is of interest to note that the flexural strength of the section for bending about only the x- or y-direction axis may be calculated to be 547,600 lb · in (61.8 kN · m).

It is evident that the manual solution of the general biaxial bending moment equations requires laborious calculations because of the trial and adjustment procedure necessary to find the depth and inclination of the neutral axis for given values of M_{ux} and M_{uy} . However, the equations can be programmed for a digital computer. A set of interaction curves, showing combinations of moments M_{ux} and M_{uy} that would cause the flexural strength to be reached for various steel contents of sections having equal steel in each corner of the section, would have the form displayed in Fig. 4.20. Design charts plotted in this form would enable the steel area to be found for particular combinations

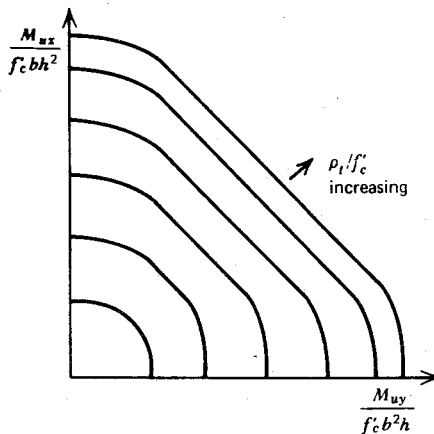


Fig. 4.20. Form of the interaction curves for a reinforced concrete section with biaxial bending moments at the flexural strength.

of $M_{ux}/(f'_c b h^2)$ and $M_{uy}/(f'_c b^2 h)$. The change of shape of the curves in Fig. 4.20 with increasing ρ_t/f'_c is of interest, where ρ_t is the total steel area divided by the concrete area. As an approximate guide, if M_{ux} and M_{uy} for a given section are known, a straight line interaction curve will always be conservative; but a circular curve (elliptical if the uniaxial flexural strengths in the two directions are different) may be unsafe, particularly at high ρ_t/f'_c values.

4.5 LATERAL INSTABILITY OF BEAMS

When slender beams are used, instability before the development of flexural strength may be the cause of failure. The instability failure takes the form of lateral buckling accompanied by twist, as illustrated in Fig. 4.21. Such instability can be important in the case of beams lacking lateral support if the

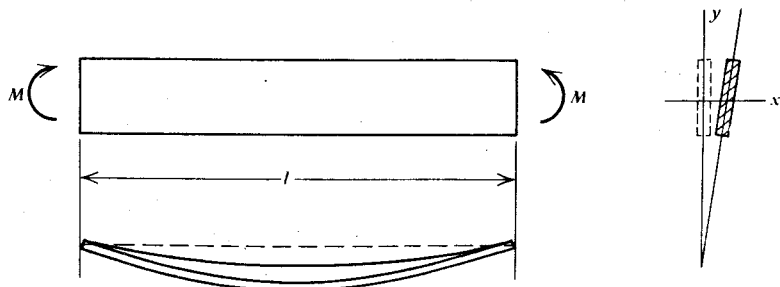


Fig. 4.21. Beam with lateral instability failure.

flexural stiffness in the plane of bending is very large compared with its lateral stiffness. The problem is rather rare because most designers intuitively choose compact sections. Critical situations may arise during erection of precast concrete structures before adequate lateral restraint to components is provided.

The analytical treatment of the problem becomes complex if an attempt is made to assess all features of reinforced concrete behavior realistically. Because there is insufficient experimental evidence against which a theoretically derived critical load could be tested convincingly, no attempt is made here to quantify the relevant parameters. This could only be done with the use of contestable assumptions.

Michell's classical solution^{4,8} for the critical moment M_{cr} producing instability in a linearly elastic, homogeneous, and isotropic prismatic beam is

$$M_{cr} = \frac{\lambda}{l} \sqrt{\frac{E_c I_x E_c I_y GJ}{E_c I_x - E_c I_y}} \left(1 - 1.74 \frac{y_w}{l} \sqrt{\frac{E_c I_y}{GJ}} \right) \quad (4.79)$$

where λ = a coefficient depending on the load pattern and having the following values:

- (a) π for uniform moment along the beam
- (b) 3.53 for uniformly distributed load
- (e) 4.24 for a central point load

E_c = modulus of elasticity of concrete

G = modulus of rigidity of concrete

I_x, I_y = moments of inertia of the concrete cross section about the major and minor axes, respectively

J = equivalent polar moment of inertia of the concrete cross section

l = unsupported length of the beam

y_w = distance of the point of application of the load above the centroid of the section

Marshall^{4,9} has investigated the applicability of each of these parameters with respect to reinforced concrete and has attempted to establish limits within which the true critical moment is likely to occur. The variations for individual quantities are very large, and in the light of this property some simplifications of Eq. 4.79 should not be objectionable. Cross sections that are sensitive to lateral buckling have a depth to width ratio of at least 2. Hence if the effect of cracking is also taken into account, the ratio I_y/I_x becomes small and may be taken to be zero. With this simplification, Eq. 4.79 becomes

$$M_{cr} = \frac{\lambda}{l} \sqrt{E_c I_y GJ} \left(1 - 1.74 \frac{y_w}{l} \sqrt{\frac{E_c I_y}{GJ}} \right) \quad (4.80)$$

In the evaluation of the critical moment, the designer must bear in mind that concrete is nonlinear in compression; hence at high stresses a reduced modulus of elasticity needs to be considered. In the assessment of the moment of inertia, the effect of flexural cracking has to be accounted for. This cracking will vary along the beam in accordance with the moment pattern. The calculation for I_y could be based on the part of the concrete cross section in the compression zone only. The value of the modulus of rigidity, G , is related to E_c , but the relative contributions of the concrete and the web reinforcement to the torsional stiffness are uncertain. Other uncertainties are: the amount of concrete cross section that should be included in the estimation of the equivalent polar moment of inertia J , and the extent to which biaxial flexure affects twisting. It is evident that there are difficulties in accurately calculating the stiffness terms.

By substituting $0.5h$ for y_w , expressing the modulus of elasticity in the nonlinear range as a fraction the compressive cylinder strength f'_c , and expressing I_x , I_y and J in terms of the section dimensions, the equation for the critical moment for a prismatic rectangular beam reduces approximately to

$$M_{cr} = k \frac{\lambda}{l} b^3 d f'_c \quad (4.81)$$

where k is a numerical constant, b is the width of the section, and d is the effective depth of the tension steel.

For an instability failure to occur, the flexural capacity of the beam M_u will be larger than the critical moment. The flexural capacity, however, depends on the steel content, and for a singly reinforced section this value lies within the approximate limits of

$$0.05 < \frac{M_u}{bd^2 f'_c} < 0.29 \quad (4.82)$$

when $\rho_{min} < \rho < \rho_{max} = 0.75\rho_b$, $40,000 \text{ psi} < f_y < 60,000 \text{ psi}$, and $f'_c \leq 4000 \text{ psi}$ ($1 \text{ psi} = 0.00689 \text{ N/mm}^2$).

An underreinforced beam is not likely to be critical with respect to buckling. Therefore, considering beams with maximum usable steel content, the critical condition is approximately

$$0.29bd^2 f'_c > k \frac{\lambda}{l} b^3 d f'_c \quad \text{or} \quad \frac{ld}{b^2} > k_1 \quad (4.83)$$

where $k_1 = k\lambda/0.29$.

By making limiting assumptions^{4,9} for the variables of Eq. 4.80, the value of k_1 is within the wide limits of 100 and 580 for beams having a uniformly distributed load. Given these limits, further refinement of the analysis, taking into account the contribution of the flexural steel,^{4,10} is not warranted.

By examining available data, Marshall^{4,9} found that the larger value for ld/b^2 was more nearly correct. It should be noted that the traditionally used span/width ratio alone, l/b , does not adequately describe instability criteria in beams.

When the effects of creep and possible initial out-of-straightness are considered, and noting that failures by instability show limited ductility, we realize that the capacity reduction factor φ used in design with M_{cr} must be small. This is borne out by the large scatter in the available experimental results.^{4,9} Alternatively, the limiting geometric parameters specified should be deliberately conservative. To prevent lateral instability, the British code CP 110^{4,11} has adopted the following limits:

1. For simply supported or continuous beams, the clear distance between lateral restraints l should be such that

$$\frac{l}{b} < 60 \quad \text{and} \quad \frac{ld}{b^2} < 250 \quad (4.84a)$$

2. For cantilevers having lateral restraints only at the supports, the values should be

$$\frac{l}{b} < 25 \quad \text{and} \quad \frac{ld}{b^2} < 100 \quad (4.84b)$$

If these limits are exceeded, the critical moment M_{cr} will govern the strength of the beam. Using Marshall's estimation,^{4,9} the approximate value of this is

$$M_{cr} = \frac{160\varphi f'_c b^3 d}{l} \quad (4.85)$$

It is suggested that $\varphi = 0.5$ be taken as the capacity reduction factor.

4.6 REFERENCES

- 4.1 C. S. Whitney, "Design of Reinforced Concrete Members Under Flexure or Combined Flexure and Direct Compression," *Journal ACI*, Vol. 33, March–April, 1937, pp. 483–498.
- 4.2 ACI Committee 318, "Building Code Requirements for Reinforced Concrete (ACI 318-71)," American Concrete Institute, Detroit, 1971, 78 pp.
- 4.3 N. J. Everard and J. L. Tanner, *Theory and Problems of Reinforced Concrete Design*, Schaum Publishing Co., New York, 1966, 325 pp.
- 4.4 C. S. Whitney and E. Cohen, "Guide for Ultimate Strength Design of Reinforced Concrete," *Journal ACI*, Vol. 53, No. 5, November 1956, pp. 455–490.
- 4.5 ACI Committee 340, *Design Handbook in Accordance with Strength Design Method of ACI 318-71*, Vol. 1, ACI Special Publication SP-17 (73), American Concrete Institute, Detroit, 1973, 432 pp.

- 4.6 ACI Committee 318, "Commentary on Building Code Requirements for Reinforced Concrete (ACI 318-71)," American Concrete Institute, Detroit, 1971, 96 pp.
- 4.7 A. H. Mattock, L. B. Kriz, and E. Hognestad, "Rectangular Stress Distribution in Ultimate Strength Design," *Journal ACI*, Vol. 57, No. 8, February 1961, pp. 875-928.
- 4.8 A. G. M. Michell, "The Elastic Stability of Long Beams Under Transverse Forces," *Phil. Mag.*, Vol. 48, No. 292, 1899.
- 4.9 W. T. Marshall, "A Survey of the Problem of Lateral Instability in Reinforced Concrete Beams," *Proceedings, Institution of Civil Engineers*, Vol. 43, July 1969, pp. 397-406.
- 4.10 J. K. Sant and R. W. Bletzacker, "Experimental Study of Lateral Stability of Reinforced Concrete Beams," *Journal ACI*, Vol. 58, No. 6, December 1961, pp. 713-736.
- 4.11 BSI, "Code of Practice for the Structural Use of Concrete, CP110: Part 1: 1972," British Standard Institution, London, 1972, 154 pp.

5

Strength of Members with Flexure and Axial Load

5.1 INTRODUCTION

Columns are structural elements used primarily to support compressive loads. A short column is one in which the ultimate load at a given eccentricity is governed only by the strength of the materials and the dimensions of the cross section. A slender column is one in which the ultimate load is also influenced by slenderness, which produces additional bending because of transverse deformations.

Concrete columns are reinforced by longitudinal and transverse steel. The transverse steel is generally in the form of ties or closely spaced spirals. (see Fig. 5.1).

5.2 AXIALLY LOADED SHORT COLUMNS

Creep and shrinkage of concrete have a strong influence on the stresses in the steel and the concrete of an axially loaded reinforced concrete column at the service load, tending to increase the longitudinal steel stress and to reduce the concrete stress. For a column having a large percentage of steel and a heavy initial load, which is later largely removed, it is even possible to have tension in the concrete and compression in the steel. Therefore it is extremely difficult to assess the safety of reinforced concrete columns using elastic theory and allowable stresses.

On the other hand, the ultimate load of a column does not vary appreciably with the history of loading. When the load is increased, the steel will normally reach the yield strength before the concrete reaches its full strength. However, at this stage the column has not reached its ultimate load. The column can carry further load because the steel sustains the yield stress while the deformations and load increase until the concrete reaches its full

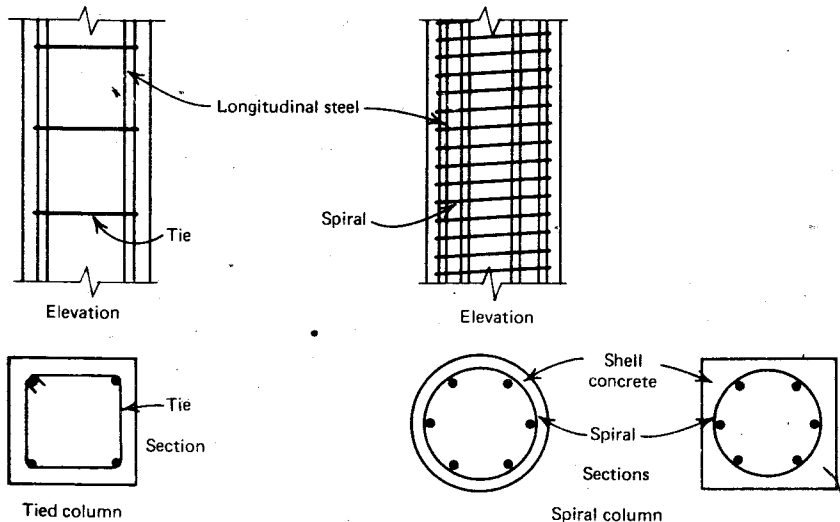


Fig. 5.1. Tied and spiral columns.

strength. Figure 5.2 illustrates this behavior. Alternatively, if the concrete approaches its strength before the steel yields, as it would when very high yield steel is used, the increased deformation of the concrete when near its full strength allows the steel to reach the yield strength. Therefore, the ultimate load of an axially loaded, reinforced concrete column (perhaps better referred to as the yield load) is the sum of the yield strength of the steel plus the strength of the concrete. It has been found (e.g., by Richart and Brown^{5.1} and Hognestad^{5.2}) that the strength of the concrete in an axially loaded column is approximately $0.85f'_c$, where f'_c is the compressive strength of a cylinder. The strength is rather lower than that of a cylinder because of the difference in specimen shape and size, and because the vertical casting of a column leads to sedimentation and water gain in the top region of the column. Thus the ultimate load of an axially loaded column may be written as

$$P_o = 0.85f'_c(A_g - A_{st}) + f_y A_{st} \quad (5.1)$$

where A_g is the gross area of the cross section, A_{st} is the total area of longitudinal steel in the section, and f_y is the yield strength of the steel.

Up to the load P_o , tied and spiral columns behave almost identically, and the transverse steel adds very little to the strength of the column. Once the load P_o is reached, a tied column with ties not closely spaced immediately fails, accompanied by breakdown of the concrete and buckling of the

4/3/16

119

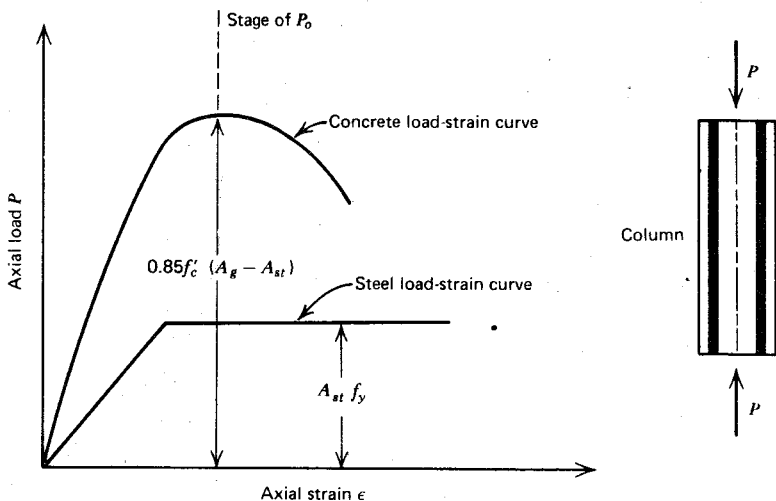


Fig. 5.2. Axial load-strain curves for the steel and concrete of an axially loaded reinforced concrete column.

longitudinal steel bars between the ties, because the spacing between the ties is generally too large to prevent general concrete failure and buckling of bars.

In a spiral column, after load P_o has been reached, the shell of concrete outside the spiral is cracked or destroyed. The load capacity is reduced because of loss of concrete area, but the spacing of the spiral steel is usually small enough to prevent buckling of the longitudinal bars between the spirals. Hence the longitudinal bars continue to carry load; large increased deformation follows, and the core concrete (which is tending to increase in volume because of internal disruption) bears against the spiral, causing the spiral to exert confining reaction on the core. The resulting radial compressive stress increases the load-carrying capacity of the core concrete, and in spite of the loss of the concrete shell, the ultimate load of a column with a heavy spiral can increase to greater than P_o . The enhancement in strength of concrete due to the confinement of a steel spiral was discussed in Section 2.1.3. Equation 2.5 gives the strength of confined concrete cylinders when the spiral reaches the yield strength. If the unconfined cylinder strength f'_c in Eq. 2.5 is replaced by the unconfined strength of concrete in a column, $0.85f'_c$, the ultimate load of a spiral column may be written as

$$P_u = \left(0.85f'_c + 8.2 \frac{f_y A_{sp}}{d_s s} \right) A_{cc} + f_y A_{st} \quad (5.2)$$

where f_y = yield strength of the steel, d_s = diameter of the spiral, A_{sp} = area of the spiral bar, s = pitch of the spiral, and A_{cc} = area of concrete in the column core.

Now

$$8.2 \frac{f_y A_{sp}}{d_s s} A_{cc} = 8.2 \frac{f_y A_{sp}}{d_s s} \left(\frac{\pi d_s^2}{4} - A_{st} \right)$$

$$= 2.05 f_y V_s - 8.2 \frac{f_y A_{sp} A_{st}}{d_s s} \quad (5.3)$$

where $V_s = A_{sp} \pi d_s / s$ = volume of spiral steel per unit length of column core
 A_{st} = total area of longitudinal steel in the section

Therefore, Eq. 5.2 may be written as

$$P_u = 0.85 f'_c A_{cc} + 2.05 f_y V_s + f_y A_{st} \left(1 - \frac{8.2 A_{sp}}{d_s s} \right) \quad (5.4)$$

If the spiral steel is replaced by an equivalent volume of longitudinal steel, V_s will equal the area of that longitudinal steel. Therefore Eq. 5.4 indicates that the steel in the spiral is approximately twice as effective as the same volume of longitudinal steel in contributing to the strength of the column. However, the high load-carrying capacity of columns having heavy spirals is available only at very large deformations and after the shell concrete has spalled. If the ultimate load carried after the spalling of the shell concrete when the spiral reaches yield is to exceed the yield load of the column before spalling, P_u from Eq. 5.4 must be greater than P_y from Eq. 5.1. This requires satisfaction of the following condition

$$0.85 f'_c A_{cc} + 2.05 f_y V_s + f_y A_{st} \left(1 - \frac{8.2 A_{sp}}{d_s s} \right) > 0.85 f'_c (A_g - A_{st}) + f_y A_{st}$$

hence we must also have

$$V_s > 0.415 \frac{f'_c}{f_y} (A_g - A_{cc} - A_{st}) + \frac{4 A_{sp} A_{st}}{d_s s}$$

which may be written as

$$\rho_s = \frac{V_s}{A_c} > 0.415 \frac{f'_c}{f_y} \left(\frac{A_g}{A_c} - 1 \right) + \frac{4 A_{sp} A_{st}}{d_s s A_c} \quad (5.5)$$

where $A_c = A_{cc} + A_{st}$, the gross area of the column core.

For spiral columns, the ACI code^{5.3} requires ρ_s to be not less than the value given by

$$\rho_s = 0.45 \frac{f'_c}{f_y} \left(\frac{A_g}{A_c} - 1 \right) \quad (5.6)$$

where A_c = core area measured to the outside diameter of the spiral. Comparison of Eqs. 5.5 and 5.6 indicates that the ACI requirement will ensure that the ultimate load of the column after spalling exceeds the load before spalling. The large ductility of spiral columns (Fig. 5.3) is of considerable

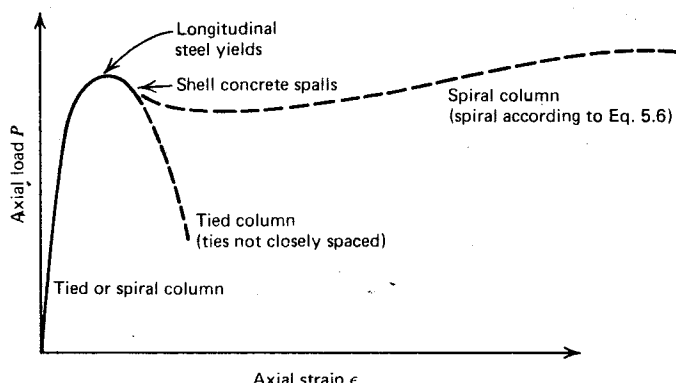


Fig. 5.3. Comparison of total axial load-strain curves of tied and spiral columns.

interest. Whereas the axially loaded tied column with ties not closely spaced shows a brittle failure, a spiral column has a large capacity for plastic deformation.

Tests have shown (see Section 2.1.3) that closely spaced rectangular ties also enhance the strength and ductility of the confined concrete, although not as effectively as circular spirals. This is because rectangular ties will apply only a confining pressure near the corners of the section, since lateral pressure from the concrete will cause lateral bowing of the tie sides, whereas circular spirals, because of their shape, are capable of applying a uniform confining pressure around the circumference. Tests by Chan^{5.4} suggested that when considering strength enhancement, the efficiency of square ties may be 50% of that of the same volume of circular spirals. Tests by many others have also indicated an enhancement of strength due to closely spaced rectangular ties, but the results reported by Roy and Sozen^{5.5} indicated no gain in strength. It is likely that the concrete strength gain from rectangular ties will be small in most cases. However, test results have always shown that a significant improvement in the ductility of the concrete resulted from the use of closely spaced rectangular ties.

5.3 ECCENTRICALLY LOADED SHORT COLUMNS WITH UNIAXIAL BENDING

5.3.1 Introduction

Axially loaded columns occur rarely in practice because some bending is almost always present, as evidenced by the slight initial crookedness of columns, the manner in which loading is applied by beams and slabs, and the moments introduced by continuous construction.

The combination of an axial load P_u and bending moment M_u is equivalent to a load P_u applied at eccentricity $e = M_u/P_u$, as in Fig. 5.4.

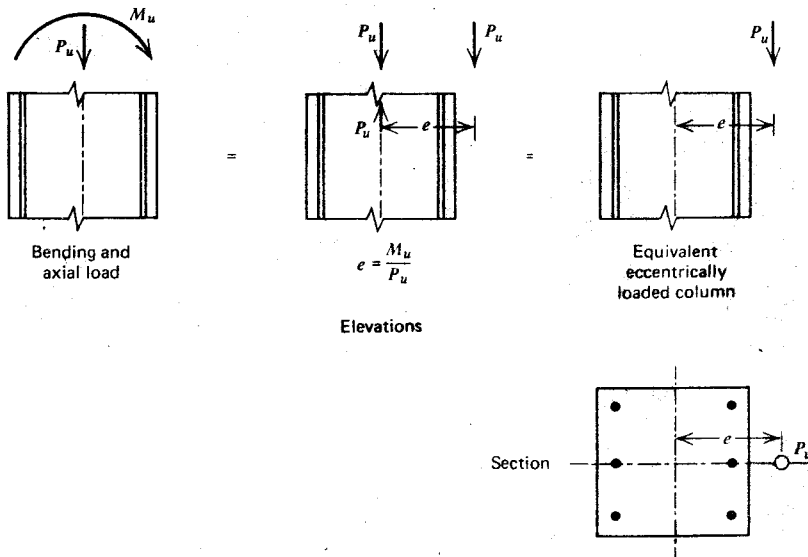


Fig. 5.4. Equivalent column loading.

Figures 5.5 and 5.6 are back and front views of tied and spirally reinforced columns that were eccentrically loaded to failure. These columns are from a series tested by Hognestad.^{5,2} The greater ductility of a spiral column is again evident from the figures. The greater ductility of spiral columns compared with columns with nominal ties has been observed in buildings damaged by earthquakes. As an example, some lower story columns of Olive View Hospital after the San Fernando earthquake of 1971 are shown in Fig. 5.7. The concrete in the tied column has been reduced to rubble, whereas

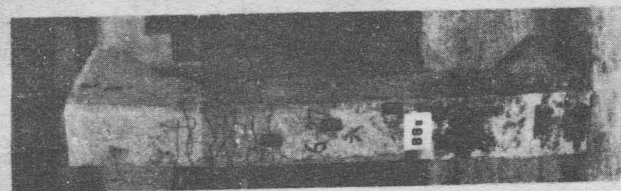
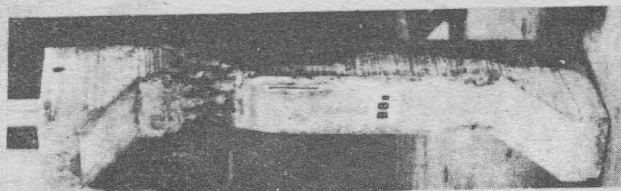
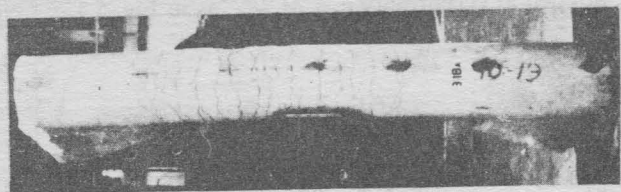
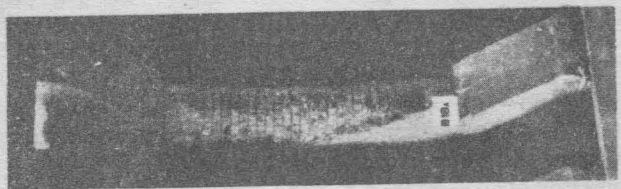


Fig. 5.5. Eccentrically loaded tied column ($e = 0.5h$) after failure. 5.2

Fig. 5.6. Eccentrically loaded spiral column ($e = 0.5h$) after failure. 5.2

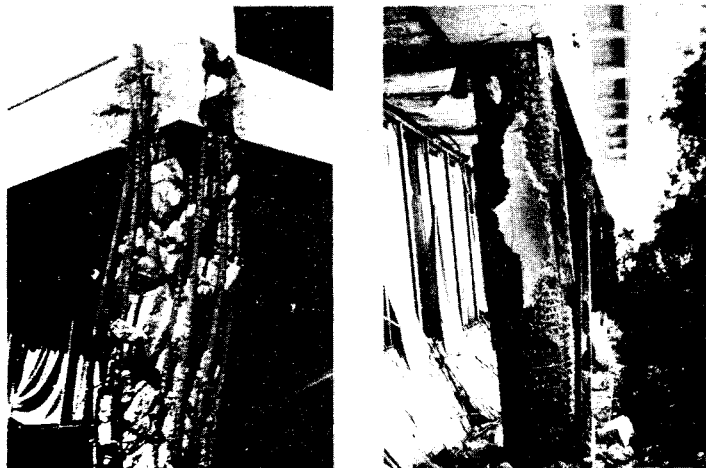


Fig. 5.7. Tied and spiral columns of Olive View Hospital after the 1971 San Fernando earthquake.

the spiral column is still intact and able to carry load, even though the shell concrete has been shed.

In practice, from the point of view of strength, both tied and spiral columns are designed as if the concrete is unconfined, but because of the greater toughness of a spiral column, the ACI code^{5.3} assigns a slightly less stringent capacity reduction factor to a spiral column ($\phi = 0.75$) than to a tied column ($\phi = 0.70$).

Strength equations for eccentrically loaded columns are derived in the following sections, assuming that the concrete is unconfined. At the ultimate load the concrete reaches its maximum capacity, but the longitudinal steel may or may not be at the yield strength. The assumptions of Section 3.1 are used in the derivation of the strength equations. Bending about one major axis of the section only (i.e., uniaxial bending) is considered in this section.

5.3.2 Analysis of Rectangular Sections with Bars at One or Two Faces

A rectangular section with bars at two faces, loaded eccentrically at the ultimate load, appears in Fig. 5.8. The neutral axis depth is considered to be less than the overall depth. As with beams, a tension failure or a compression

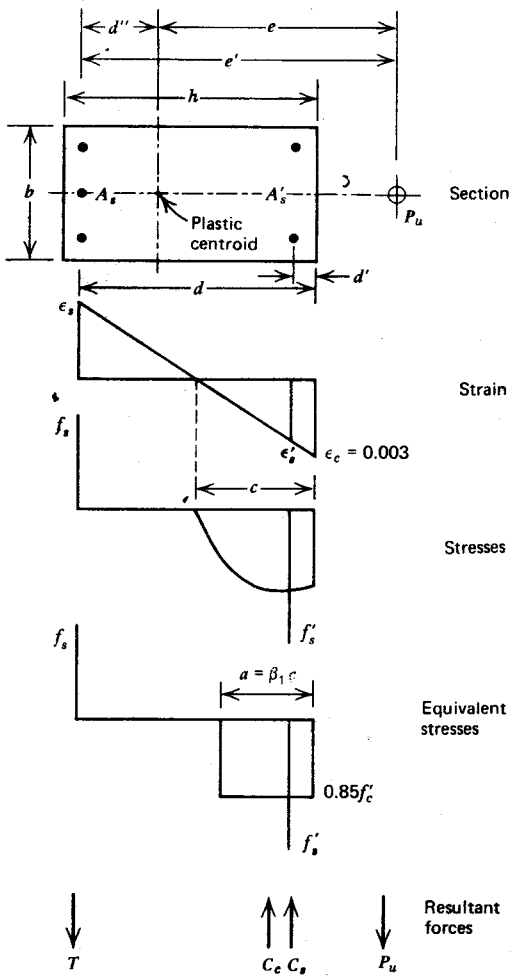


Fig. 5.8. Eccentrically loaded column section at the ultimate load.

failure can occur, depending on whether the tension steel reaches the yield strength. However, unlike beams, a compression failure cannot be avoided by limiting the steel area, since the type of failure is dependent on the axial load level. The compression steel in eccentrically loaded columns at the ultimate load generally reaches the yield strength except when the load level is low, when high strength steel is used, or when the column is small so that the dimension d' (See Fig. 5.8) is relatively large. It is usual to assume that the

compression steel is yielding, and then to check later that the yield strain has been reached. Referring to Fig. 5.8, and assuming the stress in the compression steel $f'_s = f_y$, the equilibrium equation obtained from the sum of the internal forces is

$$P_u = 0.85f'_c ab + A'_s f_y - A_s f_s \quad (5.7)$$

and the expression obtained from taking moments about the tension steel is

$$P_u e' = 0.85f'_c ab(d - 0.5a) + A'_s f_y(d - d') \quad (5.8)$$

where e' is the eccentricity of ultimate load P_u from the centroid of the tension steel, f'_c is the concrete compressive cylinder strength, f_y is the steel yield strength, f_s is the stress in the tension steel, A_s is the area of tension steel, A'_s is the area of compression steel, a is the depth of the equivalent rectangular concrete stress block, b is the column width, d is the distance from the extreme compression fiber to the centroid of the tension steel, and d' is the distance from the extreme compression fiber to the centroid of the compression steel.

Sometimes it is more convenient to use the eccentricity of P_u from the plastic centroid e . The plastic centroid is the centroid of resistance of the section if all the concrete is compressed to the maximum stress ($0.85f'_c$) and all the steel is compressed to the yield stress (f_y), with uniform strain over the section. In other words, the plastic centroid is the point of application of the external load P_o that produces an axially loaded condition at failure. This condition is represented in Fig. 5.9. Taking moments of the internal forces about the centroid of the left-hand steel and equating this to the moment of the resultant force gives

$$\begin{aligned} 0.85f'_c bh(d - 0.5h) + A'_s f_y(d - d') &= P_o d'' = [0.85f'_c bh + (A_s + A'_s)f_y]d'' \\ \therefore d'' &= \frac{0.85f'_c bh(d - 0.5h) + A'_s f_y(d - d')}{0.85f'_c bh + (A_s + A'_s)f_y} \end{aligned} \quad (5.9)$$

where d'' is the distance from the plastic centroid to the centroid of the tension steel of the column when eccentrically loaded. For symmetrically reinforced members, the plastic centroid corresponds to the centre of the cross section.

For the eccentrically loaded column of Fig. 5.8, taking moments about the plastic centroid gives

$$P_u e = 0.85f'_c ab(d - d'' - 0.5a) + A'_s f_y(d - d' - d'') + A_s f_s d'' \quad (5.10)$$

A "balanced failure" occurs when the tension steel just reaches the yield strength and the extreme fiber concrete compressive strain reaches 0.003 at the same time. For a balanced failure, from similar triangles of the strain

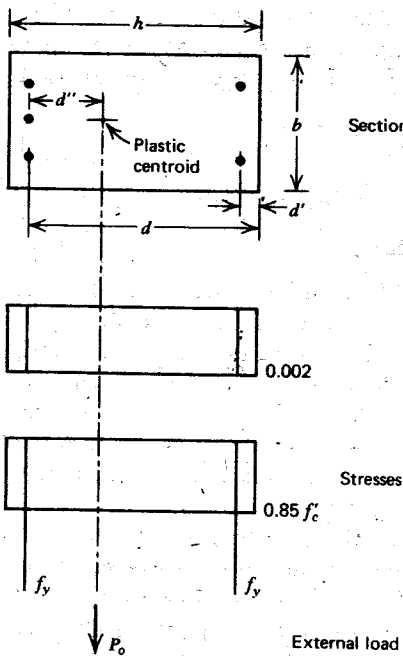


Fig. 5.9. Stresses in column section when load is applied at the plastic centroid.

diagram of Fig. 5.8, we have

$$\frac{0.003}{c_b} = \frac{f_y/E_s}{d - c_b} \quad (5.11)$$

$$\therefore c_b = \frac{0.003E_s}{f_v + 0.003E_s} d \quad (5.12)$$

and

$$a_b = \beta_i c_b = \frac{0.003E_s}{f_y + 0.003E_s} \beta_i d \quad (5.13)$$

It should be noted that a balanced failure is associated with a uniquely defined strain profile, Eq. 5.11; it is a property of the section. The load and moment at balanced failure, P_b and $P_b e_b$, may be calculated by substituting $f_s = f_y$ and a_b from Eq. 5.13 into Eqs. 5.7 and 5.10.

A tension failure occurs if $P_u < P_b$, since the smaller column load means that $c < c_b$ and reference to the strain diagram of Fig. 5.10 shows that therefore $\varepsilon_s > f_y/E_s$. In this case the tension steel yields and Eqs. 5.7 to 5.10 apply with $f_s = f_y$.

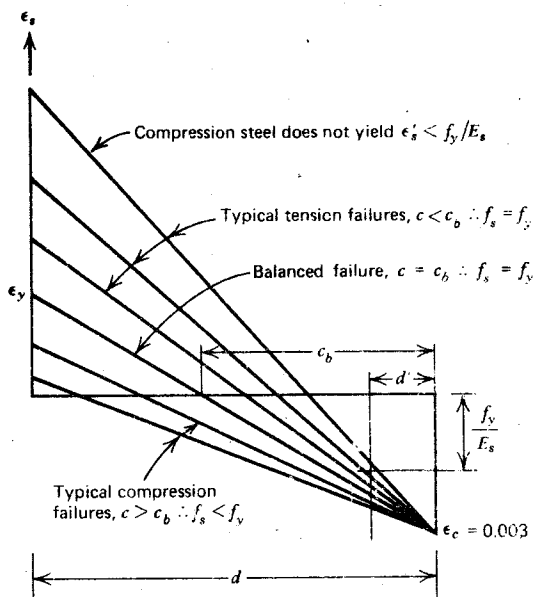


Fig. 5.10. Strain diagrams for eccentrically loaded column failures.

A compression failure occurs if $P_u > P_b$, since the larger column load means that $c > c_b$; referring to the strain diagram of Fig. 5.10, it becomes clear that therefore $\epsilon_s' < f_y/E_s$. In this case the tension steel does not reach the yield strain. The actual value of f_s may be determined from the strain diagram to be

$$f_s = \epsilon_s' E_s = 0.003 \frac{d - c}{c} E_s = 0.003 \frac{\beta_1 d - a}{a} E_s \quad (5.14)$$

For a compression failure, Eqs. 5.7 to 5.10 apply with f_s from Eq. 5.14 substituted.

It has been assumed in Eqs. 5.7 to 5.14 that the compression steel is yielding ($\epsilon_s' = f_y$). This must be checked by examining the strain diagram. For the compression steel to yield, it is required that

$$\epsilon_s' = 0.003 \frac{c - d'}{c} \geq \frac{f_y}{E_s} \quad (5.15)$$

If it is found that this steel is not yielding, the value of f_s found from the strain diagram is

$$f_s' = \epsilon_s' E_s = 0.003 \frac{c - d'}{c} E_s = 0.003 \frac{a - \beta_1 d'}{a} E_s \quad (5.16)$$

and this value, rather than f_y , should be substituted into all the foregoing equations for the stress in the compression steel.

The combinations of P_u and $P_u e$ that cause failure of a given column section are best illustrated by an interaction diagram. Figure 5.11 is such a

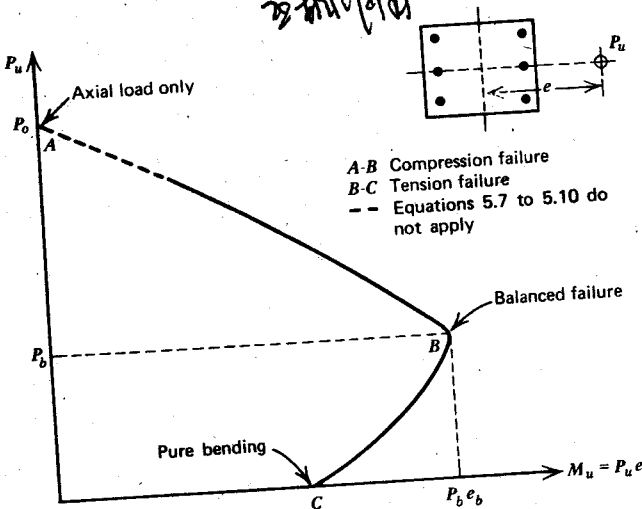


Fig. 5.11. Interaction diagram for an eccentrically loaded reinforced concrete column section, indicating the combinations of load and eccentricity that cause failure.

diagram for a typical eccentrically loaded column. Any combination of load and eccentricity giving a point on AB will cause a compression failure; any combination on BC causes a tension failure, in that yielding of the tension steel precedes crushing of the compressed concrete. At B , a balanced failure occurs. Any combination of load and eccentricity that can be plotted within the area of the interaction diagram can be supported without failure; combinations plotted outside the area cannot be supported. Note that the presence of a moderate compressive load increases the ultimate moment of resistance of the section. When $c > h$, the equations derived, Eq. 5.7-5.10, do not strictly apply because the neutral axis lies outside the section and the shape of the stress block becomes modified. This point is illustrated in Fig. 5.12, which gives a range of strain profiles for a section at the ultimate load corresponding to different neutral axis depths. For $c < h$ the extreme fiber strain is 0.003. For $c > h$, the limiting case is when $c \rightarrow \infty$, which occurs when the eccentricity is zero and the axial load is P_0 . Note that the strain profile corresponding to P_0 has a uniform strain of 0.002 over the section because at this strain an axially loaded concrete specimen reaches maximum stress (see Fig. 2.1).

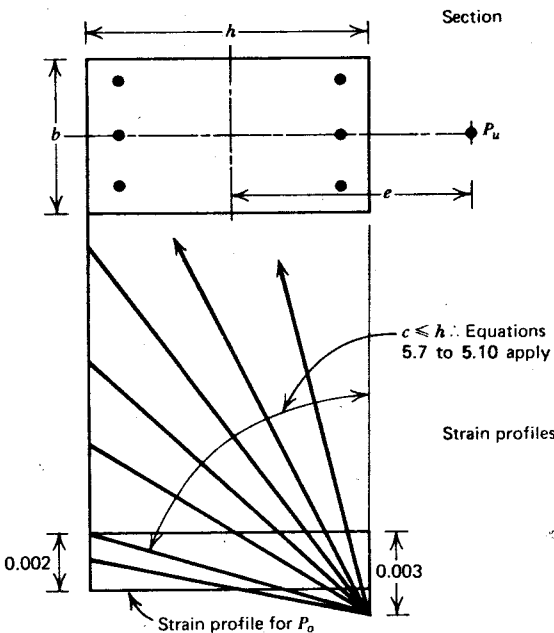


Fig. 5.12. Strain profiles for eccentrically loaded reinforced concrete column at ultimate load.

The portion of the interaction curve in Fig. 5.11 to which Eqs. 5.7 to 5.10 do not apply (dashed line) can be completed because the calculated value for P_o from Eq. 5.1 fixes the terminating point of the curve.

Also, the area of concrete displaced by the compression steel has not been allowed for in the equations. The small error thus made can be overcome by reducing the actual stress in the compression steel by $0.85f'_c$ to allow for the fact that the concrete there has been considered to be carrying this stress, i.e., the stress in the compression steel is taken to be $f'_s - 0.85f'_c$, or $f_y - 0.85f'_c$ when yielding.

Example 5.1

A 20 in (508 mm) square concrete column section is reinforced symmetrically by 4 in² (2581 mm²) of steel at each of the two critical faces. The centroid of each group of bars is 2.5 in (63.5 mm) from the near edge. The concrete has a cylinder strength of 3000 psi (20.7 N/mm²). The steel has a modulus of elasticity of 29×10^6 psi (0.20 $\times 10^6$ N/mm²) and a yield strength of 40,000 psi (276 N/mm²). The load acts eccentrically with respect to one major axis of the

column section (see Fig. 5.13). Calculate the range of possible failure loads and eccentricities for the ideal section.

Solution

Balanced failure

The tension steel is yielding, $f_s = f_y$. Assume that the compression steel is also yielding. From Eq. 5.13 we have

$$a_b = \frac{0.003 \times 29 \times 10^6}{40,000 + 0.003 \times 29 \times 10^6} 0.85 \times 17.5 = 10.19 \text{ in}$$

From Eq. 5.7, and noting that because of equal steel area at each face the steel forces cancel out, we put

$$P_b = 0.85 \times 3000 \times 10.19 \times 20 = 519,700 \text{ lb (2310 kN)}$$

From Eq. 5.10, and noting that since the reinforcement is symmetrical, the plastic centroid is at the center of the section (therefore $d'' = 7.5 \text{ in}$), we write

$$\begin{aligned} P_b e_b &= 519,700 (17.5 - 7.5 - 0.5 \times 10.19) \\ &\quad + 4 \times 40,000 (17.5 - 2.5 - 7.5) + (4 \times 40,000 \times 7.5) \\ &= 4.95 \times 10^6 \text{ lb} \cdot \text{in (559 kN} \cdot \text{m)} \end{aligned}$$

$$\text{Also } c_b = a_b / \beta_1 = 10.19 / 0.85 = 11.99 \text{ in.}$$

From Eq. 5.15, checking the compression steel stress, we find

$$\frac{f_y}{E_s} = \frac{40,000}{29 \times 10^6} = 0.00138$$

$$\epsilon'_s = 0.003 \frac{11.99 - 2.5}{11.99} = 0.00237 > 0.00138$$

Therefore compression steel is yielding as assumed.

The calculated values of P_b and $P_b e_b$ give point *B* in Fig. 5.13.

Tension failure

If $P_u < P_b$, $f_s = f_y$.

For example, let $P_u = 300,000 \text{ lb (1330 kN)} < P_b$.

Assume that the compression steel is also yielding.

Then from Eq. 5.7 write

$$300,000 = 0.85 \times 3000 \times 20a$$

$$\therefore a = 5.88 \text{ in} \quad \text{and} \quad c = \frac{a}{\beta_1} = \frac{5.88}{0.85} = 6.92 \text{ in}$$

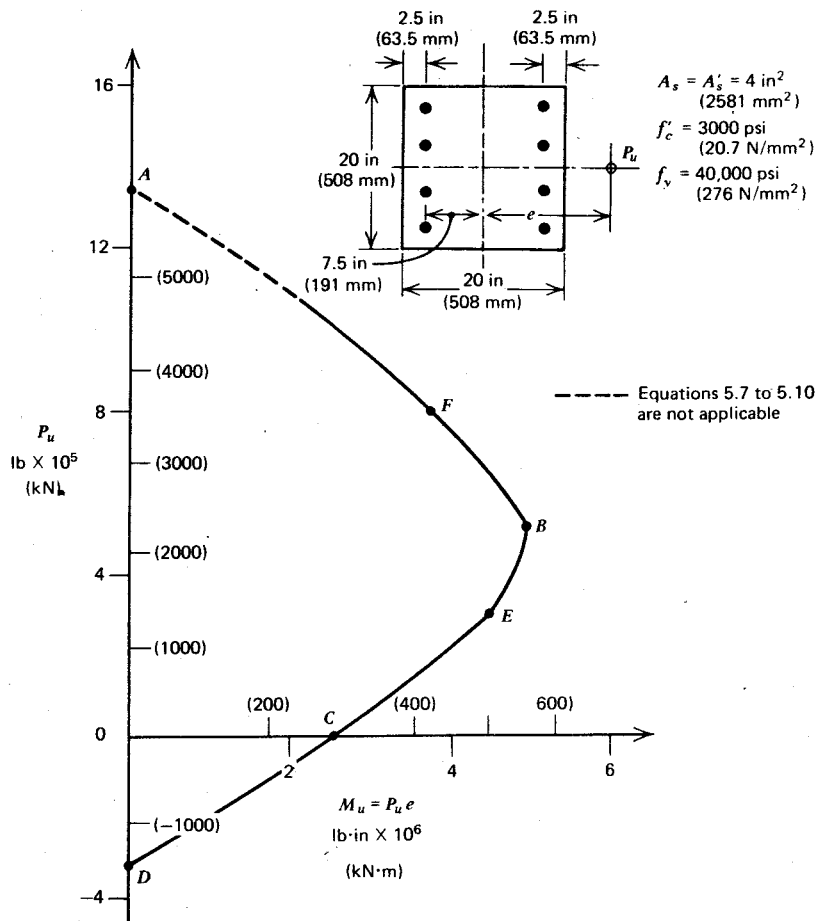


Fig. 5.13. Interaction diagram for the eccentrically loaded reinforced concrete column of Example 5.1.

Therefore, Eq. 5.15 gives

$$\varepsilon'_s = 0.003 \frac{6.92 - 2.5}{6.92} = 0.00192 > 0.00138$$

Therefore, compression steel is yielding as assumed. Hence from Eq. 5.10 we have

$$\begin{aligned} P_u e &\doteq 300,000(10 - 0.5 \times 5.88) + 2 \times 4 \times 40,000 \times 7.5 \\ &= 4.52 \times 10^6 \text{ lb} \cdot \text{in} (510 \text{ kN} \cdot \text{m}) \end{aligned}$$

This gives point *E* in Fig. 5.13.

In the limit when $P_u \rightarrow 0$ and $e \rightarrow \infty$, the case of pure flexure arises. In this case, because $A'_s = A_s$ and the concrete must carry some compression, $f'_s < f_y$. From Eq. 5.16 we can write

$$f'_s = 0.003 \frac{a - 0.85 \times 2.5}{a} 29 \times 10^6 = 87,000 \frac{a - 2.125}{a} \text{ psi}$$

From Eq. 5.7, substituting the above mentioned value for f'_s instead of the yield strength, we have

$$0 = 0.85 \times 3000 \times 20a + 4 \times 87,000 \frac{a - 2.125}{a} - 4 \times 40,000$$

$$\therefore 0 = a^2 + 3.69a - 14.51$$

Solution of this quadratic equation gives $a = 2.39$ in.

$$\therefore f'_s = 87,000 \frac{2.39 - 2.125}{2.39} = 9650 \text{ psi}$$

From Eq. 5.10, substituting the above mentioned value for f'_s instead of the yield strength, we have

$$M_u = P_u e = 0.85 \times 3000 \times 2.39 \times 20(10 - 0.5 \times 2.39)$$

$$+ 4 \times 9,650 \times 7.5 + 4 \times 40,000 \times 7.5$$

$$= 2.56 \times 10^6 \text{ lb} \cdot \text{in} (289 \text{ kN} \cdot \text{m})$$

This gives point *C* in Fig. 5.13.

Compression failure

If $P_u > P_b$, $f_s < f_y$.

For example, let $P_u = 800,000 \text{ lb}$ (3560 kN) $> P_b$.

The compression steel was yielding when $P_u = P_b$; hence it will be yielding for any load larger than this (see Fig. 5.10). However, the tension steel will not yield. Hence Eq. 5.14 gives

$$f_s = 0.003 \frac{0.85 \times 17.5 - a}{a} 29 \times 10^6 = 87,000 \frac{14.88 - a}{a} \text{ psi}$$

And from Eq. 5.7 we find

$$800,000 = 0.85 \times 3000 \times 20a + 4 \times 40,000$$

$$- 4 \times 87,000 \frac{14.88 - a}{a}$$

$$\therefore 0 = a^2 - 5.725a - 101.5$$

Solution of this quadratic equation, or a trial-and-error procedure, gives $a = 13.34$ in

$$\therefore f_s = 87,000 \frac{14.88 - 13.34}{13.34} = 10,040 \text{ psi}$$

From Eq. 5.10 we have

$$\begin{aligned} P_u e &= 0.85 \times 3000 \times 13.34 \times 20(10 - 0.5 \times 13.34) \\ &\quad + 4 \times 40,000 \times 7.5 + 4 \times 10,040 \times 7.5 \\ &= 3.77 \times 10^6 \text{ lb} \cdot \text{in} (426 \text{ kN} \cdot \text{m}) \end{aligned}$$

This gives point *F* in Fig. 5.13.

In the limit, P_u becomes a maximum when e is zero.

Then from Eq. 5.1, ignoring the area of concrete displaced by the steel, we have

$$\begin{aligned} P_u &= P_o = 0.85 \times 3000 \times 20 \times 20 + 8 \times 40,000 \\ &= 1,340,000 \text{ lb} (5960 \text{ kN}) \end{aligned}$$

This gives point *A* in Fig. 5.13.

Tensile loading

If the external load is tensile rather than compressive, the tensile strength of the column when $e = 0$ is given by

$$\begin{aligned} P_u &= -A_{st} f_y = -8 \times 40,000 \\ &= -320,000 \text{ lb} (-1420 \text{ kN}) \end{aligned}$$

This gives point *D* in Fig. 5.13.

This result ignores the tensile strength of the concrete.

The flexural strengths corresponding to other values of P_u between zero and $-320,000$ lb can be found from the tension failure equations.

Interaction diagram

The calculated results are plotted in Fig. 5.13. If sufficient points had been calculated, the curve *ABCD* could be obtained. The interaction curve *ABCD* shows the possible combinations of load and eccentricity that would cause the section to reach its strength.

5.3.3 Design of Rectangular Sections with Bars at One or Two Faces

In practice all columns are subjected to some bending moment due to initial crookedness and to unsymmetrical loading. Hence an axially loaded column

is not a practical case, and it is recommended that the eccentricity with which a compressive load is applied should not be considered to be less than some minimum value (e.g., $0.1h$ for a tied column or $0.05h$ for a spiral column^{5,3}). Indeed, one could justify adding to all columns an additional eccentricity to allow for unforeseen effects that may increase the eccentricity of the loading.

Frequently in the design of columns compression failures cannot be eliminated by limiting the proportions of the section. Therefore, design equations for both tension and compression failures are necessary. The equations for analysis may be used for design after modification to include the capacity reduction factor φ . The capacity reduction factors for columns according to ACI 318-71^{5,3} are listed in Section 1.3.1. It is to be noted that for small axial loads, reducing to zero in the tension failure range, the capacity reduction factor may be increased linearly from 0.75 for spiral columns, or 0.70 for tied columns, to 0.9 as the ultimate load decreases from approximately $0.1 f'_c A_g$ to zero, where A_g is the gross area of the column section.

The design equations for the section of Fig. 5.14 can be written using Eqs. 5.7, 5.8, and 5.10 as follows:

$$P_u = \varphi(0.85f'_c ab + A'_s f_y - A_s f_s) \quad (5.17)$$

and

$$P_u e' = \varphi[0.85f'_c ab(d - 0.5a) + A'_s f_y(d - d')] \quad (5.18)$$

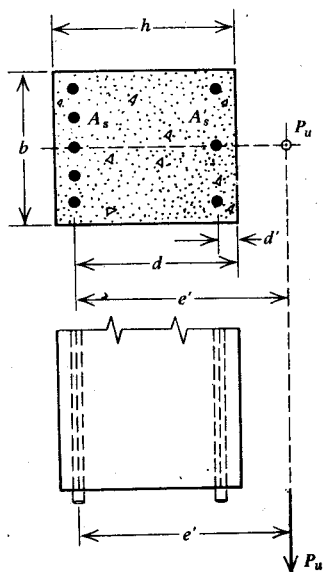


Fig. 5.14. Rectangular concrete section with bars in one or two faces.

or

$$P_u e = \phi [0.85 f'_c ab(d - d'' - 0.5a) + A'_s f_y (d - d' - d'') + A_s f_s d''] \quad (5.19)$$

At a balanced failure, $f_s = f_y$, and from Eq. 5.13 we have

$$a_b = \frac{0.003 E_s}{f_y + 0.003 E_s} \beta_1 d \quad (5.20)$$

Substituting $a = a_b$ from Eq. 5.20 and $f_s = f_y$ into Eqs. 5.17 and 5.19 gives P_b and $P_b e_b$. The type of failure then can be determined. Note that the equations assume that the compression steel is yielding ($f'_s = f_y$), and this should be checked. From Eq. 5.15, the compression steel is yielding if

$$\epsilon'_s = 0.003 \frac{a - \beta_1 d'}{a} \geq \frac{f_y}{E_s} \quad (5.21)$$

If it is found that the compression steel is not yielding, the expression

$$f'_s = \epsilon'_s E_s = 0.003 \frac{a - \beta_1 d'}{a} E_s \quad (5.22)$$

should be substituted for f_y in all the terms involving A'_s in Eqs. 5.17 to 5.19.

If it is desired to take into account the area of concrete displaced by the compression steel, the stress in the compression steel should be reduced by $0.85 f'_c$.

TENSION FAILURE

If $P_u < P_b$, tension governs ($f_s = f_y$) and the depth of the compression block a may be found from Eq. 5.17 and substituted into Eq. 5.18 to give

$$P_u = \phi 0.85 f'_c bd \left(\rho' m' - \rho m + 1 - \frac{e'}{d} + \left\{ \left(1 - \frac{e'}{d} \right)^2 + 2 \left[\frac{e'}{d} (\rho m - \rho' m') + \rho' m' \left(1 - \frac{d'}{d} \right) \right] \right\}^{1/2} \right) \quad (5.23)$$

where

$$m = \frac{f_y}{0.85 f'_c}$$

$$m' = m - 1$$

$$\rho = \frac{A_s}{bd}$$

$$\rho' = \frac{A'_s}{bd}$$

For the case of symmetrical reinforcement ($\rho = \rho'$), or no compression reinforcement ($\rho' = 0$), Eq. 5.23 becomes more simplified. This equation takes into account the area of concrete displaced by the compression steel.

COMPRESSION FAILURE

If $P_u > P_b$, compression governs ($f_s < f_y$). Then from Eq. 5.14

$$f_s = 0.003 \frac{\beta_1 d - a}{a} E_s \quad (5.24)$$

Substituting this value of f_s into Eqs. 5.17 and 5.18 or 5.19 enables a to be found and the section solved. This is not an easy solution, however, because of the lengthy calculation necessary to determine a . Two approximate methods are available when compression governs:

1. A linear relationship between P_u and $P_u e$ may be assumed. This amounts to assuming (conservatively as far as strength is concerned) that the line AB in Fig. 5.11 is straight. This approximation is illustrated in Fig. 5.15.

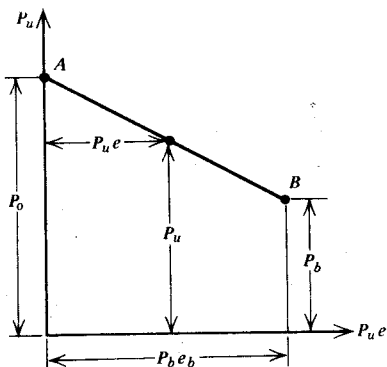


Fig. 5.15. Straight line compression failure approximation for an eccentrically loaded reinforced concrete column.

For a point on the assumed failure line AB of Fig. 5.15, from similar triangles, we find

$$P_u = P_o - (P_o - P_b) \frac{P_u e}{P_b e_b} \quad (5.25)$$

$$\therefore P_u = \frac{P_o}{1 + (P_o/P_b - 1)e/e_b}$$

where from Eq. 5.1

$$P_o = \varphi [0.85 f'_c (A_g - A_{st}) + A_{st} f_y] \quad (5.26)$$

and P_u and e_b may be found by substituting Eq. 5.20 into Eqs. 5.17 and 5.19. Thus P_u corresponding to a given e , or vice versa, may be found from Eq. 5.25. It is evident that the form of Eq. 5.25 makes the expression more useful for analysis than for design.

2. For symmetrical reinforcement ($\rho = \rho'$), a strength equation developed empirically by Whitney^{5,6} can be used. The maximum moment carrying capacity of the concrete is taken to be that found for beams failing in compression, given by Eq. 4.16. This means that at the flexural strength, the moment of the concrete force about the tension steel is given by $0.333f'_c bd^2$. On this basis, for large eccentricities, equilibrium of the moments of the forces taken about the tension steel requires

$$P_u \left(e + d - \frac{h}{2} \right) = A'_s f_y (d - d') + 0.333f'_c bd^2$$

$$\therefore P_u = \frac{A'_s f_y}{e - d' + 0.5} + \frac{f'_c bh}{\frac{3he}{d^2} + \frac{6dh - 3h^2}{2d^2}} \quad (5.27)$$

Although this equation has no real meaning for small eccentricities, it can be used under these conditions if P_u is adjusted to approach the proper value for an axially loaded column when $e \rightarrow 0$. When $e = 0$, the first term on the right-hand side of Eq. 5.27 gives $2A'_s f_y$ for the steel force as required, since $A'_s = A_s$. If the second term is to give $0.85f'_c bh$ for the concrete force when $e = 0$ the following condition must be satisfied:

$$\frac{6dh - 3h^2}{2d^2} = \frac{1}{0.85} = 1.18$$

Hence the design equation becomes

$$P_u = \varphi \left[\frac{A'_s f_y}{e - d' + 0.5} + \frac{bhf'_c}{\frac{3he}{d^2} + 1.18} \right] \quad (5.28)$$

The strain diagram should be checked to ensure that the compression steel is yielding. A plot of Whitney's design equation appears in Fig. 5.16. It is obviously inapplicable below the tension failure curve. When compared with the curve given by the more exact Eqs. 5.17, 5.18, 5.19, and 5.24, Whitney's expression does not coincide exactly. However, Eq. 5.28 is a good design approximation and is convenient to use because the steel area is given by the solution of a linear equation.

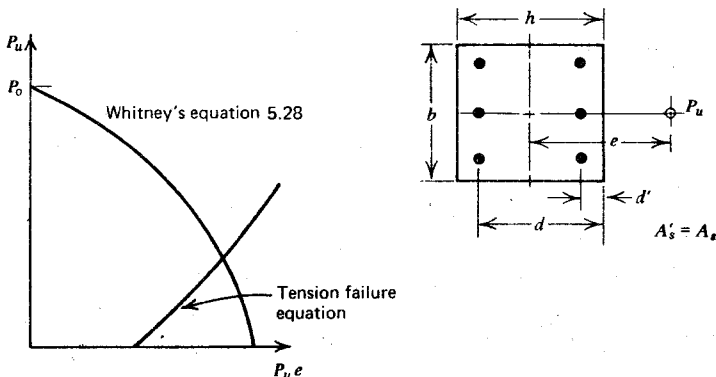


Fig. 5.16. Whitney's compression failure approximation for an eccentrically loaded reinforced concrete column with symmetrical reinforcement.

Example 5.2

An 18 in (457 mm) square tied column section is to be reinforced symmetrically by bars placed in two opposite faces of the section. The bars have their centroids at $2\frac{1}{2}$ in (64 mm) from the near edges of the section. The concrete has a cylinder strength f'_c of 4000 psi (20.7 N/mm^2). The steel has a modulus of elasticity of 29×10^6 psi ($0.20 \times 10^6 \text{ N/mm}^2$) and a yield strength of 50,000 psi (345 N/mm^2). The capacity reduction factor φ may be assumed to be 0.7, but it may be increased linearly to 0.9 as the ultimate load P_u decreases from $0.1f'_c A_g$ to zero, where A_g is the gross area of the column section. Determine the steel areas required for the column to support the following ultimate loads: (1) 250,000 lb (1110 kN) at $e = 15$ in (381 mm), and (2) 400,000 lb (1780 kN) at $e = 12$ in (305 mm).

Solution

Now $d = 18 - 2.5 = 15.5$ in, and Eq. 5.20 gives

$$a_b = \frac{0.003 \times 29 \times 10^6}{50,000 + 0.003 \times 29 \times 10^6} \times 0.85 \times 15.5 = 8.37 \text{ in}$$

Now $f_y/E_s = 50,000/(29 \times 10^6) = 0.00172$, and from Eq. 5.21 we have

$$\varepsilon'_s = 0.003 \frac{8.37 - 0.85 \times 2.5}{8.37} = 0.00224 > 0.00172$$

Therefore, compression steel is yielding, $f'_s = f_y$, at balanced failure.

Substituting a_b into Eq. 5.17, and noting that $f_s = f_y$ and $A'_s = A_s$, we have

$$P_b = 0.7(0.85 \times 4000 \times 8.37 \times 18) = 358,600 \text{ lb (1594 kN)}$$

1. $P_u = 250,000 \text{ lb} < 358,600 \text{ lb}$; therefore, $P_u < P_b$ (i.e., tension governs, $f_s = f_y$).

Also $0.1f'_c A_g = 0.1 \times 4000 \times 18^2 = 129,600 \text{ lb} < 250,000 \text{ lb}$,

$$\therefore \varphi = 0.7$$

Assume that $f'_s = f_y$. From Eq. 5.17 we have

$$250,000 = 0.7(0.85 \times 4000 \times 18a)$$

$$\therefore a = 5.84 \text{ in}$$

From Eq. 5.21 we write

$$\varepsilon'_s = 0.003 \frac{5.84 - 0.85 \times 2.5}{5.84} = 0.00191 > 0.00172$$

∴ compression steel is yielding as assumed.

From Eq. 5.19 we find

$$\begin{aligned} 250,000 \times 15 &= 0.7[0.85 \times 4000 \times 5.84 \times 18(9 - 2.92) \\ &\quad + A'_s 50,000(9 - 2.5) + A_s 50,000(9 - 2.5)] \\ \therefore A'_s &= A_s = 4.90 \text{ in}^2 \quad \therefore A_{st} = 9.80 \text{ in}^2 (6323 \text{ mm}^2) \end{aligned}$$

2. $P_u = 400,000 \text{ lb} > 358,600 \text{ lb}$; therefore, $P_u > P_b$ (i.e., compression governs, $f_s < f_y$).

Also $0.1f'_c A_g = 129,600 \text{ lb} < 400,000 \text{ lb}$; therefore, $\varphi = 0.7$.

Using the "exact theory":

From Eqs. 5.17 and 5.24 we have

$$\begin{aligned} 400,000 &= 0.7 \left[0.85 \times 4000 \times 18a + 0.5A_{st} \times 50,000 \right. \\ &\quad \left. - 0.5A_{st} \times 0.003 \left(\frac{0.85 \times 15.5 - a}{a} \right) 29 \times 10^6 \right] \end{aligned}$$

$$\therefore A_{st} = \frac{571.4a - 61.2a^2}{68.5a - 573.11} \quad (i)$$

From Eqs. 5.19 and 5.24 we have

$$400,000 \times 12 = 0.7 \left[0.85 \times 4000 \times 18 \times a(9 - 0.5a) \right. \\ \left. + 0.5A_{st} \times 50,000(9 - 2.5) + 0.5A_{st} \right. \\ \left. \times 0.003 \left(\frac{0.85 \times 15.5 - a}{a} \right) 29 \times 10^6 (9 - 2.5) \right] \\ \therefore A_{st} = \frac{4.708a^3 - 84.74a^2 + 1054.9a}{573.11 - 18.5a} \quad (ii)$$

Equating Eqs. i and ii to eliminate A_{st} gives the following cubic equation:

$$0 = a^3 - 29.876a^2 + 516.19a - 2890.1 = 0$$

from which $a = 8.71$ in.

Substituting this value for a into Eq. i gives

$$A_{st} = 14.20 \text{ in}^2 (9161 \text{ mm}^2)$$

Note that $c > c_b$, and the strain diagram shows that the compression steel is yielding in this case.

Using Whitney's equation 5.28:

$$400,000 = 0.7 \left[\frac{A'_s 50,000}{\frac{12}{13} + 0.5} + \frac{18 \times 18 \times 4000}{\frac{3 \times 18 \times 12}{15.5^2} + 1.18} \right]$$

$$\therefore A'_s = 6.75 \text{ in}^2 \quad \therefore A_s = 6.75 \text{ in}^2 \quad \text{and} \quad A_{st} = 13.50 \text{ in}^2 (8710 \text{ mm}^2)$$

Part 2 of Example 5.2 indicates the difficulty of determining the steel areas for a compression failure directly from Eqs. 5.17, 5.19, and 5.24, because of the lengthy expressions and the solution of a cubic equation for a . Hence the much more simple Whitney equation 5.28 is valuable for hand calculations, although the solution is not exact.

The example also illustrates that the calculation of steel areas may be further complicated by the compression steel not yielding. For instance, if steel with a yield strength of 60,000 psi (414 N/mm²) had been used in part 1 of Example 5.2, the compression steel would not have reached the yield strength at the ultimate load. The substitution of f'_s from Eq. 5.22 rather than f_y means that Eqs. 5.17 and 5.19 would have to be solved simultaneously, leading to a much more complicated calculation. Thus the yield strength of high-strength bars in compression may not be reached in some columns, particularly when column cross section is small. Similarly, the tension steel

may not reach yield for a large range of axial load levels if the yield strain is high. It must be remembered that a rather conservative value of $\epsilon_c = 0.003$ for the extreme fiber compressive concrete strain has been assumed (see Section 3.3). If the column is loaded to failure, however, this strain will actually be exceeded, allowing the development of higher steel stresses. Thus the actual strength of column sections with high strength steel is frequently greater than that calculated using $\epsilon_c = 0.003$.^{5,7} There is a good case for increasing ϵ_c to a more realistic value, for example 0.0035, if high-strength steel is to be used effectively.

Columns carrying a small compressive load at large eccentricity may be designed with a small area of compression steel ($A'_s < A_s$) because the internal compressive force is not required to be large. However, to ensure that such a member is reasonably ductile, it is recommended^{5,3} that when the axial load level is less than the balanced failure load P_b or $0.1f'_c A_g$, whichever is the smaller, the reinforcement ratio ρ of the tension steel (A_s/bd) should not exceed 0.75 of the ratio that would produce a balanced failure for the section under flexure without axial load. Hence Eq. 4.48 should be satisfied.

It is also recommended^{5,3} that the longitudinal steel area be not less than 0.01 nor more than 0.08 times the gross area of the section.

5.3.4 Rectangular Sections with Bars at Four Faces

When a section has bars distributed at all faces, the derivation of equations for design and analysis becomes difficult because the bars may be at various stress levels throughout the section. The analysis of such a section can be carried out using the requirements of strain compatibility and equilibrium.

Consider the symmetrically reinforced column section shown in Fig. 5.17 at the ultimate load. For a general bar i in the section, the strain diagram indicates that

$$\epsilon_{si} = 0.003 \frac{c - d_i}{c} \quad (5.29)$$

where compressive strains are positive, and tensile strains are negative. Then the stress f_{si} in bar i is given by the following relationships. If

$$\epsilon_{si} \geq \frac{f_y}{E_s}, \quad f_{si} = f_y$$

or if

$$\frac{f_y}{E_s} > \epsilon_{si} > -\frac{f_y}{E_s}, \quad f_{si} = \epsilon_{si} E_s \quad (5.30)$$

or if

$$\epsilon_{si} \leq -\frac{f_y}{E_s}, \quad f_{si} = f_y$$

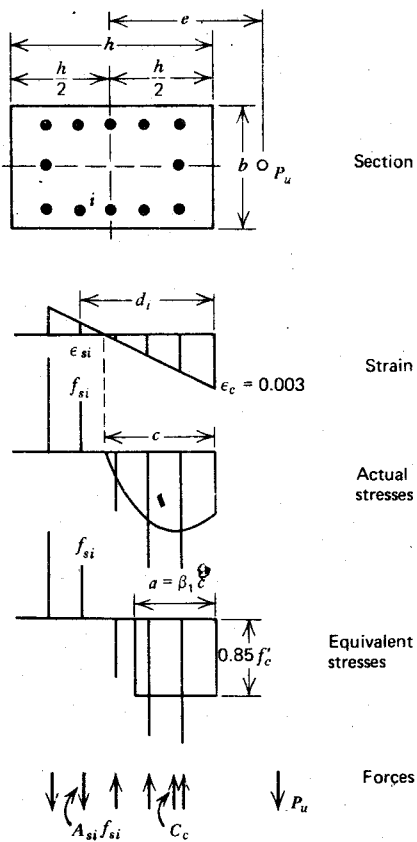


Fig. 5.17. Eccentrically loaded column section with bars at four faces at the ultimate load.

The force in the bar i is then given by $f_{si}A_{si}$ where A_{si} is the area of bar i . The equilibrium equations for a section with n bars may be written as

$$P_u = 0.85f'_c ab + \sum_{i=1}^n f_{si}A_{si} \quad (5.31)$$

$$P_u e = 0.85f'_c ab \left(\frac{h}{2} - \frac{a}{2} \right) + \sum_{i=1}^n f_{si}A_{si} \left(\frac{h}{2} - d_i \right) \quad (5.32)$$

In Eqs. 5.31 and 5.32 due regard must be given to the sign of the stress when summing the steel forces over the section.

In the general case a trial and adjustment solution is best used for analysis. For example, to calculate the ultimate load of a given section with given eccentricity, the procedure is as follows:

1. Choose a value for the neutral axis depth, c .

2. Calculate the stress in the steel in all bars using Eqs. 5.29 and 5.30.
3. Calculate P_u from Eqs. 5.31 and 5.32.
4. Repeat steps 1, 2, and 3 until the values for P_u obtained from Eqs. 5.31 and 5.32 are the same.

Note that the level of stress in the compressed reinforcement bars should be reduced by $0.85f'_c$ if the area of compressed concrete displaced by the steel is to be accounted for.

Example 5.3

Use the general method of strain compatibility and equilibrium to determine the ultimate load and eccentricity for the symmetrically reinforced column section presented in Fig. 5.18 if the neutral axis

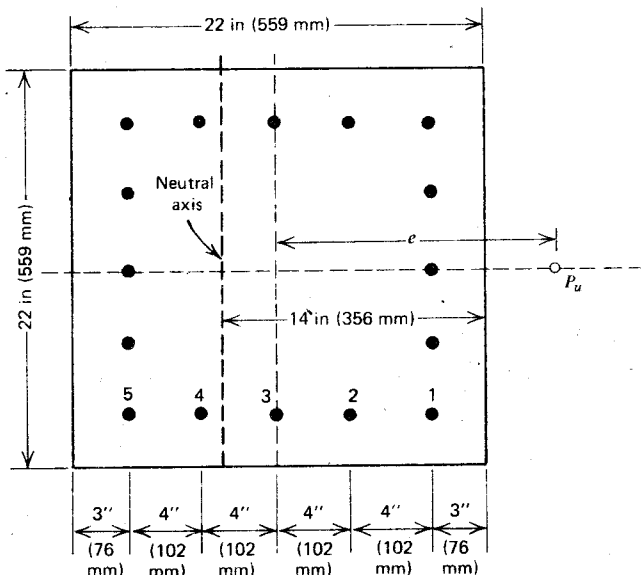


Fig. 5.18. Eccentrically loaded column section of Example 5.3.

lies at the position shown. Each of the 16 bars has a steel area of 1 in^2 (645 mm^2). The steel has a yield strength of 60,000 psi (414 N/mm^2) and a modulus of elasticity of 29×10^6 psi ($0.2 \times 10^6 \text{ N/mm}^2$). The concrete has a cylinder strength of 3000 psi (20.7 N/mm^2).

Solution

Refer to the bar levels as 1 to 5 from the compressed face as in Fig. 5.18. Now

$$\frac{f_y}{E_s} = \frac{60,000}{29 \times 10^6} = 0.00207$$

For $c = 13$ in, Eqs. 5.29 and 5.30 give

$$\varepsilon_{s1} = \frac{0.003(14 - 3)}{14} = 0.002357$$

$$\therefore f_{s1} = 60,000 \text{ psi}$$

$$\varepsilon_{s2} = \frac{0.003(14 - 7)}{14} = 0.0015$$

$$\therefore f_{s2} = 0.0015 \times 29 \times 10^6 = 43,500 \text{ psi}$$

$$\varepsilon_{s3} = \frac{0.003(14 - 11)}{14} = 0.000643$$

$$\therefore f_{s3} = 0.000643 \times 29 \times 10^6 = 18,650 \text{ psi}$$

$$\varepsilon_{s4} = \frac{0.003(14 - 15)}{14} = -0.000214$$

$$\therefore f_{s4} = -0.000214 \times 29 \times 10^6 = -6210 \text{ psi} \quad (\text{tension})$$

$$\varepsilon_{s5} = \frac{0.003(14 - 19)}{14} = -0.001071$$

$$\therefore f_{s5} = -0.001071 \times 29 \times 10^6 = -31,060 \text{ psi}$$

The compressive steel stresses given should be reduced by $0.85f'_c = 0.85 \times 3000 = 2550 \text{ psi}$ to allow for the displaced concrete.

Now $a = \beta_1 c = 0.85 \times 14 = 11.90 \text{ in.}$

Therefore, from Eq. 5.31, and using the reduced compression steel stresses, we have

$$\begin{aligned} P_u &= (0.85 \times 3000 \times 11.9 \times 22) + (57,450 \times 5) + (40,950 \times 2) \\ &\quad + (16,100 \times 2) - (6210 \times 2) - (31,060 \times 5) \\ &= 667,590 + 287,250 + 81,900 + 32,200 - 12,420 - 155,300 \\ &= 901,200 \text{ lb (4008 kN)} \end{aligned}$$

And from Eq. 5.32 we find

$$\begin{aligned}
 M_u &= P_u e = 667,590(11 - 5.95) + (287,250 \times 8) + (81,900 \times 4) \\
 &\quad + (32,200 \times 0) + (12,420 \times 4) + (155,300 \times 8) \\
 &= 7.289 \times 10^6 \text{ lb} \cdot \text{in} \text{ (823.0 kN} \cdot \text{m)}
 \end{aligned}$$

and $e = M_u/P_u = 7.289 \times 10^6/901,200 = 8.09 \text{ in (205 mm)}$. These values represent one combination of P_u and e at failure. The design values of P_u and M_u would be the same values multiplied by the capacity reduction factor ϕ .

Note that by assuming various locations of the neutral axis and by calculating the combinations of P_u and M_u that cause failure for each neutral axis position, an interaction diagram of the type represented by Fig. 5.11 can be traced out for the column section. Since there are several layers of steel however, there will not be a single sharp discontinuity in the interaction diagram at the balanced failure point; rather, a more curved diagram will result because not all the tension steel reaches the yield strength at the same time (see Fig. 5.22).

The foregoing approach for calculating interaction diagrams by determining the combinations of P_u and M_u at failure for various neutral axis locations can also be used for columns of shapes other than rectangular and for walls. However, when the neutral axis depth is small, such as in flanged walls, and the dimensions of the cross section are large, very large tensile strains can occur in the far layers of the tension steel, as indicated in Fig. 5.19. If the maximum strength of the section is to be calculated, it is important to determine whether the tensile strains in these bars is such that the bars have entered the strain-hardening range. If the full stress-strain curve for the steel is known, the actual stresses corresponding to the strain levels can be used in the strength calculations. The additional flexural strength due to strain

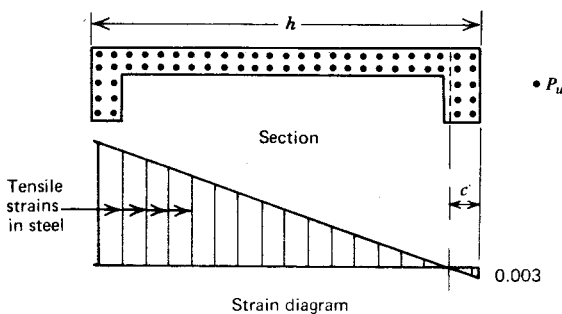


Fig. 5.19. Shear wall section with eccentrically applied ultimate load.

hardening should be taken into account when the resulting overstrength could lead to an alternative brittle failure (e.g., a shear failure rather than a flexural failure). For nonsymmetrical sections or steel arrangements, two interaction curves will result, one for each sense of the eccentricity. Such curves for a shear wall section appear in Fig. 12.12.

5.3.5 Sections with Bars in Circular Array

The ultimate load of sections with bars in a circular array can be determined using the general strain compatibility-equilibrium method of Section 5.3.4. Alternatively, the following approximate equations proposed by Whitney^{5,6,5,8} can be used. The Whitney equations should be used with care, since they do not give accurate results when steel yield strength or steel content is high. In particular, the equations apply strictly only if the compression steel is yielding.

Square Section, Steel Arrayed in a Circle

Figure 5.20 illustrates a square section with steel arrayed in a circle. Whitney suggested that the equations for this case be obtained from the equations for bars at two faces by substituting as below.

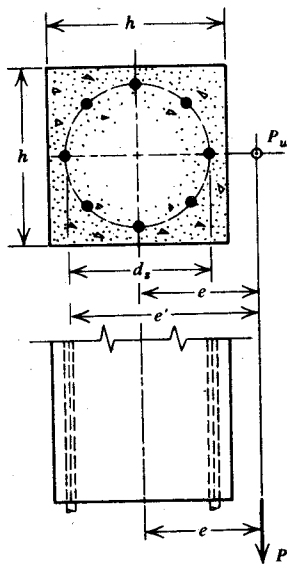


Fig. 5.20. Square section with steel arrayed in circle.

TENSION FAILURE

The equation for tension failure was obtained by substituting $0.5A_{st}$ for A_s and A'_s , f_y for f_s and f'_s , and $0.67d_s$ for $d - d'$, into Eqs. 5.17 and 5.19, ignoring the area of concrete displaced by the compression steel. Then solving Eqs. 5.17 and 5.19 simultaneously, by eliminating a , the design equation becomes

$$P_u = \varphi 0.85h^2 f'_c \left\{ \left[\left(\frac{e}{h} - 0.5 \right)^2 + 0.67 \frac{d_s}{h} \rho_t m \right]^{1/2} - \left(\frac{e}{h} - 0.5 \right) \right\} \quad (5.33)$$

where d_s = diameter of circle through centre of reinforcement, $\rho_t \neq A_{st}/h^2$, A_{st} = total steel area, h = width and depth of section, and $m = f_y/0.85f'_c$.

COMPRESSION FAILURE

The equation for compression failure was obtained by substituting $0.5A_{st}$ for A'_s , $0.67d_s$ for $d - d'$, and $0.5(h + 0.67d_s)$ for d , into Eq. 5.28. The design equation becomes

$$P_u = \varphi \left[\frac{A_{st} f_y}{\frac{3e}{d_s} + 1} + \frac{A_g f'_c}{\frac{12he}{(h + 0.67d_s)^2} + 1.18} \right] \quad (5.34)$$

where A_g is the gross area of the column.

Circular Section, Steel Arrayed in a Circle (Fig. 5.21)

Whitney suggested that the equation for a circular section, with steel arrayed in a circle, be obtained as follows.

TENSION FAILURE

The equivalent compressive stress block has a uniform stress of $0.85f'_c$ and an area A . Whitney assumed that the distance from the center of the section to the centroid of A is given by

$$\bar{x} = 0.211h + 0.293 \left(0.785h - \frac{2A}{h} \right)$$

Assuming that the total steel tension equals the total steel compression, we have

$$P_u = 0.85f'_c A \quad \text{or} \quad A = \frac{P_u}{0.85f'_c}$$

Then

$$\bar{x} = 0.211h + 0.293 \left(0.785h - \frac{2P_u}{0.85h f'_c} \right)$$

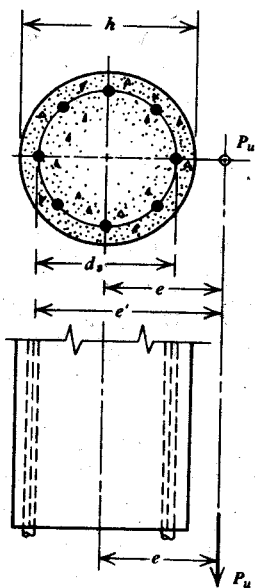


Fig. 5.21. Circular section with steel arrayed in a circle.

Then assuming that $0.4A_{st}$ is the effective steel area in tension and compression and that the effective distance between the resultant tensile and compressive forces in the steel is $0.75d_s$, taking moments about the effective centroid of the tension steel gives

$$P_u(e + 0.375d_s) = P_u(\bar{x} + 0.375d_s) + (0.4A_{st} \times 0.75d_s f_y)$$

Substituting \bar{x} into this equation and solving for P_u , the design equation becomes

$$P_u = \phi 0.85h^2 f_c \left\{ \left[\left(\frac{0.85e}{h} - 0.38 \right)^2 + \frac{\rho_t m d_s}{2.5h} \right]^{1/2} - \left(\frac{0.85e}{h} - 0.38 \right) \right\} \quad (5.35)$$

where d_s = diameter of circle through the center of the reinforcement, $\rho_t = A_{st}/A_g$, A_{st} = total steel area, A_g = gross area of column, h = diameter of column and $m = f_y/0.85f'_c$.

COMPRESSION FAILURE

Whitney adapted Eq. 5.34 for the compression failure case by the approximation of replacing h for the square section by 0.8 of h for the circular section.

The design equation is then

$$P_u = \varphi \left[\frac{A_{st} f_y}{\frac{3e}{d_s} + 1} + \frac{A_g f'_c}{\frac{9.6h}{(0.8h + 0.67d_s)^2} + 1.18} \right] \quad (5.36)$$

Example 5.4

A 20 in (508 mm) square spiral column is to be reinforced by bars arrayed symmetrically in a circle of 16 in (406 mm) diameter between centers. For the concrete, $f'_c = 3000$ psi (20.7 N/mm²) and for the steel $f_y = 40,000$ psi (276 N/mm²). Calculate the steel area required if the section is to carry an ultimate load of 380,000 lb (1690 kN) at an eccentricity of 11.55 in (293 mm) with respect to one major axis of the section. Assume a capacity reduction factor φ of 0.75.

Solution

If tension controls, Eq. 5.33 gives

$$380,000 = 0.75 \times 0.85 \times 20^2 \times 3000$$

$$\times \left\{ \left[\left(\frac{11.55}{20} - 0.5 \right)^2 + \left(0.67 \times \frac{16}{20} \times \frac{40,000}{0.85 \times 3000} \rho_t \right) \right]^{1/2} - \left(\frac{11.55}{20} - 0.5 \right) \right\}$$

$$\therefore \rho_t = 0.0385$$

$$\therefore A_{st} = 0.0385 \times 400 = 15.40 \text{ in}^2 (9935 \text{ mm}^2)$$

If compression controls, Eq. 5.34 gives

$$380,000 = 0.75 \left[\frac{\frac{A_{st} 40,000}{3 \times 11.55}}{16} + \frac{\frac{20^2 \times 3000}{12 \times 20 \times 11.55}}{\frac{(20 + 0.67 \times 16)^2}{(20 + 0.67 \times 16)^2} + 1.18} \right]$$

$$\therefore A_{st} = 17.03 \text{ in}^2 (10,987 \text{ mm}^2)$$

Therefore, compression governs. Require $A_{st} = 17.03 \text{ in}^2 (10,987 \text{ mm}^2)$.

A more exact solution of Example 5.4, involving the use of design charts^{5.9} (see Section 5.3.6), results in a steel area 7% greater than the area just calculated from the Whitney equations. The discrepancy indicates the degree of approximation of the Whitney equations for this particular case. If steel

with a yield strength of 60,000 psi (414 N/mm^2) had been used in the example, the Whitney solution would require $A_{st} = 11.35 \text{ in}^2$ (7323 mm^2), whereas the more exact solution involving the use of design charts would require 21% more steel, indicating that the Whitney solution may err seriously on the unsafe side when high strength steel is used.

5.3.6 Design Charts and Tables

In practice the design and analysis of column sections can be carried out quickly using design charts and tables. A comprehensive series of charts and tables has been published by the ACI.^{5.9, 5.10}

The design charts^{5.9} are sets of interaction diagrams that plot the ultimate load and moment in dimensionless form. Figure 5.22 is a chart for rectangular sections with bars at four faces. Known column size, material strengths, and ultimate load and moment, fix on the chart a coordinate point that defines ρ, m , from which the required area of steel can be calculated. Alternatively, for known column size, material strengths, and area of steel, the possible combinations of ultimate load and moment can be determined. The charts cover the design of rectangular tied columns with bars at two or four faces, and square and circular spiral columns with the bars arranged in a circle. The range of variables covered are $f_y = 40$ to 60 ksi (276 to 414 N/mm^2), $f'_c \leq 4$ to 5 ksi (≤ 27.6 to 34.5 N/mm^2), and $g = 0.6$ to 0.9 ; where g indicates the distance between the groups of bars as a proportion of the section dimension. The charts include the capacity reduction factor, which is taken as 0.7 for rectangular sections, or 0.75 for circular or square sections with steel in a circle. The capacity reduction factor is held constant at the quoted values for all load levels (as was the practice in the 1963 ACI code); thus the charts do not include the increase in the capacity reduction factor (permitted by ACI 318-71^{5.3}) to values up to 0.9 at low axial load. When using the charts, however, an adjustment can be made to account for this difference.

The design tables of the design handbook published in 1973 by the ACI^{5.10} are for rectangular tied columns with bars on four faces and for square and circular spiral columns with the bars arranged in a circle. The range of variables covered in the tables are $f_y = 40$ to 80 ksi (276 to 552 N/mm^2), $f'_c = 3$ to 8 ksi (20.7 to 55.2 N/mm^2), and $g = 0.45$ to 0.9 (g is given the symbol γ in the handbook). The tables list the capacity reduction factor, including the increase to values near 0.9 at low axial loads. Each table is for a given type of column with fixed f_y , f'_c , and γ values. The table gives the longitudinal steel required for various P_u/A_g and eccentricity ratios.

The ACI design charts and tables^{5.9, 5.10} were determined from first principles, using the conditions of equilibrium and compatibility of strains;

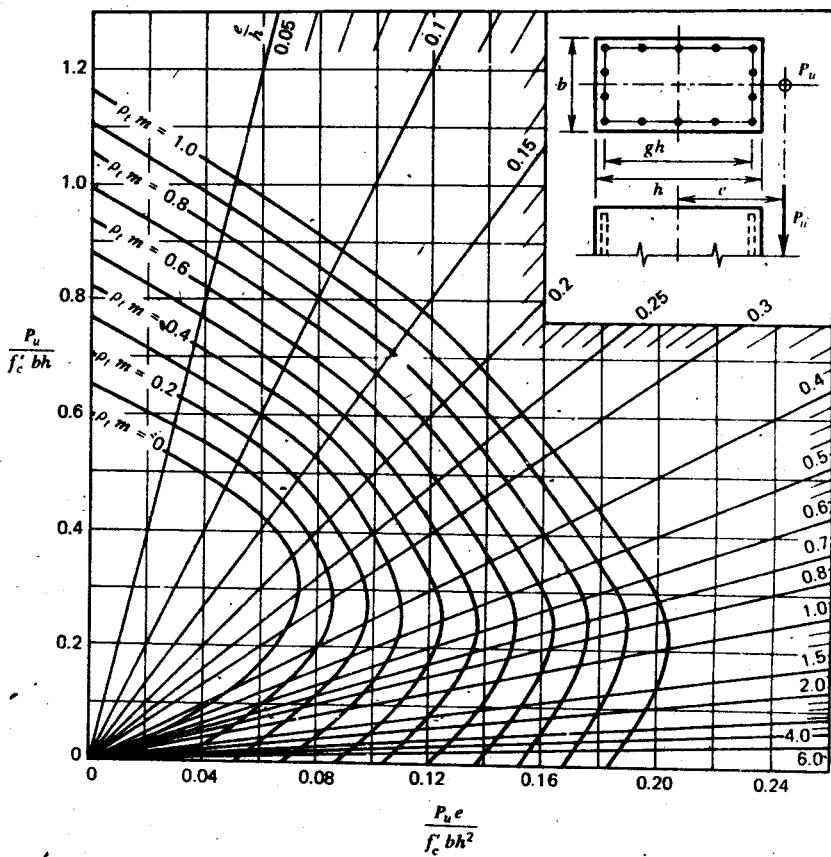


Fig. 5.22. Design chart^{5,9} for an eccentrically loaded reinforced concrete column section with $\phi = 0.7$, $0.25A_{st}$ in each face, $g = 0.7$, $f'_c \leq 4000$ psi (27.6 N/mm 2), and $f_y = 60,000$ psi (414 N/mm 2).

therefore, they take into account the possibility of steel not yielding at ultimate load. Also, the effect of the area of concrete displaced by the compression steel has been included. For all patterns of steel placement, except when it appears on two faces only in the charts for rectangular sections, the steel has been assumed to be uniformly distributed as a thin tubular shape. In square and rectangular columns with steel in four faces, one-quarter of the total steel area is assumed to be placed in each face of the column. It is claimed that the error in assuming that the steel is in the form of a thin tube rather than individual bars is 1% or less when the number of bars exceeds eight.

Example 5.5

A 20 in (508 mm) square tied column with the longitudinal steel evenly distributed at all four faces carries an ultimate load of 536,000 lb (2380 kN) at an eccentricity of 5.75 in (146 mm) with respect to one major axis of the section. The centroid of each bar is 3 in (76 mm) from the near face of the column. Calculate the steel area required if $\phi = 0.7$, $f'_c = 3000 \text{ psi}$ (20.7 N/mm^2), and $f_y = 60,000 \text{ psi}$ (414 N/mm^2).

Solution

Now $g = (20 - 6)/20 = 0.7$. Hence Fig. 5.22 may be used.

$$\frac{P_u}{f'_c b h} = \frac{536,000}{3000 \times 20 \times 20} = 0.447$$

$$\frac{P_u e}{f'_c b h^2} = 0.447 \times \frac{5.75}{20} = 0.1284$$

Referring to the point in Fig. 5.22 displaying these coordinates, and interpolating between the curves, we find $\rho_t m = 0.61$. (Note that the chart includes the required value for ϕ .)

$$\therefore \frac{A_{st}}{b h} \frac{f_y}{0.85 f'_c} = 0.61$$

$$\therefore A_{st} = 0.61 \times \frac{0.85 \times 3000}{60,000} \times 20 \times 20 = 10.4 \text{ in}^2 (6710 \text{ mm}^2)$$

5.4 ECCENTRICALLY LOADED SHORT COLUMNS WITH BIAXIAL BENDING

5.4.1 General Theory

The theory for columns treated thus far has been for loading that causes bending about one major axis of the column only, that is, uniaxial bending. In practice many columns are subjected to bending about both major axes simultaneously, especially the corner columns of buildings.

A symmetrically reinforced concrete column section with biaxial bending, and the strains, stresses, and forces on the section at the ultimate load, are illustrated in Figs. 5.23 and 5.24, respectively. The equations given by strain compatibility and equilibrium may be used to analyze the section. The approach is similar to that used for the biaxial bending of beams in Section

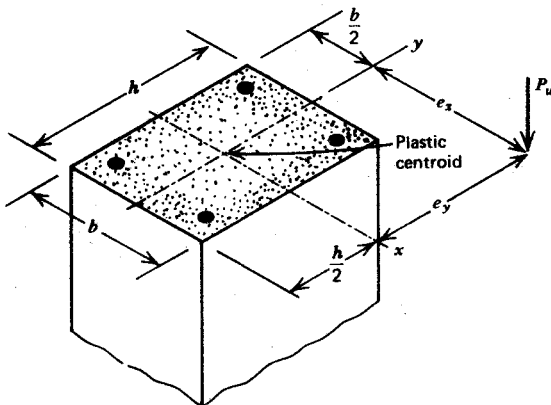


Fig. 5.23. Symmetrically reinforced concrete column section with biaxial bending.

4.4. For a given neutral axis position, the strains, stresses, and forces in the steel can be found from Eqs. 4.64 to 4.72. The resultant force in the concrete depends on the shape of the stress block (see Fig. 4.18). Equations for C_c , \bar{x} , and \bar{y} are given by Eqs. 4.73 to 4.75 and other similarly found equations. Then for symmetrical reinforcement the equilibrium equations can be written with the notation given in Fig. 5.24 as

$$P_u = C_c + S_1 + S_2 + S_3 + S_4 \quad (5.37)$$

$$M_{ux} = P_u e_y = C_c \left(\frac{h}{2} - \bar{y} \right) + (S_1 + S_2) \left(\frac{h}{2} - t_y \right) - (S_3 + S_4) \left(\frac{h}{2} - t_y \right) \quad (5.38)$$

$$M_{uy} = P_u e_x = C_c \left(\frac{b}{2} - \bar{x} \right) + (S_1 + S_3) \left(\frac{b}{2} - t_x \right) - (S_2 + S_4) \left(\frac{b}{2} - t_x \right) \quad (5.39)$$

The appropriate signs (positive for compression, negative for tension) should be substituted into these equations when they are used. If the column has more than four bars, the extra steel forces can be included.

Analysis and design of column sections with biaxial bending are difficult because a trial and adjustment procedure is necessary to find the inclination and depth of the neutral axis satisfying the equilibrium equations. The neutral axis is not usually perpendicular to the resultant eccentricity. In design, a section and reinforcement pattern could be assumed and the reinforcement area successively corrected until the section capacity approached the required value. Therefore, the direct use of the equations in design is impracticable without the aid of an electronic computer.

The strength of columns with biaxial bending can be illustrated by interaction surfaces. The failure line or interaction line of a column with uniaxial

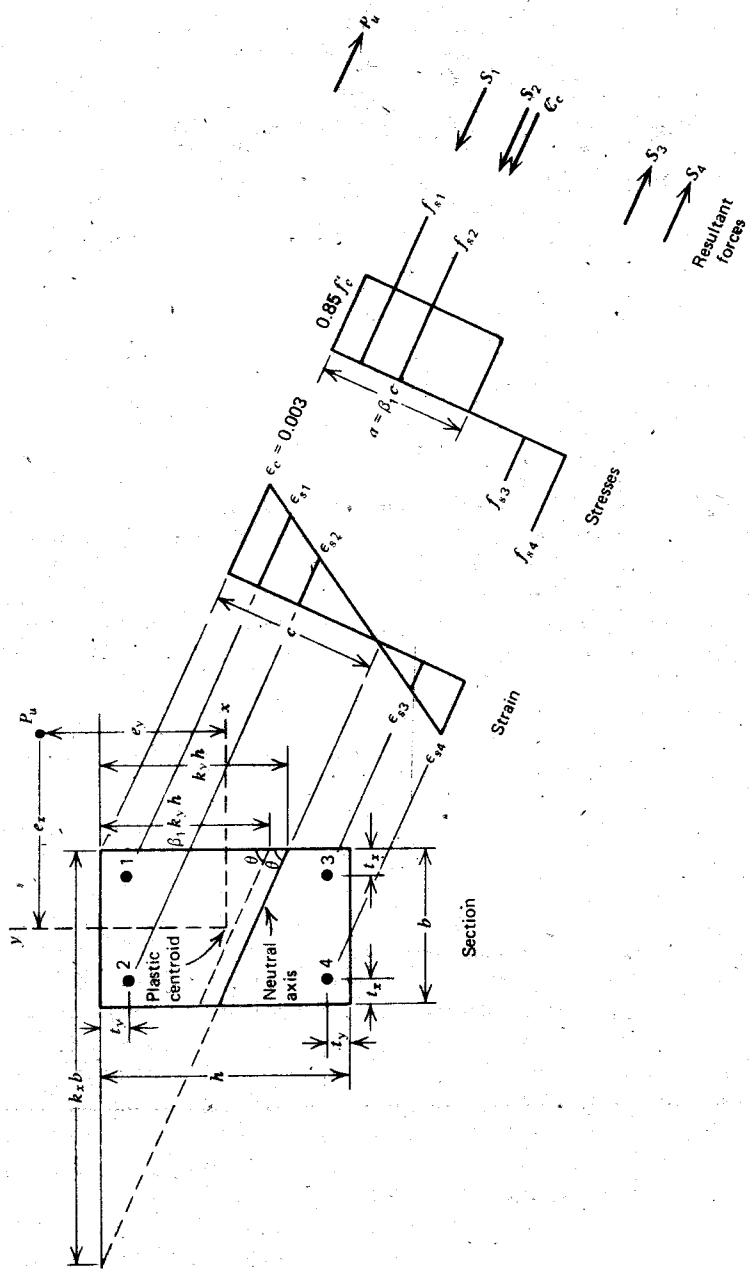


Fig. 5.24. Column section with biaxial bending at the ultimate load.

bending is displayed in Fig. 5.11. By varying the inclination of the neutral axis, it is possible to obtain a series of interaction diagrams at various angles to the major axes of the section. A typical set of interaction diagrams for a given section appears in Fig. 5.25, and a complete set of diagrams for all angles will describe the interaction surface (or the failure surface). Each point on this surface represents one particular set of axial load P_u , and moments about the major axes M_{ux} and M_{uy} , which will together produce failure of the section.

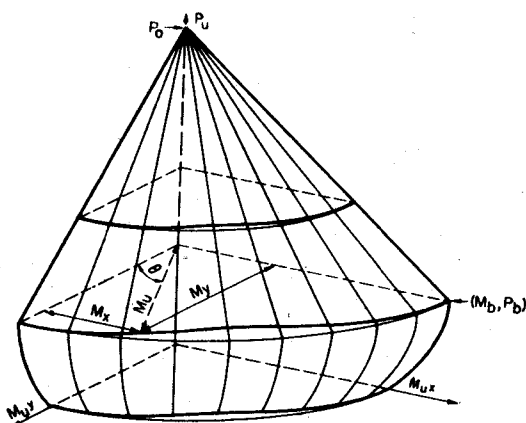


Fig. 5.25. Interaction (failure) surface for a reinforced concrete column with biaxial bending.^{5.11}

If a horizontal section is taken through the interaction surface of Fig. 5.25, the interaction line obtained gives the possible combinations of M_{ux} and M_{uy} that would cause failure at a given axial load P_u . This line is a constant load contour of the interaction surface. Such a line is drawn in Fig. 5.26, and analysis shows its shape to be different from that of an ellipse (or different from a circle in the special case of $M_{ux} = M_{uy}$). For the case of $M_{ux} = M_{uy}$, the deviation of the interaction line from a circular line is greatest for bending at 45° to the major axes. An expression for the shape of the interaction line in the general case is difficult to derive because the shape varies with the section geometry, the strength of the materials, the arrangement and content of steel, and the level of axial load.

It is evident that the preparation of design charts based on the actual interaction surfaces for columns with biaxial bending requires consideration of a large number of variables. Interaction surfaces to cover all possible design cases could not be provided without a large number of charts.

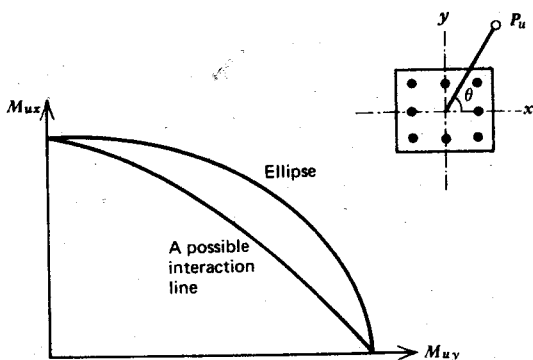


Fig. 5.26. Interaction line for a rectangular column section with biaxial bending under constant P_u .

The complications of the theory has meant that biaxial bending has been treated inadequately or ignored by many designers in practice. However, there are available design approaches for biaxial bending in which the design effort is reduced by the use of simplifying approximations. Some of these approximate methods and their accuracy are discussed in the next section.

5.4.2 Approximate Methods of Analysis and Design for Biaxial Bending

The approximate methods of analysis and design for biaxial bending fall generally under three headings. We begin by discussing methods of superposition.

Methods of Superposition

Some simplified methods of superposition have been suggested that reduce the inclined bending to bending about the major axes of the section, thus allowing the use of procedures for uniaxial bending. These methods have been discussed by Moran^{5,12} for the case of symmetrical reinforcement.

One such method is to determine the reinforcement required for each of the loading cases (P_u, M_{uy}) and (P_u, M_{ux}) separately, adding the resulting reinforcement together. This is equivalent to applying the load first at point 1 and then at point 2 in Fig. 5.27a. This method has no theoretical basis and should not be used, since it may lead to large errors on the unsafe side because the full strength of the concrete is taken into account twice in the design.

Alternatively, we can take any straight line 1-2 passing through the point where P_u is acting (see Fig. 5.27b). The reinforcement required for each of the

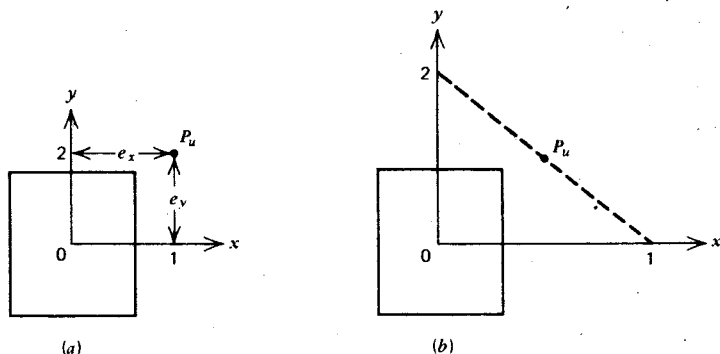


Fig. 5.27. Approximate design methods for biaxial bending.

loading cases P_u at point 1 and P_u at point 2 is determined separately and the resulting reinforcement is added together. This method has been used in the code of Venezuela. According to Moran the results will always lie on the safe side and may be excessively conservative in some cases.

In another method, we replace P_u by two statically equivalent forces P_{ux} and P_{uy} located at points 1 and 2 (see Fig. 5.27b) of the axes. The reinforcement required for each of the loading cases P_{ux} at 1, taking the concrete strength as $f'_c P_{ux}/P_u$, and P_{uy} at 2 taking the concrete strength as $f'_c P_{uy}/P_u$, are determined separately and added together. Although this method has no theoretical support, Moran comments that the solutions obtained in the considered cases seem to be satisfactory.

Method of Equivalent Uniaxial Eccentricity

Figure 5.28 shows an interaction line for a given rectangular column section with biaxial bending under constant ultimate load. Possible combinations of eccentricity for constant ultimate load P_u are given by the line. Therefore, the ultimate load for any point of application (e_y, e_x) on the line is the same as the ultimate load for a point of application with uniaxial eccentricity e_o . This illustrates a possible design approach. If the shape of the interaction line were known, it would be possible to design for the load P_u acting at equivalent uniaxial eccentricity e_o , thus allowing consideration of bending in one direction only.

A number of approximate analytical expressions have been proposed to enable the determination of the equivalent uniaxial eccentricity e_o . For example, Moran^{5,12} quotes the following equation adopted by the 1968 Spanish code.

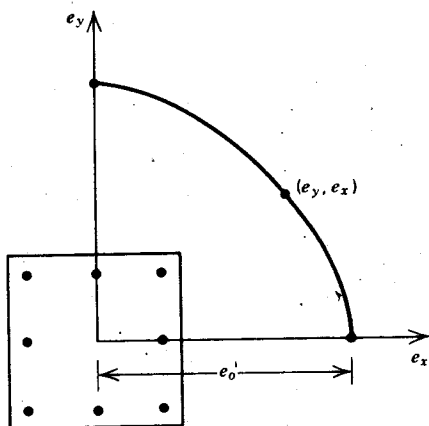


Fig. 5.28. Interaction line for column with biaxial bending under constant P_u .

$$e_o = e_x + \left(\frac{1 - \beta}{\beta} \right) e_y \quad (5.40)$$

where $e_x \geq e_y$ and β is a factor depending on the level of axial load and the steel content, tabulated in the code.

Methods Based on Approximations for the Shape of the Interaction Surface

Various suggestions have been made for the shape of the interaction surface from which, knowing the uniaxial strengths, the biaxial bending strengths may be calculated.

An expression from the Russian code and derived by Bresler^{5.13} for the strength of a biaxially loaded column is

$$\frac{1}{P_u} = \frac{1}{P_{ux}} + \frac{1}{P_{uy}} - \frac{1}{P_o} \quad (5.41)$$

where P_u = ultimate load under biaxial bending, P_{ux} = ultimate load when only eccentricity e_x is present (i.e., load applied at point 1 of Fig. 5.27a), P_{uy} = ultimate load when only eccentricity e_y is present (i.e., load applied at point 2 of Fig. 5.27a), and P_o = ultimate load when there is no eccentricity. This expression has the disadvantage of being more suitable for analysis than for design. Bresler found that the ultimate load predicted by Eq. 5.41 was in excellent agreement with the ultimate loads given by theory and by test results, the maximum deviation from test results found being 9.4%.

Bresler^{5.13} has also suggested that the family of interaction lines corresponding to the various levels of constant load P_u can be approximated by the equation

$$\left(\frac{M_{ux}}{M_{uxo}}\right)^m + \left(\frac{M_{uy}}{M_{uyo}}\right)^n = 1 \quad (5.42)$$

where $M_{ux} = P_u e_y$, $M_{uy} = P_u e_x$, e_x and e_y are the eccentricities of P_u , and M_{uxo} and M_{uyo} are the uniaxial flexural strengths about the x and y axes for the constant load under consideration. The constants m and n depend on the column properties and were determined experimentally.

Parme et al^{5.14} restated Eq. 5.42 as

$$\left(\frac{M_{ux}}{M_{uxo}}\right)^{\log 0.5/\log \beta} + \left(\frac{M_{uy}}{M_{uyo}}\right)^{\log 0.5/\log \beta} = 1 \quad (5.43)$$

where β is the parameter dictating the shape of the interaction line. The effect of different values of β on the shape of the interaction line is represented in Fig. 5.29. Values of β were calculated analytically by Parme et al and are

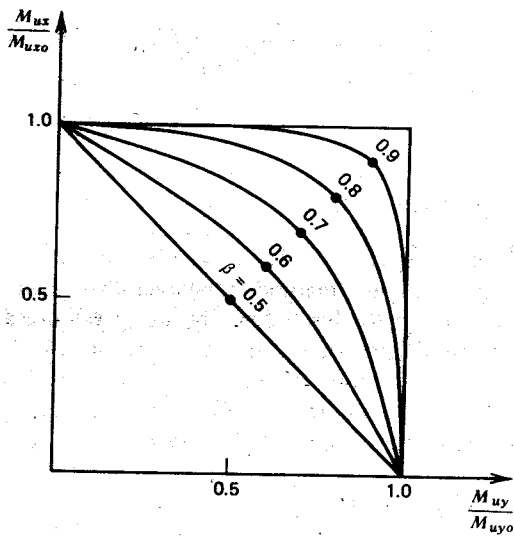


Fig. 5.29. Interaction lines for column with biaxial bending under constant P_u .^{5.14}

given in charts for a range of bar arrangements, steel yield strength, reinforcement index $\rho_t f_y/f'_c$, and P_u/P_o values. These β values, together with the uniaxial values of moment capacity and a diagram such as Fig. 5.29 can be used to determine the biaxial bending capacity of a given column section.

Other suggestions for the shape of the interaction surface have been made

by Pannell^{5.15} and Furlong^{5.11} Meek^{5.16} has suggested that the curved interaction line at constant ultimate load be replaced by two straight lines. For example, if points *A*, *B*, and *C* of Fig. 5.30 are known, the actual curve can be safely replaced by a straight line *AB* and a straight line *BC*.

The British code CP110:1972^{5.17} recommends the use of the interaction Eq. 5.42 with $m = n$ equal to 1.0 at low axial load levels, increasing linearly to 2.0 at high axial load levels. This gives a simple conservative approach.

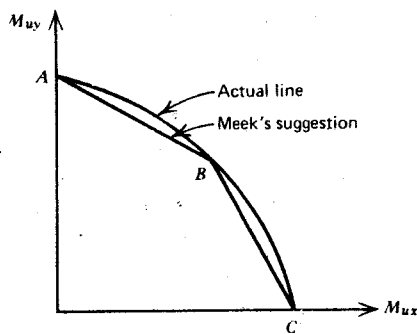


Fig. 5.30. Interaction line for column with constant P_u .

Weber^{5.18} has produced a series of design charts for square columns bending about a diagonal which allows the design or analysis of a section by linear interpolation between bending about a major axis and bending about a diagonal. This approach is similar to Meek's suggestion and appears to be the most practical design method available. Row and Paulay^{5.19} have improved the accuracy of this process by using a more accurate concrete compressive stress distribution and producing design charts for bending about axes inclined at various angles to the major axes, thus allowing linear interpolation between a number of points on the interaction lines. These design charts are described in the next section.

5.4.3 Design Charts

Design Charts of Weber

Weber^{5.18} used the conditions of equilibrium and compatibility of strains to derive from first principles interaction curves of P_u versus $P_u e$ for square columns with the load applied at various eccentricities along the line of a diagonal of the section. The equivalent rectangular stress block derived for rectangular compressed areas was used to approximate the stress block

characteristics of the triangular or near-triangular compressed concrete area. The charts are for $f'_c \leq 4000$ psi (27.6 N/mm²), $f_y = 60,000$ psi (414 N/mm²), $g = 0.6$ to 0.9, and for 4, 8, 12, and 16 bar columns (the bars are considered individually rather than as an equivalent thin tube). The charts include a capacity reduction factor $\varphi = 0.7$. One example of these charts, which have also been published by the ACI,^{5,9} appears in Fig. 5.31.

To use the charts for design given P_u , e_x , and e_y (see Fig. 5.32a) the steps are as follows:

1. Calculate the eccentricity of the resultant bending moment, $e = \sqrt{e_x^2 + e_y^2}$, and the angle θ between the y-direction axis and the direction of eccentricity e , $\theta = \tan^{-1}(e_x/e_y)$, where $e_y \geq e_x$.
2. From the charts, determine steel requirements for $P_u/f'_c h^2$ with $P_u e/f'_c h^3$ acting uniaxially and for $P_u/f'_c h^2$ with $P_u e/f'_c h^3$ acting diagonally.
3. Calculate the steel requirement for $P_u/f'_c h^2$ with $P_u e/f'_c h^3$ acting at angle θ by interpolating linearly between steel contents for $\theta = 0^\circ$ and 45° .

Similarly, when the charts are to analyze sections, the moment capacity at any angle θ can be calculated by linearly interpolating between the uniaxial and the diagonal bending moment capacities.

Good accuracy was indicated by four check calculations made by Weber,^{5,18} who obtained a maximum error of 5.3% for steel area or moment capacity compared with the full theoretical solution using the equivalent rectangular stress distribution.

Example 5.6

A 20 in (508 mm) square tied column with a total of 16 bars evenly distributed at all faces is to carry $P_u = 700,000$ lb (3113 kN) at $e_x = 2.25$ in (57.2 mm) and $e_y = 4.33$ in (110 mm). Find the required steel area if $\varphi = 0.7$, $f'_c = 4000$ psi (27.6 N/mm²), and $f_y = 60,000$ psi (414 N/mm²).

Solution

Eccentricity of the resultant bending moment

$$e = \sqrt{2.25^2 + 4.33^2} = 4.88 \text{ in}$$

Angle between the y-direction axis and the direction of e

$$\theta = \tan^{-1} \frac{2.25}{4.33} = \tan^{-1} 0.520 = 27.46^\circ$$

$$\frac{P_u}{f'_c h^2} = \frac{700,000}{4000 \times 400} = 0.438$$

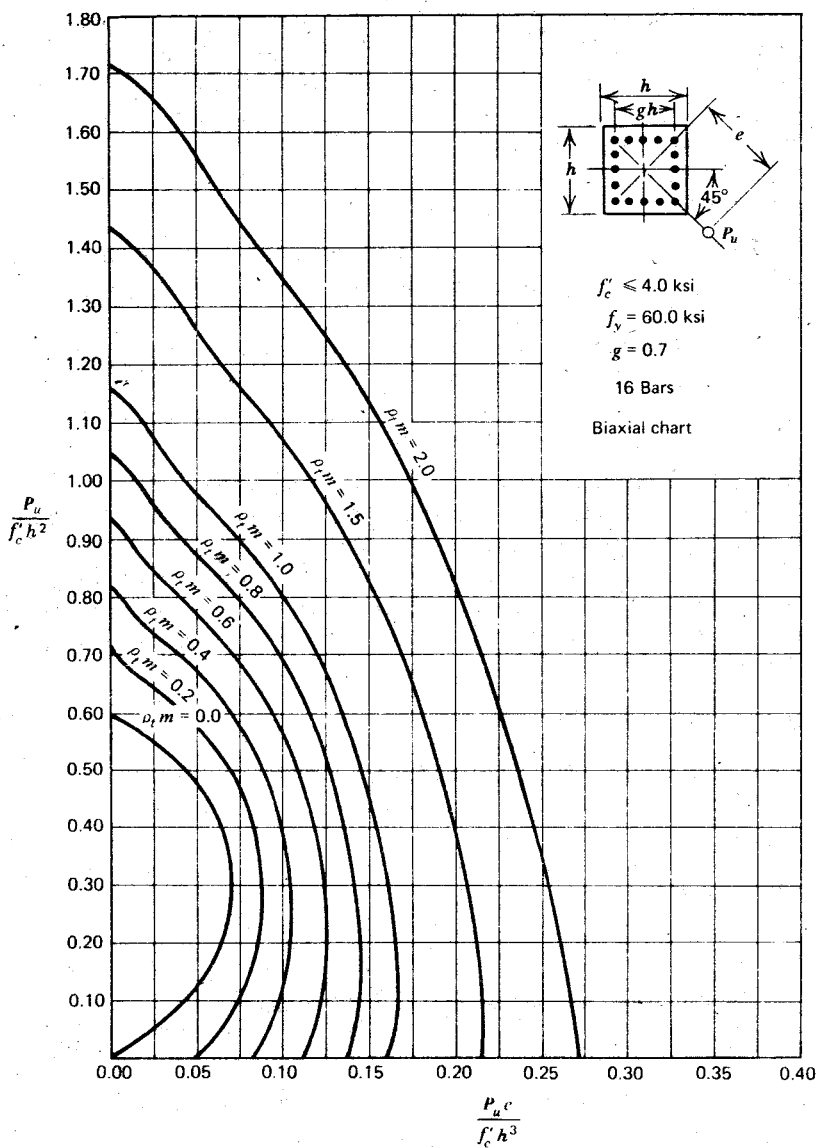


Fig. 5.31. Design chart for an eccentrically loaded square reinforced concrete column section with the load applied along a diagonal.^{5.18, 5.9}

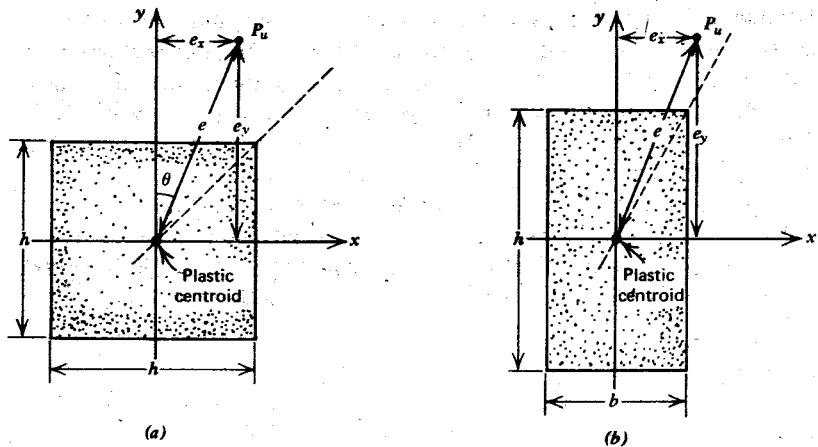


Fig. 5.32. Column sections with biaxial bending. (a) Square section. (b) Rectangular section.

$$\frac{P_u e}{f'_c h^3} = \frac{700,000 \times 4.88}{4000 \times 8000} = 0.1068$$

For the column section, assume that the centroid of each bar is 3 in from the near edge.

$$\therefore g = \frac{20 - 6}{20} = 0.7$$

Therefore, Fig 5.31 and 5.22 may be used.

From Fig. 5.31 ($\theta = 45^\circ$), $\rho_t m = 0.520$, and from Fig. 5.22 ($\theta = 0^\circ$) $\rho_t m = 0.414$. (Note that both charts include the required value for φ .) Interpolating for $\theta = 27.46^\circ$, we have

$$\rho_t m = 0.414 + (0.520 - 0.414) \times \frac{27.46}{45} = 0.479$$

But

$$m = \frac{f_y}{0.85 f'_c} = \frac{60,000}{0.85 \times 4000} = 17.65$$

$$\therefore A_{st} = h^2 \rho_t = \frac{400 \times 0.479}{17.65}$$

$$= 10.9 \text{ in}^2 (7032 \text{ mm}^2)$$

Although Weber's charts were derived for square sections, check calculations have indicated that they may be used for rectangular sections with loading on a diagonal. The ACI publication^{5,9} comments that the charts are equally applicable to rectangular sections with a depth to width ratio (or vice versa) as large as 2, but no guidance is given for the application of the charts to such sections. Fig. 5.32b presents a rectangular section with biaxial bending and indicates the directions of the axes. Note that $M_{ux} = P_u e_y$, and $M_{uy} = P_u e_x$. To use Weber's charts to determine the steel content required for the rectangular section with the loading applied on the diagonal, the following modifications to Weber's parameters could be made:

$$\text{replace } \frac{P_u}{f'_c h^2} \text{ by } \frac{P_u}{f'_c b h}$$

$$\begin{aligned} \text{replace } \frac{P_u e}{f'_c h^3} & \text{ by } \sqrt{\left[\left(P_u e_y/f'_c b h^2\right)^2 + \left(P_u e_x/f'_c b^2 h\right)^2\right]} \\ & = \frac{P_u e_y}{f'_c b h^2} \sqrt{1 + \left(e_x h/e_y b\right)^2} \end{aligned}$$

Similarly, the dimensionless load and moment terms used to find the steel content required for the rectangular section with the load applied on the major axis from uniaxial charts can be taken to be

$$\frac{P_u}{f'_c b h} \quad \text{and} \quad \frac{P_u e_y}{f'_c b h^2} \sqrt{1 + \left(e_x h/e_y b\right)^2}$$

The interpolation method used by Weber must also be modified. Instead of interpolating with respect to the true direction of the eccentricity of the loading, interpolation should be carried out with respect to the angle of the direction of eccentricity of the equivalent square section, given by $\theta' = \tan^{-1}(e_x h/e_y b)$.

Similarly, when the charts are used to analyze sections, the moment capacity at any equivalent angle θ' can be calculated by linearly interpolating between the uniaxial and diagonal values found using the dimensionless load and moment terms just given.

Example 5.7

A rectangular column section (Fig. 5.33) is to carry the loading at the position shown. The section is to be reinforced by 16 bars evenly distributed on all faces. Find the required steel area if $\phi = 0.7$, $f'_c = 4000 \text{ psi}$ (27.6 N/mm^2), and $f_y = 60,000 \text{ psi}$ (414 N/mm^2).

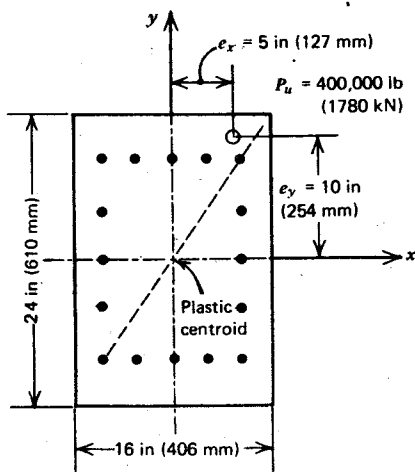


Fig. 5.33. Column section with biaxial bending of Examples 5.7 and 5.8.

Solution

For the section and loading shown we have

$$\frac{P_u}{f'_c b h} = \frac{400,000}{4000 \times 16 \times 24} = 0.260$$

$$\frac{P_u e_y}{f'_c b h^2} \sqrt{[1 + (e_x h / e_y b)^2]} = \frac{400,000 \times 10}{4000 \times 16 \times 24^2} \sqrt{1 + \left(\frac{5 \times 24}{10 \times 16} \right)^2}$$

$$= 0.1085 \times 1.25$$

$$= 0.1356$$

$$\theta' = \tan^{-1} \frac{e_x h}{e_y b} = \tan^{-1} \frac{5 \times 25}{10 \times 16} = \tan^{-1} 0.750 = 36.87^\circ$$

Assume $g = 0.7$ Therefore, Figs. 5.31 and 5.22 may be used. From Fig. 5.31 ($\theta' = 45^\circ$), $\rho_t m = 0.72$, and from Fig. 5.22 ($\theta' = 0$) $\rho_t m = 0.49$. (Note that both charts include the required value for φ .) Interpolating for $\theta' = 36.87^\circ$ gives

$$\rho_t m = 0.49 + (0.72 - 0.49) \times \frac{36.87}{45} = 0.678$$

but

$$m = \frac{f_y}{0.85f'_c} = \frac{60,000}{0.85 \times 4000} = 17.65$$

$$\therefore A_{st} = bh\rho_t = 16 \times 24 \times \frac{0.678}{17.65} \\ = 14.8 \text{ in}^2 (9,548 \text{ mm}^2)$$

It should be noted, however, that interpolation between charts for loading on a diagonal and loading on a major axis for sections with large h/b may introduce significant errors. These errors have been estimated to be as large as 10% on the unsafe side in some cases.^{5.19}

Design Charts of Row and Paulay

The accuracy of the linear interpolation method of Weber may be improved if design charts are available in which the direction of the eccentricity is inclined at various angles to the major axes, allowing interpolation between a number of points on the constant load interaction line. Also, some doubt may be felt about the accuracy of the equivalent rectangular stress block derived for rectangular compressed areas when used for column sections with nonrectangular compressed areas, as has been discussed in Section 3.4.

The direction of the eccentricity e of the load (see Fig. 5.34) may be expressed in terms of a dimensionless parameter $K = e_x h / e_y b$, where $K = 0$ implies loads on the y -direction axis, $K = 1$ implies loads on the diagonal, and $K = \infty$ implies load on the x -direction axis. Charts plotted by Row and Paulay^{5.19} for a number of values for K enable the shape of the interaction surface to be obtained accurately. The charts plot the dimensionless quantities $P_u/f'_c bh$ and $M_{ux}/f'_c bh^2 \sqrt{[1 + (e_x h / e_y b)^2]}$, where $M_{ux} = P_u e_y$, for $f'_c \leq 4000$ psi (27.6 N/mm²), $f_y = 60,000$ psi (414 N/mm²), and g and f are in the range 0.7 to 0.9. The reinforcement is assumed to be uniformly distributed as a thin tube with $0.25A_{st}$ in each face of the section. The charts were calculated from first principles, using the conditions of equilibrium and compatibility of strains and assuming a stress-strain curve for the compressed concrete which is parabolic up to a stress of $0.85f'_c$ at a strain of 0.002, and then has a constant stress of $0.85f'_c$ up to a maximum strain of 0.003 at the extreme compression fiber. The charts do not include the capacity reduction factor φ . An example chart is presented in Fig. 5.35. Interaction curves for four values of K are given in the chart, one in each quadrant of the axes.

To use the charts in design the steps are as follows:

1. Calculate the values of $P_u/f'_c bh$ and $M_{ux}/f'_c bh^2 \sqrt{[1 + (e_x h / e_y b)^2]}$.
2. Calculate $K = e_x h / e_y b$ and determine the angle between the direction

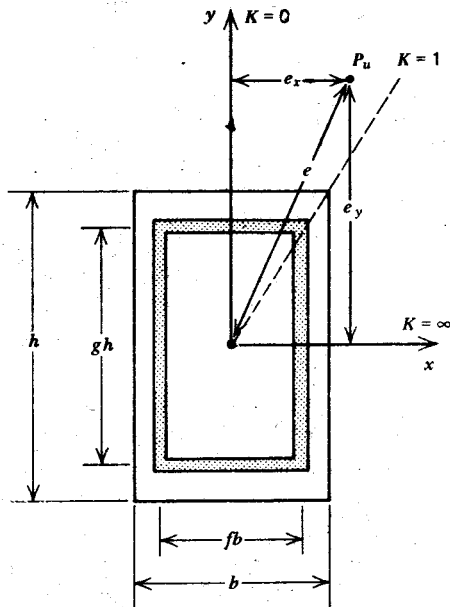


Fig. 5.34. Column section with biaxial bending.

of eccentricity for the equivalent square section and the y -direction axis from $\theta' = \tan^{-1} K$.

3. Determine the steel requirements for the K values lying each side of the calculated K value from the chart. Calculate the θ' value corresponding to each of those K values.
 4. Calculate the steel requirement for the calculated K value by interpolating linearly between the steel contents for the θ' values.

Similarly, when the charts are used to analyze sections, the moment capacity at any angle θ' can be calculated by linearly interpolating between the moment capacities of the adjacent K values. It is claimed^{5:19} that the method of interpolation is accurate to within 2.5%.

Example 5.8

The rectangular column section in Fig. 5.33 is to carry the loading at the position shown. The section is to be reinforced by bars uniformly distributed, with $A_{st}/4$ in each face. Find the required steel area if $\phi = 0.7$, $f'_c = 4000 \text{ psi}$ (27.6 N/mm^2), and $f_s = 60,000 \text{ psi}$ (414 N/mm^2).

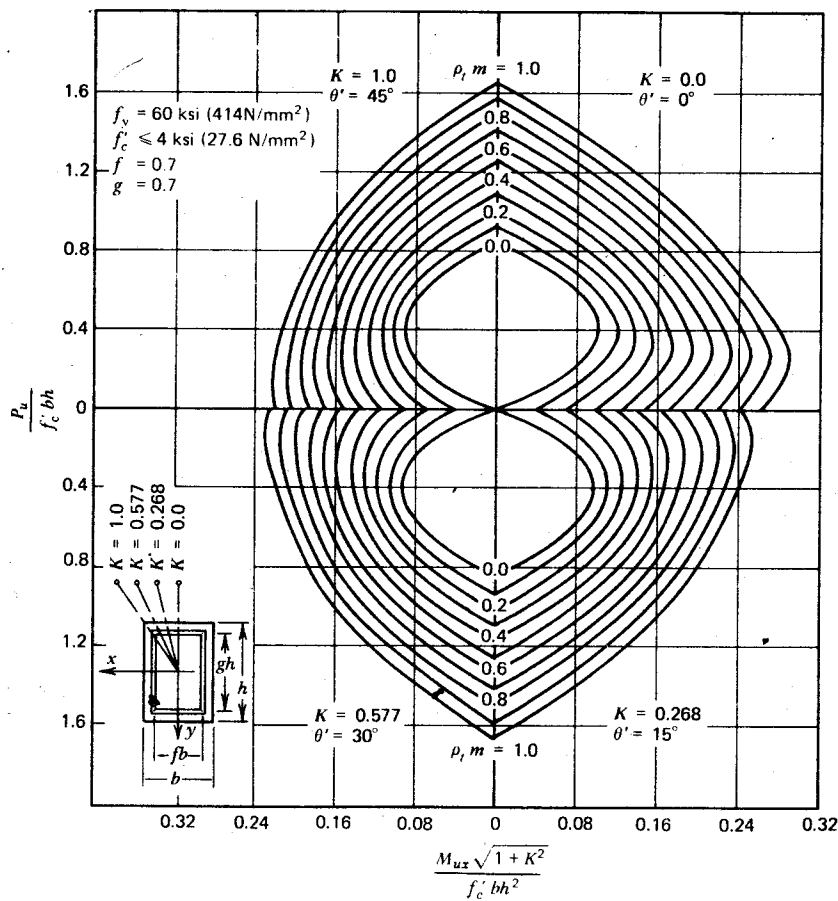


Fig. 5.35. Design chart for a reinforced concrete column section with load applied at various angles of eccentricity.^{5.19}

Solution

Design values of $P_u = 400,000/\varphi = 400,000/0.7 = 571,400$ lb

$$\frac{P_u}{f'_c b h} = \frac{571,400}{4000 \times 16 \times 24} = 0.372$$

$$\frac{M_{ux}}{f'_c b h^2} \sqrt{1 + (e_x h / e_y b)^2} = \frac{571,400 \times 10}{4000 \times 16 \times 24^2} \sqrt{1 + \left(\frac{5 \times 24}{10 \times 16}\right)^2} \\ = 0.155 \times 1.25 \\ = 0.194$$

$$K = \frac{e_x h}{e_y b} = \frac{5 \times 24}{10 \times 16} = 0.750 \quad \therefore \theta' = \tan^{-1} 0.75 = 36.87^\circ$$

Assume $g = f = 0.7$. Therefore, Fig. 5.35 may be used. The steel content for $K = 0.75$ may be obtained by interpolating between the curves for $K = 0.577$ and $K = 1.0$.

For $K = 0.577$ ($\theta' = \tan^{-1} 0.577 = 30^\circ$), from Fig. 5.35 $\rho_t m = 0.79$; for $K = 1.0$ ($\theta' = \tan^{-1} 1.0 = 45^\circ$), from Fig. 5.35 $\rho_t m = 0.83$.

Interpolating for $\theta' = 36.87^\circ$ gives

$$\rho_t m = 0.79 + (0.83 - 0.79) \frac{36.87 - 30}{45 - 30} = 0.808$$

But

$$m = \frac{f_y}{0.85 f'_c} = \frac{60,000}{0.85 \times 4000} = 17.65$$

$$\therefore A_{st} = b h \rho_t = 16 \times 24 \times \frac{0.808}{17.65} \\ = 17.6 \text{ in}^2 (11,350 \text{ mm}^2)$$

The steel content found in Example 5.8 using Row and Paulay's chart is greater than the steel content determined for the same section and loading in Example 5.7 using Weber's method. This difference is mainly due to the concrete compressive stress distribution assumed and the method of interpolation. Weber found the resultant concrete force and its position for non-rectangular compressed areas using the equivalent rectangular stress block derived for rectangular compressed areas, a procedure which may lead to some error as discussed in Section 3.4. Row and Paulay used an assumed stress-strain curve for the concrete to derive the resultant concrete force and its position, which is a more accurate approach. Note however that the stress-strain curve adopted by Row and Paulay is conservative in that the concrete compressive force given by it for uniaxial bending is $8\frac{1}{2}\%$ less than that for the equivalent rectangular stress block for $f'_c \leq 4000 \text{ psi}$ (27.6 N/mm^2). Also, Row and Paulay assumed a maximum concrete strain of 0.003, as did Weber, as this will lead to a conservative result because at the maximum load the strain at the extreme fiber of a triangular compressed area will be larger (see Section 3.4). The combined effect of error from the linear interpolation between diagonal and uniaxial loading and differences in the assumed concrete stress distribution are responsible for the 19% difference in the steel areas calculated in Examples 5.7 and 5.8. Similarly, reworking Example 5.6 using Row and Paulay's charts indicates that 20%

more steel is required than by Weber's method. It is evident that Row and Paulay's method will give a conservative result whereas Weber's method may lead to errors on the unsafe side.

5.5 SLENDER COLUMNS

5.5.1 Behavior of Slender Columns

The slenderness of a column may result in the ultimate load being reduced by lateral deflections of the column caused by bending. This effect is illustrated in Fig. 5.36 for the particular case of an initially straight column with bending in single curvature caused by load P applied with equal eccentricity e at each

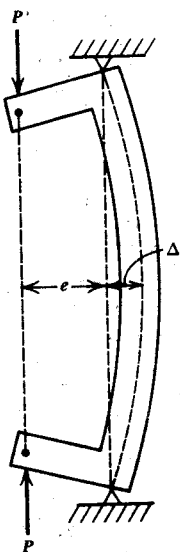


Fig. 5.36. Eccentrically loaded slender column.

end. The bending deformation of the column causes the eccentricity of the load at the critical section to become $e + \Delta$, where Δ is the additional eccentricity due to lateral deflection at that section. Hence the maximum bending moment increases to $P(e + \Delta)$. This is commonly referred to as the $P\Delta$ effect. The importance of lateral deflections due to bending depends on the type of loading on the column and the end conditions. The $P\Delta$ moment, referred to here as the additional moment, has sometimes been called the

Slender Columns

secondary moment, but that term tends to imply that the moment is of secondary importance, whereas in some cases it may be of considerable significance.

A short column is defined as one in which the ultimate load is not reduced by the bending deformations because the additional eccentricities Δ are either negligible or occur away from the critical section. A slender column is defined as one in which the ultimate load is reduced by the amplified bending moment caused by additional eccentricity.

The behavior of the column shown in Fig. 5.36 under increasing load is illustrated on the interaction diagram for the critical section of the column given in Fig. 5.37. If the additional eccentricity Δ is negligible, the maximum

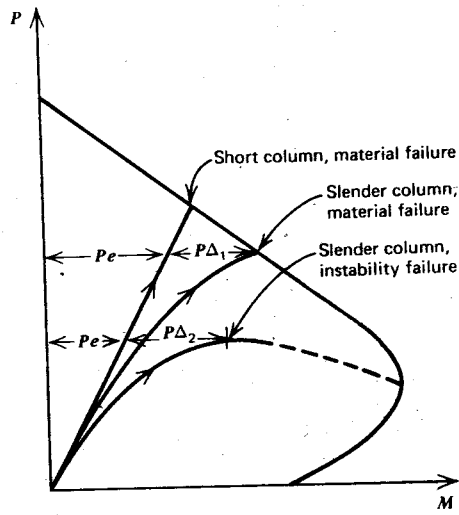


Fig. 5.37. Interaction diagram for a reinforced concrete column section illustrating short and long column P - M behavior up to failure.

moment M will equal P_e at all stages and a linear P - M path will be followed with increasing load. This is short column behavior, and a material failure of the section eventually occurs when the interaction line is reached. If the column is slender, the maximum moment M will equal $P(e + \Delta)$, and because Δ increases more rapidly at high load levels, the P - M path will be curved. Two types of slender column behavior may occur. First, a column may be stable at lateral deflection Δ_1 but having reached the interaction line a material failure of the section occurs. This type of failure generally occurs in practical columns of buildings that are braced against sway. Second, if the column is very slender it may become unstable before reaching the interaction line. This instability failure may occur in unbraced columns.

Slender column behavior for particular loading and end conditions can be illustrated further by the use of slender column interaction diagrams. Figure 5.38 reveals the construction of such a diagram as illustrated by MacGregor et al.^{5,20} Figure 5.38a is the interaction diagram for the critical section of a column of the type shown in Fig. 5.36. Short and slender column behaviors are illustrated. The slender column has an unsupported length to section thickness ratio of $l_u/h = 30$. Failure of the slender column occurs at the point *B* under the load and amplified moment. The load and primary moment P_e at failure are given by the point *A*. The point *A* can be determined for a range of e/h and l_u/h values, and the family of curves in Fig. 5.38b may be traced, giving the load P and primary moment P_e which cause failure of the column. Such diagrams are useful in indicating the reduction in strength due to slenderness for various loading cases.

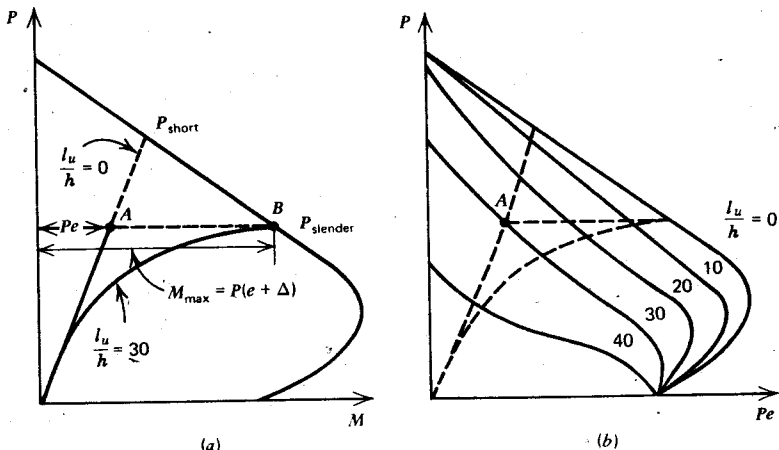
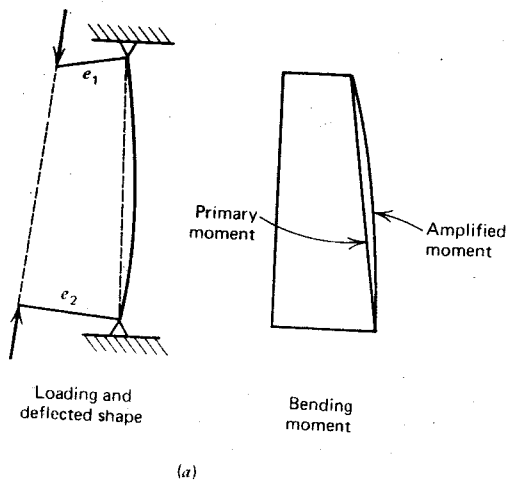
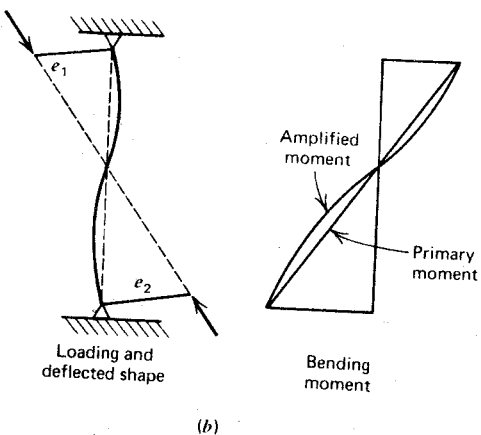


Fig. 5.38. Construction of slender column interaction diagrams.^{5,20} (a) Slender column behavior. (b) Slender column interaction diagrams.

Hinged end columns braced against sidesway with loading causing single and double curvature are illustrated in Fig. 5.39. For both cases of loading, the bending deformations cause additional moments, but the additional moments do not amplify the maximum primary moments that occur at the ends of the columns. However, if the additional moments are large, the maximum moments may move from the ends to within the height of the columns. It is evident that there is more likelihood of the maximum bending moment being increased by additional moment in the single curvature case than in the double curvature case, because in the former the lateral deflections will be greater and the primary moments are near maximum over a larger part of the



(a)

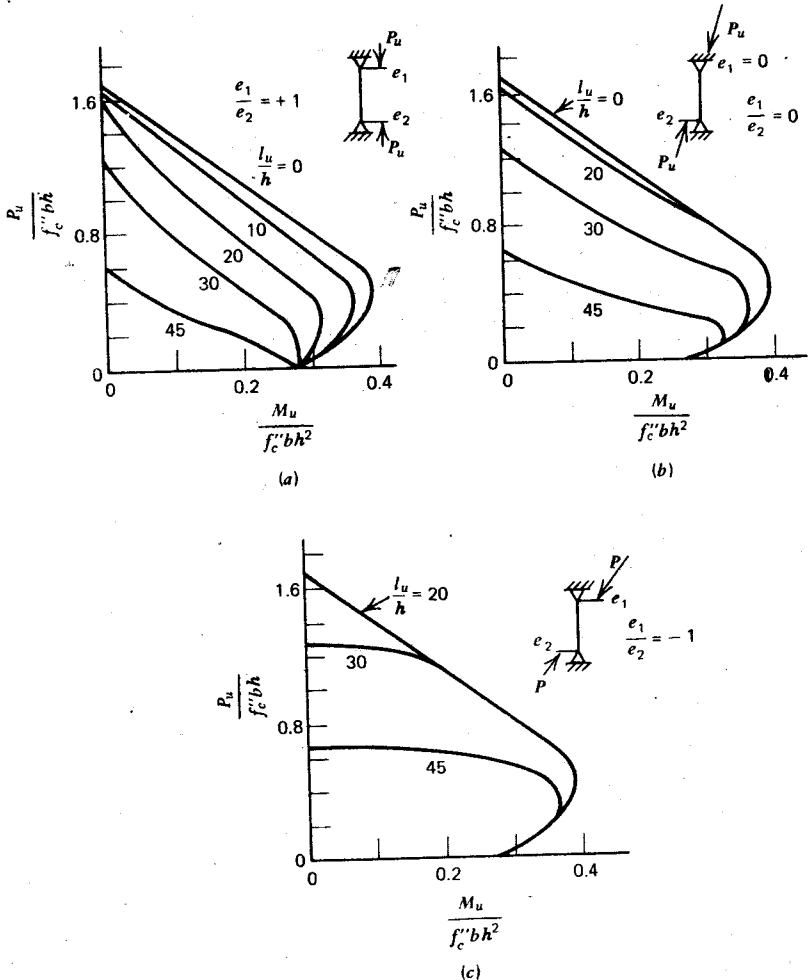


(b)

Fig. 5.39. Amplified moments in columns braced against sidesway. (a) Single curvature.
(b) Double curvature.

column. This is illustrated in the slender column interaction diagrams by MacGregor et al^{5,20} (Fig. 5.40); we can see that the greatest reduction in ultimate load occurs when the end eccentricities are equal and of the same sign, and the smallest reduction in ultimate load occurs when the end eccentricities are equal but of opposite sign.

If columns are not braced against sidesway, the maximum additional moments will be induced at the ends of the columns, and the increase in



Note: M_u = maximum end moment at failure

f_c'' = compressive strength of concrete in columns

Fig. 5.40. Effect of type of curvature on slender column interaction diagrams.^{5.20}

the maximum bending moment may be very significant. The increase in moment for a fixed end column with sidesway is illustrated in Fig. 5.41. It is evident that if the ends of the column are not fully restrained against rotation, but are elastically restrained at the ends, some end rotation will occur; then because of the increased flexibility, the sidesway displacement—hence the additional moments—will be increased.

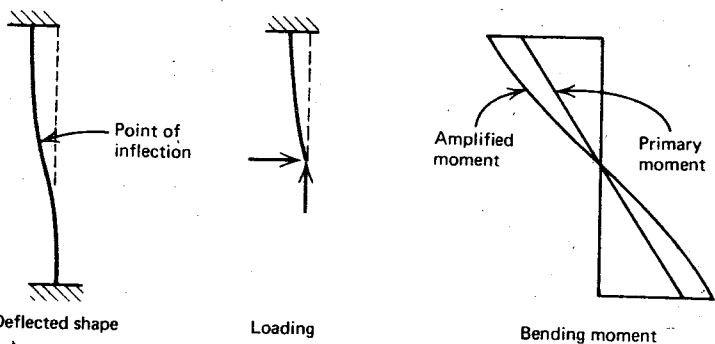
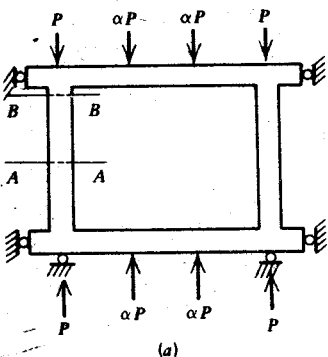
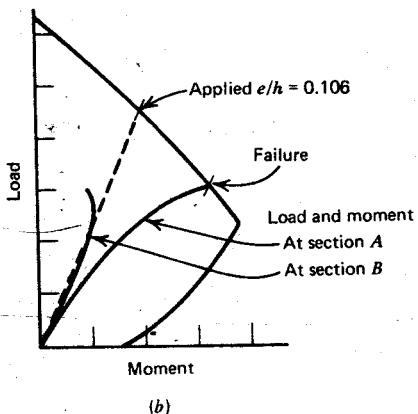


Fig. 5.41. Amplified moment in column with sidesway.

The end moments in columns of frames depend on the relative stiffnesses of the columns and the beams. During loading the stiffness of beams and columns is reduced by cracking of concrete and later by inelastic deformations. The stiffness of columns is also reduced by the additional moments caused by lateral deflection of the columns. Thus changes in column moments will occur during loading due to the additional moments caused by deflection and due to the changes in relative stiffness. The column moments may increase or decrease. For example, for a short column in a braced frame the reduction in column end moments due to the reduction in stiffness may be greater than the increase in moment due to deflections, and the maximum moment will decrease, resulting in an increase in the load capacity. For a slender column in a braced frame, however, the moments due to deflection tend to increase more rapidly than the restraint moments, and the maximum moment will increase resulting in a decrease in the load capacity. Figure 5.42a shows a braced frame tested by Furlong and Ferguson.^{5.21} The columns had an l_w/h ratio of 20 and were loaded in single curvature with $e/h = 0.106$. Failure occurred at section A at the midheight of a column. Figure 5.42b is the interaction diagram for the column section with the P - M paths



(a)



(b)

Fig. 5.42. Behavior of a column in a frame tested by Furlong and Ferguson.^{5,21} (a) Test specimen. (b) Measured load-moment response.

measured during the loading at sections *A* and *B*. Although the loads *P* and αP were proportionally applied, the variation of moment at *B* with increasing load is nonlinear, the moment eventually decreasing with increasing load because the column stiffness decreased more quickly than the beam stiffness. The moment at *A* included the additional moment due to column deflection, and as was expected for this section, there was an increase of moment at all stages with loading. It is evident that increasing the degree of rotational restraint at the ends of columns in braced frames by increasing the beam stiffness increases the strength of the columns.

In a frame in which sidesway can occur, if the beams are quite flexible the column tends to act as a rigid body, and the frame deflects laterally due primarily to bending in the beams. If the beams are stiff the amount of sway

will depend more on the bending of the columns. In frames free to sway, increasing the degree of rotational restraint at the ends of columns by increasing the beam stiffness will increase the strength of the columns. However, if the beams yield, hence cannot restrain the columns against sway, an unstable mechanism results.

The foregoing brief review of column behavior indicates that the major variables affecting the strength of slender columns are as follows:

1. The ratio of unsupported height to section depth l_u/h , the end eccentricity ratio e/h , and the ratio and signs of the end eccentricities. The effect of these variables on columns with pinned ends is illustrated in Fig. 5.40.
2. The degree of rotational end restraint. The stiffer the connecting beam system, the greater the column strength.
3. The degree of lateral restraint. A column unbraced against end displacement is significantly weaker than a braced column.
4. The content of steel reinforcement and the strength of the materials. These affect the strength and flexural rigidity of the column section.
5. The duration of loading. Creep of concrete during sustained loading increases the column deflections, hence will normally decrease the strength of slender columns.

5.5.2 "Exact" Design Approach for Slender Columns

The design of compression members can be based on the moments and forces found from a second-order analysis of the structure, taking into account the actual stiffnesses of members, the effects of deflections on moments and forces, and the effects of duration of loading. The sections may be proportioned to resist these actions without modification because the effect of column slenderness has been taken into account in the determination of the actions.

The main factor to be included in this second-order analysis is the $P\Delta$ moment due to lateral deflections of the columns of the structure. Methods for carrying out such analyses have been summarized by MacGregor.^{5.22} The structure may be idealized as a plane frame with linear elements. Realistic moment-curvature relationships must be used to provide accurate values for deflections and additional moments, and the effect of axial load on the rotational stiffness of compression members should be considered. The maximum moments determined will include the effect of frame deflections and rotations.

Use of such an analysis to determine column actions for section design is the most rational approach, but because of its complexity the analysis depends on the availability of suitably written computer programs.

5.5.3 Approximate Design Approach for Slender Columns: The Moment Magnifier Method

If conventional first-order structural analysis, based on approximate relative stiffnesses and on ignoring the effect of lateral deflections of members, is used to determine the moments and forces in a frame, the actions so found must be modified to allow for second-order effects. The sections are then proportioned to resist the modified actions. The design procedure given in ACI 318-71^{5.3} for this purpose is the moment magnifier method, which is similar to that used in the American Institute of Steel Construction specification.^{5.23}

The Method

The moment magnifier method is illustrated on the interaction diagram of Fig. 5.43. Let the ultimate column load and moment to be resisted, found using a first-order elastic frame analysis, be P_u and $M_u = P_u e$. Then the load and moment used in the design of the section are P_u and δM_u , where δ is the moment magnification factor.

The moment magnification factor δ is given by the following relationship^{5.3}

$$\delta = \frac{C_m}{1 - \frac{P_u}{\varphi P_c}} \geq 1 \quad (5.44)$$

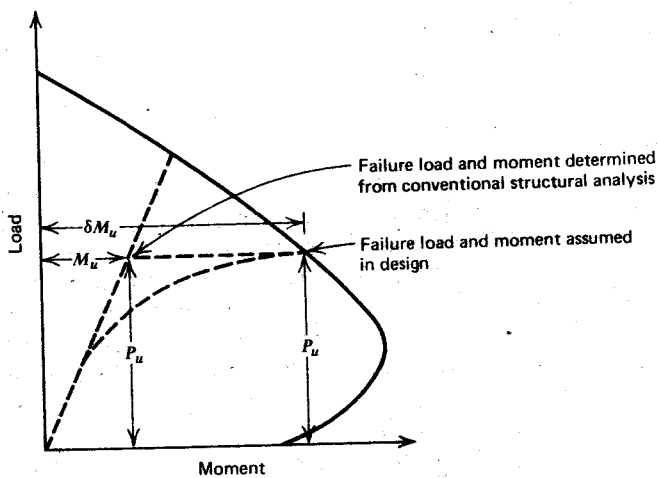


Fig. 5.43. Moment magnifier design method.

where C_m = end effect factor to be taken as $0.6 + 0.4(M_1/M_2) \geq 0.4$ for columns braced against sidesway and without transverse loads between supports, or $C_m = 1.0$ for other cases

M_1 = smaller of the ultimate moments at the ends of the column, found in the first-order analysis, positive if member is bent in single curvature, negative if bent in double curvature

M_2 = larger of the ultimate moments at the ends of the column, found in the first-order analysis, always positive

P_u = ultimate load on column

ϕ = capacity reduction factor

$$P_c = \frac{\pi^2 EI}{(kl_u)^2} \quad (5.45)$$

= theoretical Euler elastic critical buckling load

k = effective length factor for columns, varying between 0.5 and 1.0 for frames braced against sidesway and being greater than 1.0 for unbraced frames

l_u = unsupported length of column

$$EI = \frac{E_c I_g}{2.5} \frac{1}{1 + \beta_d} \quad (5.46)$$

or

$$EI = \left(\frac{E_c I_g}{5} + E_s I_s \right) \frac{1}{1 + \beta_d} \quad (5.47)$$

= flexural rigidity of column section

E_c = modulus of elasticity of concrete, given by Eq. 2.1

I_g = moment of inertia of gross concrete section of the column about centroidal axis, ignoring the reinforcement

E_s = modulus of elasticity of steel

I_s = moment of inertia of reinforcement about centroidal axis of the column cross section

β_d = concrete creep factor equal to ratio of maximum design dead load moment to maximum design total load moment, always positive, and in the range $0 \leq \beta_d \leq 1$. There are a number of cases where this definition of β_d breaks down (for example, minimum eccentricity, moments of different sign, etc) and it would appear that a more satisfactory definition would be to take β_d as the ratio of maximum design dead load to maximum design total load.

The equations for the moment magnifier factor δ and the flexural rigidity EI , and methods for calculating the effective length factor k , are briefly discussed in the following sections.

The Moment Magnification and End Effect Factors, δ and C_m

In the elastic range, an approximation for the maximum bending moment in columns with equal end moments bent in single curvature is given by

$$M_{\max} = \frac{M_o}{1 - (P/P_c)} \quad (5.48)$$

where M_o is the maximum moment from first-order analysis ($M_o = Pe$ in Fig. 5.36), P_c is the elastic critical load for buckling in the plane of the applied moment, and P is the applied load. In this case the maximum moment and the maximum column deflection occur at midheight. The exact value for M_{\max} for this case is given by the secant formula, which according to texts on the strength of materials^{5,24} is

$$M_{\max} = M_o \sec\left(\frac{\pi}{2} \sqrt{\frac{P}{P_c}}\right) \quad (5.49)$$

Equations 5.48 and 5.49 are compared for various P/P_c ratios in Table 5.1. The approximate Eq. 5.48 gives maximum moments that are somewhat on

Table 5.1 Comparison of M_{\max}/M_o Values

P/P_c	0.1	0.2	0.3	0.4	0.5	0.6	0.8	1.0
From approximate equation 5.48	1.11	1.25	1.43	1.67	2.00	2.50	5.00	∞
From secant equation 5.49	1.14	1.31	1.53	1.83	2.25	2.88	6.05	∞

the low side, but the agreement is better in the usual range of low P/P_c values, being within 11% for $P/P_c \leq 0.5$. Thus the simple approximate Eq. 5.48 has been recommended for columns bent in single curvature by equal end moments.

If the end moments are unequal, Eq. 5.48 becomes overconservative, especially when the end moments are not of the same sign. For the case of unequal end moments, the maximum column moment can be estimated by replacing M_o by an "equivalent uniform moment" $C_m M_o$, which leads to the same slender column strength as that obtained from the actual moment pattern. Thus Eq. 5.48 becomes

$$M_{\max} = \frac{C_m M_o}{1 - (P/P_c)} \quad (5.50)$$

The equation for C_m adopted,^{5.3} $0.6 + 0.4(M_1/M_2) \geq 0.4$, is from the American Institute of Steel Construction specification,^{5.23} and its accuracy may be seen compared with other relevant equations in the Column Research Council Guide.^{5.24} Equation 5.44 for δ is the design form of M_{max}/M_0 from Eq. 5.50.

The Flexural Rigidity EI

In the calculation of the critical buckling load of the column P_c for Eq. 5.44, the flexural rigidity EI of the section is required. The value of EI used should allow for the effects of cracking, creep, and nonlinearity of the concrete stress-strain curve. The values of EI given by Eqs. 5.46 and 5.47 may be used when more accurate values are not available. These equations were obtained from theoretical considerations and test results by MacGregor et al.,^{5.20} they represent lower limits to EI for practical cross sections. Hence these EI values are conservative for calculation of additional moments. In Fig. 5.44 Eqs. 5.46 and 5.47 are compared with EI values derived theoretically from moment-curvature diagrams for the case of short-term loading. The simpler Eq. 5.46 is reasonable for lightly reinforced columns, but it greatly underestimates the effect of the reinforcement in heavily reinforced columns. Equation 5.47 is more accurate but requires prior knowledge of the steel content. Creep due to sustained load reduces the EI value and is accounted for approximately by the term $(1 + \beta_d)$ in Eqs. 5.46 and 5.47.

The Effective Length of Compression Members kl

The effective length factor k used in design must take into account the degree of lateral and rotational restraint at the ends of columns. Figures 5.45 and 5.46 display effective lengths for end conditions without and with sidesway.

Figure 5.47 illustrates buckling modes for frames braced and unbraced against sidesway. Columns in frames braced against sidesway have values for k ranging between 0.5 and 1.0. The value of k always exceeds unity in frames that can sway. Because the behaviors of braced and unbraced frames are so different, values of k are normally given for frames in these two categories, and the designer must decide whether his frame is braced or unbraced. Fully braced or unbraced frames seldom occur in practice. The Commentary^{5.26} on ACI 318-71 recommends that columns be regarded as being braced against sidesway if that story contains shear walls or other types of lateral bracing having a total stiffness resisting lateral movement in the story of at least six times the sum of the stiffness of all the columns resisting lateral movements in the story. Thus the designer must exercise his judgment.

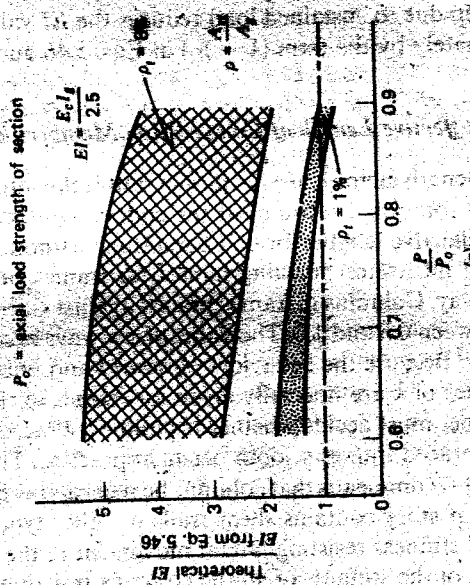
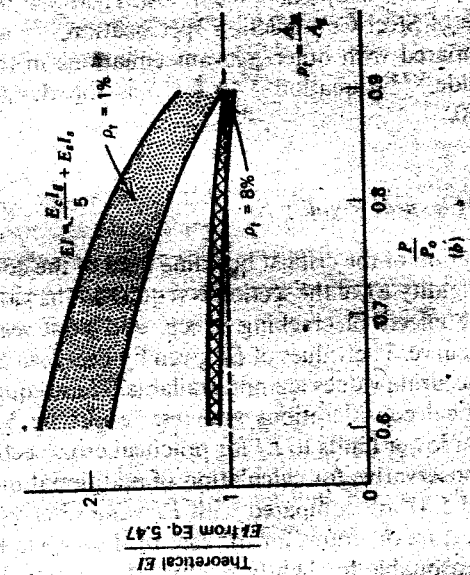


Fig. 5.44. Comparison of equations for flexural stiffness with theoretical values from moment-curvature diagrams: (a) Equation 5.46 (b) Equation 5.47.

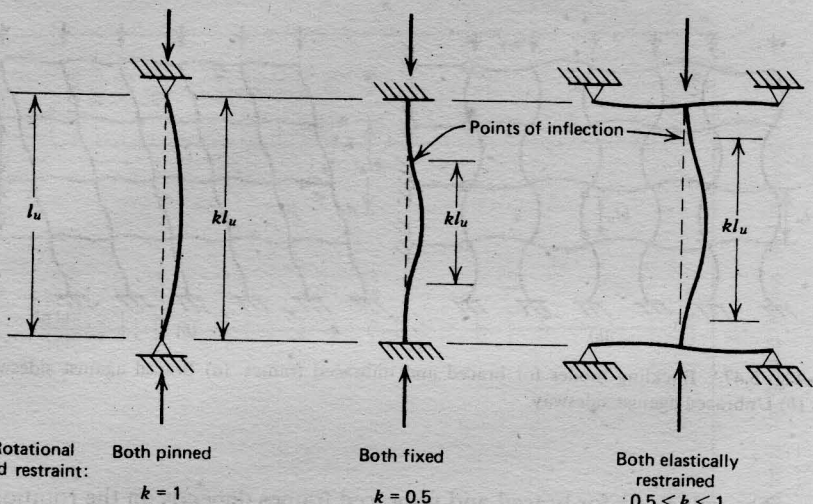


Fig. 5.45. Effective length of columns with sidesway prevented.

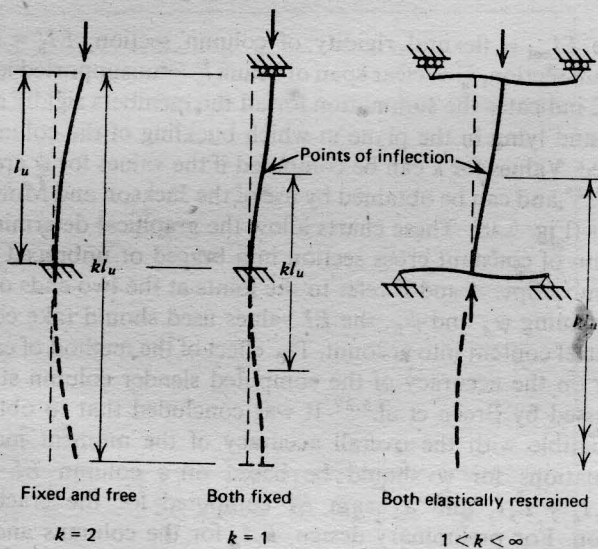


Fig. 5.46. Effective length of columns with sidesway permitted.

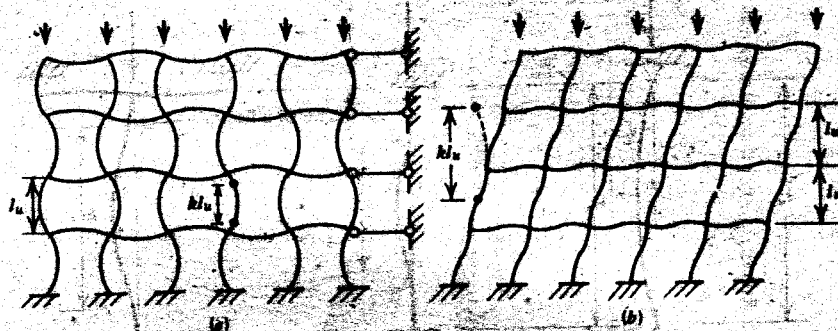


Fig. 5.47. Buckling modes for braced and unbraced frames. (a) Braced against sidesway. (b) Unbraced against sidesway.

The value of k for braced and unbraced frames depends on the rotational restraint at the joints as expressed by the parameter ψ , where

$$\psi = \frac{\sum (EI_{col}/l_u)}{\sum (EI_b/l_u)} \quad (5.51)$$

where EI_{col} = flexural rigidity of column section, EI_b = flexural rigidity of beam section, l_u = clear span of beam, l_u = unsupported length of column, and Σ indicates the summation for all the members rigidly connected at the joint and lying in the plane in which buckling of the column is being considered. Values for k can be computed if the values for ψ are known at each joint^{5.25} and can be obtained by use of the Jackson and Moreland alignment charts (Fig. 5.48). These charts allow the graphical determination of k for a column of constant cross section in a braced or unbraced multibay frame. The subscripts A and B refer to the joints at the two ends of the column. In determining ψ_A and ψ_B , the EI values used should take concrete cracking and steel content into account. The effect of the method of calculating the EI value on the accuracy of the computed slender column strength has been discussed by Breen et al.^{5.27} It was concluded that to obtain an accuracy compatible with the overall accuracy of the moment magnifier method, calculations for ψ should be based on a column EI computed from $0.2E_c I_g + E_s I_s$ and a beam EI computed for the cracked transformed section. For preliminary design, $E_c I_g$ for the columns and $0.5E_c I_g$ for the beams may be used, where I_g is the moment of inertia of the gross concrete section about the centroidal axis, ignoring the reinforcement. Calculation of the moment of inertia of concrete sections is discussed in more detail in Chapter 10.

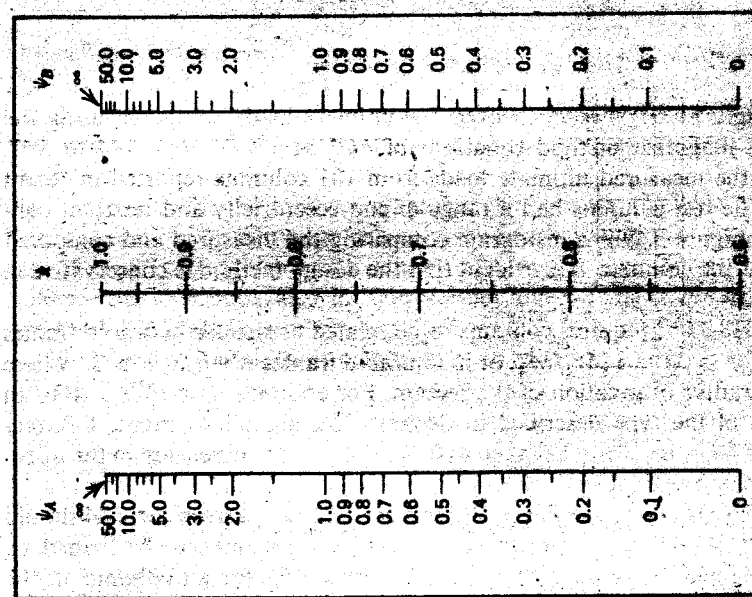
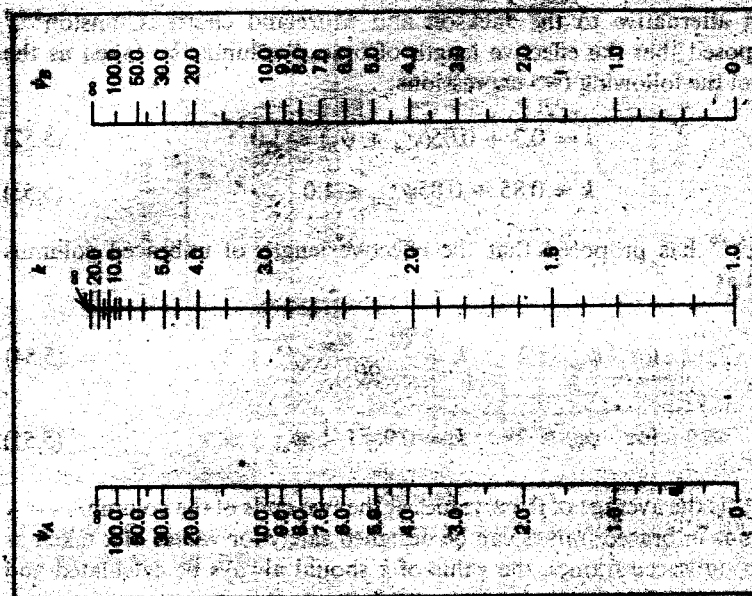


Fig. 5.48. Jackson and Moreland alignment charts for effective length factors of columns. (a) Braced frames. (b) Unbraced frames.

As an alternative to the Jackson and Moreland charts, Cranston^{5.28} has proposed that the effective length of braced columns be taken as the smaller of the following two expressions:

$$k = 0.7 + 0.05(\psi_A + \psi_B) \leq 1.0 \quad (5.52)$$

$$k = 0.85 + 0.05\psi_{\min} \leq 1.0 \quad (5.53)$$

Furlong^{5.29} has proposed that the effective length of unbraced columns be taken as

$$\text{for } \psi_{av} < 2 \quad k = \frac{20 - \psi_{av}}{20} \sqrt{1 + \psi_{av}} \quad (5.54)$$

$$\text{for } \psi_{av} \geq 2 \quad k = 0.9 \sqrt{1 + \psi_{av}} \quad (5.55)$$

where ψ_{av} is the average of the ψ values at the two ends of the column.

Columns in braced frames can be designed safely for values of k taken as unity. In unbraced frames, the value of k should always be calculated and should exceed 1.2.

Use of the Moment Magnifier Equations

MacGregor et al^{5.20} have checked the ultimate loads computed using the moment magnifier method equations of ACI 318-71,^{5.3} Eqs. 5.44 to 5.47, against the measured ultimate loads from 101 columns reported in recent years. The test columns had a range of end eccentricity and restraint conditions. Figure 5.49 is a histogram comparing the measured and computed loads for the columns. It is evident that the design method is conservative in most cases.

ACI 318-71^{5.3} requires columns to be treated as slender in braced frames when $kl_w/r \geq 34 - 12M_1/M_2$, or in unbraced frames when $kl_w/r \geq 22$, where r is the radius of gyration of the section. For columns with $kl_w/r > 100$, an analysis of the type described in Section 5.5.2 should be made. For rectangular sections, r may be taken as 0.3 of the section dimension in the direction of possible buckling.

In frames not braced against sidesway, the value of δ from Eq. 5.44 should be computed for the entire story, assuming all columns to be loaded, by taking P_u and P_c as the summation, ΣP_u and ΣP_c , for all columns in the story. In designing each individual column in the story, δ should be taken as the larger of the above-mentioned value computed for the whole story or the value computed for the individual column, assuming its ends to be

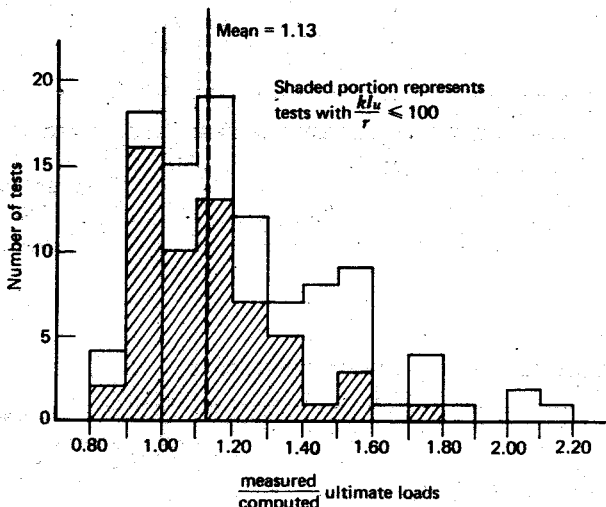


Fig. 5.49. Comparison of ultimate column load computed by the ACI 318-71 moment magnifier method with test results.^{5.20}

braced against sidesway. In structures not braced against sidesway, the beams should be designed for the magnified end moments of the columns at the joints. When columns are subjected to biaxial bending, the moment about each axis should be amplified, using the δ value computed for each axis.

Design aids for the moment magnifier method are available in the ACI handbooks.^{5.9, 5.10} Although the column design handbook^{5.9} is based on the 1963 ACI code, which used a reduction factor approach for slender column design, the handbook also includes design aids for the moment magnifier method. The more recent design handbook^{5.10} contains some examples of applications of the moment magnifier method. Some useful design aids are also given by Furlong.^{5.29}

Example 5.9

One bay of a multistory reinforced concrete frame, which is not braced against sidesway, appears in Fig. 5.50. The columns above and below the story are of similar dimensions. The actions on the column *AB*, at the ends of the unsupported length, at the ultimate load calculated by first-order structural analysis are $M_u = 289$ kip·ft (392 kN·m) and $P_u = 200$ kips (890 kN). The concrete

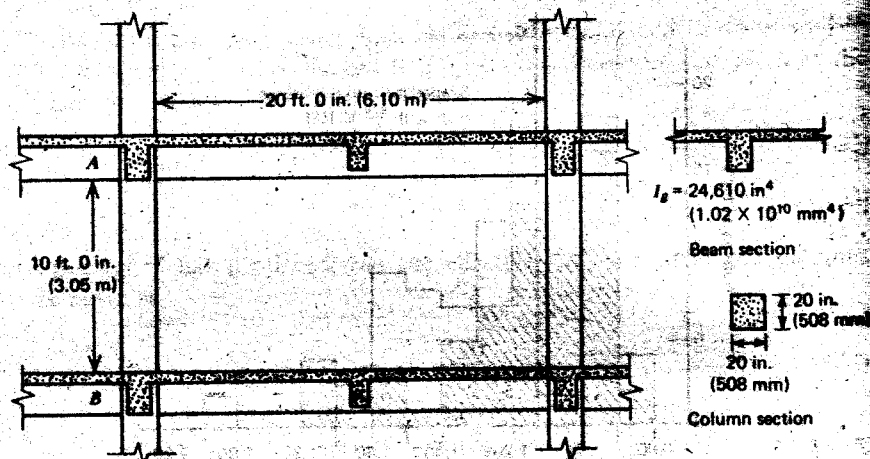


Fig. 5.50. Frame of Example 5.9.

has $f'_c = 4000$ psi (27.6 N/mm 2) and $E_c = 3.6 \times 10^6$ (24,800 N/mm 2). The steel has $f_y = 60,000$ psi (414 N/mm 2) and $E_s = 29 \times 10^6$ psi (200,000 N/mm 2). The ratio of maximum design dead load moment to maximum design total load moment β_d may be taken to be 0.2. Determine the area of longitudinal steel required for the column, using a capacity reduction factor φ of 0.7.

Solution

Effective length of column

For column $I_g = \frac{1}{12} bh^3 = \frac{1}{12} \times 20 \times 20^3 = 13,330 \text{ in}^4$

Calculate ψ using $0.5E_c I_b$ for the beams and $E_c I_g$ for the columns.

From Eq. 5.51 we have

$$\psi_A = \psi_B = \frac{\Sigma(EI_{col}/l_w)}{\Sigma(EI_w/l_w)}$$

$$= \frac{2 \times 13,330}{10 \times 12} \times \frac{20 \times 12}{2 \times 0.5 \times 24,610} = 217$$

$$\therefore \text{from Eq. 5.55} \quad k = 0.9\sqrt{1 + \psi_{av}} = 0.9\sqrt{1 + 2.17} = 1.59$$

$$\therefore kl_u = 1.59 \times 10 = 15.9 \text{ ft.}$$

Slender column check

$$r = 0.3 \times \frac{20}{12} = 0.5 \text{ ft}$$

$$\therefore \frac{kl_u}{r} = \frac{15.9}{0.5} = 31.8 > 22$$

Therefore, the column is slender.

Critical load of column

From Eq. 5.46,

$$EI = \frac{E_c I_g}{2.5(1 + \beta_d)} = \frac{3.6 \times 10^6 \times 13,330}{2.5 \times 1.2} = 1.60 \times 10^{10} \text{ lb} \cdot \text{in}^2$$

$$\therefore \text{from Eq. 5.45 } P_c = \frac{\pi^2 EI}{(kl_u)^2} = \frac{\pi^2 \times 1.60 \times 10^{10}}{(15.9 \times 12)^2} \text{ lb} = 4333 \text{ kips}$$

Moment magnification factor

From Eq. 5.44

$$\delta = \frac{C_m}{1 - P_u/\varphi P_c}$$

where $C_m = 1.0$ in frames not braced against sidesway. We assume that $\Sigma P_u / \Sigma P_c$ for the story is approximately equal to P_u / P_c for this particular column,

$$\therefore \delta = \frac{1.0}{1 - 200/(0.7 \times 4333)} = 1.07$$

Longitudinal column steel

The design actions for the column are $P_u = 200$ kips, and $M_u = 289 \times 1.07 = 309$ kip · ft

For the column, let $g = 0.7$ and design steel using Fig. 5.22, which incorporates $\phi = 0.7$.

$$\frac{P_u}{f'_c b h} = \frac{200,000}{4000 \times 20 \times 20} = 0.125$$

$$\frac{P_u e}{f'_c b h^2} = \frac{309,000 \times 12}{4000 \times 20 \times 20^2} = 0.116$$

From Fig. 5.22, we have $\rho, m = 0.42$, where $m = f_y/0.85f'_c$.

$$\begin{aligned} \therefore A_{st} &= 0.42 \times \frac{0.85 \times 4000}{60,000} \times 20^2 \\ &= 9.52 \text{ in}^2 (6140 \text{ mm}^2) \end{aligned}$$

The steel is uniformly distributed around the column perimeter. Note: The design could now be reworked more accurately using more exact EI values, including the estimated steel areas, to calculate ψ , P_c , $\Sigma P_u/\Sigma P_c$ and δ , hence to obtain a more accurate value for A_{st} . However, the procedure would not be warranted in this case because the moment magnification was only 7%, and any change in this value would result in negligible change in the required steel area.

5.6 REFERENCES

- 5.1 F. E. Richart and R. L. Brown, "An Investigation of Reinforced Concrete Columns," University of Illinois Engineering Experimental Station, Bulletin No. 267, June 1934, 91 pp.
- 5.2 E. Hognestad, "A Study of Combined Bending and Axial Load in Reinforced Concrete Members," University of Illinois Engineering Experimental Station, Bulletin No. 399, June 1951, 128 pp.
- 5.3 ACI Committee 318, "Building Code Requirements for Reinforced Concrete (ACI 318-71)," American Concrete Institute, Detroit, 1971, 78 pp.
- 5.4 W. W. L. Chan, "The Ultimate Strength and Deformation of Plastic Hinges in Reinforced Concrete Frameworks," *Magazine of Concrete Research*, Vol. 7, No. 21, November 1955, pp. 121-132.
- 5.5 H. E. H. Roy and M. A. Sozen, "Ductility of Concrete," *Proceedings of the International Symposium on the Flexural Mechanics of Reinforced Concrete*, ASCE-ACI, Miami, November 1964, pp. 213-224. Discussion on pp. 224-235.
- 5.6 C. S. Whitney, "Plastic Theory of Reinforced Concrete Design," *Proceedings of the American Society of Civil Engineers*, December 1940; *Transactions ASCE*, Vol. 107, 1942, pp. 251-326.

- 5.7 ACI Committee 439, "Uses and Limitations of High Strength Steel Reinforcement $f_y > 60$ ksi," *Journal ACI*, Vol. 70, No. 2, February 1973, pp. 77-104.
- 5.8 C. S. Whitney and E. Cohen, "Guide for Ultimate Strength Design of Reinforced Concrete," *Journal ACI*, Vol. 28, No. 5, November 1956, pp. 455-490.
- 5.9 ACI Committee 340, *Ultimate Strength Design Handbook*, Vol. 2, ACI Special Publication No. 17A, American Concrete Institute, Detroit, 1970, 226 pp.
- 5.10 ACI Committee 340, *Design Handbook in Accordance with Strength Design Method of ACI 318-71*, Vol. 1, ACI Special Publication SP-17(73), American Concrete Institute, Detroit, 1973, 432 pp.
- 5.11 R. W. Furlong, "Ultimate Strength of Square Columns Under Biaxially Eccentric Loads," *Journal ACI*, Vol. 57, No. 9, March 1961, pp. 1129-1140.
- 5.12 F. Moran, "Design of Reinforced Concrete Sections Under Normal Loads and Stresses in the Ultimate Limit State," *Bulletin d'Information* No. 83, Comité Européen du Béton, Paris, April 1972, 134 pp.
- 5.13 B. Bresler, "Design Criteria for Reinforced Concrete Columns Under Axial Load and Biaxial Bending," *Journal ACI*, Vol. 57, November 1960, pp. 481-490.
- 5.14 A. L. Parme, J. M. Nieves, and A. Gouwens, "Capacity of Reinforced Rectangular Columns Subject to Biaxial Bending," *Journal ACI*, Vol. 63, No. 9, September 1966, pp. 911-923.
- 5.15 F. N. Pannell, "Failure Surfaces for Members in Compression and Biaxial Bending," *Journal ACI*, Vol. 60, No. 1, January 1963, pp. 129-140.
- 5.16 J. L. Meek, "Ultimate Strength of Columns with Biaxially Eccentric Loads," *Journal ACI*, Vol. 60, No. 8, August 1963, pp. 1053-1064.
- 5.17 BSI, "Code of Practice for the Structural Use of Concrete, CP110: Part 1: 1972," British Standards Institution, London, 1972, 154 pp.
- 5.18 D. C. Weber, "Ultimate Strength Design Charts for Columns with Biaxial Bending," *Journal ACI*, Vol. 63, No. 11, November 1966, pp. 1205-1230.
- 5.19 D. G. Row and T. Paulay, "Biaxial Flexure and Axial Load Interaction in Short Rectangular Reinforced Concrete Columns," *Bulletin of the New Zealand Society for Earthquake Engineering*, Vol. 6, No. 2, June 1973, pp. 110-121.
- 5.20 J. G. MacGregor, J. E. Breen, and E. O. Pfrang, "Design of Slender Columns," *Journal ACI*, Vol. 67, No. 1, January 1970, pp. 6-28.
- 5.21 R. W. Furlong and P. M. Ferguson, "Tests on Frames with Columns in Single Curvature," *Symposium on Reinforced Concrete Columns*, SP-13, American Concrete Institute, Detroit, 1966, pp. 55-74.
- 5.22 J. G. MacGregor, "Stability of Reinforced Concrete Building Frames," State of Art Paper No. 1, Technical Committee 23, *Proceedings of the International Conference on Planning and Design of Tall Buildings*, Vol. 3, American Society of Civil Engineers, New York, 1973, pp. 19-35.
- 5.23 "Specification for the Design, Fabrication and Erection of Structural Steel for Buildings," American Institute of Steel Construction, New York, 1963, 97 pp.
- 5.24 E. P. Popov, *Introduction to the Mechanics of Solids*, Prentice-Hall, Englewood Cliffs, N.J., 1968, 571 pp.
- 5.25 B. C. Johnston (Ed.), *The Column Research Council Guide to Design Criteria for Metal Compression Members*, 2nd ed., John Wiley & Sons, New York, 1966, 217 pp.
- 5.26 ACI Committee 318, "Commentary on Building Code Requirements for Reinforced Concrete (ACI 318-71)," American Concrete Institute, Detroit, 1971, 96 pp.

- 5.27 J. E. Breen, J. G. MacGregor, and E. O. Pfing, "Determination of Effective Length Factors for Slender Concrete Columns," *Journal ACI*, Vol. 69, No. 11, November 1972, pp. 669-672.
- 5.28 W. B. Cranston, "Analysis and Design of Reinforced Concrete Column," Research Report 20, Paper 41.020, Cement and Concrete Association, London, 1972, 54 pp.
- 5.29 R. W. Furlong, "Column Slenderness and Charts for Design," *Journal ACI*, Vol. 68, No. 1, January 1971, pp. 9-17.

6

Ultimate Deformation and Ductility of Members with Flexure

6.1 INTRODUCTION

Types of load-deflection behavior of reinforced concrete members up to and beyond ultimate load are illustrated in Fig. 6.1. Brittle and ductile behavior are contrasted. Consideration of the load-deformation characteristics of members is necessary for the following reasons:

1. Brittle failure of members should not occur. In the extreme event of a structure being loaded to failure, it should be capable of undergoing large deflections at near-maximum load carrying capacity. This may save lives by giving warning of failure and preventing total collapse.

2. The possible distributions of bending moment, shear force, and axial load that could be used in design of statically indeterminate structures depend on the ductility of the members at the critical sections. A distribution of bending moments differing from that obtained from a linear elastic structural analysis can be achieved if moment redistribution can take place. That is, as ultimate load is approached, some sections may reach their ultimate resisting moments before others; but if plastic rotation can occur there, while the ultimate moment is maintained, additional load can be carried as the moments elsewhere increase to their ultimate value. The ultimate load of the structure is reached when, after the formation of sufficient plastic hinges, a collapse mechanism is developed. Most codes allow some redistribution of moments in design, depending on the ductility of the sections. Use of moment redistribution can convey advantages because it may reduce the congestion of reinforcement at the supports of continuous members, and it enables reduction in the peak bending moments in bending moment envelopes.

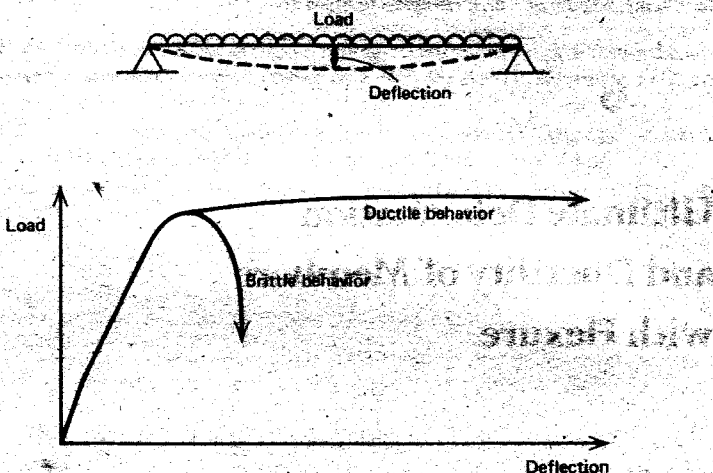


Fig. 6.1. Load-deflection behavior of a flexural member.

3. In areas subjected to earthquakes, a very important design consideration is the ductility of the structure when subjected to seismic-type loading. This is because the present seismic design philosophy relies on energy absorption and dissipation by postelastic deformation for survival in major earthquakes. Thus structures incapable of behaving in a ductile fashion must be designed for much higher seismic forces if collapse is to be avoided.

In this chapter we consider the load-deformation characteristics of flexural members at yield and at ultimate moment. Such characteristics are mainly dependent on the moment-curvature characteristics of sections, since most of the deformations of members of normal proportions arise from strains associated with flexure. Additional deformations due to shear or torsion, when important, are discussed in Chapters 7 and 8.

6.2 MOMENT-CURVATURE RELATIONSHIPS

6.2.1 Curvature of a Member

Figure 6.2 shows an initially straight element of a reinforced concrete member with equal end moments and axial forces. The radius of curvature R is measured to the neutral axis. The radius of curvature R , neutral axis depth kd , concrete strain in the extreme compression fiber ϵ_c , and tension steel strain ϵ_s , will vary along the member because between the cracks the concrete will be carrying some tension. Considering only a small element of length

dx of the member, and using the notation of Fig. 6.2, the rotation between the ends of the element is given by

$$\frac{dx}{R} = \frac{\varepsilon_c dx}{kd} = \frac{\varepsilon_s dx}{d(1 - k)}$$

$$\therefore \frac{1}{R} = \frac{\varepsilon_c}{kd} = \frac{\varepsilon_s}{d(1 - k)}$$

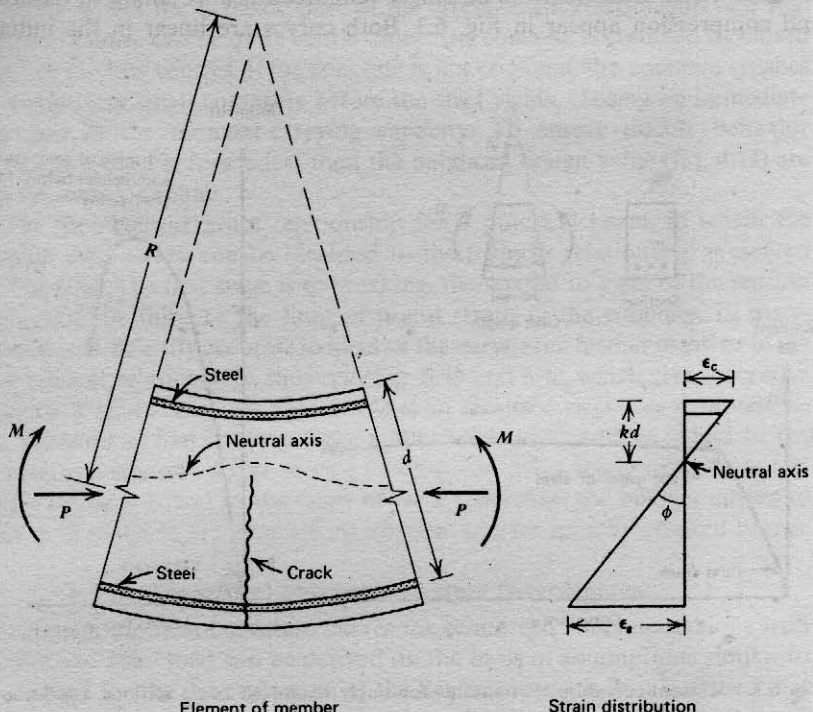


Fig. 6.2. Deformation of a flexural member.

Now $1/R$ is the curvature at the element (the rotation per unit length of member) and is given the symbol ϕ . Thus we have

$$\phi = \frac{\varepsilon_c}{kd} = \frac{\varepsilon_s}{d(1 - k)} = \frac{\varepsilon_c + \varepsilon_s}{d} \quad (6.1)$$

It is evident that the curvature ϕ is the gradient of the strain profile at the element, as in Fig. 6.2.

The curvature will actually vary along the length of the member because of the fluctuation of the neutral axis depth and the strains between the cracks. If the element length is small and over a crack, the curvature is given by Eq. 6.1, with ϵ_c and ϵ_s as the strains at the cracked section.

If the strains at the critical section of a reinforced concrete beam are measured over a short gauge length as the bending moment is increased to failure, the curvature may be calculated from Eq. 6.1, permitting the moment-curvature relationship for the section to be obtained. Two such curves obtained from measurements on singly reinforced beams failing in tension and compression appear in Fig. 6.3. Both curves are linear in the initial

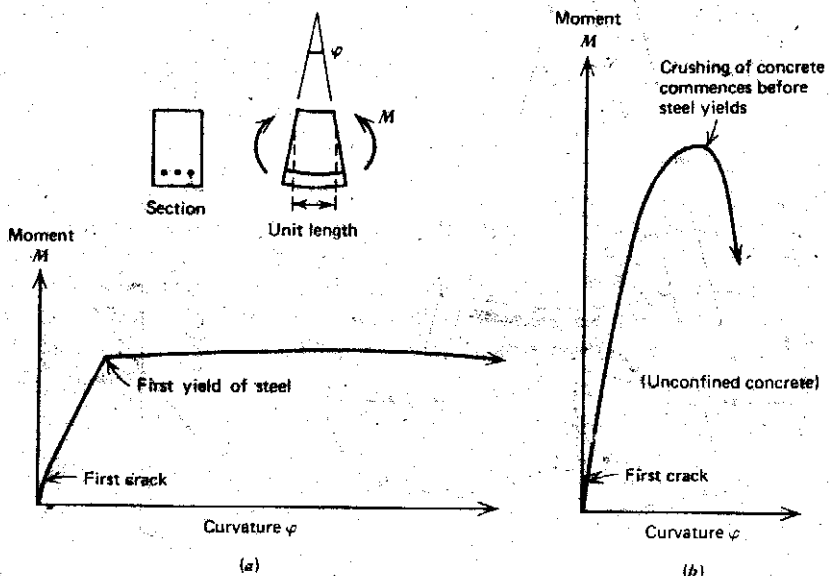


Fig. 6.3. Moment-curvature relationships for singly reinforced beam sections. (a) Section failing in tension, $\rho < \rho_s$. (b) Section failing in compression, $\rho > \rho_s$.

stages, and the relationship between moment M and curvature ϕ is given by the classical elastic equation

$$EI = MR = \frac{M}{\phi} \quad (6.2)$$

where EI is the flexural rigidity of the section. With increase in moment, cracking of the concrete reduces the flexural rigidity of the sections, the

reduction in rigidity being greater for the lightly reinforced section than for the more heavily reinforced section. The behavior of the section after cracking is dependent mainly on the steel content. Lightly reinforced sections (Fig. 6.3a) result in a practically linear $M-\phi$ curve up to the point of steel yielding. When the steel yields, a large increase in curvature occurs at nearly constant bending moment, the moment rising slowly to a maximum due to an increase in the internal lever arm, then decreasing. In heavily reinforced sections (Fig. 6.3b), on the other hand, the $M-\phi$ curve becomes nonlinear when the concrete enters the inelastic part of the stress-strain relationship (see Fig. 2.1), and failure can be quite brittle unless the concrete is confined by closed stirrups at close centres. If the concrete is not confined, the concrete crushes at a relatively small curvature before the steel yields, causing an immediate decrease in the moment-carrying capacity. To ensure ductile behavior in practice, steel contents less than the balanced design value (Eq. 4.14) are always used for beams.

The moment-curvature relationship for a practical beam, in which the tension steel yields, can be idealized to the trilinear relationship presented in Fig. 6.4a. The first stage is to cracking, the second to yield of the tension steel, and the third to the limit of useful strain in the concrete. In many cases it is sufficiently accurate to idealize the curve even further to either of the two bilinear relationships shown in Fig. 6.4b and 6.4c, which give successive degrees of approximation. Figure 6.4a is an idealized virgin curve representing behavior at first loading. Once cracks have developed, as would be the case in most beams under service loading, the $M-\phi$ relationship is nearly linear from zero load to the onset of yield. Therefore the bilinear curves of Figs. 6.4b and 6.4c are accurate approximations for initially cracked beams.

6.2.2 Theoretical Moment-Curvature Determination

Theoretical moment-curvature curves for reinforced concrete sections with flexure and axial load can be derived on the basis of assumptions similar to those used for the determination of the flexural strength. It is assumed that plane sections before bending remain plane after bending and that the stress-strain curves for concrete and steel are known. The curvatures associated with a range of bending moments and axial loads may be determined using these assumptions and from the requirements of strain compatibility and equilibrium of forces.

Figures 6.5a and 6.5b show typical stress-strain curves for steel and concrete, where f_y = yield strength of steel and f'_c = strength of concrete in a member. The stress f''_c may be less than the cylinder strength f'_c ($f''_c/f'_c = k_3$ in Fig. 3.3a and Table 3.1). Figure 6.5c displays a reinforced concrete section with axial load and flexure. For a given concrete strain in the extreme compression fiber ϵ_{cm} and neutral axis depth kd , the steel strains $\epsilon_{s1}, \epsilon_{s2}, \epsilon_{s3}, \dots$,

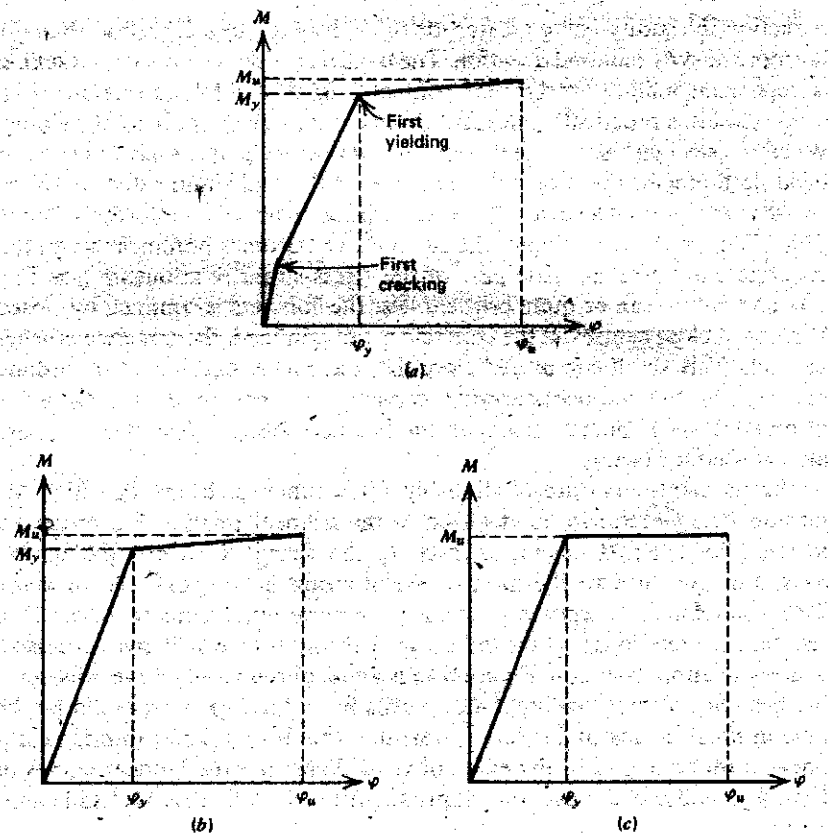


Fig. 6.4. Idealized moment-curvature curves for a singly reinforced section failing in tension.

can be determined from similar triangles of the strain diagram. For example, for bar i at depth d ,

$$\epsilon_{si} = \frac{\epsilon_{cm}}{kd} (kd - d) \quad (6.3)$$

The stresses $f_{si}, f_{s2}, f_{s3}, \dots$, corresponding to strains $\epsilon_{s1}, \epsilon_{s2}, \epsilon_{s3}, \dots$, may then be found from the stress-strain curve for the steel. Then the steel forces S_1, S_2, S_3, \dots , may be found from the steel stresses and the areas of steel. For example, for bar i , the force equation is

$$S_i = f_{si} A_{si} \quad (6.4)$$

The distribution of concrete stress over the compressed part of the section of Fig. 6.5c may be found from the strain diagram and the stress-strain curve

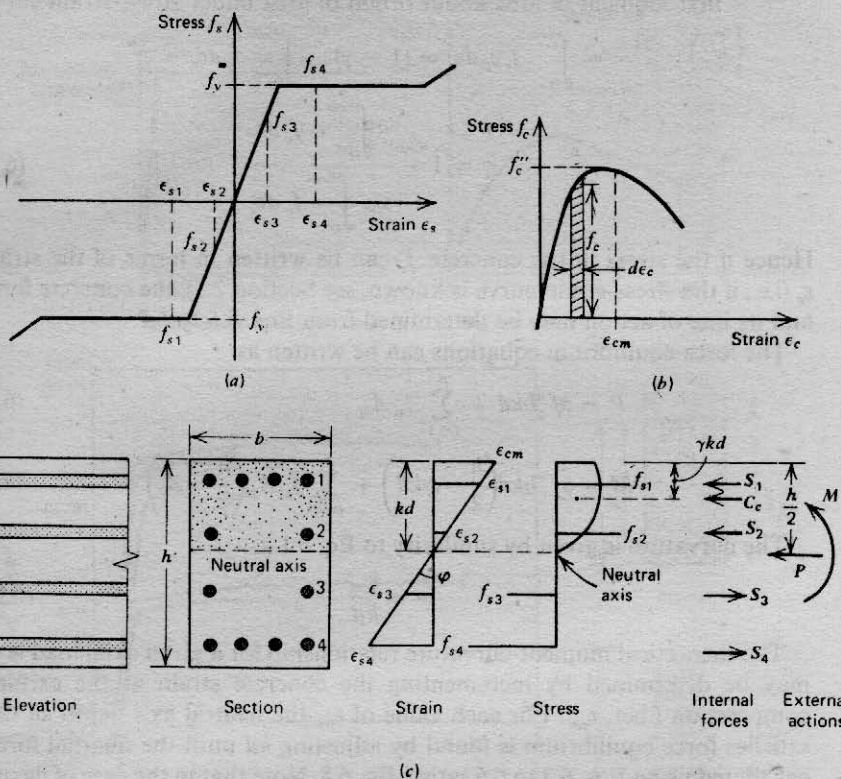


Fig. 6.5. Theoretical moment-curvature determination. (a) Steel in tension and compression. (b) Concrete in compression. (c) Section with strain, stress, and force distribution.

for the concrete. For any given concrete strain ϵ_{cm} in the extreme compression fiber, the concrete compressive force C_c and its position may be defined in terms of parameters α and γ , where

$$C_c = \alpha f_c'' b k d \quad (6.5)$$

acting at distance $\gamma k d$ from the extreme compression fiber. The mean stress factor α and the centroid factor γ for any strain ϵ_{cm} at the extreme compression fiber can be determined for rectangular sections from the stress-strain relationships as follows:

$$\text{area under stress-strain curve (see Fig. 6.5b)} = \int_0^{\epsilon_{cm}} f_c d\epsilon_c = \alpha f_c'' \epsilon_{cm}$$

$$\therefore \alpha = \frac{\int_0^{\epsilon_{cm}} f_c d\epsilon_c}{f_c'' \epsilon_{cm}} \quad (6.6)$$

first moment of area about origin of area under stress-strain curve

$$\begin{aligned}
 &= \int_0^{\varepsilon_{cm}} f_c \varepsilon_c d\varepsilon_c = (1 - \gamma) \varepsilon_{cm} \int_0^{\varepsilon_{cm}} f_c d\varepsilon_c \\
 \therefore \gamma &= 1 - \frac{\int_0^{\varepsilon_{cm}} \varepsilon_c f_c d\varepsilon_c}{\varepsilon_{cm} \int_0^{\varepsilon_{cm}} f_c d\varepsilon_c} \quad (6.7)
 \end{aligned}$$

Hence if the stress in the concrete f_c can be written in terms of the strain ε_c (i.e., if the stress-strain curve is known, see Section 2.1), the concrete force and its line of action may be determined from Eqs. 6.5 to 6.7.

The force equilibrium equations can be written as

$$P = \alpha f_c'' b k d + \sum_{i=1}^n f_{si} A_{si} \quad (6.8)$$

$$M = \alpha f_c'' b k d \left(\frac{h}{2} - \gamma k d \right) + \sum_{i=1}^n f_{si} A_{si} \left(\frac{h}{2} - d_i \right) \quad (6.9)$$

The curvature is given by similarity to Eq. 6.1 as

$$\varphi = \frac{\varepsilon_{cm}}{k d} \quad (6.10)$$

The theoretical moment-curvature relationship for a given axial load level may be determined by incrementing the concrete strain at the extreme compression fiber, ε_{cm} . For each value of ε_{cm} the neutral axis depth $k d$ that satisfies force equilibrium is found by adjusting $k d$ until the internal forces calculated using Eqs. 6.3 to 6.6 satisfy Eq. 6.8. Note that in the case of flexure only, $P = 0$. The internal forces and neutral axis depth so found are then used to determine the moment M and curvature φ from Eqs. 6.7, 6.9 and 6.10 corresponding to that value of ε_{cm} . By carrying out the calculation for a range of ε_{cm} values, the moment-curvature curve can be plotted. The calculation is lengthy and if required is best carried out using a digital computer.

Figure 6.6 gives some theoretical moment-curvature relationships that were obtained for rectangular concrete beam sections using the method just described. The assumed stress-strain curves for the steel and the concrete and the section properties appear in the figure. Most of the moment-curvature curves have been computed only for the region commencing just prior to yield of the tension steel. The moment-curvature curves exhibit a discontinuity at first yield of the tension steel and have been terminated when the extreme fiber compressive concrete strain ε_{cm} reaches 0.004. The curves show that for a given maximum concrete strain, the ductility of single reinforced sections decreases as the tension steel content is increased, and the presence of compression steel increases the ductility significantly.

Ductility of Unconfined Beam Sections

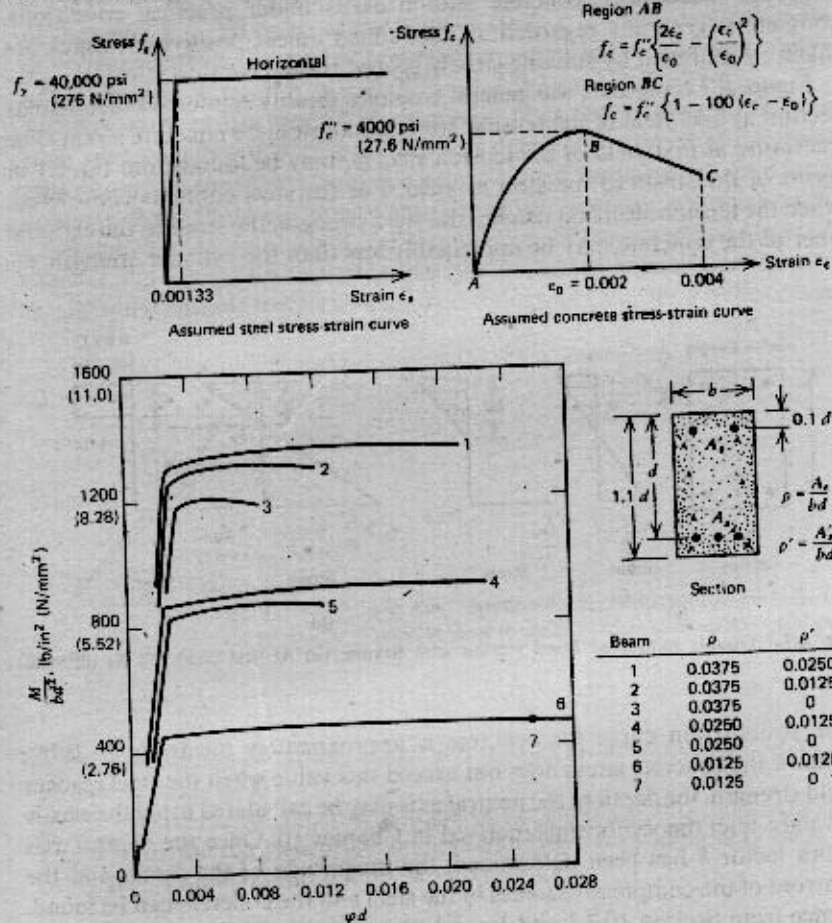


Fig. 6.6. Theoretical moment-curvature relationships.

6.3 DUCTILITY OF UNCONFINED BEAM SECTIONS

6.3.1 Yield and Ultimate Moment and Curvature

In limit and seismic design, the ductility of a member is usually expressed as the ratio of the ultimate deformation to the deformation at first yield. The relative values of moment and curvature when the tension steel first yields and the concrete reaches ultimate strain are considered below. The compressed concrete of the members will be considered to be unconfined.

Although unconfined concrete seldom exists under practical conditions, concrete is generally regarded as unconfined unless positive measures are taken to confine it by suitable closely spaced transverse steel.

Figure 6.7 represents the general case of a doubly reinforced rectangular section at first yield of the tension steel and at ultimate concrete strain. The curvature at first yield of the tension steel φ_y may be found from Eq. 6.1 in terms of the strain in the steel at yield. For the steel contents considered, when the tension steel first reaches the yield strength, the stress in the extreme fiber of the concrete may be appreciably less than the cylinder strength f_c' .

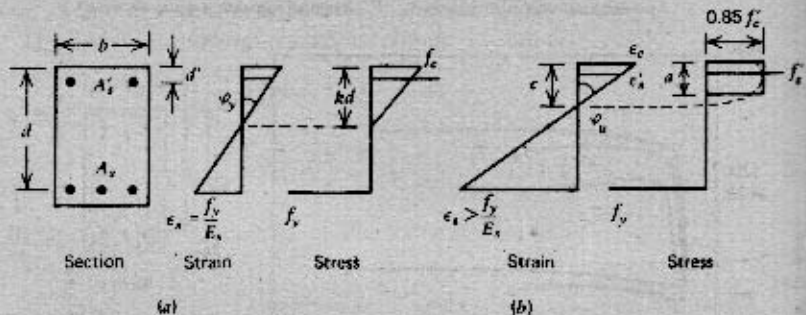


Fig. 6.7. Doubly reinforced beam section with flexure. (a) At first yield. (b) At ultimate.

The stress-strain curve for concrete is approximately linear up to $0.7f_c'$; hence if the concrete stress does not exceed this value when the steel reaches yield strength, the depth to the neutral axis may be calculated using the elastic (straight line) theory formula, derived in Chapter 10. Once the neutral axis depth factor k has been determined, the magnitude of the forces and the centroid of the compressive forces in the steel and the concrete can be found. Hence from Section 10.2.3 and Eq. 6.1, the equations defining the moment and curvature at first yield are

$$k = \left[(\rho + \rho')^2 n^2 + 2\left(\rho + \frac{\rho' d'}{d}\right)n \right]^{1/2} - (\rho + \rho')n \quad (6.11)$$

$$M_y = A_s f_y j d \quad (6.12)$$

$$\varphi_y = \frac{f_y/E_s}{d(1 - k)} \quad (6.13)$$

where A_s = area of tension steel, A'_s = area of compression steel, b = width of section, d = effective depth of tension steel, d' = distance from extreme compression fiber to centroid of compression steel, E_c = modulus of elasticity

of concrete, E_s = modulus of elasticity of steel, f_y = yield strength of steel, jd = distance from centroid of compressive forces in the steel and concrete to the centroid of tension, $n = E_s/E_c$, $\rho = A_s/bd$, and $\rho' = A'_s/bd$.

If the stress in the extreme compression fiber of the concrete is greater than approximately $0.7f'_c$, the neutral axis depth at first yield of the tension steel should be calculated using the actual curved stress-strain curve for the concrete (a parabola is a good approximation). However, an estimate may be obtained from the straight line formula even if the computed stress is as high as f'_c . Figure 6.8 indicates that the value for k calculated from the straight line formula will be smaller than the actual value for k if the concrete

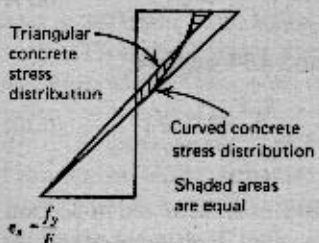


Fig. 6.8. Stress and strain distributions for same compressive force in concrete when steel reaches yield stress.

stress distribution is curved, which will lead to an underestimate of φ_y and an overestimate of M_y .

The ultimate curvature and moment of the doubly reinforced section (see Fig. 6.7) for the case where the compression steel is yielding may be found using Eqs. 4.27, 4.32, and 6.1. These equations give

$$a = \frac{A_s f_y - A'_s f_y}{0.85 f'_c b} \quad (6.14)$$

$$M_u = 0.85 f'_c a b \left(a - \frac{a}{2} \right) + A'_s f_y (d - d') \quad (6.15)$$

$$\varphi_u = \frac{\varepsilon_c}{c} = \frac{\varepsilon_c \beta_1}{a} \quad (6.16)$$

The strain in the compression steel, indicated by the strain diagram of Fig. 6.7, is given by

$$\varepsilon'_s = \varepsilon_c \left(\frac{c - d'}{c} \right) = \varepsilon_c \left(1 - \frac{\beta_1 d'}{a} \right) \quad (6.17)$$

Substituting Eq. 6.14 into Eq. 6.17 demonstrates that the compression steel is yielding when

$$\varepsilon_c \left[1 - \beta_1 d' \left(\frac{0.85 f'_c b}{A_s f_y - A'_s f_y} \right) \right] \geq \frac{f_y}{E_s} \quad (6.18)$$

Equation 6.18 must be shown to be satisfied for Eqs. 6.14 to 6.16 to be applicable.

If a check shows that Eq. 6.18 is not satisfied, the compression steel is not yielding and the actual value for compressive steel stress given by Eq. 4.34 should be substituted (instead of the yield strength). Solving Eqs. 4.33 and 4.34 simultaneously gives

$$\frac{1}{2} \left(\frac{a}{d} \right)^2 + \frac{a}{d} \left(\frac{\rho' \varepsilon_c E_s - \rho f_y}{1.7 f'_c} \right) - \frac{\rho' \varepsilon_c E_s \beta_1 d'}{1.7 f'_c d} = 0 \quad (6.19)$$

from which a is obtained. Also, from Eqs. 4.36 and 4.34 we have

$$M_u = 0.85 f'_c a b \left(d - \frac{a}{2} \right) + A'_s E_s \varepsilon_c \frac{a - \beta_1 d'}{a} (d - d') \quad (6.20)$$

and φ_u is given by Eq. 6.16.

The value of ε_c used in flexural strength calculations is discussed in Section 3.3. It is evident that a value of $\varepsilon_c = 0.004$ could be used in ultimate curvature calculations because a value of $\varepsilon_c = 0.003$ is conservative.

A measure of the increase in bending moment after yielding is given by the ratio M_u/M_y . This ratio may be obtained from Eqs. 6.14 and 6.15, or 6.19 and 6.20, and 6.12. For singly reinforced sections with $\rho \leq 0.02$, $f'_c \leq 5000$ psi (34.5 N/mm 2), and $f_y = 60,000$ psi (414 N/mm 2) or $40,000$ psi (276 N/mm 2), these equations indicate that $M_u/M_y \leq 1.06$. Hence the increase in moment after first yield is small. The increase may be more significant for doubly reinforced sections.

The ratio φ_u/φ_y gives a measure of the curvature ductility of the section. From Eqs. 6.16 and 6.13 the ratio may be written as

$$\frac{\varphi_u}{\varphi_y} = \frac{\varepsilon_c}{f_y/E_s} \frac{d(1-k)}{a/\beta_1} \quad (6.21)$$

Equation 6.21 may be used to determine the curvature ductility factor in the general case of a doubly reinforced section. If Eq. 6.18 is satisfied, the compression steel is yielding, and on substituting Eqs. 6.11 and 6.14 into Eq. 6.21, the curvature ductility factor is given as

$$\frac{\varphi_u}{\varphi_y} = \frac{0.85 \beta_1 E_s \varepsilon_c f'_c}{f_y^2 (\rho - \rho')} \left\{ 1 + (\rho + \rho')n - \left[(\rho + \rho')^2 n^2 + 2 \left(\rho + \frac{\rho' d'}{d} \right) n \right]^{1/2} \right\} \quad (6.22)$$

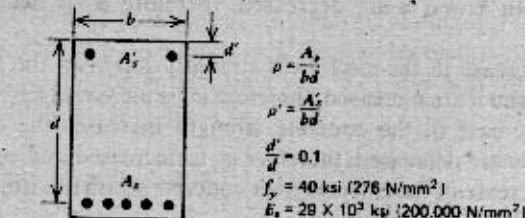
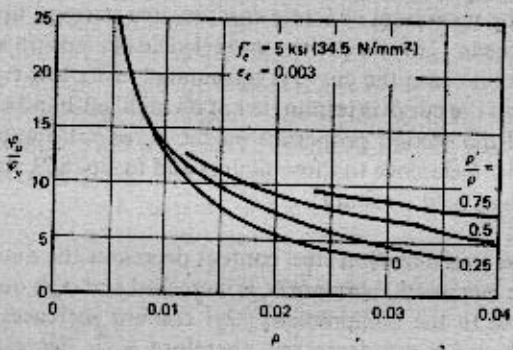
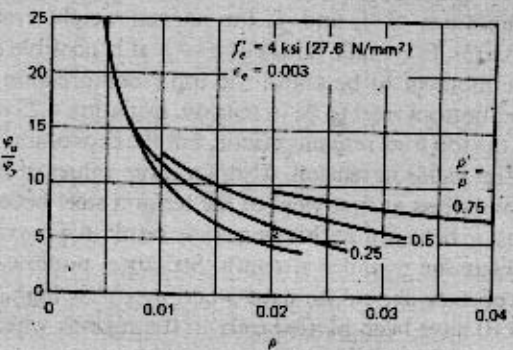
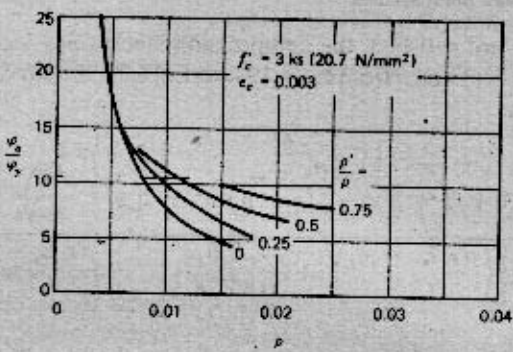
If Eq. 6.18 is not satisfied, the compression steel is not yielding, and on substituting Eq. 6.11 and a from Eq. 6.19 into Eq. 6.21, the curvature ductility factor is given as

$$\frac{\varphi_u}{\varphi_y} = \frac{\beta_1 E_s \rho_c}{f_y} \frac{1 + (\rho + \rho')n - \left[(\rho + \rho')^2 n^2 + 2\left(\rho + \frac{\rho' d'}{d}\right)n \right]^{1/2}}{\left[\left(\frac{\rho' \epsilon_c E_s - \rho f_y}{1.7 f'_c} \right)^2 + \frac{\rho' \epsilon_c E_s \beta_1 d'}{0.85 f'_c d} \right]^{1/2} - \frac{\rho' \epsilon_c E_s - \rho f_y}{1.7 f'_c}} \quad (6.23)$$

Equations 6.22 and 6.23 are plotted in Figs. 6.9 and 6.10 for a range of practical combinations of f_y and f'_c for normal weight concrete and for $\epsilon_c = 0.003$ and 0.004 . For small values of $\rho - \rho'$ it is possible for the neutral axis at ultimate moment to be above the top ("compression") steel, hence for both top and bottom steel to be in tension. Equation 6.23 can handle this situation while the top steel remains elastic, but the expression is inapplicable when the top steel yields in tension. Also, for large values of $\rho - \rho'$ the concrete compressive stress at first yield of the tension steel becomes high, and the assumed elastic behavior at this stage may result in a maximum concrete stress that exceeds the cylinder strength. Strictly a nonlinear stress-strain curve for the concrete should be used when $\rho - \rho'$ is high. The curves in Figs. 6.9 and 6.10 have been plotted only in the regions where the assumptions made in Eqs. 6.22 or 6.23 are accurate. Thus the curves have not been plotted where the maximum concrete compressive stress at first yield of the tension steel exceeds f'_c or where the top steel yields in tension at the ultimate moment. In the first case the curve is terminated at its low right-hand end, and in the second the curve is terminated at its high left-hand end.

The effects of the section properties on the φ_u/φ_y ratio appear clearly in Figs. 6.9 and 6.10. Reference to those figures and to Eq. 6.21 shows that with the other variables held constant:

1. An increase in the tension steel content decreases the ductility, because both k and a are increased, therefore φ_y is increased and φ_u is decreased.
2. An increase in the compression steel content increases the ductility, because both k and a are decreased, therefore φ_y is decreased and φ_u is increased.
3. An increase in the steel yield strength decreases the ductility because both f_y/E_s and a are increased, therefore φ_y is increased and φ_u is decreased.
4. An increase in the concrete strength increases the ductility because both k and a are decreased, therefore φ_y is decreased and φ_u is increased.
5. An increase in the extreme fiber concrete strain at ultimate increases the ductility because φ_u is increased.



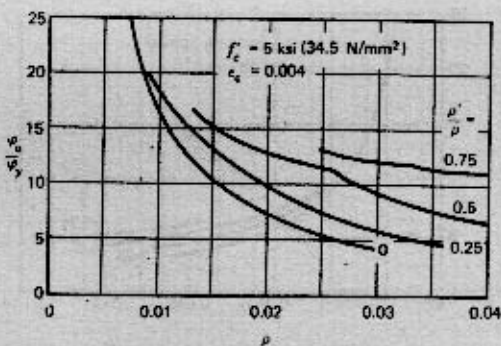
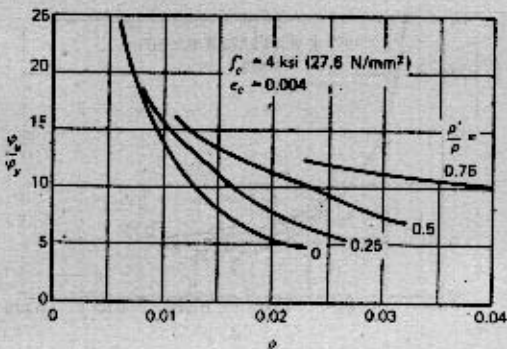
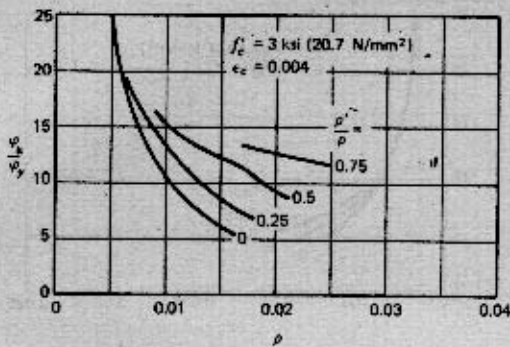
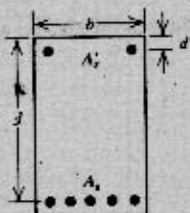
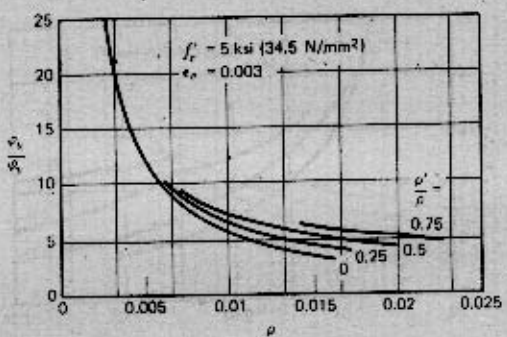
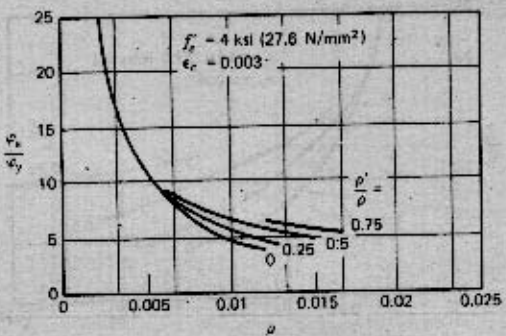
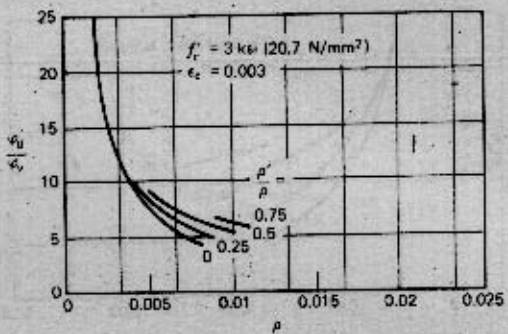


Fig. 6.9. Variation of φ_u/φ_y for beams with unconfined concrete and $f'_y = 40$ ksi (276 N/mm²).



$$\begin{aligned}
 \rho &= \frac{A_s}{bd} \\
 \rho' &= \frac{A'_s}{bd} \\
 \frac{\rho'}{\rho} &= 0.1 \\
 f'_s &= 60 \text{ ksi (414 N/mm}^2\text{)} \\
 E_s &= 29 \times 10^3 \text{ ksi (200,000 N/mm}^2\text{)}
 \end{aligned}$$

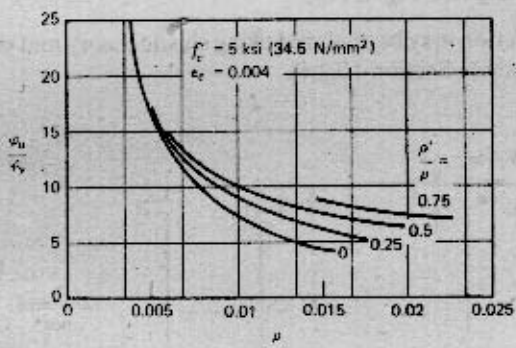
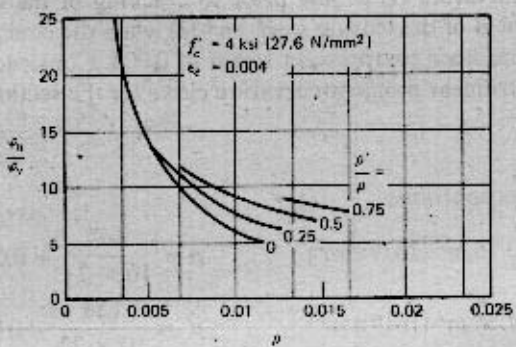
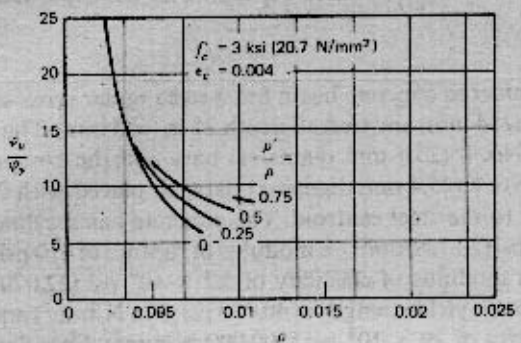


Fig. 6.10. Variation of φ_u/φ_y for beams with unconfined concrete and $f'_c = 60$ ksi (414 N/mm²).

Example 6.1

A reinforced concrete beam has a rectangular cross section of width 10 in (254 mm) and overall depth 25 in (635 mm). The tension steel is four No. 8 (25.4 mm diameter) bars and the compression steel is two No. 8 (25.4 mm diameter) bars, all placed with 2 in (51 mm) of cover to the steel centroid. The concrete has a cylinder strength of 3000 psi (20.7 N/mm²), a modulus of rupture of 410 psi (2.83 N/mm²), and a modulus of elasticity of 3.2×10^6 psi (22,070 N/mm²). The steel has a yield strength of 40,000 psi (276 N/mm²) and a modulus of elasticity of 29×10^6 psi (200,000 N/mm²). Calculate the moment and curvature (1) at just prior to cracking of the concrete, (2) at first yield of the tension steel, and (3) when the concrete reaches an extreme fiber compression strain of 0.004. Construct the approximate trilinear moment-curvature curve for the section.

Solution

Steel proportions:

$$A_s = 3.16 \text{ in}^2 (2039 \text{ mm}^2) \quad \therefore \rho = \frac{3.16}{10 \times 23} = 0.01374$$

$$A'_s = 1.58 \text{ in}^2 (1019 \text{ mm}^2) \quad \therefore \rho' = \frac{1.58}{10 \times 23} = 0.00687$$

1. *Before cracking (see Fig. 6.11b)*

The section may be analyzed using elastic theory and the transformed section (see Section 10.2.4).

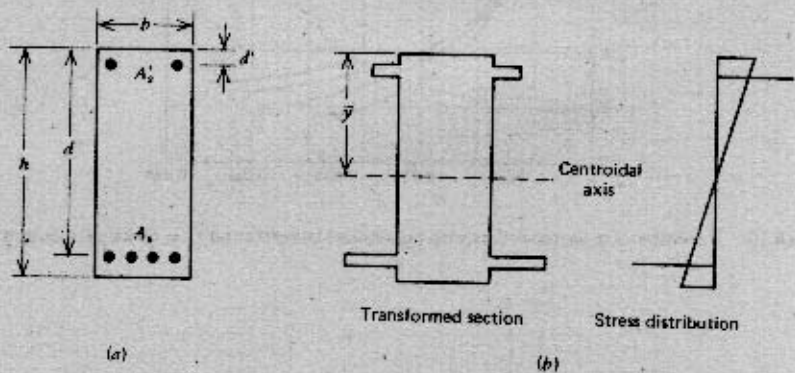
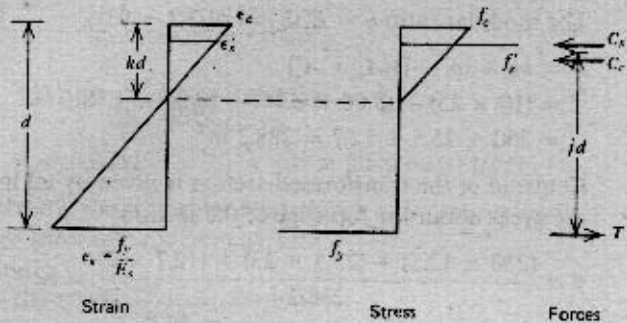
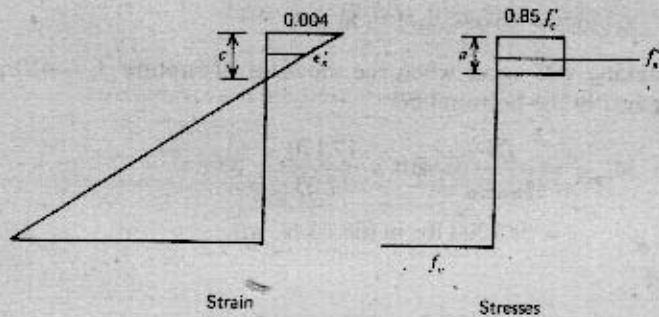


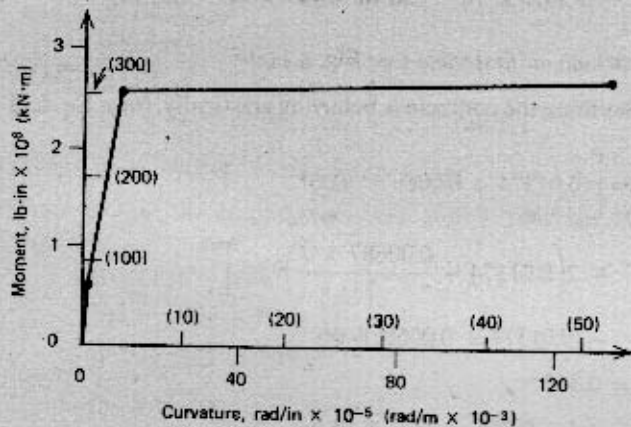
Fig. 6.11. Example 6.1. (a) Section. (b) Before cracking: elastic behavior. (c) After cracking: at first yield. (d) After cracking: at ultimate. (e) Moment-curvature curve.



(c)



(d)



(e)

The modular ratio $n = E_s/E_c = 29/3.2 = 9.06$.

$$\begin{aligned} A &= bh + (n - 1)(A_s + A'_s) \\ &= (10 \times 25) + (8.06 \times 3.16) + (8.06 \times 1.58) \\ &= 250 + 25.5 + 12.7 = 288.2 \text{ in}^2 \end{aligned}$$

Centroid of the transformed section is given by taking moments of the areas about the top edge of the section.

$$\bar{y} = \frac{(250 \times 12.5) + (25.5 \times 23) + (12.7 \times 2)}{288.2} = 12.97 \text{ in}$$

Hence the moment of inertia is given by

$$\begin{aligned} I &= \left(\frac{1}{12} \times 10 \times 25^3\right) + (250 \times 0.47^2) + (25.5 \times 10.03^2) \\ &\quad + (12.7 \times 10.97^2) = 17,170 \text{ in}^4 \end{aligned}$$

Cracking will occur when the modulus of rupture $f_r = 410 \text{ psi}$ is reached in the bottom fiber.

$$\begin{aligned} \therefore M_{\text{crack}} &= \frac{f_r I}{y_{\text{bottom}}} = 410 \times \frac{17,170}{12.03} \\ &= 585,200 \text{ lb} \cdot \text{in} (66.1 \text{ kN} \cdot \text{m}) \end{aligned}$$

and

$$\begin{aligned} \varphi_{\text{crack}} &= \frac{f_r/E_c}{y_{\text{bottom}}} = \frac{410/3.2 \times 10^6}{12.03} \\ &= 1.07 \times 10^{-5} \text{ rad/in} (0.419 \times 10^{-3} \text{ rad/m}) \end{aligned}$$

2. After cracking, at first yield (see Fig. 6.11c)

Assuming the concrete is behaving elastically, from Eq. 6.11 we write

$$\begin{aligned} k &= \left[(0.01374 + 0.00687)^2 9.06^2 \right. \\ &\quad \left. + 2 \left(0.01374 + \frac{0.00687 \times 2}{23} \right) 9.06 \right]^{1/2} \\ &\quad - (0.01374 + 0.00687) 9.06 \\ &= 0.356 \end{aligned}$$

$$\therefore kd = 0.356 \times 23 = 8.19 \text{ in}$$

$$\text{Now } \varepsilon_s = 40,000/(29 \times 10^6) = 0.00138.$$

From the strain diagram we find,

$$\epsilon_c = 0.00138 \frac{8.19}{23 - 8.19} = 0.000763$$

$$\therefore f_c = 0.000763 \times 3.2 \times 10^6 = 2440 \text{ psi} = 0.81 f'_c$$

Therefore, the triangular stress block is an approximation.
From the strain diagram we find

$$\epsilon'_s = 0.000763 \frac{8.19 - 2}{8.19} = 0.000577$$

$$\therefore f'_s = 0.000577 \times 29 \times 10^6 = 16,730 \text{ psi}$$

$$\therefore C_c = \frac{1}{2} f_c b k d = \frac{1}{2} \times 2440 \times 10 \times 8.19 = 99,920 \text{ lb}$$

$$C_s = A'_s f'_s = 1.58 \times 16,730 = 26,430 \text{ lb}$$

Therefore, total compressive force is 126,350 lb acting at \bar{y} from the top edge, where

$$\bar{y} = \frac{(2 \times 26,430) + (99,920 \times 8.19/3)}{126,350} = 2.58 \text{ in}$$

$$\therefore jd = d - \bar{y} = 23 - 2.58 = 20.42 \text{ in}$$

From Eq. 6.12

$$M_y = 3.16 \times 40,000 \times 20.42 \\ = 2.58 \times 10^6 \text{ lb} \cdot \text{in} (291 \text{ kN} \cdot \text{m})$$

and from Eq. 6.13

$$\varphi_y = \frac{0.00138}{23 - 8.19} \\ = 9.32 \times 10^{-5} \text{ rad/in} (3.67 \times 10^{-3} \text{ rad/m})$$

3. After cracking, at ultimate load (see Fig. 6.11d)

Assume that the compression steel is also yielding; from Eq. 6.14 we have

$$a = \frac{40,000(3.16 - 1.58)}{0.85 \times 3000 \times 10} = 2.48 \text{ in}$$

$$\therefore c = 2.48/0.85 = 2.92 \text{ in}$$

From the strain diagram, we find

$$\epsilon'_s = 0.004 \frac{2.92 - 2}{2.92} = 0.00126$$

But $f_y/E_s = 0.00138$; therefore, compression steel is not yielding. Actual stress in compression steel can be found from Eq. 4.34. Alternatively, use a trial-and-error approach. Try $f'_s = 38,800$ psi, then

$$a = \frac{(40,000 \times 3.16) - (38,800 \times 1.58)}{0.85 \times 3000 \times 10} = 2.55 \text{ in}$$

$$\therefore c = 2.55/0.85 = 3.00 \text{ in}$$

$$\therefore e'_s = 0.004 \times \frac{3 - 2}{3} = 0.00133$$

$$\therefore f'_s = 0.00133 \times 29 \times 10^6 = 38,600 \text{ psi}$$

which checks satisfactorily with the trial value.

$$\begin{aligned} \therefore M_u &= 0.85 f'_c ab \left(d - \frac{a}{2} \right) + A'_s f'_s (d - d') \\ &= 0.85 \times 3000 \times 2.55 \times 10 \left(23 - \frac{2.55}{2} \right) \\ &\quad + 1.58 \times 38,600 (23 - 2) \\ &= 2.69 \times 10^6 \text{ lb} \cdot \text{in} (304 \text{ kN} \cdot \text{m}) \end{aligned}$$

And from Eq. 6.16 we write

$$\begin{aligned} \varphi_u &= \frac{0.004}{3} \\ &= 133.3 \times 10^{-5} \text{ rad/in} (52.5 \times 10^{-3} \text{ rad/m}) \end{aligned}$$

The moment-curvature diagram appears in Fig. 6.11e.

6.3.2 Code-Specified Ductility Requirements for Beams

ACI 318-73^{6.1} has the following requirements affecting curvature ductilities:

1. In flexural members at all times, if the compression steel is yielding (see Eq. 4.49),

$$\rho - 0.75\rho' \leq 0.75 \frac{0.85f'_c\beta_1}{f_y} \frac{0.003E_s}{0.003E_s + f_y} \quad (6.24)$$

2. In flexural members of statically indeterminate structures where the bending moments given by elastic theory are adjusted to allow for moment redistribution

$$\rho - \rho' \leq 0.5 \frac{0.85f'_c\beta_1}{f_y} \frac{0.003E_s}{0.003E_s + f_y} \quad (6.25)$$

3. In flexural members of ductile frames in earthquake areas, if the compression steel is yielding

$$\rho - 0.5\rho' \leq 0.5 \frac{0.85f'_c\beta_1}{f_y} \frac{0.003E_s}{0.003E_s + f_y} \quad (6.26)$$

Table 6.1 shows the maximum steel contents allowed by Eqs. 6.24 to 6.26 for various steel and concrete strengths.

Table 6.1 Maximum Steel Contents for Ductility^a

f_y , psi (N/mm ²):	40,000 (276)			60,000 (414)		
f'_c , psi (N/mm ²):	3000 (20.7)	4000 (27.6)	5000 (34.5)	3000 (20.7)	4000 (27.6)	5000 (34.5)
Max ($\rho - 0.75\rho'$ from Eq. 6.24)	0.0278	0.0371	0.0437	0.0160	0.0214	0.0252
Max ($\rho - \rho'$ from Eq. 6.25)	0.0186	0.0247	0.0291	0.0107	0.0143	0.0168
Max ($\rho - 0.5\rho'$ from Eq. 6.26)	0.0186	0.0247	0.0291	0.0107	0.0143	0.0168

^a From Reference 6.1.

Reference to Figs. 6.9 and 6.10 indicates the values of φ_u/φ_y that will be ensured by Eqs. 6.24 to 6.26 for the steel and concrete strengths given in Table 6.1. For sections without compression steel, Eqs. 6.25 and 6.26 will ensure $\varphi_u/\varphi_y > 3$ for $\varepsilon_c = 0.003$ and $\varphi_u/\varphi_y > 4$ for $\varepsilon_c = 0.004$. For sections with compression steel, a greater φ_u/φ_y ratio is ensured by Eq. 6.26. For example, if $\rho'/\rho = 0.5$, Eq. 6.26 will ensure $\varphi_u/\varphi_y > 4$ for $\varepsilon_c = 0.003$ and $\varphi_u/\varphi_y > 6$ for $\varepsilon_c = 0.004$. This increase in φ_u/φ_y values with compression steel will not occur when Eq. 6.25 is used.

Thus some ductility will always be available from code-designed sections. The significance of the requirements of Eq. 6.25 and 6.26 are further discussed in other chapters.

6.4 DUCTILITY OF UNCONFINED COLUMN SECTIONS

The axial load influences the curvature; hence there is no unique moment-curvature curve for a given column section, unlike the case of a given beam section. However, it is possible to plot the combinations of axial load P and moment M which cause the section to reach the ultimate capacity and

the curvature ϕ corresponding to those combinations. Figure 6.12a, taken from Blume, Newmark, and Corning,^{6.2} plots P against M (the interaction diagram) and P against ϕh for a column section having bars on two opposite faces. The details of the section and the assumed stress-strain curve for the concrete appear in the figure. Curve 1 of the P - M diagram indicates the combinations of P and M that cause the column to reach the useful limit of strain (0.004 for the concrete) without confinement. Curve 1 in the P - ϕh diagram shows the curvature of the section corresponding to the combinations of P and M when this ultimate condition is reached. Curves 2 give the combinations of P , M , and ϕh corresponding to the points at which the tension steel first reaches the yield strength. Curves 2 do not appear above the balance point because the tension steel does not reach the yield strength above that point. Below the balance point in the P - M diagram, curves 1 and 2 lie close together, indicating little change in the load capacity after yielding. Below the balance point in the P - ϕh diagram, curves 1 and 2 separate, and indicate the amount of inelastic bending deformation that occurs once yielding has started. The ratio ϕ_u/ϕ_y obtained from these two curves for the unconfined section is plotted against the column load ratio P/P_o in Fig. 6.12b, where P_o is the axial load strength of the column when no bending is present. At the balanced point, $P/P_o = 0.31$ for this section. It is evident that the ductility of the section is significantly reduced by the presence of axial load. For example, if the column load is 15% of the axial load capacity, the ϕ_u/ϕ_y value is reduced to about 4, and is smaller at higher load levels.

Pfrang, Siess, and Sozen^{6.3} have also reported the results of an investigation into the inelastic deformations of reinforced concrete column sections. Of particular interest are the moment-curvature curves obtained for column sections with various levels of constant axial load (i.e., the column load was held constant at a particular level while the column was bent to failure). Curves for column sections with two different steel contents are presented in Fig. 6.13. The tensile strength of the concrete was ignored in the calculations, and the ultimate curvature was assumed to be reached when the maximum concrete strain was 0.0038. The curves illustrate again that at axial load levels greater than the balanced failure load, the ductility is negligible, being due only to the inelastic deformation of the concrete. At levels of load less than the balanced load, the ductility increases as the load level is reduced.

Because of the brittle behavior of unconfined columns at even moderate levels of axial compressive load, ACI 318-71^{6.1} recommends that the ends of columns in ductile frames in earthquake areas be confined by closely spaced transverse reinforcement when the axial load is greater than 0.4 of the balanced load P_b .

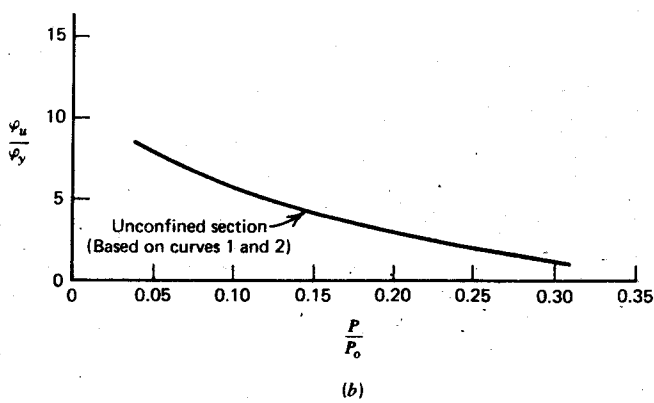
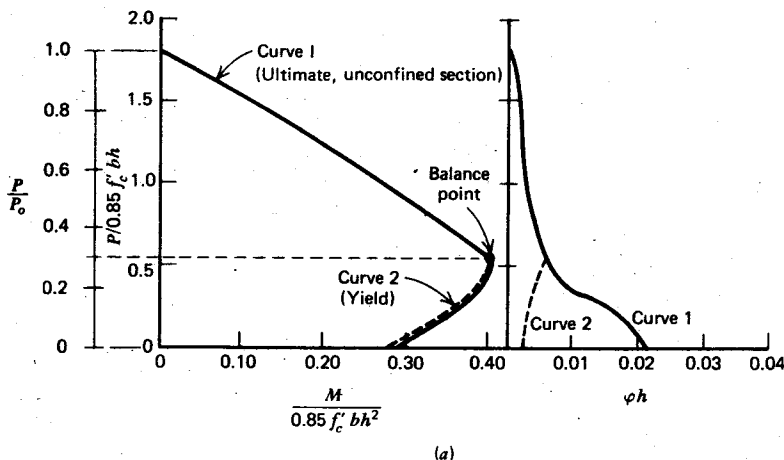
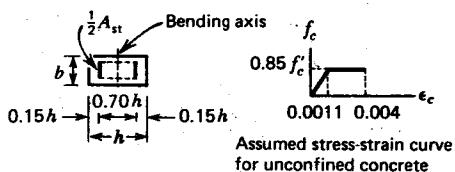
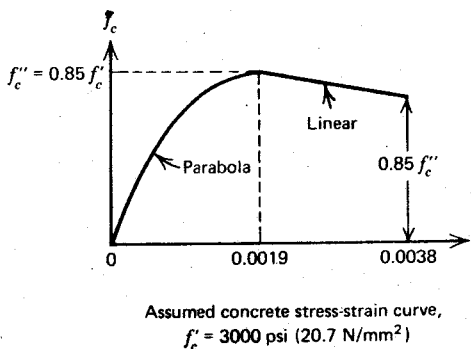
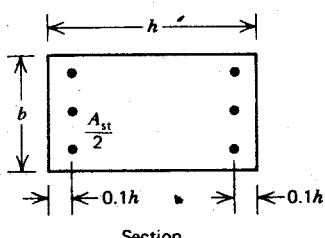
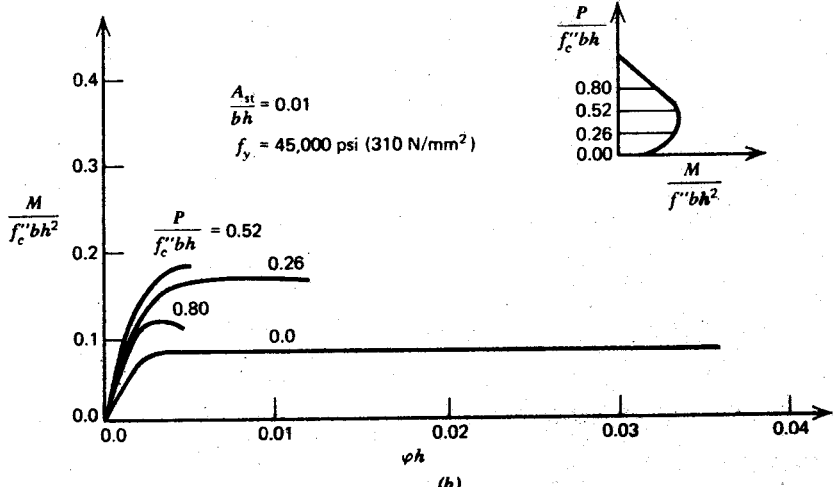


Fig. 6.12. Strength and ductility of a column section.^{6,2} (a) Interaction diagrams. (b) Curvature ductility.



(a)



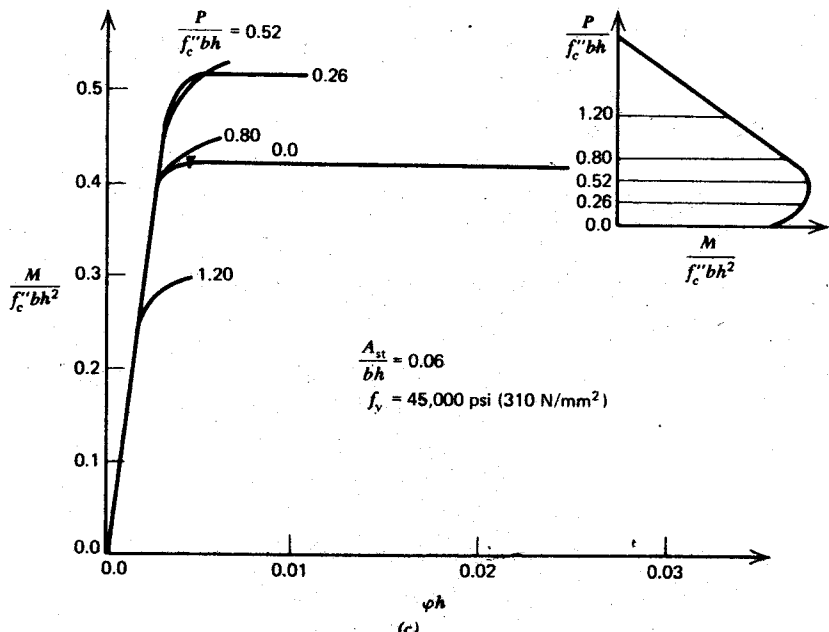


Fig. 6.13. Moment-curvature curves for column sections at various levels of axial load.^{6.3}

6.5 MEMBERS WITH CONFINED CONCRETE

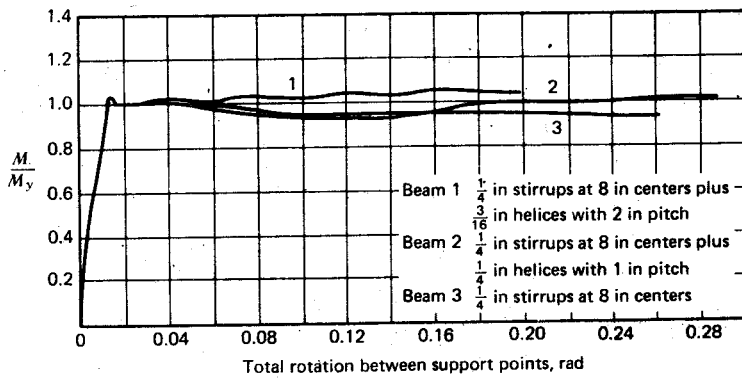
6.5.1 Effect of Confining the Concrete

If the compression zone of a member is confined by closely spaced transverse reinforcement in the form of closed stirrups, ties, hoops, or spirals, the ductility of the concrete may be greatly improved and a more ductile performance of the member at the ultimate load will result.

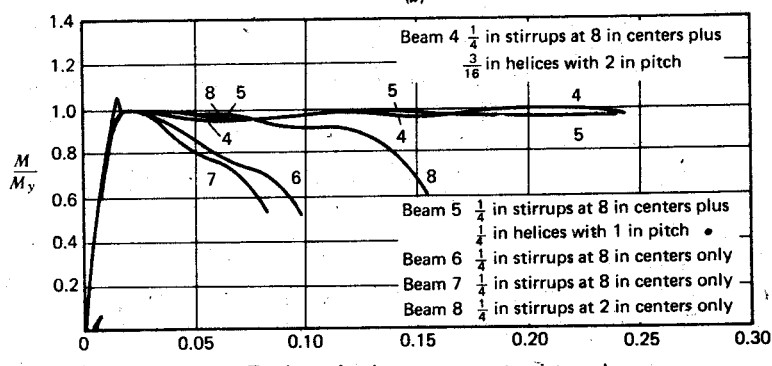
The stress-strain characteristics of concrete confined by transverse reinforcement were discussed in Section 2.1.3. At low levels of compressive stress, the transverse reinforcement is hardly stressed and the behavior of the concrete is unaffected by the reinforcement. At stresses approaching the uniaxial strength, the transverse strains in the concrete increase rapidly, because of progressive internal cracking, and the concrete expands against the transverse reinforcement. The restraining pressure applied by the reinforcement to the concrete considerably improves the stress-strain characteristics of the concrete at higher strains. Circular spirals confine the concrete more effectively than rectangular stirrups, ties, or hoops, because

confining steel in the shape of a circle applies a uniform radial pressure to the concrete, whereas a rectangle tends to confine the concrete mainly at the corners.

A number of tests that have been reported illustrate the effect of confinement of the concrete on the moment-rotation characteristics of beams. For example, Fig. 6.14 shows experimental moment-rotation curves from a series of beams tested by Base and Read.^{6,4} The beams had a rectangular section 6 in (152 mm) wide by 11 in (279 mm) deep and were loaded by a single point load at midspan over a simply supported span of 120 in (3.05 m). Figure 6.14a gives the moment-rotation curves obtained for beams having a tension steel content of approximately one-half the balanced failure value. The initial drop in moment occurred when the steel changed from the upper to the lower yield point. All beams can be seen to have a large rotation capacity



(a)



(b)

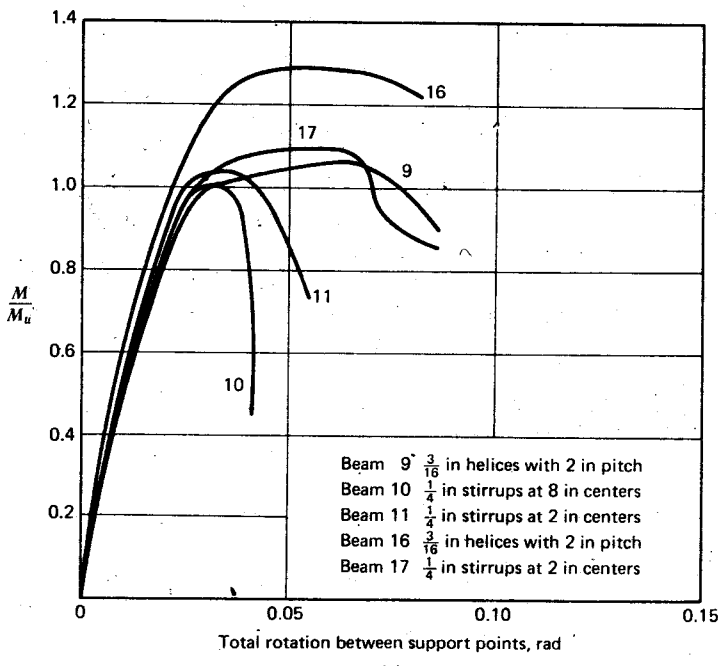


Fig. 6.14. Experimental moment-rotation curves for reinforced concrete beams.^{6,4} (a) Beams failing in tension. (b) Balanced beams. (c) Beams failing in compression.

without significant decrease in ultimate moment. Figure 6.14b. shows moment-rotation curves obtained for beams designed for a balanced failure. The helices and/or the closely spaced stirrups are shown to give a substantial increase in ductility. With curves obtained for beams that had a tension steel content greater than the balanced value (Fig. 6.14c), not only is an increase in ductility obtained from the transverse reinforcement apparent, but also an increase in strength occurs due to the large influence of the enhanced compressive strength of the concrete on this type of failure.

These tests and others have indicated qualitatively the beneficial effect of confinement by transverse reinforcement on the ductility of reinforced concrete flexural members. The effect on lightly reinforced beams is less marked because such members already have adequate ductility. The ductility of heavily reinforced beams, and of columns, can be substantially increased by confinement.

Concrete in the compression zone of members often receives some confinement from the loading or support conditions. Examples can be found

under the bearing plates of beams tested by point loads and in beams of frames at the column faces. The confinement afforded by bearing plates or adjacent members may cause the critical section to show more ductility than expected. However, one would be unwise to depend on such ductility unless positive steps are taken to ensure its availability.

The confinement of concrete in the critical sections of a member is also helped by the presence of a strain gradient across or along the member. If the strain changes rapidly with distance, because of rapid change of bending moment along the member or a small neutral axis depth, the highly stressed concrete will receive some confinement from the adjacent regions of less highly stressed concrete.

6.5.2 Compressive Stress Block Parameters for Concrete Confined by Rectangular Hoops

To develop theory for the moment-curvature characteristics of members with confined concrete, the stress-strain relationship for the concrete is required. Stress-strain relationships for confined concrete (discussed in Section 2.1.3) may be assumed to indicate the distribution of compressive stress in the compression zone of a member with confined concrete. For a given strain in the extreme compression fiber, and a given concrete stress-strain curve, the compressive stress block parameters can be determined by the method presented in Section 6.2.2. For a rectangular section, the concrete compressive force may be written as $C_c = \alpha f'_c b k d$ acting at $\gamma k d$ from the extreme compression fiber, where b = section width, $k d$ = neutral axis depth, $\alpha f'_c$ = mean stress in the stress block, and $\gamma k d$ = distance from the centroid of the stress block to the extreme compression fiber. For any given strain ϵ_{cm} in the extreme compression fiber, α and γ may be determined for rectangular sections from the stress-strain relationship of the concrete using Eqs. 6.6 and 6.7.

As an example, for the stress-strain curve for concrete confined by rectangular hoops proposed by Kent and Park^{6,5} (Fig. 2.18), there are three possible shapes for the compressive stress block, Fig. 6.15 indicates. The regions of the curve are defined by Eqs. 2.6 to 2.11. Table 6.2 shows values of α and γ computed using Eqs. 6.6 and 6.7 for stress blocks 2 and 3 (i.e., when $\epsilon_{cm} \geq 0.002$) and indicates the variation of these parameters with strain ϵ_{cm} and the parameter Z . The parameter Z is given by Eqs. 2.8 to 2.10 as

$$Z = \frac{0.5}{\frac{3 + 0.002f'_c}{f'_c - 1000} + \frac{3}{4} \rho_s \sqrt{\frac{b''}{s_h}} - 0.002} \quad (6.27)$$

where f'_c = concrete cylinder strength in psi (1 psi = 0.00689 N/mm²),

Table 6.2 Stress Block Parameters α and γ as a Function of ε_{cm} and Z^a

ε_{cm}	Z								
	10	30	50	70	100	140	200	300	400
Values of α									
0.002	0.667	0.667	0.667	0.667	0.667	0.667	0.667	0.667	0.667
0.003	0.776	0.773	0.769	0.766	0.761	0.754	0.744	0.728	0.711
0.004	0.828	0.818	0.808	0.798	0.783	0.763	0.733	0.683	0.633
0.005	0.858	0.840	0.822	0.804	0.777	0.741	0.687	0.600	0.547
0.006	0.876	0.849	0.822	0.796	0.756	0.702	0.622	0.533	0.489
0.007	0.887	0.851	0.815	0.780	0.726	0.655	0.562	0.486	0.448
0.008	0.894	0.849	0.804	0.759	0.692	0.602	0.517	0.450	0.417
0.009	0.899	0.844	0.790	0.735	0.654	0.558	0.481	0.422	0.393
0.010	0.901	0.837	0.773	0.709	0.613	0.522	0.453	0.400	0.373
0.011	0.903	0.829	0.755	0.682	0.576	0.493	0.430	0.382	0.358
0.012	0.903	0.819	0.736	0.653	0.544	0.468	0.411	0.367	0.344
0.013	0.902	0.809	0.716	0.623	0.518	0.448	0.395	0.354	0.333
0.014	0.901	0.798	0.695	0.593	0.495	0.430	0.381	0.343	0.324
0.015	0.899	0.787	0.674	0.567	0.476	0.415	0.369	0.333	0.316
Values of γ									
0.002	0.375	0.375	0.375	0.375	0.375	0.375	0.375	0.375	0.375
0.003	0.405	0.407	0.408	0.409	0.411	0.414	0.418	0.425	0.432
0.004	0.427	0.430	0.433	0.436	0.441	0.449	0.460	0.482	0.507
0.005	0.441	0.446	0.452	0.457	0.466	0.479	0.501	0.543	0.568
0.006	0.451	0.459	0.466	0.474	0.488	0.508	0.545	0.586	0.602
0.007	0.459	0.469	0.479	0.490	0.508	0.538	0.582	0.611	0.622
0.008	0.466	0.477	0.490	0.504	0.529	0.570	0.607	0.627	0.633
0.009	0.471	0.484	0.500	0.518	0.550	0.595	0.623	0.636	0.638
0.010	0.475	0.491	0.509	0.531	0.573	0.613	0.634	0.641	0.641
0.011	0.479	0.497	0.519	0.546	0.594	0.626	0.641	0.644	0.642
0.012	0.482	0.503	0.528	0.560	0.610	0.635	0.645	0.645	0.641
0.013	0.485	0.508	0.538	0.576	0.622	0.642	0.648	0.645	0.640
0.014	0.488	0.514	0.547	0.592	0.631	0.646	0.649	0.644	0.638
0.015	0.490	0.519	0.557	0.606	0.638	0.650	0.649	0.642	0.635

^a From reference 6.5.

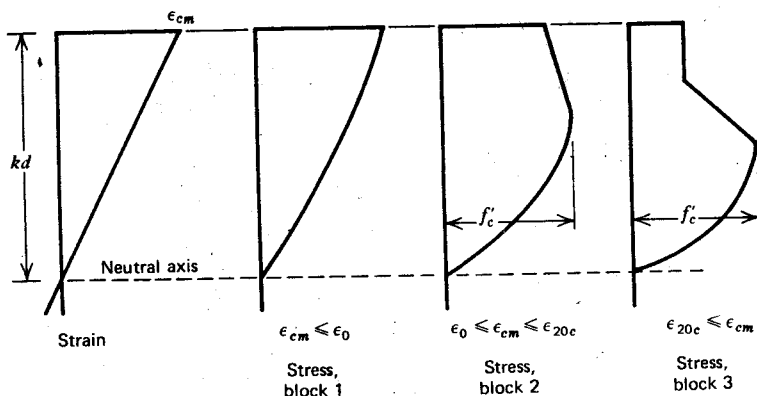


Fig. 6.15. Possible concrete compressive stress blocks.^{6.5}

ρ_s = ratio of volume of hoops to volume of concrete core measured to outside of hoops, b'' = width of confined core measured to outside of hoops, and s_h = hoop spacing. Values of Z from Eq. 6.27 are listed in Table 6.3. Note that the values of $\alpha = 0.728$ and $\gamma = 0.425$ given by Tables 6.2 and 6.3 when $f'_c = 4000$ psi (27.6 N/mm²), $\rho_s = 0$ ($\therefore Z = 300$) and $\epsilon_{cm} = 0.003$, compare well with the values of $\alpha = 0.85 \times 0.85 = 0.723$ and $\gamma = 0.5 \times 0.85 = 0.425$ given by the rectangular stress block of the ACI code.^{6.1} The improved characteristics of flexural members with confined concrete is evident from the tables. Tables 6.2 and 6.3 may be used to determine the flexural capacity and curvature of confined members at far advanced compressive strains.

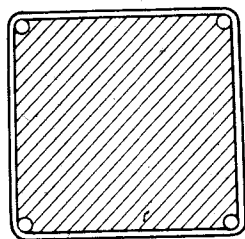
The foregoing stress-strain relationship for confined concrete was obtained from test results from concrete specimens with hoops enclosing only compressed concrete (see Fig. 6.16a). Use of a relationship based on such test data to determine the compressive stress block when part of the section is in tension (see Fig. 6.16b) may be questioned because part of the hoop is in the tension region. However, in this case the low-stressed concrete near the neutral axis will help to confine the highly stressed concrete; hence it is not of great significance that the hoop terminates in the tension zone. It is suggested conservatively that ρ_s for this case still be defined as the ratio of the volume of hoop steel to the volume of concrete enclosed by the hoops, rather than by any new definition considering an effective hoop volume and the compressed concrete volume.

In practice, various arrangements of transverse steel involving overlapping hoops, or hoops with supplementary cross ties, may be required to provide

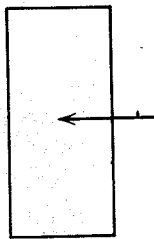
Table 6.3 Parameter Z as a Function of s_h/b'' , ρ_s , and f'_c , from Eq. 6.27

		f'_c , psi (N/mm ²)		
s_h	b''	3000 (20.7)	4000 (27.6)	5000 (34.5)
ρ_s				
0.25	0	200	300	400
	0.005	50	55	57
	0.01	29	30	31
	0.02	15	16	16
	0.03	11	11	11
	0.50	200	300	400
0.50	0.005	64	72	76
	0.01	38	41	42
	0.02	21	22	22
	0.03	15	15	15
	0.75	200	300	400
	0.005	73	83	90
0.75	0.01	45	48	51
	0.02	25	26	27
	0.03	18	18	18
	1.00	200	300	400
	0.005	80	92	100
	0.01	50	55	57
1.00	0.02	29	30	31
	0.03	20	21	21

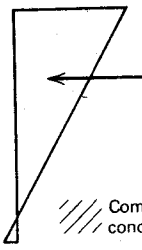
lateral support to the intermediate longitudinal bars. These additional transverse bars across the section help confine the concrete, and they must be taken into account. To include the effect of such additional transverse bars, the parameter Z in the stress-strain relationship for single hoops may be calculated for the partitioned concrete section. As an example, consider the column section with overlapping hoops shown in Fig. 6.16c. To determine Z from Eq. 6.27 for the compressive stress block of this section, it would be reasonable to assume that ρ_s is the ratio of volume of one hoop to volume of concrete core within that hoop, b'' is the width of the side of one hoop, and s_h is the spacing of sets of overlapping hoops. This definition of ρ_s is more conservative than the alternative of taking ρ_s as the ratio of total volume of hoops to total volume of concrete core, but given the lack of test data on the efficiency of overlapping hoops, it is probably wise to use the



Section



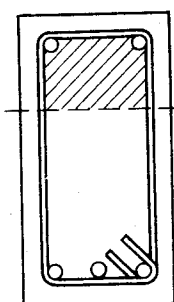
or



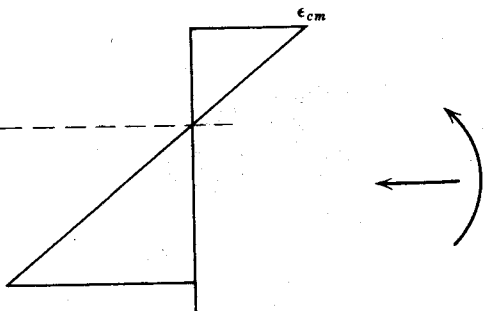
Compressed concrete

Strain profiles and external actions

(a)



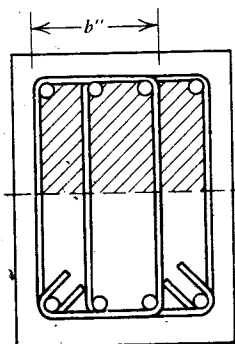
Section



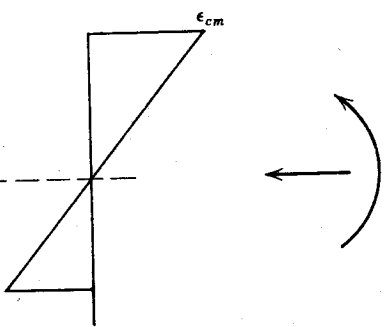
Strain profile

External actions

(b)



Section



Strain profile

External actions

(c)

Fig. 6.16. Transverse confining steel in members. (a) Type of test specimen used to determine the stress-strain curve.^{6,5} (b) Member with single hoops. (c) Member with overlapping hoops.

more conservative definition. It is evident that more experimental work is required to test the efficiency of various arrangements of transverse steel involving hoops with supplementary cross ties and overlapping hoops.

6.5.3 Theoretical Moment-Curvature Curves for Sections with Confined Concrete

Theoretical moment-curvature curves for confined reinforced concrete sections can be derived using the procedure outlined in Section 6.2.2 and the stress-strain curves for confined concrete and steel.

We shall use the stress-strain curve for confined concrete shown in Fig. 2.18, which gave the stress block parameters derived in Section 6.5.2. At large strains it is likely that the unconfined concrete outside the hoops (the cover concrete) will spall away. This is particularly true for sections containing heavy transverse hooping, since the transverse steel creates a plane of weakness that tends to precipitate spalling of the cover concrete. For small quantities of transverse steel, the cover concrete tends to act more with the core concrete. It is difficult to determine the strain at which spalling of the cover concrete commences because the spalling process occurs gradually. However, it can be assumed that the cover concrete follows the same stress-strain curve as the confined core up to a strain of 0.004, but carries no stress at higher strains. This assumption of the ineffectiveness of the cover concrete has also been made by Baker and Amarakone^{6,6} at strains greater than 0.0035, and by Blume et al^{6,2} at strains greater than 0.004. Yet others (e.g., Corley^{6,7}) have ignored spalling of cover concrete at higher strains. The actual behavior will lie somewhere between these two bounds.

At large strains it is also likely that the steel will have entered the strain-hardening range. Hence to obtain an accurate estimate of moment and curvature, the actual shape of the steel stress-strain curve must be considered. Figure 2.25c shows the general shape of the steel stress-strain curve. There are three regions, which may be represented by the following equations:

region *AB*: $\varepsilon_s \leq \varepsilon_y$

$$f_s = \varepsilon_s E_s \quad (6.28)$$

region *BC*: $\varepsilon_y \leq \varepsilon_s \leq \varepsilon_{sh}$

$$f_s = f_y \quad (6.29)$$

region *CD*: $\varepsilon_{sh} \leq \varepsilon_s \leq \varepsilon_{su}$

$$f_s = f_y \left[\frac{m(\varepsilon_s - \varepsilon_{sh}) + 2}{60(\varepsilon_s - \varepsilon_{sh}) + 2} + \frac{(\varepsilon_s - \varepsilon_{sh})(60 - m)}{2(30r + 1)^2} \right] \quad (6.30)$$

where

$$m = \frac{(f_{su}/f_y)(30r + 1)^2 - 60r - 1}{15r^2} \quad (6.31)$$

$$r = \varepsilon_{su} - \varepsilon_{sh} \quad (6.32)$$

The notation used in Eqs. 6.28 to 6.32 is illustrated in Fig. 2.25c. Equation 6.30 is similar to that obtained by Burns and Siess^{6,8} except that it follows a generalized form for steel with different f_{su}/f_y and ε_{su} values. The possibility of buckling of the compression steel is generally ignored because it is assumed that the transverse steel is at sufficiently close centers to prevent buckling. The buckling load of steel reinforcement in beams is difficult to estimate accurately (see Section 13.5). Some lateral restraint from the surrounding concrete may exist even after the cover has spalled away. Also, the curvature of the bar must change sign to buckle because it will have followed the curvature of the member.

Example 6.2

A singly reinforced concrete beam section (Fig. 6.17a) contains No. 3 (9.5 mm diameter) closed stirrups at 4 in (102 mm) centers and four No. 9 (28.7 mm diameter) longitudinal bars. The cover to the hoops is $1\frac{1}{2}$ in (38 mm). The steel has a yield strength of 52,000 psi (359 N/mm²), a modulus of elasticity of 29×10^6 psi (200,000 N/mm²), and strain hardening commences at a strain of 16 times the yield strain. The concrete has a cylinder strength of 4000 psi (27.6 N/mm²). Calculate the moment and the curvature when the concrete strain at the top of the confined concrete is 0.008, using the stress block parameters of Table 6.2.

Solution

Dimension of confined core to outside of the stirrups is 9 in by 17 in. Dimensions to center lines of stirrups is 8.63 in by 16.63 in.

$$\therefore \rho_s = \frac{0.11 \times 2(8.63 + 16.63)}{9 \times 17 \times 4} = 0.0091$$

Therefore, From Eq. 6.27 (or from Table 6.3)

$$Z = \frac{0.5}{(3 + 8)/3000 + \frac{3}{4} \times 0.0091 \sqrt{9/4 - 0.002}} = 42$$

A trial and error solution is required to determine the neutral axis depth. Estimate the neutral axis to be 7.5 in below the top of the

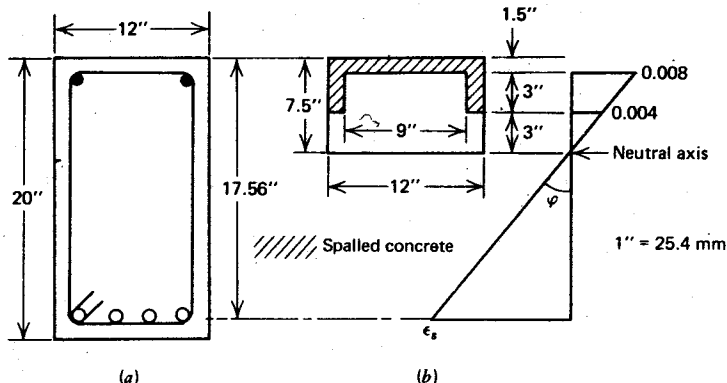


Fig. 6.17. Example 6.2. (a) Section (b) Compressed area of concrete and strain diagram for estimated neutral axis depth.

original section. Then because the strain at the top of the confined concrete is to be 0.008, the strain diagram may be drawn as in Fig. 6.17b. If unconfined concrete having a compressive strain greater than 0.004 is considered to be ineffective, the remaining compressed area resembles Fig. 6.17b. The remaining unconfined concrete will be assumed to have the same stress-strain curve as the confined concrete.

For the concrete within the stirrups

From Table 6.2 with $\epsilon_{cm} = 0.008$ and $Z = 41$, we find

$$\alpha = 0.824 \quad \gamma = 0.484$$

Therefore, the compressive force in the confined concrete

$$= 0.824 \times 4000 \times 9 \times 6 = 178,000 \text{ lb}$$

acting at distance from the tension steel

$$= 17.56 - 1.5 - 0.484 \times 6 = 13.16 \text{ in}$$

For the concrete outside the stirrups

From Table 6.2 with $\epsilon_{cm} = 0.004$ and $Z = 41$, we find

$$\alpha = 0.812 \quad \gamma = 0.432$$

Therefore, the compressive force in this concrete

$$= 0.812 \times 4000 \times 3 \times 3 = 29,200 \text{ lb}$$

acting at distance from the tension steel

$$= 17.56 - 4.5 - 0.432 \times 3 = 11.76 \text{ in}$$

$$\therefore C = 178,000 + 29,200 = 207,200 \text{ lb}$$

For the steel, from the strain diagram

$$\varepsilon_s = 0.008 \frac{17.56 - 1.5 - 6}{6} = 0.0134$$

Now

$$\varepsilon_y = \frac{52,000}{29 \times 10^6} = 0.00179 < \varepsilon_s \quad \text{and}$$

$$16\varepsilon_y = 16 \times 0.00179 = 0.0287 > \varepsilon_s$$

Therefore the steel is at the yield strength, $f_s = 52,000 \text{ psi}$.

$$\therefore T = 52,000 \times 4 = 208,000 \text{ lb}$$

Now $T \approx C$ Therefore, the correct neutral axis depth has been chosen.

$$\therefore \text{moment } M = (178,000 \times 13.16) + (29,200 \times 11.76) \\ = 2.69 \times 10^6 \text{ lb} \cdot \text{in} (304 \text{ kN} \cdot \text{m})$$

$$\text{curvature } \varphi = \frac{0.008}{6}$$

$$= 0.00133 \text{ rad/in} (0.0523 \text{ rad/m})$$

(Note: It can be shown that the above moment is 0.86 of the moment at $\varepsilon_{cm} = 0.003$, indicating the loss of moment due to concrete spalling but the curvature is 2.66 times that at $\varepsilon_{cm} = 0.003$.)

Example 6.3

Determine the postyield moment-curvature curves for square reinforced concrete column sections with the following fixed properties: $b = h = 30 \text{ in}$ (762 mm), $f'_c = 4000 \text{ psi}$ (27.6 N/mm²), $E_s = 29 \times 10^6 \text{ psi}$ (200,000 N/mm²), $f_y = 40,000 \text{ psi}$ (276 N/mm²), $f_{su} = 66,800 \text{ psi}$ (461 N/mm²), $\varepsilon_{sh} = 16\varepsilon_y$, $\varepsilon_{su} = \varepsilon_{sh} + 0.14$, cover to hoops = 1.5 in (38 mm), $P/f'_c b h = 0.3$.

The variable properties are as follows: longitudinal steel: $A_{st}/bh = 0.031$ and 0.055, distributed uniformly around the perimeter of the section; transverse steel: a range of transverse steel contents from $\frac{1}{2}$ in (12.7 mm) diameter overlapping rectangular hoops at 6 in (152 mm) centers to $\frac{3}{4}$ in (19.1 mm) diameter overlapping rectangular

hoops at 2 in (51 mm) centers. The arrangement of transverse steel appears in Fig. 6.18.

Solution

In this example, the Z values for the transverse steel contents may be calculated using Eq. 6.27 and the assumptions suggested at the end of Section 6.5.2. For the transverse steel arrangement in Fig. 6.18, with $\frac{1}{2}$ in diameter overlapping hoops at 6 in centers, we have

$$Z = \frac{0.5}{\left(\frac{3 + 8}{3000} \right) + \left(\frac{3}{4} \times \frac{90 \times 0.20}{19 \times 27 \times 6} \sqrt{\frac{19}{6}} \right) - 0.002} = 52.7$$

Similarly, for the transverse steel arrangement with $\frac{3}{4}$ in diameter overlapping hoops at 2 in centers, $Z = 5.6$. The Z values for other transverse bar diameters and spacing may also be calculated.

The moment-curvature relationships are best calculated using a digital computer. To determine the moment-curvature curves associated with different axial load levels, it is convenient to divide

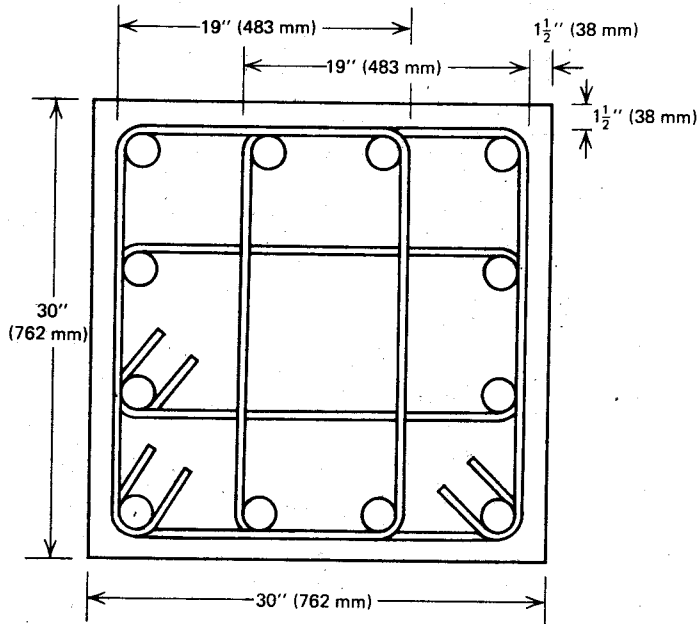


Fig. 6.18. Transverse steel arrangement, Example 6.3.

the section into a number of discrete laminae, each having the orientation of the neutral axis, and to replace the steel reinforcement by an equivalent thin tube with the appropriate wall thicknesses as in Fig. 6.19. Each lamina then contains a quantity of cover concrete, core concrete, and steel. The stresses in the concrete and steel in each lamina are found from the average strain in the lamina and the stress-strain relations. The stress-strain relations for the concrete are given by Eqs. 2.6, 2.7 with the appropriate Z value substituted, and 2.11. The stress-strain relations for the steel are given by Eqs. 6.28 to 6.32.

The theoretical moment-curvature relationship for a given load level may be determined by incrementing the concrete strain in the extreme compression fiber, ε_{cm} . For each value of ε_{cm} the neutral axis depth kd is found which satisfies the force equilibrium equation

$$P = \sum_{i=1}^n f_{ci} A_{ci} + \sum_{i=1}^n f_{si} A_{si} \quad (6.33)$$

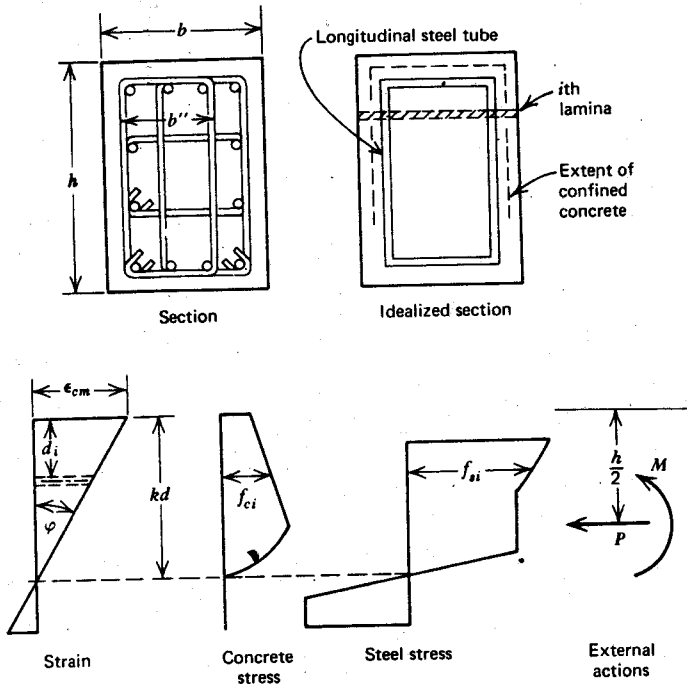


Fig. 6.19. Section with strain and stress distribution, Example 6.3.

where f_{ci} , f_{si} = stresses in the concrete and steel in the i th lamina, A_{ci} , A_{si} = areas of concrete and steel in the i th lamina, and n = number of laminae. Then the moment M corresponding to that value of ε_{cm} and load P is determined by taking the moments of the internal forces about a suitable axis

$$M = \sum_{i=1}^n f_{ci} A_{ci} d_i + \sum_{i=1}^n f_{si} A_{si} d_i - P \frac{h}{2} \quad (6.34)$$

and the curvature is given by $\varphi = \varepsilon_{cm}/kd$, where d_i = distance of the centroid of i th lamina from extreme compression fiber and h = section depth.

Figure 6.20 plots the moment-curvature relationships for the

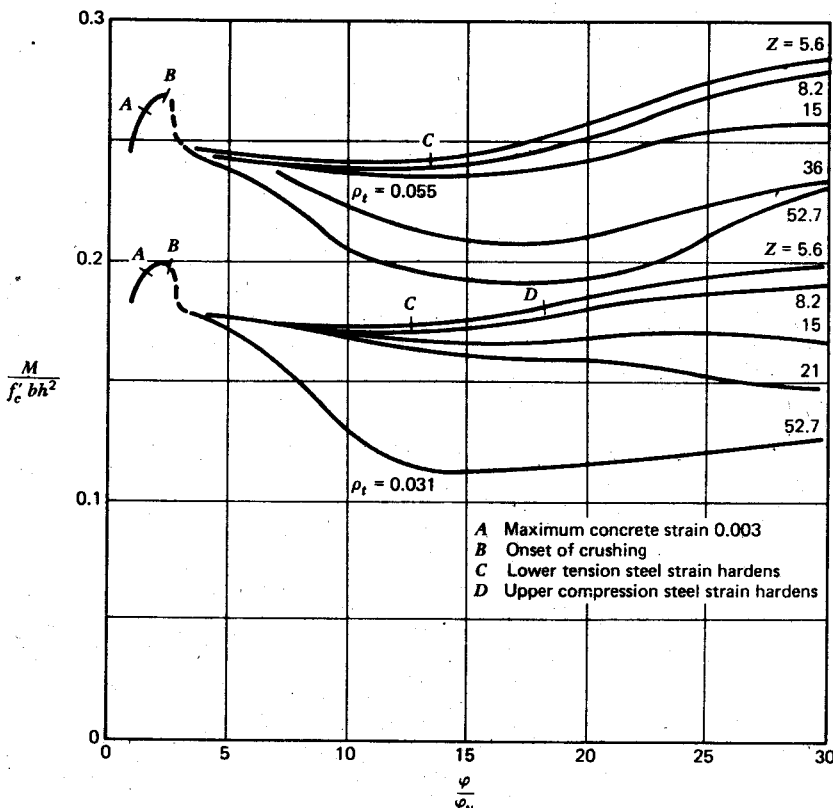


Fig. 6.20. Moment-curvature ductility curves for column section with $P = 0.3f_c'bh$, Example 6.3.

section in dimensionless form for the given level of load, the two longitudinal steel contents, and a range of Z values corresponding to various transverse steel contents. The curves display a sudden reduction in the moment capacity at the assumed onset of crushing of the concrete cover at an extreme fiber strain of 0.004. With further curvature the contribution of the concrete to the moment carrying capacity comes from such cover concrete, which is at a strain of less than 0.004, and the confined core. At curvatures high enough to cause strain hardening of the tension steel, a significant increase in moment is apparent. It has been assumed that the compression steel does not buckle.

The curves of Fig. 6.20 illustrate that good confinement (low Z values) is essential for the column of Example 6.3 if a reasonable moment capacity is to be maintained after crushing of the cover concrete has commenced. If load levels higher than $0.3f'_c b h$ had been considered, the amount of confining steel would have been even more important. In general, the higher the load level, the greater the amount of confining steel required to maintain a reasonable moment-carrying capacity at high curvatures after crushing commences.

ACI 318-71^{6.1} requires special transverse steel if the design load of the column exceeds $0.4P_b$, where P_b is the balanced failure load. A load of $0.4P_b$ corresponds to a $P/f'_c b h$ value for the section studied in Example 6.3 of approximately 0.20 to 0.23, thus special transverse steel would be required in the column of the example. The amount of special transverse steel recommended by the code for the arrangement of hoops used in the example can be obtained from $\frac{5}{8}$ in (15.9 mm) diameter hoops at 2.8 in (71 mm) centers, which is equivalent to $Z = 13$. It is evident from Fig. 6.20 that for this particular column the quantity of transverse steel specified by the code will ensure that the moment capacity after crushing of concrete has commenced is fairly well maintained at higher curvatures. The amount of transverse steel required in more general cases is examined in Chapter 11.

6.6 FLEXURAL DEFORMATIONS OF MEMBERS

6.6.1 Calculation of Deformations from Curvatures

The rotation and deflection of a member may be calculated by integrating the curvatures along the member. Since the curvature is defined as the rotation per unit length of member, the rotation between any two points A and B of the member is given by

$$\theta_{AB} = \int_A^B \varphi \, dx \quad (6.35)$$

where dx is an element of length of the member.

Figure 6.21 shows a cantilever with deformation due to rotation $d\theta$ over the element of length dx only. The rotation $d\theta$ is equal to φdx , where φ is the curvature at the element. The transverse deflection $d\Delta$ at point A from the tangent to the axis of the member at the fixed end B, due to rotation $d\theta$ between the ends of the element, is $x d\theta$ or $x\varphi dx$. Hence the transverse

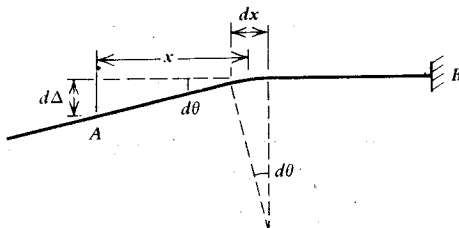


Fig. 6.21. Deflection due to flexural deformation of an element.

deflection of point A from the tangent to the axis of the member at point B due to curvature along the whole length of member between those points is given by

$$\Delta_{AB} = \int_A^B x\varphi dx \quad (6.36)$$

where x is the distance of element dx from A.

Equations 6.35 and 6.36 are generalizations of the moment-area theorems, and they apply whether elastic or plastic curvatures are involved. These two equations may be used to calculate the rotations and deflection of members when one knows the moment-curvature relationships, as calculated in previous sections, and the distribution of bending moment. Such an approach using Eqs. 6.35 and 6.36 ignores the effect of the increase in stiffness of members due to tension carried by the concrete between the cracks, as well as the additional deformations caused by diagonal tension cracks due to shear and by bond slip of the reinforcement. These additional effects are discussed in the next section.

6.6.2 Additional Effects on the Deformations of Members Calculated from Curvatures

Effects of Concrete Tension Between Flexural Cracks

Figure 6.22a represents part of a reinforced concrete flexural member. The member has cracked at discrete intervals because the tensile strength of the concrete has been exceeded. At the cracked section all the tension

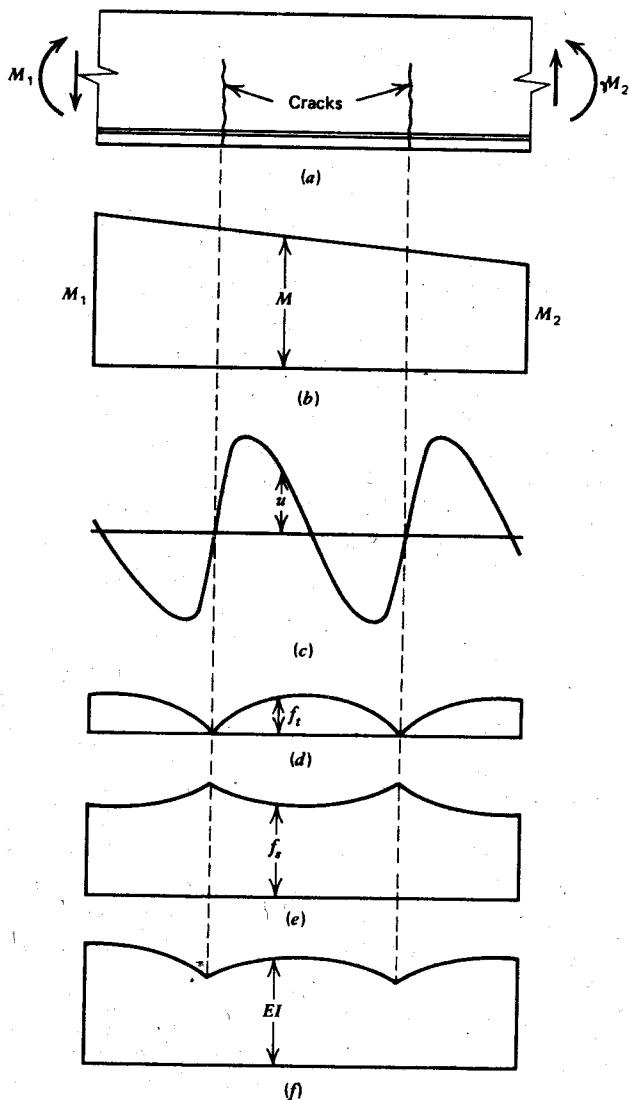


Fig. 6.22. Effect of cracking of a reinforced concrete flexural element. (a) Element of beam. (b) Bending moment distribution. (c) Bond stress distribution. (d) Concrete tensile stress distribution. (e) Steel tensile stress distribution. (f) Flexural rigidity distribution in elastic range.

is carried by the steel reinforcement. Some tensile stress will be present in the concrete between the cracks, however, because between the cracks some tension is transferred from the steel to the concrete by bond stresses. The magnitude and distribution of the bond stress between the cracks determines the distribution of the tensile stresses in the concrete and the steel between the cracks. Additional cracks can form between the initial cracks at higher moments if the tensile strength of the concrete is exceeded. The final crack spacing is reached when a tensile force of sufficient magnitude to form an additional crack between two existing cracks can no longer be transferred by bond from the steel to the concrete.

Figures 6.22c, 6.22d, and 6.22e give idealized distributions of bond stress and concrete and steel tensile stresses between cracks. Because the member is carrying some tension between cracks, the flexural rigidity clearly will be greater between the cracks than at the cracks, as indicated in Fig. 6.22f. This variation in flexural rigidity between cracks makes the accurate determination of deformations from moment-curvature relationships in the elastic range difficult because the $M-\varphi$ relationships derived in Sections 6.2 to 6.5 do not apply strictly to sections between the cracks.

Deformations in the elastic range may be estimated by substituting the relationship $\varphi = M/EI$ into Eqs. 6.35 and 6.36, where M is the moment at the element and EI is the elastic flexural rigidity at the element. The use of an EI value that lies between the uncracked and fully cracked values will lead to reasonable accuracy. As discussed in Section 10.3.3, ACI 318-71^{6.1} suggests use of the following effective moment of inertia to determine the flexural rigidity for deflection calculations of cracked members in the elastic range:

$$I_e = \left(\frac{M_{cr}}{M_a} \right)^3 I_g + \left[1 - \left(\frac{M_{cr}}{M_a} \right)^3 \right] I_{cr} \quad (6.37)$$

where M_{cr} is the moment at first cracking, M_a is the maximum moment in the member at the stage for which deflection is being calculated, I_g is the moment of inertia of the gross concrete section about the centroidal axis ignoring the reinforcement, and I_{cr} is the moment of inertia of the cracked transformed (all-concrete) section. The flexural rigidity obtained, using the effective moment of inertia of Eq. 6.37 and the modulus of elasticity of the concrete, lies between the values for uncracked and fully cracked conditions, the actual magnitude depending on the extent of cracking. The background of Eq. 6.37, which is an empirical equation, is covered in Section 10.3.3.

When the maximum moment considerably exceeds the cracking moment, Equation 6.37 indicates that the stiffening effect of tension carried by concrete between cracks has much less significance, and the cracked section value I_{cr}

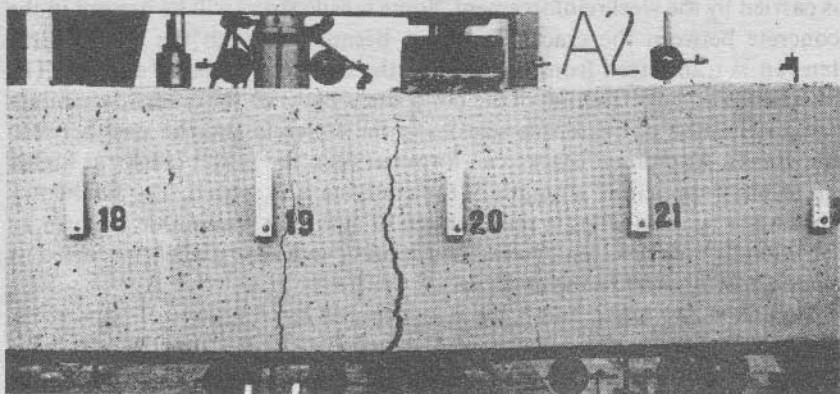


Fig. 6.23. Flexural cracks in a reinforced concrete beam near ultimate moment without significant shear force.^{6,9}

can be used with little error. In plastic regions of members, the effect of tension stiffening is particularly small.

An alternative method for dealing with the stiffening effect of concrete tension between cracks, using an assumed distribution of bond stress to compute effective moment-rotation relationships for beam elements between cracks, is discussed in Section 6.6.5.

Effect of Diagonal Tension Cracks and Bond Slip

The determination of rotations and deflections by integrating the curvatures along members using Eqs. 6.35 and 6.36 ignores the effects on the deformations of diagonal tension cracks due to shear force and of bond slip in anchorage zones.

Diagonal tension cracks form in members because of the presence of relatively large shear forces acting with flexure. The principal tensile stress developed as a result of combined shear and flexural stresses is inclined at an angle to the axis of the member and results in the diagonal tension (inclined) cracks. Figures 6.23 and 6.24 show cracks developed in reinforced concrete flexural members near ultimate moment in the absence of shear force and in the presence of shear force, respectively. The inclination of the cracks due to the presence of shear force is evident. As Fig. 6.23 indicates, when only flexural cracks occur the yielding of the tension steel concentrates across one or two critical cracks. When diagonal tension cracks are present, however, the yielding of the steel occurs over a much wider zone, as the more extensive cracking of Fig. 6.24 reveals. This effect is discussed in Section 7.5.1 in

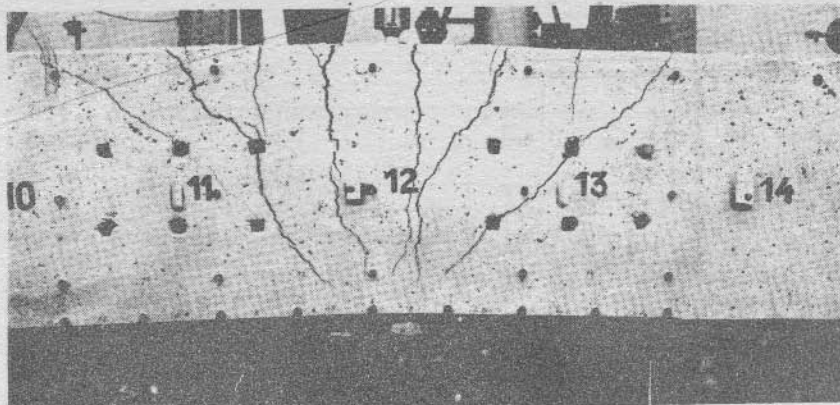


Fig. 6.24. Diagonal tension cracks in a reinforced concrete beam near ultimate moment with significant shear force.⁶⁻⁹

connection with the effect of shear force on flexural steel requirements. It is shown that when diagonal tension cracks are present in a member, the tension in the flexural reinforcement at sections away from the section of maximum moment may be larger than that computed from the bending moment diagram. This effect of diagonal tension cracking is illustrated in Fig. 7.19. It is evident that the internal tension remains nearly constant at the maximum value over a distance e_v from the critical section. The distance e_v will depend on the depth of the member and the content of web reinforcement, as shown in Fig. 7.20. Thus when diagonal tension cracks are present, the region in which the reinforcement is yielding (the plastic hinge zone) will be more extensive than the bending moment diagram implies. Use of a horizontally displaced bending moment diagram in the plastic zones, as in Figs. 7.19 and 7.20, to compute curvatures has been suggested by some investigators (e.g., Rosenblueth and Diaz de Cossio^{6,10} and Sawyer^{6,11}).

Bond slip of reinforcement in anchorage zones will also increase the deformations. The effect of bond slip can be included if the amount of slip is known. For example, if the slip of the beam tension steel through the core of the beam-column joint (Fig. 6.25) is δ , the additional rotation of the beam at the column face will be $\delta/(d - c)$, where $d - c$ is the distance from the tension steel to the neutral axis.

Notwithstanding obvious difficulties in accurately accounting for the additional deformations due to shear and bond slip, it is often possible to obtain reasonable agreement between computed and experimental rotations and displacements directly from the bending moment distribution and the

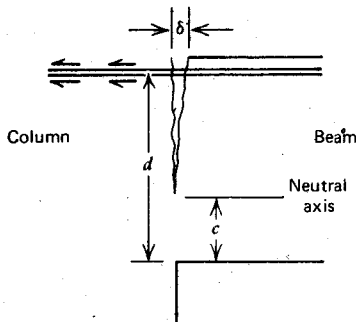


Fig. 6.25. Effect of bond slip of reinforcement on deformation.

moment-curvature relationships, since the effect of shear and bond slip is not always important. In general, plastic rotations calculated ignoring the effect of shear and bond slip will underestimate the actual plastic rotations, giving a conservative indication of the available ductility.

6.6.3 Idealized Ultimate Deformations Calculated from Curvatures

Figure 6.26 shows part of a reinforced concrete flexural member that has reached the ultimate curvature and bending moment at the critical section. End *A* of the member, for example, is the free end of a cantilever or a point of contraflexure, and end *B* is a column face. The distribution of curvature along the member is apparent. The region of inelastic curvature is spread over a length of beam, as discussed previously, this region being at least that at which the bending moment exceeds the yield moment of the section. In the regions of the beam, the curvature fluctuates because of the increased rigidity of the member between the cracks, as previously described. Each of the peaks of curvature corresponds to a crack position.

In ductility predictions it is necessary to determine the deformation that has occurred when the ultimate moment is reached. The rotation and deflection of the member in the ultimate condition can be obtained from the actual curvature distribution using Eqs. 6.35 and 6.36. The actual curvature distribution at ultimate can be idealized into elastic and inelastic regions (see Fig. 6.26c). The elastic contribution to rotation and deflection may be calculated from Eqs. 6.35 and 6.36 using $\varphi = M/EI$. The elastic contribution to the rotation over the full length of the member (the unshaded area of the curvature diagram of Fig. 6.26c) is given by

$$\theta = \int_A^B \frac{M}{EI} dx \quad (6.38)$$

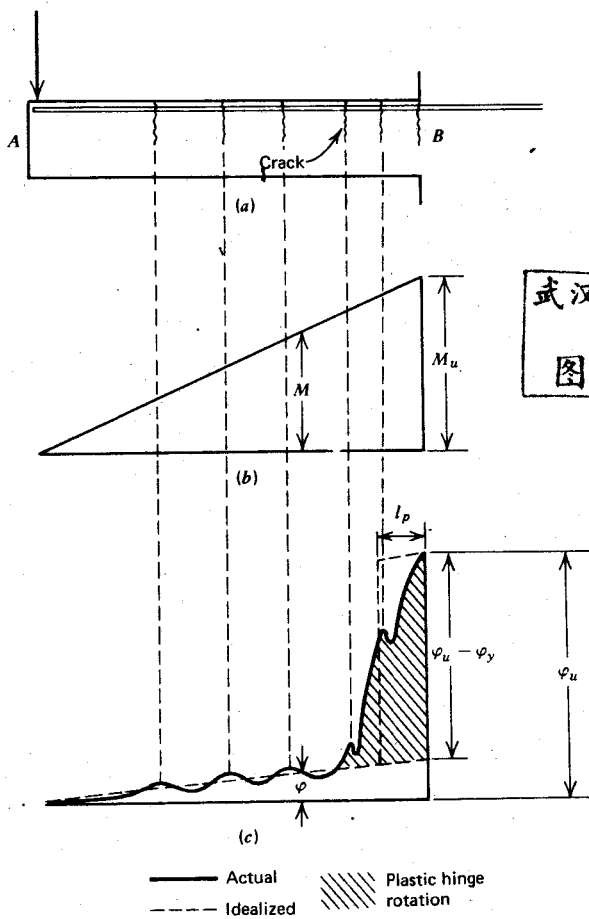


Fig. 6.26. Curvature distribution along beam at ultimate moment. (a) Beam. (b) Bending moment diagram. (c) Curvature diagram.

where the flexural rigidity EI is given by an appropriate idealization. If a fully cracked section is assumed along the whole length of the member, EI is given by $E_c I_{cr} = M_y/\varphi_y$, or approximately by M_u/φ_y . As discussed previously, these values would overestimate the elastic rotation (see also Fig. 6.27 for a comparison), and a more accurate result would be given by using $E_c I_e$ with I_e from Eq. 6.37.

The shaded area of Fig. 6.26c is the inelastic rotation that can occur at the "plastic hinge" in the vicinity of the critical section. That is, the shaded area

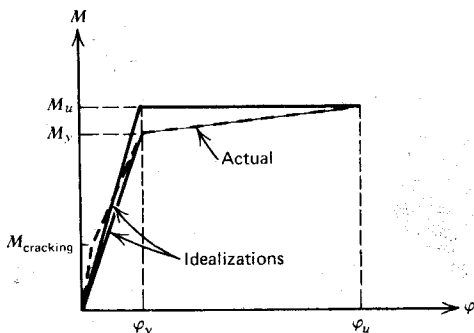


Fig. 6.27. Actual and idealized moment-curvature curves at cracked sections.

represents the plastic rotation that occurs in addition to the elastic rotation at the ultimate stage of the member. The inelastic area at the ultimate stage can be replaced by an equivalent rectangle of height $\varphi_u - \varphi_y$ and width l_p , having the same area as the actual inelastic curvature distribution, as in Fig. 6.26c. The width l_p is the equivalent length of the plastic hinge over which the plastic curvature is considered to be constant. Hence the plastic hinge rotation to one side of the critical section may be written as

$$\theta_p = (\varphi_u - \varphi_y)l_p \quad (6.39)$$

Example 6.4

For the cantilever *AB* of Fig. 6.28a with the point load, determine the rotation between the ends and the vertical end deflection when the ultimate moment is reached at the critical section. An idealized inelastic curvature distribution and a fully cracked section in the elastic region may be assumed. The effects of shear and bond slip may be ignored.

Solution

Figures 6.28b and 6.28c represent the bending moment diagram and the distribution of curvature assumed at the ultimate moment, respectively.

The rotation between *A* and *B* is given by Eq. 6.35 or Eqs. 6.38 and 6.39.

$$\begin{aligned} \therefore \theta_{AB} &= \theta_e + \theta_p \\ &= \varphi_y \frac{l}{2} + (\varphi_u - \varphi_y)l_p \end{aligned}$$

Note that θ_{AB} is the area of the curvature diagram.

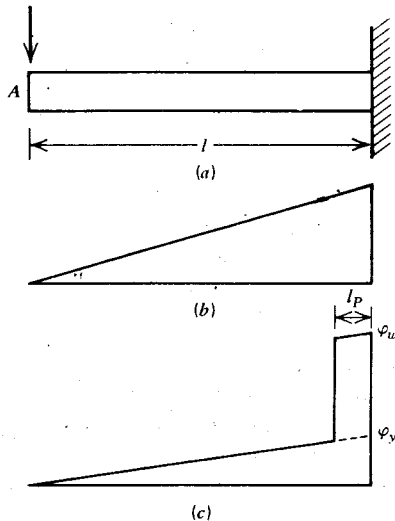


Fig. 6.28. Example 6.4. (a) Cantilever. (b) Bending moment distribution. (c) Curvature distribution.

The vertical deflection at A is given by Eq. 6.36 as the moment of the curvature diagram about A .

$$\therefore \Delta_{AB} = \left(\frac{\varphi_y l}{2} \frac{2l}{3} \right) + (\varphi_u - \varphi_y) l_p \left(1 - \frac{l_p}{2} \right)$$

6.6.4 Empirical Expressions for Ultimate Plastic Rotation Calculated from Curvatures

The Significant Variables

Equation 6.39 gives the plastic rotation in terms of the curvatures at ultimate and yield and the equivalent plastic hinge length. The strain diagrams when there is tension over part of the section at these stages appear in Fig. 6.29. From Eqs. 6.1 and 6.39 the plastic hinge rotation to one side of the critical section is

$$\theta_p = \left(\frac{\varepsilon_c}{c} - \frac{\varepsilon_{ce}}{kd} \right) l_p \quad (6.40)$$

where c is the neutral axis depth at the ultimate moment, ε_c is the concrete strain in the extreme compression fiber at the ultimate curvature, kd is the neutral axis depth when the yield curvature is reached, and ε_{ce} is the concrete strain in the extreme compression fiber when the yield curvature is reached. Usually ε_{ce} is the concrete strain when the tension steel yields, but in heavily loaded columns or overreinforced beams, the concrete may reach

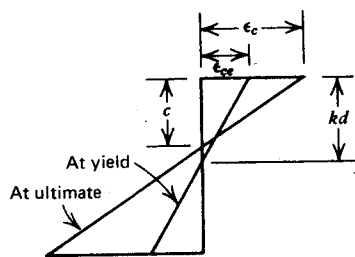


Fig. 6.29. Strain diagrams at yield and ultimate curvatures.

the inelastic range before the tension steel yields. The strain at the end of the elastic range of the concrete may be taken as 0.001 or higher, depending on the strength of the concrete (see Fig. 2.1 or 2.2). Hence ϵ_{ce} is either the concrete strain at the end of the elastic range or the concrete strain when the tension steel commences to yield, which ever is smaller.

To estimate θ_p from Eq. 6.40, the equivalent length of the plastic hinge l_p must be known. Figure 6.30a is the moment-curvature diagram for the sections of a member. Figure 6.30b gives the distribution of bending moment and internal moment Tjd along the member when the ultimate moment is reached at the critical section for two cases of cracking. The left hand diagram of Fig. 6.30b is for the case when only flexural cracks are present; the right hand diagram is for when diagonal tension cracks are present. As indicated in Section 6.6.2, diagonal tension cracks lead to higher tension forces T in the flexural reinforcement than implied by the bending moment diagram at sections away from the section of maximum bending moment. For both cases of cracking, in all regions of the beam where the internal moment exceeds the yield moment M_y , the steel is yielding. The distribution of curvature in the theoretical region of yielding ($M_y \leq M \leq M_u$) in the member without diagonal tension cracks can be calculated from the bending moment ordinates and the moment-curvature diagram, as shown in Fig. 6.30c. The value of l_p can be estimated from the determined distribution of inelastic curvature by determining the width of the rectangle having the same area as the inelastic curvature distribution. For the member with diagonal tension cracks, the moment-curvature curve applies only very approximately to the internal moment (Tjd) diagram; hence the additional inelastic curvature due to diagonal cracks cannot be estimated with accuracy. Nevertheless, Fig. 6.30 indicates the variables likely to influence the equivalent length of the plastic hinge l_p . Steel type and concrete strength affect the shape of the moment-curvature curve, hence will influence the length of yielding and distribution of curvature in the yielding zone for a given bending moment pattern. Also, the distance z from the critical section to the point of contraflexure will have

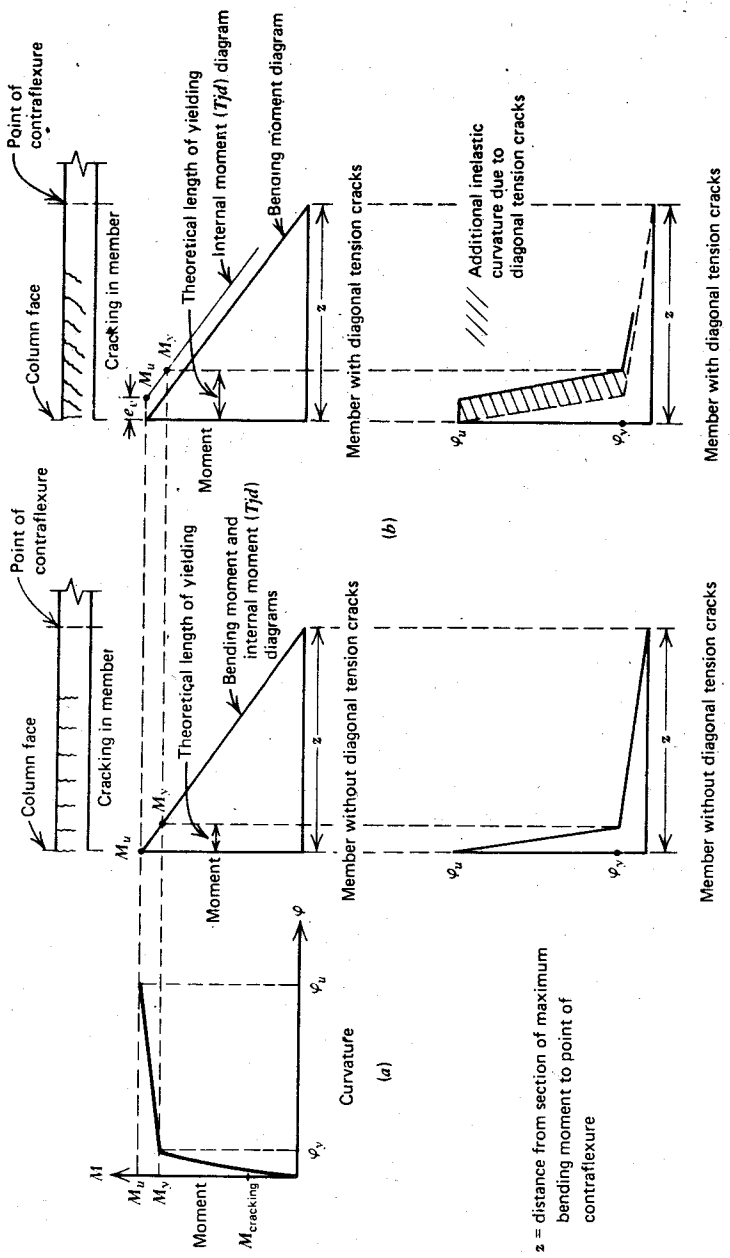


Fig. 6.30. Spread of yielding along a member at ultimate moment. (a) Moment-curvature relationship. (b) Bending and internal moment diagrams. (c) Idealized curvature diagrams.

a significant effect on l_p because, as Fig. 6.30 indicates, the greater the value of z , the greater the length of yielding. To these variables needs to be added the effect of shear, probably best expressed by the nominal shear stress intensity V/bd .

Empirical Expressions

Various empirical expressions have been proposed by investigators for the equivalent length of the plastic hinge l_p and the maximum concrete strain ε_c at ultimate curvature. These are reviewed below.

BAKER^{6.12, 6.13, 6.6}

1. For members with unconfined concrete

$$l_p = k_1 k_2 k_3 \left(\frac{z}{d} \right)^{1/4} d \quad (6.41)$$

where $k_1 = 0.7$ for mild steel or 0.9 for cold-worked steel,

$k_2 = 1 + 0.5P_u/P_0$, where P_u = axial compressive force in member and P_0 = axial compressive strength of member without bending moment

$k_3 = 0.6$ when $f'_c = 5100$ psi (35.2 N/mm 2) or 0.9 when $f'_c = 1700$ psi (11.7 N/mm 2), assuming $f'_c = 0.85 \times$ cube strength of concrete

z = distance of critical section to the point of contraflexure

d = effective depth of member

Baker has indicated that for the range of span/d and z/d ratios normally found in practice, l_p lies in the range between $0.4d$ and $2.4d$.

2. For members confined by transverse steel

More recent work reported by Baker^{6.6} proposes an expression for θ_p , implying that for members with tension over part of the section

$$l_p = 0.8k_1 k_3 \left(\frac{z}{d} \right)^{1/4} c \quad (6.42)$$

where c is the neutral axis depth at the ultimate moment and the other symbols have the previous meaning.

When Eq. 6.41 is used in conjunction with Eq. 6.40, $\varepsilon_c = 0.0035$. When Eq. 6.42 is used in conjunction with Eq. 6.40, ε_c has the following value:

$$\varepsilon_c = 0.0015 \left[1 + 150\rho_s + (0.7 - 10\rho_s) \frac{d}{c} \right] \leq 0.01 \quad (6.43)$$

where ρ_s is the ratio of the volume of the transverse confining reinforcement to the volume of the concrete core.

When these values are employed in strength calculations, Baker recommends the use of a concrete compressive stress block given by the stress-strain curve of Fig. 2.17b; where L_2 is the limiting value of strain given by 0.0035 for unconfined concrete or Eq. 6.43 for confined concrete. The maximum concrete stress f_c'' is given by

$$f_c'' = \left(0.8 + 0.1 \frac{d}{c} \right) f_c' \leq f_c' \quad (6.44)$$

Baker recommends that unconfined concrete at strains greater than 0.0035 be considered to have spalled and to be ineffective.

Test results for θ_p show considerable scatter, due mainly to the variation of the concrete strain at the ultimate curvature. The value for θ_p given by the foregoing equations is claimed by Baker to furnish a reasonable safe prediction of the available plastic rotation because safe limiting values have been used.

CORLEY^{6,7}

From the results of tests on simply supported beams, Corley has proposed the following expression for the equivalent length of the plastic hinge:

$$l_p = 0.5d + 0.2\sqrt{d} \left(\frac{z}{d} \right) \quad (6.45)$$

He also suggested the following as a lower bound for the maximum concrete strain:

$$\varepsilon_c = 0.003 + 0.02 \frac{b}{z} + \left(\frac{\rho_s f_y}{20} \right)^2 \quad (6.46)$$

where z = distance from the critical section to the point of contraflexure, b = width of beam, d = effective depth of beam in inches (1 in = 25.4 mm), ρ_s = ratio of volume of confining steel (including the compression steel) to volume of concrete core, and f_y = yield strength of the confining steel in kips per square inch (1 kip/in² = 6.89 N/mm). The plastic rotation may be calculated by substituting these values for l_p and ε_c into Eq. 6.40.

In discussing Corley's paper, Mattock^{6,14} suggested that simpler forms of Eqs. 6.45 and 6.46 that fitted the trend of the data reasonably well were

$$l_p = 0.5d + 0.05z \quad (6.47)$$

$$\varepsilon_c = 0.003 + 0.02 \frac{b}{z} + 0.2\rho_s \quad (6.48)$$

This modification to the equation for ε_c makes it more conservative for high values of ρ_s .

When using these values in strength calculations, the spalling of the cover concrete at high strains was ignored and the ACI concrete compressive stress block parameters were employed. It was also emphasized that at large ultimate curvatures the steel strains are high, and the steel may be in the strain hardening range. The increased tensile force due to strain hardening will increase the neutral axis depth and should be taken into account in calculating c , otherwise the ultimate curvature may be overestimated.

SAWYER^{6.11}

Sawyer has proposed the following expression for the equivalent length of the plastic hinge:

$$l_p = 0.25d + 0.075z \quad (6.49)$$

This equation is based on the assumptions that the maximum moment in the member is the ultimate moment, that $M_y/M_u = 0.85$, and that the zone of yielding is spread $d/4$ past the section in which the bending moment is reduced to M_y .

Example 6.5

Calculate the equivalent plastic hinge length of a reinforced concrete beam reinforced by mild steel, where $f'_c = 3000$ psi (20.7 N/mm^2) and $z/d = 5$.

Solution

$$\text{Baker's equation (6.41)} \quad l_p = 0.7 \times 1 \times 0.79(5)^{1/4}d = 0.83d$$

$$\text{Mattock's Equation (6.47)} \quad l_p = (0.5 + 0.05 \times 5)d = 0.75d$$

$$\text{Sawyer's equation (6.49)} \quad l_p = (0.25 + 0.075 \times 5)d = 0.63d$$

It is to be noted that l_p is the equivalent plastic hinge length on one side of the critical section. Thus a plastic hinge within the span of a symmetrically loaded beam will have a total equivalent length of $2l_p$.

The differences between the various empirical expressions emphasizes that the rotation capacity of plastic hinges in reinforced concrete members can only be approximated at present. More research is needed to clear the differences between the various empirical expressions.

6.6.5 Alternative Approach to the Calculation of Deformations Based on the Summation of Discrete Rotations at Cracks

In 1970 Bachmann^{6.9} proposed a method for calculating the deformations of reinforced concrete flexural members from the rotations of elements between cracks rather than from the curvatures at sections. The method takes into

account the effect of the inclination of cracks and the stiffening effects of concrete tension between cracks. In the analysis, the member is divided into "flexural crack elements" (e.g., as in the beam of Fig. 6.23, where bending moment is predominant and therefore only vertical flexural cracks can occur) and "shear crack elements" (e.g., as in the beam of Fig. 6.24, where relatively large shear forces are present with bending moment, and diagonal tension cracking occurs).

Deformations in Regions of Flexural Crack Elements

A length of member with flexural crack elements appears in Fig. 6.31. The cracks are assumed to be spaced at distance a apart. Bachmann prefers to calculate the rotation in terms of crack widths, but it is more direct to calculate the rotation in terms of the steel elongation between cracks. The total

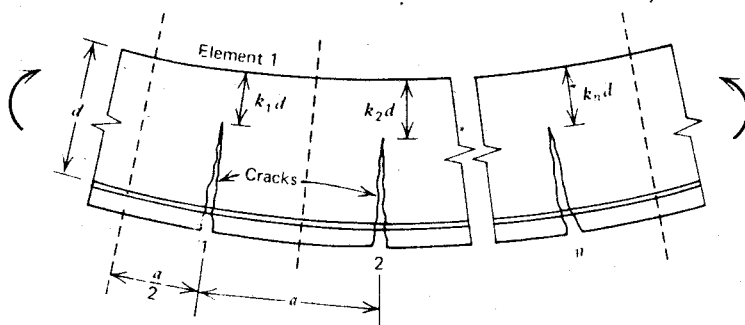


Fig. 6.31. Member with flexural crack elements.

rotation θ between the ends of a length of member consisting of n elements may be written as

$$\theta = \sum_{i=1}^n \frac{s_i}{d - k_i d} \quad (6.50)$$

where d is the effective depth to the tension steel, s_i is the elongation of the steel between the ends of element i , and $k_i d$ is the neutral axis depth at the crack in element i . An approximation made in Eq. 6.50 is that the neutral axis depth along the length of the element is constant at the cracked section value.

Considering a typical flexural crack element (Fig. 6.32), it is evident that to calculate the steel elongation, the bond characteristics for the steel reinforcement must be known. Now the change in steel force in a reinforcement

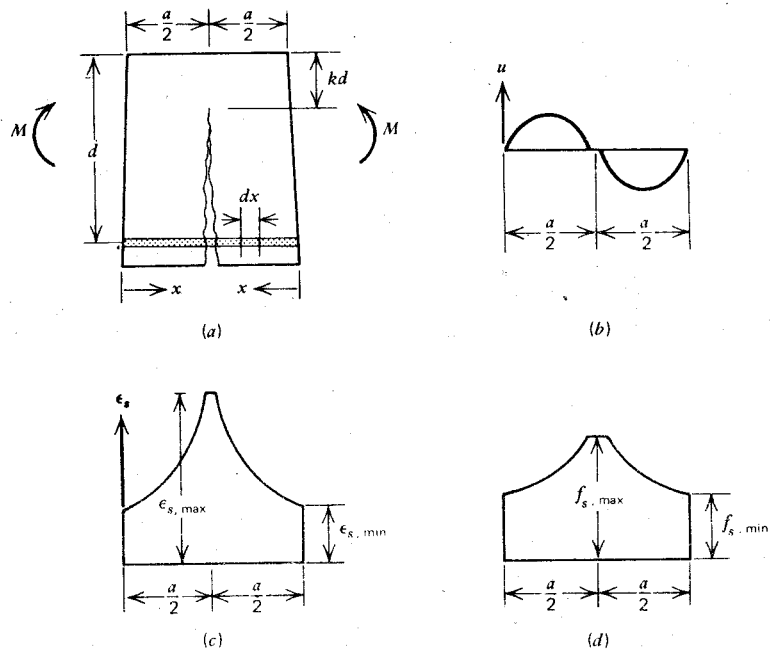


Fig. 6.32. Flexural crack element (a) with bond stress (b), steel strain (c), and steel stress (d) distributions.

bar of diameter d_b over a length dx due to change in steel stress df_s is given by

$$df_s \frac{\pi d_b^2}{4} = u \pi d_b dx$$

$$\therefore \frac{df_s}{dx} = \frac{4u}{d_b} \quad (6.51)$$

where u , the bond stress, is a function of the distance x from the midpoint between cracks. The elongation ds of the steel over length dx is given by

$$ds = \epsilon_s dx$$

$$\therefore \frac{ds}{dx} = \epsilon_s \quad (6.52)$$

where ϵ_s is a function of the steel stress f_s .

The change in steel stress between the crack and midway between the crack is given from Eq. 6.51 as

$$f_{s,\max} - f_{s,\min} = \int_0^{0.5a} \frac{4u}{d_b} dx \quad (6.53)$$

Also the elongation of the steel between two cracks is given from Eqs. 6.51 and 6.52 as

$$s = 2 \int_0^{0.5a} \varepsilon_s dx = \frac{d_b}{2} \int_{f_{s,\min}}^{f_{s,\max}} \frac{\varepsilon_s}{u} df_s \quad (6.54)$$

The steel stress at the crack $f_{s,\max}$ may be calculated from the section properties using conventional cracked section theory. Then for given crack spacing a , bond stress distribution, and steel stress-strain curve, the steel stress midway between cracks $f_{s,\min}$ may be calculated from Eq. 6.53 and the steel elongation between two cracks s may be calculated from Eq. 6.54. These calculations may be carried out for all the flexural crack elements. Then the steel elongations between cracks so found and the neutral axis depths at the cracks may be substituted into Eq. 6.50 to give the rotation θ along the length of the member.

To find the total ultimate rotation of a plastic hinge region, all flexural crack elements at which plastic steel deformations occur must be taken into account. Bachmann has shown^{6,9} that the method gives a good indication of the available plastic rotation provided the crack spacing, the bond stress distribution, and the steel stress-strain curve, are known.

Deformations in Regions of Shear Crack Elements

In Section 6.6.2 the increase in steel forces due to inclined diagonal tension cracks was discussed. Diagonal tension cracks in plastic hinge zones increase the available plastic rotation by spreading the zone of yielding along the member. For a given diagonal tension crack pattern, with known crack inclinations and positions, the steel stresses at the cracks may be estimated by statics using the equilibrium equations that take into account the effect of the shear carried by the shear reinforcement as given by Eq. 7.32. This calculation of longitudinal steel stresses is discussed in more detail in Chapter 7. Once these steel stresses have been established, the steel elongation can be calculated from the crack spacing, the bond stress distribution, and the steel stress-strain curve, using Eqs. 6.53 and 6.54; the rotation is computed from Eq. 6.50. Perhaps the greatest difficulty in the calculation is postulating the inclination and position of the diagonal tension cracks.

The foregoing considerations indicate the dependence of the ultimate rotation on the shear force present in the plastic hinge region. At a pure flexural hinge the plastic rotations are concentrated in a relatively small

zone and the resulting plastic rotation may not be large. If the shear stress is high enough to cause diagonal tension cracks, a shear crack hinge forms and the plastic rotation capacity increases, since the plastic deformations occur over a wider zone. It is evident, however, that the detailed behavior of plastic hinge zones with shear cannot yet be determined analytically and that more research is needed in this area.

6.7 DEFORMATIONS OF MEMBERS WITH CYCLIC LOADING

6.7.1 Moment-Curvature Relationships

Most of the existing evidence concerning the postelastic behavior of reinforced concrete members has been obtained from theoretical work or tests in which the loads have been applied monotonically until the maximum load is reached. Few investigators have attempted to determine the behavior of reinforced concrete beams and column sections under high-intensity loading typical of seismic motions. Examples of theoretical investigations into the behavior of members under cyclic loading are those of Aoyama,^{6.15} Agrawal, Tulin, and Gerstle,^{6.16} Bertero and Bresler,^{6.17} Brown and Jirsa,^{6.18} and Park, Kent, and Sampson.^{6.19} Most of these theories are based on an assumed linear strain profile down the depth of the section and idealized stress-strain curves for concrete and steel. The moment-curvature loop is usually obtained by calculating the moment and curvature corresponding to a range of strains in the extreme fiber of the member. For a given strain in the extreme fiber, the neutral axis depth is adjusted until the stresses in the concrete and steel, determined from the strain profile and the stress-strain curves for the materials and taking the previous strain history into account, result in internal forces that balance the external forces acting on the section. Then the moment and curvature corresponding to that strain profile are calculated. The method used by Park, Kent, and Sampson^{6.19} is presented below.

Assumed Stress-Strain Curves

The stress-strain curve for steel under cyclic loading has been discussed in Section 2.2.4. The general shape of the curve is given in Figure 6.33. The unloading path for stresses of both signs follows the initial elastic slope. After the first yield excursion the loading parts of the stress-strain curve may be represented by the Ramberg-Osgood relationship

$$\epsilon_s - \epsilon_{si} = \frac{f_s}{E_s} \left(1 + \left| \frac{f_s}{f_{ch}} \right|^{r-1} \right) \quad (6.55)$$

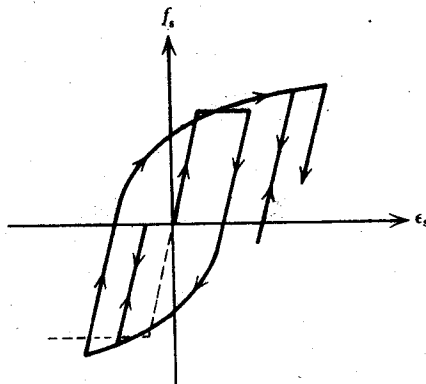


Fig. 6.33. Stress-strain curve for steel with cyclic loading illustrating the Bauschinger effect.

with the following empirical values determined by Kent and Park^{6,20} for intermediate grade steel

$$f_{ch} = f_y \left[\frac{0.744}{\ln(1 + 1,000 \epsilon_{ip})} - \frac{0.071}{1 - e^{1,000 \epsilon_{ip}}} + 0.241 \right] \quad (6.56)$$

For odd-numbered loading runs ($n = 1, 3, 5, \dots$)

$$r = \frac{4.49}{\ln(1 + n)} - \frac{6.03}{e^n - 1} + 0.297 \quad (6.57)$$

For even-numbered loading runs ($n = 2, 4, 6, \dots$)

$$r = \frac{2.20}{\ln(1 + n)} - \frac{0.469}{e^n - 1} + 3.04 \quad (6.58)$$

where ϵ_s is the steel strain, ϵ_{si} is the steel strain at beginning of loading run, f_s is the steel stress, E_s is the modulus of elasticity of steel, ϵ_{ip} is the plastic strain in steel produced in previous loading run, and n is the loading run number (first yield occurs at $n = 0$, $n = 1$ is the first postyield stress reversal, $n = 2$ is the second postyield stress reversal, etc.). It is assumed that buckling of the compression steel is prevented by the presence of closely spaced transverse steel around the longitudinal steel.

The stress-strain curve for concrete under cyclic loading appears in Fig. 6.34. The envelope curve *ABCD* for compressive stress may be represented by the relationships determined by Kent and Park^{6,5} for concrete confined by rectangular hoops under monotonic loading given by Eqs. 2.6 to 2.11. Test data have shown (see Section 2.1.1) that the envelope curve for unconfined concrete experiencing repeated inelastic loading is approximately identical to the monotonic curve. The same behavior is assumed for

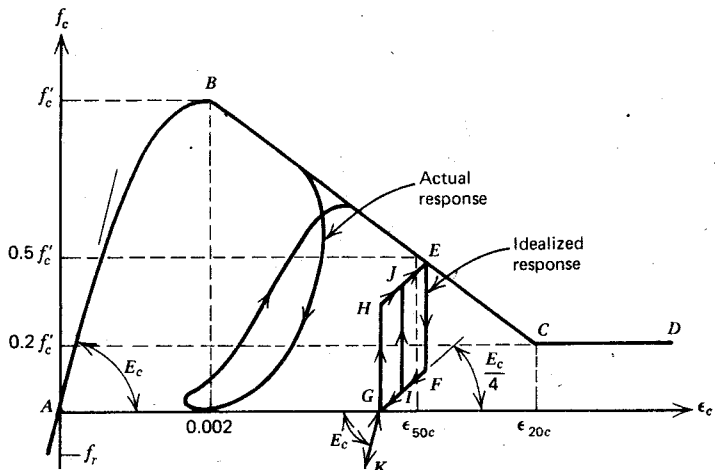


Fig. 6.34. Stress-strain behavior of concrete with cyclic loading.^{6,19}

confined concrete. A linear stress-strain curve for concrete in tension may be assumed, having the same slope as the curve for compression at zero stress. The modulus of rupture can be taken as the value given by Eq. 2.2.

The behavior of concrete under repeated loading is indicated in Fig. 2.4. The idealized behavior of Fig. 6.34 may be assumed. On unloading from point *E* it is assumed that 0.75 of the previous stress is lost without decrease in strain, whereupon a linear path of slope $0.25E_c$ is followed to point *G*. If the concrete has not cracked, it is capable of carrying tensile stress to point *K*; but if the concrete has previously cracked, or if cracks form during this loading stage, the tensile strains increase but no tensile stress develops. On reloading, the strain must regain the value at *G* before compressive stress can be sustained again. If reloading commences before unloading produces zero compressive stress, reloading follows one of the paths *IJ*. Note that the average slope of the assumed loop between *E* and *G* is parallel to the initial tangent modulus of the stress-strain curve. It is considered that a more sophisticated idealization of the loop would be unwarranted.

The stress-strain curve for the cover concrete (outside the hoops) in compression may be assumed to follow the curve for the confined core at strains less than 0.004. The cover concrete at strains greater than 0.004 may be considered to have spalled and to have zero strength. This follows because the transverse steel will lead to a plane of weakness between the core and the cover concrete, and the cover concrete may become ineffective after several reversals of high-intensity loading.

Method of Analysis

The determination of theoretical moment-curvature curves for cyclically loaded reinforced concrete sections between stipulated curvature limits is best carried out using a digital computer. Complicated distributions of concrete compressive stress occur during the loading cycles, and the most convenient method of determining the magnitude and position of the internal forces acting on the section is to sum the stresses acting on discrete elements of the section. In this approach the section is divided into a number of horizontal elements, each having the width of the section at that level. Figure 6.35 presents the arrangement for a *T* section. If there are n elements

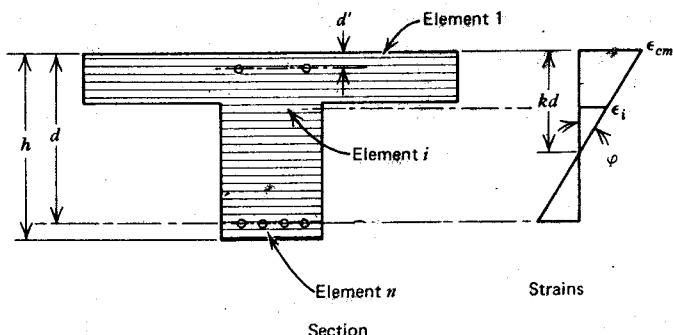


Fig. 6.35. Discrete elements for a *T* section.

numbered from the top, each will have depth h/n , where h is the overall depth of the section. The top and bottom steel reside in elements nd'/h and nd/h , respectively. If the strain in the top fiber is ϵ_{cm} and the neutral axis depth is kd , the average strain in element i is

$$\epsilon_i = \epsilon_{cm} \frac{n(kd/h) - i + 0.5}{n(kd/h)} \quad (6.59)$$

The stress in the concrete and the steel in each element is found from the assumed stress-strain curves and is taken as the stress corresponding to the average strain in the element. From the stresses and the areas of the concrete and steel in each element, the forces on the section may be determined.

An iterative technique may be used to calculate points on the moment-curvature curves. The strain ϵ_{cm} in the top concrete fiber is adjusted by a fixed amount. For each value of ϵ_{cm} , the neutral axis depth kd is estimated, and stresses in the elements are computed for this strain profile. The forces acting

on the elements are then calculated, and the equilibrium of the forces is checked by using the requirement that

$$\sum C - \sum T = P \quad (6.60)$$

in which C and T are the compressive and tensile forces acting on the elements, respectively, and P is the compressive load acting on the section (zero in the case of a beam). If the equilibrium Eq. 6.60 is not satisfied, the estimated neutral axis position is incorrect and must be adjusted until equilibrium of forces is achieved. Having obtained equilibrium, the bending moment M and curvature φ are calculated for the particular value of ε_{cm} and P .

The discrete element technique has the advantage of coping with the complex stress distributions due to cyclic loading, and it is a simple matter to alter the element force for area reductions attributable to spalling and to record the elements that have cracked. The technique has the disadvantage of being relatively slow in that to calculate the stress corresponding to a given strain, it is necessary to store for each element the parameters that record the progress along the stress-strain path.

Comparison of Moment-Curvature Responses

The theoretical approach just discussed has been checked against experimental results⁶⁻¹⁹ obtained from cyclically loaded, doubly reinforced concrete beams having a rectangular cross section 4.94 in (125 mm) wide by 8 in (203 mm) deep. The beams were pinned at each end to give a 6 ft (1.83 m) simply supported span and were loaded statically at midspan through a column stub. The load was cycled by reversing the direction of load application. Several load cycles into the inelastic range were applied. Figure 6.36 shows a beam after testing. Strains were measured on the top and bottom reinforcement over a 2 in (51 mm) gauge length in the critical region of the beam adjacent to the column stub. The experimental curvature was calculated from these strains using $(\varepsilon_s - \varepsilon'_s)/(d - d')$, where ε'_s and ε_s are the strains in the top and bottom steel, respectively (tensile strains taken as positive, compressive strains as negative), and $d - d'$ is the distance between the top and bottom steel. Figures 6.37 and 6.38 compare experimental and theoretical moment-curvature curves for two of the beams. Beam 24 contained equal top and bottom steel ($\rho = \rho' = 1.11\%$), and beam 27 contained unequal top and bottom steel ($\rho = 3.54\%$, $\rho' = 1.14\%$), where ρ is the area of bottom steel/ bd , ρ' is the area of top steel/ bd , b is the width of beam, and d is the depth of bottom steel. Both beams contained $\frac{1}{4}$ in (6.35 mm) diameter closed stirrups at 2 in (50.8 mm) centers ($\rho_s = 2.3\%$). The longitudinal reinforcement consisted of deformed steel bars with a yield strength of approximately

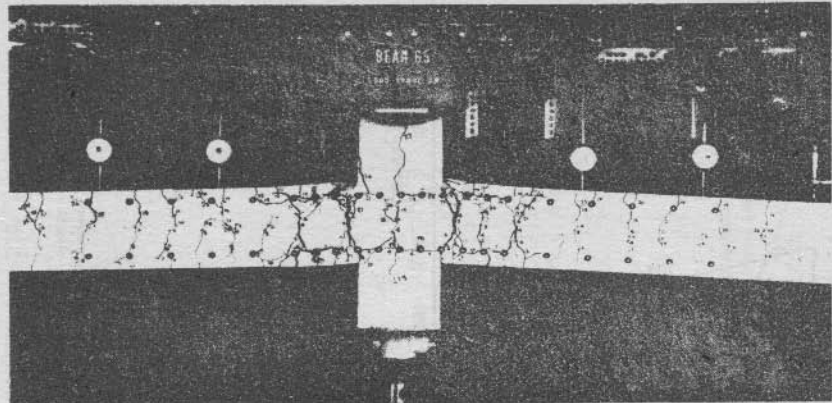
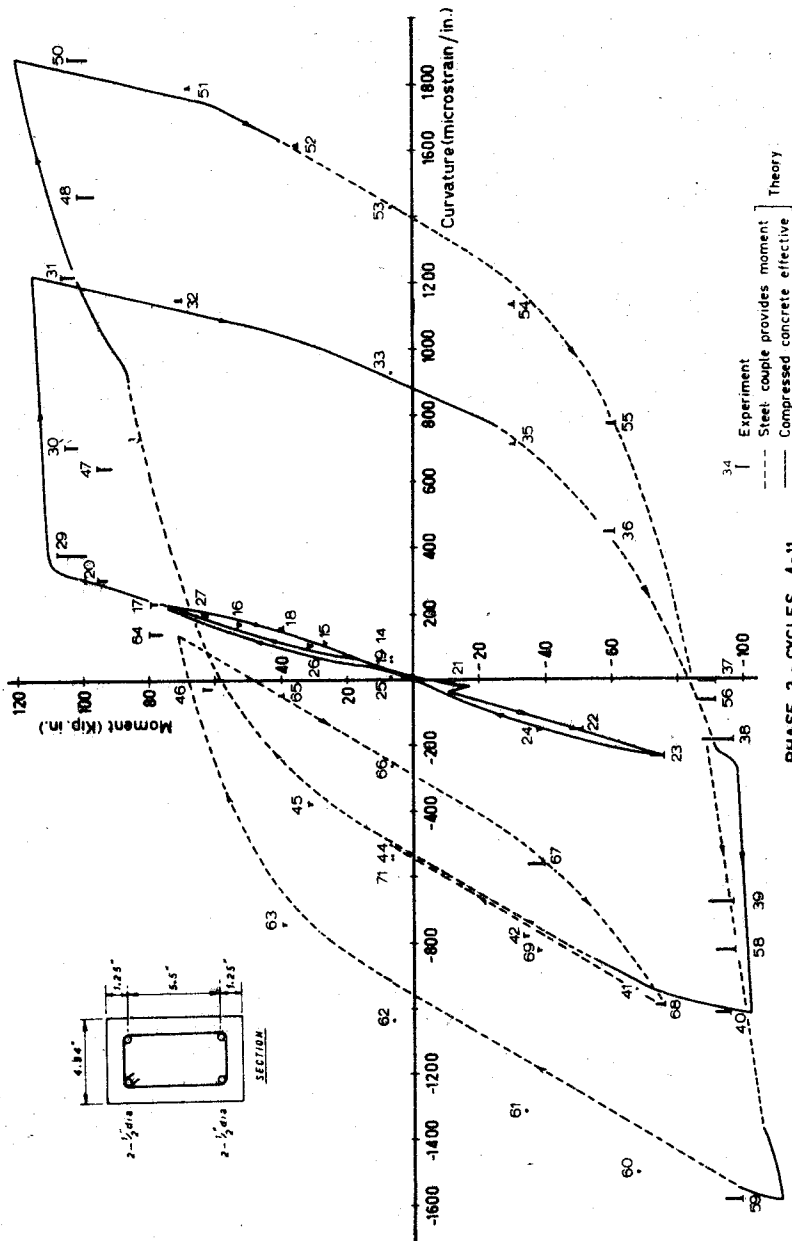


Fig. 6.36. Beam 65 with $\rho = 1.77\%$, $\rho' = 1.12\%$, and $\rho_s = 0.77\%$ after loading well into the inelastic range in each direction.^{6,19}

48 ksi (330 N/mm²). Vertical lines rather than points indicate experimental curvature in Figs. 6.37 and 6.38, reflecting the effect of creep at each increment. The theoretical curves were calculated between the experimental curvature points at which load reversal took place. The parts of the theoretical curves where moment is carried by a steel couple alone are indicated on the curves.

To assess the accuracy of the theoretical approach for column sections, the experimental results obtained by Aoyama^{6,15} for a member subjected to axial load and cyclically varying bending moment has also been checked against the theory.^{6,19} Aoyama's specimen A-2 was used, and the comparison appears in Fig. 6.39. The experimental curvatures were obtained from strain readings measured over a 6 in (152 mm) gauge length in the constant moment zone in the region of maximum bending moment. In Aoyama's paper the experimental moment-curvature points for increments 20 to 32 (the second load reversal) were drawn transferred to the symmetric position with respect to the origin, thus enabling a direct comparison with the points from the first load reversal. In Fig. 6.39 those experimental points (20 to 32) have been plotted transferred back to their actual positions.

The agreement found between the experimental and theoretical results for the beam and column sections is good. Over a large proportion of the theoretical curves for beams, the moment is carried by a steel couple alone. This behavior is due to yielding of the steel in tension, causing cracks in the tension zone that do not close when the direction of moment is reversed,



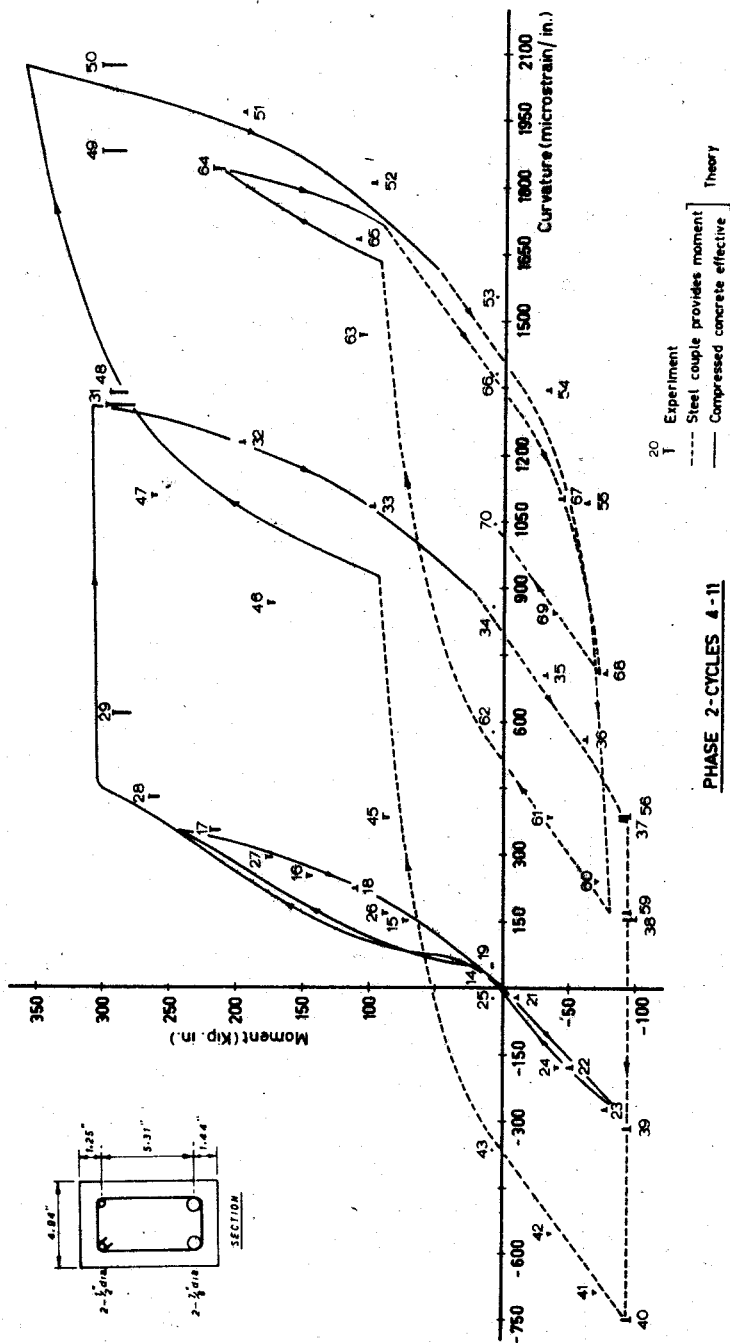


Fig. 6.38. Moment-curvature curves for critical section of beam 27 with $\rho = 3.54\%$, $\rho' = 1.14\%$, and $\rho_s = 2.30\%$.

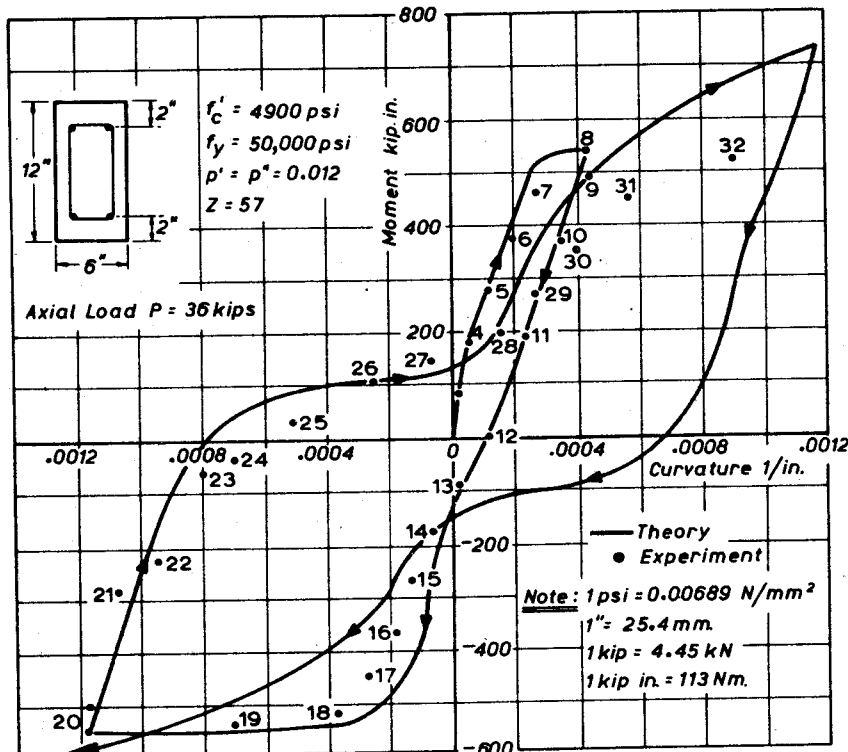


Fig. 6.39 Moment-curvature curves for Aoyama's specimen A-2 with axial load and flexure.^{6.19}

because of plastic elongation of the steel. Open cracks will exist in the compression zone until the compression steel yields and enables the cracks to close. Only then will the concrete carry some of the compressive force. In particular for beams with different reinforcement top and bottom (Fig. 6.38), once the large area of steel has yielded in tension the concrete on that side of the member may not carry compression again because there is insufficient tensile force in the small area of steel to cause the large area of steel in compression to yield. When the direction of moment is reversed, however, the small area of steel in compression will yield at a low moment. The beam of Fig. 6.37 has equal top and bottom steel, and after the first yield excursion the load is carried very largely by the steel couple. For column sections the effect of cracking may also be quite marked. In Fig. 6.39 the regions of the theoretical curve where a steel couple alone is operating

have not been indicated; but it is evident that after the first yield excursion, in the early part of the moment-curvature curves, the moment is carried only by the steel. For column sections the presence of axial compression as well as bending will mean that even for sections with equal steel in each face, the steel in compression will yield at a low moment and close the crack.

It is evident that the flexural rigidity of the section is reduced when the moment is being carried by a steel couple alone but increases when the concrete commences to carry compression. The increase in stiffness due to closing of the cracks in the compression zone is more sudden in the theoretical curves than in the tests, as Fig. 6.38 indicates. This is probably because in reality some compression can be carried across cracks before they close. Particles of concrete that flake off during cracking and small relative shear displacements along the cracks cause compression to be transferred across the cracks gradually, as high spots come into contact, rather than suddenly as the theory implies. Nevertheless it is evident that the presence in the compression zone of open cracks that eventually close, causes a marked pinching of the moment-curvature response.

The Bauschinger effect of the steel causes the moment-curvature relationships to be curved after the first yield excursion. The beam of Fig. 6.37 has equal top and bottom steel, and after the first yield excursion the load is carried very largely by the steel couple. Therefore, the shape of the moment-curvature loop is very much governed by the shape of the stress strain loop for the steel.

It is evident that both the theoretical and experimental moment-curvature loops are far removed from the normally assumed parallelogram of classical elastoplastic behavior. The rounding and pinching in of the loops means that the area within the loop is smaller than the elastoplastic assumption and thus that there will be less energy dissipation per cycle than normally assumed. This must be of significance in the dynamic analysis of reinforced concrete frames responding to severe earthquake motions and may lead to a greater response of the structure than expected. For beams, a better idealization for the actual shape of the loops would be the Ramberg-Osgood type of response or the degrading stiffness response suggested by Clough^{6,21} (see Fig. 6.40). For beams with significantly different top and bottom steel areas, and for columns, the pinching in effect shown by the experimental and theoretical curves is more marked, and a loop with smaller area than the preceding idealizations would appear to be necessary.

To summarize, it may be concluded that theoretical moment-curvature curves for reinforced concrete members subject to repeated and reversed loading can be derived assuming a linear strain profile and idealized stress-strain curves for the steel and concrete. Such theory demonstrates good agreement with test results and predicts the reduction in stiffness due to the

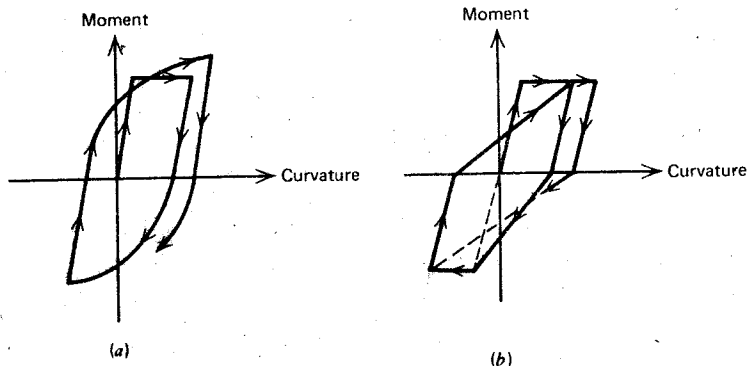


Fig. 6.40. Idealized moment-curvature responses. (a) Ramberg-Osgood response. (b) Clough's degrading stiffness response.

Bauschinger effect of the steel and due to the open cracks in the compression zone that may eventually close. Generally the flexural strength is unaffected by the reduced stiffness, but subsequently it is reached at greater deflections. The maximum moment capacity does not reduce with cyclic loading unless crushing of the concrete causes a reduction in the concrete cross section.

6.7.2 Load-Deformation Behavior

The load-deformation behavior for cyclically loaded members can be determined from the moment-curvature relationships using Eqs. 6.35 and 6.36. As an example of this procedure, theoretical moment-curvature curves were used to determine the theoretical central deflection of the simply supported beams with the centrally applied cyclic load referred to in the previous section.^{6.19} It was found convenient to divide the members into a number of short longitudinal elements and to assume the moment at the center of each element to be constant over the length of that element. Changes of deflection were obtained by adjusting the concrete strain ε_{cm} at the extreme fiber of the centermost element of the beam and by using the iterative technique described previously to find neutral axis depth, bending moment, and curvature for that value of ε_{cm} for the element. The load producing this bending moment could then be established and the bending moments in the remaining elements determined. For each of the remaining elements, the procedure was as follows: adjust the ε_{cm} value obtained for the element in the previous increment, locate the neutral axis position for strain compatibility and equilibrium, and compute the bending moment for the trial value of ε_{cm} . The computed bending moment was then compared with that required,

and ε_{cm} was adjusted until the computed and the required bending moments coincided. In this way the curvature corresponding to the bending moments for all sections were calculated. The deflection profile was computed from the curvatures. The theoretical load-deflection responses of the beams between the deflections at which load reversal took place could then be calculated.

The theoretical load-central deflection curves so calculated for beam 24 are shown in Fig. 6.41. In the theoretical analysis, each half span of the beam (each side of the column stub) was divided into 9 longitudinal elements of equal length and the section of each element into 10 discrete horizontal elements. The load-deflection response is greatly influenced by the curvature distribution at the maximum moment region; thus the choice of the length of the longitudinal element may have a marked effect on the computed deformations. Ideally, many more elements should have been taken; but because so many iteration processes are involved, considerable computer time would have been necessary. Figure 6.41 also shows the experimental points for the beam. Generally the shapes of the theoretical and experimental loops are similar.

In view of the considerable computer time required to produce the theoretical load-deflection plots, some simplification is desirable. Figure 6.42 presents the theoretical load-deflection curves calculated using Clough's degrading stiffness moment-curvature assumptions^{6.21} of Fig. 6.40b. The analysis was performed with both 10 and 100 longitudinal elements in each half-span. The agreement between theory and experiment given by this idealization in Fig. 6.42 is good. Note, however, that Clough's assumed $M-\varphi$ relationship does not simulate the pinching effect that occurs in beams when ρ and ρ' are significantly different, and in columns; thus it should be used with caution in those cases.

The preceding theoretical deflections have been calculated ignoring the stiffness effects of concrete tension between cracks. This evidently has not led to as much error as would be expected. In members under cyclic loading, the stiffness effect of the concrete between cracks may not be very important. It is certain that a gradual deterioration of bond between concrete and steel occurs in members under high intensity cyclic loading (see Fig. 9.12), which in turn reduces the influence of the concrete. Also for these simply supported beams, slip of the bars in the anchorage zones at the ends of the member would have been negligible and was not taken into account.

The theoretical calculations also ignored the effect of shear; and the curvatures were determined from the actual moment diagram rather than from the horizontally displaced diagram.

Figure 6.36 indicates that very little diagonal tension cracking occurred in the test beams analyzed, and the use of the actual moment diagram apparently was satisfactory. It should be noted, however, that other tests^{6.22}

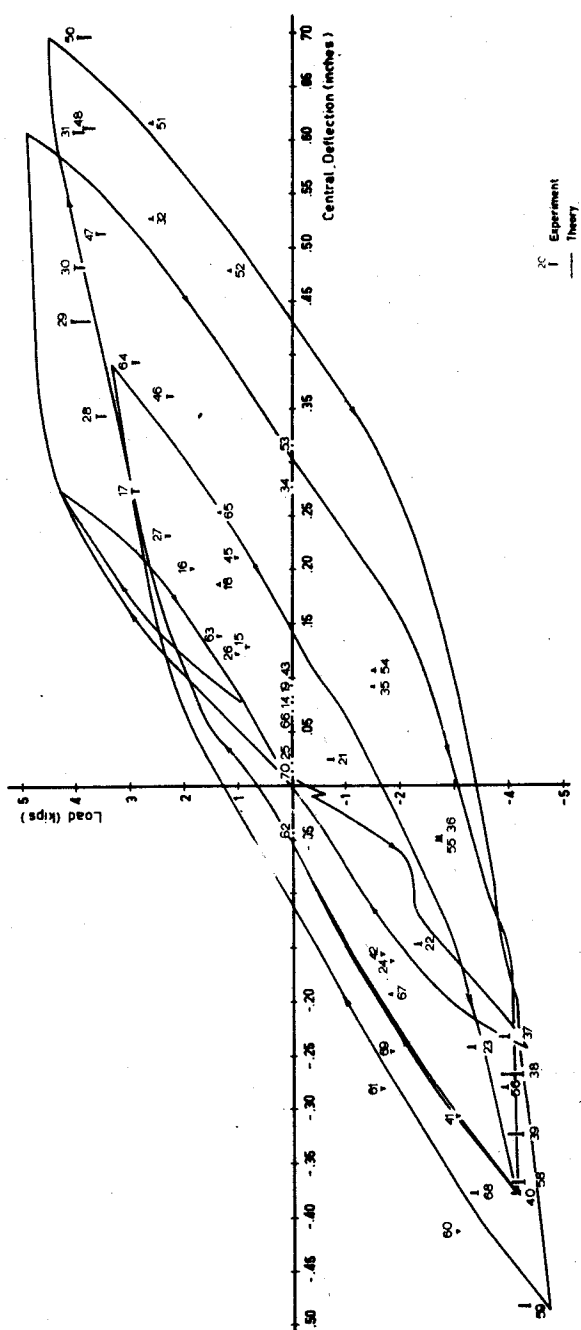


Fig. 6.41. Load-central deflection curve for beam 24 with $\rho = \rho' = 1.11\%$.

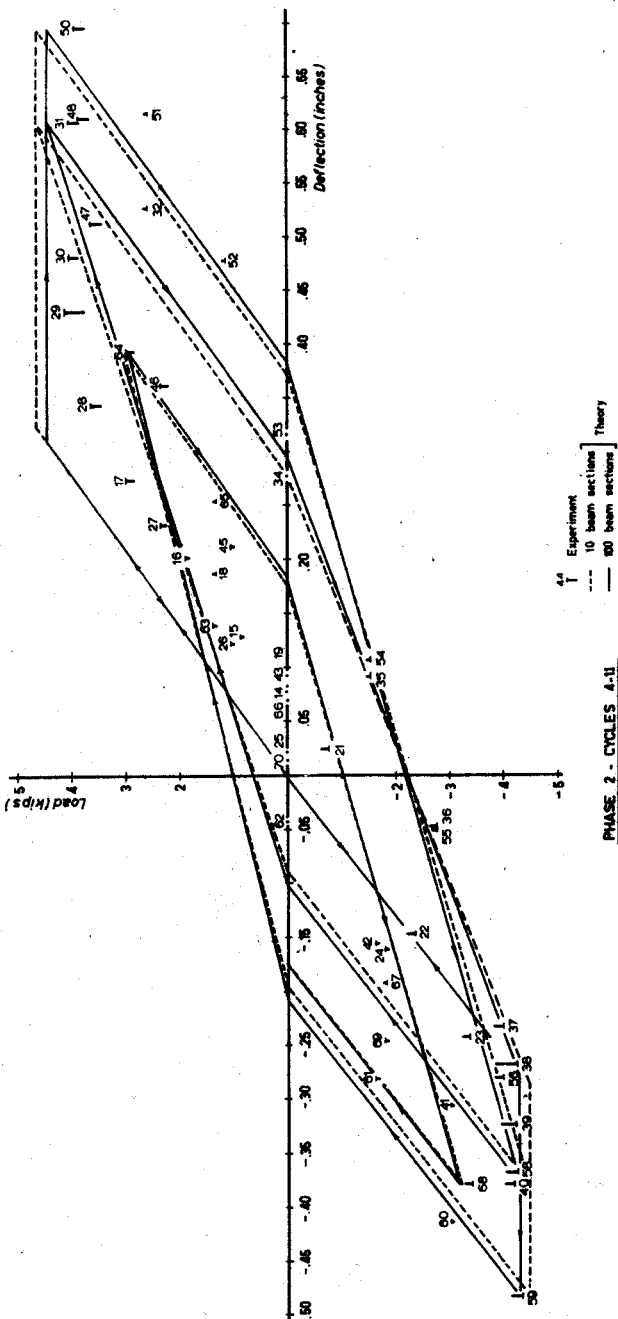


Fig. 6.42. Load-central deflection curves for beam 24 using Clough's response, 6.19

have shown that for beams in which flexure occurs with high shear [e.g., a nominal shear stress $V/bd > 3\sqrt{f'_c}$ psi ($0.25\sqrt{f'_c}$ N/mm²)], an additional reduction in stiffness may occur in each cycle of loading because of shear, and the failure may be initiated by shear. High shear causes a pinching of the load-member displacement curves, due mainly to sliding along and closing of cracks in plastic hinge zones. Thus although shear that causes diagonal tension cracks may be beneficial in spreading the yielding of flexural steel, therefore in increasing the ductility, it may produce loss of stiffness because of shear deformations in the plastic hinge zone and an eventual shear failure with cyclic loading. It must also be borne in mind that during cyclic loading open flexural cracks may exist down the full depth of the member. This condition implies that the ability of the concrete to carry shear force could be severely impaired, and splitting along the longitudinal bars may be caused by the dowel forces. Thus shear reinforcement should be provided to carry the greater part of the shear force. When flexure occurs with high shear and high axial compressive force, the reduction in the strength and stiffness with each cycle of loading may be substantial unless the column contains adequate transverse steel for shear reinforcement and concrete confinement. The behavior of members with shear force is discussed in Chapter 7.

6.8 APPLICATION OF THEORY

The determination of flexural deformations at the ultimate load has been dealt with at length in this chapter because of its relevance to considerations of ductility in limit design and seismic design. The theory outlined enables the ductility of members to be assessed and indicates how ductility may be improved. The theory has no application to design cases when the ductility of members is of no importance. The application of the theory to limit design and to seismic design is discussed in Chapter 11.

6.9 REFERENCES

- 6.1 ACI Committee 318, "Building Code Requirements for Reinforced Concrete (ACI 318-71)," American Concrete Institute, Detroit, 1971, 78 pp.
- 6.2 J. A. Blume, N. M. Newmark, and L. H. Corning, "Design of Multistory Reinforced Concrete Buildings for Earthquake Motions," Portland Cement Association, Chicago, 1961, 318 pp.
- 6.3 E. O. Pfrang, C. P. Siess, and M. A. Sozen, "Load-Moment-Curvature Characteristics of Reinforced Concrete Cross Sections," *Journal ACI*, Vol. 61, No. 7, July 1964, pp. 763-778.
- 6.4 G. B. Base and J. B. Read, "Effectiveness of Helical Binding in the Compression Zone of Concrete Beams," *Journal ACI*, Vol. 62, No. 7, July 1965, pp. 763-781.

- 6.5 D. C. Kent and R. Park, "Flexural Members with Confined Concrete," *Journal of the Structural Division, ASCE*, Vol. 97, ST7, July 1971, pp. 1969-1990.
- 6.6 A. L. L. Baker and A. M. N. Amaral, "Inelastic Hyperstatic Frames Analysis," *Proceedings of the International Symposium on the Flexural Mechanics of Reinforced Concrete*, ASCE-ACI, Miami, November 1964, pp. 85-142.
- 6.7 W. G. Corley, "Rotational Capacity of Reinforced Concrete Beams," *Journal of Structural Division, ASCE*, Vol. 92, ST5, October 1966, pp. 121-146.
- 6.8 N. H. Burns, and C. P. Siess, "Load-Deformation Characteristics of Beam-Column Connections in Reinforced Concrete," *Civil Engineering Studies, Structural Research Series No. 234*, University of Illinois, January 1962, 261 pp.
- 6.9 H. Bachmann, "Influence of Shear and Bond on Rotational Capacity of Reinforced Concrete Beams," *Publications, International Association for Bridge and Structural Engineering*, Zurich, 1970; Vol. 30, Part II, pp. 11-28.
- 6.10 E. Rosenblueth and R. Diaz de Cossio, "Instability Considerations in Limit Design of Concrete Frames," *Proceedings of the International Symposium on the Flexural Mechanics of Reinforced Concrete*, ASCE-ACI, Miami, November 1964, pp. 439-456.
- 6.11 H. A. Sawyer, "Design of Concrete Frames for Two Failure States," *Proceedings of the International Symposium on the Flexural Mechanics of Reinforced Concrete*, ASCE-ACI, Miami, November 1964, pp. 405-431.
- 6.12 A. L. L. Baker, *Ultimate Load Theory Applied to the Design of Reinforced and Prestressed Concrete Frames*, Concrete Publications Ltd, London, 1956, 91 pp.
- 6.13 ICE Research Committee, "Ultimate Load Design of Concrete Structures," *Proceedings of the Institution of Civil Engineers*, Vol. 21, February 1962, pp. 399-442.
- 6.14 A. H. Mattock, Discussion of "Rotational Capacity of Reinforced Concrete Beams," by W. G. Corley, *Journal of Structural Division, ASCE*, Vol. 93, ST2, April 1967, pp. 519-522.
- 6.15 H. Aoyama, "Moment-Curvature Characteristics of Reinforced Concrete Members Subjected to Axial Load and Reversal of Bending," *Proceedings of International Symposium on the Flexural Mechanics of Reinforced Concrete*, ASCE-ACI, Miami, November 1964, pp. 183-212.
- 6.16 G. L. Agrawal, L. G. Tulin, and K. H. Gerstle, "Response of Doubly Reinforced Concrete Beams to Cyclic Loading," *Journal ACI*, Vol. 62, No. 7, July 1965, pp. 823-836.
- 6.17 V. V. Bertero and B. Bresler, "Seismic Behaviour of Reinforced Concrete Framed Structures," *Proceedings of Fourth World Conference on Earthquake Engineering*, Vol. 1, Session B-2, Chile, 1969, pp. 109-124.
- 6.18 R. H. Brown and J. O. Jirsa, "Reinforced Concrete Beams Under Reversed Loading," *Journal ACI*, Vol. 68, No. 5, May 1971, pp. 380-390.
- 6.19 R. Park, D. C. Kent, and R. A. Sampson, "Reinforced Concrete Members with Cyclic Loading," *Journal of the Structural Division, ASCE*, Vol. 98, ST7, July 1972, pp. 1341-1360.
- 6.20 D. C. Kent and R. Park, "Cyclic Load Behaviour of Reinforcing Steel," *Strain (Journal of the British Society for Strain Measurement)*, Vol. 9, No. 3, July 1973, pp. 98-103.
- 6.21 R. W. Clough, "Effect of Stiffness Degradation on Earthquake Ductility Requirements," Report No. 66-16, Structural Engineering Laboratory, University of California, Berkeley, October 1966, 67 pp.
- 6.22 M. Celebi and J. Penzien, "Behaviour of Reinforced Concrete Beams Under Combined Moment and Shear Reversal," *Symposium on Resistance and Ultimate Deformability of Structures Acted on by Well-Defined Repeated Loads*, Reports of Working Commissions, Vol. 13, International Association for Bridge and Structural Engineering, Lisbon, 1973, pp. 193-198.

Strength and Deformation of Members with Shear

7.1 INTRODUCTION

The extensive study of the behavior of reinforced concrete flexural members has clarified the flexural failure mechanism to the extent that well-understood conclusions are now incorporated in the design codes of many countries. Progress in the understanding and quantitative assessment of the behavior of members subjected to flexure and shear has been somewhat less spectacular. Hundreds of publications, the majority having appeared in the last 15 years, speak for the complexity of the problem.

The vast majority of structural members in reinforced concrete cannot escape having to resist shearing forces. These forces seldom act on their own but rather in combination with flexure, axial load, and perhaps torsion. In addition to identifying the effect of shear forces acting alone, therefore, it is necessary to examine the possible interaction with the other structural actions. In flexural members in particular, the shear resisting mechanisms interact intimately with the bond between concrete and the embedded reinforcement and the anchorage of the latter.

Shear transfer in reinforced concrete beams relies heavily on the tensile and compressive strength of the concrete. Thus it is not surprising that a shear failure in general is nonductile. Consequently an attempt must be made to suppress such a failure. In earthquake-resistant structures in particular, heavy emphasis is placed on ductility, as outlined in other chapters, and for this reason the designer must ensure that a shear failure can never occur. This implies that when ductility is essential, the shear strength of the member must be somewhat in excess of the maximum flexural strength it could possibly develop.

It is still expedient to use the classical ^{to the} concepts of shear stresses in homogeneous, isotropic, elastic bodies when dealing with reinforced concrete members. Suitably modified, this elastic theory approach can give acceptable

predictions with respect to crack formation and strength. However, with the development of cracks an extremely complex pattern of stresses ensues, and many equations currently in use have little relevance to the actual behavior of the member at this stage. Extensive experimental work, particularly in recent years, has greatly extended the identification of various shear resisting mechanisms, however, and these will be discussed in some detail.

Bresler and McGregor prepared a very useful review of the shear problem.^{7.1} The background of the current ACI code provisions,^{7.2} widely used since 1963, was reported by ACI-ASCE Committee 326^{7.3} in 1962. A similar report on the state of the art by ACI-ASCE Joint Committee 426 was published in 1973.^{7.4} The evolution of the approach to the design for shear in reinforced concrete may be found in an interesting historical study by Hognestad.^{7.5}

7.2 THE CONCEPT OF SHEAR STRESSES

From consideration of equilibrium, the transverse or shear force across any cross section of a structural member can be derived. The intensity of this force is conveniently shown by a "shear force diagram." The sum of the shear stresses across such a cross section must naturally balance the external shear force at that section. By establishing the equilibrium of an infinitesimal element within a member, it becomes evident that the vertical and horizontal shear stress intensities at each element must be the same.

The horizontal shear stresses along any fiber of a homogeneous, isotropic, uncracked beam can be easily derived from considerations of internal equilibrium of flexural stresses. Using the notation of Fig. 7.1, the equilibrium of the cross-hatched part of the beam element will be satisfied when the horizontal shear stress is

$$\tau = \frac{V A_i \bar{y}}{b I} \quad (7.1)$$

where I is the second moment of area of the section.

It can be shown from first principles that with respect to the centroidal axis

$$z = \frac{I}{A_i \bar{y}}$$

and that there the shear flow $q = vb$ is always a maximum; that is,

$$q_{\max} = \frac{V}{z} \quad (7.2)$$

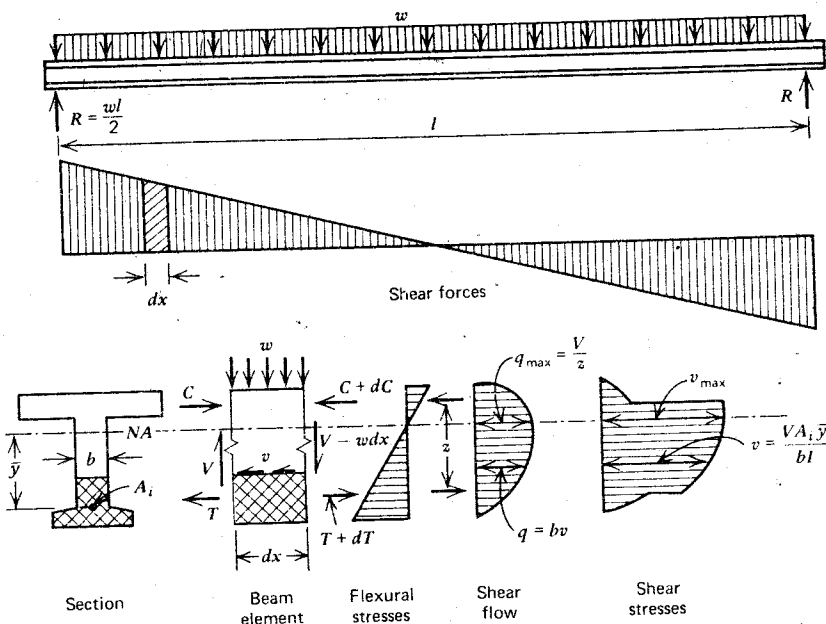


Fig. 7.1. Shear force, shear flow, and shear stresses in a homogeneous isotropic elastic beam.

where z is the internal lever arm, and this is normally the location of the maximum shear stress if the width b at that fiber is small enough (see Fig. 7.1).

The shear stresses so generated can then be combined with the flexural stresses at any fiber. Again by considering the equilibrium of an infinitesimal element, the magnitude f_1 and f_2 and the inclination φ of the principal stresses, resulting from the simultaneous application of a tensile stress f and a shear stress v illustrated in Fig. 7.2, can be obtained as follows:

$$\text{principal tension} \quad f_1 = \frac{f}{2} + \sqrt{f^2 + 4v^2} \quad (7.3a)$$

$$\text{principal compression} \quad f_2 = \frac{f}{2} - \sqrt{f^2 + 4v^2} \quad (7.3b)$$

Wif Wif The inclination of the principal tensile stress with respect to the beam's axis is found from

$$\tan 2\varphi = \frac{2v}{f} \quad \text{or} \quad \tan \varphi = \frac{v}{f_1} \quad (7.3c)$$

The inclination of the principal stresses is illustrated for the case of a uniformly loaded simply supported rectangular beam in Fig. 7.2. The stress

Wif

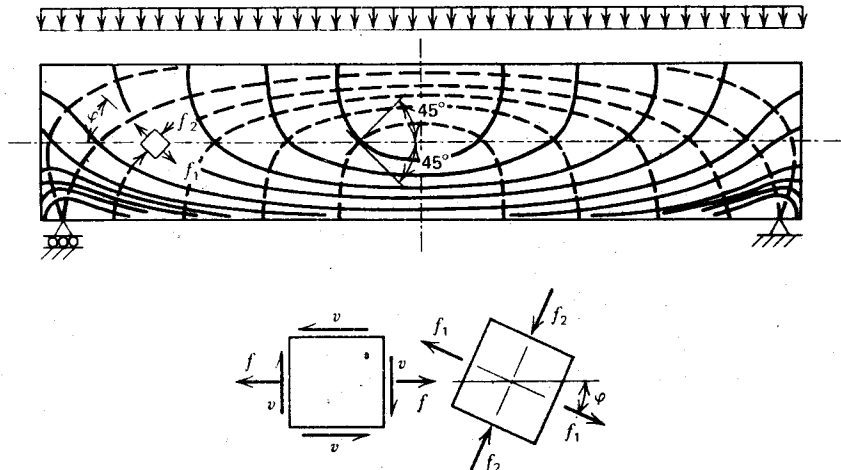


Fig. 7.2. Trajectories of principal stresses in a homogeneous isotropic beam.

trajectories intersect the neutral axis at 45° . When the principal tensile stresses become excessive, cracks develop approximately at right angles to these principal tensile stress trajectories.

These traditional concepts were extended by pioneers^{7,5} of reinforced concrete theory to the idealized section of a cracked reinforced concrete beam. As Fig. 7.3 shows, the horizontal force to be transferred across the cracked zone of the section remains constant; hence the shear flow in the tension zone is constant. Using the concepts of Fig. 7.1, the incremental tension force is $dT = vb_w dx$, and hence we have

$$v = \frac{1}{b_w} \frac{dT}{dx} = \frac{dM}{dx} \frac{1}{b_w jd} = \frac{V}{b_w jd} \quad (7.4)$$

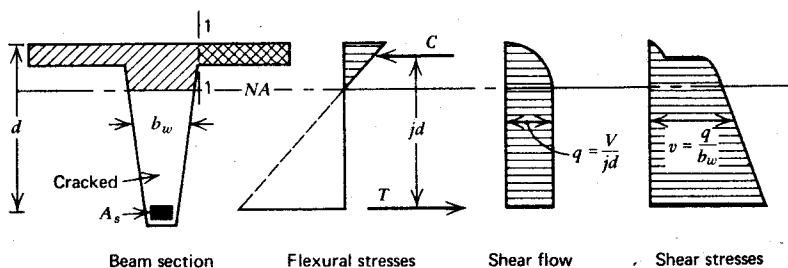


Fig. 7.3. Shear stresses across an idealized cracked reinforced concrete section.

or

$$q = \frac{V}{jd} \quad (7.4a)$$

It is evident that shear stress depends on the width of the web, illustrated for a particular example in Fig. 7.3. Since the concrete below the neutral axis (NA) is assumed to be in a state of pure shear, this equation has been used as the measure of diagonal tension in the cracked tension zone of a reinforced concrete beam. This also implies that vertical shear stresses are transmitted in this fashion across sections, irrespective of the presence of flexural cracks. ~~✓ ✓ ✓ ✓ ✓ ✓~~

In many countries this traditional shear stress equation is still used. It is a convenient "index" to measure shear intensity, but as the subsequent paragraphs reveal, it cannot be considered as giving a shear stress at any particular locality in a cracked reinforced concrete beam. For convenience the ACI adopted as an index of shear intensity the simple equation

$$v = \frac{V}{b_w d} \quad (7.5)$$

In certain cases the maximum shear stress could occur at a fiber other than at the web of the section. When the flange of a T section carries a large compression force, as over the shaded area to the right of section 1 (Fig. 7.3), the shear at the flange-web junction may become critical, and horizontal reinforcement in the flange may be needed. In beams supporting floors of buildings, the flexural reinforcement in the slab is usually adequate for this purpose.

When the depth of the member varies along its length, the magnitude of the force causing shear stresses will be affected by the internal forces induced by flexure. From Fig. 7.4 it is evident that the sloping internal compression force, $C = C'/\cos \theta'$, has a vertical component that resists some of the external shear V applied to the section. Using the notation of Fig. 7.4, the effective shear force can be expressed as

$$V_{\text{eff}} = V - C \sin \theta' = V - C' \tan \theta' = V - \frac{M_s}{jd} \tan \theta' \quad (7.6)$$

where

$$M_s = M - Ne_s \quad (7.6a)$$

The external shear is reduced only if the depth of the member increases in the same direction in which the bending moments increase. When the opposite is the case, the value of θ' in Eq. 7.6 must be taken as negative. Three typical cases of the distribution of external and effective shear for haunched beams, carrying uniformly distributed loads, are qualitatively depicted in Fig. 7.5.

274 7.5

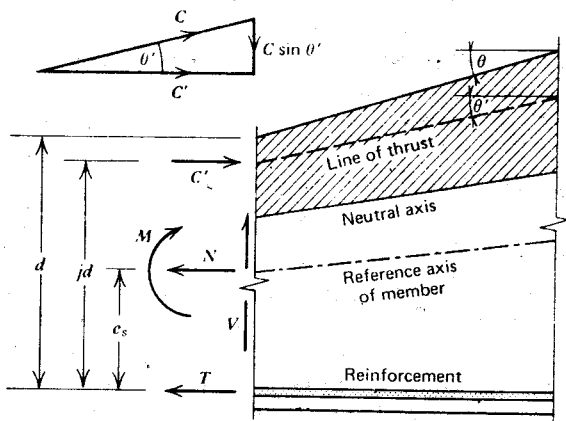


Fig. 7.4. External and internal actions in a beam with variable depth.

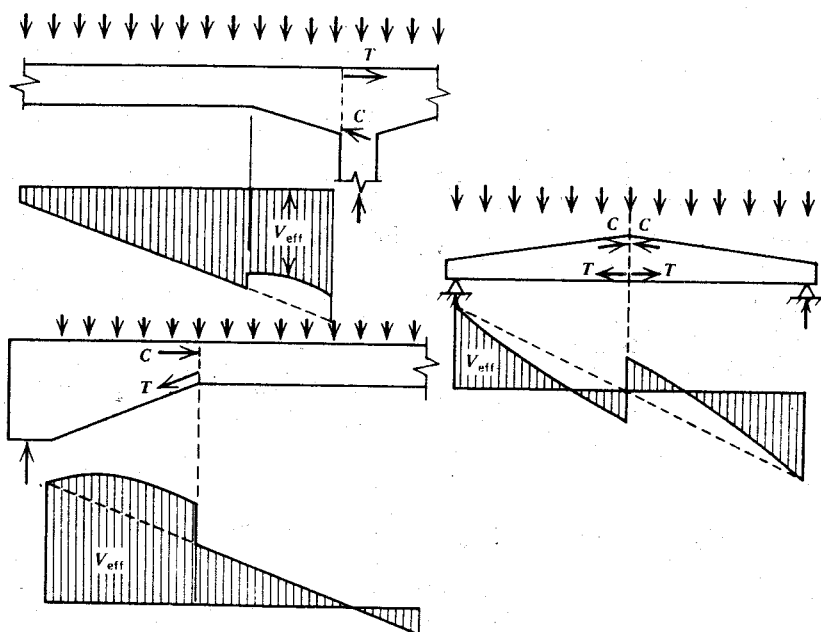


Fig. 7.5. The effective shear in haunched beams.

7.3 THE MECHANISM OF SHEAR RESISTANCE IN REINFORCED CONCRETE BEAMS WITHOUT WEB REINFORCEMENT

7.3.1 The Formation of Diagonal Cracks

In a reinforced concrete member, flexure and shear combine to create a biaxial state of stress. The principal stresses so generated are illustrated in Fig. 7.2. Cracks form when the principal tensile stresses exceed the tensile strength of the concrete. In a region of large bending moments, these stresses are greatest at the extreme tensile fiber of the member and are responsible for the initiation of flexural cracks perpendicular to the axis of the member. In the region of high shear force, significant principal tensile stresses, also referred to as diagonal tension, may be generated at approximately 45° to the axis of the member. These may result in inclined (diagonal tension) cracks. With few exceptions these inclined cracks are extensions of flexural cracks. Only in rather special cases, as in webs of flanged beams, are diagonal tension cracks initiated in the vicinity of the neutral axis. The principal stress concept is of little value in the assessment of subsequent behavior unless the complex distribution of stresses in the concrete after cracking is considered. Either a reinforced concrete flexural member collapses immediately after the formation of diagonal cracks, or an entirely new shear carrying mechanism develops which is capable of sustaining further load in a cracked beam.

The diagonal cracking load originating from flexure and shear is usually much smaller than would be expected from principal stress analysis and the tensile strength of concrete. This condition is largely due to the presence of shrinkage stresses, the redistribution of shear stresses between flexural cracks, and the local weakening of a cross section by transverse reinforcement, which causes a regular pattern of discontinuities along a beam.

In the early stages of reinforced concrete design, diagonal cracking was considered to be undesirable. However, it is now recognized that diagonal cracking under service load conditions is acceptable, provided crack widths remain within the same limits accepted for flexure.

7.3.2 Equilibrium in the Shear Span of a Beam

Figure 7.6a shows part of a simply supported beam over which the shear force is constant. The internal and external forces that maintain equilibrium for this free body, bounded on one side by a diagonal crack, can be identified.

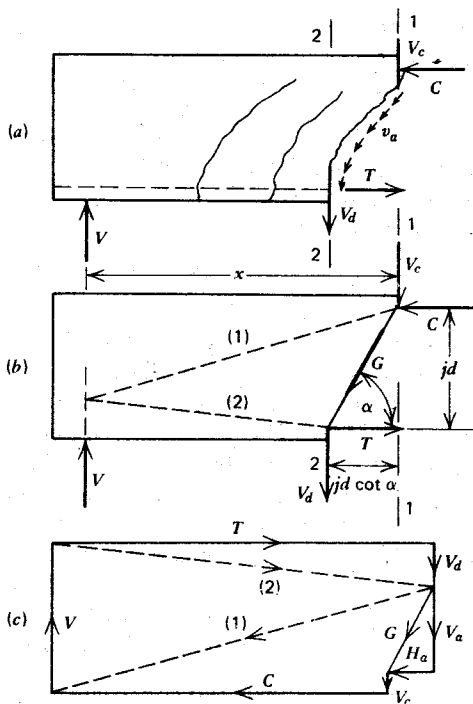


Fig. 7.6. Equilibrium requirements in the shear span of a beam.

It may be seen that the total external transverse force V , is resisted by the combination of

1. A shear force across the compression zone V_c .
2. A ~~dowel force~~ transmitted across the crack by the flexural reinforcement V_d .
3. The vertical components of inclined shearing stresses v_a transmitted across the inclined crack by means of interlocking of the aggregate particles.

To simplify the equilibrium statement, we assume that shear stresses transmitted by aggregate interlock can be lumped into a single force G , whose line of action passes through two distinct points of the section (see Fig. 7.6b). With this simplification the force polygon in Fig. 7.6c represents the equilibrium of the free body. This condition can also be stated in the form

$$V = V_c + V_a + V_d \quad (7.7)$$

representing the contribution of the compression zone, aggregate interlock, and dowel action to shear resistance in a beam without web reinforcement.

The moment of resistance of the beam is expressed by

$$M = xV = jd(T + V_d \cot \alpha) \quad (7.8)$$

If the contribution of the dowel force toward flexural resistance is ignored (a justifiable step for design purposes, particularly in the absence of stirrups), the moment of resistance simplifies to

$$M = Tjd \quad (7.9)$$

It is important to note that the moment and the tension force, related to each other in Fig. 7.6b and Eq. 7.9, do not occur at the same cross section of the beam. It is seen that the tension in the flexural reinforcement at distance $(x - jd \cot \alpha)$ from the support is governed by the moment at a distance x from the support of the beam. The increase in the steel stresses clearly depends on the slope of the idealized diagonal crack. When α is a little less than 45° , $jd \cot \alpha \approx d$. This must be taken into account when the curtailment of the flexural reinforcement is determined. This shift in the tension force distribution is examined more closely in Section 7.5.1, when the contribution of the web reinforcement is also considered.

7.3.3 The Principal Mechanisms of Shear Resistance

When the relationship between the external moment and the internal moment of resistance given by Eq. 7.9 are combined with the well-known relationship between shear and the rate of change of bending moment along a beam, the following modes of internal shear resistance result:

$$V = \frac{dM}{dx} = \frac{d}{dx}(Tjd) = jd \frac{dT}{dx} + T \frac{d(jd)}{dx} \quad (7.10)$$

The term $jd(dT/dx)$ expresses the behavior of a true prismatic flexural member in which the internal tensile force T acting on a constant lever arm jd changes from point to point along the beam, to balance exactly the external moment intensity. The term dT/dx , the rate of change of the internal tension force, is termed the bond force, q , applied to the flexural reinforcement per unit length of beam. (See also Fig. 7.3.) Should the internal lever arm remain constant (a normally accepted assumption of the elastic theory analysis of prismatic flexural members) so that $d(jd)/dx = 0$, the equation of perfect "beam action" is obtained thus

$$V = jd \frac{dT}{dx} = qjd \quad (7.11)$$

The same result was obtained in Eq. 7.4a, where q , the bond force per unit

length of the member at and immediately above the level of the flexural reinforcement, was termed the shear flow. It is evident that such simplification of behavior is possible only if the shear flow or bond force can be efficiently transferred between the flexural reinforcement and the concrete surrounding it. It gives rise to the phenomenon of bond, examined in the next chapter. For more than half a century it has been commonly believed that in the absence of web reinforcement, shear was resisted by "beam action" in this manner.

When for any reason the bond between steel and concrete is destroyed over the entire length of the shear span, the tensile force T cannot change, hence $dT/dx = 0$. Under such circumstances the external shear can be resisted only by inclined internal compression. This extreme case may be termed "arch action" Its shear resistance is expressed by the second term on the right-hand side of Eq. 7.10, namely,

$$V = T \frac{d(jd)}{dx} = C \frac{d(jd)}{dx} \quad (7.12)$$

Here the internal tension T is replaced by the internal compression force C , to signify that it is the vertical component of a compression force, with constant slope, which balances the external shear force.

In a normal reinforced concrete beam in which (owing to slip, cracking, and other causes) the full bond force q required for beam action cannot be developed, the two mechanisms, as expressed by Eq. 7.10, will offer a combined resistance against shear forces. The extent to which each mechanism contributes to shear resistance at various levels of external load intensity will depend on the compatibility of deformations associated with these actions.

Beam Action in the Shear Span

Cracks induced by load on a simply supported beam divide the tension zone into a number of blocks (see Fig. 7.6a). Each of these blocks may be considered to act as a cantilever with its base at the compression zone of the concrete and its free end just beyond the flexural tension reinforcement. Because of the analogy, the blocks will be referred to as "concrete cantilevers."

It was shown in Eq. 7.11 that for perfect beam action to take place, the full bond force q must be effectively resisted. It remains to be seen how the concrete cantilevers can fulfill such a requirement. The resistance may be examined in more detail if we first identify all the actions to which a typical cantilever is subjected. The components of the cantilever action (see Fig. 7.7), are as follows:

1. The increase of the tensile force in the flexural reinforcement between adjacent cracks produces a bond force, $\Delta T = T_1 - T_2$.

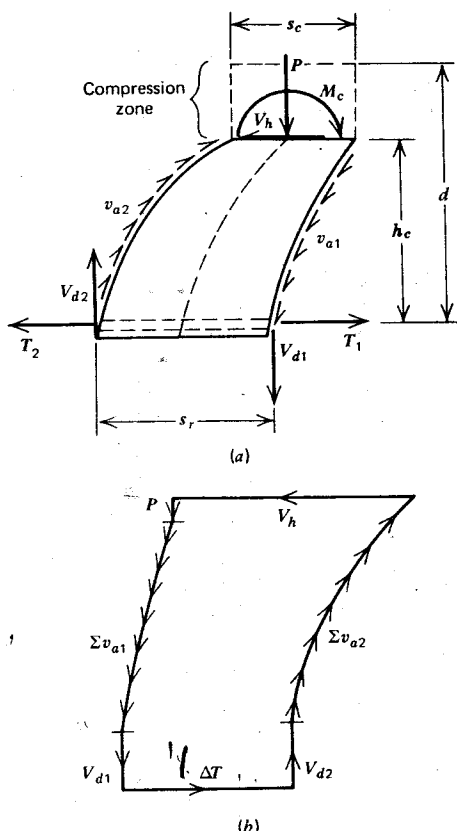


Fig. 7.7. Actions on a concrete cantilever in the shear span of a beam.

2. Provided shear displacements occur at the two faces of a crack, shear stresses v_{a1} and v_{a2} may be generated by means of aggregate interlocking.
3. The same shear displacements may also induce dowel forces V_{d1} and V_{d2} across the flexural reinforcement.
4. At the "built-in" end of the cantilever, an axial force P , a transverse shearing force V_h , and a moment M_c are induced to equilibrate the above-mentioned forces on the cantilever.

It will be noticed that the cantilever moment exerted by the bond force, ΔT , is resisted by dowel and aggregate interlock forces in addition to the flexural resistance M_c of the concrete. Tests^{7,6} have enabled a quantitative comparison between these three modes of cantilever resistance. The flexural

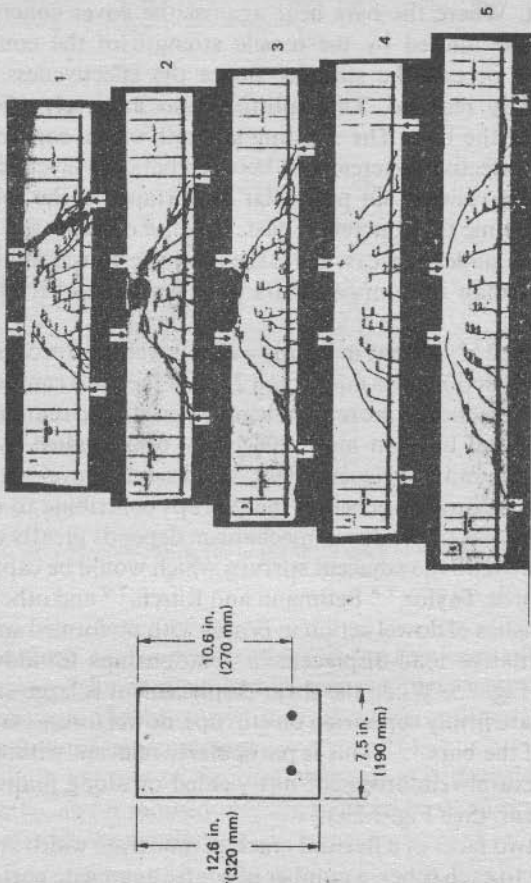
resistance of the concrete depends largely on the tensile strength of the concrete, the stress pattern resulting from the actions of P , V_h , and M_c (see Fig. 7.7), and the depth s_c of the critical cantilever section. The depth s_c is often quite small, particularly at advanced stages of cracking. Beam 5 in Fig. 7.8, which shows a series of beams tested by Leonhardt and Walther,^{7,7} is a good example of this phenomenon. Experiments^{7,6} have indicated that in beams of normal dimensions at the most 20% of the bond force could be resisted by flexure at the "built-in end" of the concrete cantilevers.

When shear displacement along an inclined crack occurs, a certain amount of shear will be transferred by means of the dowel action of the flexural reinforcement. Where the bars bear against the cover concrete, the dowel capacity will be limited by the tensile strength of the concrete. Once a splitting crack occurs, the stiffness, hence the effectiveness, of the dowel action is greatly reduced. This splitting also adversely affects the bond performance of the bars. The splitting strength of the concrete in turn will depend on the effective concrete area between bars of a layer across which the tension is to be resisted. Of particular importance is the relative position of a bar at the time the concrete is cast. Because of increased sedimentation and water gain under top-cast bars, they require considerably larger shear displacements than bottom-cast bars of a beam to offer the same dowel resistance.

Tests indicated^{7,6,7,8} that in beams without web reinforcement the contribution of dowel action does not exceed 25% of the total cantilever resistance. However, dowel action is more significant when stirrup reinforcement is used because a flexural bar can more effectively bear against a stirrup that is tightly bent around it. Nevertheless, cracks will develop approximately parallel to the flexural bars before the stirrups contribute to carrying dowel forces. The stiffness of the dowel mechanism depends greatly on the position of a crack relative to the adjacent stirrups which would be capable of sustaining a dowel force. Taylor,^{7,8} Baumann and Rüsch,^{7,9} and others have studied the characteristics of dowel action in beams with preformed smooth diagonal cracks. Qualitative load-displacement relationships for dowel action are presented in Fig. 7.9. When the shear displacement is large enough, and the flexural bars are firmly supported on stirrups, dowel forces can be transferred by kinking of the bars.^{7,10} This is particularly relevant within plastic hinges where the flexural reinforcement has yielded or along joints where sliding shear can occur. (See Fig. 7.29.)

When the two faces of a flexural crack of moderate width are given a shear displacement to each other, a number of coarse aggregate particles projecting across such a crack will enable small shear forces to be transmitted. Clearly among many variables, the width and coarseness of the crack, the shear displacement, and the strength of embedment (i.e., concrete strength), are

Mark	Span		$\frac{a}{d}$
	(in)	(m)	
1	35.4	0.90	1.0
2	41.3	1.15	1.5
3	57.0	1.45	2.0
4	66.9	1.70	2.5
5	76.7	1.95	3.0
6	92.5	2.35	4.0
7/1	112.1	3.10	5.0
8/1	141.9	3.60	6.0
10/1	185.2	4.70	8.0
9/1	228.2	5.80	7.0



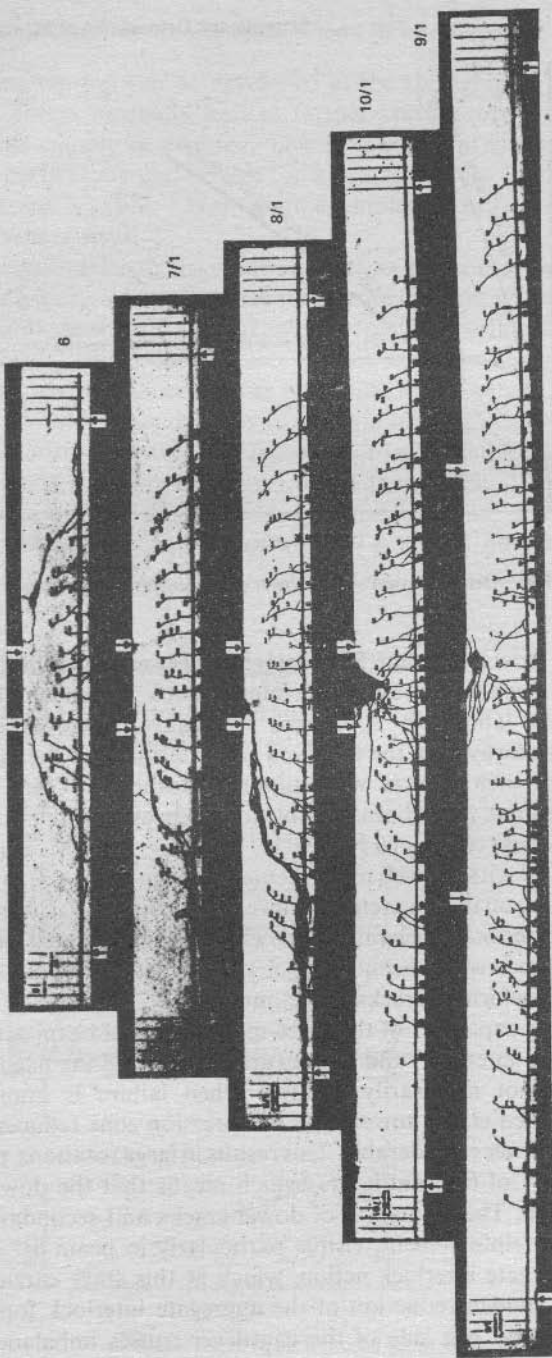


Fig. 7.8. Crack pattern in beams tested by Leonhardt and Walther.^{7,7}

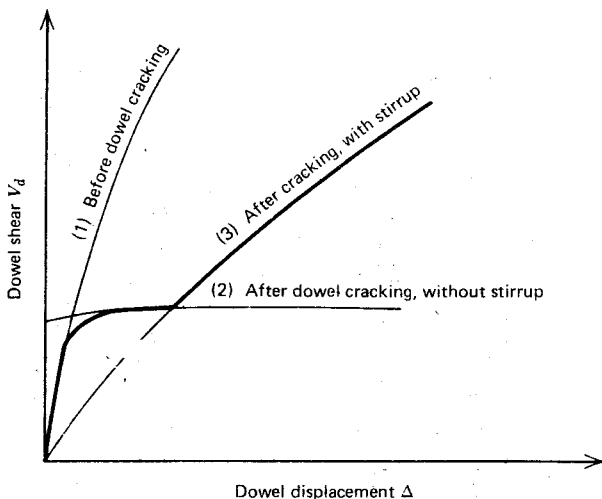


Fig. 7.9. General dowel shear-dowel displacement relationship.

likely to be the most important. Surprisingly, a very considerable force can be transmitted this way. In fact, aggregate interlock failure could not be obtained in one series of laboratory specimens^{7,6} because other causes, such as diagonal tension away from the observed crack, terminated the load carrying capacity. When such failures were suppressed and the crack width was maintained constant, it has been possible to obtain aggregate interlock shear stresses in excess of 1000 psi (69 N/mm²)^{7,11} (see Fig. 7.28). Measurements on test beams^{7,6, 7,13} without web reinforcement indicated that 50 to 70% of the bond force, acting on the concrete cantilever shown in Fig. 7.7, was resisted by the aggregate interlock mechanism. Fenwick^{7,6} demonstrated this convincingly by comparison with a beam in which the aggregate interlock mechanism across smooth preformed cracks was eliminated.

The maximum capacities of the three mechanisms of beam action (dowel action, aggregate interlock, and the flexural strength of the fixed end of the cantilever) are not necessarily additive when failure is imminent. The advance of inclined cracks toward the compression zone reduces the "fixed end" of the cantilever considerably. This results in large rotations, particularly at the "free end" of the cantilevers, which means that the dowel capacity can be exhausted. The formation of dowel cracks and secondary diagonal cracks near the reinforcement, visible particularly in beam 8/1 of Fig. 7.8, affects the aggregate interlock action, which at this stage carries the bulk of the load. A sudden reduction of the aggregate interlock force, such as Σv_{a2} in Fig. 7.7, on one side of the cantilever causes imbalance unless a

corresponding tension can be developed at the springing of the cantilever. Such tensile forces normally lead to further crack propagation, which in slender beams cannot be arrested. This is referred to as diagonal tension failure. It is particularly undesirable for it usually occurs very suddenly.

Beams 7/1 and 8/1 (Fig. 7.8) are good examples of the failure of the beam action in the shear span.

We customarily refer to the shear strength of the compression zone of a beam, on the assumption that aggregate interlock and dowel actions are not viable means of shear resistance. However, recent experiments have shown again that this is not the case. Taylor^{7,12} examined the compression zones of the concrete above diagonal cracks and found that the shear carried in this area (V_c in Fig. 7.6) increased slowly to a maximum of 25 to 40% of the total shear force across the section as the beams approached failure. The remainder of the shear must therefore be carried below the neutral axis in the tension zone of the beam. After the breakdown of the aggregate interlock and the dowel mechanisms, the compression zone is generally unable to carry the increased shear, in addition to the compression force resulting from flexure, and the beam fails.

Arch Action in the Shear Span

The second term of Eq. 7.10 signifies that shear can be sustained by inclined compression in a beam, as illustrated in Fig. 7.10. Arch action requires a

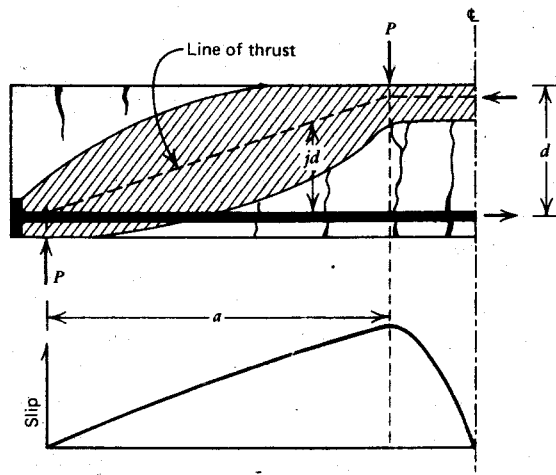


Fig. 7.10. Slip associated with arch action in an idealized beam.

substantial horizontal reaction at the support, which in simply supported beams is provided by the flexural reinforcement. This imposes heavy demands on the anchorages, and indeed it accounts for the most common type of arch failure. In the idealized beam of Fig. 7.10, full anchorage is assumed, thus a constant tensile force can develop in the bottom reinforcement over the full length as required. The shaded area indicates the extent of the compressed concrete outside which cracks can form. By considering the requirements of strain compatibility, and by assuming linear strain distribution across the full concrete section, a unique position of the line of thrust may be determined. The total extension of the reinforcement between anchorages must equal the total elongation of the concrete fiber situated at the same level. Where the concrete is cracked, the elongation can be derived from linear extrapolation of the strains in the compression zone. Having satisfied these criteria, the translation displacement of the steel relative to its surrounding concrete (i.e., the slip), can be determined. A typical slip distribution along the shear span is shown in Fig. 7.10.

Three points worth noting emerged from the study of such an idealized beam:^{7,6}

1. Arch action can only occur at the expense of slip (i.e., of complete loss of bond transfer).
2. The translational displacements required for complete arch action increase toward the load point and attain a value approximately equal to the total extension of the steel in the shear span.
3. In the vicinity of the load point the line of thrust, hence the neutral axis, rises well above the position predicted by standard flexural theory.

In real beams, particularly when deformed bars are used, no appreciable slip can take place between steel and concrete. The translational displacement occurs mainly as a result of the flexural deformation or the failure of the concrete cantilevers formed between diagonal cracks and the bending of the compression zone above the top of these cracks. Also in a real beam, the transition from beam action to arch action is gradual, and this can be determined if the development of the tension force along the reinforcement, hence the variation of the internal lever arm in test beams, is observed. The full strength of arch and beam actions cannot be combined because of the gross incompatibility of the deformations associated with the two mechanisms.

The available strength from arch action is largely dependent on whether the resulting diagonal compression stresses can be accommodated. For a given steel force and beam width, the intensity of the diagonal compression stresses depends on the inclination of the line of thrust. The shear span to depth ratio (a/d in Fig. 7.10) is a measure of this inclination. It can also be

expressed in terms of the moment and the shear as follows

$$\frac{a}{d} = \frac{Va}{Vd} = \frac{M}{Vd} \quad (7.13)$$

Excluding loss of anchorage, arch failures may be placed in three groups.

1. After the failure of the beam action, the propagation of an inclined crack reduces the compression zone excessively. A slope is reached when the available area of concrete in the vicinity of the load point becomes too small to resist the compression force and it crushes. This is known as a "shear compression" failure. Beams 4, 5, and 6 of Fig. 7.8 are good examples of such a failure.

2. The line of thrust may be so eccentric that a flexural tension failure occurs in the "compression zone." An example of such behavior is beam 7/1 in Fig. 7.8. The failure is very sudden.

3. When the line of thrust is steeper (i.e., when a/d is less than 2), considerable reserve strength may be available owing to more efficient arch action. Failure may eventually be due to diagonal compression crushing or splitting, which can be likened to a transverse splitting test performed on a standard concrete cylinder (see beam 1 in Fig. 7.8). Frequently the flexural capacity of a beam is attained because the arch mechanism is sufficient to sustain the required shear force (see beam 2 in Fig. 7.8).

It is important to note that arch action in beams without web reinforcement can occur only if loads are applied to the compression zone of the beam. This was the case for all the test beams in Fig. 7.8. The load situation may be more serious when a girder supports secondary beams near its bottom edge. It is evident that effective arch action cannot develop in a beam when the external shear force is transmitted to the tension zone. Precautionary measures for such situations are discussed in Chapter 13. The foregoing material has clearly indicated that arch action must be the dominant mode of shear resistance in deep beams loaded in the compression zone.

7.3.4 Size Effects

For obvious reasons most shear tests have been carried out on relatively small beams. Recently it has been found that the results of such laboratory tests cannot be directly applied to full size beams. The shear strength of beams without web reinforcement appears to decrease as the effective depth increases. Kani, in his experiments, has demonstrated this very effectively.^{7.14} If proper scaling of all properties is taken into account, the effect of the absolute size of a beam on its shear strength is not so large.^{7.15} Dowel and aggregate interlock actions in particular can be considerably reduced in

large beams if aggregate and reinforcing bar sizes are not correctly scaled. Experiments at the University of Stuttgart indicated, however, that the relative loss of shear strength of large beams was not significant when beams with web reinforcement were compared.^{7,16}

7.3.5 Shear Failure Mechanisms

Shear failure mechanisms of simply supported beams, loaded with point loads of the types previously described, fall into three approximate bands of a/d ratios. These can be observed on the beams tested by Leonhardt and Walther^{7,7} (Fig. 7.8). The failure moments and the ultimate shear forces for the 10 beams of Fig. 7.8 are plotted against the shear span to depth ratio (Eq. 7.13) in Fig. 7.11. The beams contained no stirrups and the material properties of all specimens were nearly identical.

Type I. Failure of the beam mechanism at or shortly after the application of the diagonal cracking load, when $3 < a/d < 7$. The subsequent arch mechanism is not capable of sustaining the cracking load.

Type II. Shear compression or flexural tension failure of the compression zone above diagonal cracking load. This is usually a failure of arch action when $2 < a/d < 3$.

Type III. Failure by crushing or splitting of the concrete (i.e., a failure of arch action), when a/d is smaller than 2.5.

Figure 7.11 reveals that when $1.5 < a/d < 7$, the flexural capacity of the beams is not attained. Hence shear governs the design.

By considering the beam action of shear resistance, as outlined previously, it becomes clear that the magnitude of the bond force ΔT , transmitted between two adjacent cracks, is limited by the strength of the cantilever block (Fig. 7.7) formed between the cracks. By assuming that the strength of each cantilever in the shear span of a prismatic beam is the same, $\Delta T_{\max} = q_{\max} \Delta x$, the maximum moment that can be developed by beam action becomes

$$M_{\max} = jdT_{\max} = jd \sum_0^x q_{\max} \Delta x = q_{\max} jdx \quad (7.14)$$

where q_{\max} is the maximum bond force per unit length of beam, Δx is the distance between cracks and x is the distance of the maximum moment section from the support. When this moment is less than the flexural strength of the section M_u , shear strength, associated with beam action, governs the capacity of the beam. From Eq. 7.14 it is evident that the moment sustained by the concrete cantilevers of the beam action in the shear span increases with the distance x from the support. Beam action also implies constant

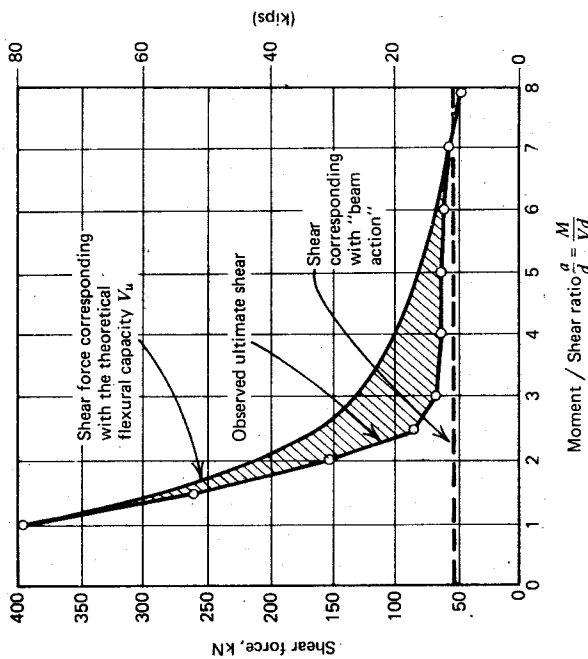
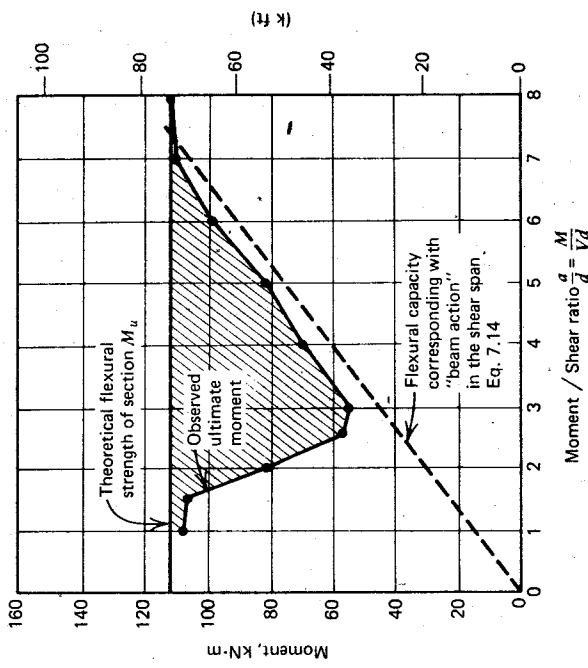


Fig. 7.11. Moments and shears at failure plotted against shear span to depth ratio.

shear strength, limited by q_{\max} , which is independent of the shear span to depth ratio a/d .

The flexural and shear capacities of "beam action" are designated by dashed lines in Fig. 7.11. When compared with observed ultimate values, they demonstrate that beam action governs the behavior when a/d is larger than 3. When a/d is larger than 7, the shear strength exceeded the flexural strength of these beams; hence flexure governed their strength. The discrepancy between the theoretical flexural capacity and the observed shear strength of these beams is indicated by the shaded area in Fig. 7.11.

The flexural steel content for the beams represented in Fig. 7.11 was 2%. For higher steel content the "valley" at $a/d \approx 2.5$ will be deeper and for a

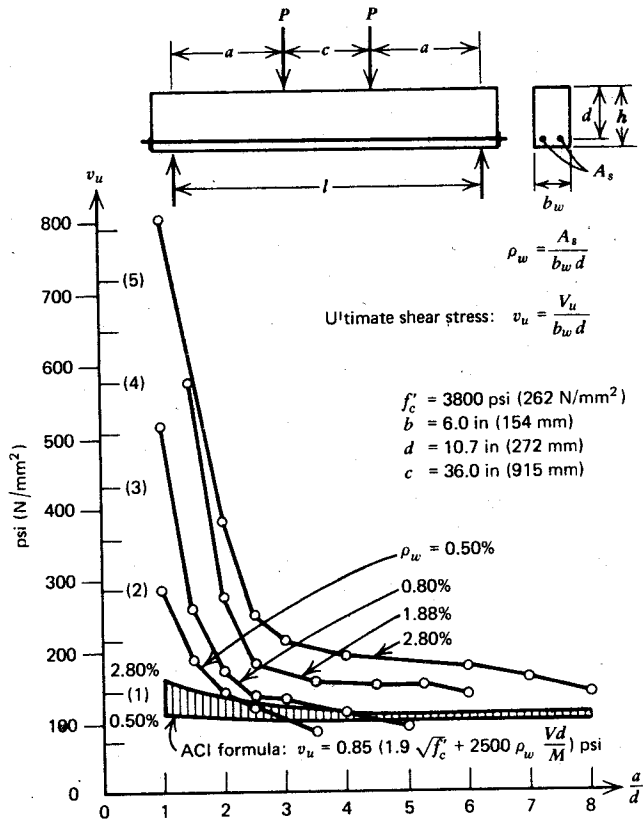


Fig. 7.12. Shear stress at failure as a function of the shear span to depth ratio. ^{7.17}

smaller steel percentage it will be shallower. Kani has demonstrated this change with flexural steel content in tests on a large number of beams.^{7,17}

A high steel content in the shear span, however, will mean narrower flexural cracks at a given load, and this will enable aggregate interlock and dowel actions to carry larger load. The increased strength of the beam action, resulting from larger flexural steel content, has been demonstrated also by tests^{7,17} (see Fig. 7.12).

7.3.6 The Design for Shear of Beams Without Web Reinforcement

The previous pages have discussed the nature of shear resistance in simply supported beams without web reinforcement subject to concentrated loadings. It was seen that the shear failure mechanism, particularly of beams with $2.5 < a/d < 7$, depends greatly on the tensile strength of the concrete. Thus it is not surprising that there is a great scatter of test data from apparently similar members. For beams subjected to uniformly distributed load along the compression edges, slightly more favorable results are obtained. In continuous beams, on the other hand, the a/d ratio does not represent the same situation encountered in simply supported beams because the sections do not coincide with the supports at which reactions are applied. For this reason a relatively simple semiempirical design equation has been adopted by the ACI, based on the results of numerous tests. This conservatively predicts the shear strength of beams in most situations.^{7,3} It also takes into account the major factors influencing shear resistance, such as the tensile strength of the concrete, as measured by the parameter $\sqrt{f'_c}$, crack control as expressed by $\rho_w = A_s/b_w d$, and the shear span to depth ratio M/Vd , in this form

$$v_c = \frac{V_c}{b_w d} = 1.9\sqrt{f'_c} + 2500\rho_w \frac{V_u d}{M_u} \leq 3.5\sqrt{f'_c} \quad (7.15)$$

where all quantities are in pound and inch units and $(V_u d/M_u) \leq 1.0$ at any section.

Often the use of the second term of Eq. 7.15 is not warranted (see the shaded area of Fig. 7.12), and equally satisfactory design may be achieved by using the simpler and slightly more conservative expression

$$v_c = 2.0\sqrt{f'_c} \text{ (psi)} \quad \text{or} \quad v_c = 0.166\sqrt{f'_c} \text{ (N/mm}^2\text{)} \quad (7.16)$$

Figure 7.13 compares Eqs. 7.15 and 7.16 with experimental results.

However small the nominal shear stress may be, it is good practice to provide a minimum amount of web reinforcement in all beams, as suggested in Section 7.4.3, to ensure that a possible diagonal crack is not followed by an immediate collapse. This is important because in addition to Kani's

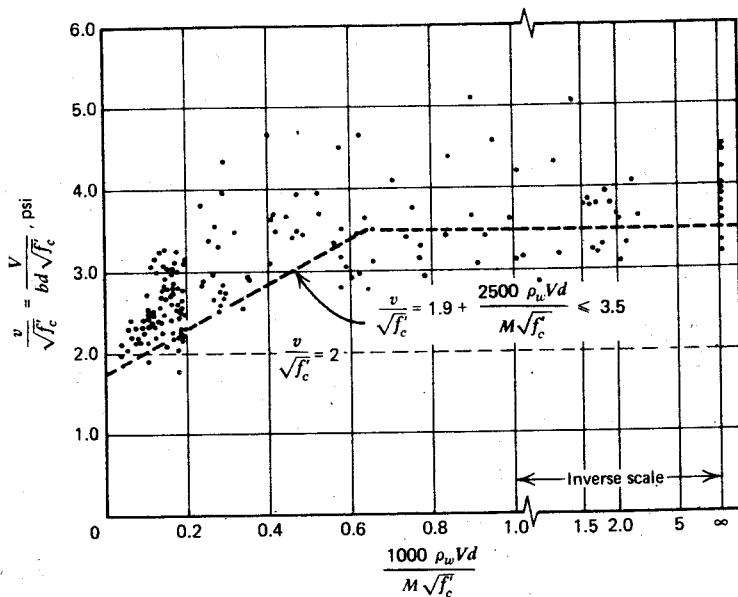


Fig. 7.13. Comparison of Eqs. 7.15 and 7.16 with experimental results.^{7.3}

tests (Fig. 7.12), there is other evidence^{7.18} that Eq. 7.15 might not be conservative when the flexural steel content is small. Also, unforeseen axial tension in a member could reduce v_c .

Inevitably, a general expression such as Eq. 7.15, which attempts to predict the strength of two mechanisms so different as beam action and arch action, will have shortcomings. Thus far, however, it has not been possible to rationally allow for all factors affecting each of the components of the shear resisting mechanisms and their interaction. One of the best correlations between the shear strength of different experimental slender beams ($a/d > 2.5$) and the three most important parameters governing shear (diagonal cracking) strength

$$v_c = 59 \left(\frac{f'_c \rho_w d}{a} \right)^{1/3} \quad (\text{psi}) \quad (7.17)$$

was derived by Zsutty^{7.19} using dimensional and statistical regression analyses. A semiempirical approach yielded very similar results for Regan^{7.20} and Placas^{7.21} in their extensive work at Imperial College. In beams with a/d ratios less than 2.5, loaded at the top and bottom edge, Zsutty proposed the

following equation

$$v_c = \text{Eq. 7.17} \left(\frac{2.5d}{a} \right) \quad (7.17a)$$

to account for arch action.^{7.22}

7.4 THE MECHANISM OF SHEAR RESISTANCE IN REINFORCED CONCRETE BEAMS WITH WEB REINFORCEMENT

7.4.1 The Role of Web Reinforcement

The inclusion of web reinforcement such as stirrups does not change fundamentally the previously described mechanism of shear resistance. The concrete cantilevers, which are the principal elements of the beam mechanism, will act as tied cantilevers. In addition to the bond force ΔT , resisted by the combination of aggregate interlock, dowel, and flexural action of the cantilevers, another bond force $\Delta T'$ can be sustained by what is traditionally termed "truss action." In this truss the cantilevers act as diagonal compression members (see Fig. 7.14).

The presence of stirrups is beneficial to beam action in a number of other aspects, as well. Stirrups contribute to the strength of the shear mechanisms by the following means:

1. Improving the contribution of the dowel action. A stirrup can effectively support a longitudinal bar that is being crossed by a flexural shear crack close to a stirrup.
2. Suppressing flexural tensile stresses in the cantilever blocks by means of the diagonal compression force C_d , resulting from truss action.

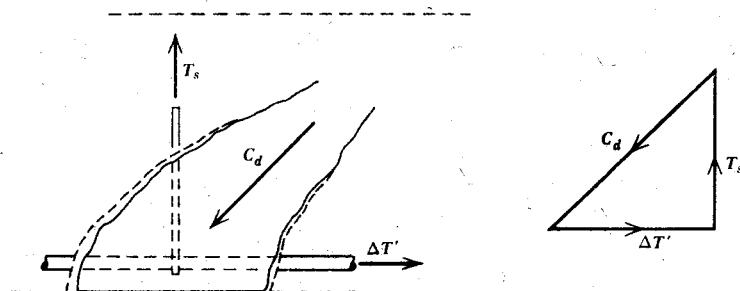


Fig. 7.14. Concrete cantilevers acting as struts.

3. Limiting the opening of diagonal cracks within the elastic range, thus enhancing and preserving shear transfer by aggregate interlock.
4. Providing confinement, when the stirrups are sufficiently closely spaced, thus increasing the compression strength of localities particularly affected by arch action.
5. Preventing the breakdown of bond when splitting cracks develop in anchorage zones because of dowel and anchorage forces.

It may be said that suitably detailed web reinforcement will preserve the integrity, therefore the strength, of the previously defined beam mechanism V_c , allowing additional shear forces V_s to be resisted by the truss mechanism.

7.4.2 The Truss Mechanism

The analogy between the shear resistance of a parallel chord truss and a web-reinforced concrete beam is an old concept of concrete structures. The analogy, postulated by Mörsch at the beginning of the century,^{7,23} implies that the web of the equivalent truss consists of stirrups acting as tension members and concrete struts running parallel to diagonal cracks, generally at 45° to the beam's axis. The flexural concrete compression zone and the flexural reinforcement form the top and bottom chords of this analogous pin-jointed truss. The forces in the truss can be determined from considerations of equilibrium only. The behavior of the truss is similar to the previously defined "perfect beam action" to the extent that it can sustain discrete bond forces $\Delta T'$ at the hypothetical pin joints along the flexural reinforcement, thus resisting variable external moments on a constant internal lever arm.

The deformations associated with beam or arch action and the truss mechanism within the beam are not compatible. This strain incompatibility, traditionally ignored, becomes progressively less significant as ultimate (i.e., plastic) conditions are approached.

The analogous truss appearing in Fig. 7.15 depicts the general case of web reinforcement inclined at an angle β to the horizontal. It will serve to illustrate the relation between the external shear force V_s , to be resisted by the truss, and the various internal forces. The diagonal compression struts, resisting a force C_d , are inclined at an angle α to the horizontal. From the equilibrium force polygon drawn for joint X in Fig. 7.15 it is evident that

$$V_s = C_d \sin \alpha = T_s \sin \beta \quad (7.18)$$

where T_s is the resultant of all stirrup forces across the diagonal crack. The web steel force per unit length of beam is T_s/s , where from the geometry of the analogous truss, the spacing between stirrups is

$$s = jd(\cot \alpha + \cot \beta) \quad (7.19)$$

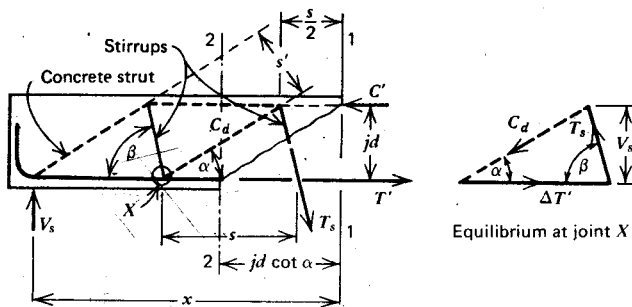


Fig. 7.15. Internal forces in an analogous truss.

From Eqs. 7.18 and 7.19, the stirrup force per unit length is

$$\frac{T_s}{s} = \frac{V_s}{jd \sin \beta (\cot \alpha + \cot \beta)} = \frac{A_v f_s}{s} \quad (7.20)$$

where A_v is the area of the web reinforcement spaced at a distance s along the beam and f_s is the stirrup stress.

For design purposes it is convenient to express shear in terms of nominal stresses, as in Eq. 7.15. The total shear V_u is assumed to be resisted partly by the truss mechanism (V_s) and partly by the previously described beam or arch mechanisms (V_c). In terms of stresses, this is expressed as

$$v_u = v_c + v_s \quad (7.21)$$

where

$$v_s = \frac{V_s}{b_w jd} \approx \frac{V_s}{b_w d} \quad (7.22)$$

By combining Eqs. 7.20 and 7.22, the required area of web reinforcement at ideal strength, when $f_s = f_y$, becomes

$$A_v = \frac{v_s}{\sin \beta (\cot \alpha + \cot \beta)} \frac{s b_w}{f_y} \quad (7.23)$$

The diagonal compression force C_d is assumed to generate uniform stresses in the struts of the truss. The struts have an effective depth of $s' = s \sin \alpha = jd \sin \alpha (\cot \alpha + \cot \beta)$. Thus the diagonal compression stresses due to the truss mechanism can be approximated by

$$f_{cd} = \frac{C_d}{b_w s'} = \frac{V_s}{b_w jd \sin^2 \alpha (\cot \alpha + \cot \beta)} = \frac{v_s}{\sin^2 \alpha (\cot \alpha + \cot \beta)} \quad (7.24)$$

For the common cases of web steel arrangements, Eqs. 7.23 and 7.24 simplify as follows:

1. VERTICAL STIRRUPS, $\beta = 90^\circ$

Compression diagonals at $\alpha = 45^\circ$

$$A_v = v_s \frac{sb_w}{f_y} \quad (7.23a)$$

$$f_{cd} = 2v_s \quad (7.24a)$$

Compression diagonals at $\alpha = 30^\circ$

$$A_v = 0.58v_s \frac{sb_w}{f_y} \quad (7.23b)$$

$$f_{cd} = 2.31v_s \quad (7.24b)$$

2. SLOPING WEB REINFORCEMENT, $\beta < 90^\circ$

Compression diagonals at $\alpha = 45^\circ$

$$A_v = \frac{v_s}{(\sin \beta + \cos \beta)} \frac{sb_w}{f_y} \quad (7.23c)$$

$$f_{cd} = \frac{2v_s}{1 + \cot \beta} \quad (7.24c)$$

Web reinforcement and struts at 45°

$$A_v = 0.50 \frac{sb_w}{f_y} \quad (7.23d)$$

$$f_{cd} = v_s \quad (7.24d)$$

The slope of the compression diagonals has been traditionally assumed to be 45° to the beam axis. It has been observed, however, that the slope of the diagonal cracks at the boundaries of the struts vary along the beam. Studies^{7,24} based on strain energy considerations show that the optimum angle of the struts is about 38° . From Eq. 7.23 it is evident that the web steel demand is reduced as the angle of the compression diagonals becomes less than 45° , because more stirrups are encountered across a flat crack. This is often the case, and design equations based on compression struts at 45° are conservative. On the other hand, the struts are steeper in the vicinity of point loads. However, in these areas local arch action boosts the capacity of the other shear carrying mechanisms. Generally in a beam having high concrete strength and low web steel content, representing a less rigid tension system, the compression struts are at an angle less than 45° , hence the stirrups are more effective than in a 45° truss. Conversely with large web steel content

and lower concrete strength, the load on the concrete will be relieved at the expense of larger stirrup participation.^{7,24} The slopes of the diagonal cracks in the vicinity of point loads and a point of contraflexure are displayed in Fig. 7.16.

Flat diagonal compression struts and steep stirrups imply larger concrete compression stresses (cf. Eqs. 7.24d and 7.24b). This indicates that the web steel content cannot be increased indefinitely. Figure 7.16 shows a continuous, thin-webbed flanged beam with heavy web reinforcement. In such beams, shear failure may be brought about by web crushing caused by diagonal compression (Eq. 7.24). When assessing the compression strength of the web of beams, it is necessary to consider the following additional factors:

1. The diagonal struts are also subjected to bending moments if they are to participate in beam action (see Fig. 7.7). Secondary moments are introduced because of the absence of true "pin joints" in the truss.
2. Stirrups passing through transmit tension to these struts by means of bond, so that generally a biaxial state of strains prevails. The compression capacity of concrete is known to be drastically reduced when simultaneous transverse tensile strains are imposed (see Fig. 2.8).
3. The compression forces are introduced at the "joints" of the analogous truss, and these forces are far from being evenly distributed across the web. Eccentricities and transverse tensile stresses may be present.
4. Some diagonals may be inclined at an angle considerably smaller than 45° to the horizontal, and this will result in significant increase in diagonal compression stresses (see Eq. 7.24 and Fig. 7.16).

These observations point to the need to limit diagonal concrete stresses to a value well below the crushing strength of the concrete. For this reason the ACI limits the contribution of the truss mechanism to shear strength to a very conservative value of $v_s = 8\sqrt{f'_c}$ (psi). Thus from Eqs. 7.15 and 7.21 the absolute maximum nominal shear stress in a beam (in psi units) is $10\sqrt{f'_c} < v_{u,\max} < 11.5\sqrt{f'_c}$, depending on the value of v_c . However, Kupfer and Baumann^{7,24} and others have shown that with closely spaced stirrups, as used in the double-flanged precast concrete beam in Fig. 7.16, nominal shear stresses of the order of $20\sqrt{f'_c}$ (psi) could be reached even after 50 applications of load to one-half that intensity. As a rule, shear stresses of this magnitude could not be attained in beams of rectangular cross section.

Stirrups can develop their assigned strength only if they are adequately anchored. A stirrup may be crossed by a diagonal crack at any point along its length. Since the crack may be very close to the tension or compression edge of the member, a stirrup must be capable of developing its yield strength

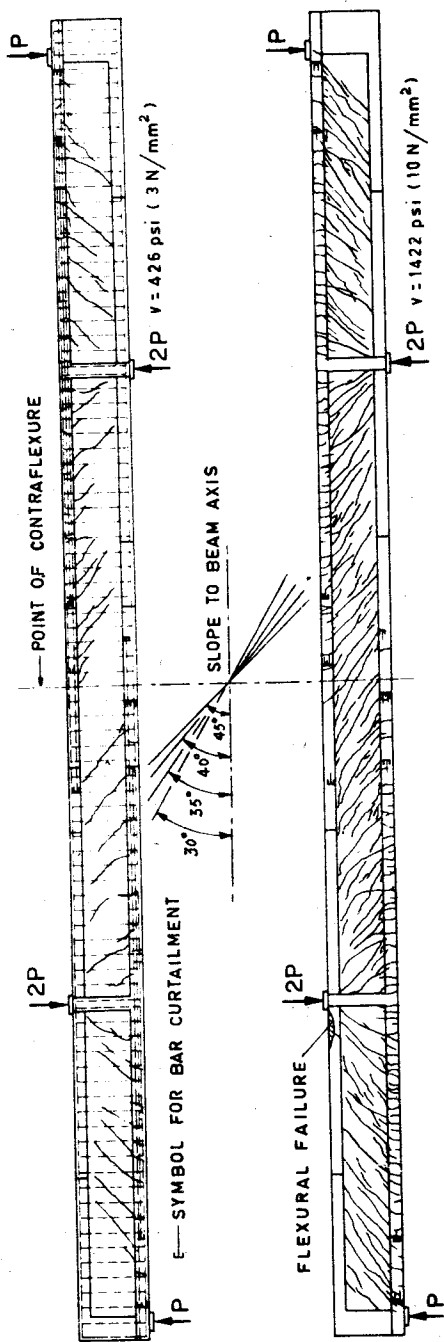


Fig. 7.16. Crack formation in a thin webbed beam. 7.24

over the full extent of its length. Therefore it is important that stirrups be bent around larger longitudinal bars and be extended beyond them, by an adequate development length. Codes stipulate various forms of satisfactory anchorage. For effective truss action the stirrup has to dispose of its load at or near the "pin joint." Careful detailing, as outlined in Chapter 13, must ensure this load transfer. The concentration of load transfer at the corners of stirrups may lead to local crushing of the concrete if a good fit to a longitudinal flexural bar is not assured. Stirrup slips as large as 0.02 in (0.5 mm) have been observed in some members. In shallow beams these slips can increase considerably the width of diagonal cracks.

Sometimes a set of stirrups, crossed by a continuous diagonal crack, yields; unrestricted widening of that crack then commences, and one of the important components of shear resistance, aggregate interlock action, becomes ineffective. The shear resistance so lost cannot be transferred to the dowel and the truss mechanisms, because they are already exhausted, hence failure follows, with little further deformation. To prevent such nonductile failure it is good practice—indeed, in seismic design it is mandatory—to ensure that stirrups will not yield before the flexural capacity of the member is fully exhausted.

A truss mechanism in beams can function only after the formation of diagonal cracks (i.e., after the disappearance of diagonal tension in the concrete). The prime role of stirrups is to transfer the transverse (vertical) shear across a potential diagonal failure crack. The use of a mesh reinforcement in the web is advocated from time to time and this is capable of resisting both horizontal and vertical forces, but it is no more effective in resisting shear. This is because horizontal reinforcement in the web of normal beams cannot contribute to the resistance of transverse (vertical) forces^{7,20} apart from aiding crack control and increasing dowel action. Horizontal web reinforcement will strengthen the "contribution of the concrete" v_c but will not affect the shear strength of the truss mechanism v_s (see Eq. 7.21). In deep beams, however (examined in Chapter 13), the arch mechanism can be substantially boosted by the addition of horizontal bars well anchored in the support zone.

7.4.3 The Design for Shear of Beams with Web Reinforcement

It has been shown that the shear resisting mechanism of a beam without web reinforcement, particularly aggregate interlock action, will function as long as the width of cracks does not become excessive. Hence in the presence of web reinforcement, beam action resists shearing forces, provided the strains in the web reinforcement do not become large (i.e., the stirrups do not yield). Before or at the onset of yielding of the stirrups, therefore, it is possible to

superimpose the strength of the two actions thus

$$v_u = v_c + v_s \quad (7.21)$$

A conservative value for v_c , specified by the ACI, was given by Eq. 7.15 or Eq. 7.16, this quantity being essentially a function of the tensile strength of the concrete. Hence the remaining shear $v_s = v_u - v_c$, is to be allocated to web reinforcement in accordance with Eq. 7.23 using vertical stirrups, bent-up bars, or the combination of both. The simple relationship between the total required shear strength v_u and the required strength of vertical stirrups v_s is represented in Fig. 7.17. It must be remembered that in the ACI specification compression struts are assumed to be inclined at $\alpha = 45^\circ$. An alternative view is^{7,24} that the contribution of the concrete v_c is negligible and the inclination of the diagonal concrete struts is less than 45° , therefore, more stirrups cross the potential crack. (See e.g., Fig. 7.16.) The broken lines in Fig. 7.17 indicate the corresponding relationships for various values of α . For most beams the shear strength predicted by the two approaches is very similar.

The ACI design approach is compared in Fig. 7.18 with the behavior of beams tested by Leonhardt and Walther.^{7,7} It is seen that the contribution of the concrete at ultimate load, v_c , is underestimated by the ACI. The theoretical relationship (Eq. 7.23a) rewritten to express the stirrup stress as

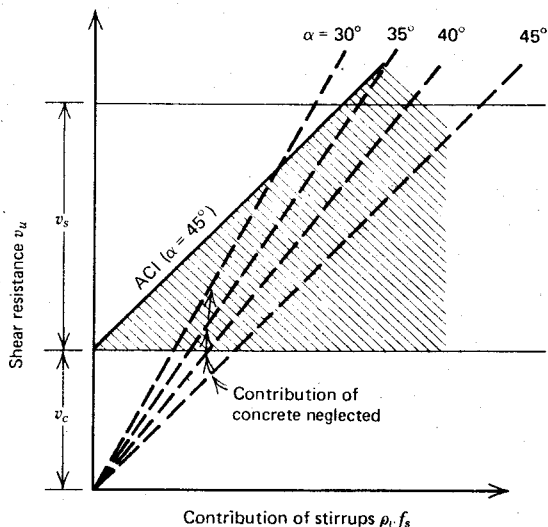


Fig. 7.17. The contribution of stirrups to shear strength.

$f_s = (v_u - v_c)/\rho_v$, where $\rho_v = A_v/sb_w$, is shown by dashed lines. Figure 7.18a compares the ACI approach with test results from four beams with identical web reinforcement. Only the web width varied in these beams; the flange width to web width ratio varied between 1 and 6. Accordingly, the contribution of the concrete, v_c , may be expected to increase proportionally as the web thickness increases (see Eq. 7.15). This supposition is borne out by the tests. Moreover, it will be seen that the shear prior to the significant rise of stirrup stresses, previously referred to as shear causing diagonal cracking, is maintained while the stirrup stresses rise to yield level (i.e., v_c remains almost constant). The same behavior is illustrated by four identical T beams^{7,7} in Fig. 7.18b, in which the theoretical share of the stirrups in the total shear strength, $\eta = v_s/v_u$, varied between 27 and 93%.

Irrespective of the shear intensity, a minimum web reinforcement, corresponding with at least $v_s = 50$ psi (0.35 N/mm^2), should be provided in every beam^{7,2} (Eq. 7.23a). Also, to ensure that every potential crack is effectively crossed by stirrups, the spacing, s , should not exceed $d/2$. Where plastic hinges may form, the stirrup spacing should not be more than $d/4$. When the flexural steel yields, it is inevitable that diagonal cracks, being a continuation of flexural cracks, will also increase. In these areas the contribution of the concrete toward shear resistance v_f should be ignored and web reinforcement provided for the whole of the shear (i.e., $v_s = v_u$).

When moment reversals are to be expected, as under seismic loading, the close spacing of closed stirrups (ties) is particularly important. Such stirrups will provide confinement to the compressed concrete and lateral support to the compression bars in regions where the flexural strength is developed. Diagonal web reinforcement is effective only in one direction; therefore, it should not be used when the loading may be reversed unless it is provided in both directions.

An example, given at the end of this chapter, illustrates the application of these principles. Further aspects of shear, as they affect the detailing of structural members, are discussed in Chapter 13.

7.5 THE INTERACTION OF FLEXURE AND SHEAR

Experiments with normal reinforced concrete beams with adequate web reinforcement indicate that the shear force has no recognizable influence on the development of flexural capacity. This enables the designer to ignore interaction and to deal with flexure and shear separately. The previous discussion shows, however, that an intimate relation does exist between flexure, shear, bond, and anchorage in the shear span of a beam. This is evident from an examination of the behavior of the flexural reinforcement along the beam. When large shear forces are to be transmitted across a

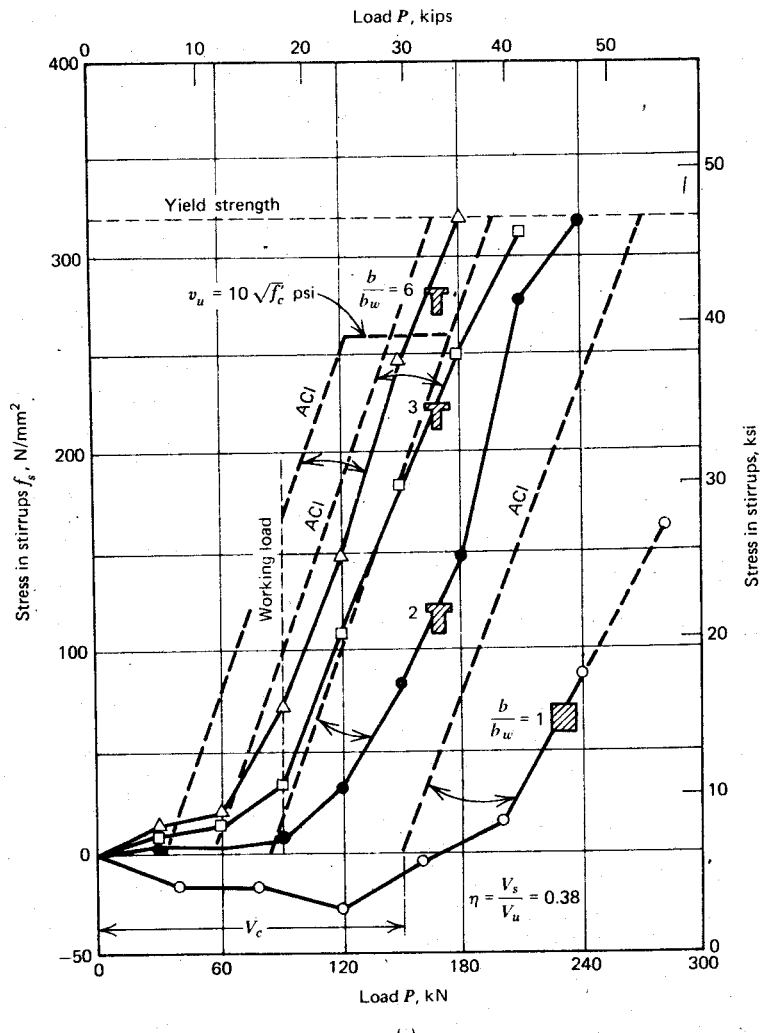
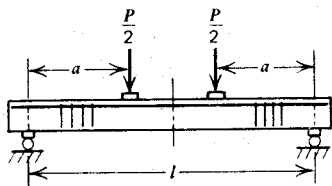
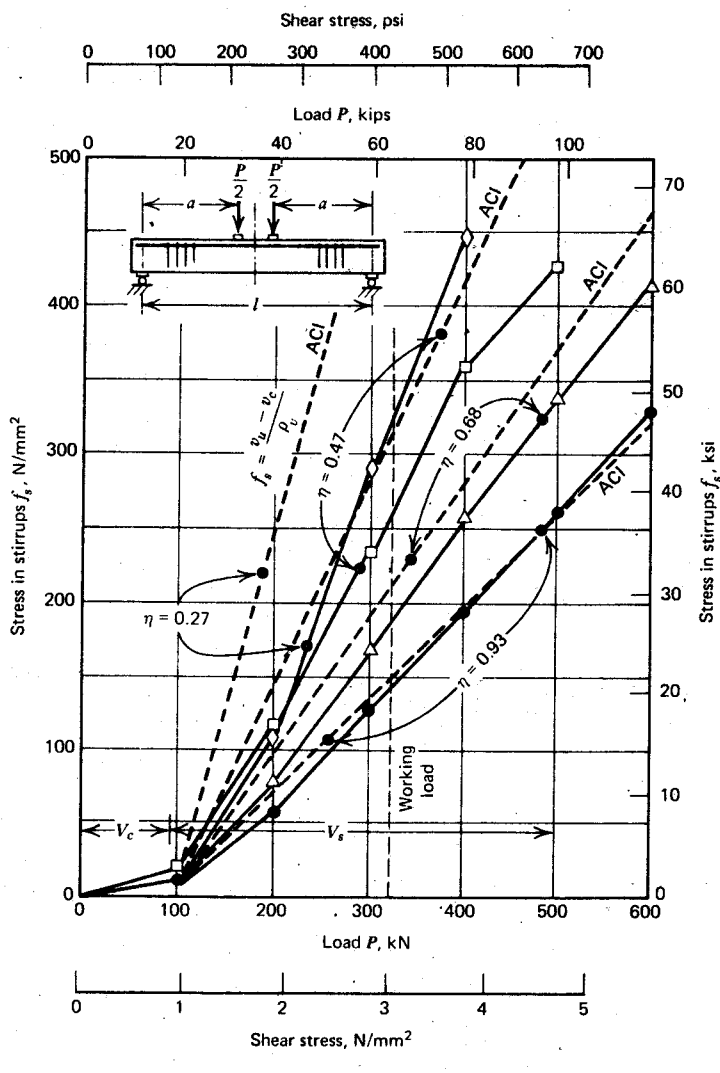


Fig. 7.18. Stirrup stress-load relationship. (a) Beams with constant web steel content. (b) Beams with variable web steel content.^{7,7}



(b)

section at ultimate moment, the distribution of the flexural strains in the concrete and the steel can be affected. Shear forces in deep beams can be so dominant that they govern the strength of the member by inhibiting the development of the full flexural capacity as derived from the principles presented in earlier chapters.

7.5.1 The Effect of Shear on Flexural Steel Requirements

The tension induced in the flexural reinforcement by the forces associated with the truss mechanism only can be established with reference to Fig. 7.15. Taking moment about the compression resultant C' at section 1-1, gives the following relationship:

$$M'_1 = V_s x = M'_2 + V_s j d \cot \alpha = T' j d + \frac{s}{2} T_s \sin \beta \quad (7.25)$$

where M'_1 and M'_2 are the bending moments generated by the external forces at sections 1 and 2, respectively. By substituting for T_s and s from Eqs. 7.18 and 7.19, we obtain

$$T' = \frac{M'_2}{j d} + \frac{V_s}{2} (\cot \alpha - \cot \beta) \quad (7.26)$$

Similarly, by considering beam action of a beam without web reinforcement in which diagonal cracks develop at an angle, α , to the axis of the beam, the moment equilibrium at sections 1 and 2 (Fig. 7.6) requires that

$$M''_1 = T'' j d = M''_2 + V_c j d \cot \alpha \quad (7.27)$$

Note that in this case the shear V_c is resisted by mechanisms other than the web reinforcement (i.e., $T_s = 0$ in Fig. 7.15). It is important to note that from Eq. 7.27

$$T'' = \frac{M''_1}{j d} = \frac{M''_2}{j d} + V_c \cot \alpha \quad (7.27a)$$

which shows that the tension force at section 2, T'' , is governed by the bending moment at section 1.

Let us combine the two mechanisms in accordance with Eq. 7.21, whereby

$$V_u = V_c + V_s \quad \therefore \quad M_u = M'_2 + M''_2 \quad \text{and} \quad T_u = T' + T''$$

Then the total tension force in the flexural reinforcement at section 2 is obtained thus

$$T_u = \frac{M_u}{j d} + V_c \cot \alpha + \frac{V_s}{2} (\cot \alpha - \cot \beta) \quad (7.28)$$

It is convenient to introduce the factor

$$\eta = \frac{V_s}{V_u} = \frac{v_s}{v_u} \quad (7.29)$$

which expresses the share of the web reinforcement in resisting the total shear force. Using this factor, the tension force becomes

$$T_u = \frac{M_u}{jd} + \frac{e_v}{d} V_u \quad (7.30)$$

where

$$\frac{e_v}{d} = \cot \alpha - \frac{\eta}{2} (\cot \alpha + \cot \beta) \geq 0 \quad (7.30a)$$

It is evident from Eq. 7.30 that after the formation of diagonal cracks, the tension force T_u in the flexural steel becomes greater than that required to resist the external moment at that section. The increase is largely dependent on the inclination of the cracks (i.e., the angle, α , of the diagonal struts).

This finding is particularly relevant to the curtailment of the flexural reinforcement. Figure 7.19 illustrates a simple beam and the bending moment diagram M associated with the given loading. We assume that it is practical to curtail at a suitable position one-third of the flexural reinforcement (say, two bars), which is required under the midspan load P_1 (six bars). At first it seems that only two-thirds of the positive flexural reinforcement is required at its full capacity at section 2. However, because of diagonal cracking, the required moment of resistance has increased by $e_v V_u$ there and over the whole of the left-hand shear span. This is shown by the dashed line envelope. Therefore, two-thirds of the flexural reinforcement will be required at full strength capacity (f_y) at section 3, which is located at distance e_v away from section 2, in the direction of decreasing moments. If a further two bars of the positive flexural bars are to be terminated, these must extend by the full development length l_d beyond section 3. (Anchorage and development lengths are examined in Chapter 9.) The same (two) bars must also extend at least to section 4 because the remaining one-third of the positive moment steel is insufficient to supply the moment of resistance required at section 4 (i.e., over the length of the small shaded triangle). The latter requirement does not apply at the other end of the bars in question, since their end is well past section 5. By similar considerations the curtailed ends of the shortest bars in the span, shown in Fig. 7.19 in elevation only, were also determined. The curtailment of the negative reinforcement, over the right-hand support, was determined on the assumption that eight smaller size bars can be cut off in pairs.

The curtailment of the flexural reinforcement may be conveniently determined from the envelope of the moment of resistance Tjd , shown by

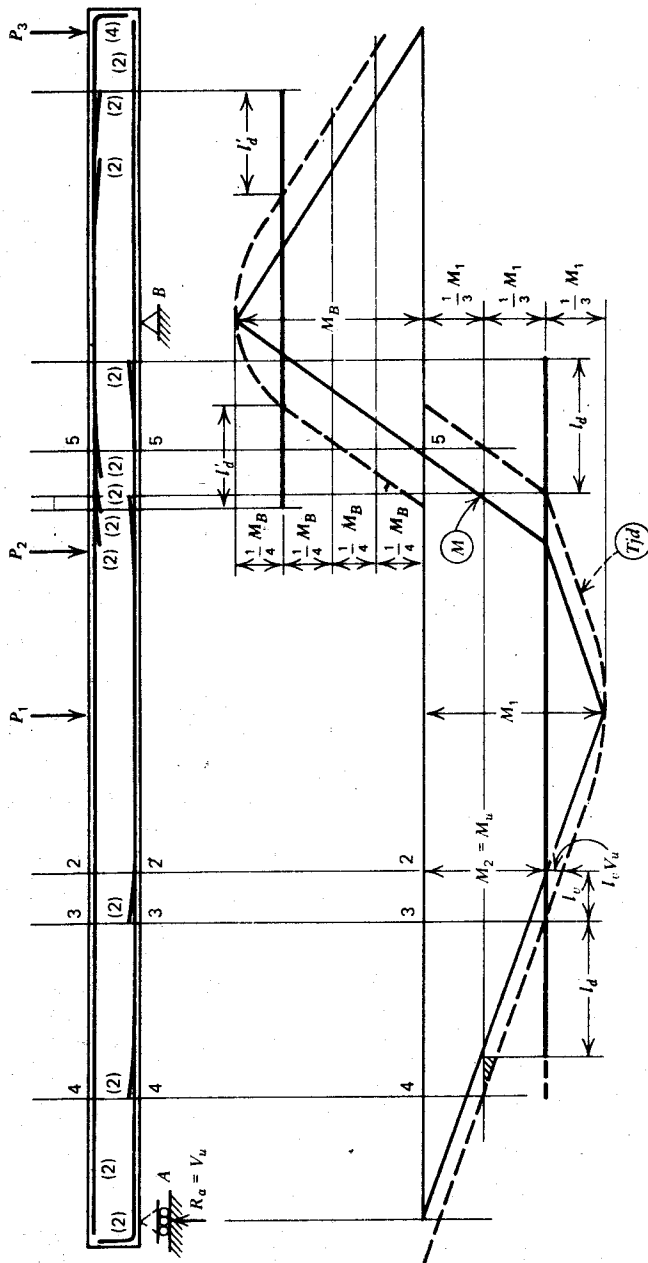


Fig. 7.19. The relationship between the external bending moment M and requirements of moment of resistance Tid .

the dashed line in Fig. 7.19. This is simply the bending moment diagram displaced horizontally by a distance e_v , whose magnitude depends on the web reinforcement factor η and the inclination of the cracks α .

The value of e_v/d from Eq. 7.30a is given for different values of α , β , and η in Table 7.1. It may be noted that for moderate web steel contents, $\eta < 0.5$.

Table 7.1 The value of e_v/d

Cracks, α	Web Steel, β	Inclination			Web Reinforcement Factor η
		1.00	0.50	0.00	
45°	45°	0.00	0.45	0.90	
45°	90°	0.45	0.68	0.90	
38°	90°	0.58	0.86	1.15	
30°	90°	0.78	1.17	1.56	

and a crack inclination a little less than 40°, the value of e_v is approximately equal to the effective depth d .

To simplify the design procedure, the ACI code^{7.2} requires that flexural bars be extended beyond the point at which they no longer need to resist flexure for a distance equal to the effective depth of the member. This implies that e_v , as shown in Fig. 7.19, is d . The development length l_d has to be provided beyond this point.

Figure 7.19 demonstrates another phenomenon, often overlooked. After the development of diagonal cracks, both the top and bottom reinforcement will be in tension at the point of contraflexure. (i.e., at the point of theoretical zero moment). To equilibrate these tension forces, an equal and opposite compression force will develop near the middepth of the section. These phenomena have been verified in experiments.

7.5.2 Shear at Plastic Hinges

Figure 7.16 illustrates that at the interior support of a beam the diagonal cracks, instead of being parallel, tend to radiate from the compression zone at the load point. When the flexural reinforcement has yielded, these cracks increase in width, and it is prudent to assume that very little shear can be transferred by either aggregate interlock or dowel action. Consequently, nearly the whole shear force will have to be transferred across the compression zone of the vertical section adjacent to the support. An idealized situation at the junction of a beam and the face of a column appears in Fig. 7.20a.

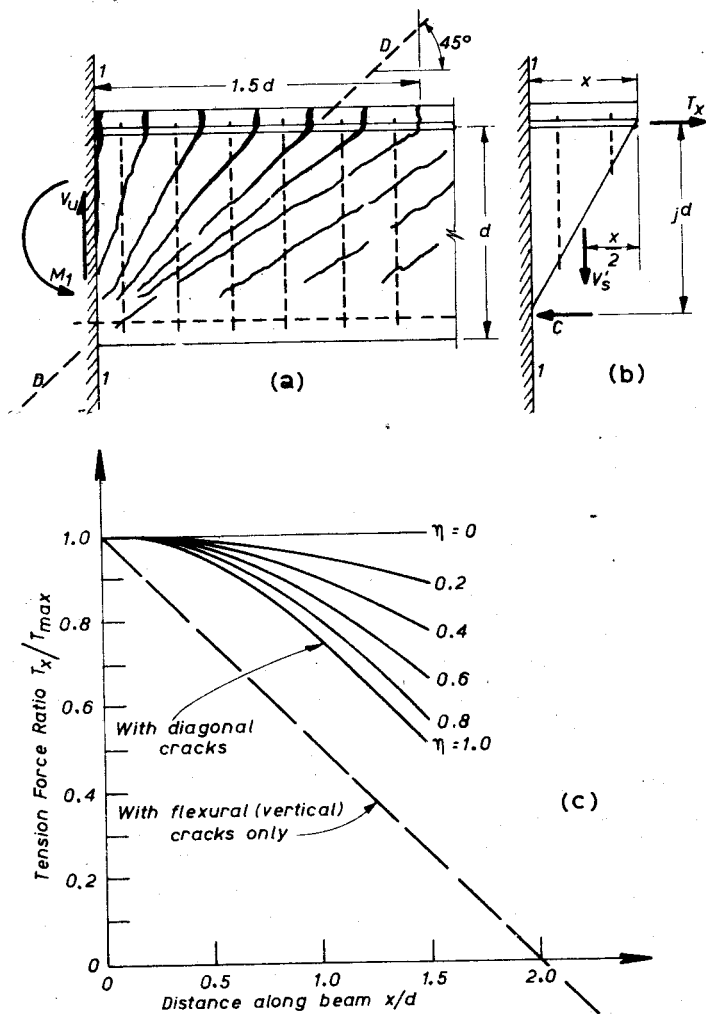


Fig. 7.20. The distribution of steel forces at a plastic hinge as affected by shear.

Each of the radiating cracks, to a minimum slope of 1:1.5, may be assumed to form the boundary of an inclined strut. Nearly all the diagonal compression forces in these struts pass through the compression zone of the beam at section 1; thus it is justifiable to assume that the total shear force is transferred across the compression zone between the last stirrup and the face of the column. It is evident that the capacity of the flexural compression zone of a

beam is reduced when the shear force across the plastic hinge is large. However, the confinement provided by stirrup ties and the adjacent tied column strengthens the concrete and enables the compression in the beam, generated by flexure M_1 and shear V_u , to be transmitted. Also in common situations, under monotonic loading, the transfer of flexural compression is assisted by the presence of compression reinforcement in the beam, and this adverse effect of shear is not observed.

A free body bounded by one of the diagonal cracks is shown in Fig. 7.20b. The stirrups crossing this particular crack are assumed to resist a force $V'_s = V_s x/d$, where V_s is the total force resisted by the stirrups crossing a 45° diagonal, section D-D, in accordance with the previously discussed truss analogy. This may or may not be the total shear force, depending on the value of η (i.e., $0 < \eta < 1$). From the equilibrium requirement for the free body shown, we have

$$M_1 = T_x jd + \frac{x}{2} V'_s \quad (7.31)$$

where $x < 1.5d$ for the example in Fig. 7.20a. Hence Eq. 7.31 gives

$$T_x = \frac{1}{jd} \left(M_1 - \frac{x^2 \eta}{2d} V_u \right) \quad (7.32)$$

The corresponding variation of the tension force in the vicinity of the column face, in terms of the maximum value, is displayed for various relative web steel capacities η in Fig. 7.20c. In this example it was arbitrarily assumed that $M/Vd = 2$.

If only vertical flexural cracks had formed, the tension force at any section would have been

$$T_x = \frac{M_x}{jd} = \frac{1}{jd} (M_1 - x V_u) \quad (7.33)$$

as indicated by the dashed line in Fig. 7.20c. It is thus evident that diagonal cracking, caused by shear, can have a marked effect on the distribution of steel stresses in the vicinity of a potential plastic hinge, particularly when only a small fraction of the shear is resisted by stirrups. This means that yielding of flexural reinforcement will spread over a considerable length of the beam, thus increasing significantly the plastic hinge length. This increase of plastic rotational ability enables the occurrence of larger redistribution of moments (see Chapter 6) in continuous reinforced concrete structures.^{7.25}

In T beams large shear forces cause the diagonal cracks to penetrate up to the underside of the compression flanges. This implies that in such cases a portion of the web that may be required to carry compression cannot be utilized for this purpose.^{7.24}

7.5.3 Interaction Effects in Deep Beams

In simply supported or continuous deep beams, where the external loads and reactions are applied to the top and bottom compression face of the beam, the mode of shear transfer after the formation of diagonal cracks is mainly by arch action. The behavior and design of such beams are discussed in Chapter 13.

The redistribution of the forces along the flexural reinforcement, examined in the previous section, can dominate the behavior of short and relatively deep spandrel beams. Such beams commonly occur in coupled shear walls. Because approximately equal but opposite bending moments are introduced at both ends, the point of zero moment occurs at the midspan of such beams. The distribution of the internal tension forces will therefore be similar to that indicated by the T_{jd} envelope at and in the immediate vicinity of the point of contraflexure of the beam shown in Fig. 7.19. When the distance e_r is equal to or greater than the half-span, tension will occur in the top and bottom reinforcement over the entire clear span of such a spandrel beam. Experimental evidence to this effect,^{7,26} and its consequences with respect to behavior, are more fully examined in Section 12.5.3.

7.6 THE INTERACTION OF SHEAR, FLEXURE, AND AXIAL FORCES

The combination of shear, flexure, and axial force is seldom critical when the loading on the structure originates from gravity. Under seismic load conditions, however, the columns of a multistory structure are subjected to large shear forces and flexure in addition to axial compression. In certain columns, particularly at the corners of buildings, seismic disturbances may even generate net tension. Figure 7.21 presents a typical example of a shear-compression failure, which occurred in the 43 in (1092 mm) diameter columns of the Macuto-Sheraton Hotel during the 1967 Caracas earthquake.^{7,27}

Since shear is associated with the phenomenon of diagonal tension, it is to be expected that axial compression will increase—or conversely, axial tension will decrease—the shear capacity of reinforced concrete members.

7.6.1 Shear and Axial Compression

It was shown previously that in web reinforced members a shear force V_c approximately equal to the diagonal cracking load, can be carried together with the shear resisted by the truss mechanism with 45° diagonal struts. This is also the basis for the current ACI approach to the design of flexural members subjected to axial forces. The semiempirical Eq. 7.15, based on principle

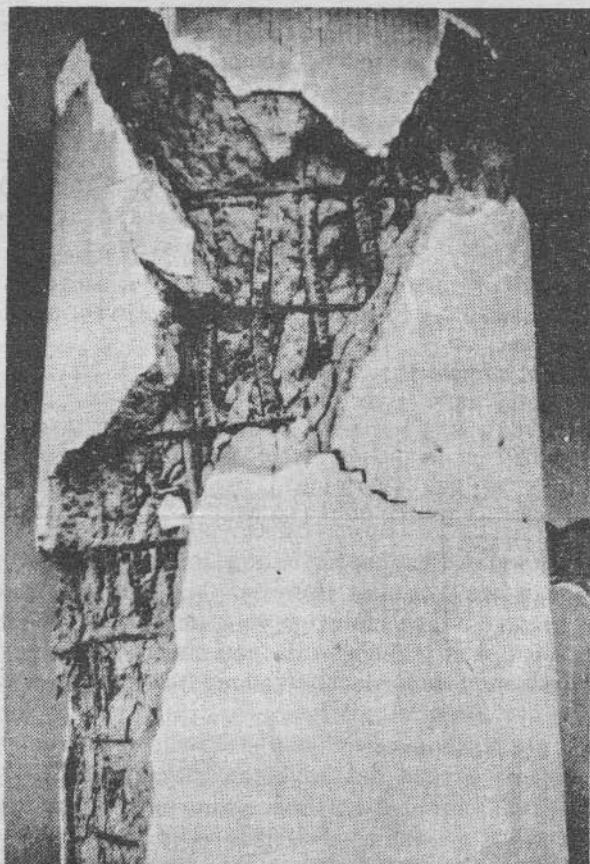


Fig. 7.21. Shear failure in large column during the 1967 Venezuela earthquake. Courtesy American Iron and Steel Institute.

stress concepts, which conservatively predicts the diagonal cracking load and incorporates the major parameters of shear strength, can be suitably modified^{7,3} to take into account the effect of axial forces. The axial force N_u , acting with the appropriate eccentricity, is considered when deriving the tensile stresses causing diagonal cracking in the section. The moment M_u in Eq. 7.15 can be replaced by an equivalent moment M_m , which produces the same effect on diagonal cracking as the moment M_u acting with the axial force N_u .^{7,3} This is approximately

$$M_m = M_u - \frac{(4h - d)}{8} N_u \quad (7.34a)$$

where h is the overall depth of the member. Thus the nominal shear stress at diagonal cracking becomes from Eq. 7.15

$$v_c = 1.9\sqrt{f'_c} + \frac{2500\rho_w V_u d}{M_m} \quad (\text{psi}) \quad (7.34b)$$

Because Eq. 7.34b is frequently difficult to apply in design, the ACI code^{7.2} allows the use of the following simplified equations to compute the shear carried by the concrete in beams subjected to axial forces

$$v_c = 2\left(1 + 0.0005 \frac{N_u}{A_g}\right)\sqrt{f'_c} \quad (\text{psi}) \quad (7.35a)$$

However, v_c shall not exceed

$$v_c = 3.5\sqrt{f'_c} \sqrt{1 + 0.002 \frac{N_u}{A_g}} \quad (\text{psi}) \quad (7.35b)$$

where A_g is the gross concrete area of the section and the quantities N_u/A_g and f'_c are expressed in psi. (1 psi = 0.00689 N/mm².)

One might expect the foregoing equations to be suitable predictions also for prestressed concrete beams. However, this is not the case. Mattock studied this question^{7.28} and found from a comparison of numerous test results that the product of the modular ratio and steel content, $n\rho$, was a more suitable parameter to predict shear strength because it is a good measure of the position of the neutral axis, hence the depth to which flexural cracks penetrate. The greater the penetration of the flexural cracks into the web, the greater the principal stress at the root of the cracks responsible for diagonal cracking at a given applied shear. Hence with small flexural steel content (i.e., small $n\rho$ value), a much smaller shear force increment is required to initiate diagonal cracking. This is often the case in prestressed concrete beams. The adverse effect of low flexural steel content and the unconservative nature of Eqs. 7.15 or 7.34b for such a situation has also been pointed out by Rajagopalan and Ferguson.^{7.18} It was also found^{7.28} that axial load affects the magnitude of shear at the onset of flexural cracking, but apparently it does not affect the increment of shear between flexural cracking and the onset of diagonal tension cracking.

In the presence of axial compression, the diagonal cracks tend to be flatter than 45°, therefore, the current design approach for web reinforcement, based on the truss analogy with 45° struts, is conservative.

7.6.2 Shear and Axial Tension

If the previous assumptions with respect to diagonal cracking are correct, Eqs. 7.34b and 7.35 should also predict the shear cracking capacity of

members in the presence of axial tension, taking the value of N_u as negative in this case. In tests at the University of Washington,^{7.29} beams with web reinforcement, subjected to shear and axial tension, covering the wide range of shear stresses permitted by the ACI Code,^{7.2} and designed in accordance with Eqs. 7.23a and 7.34b, carried loads that were at least 30% in excess of the theoretical failure load. It appears that axial tension does not affect the performance of truss action but only reduces the shear resistance of the other mechanisms (i.e., v_c is reduced).

From considerations of principal stresses, one could expect diagonal cracks to form at an angle greater than 45° to the axis of the member. In this case the number of stirrups encountered by a diagonal crack would be smaller than is assumed in the truss analogy. However, tests^{7.29} have consistently demonstrated that the angle of inclination of the diagonal cracks is not noticeably affected by axial tension and that the shear resisting mechanism of truss action remains operative. Figure 7.22 shows a beam from a test series^{7.10} in which the axial tension force to shear force ratio was varied between 1 and 3. The stirrups were deliberately spaced far apart ($s = 0.8d$) to determine whether a potential diagonal failure crack would form between two adjacent stirrups. It can be seen that the crack pattern is essentially the same as that encountered in beams without axial load, except that inclined cracks crossed flexural cracks that developed at lower loads.

The axial load and the bending moment may not be applied simultaneously in real structures. It is possible that a large axial tension (e.g., shrinkage strains) may cause cracks to form over the full depth of a member, at right angles to its axis, before any shear force is applied. An example of such a region is a point of inflection at which moments will not close tension cracks or, worse, the flexural steel may be in tension near both faces of the beams, as in Fig. 7.19. It is sometimes thought that such a fully cracked beam will not be effective in resisting shear forces applied subsequently. In this situation aggregate interlock action has proved to be effective in transferring shear. In a series of tests, Sayani^{7.30} found that after the application of moment and shear new diagonal cracks formed and the previously developed tension cracks had no effect on the strength of test beams.

A similar situation can arise in the columns of multistory buildings during severe seismic disturbances. At the point of contraflexure, large concurrent axial tension and shear forces may be generated. Since the column bars are not normally curtailed, however, the axial stresses at these localities will be low; thus a widening of a tension crack is not possible. Hence aggregate interlock shear transfer, which is examined in greater detail in Section 7.8, will remain operative, and the shear capacity should not be less than that in the high moment regions of the same column, where the cracking will always be more extensive.

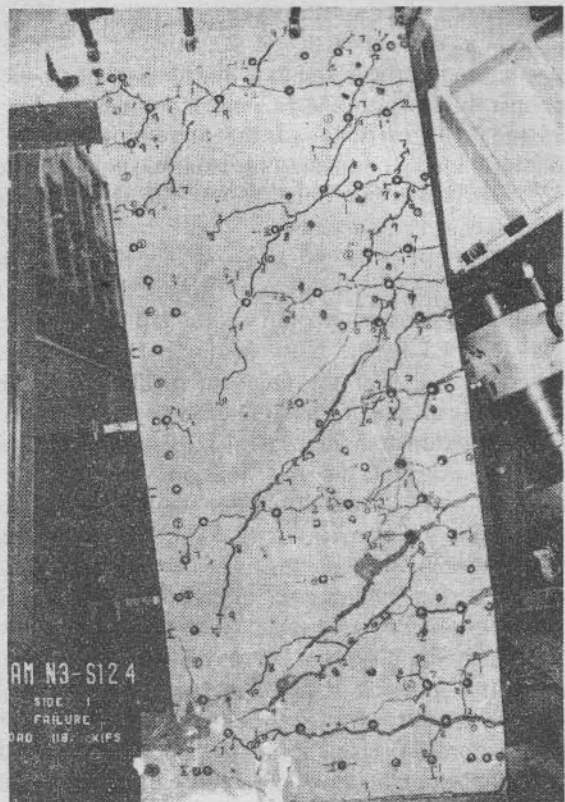


Fig. 7.22. Crack pattern in a beam with widely spaced stirrups when the axial tension to shear force ratio was 3.^{7.10}

There is some evidence that after reversed cyclic loading the potential diagonal crack, induced by shear and axial tension, may form at an angle larger than 45° to the axis of the member. This is because diagonal cracks propagating from one face of a member may link up with flexural cracks that formed during a previous cycle of reversed load at the opposite face of that member.

In some beams subjected to tension the diagonal cracking load fell below that predicted by the appropriate application of Eq. 7.34. Hence ACI Committee 426 suggested a simple and conservative linear interpolation^{7.31} between $v_c = 2\sqrt{f'_c}$ with no tension and $v_c = 0$ for an axial tensile stress

of 500 psi. Thus we have

$$v_c = 2 \left(1 + 0.002 \frac{N_u}{A_g} \right) \sqrt{f'_c} \text{ (psi)} \quad (7.36)$$

where N_u is negative for tension.

7.7 SHEAR DEFORMATIONS

For short, deep rectangular beams and for continuous *T* beams, the deformations caused by shear may become significant. Hence when service conditions are examined, the designer also needs to be able to assess the order of expected shear deflections. For most relatively slender members, subject to low shear, the effect of shear on deflection is negligible.

7.7.1 Uncracked Members

Before the formation of flexural or diagonal cracks, the behavior of a beam can be satisfactorily predicted by using the principles of elasticity. The modulus of rigidity (modulus of elasticity in shear) for concrete can be approximated from the well-known relationship

$$G = \frac{E_c}{2(1 + \mu)} \quad (7.37)$$

where $E_c = 57,000\sqrt{f'_c}$ psi is Young's modulus for normal weight concrete and μ is Poisson's ratio, which is approximately 0.16 to 0.30 for normal weight concrete.

The shear stiffness K'_v is the magnitude of the shear force that when applied to a beam of unit length, will cause unit shear displacement of one end of the beam relative to the other. The cross-sectional area of the beam normally to be considered when determining the shear stiffness is the area of the web only, $b_w d$.

With $G = 0.4E_c$, the shear stiffness of an uncracked beam of unit length will be

$$K'_v = \frac{0.4E_c b_w d}{f} \quad (7.38)$$

The factor f allows for the nonuniform distribution of the shear stresses. For rectangular sections $f = 1.2$ and for *T* and *I* sections it may be taken as unity.

7.7.2 Shear Deformations in Cracked Members

In beams that are subject to large shear forces and are web reinforced accordingly, diagonal cracks must be expected during service conditions. These cracks can increase the shear deformation of the beam considerably. The greater proportion of the load is likely to be carried by truss action, therefore, the deformation characteristics of this mechanism are of interest.

Shear distortions, occurring in the web of most conventionally reinforced concrete beams, may be approximated by using the model of the analogous truss presented in Figure 7.15. For the sake of simplicity, vertical stirrups and 45° diagonal concrete struts are assumed to form the web members (Fig. 7.23a). For the purpose of determining the web distortions only, the

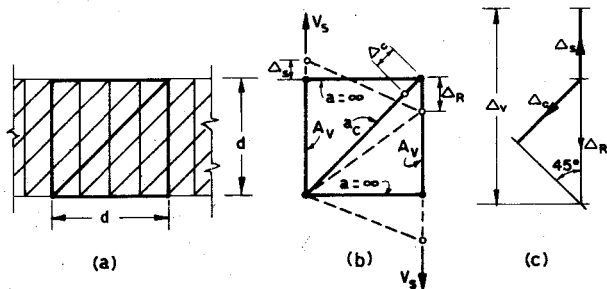


Fig. 7.23. Shear distortions in the web of a reinforced concrete beam modeled on the web members of an analogous truss.

chord members are assumed to be infinitely rigid; that is, the area of chord a is infinity (Fig. 7.23b). The elongation of the stirrups is Δ_s and the shortening of the compression strut is Δ_c . Applying Williot's principles, the shear distortion can be found from Figs. 7.23b and 7.23c as follows:

$$\Delta_v = \Delta_s + \Delta_c = \Delta_s + \sqrt{2\Delta_c} \quad (7.39)$$

Using Eqs. 7.22 and 7.23a, the stirrup stress can be expressed as

$$f_s = \frac{V_s s}{jdA_v} \approx \frac{V_s s}{dA_v} \quad (7.40)$$

Hence the elongation of the stirrups becomes

$$\Delta_s = \frac{f_s}{E_s} d = \frac{V_s s}{E_s A_v} \quad (7.41)$$

Similarly from Eq. 7.24a the diagonal concrete compression stress is obtained

$$f_{cd} = 2v_s = 2 \frac{V_s}{b_w d}$$

Hence the shortening of the diagonal strut is

$$\Delta_c = \frac{f_{cd}}{E_c} \sqrt{2}d = \frac{2\sqrt{2}V_s}{E_c b_w} \quad (7.42)$$

Therefore the shear distortion per unit length of beam becomes

$$\theta_v = \frac{\Delta_v}{d} = \frac{1}{d} \left(\frac{V_s s}{E_s A_v} + \sqrt{2} \frac{2\sqrt{2}V_s}{E_c b_w} \right) = \frac{V_s}{E_s b_w d} \left(\frac{s b_w}{A_v} + \frac{4E_s}{E_c} \right) \quad (7.43a)$$

By making the appropriate substitution for web steel content $\rho_v = A_v/sb_w$, and modular ratio $n = E_s/E_c$, it is found that

$$\theta_v = \frac{V_s}{E_s b_w d} \left(\frac{1}{\rho_v} + 4n \right) \quad (7.43b)$$

The shear stiffness of beam with 45° diagonal cracks, in accordance with truss action, is the value of V_s when $\theta_v = 1$, and is thus given by

$$K_{v, 45} = \frac{\rho_v}{1 + 4n\rho_v} E_s b_w d \quad (7.44)$$

The similarity between Eqs. 7.38 and 7.44 is apparent.

Similar expressions can be derived for other inclinations of compression struts α and stirrups β . Using the notation of Fig. 7.15 it may be easily shown for the general case that the stirrup stress will be

$$f_s = \frac{v_s}{\rho_v (\cot \alpha + \cot \beta) \sin^2 \beta} \quad (7.45)$$

where the stirrup length is $d/\sin \beta$.

The compression stresses for the $d/\sin \alpha$ long struts are given by Eq. 7.24.

By combining the foregoing relationships, the shear stiffness can be defined by the following expression:

$$K_v = \frac{\rho_v \sin^4 \alpha \sin^4 \beta (\cot \alpha + \cot \beta)^2}{\sin^4 \alpha + n \rho_v \sin^4 \beta} E_s b_w d \quad (7.46)$$

where $\rho_v = A_v/(s b_w \sin \beta)$ for the general case.

Dilger has further refined these expressions by computing the inclination of the compression struts from strain energy considerations of the analogous truss.^{7,32} His experiments show that this approach underestimates somewhat

the shear distortion in beams. The analysis is based on the greatly simplified model of the analogous truss, and deformations at the anchorages of the stirrups have not been taken into account. Slips at the ends of stirrups (see Section 9.4.2) can considerably increase shear deformations, particularly in shallow beams where the anchorage slip represents a greater fraction of the total distortion.

Comparison of Eqs. 7.38 and 7.44 indicates that the shear stiffness of a diagonally cracked member is approximately 10 to 30 % of the shear stiffness of the uncracked member, depending on the amount of web steel provided. It is thus evident that cracking can have a much larger effect on shear stiffness than on flexural stiffness.

Analytical and experimental studies have verified that the stiffness of cracked deep beams (e.g., as in Fig. 12.28), in which shear deformations dominate, is only about 15 % of the stiffness in the uncracked state when

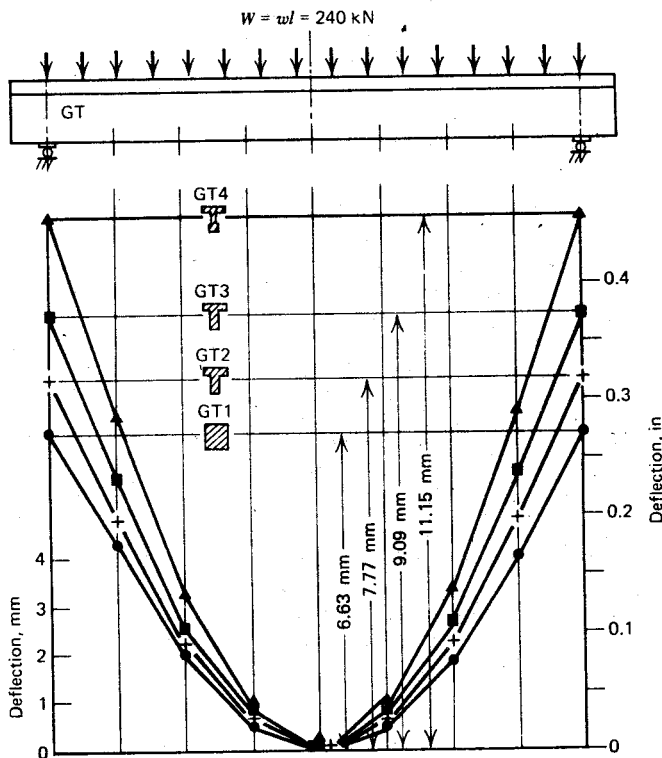


Fig. 7.24. Observed deflections under the same load with varying web width.^{7.7}

shear and flexure distortions are considered. The truss mechanism in such beams will consist of a series of radiating struts rather than parallel 45° members, and this needs to be taken into account in the analysis.^{7,26} Loss of stiffness is significant when assessing service load distortions in structures or their response to dynamic excitation.

The deflections of four beams,^{7,7} similar to those in Fig. 7.18a, are compared in Fig. 7.24. All beams carry the same uniformly distributed load and contain the same flexural and web reinforcement but have different web widths. The flexural stiffness of the thin-webbed T beam GT4 is only a little less than that of beam GT1 after flexural cracking has occurred. The difference of deflections as shown in Fig. 7.24 is largely because of the shear distortions, which become more significant as the web area is reduced.

The contribution of shear distortions to the total deflection of continuous T beams becomes particularly significant when a large proportion of the shear is resisted by web reinforcement ($\eta \approx 1.0$).

7.8 INTERFACE SHEAR

In all situations examined so far the applied shear forces have produced inclined cracking across a member. It is also possible that shear stresses may cause a sliding type of failure along a well-defined plane. Because of external tension, shrinkage, or accidental causes, a crack may form along such a plane even before shear occurs. Thus the possibility of shear transfer by aggregate interlock and dowel action, discussed previously, arises. For example, shear may have to be transferred in this way in deep beams, corbels (to be examined in Chapter 13), joints between precast concrete elements, and shear walls. The term "interface shear transfer" is used to designate the mechanism, and its possible components are discussed subsequently.

Interface shear transfer in flexural members can be critical only if the shear span to depth ratio is very small (say, < 0.5) or when a particular section, along which shear displacement (hence tangential shear transfer) can occur, is weakened (e.g., by the formation of a tension crack). The mechanism of interface shear is different in initially uncracked and initially cracked concrete, even though the design approach to both will be the same.

When required, reinforcement is provided, generally at right angles to the shear plane, primarily to supply a clamping force between the two potential sliding faces. To ensure the development of the yield stress, these bars must be adequately anchored at both sides of the potential shear plane. It is also evident that to engage the clamping action of the reinforcement, the faces

of the crack must separate slightly. This type of clamping force can be supplemented by externally applied compression forces across a shear plane. Conversely an externally applied tension may diminish the clamping force available for the shear transfer mechanism.

A number of studies of interface shear have been made recently. Only those of Mast,^{7.33} Mattock and Hawkins,^{7.34} and work at the University of Canterbury^{7.11, 7.35} are referred to here. The report of Mattock and Hawkins contains significant additional references. Figure 7.25 represents typical pushoff specimens used to determine experimentally the mechanism of interface shear transfer.

7.8.1 Shear Transfer Across Uncracked Concrete Interfaces

When a shear force is being transmitted along an uncracked potential shear plane, diagonal principal stresses will be generated. Subsequently developing across the shear plane are short, 45° or flatter, cracks, which in

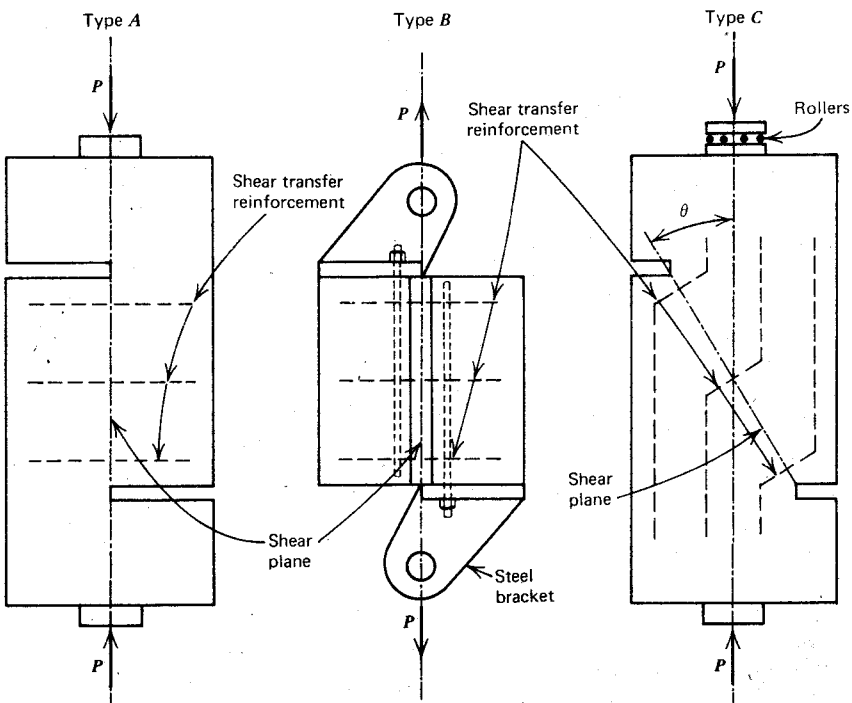


Fig. 7.25. Typical pushoff interface shear transfer specimens.^{7.34}

the presence of transverse steel results in shear being transferred by a truss mechanism as indicated in Fig. 7.26. The short diagonal struts are subjected to compression σ and shear stresses τ (see detail, Fig. 7.26). The resulting principal stresses will govern the failure criteria for the concrete as indicated

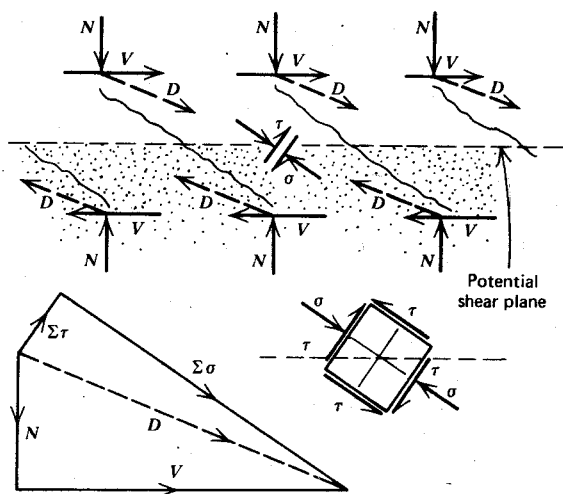


Fig. 7.26. The mechanism of interface shear transfer across an uncracked shear plane.

by the failure envelope discussed in Chapter 2 (see Fig. 2.10). The clamping force N must be developed by the reinforcement within its yield range after the formation of cracks and by any available external compression. Very small shear displacements will occur before and at the development of cracks. Failure normally occurs when the transverse steel yields permitting the concrete struts to rotate and the cracks to propagate at a flat angle, nearly parallel with the shear plane. Mattock and Hawkins^{7,34} found good experimental correlation with the failure envelope hypothesis for concrete (Fig. 2.10). For design purposes it is assumed that a crack may exist along the shear plane; hence designers rely on a lower shear strength, set out in the following section.

7.8.2 Shear Transfer Across Precracked Concrete Interfaces

The mechanism of shear transfer by aggregate interlock was briefly outlined in Section 7.3.3. Consideration of two rough, interlocking faces along a crack in the general shear plane (Fig. 7.27) indicates that shear displacements much

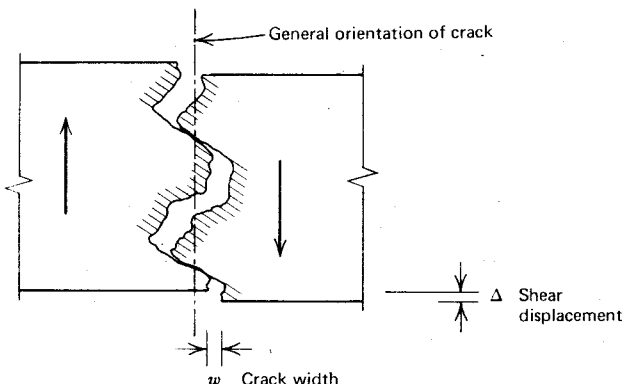


Fig. 7.27. Displacement along a cracked shear plane.

larger than those to be encountered along initially uncracked interfaces, will now be required to effectively engage aggregate particles protruding across the shear plane. The larger the crack width, w , the larger the shear displacement, Δ , and the smaller the attainable ultimate strength. It is also evident that as the shear displacement increases, the concrete masses on either side of the crack will be pushed apart; hence the crack width will tend to increase. Unless the tendency of the crack width to increase is controlled by an effective clamping or restraining force, very little shear can be transmitted.

Typical shear stress-shear displacement relationships, obtained by Loeber^{7,11} with specimens similar in form to type *A* illustrated in Fig. 7.25, appear in Fig. 7.28. No reinforcement crossed the crack. However, its width was maintained constant by external clamping forces. Up to an average shear stress of approximately 1000 psi (6.9 N/mm²), a bilinear response was observed. At low loads a larger slip is required before the larger particles come into contact, whereupon the joint becomes stiffer. No significant difference in the response of the specimens was noted when the investigators used different coarse aggregates, with $\frac{3}{8}$ in (9 mm) and $\frac{3}{4}$ in (19 mm) nominal sizes. In an actual structure both the crack width and the clamping force will vary as the load and shear displacement increase, but Loeber's work gives a good indication of the shear strength available from aggregate interlock.

The opening of the crack can be controlled by reinforcement that normally crosses the shear plane at right angles. Such bars will also be subjected to shear displacement, hence a certain amount of additional shear can be transmitted by dowel action. Early designers often intuitively relied on this dowel action, just as they did on rivets and bolts in steel construction.

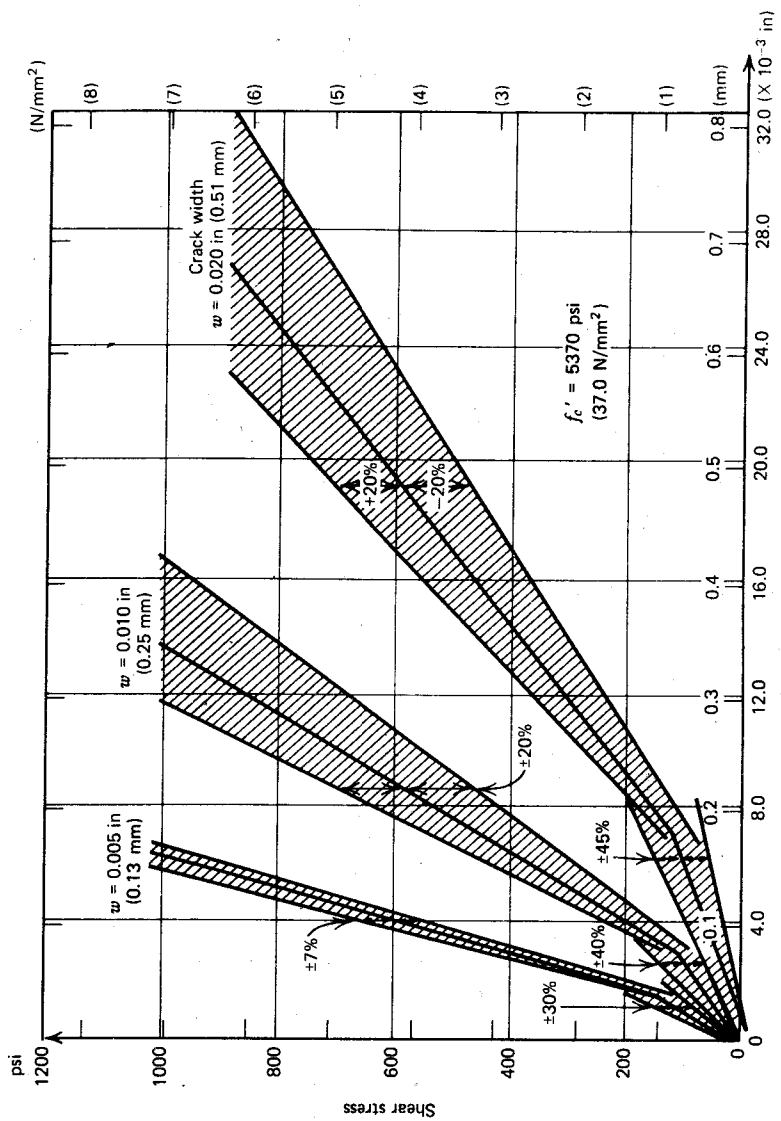


Fig. 7.28. Typical mean shear stress-shear displacement relationships for aggregate interlock mechanism.^{7.11}

Dowel strength across a shear plane can be developed by three mechanisms: the flexure of the reinforcing bars, the shear strength across the bars, and the kinking of the reinforcement. These mechanisms are illustrated in Fig. 7.29, where the associated shear force V_d is also expressed in terms of the yield strength of the bar. It is to be noted, however, that the yield strength of a bar in flexure and shear cannot be fully utilized for dowel action if the same

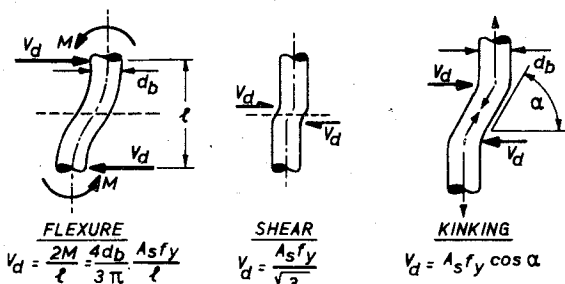


Fig. 7.29. The mechanism of dowel action across a shear interface.

bar is to provide a clamping force, as well. Hence the V_d values given in Fig. 7.29 for flexure and shear are upper limits. Tests by Phillips^{7,35} indicated that kinking is likely to be the major source of dowel strength, particularly when small size bars are used. Figure 7.30 shows the typical response of small diameter bars to dowel action obtained from pushoff tests^{7,35} on specimens in which shear transfer along the interface by mechanisms other than dowel action was prevented by applying wax to the smooth surface. Figure 7.30a indicates the effect of variable steel content across the interface, and Fig. 7.30b compares three different bar sizes used to make up the same steel content of $\rho_{v,f} = 0.0123$.

To develop dowel strength of some significance (Fig. 7.30), large displacements along the shear plane are necessary. This slip may well exceed what could be considered to be acceptable within the limits of structural usefulness. If a shear slip of 0.01 in (0.25 mm) is considered acceptable, and 1.23% transverse steel is used, about 150 psi (1 N/mm²) shear stress in dowel action could be developed by reasonable bar arrangement according to Fig. 7.30b. For the same slip, however, considerably larger aggregate interlock shear stresses would be generated, as in Fig. 7.28, unless the crack width were very large. Hence dowel action is not a major component of the shear-resisting mechanism across cracked interfaces at acceptable shear displacements.

The design for interface shear transfer can be based on traditional concepts

of friction. The coefficient of friction μ of the cracked surface has been found experimentally to be at least 1.4.^{7,33} The normal force can be provided by the reinforcement A_{vf} at yield. Therefore, the shear stress v_{uf} , transferable across a cracked concrete surface of area A_g , is

$$v_{uf} = \mu \frac{A_{vf} f_y}{A_g} = \mu \rho_{vf} f_y \quad (7.47)$$

At moderate levels of loading this relationship has been found to be independent of the concrete strength.^{7,34} When large shear stresses are applied, the concrete in the interlock mechanism can be expected to break down. Such load will require heavy reinforcement and/or external transverse compression. The strength will then be governed by the same failure mechanism controlling initially uncracked interfaces, discussed in Section 7.8.1. The ACI code^{7,2} sets a conservative upper limit of $v_{uf} = 0.2f'_c$ or 800 psi (5.5 N/mm²) to guard against a concrete failure. The code recommends that $\mu = 1.0$ be used when concrete is placed against hardened concrete and $\mu = 1.4$ be used for concrete cast monolithically.

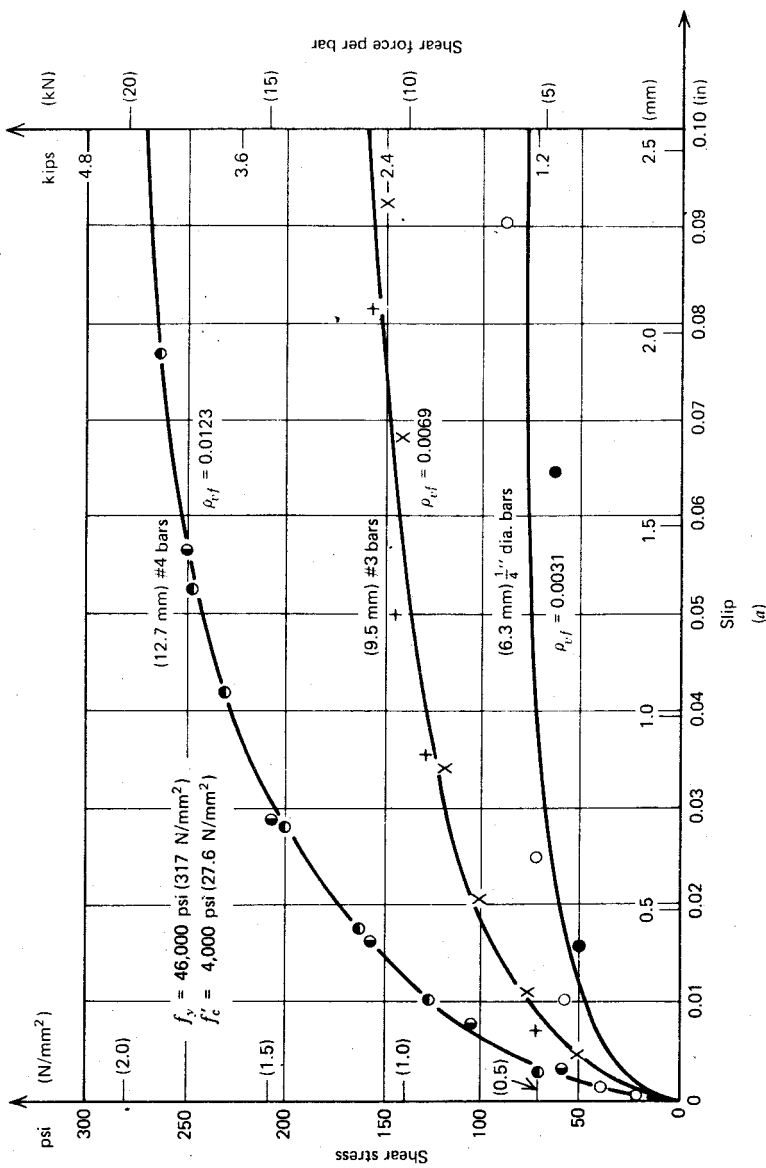
The University of Washington tests^{7,34} resulted in the following equation

$$v_{uf} = 200 + 0.8 \left(\rho_{vf} f_y + \frac{N}{A_g} \right) < 0.3f'_c \quad (7.48)$$

where stresses are in psi units and N is the externally applied compression force normal to the interface. If N is a tensile force, it should be taken as negative. Evidence for the case of tension was obtained from tests on corbels. These are discussed in Chapter 13.

7.8.3 Shear Transfer Across Construction Joints

Construction joints in beams, columns, and walls can present a potential weakness if large shear forces need to be transmitted across them. In slender beams a well-prepared construction joint does not normally present any problem because the shear or flexural strength of these members is considerably less than the interface shear capacity at a construction joint across the members. Recent earthquakes have shown, however, that construction joints in some members, particularly shear walls, can form the weakest link in the load-resisting mechanism of the structure. Horizontal construction joints in both medium and low rise buildings became visible during the 1964 Alaska and the 1971 San Fernando earthquakes. Some of the damage at construction joints was almost beyond repair. Lightweight concrete floor slabs, giving two construction joints at each floor level, represent a particular weakness in normal weight concrete shear walls. The design of a construction



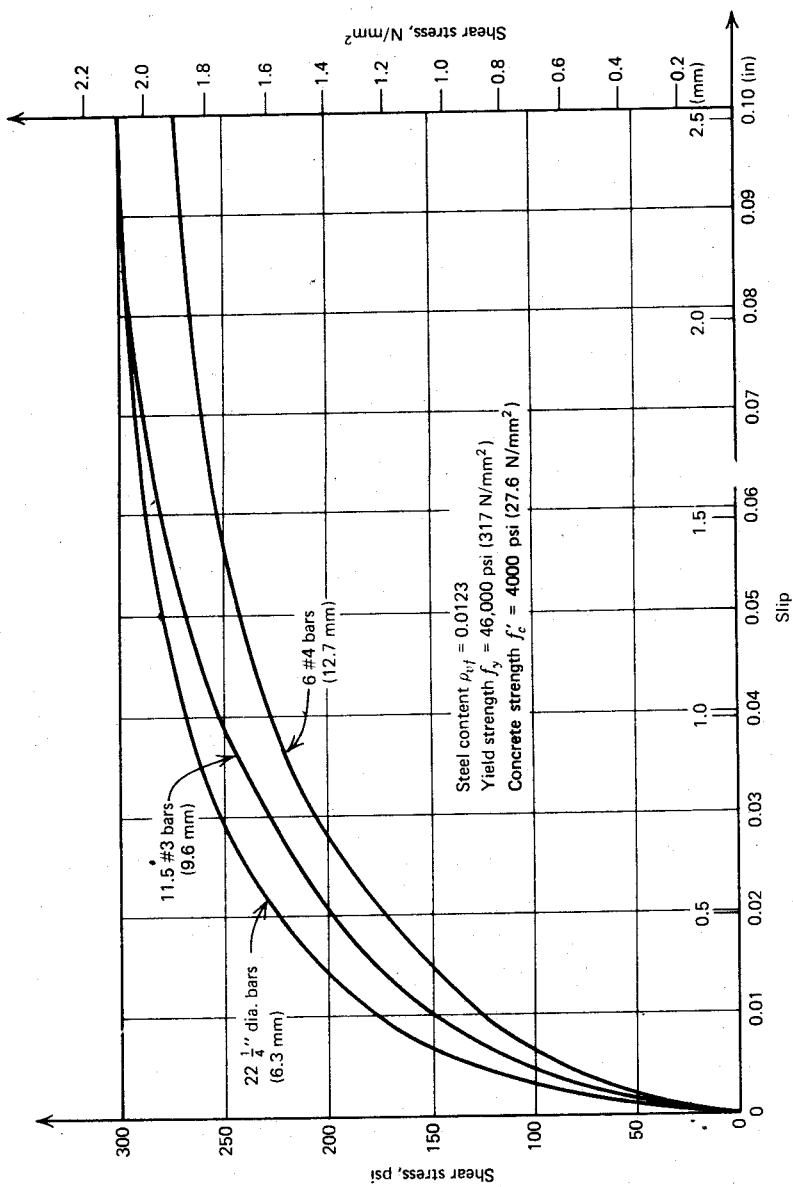
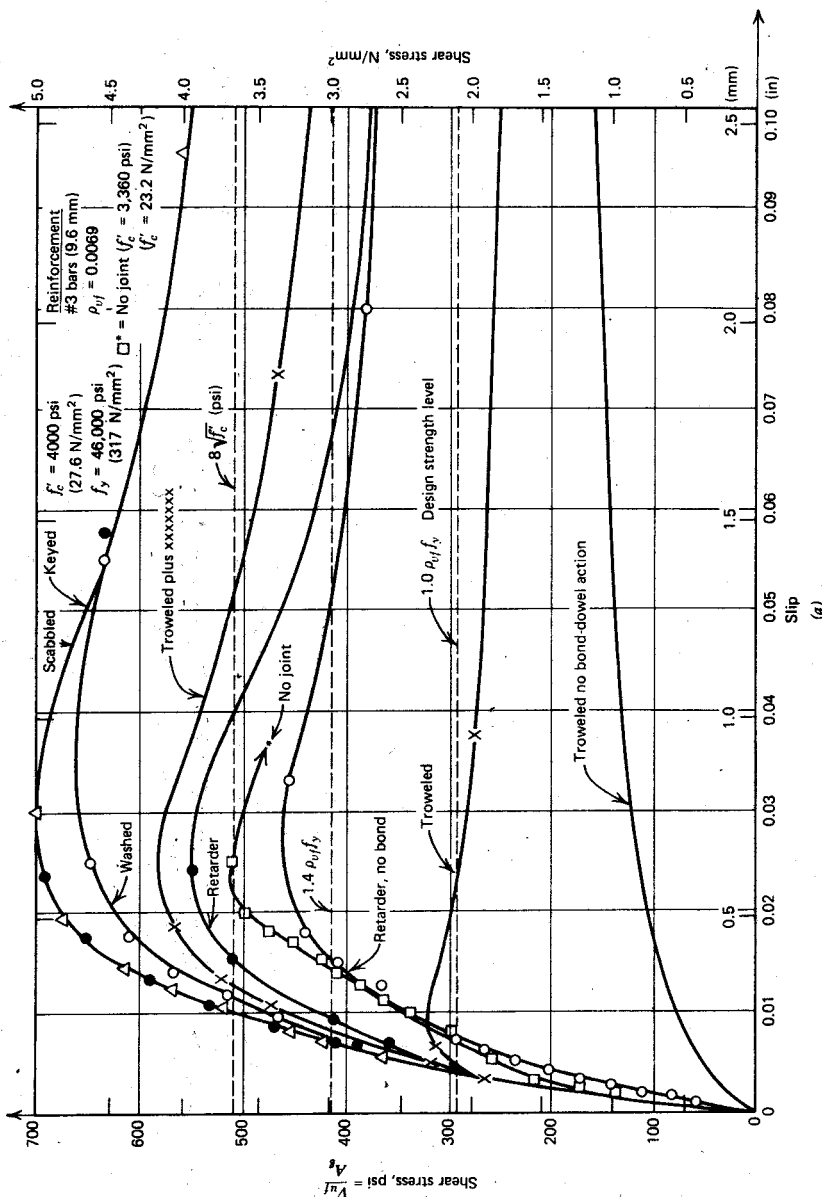


Fig. 7.30. Load-slip relationship for dowel action alone.^{7,35} (a) Using different steel contents. (b) Using 1.23% steel and different bars.



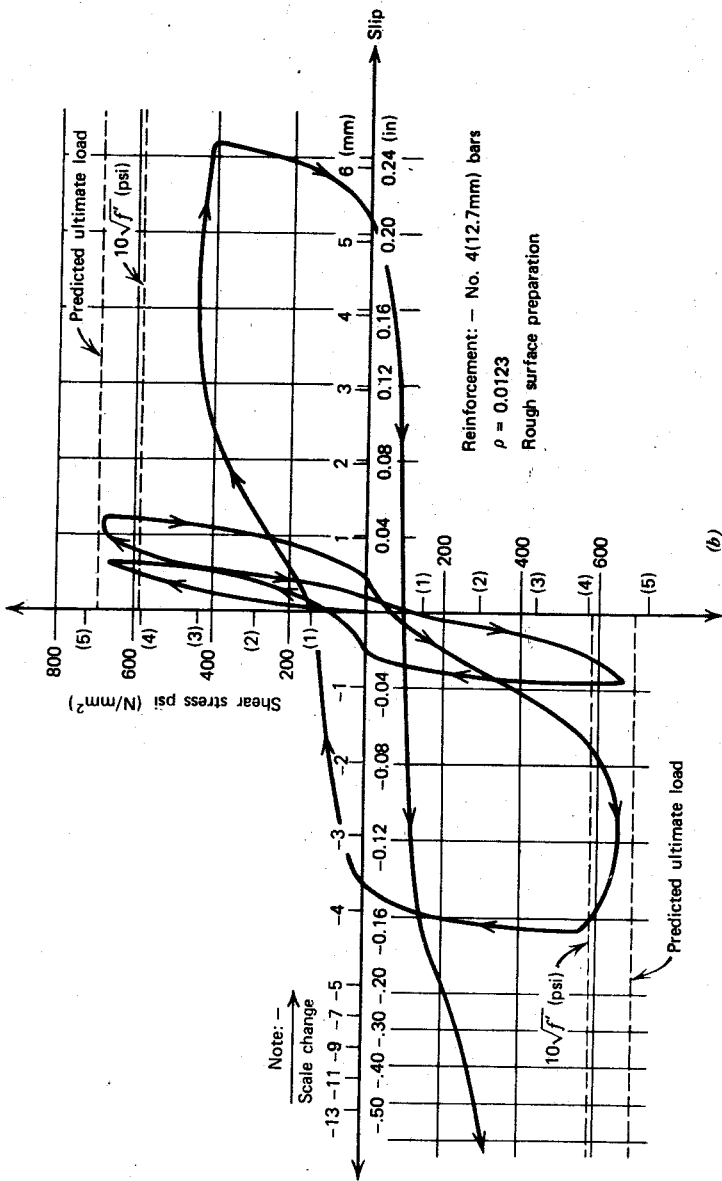


Fig. 7.31. Load-slip curves for shear transfer across construction joints.^{7,3,5} (a) Concrete shear transfer with different surface preparations. (b) Total shear transfer with reversed cyclic loading.

joint must be based on the premise that its capacity must at least equal the shear (diagonal tension) capacity of the adjoining parts.

The concrete of a construction joint may possess little tensile strength across the interface, therefore, it is advisable to assume that a crack is present at the joint before any shear is applied. Consequently, the shear friction concept, outlined in the previous section, can be applied. However, the shear capacity of such an interface could be influenced by type of surface preparation used for the joint. Since the interface capacity could be less than that encountered along cracks formed in monolithic concrete, the use of a lower coefficient of friction is appropriate.

From experimental studies conducted on the performance of construction joints at the University of Canterbury^{7,35} the following observations emerged:

1. Adequately reinforced horizontal construction joints with a clean and rough surface, to which the freshly placed concrete can bond, can develop an interface shear strength equal to or larger than the diagonal tension capacity of the structure. Rough surfaces were obtained in several ways: by removing the mortar from between the larger aggregate particles with a water jet and soft brush when the concrete was in a semihardened state, by first applying a chemical retarder to the surface, by scabbling, by providing keyes (see Fig. 7.32), or by forming cruciform grooves with a sharp tool along the troweled wet surface.
2. The lack of bond to the old concrete, in specimens in which the surface was varnished, resulted in approximately twice as much initial slip than occurred in construction joints with bond.
3. Troweled surfaces with small roughness resulted in failures shortly after the development of a crack, when bond between the interfaces broke down.
4. The responses of construction joints with different surface preparations and with a reinforcement content corresponding to $\rho_{vf} f_y = 295$ psi (2.03 N/mm²) appear in Fig. 7.31a. The lowest curve shows the contribution of dowel action only, the upper curves represent the contribution of the concrete only, the shear stress carried by the dowel action being subtracted. Three significant design stress levels are also presented. It is evident that the design strength without the dowel contribution, based on a coefficient of friction $\mu = 1.0$, could be comfortably developed in all rough joints after a slip of approximately 0.005 in (0.12 mm). This load intensity will never be exceeded in a well-designed structure, because other, more desirable failure modes (flexural yielding) should limit the load level.
5. In a well-designed and well-executed construction joint, the plane of the sliding shear failure is likely to be located below the level of the joint

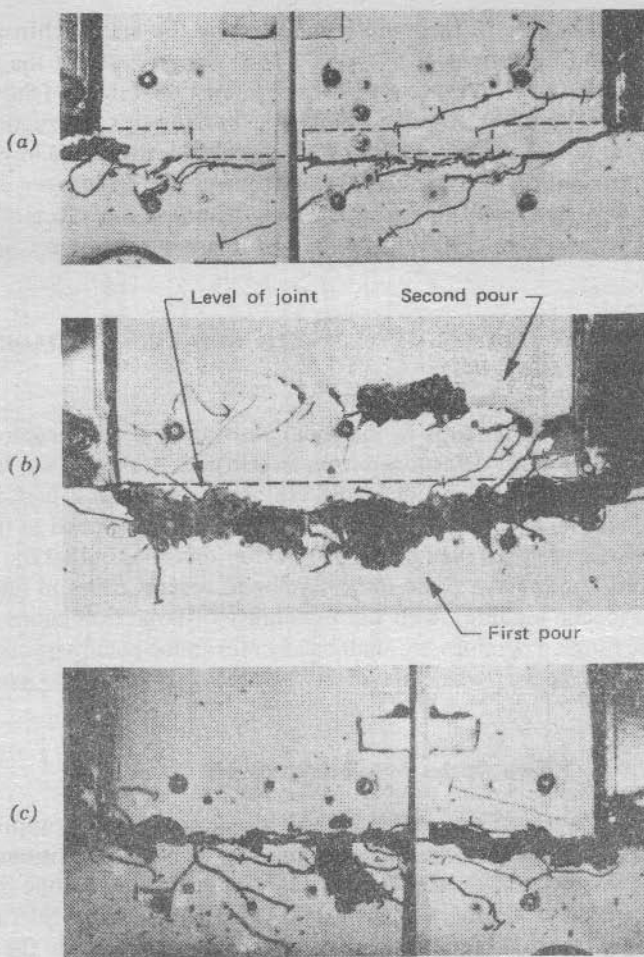


Fig. 7.32. The failure of construction joints with 0.60% steel content.^{7,35} (a) Keyed joint. (b) Rough surface obtained with chemical retarder, cyclic loading. (c) New concrete placed on troweled surface.

in a layer of inferior concrete. This forms at the top of a "pour" as a result of the accumulation of particles with low specific gravity, water gain, and consequent increase in water/cement ratio, and in particular, the entrapment of air under the coarse aggregate. The bond between the coarse aggregate particles and the mortar matrix, a potentially weak link in the aggregate interlock mechanism, may be further weakened by sedimentation in the

fresh concrete, which in turn will be affected by the watertightness of the formworks and the height of a "pour." Thus the strength of the concrete used in the structure is likely to give a very optimistic estimate of the strength available immediately below the plane of a horizontal construction joint. Some typical failure modes of construction joints are displayed in Fig. 7.32.

The determination of the vertical reinforcement placed across a construction joint in a shear wall in seismic design, including the effects of gravity loads and vertical accelerations, is discussed in greater detail in Chapter 12.

7.9 THE EFFECTS OF REPEATED AND CYCLIC LOADING ON SHEAR STRENGTH

The contribution of stirrups in the shear resistance of reinforced concrete beams has been mainly determined from tests in which the load was increased monotonically until failure occurred. In many situations high-intensity repeated loading, resulting from traffic or wind, can be applied to the structure. In seismic areas an even more severe criterion exists in that the strength of a structure may have to be fully developed several times in alternating directions (cyclic loading), with the possibility of large excursions into the postelastic range. Therefore, we shall briefly reexamine some aspects of shear resistance that appear when the effects of repeated and cyclic loading are present.

7.9.1 Effects on the Web Reinforcement

A study by Mayer^{7.36} has indicated that the current design approach for shear is also applicable when a large number of load repetitions occurs. Figure 7.33 shows the stresses measured in plain stirrups in one of several rectangular beams during some 900,000 cycles of loading. Stirrups were provided to resist 114% of the shear force associated with the flexural strength of the beam. The load was cycled between 13 and 71% of the flexural strength, thus the nominal shear stress in the shear span varied between 70 psi (0.48 N/mm^2) and $400 \text{ psi} = 5.3\sqrt{f_c}$ (2.76 N/mm^2). This corresponded with a theoretical change in the flexural steel stress of 34,000 psi (234 N/mm^2). After each 100,000 cycles (approximately), the beam was left unloaded for 15 hours. As may be expected, shear-resisting mechanisms other than the truss action of the web steel deteriorated as the repeated load continued. As Fig. 7.33 reveals, the contribution of the stirrups increased considerably in the first 100,000 cycles, but the shear-resisting mechanism stabilized after 400,000 cycles.

Assuming that in the elastic range the shear stress resisted by the concrete

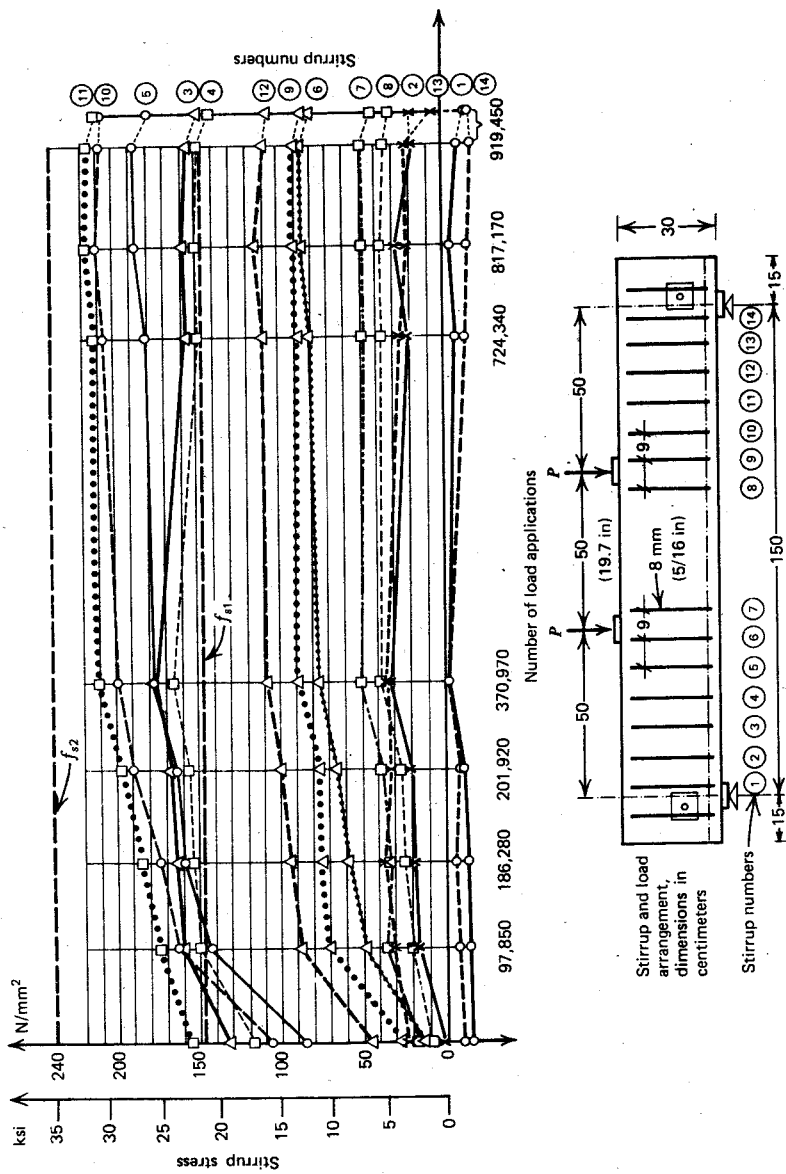


Fig. 7.33. The increase of stirrup stresses during repeated loading. 7.36

v_c is that given by Eq. 7.15 and that the shear stress resisted by the truss action can be obtained from Eq. 7.23a, in which f_y is replaced by the required stirrup stress f_s (this may be justified by reference to Fig. 7.18), the average stress in the stirrups, when 71% of the flexural strength was applied, may be calculated to be $f_{s1} = 21$ ksi (145 N/mm 2). When the contribution of the concrete (Eq. 7.15) is ignored, leaving all the shear to be carried by the truss mechanism, the stirrup stresses at this load level would have to increase to $f_{s2} = 36.0$ ksi (250 N/mm 2). These two limits are designated by dashed lines in Fig. 7.33. When comparing these theoretical stress limits with measured values, the mean stress in three adjacent stirrups, corresponding with a potential diagonal crack, should be considered. Failure eventually occurred as a result of fracture of the flexural reinforcement in the shear span after more than 10^6 repetitions of load. The increases of stirrup stresses with repeated loading, in an identical beam in which deformed bars were used for stirrups, were even smaller. This is probably because of the better crack control provided by deformed bars, hence less deterioration of shear-resisting mechanism of the concrete. The efficient participation of the web reinforcement with only a small increase in measured stresses after 50 cycles of service load applied, with a nominal shear stress of 710 psi (4.9 N/mm 2), has also been verified for thin webbed flanged beams.^{7.24}

The deterioration of the concrete shear-resisting mechanisms is much more rapid if the flexural reinforcement yields as a result of high-intensity cyclic reversed loading. Figure 7.34 shows the total shear force carried across the potential diagonal failure crack by all the stirrups, in an approximately square spandrel beam, similar to that shown in Fig. 12.28. The largest strains measured occurred in each stirrup where it was crossed by the potential failure crack. It is seen that during the first five cycles of loading some 40 kips (178 kN) were resisted by mechanisms not involving stirrups. Up until this stage no yield occurred in the flexural reinforcement. After the fifth cycle, alternating yielding was imposed on the main reinforcement, and as Fig. 7.34 reveals, nearly the entire applied shear was resisted by the stirrups in the ninth cycle. The percentages given in Fig. 7.34 show the proportion of the total applied shear resisted by the stirrups. The test results point to the necessity for ignoring the concrete shear-resisting mechanisms and for providing web reinforcement to resist the total shear force over regions where yielding of the flexural reinforcement under cyclic reversed loading is a possibility.

We must expect high-intensity cyclic loading to cause some stiffness degradation. This effect is particularly evident when diagonal cracks are permitted to widen.^{7.26} In general, the reduction in stiffness depends primarily on the magnitude of the previously imposed loading rather than on the number of cycles applied.^{7.37}

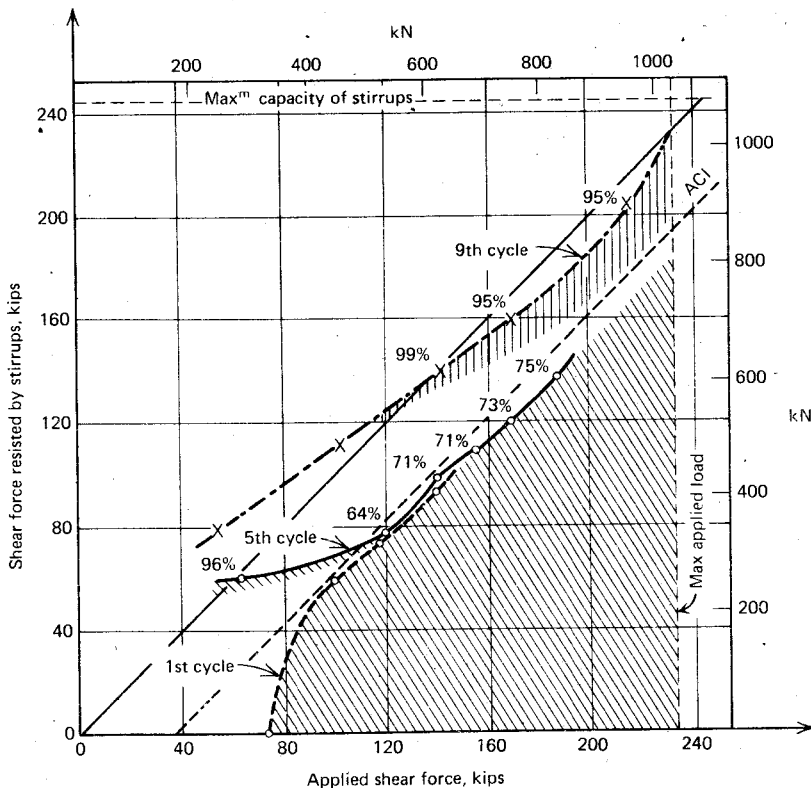


Fig. 7.34. The total shear force carried across the potential diagonal failure crack across a deep spandrel beam.

7.9.2 Effects on Interface Shear Transfer

When cracks do not develop along the shear plane during interface shear transfer, no deterioration of shear capacity can be expected after a few cycles of repeated high-intensity loading. This has been observed in a limited number of tests on horizontal construction joints.^{7,35} Shear friction by aggregate interlock does not become operative until cracks develop; therefore, before cracking, the transverse steel crossing the interface has no significant role in the load transfer. After the development of cracks, however, repeated loading will cause a deterioration of the interface roughness, with a corresponding reduction in the equivalent coefficient of friction.

In Fig. 7.35, a typical shear stress-shear displacement relationship is illustrated from an aggregate interlock test^{7,11} in which a few repetitions of

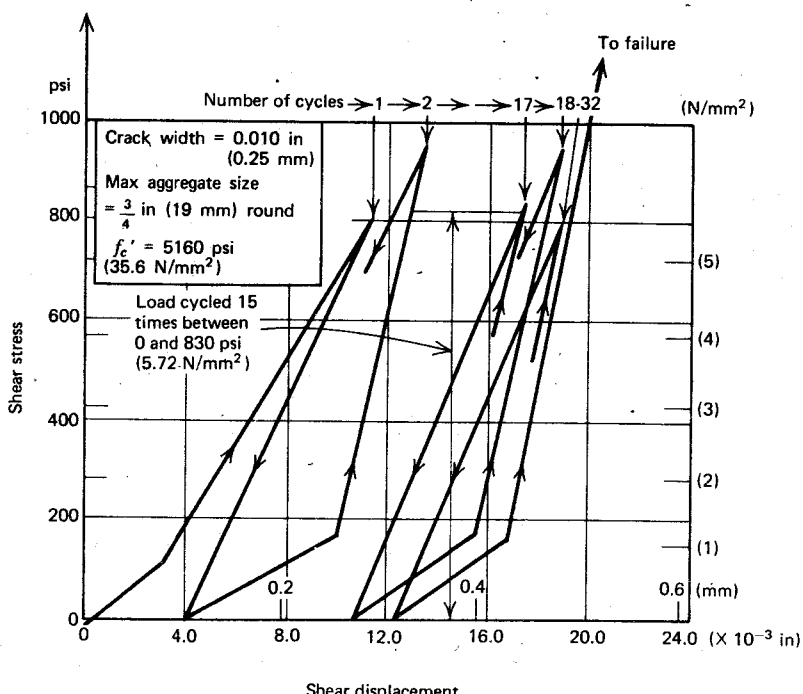


Fig. 7.35. Shear stress-shear displacement relationships for repeated loading of aggregate interlock specimens.^{7.11}

large shear loads ($v_u \approx 12.5\sqrt{f'_c}$ psi, $\approx 1.04\sqrt{f'_c}$ N/mm²) were applied while a constant crack width was maintained by external clamping. It is seen that the residual slip increases at a diminishing rate, and some increase in the stiffness of the system occurs. When the clamping force is provided internally by transverse reinforcement, the opening of the crack will not be so well controlled, and a more rapid deterioration must be expected. In tests on construction joints, very large residual slips occurred with a marked loss of shear strength across the interface after the reinforcement had yielded.^{7.35} As Fig. 7.31b shows the interface deterioration is particularly significant when high-intensity reversed loading is applied. This type of action tends to dislodge the embedded aggregate particles more easily. The load intensity required to cause this deterioration was found to be higher than the maximum values specified in the shear friction provisions of the ACI code.^{7.2}

With low intensity of shear transfer, the interface deterioration is much less, as can be expected. The joint effectiveness in concrete pavement slabs, as a

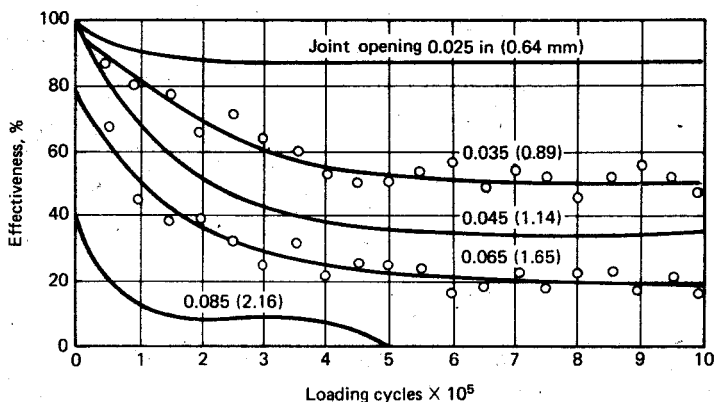


Fig. 7.36. Joint effectiveness in pavements under repeated loading.^{7.38}

function of the crack width, was studied by the Portland Cement Association.^{7.38} Some results appear in Fig. 7.36: 100% effectiveness indicates that there is no relative displacement along the interface. The shear transferred was 28 psi (0.19 N/mm²). The drastic loss of effectiveness with increased joint opening (crack width) is most evident. The effect of cyclic loading on clamping force and slip, at moderate shear stress intensities along an interface with

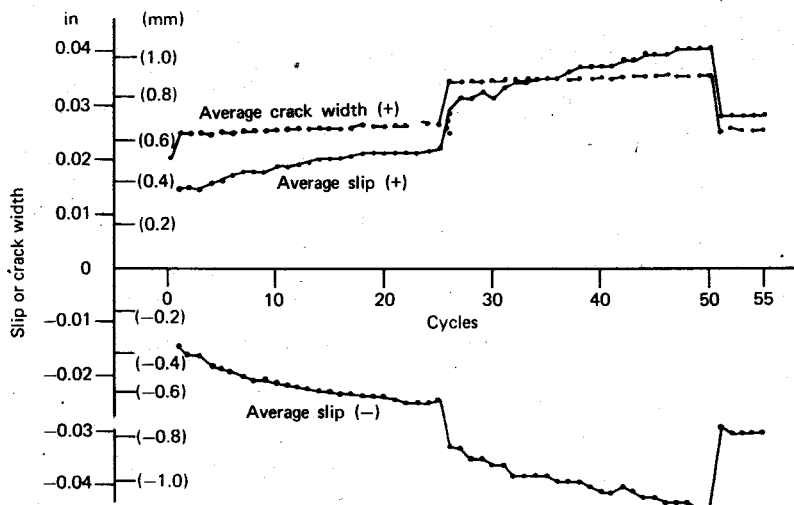


Fig. 7.37. Effect of load cycling on slip and crack width in interface shear tests.^{7.39}

preset crack widths, has also been studied by White and Holley,^{7,39} to establish safe levels for membrane stresses in cracked concrete containment vessels. The observed increase in slip for two preset crack widths during 50 cycles of complete stress reversals with $v = 164$ psi (1.11 N/mm 2) is given in Fig. 7.37.

7.10 SPECIAL MEMBERS AND LOADINGS

In previous sections of this chapter the phenomenon of shear has been discussed mainly in connection with beams. However, shear may become a critical design item in other situations when one or another aspect of the predominant shear resisting mechanisms must be determined. A detailed examination of such cases is beyond the scope of this book.

A designer who is familiar with the basic concepts of shear in reinforced concrete beams will have no difficulty in identifying the predominant mode of shear resistance in another structural component. The major task will then be to arrange the reinforcement to enable this particular mechanism to function efficiently. For this reason, a number of cases in which the arrangement of reinforcement may have a major effect on shear performance are briefly examined in Chapter 13.

The load applied to a beam may be such that truss or arch action cannot develop without the introduction of additional reinforcement. This situation can arise in girders that support secondary beams. Also, the web of beams must be carefully examined for shear resistance when openings are to be provided in them. The arch mechanism will require special attention in deep beams in which diagonal cracks may form at steep angles. Corbels and brackets may carry very large forces on a short lever arm, permitting arch action and interface shear transfer to become the major modes of shear resistance. Deep beam effects may dominate the behavior of certain shear walls. These are discussed in Chapter 12. A particularly severe shear problem can arise in beam-column joints of reinforced concrete frames, and this situation is examined in some detail in Chapter 13.

Example 7.1. The Design of the Web Reinforcement and the Curtailment of the Flexural Reinforcement in a Foundation Beam

A symmetrical foundation beam (half of it shown in Fig. 7.38a) supports two axially loaded columns at 30 ft (9.14 m) centres. The ultimate load on each column is 480 k (2136 kN) and the corresponding reactive upward pressure of 20 k/ft (292 kN/m) is assumed to be uniformly distributed over the full 48 ft (14.63 m) length of the

beam. The corresponding bending moments have been computed, and these are plotted in Fig. 7.38b.

Properties

The dimensions of the cross section of the inverted *T* beam are shown in section *A-A*. The top reinforcement at midspan consists of nine No. 9 (28.6 mm) bars, and seven No. 8 (25.4 mm) bars under the columns make up the bottom (positive) flexural reinforcement; No. 4 (12.7 mm) bars are used for the stirrups.

Materials: $f'_c = 3600 \text{ psi} (24.8 \text{ N/mm}^2)$; $f_y = 60,000 \text{ psi} (414 \text{ N/mm}^2)$.

Adequacy of flexural reinforcement

1. Top steel at midspan, nine No. 9, $A_s = 9.0 \text{ in}^2$.

Total tension force $T = A_s f_y = 9.0 \times 60 = 540 \text{ k}$. Hence $a = T/0.85f'_c b = 540/(0.85 \times 3.6 \times 48) = 3.7 \text{ in}$, $d = 42 - 4.75 = 37.25 \text{ in}$, $jd = d - a/2 = 37.25 - 0.5 \times 3.7 = 35.4 \text{ in}$.

$$M_u = Tjd = 540 \times 35.4 = 19,120 \text{ k} \cdot \text{in}$$

Dependable $M_u = \varphi M_u = 0.9 \times 19,120 = 17,204 \approx 17,280 \text{ k} \cdot \text{in}$ (Fig. 7.38b)

2. Bottom reinforcement at columns, eight No. 8, $A_s = 5.5 \text{ in}^2$,

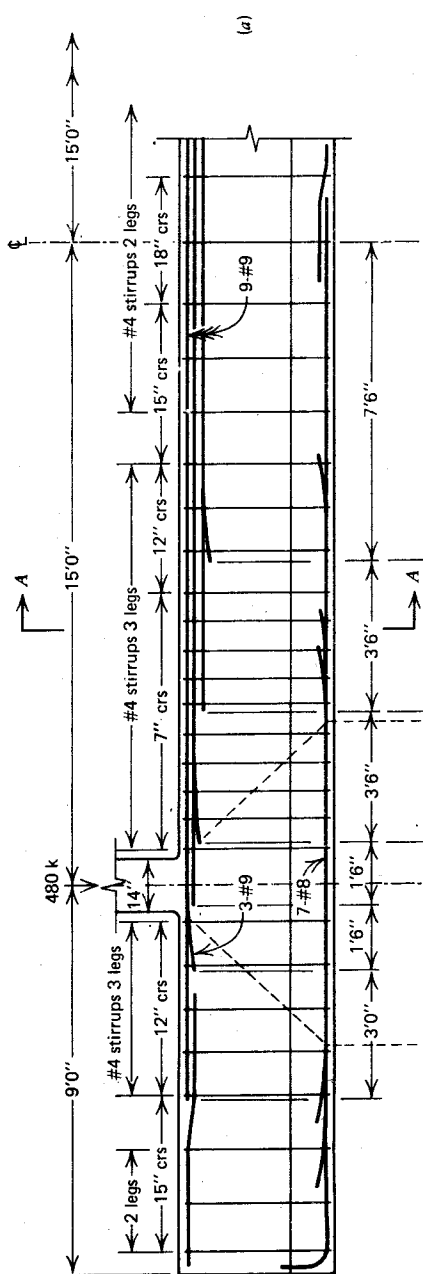
$a = 5.5 \times 60/(0.85 \times 3.6 \times 14) = 7.7 \text{ in}$, $d = 42 - 3 = 39 \text{ in}$, $jd = 35.15 \text{ in}$.

$$M_u = 5.5 \times 60 \times 35.15 = 11,600 \text{ k} \cdot \text{in}$$

$$\therefore \text{dependable } M_u = 0.9 \times 11,600 = 10,440 > 9720 \text{ k} \cdot \text{in}$$

Shear forces and stresses

The critical section for shear is at a distance d to the right of the columns, as indicated by the 45° broken line. For the purpose of stress calculations, a mean effective depth of 38 in will be assumed. Thus the maximum shear, causing diagonal tension, will be $V_{\max} = [15 - (7 + 38)/12] 20 = 225 \text{ k}$. Shear strength to be provided $V_u = V_{\max}/\varphi = 225/0.85 = 265 \text{ k}$. Hence from Eq. 7.5 $v_u = V_u/b_w d = 265,000/(14 \times 38) \approx 500 \text{ psi}$. The concrete can resist at least $v_c = 2.0\sqrt{f'_c} = 120 \text{ psi}$ (Eq. 7.16). Hence the maximum shear stress that could be allocated to this section should not be more (see Section 7.4.2) than $10\sqrt{f'_c} = 600 \text{ psi} > 500 \text{ psi}$. Thus the concrete dimensions are adequate. The stirrups need to resist equivalent shear stresses



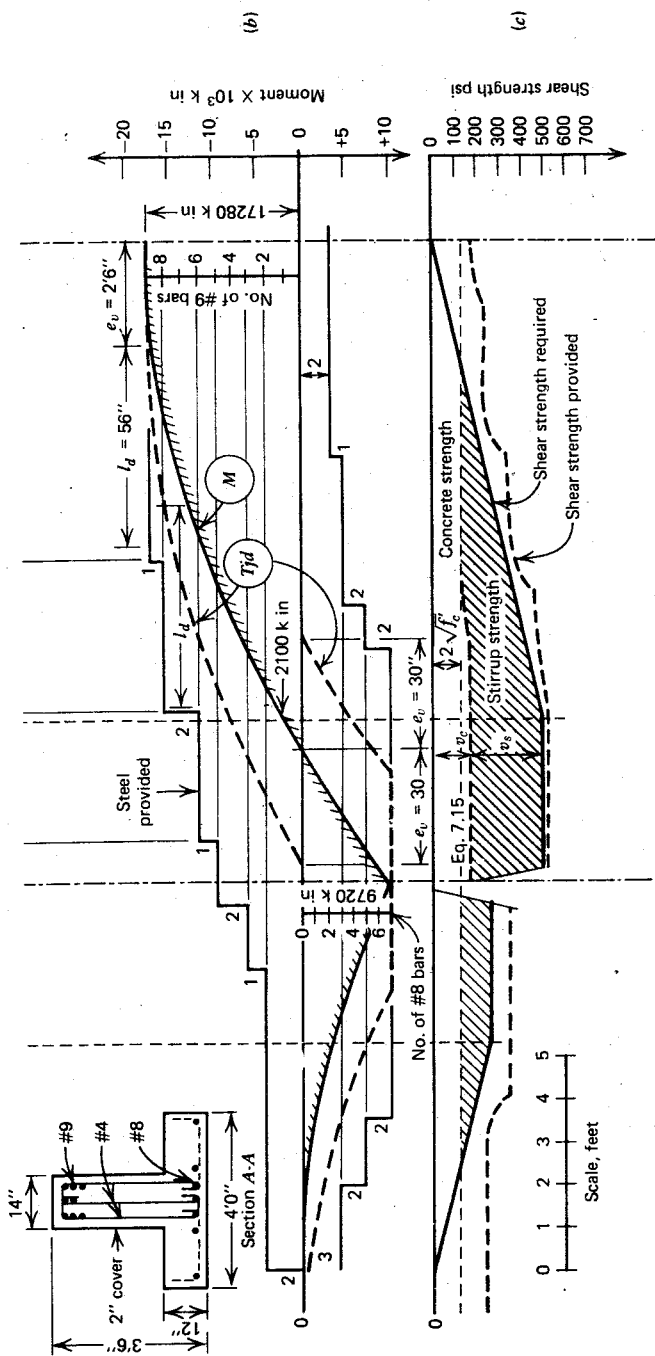


Fig. 7.38. The reinforcement in a foundation beam (1 in = 25.4 mm, 1 foot = 0.305 m, 1 psi = 0.0069 N/mm², 1 k · in = 0.113 kN · m).

(Eq. 7.21) of $v_s = v_u - v_c = 500 - 120 = 380$ psi. From Eq. 7.29 this corresponds to $\eta = v_s/v_u = 380/500 = 0.76$. The design will be based on 45° diagonal struts, $\alpha = 45^\circ$, and vertical stirrups $\beta = 90^\circ$ (see Fig. 7.15).

Curtailment of the flexural reinforcement

The flexural steel will be terminated in accordance with a "Tjd" diagram like Fig. 7.19. The amount, e_v , by which the Tjd diagram is displaced from the bending moment diagram is obtained from Eq. 7.30a as

$$e_v = [\cot \alpha - 0.5\eta(\cot \alpha + \cot \beta)] d \\ = [1 - 0.5 \times 0.76(1 + 0)] d = 0.62d$$

Toward the center of the beam, however, stirrups are assigned a smaller fraction of the total shear; hence $\eta < 0.76$. For this reason it will be assumed that $e_v \approx 0.8d \approx 30$ in. (Note that the ACI code implies that $e_v = d = 38$ in). Accordingly, the Tjd diagram is shown by the broken curves in Fig. 7.38b. Bars must extend beyond this curve by the full development length l_d . For the top No. 9 bars, $l_d = 1.4 \times 40 = 56$ in, for the bottom No. 8 bars, $l_d = 1.0 \times 32 = 32$ in (see Chapter 9).

Figure 7.38b shows where the flexural bars can be stopped. The steel so provided is designated by the stepped moment envelope. Two bars are spliced and carried right to the end of the cantilever. The same procedure can be followed for the curtailment, generally in pairs, of the bottom No. 8 bars. Again two bars are carried to the midspan and lapped with similar bars from the other half of the beam. In each case the cutoff point has been conservatively selected, to give a bar cutting length to the nearest 6 in.

Stirrup reinforcement

Preliminary computations or experience will indicate that stirrups consisting of two or three No. 4 legs can be used; thus one set of stirrups will give 0.40 in^2 or 0.60 in^2 of steel area.

From Eq. 7.15, the shear stresses resisted by the concrete mechanisms at the critical section are $v_c = 1.9\sqrt{f'_c} + 2500 \rho_w V_u d/M_u$ where $\rho_w = 5.5/(14 \times 38) \approx 0.01$, $d = 38$ in, and $M_u \approx 2100 \text{ k} \cdot \text{in}$ as scaled from the bending moment diagram; thus

$$V_u d/M_u = 225 \times 38/2100 > 1$$

$$v_c = 1.9\sqrt{3600} + (2500 \times 0.01 \times 1) = 114 + 25 = 139 \text{ psi}$$

or

$$v_c = 3.5\sqrt{f'_c} = 210 \text{ psi} > 139 \text{ psi}$$

At a section 7 feet from the centerline of the beam, it will be found from Eq. 7.15 that

$$v_c = 114 + 2500 \times 0.015 \times 140 \times \frac{38}{11,400} = 114 + 17 = 131 \text{ psi}$$

Hence in this region, and toward the center of the span, the more simple estimate of Eq. 7.16 will be quite satisfactory; that is,

$$v_c = 2\sqrt{f'_c} = 120 \text{ psi}$$

Both Eqs. 7.15 and 7.16, as applied to the example beam, are plotted in Fig. 7.38c.

Stirrup reinforcement at the critical area, near the column, will need to be provided for $v_s = v_u - v_c = 500 - 139 = 361$ psi. Hence from Eq. 7.23a the required stirrup area per 1-foot ($s = 12$ in) length of beam is $A_v = v_s b_w / f_y = 361 \times 12 \times 14 / 60,000 = 1.01$ in²/ft. Using three No. 4 legs, $s = 0.60 \times 12 / 1.01 = 7.2$ in; say, use 7-in spacing.

At 7 feet from the center line of the beam, Fig. 7.38c gives $v_s \approx 310 - 120 = 190$ psi; thus the spacing can be increased to $361 \times 7.2 / 190 = 13.5$ in; say, use 12-in spacing.

At 5 feet from the centerline, from the same diagram, $v_s \approx 220 - 120 = 100$ psi. Using only two No. 4 legs, $s = A_v f_y / v_s b_w = 0.4 \times 60 / (0.1 \times 14) = 17.1$ in. Thus the spacing could be 15 in.

The minimum web reinforcement (see section 7.4.3) should correspond with $v_s = 50$ psi, so that $A_{v,\min} = 50 \times 12 \times 14 / 60,000 = 0.14$ in²/ft. Two No. 4 legs are required at $s = 0.40 \times 12 / 0.14 = 34$ in, but the maximum spacing should not exceed $d/2 = 38/2 = 19$ in. Nominal stirrup at 18-in centers will be used.

The shear strength so provided is represented by the broken line envelope in Fig. 7.38c. A few stirrups comfortably cope with the less critical situation in the cantilever portion of the beam.

7.11 REFERENCES

- 7.1 B. Bresler and J. G. MacGregor, "Review of Concrete Beams Failing in Shear," *Journal of the Structural Division, ASCE*, Vol. 93, ST1, February 1967, pp. 343-372.
- 7.2 "Building Code Requirements for Reinforced Concrete (ACI 318-71)," American Concrete Institute, Detroit, 1971, 78 pp.

- 7.3 ACI-ASCE Committee 326, "Shear and Diagonal Tension," *Journal ACI*, Vol. 59, January, February, March 1962, pp. 1-30, 277-334, 352-396.
- 7.4 Joint ASCE-ACI Task Committee 426, "The Shear Strength of Reinforced Concrete Members," *Journal of the Structural Division, ASCE*, Vol. 99, ST6, June 1973, pp. 1091-1187.
- 7.5 E. Hognestad, "What Do We Know About Diagonal Tension and Web Reinforcement in Concrete? A Historical Study," *University of Illinois Bulletin*, Vol. 49, No. 50, March 1952, 47 pp.
- 7.6 R. C. Fenwick and T. Paulay, "Mechanisms of Shear Resistance of Concrete Beams," *Journal of the Structural Division, ASCE*, Vol. 94, ST10, October 1968, pp. 2235-2350.
- 7.7 F. Leonhardt, "Reducing the Shear Reinforcement in Reinforced Concrete Beams and Slabs," *Magazine of Concrete Research*, Vol. 17, No. 53, December 1965, pp. 187-198. (This is a brief summary of tests carried out in Stuttgart from 1961 to 1963 only. References give the source for the main body of the work of Leonhardt and Walther as it appeared in bulletins of the Deutscher Ausschuss für Stahlbeton, the German Committee for Reinforced Concrete.)
- 7.8 H. P. J. Taylor, "Investigation of the Dowel Shear Forces Carried by the Tensile Steel in Reinforced Concrete Beams," Cement and Concrete Association, London, TRA 431, 1969, 24 pp.
- 7.9 T. Baumann and H. Rüsch, "Versuche zum Studium der Verdübelungswirkung der Biegezugbewehrung eines Stahlbetonbalkens," Deutscher Ausschuss für Stahlbeton, Bulletin No. 210, Berlin, 1970, pp. 42-83.
- 7.10 A. J. O'Leary, "Shear, Flexure and Axial Tension in Reinforced Concrete Members." Ph.D. Thesis, University of Canterbury, Christchurch, New Zealand, 1970, 380 pp.
- 7.11 T. Paulay and P. J. Loeber, "Shear Transfer by Aggregate Interlock," *Shear in Reinforced Concrete*, ACI Special Publication 42, Vol. 1, Detroit, 1974, pp. 1-15.
- 7.12 H. P. J. Taylor, "Further Tests to Determine Shear Stresses in Reinforced Concrete Beams," Cement and Concrete Association, London, TRA 438, February 1970, 27 pp.
- 7.13 H. P. J. Taylor, "Investigation of the Forces Carried Across Cracks in Reinforced Concrete Beams in Shear by Interlock of Aggregate," Cement and Concrete Association, London, TRA 42.447, 1970, 22 pp.
- 7.14 G. N. J. Kani, "How Safe Are our Large Reinforced Concrete Beams?" *Journal ACI*, Vol. 64, March 1967, pp. 128-141.
- 7.15 H. P. J. Taylor, "Shear Strength of Large Beams," *Journal of the Structural Division, ASCE*, Vol. 98, ST11, November 1972, pp. 2473-2490.
- 7.16 N. S. Bhal, "Über den Einfluss der Balkenhöhe auf die Schubtragfähigkeit von einfeldrigen Stahlbetonbalken mit und ohne Schubbewehrung." Dr.-Ing. Thesis, University of Stuttgart, 1968, 124 pp.
- 7.17 G. N. J. Kani, "Basic Facts Concerning Shear Failure," *Journal ACI*, Vol. 63, June 1966, pp. 675-692.
- 7.18 K. S. Rajagopalan and P. M. Ferguson, "Exploratory Shear Tests Emphasizing Percentage of Longitudinal Steel," *Journal ACI*, Vol. 65, August 1968, pp. 634-638; Vol. 66, February 1969, pp. 150-154.
- 7.19 T. C. Zsutty, "Beam Shear Strength Prediction by Analysis of Existing Data," *Journal ACI*, Vol. 65, November 1968, pp. 943-951.
- 7.20 P. E. Regan, "Behaviour of Reinforced and Prestressed Concrete Subjected to Shear Force," *Proceedings, Institution of Civil Engineers*, Paper 7441S, 1971 Supplement (XVII), pp. 337-364.

- 7.21 A. Placas and P. E. Regan, "Shear Failure of Reinforced Concrete Beams," *Journal ACI*, Vol. 68, October 1971, pp. 763-773.
- 7.22 T. Zsutty, "Shear Strength Prediction for Separate Categories of Simple Beam Tests," *Journal ACI*, Vol. 68, February 1971, pp. 138-143.
- 7.23 E. Mörsch, "Der Eisenbeton. Seine Theorie und Anwendung," Wittwer, Stuttgart, 1908.
- 7.24 H. Kupfer and T. Baumann, "Staffelung der Biegezugbewehrung bei hohen Schubspannungen in Schlanken Stahlbetonträgern mit I-Querschnitt," *Beton- und Stahlbetonbau*, Vol. 64, December 1969, pp. 278-283.
- 7.25 H. Bachmann, "Influence of Shear and Bond on Rotational Capacity of Reinforced Concrete Beams," Publications, International Association for Bridge and Structural Engineering, Vol. 30, Part II, Zürich, 1970, pp. 11-28.
- 7.26 T. Paulay, "Coupling Beams of Reinforced Concrete Shear Walls," *Journal of the Structural Division, ASCE*, Vol. 97, ST3, March 1971, pp. 843-862.
- 7.27 M. A. Sozen, "The Caracas Earthquake of July 29, 1967," *Journal ACI*, Vol. 65, May 1968, pp. 394-401.
- 7.28 A. H. Mattock, "Diagonal Tension Cracking in Concrete Beams with Axial Forces," *Journal of the Structural Division, ASCE*, Vol. 95, ST9, September 1969, pp. 1887-1900.
- 7.29 M. J. Haddadin, S. T. Hong, and A. H. Mattock, "Stirrup Effectiveness in Reinforced Concrete Beams with Axial Force," *Journal of the Structural Division, ASCE*, Vol. 97, ST9, September 1971, pp. 2277-2297.
- 7.30 F. H. N. Sayani, "Influence of Axial Tension on the Shear Strength of Reinforced Concrete Beams." M.Phil. Thesis, Imperial College of Science and Technology, University of London, 1968, 118 pp.
- 7.31 J. G. MacGregor and J. M. Hanson, "Proposed Changes in Shear Provisions for Reinforced and Prestressed Concrete Beams," *Journal ACI*, Vol. 66, April 1969, pp. 276-288.
- 7.32 W. Dilger, "Veränderlichkeit der Biege- und Schubsteifigkeit bei Stahlbetontragwerken und ihr Einfluss auf Schnittkraftverteilung und Traglast bei statisch unbestimmter Lagerung," Deutscher Ausschuss für Stahlbeton, Bulletin No. 179, Berlin, 1966, 101 pp.
- 7.33 R. F. Mast, "Auxiliary Reinforcement in Concrete Connections," *Journal of the Structural Division, ASCE*, Vol. 94, ST6, June 1968, pp. 1485-1504.
- 7.34 A. H. Mattock and N. M. Hawkins, "Shear Transfer in Reinforced Concrete—Recent Research," *PCI Journal*, March-April, 1972, pp. 55-75.
- 7.35 T. Paulay, R. Park, and M. H. Phillips, "Horizontal Construction Joints in Cast in Place Reinforced Concrete," *Shear in Reinforced Concrete*, ACI Special Publication 42, Vol. 2, Detroit, 1974, pp. 599-616.
- 7.36 H. Mayer, "Versuche zum Studium von Grösse und Verteilung der Bügelkräfte im Stahlbeton-Rechteckbalken." Materialprüfungsamt für das Bauwesen der Technischen Hochschule München, Report No. 72, 1967 (2 vols).
- 7.37 G. Alatorre and J. Casillas, "Shear Strength Behaviour of Concrete Beams Subjected to Alternate Loading," *RILEM International Symposium on the "Effects of Repeated Loading of Materials and Structures*, Mexico, 1966, Vol. 4, 26 pp.
- 7.38 B. E. Colley and H. A. Humphrey, "Aggregate Interlock at Joints of Concrete Pavements," Portland Cement Association Research and Development Laboratories, Bulletin D124, 1967, 18 pp.
- 7.39 R. N. White and M. J. Holley, "Experimental Studies of Membrane Shear Transfer," *Journal of the Structural Division, ASCE*, Vol. 98, ST8, August 1972, pp. 1835-1852.

Strength and Deformation of Members with Torsion

8.1 INTRODUCTION

Torsion in reinforced concrete structures often arises from continuity between members. For this reason torsion received relatively scant attention during the first half of this century, and the omission from design considerations apparently had no serious consequences. During the last 10 to 15 years, a great increase in research activity has advanced the understanding of the problem significantly. Numerous aspects of torsion in concrete have been, and currently are being, examined in various parts of the world. The first significant organized pooling of knowledge and research effort in this field was a symposium sponsored by the American Concrete Institute. The symposium volume^{8.1} also reviews much of the valuable pioneering work.

Most code references to torsion to date have relied on ideas borrowed from the behavior of homogeneous isotropic elastic materials. The current ACI code^{8.2} incorporates for the first time detailed design recommendations for torsion. These recommendations are based on a considerable volume of experimental evidence, but they are likely to be further modified as additional information from current research efforts is consolidated.

Torsion may arise as a result of primary or secondary actions. The case of primary torsion occurs when the external load has no alternative to being resisted but by torsion. In such situations the torsion, required to maintain static equilibrium, can be uniquely determined. This case may also be referred to as equilibrium torsion. It is primarily a strength problem because the structure, or its component, will collapse if the torsional resistance cannot be supplied. A simple beam, receiving eccentric line loadings along its span, cantilevers and eccentrically loaded box girders, as illustrated in Figs. 8.1 and 8.8, are examples of primary or equilibrium torsion.

In statically indeterminate structures, torsion can also arise as a secondary action from the requirements of continuity. Disregard for such continuity

in the design may lead to excessive crack widths but need not have more serious consequences. Often designers intuitively neglect such secondary torsional effects. The edge beams of frames, supporting slabs or secondary beams, are typical of this situation (see Fig. 8.2). In a rigid jointed space structure it is hardly possible to avoid torsion arising from the compatibility of deformations. Certain structures, such as shells elastically restrained by edge beams,^{8,3} are more sensitive to this type of torsion than are others. The present state of knowledge allows a realistic assessment of the torsion

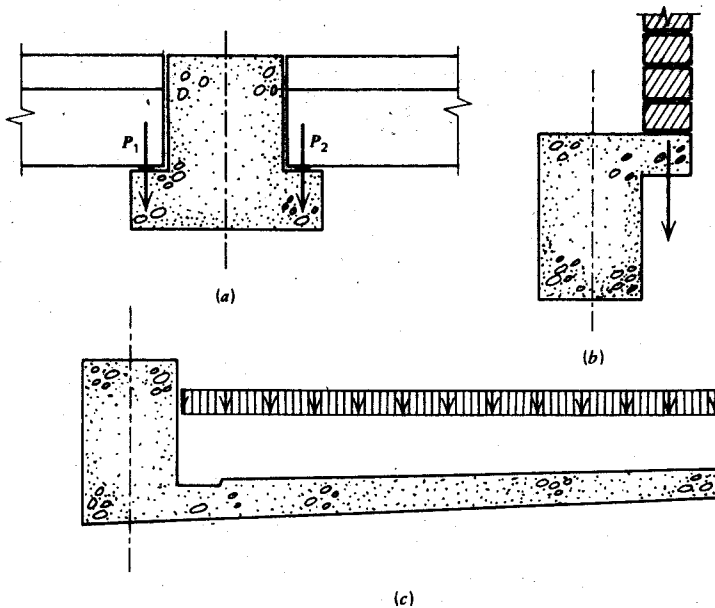


Fig. 8.1. Examples of primary or equilibrium torsion.

that may arise in statically indeterminate reinforced concrete structures at various stages of the loading.

Torsion in concrete structures rarely occurs without other actions. Usually flexure, shear, and axial forces are also present. A great many of the more recent studies have attempted to establish the laws of interactions that may exist between torsion and other structural actions. Because of the large number of parameters involved, some effort is still required to assess reliably all aspects of this complex behavior.

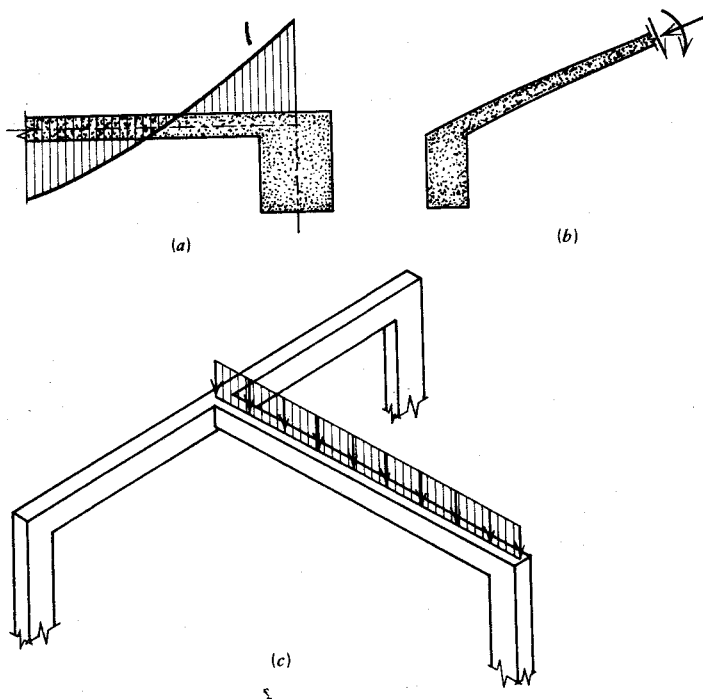


Fig. 8.2. Torsion in statically indeterminate structures.

8.2 PLAIN CONCRETE SUBJECT TO TORSION

The behavior of reinforced concrete in torsion, before the onset of cracking, can be based on the study of plain concrete because the contribution of reinforcement at this stage is negligible.

8.2.1 Elastic Behavior

For the assessment of torsional effects in plain concrete, we can use the well-known approach presented in most texts on structural mechanics. The classical solution of St. Venant can be applied to the common rectangular concrete section. Accordingly, the maximum torsional shearing stress v_t is generated at the middle of the long side and can be obtained from

$$v_t = \psi_t \frac{T}{x^2 y} \quad (8.1)$$

where T = torsional moment at the section

y, x = overall dimensions of the rectangular section, $x < y$

ψ_t = a stress factor being a function y/x , as given in Fig. 8.3

It may be equally as important to know the load-displacement relationship for a particular torsion member. This can be derived from the familiar relationship^{8,4}

$$\frac{d\theta_t}{dz} = \frac{T}{GC} \quad (8.2)$$

where θ_t = the angle of twist

T = the applied torque, which may be a function of the distance along the span

G = the modulus in shear as defined in Eq. 7.37

C = the torsional moment of inertia, sometimes referred to as torsion constant or equivalent polar moments of inertia

z = distance along member

For rectangular sections, we have

$$C = \beta_t x^3 y \quad (8.3)$$

in which β_t , a coefficient dependent on the aspect ratio y/x of the section (Fig. 8.3), allows for the nonlinear distribution of shear strains across the section.

These terms enable the torsional stiffness of a member of length l to be

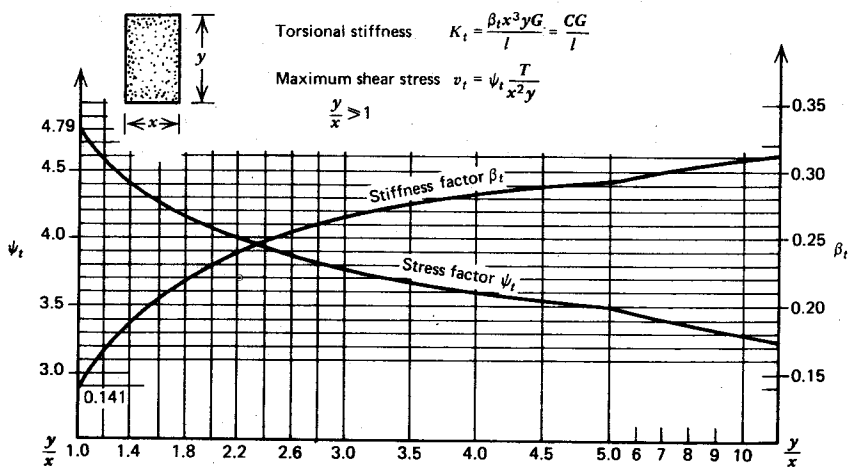


Fig. 8.3. Stiffness and stress factors for rectangular sections subjected to torsion.

defined as the magnitude of the torque required to cause unit angle of twist over this length as

$$K_t = \frac{GC}{l} \quad (8.4)$$

In the general elastic analysis of a statically indeterminate structure, both the torsional stiffness and the flexural stiffness of members may be required. Equation 8.4 for the torsional stiffness of a member may be compared with the equation for the flexural stiffness of a member with far end restrained, defined as the moment required to cause unit rotation, $4EI/l$, where EI = flexural rigidity of a section.

The behavior of compound sections, *T* and *L* shapes, is more complex. However, following Bach's suggestion,^{8.5} it is customary to assume that a suitable subdivision of the section into its constituent rectangles is an acceptable approximation for design purposes. Accordingly it is assumed that each rectangle resists a portion of the external torque in proportion to its torsional rigidity. As Fig. 8.4a shows, the overhanging parts of the flanges should be taken without overlapping. In slabs forming the flanges of beams, the effective length of the contributing rectangle should not be taken as more than three times the slab thickness.^{8.6} For the case of pure torsion, this is a conservative approximation.

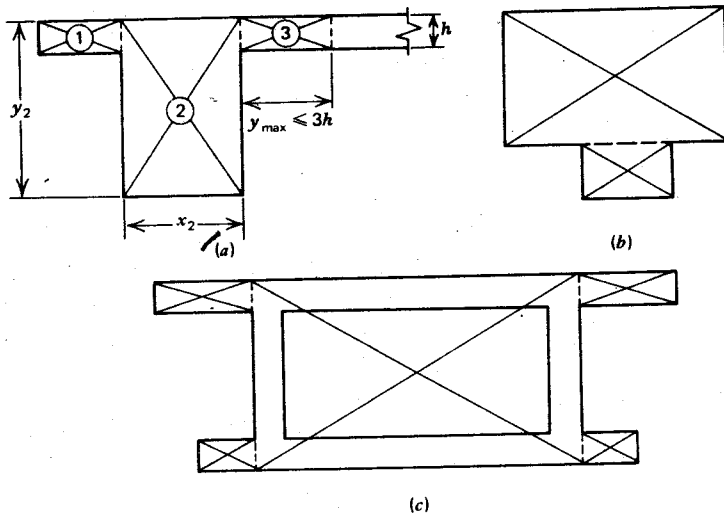


Fig. 8.4. The subdivision of compound sections for torsional analysis.

Using Bach's approximation,^{8,5} the portion of the total torque T resisted by element 2 in Fig. 8.4a is

$$T_2 = \frac{K_{t2}}{\sum_{i=1}^3 K_{ti}} T \quad (8.5)$$

and the resulting maximum torsional shear stress is from Eq. 8.1

$$v_{t2} = \psi_{t2} \frac{T_2}{x_2^2 y_2}$$

The approximation is conservative because the "junction effect" has been neglected.

Compound sections in which shear flow can occur, as in box sections, must be subdivided in a different way. Figure 8.4c illustrates the procedure.

The elastic torsional shear stress distribution over compound cross sections may be best visualized by Prandtl's membrane analogy, the principles of which may be found in standard works on elasticity.^{8,4} In reinforced concrete structures, we seldom encounter the conditions under which the foregoing assumptions associated with linear elastic behavior are satisfied.

8.2.2 Plastic Behavior

In ductile materials it is possible to attain a state at which yield in shear will occur over the whole area of a particular cross section. If yielding occurs over the whole section, the plastic torque can be computed with relative ease.

Consider the square section appearing in Fig. 8.5, where yield in shear v_{ty} , has set in the quadrants. The total shear force V_t acting over one quadrant is

$$V_t = b \frac{b}{2} \frac{1}{2} v_{ty} = \frac{b^2}{4} v_{ty}$$

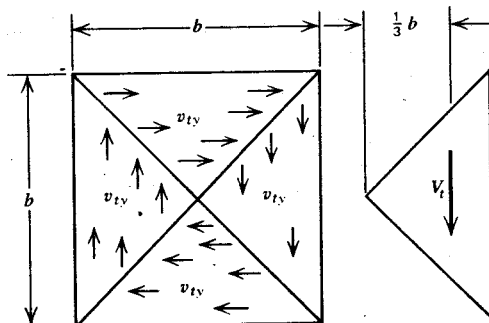


Fig. 8.5. Torsional yielding of a square section.

Thus the total torque resisted is

$$T = 4V_t \frac{b}{3} = \frac{b^3}{3} v_{ty} \quad (8.6)$$

The same results may be obtained using Nádai's "sand heap analogy."^{8/1} According to this analogy the volume of sand placed over the given cross section is proportional to the plastic torque sustained by this section. The heap (or roof) over the rectangular section (see Fig. 8.6) has a height xv_{ty} ,

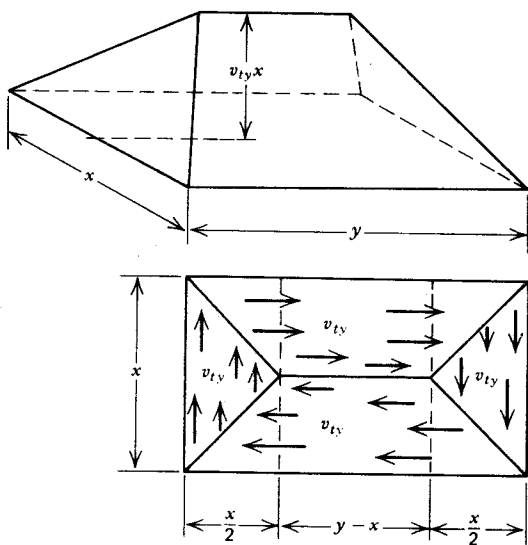


Fig. 8.6. Nádai's sand heap analogy.

where x = small dimension of the cross section. Thus the volume of the pyramid over the square section (Fig. 8.5) is

$$T = b^2 \frac{bv_{ty}}{3} = \frac{b^3}{3} v_{ty} \quad (8.6)$$

The volume of the heap over the oblong section (Fig. 8.6) is

$$\begin{aligned} T &= x^2 \frac{xv_{ty}}{3} + (y-x)x \frac{xv_{ty}}{2} \\ &= \frac{x^2}{2} \left(y - \frac{x}{3} \right) v_{ty} \end{aligned}$$

Hence

$$v_{ty} = \psi_{ty} \frac{T}{x^2 y} \quad (8.7)$$

where

$$\psi_{ty} = \frac{2}{1 - x/3y} \quad (8.7a)$$

It is evident that $\psi_{ty} = 3$ when $x/y = 1$ and $\psi_{ty} = 2$ when $x/y = 0$.

It may be seen that Eq. 8.7 is similar to the expression obtained for elastic behavior, Eq. 8.1.

Concrete is not ductile enough, particularly in tension, to permit a perfect plastic distribution of shear stresses. Therefore the ultimate torsional strength of a plain concrete section will be between the values predicted by the membrane (fully elastic) and sand heap (fully plastic) analogies. Shear stresses cause diagonal (principal) tensile stresses, which initiate the failure. In the light of the foregoing approximations and the variability of the tensile strength of concrete, the simplified design equation for the determination of the nominal ultimate shear stress induced by torsion in plain concrete sections, proposed by ACI 318-71^{8.2}, is acceptable:

$$v_{ty} = v_{tu} = \frac{3T_u}{x^2 y} \quad (8.8)$$

where $x \leq y$.

The value of 3 for ψ_t or ψ_{ty} is a minimum for the elastic theory and a maximum for the plastic theory (see Fig. 8.3 and Eq. 8.7a).

The ultimate torsional resistance of compound sections can be approximated by the summation of the contribution of the constituent rectangles. For sections such as those in Fig. 8.4, the approximation is

$$v_{tu} = \frac{3T_u}{\Sigma x^2 y} \quad (8.8a)$$

where $x \leq y$ for each rectangle.

In Eq. 8.8a, contributions from the junctions (the sand that could be heaped in the valleys between adjacent roofs) are neglected.

The value of v_{tu} cannot be directly related to a strength property of the concrete. However, numerous tests^{8.8-8.11} indicate that its value, when computed from Eq. 8.8 or 8.8a is between $4.0\sqrt{f'_c}$ psi and $7.0\sqrt{f'_c}$ psi ($0.33\sqrt{f'_c}$ and $0.58\sqrt{f'_c}$ N/mm²). This value will also depend on the absolute size of the test specimen from which v_{tu} was obtained. It is believed that these stresses are also reached in reinforced concrete beams when diagonal tension cracks due to torsion are about to develop. Hence ACI Committee 438

adopted the value of $6.0\sqrt{f'_c}$ psi ($0.5\sqrt{f'_c}$ N/mm²) for the estimation of the diagonal cracking load.

The principal stress (tensile strength) concept would suggest that failure cracks should develop at each face of the beam along a spiral running at 45° to the beam axis. However, this is not possible because the boundary of the failure surface must form a closed loop. Hsu has suggested that bending occurs about an axis that is at approximately 45° to the beam axis and parallel to the planes of the long faces of a rectangular beam.^{8,12} This bending causes compression and tensile stresses in the 45° plane across the beam. The latter eventually initiates a surface crack. As soon as flexural tension cracking occurs, the flexural strength of the section is reduced, the crack rapidly propagates, and sudden failure follows. Hsu observed this sequence of failure with the aid of high-speed motion pictures.^{8,12} For most structures little use can be made of the torsional (tensile) strength of unreinforced concrete members.

8.2.3 Tubular Sections

Because of the advantageous distribution of shear stresses, tubular sections are most efficient in resisting torsion. They are widely used in bridge construction. Figure 8.7 illustrates the basic forms used for bridge girders. The

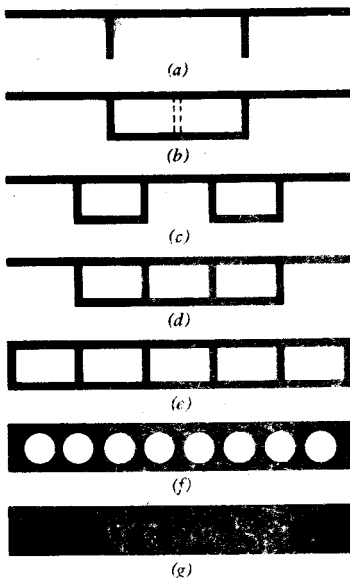


Fig. 8.7. Basic forms used for bridge cross sections.^{8,3}

torsional properties of the girders improve in progressing from Figs. 8.7a to 8.7g.

When the wall thickness h is small relative to the overall dimensions of the section, uniform shear stresses v_t across the thickness can be assumed. By considering the moments exerted about a suitable point by the shear stresses, acting over infinitesimal elements of the tube section, as in Fig. 8.8a, the torque of resistance can be expressed as

$$T = \int h v_t r \, ds \quad (8.9a)$$

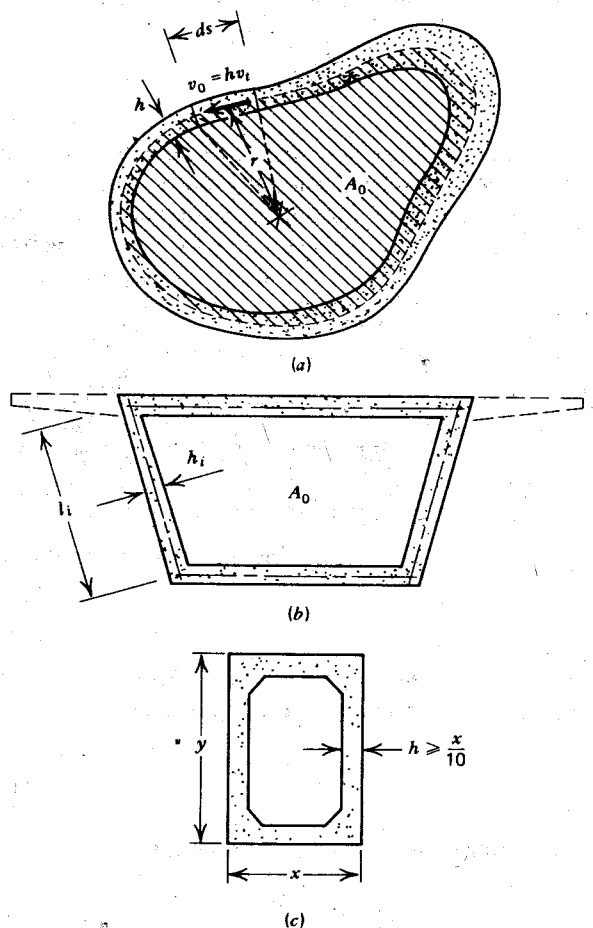


Fig. 8.8. Hollow sections.

The product $hv_t = v_0$ is termed the shear flow, and this is constant; thus

$$v_0 = \frac{T}{\oint r \, ds} \quad \text{or} \quad v_t = \frac{T}{2A_0 h} \quad (8.9b)$$

where A_0 = the area enclosed by the center line of the tube wall (shaded area in Fig. 8.8).

The concept of shear flow around the thin wall tube is useful when the role of reinforcement in torsion is considered.

The ACI code^{8.2} suggests that the equation relevant to solid sections, Eq. 8.8, be used also for hollow sections, with the following modification when the wall thickness is not less than $x/10$ (see Fig. 8.8c):

$$v_{tu} = \left(\frac{x}{4h} \right) \frac{3T_u}{x^2 y} \quad (8.10)$$

where $x \leq y$.

Equation 8.9b follows from first principles and has the advantage of being applicable to both the elastic and fully plastic state of stress.

The torque-twist relationship for hollow sections may be readily derived from strain energy considerations. By equating the work done by the applied torque (external work) to that of the shear stresses (internal work), the torsion constant C_0 for tubular sections can be found thus:

$$\text{internal work} = \frac{1}{2} \times (\text{sum of shear stress}$$

× shear strain acting on the tube elements)

$$\times (\text{unit length}) = \frac{1}{2} \times \oint v_t \frac{v_t}{G} h \, ds \times 1$$

$$\text{external work} = \frac{1}{2} \times (\text{applied torque})$$

× (angle of twist per unit length of member)

$$= \frac{1}{2} \times T \times \frac{\theta}{l}$$

Hence by equating the two expressions and using Eq. 8.9b, the relationship between torque and angle of twist is found to be

$$T = \frac{GC_0}{l} \theta$$

and the torsional stiffness of such member is therefore

$$K_t = \frac{GC_0}{l} \quad (8.4a)$$

where C_0 is the equivalent polar moment of inertia of the tubular section and is given by

$$C_0 = \frac{4A_0^2}{\oint ds/h} \quad (8.11)$$

where s is measured around the wall centerline. The same expression for the more common form of box section (Fig. 8.8b) becomes

$$C_0 = \frac{4A_0^2}{\sum l_i/h_i} \quad (8.11a)$$

For uniform wall thickness Eq. 8.11 reduces further to

$$C_0 = \frac{4A_0^2 h}{p} \quad (8.11b)$$

where p is the perimeter measured along the tube centerline.

It is emphasized that the preceding discussion on elastic and plastic behavior relates to plain concrete, and the propositions are applicable only at low load intensities before cracking. They may be used for predicting the onset of diagonal cracking.

8.3 BEAMS WITHOUT WEB REINFORCEMENT SUBJECT TO FLEXURE AND TORSION

The failure mechanism of beams subjected to torsion and bending depends on the predominance of one or the other. The ratio of ultimate torque to moment, T_u/M_u , is a suitable parameter to measure the relative magnitude of these actions. The flexural resistance depends primarily on the amount of flexural reinforcement. The torsional behavior of a concrete beam without web reinforcement is more difficult to assess in the presence of flexure.

Flexural stresses initiate diagonal cracks in the case of torsion, much as they do in the case of shear. In the presence of flexure these cracks are arrested in the compression zone. For this reason a diagonally cracked beam is capable of carrying a certain amount of torsion. The manner in which this torsion is resisted is, at present, a matter of speculation. Clearly the compression zone of the beam is capable of resisting a limited amount of torsion, and horizontal reinforcement can also contribute to torsional resistance by means of dowel action.

It has been found (e.g., by Mattock⁸⁻¹³) that the torsional resistance of a cracked section is approximately one-half the ultimate torsional strength of the uncracked section, provided a certain amount of bending is present.

Thus one half the torque causing cracking can be sustained after the formation of cracks. The torque thus carried is so small that its influence on flexure can be ignored.

The nominal torsional shear stress, corresponding to this limited torsion, is conservatively assumed by ACI 318-71^{8,2} to be 40% of a cracking stress of $6\sqrt{f'_c}$ psi ($0.5\sqrt{f'_c}$ N/mm²).

$$\therefore v_{tc} = 0.4(6\sqrt{f'_c}) = 2.4\sqrt{f'_c} \text{ psi } (0.2\sqrt{f'_c} \text{ N/mm}^2) \quad (8.12)$$

and the torque supplied by the concrete section only, after the onset of cracking, is revealed by Eq. 8.8 to be

$$T_c = \frac{x^2 y}{3} v_{tc} \quad (8.13)$$

Similarly, for compound sections, Eq. 8.8a gives

$$T_c = \sum \frac{x^2 y}{3} v_{tc} \quad (8.13a)$$

with the limitations on overhanging parts as indicated in Fig. 8.4.

When $T_u/M_u > 0.5$ (i.e., when torsion is significant), brittle failure has been observed.^{8,8} When the bending moment is more pronounced, (i.e., when $T_u/M_u < 0.5$), a more ductile failure can be expected. The torsional strength of a beam can be increased only with the addition of web reinforcement. The amount of flexural reinforcement appears to have no influence on the torsional capacity of the concrete section, T_c .

In T or L beams the overhanging part of the flanges contribute to torsional strength. This has been verified on isolated beams.^{8,14, 8,15} The effective width of flanges, when these are part of a floor slab, is difficult to assess. When a yield line can develop along an edge beam because of negative bending moment in the slab, as illustrated in Fig. 8.9, it is unlikely that much of the flange can contribute toward torsional strength. In such cases, it is advisable to rely only on the rectangular section.

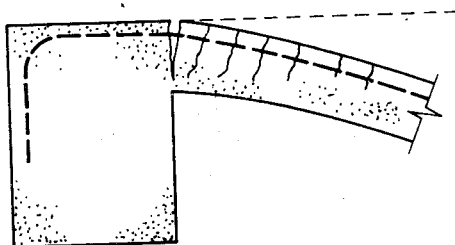


Fig. 8.9. Yield line along an edge beam.

8.4 TORSION AND SHEAR IN BEAMS WITHOUT WEB REINFORCEMENT

It is evident that in superposition, the shear stresses generated by torsion and shearing force are additive along one side and subtractive along the opposite side of a rectangular beam section. The critical diagonal tensile stresses that ensue are further affected by flexural tensile stresses in the concrete, because it is impossible to apply shearing forces without simultaneously inducing flexure. A fully rational theory for the interaction of shear and torsion in the presence of bending is not known to have yet been developed. For this reason reliance must be placed on empirical information derived from tests. By providing more than adequate flexural reinforcement, it is possible to experimentally study the failure criteria for combined shear and torsion. It is usual in such tests to keep the torsion to shear ratio constant while the load is being increased to failure. However, in practice one action may occur first, imposing its own crack pattern before the other action becomes significant. For the time being, it is advisable to be conservative in the interpretation of test results.

Figure 8.10 plots the scatter obtained in typical combined torsion-shear tests. It also indicates that a circular interaction relationship (normalized for this particular group of tests) can be useful for design purposes, provided sufficiently low stress values for diagonal cracking by shear and torsion are chosen. For these beams,^{8.10} which contained no web reinforcement, the shear and torsional stresses which formed an approximate lower bound for the plotted experimental points, as computed from Eqs. 7.5 and 8.8, were found to be, respectively,

$$v_c = 2.68\sqrt{f'_c} \text{ psi (0.22}\sqrt{f'_c} \text{ N/mm}^2)$$

and

$$v_{tc} = 4.80\sqrt{f'_c} \text{ psi (0.4}\sqrt{f'_c} \text{ N/mm}^2)$$

The circular interaction relationship is the basis of the current ACI code provisions.^{8.2} For convenience, the magnitude of the interaction shear and torsional forces carried by a cracked section at ultimate load can be expressed in terms of nominal stress as

$$\left(\frac{v_{tu}}{2.4\sqrt{f'_c}}\right)^2 + \left(\frac{v_u}{2\sqrt{f'_c}}\right)^2 = 1 \quad (8.14)$$

where v_{tu} = induced nominal torsional stress carried by the concrete at ultimate, given by Eq. 8.8

v_u = induced nominal shear stress carried by the concrete at ultimate, given by Eq. 7.5

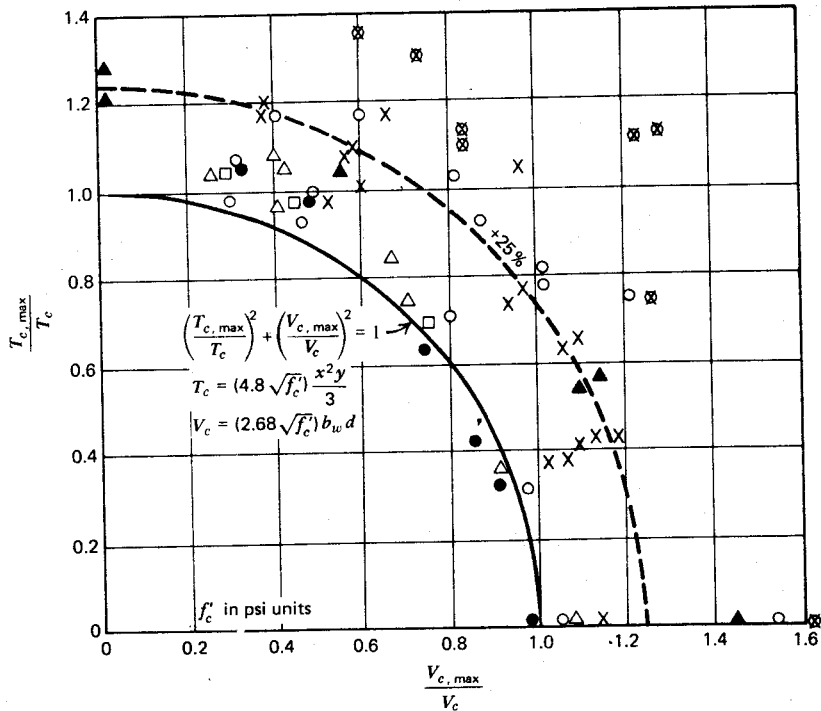


Fig. 8.10. Interaction of torsion and shear.^{8.10}

The $2.4\sqrt{f'_c}$ and $2.0\sqrt{f'_c}$ terms in Eq. 8.14 are the proposed values for the nominal ultimate torsional shear strength of the concrete after cracking without the presence of shear, and the nominal ultimate shear strength of the concrete without the presence of torsion, respectively, both in psi units. In SI units, $2.4\sqrt{f'_c}$ psi would be replaced by $0.2\sqrt{f'_c}$ N/mm², and $2.0\sqrt{f'_c}$ psi by $0.166\sqrt{f'_c}$ N/mm². Equation 8.14 controls the design of beams with only nominal web reinforcement, the above-mentioned stresses being assumed to be carried across a cracked section by mechanisms not involving the web reinforcement.

Now from Eq. 8.14 we have

$$v_{tu}^2 \left[1 + \left(\frac{2.4\sqrt{f'_c}}{2.0\sqrt{f'_c}} \frac{v_u}{v_{tu}} \right)^2 \right] = (2.4\sqrt{f'_c})^2$$

Therefore, the permissible nominal ultimate torsion shear stress that can be carried by the concrete alone in the presence of a shear force is

$$v_{tc} = \frac{2.4\sqrt{f'_c}}{\sqrt{[1 + (1.2v_u/v_{tu})^2]}} \text{ psi} \quad (8.15a)$$

Similarly, it may be shown that the permissible nominal ultimate shear stress that can be carried by the concrete alone in the presence of torsion is

$$v_c = \frac{2.0\sqrt{f'_c}}{\sqrt{[1 + (v_{tu}/1.2v_u)^2]}} \text{ psi} \quad (8.15b)$$

In design, only one of these equations need be computed because it is evident that the permissible stresses v_{tc} and v_c are related to the induced stresses v_{tu} and v_u by

$$\frac{v_{tu}}{v_u} = \frac{v_{tc}}{v_c} \quad (8.15c)$$

Additional torsional and shear strength can be derived from appropriate web reinforcement.

8.5 TORSION MEMBERS REQUIRING WEB REINFORCEMENT

The role of web reinforcement in torsion members is similar to that of stirrups in flexural members subject to shear. After the formation of diagonal cracks, torsional shear stresses can no longer be resisted unless a different mechanism, such as a space truss, is formed to enable stresses to be transferred in a manner essentially different from St. Venant's concept.

A space truss, consisting of stirrup tension members and diagonal concrete compression struts, is the traditional model on which the design of web reinforcement has been based.^{8,16} Such a truss appears in Fig. 8.11a. The full lines indicate tension chords and the strips between the diagonal crack lines, inclined at an angle α_c , suggest compression struts. All early studies assumed $\alpha_c = 45^\circ$.

A potential diagonal failure crack, as in Fig. 8.11b, is crossed by $n_1 = y_0/(s \tan \alpha_c)$ number of stirrup legs, where y_0 is the straight portion of the vertical stirrup leg that can effectively cross diagonal cracks, as in Fig. 8.11e. Therefore, the tension developed across this crack at ultimate is

$$N_1 = n_1 A_t f_y \quad (8.16a)$$

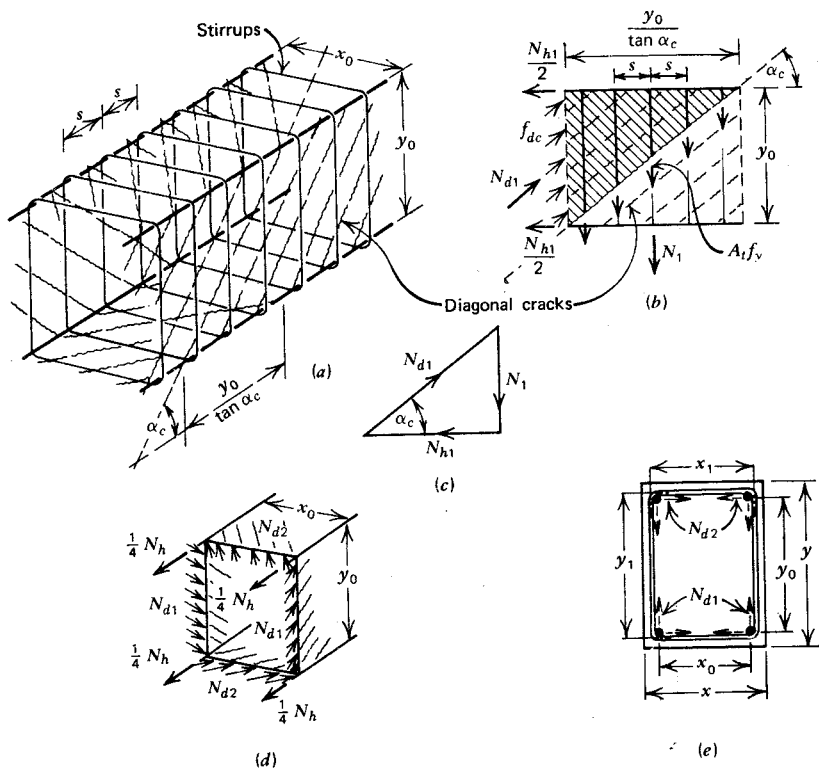


Fig. 8.11. Torsional resistance by the space truss model.

where A_t is the area of one leg of a closed stirrup and f_y is the yield stress in the stirrups. Similarly, the tension developed across a corresponding diagonal crack in the top plane of the space truss is

$$N_2 = n_2 A_t f_y \quad (8.16b)$$

where the number of stirrup legs affected is $n_2 = x_0/(s \tan \alpha_c)$.

The vertical stirrup forces resolve themselves at the "joints" of the truss into horizontal and diagonal components. These forces, acting on a transverse section of a space truss, are represented in Figs. 8.11b through 8.11d. It will be seen that

$$N_{d1} = \frac{N_1}{\sin \alpha_c} \quad \text{and} \quad N_{d2} = \frac{N_2}{\sin \alpha_c}$$

The total horizontal force, which is the sum of the horizontal components of the diagonal compression forces, is found from Fig. 8.11d and Eqs. 8.16a and 8.16b as

$$N_h = 2 \frac{N_{d1} + N_{d2}}{\sec \alpha_c} = 2 \frac{N_1 + N_2}{\tan \alpha_c} = 2A_t f_y \frac{x_0 + y_0}{s \tan^2 \alpha_c} \quad (8.17)$$

This compression force must be balanced by an equal and opposite tension force requiring a total horizontal steel area, represented in the model of Fig. 8.11 by four longitudinal corners bars, of

$$A_t = 2A_t \frac{f_y}{f_{ly}} \frac{(x_0 + y_0)}{s \tan^2 \alpha_c} \quad (8.18)$$

where f_{ly} is the yield strength of the longitudinal bars.

The inclination of the compression struts α_c can be determined from the effective volumetric ratio of the longitudinal and transverse tension members of the space truss thus

$$m_t = \frac{\text{Vol}_l}{\text{Vol}_t} = \frac{A_l}{2(x_0 + y_0)} \times \frac{s}{A_t} = \frac{f_y}{f_{ly} \tan^2 \alpha_c} \quad (8.19)$$

so that

$$A_l = \frac{2(x_0 + y_0)}{s} A_t m_t \quad (8.18a)$$

The contribution of the transverse members (stirrups) of the space truss can be derived from consideration of the diagonal concrete compression forces (Fig. 8.11d). These forces are transmitted from the stirrups, through the four horizontal corner bars, by means of bearing.^{8.17} The positions of the diagonal compression forces N_{d1} and N_{d2} relative to the cross section, are indicated in Fig. 8.11e. The transverse components of these compression forces generate the torsion and by reference to Figs. 8.11d and 8.11c it is evident that

$$T_s = (x_0 N_{d1} + y_0 N_{d2}) \sin \alpha_c = x_0 N_1 + y_0 N_2$$

and from Eqs. 8.16a and 8.16b we have

$$T_s = 2 \frac{A_t f_y}{s \tan \alpha_c} x_0 y_0 \quad (8.20)$$

This equation, developed by Lampert,^{8.17} gives the torsional resistance of a tube section in which the center lines of the tube walls pass through the four longitudinal corner bars. Equation 8.20 is the basis of the current CEB recommendations.^{8.18} The corresponding equations of the ACI code^{8.2} are

based on the traditional space truss, which has its panels in the planes of the stirrup legs,^{8.16} so that the tube area is defined by the product $x_1 y_1$ (see Fig. 8.11e) rather than $x_0 y_0$.

By combining Eqs. 8.19 and 8.20, the torsional resistance of the space truss is obtained^{8.17} in terms of the area of a stirrup leg A_t and the total area of longitudinal reinforcement A_l as

$$T_s = 2x_0 y_0 \sqrt{\frac{A_t f_y}{s} \frac{A_l f_{ly}}{2(x_0 + y_0)}} \quad (8.21)$$

Lampert showed^{8.17} that this equation is valid for any compact non-symmetrical section in the form

$$T_s = 2A_0 \sqrt{\frac{A_t f_y}{s} \frac{A_l f_{ly}}{P_0}} \quad (8.21a)$$

where A_0 = area enclosed by the connecting lines between the centers of longitudinal bars

P_0 = perimeter formed by the same set of lines

Comparison with tests carried out at various research establishments indicates very good agreement between observed ultimate strength and the predictions of Eq. 8.21.^{8.19} It is to be noted that Eq. 8.21 is intended to predict the total torque T_u and does not imply any contribution to the torsional strength from other sources.

In a beam subjected to pure torsion, cracks form initially at 45° to the axis of the beam, irrespective of the shape of the cross section or the amount and arrangement of reinforcement. As the load approaches ultimate, however, this angle changes if the volumes of horizontal and transverse reinforcement are different (i.e., where $m_t \neq 1$).^{8.20}

For steel with equal yield strength in both directions (i.e., $f_y = f_{ly}$), the theoretical minimum steel content for a given torque is obtained when the volumes of the horizontal and transverse reinforcement are made equal.^{8.17} This corresponds to $m_t = 1$ and $\alpha_c = 45^\circ$ (see Eq. 8.19).

A corresponding simplification obtained from Eqs. 8.21 and 8.18a with $m_t = 1$ results in a design expression that gives the required area of one closed stirrup A_t to resist a given torque T_s as

$$A_t = \frac{T_s s}{2f_y x_0 y_0} \quad (8.22)$$

The spacing of the closed stirrups should not exceed $(x_1 + y_1)/4$ or 12 in (250 mm), whichever is smaller.^{8.21}

It does not seem to matter how the longitudinal steel is distributed in a cross section, provided this steel is symmetrically arranged and is well anchored beyond the section at which the torsion is introduced into the beam. This steel enables the longitudinal tension N_h (see Fig. 8.11d), necessary for truss action, to be developed over the length subjected to torsion. The stressing of the longitudinal steel implies that a torsion member must elongate after diagonal cracking, that is, when the space truss commences to contribute toward strength. Any restraint against lengthening of a torsion member or precompression has the same effect as providing additional longitudinal steel.^{8.21}

To enable the diagonal compression forces to resolve themselves at the node points of the space truss, it is advisable to provide a substantial longitudinal bar at each of the four corners of the section. Otherwise the outward pointing components of the diagonal concrete compression stresses may push off the concrete located between stirrups, especially when these are widely spaced. It is suggested that the minimum diameter of the longitudinal bars be not less than one-sixteenth of the stirrup spacing.^{8.21}

The analysis of the space truss (Fig. 8.11) demonstrates the similarity of the behavior of a torsion member to the behavior of the thin-walled tube, discussed in Section 8.2.3. Indeed, an experimental verification of this analysis comes from the tests of Lampert,^{8.22} who used rectangular hollow sections. Nowhere in the evaluation of the torque sustained by torsion reinforcement were the properties of the concrete, or even the configuration of the section, considered. Obviously some limit must be placed on the amount of reinforcement, to ensure that the diagonal concrete struts do not become the weakest link of the mechanism. It appears that a workable mechanism exists as long as the diagonal compression between node points of these struts can be developed. This can be achieved efficiently in both solid and hollow sections, provided the effective wall thickness is not too small. Hsu^{8.20} and Lampert^{8.22} found that the ultimate torque was essentially the same for thick-walled hollow sections as for solid rectangular sections, having identical overall dimensions and the same reinforcement. The same conclusion may be reached by examining Fig. 8.11. Therefore, it is evident that the core of solid reinforced concrete sections does not significantly contribute toward torsional strength.

The thin-walled tube or the equivalent space truss with 45° diagonals was the mathematical model for torsional resistance generally used by early researchers, such as Rausch.^{8.16} The principal sectional dimensions of this model were x_1 and y_1 , shown in Fig. 8.11. These dimensions were used in many of the proposed torsion theories (a very good review of these is given by Zia^{8.23}) and in the formulation of the present ACI recommendations.

The equation for the amount of closed stirrup reinforcement adopted by the present ACI code^{8.2} has similarities to Eq. 8.22. The ACI equation is

$$A_t = \frac{s T_s}{\alpha_t f_y x_1 y_1} \quad (8.23)$$

where

$$\alpha_t = 0.66 + 0.33 \left(\frac{y_1}{x_1} \right) \leq 1.50 \quad (8.23a)$$

and $y_1 \geq x_1$.

When equal volumes of longitudinal and transverse torsion steel are used (i.e., when $m_t = 1$), $x_0 = x_1$, and $y_0 = y_1$, it is clear that the truss or tube analogy, Eq. 8.22, would give $\alpha_t = 2.0$. The ACI value for α_t was determined experimentally by Hsu.^{8.20} Typical findings of Hsu are presented in Fig. 8.12, where the relationship between the observed ultimate torque and the stirrup contribution parameter ($x_1 y_1 A_t f_y / s$) is compared with the CEB recommendations^{8.18} for rectangular and hollow beams with identical overall dimensions,

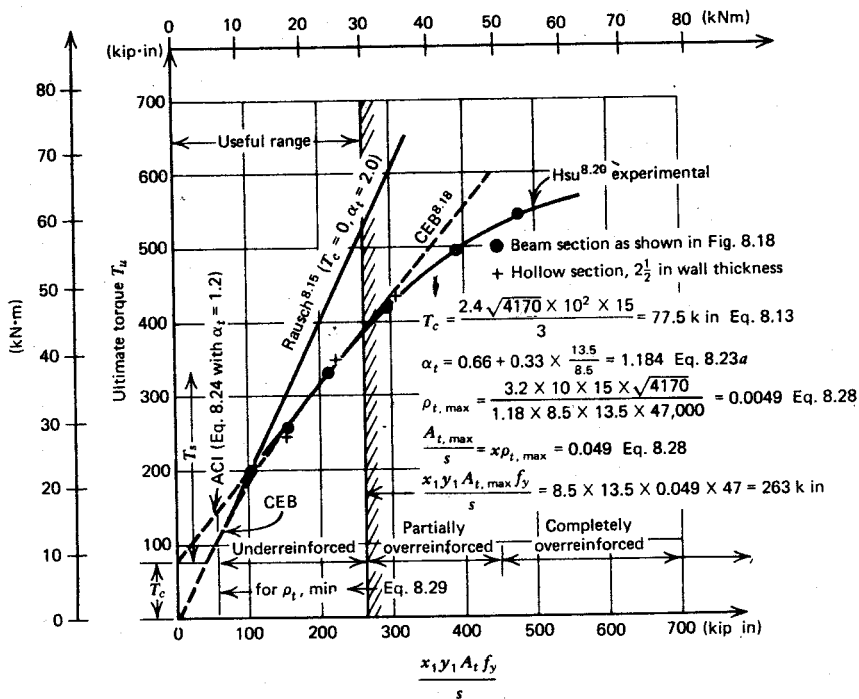


Fig. 8.12. The increase of ultimate torque with reinforcing content.

concrete strengths, and variable steel contents with $m_t = 1$. In the "under-reinforced" beams, both the stirrups and the longitudinal steel reached yield strength, and the failure was very ductile. In the partially overreinforced members, the stirrups or the longitudinal bars did not reach yield. In the completely overreinforced beams, both types of bar failed to reach yield.

Figure 8.12 serves as a basis for discussing the current ACI design philosophy for pure torsion. The straight portion of the curve may be expressed, when Eqs. 8.13 and 8.23 are combined, as follows:

$$T_u = T_c + T_s = T_c + \alpha_t \frac{x_1 y_1 A_t f_y}{s} \quad (8.24)$$

This equation predicts the ultimate torque T_u , carried when both the transverse and the longitudinal steel yield. The downward extension of the straight line, fitted to the experimental results,^{8.20} indicates that a portion of the torque T_c is resisted by a mechanism other than the reinforcement. It is convenient to call this the torque contribution of the concrete, as discussed in Section 8.3. The results appearing in Fig. 8.12 were obtained from test beams subjected to monotonic loading. It is likely that several cycles of service load application would diminish this contribution of the concrete and would result in a consequent increase in stirrup stresses.

Comparison of the solid and hollow sections reveals that the absence of a core in the latter did not affect the strength of these members. It was previously thought that the contribution of the core, perhaps not fully cracked, accounted mainly for the torsion contribution of the concrete T_c . This experimental evidence justifies a design approach based entirely on the behavior of hollow sections.^{8.18}

The ACI design equation for stirrups to resist torsion, Eq. 8.23, is based on the condition that at least an equal amount of longitudinal bars will be provided. Accordingly, $m_t \geq 1$; hence, from the similarity to Eq. 8.18a, we write

$$A_t = 2A_s \frac{x_1 + y_1}{s} \quad (8.25)$$

The failure of "overreinforced" beams originates from the premature crushing of the concrete in compression. The compression stresses result mainly from strut action, as part of the space truss illustrated in Fig. 8.11. Using the analogy for a hollow section, similar to that in Fig. 8.11d, the diagonal compression stress can be derived from Eq. 8.16a thus

$$f_{dc} = \frac{N_{d1}}{h y_0 \cos \alpha_c} = \frac{N_1}{h y_0 \sin \alpha_c \cos \alpha_c} = \frac{A_t f_y}{h s \sin^2 \alpha_c}$$

or when $\alpha_c = 45^\circ$ and Eq. 8.20 is considered,

$$f_{dc} = 2 \frac{A_t f_y}{hs} = \frac{T_s}{hx_0 y_0} \quad (8.26)$$

where h is the wall thickness of the hollow section.

This amount is twice the stress one would obtain using conventional analysis, such as Eq. 8.9b, and the concept of principal stresses. Strain measurements on the surface of test beams have demonstrated that in fact compression stresses considerably in excess of the value given by Eq. 8.26 are generated. Lampert and Thürlmann^{8.22} have drawn attention to the twisted surface of a torsion member (see Fig. 8.13). The compression struts

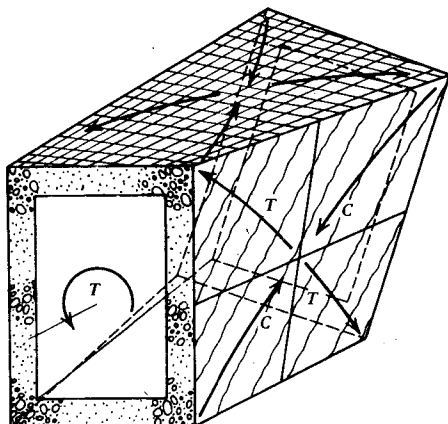


Fig. 8.13. Bending of the diagonal struts due to torsion.

formed between diagonal cracks, being part of a hyperbolic paraboloid surface, are clearly subject to curvature. The bending moment so generated induces additional compression in them, thus reduces their strut capacity. In addition, these compression struts are being crossed by the stirrup reinforcement, thus are simultaneously subject to transverse tensile strain. The loss of compression strength due to this effect was discussed in connection with the shear strength of beams in Chapter 7.

It is evident that if a premature compression (brittle) failure is to be avoided, the intensity of the ultimate torque must be limited. The ACI code^{8.2} expresses this limit in terms of a nominal torsional shearing stress that should

not be exceeded. The requirement is

$$v_{tu} \leq 12\sqrt{f'_c} \text{ psi} \quad (v_{tu} \leq 1.0\sqrt{f'_c} \text{ N/mm}^2) \quad (8.27)$$

To ensure a ductile type of failure, the torsion member must be under-reinforced. This is achieved when Eqs. 8.12, 8.13, 8.23, and 8.27 are combined. Hence using the notation of Fig. 8.11, we find that the content of the closed stirrup reinforcement for pure torsion is limited to

$$\rho_t = \frac{A_t}{sx} \leq \frac{3.2xy\sqrt{f'_c}}{\alpha_t x_1 y_1 f_y} = \rho_{t,\max} \quad (8.28)$$

in the presence of an equal volume of longitudinal reinforcement. (In Eq. 8.28 the numerical 3.2 should be replaced by 0.266 when f'_c is expressed in newtons per square millimeter). The relevance of this equation to some test beams is shown in Fig. 8.12 and Fig. 8.18, where the torsion theoretically developed with maximum steel content, as given by Eq. 8.28, is compared with observed maximum torques. These tests^{8,20} show (see Fig. 8.18) that the ACI design approach outlined in this section is unconservative when the web steel content ρ_t exceeds the maximum value specified by Eq. 8.28.

It is also evident that a minimum amount of torsion reinforcement must be provided to ensure that no immediate collapse follows if the cracking torque of an unreinforced member is attained. For this, the ACI code^{8,2} recommends

$$\begin{aligned} \rho_{t,\min} &\leq \frac{A_t}{sx} = \frac{50}{f_y}, \quad \text{with } f_y \text{ in psi} \\ &= \frac{0.345}{f_y}, \quad \text{with } f_y \text{ in N/mm}^2 \end{aligned} \quad (8.29)$$

Because the torsion sustained by the concrete after diagonal cracking is much less than the torsion at the onset of cracking, the above-mentioned minimum stirrup reinforcement, which for convenience has been kept the same as specified for shear, would not be adequate. However, with an increase of the longitudinal steel (i.e., with $m_t > 1$), the torsional resistance can be boosted. Therefore, to increase the minimum amount of longitudinal steel, when only a small amount of torsion stirrup is required, the ACI code^{8,2} stipulates that

$$A_{t,\min} = \left[\frac{400xs}{f_y} \left(\frac{v_{tu}}{v_{tu} + v_u} \right) - 2A_t \right] \frac{x_1 + y_1}{s} \quad (8.25a)$$

where $2A_t$ need not be taken as less than $50xs/f_y$. (The numerical 400 should be replaced by 2.76 when stresses are expressed in newtons per square millimeter.)

8.6 COMBINED SHEAR AND TORSION IN BEAMS WITH WEB REINFORCEMENT

The current ACI recommendations^{8.2} are based on the premise that a portion of either the shear force or the torsion is carried by mechanisms other than the web reinforcement. We do not know precisely how these mechanisms interact in the case of combined torsion and shear. However, satisfactory approximations can be made in terms of ultimate strength, using circular or bilinear interaction relationships. Because of the large scatter of experimental data, neither approach can be considered to be more justifiable than the other.

Liao and Ferguson^{8.24} have found from tests on a number of beams with various cross sections that a circular interaction relationship, based on strength including the contribution of web reinforcement, can be used.

The current ACI code^{8.2} requires that the contribution of the concrete toward shear and torsion, as outlined in Section 8.4, be supplemented by web reinforcement. This is carried out by computing the stirrup requirements for shear and torsion separately and providing web steel for the total quantity. The application of this principle is illustrated and discussed at the end of this section.

To ensure that under combined torsion and shear a diagonal concrete compression failure is preceded by yielding of the web reinforcement, it is essential to set an upper limit to the combined load. For the sake of simplicity, the maximum nominal stress requirements for shear (discussed in Section 7.4.2) and for torsion (Eq. 8.27), were combined to give again a circular interaction relationship thus

$$\left(\frac{v_{tu}}{12\sqrt{f'_c}} \right)^2 + \left(\frac{v_u}{10\sqrt{f'_c}} \right)^2 \leq 1 \quad (8.30)$$

The terms of this equation are as for Eq. 8.14 in psi. In SI units (N/mm²) the numericals 12 and 10 are replaced by 1.0 and 0.83. The indications are that Eq. 8.30 is safe. However, there is little evidence, particularly in the intermediate ranges of torsion and shear, to show the validity^{8.25} of this equation.

For convenience, Eq. 8.30 can be rearranged in the following form to suit design procedures:

$$v_{tu} \leq \frac{12\sqrt{f'_c}}{\sqrt{[1 + (1.2v_u/v_{tu})^2]}} \text{ psi} \quad (8.31a)$$

or

$$v_u \leq \frac{10\sqrt{f'_c}}{\sqrt{[1 + (v_{tu}/1.2v_u)^2]}} \text{ psi} \quad (8.31b)$$

The numericals 12 and 10 should be replaced by 1.0 and 0.83 when stresses are expressed in SI units. Only one of these equations need be used to satisfy Eq. 8.30.

Example 8.1

A small bridge in an industrial plant, supporting a conveyor and spanning continuously over 40 ft (12.2 m), has a single *T* cross section 10 ft (3.05 m) wide (see Fig. 8.14). The bridge is to carry a service live load of 100 lb/ft² (4.79 kN/m²) over its entire width; when only one-half the width of the bridge is loaded, a service live load of 150 lb/ft² (7.19 kN/m²) shall be considered. The side spans of the bridge are of such lengths that we may assume that under a uniformly distributed load, the negative and positive bending moments for this 40 ft (12.2 m) span are equal. Design the web reinforcement at the support section of the beam using the following material properties and section dimensions (see also Fig. 8.14):

Dimensions:	
$f'_c = 3600 \text{ psi (24.8 N/mm}^2)$	$x = b_w = 16.0 \text{ in (406 mm)}$
$f_y = 40,000 \text{ psi (276 N/mm}^2)$	$d = 21.5 \text{ in (546 mm)}$
$(f'_c)^{1/2} = 60 \text{ psi (0.414 N/mm}^2)$	$x_1 = 12.5 \text{ in (317 mm)}$
	$y_1 = 20.5 \text{ in (521 mm)}$

Weight of concrete: $1.04 \times 144 = 150 \text{ lb/ft}^3 (2400 \text{ kg/m}^3)$

$\varphi = 0.85$ for torsion and shear

$\varphi = 0.90$ for flexure

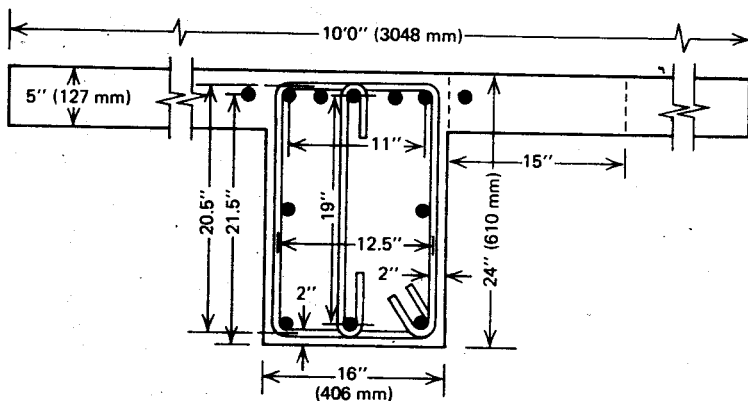


Fig. 8.14. Reinforcement and dimensions of the beam section subject to torsion, shear, and flexure for Example 8.1.

Solution

1. *Loading*

$$\begin{aligned} \text{Service dead load:} \quad & \text{slab } 120 \times 5 \times 1.04 = 624 \text{ lb/ft} \\ & \text{web } (24 - 5) \times 16 \times 1.04 = 316 \text{ lb/ft} \\ & \text{total} = \underline{940 \text{ lb/ft}} \end{aligned}$$

Service live load over whole width $10 \times 100 = 1000 \text{ lb/ft}$
 Service live load over half-width $5 \times 150 = 750 \text{ lb/ft}$, introducing a torque about the beam center line of

$$0.750 \times 0.5 \times 5 \times 12 = 22.5 \text{ kip} \cdot \text{in/ft}$$

Design torque and shear at end support section:

Case i. Full dead and live load

$$V_u = (1.4 \times 0.94 + 1.7 \times 1.00) \times 20 = 60.3 \text{ kips}$$

$$T_u = 0$$

Case ii. Full dead load and live load over half-width

$$V_u = (1.4 \times 0.94 + 1.7 \times 0.75) \times 20 = 51.8 \text{ kips}$$

$$T_u = (1.7 \times 22.5) \times 20 = 765 \text{ kip} \cdot \text{in}$$

Design for case ii and check for case i.

2. *Estimation of flexural reinforcement*

Case i. Support moment

$$M_u = \frac{1}{2} \times \frac{Wl}{8} = \frac{2 \times 60.3 \times 40 \times 12}{16} = 3620 \text{ kip} \cdot \text{in}$$

Assume the internal lever arm is $0.9 \times 21.5 = 19.3 \text{ in}$, and neglect compression steel. Then find

$$A_s = \frac{M_u}{\varphi f_y jd} = \frac{3620}{0.9 \times 40 \times 19.3} = 5.21 \text{ in}^2 (3361 \text{ mm}^2)$$

Check: $a = 5.21 \times 40 / (0.85 \times 3.6 \times 16) = 4.3 \text{ in}$ (depth of compression stress block); hence $21.5 - 4.3/2 = 19.4 \approx 19.3 \text{ in}$, a satisfactory approximation.

Case ii. Flexural steel required is approximately by proportion

$$A_s = 5.21 \times \frac{51.8}{60.3} = 4.48 \text{ in}^2 (2890 \text{ mm}^2)$$

Additional steel will be required for torsion. The total steel in the top of the section must be at least 5.21 in^2 , as required by case i.

3. Nominal shear stresses

$$\text{Shear: } v_u = \frac{V_u}{\phi b_w d} = \frac{51,800}{0.85 \times 16 \times 21.5} = 177 \text{ psi for case ii,}$$

Eq. 7.5

$$\text{Torsion: } \frac{1}{3} \sum x^2 y = \frac{(16^2 \times 24) + (2 \times 5^2 \times 15)}{3} = 2298 \text{ in}^3,$$

$$v_{tu} = \frac{T_u}{\phi \frac{1}{3} \sum x^2 y} = \frac{765,000}{0.85 \times 2298} = 392 \text{ psi,} \quad \text{Eq. 8.8a}$$

Check maximum allowable nominal combined stresses

$$\frac{v_{tu}}{1.2v_u} = \frac{392}{1.2 \times 177} = 1.85, \quad \text{Eq. 8.31b}$$

$$v_{u,\max} = \frac{10\sqrt{f'_c}}{\sqrt{[1 + (v_{tu}/1.2v_u)^2]}} = \frac{10 \times 60}{\sqrt{(1 + 1.85^2)}} = 285 > 177 \text{ psi,}$$

Eq. 8.31b

Hence section will not be overreinforced.

Allocate actions to resistance of concrete

$$v_c = \frac{2.0\sqrt{f'_c}}{\sqrt{[1 + (v_{tu}/1.2v_u)^2]}} = \frac{2 \times 60}{\sqrt{(1 + 1.85^2)}} = 57 \text{ psi,} \quad \text{Eq. 8.15b}$$

$$v_{tc} = \frac{v_{tu}}{v_u} v_c = \frac{392}{177} 57 = 126 \text{ psi,} \quad \text{Eq. 8.15c}$$

4. The web reinforcement for shear and torsion

Stirrup area required for shear resistance:

$$A_v = \frac{b_w s}{f_y} (v_u - v_c) = \frac{16 \times 12}{40000} (177 - 57) = 0.576 \text{ in}^2/\text{ft,}$$

Eqs. 7.21 and 7.23a

Torsion to be resisted by steel:

$$T_s = (v_{tu} - v_{tc}) \sum \frac{x^2 y}{3} = (392 - 126) 2298 = 611 \text{ kip}\cdot\text{in,}$$

Eqs. 8.8 and 8.24

$$\alpha_t = 0.66 + 0.33 \left(\frac{y_1}{x_1} \right) = 0.66 + 0.33 \times \frac{20.5}{12.5} = 1.20 < 1.50,$$

Eq. 8.23a

Stirrups required for torsion:

$$A_t = \frac{sT_s}{\alpha_t f_y x_1 y_1} = \frac{12 \times 611}{1.20 \times 40 \times 12.5 \times 20.5} = 0.596 \text{ in}^2/\text{ft},$$

Eq. 8.23

If two-legged stirrups are used, the area of one leg is

$$A_{v, \text{outer}} = \frac{1}{2} A_v + A_t = \frac{0.576}{2} + 0.596 = 0.884 \text{ in}^2/\text{ft} (1870 \text{ mm}^2/\text{m})$$

Use No. 5 at 4 in crs = 0.918 in²/ft.

If three-legged stirrups are used, as shown in Fig. 8.14, the area of the outer legs would be $0.576/3 + 0.596 = 0.788 \text{ in}^2/\text{ft}$, (i.e., No. 5 at $4\frac{1}{2}$ in crs = 0.816 in²/ft).

Thus the area required for the inner leg would be

$$0.576 - 2(0.816 - 0.596) = 0.136 \text{ in}^2/\text{ft}$$

Provide No. 4 at $13\frac{1}{2}$ in crs = 0.174 in²/ft.

5. Longitudinal steel for torsion

$$A_l = 2A_t \frac{x_1 + y_1}{s} = 2 \times 0.596 \frac{12.5 + 20.5}{12} = 3.28 \text{ in}^2 (2116 \text{ mm}^2),$$

Eq. 8.25

This steel could be divided into two or three equal parts and distributed along the depth of the section. Following the arrangement in Fig. 8.14, provide total:

- (i) Top steel = $3.28/3 + 4.48 = 5.57 > 5.21 \text{ in}^2$;
use six No. 8 bars and one No. 9 bar = 5.71 in².
- (ii) Steel at middepth = $3.28/3 = 1.09 \text{ in}^2$, say, two No. 7 bars = 1.20 in².
- (iii) At the bottom of the section compression prevails; thus the longitudinal tension steel for torsion would not be required. However, from considerations of flexure, two or three bars from the positive midspan reinforcement would be carried to the supports.

6. Minimum reinforcement

It may be easily shown that the requirements of Eqs. 8.29 and 8.25a are comfortably satisfied at this critical section.

7. Web reinforcement for shear

Considering loading case i, it may be shown that the web steel requirement for 60.3 kip shear alone is considerably less than that calculated for case ii, $v_u = 60300/(0.85 \times 16 \times 215) = 206 \text{ psi}$.

8. An examination of the shear-torsion interaction relationship

The design of this beam for all combinations of torsion and shear could have been obtained with the aid of an interaction chart like Fig. 8.15, which was constructed to demonstrate the interpretation of the ACI code^{8.2} more clearly. The chart indicates the combinations of ultimate shear and torsion that could be carried by a beam section for various steel contents. The following observations may be made:

- (i) The shaded area shows the circular interaction relationship for the resisting mechanisms other than web reinforcement. Only the additional actions need be resisted by stirrups.
- (ii) The additional strength obtained from stirrups approaches a linear interaction relationship as the steel content increases. This

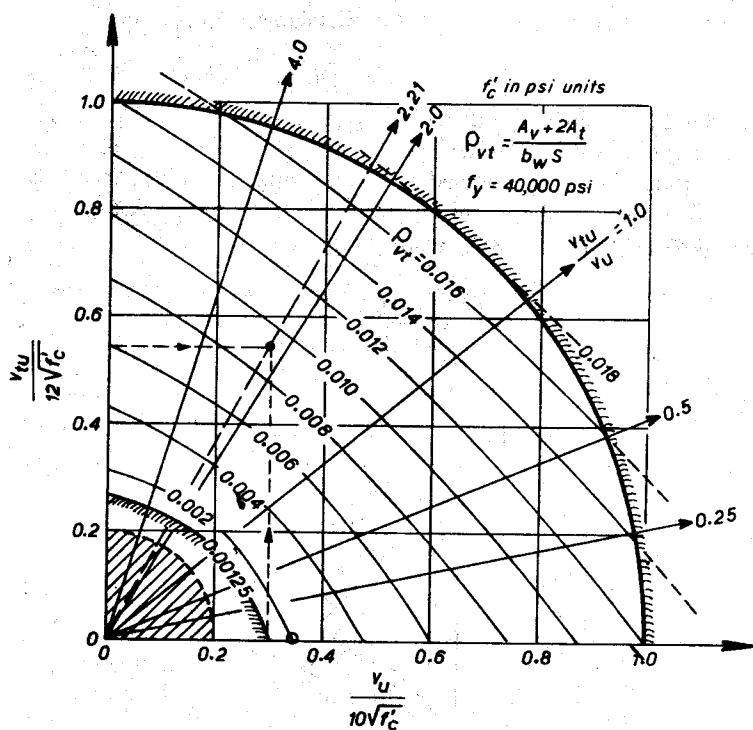


Fig. 8.15. An interaction diagram for shear and torsion.

suggests an anomalous situation. The maximum content of transverse steel ρ_{vt} is 1.2% if only shear is to be resisted, but $\rho_{vt} = 1.8\%$ could be used when the ratio of the maximum possible nominal torsional and shear stresses is about 1.5. This anomaly arises from the arbitrary circular interaction limitation for the maximum shear and torque, shown by the shaded outer circle.

(iii) The minimum web reinforcement to be used in this beam (Eq. 8.29) is $\rho_{min} = 50/f_y = 0.00125$, and its contribution is indicated by the inner shaded curve.

(iv) The required steel for the example beam could have been obtained as follows:

$$\frac{u_{tu}}{12\sqrt{f'_c}} = \frac{392}{12 \times 60} = 0.544$$

$$\frac{v_u}{10\sqrt{f'_c}} = \frac{177}{10 \times 60} = 0.295 \quad \text{or} \quad \frac{v_{tu}}{v_u} = \frac{392}{177} = 2.21$$

gives a radial direction.

The point of intersection of the above values on the figure gives $\rho_{vt} = 0.0092$. Hence

$$A_{v,\text{total}} = 0.0092 \times 16 \times 12 = 1.766 \text{ in}^2/\text{ft}$$

that is, 0.883 in²/ft for one leg of the stirrups as obtained previously.

(v) With $v_u/10\sqrt{f'_c} = 206/(10 \times 60) = 0.343$, pure shear is obviously not critical as Fig. 8.15 reveals ($\rho_{vt} = 0.002 < 0.0092$).

9. Design of the web reinforcement in accordance with the CEB recommendations^{8.18}

The relevant dimensions of the equivalent tube (Fig. 8.11e) are approximately from Fig. 8.14: $x_0 = 11$ in (279 mm) and $y_0 = 19$ in (483 mm). Equation 8.22 was derived on the assumption that the equivalent space truss is to resist the whole of the torsion. The stirrup area required on this basis is

$$A_t = \frac{T_s s}{\varphi 2 f_y x_0 y_0} = \frac{765 \times 12}{0.85 \times 2 \times 40 \times 11 \times 19} = 0.646 \text{ in}^2/\text{ft}, \quad \text{Eq. 8.22}$$

Since the web steel for shear alone is as derived in paragraph 4 of this example, the total area of one leg of a closed stirrup required for combined shear and torsion is

$$A_v = \frac{0.576}{2} + 0.646 = 0.934 \text{ in}^2/\text{ft} (1976 \text{ mm}^2/\text{m})$$

which is 5.7% more than the amount obtained from the ACI code requirements.

Longitudinal steel in a correspondingly larger amount would also be required for torsion alone.

8.7 COMBINED FLEXURE AND TORSION

Considerable work has been carried out recently to assess the ultimate torsional strength of reinforced concrete members subjected to combined torsion and flexure. The theories put forward differ mainly in the formulation of the failure mechanisms and the number of components of the resisting system being considered. Using the postulated failure mechanism, equilibrium statements can be established for the ultimate torsional and the flexural actions. The internal compression forces are usually assumed to be resisted along an inclined compression hinge, whereas the required tensile forces are supplied by the longitudinal and transverse bars at yield.^{8.8, 8.26} Much pioneering work related to this concept was done in the USSR by Lessig, Yudin, Lialin^{8.27} and others.

A typical idealization of a failure mode in *T* beams appears in Fig. 8.16. Using this model, observed capacities in bending, torsion, and shear can be predicted satisfactorily,^{8.28} but the equations seldom lend themselves easily to design office use. Also, depending on the relative magnitude of bending,

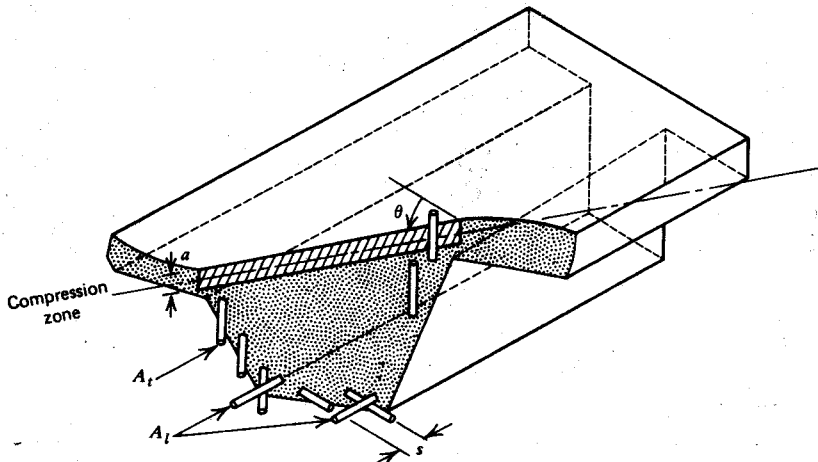


Fig. 8.16. Idealized *T*-beam failure mode in bending and torsion.

torsion, and shear, the compression hinge may form across the bottom or along the side of the beam.^{8.26}

Lampert and Collins^{8.19} approached the problem by using both the space truss analogy and a skew bending theory. In the evaluation of the flexural resistance, the internal lever arm (which in this case is a dimension of the truss) is assumed to be constant throughout the prismatic member and is independent of the reinforcing content. The derived interaction relationship is based on the premise that beams in combined torsion and flexure fail along an inclined plane in bending. The capacity of such a beam for each inclined plane can be expressed in terms of the moment capacity in the longitudinal and transverse directions. In both the truss analogy and skew bending theory approaches, a parabolic interaction between flexure and torsion was found. The former predicts torsion accurately because the correct torsion lever arms x_0 and y_0 , are used. The latter is accurate for pure flexure when the appropriate internal moment arm ($d - a/2$), is used. As a result of this work, Lampert and Collins^{8.19} suggest an interpolated parabolic interaction relationship for pure torsion and pure flexure in the following form:

$$\left(\frac{T_u}{T_{u0}}\right)^2 = r \left(1 - \frac{M_u}{M_{u0}}\right) \quad (8.32a)$$

when yielding of the longitudinal steel occurs in the flexural tension zone and

$$\left(\frac{T_u}{T_{u0}}\right)^2 = 1 + r \frac{M_u}{M_{u0}} \quad (8.32b)$$

when tension yielding of the longitudinal steel occurs in the flexural compression zone,

where T_u = applied ultimate torque

M_u = applied ultimate bending moment

T_{u0} = pure ultimate torsional capacity of the section, Eq. 8.21, if $r = 1$

M_{u0} = pure ultimate flexural capacity of the section, Eq. 4.36

r = ratio of yield forces of flexural tension and compression reinforcement, given as follows

$$r = \frac{A_s f_y}{A'_s f'_y} \quad (8.33)$$

These relationships show good agreement with experiments.^{8.19}

The corresponding interaction diagrams are given in Fig. 8.17. Clearly the flexural compression steel can considerably boost the torsion capacity of a section when only small bending is present. Before this steel can yield in tension, the compression force induced by flexure in the surrounding

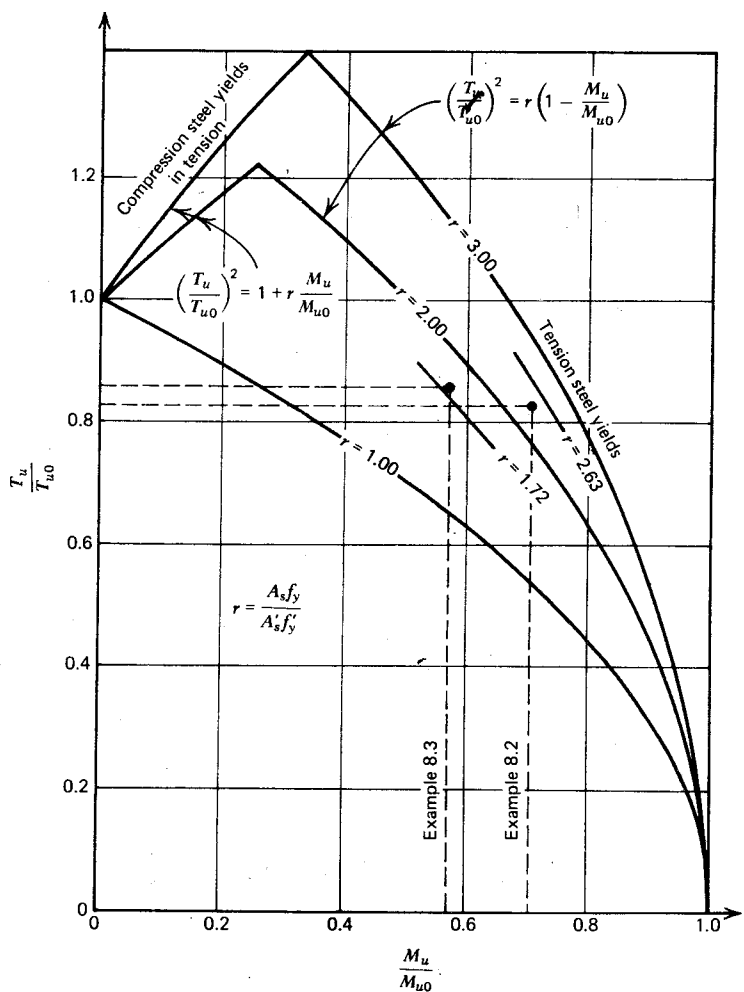


Fig. 8.17. An interaction diagram for bending and torsion.^{8.19}

concrete must be overcome. This gives the longitudinal steel ($A_l f_{ly}$ in Eq. 8.21) apparent extra strength. The larger the flexural compression in the concrete (i.e., the larger the flexural tensile steel content of the beam A_s), the larger will be the apparent strength increase of the longitudinal compression steel in torsion.

The role of the longitudinal reinforcement in the resistance of torsion was discussed previously. If other actions, such as bending or axial tension, reduce

the capacity of the longitudinal steel, the web reinforcement cannot fully contribute toward the intended torsional resistance of the truss mechanism (see Eq. 8.21). Conversely, if some of the longitudinal steel in a beam is being used for torsion, the flexural contribution of these bars is reduced. Therefore each action could reduce the capacity of the other. The interaction diagram in Fig. 8.17 shows that in a symmetrically reinforced beam ($r = 1$) even a small moment will decrease the torsional strength by causing earlier yield in the longitudinal steel. In an unsymmetrically reinforced beam, on the other hand, a small amount of bending will increase the torsional strength, because the longitudinal bars in the flexural compression zone will yield much later as a result of the tension generated by torsion in the space truss mechanism. The current design approach proposed by the ACI and the CEB is based on the premise that a simple superposition of the longitudinal flexural and torsional reinforcement is likely to result in excess strength, thus permitting the designer to omit the examination of the actual interaction of bending and torsion. The application of this proposition was shown in Example 8.1. The simplicity of the approach^{8.13} seems to outweigh the advantages of a more sophisticated analysis that could offer some economic benefits. However, the interaction relationship,^{8.19} as shown in Fig. 8.17, is very simple. Its application and a comparison with the ACI procedure are presented in the next section. For design, Eqs. 8.32a and 8.32b can be rearranged to give the required reinforcing steel area for torsion and bending with simple superposition of the requirements.

These considerations assume that yielding of the reinforcement will be the primary cause of failure which, therefore, will be ductile. It is essential to ensure that by limiting the flexural (Eq. 4.49) and torsional (Eq. 8.28) steel content, premature crushing of the concrete cannot occur.

Example 8.2

Check the adequacy of the beam section designed for torsion and shear in Example 8.1 using the interaction relationship of Fig. 8.17. Note that in establishing this interaction relationship Lampert and Collins considered the torsional contribution of the space truss (Eq. 8.21) only;^{8.19} neglecting the contribution of the concrete T_c . The dimensions of the section appear in Fig. 8.14.

Solution

1. *The approximate flexural capacity*

Tension steel, $A_s = 5.71 \text{ in}^2$ in top of beam. Compression steel, $A'_s = \text{assume three No. 7 bars} = 1.80 \text{ in}^2$ in bottom of beam.
 Steel at middepth, $\frac{1}{3}A_s = 1.20 \text{ in}^2$

For the purpose of the flexural and torsion computation, one-half this steel may be allocated to both the top and the bottom reinforcement.

Estimate internal lever arm:

$$a_{\max} = \frac{A_s f_y}{0.85 f'_c b_w} = \frac{(5.71 + 0.5 \times 1.20) \times 40}{0.85 \times 3.6 \times 16} = 5.16 \text{ in}$$

$$a_{\min} = \frac{A_s - A'_s}{A_s} a_{\max} = \frac{6.31 - 2.40}{6.31} \times 5.16 = 3.20 \text{ in}$$

$$a \approx 0.5(5.16 + 3.20) = 4.2 \text{ in}$$

$$\left(d - \frac{a}{2} \right) \approx 21.5 - 0.5 \times 4.2 = 19.4 \text{ in}$$

$M_{u0} = 6.31 \times 40 \times 19.4 = 4897 \text{ kip} \cdot \text{in}$, the pure flexural capacity of the section. The bending moment resulting from dead and live load is for case ii

$$M_u = \frac{Wl}{\varphi 16} = \frac{2 \times 51.8 \times 40 \times 12}{0.9 \times 16} = 3453 \text{ kip} \cdot \text{in}$$

$$\therefore \frac{M_u}{M_{u0}} = \frac{3453}{4897} = 0.705$$

2. The torsional capacity

From Example 8.1

Stirrup steel provided No. 5 at 4 in crs = 0.918 in²/ft

Stirrup steel required for shear $0.576/2 = 0.288 \text{ in}^2/\text{ft}$

\therefore Stirrup steel available for torsion = $\overline{0.630} \text{ in}^2/\text{ft}$

Longitudinal steel is provided as in paragraph 1. For pure torsion the weaker of the top or bottom steel will determine the beginning of yielding. Hence assume

$$A_t = 1.80 + 1.20 + 1.80 = 4.80 \text{ in}^2$$

Note that this is in excess of that computed in Example 8.1, (i.e., 3.28 in²).

As a matter of interest compute, m_t :

$$m_t = \frac{sA_t}{2(x_0 + y_0)A_t} = \frac{12 \times 4.80}{2(11 + 19) \times 0.63} = 1.524 = \frac{1}{\tan^2 \alpha_c},$$

Eq. 8.19

where $x_0 \approx 16 - 4 - 1 = 11$ in and $y_0 \approx 24 - 4 - 1 = 19$ in. Therefore, $\alpha_c = 39^\circ$; thus more stirrups would be encountered by a diagonal crack than in the case of 45° cracks.

$$T_s = T_{u0} = 2x_0 y_0 f_y \sqrt{\frac{A_t A_l}{2s(x_0 + y_0)}} \\ = \frac{2 \times 11 \times 19 \times 40 \sqrt{0.63 \times 4.8}}{\sqrt{2 \times 12(11 + 19)}}, \quad \text{Eq. 8.21} \\ = 1084 \text{ k} \cdot \text{in}$$

Torsion to be resisted $= T_u = 765/0.85 = 900 \text{ kip} \cdot \text{in}$

$$\therefore \frac{T_u}{T_{u0}} = \frac{900}{1084} = 0.830$$

3. Interaction

$$r = \frac{A_s}{A'_s} = \frac{5.71 + 0.60}{1.80 + 0.60} = 2.63, \quad \text{Eq. 8.33}$$

As $M_u/M_{u0} = 0.705$, it is evident from Fig. 8.17 that Eq. 8.32a is applicable.

$$\left(\frac{T_u}{T_{u0}}\right)^2 = r \left(1 - \frac{M_u}{M_{u0}}\right) = 2.63(1 - 0.705) = 0.776, \quad \text{Eq. 8.32a}$$

Therefore, the maximum torque permitted to act together with the given bending moment is $T_u = \sqrt{0.776} T_{u0} = 0.881 \times 1084 = 955 \text{ kip} \cdot \text{in} > 900 \text{ kip} \cdot \text{in}$. This indicates that according to the proposed interaction approach, the section is satisfactory, but it is nearly exhausted in flexure and torsion. Since the steel areas theoretically required in Examples 8.1 have been rounded up to achieve a practical arrangement of reinforcement, a direct comparison with the ACI "no interaction" approach cannot be made.

The relationship is also illustrated in Fig. 8.17. Any point lying within the area bound by the appropriate interaction curve indicates a safe design.

Example 8.3

To illustrate the relationship between the "interaction" and "no interaction" design approach once more, the same section studied in Examples 8.1 and 8.2 is considered under reduced bending moment.

We assume that the previously considered beam (Fig. 8.14) is subjected to a negative support moment of only $M_u = \frac{1}{2}WI/16$.

Solution

$$\frac{M_u}{\varphi} = 0.5 \times 3453 = 1727 \text{ kip} \cdot \text{in}$$

Hence flexural steel required is approximately $1727/(40 \times 19.4) = 2.23 \text{ in}^2$. If one-half the longitudinal torsion steel is provided in the top of the beam, then according to previous calculations, $A_t/2 = 1.64 \text{ in}^2$. The total top steel is thus $A_s = 3.87 \text{ in}^2$.

The positive midspan steel for this beam would be approximately 9 in^2 , and at least one-quarter of this would be carried into the support section. Thus assume $A'_s = 2.25 \text{ in}^2$, therefore $r = 3.87/2.25 = 1.72$.

The horizontal steel considered to be available for pure torsion would be $A_t = 2 \times 2.25 = 4.50 \text{ in}^2$ and, with the stirrup arrangement unaltered, the torsional capacity of the section is

$$T_{uo} = 2 \times 11 \times 19 \times 40 \sqrt{\left[\frac{0.63 \times 4.5}{2 \times 12(11 + 19)} \right]} = 1049 \text{ kip} \cdot \text{in}$$

Eq. 8.21

Hence $T_u/T_{uo} = 900/1049 = 0.858$.

The increased top steel would increase the ultimate flexural capacity of the section to approximately $M_{uo} \approx 3.87 \times 40 \times 19.4 = 3003 \text{ kip} \cdot \text{in}$.

Therefore $M_u/M_{uo} = 1727/3003 = 0.575$, and from the interaction relationship, Eq. 8.32a, we have

$$\left(\frac{T_u}{T_{uo}} \right)^2 = 1.72(1 - 0.575) = 0.731 \quad \text{and}$$

$$T_u = \sqrt{0.731} \times 1049 = 897 \text{ kip} \cdot \text{in} \approx 900 \text{ kip} \cdot \text{in}$$

For design purposes this gives satisfactory agreement between the "interaction" and "no interaction" approaches.

8.8 TORSIONAL STIFFNESS

Considerations of the classical theory of elasticity led to the derivation of the torsional stiffness of homogeneous beams having various cross sections (see Eqs. 8.3 and 8.4). Experiments on reinforced or prestressed concrete

beams indicate a satisfactory degree of agreement with theory.^{8.22, 8.29} However, the property is of little use to the designer unless he takes into account diagonal cracking, which sets in at an early stage of the loading.

Typical observed torque-twist relationships for 15 × 10 in (381 × 254 mm) rectangular beams^{8,20} (Fig. 8.18) reveal the sudden increase of twist at the onset of diagonal cracking. At this stage a new mechanism, such as the space truss, takes over the load. Instead of shear strains, diagonal

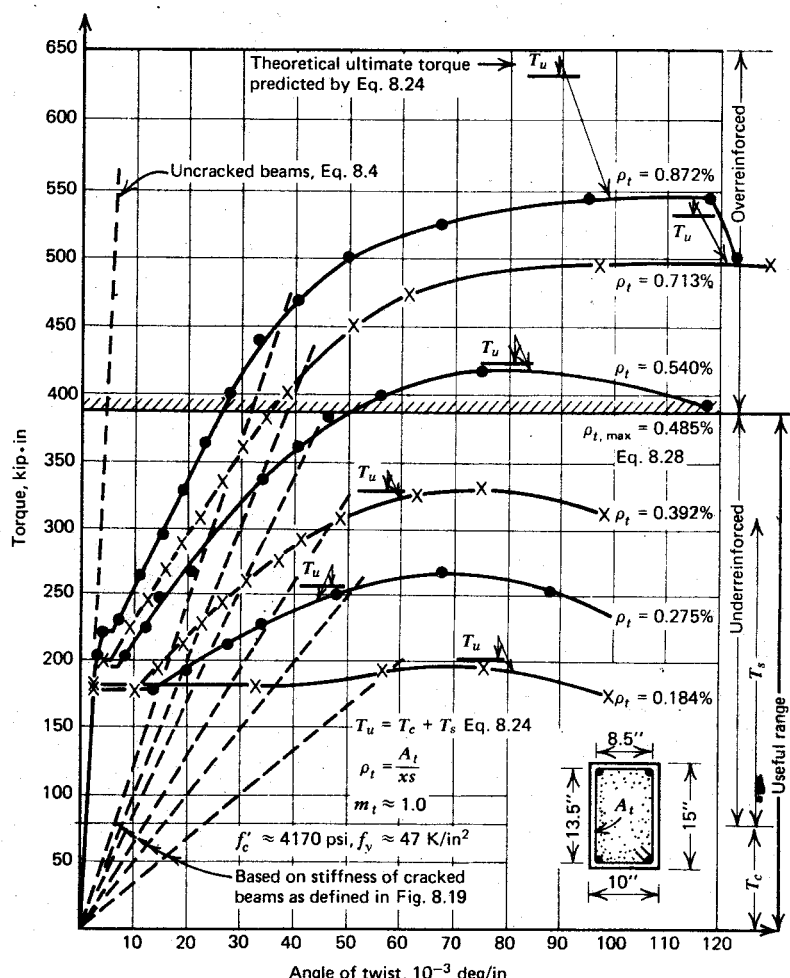


Fig. 8.18. Typical torque-twist relationships for beams tested by Hsu.^{8,20}

concrete compression strains and steel tensile strains in the longitudinal and transverse directions determine the angle of twist. The deformations of the space truss (Fig. 8.11) or the equivalent hollow section can be derived the same way as the shear deformations of the equivalent truss in an ordinary beam, outlined in Chapter 7.

The core of a solid section does not contribute significantly to torsional resistance; therefore, the solid section in the cracked state may be replaced by a hollow section for the purpose of determining its stiffness. Rahlwes, who compared the theoretical torsional stiffnesses of rectangular sections in the cracked and uncracked state,^{8.30} found that the aspect ratio y/x was not a significant variable in determining the loss of stiffness caused by cracking. Experimental beams with the same core area ($x_0 y_0 = \text{constant}$) and with aspect ratios $1 \leq y/x \leq 6$, exhibited approximately the same stiffness at all stages of cracking.^{8.29} The stiffness of the space truss depends largely on the torsional steel content. The more important assumptions and the results of the analytical study of Rahlwes,^{8.30} for the common case of equal transverse and longitudinal steel content (i.e., $m_t = 1$), are present in Fig. 8.19.

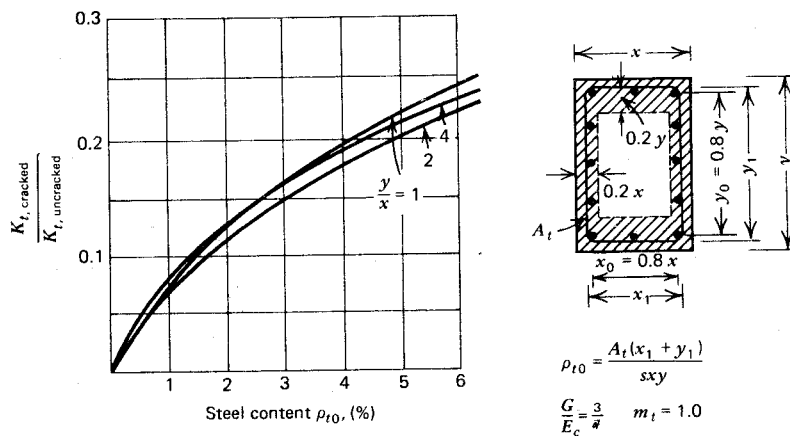


Fig. 8.19. The torsional stiffness of diagonally cracked rectangular and hollow reinforced concrete beams.^{8.30}

The effect of transverse and longitudinal torsion reinforcement on twisting has also been considered by Lampert.^{8.31} For beams of practical dimensions, his findings agree satisfactorily with theoretical results derived from a thin-walled tube analogy. Equations based on this analogy, suggested by Collins,^{8.31} may be derived as follows. When we compare Eq. 8.21, defining

the torque sustained by the space truss, and Eq. 8.9b, giving the shear flow in a tube, the similarity in form as well as in behavior is easily recognised. This suggests that for the purpose of stiffness predictions the space truss could be replaced by a tube of similar dimensions, having a wall thickness of

$$h = \sqrt{\left[\frac{A_t}{s} \frac{A_l}{2(x_0 + y_0)} \right]} \quad (8.34)$$

This is the root mean square of the transverse and longitudinal torsional steel contents. Using the ratio m_t defined in Eq. 8.19, this hypothetical thickness becomes

$$h = \frac{A_t}{s} \sqrt{m_t} \quad (8.34a)$$

Thus the equivalent polar moment of inertia of the tube can be expressed from Eq. 8.11b as

$$C_{0, \text{cracked}} = \frac{4A_0^2 h}{p} = \frac{4(x_0 y_0)^2}{2(x_0 + y_0)} \frac{A_t \sqrt{m_t}}{s} \quad (8.35)$$

By making the approximation $G = \frac{1}{2}E_s$, the corresponding torsional stiffness of a diagonally cracked reinforced concrete beam becomes

$$K_{t, \text{cracked}} = \frac{E_s (x_0 y_0)^2 A_t}{l(x_0 + y_0) s} \sqrt{m_t} \quad (8.36)$$

Properties of the concrete do not enter Eq. 8.36. In usable beams, which need to be underreinforced for torsion, the concrete deformation is insignificant and the twist is largely governed by the elongation of the reinforcing bars.

Using the stiffness information of Fig. 8.19, the theoretical torque-twist behavior of some rectangular beams tested by Hsu^{8.20} has been plotted (by dashed lines) on the experimental torque-twist relationship for the beams in Fig. 8.18. It appears that good stiffness agreement exists for most usable beams at an angle of twist of 45×10^{-3} deg/in, which occurs at about 93% of the ultimate torque. Once a beam has cracked, when the load is reapplied from zero, the torque-twist relationship is close to linear within the elastic range (i.e., similar to that shown by the dashed lines in Fig. 8.18).

The relationship between torsional stiffness and steel content, shown in Fig. 8.19 or given by Eq. 8.36, may also be useful in checking the angle of twist to be expected under full service load conditions. This is illustrated in Example 8.4.

Further refinement of stiffness calculations in the cracked state is not warranted because several other factors (anchorage slip of horizontal bars

and stirrups in particular, and the effects of flexural cracking and shear forces on torsional stiffness) cannot yet be adequately allowed for.

Example 8.4

Determine the maximum angle of twist to be expected under full service load conditions for the beam of Example 8.1 (Fig. 8.14).

Solution

$$G = \frac{3}{7}E_c = 0.43 \times 57000\sqrt{f'_c} = 1470 \text{ kip} \cdot \text{in}^2, \quad \text{Eqs. 7.37 and 2.1}$$

$$C = \beta_t x^3 y = 0.195 \times 16^3 \times 24 = 19,170 \text{ in}^4,$$

from Fig. 8.3 and Eq. 8.3

The inclusion of part of the flanges of the *T* beam, Eq. 8.5, would increase the torsional stiffness by only 5%. The contribution of the flanges will therefore be neglected.

The angle of twist is

$$\theta_t = \frac{1}{GC} \int_0^z T(z) dz, \quad \text{Eq. 8.2}$$

The beam is subjected to a uniformly distributed transverse moment, m_{u1} , when one-half the flange width is subjected to live load; therefore the maximum torsion at the supports of the beam is $T(0) = \frac{1}{2}m_{u1}l$. Hence the torque at any section at distance z from the support is

$$T(z) = T(0) - m_{u1}z = m_{u1}\left(\frac{l}{2} - z\right)$$

whence

$$GC\theta_t = \int_0^z m_{u1}\left(\frac{l}{2} - z\right) dz = \frac{m_{u1}}{2}(lz - z^2)$$

The maximum angle of twist will occur at midspan, when $z = l/2$, therefore

$$GC\theta_{t, \max} = \frac{m_{u1}l^2}{8}$$

For a uniformly distributed live load of 150 lb/ft² on one side of the 10 ft wide beam of 40 ft span, the transverse moment per inch length of beam is

$$m_{u1} = 5 \times 0.150 \times 2.5 \times \frac{12}{12} = 1.875 \text{ kip} \cdot \text{in/in}$$

Therefore, we write

$$\theta_{t, \max} = \frac{1.875 \times (40 \times 12)^2}{8 \times 1470 \times 19,170} = 1.916 \times 10^{-3} \text{ rad}$$

assuming that the beam has not cracked.

When allowing for cracking, the reduction factor from Fig. 8.19 is obtained thus:

No. 5 stirrups are provided at 4 in centers. Hence

$$\rho_{t,0} \% = \frac{2 \times 0.306 \times (12.5 + 20.5)}{4 \times 16 \times 24} 100 = 1.31 \%$$

From Fig. 8.19

$$\frac{K_{t, \text{cracked}}}{K_{t, \text{uncracked}}} = 0.09$$

$$\begin{aligned} \therefore \theta_{t, \max(\text{cracked})} &= \frac{0.001916}{0.09} = 0.022 \text{ rad} \\ &= 1.22^\circ \end{aligned}$$

Alternatively, using Eq. 8.36 and the information given in Example 8.2, and putting $E_s = 29,000 \text{ kip/in}^2$,

$$\begin{aligned} GC_{0, \text{cracked}} &= \frac{29,000(11 \times 19)^2 \times 0.63}{(11 + 19) \times 12} \sqrt{1.524} \\ &= 2.737 \times 10^6 \text{ kip} \cdot \text{in}^2 \end{aligned}$$

Therefore from proportions

$$\begin{aligned} \theta_{t, \max(\text{cracked})} &= \frac{GC}{GC_{0, \text{cr}}} 1.916 \times 10^{-3} \\ &= \frac{1470 \times 19,170 \times 1.916 \times 10^{-3}}{2.737 \times 10^6} \\ &= 0.0197 \text{ rad} = 1.13^\circ \end{aligned}$$

This is of the same order as the angle obtained from Fig. 8.19. The torsion increases linearly from the midspan toward the supports, and the beam is not likely to have diagonal cracks in its middle portion. Therefore, the foregoing result will overestimate the

maximum order of tilt the designer would have to allow for. The computed twist indicates a possible transverse fall of 1 in 50 across the midspan of the bridge, a value that is not likely to be acceptable.

8.9 TORSION IN STATICALLY INDETERMINATE STRUCTURES

The conclusions of the previous section on torsional stiffness are most relevant to the analysis of statically indeterminate structures. When one member offers restraint by virtue of its torsional stiffness, the ensuing torsion will be greatly affected by the value of that stiffness. Because the reduction of stiffness, owing to diagonal cracking, is so much greater in torsion than it is in flexure, the effect of cracking on stiffness should be taken into account when the bending moments and torques are determined in a statically indeterminate structure.

When ductile failure mechanisms are assured, great latitude exists in adopting a statically admissible moment pattern. Torque-twist characteristics of members underreinforced for torsion are ductile (see Fig. 8.18); therefore, virtually any value of stiffness between the theoretical maximum, corresponding with the uncracked state, and zero would lead to the same ultimate load on the structure. However, considerations of crack width control at service loads suggest that an analysis based on the stiffness in the cracked state for both flexure and torsion, as appropriate, would lead to the most satisfactory moment pattern under the service loading.

It has been observed^{8,31} that in spandrel beams supporting secondary floor beams in flexure and torsion (similar to the arrangement in Fig. 8.2c), about the same amount of twist occurs at the service load level regardless of the amount of torsion steel provided. It is evident that this twist will generate high torques in spandrels with more torsion reinforcement. Satisfactory agreement with values based on the properties of cracked members was observed.^{8,31}

A suitable design procedure for statically indeterminate structures would avoid the introduction of high torques, resulting in the use of minimum torsion reinforcement. In any case, large torques can be sustained only at the expense of large twists, which seldom can be supplied under service conditions. It appears that for most situations the assumption of zero torsional stiffness can be made.^{8,31} This greatly simplifies analysis. However, it is important to provide at least minimum closely spaced longitudinal and transverse web reinforcement in the members subjected to torsion, to ensure that the member is able to twist in a ductile manner without displaying excessive crack widths at service load.^{8,31}

8.10 REFERENCES

- 8.1 *Torsion of Structural Concrete*, American Concrete Institute, Detroit, Special Publication 18, 1968, 505 pp.
- 8.2 "Building Code Requirements for Reinforced Concrete, (ACI 318-71)," American Concrete Institute, Detroit, 1971, 78 pp.
- 8.3 K. G. Tamberg, "Aspects of Torsion in Concrete Structure Design"; pp. 7-68 of Ref. 8.1.
- 8.4 E. P. Popov, *Introduction to Mechanics of Solids*, Prentice-Hall, Englewood Cliffs, N.J., 1968, 571 pp.
- 8.5 C. Bach, *Elastizität und Festigkeit*, Springer, Berlin, 1911.
- 8.6 D. J. Victor, "Effective Flange Width in Torsion," *Journal ACI*, Vol. 68, No. 1, January 1971, pp. 42-46.
- 8.7 A. Nádai, *Plasticity*, McGraw-Hill, New York, 1931, 349 pp.
- 8.8 P. F. Walsh, M. P. Collins, F. E. Archer, and A. S. Hall, "Experiments on the Strength of Concrete Beams in Combined Flexure and Torsion," UNICIV Report No. R-15, February 1966, University of New South Wales, Kensington, Australia, 59 pp.
- 8.9 D. J. Victor, "Reinforced Concrete *T*-Beams Without Stirrups Under Combined Moment and Torsion," *Journal ACI*, Vol. 65, No. 1, January 1968, pp. 29-36.
- 8.10 U. Ersoy and P. M. Ferguson, "Concrete Beams Subjected to Combined Torsion and Shear—Experimental Trends"; pp. 441-460 of Ref. 8.1.
- 8.11 M. S. Mirza and J. O. McCutcheon, "Ultimate Strength Design of Reinforced Concrete Beams Subjected to Combined Loadings," *Transactions of the Engineering Institute of Canada*, Vol. 12, No. A-3, March 1969, pp. I-VIII.
- 8.12 T. T. C. Hsu, "Torsion of Structural Concrete—Plain Concrete Rectangular Sections"; pp. 203-238 of Ref. 8.1.
- 8.13 A. H. Mattock, "How to Design for Torsion"; pp. 469-495 of Ref. 8.1.
- 8.14 L. E. Farmer and P. M. Ferguson, "T-Beams Under Combined Bending, Shear and Torsion," *Journal ACI*, Vol. 64, No. 11, November 1967, pp. 757-766.
- 8.15 U. Ersoy and P. M. Ferguson, "Behavior and Strength of Concrete *L*-Beams Under Combined Torsion and Shear," *Journal ACI*, Vol. 64, No. 12, December 1967, pp. 793-801.
- 8.16 E. Rausch, *Drillung (Torsion), Schub und Scheren im Stahlbetonbau*, Deutscher Ingenieur-Verlag, Berlin, 1953, 168 pp.
- 8.17 P. Lampert, "Bruchwiderstand von Stahlbetonbalken unter Torsion (und Biegung)," Bericht No. 26, Institut für Baustatik, ETH Zürich, 1970, 189 pp.
- 8.18 CEB-FIP, *International Recommendations for the Design and Construction of Concrete Structures*, Comité Européen du Béton, Paris, June 1970. (English edition published by Cement and Concrete Association, London, 80 pp.)
- 8.19 P. Lampert and M. P. Collins, "Torsion, Bending and Confusion—An Attempt to Establish the Facts," *Journal ACI*, Vol. 69, No. 8, August 1972, pp. 500-504.
- 8.20 T. T. C. Hsu, "Torsion of Structural Concrete—Behaviour of Reinforced Concrete Rectangular Members"; pp. 261-306 of Ref. 8.1.
- 8.21 D. Mitchell, P. Lampert, and M. P. Collins, "The Effects of Stirrup Spacing and Longitudinal Restraint on the Behaviour of Reinforced Concrete Beams Subjected to Pure Torsion," Publication 71-22 University of Toronto, Department of Civil Engineering, October 1971, 75 pp.

- 8.22 P. Lampert and B. Thürlmann, "Torsionsversuche an Stahlbetonbalken," Bericht No. 6506-2, Institut für Baustatik, ETH Zürich, June 1968, 101 pp.
- 8.23 P. Zia, "Torsion Theories for Concrete Members"; pp. 103-132 of Ref. 8.1.
- 8.24 H. M. Liao and P. M. Ferguson, "Combined Torsion in Reinforced L-Beams with Stirrups," *Journal ACI*, Vol. 66, No. 12, December 1969, pp. 986-993.
- 8.25 "Tentative Recommendations for the Design of Reinforced Concrete Members to Resist Torsion," Reported by ACI Committee 438, *Journal ACI*, Vol. 66, No. 1, January 1969, pp. 1-23; No. 7, July 1969, pp. 576-588.
- 8.26 M. P. Collins, P. F. Walsh, F. E. Archer, and A. S. Hall, "Reinforced Concrete in Torsion," UNICIV Report No. R-31, March 1968, University of New South Wales, Kensington, Australia, 339 pp.
- 8.27 H. J. Cowan and I. M. Lyalin, *Reinforced and Prestressed Concrete in Torsion*, Edward Arnold, London, 1965, 138 pp.
- 8.28 D. W. Kirk and S. D. Lash, "T-Beams Subject to Combined Bending and Torsion," *Journal ACI*, Vol. 68, No. 2, February 1971, pp. 150-159.
- 8.29 F. Leonhardt, "Shear and Torsion in Prestressed Concrete," *European Civil Engineering*, Vol. 4, 1970, pp. 157-181.
- 8.30 K. Rahlwes, "Zur Torsionssteifigkeit von Stahlbetonrechteckquerschnitten," *Beton und Stahlbetonbau*, Vol. 65, No. 9, September 1970, pp. 226-228.
- 8.31 M. P. Collins and P. Lampert, "Redistribution of Moments at Cracking—The Key to Simpler Torsion Design?" University of Toronto, Department of Civil Engineering, Publication '1-21, February 1971, 49 pp.

Bond and Anchorage

9.1 INTRODUCTION

9.1.1 Basic Considerations

Since external load is very rarely applied directly to the reinforcement, steel can receive its share of the load only from the surrounding concrete. "Bond stress" is the name assigned to the shear stress at the bar-concrete interface which, by transferring load between the bar and the surrounding concrete, modifies the steel stresses. This bond, when efficiently developed, enables the two materials to form a composite structure. The attainment of satisfactory performance in bond is the most important aim of the detailing of reinforcement in structural components.

Bond forces are measured by the rate of change in the force in reinforcing bars. Bond stress will not exist unless the steel stresses change between any two sections. Bond stress u , customarily defined as a shear force per unit area of bar surface, is given by

$$u = \frac{q}{\Sigma o} = \frac{\Delta f_s A_b}{\Sigma o} = \frac{d_b}{4} \Delta f_s \quad (9.1)$$

where q = change of bar force over unit length

Σo = nominal surface area of a bar of unit length

d_b = nominal diameter of the bar

Δf_s = change of steel stress over unit length

A_b = area of bar

Bond strength was a more serious problem when only plain reinforcing bars were used. Bars with a deformed surface provide an extra element of bond strength and safety. On the other hand, the behavior of deformed bars, in particular the introduction of high-strength steels and large diameter bars, presented some new problems. This has necessitated a reexamination of the conventional considerations of bond.^{9,1}

Since existing code requirements are entirely empirical, the full background

to numerous design rules is not discussed in this chapter. However, the designer must be aware of the aspects of bond and anchorage that can critically affect structural behavior. Therefore, these are examined in some depth to enable the designer to effectively detail reinforcement.

Several problems in bond that require clarification, have been reported by ACI Committee 408.^{9,2} The report includes a good bibliography.

Bond stresses in reinforced concrete members arise from two distinct situations: from the anchorage of bars, and from the change of bar force along its length, due to change in bending moment along the member.

9.1.2 Anchorage or Development Bond

A bar must extend a distance l_d beyond any section at which it is required to develop a given force, the distance l_d being required to transmit the bar force to the concrete by bond. If the average bond stress u , assumed to be uniformly distributed over this length, is specified, then considerations of equilibrium (Fig. 9.1a) yield the following relationship:

$$T = A_b f_s = u \Sigma o l_d \quad (9.2a)$$

Hence the development length becomes

$$l_d = \frac{d_b}{4u} f_s \quad (9.2b)$$

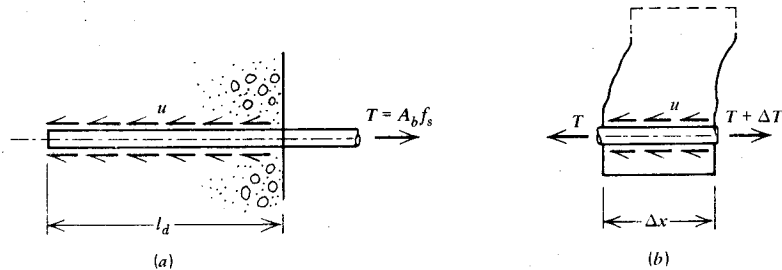


Fig. 9.1. The generation of anchorage and flexural bond.

Some codes specify safe values for the anchorage bond stress u , permitting the development length to be calculated from Eq. 9.2b. The ACI code^{9,3} prescribes the minimum development length l_d for various design/situations. The ACI recommendations for l_d are given in Section 9.4.

9.1.3 Flexural Bond

In Chapter 7 it was shown that bond forces ΔT are developed along the flexural reinforcement in the shear span of any beam (see Figs. 7.7 and 7.14). If it is assumed that the bond stresses u are uniformly distributed between any two sections, close to each other, the equilibrium of a short length of bar (Fig. 9.1b) requires that $\Delta T = u \Sigma o \Delta x$. However, if ideal beam action is to take place, as discussed in Section 7.3.3, the internal tension force T must vary at the same rate as the external bending moment M . (See also Eq. 7.10.) Therefore,

$$\Delta T = \frac{\Delta M}{jd} = \frac{V}{jd} \Delta x$$

hence

$$u = \frac{V}{jd\Sigma o} \quad (9.3)$$

This equation indicates that when the rate of change of external bending moment (i.e., the shear force) is high, the flexural bond stress can also exhibit high intensity. However, Eq. 9.3 grossly oversimplifies the situation, and it does not even approximately predict the magnitude of the actual bond stress. This is because the presence of cracks in the concrete at discrete intervals along a member results in additional bond stresses due to the tension carried by the concrete between the cracks (see Fig. 6.22). Even when the shear force is zero (region of constant bending moment), bond stress will be developed. It has been observed, however, that provided sufficient anchorage length is available for the bars, failure originating from flexural bond stress does not occur. Flexural bond considerations require the anchorage length to be checked in regions of members where the bending moment is zero (at simple supports and at points of contraflexure). In such regions the area of tension steel may be small and the shear force large, resulting in high flexural bond stresses. The ACI code^{9.3} recommendations for anchorage to satisfy flexural bond conditions are given in Section 9.5.

9.2 THE NATURE OF BOND RESISTANCE

9.2.1 Basic Features of Bond Resistance

The bond resistance of plain bars is often thought of as chemical adhesion between mortar paste and bar surface. However, even low stresses will cause sufficient slip to break the adhesion between the concrete and the steel. Once slip occurs, further bond can be developed only by means of friction and by the

wedging action of small dislodged sand particles between the bar and the surrounding concrete. The frictional resistance depends on the surface conditions of the steel. Figure 9.2, taken from Rehm's work,^{9,4} displays typical surface profiles for plain round bars under different conditions of rusting. The variation in pitting is significant, and it is not surprising that most designers prefer to use steel in a mildly rusted condition. When plain round bars are subjected to standard load tests, failure occurs when the adhesion and frictional resistance is overcome, and the bars usually pull out from the encasing concrete.

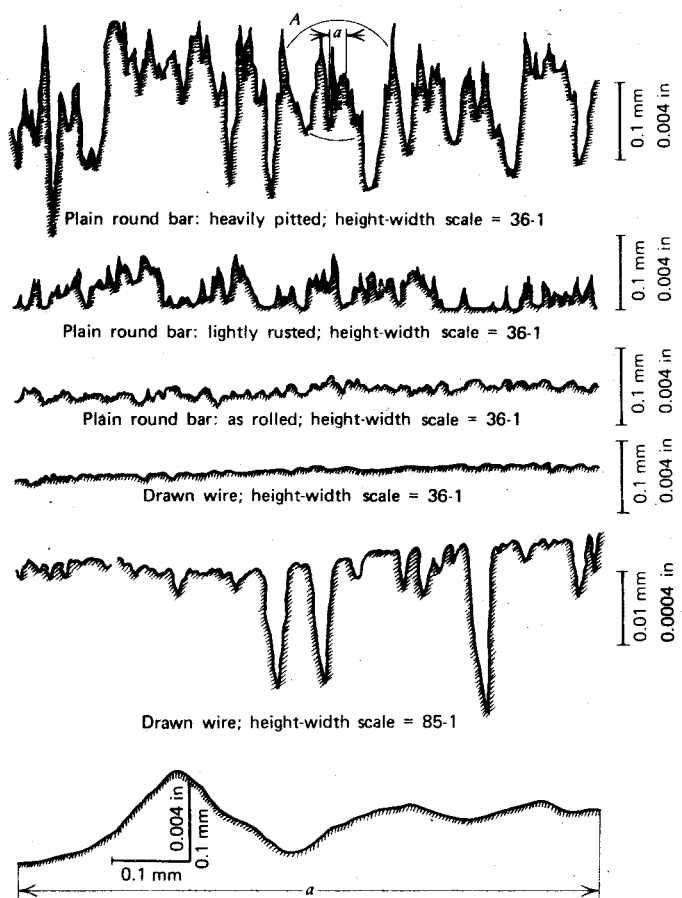


Fig. 9.2. The magnified surface of plain reinforcing bars.^{9,4}

Deformed bars have greatly increased bond capacity because of the interlocking of the ribs with the surrounding concrete. The bond strength developed between two ribs of a bar (see Fig. 9.3) is associated with the following stresses:

1. Shear stresses v_a , developed through adhesion along the surface of the bar.
2. Bearing stresses f_b , against the face of the rib.
3. Shear stresses v_c , acting on the cylindrical concrete surface between adjacent ribs.

The relation between these stresses and the force to be transferred to the concrete by bond over a short length of bar between centers of ribs can be obtained from a simple equilibrium requirement as follows:

$$\Delta T = \pi d_b'(b + c)v_a + \pi \frac{d_b''^2 - d_b'^2}{4} f_b \approx \pi d_b'' c v_c \quad (9.4)$$

where each term can be identified in Fig. 9.3.

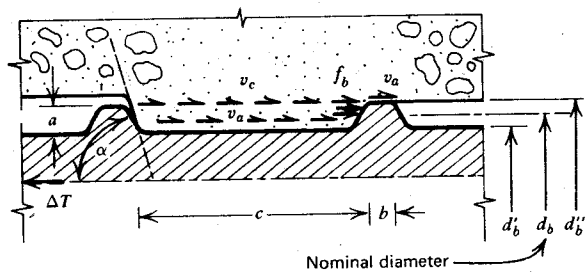


Fig. 9.3. The stresses between two ribs of a deformed bar.

As the load is being increased, the adhesion along the bar surface inevitably breaks down. The remaining frictional shear strength is very small in comparison with the bearing strength developed around the ribs; therefore v_a can be ignored for practical purposes. The relationship between the remaining two important components of bond force development, f_b and v_c , can be simplified as follows:

1. Since $b \approx 0.1c$, the rib spacing is approximately c .
2. Since $a \approx 0.05d_b'$, the bearing area of one rib is

$$\pi \frac{d_b''^2 - d_b'^2}{4} \approx \pi d_b a$$

where d_b is the nominal diameter of the bar.

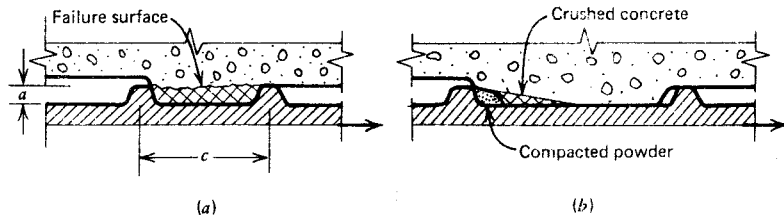


Fig. 9.4. Failure mechanisms at the ribs of deformed bars. (a) $a/c > 0.15$. (b) $a/c < 0.10$.

Hence from Eq. 9.4 we have $\Delta T = \pi d_b a f_b \approx \pi d_b c v_c$; therefore,

$$v_c \approx \frac{a}{c} f_b \quad (9.5)$$

Rehm^{9,4} succeeded in relating several aspects of the bond problem to the geometric parameter a/c . He found the most satisfactory performance of a bar embedded in concrete over the short length c when a/c was in the vicinity of 0.065.* When the ribs are high and spaced too closely, the shear stress v_c will govern the behavior and the bar will pull out. When the rib spacing is larger than approximately 10 times the rib's height, the partly crushed concrete may form a wedge in front of the rib, and failure is normally brought about by splitting of the surrounding concrete. The concrete in front of the rib can sustain a bearing pressure several times the cylinder crushing strength because of the confined condition of the concrete. The two types of failure mechanism, associated with the rib, are illustrated in Fig. 9.4. Clearly the geometry of deformed bars must be such that a shear pullout failure (Fig. 9.4a) cannot occur. The factors that may affect the ultimate capacity and service behavior of deformed bars, which conform with the conditions in Fig. 9.4b, are examined in subsequent sections.

One of the most important aspects of bond performance is its effect on crack development. This is closely related to the bond slip characteristics of a particular type of bar in various situations. Generally speaking, the smaller the slip associated with a usable bond force, the better the quality of the bond.

9.2.2 The Position of Bars with Respect to the Placing of the Surrounding Concrete

The load–bond slip relationship for deformed bars is primarily affected by the behavior of the concrete immediately in front of the ribs. The quality of

* The deformation requirements of ASTM A 305 are such^{9,6} that $0.057 < a/c < 0.072$.

the concrete in this region depends on its relative position when cast. In connection with dowel action, attention was drawn in Chapter 7 to the effect of water gain and sedimentation under reinforcing bars and under coarse aggregate particles. As a result, a soft and spongy layer of concrete can form under the ribs. When bearing stresses of high intensity are to be developed against such a soft zone, large slips may occur. Figure 9.5 shows how three bars are affected in different ways by a porous layer of concrete, even though all tend toward the development of the same ultimate load. In these tests^{9.4} the computed bearing stress in front of one rib was in excess of 7 times the compressive cube strength of the concrete.

The effect of casting position on bond is even more severe for plain round bars. Figure 9.6 indicates that the ultimate bond strength is drastically reduced in the case of horizontal bars as compared with vertical bars.^{9.4} The upper curves of each pair was obtained for heavily rusted and pitted bars. The lower curve of each pair is for smooth surfaced bars.

It is to be expected that the top bars of a beam will have poorer bond qualities than bottom bars, since the water and air gain will be greater under top bars. In addition, the relative downward movement of the surrounding concrete, caused by settlement of the fresh mixture, can be large. The amount of settlement that occurs will depend on the extent of bleeding of the fresh concrete and the rate at which water is permitted to escape from the form-work. Welch and Patten studied this effect and compared the bond performance of bars surrounded by concrete in leaky timber moulds and in well-sealed steel moulds.^{9.5} In the latter they also delayed the placing of the concrete by 40 minutes. Their results (Fig. 9.7) demonstrate the profound effect of settlement on bond, particularly for top bars. The ACI code^{9.3} recognizes this phenomenon by requiring 40% excess development length for top-cast deformed bars.

9.2.3 Bar Profiles and Surface Conditions

Variation in the angle between the face of the rib and the axis of the bar (angle α in Fig. 9.3) does not seem to affect the bond strength provided this angle is more than 70° . When the angle α is between 45 and 70° , the deformations must be reversed in direction on each side or on opposite sides of the bar.^{9.6} Special pullout tests, using bar specimens with a single rib, indicated that if the angle α is greater than 40° , the friction between the rib face and the concrete is sufficient to restrict slip along this interface.^{9.7} Then the slip of the bar is likely to be mainly attributable to the crushing of the concrete in front of the bar ribs (see Fig. 9.4b). On the other hand, if the angle α is small and the surface is smooth, slip can occur along the face of the rib, and the rib tends to push the concrete away from the bar.^{9.8} This wedging action can be a major cause of longitudinal splitting along the bar.

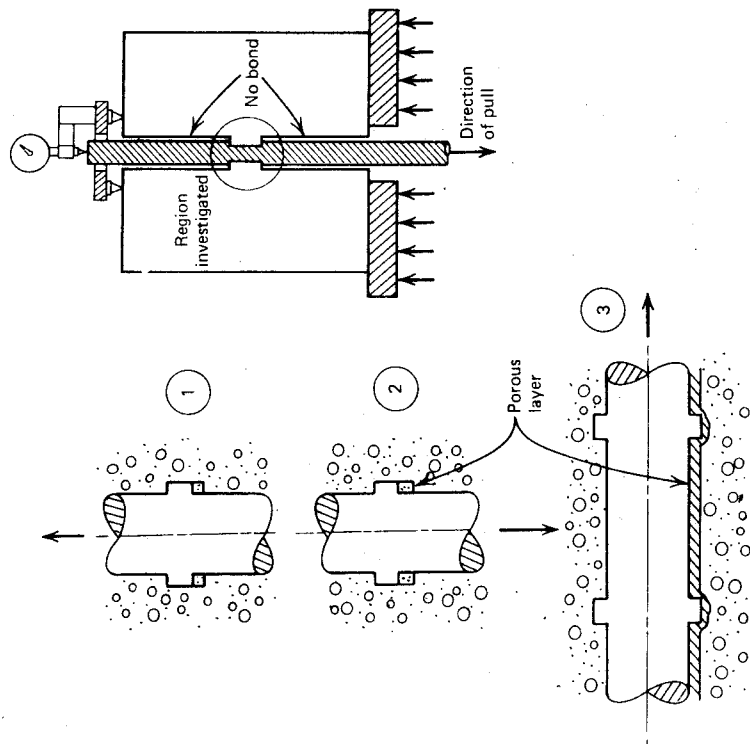
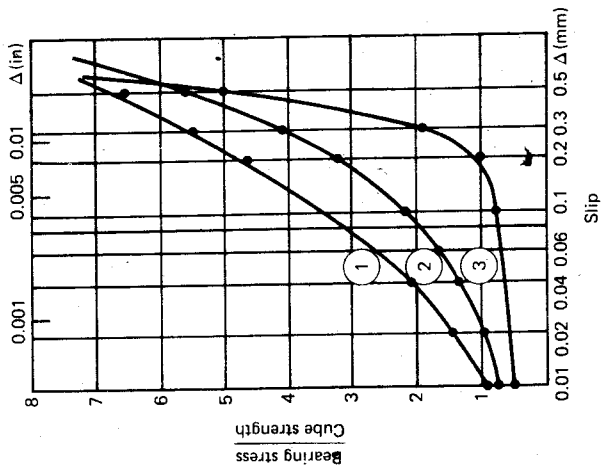


Fig. 9.5. The influence of casting positions on bond performance.^{9.4}

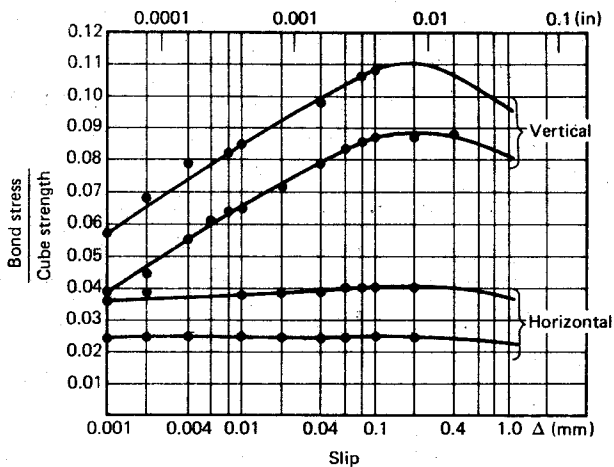


Fig. 9.6. The load-slip relationship for a No. 5 (16 mm) plain round bar in different casting positions.^{9.4}

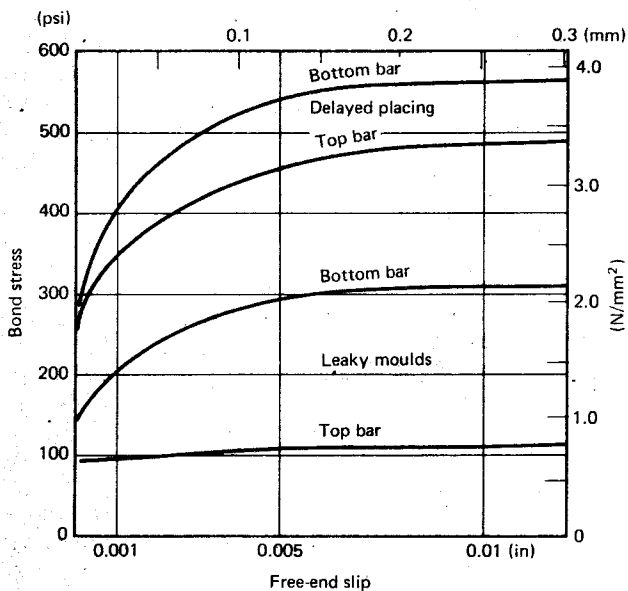


Fig. 9.7. Bond stress-slip relationship for plain round bars, as affected by the settlement of fresh concrete.^{9.5}

The bond characteristics of deformed bars do not appear to be adversely affected by varying degrees of surface rust or ordinary mill scale, provided the unit weight of a cleaned piece of bar meets the minimum requirements of standard specifications. Kemp et al^{9,9} found that it is not necessary to clean or wipe the bar surface before using it in concrete construction. For a given environment causing rust, the thickness of rust will be about the same for all bar sizes. Therefore, larger diameter bars, which have higher ribs, will be less affected by rust.

9.2.4 The State of Stress in the Surrounding Concrete

In the previous sections we examined the conditions prevailing in the immediate vicinity of one rib of a deformed bar. To enable the full strength of a bar to be developed, bond forces across numerous adjacent ribs need to be transferred. Therefore, the stress conditions in the surrounding concrete fluctuate along an embedded bar and affect the bond performance. The bond or anchorage strength of a bar cannot be obtained from the simple summation of the bond strength of a given number of individual ribs.

The stresses in the concrete surrounding a deformed bar lead to cracks and deformations of the concrete, as illustrated in Fig. 9.8. The bond stresses u ,

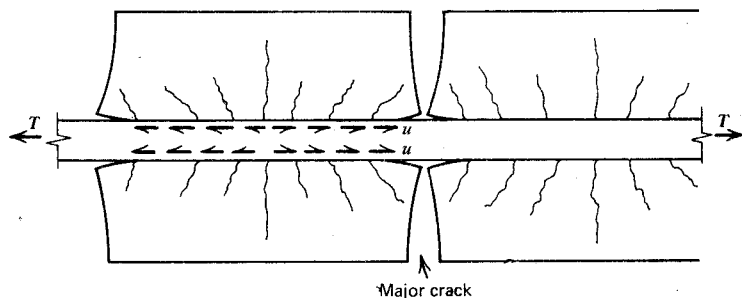


Fig. 9.8. Deformed concrete between transverse cracks of a tension member.^{9,8}

transmitted to the concrete, subjects the cover thickness of concrete to eccentric tension. The deformations of the concrete resulting from the stresses so generated tend to pull the concrete away from this steel in the vicinity of the major crack. The tensile strength of the adhesive bond between steel and the mortar is then reached, and the surrounding concrete separates from the steel. Also numerous internal secondary cracks can form which may not propagate to the external surface of the concrete. In plain bars the bond stresses can be expected to disappear completely where separation between

steel and concrete occurred. With deformed bars, bond forces have to be transmitted in this area solely by rib bearing. This is indicated in Fig. 9.9. Some of the tension in the concrete is lost when a primary crack opens near the surface of the bar. By injecting ink between the bar and the surrounding concrete, Goto^{9,10} found sloping secondary cracks radiating from each rib (see Fig. 9.9). He also verified experimentally the separation between the bar and the concrete in the vicinity of the primary crack.

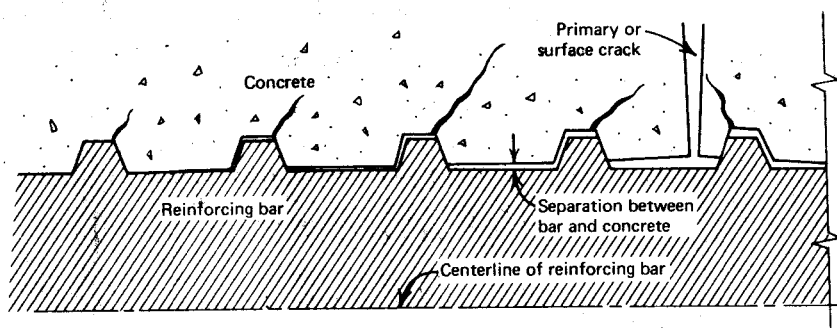


Fig. 9.9. Section through reinforcing bar and concrete, showing separation that occurs near a primary crack.^{9,8}

When the concrete separates itself from around a bar at a primary crack, the circumference of the concrete surface, previously in contact with the bar, increases; hence circumferential tensile stresses are induced. These stresses can lead to longitudinal splitting cracks. Lutz and Gergely determined the likely magnitude of these stresses from finite element studies of corresponding models.^{9,8}

When the ultimate capacity in bond transfer is being approached, there is crushing in front of the ribs. The compacted concrete powder, extending in front of the rib at a distance of up to three times the rib height, forms a flat wedge (Fig. 9.4b), and this tends to push the concrete further away from the bar. Hence additional circumferential tensile stresses are generated which may bring about a splitting failure.

The concrete surrounding a particular bar may be subjected to stresses in addition to those generated by bond, because it participates in other structural actions. At the intersection of beams in building frames, compression or tension is induced transversely to the bars. Similarly, transverse tension may be induced in the concrete around the top bars of beams that

support continuous slabs. Such transverse tensile stresses could lead to early cracking along principal bars and could adversely affect their bond performance. Conversely, transverse compression can provide beneficial confinement to embedded bars.

9.2.5 The Splitting Failure

Where adequate embedment length is provided in a large mass of concrete, it is not possible to produce a bond (pullout) failure with standard deformed bars. Rather, the bar will fracture at its loaded end. In most structural components, however, the area of concrete surrounding a bar or group of bars is relatively small. In such a situation the common mode of failure is splitting, since the surrounding concrete cannot sustain the circumferential, tensile stresses.

A particularly severe situation arises in the shear span of beams, where splitting can be induced along the flexural reinforcement by the combination of the following events:

1. Circumferential tensile stresses generated in the vicinity of each flexural crack.
2. Circumferential or transverse tensile stresses induced by wedging action of the deformations and by the compressed concrete at the ribs (Fig. 9.4b) when large bond forces need to be transferred.
3. Transverse tensile stresses resulting from dowel action of the flexural reinforcement. This event is associated with shear displacement along diagonal cracks. Gergely found that dowel forces reduce the bond strength if no confining pressure is present, resulting in larger slips for a given load.^{9.7} Beams with splitting cracks caused by dowel action were shown in Fig. 7.8.

A group of bars, particularly when closely spaced, will create a more adverse situation than a single bar. This is illustrated in Fig. 9.10 which presents typical observed splitting cracks.^{9.1}

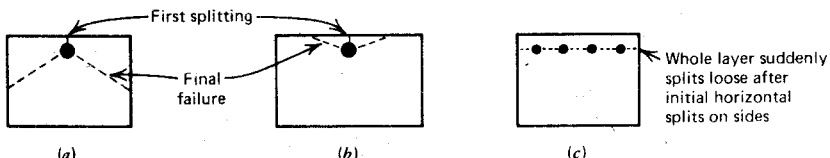


Fig. 9.10. Splitting cracks at failure.^{9.1} (a) Typical case. (b) In very wide beams. (c) With closely spaced bars.

9.2.6 Confinement

The widening of splitting cracks can be restricted if the concrete that surrounds a bar can be confined. In certain areas, such as at the simply supported ends of beams, transverse compression is normally available from the reaction force. Transverse compression is beneficial to the anchorage of reinforcement. More attention is paid to this subject when various aspects of the detailing of reinforcement are discussed in Chapter 13.

Increased concrete cover has been found to produce some increased resistance against splitting. However, the improved bond performance is not proportional to the additional cover thickness. For large size bars, the beneficial effect is not very significant.^{9.11} For these bars, as a rule, the effect on the formation and widths of cracks under service load condition is the governing criterion in selecting an appropriate value for allowable average bond stresses. Extra cover does not provide protection against excessive surface crack width^{9.11} (see Chapter 10). Medium sized top bars appear to benefit more from added cover,^{9.12} as Fig. 9.11 indicates. When dowel action affects bond, the influence of cover is eliminated.

Stirrups, particularly when closely spaced, prevent the opening of cracks that form along embedded bars and enable greater bond forces to be transmitted. In many situations (Fig. 9.10c) this is only possible if shearing stresses, by means of aggregate interlock, are transmitted across splitting cracks. Stirrups cannot prevent splitting cracks, which always form when large bars (e.g., No. 11; 35.8 mm diameter) are used in beams, but they enable friction to be transferred along cracks as outlined in Chapter 7. Stirrups do not appear to improve crack width control,^{9.11} but they ensure that a more ductile type of bond failure occurs.

Special reinforcement in the form of spirals or hoops may be required when splices are situated in critical zones. The performance of such reinforcement can be assessed using the concept of interface shear transfer (see Section 7.8).

The aim of confinement by means of transverse compression or transverse reinforcement is to prevent a failure along a potential splitting crack and to enforce, if necessary, a shear failure (Fig. 9.4a), which is associated with the maximum attainable bond strength. Larger bars benefit more from confinement than smaller ones.

9.2.7 Repeated and Cyclic Reversed Loading

When the tensile force in a bar is increased and the adhesive bond between the steel and the concrete is broken, some frictional slip takes place before the full bearing capacity at a rib is mobilized. After removal of the load from a bar, negative frictional resistance is developed, accounting for some residual

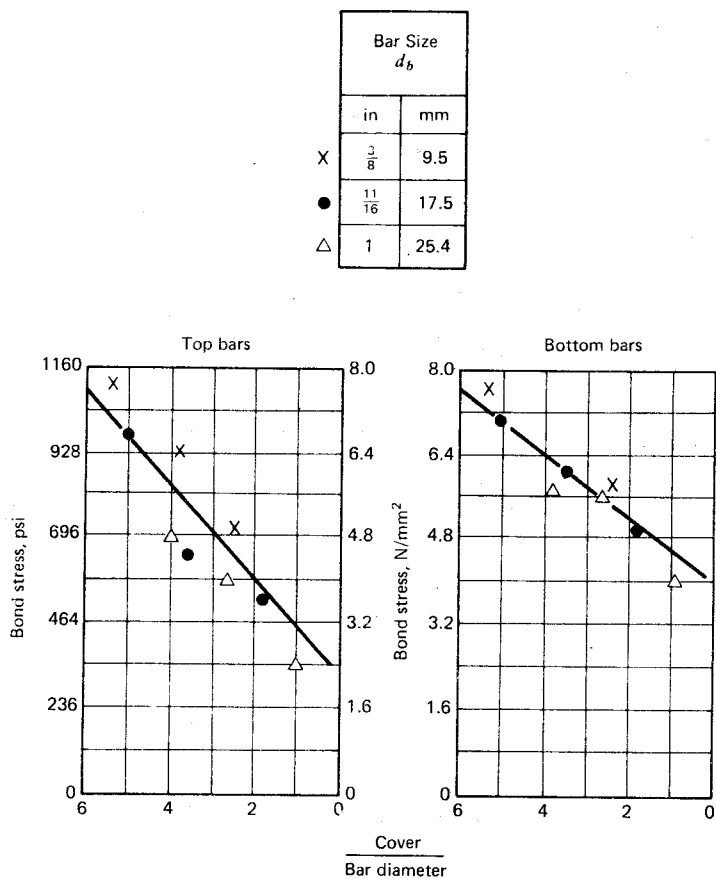


Fig. 9.11. The effect of cover on bond strength.^{9.12}

tension in the bar and corresponding compression in the surrounding concrete. Inelastic deformation in the vicinity of the ribs, microcracking in the concrete, and the release of shrinkage strains result in some permanent slip, its magnitude primarily depending on the intensity of the previously applied load. For this reason cracks formed during the tensioning of a bar do not close completely after the removal of the load. With repeated loading, the frictional resistance diminishes, resulting in a deterioration of the stiffness of the bond mechanism. Bresler and Bertero^{9.13} have used carefully instrumented experiments to observe the loss of bond under repeated loading. Figure 9.12 plots the strain distribution along a 16 in (406 mm) length of a

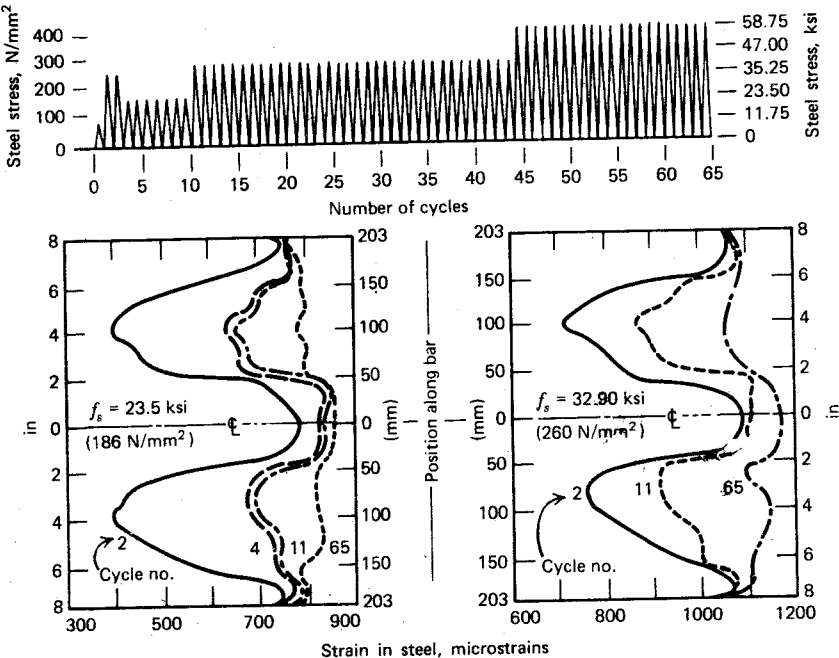


Fig. 9.12. Steel strains at two levels of stress along a bar after cyclic loading.^{9,13}

No. 9 (28.6 mm diameter) deformed bar that was embedded in a 6 in (150 mm) diameter concrete cylinder. A circular notch midway along the cylinder acted as a crack initiator. The tensile strain distribution along this specimen is representative of the bond conditions around a bar in the constant moment zone of a beam, when cracks are spaced at 8 in (203 mm) centers. The curves show the existence of high bond stresses a small distance away from the cracks, as well as the loss of bond between cracks after several cycles of loading as the tensile stress tends to become uniform over the full length of the bar. This loss of bond would contribute to the overall loss of stiffness in a reinforced concrete structure.

The consequences of the deterioration of bond in a constant moment area are not serious, for they affect stiffness and crack widths only. The behavior of the anchorage zone under repeated load is much more important, because it may affect strength. Subjecting No. 6 (19 mm diameter) bars to repeated static and dynamic loading in eccentric pullout tests, Perry and Jundi^{9,14} found that a gradual redistribution of bond stresses occurred from the loaded to the unloaded ends of the specimens. In their tests 80% of the ultimate static strength was attained for several hundred load cycles.

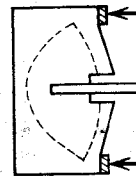
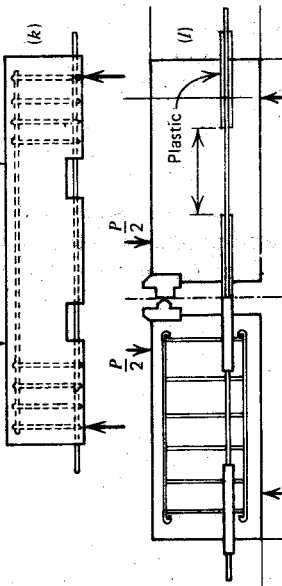
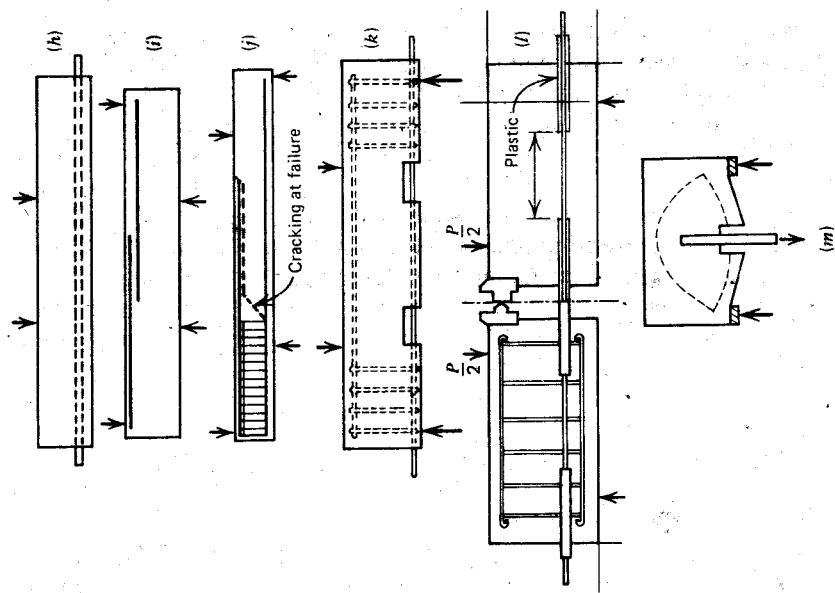
During earthquakes, alternate yielding in tension and compression at a critical section, such as a column-beam interface, can occur. The gradual loss of bond can result in penetration of yielding into the anchorage zone, drastically diminishing the effective development length, available to absorb the yield strength of the bar. Ismail and Jirsa^{9,15} observed yield penetration under cyclic overload to a distance of 14 to 18 bar diameters when the concrete in the anchorage zone was simultaneously subjected to 1000 psi (6.9 N/mm²) transverse compression. Yield penetration into the anchorage zone was found to account for up to 60% of the total deflection in test cantilevers.^{9,15} Less favorable conditions of transverse stress than existed in this test are often encountered in structures. This problem is examined with respect to joints in Chapter 13.

9.3 THE DETERMINATION OF USABLE BOND STRENGTH

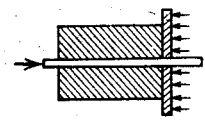
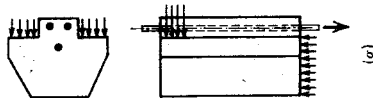
Traditionally the bond performance of various reinforcing bars, embedded in concrete of different strengths, has been determined from pullout tests. Generally the bars were pulled from the surrounding concrete in such a way that transverse compression against the bars was also induced. This transverse compression had a beneficial effect on the bond strength and was not therefore typical of situations encountered in structures. For this reason various forms of test specimen have been proposed to eliminate transverse compression. Representative test arrangements are depicted in Fig. 9.13. In these tests the bond strength is expressed in terms of the average bond stress developed by the pullout force around the embedded surface. The peak bond stress values, which have been determined in some studies,^{9,17} are known to be well in excess of the mean stress.

The pullout tests (Figs. 9.13a, through 9.13e) are atypical of situations encountered in beams. The major parameters affecting bond in reinforced concrete beams are shear forces and consequent diagonal cracks, concrete cover, and splitting cracks initiated by dowel action. Thus other forms of test arrangement (see Figs. 9.13f and 9.13g) have been advocated. ACI Committee 408 has prepared a detailed guide for the determination of bond strength in beam specimens.^{9,18} This document allows greater flexibility for the application of the relevant ACI standard.^{9,19}

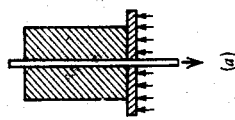
The usable bond strength is seldom a given fraction of the ultimate bond strength developed in a particular pullout test. Generally the slip at the loaded or unloaded end of the bar governs the "critical" bond intensity that can be developed under working load conditions, since this slip will significantly affect crack widths. It is important, therefore, that the full load-slip history be determined when such a test is carried out. According to Mathey and Watstein,^{9,20} the "critical" bond stress may be defined as the lesser of the



(m)



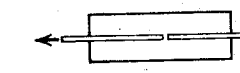
(b)



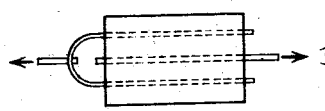
(a)



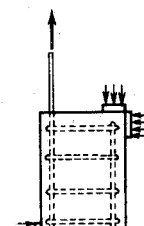
(c)



(d)



(e)



(f)

Fig. 9.13. Various bond test methods. 9.16

bond stresses associated with either a free-end slip of 0.002 in (0.05 mm) or a loaded-end slip of 0.01 in (0.25 mm) in beam tests like that in Fig. 9.13k. This slip can be considerably affected by the position of the bars when cast. In pullout tests,^{9,21} some slip at the free end of top-cast bars has been observed before the development of significant strength or of any cracking.

The slip at the loaded end of an embedded bar (i.e., at the face of a crack) is largely governed by the concentration of bond stresses in its immediate vicinity. An increase of embedment length and a consequent lowering of the average bond stress has little effect on the slip at the loaded end before it exceeds 0.01 in (0.25 mm).^{9,21}

The limitation on slip at the loaded end, taken as one-half an acceptable crack width of 0.02 in (0.5 mm), may set an upper limit to the usable strength of large bars. Figure 9.14 presents the findings of Ferguson et al^{9,21} from pullout tests. The lower band indicates the tensile stresses developed in top

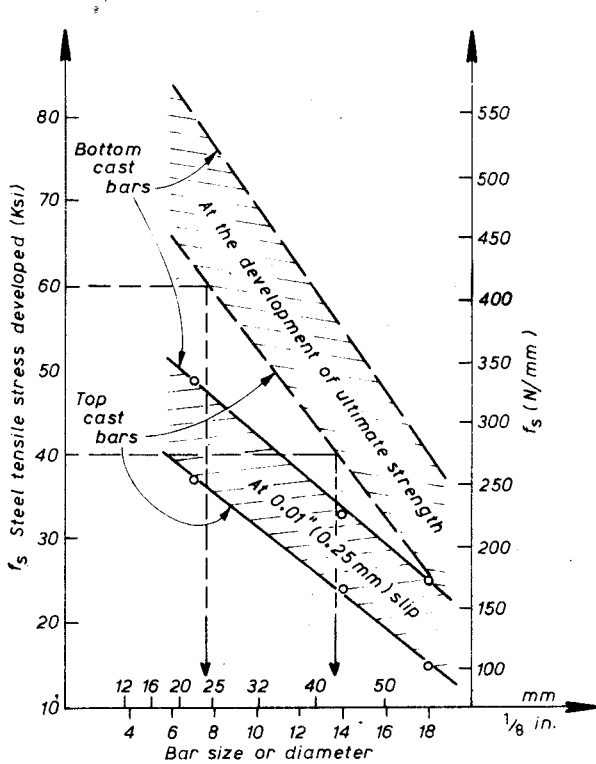


Fig. 9.14. Stresses developed in pullout specimens at 0.01 in (0.25 mm) slip.^{9,21}

and bottom cast bars of different sizes at a loaded end slip of 0.01 in (0.25 mm). If it is assumed that the ultimate load on the structure will produce steel stresses 1.65 times those induced at 0.01 in (0.25 mm) slip, the upper shaded band of Fig. 9.14 will result. These observations are not necessarily representative of the situation encountered in beams, but the plot indicates that the development of a yield strength of 60 ksi (414 N/mm²) or 40 ksi (276 N/mm²) in top cast bars, larger than No. 8 (25.4 mm diameter) or No. 14 (43 mm diameter), respectively, is likely to produce excessive crack widths at the service load.

9.4 THE ANCHORAGE OF BARS

9.4.1 Straight Anchorages for Bars with Tension

The full tensile strength of a deformed bar can usually be developed at a section, provided the bar extends in the concrete a sufficient distance beyond that section. The length of bar beyond the section required to develop the strength of the bar is known as the anchorage length or the development length. Development length is a consideration at sections of maximum moment along a beam and where a neighboring bar is cut off. The point beyond which a straight development length is required cannot always be determined with great precision. For this reason liberal allowance must be made, in addition to the moment shift referred to in Section 7.5.1, for establishing the reference points from which the development length is to be measured. The development length l_d is proportional to the force to be developed and inversely proportional to the tensile strength of the concrete, since these two factors control concrete splitting. For No. 5 (16 mm diameter) to No. 11 (35.8 mm diameter) deformed bars in tension, the ACI code^{9,3} indicates that

$$l_d = (m_f) \frac{0.04 A_b f_y}{\sqrt{f'_c}} \quad (\text{in}) \quad (9.6)$$

where all units are in lb and in.

The modification or judgment factor m_f allows for: (1) the adverse effect on top-cast bars [l_d is increased by 40% in the case of bars with more than 12 in (305 mm) of concrete cast below the bars], (2) yield strength of steel greater than 60,000 psi (414 N/mm²), (3) the reduced strength of lightweight aggregate concrete, (4) the effect of cover and lateral spacing between bars, (5) the use of excess flexural reinforcement at a section, and (6) the effect of spiral reinforcement (l_d is reduced by 25% if the bar is enclosed in an appropriate steel spiral).

Similar provisions are made for very large bars and for bars smaller than

No. 6 (18 mm diameter). The same development length (Eq. 9.6) could have been obtained using Eq. 9.2b by specifying that $u = 8\sqrt{f'_c m_f d_b}$ (psi).

Example, 7.1, featured in Fig. 7.38, demonstrates the curtailment of top-cast bars, with allowance for the development length l_d , in accordance with ACI requirements.^{9.3}

9.4.2 Hook Anchorages for Bars with Tension

When the straight length of bar available for anchorage is insufficient, the reinforcement can be bent, or a hook may be formed to aid anchorage. Hooked anchorages for plain round bars have distinct advantages that were recognized by the pioneers of structural concrete.

In pullout tests specifically designed to obtain the strength of hooked anchorages, the bond along the straight portion of the bar in front of the hook was eliminated (see Fig. 9.15). Load-slip relationships obtained from such tests indicate the usable anchorage loads available from various types of hooks. The slip is measured at the point where the bar enters the concrete. For deformed bars the strain distribution in the steel measured along the hook in such a test reveals that the bar force is transferred rapidly into the

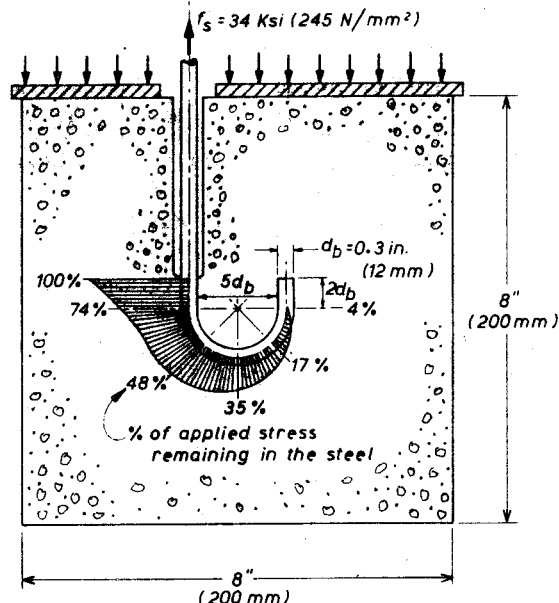


Fig. 9.15. Pullout test for hooked deformed bars.^{9.22}

concrete and the straight portion following a hook is generally ineffective^{9.22} (see Fig. 9.15). For plain bars the tensile stresses reduce more slowly along the hook; therefore extra anchorage strength may be obtained by extending the straight portion of the bar following the hook.

The useful strength of a hook is also related to an acceptable slip at the loaded end. Provided no splitting failure occurs in the plane of the hook, slip appears to be the governing criterion. A linear relationship between load and slip can be expected for slips up to 0.001 in (0.025 mm).^{9.23} A suitable comparison of the load-carrying capacity of various types of hooked anchorages can be made at a slip of 0.01 in (0.25 mm).

The largest bearing stresses on the concrete are developed along the inside of the hook near the loaded part of the bar. In these areas, therefore, such properties of the surrounding concrete as porosity and strength, can significantly affect the slip at any given load. Figure 9.16 displays typical load-slip curves for 180° hooks, at various positions when cast. The load is expressed in terms of the f_s/f'_{cu} ratio, where f_s is tensile stress applied to the bar in front of the hook and f'_{cu} is the cube strength of the surrounding concrete. Each curve represents the mean of 6 to 35 tests. Because of the random variation of the concrete quality (i.e., the degree of water gain) under the critical

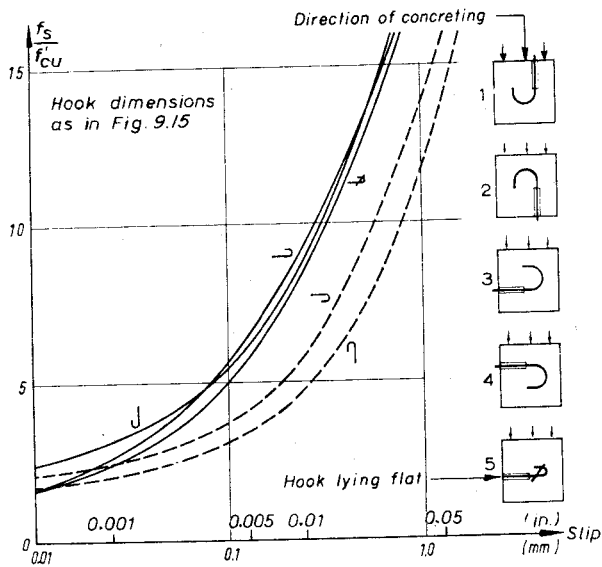


Fig. 9.16. Load-slip relationship for hooked anchorages of deformed bars.^{9.24}

bearing area, considerable scatter has been observed in such tests. However, the inferior performance of topcast bars, such as types 2 and 4 in Fig. 9.16, is clearly evident. The average anchorage capacity of hooks, in terms of f_s/f'_{cu} for three different bar sizes at various slips, are compared in Fig. 9.17.^{9,24} For the tests featured in Figs. 9.16 and 9.17 deformed bars were used.

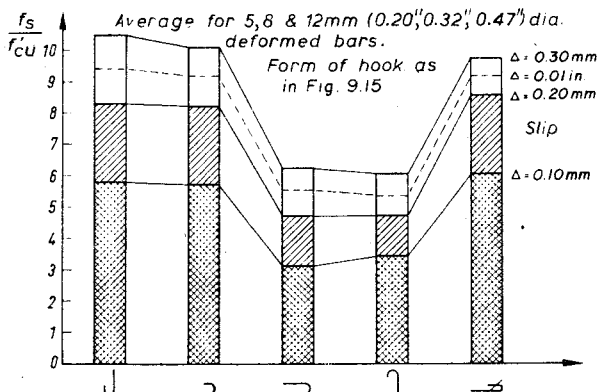


Fig. 9.17. The influence on bond strength at given slip of hook position at the casting of concrete.^{9,24}

Rehm's pullout tests of hooked anchorages also demonstrated that a bend with less than 180° turn does not necessarily provide anchorage superior to a straight bar of the same length.^{9,24} When it is realized that a bend introduces stress concentrations, consequently large local deformations in the concrete, which in turn lead to increased slip at the loaded end of an embedded bent bar, it is not surprising that for the same embedded length of bar, the straight vertical bar gives the best performance. Figure 9.18a, in which bars with different bend angles but identical embedded lengths (i.e., 10 bar diameters) are compared, illustrates this observation. The differences in performance between various bend angles become less significant when the bar pull is against the direction of concrete casting (see Fig. 9.18b), since in this case the anchored bars bear against concrete not affected by water gain and sedimentation.

A smaller bar curvature at a bend or a hook will mean a smaller load concentration, consequently a smaller slip, at the loaded end of the anchorage. Therefore, a large diameter hook will transmit a larger load for a given acceptable slip. Typical data relating to this observation^{9,24} appear in Fig. 9.19.

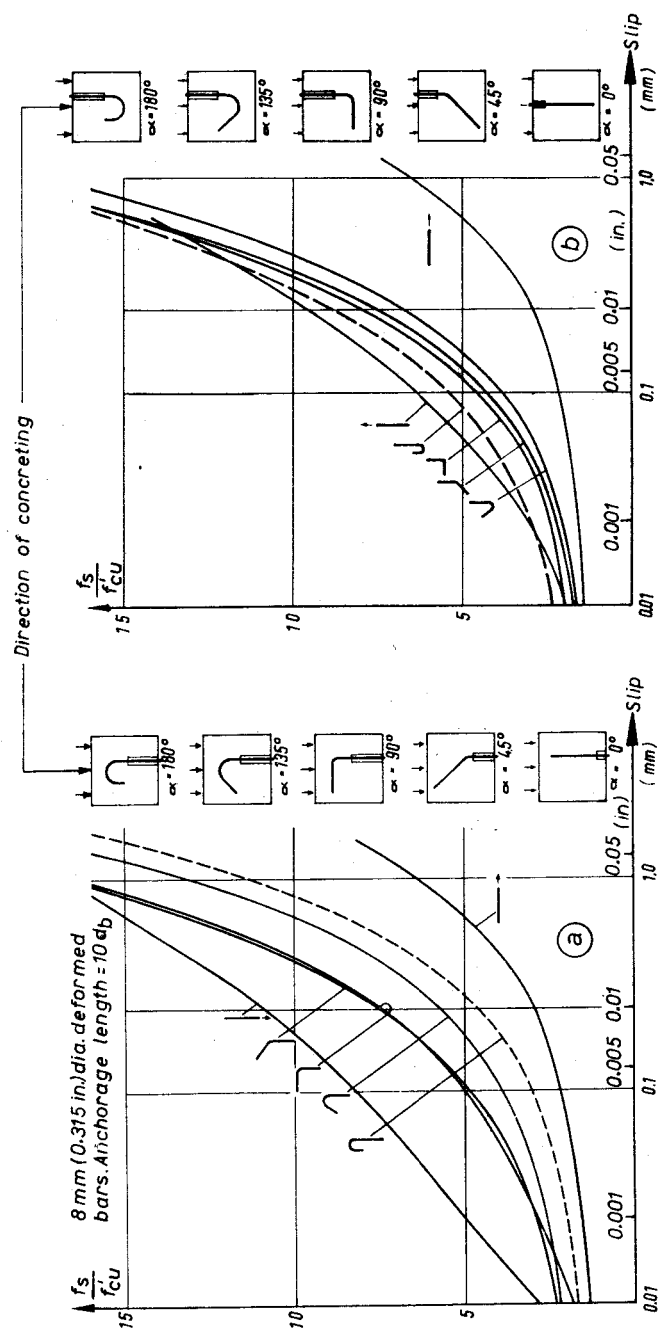


Fig. 9.18. The performance of anchorages of deformed bars with various degrees of bends.^{9,24} (a) Top-cast bars. (b) Bottom-cast bars.

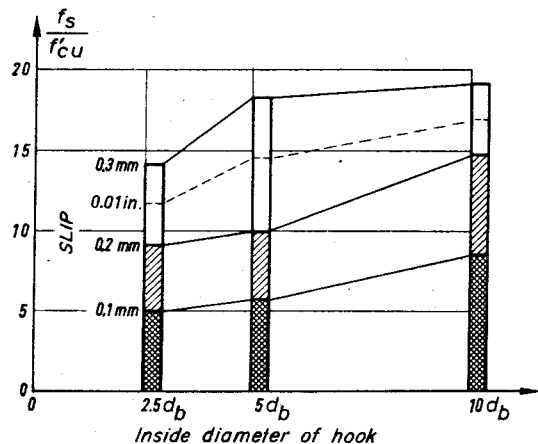


Fig. 9.19. The effect of hook curvature on anchorage performance.^{9,24}

When a bar is bent around a transverse bar, as is the case of stirrup anchorages, 10 to 30% larger tensile stresses can be developed for the same amount of slip.^{9,22} However, this benefit can be obtained only if direct contact between the hook and the transverse bar exists. Under normal site conditions, contact between stirrups and main beam reinforcement cannot be assured (see Fig. 9.20). Also, in the vicinity of the contact point between a stirrup and a longitudinal bar, some deterioration in the quality of the concrete can be expected. These two factors are likely to lead to larger slips at relatively low stirrup stresses. The effect of this slip on the width of diagonal cracks and on the participation of stirrups in shear resistance, particularly in shallow beams, could be significant.

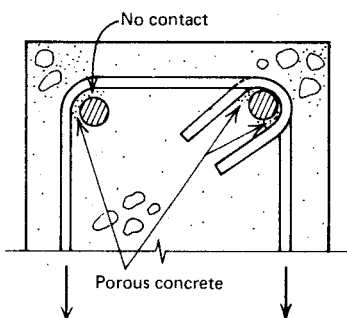


Fig. 9.20. The anchorage of stirrups.

For a hook of the type shown in Fig. 9.15, the bar diameter does not appear to influence the steel stress-slip relationship^{9.22} up to a slip of 0.02 in (0.5 mm). For a given slip, in the usual grades of concrete, the hook capacity is proportional to the concrete strength. Experiments at the Technical University of Munich^{9.22} established the following relationship

$$f_s^* = k_h f'_{cu} \quad (9.7)$$

where f_s^* = steel stress at the loaded end of the hook at a slip of 0.004 in (0.01 mm)

f'_{cu} = compressive cube strength of the concrete

k_h = experimental constant given in Table 9.1

Table 9.1 Value of k_h

Position of Hooks	Type ^a	Plain Bars	Deformed Bars
Bottom-cast hooks	1, 3	1.70	3.75
Top-cast hooks	2, 4	1.20	2.00

^a For identification of hook type, see Fig. 9.16.

At ultimate load the tensile strength of the concrete might limit the capacity of a hook, unless transverse compression or appropriate confining reinforcement prevents a splitting failure in the plane of a hook. This is why the ACI code^{9.3} indicates that the hook capacity is dependent on the tensile strength of the surrounding concrete and considers that standard hooks can anchor a bar with a tensile stress equal to $f_h = K \sqrt{f'_c}$ psi, where f'_c is in psi (1 psi = 0.00689 N/mm²) and K is given in Table 9.2. The value of K may be increased by 30% when enclosure is provided perpendicular to the plane of the hook. The code^{9.3} also specifies the shapes and dimensions of standard hooks.

9.4.3 Anchorage for Bars with Compression

The mechanisms by which tensile and compressive bar forces are anchored differ significantly. There is less tendency for splitting to occur along a bar in compression, and a part of the compression force can be transferred to the concrete by end bearing.^{9.25} However, significant bearing stresses at the end of a square-cut bar can be developed only if there is sufficient mass of concrete behind the end of the bar. Codes recognize the improved development conditions for bars in compression and accordingly specify considerably smaller

Table 9.2 *K* Values^a

Bar Size (mm)	Top Bars		Other Bars	
	$f_y = 60$ ksi (414 N/mm ²)	$f_y = 40$ ksi (276 N/mm ²)	$f_y = 60$ ksi (414 N/mm ²)	$f_y = 40$ ksi (276 N/mm ²)
No. 18 (57)	220 (18.3)	220 (18.3)	220 (18.3)	220 (18.3)
No. 14 (43)	330 (27.4)	330 (27.4)	330 (27.4)	330 (27.4)
No. 11 (36)	360 (29.9)	360 (29.9)	420 (34.9)	360 (29.9)
No. 10 (32)	360 (29.9)	360 (29.9)	480 (39.9)	360 (29.9)
No. 9 (29)	360 (29.9)	360 (29.9)	540 (44.8)	360 (29.9)
No. 8 (25)	360 (29.9)	360 (29.9)	540 (44.8)	360 (29.9)
No. 7 (22)	360 (29.9)	360 (29.9)	540 (44.8)	360 (29.9)
No. 6 (19)	450 (37.4)	360 (29.9)	540 (44.8)	360 (29.9)
Nos. 3 to 5 (9.5 to 16)	540 (44.8)	360 (29.9)	540 (44.8)	360 (29.9)

^a Values in parentheses are applicable when SI units are used.

development lengths.^{9,3} Certain problems that may arise in connection with end bearing are discussed in Section 9.6.3, which treats compression splices.

9.5 ANCHORAGE REQUIREMENTS FOR FLEXURAL BOND

In the regions of members where the external bending moment is near zero (e.g., near the supports of simply supported beams and near points of contraflexure), the external shear force may be large and the area of flexural reinforcement may be small, possibly making flexural bond strength requirements (see Section 9.1.3) critical. By equating the bond stresses given by Eqs. 9.2a and 9.3, we find

$$u = \frac{V_u}{jd\Sigma o} = \frac{A_s f_y}{l_d \Sigma o}$$

where Σo is the sum of the bar perimeters

$$\therefore l_d = \frac{A_s f_y j d}{V_u} = \frac{M_t}{V_u} \quad (9.8a)$$

where M_t is the theoretical flexural capacity of the section at the support or point of contraflexure provided by the bars in the tension face. If the specified bond strength u is not to be exceeded, the ratio M_t/V_u must be equal to or

larger than the required development length l_d . According to the ACI code,^{9,3} locally exceeding the bond strength u will not lead to failure if an additional anchorage length l_a is provided. At a simple support, l_a is the embedment length beyond the center of a support, plus any equivalent embedment length from a furnished hook or mechanical anchorage. At a point of contraflexure, the embedment length to be considered, l_a , shall be limited to the effective depth of the member or $12d_b$, whichever is greater. Accordingly, Eq. 9.8a is modified so that

$$l_d \leq \frac{M_t}{V_u} + l_a \quad (9.8b)$$

When the reaction at the supports of members is introduced so that the member is compressed transversely, resulting in confinement of the ends of the bars, the ACI code^{9,3} allows the value of M_t/V_u , used in Eq. 9.8b, to be increased by 30% to allow for the improved anchorage conditions.

When Eq. 9.8b is not satisfied, the designer needs to undertake one of the following steps:

1. Increase the total steel area A_s at the section by bringing more bars to the section. The theoretical ultimate moment capacity M_t is thus increased.
2. Increase the anchorage length l_a beyond the section by bending up bars if necessary, or by other means (see support A in Fig. 7.19).
3. Reduce the required development length l_d , given by Eq. 9.6 by using a larger number of smaller size bars.

9.6 SPLICES

9.6.1 Introduction

A lapped splice transfers the force from one bar to another through the concrete surrounding both bars. At any point along a splice, forces are being transferred from one bar by bond to the surrounding concrete and simultaneously, also by bond, to the other bar of the pair forming the splice. Within the concrete, these forces can generate high shear stresses as well as splitting forces. The integrity of a lapped splice depends on the development of adequate bond along the surfaces of the bars and on the ability of the concrete around the two bars to transfer shear without disintegration or excessive deformation. The nature of bond was discussed in the preceding sections. The behavior of the concrete in the vicinity of a lapped splice deserves further study.

9.6.2 Tension Splices

The danger of concrete splitting is particularly great in the vicinity of tension splices. Two spliced bars generate diagonal compression in the space between them, and a clamping force is required to prevent a possible separation. The wedging effect of each of the two spliced bars may lead to a splitting crack along a line passing through the centers of lapped bars. Such a horizontal crack is drawn in Fig. 9.21, which illustrates the splicing of four bars in a

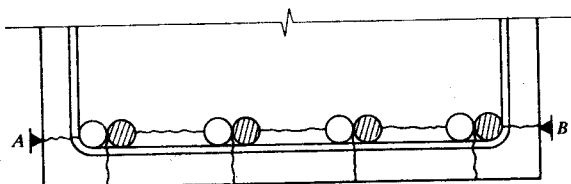


Fig. 9.21. Possible cracks at a lapped splice.

beam. It is evident that only the outer stirrup legs would offer resistance against the separation of the narrow concrete block below the reinforcement. The horizontal leg of a stirrup is effective in controlling the opening of longitudinal cracks (vertical cracks in Fig. 9.21) caused by the combination of shear, diagonal tension, and wedging effects. The role of such transverse reinforcement is similar to that encountered when interface shear is transmitted, as in Fig. 7.26.

The free ends of spliced bars, being sources of discontinuity, act as crack initiators across a tension zone. This transverse crack in turn triggers splitting cracks. During tests, the increase of the sectional dimensions of a member, such as the distance $A-B$ in Fig. 9.21, can be measured with suitable instruments while loading is proceeding. A sudden increase in sectional dimensions indicates the onset of splitting along lapped bars. Stöckl observed^{9.26} that such a transverse expansion was much greater at the free ends than anywhere else along the lapped length of bars. When several highly stressed bars are terminated across the same section, the splitting effects at their free ends are cumulative, unless the lateral dimension between splices is large. Therefore, it is beneficial to stagger lapped splices in such a way that no free ends line up at the same section, unless the bars are further than $12d_b$ apart. A stagger by half a lap length, or by more than 1.3 lap lengths, (Fig. 9.22) is to be preferred. Figure 9.22 presents observed^{9.26} transverse expansion and transverse cracks for three different arrangements of lapped splices.

Because of the adverse conditions that prevail at a splice, the lap length l_{sl} required must be larger than the development length for a single bar

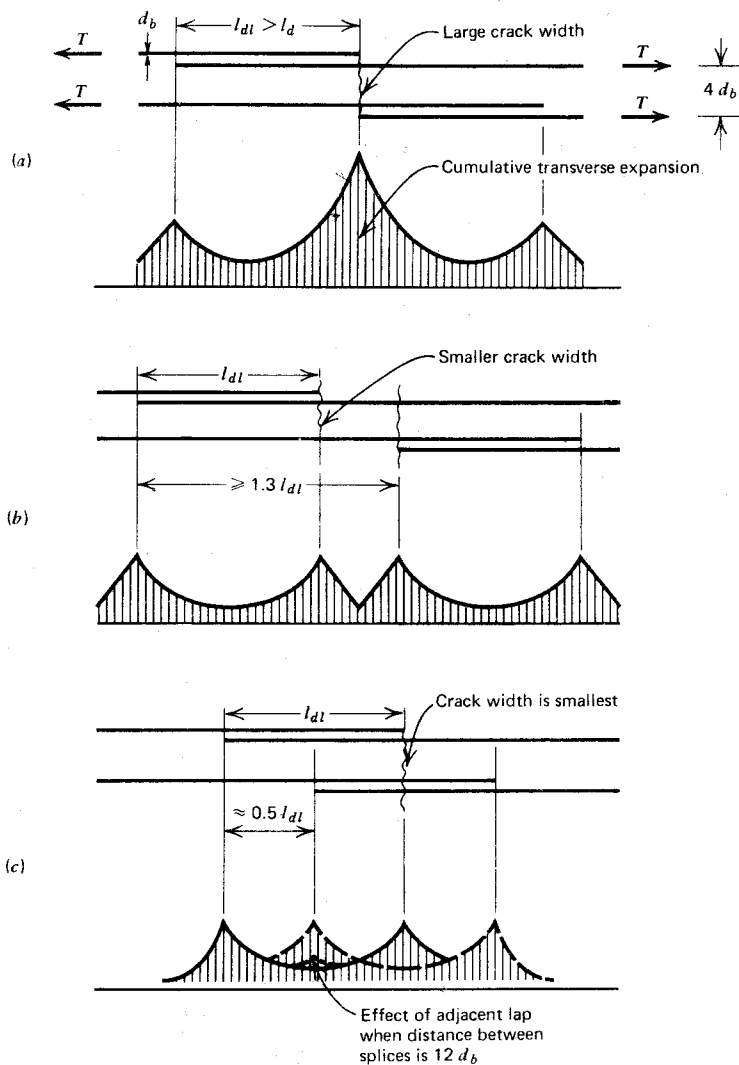


Fig. 9.22. Transverse expansion and crack widths at staggered lapped splices.^{9,26} (a) Overlapping transverse expansion (b) Transverse expansion does not overlap. (c) Overlapping of transverse expansion is not critical.

l_d (Fig. 9.22). Codes have certain restrictions to discourage designers from placing splices in critical zones. Also, when bars are in contact, are spaced transversely within a limited distance, or are welded together, the splice must be able to develop at least 125% of the yield strength of the bars, if a positive connection is to be achieved.

The most severe conditions exist in a tension tie or at the section of maximum tensile stresses in a flexural member. For a tension tie member, the ACI code^{9.3} requires a lap length equal to twice the development length and spiral reinforcement around the splice. It also requires hooks for bars larger than No. 4 (13 mm diameter). In regions of maximum bending moment in flexural members, the code calls for a lap length of 1.7, 1.3, or 1.0 times the development length, depending on the lap arrangement. The code^{9.3} implicitly prefers staggered splice layouts, located away from the sections of maximum tension.

In Section 9.2.6 we outlined the role of transverse reinforcement (e.g., stirrups, ties, or spirals) in providing bond strength. The failure of a tension splice is violent and complete if stirrups or transverse reinforcement of another type are absent from the member. Even a minimum stirrup content ($\rho_v = 0.15\%$) will increase the splice strength, restrict the growth of splitting cracks, and ensure a ductile failure.^{9.27}

9.6.3 Compression Splices

The transmission of compression forces by splicing reinforcing bars has received less attention than the tension case. The splice length in compression may be specified either in terms of an acceptable bond stress u (Eq. 9.2b) or in terms of the development length l_d .^{9.3} Because of the better bond conditions for bars in compression, codes allow higher bond stresses and correspondingly lower development lengths for these bars than for bars in tension. In axially loaded columns, the transverse reinforcement, consisting of ties, hoops, or spirals, gives added protection against splitting along a splice, and this property is recognized by codes. Because transverse cracking does not occur in compression zones, the harmful effect of such cracks in initiating splitting is also absent. The major difference between a tension and a compression splice comes from the ability of the bars in a compression splice to transfer load to the concrete directly by end bearing. In tests conducted by Pfister and Mattock,^{9.25} bearing stresses equal to 5 times the cylinder strength of the concrete were attained at the square-cut ends of bars in compression splices.

From recent experiments, at the Otto-Graf-Institute of the University of Stuttgart,^{9.28} the following factors affecting the behavior of compression splices became evident.

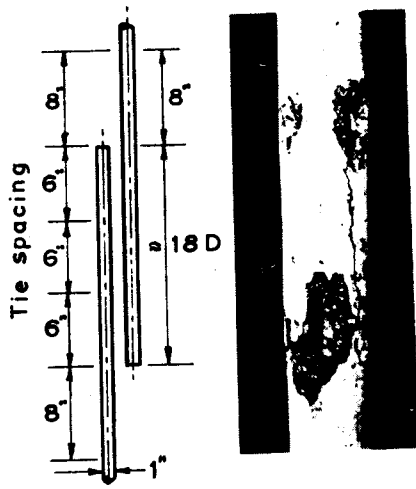


Fig. 9.23. Failure of a compression splice caused by end bearing.^{9,28}

1. End bearing was found to be responsible for the majority of splice failures, irrespective of the splice length tested. The splice lengths in the tests varied between 9 and 38 times the bar diameter. The crushing of the concrete at the square ends of bars becomes particularly severe when the bar size is increased. A typical example of end bearing failure appears in Fig. 9.23.

2. The bearing capacity of the concrete at the cut ends of the column bars was increased by the presence of confining reinforcement, which prevented the lateral expansion of the concrete in these areas. Under such conditions concrete bearing stresses of the order of 17,000 psi (120 N/mm²) were measured.

3. An increase in the thickness of concrete cover over a compression splice resulted in insignificant improvement.

4. When column bars smaller than 0.55 in (14 mm) diameter are spliced, end bearing is unlikely to influence behavior, and the standard transverse reinforcement, used outside the splice area, is likely to be adequate also at the splice.

5. Under long-term loading, the bearing pressure under the ends of the bars diminishes because of creep; hence the splice performance improves.

Compressive forces in steel bars can be directly transferred from bar to bar by end bearing. Force transfer by end bearing can be used only when the designer is certain that under the most adverse load combination, the bars are never required to carry tension. In such cases it is necessary that square-cut or sawn ends be obtained so that the bars in contact can bear

uniformly against each other. Experiments indicate, however, that small inaccuracies in the bearing faces are not detrimental. The ACI code^{9,3} permits a maximum deviation of 1.5° from a right angle at the end surfaces of the bars. This means that instead of perfectly uniform bearing, a 3° angle between contact end surfaces of bars is still acceptable. However, the bars must be held firmly in position relative to each other by a suitable sleeve or other device.^{9,3} In the tests at the University of Stuttgart,^{9,28} compressive force transfer by contact end bearing was found to be superior to lapped compression splices in every case, even without the use of additional ties at the splice.

9.6.4 Mechanical or Contact Splices

It is evident that the weakest link in a lapped splice is the concrete between the bars. When the full strength of the bars is to be transferred, the splice length (which is equal to or larger than the development length l_d) can be large. When a considerable amount of reinforcement is required in a member and large size bars are used, a significant weight of steel may be needed to satisfy splice requirements. For example, lapped splices may extend over one-third the height of a column in a multistory, reinforced concrete frame. Moreover, lapped splices may produce congestion, and they may interfere with the proper compaction of the concrete.

To overcome these difficulties, methods that allow the transfer of the tension or compression forces directly from bar to bar without assistance from the concrete have been employed. The butt welding of two bars, end to end, by electric arc welding has been used extensively. More recently, a gas pressure welding process has been developed in which the ends of bars, heated to the correct temperature, are pressed against each other; thus fusion is achieved while a bulb at the contact section is being formed. For deformed bars, a mechanical splice technique is available involving an annular sleeve that is cold pressed against the bars, forcing the ribs of the deformed bars to become embedded in the wall thickness of the sleeve. With suitable bar deformations, a sleeve embedment length of as little as $2d_b$ for each of the two bars may be sufficient to transfer the breaking load of the bar in tension.^{9,27} An alternate splicing device consists of an annular sleeve somewhat larger than the bars, placed around the two bars. A thermal process is employed to fill the space between the sleeve and the deformed bars with a metallic compound. The techniques in which a steel sleeve is used are particularly useful when high strength reinforcement is to be spliced, because the welding of such bars may cause embrittlement.

Mechanical splice devices must be subjected to rigorous test procedures before they can be adopted for use in the structure.

9.7 REFERENCES

- 9.1 "Bond Stresses—The State of the Art," Reported by ACI Committee 408, *Journal ACI*, Vol. 63, No. 11, November 1966, pp. 1161-1190.
- 9.2 "Opportunities in Bond Research," Reported by ACI Committee 408, *Journal ACI*, Vol. 67, No. 11, November 1970, pp. 857-867.
- 9.3 "Building Code Requirements for Reinforced Concrete (ACI 318-71)," American Concrete Institute, Detroit, 1971, 78 pp.
- 9.4 G. Rehm, "The Basic Principles of the Bond Between Steel and Concrete," Translation No. 134, Cement and Concrete Association, London, 1968, 66 pp.
- 9.5 G. B. Welch and B. J. F. Patten, "Reduction in Concrete-Steel Bond with Horizontally Embedded Reinforcement," UNCIV Report No. R-8, February 1967, University of New South Wales, 26 pp.
- 9.6 "Standard Specification for Deformed and Plain Billet-Steel Bars for Concrete Reinforcement," ASTM: A 615-72, American Society for Testing and Materials, 1972.
- 9.7 P. Gergely, "Splitting Cracks Along the Main Reinforcement in Concrete Members," Report to Bureau of Public Roads U.S. Department of Transportation, Cornell University, Ithaca, N.Y., April 1969, 90 pp.
- 9.8 L. A. Lutz and P. Gergely, "Mechanics of Bond and Slip of Deformed Bars in Concrete," *Journal ACI*, Vol. 64, No. 11, November 1967, pp. 711-721.
- 9.9 E. L. Kemp, F. S. Brezny, and J. A. Unterspan, "Effect of Rust and Scale on the Bond Characteristics of Deformed Reinforcing Bars," *Journal ACI*, Vol. 65, No. 9, September 1968, pp. 743-756.
- 9.10 Y. Goto, "Cracks Formed in Concrete Around Deformed Tension Bars," *Journal ACI*, Vol. 68, No. 4, April 1971, pp. 244-251.
- 9.11 P. M. Ferguson and J. N. Thompson, "Development Length for Large High Strength Reinforcing Bars," *Journal ACI*, Vol. 62, No. 1, January 1965, pp. 71-93.
- 9.12 "An Investigation of the Bond of Deformed Steel Bars with Concrete," Translation No. 112, Cement and Concrete Association, London, 1964, 28 pp.
- 9.13 B. Bresler and V. Bertero, "Behaviour of Reinforced Concrete Under Repeated Load," *Journal of the Structural Division, ASCE*, Vol. 94, ST6, June 1968, pp. 1567-1589.
- 9.14 E. S. Perry and N. Jundi, "Pullout Bond Stress Distribution Under Static and Dynamic Repeated Loadings," *Journal ACI*, Vol. 66, No. 5, May 1969, pp. 377-380.
- 9.15 H. A. F. Ismail and J. O. Jirsa, "Behaviour of Anchored Bars Under Low Cycle Over-loads Producing Inelastic Strains," *Journal ACI*, Vol. 69, No. 7, July 1972, pp. 433-438.
- 9.16 R. Baus and M. G. Claude, "État des Connaissances sur le Mécanisme de l'Adhérence et des Ancrages," *Essai de Synthèse Bibliographique*, October 1966, CEB Bulletin No. 66, April 1968, pp. 185-213.
- 9.17 R. M. Mains, "Measurement of the Distribution of Tensile and Bond Stresses Along Reinforcing Bars," *Journal ACI*, Vol. 23, No. 3, November 1951, pp. 225-252.
- 9.18 "A Guide for the Determination of Bond Strength in Beam Specimens," Reported by ACI Committee 408, *Journal ACI*, Vol. 61, No. 2, February 1964, pp. 129-135.
- 9.19 "Test Procedure to Determine Relative Bond Value of Reinforcing Bars" (ACI 208-58), *Journal ACI*, Vol. 55, No. 1, July 1958, pp. 1-6.

- 9.20 R. G. Mathey and D. Watstein, "Investigation of Bond in Beam Pull-Out Specimens with High-Yield-Strength Deformed Bars," *Journal ACI*, Vol. 57, No. 9, March 1961, pp. 1071-1090.
- 9.21 P. M. Ferguson, J. E. Breen, and J. N. Thompson, "Pullout Tests on High Strength Reinforcing Bars," Part 1, *Journal ACI*, Vol. 62, No. 8, August 1965, pp. 933-950.
- 9.22 H. H. Müller, "Ausziehversuche mit Betonstahlhaken," Aus unseren Forschungsarbeiten. Bericht No. 80, December 1968, Materialsprüfungsamt für das Bauwesen der Technischen Hochschule München, pp. 70-75.
- 9.23 J. A. Hribar and R. C. Vasko, "End Anchorage of High Strength Steel Reinforcing Bars," *Journal ACI*, Vol. 66, No. 11, November 1969, pp. 875-883.
- 9.24 G. Rehm, "Kriterien zur Beurteilung von Bewehrungsstäben mit hochwertigen Verbund," *Stahlbetonbau, Berichte aus Forschung und Praxis, Festschrift Rüsch*. Wilhelm Ernst & Sohn, Berlin, 1969, pp. 79-96.
- 9.25 J. F. Pfister and A. H. Mattock, "High Strength Bars as Concrete Reinforcement, Part 5. Lapped Splices in Concentrically Loaded Columns," *Journal of the PCA Research and Development Laboratories*, Vol. 5, No. 2, May 1963, pp. 27-40.
- 9.26 S. Stöckl, "Übergreifungsstöße von zugbeanspruchten Bewehrungsstäben," *Beton und Stahlbetonbau*, Vol. 67, No. 10, October 1972, pp. 229-234.
- 9.27 P. M. Ferguson and J. E. Breen, "Lapped Splices for High Strength Reinforcing Bars," *Journal ACI*, Vol. 62, No. 9, September 1965, pp. 1063-1078.
- 9.28 F. Leonhardt and K-T. Teichen, "Druck-Stöße von Bewehrungsstäben," Deutscher Ausschuss für Stahlbeton Bulletin No. 222, W. Ernst and Sohn, Berlin 1972, pp. 1-53.

Service Load Behavior

10.1 SERVICE LOAD PERFORMANCE

The performance of structures at the service loads is an important design consideration. If sections are proportioned by strength requirements alone, there is a danger that although the degree of safety against collapse will be adequate, the performance of the structure at the service loads may be unsatisfactory. For example, at the service loads the deflections of the members may be excessively large, or the cracking of the concrete may be unacceptably great.

In European terminology, the structure should be designed with reference to several limit states, the most important being strength at ultimate load, deflection at service loads, and crack width at service loads. Other possible limit states are vibrations and fatigue at service loads. The aim in design should be to ensure an adequate margin of safety against collapse and against the possibility that the structure will become unfit for use at service loads.

Therefore, to produce a satisfactory design, it must be ascertained that the magnitude of deflections and the extent of cracking at the service loads lie within reasonable limiting values. This check requires the use of elastic theory. The 1971 ACI code^{10.1} emphasizes design based on strength with serviceability checks; but the code also allows an alternate design method based on elastic theory, with specified allowable stresses at the service loads for flexural members without axial load.

This chapter considers service load behavior. Elastic theory is developed for the determination of stresses in members due to flexure at the service loads and for use in the alternate design method; the method of calculation of deflections and crack widths at the service loads is outlined, as well.

10.2 ELASTIC THEORY FOR STRESSES IN MEMBERS DUE TO FLEXURE

10.2.1 Effective Modulus of Elasticity

A major difficulty in the application of elastic theory to reinforced concrete is the inelasticity of concrete. The modulus of elasticity of concrete is dependent on both the level of stress and the time of loading. The modulus of elasticity given by Eq. 2.1, determined from short-term loading tests, gives the secant modulus at approximately $0.5f'_c$. For slow loading rates the modulus is reduced because of creep strains, as indicated in Fig. 2.5.

The creep deformation of concrete under constant axial compressive stress is illustrated in Fig. 2.20. For an applied stress, which does not exceed about $0.5f'_c$, the creep strain that occurs over a given period is almost proportional to the applied stress. Hence the creep strain under constant compressive concrete stress f_c may be written as

$$\varepsilon_{\text{creep}} = C_t \frac{f_c}{E_c} \quad (10.1)$$

where E_c = secant modulus of elasticity of the concrete at the instant of loading and C_t = creep coefficient of concrete, which is an empirical factor dependent on the age of the concrete on loading, the duration of loading, the concrete mix proportions, the thickness of the member, and the humidity, as described in Section 2.1.4. Note that because of the linearity assumption, C_t is independent of the level of stress. The total strain is given by

$$\varepsilon_{\text{total}} = \frac{f_c}{E_c} + C_t \frac{f_c}{E_c} = \frac{f_c}{E_c} (1 + C_t) \quad (10.2)$$

The effective secant modulus of elasticity of the concrete, including creep, is $f_c/\varepsilon_{\text{total}}$, which from Eq. 10.2 may be written as

$$E_{\text{eff}} = \frac{f_c}{\varepsilon_{\text{total}}} = \frac{E_c}{1 + C_t} \quad (10.3)$$

The effective modulus of elasticity may be used to relate stress and strain when the creep coefficient is known, normally under assumed constant stress conditions.

Average values for the creep coefficient C_t under typical design conditions after very long-term loading are 1.5 to 2.0, but large variations can occur. Section 2.1.4 gives a method for calculating the creep coefficient as a function of the many variables that affect it.

As Fig. 2.20 illustrates, if the load is removed, the elastic strain is recovered immediately, and some creep recovery occurs with time.

10.2.2 Elastic Theory Assumptions

Three assumptions are made in the elastic theory for members subjected to flexure:

1. Plane sections before bending remain plane after bending.
2. The tensile strength of concrete may be ignored if cracking has commenced at the extreme tension fiber.
3. The stress-strain relationships for concrete and steel are linearly elastic.

The first assumption, made in strength theory, was discussed in Section 3.1.

The second assumption implies that when the stress in the extreme tension fiber exceeds the modulus of rupture of the concrete, the concrete will crack up to the neutral axis. This assumption is reasonable because once cracking commences, the stresses in the tension steel and compressed concrete increase significantly owing to the redistribution of stresses, and only a little concrete, if any, will be left carrying tension between the stress concentration at the tip of the crack and the neutral axis.

The third assumption, which is true for steel at stresses less than the yield strength, is reasonable for concrete at service load stresses. Creep can be taken into account by use of an effective modulus of elasticity for the concrete. However, the direct proportionality between creep strain and applied stress, which has been assumed in determining the effective modulus of elasticity, strictly applies only when the concrete compressive stress does not exceed about one-half the cylinder strength. Nevertheless, the departure from proportionality becomes large only under stresses a great deal higher.

In the analysis of sections, when the neutral axis depth changes because of a redistribution of stresses due to the creep of concrete, the use of the effective modulus of elasticity for the concrete with a constant creep factor gives only an approximation for the stresses. This follows because the effective modulus of elasticity applies to constant stress conditions, whereas the magnitude and distribution of stresses changes over the cross section with time. However, use of the effective modulus of elasticity will give a reasonable approximation for the stresses.

If a more accurate approach is required which considers the effect of variable stress history, the rate-of-creep method^{10.2} or the superposition method^{10.3} may be used when creep-time data and load-history information are available.

10.2.3 Analysis of Beams Using the Internal Couple Approach

Rectangular Sections

Figure 10.1 depicts a doubly reinforced concrete rectangular beam section in the service load range after cracking. The dimensions of the concrete section

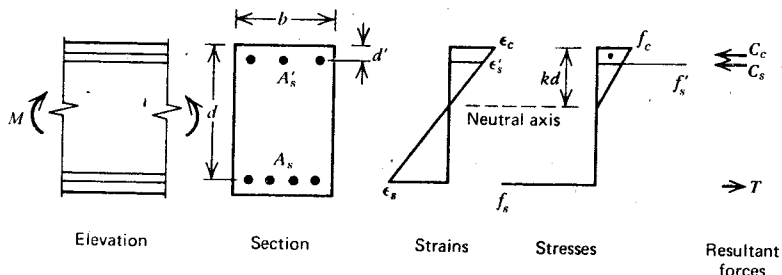


Fig. 10.1. Doubly reinforced concrete rectangular beam section in service load range after cracking.

and the steel areas and positions are considered to be known quantities. The section can be analyzed using the internal couple concept and the requirements of strain compatibility and equilibrium of forces.

The strains ϵ_c , ϵ'_s , and ϵ_s may be written in terms of the stresses as follows;

$$\epsilon_c = \frac{f_c}{E_c} (1 + C_t), \quad \epsilon'_s = \frac{f'_s}{E_s}, \quad \epsilon_s = \frac{f_s}{E_s}$$

where E_c = modulus of elasticity of the concrete (at instant of loading), E_s = modulus of elasticity of the steel, and C_t = creep coefficient of concrete. From the similar triangles of the strain diagram, we have

$$\frac{\epsilon_c}{kd} = \frac{\epsilon'_s}{kd - d'} = \frac{\epsilon_s}{d - kd} \quad (10.4)$$

On substituting for ϵ_c , ϵ'_s , and ϵ_s in Eq. 10.4, the following equations for steel stress are obtained:

$$f'_s = \frac{kd - d'}{kd} nf_c \quad (10.5)$$

$$f_s = \frac{1 - k}{k} nf_c \quad (10.6)$$

where

$$n = \frac{E_s}{E_c}(1 + C_t) \quad (10.7)$$

The ratio n is known as the modular ratio.

The resultant compressive force in the concrete, ignoring the small area of concrete displaced by the compression steel, is $0.5f_c bkd$. The equation for equilibrium of internal forces may be written as

$$C_c + C_s = T \quad \text{or} \quad 0.5f_c bkd + f'_s A'_s = f_s A_s \quad (10.8)$$

Substituting the steel stresses from Eqs. 10.5 and 10.6 into Eq. 10.8 gives

$$0.5f_c bkd + \frac{kd - d'}{kd} nf_c A'_s = \frac{1 - k}{k} nf_c A_s$$

$$\therefore 0 = k^2 + 2k(\rho + \rho')n - 2\left(\rho + \rho' \frac{d'}{d}\right)n$$

where

$$\rho = \frac{A_s}{bd} \quad \text{and} \quad \rho' = \frac{A'_s}{bd}$$

Solution of the quadratic equation for k gives

$$k = \left[(\rho + \rho')^2 n^2 + 2\left(\rho + \rho' \frac{d'}{d}\right)n \right]^{1/2} - (\rho + \rho')n \quad (10.9)$$

The centroid of the triangular concrete stress block is at $kd/3$ from the extreme compression fiber; therefore the lever arm of the resultant concrete force about the tension steel is $d(1 - k/3)$, where k is given by Eq. 10.9.

The moment of resistance of the section can be obtained by taking moments of the internal compressive forces about the tension steel.

$$M = 0.5f_c bkd \left(d - \frac{kd}{3} \right) + f'_s A'_s (d - d') \quad (10.10)$$

Equations 10.5 to 10.10 can be used to determine the stresses in the concrete and steel for a given moment, or the moment for a given stress, when the dimensions of the concrete section, the steel areas, and bar positions, are known. Note that the equations can be used to analyze singly reinforced sections by putting $A'_s = 0$.

Example 10.1

A doubly reinforced concrete beam has a rectangular cross section 16 in (406 mm) wide; it has an effective depth to the centroid of the tension steel of 28.37 in (721 mm), a depth to the centroid of the

compression steel of 2.82 in (71.6 mm), an area of tension steel of 4.71 in² (3039 mm²), and an area of compression steel of 2.40 in² (1548 mm²). The modulus of elasticity of the concrete at first loading is 3.86×10^6 psi (26,600 N/mm²) and of the steel is 29×10^6 psi (200,000 N/mm²). Calculate the stresses in the steel and the concrete due to a bending moment of 2.28×10^6 lb · in (257 kN · m) (1) at first loading and (2) after long-term loading, if the creep coefficient is 1.0.

Solution

$$\rho = \frac{4.71}{16 \times 28.37} = 0.0104 \quad \rho' = \frac{2.40}{16 \times 28.37} = 0.00529$$

1. *At first loading*

Creep is zero, $C_t = 0$.

From Eq. 10.7 we have

$$n = \frac{29 \times 10^6}{3.86 \times 10^6} = 7.51$$

From Eq. 10.9 we have

$$\begin{aligned} k &= \left[(0.0104 + 0.00529)^2 7.51^2 \right. \\ &\quad \left. + 2 \left(0.0104 + 0.00529 \times \frac{2.82}{28.37} \right) 7.51 \right]^{1/2} \\ &\quad - 7.51(0.0104 + 0.00529) \\ &= 0.304 \end{aligned}$$

$$\therefore kd = 0.304 \times 28.37 = 8.62 \text{ in}$$

From Eqs. 10.5 and 10.6 we write

$$f'_s = \frac{8.62 - 2.82}{8.62} \times 7.51 f_c = 5.05 f_c$$

$$f_s = \frac{1 - 0.304}{0.304} \times 7.51 f_c = 17.19 f_c$$

Hence Eq. 10.10 gives

$$\begin{aligned} 2.28 \times 10^6 &= 0.5 f_c \times 16 \times 8.62 \left(28.37 - \frac{8.62}{3} \right) \\ &\quad + 5.05 f_c \times 2.40 (28.37 - 2.82) \end{aligned}$$

from which $f_c = 1100 \text{ psi (7.59 N/mm}^2\text{)}$.

$$\therefore f'_s = 5.05 \times 1100 = 5560 \text{ psi (38.3 N/mm}^2\text{)} \quad \text{and}$$

$$f_s = 17.19 \times 1100 = 18,910 \text{ psi (130.4 N/mm}^2\text{)}$$

2. After long-term loading when $C_t = 1$

From Eq. 10.7, $n = 7.51 (1 + 1) = 15.02$.

From Eq. 10.9, $k = 0.383$.

From Eqs. 10.5, 10.6, and 10.10,

$$f_c = 810 \text{ psi (5.59 N/mm}^2\text{)}$$

$$f'_s = 8950 \text{ psi (61.7 N/mm}^2\text{)}$$

$$f_s = 19,480 \text{ psi (134.3 N/mm}^2\text{)}$$

The effect of concrete creep on the stresses is indicated in this example. Concrete creep under constant bending moment results in an increase in the neutral axis depth, and leads to a decrease in the maximum concrete compressive stress, an increase in the steel compressive stress, and a slight increase in the steel tensile stress. Of these, the rise in the steel compressive stress is the most significant. In Example 10.1 the doubling of the modular ratio has resulted in a 61% increase in the compressive steel stress, a 26% decrease in the concrete compressive stress, and a 3% increase in the steel tensile stress. Note that the concrete creep has caused some of the internal compressive force to be transferred from the concrete to the steel.

T-Sections

Figure 10.2 displays a singly reinforced concrete *T*-beam section in the service load range after cracking. The dimensions of the concrete section and the steel areas and positions are considered to be known quantities. In the case illustrated, the neutral axis lies in the web. When the neutral axis lies in the flange, the case can be analyzed using the equations for a rectangular section of width b .

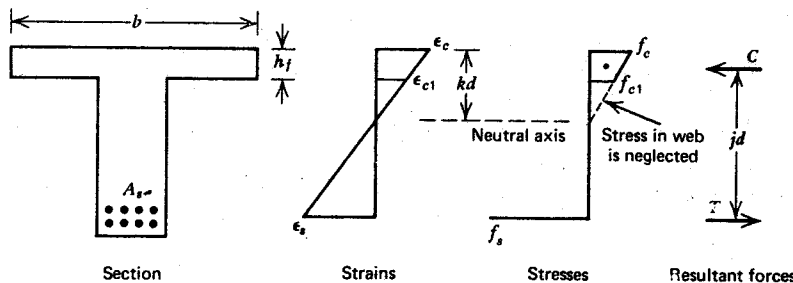


Fig. 10.2. Reinforced concrete *T*-beam section in service load range after cracking.

The section of Fig. 10.2 with neutral axis in the web can be analyzed using the requirements of strain compatibility and equilibrium of forces.

The strains may be written in terms of the stresses as follows:

$$\epsilon_c = \frac{f_c}{E_c} (1 + C_t), \quad \epsilon_{c1} = \frac{f_{c1}}{E_c} (1 + C_t), \quad \epsilon_s = \frac{f_s}{E_s}$$

where E_c = modulus of elasticity of concrete (at instant of loading), E_s = modulus of elasticity of steel, and C_t = creep coefficient of concrete.

From the similar triangles of the strain diagram, we have

$$\frac{\epsilon_c}{kd} = \frac{\epsilon_{c1}}{kd - h_f} = \frac{\epsilon_s}{d - kd} \quad (10.11)$$

On substituting for the strains in Eq. 10.11, the following equations for concrete and steel stress are obtained:

$$f_{c1} = \frac{kd - h_f}{kd} f_c \quad (10.12)$$

$$f_s = \frac{1 - k}{k} nf_c \quad (10.13)$$

where

$$n = \frac{E_s}{E_c} = (1 + C_t)$$

The compressive force in the concrete in the web is ignored, since it is relatively small because of the small stress and width of section there. The resultant compressive force in the concrete is then $0.5(f_c + f_{c1})bh_f$. On substituting Eq. 10.12, the resultant compressive force becomes

$$\begin{aligned} C &= 0.5 \left(f_c + \frac{kd - h_f}{kd} f_c \right) bh_f \\ &= bh_f f_c \left(1 - \frac{h_f}{2kd} \right) \end{aligned} \quad (10.14)$$

The equation for equilibrium of the internal forces $C = T$ may be written as

$$bh_f f_c \left(1 - \frac{h_f}{2kd} \right) = A_s f_s \quad (10.15)$$

Substituting f_s from Eq. 10.13 into Eq. 10.15 gives

$$bh_f f_c \left(1 - \frac{h_f}{2kd} \right) = A_s \frac{1 - k}{k} nf_c$$

from which we write

$$k = \frac{\rho n + \frac{1}{2}(h_f/d)^2}{\rho n + h_f/d} \quad (10.16)$$

where $\rho = A_s/bd$.

The value for k found from Eq. 10.16 applies providing the neutral axis lies in the web (i.e., $k \geq h_f/d$). If k from Eq. 10.16 is less than h_f/d , the neutral axis lies in the flange, and the rectangular section Eqs. 10.4 to 10.10 should be used instead.

The lever arm depends on the position of the centroid of the trapezoidal stress block (see Fig. 10.3). Treating the block as if it were composed of two

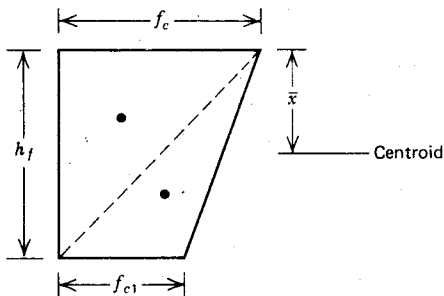


Fig. 10.3. Centroid of compressive stress block.

triangles, and taking the moments of the areas of the triangles about the top of the block, we find

$$\begin{aligned} \frac{1}{2}(f_c + f_{c1})h_f b \bar{x} &= \frac{f_{c1}h_f b}{2} \frac{2}{3}h_f + \frac{f_c h_f b}{2} \frac{h_f}{3} \\ \therefore \bar{x} &= \frac{h_f}{3} \left(\frac{2f_{c1} + f_c}{f_{c1} + f_c} \right) \end{aligned}$$

On substituting f_{c1} from Eq. 10.12

$$\bar{x} = \frac{h_f}{3} \frac{\left\{ 2 \left(\frac{kd - h_f}{kd} \right) + 1 \right\} f_c}{\left(\frac{kd - h_f}{kd} + 1 \right) f_c} = \frac{h_f}{3} \left(\frac{3kd - 2h_f}{2kd - h_f} \right) \quad (10.17)$$

$$\therefore jd = d - \bar{x} = d - \frac{h_f}{3} \left(\frac{3kd - 2h_f}{2kd - h_f} \right) \quad (10.18)$$

The moment of resistance of the section is then

$$M = A_s f_s j d \quad (10.19)$$

or

$$M = b h_f f_c \left(1 - \frac{h_f}{2kd}\right) j d \quad (10.20)$$

with jd from Eq. 10.18.

Equations 10.12 to 10.20 can be used to determine the stresses in the concrete and steel for a given moment, or the moment for a given stress, when the section dimensions and the steel area are known.

Example 10.2

A reinforced concrete *T*-beam has a flange width of 50 in (1270 mm), a flange thickness of 5 in (127 mm), an effective depth to the steel of 20 in (508 mm), and a cross-sectional area of tension steel of 6 in² (3871 mm²). The modular ratio is 9. Determine (1) the stresses in the steel and concrete when the section carries a bending moment of 2×10^6 lb · in (226 kN · m), and (2) the maximum bending moment the section can carry if the maximum concrete stress is not to exceed 1350 psi (9.31 N/mm²) and the steel stress is not to exceed 24,000 psi (165.5 N/mm²).

Solution

Assume that the neutral axis lies in the web.

$$\rho n = \frac{6}{50 \times 20} \times 9 = 0.054 \quad \frac{h_f}{d} = \frac{5}{20} = 0.25$$

From Eq. 10.16 we have

$$k = \frac{0.054 + \frac{1}{2}(0.25)^2}{0.054 + 0.25} = 0.280$$

$$\therefore kd = 0.28 \times 20 = 5.60 \text{ in} > h_f$$

Therefore the neutral axis lies in the web as assumed.

From Eq. 10.18 we have

$$jd = 20 - \frac{5}{3} \left(\frac{3 \times 5.6 - 2 \times 5}{2 \times 5.6 - 5} \right) = 18.17 \text{ in}$$

1. *Stresses for $M = 2 \times 10^6$ lb · in*

From Eq. 10.19 we write

$$f_s = \frac{2 \times 10^6}{6 \times 18.17} = 18,350 \text{ psi (126.6 N/mm}^2\text{)}$$

From Eq. 10.20 we write

$$f_c = \frac{2 \times 10^6}{50 \times 5[1 - 5/(2 \times 5.6)]18.17} = 795 \text{ psi (5.52 N/mm}^2\text{)}$$

or, from Eq. 10.13,

$$f_c = \frac{0.280}{1 - 0.280} \frac{18,350}{9} = 795 \text{ psi (5.52 N/mm}^2\text{)}$$

2. *Maximum bending moment if $f_s \leq 24,000$ psi and $f_c \leq 1,350$ psi*

If $f_s = 24,000$ psi, Eq. 10.19 gives us

$$\begin{aligned} M &= 6 \times 24,000 \times 18.17 \\ &= 2.62 \times 10^6 \text{ lb · in} \end{aligned}$$

If $f_c = 1,350$ psi, Eq. 10.20 gives us

$$\begin{aligned} M &= 50 \times 5 \times 1350 \left(1 - \frac{5}{2 \times 5.6}\right) 18.17 \\ &= 3.39 \times 10^6 \text{ lb · in} \end{aligned}$$

Therefore, the steel stress controls. The maximum permissible bending moment is $M = 2.62 \times 10^6$ lb · in (296 kN · m), with $f_s = 24,000$ psi (165.5 N/mm²) and $f_c = 1350 \times 2.62/3.39 = 1040$ psi (7.17 N/mm²).

10.2.4 Analysis of Beams Using the Transformed Section Approach

An alternative elastic theory approach employs transformed section theory, in which the steel is transformed into an equivalent concrete area and the "all concrete" section is analyzed by conventional elastic theory.

Consider an element of concrete area with a steel bar at its centroid, as in Fig. 10.4. If an external axial load P is applied to the element, the resulting steel and concrete strain will be equal, $\varepsilon_s = \varepsilon_c$, giving

$$\begin{aligned} \frac{f_s}{E_s} &= \frac{f_c}{E_c} (1 + C_t) \\ \therefore f_s &= \eta f_c \end{aligned} \tag{10.21}$$

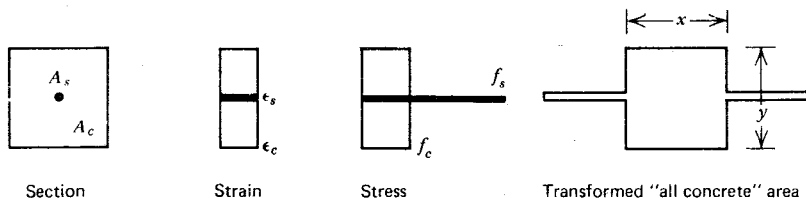


Fig. 10.4. Transformed area of reinforced concrete element.

where

$$n = \frac{E_s}{E_c} (1 + C_t)$$

The load carried by the element is therefore

$$\begin{aligned} P &= A_c f_c + A_s f_s \\ &= f_c (A_c + n A_s) \end{aligned} \quad (10.22)$$

where A_c = concrete area and A_s = steel area. It is evident that the steel area A_s acts identically to a concrete area $n A_s$, and hence could be replaced by a concrete area $n A_s$. This equivalent concrete area $n A_s$ is referred to as the transformed area of steel. Thus the total area of the transformed element is $A_c + n A_s = xy + (n - 1) A_s$. The effective added area is $(n - 1) A_s$ because the steel displaces an area of concrete A_s . The transformed section is represented in Fig. 10.4. The transformed section may be pictured in any way that results in the transformed area of steel having the same level of strain as the steel it replaces. The transformed area of steel is also placed symmetrically about the steel it replaces. Replacing the steel by its transformed area is advantageous because conventional elastic theory for a homogeneous material can be used to analyze the element. The steel stress may be determined from $n f_c$, where f_c is the concrete stress at that point.

If the element of area is part of a section subjected to flexure, the concrete area that replaces the steel must be placed in a symmetrical manner parallel to the neutral axis, to have the same level of strain as the steel (see Figs. 10.5 and 10.6). For the uncracked section, the steel areas A'_s and A_s are replaced by transformed areas $(n - 1) A'_s$ and $(n - 1) A_s$. For the cracked section, the compression steel area A'_s is replaced by $(n - 1) A'_s$, but the tension steel area A_s is replaced by $n A_s$ because the actual concrete section below the neutral axis cannot carry tension, hence the tension steel does not displace any effective concrete.

Conventional elastic theory for a section of homogeneous material may be used to analyze the transformed section. For a beam, the stress f and

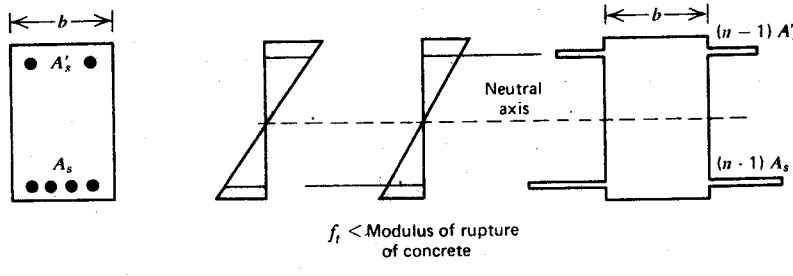


Fig. 10.5. Transformed section for flexure before cracking.

bending moment M are related by the equation (see any text on strength of materials)

$$f = \frac{My}{I} \quad (10.23)$$

where y = distance from the neutral axis to the fiber concerned and I = moment of inertia (second moment of area) of the transformed section about the neutral axis. Since the neutral axis is located at the centroid of the transformed section, the neutral axis position may be found by taking moments of the areas about any convenient axis. The moment of inertia is given by $\int y^2 dA$, where y = distance from the neutral axis to an element of area and dA = area of the element.

Example 10.3

A singly reinforced concrete beam with the cross section indicated in Fig. 10.7 has concrete with a modulus of rupture of 450 psi (3.1 N/mm^2). The modular ratio is $n = 8$. Calculate the stresses in the steel and the concrete when the bending moment is (1) 300,000 lb · in (33.9 kN · m), and (2) 900,000 lb · in (101.6 kN · m).

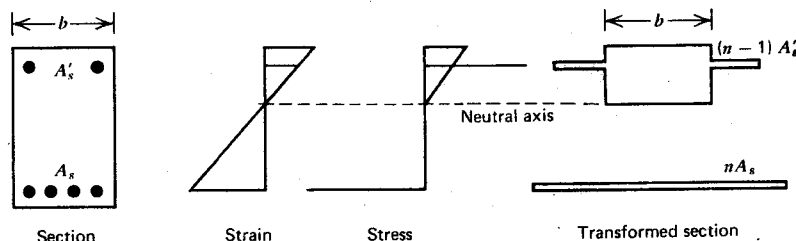


Fig. 10.6. Transformed section for flexure after cracking.

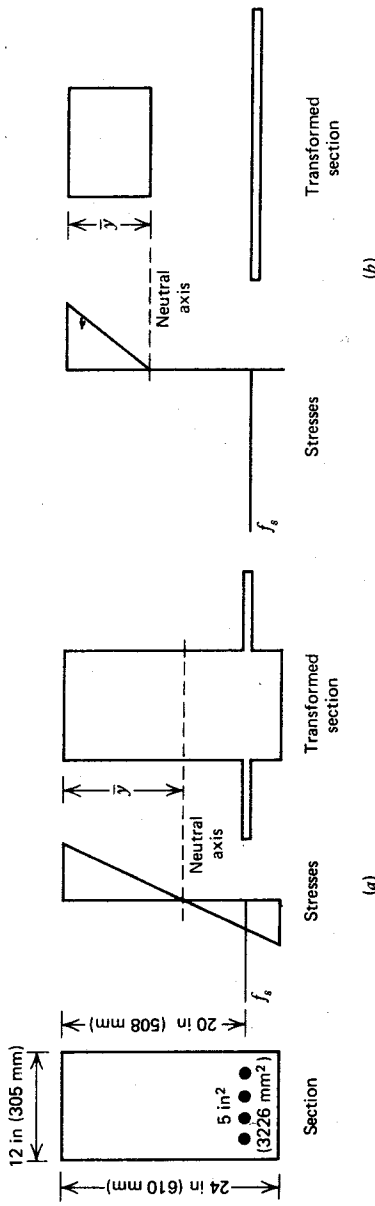


Fig. 10.7. Example 10.3. (a) Before cracking. (b) After cracking.

Solution**Transformed section properties****Before cracking (Fig. 10.7a)**

$$(n - 1)A_s = (8 - 1) \times 5 = 35 \text{ in}^2$$

$$\therefore A = (12 \times 24) + 35 = 288 + 35 = 323 \text{ in}^2$$

Taking moments about the top edge to find \bar{y} :

$$323\bar{y} = (288 \times 12) + (35 \times 20) \quad \therefore \bar{y} = 12.87 \text{ in}$$

$$\begin{aligned} \therefore I &= \frac{12 \times 24^3}{12} + (288 \times 0.87^2) + (35 \times 7.13^2) \\ &= 15,820 \text{ in}^4 \end{aligned}$$

After cracking (Fig. 10.7b)

$$nA_s = 8 \times 5 = 40 \text{ in}^2$$

$$\therefore A = 12\bar{y} + 40$$

Taking moments about the neutral axis to find \bar{y} :

$$12\bar{y} \frac{\bar{y}}{2} = 40(20 - \bar{y})$$

$$\therefore \bar{y}^2 + 6.67\bar{y} - 133.3 = 0 \quad \therefore \bar{y} = 8.68 \text{ in}$$

$$\begin{aligned} \therefore I &= \frac{12 \times 8.68^3}{12} + (12 \times 8.68 \times 4.34^2) + (40 \times 11.32^2) \\ &= 7740 \text{ in}^4 \end{aligned}$$

Note that it is assumed that the transformed area of steel has negligible thickness; hence the moment of inertia about its own centroid can be ignored. Also, for the section of this example the effect of cracking is to reduce the I value by 51%.

Moment to cause cracking

$$M_{\text{cracking}} = \frac{f_r I_{\text{uncracked}}}{y_{\text{bottom}}}$$

where f_r = modulus of rupture of concrete

$$\begin{aligned} \therefore M_{\text{cracking}} &= \frac{450 \times 15,820}{11.13} \\ &= 639,600 \text{ lb} \cdot \text{in} \end{aligned}$$

1. $M = 300,000 \text{ lb} \cdot \text{in}$; therefore, section is uncracked.

$$f = \frac{My}{I}$$

$$\text{top } f_c = 300,000 \times 12.87/15,820 = 244 \text{ psi (1.68 N/mm}^2)$$

$$\text{bottom } f_c = 300,000 \times 11.13/15,820 = 211 \text{ psi (1.46 N/mm}^2)$$

$$\begin{aligned} f_s &= nf_c = 8 \times 300,000 \times 7.13/15,820 \\ &= 1080 \text{ psi (7.45 N/mm}^2) \end{aligned}$$

2. $M = 900,000 \text{ lb} \cdot \text{in}$; therefore, section is cracked.

$$\text{top } f_c = 900,000 \times 8.68/7740 = 1010 \text{ psi (6.96 N/mm}^2)$$

$$f_s = 8 \times 900,000 \times 11.32/7740 = 10,530 \text{ psi (72.6 N/mm}^2)$$

Note the significant increase in steel stress after cracking. When cracking occurs at a bending moment of 639,600 lb · in (72.2 kN · m) the maximum concrete stress increases from 520 to 720 psi (3.6 to 5.0 N/mm²) and the steel stress increases from 2300 to 7480 psi (15.9 to 51.6 N/mm²).

10.2.5 Design of Beams Using the Alternative (Elastic Theory) Method

The 1971 ACI code^{10.1} allows the design of flexural members without axial load by the elastic theory approach (straight line theory). This design method proportions members so that at the service loads the specified allowable stresses are not exceeded. The allowable compressive stress in the concrete is $0.45f'_c$. The allowable tensile stress in the steel is 20,000 psi (138 N/mm²) for Grade 40 or Grade 50 steel ($f_y = 276$ or 345 N/mm²), or 24,000 psi (166 N/mm²) for Grade 60 steel ($f_y = 414$ N/mm²) or higher grade steel. The modular ratio n stipulated by the code is E_s/E_c , except that in doubly reinforced members, an effective modular ratio of $2E_s/E_c$ is used when considering the compression steel. The value taken for E_s is 29×10^6 psi (200,000 N/mm²), and for both normal weight and lightweight concrete E_c is $57,000\sqrt{f'_c}$ psi (4730 $\sqrt{f'_c}$ N/mm²). The modular ratio n may be taken as the nearest whole number.

The recommended value for the modular ratio ignores the effect of concrete creep except as it effects the compression steel, whereupon the creep coefficient is taken as $C_t = 1$. The reason for this is revealed in Example 10.1. Comparison of stresses after creep with stresses before creep indicates a very significant increase in the compressive steel stress, but only a very slight increase in the tensile steel stress and a decrease in the compressive concrete stress. This approach means that when a doubly reinforced section is first loaded, the concrete will be more highly stressed than calculated, but the

compressive concrete stress will decrease with time because of creep, and the compression steel stress will gradually increase and approach the design value.

Design of Singly Reinforced Rectangular Sections for Simultaneous Development of the Allowable Steel and Concrete Stresses

A convenient approach, which makes good use of the materials, is to design for simultaneous development of the allowable stresses of the steel and concrete at the service load bending moment.

Equation 10.6 shows that

$$\frac{f_s}{nf_c} = \frac{1 - k}{k}$$

where

$$n = \frac{E_s}{E_c}$$

or

$$k = \frac{nf_c}{nf_c + f_s} \quad (10.24)$$

Thus k for given allowable stresses may be found from Eq. 10.24. The design equations then are

$$M = 0.5f_c bkd \left(d - \frac{kd}{3} \right) \quad (10.25)$$

and

$$M = A_s f_s \left(d - \frac{kd}{3} \right) \quad (10.26)$$

Equation 10.25 may be written as

$$bd^2 = \frac{2M}{f_c k (1 - k/3)} \quad (10.25a)$$

which enables the selection of section dimensions for a given moment and simultaneous development of allowable stresses. Also Eq. 10.26 may be rewritten as

$$A_s = \frac{M}{f_s d (1 - k/3)} \quad (10.26a)$$

which enables the required steel area to be found.

A design in which the allowable stresses of the steel and concrete are developed simultaneously has in the past been referred to as a "balanced design." That terminology is not used here because of possible confusion with a "balanced failure" of the strength design method. The simultaneous development of the allowable steel and concrete stresses at the service load does not mean that such a section would undergo a balanced failure if loaded to its flexural strength. Such a section would invariably undergo a tension failure because the curved shape of the concrete compressive stress block at high stresses means that a large compressive force can be developed by the concrete. Also, the chosen ratios of allowable stress to yield or ultimate strength will influence the balance of steel and concrete strength.

Example 10.4

Design a singly reinforced rectangular section with a width of 10 in (254 mm) to carry a service load bending moment of 1.2×10^6 lb · in (135 kN · m). The allowable steel and concrete stresses, $f_s = 0.5f_y$ and $f_c = 0.45f'_c$, are to be developed simultaneously. The material strengths are $f_y = 40,000$ psi (276 N/mm²) and $f'_c = 3000$ psi (20.7 N/mm²).

Solution

Allowable stresses are $f_s = 20,000$ psi and $f_c = 0.45 \times 3000 = 1350$ psi. Also, $E_c = 57,000\sqrt{3000} = 3.12 \times 10^6$ psi. Hence $n = E_s/E_c = 29 \times 10^6/(3.12 \times 10^6) = 9.29$. Therefore, use $n = 9$.

From Eq. 10.24 we have

$$k = \frac{9 \times 1350}{9 \times 1350 + 20,000} = 0.378$$

From Eqs. 10.25 or 10.25a we have

$$1.2 \times 10^6 = 0.5 \times 1350 \times 10 \times 0.378 \left(1 - \frac{0.378}{3}\right) d^2$$

$$\therefore d = 23.2 \text{ in (589 mm)}$$

From Eqs. 10.26 or 10.26a we put

$$1.2 \times 10^6 = A_s 20,000 \times 23.2 \left(1 - \frac{0.378}{3}\right)$$

$$\therefore A_s = 2.96 \text{ in}^2 (1910 \text{ mm}^2)$$

Design of Singly Reinforced Rectangular Sections Without Simultaneous Development of the Allowable Stresses

A section in which the allowable steel and concrete stresses are developed simultaneously is not necessarily the most economical section. The relative costs of steel and concrete, the necessity to standardize sizes throughout a structure, and other reasons, may make it more convenient to have a section of such proportions that the allowable stresses are not developed simultaneously. The design will then be governed either by the stress in the steel or in the concrete. The critical stress will depend on the allowable stresses and the steel ratio $\rho = A_s/bd$.

For a given ρ the neutral axis depth of a singly reinforced section is given by Eq. 10.9 as

$$k = \sqrt{\rho^2 n^2 + 2\rho n} - \rho n \quad (10.27)$$

The value of k for the simultaneous development of the allowable steel and concrete stresses is given by Eq. 10.24, with the allowable stresses substituted for f_c and f_s .

If it is found that the actual value of k for the section is less than the value of k for the simultaneous development of the allowable stresses, then at the allowable bending moment f_s equals allowable steel stress but f_c is less than allowable concrete stress (see Fig. 10.8). The allowable bending moment is given by Eq. 10.26 as

$$M = A_s f_s \left(d - \frac{kd}{3} \right)$$

with f_s at the allowable value.

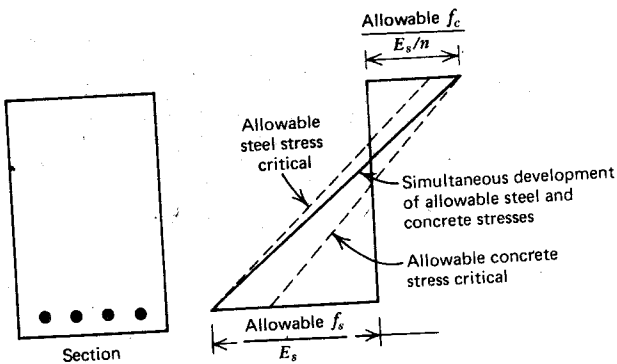


Fig. 10.8. Strain diagrams for section with allowable steel and concrete stresses critical.

Alternatively, if k exceeds the value of k for the simultaneous development of the allowable stresses, Fig. 10.8 shows that at the allowable bending moment f_c equals allowable concrete stress but f_s is less than allowable steel stress. The allowable bending moment is given by Eq. 10.25 as

$$M = 0.5f_c bkd \left(d - \frac{kd}{3} \right)$$

with f_c at the allowable value.

From Eq. 10.25 it is evident that

$$\frac{M}{bd^2} = 0.5f_c k \left(1 - \frac{k}{3} \right) \quad (10.28)$$

In design, if the dimensions of the concrete section are known, the best way to check whether the steel or the concrete stress will be critical is to calculate the value of $0.5f_c k(1 - k/3)$ for simultaneous development of the allowable stresses and to compare it with the M/bd^2 value for the section, where M is the service load bending moment. If $M/bd^2 < 0.5f_c k(1 - k/3)$ for the simultaneous development of the allowable stresses, the steel stress is critical; and if $M/bd^2 > 0.5f_c k(1 - k/3)$ for the simultaneous development of the allowable stresses, the concrete stress is critical.

Example 10.5

A reinforced concrete rectangular section with an 18 in (457 mm) width and a 32 in (813 mm) effective depth to the tension steel is to carry a service load bending moment of 2.8×10^6 lb · in (316 kN · m). The modular ratio is $n = 9$, and the allowable stresses are 1350 psi (9.31 N/mm²) for the concrete and 24,000 psi (166 N/mm²) for the steel. Calculate the required steel area.

Solution

From Eq. 10.24 the value of k for the simultaneous development of the allowable stresses is

$$k = \frac{9 \times 1350}{9 \times 1350 + 24,000} = 0.336$$

$$\therefore 0.5f_c k \left(1 - \frac{k}{3} \right) = 0.5 \times 1350 \times 0.336 (1 - 0.112) = 201$$

Now

$$\frac{M}{bd^2} = \frac{2.8 \times 10^6}{18 \times 32^2} = 152 < 201$$

Therefore the steel stress will be critical (i.e., f_s = allowable steel stress and $f_c <$ allowable concrete stress).

Now the actual value for k will be smaller than $k = 0.336$. However the use of $k = 0.336$ to find the lever arm will give a very good approximation, slightly on the safe side (the actual lever arm will be a little larger).

$$\therefore jd = 32 \left(1 - \frac{0.336}{3} \right) = 28.42 \text{ in}$$

$$\therefore A_s = \frac{M}{jdf_s}$$

$$= \frac{2.8 \times 10^6}{28.42 \times 24,000} = 4.11 \text{ in}^2 (2648 \text{ mm}^2)$$

Design of Doubly Reinforced Rectangular Sections

In the design of sections where M/bd^2 exceeds the value of $0.5f_c k(1 - k/3)$ for the simultaneous development of the allowable stresses, the concrete stress is critical. It is best to use both compression and tension steel in this case, since tension steel alone could require a large area of steel working at less than the allowable stress.

To design a doubly reinforced section (see Fig. 10.9) the most convenient first step is to calculate the bending moment that a singly reinforced beam with the given dimensions could carry if the allowable steel and concrete stresses are developed simultaneously.

$$M_1 = 0.5f_c bkd \left(d - \frac{kd}{3} \right) \quad (10.29)$$

where f_c is the allowable value and k is found using the allowable stresses.

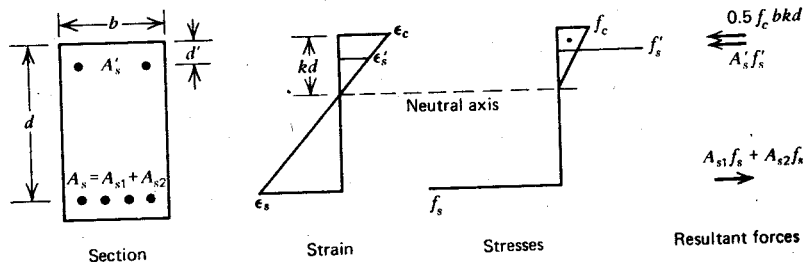


Fig. 10.9. Design of doubly reinforced concrete section.

Then the area of tension steel A_{s1} required for M_1 may be calculated

$$A_{s1} = \frac{M_1}{f_s(d - kd/3)} \quad (10.30)$$

where f_s is the allowable value. The remainder of the bending moment, $M - M_1$, must be resisted by an internal couple formed by compression steel area A'_s and additional tension steel area A_{s2} with a lever arm of $d - d'$.

$$\therefore A_{s2} = \frac{M - M_1}{f_s(d - d')} \quad (10.31)$$

where f_s is the allowable value, and

$$A'_s = \frac{M - M_1}{f'_s(d - d')} \quad (10.32)$$

where f'_s is governed by the strain in the adjacent concrete. From the strain diagram of Fig. 10.9, we can write

$$\begin{aligned} \frac{\varepsilon'_s}{\varepsilon_c} &= \frac{kd - d'}{kd} \\ \therefore f'_s &= \varepsilon'_s E_s = \varepsilon_c \left(\frac{kd - d'}{kd} \right) E_s \end{aligned}$$

But

$$\begin{aligned} \varepsilon_c &= \frac{f_c}{E_c} (1 + C_t) \\ \therefore f'_s &= n f_c \left(\frac{kd - d'}{kd} \right) \end{aligned} \quad (10.33)$$

where

$$n = \frac{E_s}{E_c} (1 + C_t)$$

Example 10.6

A rectangular concrete section has $b = 15$ in (381 mm), $d' = 3.6$ in (91 mm), and $d = 35.6$ in (904 mm), the allowable stresses are 1125 psi (7.76 N/mm^2) for the concrete and 20,000 psi (138 N/mm^2) for the steel. The ratio E_s/E_c is 10. Calculate the steel areas required for a service load moment of 5×10^6 lb · in (565 kN · m).

Solution

According to ACI 318-71,^{10.1} $n = E_s/E_c = 10$; except when determining the area of compression steel, $n = 2E_s/E_c = 20$.

From Eq. 10.24, the value of k for simultaneous development of the allowable stresses is

$$k = \frac{10 \times 1125}{10 \times 1125 + 20,000} = 0.360 \quad 1 - \frac{k}{3} = 1 - 0.12 = 0.88$$

From Eqs. 10.29 and 10.30 we have

$$M_1 = 0.5 \times 1125 \times 15 \times 0.36 \times 35.6 \times 35.6 \times 0.88 \\ = 3.39 \times 10^6 \text{ lb} \cdot \text{in}$$

$$A_{s1} = \frac{3.39 \times 10^6}{20,000 \times 35.6 \times 0.88} = 5.41 \text{ in}^2$$

From Eqs. 10.31 to 10.33 we have

$$A_{s2} = \frac{(5 - 3.39) \times 10^6}{20,000(35.6 - 3.6)} = 2.52 \text{ in}^2$$

$$f'_s = 20 \times 1125 \times \left(\frac{0.36 \times 35.6 - 3.6}{0.36 \times 35.6} \right) = 16,180 \text{ psi} < 20,000 \text{ psi}$$

$$\therefore A'_s = \frac{(5 - 3.39) \times 10^6}{16,180(35.6 - 3.6)} = 3.11 \text{ in}^2 (2006 \text{ mm}^2)$$

$$\therefore A_s = A_{s1} + A_{s2} = 5.41 + 2.52 = 7.93 \text{ in}^2 (5116 \text{ mm}^2)$$

Note that the stress in the compression steel should not exceed the allowable steel stress. If the calculated value for f'_s goes beyond the allowable stress, the allowable stress should be used instead of the calculated stress.

Design of T-Beam Sections

A T-beam section in which the allowable steel and concrete stresses develop simultaneously will have k as given by Eq. 10.24 with the allowable stresses substituted. From Eqs. 10.18 and 10.20 we find

$$M = bh_f f_c \left(1 - \frac{h_f}{2kd} \right) \left[d - \frac{h_f}{3} \left(\frac{3kd - 2h_f}{2kd - h_f} \right) \right]$$

$$\therefore \frac{M}{bh_f f_c} = \left(\frac{2kd - h_f}{2kd} \right) \left[\frac{6kd^2 - 3h_f d - 3kdh_f + 2h_f^2}{3(2kd - h_f)} \right]$$

$$= d - \frac{1}{2} \frac{h_f}{k} - \frac{h_f}{2} + \frac{1}{3} \frac{h_f^2}{kd}$$

$$\therefore 0 = d^2 - d \left[\frac{M}{bh_f f_c} + \frac{h_f}{2k} (1 + k) \right] + \frac{h_f^2}{3k} \quad (10.34)$$

Equation 10.34 allows the determination of the effective depth of a *T*-beam section in which the allowable stresses develop simultaneously. Then the steel area may be found, using Eqs. 10.18 and 10.19.

Example 10.7

A *T*-beam section has a flange width of 48 in (1220 mm) and a flange thickness of 5 in (127 mm). The service load bending moment is 6×10^6 lb · in (677 kN · m). Calculate the effective depth and steel area if $n = 9$ and the allowable stresses of 1350 psi (9.31 N/mm²) for the concrete and 20,000 psi (138 N/mm²) for the steel develop simultaneously.

Solution

From Eq. 10.24, the value of k for simultaneous development of the allowable stresses is

$$k = \frac{9 \times 1350}{9 \times 1350 + 20,000} = 0.378$$

From Eq. 10.34 we have

$$\begin{aligned} 0 &= d^2 - d \left(\frac{6 \times 10^6}{48 \times 5 \times 1350} + \frac{5 \times 1.378}{2 \times 0.378} \right) + \frac{5^2}{3 \times 0.378} \\ &= d^2 - 27.63d + 22.05 \\ \therefore d &= 28.4 \text{ in (721 mm)} \end{aligned}$$

From Eqs. 10.18 and 10.19 we have

$$\begin{aligned} jd &= 28.4 - \frac{5}{3} \left(\frac{3 \times 0.378 \times 28.4 - 2 \times 5}{2 \times 0.378 \times 28.4 - 5} \right) = 26.15 \text{ in} \\ \therefore A_s &= \frac{6 \times 10^6}{20,000 \times 26.15} \\ &= 11.47 \text{ in}^2 (7400 \text{ mm}^2) \end{aligned}$$

A design for *T*-beams based on the simultaneous development of the allowable stresses usually results in a relatively shallow section with a large area of steel to be placed in the web. A deeper section may be more desirable. A *T*-beam section deeper than that for simultaneous development of the allowable stresses will have $f_s = \text{allowable steel stress}$ and $f_c < \text{allowable concrete stress}$. For such a section, the steel area can be found from $A_s = M/f_s jd$. A reasonable approximation for jd is $d - 0.5h_f$.

10.2.6 Analysis of Short Columns

Axially Loaded Short Columns

If an axial load P is applied to the centroid of the section of a reinforced concrete short column with concrete area A_c and steel area A_s , the load is shared between the concrete and the steel.

$$P = A_c f_c + A_s f_s$$

The steel and concrete will have the same strain over the whole section, and from Eq. 10.21, $f_s = n f_c$, where $n = (E_s/E_c)(1 + C_t)$.

$$\therefore P = f_c(A_c + A_s n) \quad (10.35)$$

or

$$P = f_s \left(\frac{A_c}{n} + A_s \right) \quad (10.36)$$

In a column under sustained load, n will increase with time because of increase in the creep coefficient C_t , and a large redistribution of stress between the concrete and the steel will result.

Example 10.8

A 10 in (254 mm) square reinforced concrete column is symmetrically reinforced by 1.76 in² (1135 mm²) of steel; $E_s/E_c = 10$. The column is to carry an axial load of 200 kips (890 kN). Calculate the stresses (1) at the first application of the load, (2) after a long period of loading if the creep coefficient is $C_t = 2$, and (3) when the load is removed after the long period of loading.

Solution

$$A_s = 1.76 \text{ in}^2 \quad A_c = 100 - 1.76 = 98.24 \text{ in}^2$$

1. At first application of loading, $C_t = 0$

$$\therefore n = 10$$

From Eqs. 10.35 and 10.36 we write

$$f_c = \frac{200,000}{98.24 + 1.76 \times 10} = 1727 \text{ psi (11.9 N/mm}^2\text{)}$$

$$f_s = \frac{200,000}{98.24/10 + 1.76} = 17,270 \text{ psi (119 N/mm}^2\text{)}$$

2. After a long period of loading, $C_t = 2$.

$$\therefore n = 10(1 + 2) = 30$$

From Eqs. 10.35 and 10.36 we have

$$f_c = \frac{200,000}{98.24 + 1.76 \times 30} = 1324 \text{ psi (9.12 N/mm}^2)$$

$$f_s = \frac{200,000}{98.24/30 + 1.76} = 39,720 \text{ psi (274 N/mm}^2)$$

3. On removal of loading after the long period of application

The change in stress on the removal of the loading will be due to elastic behavior with $n = 10$. The residual stresses when the load is removed are therefore found from case 2 minus case 1.

$$f_c = 1320 - 1730 = -410 \text{ psi (2.83 N/mm}^2), \text{ tension}$$

$$f_s = 39,760 - 17,270 = 22,490 \text{ psi (155 N/mm}^2), \text{ compression}$$

It is to be noted that creep recovery of the concrete will cause these residual stresses to reduce with time.

Fig. 10.10 illustrates the changes of stresses in the column with time.

The foregoing example illustrates that creep of concrete with sustained load results in a decrease in the concrete compressive stress and a considerable increase in the steel compressive stress. The increase in steel stress may even be sufficient to cause the steel to reach the yield strength at the service load.

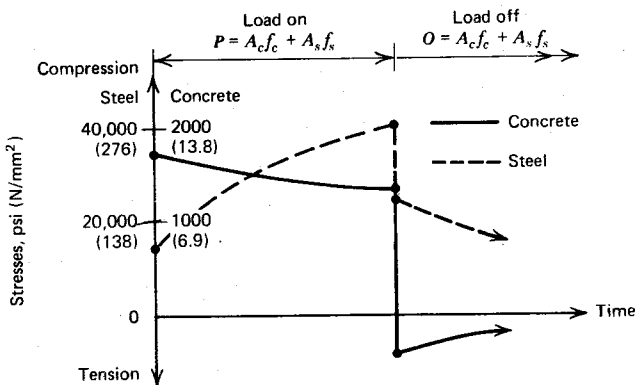


Fig. 10.10. Stresses of Example 10.8.

Creep of concrete at a sustained service load will not affect the safety of the column, however. The ultimate load of a short column is not reached until both the steel and the concrete have attained their strengths. That is, sufficient load must be applied to cause the steel to reach its yield strength and the concrete to reach its crushing strength before the ultimate load is attained (see Section 5.2). Some loss in concrete strength may arise from the effect of sustained loading (see Section 2.1.1), but since the concrete stress level at service loads is relatively low, this effect would be negligible.

Example 10.8 also illustrates that if the load is removed, the concrete may be left with a residual tension, and the steel with considerable residual compression, which will reduce with time due to creep.

It is evident that it is extremely difficult to realistically assess the safety of reinforced concrete columns using elastic theory. ACI 318-71^{10.1} does not allow elastic theory for column design. However an elastic analysis, including an allowance for the likely order of the creep effect, is necessary when deformation under service load conditions are to be evaluated.

Eccentrically Loaded Short Columns

Depending on the magnitude of the eccentricity of load, tension may or may not exist in the concrete.

COMPRESSION OVER WHOLE SECTION

The transformed section approach is best for the case of compression over whole section. The concrete stresses for a short column with bending about one major axis due to load P acting at eccentricity e from the centroid of the transformed section are given by

$$f = \frac{P}{A} \pm \frac{Pey}{I} \quad (10.37)$$

where y = distance from the centroid of the transformed section to the fiber concerned, A = area of the transformed section, and I = moment of inertia (second moment of area) of the transformed section about the centroidal axis. The steel stress is given by n times the stress in the adjacent concrete.

Example 10.9

The concrete column section in Fig. 10.11 is unsymmetrically reinforced by five No. 8 (25.4 mm diameter) bars, each placed with its centroid at 2 in (51 mm) from the adjacent faces of the column. Find the stresses due to a 100 kip (445 kN) load placed as shown, if the modular ratio is $n = 20$.

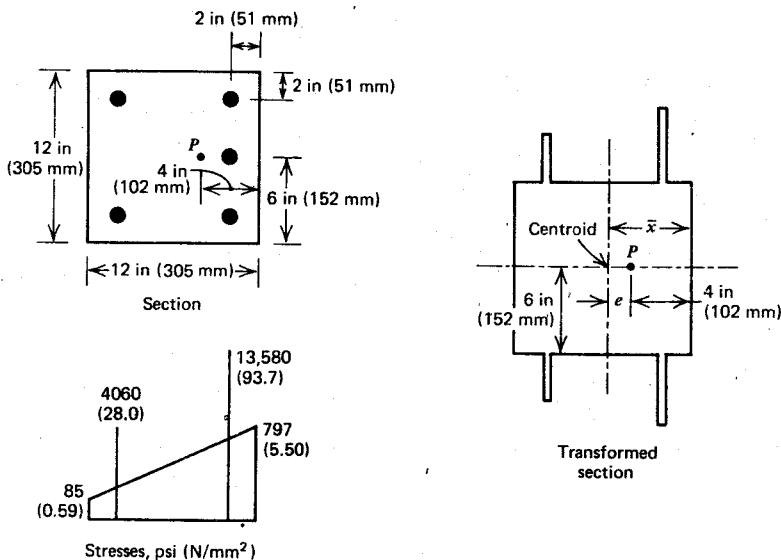


Fig. 10.11. Example 10.9.

Solution

Area of each bar is 0.79 in^2 .

Transformed area of section is

$$A = 12 \times 12 + (20 - 1)3 \times 0.79 + (20 - 1)2 \times 0.79 \\ = 144 + 45.0 + 30.0 = 219 \text{ in}^2$$

Position of centroid \bar{x} may be found by taking moments about right hand edge

$$219 \bar{x} = (144 \times 6) + (45 \times 2) + (30 \times 10)$$

$$\therefore \bar{x} = 5.73 \text{ in}$$

$$\therefore \text{eccentricity of load } e = 5.73 - 4 = 1.73 \text{ in}$$

Moment of inertia is

$$I = \left(\frac{1}{12} \times 12 \times 12^3 + 144 \times 0.27^2\right) + (45 \times 3.73^2) + (30 \times 4.27^2) \\ = 2912 \text{ in}^4$$

Therefore, from Eq. 10.37, we have

$$f = \frac{100,000}{219} \pm \frac{100,000 \times 1.73x}{2912} = 457 \pm 59.4x$$

$$\begin{aligned}
 \text{At left edge, } f_c &= 457 - 59.4 \times 6.27 = 85 \text{ psi (0.59 N/mm}^2\text{)}, \\
 \text{At right edge, } f_c &= 457 + 59.4 \times 5.73 = 797 \text{ psi (5.50 N/mm}^2\text{)} \\
 \text{At left steel, } f_s &= 20(457 - 59.4 \times 4.27) \\
 &= 4060 \text{ psi (28.0 N/mm}^2\text{)}
 \end{aligned}$$

$$\text{At right steel, } f_s = 20(457 + 59.4 \times 3.73) \\ = 13,580 \text{ psi (93.7 N/mm}^2\text{)}$$

Compression exists over the whole section.

TENSION OVER PART OF SECTION

If the eccentricity of the loading is large, significant tensile stress will be induced in the concrete and the concrete will crack. This case can be analyzed using the transformed section approach, ignoring the concrete in tension. Alternatively, the internal couple approach can be used.

The strain and stress diagrams for a cracked section reinforced symmetrically by bars in two opposite faces appear in Fig. 10.12. The stresses can be related by the strain diagram and the modular ratio in the same manner.

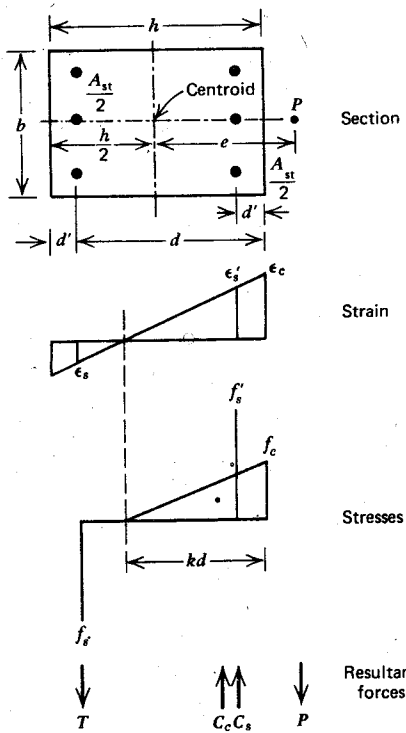


Fig. 10.12. Symmetrically reinforced column with eccentric loading.

employed for a doubly reinforced beam (see Eqs. 10.4 to 10.7). The stresses are given by

$$f'_s = \left(\frac{kd - d'}{kd} \right) nf_c \quad \text{and} \quad f_s = \frac{1 - k}{k} nf_c$$

where

$$n = \frac{E_s}{E_c} (1 + C_t)$$

The equilibrium equations for the section are

$$P = 0.5f_c bkd + f'_s 0.5A_{st} - f_s 0.5A_{st} \quad (10.38)$$

$$Pe = 0.5f_c bkd \left(\frac{h}{2} - \frac{kd}{3} \right) + f'_s 0.5A_{st} \left(\frac{h}{2} - d' \right) + f_s 0.5A_{st} \left(\frac{h}{2} - d' \right) \quad (10.39)$$

On substituting for f'_s and f_s from Eqs. 10.5 and 10.6, we write

$$\begin{aligned} P &= 0.5f_c bkd + \frac{kd - d'}{kd} nf_c 0.5A_{st} - \frac{1 - k}{k} nf_c 0.5A_{st} \\ &= 0.5f_c bkd + 0.5 \left(\frac{2kd - d' - d}{kd} \right) nf_c A_{st} \end{aligned} \quad (10.40)$$

$$\begin{aligned} Pe &= 0.5f_c bkd \left(\frac{h}{2} - \frac{kd}{3} \right) + \frac{kd - d'}{kd} nf_c 0.5A_{st} \left(\frac{h}{2} - d' \right) \\ &\quad + \frac{1 - k}{k} nf_c 0.5A_{st} \left(\frac{h}{2} - d' \right) \\ &= 0.5f_c bkd \left(\frac{h}{2} - \frac{kd}{3} \right) + 0.5 \left(\frac{d - d'}{kd} \right) nf_c A_{st} \left(\frac{h}{2} - d' \right) \end{aligned} \quad (10.41)$$

The use of Eqs. 10.40 and 10.41 to solve a given column section is difficult, requiring the solution of a cubic equation for the neutral axis depth. The solution is best carried out by use of design charts.

Example 10.10

A 12 in (305 mm) square column section is symmetrically reinforced by four No. 6 (19.1 mm diameter) bars, one bar being placed in each corner of the section. The centroid of each bar is 2 in (51 mm) from the adjacent sides of the column. The column carries a load of 50 kips (222 kN) at an eccentricity of 4 in (102 mm) with respect to one major axis of the section. The modular ratio n is 15. Calculate the stresses in the steel and the concrete.

Solution

$$A_{st} = 4 \times 0.44 = 1.76 \text{ in}^2$$

From Eq. 10.40 we have

$$50,000 = 0.5 \times 12 \times 10f_c k + 0.5 \left(\frac{2 \times 10k - 2 - 10}{10k} \right) 15 \times 1.76f_c$$

$$\therefore f_c = \frac{50,000}{60k + 5.28(5k - 2)/k}$$

From Eq. 10.41 we find

$$50,000 \times 4 = 0.5 \times 12 \times 10f_c k \left(6 - \frac{10k}{3} \right) + 0.5 \left(\frac{10 - 2}{10k} \right) 15 \times 1.7f_c (6 - 2)$$

$$200,000 = 60f_c k(6 - 3.333k) + 42.24 \frac{f_c}{k}$$

$$\therefore f_c = \frac{200,000}{60k(6 - 3.333k) + 42.24/k}$$

Equating the two equations for f_c gives

$$k^3 - 0.600k^2 + 0.528k - 0.422 = 0$$

which on solving by trial and error gives $k = 0.715$.

$$\therefore f_c = \frac{50,000}{60 \times 0.715 + 5.28(5 \times 0.715 - 2)/0.715} = 920 \text{ psi (6.34 N/mm}^2\text{), compression}$$

$$f_s' = \left(\frac{10 \times 0.715 - 2}{10 \times 0.715} \right) 15 \times 920 = 9940 \text{ psi (68.6 N/mm}^2\text{)},$$

compression

$$f_s = \left(\frac{1 - 0.715}{0.715} \right) 15 \times 920 = 5500 \text{ psi (37.9 N/mm}^2\text{)}, \quad \text{tension}$$

Again the stresses, particularly in the compression steel, are very much dependent on the value used for the modular ratio. ACI 318-71^{10.1} requires columns to be designed by the strength method.

10.2.7 Shrinkage Stresses

Stresses will be induced by shrinkage of the concrete if strains due to shrinkage cannot occur without restraint. Reinforcement bars restrain concrete shrinkage and may cause significant stresses to be developed in the concrete. The magnitude of the shrinkage strain that concrete will undergo if free to shrink without restraint is discussed in Section 2.1.5.

The main purpose of evaluating the shrinkage stresses is to obtain the intensity of concrete tensile stress induced. This value may exceed the tensile strength of the concrete, particularly at the early stages of hardening. Cracks will result if the tensile strength is exceeded. Stresses due to shrinkage are determined for symmetrical and unsymmetrical cases below, assuming that the section remains uncracked.

Symmetrical Reinforcement and Section

Consider the element of length of the symmetrically reinforced concrete member in Fig. 10.13. Let ε_{sh} be the shrinkage strain the concrete would undergo if unrestrained. Because of the restraint of the steel, the actual

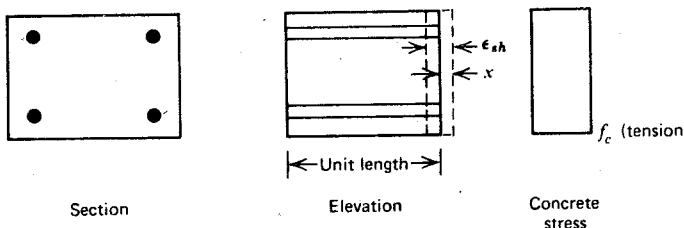


Fig. 10.13. Shrinkage of a symmetrically reinforced member.

shrinkage strain will only be x . Hence the reinforcement undergoes a compressive strain x causing compressive stress f_s , and the concrete undergoes tensile strain $\varepsilon_{sh} - x$ causing tensile stress f_c .

$$\therefore f_s = xE_s \quad \text{and} \quad f_c = (\varepsilon_{sh} - x) \frac{E_c}{1 + C_t}$$

$$\therefore x = \frac{f_s}{E_s} \quad \text{and} \quad f_c = \left(\varepsilon_{sh} - \frac{f_s}{E_s} \right) \frac{E_c}{1 + C_t}$$

The internal forces must be in equilibrium,

$$\therefore f_s A_s = f_c A_c$$

where A_s = steel area and A_c = concrete area.

$$\therefore f_s = f_c \frac{A_c}{A_s} \quad (10.42)$$

and

$$f_c = \left(\varepsilon_{sh} - \frac{f_c A_c}{E_s A_s} \right) \frac{E_c}{1 + C_t} = \frac{\varepsilon_{sh} E_c}{1 + C_t} - \frac{f_c A_c}{A_s E_s} \frac{E_c}{1 + C_t}$$

$$\therefore f_c = \frac{\varepsilon_{sh}}{\frac{1 + C_t}{E_c} + \frac{A_c}{A_s E_s}} \quad (10.43)$$

It is evident that the concrete tensile stress induced by shrinkage is proportional to the unstrained shrinkage strain ε_{sh} and that the tensile stress increases with increased steel content. Steel placed in concrete to control shrinkage cracks will actually increase the concrete tensile stress.

Example 10.11

A reinforced concrete slab section is symmetrically reinforced. The ratio of reinforcement area to concrete area is 0.03. The modulus of elasticity of the steel is 29×10^6 psi ($200,000$ N/mm 2), the modulus of elasticity of the concrete is 2.9×10^6 psi ($20,000$ N/mm 2), the creep coefficient is 2, and the unrestrained shrinkage strain of the concrete is 0.0005. Estimate the stresses in the steel and the concrete due to shrinkage.

Solution

From Eq. 10.43, write

$$f_c = \frac{0.0005}{\frac{1 + 2}{2.9 \times 10^6} + \frac{1}{0.03 \times 29 \times 10^6}}$$

$$= 228 \text{ psi (1.57 N/mm}^2\text{)}, \quad \text{tension}$$

From Eq. 10.42, write

$$f_s = \frac{228}{0.03}$$

$$= 7600 \text{ psi (52.4 N/mm}^2\text{)}, \quad \text{compression}$$

Unsymmetrical Reinforcement and Section

When the reinforcement and/or the section are unsymmetrical the restrained shrinkage is not uniform over the section (see Fig. 10.14). It is assumed that plane sections before shrinkage remain plane after shrinkage.

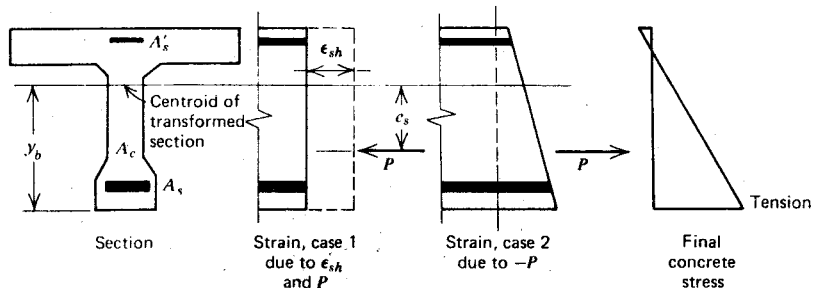


Fig. 10.14. Shrinkage of an unsymmetrically reinforced member.

The effect of shrinkage in this general case can be assessed by a general approach based on the properties of transformed areas (see Section 10.2.4) and the principle of superposition. Let the section in Fig. 10.14 have a transformed section with area A , moment of inertia about the centroid I , and distance from the bottom fiber to the centroid y_b . Let the full unrestrained shrinkage strain of the concrete ϵ_{sh} take place as in strain case 1 of Fig. 10.14. It is evident that this is only possible if an external force P is applied to the reinforcement so as to shorten it by the same amount. This force is

$$P = A_{st} E_s \epsilon_{sh}$$

where $A_{st} = \text{total area of reinforcement} = A'_s + A_s$. The force P acts at the centroid of the total steel area, situated at distance e_s from the centroid of the transformed section, as in Fig. 10.14. The stresses at this hypothetical load stage are zero in the concrete and

$$f_{s1} = \frac{P}{A_{st}} = \epsilon_{sh} E_s \quad (10.44)$$

compression in the steel. To remove the artificial external load P , an equal and opposite force may be applied to the section, as in strain case 2 of Fig. 10.14. This represents an eccentric tension, and the resulting concrete stresses (tension positive) can be obtained from

$$f_{c2} = \frac{P}{A} \pm \frac{Pe_s y}{I} \quad (10.45)$$

where y = distance of the fiber considered from the neutral axis; the resulting steel stresses may be obtained from

$$f_{s2} = nf_{c2} \quad (10.46)$$

where f_{c2} = concrete stress at fiber where steel stress is to be determined. The final stresses induced by shrinkage are obtained from the summation of these two stress systems, $f_s = f_{s1} + f_{s2}$ and $f_c = f_{c2}$.

Example 10.12

A singly reinforced concrete slab section has an overall depth of 10 in (254 mm), an effective depth of 8 in (203 mm), and is reinforced by 1.92 in² (1239 mm²) of steel per 12 in (305 mm) width. The modulus of elasticity of the steel is 29×10^6 psi (200,000 N/mm²), the modulus of elasticity of the concrete is 2.9×10^6 psi (20,000 N/mm²), the creep coefficient is 2, and the unrestrained shrinkage strain of the concrete is 0.0005. Estimate the stresses in the steel and the concrete due to shrinkage.

Solution

The modular ratio including creep is

$$n = \frac{E_s}{E_c}(1 + C_t) = \frac{29}{2.9}(1 + 2) = 30$$

Transformed area is

$$A = (12 \times 10) + (30 - 1)1.92 = 175.7 \text{ in}^2 \text{ per ft. width}$$

The position of the centroidal axis of the transformed section above the level of the reinforcement is

$$\bar{y} = 12 \times 10 \frac{5 - 2}{175.7} = 2.05 \text{ in} (= e_s)$$

Therefore, moment of inertia about the centroid is

$$I = \left(12 \times \frac{10^3}{12}\right) + (30 - 1)1.92 \times 2.05^2 + 12 \times 10(5 - 2 - 2.05)^2 = 1342 \text{ in}^2 \text{ per ft. width}$$

The compressive stress and the force that would be developed in the steel by a strain ϵ_{sh} of 0.0005 are found from Eq. 10.44 as

$$f_{s1} = 0.0005 \times 29 \times 10^6 = 14,500 \text{ psi, compression}$$

and

$$P = 14,500 \times 1.92 = 27,840 \text{ lb per ft. width}$$

To eliminate this, apply a tensile force P and a moment Pe_s to the transformed section. Then the stresses induced in the concrete are found from Eqs. 10.45 and 10.46 in the top fiber

$$f_{c2} = \frac{27,840}{175.7} - \frac{27,840 \times 2.05 \times 5.95}{1342}$$

$$= 158 - 253 = -95 \text{ psi, compression}$$

in the bottom fiber

$$f_{c2} = 158 + 253 \times \frac{4.05}{5.95} = 330 \text{ psi, tension}$$

and in the steel

$$f_{s2} = 30 \left(158 + 253 \times \frac{2.05}{5.95} \right) = 7360 \text{ psi, tension}$$

Hence the final stresses are by summation

$$f_s = 14,500 - 7360 = 7140 \text{ psi (49.2 N/mm}^2\text{), compression}$$

$$\text{top fiber } f_c = -95 \text{ psi } (-0.66 \text{ N/mm}^2\text{), compression}$$

$$\text{bottom fiber } f_c = 330 \text{ psi (2.28 N/mm}^2\text{), tension}$$

The effective modulus of elasticity $E_c/(1 + C_t)$ has been used in the calculation of stresses due to concrete shrinkage because sustained stresses are involved. However, the use of values for the creep coefficient C_t obtained for concrete under constant compressive stress is only an approximation, because the shrinkage stresses in the concrete increase with time and are mainly tensile. Thus these calculations can be expected to provide only an approximation to the actual shrinkage stresses.

10.3 CONTROL OF DEFLECTIONS

10.3.1 The Need for Deflection Control

With the use of concrete and steel of higher strengths, and the introduction of strength design, the design of more slender structural elements has become possible. Also, modern building structures often lack substantial walls and partitions, and the nonstructural elements may be prone to damage caused

by deformations of the structural members. Hence the control of the deflections of flexural members under service load is assuming greater importance.

A report by ACI Committee 435^{10.4} on allowable deflections classifies effects of deflections under four broad headings, as follows.

Sensory Acceptability

Sensory acceptability tends to be a matter for personal judgment and depends a great deal on the social background of the users and the type of structure. Under this heading come visual effects such as sagging beams or drooping cantilevers, tactile effects such as vibrations due to dynamic effects of live load or wind, and auditory effects such as noise from vibrations. Deflection limits on sensory acceptability are difficult to establish because of the variability of personal opinion.

Serviceability of the Structure

Serviceability limits are related to the intended use of the structure. Examples in this category are roof surfaces that should drain water, floors that should remain plane (e.g., gymnasia), and members supporting sensitive equipment. Deflection limits on serviceability are more easy to define.

Effect on Nonstructural Elements

Deflections must be limited to prevent cracking, crushing, bulging, or other types of damage to nonstructural elements such as walls, partitions, and ceilings. Deflections should not prevent moving elements such as doors and windows from operating properly. Thermal and shrinkage effects may be important, as well as deflections due to gravity and lateral loads. The deflection limits to be applied depend on the type of nonstructural element and the method of installation.

Effect on Structural Elements

Deflections may need to be limited to prevent the structural behavior from being different from that assumed in the design. Examples in this category are deflections causing instability, such as in arches and shells or long columns; deflections causing a change in the stress system, such as a change in the bearing area due to beam end rotation, and deflections causing dynamic effects that increase stresses, such as resonant vibrations due to moving loads. When possible, the effects of deflections on the structural behavior should be included in the design of the element.

10.3.2 Method of Deflection Control

Deflections may be controlled by ensuring that members have sufficient stiffness to limit the deformations at the service loads. Structural deflections are normally thought of as vertical or horizontal displacements of members.

ACI 318-71^{10.1} has two methods for controlling the deflections:

Use of Limiting Span/Thickness Ratios

For beams and one-way slabs that are not supporting or not attached to partitions or other construction likely to be damaged by large deflections, the deflection requirements may be considered to be satisfied if the minimum overall thickness is not less than those specified in Table 10.1.

Table 10.1 Minimum Thickness of Beams and One-Way Slabs Unless Deflections Are Computed^{a,b}

Member	Minimum Thickness, <i>h</i>			
	Simply Supported	One End Continuous	Both Ends Continuous	Cantilever
Members not supporting or attached to partitions or to other construction likely to be damaged by large deflections ^c				
Solid one-way slabs	<i>l</i> /20	<i>l</i> /24	<i>l</i> /28	<i>l</i> /10
Beams or ribbed one-way slabs	<i>l</i> /16	<i>l</i> /18.5	<i>l</i> /21	<i>l</i> /8

^a From Reference 10.1.

^b These minimum thickness values are for members made with normal weight concrete ($w = 145 \text{ lb/ft}^3 = 2320 \text{ kg/m}^3$) and Grade 60 reinforcement ($f_y = 60,000 \text{ psi} = 414 \text{ N/mm}^2$). For other members the values should be modified as follows:

1. For structural lightweight concrete, where $w = 90 \text{ to } 120 \text{ lb/ft}^3 (1440 \text{ to } 1920 \text{ kg/m}^3)$, the values shall be multiplied by $(1.65 - 0.005w)$, but not less than 1.09, where w is in pounds per cubic foot.

2. For reinforcement having a yield strength f_y other than 60,000 psi (414 N/mm^2), the values shall be multiplied by $(0.4 + f_y/100,000)$, where f_y is in psi.

^c l = span length of member.

Use of Limiting Computed Deflections

For beams and one-way slabs that support or are attached to partitions or other construction likely to be damaged by large deflections, or do not meet the minimum thickness requirements of Table 10.1, the deflections must be calculated and are limited to the values listed in Table 10.2.

Note that Table 10.1 is for members constructed using normal weight concrete and reinforced by steel with yield strength $f_y = 60,000$ psi (414 N/mm 2). The notes accompanying the table indicate the modifications for structural lightweight concrete and for other grades of steel. The modification for lightweight concrete is based on the report of ACI Committee 213 and

Table 10.2 Maximum Allowable Computed Deflections^a

Type of Member	Deflection to be Considered	Deflection Limitation
Flat roofs not supporting or attached to nonstructural elements likely to be damaged by large deflections	Immediate deflection due to live load, L	$l/180^b$
Floors not supporting or attached to nonstructural elements likely to be damaged by large deflections	Immediate deflection due to live load, L	$l/360$
Roof or floor construction supporting or attached to nonstructural elements likely to be damaged by large deflections	That part of the total deflection which occurs after the attachment of the non-structural elements, the sum of the long-term deflection due to all sustained loads, and the immediate deflection due to any additional live load	$l/480^c$
Roof or floor construction supporting or attached to nonstructural elements not likely to be damaged by large deflections		$l/240^d$

^a From Reference 10.1.

^b This limit is not intended to safeguard against ponding. Ponding should be checked by suitable deflection calculations.

^c This limit may be exceeded if adequate measures are taken to prevent damage to supported or attached elements.

^d But not greater than the tolerance provided for the nonstructural elements. This limit may be exceeded if camber is provided so that the total deflection minus the camber does not exceed the limitation.

the accompanying discussions.^{10.5} For concrete with w between 120 and 145 lb/ft³ (1920 and 2320 kg/m³) no correction is necessary, since the correction term is close to unity. The modification for steel yield strength is based on judgment, experience, and studies, and it should give conservative results for typical members with f_y in the range 40,000 to 80,000 psi (276 to 552 N/mm²), according to the Commentary on ACI 318-71.^{10.6} The designer may use a smaller thickness than that specified in Table 10.1 if calculations demonstrate that the service load deflection would be less than that specified in Table 10.2.

Table 10.2 is a simplification of the extensive range of limitations that would be necessary to cover all types of construction and conditions of loading (see Section 10.3.1). It is assumed that deflections likely to affect the strength of structural elements have been taken into account in the design of structures. The designer must be careful to ensure the consideration of any unusual aspects of the structure (e.g., particular serviceability requirements or response to vibrations) not covered by the table.

10.3.3 Calculation of Deflections

The accurate prediction of the deflections of reinforced concrete members at the working load is difficult. Unsymmetrical reinforcement in beams ($A_s > A'_s$) leads to deflections due to shrinkage of the concrete, which add to the gravity load deflections. Creep of concrete leads to a gradual increase of deflection of members under sustained service loads. The shrinkage and creep that occur are influenced by temperature and humidity, curing conditions, age of concrete at time of loading, and other factors as outlined in Sections 2.1.4 and 2.1.5. The decrease in flexural stiffness caused by cracking of the concrete also has an appreciable effect on the deflection, and the uncertainty of the extent of cracking makes the effective moment of inertia of members difficult to estimate. It is possible, however, to estimate the deflections with a margin of error of $\pm 20\%$, which is sufficiently accurate for most practical purposes. The deflections can be estimated in two steps: (1) the immediate deflection that occurs at first loading, and (2) the additional deflection that occurs with time, because of creep and shrinkage of the concrete. The following comments explain the method of deflection calculation given in ACI 318-71.^{10.1}

Immediate Deflection

The immediate deflection caused by the service loads may be calculated using the usual elastic theory equations for deflections. For example, the central deflection of a simply supported beam with span l and flexural rigidity EI , carrying a uniform load w per unit length, is $5wl^4/384EI$. This

deflection for a simply supported beam is 5 times that of the same beam with the same load but fully restrained against rotation at both ends. Hence if the ends of a beam are continuous, as they are in most reinforced concrete construction, it is essential to consider the reduction in deflection due to end restraint. To account for end restraint it is usually sufficiently accurate to calculate the central deflection of the member as if simply supported, and to subtract from it the opposite deflection caused by the average of the negative moments at the two ends. Thus if these end moments are M_1 and M_2 , so that $M_{av} = (M_1 + M_2)/2$, the amount to be subtracted from the simple beam deflection is $M_{av}l^2/8EI$.

To obtain the flexural rigidity EI of the section, E may be taken as the value for concrete given by Eq. 2.1, i.e. $E_c = w^{1.5} 33\sqrt{f'_c}$ psi, with f'_c in psi, for values of w between 90 and 155 lb/ft³ (1 psi = 0.00689 N/mm², 1 lb/ft³ = 16.02 kg/m³). For normal weight concrete, E_c may be taken as $57,000\sqrt{f'_c}$ psi ($4730\sqrt{f'_c}$ N/mm²).

The moment of inertia I depends on the amount of cracking that has taken place in the member. If at the service load the maximum tensile stress in the concrete, calculated on the basis of the uncracked section, is less than the modulus of rupture of the concrete, it can be assumed that no tension cracks will have formed. In this case I may be taken as I_g , where I_g is the moment of inertia of the uncracked gross section about the centroidal axis, ignoring the transformed area of the reinforcement. More accurately, the moment of inertia of the uncracked section taking into account the transformed area of the reinforcement may be used, since the steel can increase the moment of inertia of the uncracked section by as much as 30%. The method of calculating the moment of inertia of the transformed section was described in Section 10.2.4. In regions of the member where the bending moment is great enough for the tensile stress to exceed the modulus of rupture of the concrete, cracks will form at discrete intervals along the member. The moment of inertia of a section is reduced by cracking, the reduction being greater for lightly reinforced sections than for heavily reinforced sections. At a cracked section the moment of inertia is I_{cr} , based on the cracked section transformed to concrete area. Between the cracks the concrete will be carrying some tension because tension is transferred from the steel to the concrete by bond and sufficient length is required for the tensile stress in the concrete to reach the modulus of rupture before the concrete will crack again (see Section 6.6.2). The tension carried by the concrete between cracks will tend to stiffen the member. Also in regions of the member where the bending moment is low the concrete will not have cracked. Hence in a cracked member it is desirable to take an effective moment of inertia I_e that will have a value between those derived for cracked and uncracked sections. ACI 318-

71^{10.1} recommends the use of the following expression for the effective moment of inertia

$$I_e = \left(\frac{M_{cr}}{M_a} \right)^3 I_g + \left[1 - \left(\frac{M_{cr}}{M_a} \right)^3 \right] I_{cr} \quad (10.47)$$

where I_g = moment of inertia of the gross uncracked section, I_{cr} = moment of inertia of the cracked section transformed to concrete, M_a = maximum moment in member at stage at which the deflection is being computed, and M_{cr} = moment at first cracking, given by

$$M_{cr} = \frac{f_r I_g}{y_t} \quad (10.48)$$

where y_t = distance from centroidal axis of gross section to the extreme tension fiber, and f_r = modulus of rupture of the concrete. In terms of cylinder strengths, f_r may be taken as $7.5\sqrt{f'_c}$ psi for normal weight concrete, $6.38\sqrt{f'_c}$ psi for "sand-lightweight" aggregate concrete, or $5.63\sqrt{f'_c}$ psi for "all lightweight" aggregate concrete, where f'_c is in psi (1 psi = 0.00689 N/mm²). Equation 10.47 for I_e has two limits of I_g and I_{cr} , thus gives a transition expression that depends on the extent of cracking. As M_a/M_{cr} becomes large, the value for I_e rapidly tends toward I_{cr} . Equation 10.47 is an empirical expression developed by Branson^{10.7} which has been shown to give good accuracy. The value for I_e may be thought of as being proportional to the slope of the secant line to the appropriate point on the load-deflection curve above the load at first cracking. For continuous beams the moment of inertia may be taken as the average of the I_e values obtained for the positive and negative moment regions.

Immediate deflections calculated by the above ACI code method for simply supported and continuous beams are shown compared with test data in Fig. 10.15, which is from a report^{10.8} by ACI Committee 435.

The calculation of the moment of inertia of sections may be tedious, especially in the case of cracked transformed sections. The *ACI Design Handbook*, Volume 1,^{10.9} contains a number of useful design tables that enable I_{cr} to be found for rectangular and *T* sections. Tables and charts for I_{cr} can be prepared from the moment-curvature relationship.

$$\frac{M}{E_c I_{cr}} = \phi = \frac{\varepsilon_c}{kd} \quad \therefore \quad I_{cr} = \frac{Mkd}{E_c \varepsilon_c} = \frac{Mkd}{f_c} \quad (10.49)$$

where M = bending moment, kd = neutral axis depth, E_c = modulus of elasticity of the concrete, ε_c = strain in extreme compression fiber of the

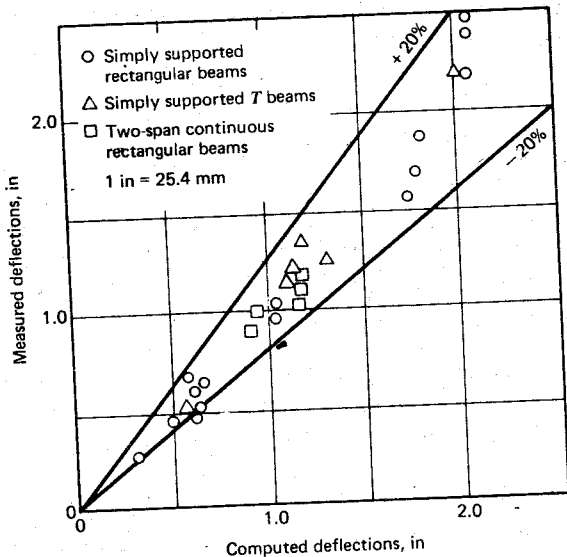


Fig. 10.15. Comparison of computed immediate deflections by the ACI 318-71 method with experimental deflections.^{10.8}

concrete, and f_c = stress in extreme compression fiber of the concrete. If M in terms of the concrete and steel stresses, areas, and lever arms is substituted into this equation, an expression for I_{cr} can be determined and plotted in the form of charts. T beams may be treated as doubly reinforced beams by replacing the overhanging flanges of the section by an equivalent area of compression steel.

The ACI handbook^{10.9} also gives tables that enable a relatively quick determination of the deflection for various types of loading.

Long-Term Deflection

The deflection of reinforced concrete beams increases with time. The additional deflections are caused by creep and shrinkage of the concrete. The rate of additional deflection decreases as time proceeds. The magnitude of concrete creep and shrinkage strains was discussed in Sections 2.1.4 and 2.1.5. Additional deflections two or three times as large as the immediate deflection may eventually be reached.

Concrete shrinkage is unsymmetrically reinforced members causes a nonuniform strain distribution down the section (see Fig. 10.14), hence results in shrinkage curvature. The curvature is greater in singly reinforced

members because the concrete shrinkage is unrestrained in the compression zone. In flexural members the reinforcement is mainly in the tension zone of the sections. Therefore, shrinkage curvatures will have the same sign as the curvatures due to transverse loads; therefore, they will increase the deflections due to transverse load. Also the concrete tensile stresses induced by shrinkage combine with the tensile stresses due to transverse loading to produce additional cracking.

Concrete creep results in a shortening of the compressed part of the concrete cross section, hence also causes additional curvature.

It is evident that the additional deflections due to shrinkage and creep can be substantially reduced by the presence of compression reinforcement. Such reinforcement reduces the shrinkage curvature by providing restraint to shrinkage in the compression zone of the section. In the limit, if a member with a symmetrical cross section is equally reinforced top and bottom, the shrinkage curvature will be zero. In the general case of an unsymmetrical section, the shrinkage curvature will be zero if the centroids of the reinforcement and the transformed section coincide. This observation is confirmed by inspection of Fig. 10.14. Compression reinforcement also reduces the influence of concrete creep because as the concrete compressive strains increase with time, some compressive stress is transferred gradually to the steel, resulting in reduced concrete compressive stress and reduced creep strains.

In addition to the content of compression steel, the amount of long-term deflection depends on the humidity, temperature, curing conditions, age of concrete at time of loading, ratio of stress to strength, and other factors, as outlined in Sections 2.1.4 and 2.1.5. For this reason only estimates can be made of long-term deflections, any more accuracy being unwarranted unless the service load conditions and concrete properties are known exactly. A paper by Yu and Winter^{10.10} forms the basis of the recommended method of estimation. The additional long-term deflections for both normal weight and lightweight concrete flexural members may be obtained by multiplying the immediate deflection caused by the sustained load by the factor

$$2 - 1.2 \frac{A'_s}{A_s} \geq 0.6 \quad (10.50)$$

where A'_s = area of compression steel and A_s = area of tension steel.

For shorter periods of loading the multipliers in Fig. 10.16 may be used. This figure was prepared from Yu and Winter's results^{10.10} and published in the Commentary^{10.6} on the ACI code. According to Yu and Winter the long-term deflections may be predicted to an accuracy of $\pm 20\%$, using the multipliers given. The multipliers should be applied only to that part of the immediate deflection which is caused by the sustained load. Hence the full dead load falls into this category, but the type of occupancy will determine

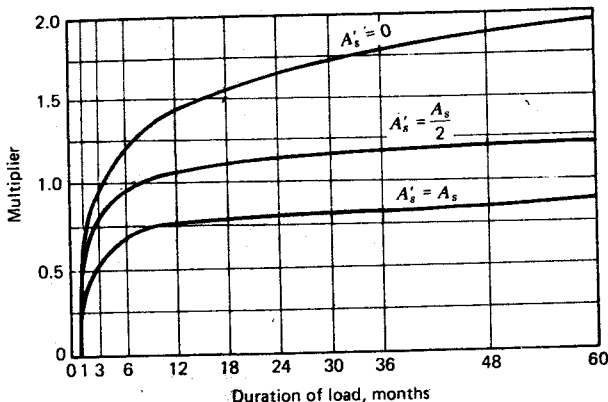


Fig. 10.16. Multipliers for long term deflections.^{10.6}

the portion of the live load that should be considered to remain sustained for long periods. For instance, perhaps only 20% of the service live load in an apartment building will fall into this category, but in a warehouse it may be necessary to assume that about 80% or more of the live load is sustained over long periods. For example, if a uniformly loaded, simply supported beam with $A'_s = 0.25A_s$ is designed for service dead load D and service live load L , both per unit length, and if 50% of the live load is considered to be sustained, the multiplier from Eq. 10.50 is $2 - 1.2 \times 0.25 = 1.7$, and the total maximum deflection would be equal to the sum of the immediate plus additional deflection due to $D + 0.5L$ and the immediate deflection due to $0.5L$. Thus the total maximum deflection would be

$$\frac{5}{384} \frac{l^4}{E_c I_{e1}} (D + 0.5L)(1 + 1.7) + \frac{5}{384} \frac{l^4}{E_c I_{e2}} 0.5L$$

where $I_{e1} = I_e$ from Eq. 10.47 with M_a from $D + 0.5L$, and $I_{e2} = I_e$ with M_a from $D + L$. Figure 10.16 is useful for estimating deflections during different periods. For example, the deflection of the same beam at age 3 months would be obtained by changing the multiplier in the formula from 1.7 to 0.85. The difference in the deflections would be the amount of future deflection the beam would undergo.

10.3.4 More Accurate Methods for Calculating Deflections

The report^{10.8} of ACI Committee 435 gives a summary of methods available for calculating deflections and compares their accuracy. The ACI code

method should normally lead to sufficient accuracy for design purposes; if accuracy greater than $\pm 20\%$ is required, however, a more comprehensive analysis could be carried out. Such an analysis can only be justified if experimental data are available for the modulus of rupture and the modulus of elasticity of the concrete, and for the shrinkage and creep characteristics of the concrete in the environment in which the member is in service. Some suggestions of Subcommittee 1 ACI Committee 435^{10.4} for more accurate calculations of immediate deflection, and methods due to Branson^{10.7, 10.8} for calculating the additional long-term deflections due to creep and shrinkage, are outlined below.

Immediate Deflections

Almost all beams designed as simply supported spans have some restraint against rotation at the ends. A small end moment will reduce the central deflection significantly. Therefore, some assessment could be made of the degree of end restraint available from elements such as masonry walls and concrete topping and included in the deflection calculations.

The modulus of rupture and the modulus of elasticity for the deflection calculations could be obtained from the concrete used for the structure. For example, the modulus of elasticity could be calculated from the average measured cylinder strength rather than from the specified minimum cylinder strength used in the design. The modulus of rupture may exceed the value recommended by the code for use in Eq. 10.48, and the average measured value could be used.

Also possible is more realistic assessment of the manner in which non-structural elements, particularly walls, affect structural behavior. For example, partition walls may span from end to end when the structural member deflects, beams may come to rest on walls below, and infill walls may stiffen frames considerably.

Flanges of *T* beams on the tension side should be included in moment of inertia calculations. Also, the transformed area of reinforcing steel in un-cracked sections should not be ignored, particularly in the case of heavily reinforced members, because it can increase the moment of inertia significantly.

In continuous members a more realistic assessment of the flexural rigidity along the member could be made, rather than simple averaging of the negative and positive moment of flexural rigidities.

Shear deflections should be accounted for when thin-webbed members are used, or when a large proportion of the shear stresses is resisted by web reinforcement resulting in diagonal tension cracks under service load conditions.

Long-Term Deflections due to Concrete Shrinkage

Concrete shrinkage causes a shortening of the member that is resisted by the reinforcing steel, inducing compressive stresses in the steel and mainly tensile stresses in the concrete. Symmetrical sections with symmetrical reinforcement will undergo uniform strain, hence no shrinkage curvature occurs. Generally, when the section or the reinforcement is unsymmetrical, shrinkage causes a nonuniform strain distribution and will result in curvature of the member. Equations for curvatures due to shrinkage for uncracked and cracked sections can be developed using elastic theory. For example, in Section 10.2.7 the stresses in uncracked reinforced sections due to shrinkage were determined. The strains may be determined from the stresses and the shrinkage curvature is given by $\varphi_{sh} = (\varepsilon_{ct} + \varepsilon_{cb})/h$, where ε_{ct} and ε_{cb} are the strains in the concrete at the extreme top and bottom fibers (added if one is tensile and the other is compressive; subtracted if both are tensile or compressive), and h is the overall depth of the section. However, such solutions are not exact because of the difficulty of dealing accurately with the effects of concrete creep. Also, shrinkage deflections are normally of the order of 30% or less of the total deflections. Hence simplified approaches suffice.

Branson^{10.7, 10.8} has suggested the following empirical expressions for the shrinkage curvature φ_{sh} of doubly reinforced rectangular concrete members. For $\rho - \rho' < 0.03$

$$\varphi_{sh} = 0.7 \frac{\varepsilon_{sh}}{h} [100(\rho - \rho')]^{1/3} \left(\frac{\rho - \rho'}{\rho} \right)^{1/2} \quad (10.51)$$

and for $\rho - \rho' > 0.03$

$$\varphi_{sh} = \frac{\varepsilon_{sh}}{h} \quad (10.52)$$

where ε_{sh} = unrestrained shrinkage strain, h = overall depth of member, $\rho = A_s/bd$, $\rho' = A'_s/bd$, A_s = tension steel area, A'_s = compression steel area, b = member width, and d = effective depth of tension steel. Equations 10.51 and 10.52 have been found to give reasonable agreement with experimental results.^{10.8}

When the shrinkage curvature φ_{sh} is constant along a simply supported span l , or is the same in the positive and negative moment regions of a continuous beam of span l , the maximum shrinkage deflection is given as for cantilever beams

$$\Delta_{sh} = 0.5\varphi_{sh}l^2 \quad (10.53a)$$

for simply supported beams

$$\Delta_{sh} = 0.125\varphi_{sh}l^2 \quad (10.53b)$$

for beams fully restrained against rotation at both ends

$$\Delta_{sh} = 0.063\varphi_{sh}l^2 \quad (10.53c)$$

When the shrinkage curvature varies along the span, the deflections can be computed from first principles or approximated using a weighted average φ_{sh} value in Eqs. 10.53.

The shrinkage strain ε_{sh} to be used may be assessed using existing data^{10.8, 10.11, 10.12} as outlined in Section 2.1.5.

Example 10.13

A singly reinforced concrete slab has an overall depth of 10 in (254 mm), an effective depth of 8 in (203 mm), and is reinforced by 1.92 in² (1239 mm²) of steel per 12 in (305 mm) width. The modulus of elasticity of the steel is 29×10^6 psi (200,000 N/mm²), the modulus of elasticity of the concrete is 2.9×10^6 psi (20,000 N/mm²), the creep coefficient is 2, and the unrestrained shrinkage strain of the concrete is 0.0005. The slab is simply supported over a span of 15 ft (4.57 m). Estimate the maximum deflection due to shrinkage.

First Principles Solution

In Example 10.12 the concrete stresses for this slab were calculated to be 95 psi compression in the top fiber and 330 psi tension in the bottom fiber, due to shrinkage. The effective modulus of elasticity of the concrete is $E_c/(1 + C_c) = 2.9 \times 10^6/(1 + 2) = 0.976 \times 10^6$ psi. Hence the strains in the top and bottom concrete fibers are

$$\varepsilon_{ct} = \frac{95}{0.976 \times 10^6} = 97 \times 10^{-6} \quad \varepsilon_{cb} = \frac{330}{0.976 \times 10^6} = 338 \times 10^{-6}$$

$$\therefore \text{shrinkage curvature } \varphi_{sh} = \frac{\varepsilon_{ct} + \varepsilon_{cb}}{h} = \frac{97 + 338}{10} \times 10^{-6} \\ = 43.5 \times 10^{-6} \text{ rad/in}$$

From Eq. 10.53b, maximum deflection is

$$\Delta_{sh} = 0.125 \varphi_{sh} l^2 \\ = 0.125 \times 43.5 \times 10^{-6} \times (15 \times 12)^2 \\ = 0.176 \text{ in (4.47 mm)}$$

Branson's Approximate Solution

$$\rho = \frac{A_s}{bd} = \frac{1.92}{12 \times 8} = 0.02, \quad \rho' = 0$$

$$\therefore \rho - \rho' = 0.02 < 0.03$$

Therefore, Eq. 10.51 gives

$$\begin{aligned}\varphi_{sh} &= 0.7 \times \frac{0.0005}{10} \times (100 \times 0.02)^{1/3} \\ &= 44.1 \times 10^{-6} \text{ rad/in}\end{aligned}$$

$$\begin{aligned}\therefore \text{maximum deflection } \Delta_{sh} &= 0.125 \times 44.1 \times 10^{-6} \times (15 \times 12)^2 \\ &= 0.178 \text{ in (4.53 mm)}\end{aligned}$$

Note that Branson's approximate equation has given excellent agreement with the exact solution in this example.

Long-Term Deflections due to Concrete Creep

Long-term deflections due to concrete creep are often greater than the sum of the deflections from the other effects and therefore are of primary interest. An accurate analysis including the effect of variable loading is extremely difficult because of the need for data on the creep strain-time characteristics of the concrete, and the loading history. The rate-of-creep method^{10.2} or the superposition method^{10.3} may be used if such data are available. Usually the analysis cannot be justified, and a more approximate approach is chosen.

One approximate method uses the effective modulus of elasticity of the concrete for calculating the immediate plus creep deflections. The effective modulus is given by $E_c/(1 + C_i)$, where E_c is the modulus of elasticity at the instant of loading and C_i is the creep coefficient of the concrete (see Section 10.2.1). Since the creep coefficient C_i is the ratio of the creep strain to initial

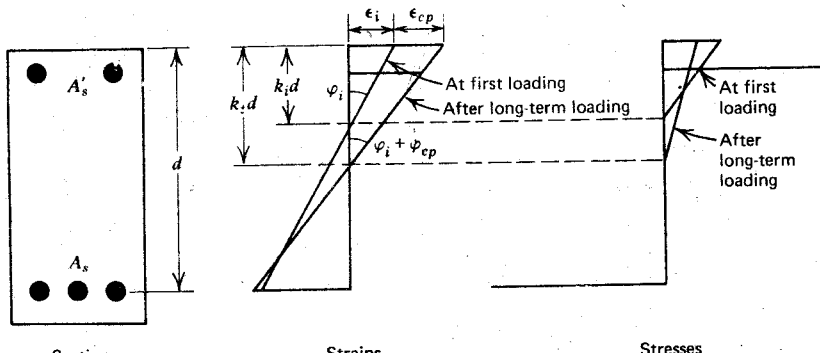


Fig. 10.17. Strain and stress distributions at first loading and after long-term loading in a flexural member subjected to creep of concrete.

(elastic) strain, it is evident that in this approach the deflection due to creep is equal to the immediate deflection multiplied by the creep coefficient. However this approach is very approximate. Figure 10.17 identifies the strain and stress distributions for a reinforced concrete beam section immediately on the application of the service load and after long-term loading. The changes in strain and stress with time were noted in Example 10.1 of Section 10.2.3. Concrete creep under constant bending moment results in a significant increase in the extreme fiber compression strain, an increase in the neutral axis depth, an increase in the steel compressive stress, and a decrease in the concrete compressive stress. The tensile stress in the steel increases slightly because the lever arm is reduced. The ratio of curvature due to creep to immediate curvature (see Fig. 10.17) may be written as

$$\begin{aligned}
 \frac{\varphi_{cp}}{\varphi_i} &= \frac{\frac{\varepsilon_i + \varepsilon_{cp}}{k_t d} - \frac{\varepsilon_i}{k_i d}}{\frac{\varepsilon_i}{k_i d}} \\
 &= \frac{\frac{\varepsilon_{cp}}{\varepsilon_i} \frac{k_i}{k_t} - \left(1 - \frac{k_i}{k_t}\right)}{\frac{k_i}{k_t}} \\
 &= k_r C_t
 \end{aligned} \tag{10.54}$$

where ε_i and ε_{cp} are the immediate and creep extreme compression fiber concrete strains, $k_t d$ and $k_i d$ are the immediate and eventual neutral axis depths, C_t is the creep coefficient, and k_r is a factor. The factor k_r is less than unity because the analysis of the section shows that $k_i/k_t < 1$ and $\varepsilon_{cp}/\varepsilon_i < C_t$, because of the redistribution of compressive stress resulting from creep. Thus the curvature caused by creep will be less than the immediate curvature multiplied by the creep coefficient.

Given the influences just mentioned, Branson^{10.7, 10.8} has suggested that the deflection due to creep may be determined from

$$\Delta_{cp} = k_r C_t \Delta_i \tag{10.55}$$

where Δ_i = deflection occurring immediately on loading and k_r is the same kind of factor as in Eq. 10.54, which takes into account the effect of redistribution of compressive stress resulting from creep and additional progressive cracking due to creep loading. Values suggested for k_r were $k_r = 0.85$ when $A'_s = 0$, $k_r = 0.6$ when $A'_s = 0.5A_s$, and $k_r = 0.4$ when $A'_s = A_s$.

The creep coefficient C_t to be used can be assessed using existing data,^{10.8, 10.11, 10.12} as outlined in Section 2.1.4.

10.4 CONTROL OF CRACKING

10.4.1 The Need for Crack Control

The occurrence of cracks in reinforced concrete structures is inevitable because of the low tensile strength of concrete. The tensile resistance of concrete is normally neglected in design. Structures designed with low steel stresses at the service load serve their intended function with very limited cracking. In many cases no cracking is visible at all because many members are not subjected to their full service load and the concrete has some tensile strength. However with high service load steel stresses, particularly as a result of the use of high-strength steel, some cracking must be expected at the service load. The cracking of a reinforced concrete structure at the service load should not be such as to spoil the appearance of the structure or to lead to corrosion of the reinforcement. These two requirements are considered next.

Aesthetic Considerations

The maximum size of a crack that may be considered nondetrimental to the appearance of a member, or nonconducive to feelings of alarm, depends on the position, length, width, illumination, and surface texture of the crack. The social background of the users and the type of structure also exert an influence. The limits on aesthetic acceptability are difficult to set because of the variability of personal opinion. The maximum crack width that will neither impair a structure's appearance nor create public alarm is probably in the range 0.010 to 0.015 in (0.25 to 0.38 mm), but larger crack widths may be tolerated.

Protection Against Corrosion

Portland cement concrete usually provides good protection for embedded reinforcing steel against corrosion. The protective value of the concrete is due mainly to its high alkalinity. If chemical agents such as carbon dioxide (producing carbonic acid) penetrate to the concrete surrounding the steel, the alkalinity is neutralized and the corrosion-inhibiting properties are reduced. Chlorides from deicing salts, sea spray, and so on, are also extremely active corrosion agents. Concrete of low permeability resists the penetration of corrosion agents. The main factors affecting the rate of diffusion of corrosion agents to the steel are the permeability of the concrete, the thickness of the concrete cover, the width, shape, and length of cracks, and the period of time the cracks are open.

The permeability of the concrete is a major factor affecting the corrosion of reinforcing steel. It is extremely important to avoid the presence of inferior concrete around the steel. The thickness of concrete cover also affects the rate of penetration of the corrosion agents. In many publications cracking is assessed only in terms of crack widths on the concrete surface. However, it is evident that the shape of the crack (i.e., the variation in the crack width between the concrete surface and the bar surface) and the length of the crack are as important as the surface width of the crack in assessments of the reduction in the effectiveness of the cover concrete due to cracking. Thus the importance of surface crack width has been overemphasized by many publications. Ideally the durability of a reinforced concrete member should be assessed by estimating the rate of corrosion in terms of the thickness and permeability of the cover concrete, the width, shape, and length of cracks, the period of time the cracks are open, and in terms of the corrosive nature of the environment. The bar diameter is also a consideration in that for a given depth of corrosion in the bar, the percentage loss in bar area will be greater for small diameter bars. However, the full assessment appears to be impracticable at present, particularly because of the difficulty of determining the important parameters. The influence of cracking on corrosion of the reinforcement is still the subject of research, and conflicting data have been reported. It is possible that the effect of crack shape has not been appreciated in many cases because results have invariably been reported in terms of the crack width at the surface of the concrete. Some studies have indicated that surface crack widths of up to 0.016 in (0.41 mm) have produced little or no corrosion, even in aggressive environments, whereas other reports have not been so optimistic.

At present cracking is controlled by specifying maximum allowable crack widths at the surface of the concrete for given types of environment.

10.4.2 Causes of Cracking

The causes of cracking in concrete are numerous, but most cracks occur as a result of one or more of the following actions.

Cracking due to Settlement of Plastic Concrete

As concrete sets, it tends to settle slightly in the mould when in the plastic state. This causes the concrete to drop away slightly on each side of bars near the top surface of the concrete, because the bars are normally fixed in position. Lines of cracking following the reinforcement may result. Such cracks may sometimes be observed in beams over stirrups and other top steel. This type of cracking can be avoided by good mix design and by vibration and screeding of the plastic concrete.

Cracking due to Volumetric Change

Drying shrinkage and thermal stresses cause volumetric changes that will introduce tensile stresses in the concrete if restrained, and therefore can lead to cracking. The restraint can arise in a number of ways. For example, concrete near the surface of members shrinks more than the concrete further inside the member; therefore, the inner concrete will restrain the outer concrete, causing tensile stresses to develop near the surface, which may cause surface cracking. Also, shrinkage of members may be restrained by other members, foundations, or reinforcement, thus introducing tension. Similarly, temperature change will cause tension if the movements cannot occur unrestrained. Cracking due to shrinkage may be controlled by reducing the shrinkage of concrete by good mix design (e.g., by keeping the water content as low as possible) and by properly placed reinforcement. The reinforcement will not prevent cracking. Indeed the restraint of the reinforcement will tend to encourage cracking, but the shrinkage strains are distributed along the bars by bond, and a number of fine cracks should occur (instead of a few wide cracks). The minimum amount and spacing of reinforcement that may be used in slabs and walls is given in ACI 318-71.^{10.1} This reinforcement is intended to be adequate to control crack widths due to shrinkage and temperature stresses. Control joints in walls and slabs are an effective method of preventing unsightly shrinkage cracking in large expanses of concrete. Such joints consist normally of grooves in the concrete along which the concrete is encouraged to crack. This controlled cracking relieves the stresses elsewhere in the concrete. Sawed joints are commonly used in pavements for this purpose.

Cracking due to Direct and Flexural Stresses Resulting from Applied Load or Reactions

Cracking may occur in the tension zone of members subjected to flexure or axial tension. Such tension may arise from external loads or reactions. The cracks may form perpendicular to the axis of the member, as in the case of axial tension or flexure without significant shear force; or when the shear force is significant, they may form inclined to the axis of the member. Such inclined cracks, known as diagonal tension cracks, are generally considered to be controlled adequately by shear reinforcement. Little analytical work is available on the control of diagonal tension cracks, but there is evidence that the control mechanism for diagonal tension cracking is similar to that for flexural cracking. Sections 10.4.3 and 10.4.4 deal with the mechanism of flexural crack formation and with flexural crack control.

10.4.3 Mechanism of Flexural Cracking

Many variables influence the width and spacing of cracks in reinforced concrete members. Because of the complexity of the problem, we now have a number of approximate, semitheoretical and empirical approaches for the determination of the width of cracks, each approach containing a selection of the variables. Some of the methods are reviewed below to indicate their background.

Classical Theory

In the mechanism of cracking of axially loaded reinforced concrete members, proposed in most of the early studies on cracking, crack control was believed to depend largely on the quality of the bond between the concrete and steel. Consider the axially loaded tension member in Fig. 10.18. Initial tension

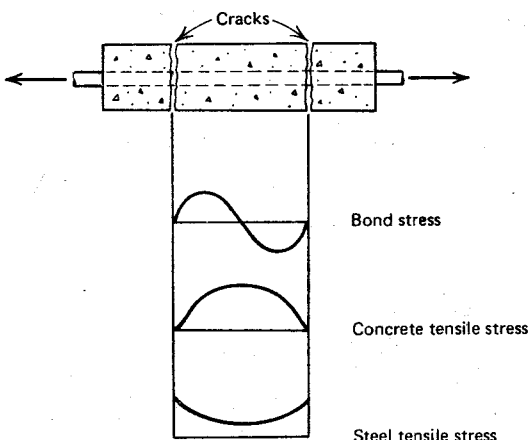


Fig. 10.18. Cracking of a member with axial tension.

cracks form when the tensile strength of the concrete is exceeded at weak sections that are distributed at random. Slip occurs between the concrete and steel at the cracks. At the cracks the concrete is free from stress, and the reinforcement alone carries the external load. Tensile stress is present in the concrete between the cracks, however, because tension is transferred from the steel to the concrete by bond. The magnitude and distribution of bond stress between the cracks determines the distribution of tensile stress in the concrete and the steel between the cracks. Additional cracks can form

between the initial cracks at higher loads when the tensile strength of the concrete is exceeded.

The foregoing hypothesis was formalized in 1943 by Watstein and Parsons,^{10,13} and several other theories appeared later. Hognestad^{10,14} has described the derivation of the theoretical equations as follows. For a reinforced concrete member loaded in axial tension (see Fig. 10.19a), initial

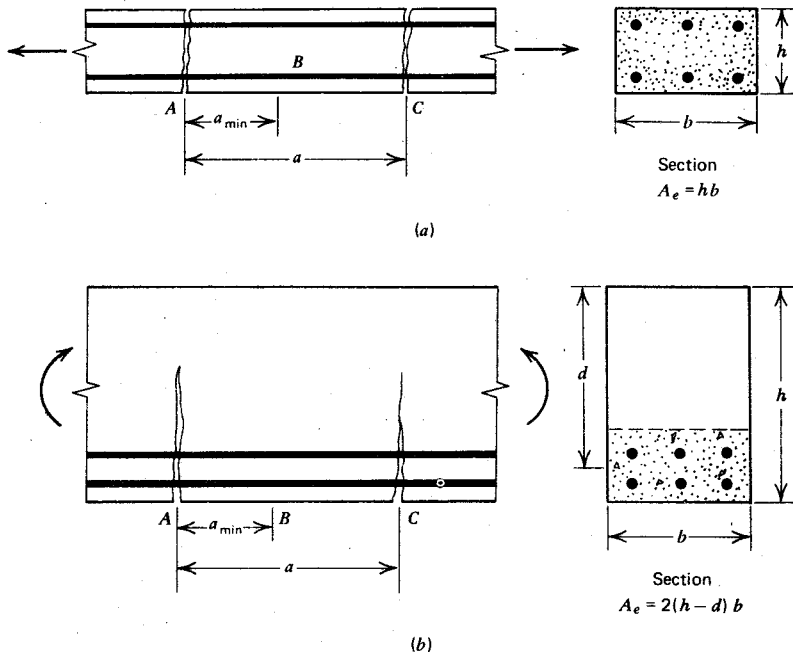


Fig. 10.19. Members with cracking. (a) Member with axial tension. (b) Member with flexure.

tension cracks form at irregular spacing when the tensile strength of the concrete is exceeded at weak sections. Additional cracks form between the initial cracks at higher loads, but the crack spacing can only be reduced down to a certain minimum spacing a_{min} . This limit is reached when a tensile force great enough to form an additional crack between two existing cracks can no longer be transferred by bond from steel to concrete. Say in Fig. 10.19a that two cracks form initially at sections A and C, which are distance a apart. If an additional crack is to form at B at minimum distance from A, the bond between the steel and the concrete along the length AB must transfer

sufficient tension from the steel to the concrete to crack the concrete at *B*. The tensile force required to crack the concrete is $A_e f'_t$, where A_e is the effective area of concrete in tension and f'_t is the tensile strength of the concrete. The tension transferred to the concrete is $a_{\min} u \Sigma o$, where a_{\min} is the minimum crack spacing, u is the average bond stress, and Σo is the sum of the perimeters of the bars. Equating the two values of tension gives

$$a_{\min} = \frac{A_e f'_t}{u \Sigma o} \quad (10.56)$$

Now the spacing between the initial cracks *A* and *C* is a . Therefore, if $a \geq 2a_{\min}$, a new crack can form at *B*; and if $a < 2a_{\min}$, a new crack cannot form at *B*. This means that the crack spacing can be expected to vary between a_{\min} and $2a_{\min}$, with an average spacing of approximately $1.5a_{\min}$. This reasoning indicates that in practice there will be a large scatter in crack spacing; crack spacings ranging between 0.67 and 1.33 of the average spacing are theoretically possible.

For bars of the same diameter, $\Sigma o = 4A_s/d_b$, where A_s is the steel area and d_b is the bar diameter. Also, substituting $\rho_e = A_s/A_e$ into Eq. 10.56 gives

$$a_{\max} = 2a_{\min} = \frac{f'_t d_b}{2u \rho_e} \quad (10.57)$$

The crack width is given by the elongation of the steel between two cracks minus the elongation of the concrete. Ignoring the elongation of the concrete as small, the maximum crack width is given by $a_{\max} f_s/E_s$, where f_s is the steel stress and E_s is the modulus of elasticity of the steel. Substituting a_{\max} from Eq. 10.57 gives the maximum crack width as

$$w_{\max} = \frac{d_b f_s}{\rho_e K_1} \quad (10.58)$$

where $K_1 = 2uE_s/f'_t$.

This basic equation for maximum crack width has been modified by many workers. The foregoing derivation involves the assumption that the tensile stress in the concrete at section *B* of Fig. 10.19a is uniform, and the effective area of concrete in tension A_e is therefore the whole cross section of the member. This assumption is questionable because the actual distribution of tensile stress may be highly nonuniform. It is also assumed that the opening of cracks is due to slip of the concrete relative to the reinforcement, that the spacing of cracks is determined by the force that can be transmitted from the steel to the concrete by bond, and that the crack has parallel sides (i.e., a constant width) through the thickness of the member.

The application of Eq. 10.58 to the bending of a beam as in Fig. 10.19b involves further assumptions. The effective area of concrete in tension A_e

must be suitably defined. Generally A_e is taken to be the area of concrete having the full width of the beam and having the same centroid as the main reinforcement, as in Fig. 10.19b. Attempts to apply Eq. 10.58 to beams have demonstrated the need to reduce the effect of d_b and ρ_e . Modified forms of Eq. 10.58 have been suggested based on comparison with test results. For example, an early CEB^{10.15} equation for the maximum crack width at the level of the reinforcement on the concrete surface is

$$w_{\max} = \left(4.5 + \frac{0.4}{\rho_e} \right) d_b \frac{f_s}{K_2} \quad (10.59)$$

where $K_2 = 47.5 \times 10^6$ psi ($328,000$ N/mm 2) for deformed bars. Kaar and Mattock^{10.16} of the Portland Cement Association further modified Eq. 10.59 to express the maximum crack width at the level of deformed bar reinforcement on the concrete surface as

$$w_{\max} = 0.115 \sqrt[4]{A} f_s \times 10^{-6} \text{ in} \quad (10.60)$$

where A = area of concrete surrounding each bar ($A = A_e/n$, where n is the number of bars) in square inches, and the steel stress f_s is in psi (1 in = 25.4 mm; 1 psi = 0.00689 N/mm 2). The measured maximum crack widths from which Eq. 10.60 was derived showed a scatter of up to $\pm 40\%$ from the equation. To obtain the maximum crack width at the extreme tension fiber for beams reinforced by deformed bars, Kaar and Hognestad^{10.17} modified Eq. 10.60 to

$$w_{\max} = 0.115 \sqrt[4]{A} f_s \frac{h_2}{h_1} \times 10^{-6} \text{ in} \quad (10.61)$$

where h_1 = distance from the centroid of tension steel to the neutral axis and h_2 = distance from the extreme tension fiber to the neutral axis.

No-Slip Theory

Base et al^{10.18} of the Cement and Concrete Association proposed a fundamentally different approach in which they assumed that for the range of crack widths normally permitted in reinforced concrete, there is no slip of the steel relative to the concrete. The crack is therefore assumed to have zero width at the surface of the reinforcing bar and to increase in width as the surface of the member is approached. This means that the crack width is dependent on the deformations of the surrounding concrete. The theory of elasticity can be used to determine the distribution of stress and strain in the concrete between the cracks. The stresses so calculated indicate when further cracking is likely; the strains indicate the deformed shape of the concrete

surface, hence the likely width of cracking. On the basis of tests conducted at the Cement and Concrete Association, the following formula for the prediction of the maximum crack width on the surface of concrete beams reinforced by deformed bars was proposed by Base et al.:

$$w_{\max} = 3.3c \frac{f_s}{E_s} \frac{h_2}{h_1} \quad (10.62)$$

where c = distance from the point at which the crack width is to be determined to the surface of the nearest reinforcement bar, f_s = stress in the steel, E_s = modulus of elasticity of the steel, h_2 = distance from the point at which the crack width is to be determined to the neutral axis, and h_1 = distance from the centroid of the tension steel to the neutral axis. Some of the notation appears in Fig. 10.20a.

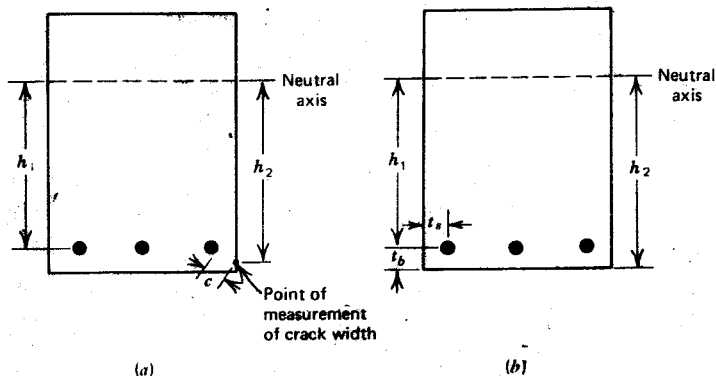


Fig. 10.20. Notation for crack width equations. (a) Base et al. approach. (b) Gergely-Lutz approach.

The Cement and Concrete Association tests also revealed that the type of reinforcing steel had a much smaller influence on the crack width than had previously been thought. It was found that for beams reinforced by plain bars, the surface crack widths may only be 20% greater than those in beams reinforced by deformed bars, for the same steel stress and beam proportions.

A Statistical Approach

Gergely and Lutz^{10.19} have subjected the data from previous investigations to statistical analysis to determine the importance of the variables involved.

Many combinations of variables were tried, and it was very difficult to obtain an equation that fitted all sets of data well. The important variables were found to be the effective area of concrete in tension A_e , the number of bars, the side or bottom cover, the strain gradient from the level of the steel to the tension face, and the steel stress. Of these, the steel stress was the most important. The following equations were developed for predicting the maximum crack widths on the surface of members reinforced by deformed bars. At the extreme tension fiber we have

$$w_{\max} = 0.076 \sqrt[3]{t_b A} \frac{h_2}{h_1} f_s \times 10^{-6} \text{ in} \quad (10.63)$$

At the level of the reinforcement we have

$$w_{\max} = \frac{0.076 \sqrt[3]{t_s A}}{1 + \frac{2}{3} \frac{t_s}{h_1}} f_s \times 10^{-6} \text{ in} \quad (10.64)$$

where t_b = distance from extreme tension fiber to the center of the adjacent bar (in), t_s = distance from the side of the beam to the center of the adjacent bar (in), A = average effective area of concrete in tension around each reinforcing bar ($= A_e/n$, where n is the number of bars) (in^2), f_s = steel stress (psi), h_1 = distance from the centroid of the tension steel to the neutral axis (in), and h_2 = distance from the extreme tension fiber to the neutral axis (in): 1 in = 25.4 mm, 1 psi = 0.00689 N/mm². Some of the notation is given in Fig. 10.20b.

Nawy^{10.20} has compared the accuracy of a form of Eq. 10.64 with experimental maximum crack width data from the tests conducted by himself, the Portland Cement Association,^{10.14, 10.16} and the Cement and Concrete Association.^{10.18} The scatter of data about the predicted maximum crack widths was very considerable, as Fig. 10.21 indicates. Navy^{10.20} also compared the maximum crack widths predicted by the Portland Cement Association equation (10.60) and the Cement and Concrete Association equation (10.62) with the experimental data and found a wide scatter. Lloyd et al^{10.21} have measured maximum crack widths on one-way slabs reinforced by deformed bars, deformed wires, deformed wire fabric, and smooth wire fabric, concluding that the Gergely-Lutz equations (10.63 and 10.64) satisfactorily predicted the maximum crack width. Comparison of their experimental data with Eq. 10.64 (Fig. 10.22) reveals considerable deviation from the equation in some cases.

More General Approach

The previous brief survey shows that no satisfactory theory exists to enable the accurate prediction of the cracking behavior of reinforced concrete

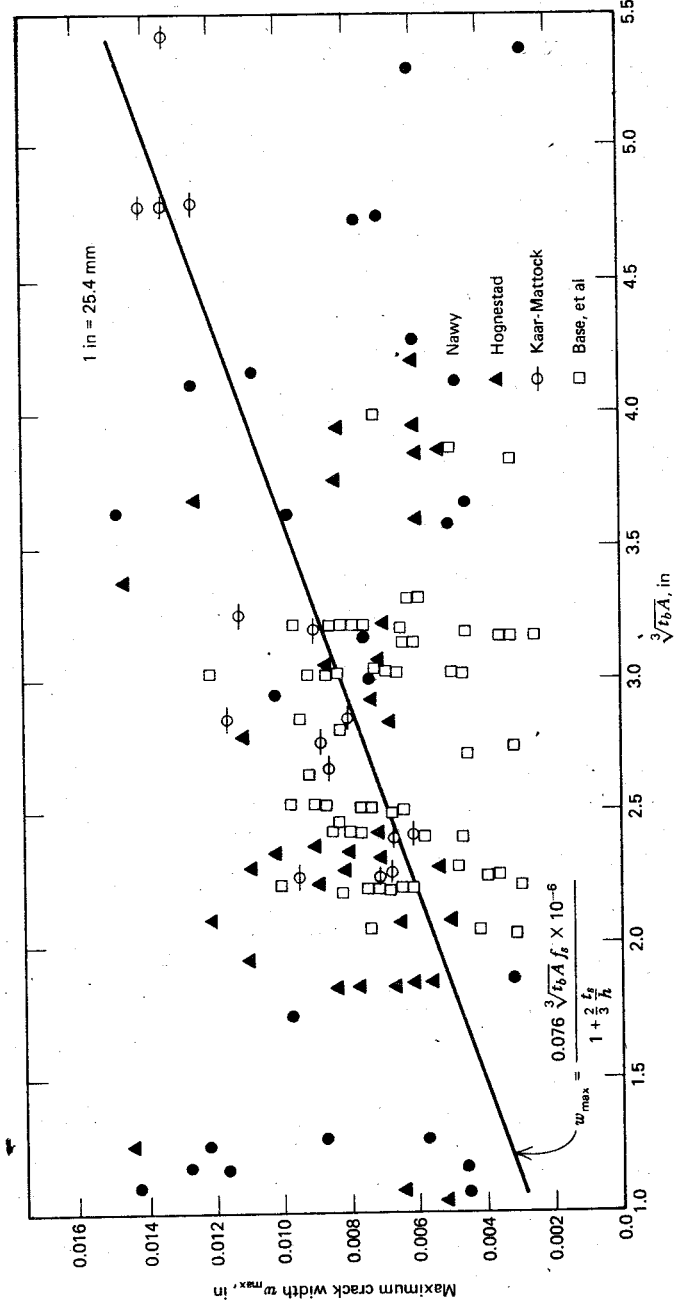


Fig. 10.21. Maximum crack width in beams at level of reinforcement at 40 ksi (276 N/mm²) compared with a form of the Gergely-Lutz equation. 10.20

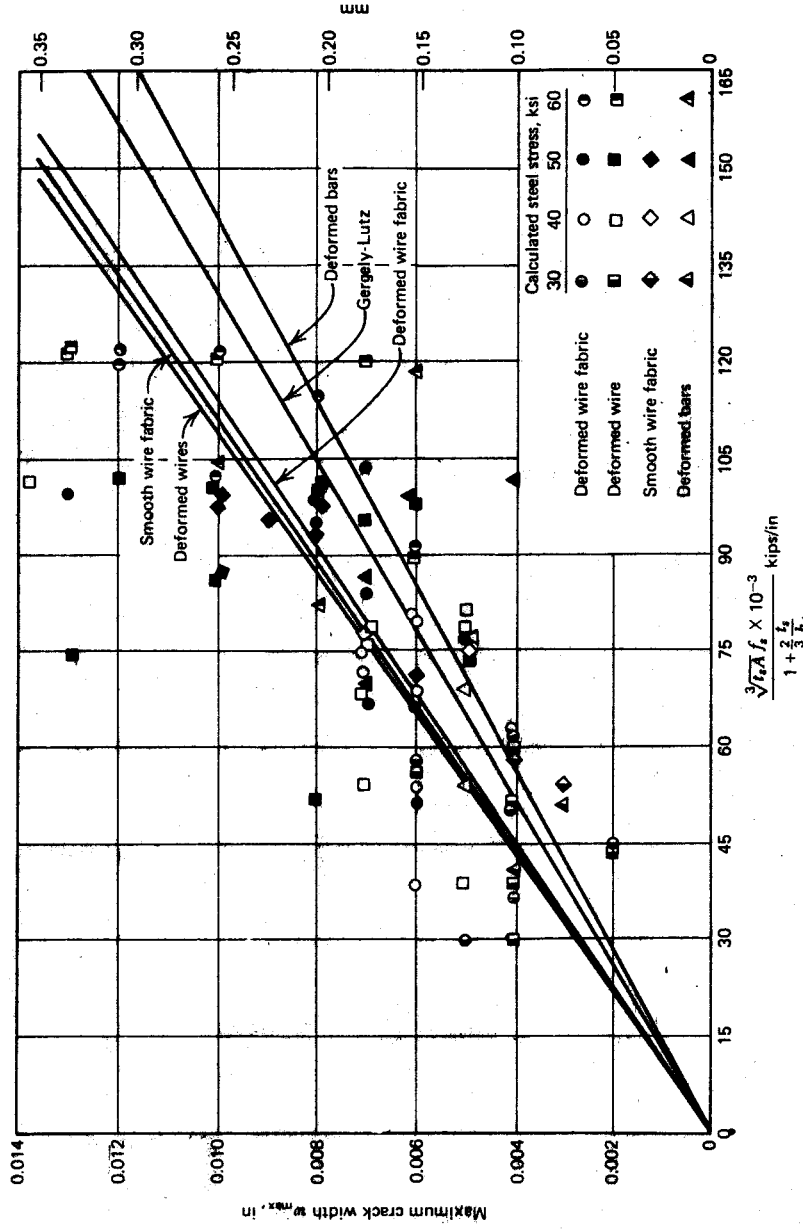


Fig. 10.22. Maximum crack width in one-way slabs at level of reinforcement compared with the Gergely-Lutz equation.^{10.21} (1 ksi = 6.89 N/mm², 1 kip/in = 175 kN/m).

members. However, recent work by Beeby^{10.22} at the Cement and Concrete Association has resulted in a clearer understanding of the mechanism of cracking. Beeby measured crack widths and spacing at various points across the bottom of one-way reinforced concrete slabs, that is, for various values of c as in Fig. 10.23a. It was found that the crack spacing and width increased with distance from the bar and at some distance from the bar approached constant values, which were dependent on the crack height rather than the distance from the bar. Beeby therefore concluded that the crack pattern at any point was the result of interaction between two basic crack patterns.

CRACKING AT A POINT DISTANT FROM A REINFORCING BAR

The crack pattern illustrated in Fig. 10.23b is controlled by the crack height, h_o . The crack will penetrate nearly to the neutral axis, and its height may be calculated by standard elastic theory using the steel content and the modular ratio. From St. Venant's principle it is evident that the concrete tensile stresses between the cracks are substantially unaffected by the crack at distances greater than h_o from the crack. Hence the next crack will form at a distance from the crack equal to or greater than h_o . Therefore, the minimum spacing of the cracks is h_o and the maximum is $2h_o$, giving a mean crack spacing of $1.5h_o$. A mean value of $1.33h_o$ was actually measured by Beeby in the tests. The crack width and the spacing were found to be directly proportional to the initial crack height h_o . Therefore this type of cracking is controlled by the initial crack height h_o .

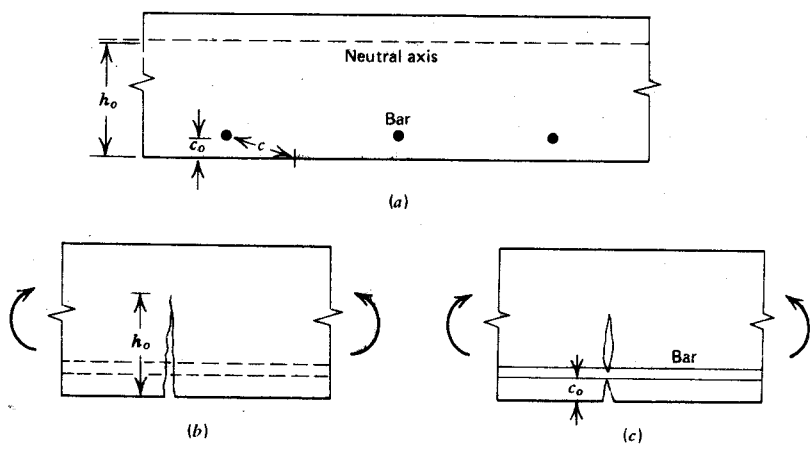


Fig. 10.23. Effect of bar proximity on cracking.^{10.22} (a) Section (b) Crack at distance from a bar, h_o controlled. (c) Crack at a bar, c_o controlled.

CRACKING DIRECTLY OVER A REINFORCING BAR (Fig. 10.23c)

The "no-slip" theory discussed previously predicts wedge-shaped cracks with zero width at the bar. That is, a linear relationship is predicted between crack width and distance from the bar. Thus directly over the bar the effective crack height is c_o ; using the same reasoning as before, the crack spacing will vary between c_o and $2c_o$, with a mean spacing of $1.5c_o$. Slip or deformations at the bar surface that occur before the crack pattern has fully developed will result in the crack having some width at the surface of the bar and will increase the effective crack height, causing larger crack spacings and widths. If there was no bond between concrete and steel, the crack pattern would be controlled by the initial crack height, h_o . Thus the effect of slip and internal deformations is to modify the c_o controlled crack pattern toward the h_o controlled crack pattern, and the widths of cracks in this general case will be a function of c_o , to take the wedge shape into account, and c_o/h_o , to take slip and internal fracturing at the bar surface into account.

Beeby found that the following equations gave the best fit to his experimental data.

maximum crack width directly over a bar

$$\frac{w_{\max o}}{\varepsilon_m} = K_1 c_o + K_2 \frac{A}{d_b} e^{-K_3(c_o/h_o)} \quad (10.65)$$

maximum crack width at a distance from a bar

$$\frac{w_{\max l}}{\varepsilon_m} = K_1 h_o \quad (10.66)$$

maximum crack width for intermediate positions

$$w_{\max} = \frac{c w_{\max l} w_{\max o}}{c_o w_{\max l} + (c - c_o) w_{\max o}} \quad (10.67)$$

where c = distance from point of measurement of crack to surface of the nearest bar, c_o = minimum cover to steel, d_b = bar diameter, A = effective area of concrete in tension surrounding one bar, h_o = initial height of crack, ε_m = average longitudinal strain at the level where cracking is being considered, e = base of the natural logarithm, and K_1 , K_2 , and K_3 are constants that depend on the probability of the crack width being exceeded.

Equations 10.65 to 10.67 are too complex for practical use. The equations can be simplified, as Beeby^{10.23} has done, giving the crack width that will be exceeded by approximately 20% of the results as

$$w_{\max} = \frac{3c\varepsilon_m}{1 + 2(c - c_o)/(h_o - kd)} \quad (10.68)$$

where h = overall depth of the section, kd = neutral axis depth and

$$\varepsilon_m = \left(\varepsilon_s - \frac{2.5bh}{A_s} \times 10^{-6} \right) \frac{h - kd}{d - kd} \quad (10.69)$$

where ε_s = strain in the steel at a crack, b = section width, h = overall depth of the section, A_s = area of tension steel, d = effective depth, and kd = neutral axis depth. Equation 10.69 for ε_m is the steel strain at a crack, less an empirical term due to the stiffening effect of concrete tension between cracks, and modified by the strain gradient term to obtain the average strain at the extreme tension fiber of the member.

Equation 10.65 has similarities to the following equation developed by Ferry Borges^{10.24} for the maximum crack width in beams reinforced by deformed bars

$$w_{\max} = \frac{1}{E_s} \left(2.5c + 0.066 \frac{d_b}{\rho_w} \right) \left(f_s - \frac{107}{\rho_w} \right) \text{ in} \quad (10.70)$$

where E_s = modulus of elasticity of steel (psi), c = thickness of concrete cover over bar (in), d_b = bar diameter (in), $\rho_w = A_s/b_w d$; A_s = steel area (in^2), b_w = web width (in), d = beam effective depth (in), and f_s = steel stress at crack (psi): 1 in = 25.4 mm, 1 psi = 0.00689 N/mm². In Eq. 10.70 the $2.5c$ term takes the wedge shape of the crack into account, the $0.066d_b/\rho_w$ term takes the bond slip effect at the bars into account (similar term to the classical theory), and the $107/\rho_w$ term reduces the steel stress at a crack to give the average steel stress to account for tension carried by the concrete between cracks.

Long-Term Cracking

All the previously described equations were obtained from relatively short-term loading tests. Very little information is available on the effect of long-term loading on crack widths. Illston and Stevens^{10.25} found that the spacing of cracks does not change with time under sustained loading, but the average crack width does increase with time. The increase in width occurred at a decreasing rate with time, and in the tests the crack widths doubled in two years. The increase in widths is caused by shrinkage of the concrete and by time-dependent change of curvature. It was also found that there was a breakdown of bond with sustained loading, and the cracks tended to become more parallel sided. In terms of Beeby's work, this probably means that sustained loading tends to modify the c_o controlled cracks to h_o controlled cracks.

10.4.4 Control of Flexural Cracks in Design

The permissible values for the width of flexural cracks in practice depend mainly on the environment in which the structure has to serve, particularly from the point of view of the possibility of corrosion of the reinforcement. The permissible values recommended by ACI Committee 224^{10.26} are listed in Table 10.3. In comparison with these values, ACI 318-71^{10.1} recommends

Table 10.3 Permissible Crack Widths in Reinforced Concrete^a

Exposure Condition	Maximum Allowable Crack Width, in (mm)
Dry air or protective membrane	0.016 (0.41)
Humidity, moist air, soil	0.012 (0.30)
Deicing chemicals	0.007 (0.18)
Seawater and seawater spray, wetting and drying	0.006 (0.15)
Water-retaining structures	0.004 (0.10)

^a From Reference 10.26

only two maximum allowable crack widths, 0.016 in (0.41 mm) for interior exposure and 0.013 in (0.33 mm) for exterior exposure. The ACI 318-71 method for beams and one-way slabs is based on the Gergely-Lutz equation 10.63, with h_2/h_1 put at 1.2. The requirement may be written as permissible maximum crack width $\geq 0.076\sqrt[3]{t_b A} \times 1.2f_s \times 10^{-6}$ in, with t_b in inches, A in square inches, and f_s in psi (1 in = 25.4 mm, 1 psi = 0.00689 N/mm²). Substituting the permissible values for crack widths into the equation gives

$$f_s \sqrt[3]{t_b A} \leq 175,000 \text{ lb/in} \quad \text{for interior exposure} \quad (10.71a)$$

and

$$f_s \sqrt[3]{t_b A} \leq 145,000 \text{ lb/in} \quad \text{for exterior exposure} \quad (10.71b)$$

where again the units are inches and pounds. ACI 318-71 requires the section to be proportioned so that either Eq. 10.71a or 10.71b is satisfied. This check need only be carried out when the design yield strength for the reinforcement exceeds 40,000 psi (276 N/mm²). In structures subjected to very aggressive environment or designed to be watertight, Eq. 10.71b does not apply, since a smaller maximum allowable crack width needs to be adopted (see Table 10.3).

To use Eq. 10.71a or 10.71b, the steel stress f_s at the service load is required. This steel stress may be found from $f_s = M/(jdA_s)$, where M = service load

bending moment, jd = level arm of the internal moment, and A_s = steel area. Alternatively, f_s may be taken as 60% of the specified yield strength of the steel.

By comparison, the British code of practice CP 110:1972^{10.27} requires in general that the surface crack widths at the service load not exceed 0.3 mm (0.012 in). The code gives rules for clear distances between bars for crack control and quotes a formula similar to Eq. 10.68 for use when crack widths have to be checked. The recommendations of the European Concrete Committee—International Federation of Prestressing^{10.12} require that the surface crack widths at the service load not exceed 0.1 mm (0.004 in) in a very exposed (particularly aggressive) environment, 0.2 mm (0.008 in) in an unprotected environment (external member in bad weather conditions or internal member in a damp or aggressive environment), or 0.3 mm (0.012 in) in a protected environment (internal member in normal surroundings). The maximum crack widths are calculated using a formula based on the Ferry Borges equation 10.70.

Example 10.14

The rib of the *T* beam in Fig. 10.24 contains six No. 9 (28.7 mm diameter) deformed steel bars as longitudinal tension reinforcement. The cover and vertical spacing between bars are indicated in the figure. The overall depth of the section is 27 in (686 mm), and the neutral axis lies at 5.25 in (133 mm) from the extreme compression fiber. The steel has a stress of 30,000 psi (207 N/mm^2) at the service load and a modulus of elasticity of 29×10^6 psi ($200,000 \text{ N/mm}^2$).

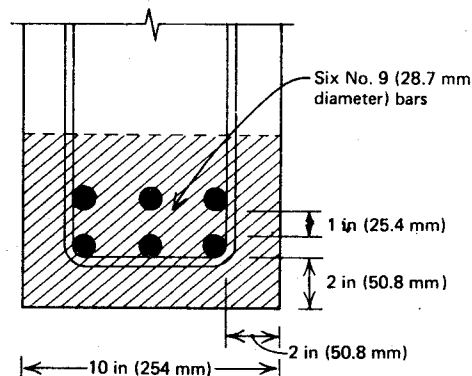


Fig. 10.24. Example 10.14.

- (1) Check that the reinforcement arrangement is adequate for exterior exposure using the ACI 318-71 approach, and (2) calculate the maximum likely crack width using the various crack width formulas.

Solution

1. ACI 318-71 approach. Equation 10.71b applies

The effective area of concrete in tension A_e is shaded in Fig. 10.24 (see also Fig. 10.19b).

$$A_e = 10(2 + 1.13 + 1 + 1.13 + 2) = 72.6 \text{ in}^2$$

$$\therefore A = \frac{72.6}{6} = 12.10 \text{ in}^2/\text{bar}$$

Also $t_b = 2 + 0.56 = 2.56$ in and $f_s = 30,000$ psi.

$$\therefore f_s \sqrt[3]{t_b A} = 30,000 \sqrt[3]{2.56 \times 12.1} = 94,200 \text{ lb/in}$$

which is less than 145,000 lb/in. Therefore, the arrangement of reinforcement is satisfactory.

If the arrangement had not been satisfactory, it would have been necessary to use a larger number of smaller diameter bars to make up the steel area to reduce A .

2. Maximum likely crack width according to the various formulas

For the beam section, $h_2 = 27 - 5.25 = 21.75$ in, and $h_1 = 21.75 - (2 + 1.13 + 0.5) = 18.12$ in

Kaar-Hognestad equation 10.61; at the extreme tension fiber

$$w_{\max} = 0.115 \sqrt[4]{12.1} \times 30,000 \times \frac{21.75}{18.12} \times 10^{-6}$$

$$= 0.0077 \text{ in (0.20 mm)}$$

Base et al equation 10.62; at the extreme tension fiber at one corner of the section, where c is a maximum, we have

$$c = \sqrt{2}(2 + 0.56) - 0.56 = 3.06 \text{ in}$$

$$w_{\max} = 3.3 \times 3.06 \frac{30,000}{29 \times 10^6} \times \frac{21.75}{18.12}$$

$$= 0.0125 \text{ in (0.32 mm)}$$

(Note: directly under the bar $c = 2$ in and $w_{\max} = 0.0082$ in.)

Gergely-Lutz equation 10.63: at the extreme tension fiber

$$w_{\max} = 0.076 \sqrt[3]{2.56 \times 12.1} \times \frac{21.75}{18.12} \times 30,000 \times 10^{-6}$$

$$= 0.0086 \text{ in (0.22 mm)}$$

Beeby equations 10.68 and 10.69: at the extreme tension fiber at one corner of the section, where c is a maximum, $c = 3.06$ in and $c_0 = 2$ in,

$$w_{\max} = \frac{3 \times 3.06}{1 + 2(3.06 - 2)/21.75}$$

$$\times \left(\frac{30,000}{29 \times 10^6} - \frac{2.5 \times 10 \times 27}{6} \times 10^{-6} \right) \frac{21.75}{18.12}$$

$$= 0.0092 \text{ in (0.23 mm)}$$

(Note: directly under the bar $c = 2$ in and $w_{\max} = 0.0066$ in.)

Ferry Borges equation 10.70: at the extreme tension fiber at one corner of the section, where c is a maximum, $c = 3.06$ in, and

$$w_{\max} = \frac{1}{29 \times 10^6} \left[2.5 \times 3.06 + 0.066 \frac{1.13}{6/(10 \times 23.37)} \right]$$

$$\times \left[30,000 - \frac{107}{6/(10 \times 23.37)} \right] = 0.0094 \text{ in (0.23 mm)}$$

(Note: directly under the bar $c = 2$ in and $w_{\max} = 0.0070$ in.) The equation by Base et al has given a rather higher maximum crack width than the other equations, but Eq. 10.62 may be regarded as having been superseded by Beeby's equations. It should be noted that the equations of Beeby, Ferry Borges, and Kaar-Hognestad gives results that lie within 11% of the Gergely-Lutz equation in Example 10.14.

It is evident that crack widths will not normally be a problem in design unless the steel stresses at service load are very high or the crack widths are to be kept very small. In view of the wide scatter of measured crack widths on structural elements, great accuracy in calculations for crack control cannot be justified. The best crack control is obtained when the reinforcing bars are well distributed over the zone of concrete tension. The aim is to ensure that fine, closely spaced cracks form, rather than a few wide cracks. For relatively deep beams, reinforcement should also be added near the vertical faces in the tension zone to control cracking in the web.^{10.1} Without such face steel, a few wide cracks may extend into the web even though the zone of maximum

tension may contain only fine cracks. To achieve crack control in the flanges of *T* beams with negative moment, the reinforcement should be well distributed throughout the flange. If the reinforcement is placed only over the web, a few wide cracks may extend into the slab even though only fine and well-distributed cracks may exist over the web.^{10,17}

It should also be emphasized that protection against corrosion is not just a matter of limiting the crack width on the surface of the concrete. A reasonable thickness of good quality, well-compacted concrete is also essential for durable structures.

The control of cracking by correct construction practices, and the effects of drying shrinkage, are discussed by ACI Committee 224.^{10,26}

10.5 REFERENCES

- 10.1 ACI Committee 318, "Building Code Requirements for Reinforced Concrete, (ACI 318-71)", American Concrete Institute, Detroit, 1971, 78 pp.
- 10.2 A. D. Ross, "Creep of Concrete Under Variable Stress," *Journal ACI*, Vol. 54, No. 9, March 1958, pp. 739-758.
- 10.3 D. McHenry, "A New Aspect of Creep in Concrete and its Applications to Design," *Proceedings American Society for Testing and Materials*, Vol. 43, 1943, pp. 1969-1984.
- 10.4 Subcommittee 1, ACI Committee 435, "Allowable Deflections," *Journal ACI*, Vol. 65, No. 6, June 1968, pp. 433-444.
- 10.5 ACI Committee 213, "Guide for Structural Lightweight Aggregate Concrete," *Journal ACI*, Vol. 64, No. 8, August 1967, pp. 433-464. Also discussion by R. N. McManus and Committee Closure, *Journal ACI*, Vol. 65, No. 2, February 1968, pp. 151-155.
- 10.6 ACI Committee 318, "Commentary on Building Code Requirements for Reinforced Concrete, (ACI 318-71)," American Concrete Institute, Detroit, 1971, 96 pp.
- 10.7 D. E. Branson, "Instantaneous and Time-Dependent Deflections of Simple and Continuous Reinforced Concrete Beams," HPR Report No. 7, Part 1, Alabama Highway Department, Bureau of Public Roads, August 1963 (1965), pp. 1-78.
- 10.8 ACI Committee 435, "Deflections of Reinforced Concrete Flexural Members," *Journal ACI*, Vol. 63, No. 6, June 1966, pp. 637-674.
- 10.9 ACI Committee 340, *Design Handbook in Accordance with the Strength Design Method of ACI 318-71*, Vol. 1. Publication SP-17(73), American Concrete Institute, Detroit, 1973, 403 pp.
- 10.10 W. W. Yu and G. Winter, "Instantaneous and Long-Time Deflections of Reinforced Concrete Beams Under Working Loads," *Journal ACI*, Vol. 57, No. 1, July, 1960, pp. 29-50.
- 10.11 ACI Committee 209, "Prediction of Creep, Shrinkage and Temperature Effects in Concrete Structures," *Designing for the Effects of Creep, Shrinkage, and Temperature in Concrete Structures*, SP-27, American Concrete Institute, Detroit, 1971, pp. 51-93.
- 10.12 CEB-FIP, "International Recommendations for the Design and Construction of Concrete Structures," Comité Européen du Béton/Fédération Internationale de la Précontrainte, Paris, (English edition published by the Cement and Concrete Association, London.) 1970, 80 pp.

- 10.13 D. Watstein and D. E. Parsons, "Width and Spacing of Tensile Cracks in Axially Reinforced Concrete Cylinders," *Journal of Research of the National Bureau of Standards*, Vol. 31, No. RP 545, July 1943, pp. 1-24.
- 10.14 E. Hognestad, "High Strength Bars as Concrete Reinforcement, Part 2. Control of Flexural Cracking," *Journal*, Portland Cement Association Research and Development Laboratories, Vol. 4, No. 1, January 1962, pp. 46-63.
- 10.15 CEB, "Compte-Rendu de la 5ème Session de Travail," Comité Européen du Béton, Bulletin d'Information No. 24, Paris, 1960.
- 10.16 P. H. Kaar, and A. H. Mattock, "High Strength Bars as Concrete Reinforcement, Part 4. Control of Cracking," *Journal*, Portland Cement Association Research and Development Laboratories, Vol. 5, No. 1, January 1963, pp. 15-38.
- 10.17 P. H. Kaar and E. Hognestad, "High Strength Bars as Concrete Reinforcement, Part 7. Control of Cracking in T-Beam Flanges," *Journal*, Portland Cement Association Research and Development Laboratories, Vol. 7, No. 1, January 1965, pp. 42-53.
- 10.18 G. D. Base, J. B. Read, A. W. Beeby, and H. P. J. Taylor, "An Investigation of the Crack Control Characteristics of Various Types of Bar in Reinforced Concrete Beams," Research Report No. 18, Part I, Cement and Concrete Association, London, December 1966, 44 pp.
- 10.19 P. Gergely, and L. A. Lutz, "Maximum Crack Width in Reinforced Flexural Members," *Causes, Mechanism and Control of Cracking in Concrete*, SP-20, American Concrete Institute, Detroit, 1968, pp. 87-117.
- 10.20 E. G. Navy, "Crack Control in Reinforced Concrete Structures," *Journal ACI*, Vol. 65, No. 10, October 1968, pp. 825-836.
- 10.21 J. P. Lloyd, M. R. Hassan, and C. E. Kesler, "Crack Control in One-Way Slabs Reinforced with Deformed Welded Wire Fabric," *Journal ACI*, Vol. 66, No. 5, May 1969, pp. 366-376.
- 10.22 A. W. Beeby, "An Investigation of Cracking in Slabs Spanning One Way," Technical Report TRA 433, Cement and Concrete Association, London, April 1970, 33 pp.
- 10.23 A. W. Beeby, "Prediction and Control of Flexural Cracking in Reinforced Concrete Members," *Cracking, Deflection and Ultimate Load of Concrete Slab Systems*, SP-20, American Concrete Institute, Detroit, 1971, pp. 55-75.
- 10.24 J. Ferry Borges, "Cracking and Deformability of Reinforced Concrete Beams," *Publications*, Vol. 26, International Association for Bridge and Structural Engineering, Zurich, 1966, pp. 75-95.
- 10.25 J. M. Illston and R. F. Stevens, "Long-Term Cracking in Reinforced Concrete Beams," *Proceedings of the Institution of Civil Engineers*, Part 2, *Research and Theory*, Vol. 53, December 1972, pp. 445-459.
- 10.26 ACI Committee 224, "Control of Cracking in Concrete Structures," *Journal ACI*, Vol. 69, No. 12, December 1972, pp. 717-753.
- 10.27 BSI, "Code of Practice for the Structural Use of Concrete," CP110: Part 1: 1972," British Standards Institution, London, 1972, 154 pp.

Strength and Ductility of Frames

11.1 INTRODUCTION

Consideration of the behavior of reinforced concrete frames at and near the ultimate load is necessary to determine the possible distributions of bending moment, shear force, and axial force that could be used in design. It is possible to use a distribution of moments and forces different from that given by linear elastic structural analysis if the critical sections have sufficient ductility to allow redistribution of actions to occur as the ultimate load is approached. Also, in countries that experience earthquakes, a further important design aspect is the ductility of the structure when subjected to seismic-type loading, since present seismic design philosophy relies on energy dissipation by inelastic deformations in the event of major earthquakes.

Both these aspects of behavior at ultimate load depend on the deformation characteristics of the members, which for frames depend mainly on the relationship between moment and curvature. Moment-curvature relationships for beam and column sections, and the calculation of flexural deformations at and near the ultimate load of members, have been discussed in Chapter 6. Figure 11.1 gives a typical moment-curvature curve for a section in which the tension steel is at the yield strength at the ultimate moment. The curve is marked to indicate points at which the concrete starts to crack, the tension steel begins to yield, and spalling and crushing of the concrete commences. A ductile section is capable of maintaining moment capacity at near the ultimate value for large curvatures beyond the curvature at first yield.

11.2 MOMENT REDISTRIBUTION AND PLASTIC HINGE ROTATION

It is evident that the nonlinear nature of the moment-curvature relationship for reinforced concrete sections will cause some adjustment to the relative values of the bending moments if the structure is loaded into and beyond the

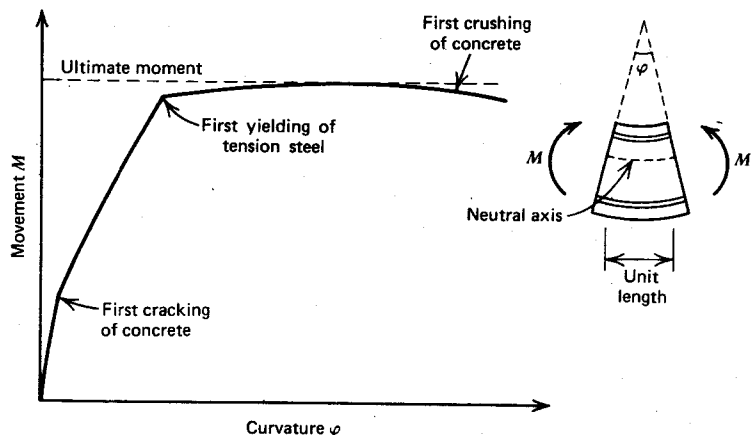


Fig. 11.1. Typical moment-curvature relationship for reinforced concrete flexural member.

service load range. In particular, because of plastic rotations at some sections, it is possible for the bending moments to assume a pattern different from that derived from linear elastic structural analysis, and for all the critical positive and negative moment sections to reach their ultimate moments of resistance at the ultimate load. Thus moment redistribution can have a marked influence on the ultimate load of a statically indeterminate structure.

Consider, for example, a two-span continuous beam, having a uniform cross section (Fig. 11.2a). Let M'_u be the ultimate moment of resistance of the negative bending moment sections, and M_u be the ultimate moment of resistance of the positive bending moment sections. We assume that the sections are adequately reinforced for shear, allowing the ultimate moments to be attained without shear failure. We also assume that the moment-curvature relationship for the sections is the idealized bilinear relationship for a ductile section shown in Fig. 11.2b, all sections having the same constant flexural rigidity up to the ultimate moment and the moment remaining constant at the ultimate value at higher curvatures. At low loads the distribution of bending moment due to the two concentrated loads will be in accordance with the elastic theory distribution (see Fig. 11.2c). The dead load of the beam has been neglected. As the applied loads are increased further, the ultimate moment of resistance will be reached at one critical section, say over the center support, before it is reached at the other sections. Then the moment at the center support will be M'_u , as in Fig. 11.2d. The extent to which further load can be carried by the beam depends on the capacity for plastic rotation at the center support. If the section is brittle, the moment will

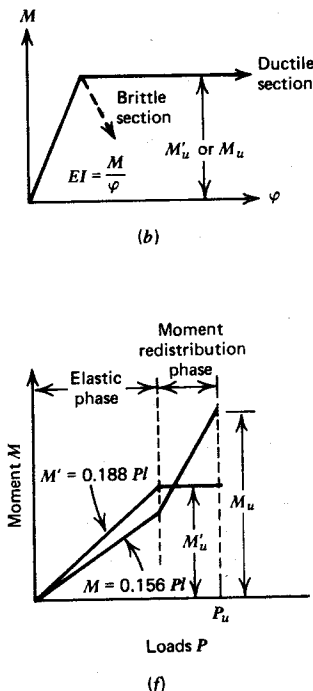
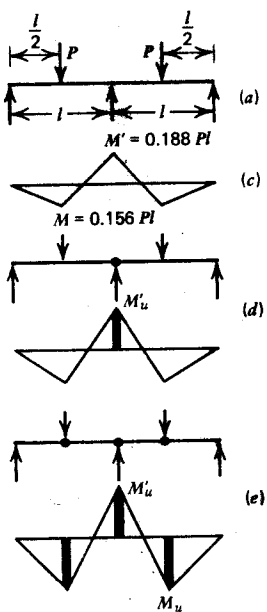


Fig. 11.2. Moment redistribution and formation of a collapse mechanism for a continuous beam. (a) Beam. (b) Idealized moment-curvature relationship for the sections. (c) Elastic theory bending moment diagram. (d) At formation of first plastic hinge. (e) At formation of collapse mechanism. (f) Change of bending moment with load.

decrease rapidly after reaching the maximum (see Fig. 11.2b), and the beam will fail suddenly without carrying any additional load. If the section is ductile, additional load can be carried because the plastic hinge at the center support rotates while maintaining its moment of resistance constant at M'_u , and moment redistribution will occur until the maximum positive moment in the spans increases to M_u . Then the collapse mechanism in Fig. 11.2e is formed. Figure 11.2f traces the variation of bending moment at the critical sections with load on the beam, assuming that the plastic hinge forms first at the center support (this requires $M'_u/M_u < M'/M = 1.2$). Note that at all stages equilibrium requires

$$M + \frac{M'}{2} = \frac{Pl}{4}$$

$$\therefore P = \frac{4}{l} \left(M + \frac{M'}{2} \right) \quad (11.1)$$

And, if the moment at the center support remains at M'_u until M_u develops at the midspan sections, we have

$$P_u = \frac{4}{l} \left(M_u + \frac{M'_u}{2} \right) \quad (11.2)$$

Therefore, if sufficient rotation capacity of the plastic hinges is available, the bending moment distribution at the ultimate load may be quite different from that calculated using elastic theory and will depend on the ultimate moments of resistance of the sections. In reinforced concrete structures, the ductility at the first plastic hinges to form may be insufficient to enable full redistribution of moments to take place with the ultimate moment at each critical section. Thus if moment redistribution is to be relied on, the availability of sufficient ductility at the plastic hinges must be ensured.

As an example, let us calculate the required plastic rotation for the two-span continuous beam of Fig. 11.2 for the case of the plastic hinge forming first at the center support. The beam and the curvature diagrams of Figs. 11.3a and 11.3b show the stage at which sufficient plastic rotation has occurred at the center support B to enable the ultimate moment M_u to be just developed at midspan. Hence Figs. 11.3a and 11.3b indicate the stage when P_u is just reached. The plastic curvature is considered to occur over the equivalent plastic hinge length l_p each side of the critical section (see Section 6.6.3). The elastic curvature along the length of the member may be calculated from the distribution of bending moments and the assumed constant flexural rigidity EI . The plastic rotation θ_p at the center support B is the discontinuity of slope between the ends of the adjacent members, and $\theta_p = 2\theta_B$ as indicated in Fig. 11.3a. To find θ_p , we must consider the elastic deformations of the members supporting the loads P_u . First, replace the plastic hinge at B by a frictionless hinge as in Fig. 11.3c. Then from the moment area theorem the rotation at B due to the load P_u alone on one span is

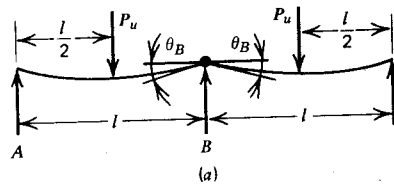
$$\theta'_B = \frac{(M_u + 0.5M'_u)l}{4EI} \quad (11.3)$$

Now consider the effect of the ultimate support moment M'_u acting at the frictionless hinge as in Fig. 11.3d. The rotation at B due to M'_u alone is

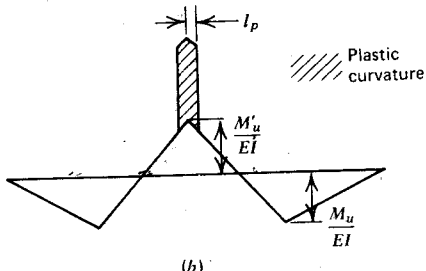
$$\theta''_B = \frac{M'_u l}{3EI} \quad (11.4)$$

$$\therefore \theta_B = \theta'_B - \theta''_B = \frac{l}{4EI} (M_u - \frac{5}{6}M'_u)$$

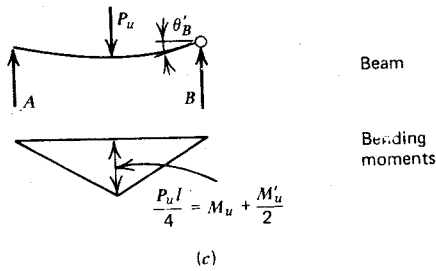
$$\therefore \theta_p = 2\theta_B = \frac{l}{2EI} (M_u - \frac{5}{6}M'_u) \quad (11.5)$$



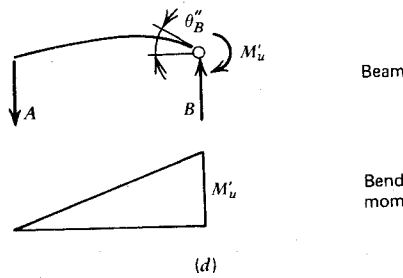
(a)



(b)



(c)



(d)

Fig. 11.3. Calculation of plastic hinge rotation for beam of Fig. 11.2. (a) Deflected shape when ultimate load is reached. (b) Idealized curvature distribution when ultimate load is reached. (c) P_u acting without M'_u . (d) M'_u acting without P_u .

Equation 11.5 gives the rotation required at the plastic hinge at the center support B for the case when $M_u > \frac{5}{6}M'_u$. If $M_u = \frac{5}{6}M'_u$ (i.e., if $M'_u/M_u = 1.2$), the required θ_p is zero because this is the ratio of moments given by elastic theory, and no redistribution of bending moments is required. Also, if $M_u < \frac{5}{6}M'_u$ the value given for θ_p is negative, in that case, the foregoing calculation does not apply because the first plastic hinge forms at the load points at midspan and the required plastic rotation at those sections would have to be calculated. From Section 6.6.4 and Fig. 11.3b, the available plastic hinge rotation at the plastic hinge may be seen to be $(\varepsilon_c/c - \varepsilon_{ce}/kd)2l_p$, where ε_c = concrete strain at extreme compression fiber at the ultimate curvature, ε_{ce} = concrete strain at the extreme compression fiber when the yield curvature is reached, c = neutral axis depth at the ultimate moment, kd = neutral axis depth when the yield curvature is reached, and l_p = equivalent plastic hinge length, each side of the critical section. Therefore, in the example, when $M_u > \frac{5}{6}M'_u$, redistribution of bending moments can take place until the ultimate moment develops at each critical section if

$$\frac{l}{2EI}(M_u - \frac{5}{6}M'_u) \leq \left(\frac{\varepsilon_c}{c} - \frac{\varepsilon_{ce}}{kd}\right)2l_p \quad (11.6)$$

Whether the full moment redistribution can take place can be checked from the section properties using Eq. 11.6.

The calculations for the foregoing example involved several assumptions, which are discussed below.

All sections were assumed to have the same constant flexural rigidity EI up to the ultimate moment. This assumption is only accurate at low loads before cracking of the concrete commences. When the beam cracks, the flexural rigidity reduces in the cracked regions and the variation of flexural rigidity along the member causes the distribution of bending moments to change from that calculated by elastic theory using a constant flexural rigidity. With further loading the extent of cracking increases and the distribution of flexural rigidity, hence bending moment, will be again modified. This effect is particularly noticeable when members contain different amounts of negative and positive moment steel; it is even more noticeable in T beams because cracking of the flange in the negative moment region reduces the flexural rigidity there much more than cracking of the web in the positive moment region. This variation of the flexural rigidity along the beam will affect the amount of plastic rotation required for full moment redistribution at the ultimate load. Strictly, the effect of cracking on the flexural rigidity EI of the sections needs to be taken into account in the determination of the plastic hinge rotation at the ultimate load.

The moment-curvature relationship chosen was assumed to have a horizontal branch beyond yield, with the moment remaining constant at

the ultimate value. This assumption only approximates the actual moment-curvature relationship after first yielding (see Fig. 11.1), for this curve has an ascending portion to the ultimate (maximum) moment after first yield of the tension steel. Therefore, both the negative and positive moment critical sections cannot develop the ultimate moments simultaneously because the curvatures at those sections will be at different points on the moment-curvature curves. It is evident that the assumption that the ultimate moment exists at all critical sections simultaneously will give a nonconservative value for the ultimate load. If, for example, the moment capacity at first yield is $M_y = 0.9M_u$, where M_u is the ultimate moment, the error in ultimate load calculated (assuming that all critical sections are at the ultimate moment) may be about 5%. Clearly, if the attainment of yield (M_y) at the last hinge to form is taken as the ultimate moment, and if M_y is significantly less than the ultimate moment M_u , the error in calculating the ultimate load (assuming the ultimate moments at all hinges) may be significant.

It is difficult, as we have seen, to calculate accurately the required plastic hinge rotation in reinforced concrete frames for full moment redistribution and the ultimate load. However, if moment redistribution is to be relied on in design, we need assurance that the ductility available at the critical sections is in excess of the ductility demand calculated from theoretical considerations such as those just discussed.

It has been known for many years that some moment redistribution can take place in reinforced concrete structures at high loads. The first extensive investigation of this problem in the English-speaking countries was conducted by Glanville and Thomas^{11.1} in 1935 at the Building Research Station, England.

11.3 COMPLETE ANALYSIS OF FRAMES

The bending moments, shear and axial forces, and deflections of reinforced concrete frames at any stage of loading from zero to ultimate load can be determined analytically using the conditions of static equilibrium and geometric compatibility, if the moment-curvature relationships of the sections are known. However, difficulties are caused by the nonlinearity of the moment-curvature relationships, and a step-by-step procedure, with the load increased increment by increment, is generally necessary. Also, the moment-curvature relationship of sections carrying moment and axial force is dependent not only on the section geometry and the material properties but also on the level of axial force. This interdependence means that the moment-curvature relationship for each section must be recomputed at

each increment of loading. A successive linear approximation method based on the stiffness method of analysis can be used to follow through the behavior of the frame from zero to ultimate load. In this method the members of the frame are divided along their length into small elements. At each load level the flexural rigidity ($EI = M/\phi$), corresponding to the particular bending moment and axial force at each element, is obtained from the appropriate point on the moment-curvature relationship. Members are assumed to be uncracked for the initial load increments, and the deformations are determined using the uncracked section flexural rigidity. The elements are searched at each load increment to ascertain whether the cracking moment has been reached. When it is found that the cracking moment has been reached, the flexural rigidity of the element is recomputed on the basis of the cracked section, and the actions in the frame are recomputed. This procedure is repeated at the load level until all flexural rigidities are correct. At higher loads, when the stresses at the elements enter the inelastic range, the flexural rigidity of each element is adjusted to that corresponding to the appropriate point of the moment-curvature curve calculated for that moment and axial force level. Eventually, with further increments, plastic hinges spread throughout the frame, and the ultimate load is reached when a mechanism forms and no further load can be carried.

An example of the foregoing type of analytical approach is the work of Lazaro and Richards.^{11,2} One of their comparisons of results of analysis with experimental results appears in Fig. 11.4. The experimental results were obtained from tests conducted by Cranston^{11,3} on a hinged-base rectangular portal frame with a clear span of 104 in (2.64 m) and a height to the bottom of the beam of 73 in (1.85 m). The analytical and experimental load-deflection and moment-deflection results compared in the figure show good agreement. The analytical ultimate load was 0.97 of the experimental ultimate load. In this frame the analysis predicted a failure load 29% higher than the load at the formation of the first plastic hinge, indicating the degree of moment redistribution necessary to reach ultimate load in this case. The analysis predicted an overly flexible behavior in the region between first tensile cracking and first yielding because it was assumed that when the moment at first cracking was reached at an element, all the concrete in tension throughout the element cracked. In reality, however, some uncracked concrete will be carrying tension between the cracks, and this will increase the flexural rigidity. The tension stiffening effect may be taken into account by using an effective flexural rigidity part way between the uncracked and fully cracked value (see, e.g., Section 6.6.2).

It is evident that the full analytical approach to the behavior of reinforced concrete frames at all stages of loading is lengthy and can be successfully undertaken only with the aid of a computer having large storage. For such

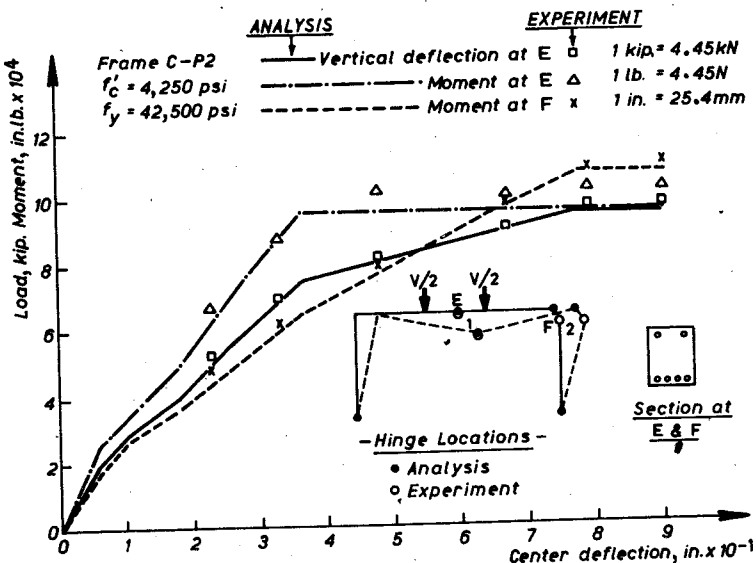


Fig. 11.4. Comparison of experimental and analytical results by Lazaro and Richards.^{11,2}

a general computer program, the input necessary includes the frame geometry, cross-sectional properties, material properties, and type of loading. The output could be the bending moment, shear force and axial force distributions and the deflections at any load level, and the ultimate load and the plastic hinge locations. Such an analytical approach for the determination of the ultimate load avoids the trial-and-error procedure, necessary in normal upper-bound plastic analysis, to determine the correct failure mechanism. In a normal upper-bound plastic analysis all the possible failure mechanisms must be examined to determine the mechanism giving the smallest ultimate load. Also, a more accurate prediction of the ultimate load is obtained by the full analytical approach because the moments of resistance at the critical sections at the ultimate load are known. Thus the approach will avoid errors arising from assuming that the ultimate moments of resistance exist simultaneously at all the critical sections. Also, the effect of axial force on moment capacity can be included accurately because the magnitude of the axial force is known, whereas in normal upper-bound plastic analysis the axial force level would have to be estimated in the first instance.

Since the full approach is an analysis procedure, it would require a trial-and-error solution if used in design. Hence the approach could hardly be

regarded as suitable for design. Nevertheless, when more computer programs are readily available, the approach will become a powerful analytical tool for evaluating or checking structural performance over the full range of loading, including behavior at the service loads and at the ultimate load. Geometric changes in the frame under load can also be included in such programs to allow for the effect of deflections on the internal actions. This would account for moment magnification due to column deflections, indicating any instability effects, as well.

Computer programs for the complete analysis of reinforced concrete frames are under development in many parts of the world. Examples of existing analyses are those of Cranston,^{11.4} Becker,^{11.5} Blaauwendraad,^{11.6} Menegotto and Pinto,^{11.7} and Lazaro and Richards.^{11.2} Programs suitable for general application are still awaited.

11.4 METHODS FOR DETERMINING BENDING MOMENT, SHEAR FORCE, AND AXIAL FORCE DISTRIBUTIONS AT THE ULTIMATE LOAD FOR USE IN DESIGN

We now consider methods for determining the distributions of bending moments and shear and axial forces at the ultimate load, which could be used in the strength design of reinforced concrete frames. These methods are the elastic bending moment diagram method, with or without some moment redistribution, and the various limit design methods.

11.4.1 The Elastic Bending Moment Diagram

The bending moments and the forces in the structure at the ultimate load, for the various load combinations, may be calculated using linear elastic structural analysis. The sections are designed to have ultimate capacities that at least equal the bending moments and forces obtained from such an analysis. This is the method recommended by ACI 318-71^{11.8} and by most other building codes. The ACI code allows any reasonable assumptions in the computation of the relative flexural and torsional stiffness of the members, provided the assumptions are consistent throughout the analysis.

It might seem incongruous that although the sections are designed by the strength method, taking into account inelastic behavior of the concrete and the steel, the bending moments and forces at the ultimate load are calculated assuming linear elastic behavior of the members. However, this approach is valid because the distribution of the bending moments and forces so found satisfies the conditions of static equilibrium and the boundary conditions. That is, the bending moment distribution is statically admissible.

Such a design could in fact be regarded as a valid lower-bound (limit design) solution.

Assuming linear elastic structural behavior has the following advantage: it ensures that only a small amount of redistribution of bending moments will occur before the ultimate load is reached, because the critical sections will tend to reach their ultimate capacities together. Therefore, the plastic rotation required at the critical sections will be small and the plastic rotation capacity of sections need not be checked. It is evident that some moment redistribution will always be necessary, however. This is because once cracking and inelastic strains commence, the flexural stiffness of the members will change, and unless the bending moments calculated by linear elastic structural analysis are based on the final complex distribution of flexural stiffnesses, some moment redistribution will be necessary before all the critical sections can attain their flexural strength.

There are at least two more advantages of assuming linear elastic behavior of members: one is that it ensures that the steel and concrete stresses at the service load are kept as low as possible, thus minimizing the widths of cracks in the concrete; and the other is that the design moments and forces can be found using relatively simple and well-established structural theory.

Commonly, the flexural stiffness values used in the structural analysis are based on the gross concrete section: no allowance is made for concrete cracking, and the steel is ignored. It may seem that this is a crude approximation because when members crack the flexural stiffnesses change. For example, for a rectangular section with a modular ratio of 10, the reduction in flexural rigidity from the gross section value on cracking may be 30 to 60% for sections with $\rho = \rho' = 0.01$, and 40 to 60% for sections with $\rho = 0.01$ and $\rho' = 0$, depending on the steel positions in the section. (The calculation of the flexural rigidity of sections was discussed in Section 10.2.4 and 10.3.3, and reference can be made to the *ACI Design Handbook*, Vol. 1,^{10.9} for tables allowing a quick determination of flexural rigidity values.) However, it must be remembered that the distribution of bending moments depends on the ratios of the flexural stiffnesses of the members. Sometimes after cracking of the members, the ratios of the flexural stiffness are still approximately as initially assumed, because similar changes in the flexural rigidity may occur at all sections; then relatively little moment redistribution is necessary at high loads to develop the assumed bending moment pattern. However, the change in the ratios of the flexural stiffnesses resulting from cracking may be significant in some cases. In continuous *T* beams, for example, cracking causes a greater reduction in the flexural rigidity of the negative moment regions than the positive moment regions; after cracking, therefore, the ratio of the maximum negative to positive moments will be lower than the ratio obtained assuming a uniform flexural rigidity. Also, in frames the changes of

flexural rigidity of the columns may not be as great as for beams, because columns are generally more heavily reinforced than beams and they normally carry axial compressive loads. Hence for columns the change in flexural rigidity from the gross section value to the cracked section value will not be so great. In fact, in many frames the beams will be cracked but the columns will remain uncracked in the service load range. The reduced flexural rigidity of cracked beams may lead to a bending moment to the columns larger than that calculated on the basis of gross section stiffnesses: Near ultimate load, the flexural rigidity of the columns will reduce, and the moment will be redistributed back to the beams. To avoid significant moment redistribution, it may be better to base the moment of inertia of the beams on an approximate transformed cracked section value (e.g., $0.5I_g$) and the moment of inertia of the columns on the gross section value I_g . Okamura et al^{11,9} recommend use of the transformed cracked section for the beam and the transformed uncracked section for the column, with modified (increased) modular ratios to reflect inelastic behavior. Probably the greatest variations in flexural rigidity from gross section values occurs in frames in which both the torsional and the flexural stiffnesses of members are considered, because cracking results in a much greater reduction in the torsional stiffness than in the flexural stiffness. For example, cracking may reduce the torsional stiffness of a member by more than 90%. Therefore, very often the torsion stiffness may be ignored (see Section 8.9).

The foregoing discussion again emphasizes that unless the final complex distribution of stiffnesses is used in design, some moment redistribution will always be necessary, the extent of the redistribution depending on the designer's assumptions about the flexural stiffnesses. Hence although linear elastic structural analysis gives a convenient approach for determining the distribution of moments and forces in strength design, it should be kept in mind that the critical sections will require some ductility to attain the design ultimate load. Therefore, reasonably realistic approximations for the stiffnesses of member should be used.

11.4.2 The Elastic Bending Moment Diagram Modified for Moment Redistribution

Some codes permit the bending moment patterns obtained from linear elastic structural analysis to be modified when the sections are ductile enough to allow for moment redistribution. ACI 318-71^{11,8} allows the negative moments at the supports of continuous flexural members, for any loading combination, to be increased or decreased by not more than

$$20 \left(1 - \frac{\rho - \rho'}{\rho_b} \right) \% \quad (11.7)$$

where $\rho = A_s/bd$, $\rho' = A'_s/bd$, and from Eq. 4.14

$$\rho_b = \frac{0.85\beta_1 f'_c}{f_y} \frac{0.003E_s}{0.003E_s + f_y}$$

The modified negative moments are used to calculate the moments within the spans. That is, static equilibrium between the internal forces and the external loads must be maintained. Such an adjustment can only be made if the section at which the moment is reduced is designed so that

$$\rho - \rho' \leq 0.5\rho_b \quad (11.8)$$

It is evident from Eqs. 11.7 and 11.8 that the ACI code allows support moments to be changed by up to 20%, depending on the ductility of the section where the moment is reduced, provided static equilibrium between internal forces and external loads is maintained.

Reference to Section 6.3.2, and to Figs. 6.9 and 6.10, indicates that for the range $f'_c = 3000$ to 5000 psi (20.7 to 34.5 N/mm 2) and $f_y = 40,000$ to $60,000$ psi (276 to 414 N/mm 2), Eq. 11.8 will ensure that $\varphi_u/\varphi_y > 3$ for $\varepsilon_c = 0.003$ and $\varphi_u/\varphi_y > 4$ for $\varepsilon_c = 0.004$.

The term $(\rho - \rho')/\rho_b$ in Eqs. 11.7 and 11.8 is related to curvature ductility through its effect on the neutral axis depth at the ultimate moment. If the compression steel yields, the equilibrium equation $C = T$ for the section shows that

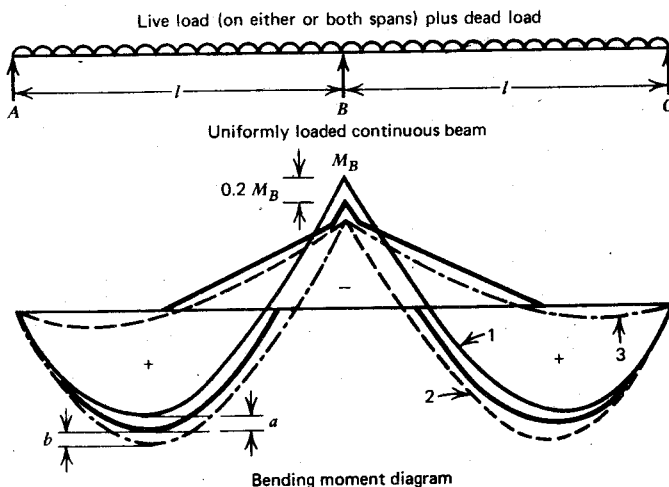
$$\begin{aligned} (\rho - \rho')bd f_y &= 0.85f'_c ab \quad \text{or} \quad \rho - \rho' = \frac{0.85f'_c}{f_y d} a \\ \rho_b b d f_y &= 0.85f'_c a_b d \quad \text{or} \quad \rho_b = \frac{0.85f'_c}{f_y d} a_b \\ \therefore \frac{\rho - \rho'}{\rho_b} &= \frac{a}{a_b} \end{aligned} \quad (11.9)$$

where a and a_b = depth of equivalent rectangular compressive stress block of concrete for $\rho - \rho'$ and ρ_b , respectively.

Hence if the compression steel yields, the ACI limit of $\rho - \rho' \leq 0.5\rho_b$ given by Eq. 11.8 may be thought of as requiring $a \leq 0.5a_b$. Now for the ranges $f'_c = 3000$ to 5000 psi (20.7 to 34.5 N/mm 2) and $f_y = 40,000$ to $60,000$ psi (276 to 414 N/mm 2), a_b/d may be shown by Eq. 4.12 to be in the range 0.583 to 0.473. Therefore, reference to Eq. 11.8 shows that for the ranges of f'_c and f_y just given, 10% moment redistribution is allowed when $a/d = 0.29$ to 0.24, and higher percentage moment redistribution is allowed at lower a/d values.

The adjustment to the elastic bending moment diagram allowed by moment redistribution leads to a reduction in the peak design bending moments

when combinations of loading are considered. The adjustment is illustrated in Fig. 11.5 for a uniformly loaded two-span continuous beam. The maximum adjustment of 20% is assumed in the figure. Bending moment curves 1, 2, and 3 are for the load cases with live load on both spans, right-hand span only, and left-hand span only, respectively. The heavy line represents the bending moment envelope permissible in design. It is obtained by moving down the bending moment curve with the peak negative moment, and by moving up the bending moment curves with the peak positive moments, while at the same time maintaining static equilibrium. In Fig. 11.5 the peak negative bending moment at the center support due to load case 1 has been reduced by 20% to give the peak of the negative moment design envelope. The negative moments at the center support for load cases 2 and 3 have been increased by 20% or up to the design envelope there, whichever is less, to give the other parts of the negative moment design envelope. To satisfy static equilibrium,



a = not less than increase resulting from reduction of support moment for load case 1 by 20%

b = not more than the reductions resulting from an increase of support moment for load cases 2 and 3 by 20% or up to design envelope, whichever is less

- Load case 1: dead load and live load on both spans
- Load case 2: dead load on both spans, live load on right-hand span
- Load case 3: dead load on both spans, live load on left-hand span.
- Bending moment envelope for design

Fig. 11.5. Adjustment of elastic theory bending diagram for allowable moment redistribution.

the midspan positive moment plus the average of the negative moments at the two adjacent supports of the span should equal $Wl/8$, where W is the total load uniformly distributed on span l . Hence the positive moments for load case 1 are increased (by 0.5 of $0.2M_B = 0.1M_B$ at midspan), and the positive moments for load cases 2 and 3 are decreased. The positive moment design envelope will be given by the greatest of these adjusted moment ordinates, as indicated in the definitions for a and b in Fig. 11.5. Note that the allowable moment redistribution means a reduction in both the maximum negative and positive moments obtained from elastic analysis, hence leads to a more economical design.

The percentage of moment redistribution from the elastic moment diagram allowed in design by ACI 318-71^{11,8} has been limited to ensure that the sections have sufficient reinforcement to prevent excessive crack widths at the service load due to high steel stresses, and to ensure that the sections have adequate ductility at the plastic hinges at the ultimate load to enable the design moment distribution to be reached. According to the Commentary on ACI 318-71,^{11,10} the allowable moment redistribution is based on knowledge of service and ultimate load behavior obtained from tests and analytical studies. Figure 11.6, taken from the Commentary, plots the calculated avail-

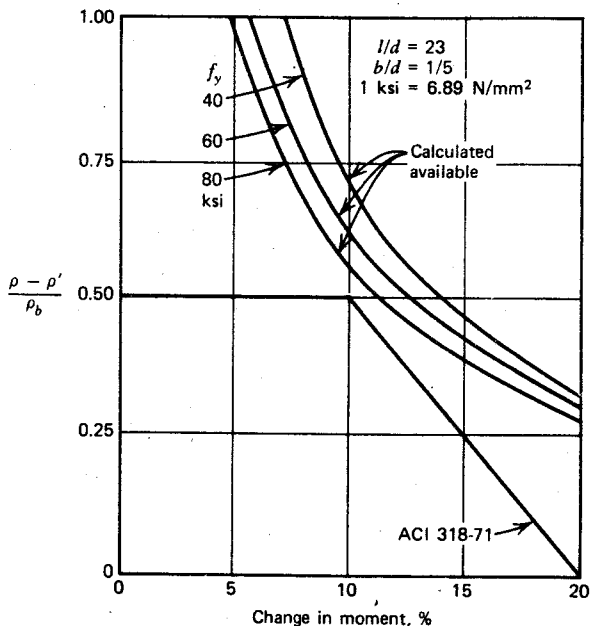


Fig. 11.6. Allowable moment redistribution for minimum plastic rotation capacity.^{11,10}

able percentage change in moment against the reinforcement index $(\rho - \rho')/\rho_b$. According to the Commentary, the curves were calculated using conservative values of ultimate concrete strain and equivalent plastic hinge lengths. The ACI 318-71 allowable percentage change of moment, from Eqs. 11.7 and 11.8, also appears in the figure and is seen to be conservative. The Commentary also states that studies by Cohn^{11.11} and Mattock^{11.12} indicate that adequate plastic rotation capacity is available for the redistribution allowed by ACI 318-71. These two studies also assert that cracking and deflections of beams designed in accordance with the allowed moment redistribution are no more severe than they are for beams designed to the elastic theory moment patterns.

It is of interest to note that the elastic theory pattern of moments, from which the moment redistribution is permitted, is not clearly defined by ACI 318-71. By making various assumptions about the flexural rigidity of the sections, a number of "elastic bending moment patterns" are possible. The variations between these diagrams may be larger than the redistributions allowed by Eqs. 11.7 and 11.8. However, the conservative nature of Eqs. 11.7 and 11.8 should mean that the permitted redistribution is safe when applied to any elastic bending moment pattern obtained, making reasonable and consistent assumptions for the flexural rigidities of the members.

Most codes of practice permit the use of the bending moment diagram derived from linear elastic structural analysis on the basis of approximate flexural stiffnesses and modified for a small amount of moment redistribution. Some codes however, allow extensive moment redistribution to be taken into account. The British code of practice CP110:1972^{11.13} allows the peak elastic moments to be reduced by up to $(0.6 - c/d)100\%$, but not more than 30% (c = neutral axis depth at the section of reduced moment, d = effective depth of the tension steel), provided the static equilibrium between internal forces and external loads is maintained and the elastic moment at the section is not reduced by more than 30% of the numerically largest elastic moment anywhere in the member. Thus as much as 30% reduction in moment is allowed by the British code for neutral axis depths equal to or less than $0.3d$. For neutral axis depths greater than $0.3d$ the allowable redistribution reduces linearly to 10% at a neutral axis depth of $0.5d$. For structures more than four stories high, in which the frame provides the lateral stability, the reduction in moment is restricted to 10%. The Russian regulations apparently have allowed^{11.14} the intermediate spans of uniformly loaded continuous beams of equal span to be designed for equal positive and negative moments ($Wl/16$, where W = total load on span l), and have allowed 30% moment redistribution from the elastic bending moment diagram in the other cases, provided the neutral axis depth is less than 0.3 of the effective depth.

By comparison to the British and Russian recommendations, the ACI 318-71 Equations 11.7 and 11.8 are conservative. The curves for calculated available percentage change in moment in Fig. 11.6 indicate that up to 30% is available at low $(\rho - \rho')/\rho_b$ values. The code is being rather restrictive in not allowing moment redistribution of this order. Possible variations in the elastic bending moment patterns due to the approximate stiffnesses used in design may cause caution, but such variations on the unconservative side may be offset by the conservative values used for ultimate concrete strain and equivalent plastic hinge length in the calculated curves of Fig. 11.6. The use of large amounts of moment redistribution is often thought to mean high steel stresses at some sections at service load, which may lead to excessive cracking and deflections. However, many investigators have shown this to be untrue. For example, in Mattock's tests^{11,12} the cracking at the service load of continuous T beams designed on the basis of 25% redistribution of bending moments from the elastic bending moment diagram was no more severe than that of T beams designed for the elastic distribution. Hence it is evident that moment redistribution similar to that allowed by the Russian regulations and the British code could well be permitted in general.

There are two main advantages associated with the use of moment redistribution: the designer can select patterns of bending moment that avoid congestion of the reinforcement at the supports of beams, and economies result from the reduction of the peaks of bending moment in the envelope of bending moment drawn for different positions of live load. The point about economy may be illustrated by reference to Fig. 11.5. If large adjustments to the peaks of bending moment can be made, significant savings will result, particularly if the ratio of live load to dead load is high.

11.4.3 Limit Design

The limit design approach allows any distribution of bending moments at ultimate load to be used, provided the following conditions are met.

1. The distribution of bending moments is statically admissible. That is, the bending moment pattern chosen does not violate the laws of equilibrium for the structure as a whole or for any member of it. Such a distribution of bending moments may be obtained, for example, by assuming the positions of sufficient points of contraflexure to make the structure statically determinate and finding the resulting bending moments and forces from the equations of static equilibrium.

2. The rotation capacity of the plastic hinge regions is sufficient to enable the assumed distribution of moments to be developed at the ultimate load.

3. The cracking and deflections at the service load are not excessive.

The requirements of items 1 to 3 can be stated as limit equilibrium, rotation compatibility, and serviceability. This method takes the elastic moment pattern method a stage further and allows extensive moment redistribution; however, it must be shown to be achievable, and it must not impair the serviceability of the structure.

Figure 11.7 is a possible limit bending moment diagram for a continuous beam with ultimate uniformly distributed load w_u per unit length. In the

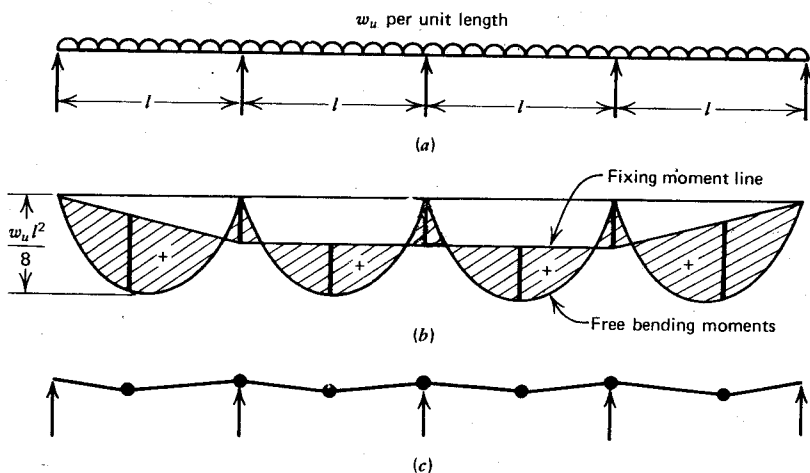


Fig. 11.7. Continuous beam at ultimate load. (a) Beam. (b) Limit bending moment diagram. (c) Collapse mechanism.

limit bending moment diagram, the free (static) bending moments in each span, due to the external loads acting with the ends of each span free of rotational restraint, have a maximum ordinate of $w_u l^2 / 8$. The fixing moment line, due to the end restraint moments at the supports, may be chosen to lie anywhere within the free moment diagrams. The required magnitudes of the ultimate moments of resistance of the sections may be calculated from the bending moment ordinates at the plastic hinges. For instance, if the position of the fixing moment line is chosen so that the support moments are all $w_u l^2 / 16$, the required maximum positive moments for the interior spans and for the end spans are $w_u l^2 / 16$ and $0.0958 w_u l^2$, respectively. Thus we have an infinite number of usable positions for the fixing moment line, because a section can be reinforced to give ultimate resisting moment as required. This situation can be compared with the plastic design of continuous steel beams: unless

cover plates are used, a steel section has the same plastic moment of resistance for both positive and negative moments, hence the fixing moment line can have only one position in the collapse moment diagram. In the general case, for reinforced concrete members, the elastic moment diagram is one of the possible moment diagrams that could be used.

Since the live load placed on all spans results in the greatest free bending moments, it gives the worst case for the magnitude of positive and negative moments. However, to calculate the extent of negative moment steel required in a span, the live load should be taken off that span. For example, consider a uniformly loaded two-span beam, where the chosen limit moment diagram for dead load and live load acting appears in Fig. 11.8a. To

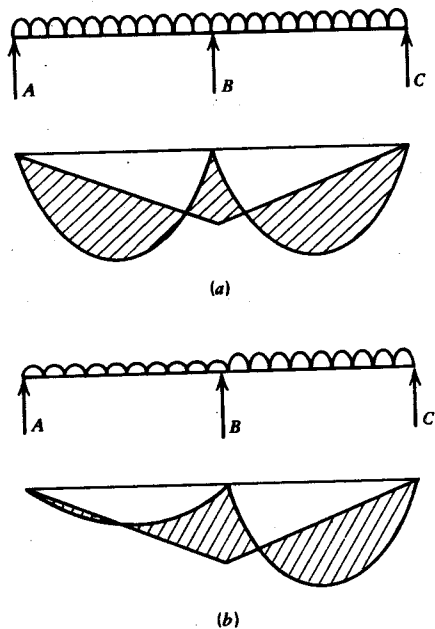


Fig. 11.8. Limit bending moment diagrams for full and partial loadings. (a) Beam with live load on both spans plus dead load, and limit moment diagram. (b) Beam with live load on right-hand span only plus dead load, and limit moment diagram.

find the extent of top steel required in span AB the live load is removed from that span. Only the dead load bending moment remains (see Fig. 11.8b), indicating the extent to which reinforcement should be provided in the span to prevent failure by this mode of loading.

The main advantages resulting from limit design are similar to those resulting from moment redistribution. Patterns of moments can be chosen to avoid congestion of reinforcement at the supports of members. Also,

substantial economies can result from designing to moments obtained by dividing the free bending moments between the negative and positive moments, rather than designing to the peaks of bending moment found from the elastic theory moment envelope for different positions of loading. The method also gives the designer an appreciation of the real behavior of the structure. However, formulations of the present knowledge of plastic rotation capacity and of serviceability into simple rules for limit design are not generally included in building codes. For example, ACI 318-71^{11,8} and the British CP110^{11,13} do not have recommendations for limit design. The greatest restraints against the acceptance of limit design have been the concern that the service load behavior with regard to cracking and deflections may not be satisfactory, the complexities of some of the available limit design procedures, and the lack of precise experimental data concerning the plastic rotation capacity of members.

11.5 LIMIT DESIGN METHODS

An ACI-ASCE committee report^{11,15} on limit design and some proposed limit design methods are considered next, to indicate possible limit design approaches.

11.5.1 ACI-ASCE Committee 428 Report

ACI-ASCE Committee 428, in a progress report^{11,15} on limit design, has presented model clauses suitable for inclusion in a building code. Rather than recommending a single method of limit design, the clauses define envelope values, or upper and lower limits, of factors defining the moment-curvature relationships. These clauses, summarized below, enable the designer to use any of the acceptable methods of limit design published in recent years.

The Distribution of Moments

The inelastic distribution of moments at the ultimate load may be found using any consistent set of assumptions that fall within the following conditions:

1. The elastic flexural rigidity of the sections $E_c I$ shall be determined from the gross section or the transformed cracked section using values of E_c and n within 25% of the ACI code values, where E_c = modulus of elasticity of concrete, n = modular ratio, and I = moment of inertia of the section. The elastic limit moment M_y shall not be assumed to be less than $0.8M_u$, where M_u = ultimate resisting moment.

2. The assumptions of the strength theory of the ACI code shall be used to calculate the ultimate resisting moment M_u and ultimate axial load P_u . The same assumptions shall be used to determine the curvature φ_u at M_u and P_u , except that the extreme fiber compressive strain in the concrete ε_c at φ_u shall be ε_{co} for members with flexure and axial load, and in the range

$$\varepsilon_{co} \leq \varepsilon_c \leq \varepsilon_{co} + 0.02 \frac{b}{z} + \left(\frac{\rho_s f_y}{20} \right)^2 \quad (11.10)$$

for members without significant axial load, where ε_{co} = basic ultimate compressive concrete strain neglecting the influence of confinement, loading rate, and strain gradient, to which a value in the range 0.003 to 0.004 shall be assigned; b = width of compression face of section; z = shear span defined by Eq. 11.16, ρ_s = ratio of total volume of stirrups and compression steel in length s to volume of concrete bds , where d = effective depth of member and s = stirrup spacing, and f_y = steel yield strength in ksi (1 ksi = 6.89 N/mm²).

3. The moment-curvature relationship between M_y and M_u shall lie within the straight line BC and the lines $BB'C$ of Fig. 11.9.

4. The length along a member from the section of maximum bending moment M_m over which the inelastic curvatures are assumed to occur, l_p , shall exceed the lesser of

$$R_e(0.25d + 0.03zR_m) \quad (11.11)$$

and

$$R_e d \quad (11.12)$$

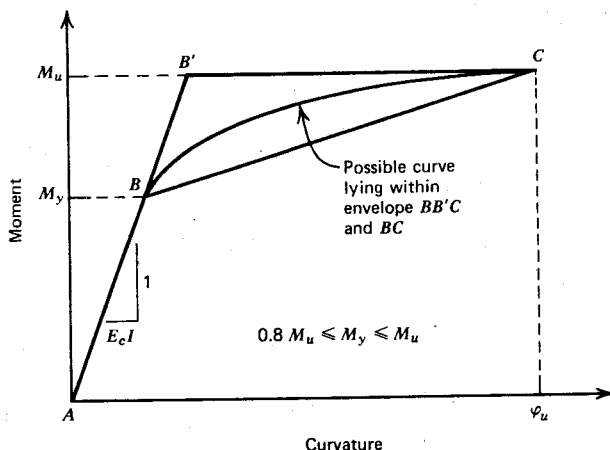


Fig. 11.9. Assumed moment-curvature relationship.^{11.15}

but shall not exceed

$$R_e(0.5d + 0.1zR_m) \quad (11.13)$$

in which

$$R_e = \frac{0.004 - \varepsilon_{ce}}{\varepsilon_{co} - \varepsilon_{ce}} \quad (11.14)$$

$$R_m = \frac{M_m - M_y}{M_u - M_y} \quad (11.15)$$

$$z = \frac{4M_m}{4V_z + \sqrt{wM_mR_m}} \quad (11.16)$$

or

$$z = \infty \text{ in region of constant moment}$$

where ε_{ce} = elastic component of ε_c either calculated or assumed in the range 0.001 to 0.002, V_z = shear force adjacent to concentrated load or reaction at section of maximum moment, and w = uniformly distributed load per unit length at section of maximum moment (taken as zero if a concentrated load or reaction at the section acts in the opposite direction).

5. The conditions of equilibrium and geometric compatibility shall be satisfied throughout.

The Design

The members designed according to the inelastic distribution of moments shall satisfy the following requirements:

1. Elastically calculated stresses in the reinforcement at the service loads multiplied by 1.2 for gravity loads, or 1.0 if lateral loads are included, shall not exceed $0.9f_y$ or 60 ksi (414 N/mm^2), whichever is smaller.
2. For portions of lengths of members where the moment at the ultimate load exceeds $0.8M_u$, closed stirrups shall be provided to resist shear force exceeding $bd\sqrt{f'_c}$ 1b, where b and d are in inches and f'_c is in psi ($1 \text{ lb} = 4.45 \text{ N}$, $1 \text{ in} = 25.4 \text{ mm}$, $1 \text{ psi} = 0.00689 \text{ N/mm}^2$).
3. For the design of unbraced frames, the effect of deflections on internal forces shall be considered with elastic and inelastic deflections from sustained loads increased by a factor of 3.

4. The load factors used to determine the required ultimate load calculated from the service loads shall be multiplied by the factor

$$\frac{\gamma + 1}{\gamma + M_y/M_u} \quad (11.17)$$

where γ is the power of the parabola defining curve BC of Fig. 11.9 ($= 1$ for straight line BC , $= 2$ for curved line BC shown, $= \infty$ for lines $BB'C$).

Comments

In the section on distribution of moments, item 1 defines the elastic stiffness and the end of the elastic range. Item 2 indicates the method to calculate the ultimate moment and axial load and the corresponding curvature. The upper bound of Eq. 11.10 was obtained from Corley's equation (6.46). Item 3 allows use of a bilinear sloping top or curved top or flat top to the moment-curvature relationship. Item 4 gives the equivalent plastic hinge length covering the range of values obtained from the equations of Corley (6.45), Sawyer (6.49), and Baker (6.41). The R_m term is necessary to take the effect of the magnitude of maximum moment into account. The R_e term is necessary to adjust the length according to the assumed ultimate concrete strain to obtain a practically constant inelastic rotation for the possible range of assumed ϵ_{co} values. Equation 11.16 gives z in regions where the moment/shear force ratio is varying. Item 5 restates the conditions that must be complied with in an inelastic analysis, as in an elastic analysis.

In the section on design, the purpose of item 1 is to ensure that the steel does not yield at the service loads and lead to excessive cracking and deflection. To calculate the steel force, the service load moment may be divided by an assumed internal moment lever arm of $7/8d$. Item 2 requires the designer to take more shear on the stirrups in regions where yielding of the flexural tension steel may cause wide cracking and loss of shear carried by the concrete. Also, the stirrups will provide confinement for the concrete. Item 3 requires him to take into account changes of moments due to deflections, replacing any other need to consider column slenderness. Item 4 accounts for the nonsimultaneous development of the ultimate moments at the critical sections. It is assumed that at the ultimate load, the moments at the critical sections are distributed uniformly along the curve between B and C in Fig. 11.9 and that all moments contribute equally to the ultimate load. For example, if the straight line BC is used and $M_y/M_u = 0.9$, the multiplication factor for the load factors given by Eq. 11.17 is $2/1.9 = 1.05$.

11.5.2 Available Limit Design Methods

A limit design procedure aims to satisfy three conditions: (1) limit equilibrium, (2) rotational compatibility, and (3) serviceability. Most of the avail-

able limit design methods consider one or two of these conditions initially, the remaining condition or conditions being the object of a subsequent check. The most economical distribution of bending moments may also be sought, that being the distribution of moments which results in the greatest moment reduction when compared with the elastic envelope moments obtained from the various design loading combinations. Of the limit design methods that have been proposed, probably the methods deserving the most attention are those due to Baker,^{11.14, 11.16, 11.17} Cohn,^{11.11, 11.18} Sawyer,^{11.19} and Furlong,^{11.20} These four methods are briefly described below.

Baker's Method

Baker^{11.14, 11.16, 11.17} has been developing a method of limit design since the 1940s. The design is based on the requirements of limit equilibrium. The requirements of rotational compatibility and serviceability are checked as subsequent steps. The design is commenced by determining a distribution of ultimate bending moments which is in equilibrium with the ultimate loads. This may be obtained by drawing the free bending moment diagram for the members supporting the ultimate loads when the ends are free of rotational restraint, and drawing the fixing moment line at some convenient position, as in Fig. 11.7. The sections are reinforced for those ultimate moments. Note that a collapse mechanism has developed at the ultimate load. The rotation capacity of the plastic hinge regions is then checked to ensure that the chosen distribution of bending moments can be developed at the ultimate load, and the pattern of moments at the service load is determined and the stresses checked to ensure that the members are serviceable. The assumed distribution of ultimate moments may need to be modified if inadequate rotation capacity or unsatisfactory serviceability is found.

Cohn's Method

Cohn^{11.11, 11.18} has developed a method based on the requirements of limit equilibrium and serviceability. The requirement of rotational compatibility is checked as a subsequent step. The solution is obtained by scaling down the elastic envelope moments, obtained from the various ultimate load combinations, by multiplying by appropriate parameters $x_j \leq 1$, where x_j is the yield safety parameter for section j . The value of x_j is set by the following requirements: at the service load, the critical sections of the frame must remain in the elastic range; at the ultimate load, the internal forces must be in equilibrium with the external loads and one or more collapse mechanisms must form; and the overall moment reductions from the elastic envelope must be a maximum. A typical design seeks the minimum value for x_j consistent with acceptable service load behavior and the equilibrium conditions at the

ultimate load. The sections are designed on the basis of the determined distribution of bending moments, and the plastic hinge regions are checked to ensure that they have sufficient rotation capacity to develop the assumed moment distribution at the ultimate load.

Sawyer's Method

Sawyer^{11,19} has presented an approach based on the requirements of limit equilibrium and rotational compatibility. The requirement of serviceability is checked by a subsequent step. The method uses a rotational compatibility analysis indirectly by adjusting a given design by successive approximations. The design is commenced by adjusting the elastic envelope moments obtained from the various design loading combinations at ultimate load, to establish a bending moment pattern for which reinforcement is provided. For each possible loading combination at ultimate load, using any set of adjusted moments that satisfies static equilibrium and falls within the ultimate resisting moments of the sections, the inelastic rotation at each plastic region is calculated. A moment-curvature curve with a yield moment of 0.85 of the ultimate moment may be assumed. Elastic theory is then used to calculate the moments resulting from these inelastic bending angles and the external loading imposed on the structure. If the calculated moments exceed the ultimate resisting moments of the sections, the reinforcement is revised by adding reinforcement to regions in which the ultimate moment is exceeded or to regions in which the inelastic angle developed is excessive. The moments introduced by the inelastic angles and the external loading are recalculated, and the reinforcement is adjusted, until the adequacy of the ultimate moments of resistance has been demonstrated. The design is then checked by elastic theory to ensure that the steel stresses at the service load are not excessive.

Furlong's Method

The limit design method of Furlong^{11,20} involves assigned ultimate moments for structures braced against sway. The worst cases of different types and arrangements of loading on various arrangements of spans were analyzed by Furlong to determine the possible patterns of design moments in continuous beams that would satisfy the requirements of serviceability (tension steel not to yield at the service loads) and limit equilibrium. Then the plastic rotations resulting from these distributions of ultimate moments were analyzed to determine the curvature ductility requirements. The possible distributions of design moments so found were tabulated, and a simple equation was given for the curvature ductility requirements. A convenient design approach results. To design a beam, the sections are reinforced so that in each span the ultimate moments of resistance are in equilibrium with the ultimate load to be

supported and the ultimate moments of resistance are equal to or greater than the product of M_F and the appropriate coefficient given in Table 11.1, where M_F = maximum bending moment in the span due to the ultimate loads when the ends are free of rotational restraint. The sections are also proportioned so that

$$\frac{\varphi_u}{\varphi_y} \geq 1 + 0.25 \frac{l_n}{d} \quad (11.18)$$

where φ_u = ultimate curvature, φ_y = curvature at first yield, l_n = clear span and d = effective depth of section.

Table 11.1 Beam Moment Coefficients for Various End Restraints^{11.20}

End Restraint	Type of Moment	Beams Loaded Only by One Force at Midspan	All Other Beams
Span with two ends restrained	Negative moment	0.37	0.50
	Positive moment	0.42	0.33
Span with one end restrained	Negative moment	0.56	0.75
	Positive moment	0.50	0.46

An example of the determination of the ultimate resisting moments for an interior span of a continuous beam carrying a uniform load w_u per unit length is represented in Fig. 11.10. The sections would be proportioned to satisfy Eq. 11.18 using charts similar to Figs. 6.9 and 6.10. It is apparent that Furlong's method gives a simple direct design approach. The use of assigned ultimate moments means that the designer avoids the complexities of trial-and-error solutions and does not have to check for plastic rotation capacity and serviceability.

11.5.3 General Method for Calculating Required Plastic Hinge Rotations

To develop the pattern of ultimate moments used in design, Baker's and Cohn's methods call for the checking of the inelastic rotation required at the plastic hinge regions. The plastic hinge regions will occur at the maximum positive and negative moment regions. Between the plastic hinge regions, the members will be acting elastically, since normally the reinforcement does not follow the bending moment pattern exactly and provides a greater flexural

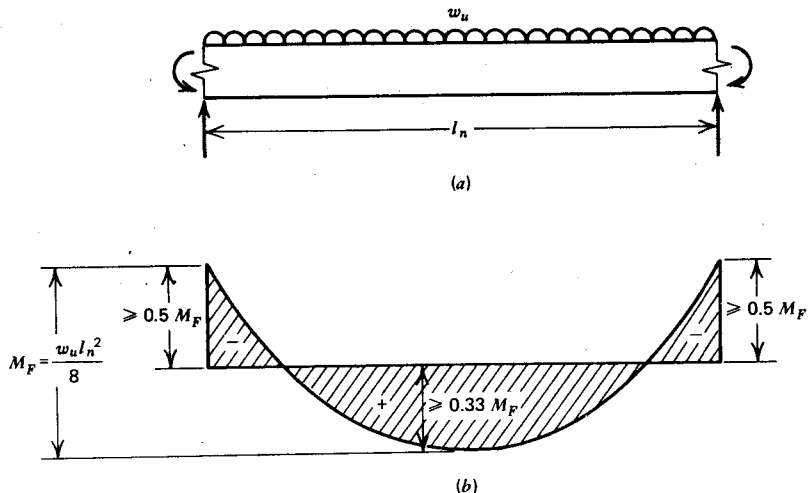


Fig. 11.10. Assigned limit moments for a uniformly loaded interior span.^{11.20} (a) Interior span of continuous beam. (b) Limit bending moment diagram.

strength than required outside the plastic hinge regions. The plastic hinge rotations needed to achieve the ultimate load may be calculated by the flexibility method (also known as the δ_{ik} method) using a procedure developed mainly by Baker.^{11.16}

The ultimate load of a statically indeterminate structure is reached when the last plastic hinge is just about to form. Ideally, for a structure that is statically indeterminate to the n th degree, the ultimate load is reached when n plastic hinges have formed and the remaining plastic hinge or hinges are just about to develop. The n plastic hinges are positioned where plasticity originates. To calculate the plastic rotation required of the plastic hinge regions when the ultimate load is just reached, the following assumptions can be made:

1. The moment-curvature relationships are bilinear, having a horizontal top portion as represented by curve ABC in Fig. 11.9.

2. The elastic flexural rigidity EI is constant along the span.

The method may be developed by considering a three-span continuous beam (Fig. 11.11). The beam is statically indeterminate to the second degree. Consider the plastic hinges to form first at the supports 1 and 2, and let the ultimate moments at 1 and 2 be M_1 and M_2 , respectively. To find the plastic

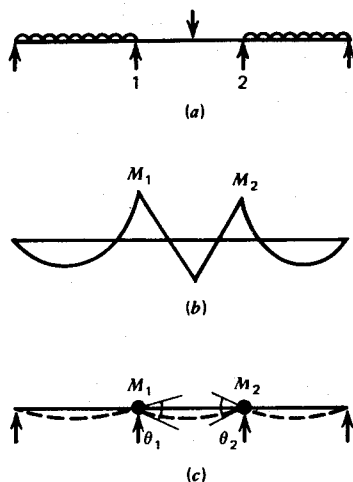


Fig. 11.11. Continuous beam when ultimate load is just reached. (a) Beam. (b) Bending moment diagram at ultimate load. (c) Beam when ultimate load is just reached.

rotations θ_1 and θ_2 at the plastic hinges 1 and 2 when the ultimate load is on the structure, replace the plastic hinges by frictionless hinges. The ultimate moments at the hinges can be simulated by applying external couples M_1 and M_2 at the hinges. Consider the effects of applying the external loading, M_1 and M_2 separately. The resulting bending moment diagrams appear in Fig. 11.12. The bending moment at any point in the structure at the ultimate load is

$$M = M_0 + X_1 M_1 + X_2 M_2 \quad (11.19)$$

where M_0 = bending moment at any point when the members are free of rotational restraint at the supports (Fig. 11.12a), X_1 = bending moment at any point when $M_1 = 1$ (Fig. 11.12b), and X_2 = bending moment at any point when $M_2 = 1$ (Fig. 11.12c). Between the hinges, the member is behaving elastically. The elastic strain energy stored in the beam is

$$U = \int \frac{M^2}{2EI} dx = \int (M_0 + X_1 M_1 + X_2 M_2)^2 \frac{dx}{2EI} \quad (11.20)$$

where dx = element of length of member, and the integrations are carried out along the whole length of the beam. The rotations at hinges 1 and 2 due to the elastic deformations between the hinges may be found using Castiglione's theorem. The calculated rotations at the frictionless hinges when the ultimate load is applied to the structure will be the required

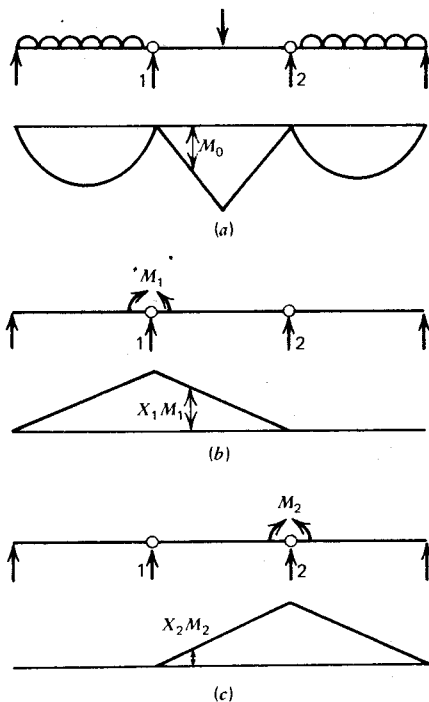


Fig. 11.12. Bending moments in beam of Fig. 11.11 with frictionless hinges at the supports, due to external loading and support moments applied separately. (a) External transverse loading acting on beam with frictionless hinges at 1 and 2, and resulting bending moment diagram. (b) Couples M_1 acting on beam with frictionless hinges at 1 and 2, and resulting bending moment diagram. (c) Couples M_2 acting on beam with frictionless hinges at 1 and 2, and resulting bending moment diagram.

rotations of the plastic hinges of the real structure. Now we have

$$-\theta_1 = \frac{\partial U}{\partial M_1} = \int \frac{X_1}{EI} (M_0 + X_1 M_1 + X_2 M_2) dx$$

$$\therefore -\theta_1 = \int \frac{X_1 M_0}{EI} dx + M_1 \int \frac{X_1^2}{EI} dx + M_2 \int \frac{X_1 X_2}{EI} dx \quad (11.21)$$

and

$$-\theta_2 = \frac{\partial U}{\partial M_2} = \int \frac{X_2}{EI} (M_0 + X_1 M_1 + X_2 M_2) dx$$

$$\therefore -\theta_2 = \int \frac{X_2 M_0}{EI} dx + M_1 \int \frac{X_1 X_2}{EI} dx + M_2 \int \frac{X_2^2}{EI} dx \quad (11.22)$$

The negative signs are necessary for θ_1 and θ_2 in Eqs. 11.21 and 11.22 because the rotations occur in the direction opposite to the direction of M_1 and M_2 .

Now if $M_0 = 0$ and $M_2 = 0$ (external transverse loads and couple M_2 removed), we can write

$$-\theta_1 = M_1 \int \frac{X_1^2}{EI} dx = M_1 \delta_{11} \quad (11.23)$$

where δ_{11} = rotation at 1 due to unit couple at 1.

And if $M_0 = 0$ and $M_1 = 0$, we have

$$-\theta_1 = M_2 \int \frac{X_1 X_2}{EI} dx = M_2 \delta_{12} \quad (11.24)$$

where δ_{12} = rotation at 1 due to unit couple at 2.

And if $M_1 = 0$ and $M_2 = 0$, we find

$$-\theta_1 = \int \frac{X_1 M_0}{EI} dx = \delta_{10} \quad (11.25)$$

where δ_{10} = rotation at 1 due to external loads.

Hence Eqs. 11.21 and 11.22 may be written

$$-\theta_1 = \delta_{10} + M_1 \delta_{11} + M_2 \delta_{12} \quad (11.26)$$

$$-\theta_2 = \delta_{20} + M_1 \delta_{21} + M_2 \delta_{22} \quad (11.27)$$

In general, the solution of a structure that is statically indeterminate to the n th degree will involve finding the plastic hinge rotations $\theta_1, \theta_2, \dots, \theta_i, \dots, \theta_n$ at plastic hinges 1, 2, ..., i , ..., n . The rotation θ_i at hinge i is

$$-\theta_i = \delta_{i0} + M_1 \delta_{i1} + M_2 \delta_{i2} + \dots + M_i \delta_{ii} + \dots + M_n \delta_{in}$$

or

$$-\theta_i = \delta_{i0} + \sum M_k \delta_{ik} \quad (11.28)$$

where

$$\delta_{i0} = \int \frac{X_i M_0}{EI} dx \quad (11.29)$$

= rotation at hinge i due to external loads alone

$$\delta_{ik} = \int \frac{X_i X_k}{EI} dx \quad (11.30)$$

= rotation at hinge i due to $M_k = 1$ acting at hinge k alone, and M_i and M_k = ultimate moments at hinges i and k , X_i = bending moment at any point when $M_i = 1$, X_k = bending moment at any point when $M_k = 1$, EI = flexural rigidity, and dx = element of length of member. The integrations are carried out along the whole length of the beam.

Hence the method involves making the structure statically determinate by placing frictionless hinges at the estimated plastic hinge points and finding the rotations caused at the hinges by the external loads and the ultimate moments acting at the hinges. The plastic hinges are chosen at the positions of the origin of plasticity. If the positions are incorrectly chosen, a negative value will be obtained for the rotation when calculated, and the hinge positions must be adjusted. It is also to be noted that in Eq. 11.28, δ_{i0} , M_k , and δ_{ik} may all be determined independently, hence the calculation of θ_i does not involve the solution of simultaneous equations.

The calculation of the flexibility (or influence) coefficient δ_{ik} requires the solution of a product integral involving the bending moments X_i and X_k . In most cases either X_i or X_k varies linearly along the member. Consider a member AB of length l with constant flexural rigidity EI . Let the moment X_i have a general variation along the member and the moment X_k have a linear variation along the member, as in Fig. 11.13. Now we have

$$X_k = \frac{x}{l} X_B + \frac{l-x}{l} X_A$$

$$\therefore \delta_{ik} = \int_0^l \frac{X_i X_k}{EI} dx = \frac{1}{EI} \int_0^l X_i \frac{x}{l} X_B dx + \frac{1}{EI} \int_0^l X_i \frac{l-x}{l} X_A dx$$

But $\int_0^l X_i x dx$ = first moment of area of X_i diagram about $A = A_i \bar{x}_i$, and $\int_0^l X_i (l-x) dx$ = first moment of area of X_i diagram about $B = A_i (l - \bar{x}_i)$

$$\begin{aligned} \therefore \delta_{ik} &= \int_0^l \frac{X_i X_k}{EI} dx = \frac{1}{EI} \left\{ \frac{X_B}{l} A_i \bar{x}_i + \frac{X_A}{l} A_i (l - \bar{x}_i) \right\} \\ &= \frac{A_i}{EI} \left(X_B \frac{\bar{x}_i}{l} + X_A \frac{l - \bar{x}_i}{l} \right) \\ &= \frac{A_i}{EI} \eta \end{aligned} \quad (11.31)$$

where A_i = area of the moment diagram with general variation, η = ordinate of the moment diagram with linear variation at the point vertically opposite the centroid of the moment diagram with general variation, and EI = flexural rigidity of the member section.

In the case of multispan continuous beams, the δ_{ik} values reduce to simple expressions. Consider the uniformly loaded continuous beam shown in Fig. 11.14 at the ultimate load. Assume that the plastic hinges form at the supports first and insert frictionless hinges at the supports to make the beam statically determinate. Then from Eqs. 11.28 the rotation at hinge 1 is

$$-\theta_1 = \delta_{10} + M_1 \delta_{11} + M_2 \delta_{12} + M_3 \delta_{13} + M_4 \delta_{14}$$

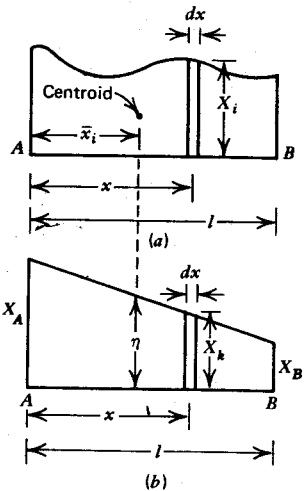


Fig. 11.13. Bending moment diagrams. (a) X_i bending moment diagram (general variation). (b) X_k bending moment diagram (linear variation).

where from Eqs. 11.29 to 11.31 we have

$$\begin{aligned}\delta_{10} &= \int \frac{X_1 M_0}{EI} dx = \frac{1}{EI_A} \left(\frac{2}{3} M_{FA} l_A \times -\frac{1}{2} \right) + \frac{1}{EI_B} \left(\frac{2}{3} M_{FB} l_B \times -\frac{1}{2} \right) \\ &= -\frac{M_{FA} l_A}{3EI_A} - \frac{M_{FB} l_B}{3EI_B}\end{aligned}\quad (11.32)$$

$$\begin{aligned}\delta_{11} &= \int \frac{X_1^2}{EI} dx = \frac{1}{EI_A} \left(-\frac{l_A}{2} \times -\frac{2}{3} \right) + \frac{1}{EI_B} \left(-\frac{l_B}{2} \times -\frac{2}{3} \right) \\ &= \frac{l_A}{3EI_A} + \frac{l_B}{3EI_B}\end{aligned}\quad (11.33)$$

$$\begin{aligned}\delta_{12} &= \int \frac{X_1 X_2}{EI} dx = 0 + \frac{1}{EI_B} \left(-\frac{l_B}{2} \times -\frac{1}{3} \right) + 0 \\ &= \frac{l_B}{6EI_B}\end{aligned}\quad (11.34)$$

$$\delta_{13} = \delta_{14} = 0 \quad (11.35)$$

where I_A, I_B, \dots = moments of inertia of the sections of spans l_A, l_B, \dots , M_1, M_2, M_3, \dots = ultimate moments at 1, 2, 3, ..., and M_{FA}, M_{FB}, \dots = maximum values of M_0 for spans l_A, l_B, \dots . Therefore θ_1 may be found. Similarly θ_2, θ_3 , and θ_4 may be found. Note that the determination of the

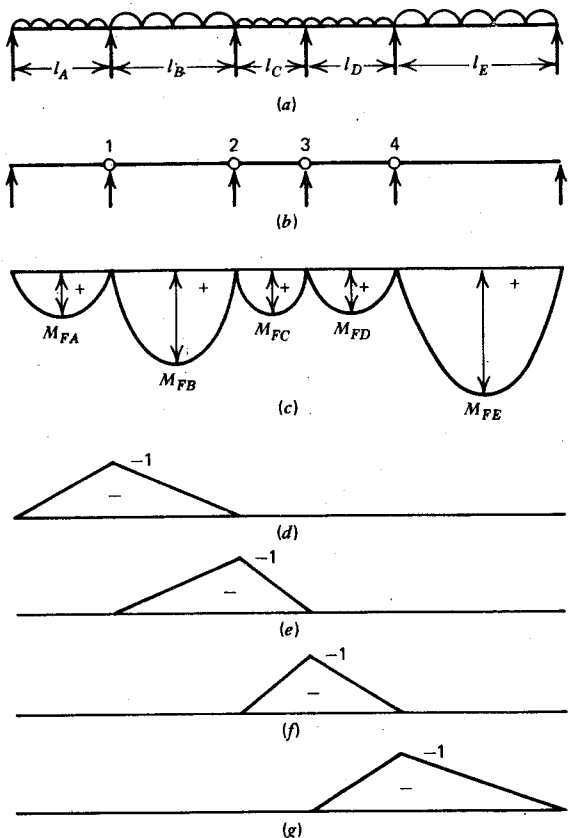


Fig. 11.14. Moment diagrams for continuous beam with frictionless hinges inserted at the interior supports. (a) Beam with uniform ultimate loading. (b) Structure released by frictionless hinges. (c) M_0 moment diagrams due to uniform loading. (d) X_1 moment diagram due to $M_1 = 1$. (e) X_2 moment diagram due to $M_2 = 1$. (f) X_3 moment diagram due to $M_3 = 1$. (g) X_4 moment diagram due to $M_4 = 1$.

coefficients is helped by the reciprocal relationship $\delta_{ik} = \delta_{ki}$. Hence $\delta_{12} = \delta_{21}$, $\delta_{34} = \delta_{43}$, and so on.

The foregoing equations assume that plasticity commences at the supports. This will be the case when the ultimate negative to positive moment ratios used in design are less than the elastic theory ratio. If it is found that the plastic hinges form first at the midspan sections (as shown by a negative value for θ_i from Eq. 11.28), a new set of equations must be derived for that case.

Note that the required plastic hinge rotations given by Eq. 11.28 vary inversely with the flexural rigidity EI of the section, a low flexural rigidity resulting in a high required plastic rotation. Therefore, to ensure that the required plastic hinge rotations are not underestimated, the flexural rigidity should not be overestimated. Hence safe computations for required plastic hinge rotations will use cracked section EI values. A safe estimate can also be obtained from $EI = M_y/\varphi_y$ or M_u/φ_y , where M_y = moment of resistance at first yield of tension steel, M_u = ultimate moment of resistance, and φ_y = curvature at first yield of the tension steel.

11.5.4 Calculation of Service Load Moments and Stresses

The serviceability check of a structure designed by limit design requires determination of the stresses at the service loads to ensure particularly that the steel is in the elastic range and at a level of stress that is not likely to cause unacceptable cracking of the concrete.

An analysis based on linear elastic theory is necessary to calculate the moments in the structure at the service loads. The moments can be calculated by any of the commonly accepted methods. If the δ_{ik} method of Section 11.5.3 has been used to calculate the plastic hinge rotations, it may be convenient to use the same method to find the service load bending moments. This can be carried out by putting the plastic hinge rotations equal to zero and solving simultaneously the set of equations for supports 1, 2, 3, ..., given by Eq. 11.28

$$0 = \delta_{i0} + \sum M_k \delta_{ik} \quad (11.36)$$

with the service loads on the structure to find the service load support moments M_k , thus allowing the complete service load bending moment diagram to be obtained.

A good approximation for the steel stress is obtained by dividing the moment by the product of the area of steel and a lever arm of $\frac{7}{8}$ of the effective depth.

Example 11.1

A continuous reinforced concrete beam with at least four equal spans, each of length l , is seated on simple supports and carries a uniform load over all spans. At the ultimate load the sum of the midspan positive moment and the average maximum negative moments for each span is M (i.e., the maximum ordinate of the free or static bending moment diagram is M), and the beam is reinforced so that the moments at the interior supports are all $0.5M$. The moment-curvature relationship may be assumed to be bilinear with a horizontal top. The sections at the interior supports have an ultimate moment of resistance of $400bd^2$ lb · in with a neutral axis

depth of $0.2d$, where b = width of section and d = effective depth of section in inches (1 lb = 4.45 N and 1 in = 25.4 mm). The equivalent length of the plastic hinge zones each side of the critical maximum moment sections is $0.5d$ and the extreme fiber compressive concrete strains at the end of the idealized elastic and inelastic stages are 0.001 and 0.004, respectively. The flexural rigidity EI of the members in the elastic range is $150,000bd^3$ lb · in 2 with a neutral axis depth of $0.375d$. Calculate the maximum allowable l/d ratio for the beam if full redistribution of bending moments is to occur at the ultimate load.

Solution

Figure 11.15 shows the beam and the bending moment diagram at the ultimate load. Since the ratio of maximum negative to maximum positive moments is less than the elastic theory value, the plastic hinges will form first at the supports. Insert frictionless hinges at the interior supports. Now from Eq. 11.28 we have

$$-\theta_1 = \delta_{10} + M_1 \delta_{11} + M_2 \delta_{12} + M_3 \delta_{13}$$

where from Eqs. 11.32 to 11.34

$$\delta_{10} = -\frac{2}{3} \frac{Ml}{EI} \quad \delta_{11} = \frac{2}{3} \frac{l}{EI} \quad \delta_{12} = \frac{1}{6} \frac{l}{EI} \quad \delta_{13} = 0$$

$$\therefore -\theta_1 = -\frac{2}{3} \frac{Ml}{EI} + 0.5M \frac{2}{3} \frac{l}{EI} + 0.5M \frac{1}{6} \frac{l}{EI} + 0 = -\frac{Ml}{4EI}$$

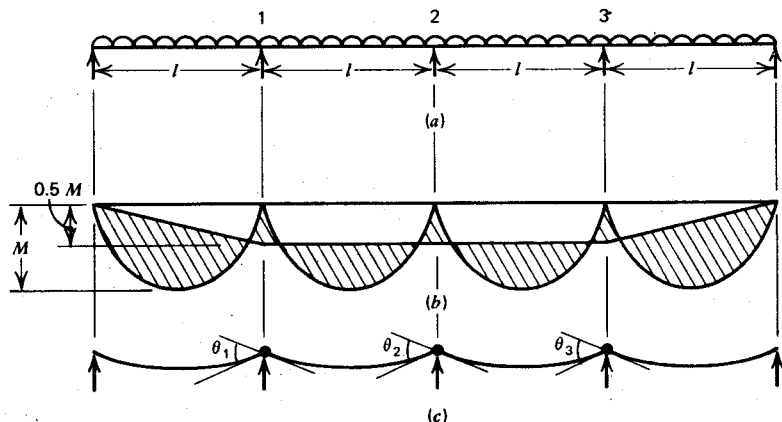


Fig. 11.15. Continuous beam of Example 11.1. (a) Beam at ultimate load. (b) Limit bending moment diagram. (c) Plastic hinge rotation when ultimate load is just reached.

Also

$$-\theta_2 = \delta_{20} + M_1 \delta_{21} + M_2 \delta_{22} + M_3 \delta_{23}$$

where from Eqs. 11.29 to 11.31

$$\delta_{20} = \frac{1}{EI} \left(\frac{2}{3} Ml \times -\frac{1}{2} \right) + \frac{1}{EI} \left(\frac{2}{3} Ml \times -\frac{1}{2} \right) = -\frac{2}{3} \frac{Ml}{EI}$$

$$\delta_{21} = \frac{1}{EI} \left(-\frac{l}{2} \times -\frac{1}{3} \right) = \frac{1}{6} \frac{l}{EI}$$

$$\delta_{22} = \frac{1}{EI} \left(-\frac{l}{2} \times -\frac{2}{3} \right) + \frac{1}{EI} \left(-\frac{l}{2} \times -\frac{2}{3} \right) = \frac{2}{3} \frac{l}{EI}$$

$$\delta_{23} = \frac{1}{EI} \left(-\frac{l}{2} \times -\frac{1}{3} \right) = \frac{1}{6} \frac{l}{EI}$$

$$\begin{aligned} \therefore -\theta_2 &= -\frac{2}{3} \frac{Ml}{EI} + 0.5M \frac{1}{6} \frac{l}{EI} + 0.5M \frac{2}{3} \frac{l}{EI} + 0.5M \frac{1}{6} \frac{l}{EI} \\ &= -\frac{Ml}{6EI} \end{aligned}$$

Therefore, the required plastic hinge rotations at the supports are

$$\theta_1 = \frac{Ml}{4EI} = \theta_3 \quad \text{by symmetry} \quad \text{and} \quad \theta_2 = \frac{Ml}{6EI}$$

Note that the positive values for θ_1 , θ_2 , and θ_3 imply that the positions of the first plastic hinges to form have been correctly chosen.

Now $M = 2 \times 0.5M = 2 \times 400bd^2 = 800bd^2$ and $EI = 150,000bd^3$. Therefore, the required plastic hinge rotations are

$$\theta_1 = \theta_3 = \frac{800bd^2l}{4 \times 150,000bd^3} = \frac{1}{750} \frac{l}{d} \text{ rad}$$

$$\theta_2 = \frac{800bd^2l}{6 \times 150,000bd^3} = \frac{1}{1125} \frac{l}{d} \text{ rad}$$

Now from Eq. 6.40 the total available plastic rotation at each plastic hinge is

$$\theta_a = \left(\frac{\varepsilon_c}{c} - \frac{\varepsilon_{ce}}{kd} \right) 2l_p$$

where l_p = equivalent plastic hinge length each side of the critical section.

$$\therefore \theta_a = \left(\frac{0.004}{0.2d} - \frac{0.001}{0.375d} \right) 2 \times 0.5d = 0.0173 \text{ rad}$$

Therefore, for full moment redistribution we require

$$\frac{1}{750} \frac{l}{d} \leq 0.0173 \quad \text{and} \quad \frac{1}{1125} \frac{l}{d} \leq 0.0173$$

or

$$\frac{l}{d} \leq 13.0 \quad \text{and} \quad \frac{l}{d} \leq 19.5$$

Hence the rotational capacity of the plastic hinges requires that for full moment redistribution $l/d \leq 13.0$.

Note that the required plastic hinge rotation for various cases of live load positions may be found by adjusting the free (static) moment values to suit the loading on the span.

Example 11.2

A beam of span l with ends restrained against rotation carries a uniformly distributed load w_u per unit length at the ultimate load. The moment-curvature relationship of the sections may be assumed to be bilinear, having a horizontal top. The sections have a uniform flexural rigidity EI along the length of the member. Calculate the allowable redistribution of bending moments at ultimate load from the elastic moment distribution in terms of the required ductility φ_u/φ_y at the plastic hinge sections, where φ_u = ultimate curvature and φ_y = curvature at first yield of the tension steel.

Solution

Let M'_u and M_u be the negative and positive ultimate moments of resistance, respectively. Referring to the bending moment diagram of Fig. 11.16b, and using the moment-area theorem, the change in slope of the beam between the support and midspan is

$$\begin{aligned} \theta &= \frac{2}{3} \frac{(M'_u + M_u)}{EI} \frac{l}{2} - \frac{M'_u}{EI} \frac{l}{2} \\ &= \frac{l}{6EI} (2M_u - M'_u) \end{aligned} \quad (i)$$

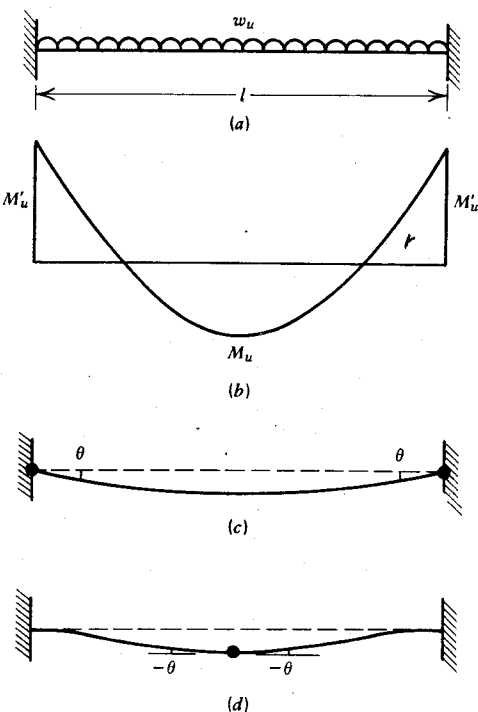


Fig. 11.16. Beam of Example 11.2. (a) Beam. (b) Limit bending moment diagram. (c) Ultimate load just reached with plastic hinges at supports and about to form at midspan. (d) Ultimate load just reached with plastic hinge at midspan and about to form at supports.

Also, for equilibrium

$$M'_u + M_u = \frac{w_u l^2}{8} \quad (ii)$$

If the beam behaves elastically, the slope of the member at the support and at midspan is horizontal. Then Eqs. *i* and *ii* give

$$\theta = 0 = \frac{l}{6EI} (2M_u - M'_u)$$

$$\therefore M'_u = 2M_u = \frac{w_u l^2}{12} \quad (iii)$$

If $M'_u < 2M_u$, plastic hinges will develop at the supports before at midspan (see Fig. 11.16c). When the ultimate load is just reached, the

slope of the member is horizontal at midspan and the plastic rotation required at the supports is found from Eqs. i and ii:

$$\theta = \frac{l}{6EI} (2M_u - M'_u) = \frac{l}{6EI} \left(\frac{w_u l^2}{4} - 3M'_u \right) \quad (\text{iv})$$

If $M'_u > 2M_u$, a plastic hinge will develop at midspan before at the supports (see Fig. 11.16d). Then when the ultimate load is just reached, the slope of the member is horizontal at the supports, and Eqs. i and ii give the plastic rotation required to each side of the critical section at midspan:

$$\theta = \frac{l}{6EI} (2M_u - M'_u) = \frac{l}{6EI} \left(\frac{w_u l^2}{4} - 3M'_u \right) \quad (\text{v})$$

Now if β is the percentage of the elastic theory negative moment that can be redistributed at the ultimate load, we have

$$\beta = \frac{w_u l^2 / 12 - M'_u}{M'_u} \times 100 = 100 \left(\frac{w_u l^2}{12M'_u} - 1 \right)$$

$$\therefore M'_u = \frac{w_u l^2}{12} \left(\frac{100}{100 + \beta} \right) \quad (\text{vi})$$

Also it may be assumed that

$$EI = \frac{M'_u}{\varphi_y} \quad (\text{vii})$$

where φ_y = curvature at first yield at the critical section. Substituting M'_u and EI from Eqs. vi and vii into Eqs. iv and v gives the required plastic rotation to one side of the critical section:

$$\theta = \frac{\varphi_y l}{2} \frac{\beta}{100} \quad (\text{viii})$$

Now from Eq. 6.39 the available plastic rotation to one side of the critical section is

$$\theta_a = (\varphi_u - \varphi_y) l_p \quad (\text{ix})$$

where φ_u = ultimate curvature and l_p = equivalent length of plastic hinge to one side of the critical section.

For the required moment redistribution to occur, we must have when β is positive $\theta \leq \theta_a$.

$$\therefore \frac{\varphi_y l}{2} \frac{\beta}{100} \leq (\varphi_u - \varphi_y) l_p$$

$$\therefore \frac{\varphi_u}{\varphi_y} \geq 1 + \frac{\beta}{200} \frac{l}{d} \frac{d}{l_p} \quad (\text{x})$$

and similarly when β is negative we must have $-\theta \leq \theta_a$

$$\therefore \frac{\phi_u}{\phi_y} \geq 1 - \frac{\beta}{200} \frac{l}{d} \frac{d}{l_p} \quad (\text{xi})$$

Note that the required curvature ductility depends on β , l/d , and l_p/d . For example, if $\beta = 30\%$, $l/d = 30$, and $l_p/d = 0.5$, Eq. x indicates that the required $\phi_u/\phi_y = 1 + (0.15 \times 30/0.5) = 10$. Since $l/d = 30$ is approximately the maximum likely value for a continuous beam (see Table 10.1) and $l_p/d = 0.5$ is about the minimum likely equivalent plastic hinge length (see Eqs. 6.41 and 6.49), $\phi_u/\phi_y = 10$ is the maximum likely required curvature ductility for 30% moment redistribution in the case of ends fully restrained against rotation and the member uniformly loaded. The required ϕ_u/ϕ_y values for other values of β , l/d , and l_p/d can be calculated from Eq. x. Whether a section has sufficient ductility can be checked using Figs. 6.9 and 6.10.

A more general result for spans of continuous beams carrying various combinations of dead and live loading where some rotation occurs at ends of spans can be obtained using Eq. 11.28.

Example 11.3

A one-way reinforced concrete slab is continuous over two 20 ft (6.10 m) spans. The slab is to carry a service live load of 150 lb/ft² (7.18 kN/m²). The concrete is normal weight with a cylinder strength of 3000 psi (20.7 N/mm²), and the steel has a yield strength of 60,000 psi (414 N/mm²). Determine a suitable slab thickness and steel arrangement by limit design.

Solution

A number of possible negative to positive ultimate moment ratios could be used. In this design we will use equal negative and positive ultimate moments, which results in a convenient steel arrangement, and the minimum thickness allowed in Table 10.1 without a deflection check.

$$\therefore h = 20 \times \frac{12}{24} = 10 \text{ in}$$

\therefore service loads are

$$D = \frac{10}{12} \times 150 = 125 \text{ lb/ft}^2 \quad \text{and} \quad L = 150 \text{ lb/ft}^2$$

ultimate loads are from Eq. 1.1

for D alone, $U = 1.4 \times 125 = 175 \text{ lb/ft}^2$

for $D + L$, $U = 1.4 \times 125 + 1.7 \times 150 = 430 \text{ lb/ft}^2$.

SECTION DESIGN FOR STRENGTH

Figure 11.17a is the limit bending moment diagram with the ultimate dead plus live load on each span. To find the relationship between the ultimate loads and moments, let x_0 be the distance from the end support to the section of maximum positive bending moment and zero shear force, and R the left-hand support reaction. Considering actions between the end support and the maximum positive

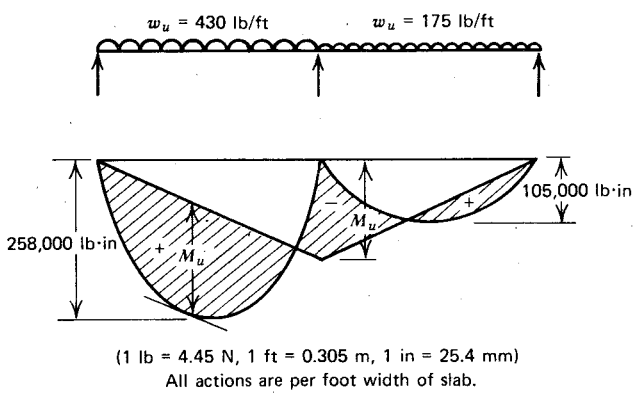
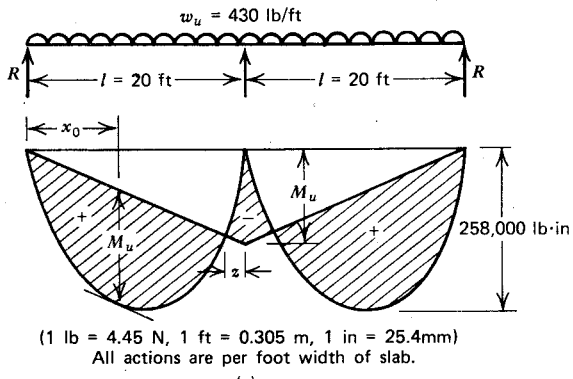


Fig. 11.17. Bending moment diagrams for limit design of slab of Example 11.3. (a) Loading and limit bending moment diagram for ultimate live load on both spans plus dead load for calculation of section strengths. (b) Loading and limit bending moment diagram for ultimate live load on left-hand span plus dead load for calculation of negative moment steel in right-hand span.

moment section, we have

$$0 = R - w_u x_0 \quad \therefore \quad x_0 = \frac{R}{w_u}$$

$$M_u = Rx_0 - \frac{w_u x_0^2}{2} = \frac{R^2}{w_u} - \frac{R^2}{2w_u} = \frac{R^2}{2w_u}$$

$$\therefore R = \sqrt{2w_u M_u}$$

Also, considering sections between the end and the center supports, we put

$$M_u = -Rl + \frac{w_u l^2}{2} = -l\sqrt{2w_u M_u} + \frac{w_u l^2}{2}$$

$$\therefore M_u^2 - 3w_u l^2 M_u + \frac{w_u l^4}{4} = 0$$

from which

$$M_u = \frac{w_u l^2}{11.65} \quad (i)$$

and

$$R = \sqrt{2w_u \frac{w_u l^2}{11.65}} = 0.414 w_u l$$

At section of zero moment, we have

$$0 = 0.414 w_u l(l - z) - \frac{w_u}{2} (l - z)^2$$

$$\therefore z = 0.172l \quad (ii)$$

Note that a good approximation for the ultimate moment M_u could have been obtained by assuming that the maximum positive moment occurs at midspan. This would mean that

$$M_u + 0.5M_u = \frac{w_u l^2}{8}$$

$$\therefore M_u = \frac{w_u l^2}{12}$$

which is only 3% less than the exact value given by Eq. i.

From Eq. i the positive and negative ultimate moments are

$$M_u = \frac{430 \times 20^2}{11.65} \times 12 \\ = 177,000 \text{ lb} \cdot \text{in/ft width}$$

Use, say, No. 5 bars with $\frac{3}{4}$ in cover.

$$d = 10 - \frac{3}{4} - \frac{5}{16} = 8.94 \text{ in}$$

$$\therefore \frac{M_u}{\varphi f'_c bd^2} = \frac{177,000}{0.9 \times 3000 \times 12 \times 8.94^2} = 0.0684$$

Therefore, from Table 4.2, $\omega = 0.0714$.

$$\therefore \rho = \frac{f'_c}{f_y} \omega = \frac{3000}{60,000} \times 0.0714 = 0.00357$$

Now from Table 4.1

$$\rho_{\max} = 0.016 > \rho \quad \therefore \text{satisfactory}$$

and according to ACI 318-71^{11.8}

$$\rho_{\min} = 0.0018 < \rho \quad \therefore \text{satisfactory}$$

$$A_s = 0.00357 \times 8.94 \times 12 = 0.383 \text{ in}^2/\text{ft width.}$$

Therefore, we can use No. 5 bars at $0.31/0.383 \times 12 = 9.7$ in centers.

Use, say, No. 5 (15.9 mm diameter) bars at 10 in (254 mm) centers.

To find the region of the slab over which negative moment steel is required, the live load is taken off that span. The maximum free bending moment ordinates ($w_u l^2/8$) at the ultimate load are for dead plus live load $430 \times 20^2 \times 12/8 = 258,000 \text{ lb} \cdot \text{in/ft width}$ and for dead load alone $175 \times 20^2 \times 12/8 = 105,000 \text{ lb} \cdot \text{in/ft width}$. To find the extent of negative moment steel required in the right-hand span, the live load is taken off that span, as in Fig. 11.17b, and the resulting moment diagram is used to calculate possible cutoff points for those bars. Similar cutoff points will apply to the left hand span.

CHECK OF PLASTIC ROTATION CAPACITY

For the section $n = 9$ and $\rho n = 0.00357 \times 9 = 0.0321$, therefore, Eq. 10.9 gives

$$k = \sqrt{\rho^2 n^2 + 2\rho n} - \rho n \\ = \sqrt{0.0321^2 + 2 \times 0.0321} - 0.0321 = 0.223 \\ \therefore \varphi_y = \frac{f_y/E_s}{d(1 - k)} = \frac{60,000/29,000,000}{8.94(1 - 0.223)} = 0.000298 \text{ rad/in.} \quad (\text{iii})$$

and

$$EI = M_u/\varphi_y = 177,000/0.000298 = 594 \times 10^6 \text{ lb} \cdot \text{in}^2/\text{ft width} \quad (\text{iv})$$

The slab is statically indeterminate to the first degree. Assume that the first plastic hinge forms at the center support and that the ultimate moment there is $M_u = M_1 = 177,000 \text{ lb} \cdot \text{in}/\text{ft width}$. Insert a frictionless hinge at the center support. Figure 11.18 shows the bending moments in the slab for the loading cases with live load on both spans or one span. Now from Eq. 11.28, if the subscript 1 refers to the center support, we have

$$-\theta_1 = \delta_{10} + M_1 \delta_{11} \quad (\text{v})$$

where

$$\begin{aligned} \delta_{11} &= \int \frac{X_1^2}{EI} dx = \frac{2}{EI} \left(-\frac{l}{2} \times -\frac{2}{3} \right) = \frac{2l}{3EI} \\ &= \frac{2 \times 240}{3 \times 594 \times 10^6} = 0.269 \times 10^{-6} \text{ rad}/(\text{lb} \cdot \text{in}/\text{ft width}) \end{aligned}$$

$$\begin{aligned} \delta_{10} &= \int \frac{X_1 M_0}{EI} dx = \frac{1}{EI} \left(\frac{2}{3} M_{FA} l \times -\frac{1}{2} \right) + \frac{1}{EI} \left(\frac{2}{3} M_{FB} l \times -\frac{1}{2} \right) \\ &= -\frac{l}{3EI} (M_{FA} + M_{FB}) \end{aligned}$$

For live load on both spans, we write

$$\delta_{10} = -\frac{240}{3 \times 594 \times 10^6} (258,000 + 258,000) = -0.0695 \text{ rad}$$

Therefore, Eq. v gives

$$-\theta_1 = -0.0695 + 177,000 \times 0.269 \times 10^{-6} = -0.0219 \text{ rad}$$

∴ required plastic rotation $\theta_1 = 0.0219 \text{ rad}$

For live load on one span only, we have

$$\delta_{10} = -\frac{240}{3 \times 594 \times 10^6} (258,000 + 105,000) = -0.0489 \text{ rad}$$

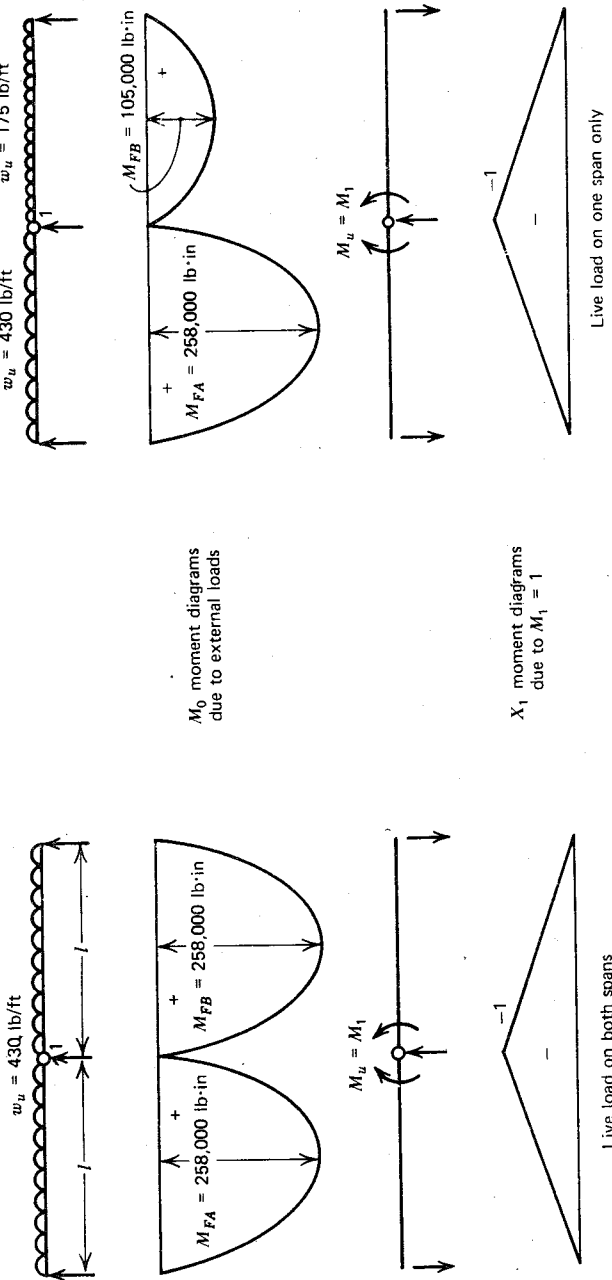
Therefore, Eq. v gives

$$-\theta_1 = -0.0489 + 177,000 \times 0.269 \times 10^{-6} = -0.0013 \text{ rad}$$

∴ required plastic rotation $\theta_1 = 0.0013 \text{ rad}$

Now from Eq. 6.39 available plastic rotation is

$$\theta_a = (\varphi_u - \varphi_y) 2l_p \quad (\text{vi})$$



(1 lb = 4.45N, 1 ft = 0.305 m, 1 in = 25.4 mm)
All actions are per foot width of slab.

Fig. 11.18. Bending moment diagrams for check of rotation capacity of plastic hinge for limit design of slab of Example 11.3.

where l_p is the equivalent plastic hinge length each side of the critical section. Now from Eq. ii, $z = 0.172l = 0.172 \times 240 = 41.3$ in and $z/d = 41.3/8.94 = 4.62$. Equations 6.47 and 6.49 indicate that $l_p = 0.5d + (0.05 \times 4.62d) = 0.73d$ or $l_p = 0.25d + (0.075 \times 4.62d) = 0.60d$. Conservatively, we estimate l_p to be $0.6d$. Also, the depth of the equivalent rectangular concrete stress block at the ultimate moment is

$$a = \frac{A_s f_y}{0.85 f'_c b} = \frac{0.383 \times 60,000}{0.85 \times 3000 \times 12} = 0.751 \text{ in}$$

$$c = \frac{a}{\beta_1} = \frac{0.751}{0.85} = 0.884 \text{ in}$$

If $\epsilon_c = 0.003$, $\phi_u = \epsilon_c/c = 0.003/0.884 = 0.00339 \text{ rad/in}$. Therefore, available plastic rotation from Eqs. iii and vi is

$$\theta_a = (0.00339 - 0.000298)2 \times 0.6 \times 8.94 \\ = 0.0332 \text{ rad}$$

Since θ_a is greater than the θ_1 values, the required plastic rotation capacity is available.

CHECK OF SERVICEABILITY

The deflection at service load has been controlled by using a span/thickness ratio not greater than 24, as recommended by Table 10.1.

The extent of cracking at the service loads may be checked from the maximum service load bending moments found from linear elastic theory.

Live load L on both spans plus dead load D gives a maximum negative moment (see Fig. 11.19) of

$$M = \frac{(L + D)l^2}{8} = \frac{(150 + 125)20^2 \times 12}{8} = 165,000 \text{ lb} \cdot \text{in/ft width.}$$

Maximum steel stress for this loading is

$$f_s = \frac{M}{A_s(1 - k/3)d} = \frac{165,000}{0.383 \times (1 - 0.223/3)8.94} \\ = 52,000 \text{ psi} < 60,000 \text{ psi}$$

Hence steel is not yielding at service load.

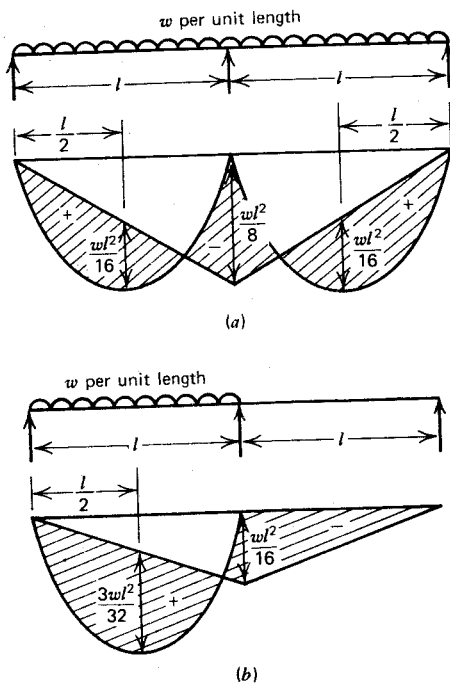


Fig. 11.19. Bending moment diagrams from elastic theory for check of service load stresses for limit design of slab of Example 11.3. (a) Load on both spans. (b) Load on one span only.

Live load L on one span plus dead load D gives a midspan positive moment (close to maximum, see Fig. 11.19) of

$$M = \frac{3Ll^2}{32} + \frac{Dl^2}{16} = \left(\frac{3 \times 150}{32} + \frac{125}{16} \right) 20^2 \times 12 = 105,000 \text{ lb} \cdot \text{in}/\text{ft width}$$

Maximum steel stress for this loading is

$$f_s = \frac{105,000}{0.383 \times (1 - 0.223/3)8.94} = 33,100 \text{ psi}$$

Equation 10.71 indicates that the maximum crack widths depend on the value for $f_s \sqrt[3]{t_b A}$, where t_b = thickness of concrete cover measured to bar center, and A = effective area of concrete in tension surrounding each bar. Now

$$t_b = \frac{3}{4} + \frac{5}{16} = 1.06 \text{ in}$$

$$A = 10 \times 2 \times 1.06 = 21.2 \text{ in}^2/\text{bar}$$

$$\max f_s = 52,000 \text{ psi}$$

$$\therefore f_s \sqrt[3]{t_b A} = 52,000 \sqrt[3]{1.06 \times 21.2} \\ = 146,600 \text{ lb/in} < 170,000 \text{ lb/in}$$

Thus according to Eq. 10.71 the cracking in the slab at the service loads is not greater than allowed for interior exposure and is close to being satisfactory for exterior exposure.

CHECK OF SHEAR STRENGTH

The maximum shear force at the ultimate load is adjacent to the center support with the span fully loaded. The maximum is

$$V_u = \frac{w_u l}{2} + \frac{M_u}{l} \\ = \frac{430 \times 20}{2} + \frac{177,000}{20 \times 12} = 5040 \text{ lb/ft width}$$

$$\therefore \frac{V_u}{bd\sqrt{f'_c}} = \frac{5040}{12 \times 8.94\sqrt{3000}} = 0.859$$

Therefore shear reinforcement is not required.

COMMENTS ON THE DESIGN

Had the envelope of elastic bending moments at ultimate load been used for the design of the sections, the maximum ultimate negative moment would have been

$$\frac{(1.4D + 1.7L)l^2}{8} = \frac{430 \times 20^2 \times 12}{8} = 258,000 \text{ lb} \cdot \text{in/ft width}$$

and the maximum (midspan) ultimate positive moment would have been

$$\frac{1.4Dl^2}{16} + \frac{3 \times 1.7Ll^2}{32} = \left(\frac{175}{16} + \frac{3 \times 255}{32} \right) 20^2 \times 12 \\ = 167,000 \text{ lb} \cdot \text{in/ft width}$$

The limit design ultimate moments used were 177,000 lb · in/ft width. Thus the limit design negative moment is 31% less than the elastic envelope moment and the limit design positive moment is 6% greater than the elastic envelope moment, indicating the extent of the saving in steel. Note that the ultimate negative moment used

in the limit design cannot be achieved without a 31 % redistribution of elastic negative moment. This was checked, and the curvature ductility was found to be adequate. ACI 318-71^{11,8} would allow approximately 17 % redistribution according to Eq. 11.7, illustrating the conservative nature of the ACI equation.

The maximum steel stress at the service loads in the limit design is high ($0.87f_y$), but provided the steel is not yielding, the crack widths can be shown to be acceptable if a reasonable arrangement of steel is used. This requires bars at reasonably close centers. The small thickness of concrete cover to steel used in a slab is also helpful in keeping surface crack widths small.

A design procedure such as outlined in this example may require a trial-and-error approach, since sometimes the rotation required of plastic hinges at the ultimate load is excessive; the steel stresses at the service loads, too, may be excessive. This may require the chosen limit bending moment diagram to more closely approach the elastic pattern of bending moments. Also, the critical plastic hinge in the example was at the center support, but in other cases, particularly when the live load to dead load ratio is high and the live load is on alternate spans only, the critical plastic hinges may occur at midspan. Checking the required rotation at positive moment plastic hinges requires equations additional to those derived in Section 11.5.3.

11.5.5 Comments on Limit Design

The theory and examples of the preceding sections indicate that the complexities of limit design, and the computational effort involved, are much greater than those associated with design based on the elastic bending moment distribution. Hence the additional burden placed on the designer by limit design may not be acceptable except in special cases.

To some extent, the advantages of limit design of alleviating steel congestion and of saving some steel, can be obtained simply and safely by the limited moment redistribution from the elastic moment diagram allowed by current design codes. Thus the design approach based on the elastic bending moment patterns, with or without some moment redistribution, is likely to remain the only practical approach for some time. The future use of limit design procedures appears to depend on the ready availability of comprehensive computer programs capable of taking into account elastic and inelastic behavior and able to design structures and check behavior at all loading stages.

11.6 DESIGN FOR SEISMIC LOADING

11.6.1 Basic Concepts

During an earthquake, ground motions occur in a random fashion in all directions. Measurements of horizontal and vertical ground accelerations, made as a function of time, have indicated that the ground accelerations can be considerable. For example, during the 1940 El Centro earthquake the peak recorded horizontal ground acceleration was 0.33 g . An extreme example was the 1971 San Fernando earthquake, during which peak ground accelerations exceeding 1 g were measured at the Pacoima dam site.

When a structure is subjected to ground motions in an earthquake, it responds in a vibratory fashion. When the structure is behaving elastically, the maximum response acceleration will depend on the structure's natural period of vibration and the magnitude of the damping present. Dynamic analyses of structures responding elastically to typical earthquake records have indicated the order of response acceleration the structures may experience. Results of such dynamic analyses may be seen in texts by Wiegel^{11.21} and Newmark and Rosenblueth.^{11.22} For example, Fig. 11.20a illustrates a simple structure in the form of a single degree of freedom oscillator subjected to ground vibrations. Figure 11.20b shows the maximum acceleration response of the structure behaving elastically, as obtained by Housner,^{11.21} when the structure is subjected to recorded ground motions from some United States earthquakes. The maximum response acceleration S_a is plotted as a function of the natural period of vibration of the structure and the magnitude of the damping, which is expressed as a percentage of the critical viscous damping. The curves are idealized ("smoothed") from the more irregular actual curves; $S_a = 1$ may be taken to be the maximum ground acceleration. For example, if Fig. 11.20b is used to idealize an earthquake in which the maximum ground acceleration was 0.33 g , the S_a values in the figure would be multiplied by 0.33 g . It is evident that for a range of periods, the maximum response acceleration of the structure may be several times the ground acceleration. The maximum response acceleration of structures with a very small period (i.e., very rigid structures) approaches the maximum ground acceleration. The maximum response acceleration of structures with large periods of vibration may experience little more than the maximum ground acceleration, and at greater periods they may experience less than the maximum ground acceleration. An increase in damping will always result in a decrease in response acceleration. Using Fig. 11.20, the maximum inertia loads acting on the simple structure during the earthquake may be obtained by multiplying the acceleration by the mass.

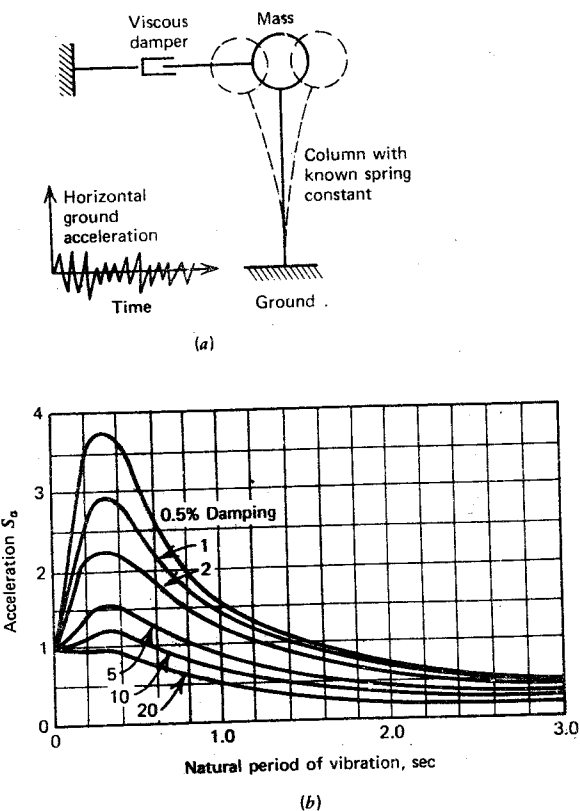


Fig. 11.20. Design spectrum giving acceleration as a function of damping and period of vibration for a single degree of freedom linear oscillator responding elastically to some earthquake ground motions.^{11.21} (a) Oscillator. (b) Design spectrum.

The design seismic loading recommended by building codes, for example the SEAOC^{11.23} and the ICBO^{11.24} codes, is in the form of static lateral loading. Equivalent static lateral loading for multistory structures is normally applied with a near-triangular distribution to the structure, placing the greatest load at the top, thus simulating the deflected shape of the first mode of vibration in Fig. 11.20a. These codes use static design loads to determine the strength of structure necessary to withstand the dynamic loads induced by the earthquake. However, the recommended level of static design lateral load is generally quite low. Dynamic analyses of structures, responding elastically to ground motions recorded during severe earthquakes, have

shown that the theoretical response inertia loads may be much greater than the static design lateral loads recommended by such codes. Although this difference is too large to be reconciled by safety factors in design, it is well known that structures designed to the lateral loads of codes have survived severe earthquakes. This apparent anomaly has been attributed mainly to the ability of ductile structures to dissipate energy by postelastic deformations, helped by such other factors as a reduced response due to increased damping, and to soil-structure interaction. The ductility of the members may be the most important factor.

It is evident that it would be uneconomical to design a structure to withstand the greatest likely earthquake without damage. The cost of providing strength to resist very high intensity lateral vibrations must be weighed against the importance of the structure and the probability of the earthquakes. The criteria for the level of loading of the SEAOC code^{11,23} are as follows: buildings should be able to resist minor earthquakes without damage, to resist moderate earthquakes without structural damage but with some nonstructural damage, and to resist major earthquakes without collapse but with some structural and nonstructural damage. Hence the possibility of damage is accepted, but not loss of life. The code objective is to have structures that will behave elastically under earthquakes that can be expected to occur more than once in the life of the building; the structures, moreover, should be able to survive without collapse the major earthquake that might occur during the life of the building. To avoid collapse during the major earthquake, members must be ductile enough to absorb and dissipate energy by postelastic deformations. The order of ductility involved may be associated with very large permanent deformations. Thus although the structure should not collapse, the resulting damage might be beyond repair, and the structure might become a total economic loss.

11.6.2 Displacement Ductility Requirements

In earthquake-resistant design, a prime consideration is clearly the need to have a structure capable of deforming in a ductile manner when subjected to several cycles of lateral loading well into the inelastic range. Nonlinear dynamic analysis of code-designed structures responding to typical earthquake motions have given an indication of the order of postelastic deformations required.^{11.21, 11.22, 11.25}

The effect of nonlinear behavior on the response of a structure to severe earthquake motions may be seen with reference to a single degree of freedom oscillator. Such an oscillator, responding elastically, will have a load-deflection relationship as represented in Fig. 11.21a, where point *b* is the maximum response. The area *abc* under the curve represents the potential

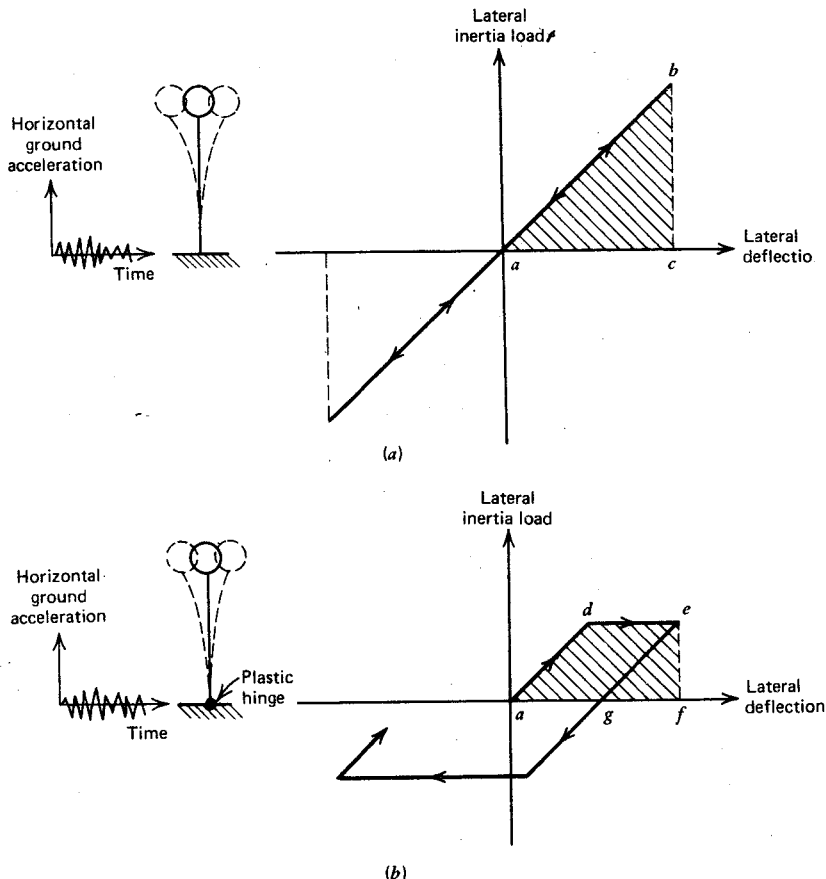


Fig. 11.21. Response of oscillators to earthquake motions. (a) Elastic response. (b) Elasto-plastic response.

energy stored at the maximum deflection; and as the mass returns to the zero position, the energy is converted into kinetic energy. If the oscillator is not strong enough to carry the full elastic response inertia load and develops a plastic hinge with elastoplastic characteristics, the load-deflection curve will be as in Fig. 11.21b. When the plastic hinge capacity is reached, the deflection response proceeds along line de , and point e represents the maximum response. The potential energy stored at maximum deflection in this case is represented by the area $adef$: note that the forces acting on the structure have been limited by the plastic hinge capacity. When the mass returns to the zero

position, the energy converted to kinetic energy is represented by the small triangular area efg , because the energy represented by the area $adeg$ is dissipated by the plastic hinge by being converted into heat and other irrecoverable forms of energy. Thus it is evident that in the elastic structure the full stored energy is returned as velocity energy in each cycle, whereas in the elastoplastic structure only part of the energy is returned. Hence the potential energy stored in the elastoplastic structure in each cycle is not required to be so great as in the elastic structure, and the maximum deflection of the elastoplastic structure is not necessarily much greater than that of the elastic structure. In fact, a number of dynamic analyses^{11.25, 11.21} have indicated that the maximum deflection reached by the two structures may be approximately the same. Behavior based on the assumption of equal maximum deflections is illustrated in Fig. 11.22a.

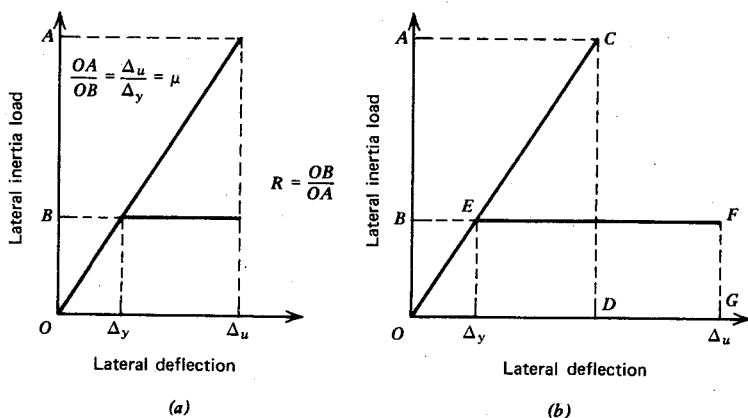


Fig. 11.22. Assumed responses of elastic and elastoplastic structures. (a) Equal maximum deflection response. (b) Equal maximum potential energy response.

A measure of the ductility of a structure is the displacement ductility factor μ defined as

$$\mu = \frac{\Delta_u}{\Delta_y} \quad (11.37)$$

where Δ_u is the lateral deflection at the end of the postelastic range and Δ_y is the lateral deflection when yield is first reached. When a number of load cycles are involved, Δ_y is taken as the lateral deflection when yield is first reached in the first load excursion into the postelastic range.

The Commentary on the SEAOC code^{11.23} indicates that the displacement ductility factor required in design may be estimated on the basis of the ratio

of elastic response inertia load to code static design load (as may be seen from similar triangles of Fig. 11.22a) and that typical values for the displacement ductility factor μ may range from 3 to 5.

The ratio of the code static design load to the elastic response inertia load may be referred to as the load reduction factor R . In the equal maximum deflection assumption of Fig. 11.22a this would mean

$$R = \frac{1}{\mu} \quad (11.38)$$

Some dynamic analyses have indicated that the equal maximum deflection assumption of Fig. 11.22a may be unconservative. In particular, reinforced concrete may show a deterioration of stiffness under load reversals, and this causes a reduction in the energy dissipating characteristics. Blume^{11.21} has shown that a value for the reduction factor R that gives a probable upper limit is

$$R = \frac{1}{\sqrt{2\mu - 1}} \quad (11.39)$$

Equation 11.39 is based on the equal energy concept, which implies that the potential energy stored by the elastic system at maximum deflection is the same as that stored by the elastoplastic system at maximum deflection. This is illustrated in Fig. 11.22b and requires area OCD equal to area $OEGF$.

$$\therefore \frac{OA \times OD}{2} = \frac{OB \times \Delta_y}{2} + (\Delta_u - \Delta_y)OB$$

But $OD = \Delta_y OA / OB$.

$$\therefore \frac{\Delta_y}{2} \frac{OA^2}{OB} = OB \left(\Delta_u - \frac{\Delta_y}{2} \right)$$

$$\therefore \left(\frac{OB}{OA} \right)^2 = \frac{\Delta_y}{2(\Delta_u - \Delta_y/2)} = \frac{1}{2\Delta_u/\Delta_y - 1}$$

which gives Eq. 11.39, since $OB/OA = R$ and $\Delta_u/\Delta_y = \mu$.

A comparison between the μ values obtained from Eqs. 11.38 and 11.39 for a range of R values is given below.

$R = \frac{\text{Design load}}{\text{Elastic response load}}$	0.2	0.4	0.6	0.8	1.0
μ from Eq. 11.38	5.0	2.5	1.67	1.25	1.0
μ from Eq. 11.39	13.0	3.63	1.89	1.28	1.0

It is evident that the elastoplastic system responding at a lower strength level will suffer larger displacements if it is to absorb the same energy as the elastic system. It is also evident that the difference between Eqs. 11.38 and 11.39 can be substantial at low values for R .

Figure 11.23, plotted by Blume,^{11.21} compares Eqs. 11.38 and 11.39 with results obtained from dynamic analyses on single degree of freedom systems conducted by Clough.^{11.26} Elastoplastic and degrading stiffness systems were compared with elastic systems. It is evident from Fig. 11.23 that Eq. 11.39 may be an upper bound, and a more realistic value for R may approach that given by Eq. 11.38.

The foregoing considerations apply approximately to multistory frames. It is apparent that in severe earthquakes considerable ductility may be required of buildings designed to code static loads, but of course the ductility demand can be reduced by designing to higher static lateral loads. Using a design spectrum such as that in Fig. 11.20b, and the reduction factor as defined by Eqs. 11.38 or 11.39, the designer can approximately relate the earthquake to be survived to the static design load and the displacement ductility factor. For a multistory building, the displacements Δ_y and Δ_u giving the displacement ductility factor are measured at a suitable position (e.g., at the roof level). In a multistory frame, plastic hinges will tend to develop at the critical sections throughout the structure but will not all develop at the same

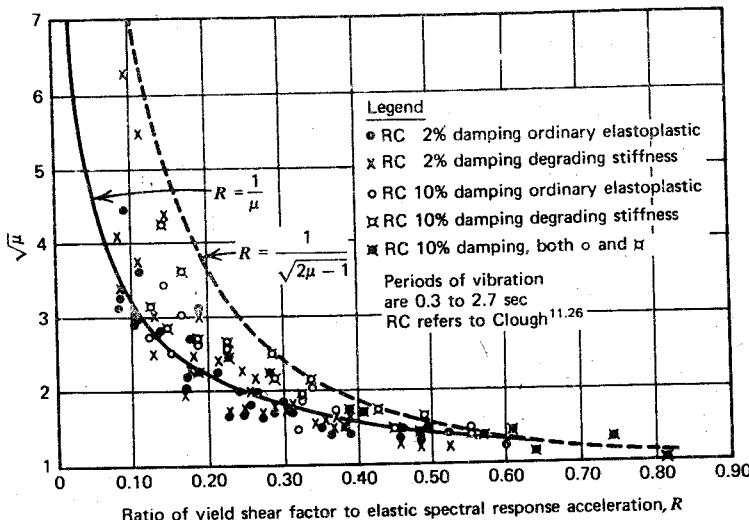


Fig. 11.23. Displacement ductility versus ratio of strength to elastic demand for single degree of freedom oscillators responding to the 1940 El Centro N-S earthquake.^{11.21}

load. Hence the lateral load-deflection relationship will not be bilinear as in Fig. 11.21b but will tend to be more curved because of the stiffness decreasing gradually as the plastic hinges develop at various load levels. To assess the displacement ductility factor in such a case, and approximate bilinear lateral load-deflection curve can be assumed, taking the deflection at first yield as the deflection due to the static design load applied to the frame behaving elastically. However, the approximations are such that accurate assessment of the ductility demand in important cases may require nonlinear dynamic analyses of the structure responding to the major earthquake.

It is emphasized that ductility is associated with plastic deformations, hence is associated with permanent structural damage. This means that a structure designed using a low load reduction factor R is susceptible to permanent damage during earthquakes of smaller intensity. For buildings of importance, particularly those which need to function after a seismic disaster, the potential ductility of the structure may not be utilized, because damage control will be the overriding design criterion. For such a structure, a larger load reduction factor could be used—for example, $R = 0.5$, requiring $\mu = 2$ according to Eq. 11.38.

11.6.3 Curvature Ductility Requirements

The ductility of reinforced concrete sections can be expressed by the curvature ductility ratio φ_u/φ_y , where φ_u = curvature at the end of the post-elastic range and φ_y = curvature at first yield. This assumes that flexural deformations predominate. Values for the curvature ductility factor φ_u/φ_y available from typical members were discussed in Chapter 6. The available curvature ductility factor is quite large in many cases, but it is important to recognize that there is a significant difference between the displacement ductility factor Δ_u/Δ_y and the curvature ductility factor φ_u/φ_y . This is because once yielding has commenced in a frame, the deformations concentrate at the plastic hinge positions; hence when a frame is deflected laterally in the post-elastic range, the required φ_u/φ_y ratio at a plastic hinge may be greater than the Δ_u/Δ_y ratio.

The relationship between curvature ductility and displacement ductility in a simple case can be illustrated with reference to the cantilever column with a lateral load at the end in Fig. 11.24. (The idealized distribution of curvature at the ultimate moment also shown.) The lateral deflection at the top of the column may be determined by taking moments of the curvature diagram about the top. The calculation of deflections from curvatures was discussed in Section 6.6. The lateral deflection at the top at the ultimate moment is

$$\Delta_u = \left(\frac{\varphi_y l}{2} \frac{2l}{3} \right) + (\varphi_u - \varphi_y) l_p (l - 0.5l_p)$$

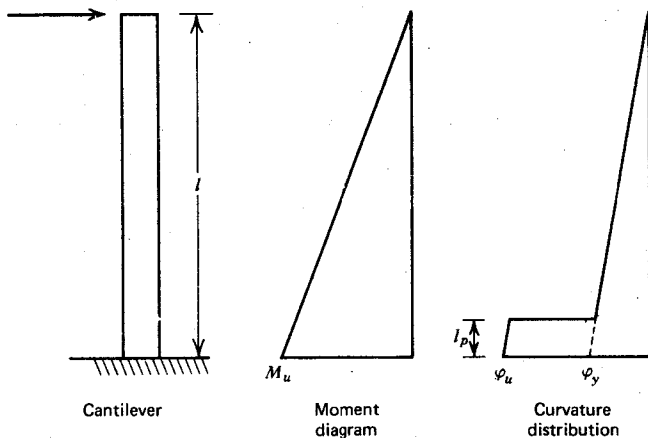


Fig. 11.24. Cantilever column with lateral loading at ultimate moment.

where l = length of column and l_p = equivalent length of the plastic hinge. The lateral deflection at the top at first yield is

$$\Delta_y = \frac{\varphi_y}{2} \frac{l}{3} 2l$$

$$\begin{aligned} \therefore \mu &= \frac{\Delta_u}{\Delta_y} = 1 + \left(\frac{\varphi_u - \varphi_y}{\varphi_y} \right) \frac{l_p(l - 0.5l_p)}{l^2/3} \\ \therefore \frac{\varphi_u}{\varphi_y} &= \frac{l^2(\mu - 1)}{3l_p(l - 0.5l_p)} \end{aligned} \quad (11.40)$$

For example, if $\mu = 4$ the required φ_u/φ_y values from Eq. 11.40 are:

l_p/l	0.05	0.1	0.15	0.20	0.25	0.30	0.35
φ_u/φ_y	20.5	10.5	7.2	5.6	4.6	3.9	3.5

Since the equivalent length of the plastic hinge l_p is typically in the range 0.5 to 1.0 times the member depth (see Section 6.6.4), it is evident that the φ_u/φ_y ratio required for a cantilever column will generally exceed the Δ_u/Δ_y ratio and that if the equivalent plastic hinge length is a small proportion of the length l , the φ_u/φ_y demand will be particularly high. On the other hand, for squat shear walls in which the height l to depth ratio is such that the equivalent

plastic hinge length is about 0.3 of the height, the curvature and displacement ductility factors will be of the same order.

In the more complex case of a multistory frame, the ϕ_u/ϕ_y ratio required of members, designed according to present code seismic loading, has not yet been clearly established. The relationship between displacement and curvature ductilities is complex because for most multistory frames, yielding will not occur at the critical sections at the same load, and the distribution of inertia loads is more complicated than the distribution of static loads recommended by codes. Some attempts at relating Δ_u/Δ_y and ϕ_u/ϕ_y ratios for multistory frames are discussed in the following sections.

11.6.4 Determining Curvature Ductility Demand of Multistory Frames Using Static Collapse Mechanisms

Assumptions

An approximate assessment of the order of curvature ductility required of multistory frames to achieve a given displacement ductility factor can be made on the basis of static collapse mechanisms and simplifying assumptions. We consider a framed structure (Fig. 11.25) that is subjected to both gravity

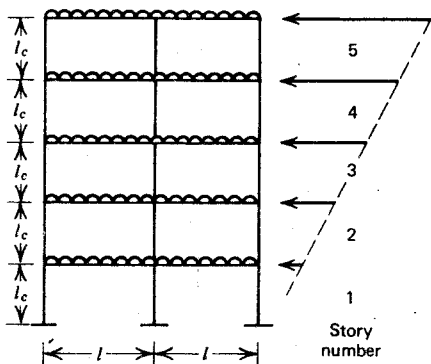


Fig. 11.25. Frame with gravity and seismic loading.

and seismic loading while responding to an acceleration pulse of an earthquake. The following assumptions are made.^{11.27}

1. The sections of the frame will have bilinear moment-curvature characteristics as in Fig. 11.26, but not necessarily with the same M_u , ϕ_y , or ϕ_u values. For beams, the values of these quantities will depend on the section properties; for columns, however, the level of axial load at the commencement of yielding will also have an influence. This assumption ignores the

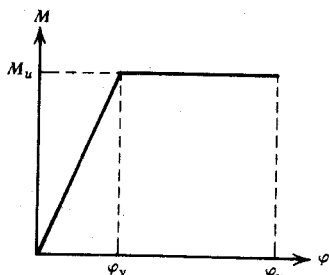


Fig. 11.26. Assumed moment-curvature relationship.

greater flexural rigidity of members that have not cracked and the greater flexural rigidity between cracks. Therefore, the elastic deformations due to flexure will be somewhat overestimated.

2. Only the deformations of the members due to flexure will be considered. This is a reasonable assumption for framed structures lacking deep members and for frames having no extensive diagonal tension cracking. The neglect of displacements due to shear will compensate to some extent for the overestimate of elastic flexural displacements.

3. When the seismic loading on the frame is increased until yielding occurs, yielding will commence at all the critical sections at the same load and at sufficient sections to form a mechanism. This condition will rarely occur in practice because of variations in the actual strengths of the steel and the concrete, differences between the approximate triangular code-specified seismic loading and the actual distribution of inertia loading induced in the structure by an earthquake, and the various factors affecting the strength of members as discussed in Chapter 1. However, the assumption will enable a reasonably simple solution to be obtained.

Lateral Displacement at First Yield

Figure 11.27 shows the curvature distribution in a typical column, when the lateral loading has increased to the extent of just causing yield in the frame. This curvature distribution in the column follows the shape of the bending moment diagram because the moments are still in the initial linear region of the moment-curvature relationships. The curvature in the columns will differ from story to story because of different section properties and axial load levels. The lateral deflection at any level of the columns relative to the ground may be calculated by taking moments about that level of the curvature diagram below that level. Let the stories of the frame be numbered $1, 2, 3, \dots, i, \dots, r, \dots$, from the bottom. Noting that both positive and negative curvatures are present in the column, the lateral deflection at the top of the r th story at

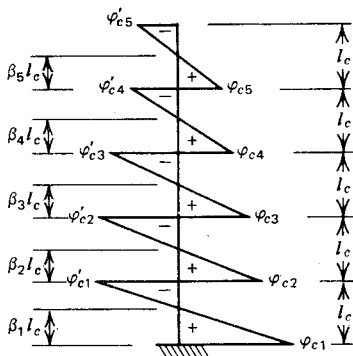


Fig. 11.27. Curvature distribution in a typical column at first yielding in the frame.

first yield relative to the bottom of the structure is

$$\begin{aligned}
 \Delta_y = & \varphi_{c1} l_c \left(r l_c - \frac{l_c}{2} \right) - \varphi_{c1} \left(1 + \frac{1 - \beta_1}{\beta_1} \right) \frac{l_c}{2} \left(r l_c - \frac{2 l_c}{3} \right) \\
 & + \varphi_{c2} l_c \left(r l_c - \frac{3 l_c}{2} \right) - \varphi_{c2} \left(1 + \frac{1 - \beta_2}{\beta_2} \right) \frac{l_c}{2} \left(r l_c - \frac{5 l_c}{3} \right) + \dots \\
 & + \varphi_{ci} l_c \left[r l_c - \left(i - \frac{1}{2} \right) l_c \right] - \varphi_{ci} \left(1 + \frac{1 - \beta_i}{\beta_i} \right) \frac{l_c}{2} \left[r l_c - \left(i - \frac{1}{3} \right) l_c \right] + \dots \\
 & + \varphi_{cr} \frac{l_c^2}{2} - \varphi_{cr} \left(1 + \frac{1 - \beta_r}{\beta_r} \right) \frac{l_c^2}{6} \\
 = & \frac{l_c^2}{6} \sum_{i=1,2,\dots,r} \frac{\varphi_{ci}}{\beta_i} [6\beta_i(r - i + 0.5) - 3(r - i) - 1] \quad (11.41)
 \end{aligned}$$

where $\varphi_{c1}, \varphi_{c2}, \dots, \varphi_{ci}, \dots, \varphi_{cr}$ are the column curvatures at the bottom of the 1st, 2nd, \dots , i th, \dots , r th story when yield is first reached in the frame, and $\beta_1, \beta_2, \dots, \beta_i, \dots, \beta_r$ refer to the positions of the points of contraflexure in those stories. When taking moments of the curvature diagrams to obtain Eq. 11.41, the curvature distribution in each story has been treated as if composed of a rectangular block and a triangular block, as illustrated in Fig. 11.28 for story i . That is, the contribution of that story to the deflection is equal to the moment of rectangle $BCDE$ minus the moment of triangle ACD , both taken about the top of the r th story.

If it is assumed that the points of contraflexure occur at 0.6 of the column height from the bottom of the columns of the bottom story, and at mid-height in the columns of all other stories, then

$$\beta_1 = 0.6 \quad \text{and} \quad \beta_2 = \beta_3 = \dots = \beta_r = 0.5$$

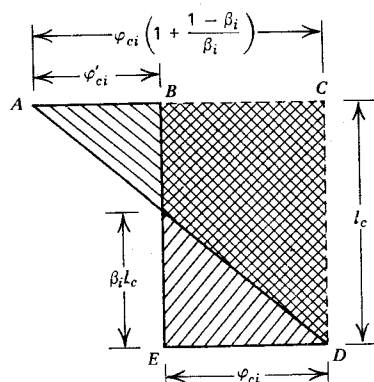


Fig. 11.28. Curvature distribution in column of story i .

and from Eq. 11.41 the deflection at the top of the r th story at first yield relative to the bottom of the structure becomes

$$\Delta_y = \frac{l_c^2}{6} \left[\varphi_{c1} \left(r + \frac{1}{3} \right) + \varphi_{c2} + \varphi_{c3} + \cdots + \varphi_{cr} \right] \quad (11.42)$$

Lateral Displacement in the Postelastic Range and Curvature Ductility Requirement

The lateral displacement that occurs after yielding commences is due to rotation at the plastic hinge positions. Two possible types of collapse mechanism may develop.

CASE 1 COLUMN SIDESWAY MECHANISM

If yielding has commenced at the critical sections of the columns before the beams reach yield curvature, then we have in Eq. 11.41 $\varphi_{c1} = \varphi_{yc1}$, $\varphi_{c2} = \varphi_{yc2}$, ..., $\varphi_{cr} = \varphi_{ycr}$, where $\varphi_{yc1}, \dots, \varphi_{ycr}$ are the yield curvatures in columns 1, ..., r , respectively. In this case further deflection will take place at constant lateral load by plastic deformation at the critical sections of the columns. In the worst case, this further deflection may occur because of a column sidesway mechanism developing in only one story, since the columns of the other stories are stronger. In Fig. 11.29, which shows the mechanism developing only in the i th story, only the plastic deformations are illustrated. All the postelastic deformation that occurs is due to the plastic rotations at the hinges in the columns of the critical story. The distribution of curvature in a typical column of the i th story when the ultimate curvature is reached at both hinges in the column is plotted in Fig. 11.30. In general, the plastic rotation permissible at the column hinges, θ_{pc} , is either $(\varphi'_{uci} - \varphi'_{yci})l'_{pc}$ or $(\varphi_{uci} - \varphi_{yci})l_{pc}$, whichever is least, where φ'_{uci} and φ_{uci} are the ultimate curvatures at the top

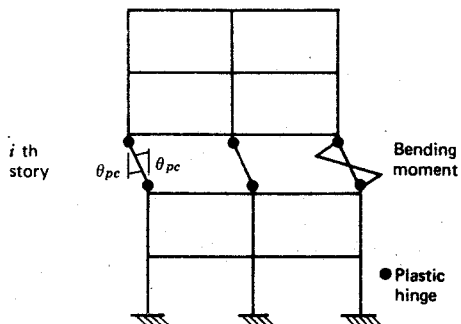


Fig. 11.29. Column sidesway mechanism in i th story.

and the bottom of the i th-story column, φ'_{uci} and φ_{yci} are the yield curvatures at the top and the bottom of the i th-story column, and l'_pc and l_{pc} are the equivalent plastic hinge lengths.

The lateral deflection at the top of the i th story when the ultimate curvature is reached in the i th story columns for this mechanism is

$$\Delta_u = \Delta_y + \theta_{pc}[l_c - 0.5(l_{pc} + l'_pc)] \quad (11.43)$$

Therefore, the displacement ductility factor is given by Eqs. 11.37 and 11.43, as

$$\mu = 1 + \frac{\theta_{pc}}{\Delta_y} [l_c - 0.5(l_{pc} + l'_pc)] \quad (11.44)$$

where Δ_y is given by Eq. 11.41 and θ_{pc} is either $(\varphi'_{uci} - \varphi'_{yci})l'_pc$ or $(\varphi_{uci} - \varphi_{yci})l_{pc}$, whichever is least; here the terms with a prime apply to the plastic hinge at the top of the column and the terms without a prime apply to the plastic

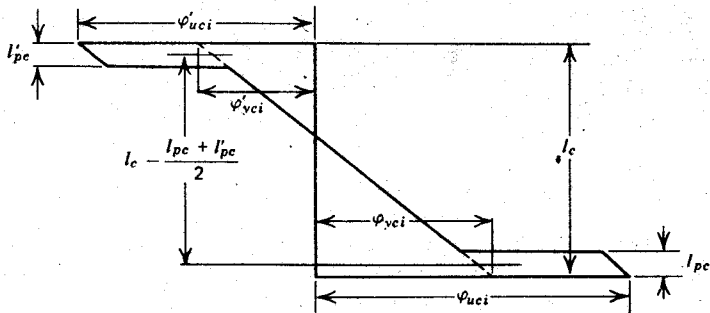


Fig. 11.30. Curvature distribution in a typical column at first yielding in frame.

hinge at the bottom of the column. For example, if the required ductility factor μ is 4, $l_{pc} = l'_{pc} = 0.7h$ where h = column depth, $l_c = 8h$, $\beta_1 = 0.6$, $\beta_2 = \beta_3 = \dots = \beta_i = \dots = \beta_r = 0.5$, and $\varphi_{yc1} = \varphi_{yc2} = \dots = \varphi_{yci} = \dots = \varphi_{ycr}$, Eq. 11.44 indicates that the requirement is $\varphi_{uci}/\varphi_{yci} = 12.54r - 3.2$, where r is the number of the story to the top of which the deflections are being measured. It is evident that very large curvature ductility factors of column sections are required if this mechanism develops, particularly in tall buildings. For instance, for the example given, the requirement for the column curvature ductility factor would be $\varphi_{uci}/\varphi_{yci} = 122$ if $r = 10$, or 34 if $r = 3$. It is also to be noted that for the same example, the requirement for $\varphi'_{uci}/\varphi'_{yci}$ would be more severe than that for $\varphi_{uci}/\varphi_{yci}$ if the mechanism forms in the columns of the first story, but identical if the mechanism forms in any other story of the frame.

In Eq. 11.44, the displacement ductility factor μ has been taken as the ratio of ultimate to yield displacements relative to the ground. If for the top story $\mu = 4$, Eq. 11.44 shows that for stories below the top of the frame (but above the plastic hinges) μ will be greater than 4, since for the lower stories Δ_y is smaller. If for an n -story building an average μ value of 4 is required for all stories, and if the plastic hinges develop in the columns of the bottom story, $r = 0.5n$ should be substituted into Eq. 11.44 to find the required curvature ductility factor. This is because the center of mass of the building will be below half the height, and if the required μ value of 4 is obtained at about half the building height, a reasonable approximation for the displacement ductility factor of the building as a whole is obtained. If the plastic hinges develop in higher columns, the curvature ductility factor will have to be higher, however.

It is evident that the curvature ductility factor available from column sections will generally be insufficient to meet the ductility demand of a column sidesway mechanism if the frame is several stories high.

CASE 2 BEAM SIDESWAY MECHANISM

If yielding has commenced at the critical sections of the beams before the columns reach yield curvature, further lateral deformation will take place at constant lateral load by plastic deformation at plastic hinges in the beams. It will also be necessary to develop a plastic hinge at the base of each column, but the remainder of the columns can remain elastic. Figure 11.31 displays the resulting beam sidesway mechanism. Only the plastic deformations are illustrated. Consideration of the deformations indicated in Fig. 11.31 shows that at the base of each column, the plastic rotation is

$$\theta_{pc} = \frac{\Delta_u - \Delta_y}{rl_c} \quad (11.45)$$

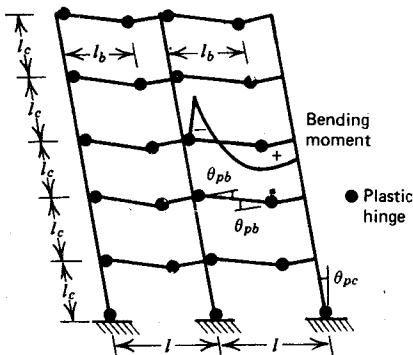


Fig. 11.31. Beam sidesway mechanism.

Figure 11.32 details the geometry of the plastic deformation of the beams and columns. Since the deformations are small, the plastic rotations in the beams and at the base of each column can be related as follows

$$\delta = l\theta_{pc} = l_b\theta_{pb}$$

And on substituting θ_{pc} from Eq. 11.45, we have

$$\theta_{pb} = \theta_{pc} \frac{l}{l_b} = \frac{\Delta_u - \Delta_y}{rl_c} \frac{l}{l_b} \quad (11.46)$$

In Eqs. 11.45 and 11.46, the lateral displacements are measured to the top of the r th story relative to the ground. Also, in these two equations rl_c has been written as an approximation for $rl_c - 0.5l_{pc}$; but since l_{pc} is small compared with rl_c , the approximation is justified. Rearranging Eq. 11.46 shows that the lateral displacement at the top of the r th story, relative to the ground at ultimate curvature, may be written in terms of the rotation of the beam hinges as

$$\Delta_u = \Delta_y + \frac{rl_c l_b}{l} \theta_{pb} \quad (11.47)$$

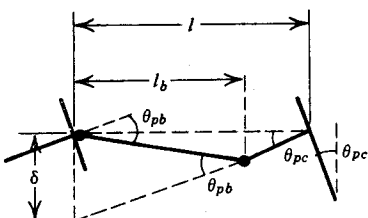


Fig. 11.32. Geometry of plastic deformations in beam sidesway mechanism.

where θ_{pb} is either $(\varphi'_{ub} - \varphi'_{yb})\Sigma l'_{pb}$ or $(\varphi_{ub} - \varphi_{yb})l_{pb}$, whichever is least, where the terms in the equations for θ_{pb} with a prime refer to the positive moment plastic hinges and the terms without a prime refer to the negative moment plastic hinges. The positive moment plastic hinges are seldom critical because of the greater total equivalent plastic hinge lengths ($\Sigma l'_{pb}$ = sum of equivalent plastic hinge lengths each side of the critical section) and the more ductile section primarily attributable to the presence of a compression flange (due to the slab). Therefore θ_{pb} is generally limited by the negative moment plastic hinge.

Also, in terms of the plastic hinges at the bases of the columns, we have from Eq. 11.45

$$\Delta_u = \Delta_y + rl_c \theta_{pc} \quad (11.48)$$

where $\theta_{pc} = (\varphi_{uc1} - \varphi_{yc1})l_{pc}$.

Hence from Eqs. 11.37 and 11.47, the displacement ductility factor in terms of the beam hinges is

$$\mu = 1 + \frac{rl_c l_b}{l} \frac{\theta_{pb}}{\Delta_y} \quad (11.49)$$

where Δ_y is given by Eq. 11.41, and θ_{pb} is generally the plastic rotation at the negative moment plastic hinge $(\varphi_{ub} - \varphi_{yb})l_{pb}$.

For example, let the required displacement ductility factor be $\mu = 4$, $l_c = 8d$ where d = effective depth of beam, $l_b = \frac{2}{3}l$, $l_{pb} = 0.7d$, $\beta_1 = 0.6$, $\beta_2 = \beta_3 = \dots = \beta_r = 0.5$, and $\alpha\varphi_{yb} = \varphi_{c1} = \varphi_{c2} = \dots = \varphi_{cr}$, where α relates the beam yield curvature and the column curvatures at that stage. Then Eq. 11.49 indicates that the required value for the curvature ductility factor in the beams $\varphi_{ub}/\varphi_{yb}$ when $\alpha = 1$ is 16.2 when $r = 3$ and 17.6 when $r = 10$. It is apparent that the required ductility of such beam sections can be obtained in practice; moreover, the required curvature ductility factor does not increase significantly when the number of stories increases. If the beams are deeper and the columns are near yield when the beams yield, $\alpha > 1$. If $\alpha = 3$, the required beam curvature ductility factor $\varphi_{ub}/\varphi_{yb}$ for the foregoing example becomes 46.7 when $r = 3$ and 50.7 when $r = 10$. This indicates the danger of having columns that are far more flexible than the beams, even if yield commences first in the beams. In addition, the requirement for $\varphi'_{ub}/\varphi'_{yb}$ will not be as severe as that for $\varphi_{ub}/\varphi_{yb}$ because a greater plastic hinge length is available at the positive moment hinge.

Also from Eqs. 11.37 and 11.48, the displacement ductility factor in terms of the hinge at the base of each column is

$$\mu = 1 + rl_c \frac{\theta_{pc}}{\Delta_y} \quad (11.50)$$

where Δ_y is given by Eq. 11.41 and $\theta_{pc} = (\varphi_{uc1} - \varphi_{yc1})l_{pc}$. For example, if the required displacement ductility factor is 4, $l_{pc} = 0.7h$ where h = column depth, $l_c = 8h$, $\beta_1 = 0.6$, $\beta_2 = \beta_3 = \dots = \beta_r = 0.5$, and $\varphi_{yc1} = \varphi_{c1} = \varphi_{c2} = \dots = \varphi_{cr}$, Eq. 11.50 indicates that the required value for the curvature ductility factor in the column bases $\varphi_{uc1}/\varphi_{yc1}$ is 11.2 when $r = 3$ and 12.1 when $r = 10$. Hence the curvature ductility required at the column bases is not as high as that required for the columns in the column sidesway mechanism.

Discussion of Results of Static Collapse Mechanism Analysis

The derived equations 11.44, 11.49, and 11.50 indicate the order of curvature ductility factor required for static lateral loading to achieve a given displacement ductility factor. Given the details of a frame, the equations could be used to assess the adequacy of a design. The column sidesway mechanism in Fig. 11.29 is dangerous because the plastic deformations may occur only in the columns of one story; in a tall building it is unlikely that sufficient curvature ductility would be available for this mechanism to survive a major earthquake. It is apparent that it is much better to ensure that the beam sidesway mechanism of Fig. 11.31 occurs, since the required ductility of the beam sections is lower and can be provided more easily. To ensure that the beam sidesway mechanism occurs, the columns should be made strong enough to avoid the formation of plastic hinges in the columns. The column bases in this mechanism would have to be carefully detailed, with transverse hoops or spirals, to develop the required plastic rotation.

The derived equations are based on the simplifying assumption that the frame reaches yield at all the plastic hinge sections simultaneously. If moment redistribution is necessary before all the plastic hinges develop, the curvature ductility required at the first hinges to form will need to be larger. Also, it has been assumed that the bending moment patterns are as obtained from the equivalent static lateral loading recommended by codes. This code static loading, such as shown in Fig. 11.25, corresponds predominantly with the first mode of vibration response. For tall buildings, the higher modes of vibration may have a significant influence and may result in a radical change in the bending moment patterns. Thus fewer plastic hinges may form simultaneously in the beams in the actual dynamic situation than the approach based on the code static loading suggests. Therefore the static approach just presented can be taken only as a guide.

Nevertheless our static analysis indicates the desirability of having strong columns, to avoid, if possible, the formation of plastic hinges in the columns (because the energy is dissipated more efficiently by plastic hinges in the beams). In general, it appears that sections at plastic hinges in beams and column bases should be capable of reaching curvature ductility factors of at least 4 times the required displacement ductility factor (i.e., $\varphi_u/\varphi_y \geq 4\mu$).

11.6.5 Determining Curvature Ductility Demand of Multistory Frames Using Nonlinear Dynamic Analyses

The foregoing approximate method based on static collapse mechanisms cannot be claimed to give an accurate assessment of the curvature ductility factor required in the complex case of a multistory frame responding nonlinearly to a major earthquake. A number of multistory frames responding nonlinearly to earthquakes have been analyzed dynamically (see, e.g., Refs. 11.28 and 11.21), but it is difficult to draw general conclusions. The number of variables involved in the nonlinear response of multistory structures is so high that no more than qualitative statements can be made at present. For example, the type of ground motion has a considerable influence, and a structure designed to develop near-uniform curvature ductilities in its members when responding to one ground motion may develop locally high curvature ductilities when responding to a different ground motion. There would appear to be a need for many more nonlinear dynamic analyses to be conducted on a range of multistory frames to give a better indication of the order of the curvature ductility factors required. Some results from available nonlinear dynamic analyses are discussed below.

Analyses of multistory frames have indicated that the displacement ductility factor of a frame is of the same order as for a single degree of freedom system having the same force-displacement characteristics and designed for the same fraction of the elastic response loading. The rotational ductility factor θ_u/θ_y of members has been obtained from such analyses, where θ_u = rotation at end of the member at the maximum response and θ_y = rotation at the end of the member at first yield. The required curvature ductility factor from such analyses can be obtained from the curvature distribution with an assumed plastic hinge length. For example, if the moments M at the ends of a member are equal but of opposite sign and the member is not subjected to transverse loads along its length (i.e., the member is in symmetrical double curvature as in Fig. 11.33), elastic theory shows that the end rotation is

$$\theta = \frac{Ml}{6EI}$$

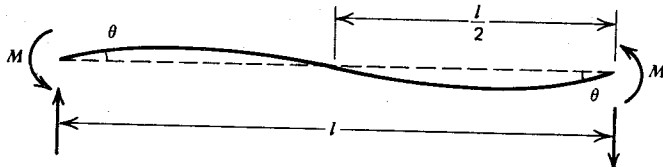


Fig. 11.33. Member in symmetrical double curvature.

where l = length of member and EI = flexural rigidity of section. When yield is just reached at the ends, $\theta = \theta_y$ and $M = M_y$, where M_y = moment at first yield. The yield curvature is $\varphi_y = M_y/EI$.

$$\therefore \theta_y = \frac{\varphi_y l}{6}$$

Further rotation at the ends of the member will impose plastic rotation θ_p , where

$$\theta_p = (\varphi_u - \varphi_y)l_p$$

where φ_u = curvature at end of postelastic range and l_p = equivalent length of plastic hinge. The total end rotation is then

$$\begin{aligned} \theta_u &= \theta_y + \theta_p \\ \therefore \frac{\theta_u}{\theta_y} &= 1 + \frac{\theta_p}{\theta_y} = 1 + 6 \frac{l_p}{l} \left(\frac{\varphi_u}{\varphi_y} - 1 \right) \\ \therefore \frac{\varphi_u}{\varphi_y} &= 1 + \frac{l}{6l_p} \left(\frac{\theta_u}{\theta_y} - 1 \right) \end{aligned} \quad (11.51)$$

For example, if $\theta_u/\theta_y = 8$ and $l_p/l = 0.1$, Eq. 11.51 gives $\varphi_u/\varphi_y = 12.7$. Higher φ_u/φ_y values arise from smaller l_p/l ratios. Transverse loading on members will cause the symmetry of deformation of the member to change, and the yield rotation θ_y will change from the value just calculated making the definition of θ_y more difficult. Nevertheless, the required φ_u/φ_y values corresponding to given moment patterns and plastic deformations can be found. It is evident that the curvature ductility factor φ_u/φ_y is a far more meaningful index for member ductility than the rotational ductility factor θ_u/θ_y because the dependence of θ_y on the loading as well as the member properties means that no unique expression for θ_y can be written.

For the case of symmetrical deformation illustrated in Fig. 11.33, dynamic analyses of frames have often found rotational ductility factors θ_u/θ_y of members of about twice the displacement ductility factor, in the case of well-proportioned frames. However, the presence of weak stories will result in a rotational ductility demand in those stories many times greater than for well-proportioned frames.

The concentration of ductility demand in weak parts of structures, shown both by nonlinear dynamic analyses and by the static collapse mechanism approach, points to an extremely important principle in seismic design. In ordinary design for static loads, the presence of overstrong parts of the structure will never decrease the strength of the structure. In seismic design, however, when a structure relies on energy dissipation by ductile plastic hinges to survive earthquakes, the presence of overstrong parts of the structure will

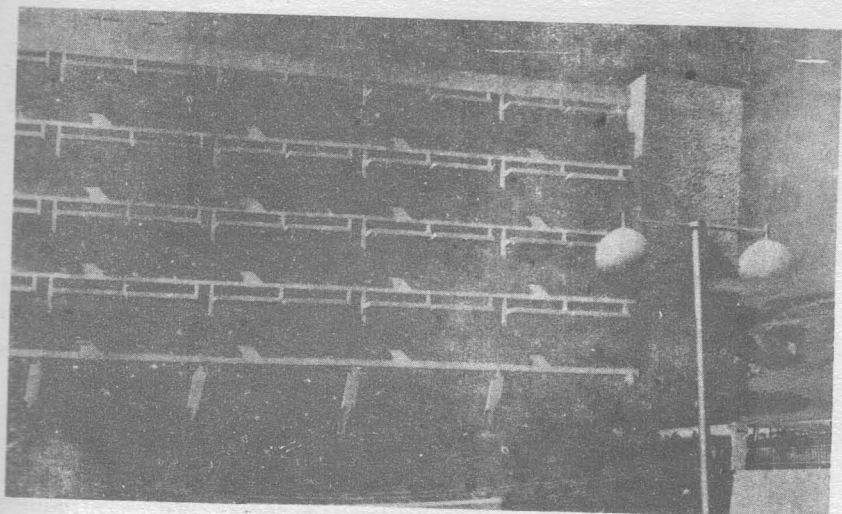
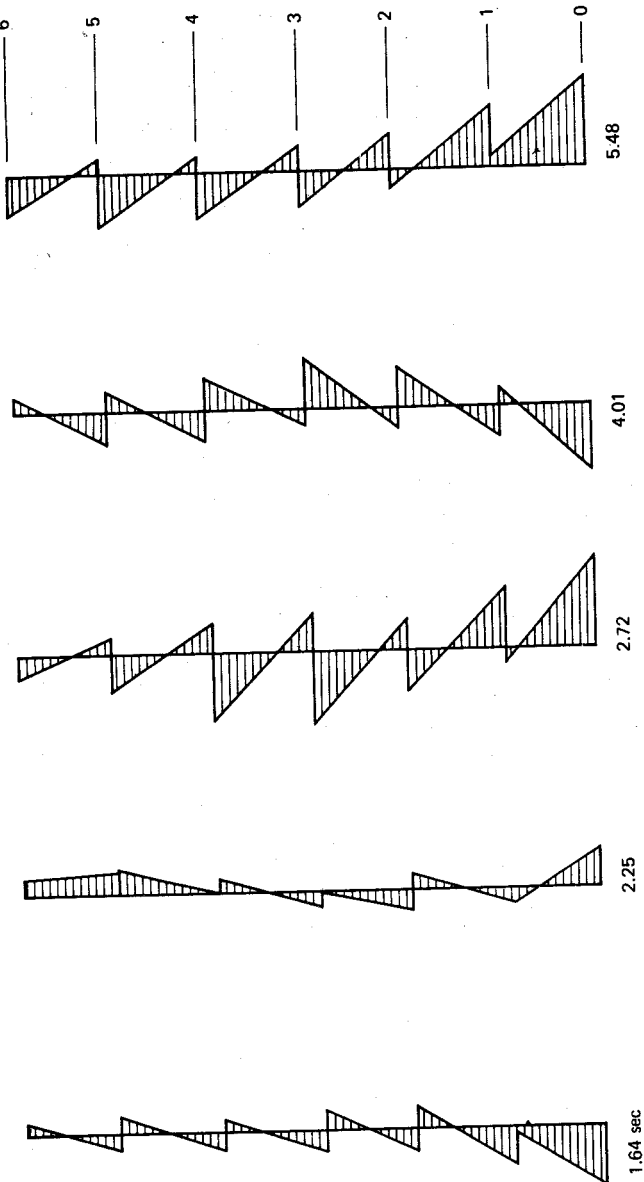


Fig. 11.34. Part of Olive View Hospital after the 1971 San Fernando earthquake.

mean that the curvature ductility demand is concentrated into local regions of the structure and may lead to collapse because of the very high inelastic deformations enforced there. Note that a weak part of a structure acts as a fuse. Once the strength of that part of the structure is reached (e.g., in the case of a column sidesway mechanism), the rest of the frame may remain in the elastic range. Weak parts of structures may be attributable to underdesign of that part of the structure and/or overdesign of other parts of the structure. Thus in seismic design dangers exist from both understrong and overstrong elements. A common cause of overstrength is the presence of walls that have not been accounted for in the structural response. The presence of walls in some stories only could enforce a column sidesway mechanism to form in other stories. For example, if a building's first floor is open and its upper stories are enclosed by walls, damage could concentrate in the first story. To avoid this problem, separation gaps between such walls and the structural elements could be used. For a recent example of damage concentrating mainly in one story of a structure, consider the Olive View Hospital after the 1971 San Fernando earthquake in California (see Fig. 11.34). In this structure shear walls and columns were present in the upper four stories. In the first story the resistance to lateral loading came only from the columns, and the damage concentrated mainly in the columns of that story. The permanent lateral displacement of the structure after the earthquake, which was almost 2 ft (0.6 m), was due almost entirely to deformations in the first story. Examples

Fig. 11.35. Bending moments in columns of a 12-story frame responding nonlinearly to El Centro earthquake 1940 N-S component.^{11,29}



of tied and spiral columns from this story are illustrated in Fig. 5.7, and it is apparent that only extremely well-confined concrete is capable of deforming to this extent and maintaining load-carrying capacity. Figures 11.34 and 5.7 illustrate another point regarding earthquake damage. Columns are much more difficult to repair than beams because the structure has to be straightened and propped during the repair. Extensive column damage may mean the structure has to be demolished, as was the case of Olive View Hospital.

Nonlinear dynamic analyses also indicate that unexpected distributions of bending moment may occur in columns of multistory frames, compared with the distribution obtained from static code lateral loading. Static lateral load analysis indicates that points of contraflexure exist generally close to mid-height of the columns, unless the beams are much more flexible than the columns, except in the stories near the top and bottom of the frame. However, nonlinear dynamic analysis suggests that at certain times during the response of the structure to earthquake ground motions, the point of contraflexure in a column between floors may be close to the beam-column joint, and the column may even be in single curvature at times. Some column bending moment diagrams (Fig. 11.35) were obtained by Kelly^{11,29} for a 12-story frame designed according to the New Zealand seismic loading code responding to the N-S component of the El Centro 1940 earthquake. The analysis, a step-by-step procedure through the time history of the earthquake, solved directly for the incremental displacement and took into account the elasto-plastic behavior of the members. The reason for the unexpected distribution of column bending moments at some instants of time is the strong influence of the higher modes of vibration, particularly the second and third modes. Deflected shapes of a vibrating frame are approximated in Fig. 11.36. Code static lateral loading normally has a triangular distribution corresponding

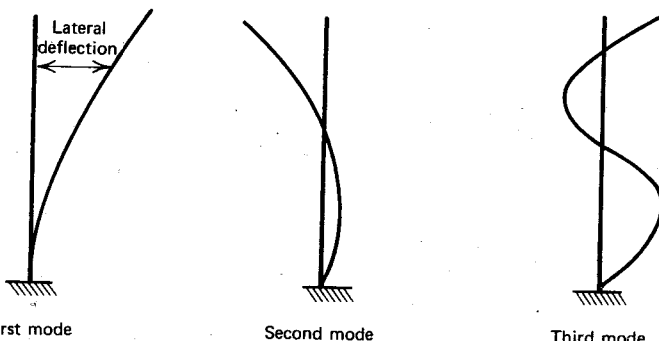


Fig. 11.36. Approximate modal shapes of vibrating frame.

to lateral loads varying linearly from zero at the column base to a maximum at the top of the structure, sometimes with an additional concentrated load at the top. This load distribution corresponds approximately to the fundamental (first) mode of vibration. If the other modes of vibration are significant, it is evident that the distribution of inertia loads on the structure at certain instants could differ appreciably from that assumed and result, for example, in the distribution of bending moments shown in Fig. 11.35. The shift of the point of contraflexure in the columns to well away from the mid-height position in some cases means that the column moments induced may be very much higher than the moment obtained from a static lateral load analysis and may lead to plastic hinges forming in the columns.

Dynamic analysis also indicates that plastic hinges are not generally present in all beams at the same interval of time. The development of plastic hinges tends to move up the frame in waves involving a few stories at a time, but there may be instants in low-rise buildings when all beams have plastic hinges formed simultaneously.

11.6.6 Additional Factors in Analysis for Ductility

Rate of Loading Effects

Since earthquake loads are dynamic, it is necessary to consider the effect of rapid loading on a structure. Extremely rapid loading can result in a significant increase in the strength of both concrete and steel. Table 11.2

Table 11.2 Effect of Strain Rate on Material Strength^{11.30}

Average Strain rate in/(in)(sec) [mm/(mm)(sec)]	Ratio of Strength to Static Strength		
	Concrete $f'_c = 2500 \text{ psi}$ (17.2 N/mm ²)	Concrete $f'_c = 6500 \text{ psi}$ (44.8 N/mm ²)	Steel Lower Yield Point $f_y = 45, 51, \text{ and } 57 \text{ ksi}$ (310, 352, and 393 N/mm ²)
0.001	1.05	1.11	1.02–1.05
0.01	1.17	1.16	1.07–1.14
0.1	1.39	1.23	1.16–1.21
1.0	1.62	1.40	1.25–1.28

summarizes some data presented by an ACI report^{11.30} and indicates the effect of rate of strain on the compressive strength of concrete and the lower yield strength of steel. A range of strain rates can be caused by earthquake

motions, depending on the period of vibration of the structure and the ductility demand. For structures having a small period of vibration and a high ductility demand, the strain rates are surprisingly high and may result in significant strength increase of the materials. For example, Fig. 11.37 presents an idealized stress-time plot for a steel reinforcing bar at a plastic hinge in a flexural member for a period of vibration T seconds long. If the

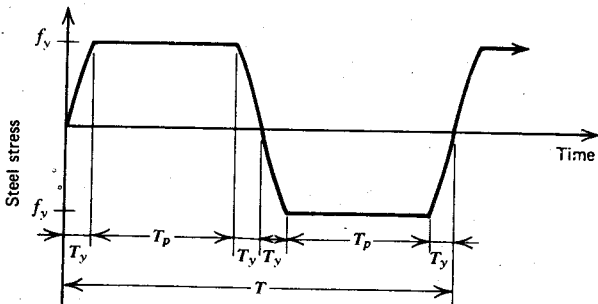


Fig. 11.37. Idealized stress-time history for a reinforcing bar.

curvature ductility demand is high, the time in the plastic range in the half-cycle T_p may considerably exceed the time required to load to yield T_y ; therefore, T_y may be small. In an extreme case, if $T_p = 15T_y$ and $T = 0.1$ sec, it is evident that $T_y = 0.1 \times 1/34 = 0.0029$ sec. For steel with a yield strength of 60 ksi (414 N/mm^2) and a modulus of elasticity of $29 \times 10^6 \text{ psi}$ ($200,000 \text{ N/mm}^2$), the strain at yield is $60,000/29 \times 10^6 = 0.00207$, and the average strain rate during interval T_y in our example would be $0.00207/0.0029 = 0.71$ in per in/second, which would certainly cause a significant strength increase, as Table 11.2 indicates. However, it is customary in design to ignore any strength increase due to strain rate. It should be borne in mind that neglect of such strength increase is not necessarily a conservative step for small period structures with high ductility demands.

Reversed Load Effects on Structures

Frames subjected to severe earthquake motions will undergo several reversals of loading well into the inelastic range during an earthquake. The moment-curvature relationships at the critical sections of frames under repeated reversed loading into the yield range are usually assumed to be bilinear elastoplastic (as in Fig. 11.38) in dynamic studies of frame behavior. It should be noted, however, that the actual behavior of reinforced concrete

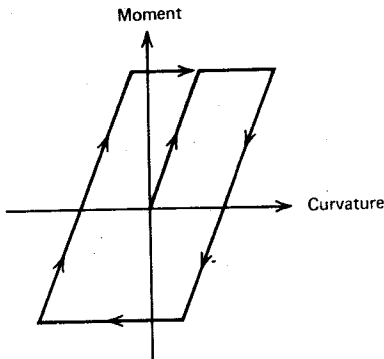


Fig. 11.38. Idealized bilinear elastoplastic behavior.

members is quite different from this assumed elastoplastic relationship. In particular, a significant reduction in stiffness occurs with reversed loading. The reduction in stiffness does not prevent a properly detailed member from reaching its design flexural strength, but the deformation at which the flexural strength is reached is increased. A reduction in stiffness resulting from inelastic deformation will cause an increase in the period of vibration of the structure, which will alter its response to the earthquake.

The behavior of members subjected to cyclic (reversed) bending moment was discussed in Section 6.7, and theoretical moment-curvature relationships were obtained. Discussion of the effect of cyclic flexure on shear and bond has also been presented previously. The factors that affect the load-deflection relationships of members subjected to large reversed inelastic deformations, may be summarized as follows:

1. The inelastic behavior of the steel reinforcement. Steel with reversed loading in the yield range shows the Bauschinger effect, in which the stress-strain curve becomes nonlinear at a much lower stress than the initial yield strength (see Section 2.2.4 and Figs. 2.27 to 2.29).
2. The extent of cracking of concrete. The opening and closing of cracks will cause a deterioration of the concrete, hence will result in stiffness degradation. The larger the proportion of load carried by the concrete, the larger the stiffness degradation.
3. The effectiveness of bond and anchorage. A gradual deterioration of bond between concrete and steel occurs under high-intensity cyclic loading.
4. The presence of shear. High shear forces will cause further loss of stiffness because of increased shear deformation in plastic hinge zones under reversed loadings.

The influences of some of these factors on the stiffness of a doubly reinforced beam may be seen with reference to Fig. 11.39. When the beam is loaded

downward well into the postelastic range of the tension steel, the large cracks in Fig. 11.39a will not close completely on unloading but will remain open, as in Fig. 11.39b, because of the residual plastic strains in the steel. If the member is then loaded in the opposite direction, as in Fig. 11.39c, the resistance to rotation will be less than that during the first loading because the presence of open cracks in the compression zone means that the whole of the compression is carried by the compression steel. Thus the flexural rigidity of the section is only that of the steel, and this is further reduced when the compression steel reaches the stress level at which the Bauschinger effect commences and behaves inelastically. The cracks in the compression zone may eventually close, as in Fig. 11.39d, depending on the magnitude of the load and the relative amounts of top and bottom steel. When the cracks close, the stiffness of the member increases, since at that time some compression

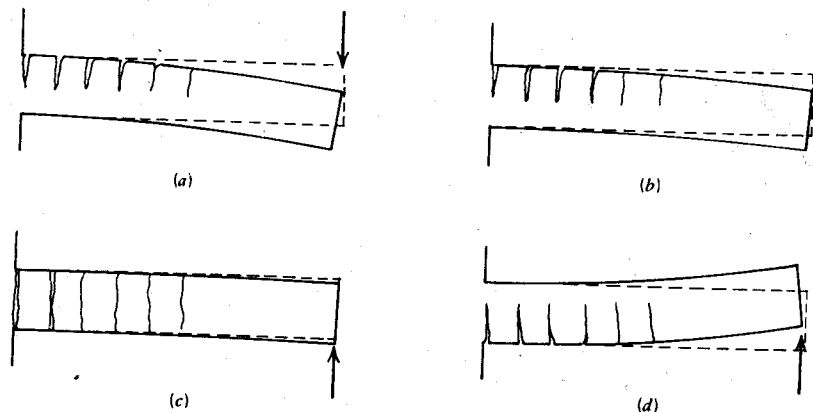


Fig. 11.39. Effect of reversed load on reinforced concrete cantilever beam. (a) At end of first loading. (b) After unloading. (c) At start of reversed loading. (d) At end of reversed loading.

is again transferred by the concrete. If the cracks do not close and the member is unloaded, the critical section may be cracked throughout its whole depth. The width of this full-depth cracking will depend on the amount of yielding and the effectiveness of the bond. If the member is then loaded down, the member will initially act again as a steel beam, since the concrete is not in contact at the face of the crack.

The opening and closing of cracks in zones that alternate between tension and compression may eventually lead to a deterioration in the compressive strength of the concrete because the faces of the crack might not come into even contact, owing to slight relative lateral movement or debris in the crack.

Another cause for deterioration of strength and stiffness is the presence of full-depth cracking at a section, since under these conditions the whole shear force at the section must be carried by dowel action of the main reinforcement and by greatly diminished aggregate interlock shear. It was pointed out in Chapter 7 that significant shear transfer by dowel action is associated with large shear displacements (see Fig. 7.30). These will cause longitudinal splitting of the concrete along the flexural bars and will lead to further loss of bond and consequent stiffness degradation. If the shear force to be transferred across the plastic hinge region is large, the phenomenon discussed may lead to a failure by sliding shear along a continuous wide crack across the critical section. Additional web reinforcement will do little in alleviating this situation.

The effect of the opening and closing of cracks, and the Bauschinger effect of the steel, on the moment-curvature relationship for a doubly reinforced section is illustrated in Fig. 11.40. The rounding and pinching in of the loop

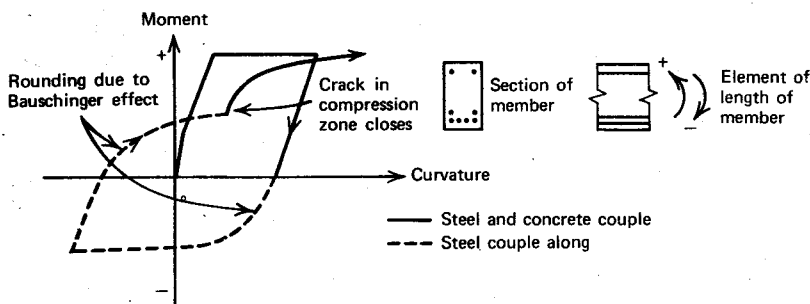


Fig. 11.40. Moment-curvature relationship for doubly reinforced section with reversed flexure.

indicates that the often-used elastoplastic idealization of Fig. 11.38 is no more than a crude assumption. The rounding and pinching of the loops means that the area within the loops is smaller than the corresponding area based on the elastoplastic assumption; thus there will be less energy dissipation per cycle than normally assumed. This will influence the response of frames to severe earthquake motions. Realistic dynamic analyses should be based on more accurate moment-curvature loops. For beams, a better idealization would be a Ramberg-Osgood type of response, suggested by Jennings,^{11.31} or the degrading stiffness response suggested by Clough^{11.26} (see Fig. 11.41). The Ramberg-Osgood skeleton curve is defined by the equation

$$\frac{\phi}{\phi_{ch}} = \frac{M}{M_{ch}} \left(1 + \left| \frac{M}{M_{ch}} \right|^{r-1} \right) \quad (11.52)$$

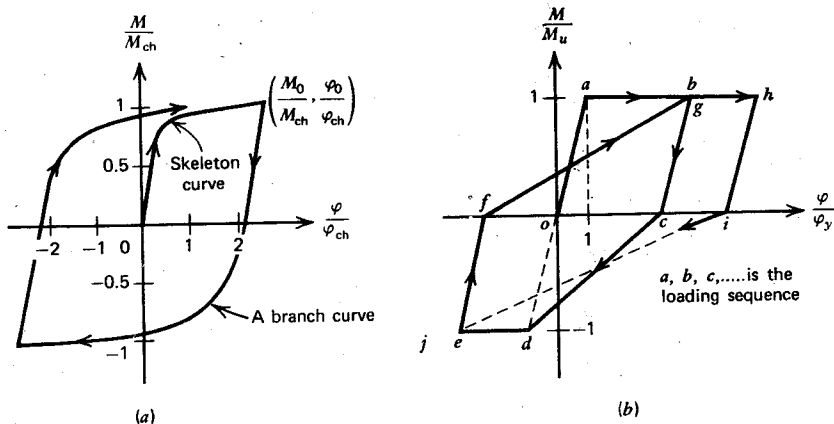


Fig. 11.41. Idealized moment-curvature relationships. (a) Ramberg-Osgood relationship. (b) Clough's degrading stiffness relationship.

where φ_{ch} , M_{ch} , and r are empirical parameters defining the skeleton curve. The branch curve commencing from a point with coordinates M_0/M_{ch} , φ_0/φ_{ch} is given by

$$\frac{\varphi - \varphi_0}{2\varphi_{ch}} = \frac{M - M_0}{2M_{ch}} \left(1 + \left| \frac{M - M_0}{2M_{ch}} \right|^{r-1} \right) \quad (11.53)$$

The degrading stiffness curve of Clough assumes that the stiffness on loading in each cycle is dependent on the deformation reached in the previous cycle. This model was based on observed test results. For beams having significantly different top and bottom steel areas, and for columns, the pinching effect is more marked, and a loop whose enclosed area is even smaller than the idealizations of Fig. 11.41b may be necessary.

The shape of the moment-curvature loops illustrated in Figs. 11.40 and 11.41 indicates that the deformation when yielding commences changes from cycle to cycle. The displacement ductility factor, as previously defined, is the ratio of the maximum displacement to the displacement at first yield. That is, the displacement when yielding commences in the first yield excursion is used as the reference displacement, not the displacement when yielding commences in each cycle. The same type of definition applies to curvature and rotational ductility. This allows the ductility factor to clearly indicate the maximum deformation.

Clough^{11.26} in studies of single degree of freedom systems compared simple structures with elastoplastic and degrading stiffness properties. For long period structures it was found that the degrading stiffness property

does not significantly affect the initial amplitudes of vibration during earthquakes, but the loss of stiffness caused by the large yield displacements reduced the subsequent displacement response of the degrading stiffness structure. However, short period structures ($T = 0.3$ sec) having degrading stiffness properties were found to have significantly larger displacement ductility requirements than the corresponding elastoplastic structure. Thus degrading stiffness properties may not materially affect the earthquake resistance of long period multistory frames; indeed the loss of stiffness reduces the subsequent response of frames. However the resistance of short period structures may be reduced by degrading stiffness behavior. The reason for this may be seen from Fig. 11.20. A reduction in stiffness will cause an increase in period which for a long period structure will cause a reduction in the response acceleration but for a short period structure may cause a substantial increase in the response acceleration.

The degradation of stiffness of frames under reversed lateral loading has been observed during tests. A one-fifth scale model of a one bay by one bay six-story building structure (Fig. 11.42) tested at the University of

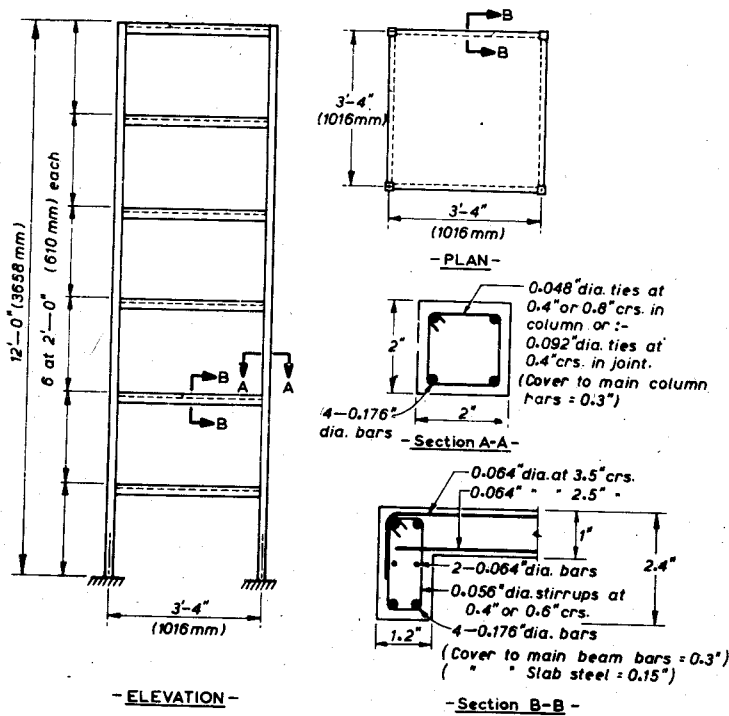


Fig. 11.42. Model reinforced concrete building structure. 11.32

Canterbury^{11,32} was designed according to the 1971 ACI code^{11,8} requirements for ductile frames in seismic zones. The design seismic loading followed the New Zealand loading code. The model structure was subjected to a gravity load of 27 lb/ft² (1290 N/m²) on each floor, in addition to its own weight, and it was subjected to reversed static loading with the distribution shown in Fig. 11.43. The structure under test appears in Fig. 11.44. The

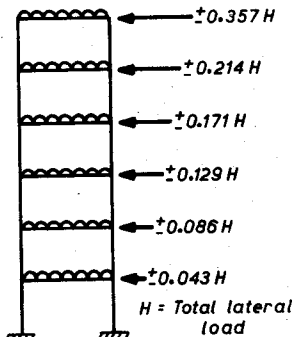


Fig. 11.43. Load on model reinforced concrete building structure.^{11,32}

curves for measured lateral load versus lateral deflection at the top of the frame (Fig. 11.45) show considerable degradation of stiffness during the cycles of lateral loading. The slope of lines connecting the extremities of the load-deflection loops indicates that the stiffness of the frame with respect to lateral loading at the last cycle of loading was only approximately 20% of the initial stiffness. The shape of the loops is also very different from elastoplastic behavior and show rounding and pinching due to the Bauschinger effect and the closing of cracks.

In frames the shape of load-deflection hysteresis loops is also affected by shear deformations and anchorage slippage that occur in the core of beam-column joints. Beam-column joints cores are usually subjected to very high shear stresses when a frame is subjected to high-intensity lateral loading. Reversed lateral loading causes the direction of the shear stresses to alternate, and the opening and closing of diagonal tension cracks in the joint core may lead to a reduction in the shear strength and a deterioration of the shear stiffness of the joint core. Such joints need to be reinforced by transverse steel to help carry the shear and to confine the concrete. Another feature of beam-column joint behavior is the possible reduction in the effectiveness of compression reinforcement. A bar in a member passing through the joint core will be in tension on one side of the joint core and in compression on the other side, as indicated by the bending moment diagram. In the limit, the bar may be stressed to yield in tension on one side of the joint core and to

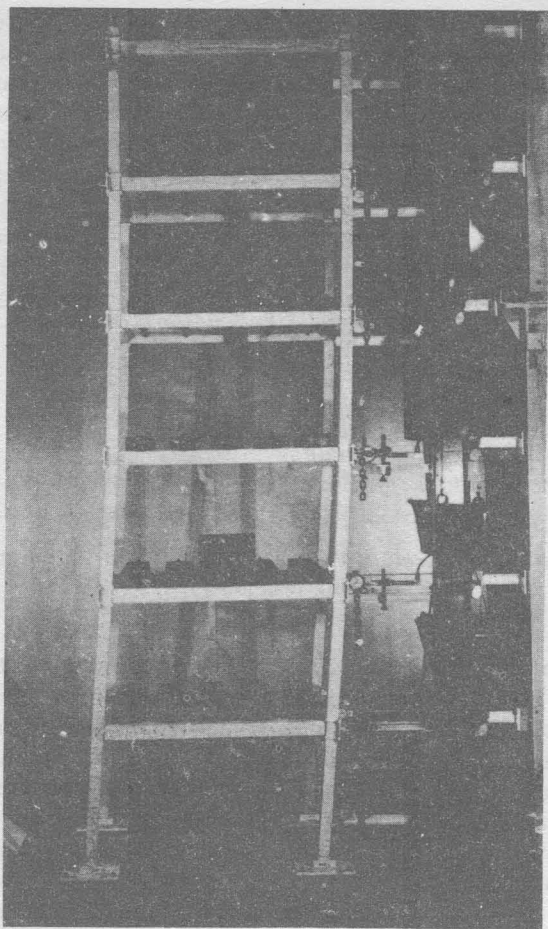


Fig. 11.44. Model reinforced concrete building structure under test.^{11.32}

yield in compression on the other side. For such a bar, twice the yield force of the bar has to be developed by bond within the joint core, which in turn requires very high bond stresses, and deterioration of bond under reversed loading may result in slip of reinforcement through the joint core. If slip occurs, the tension in the bar may become anchored in the beam on the other side of the joint core. Thus the "compression steel" in the beam at the column face may actually be in tension. This will reduce the strength, stiffness, and ductility of the section. The strength and behavior of beam-column joints under seismic load conditions are discussed in detail in Chapter 13.

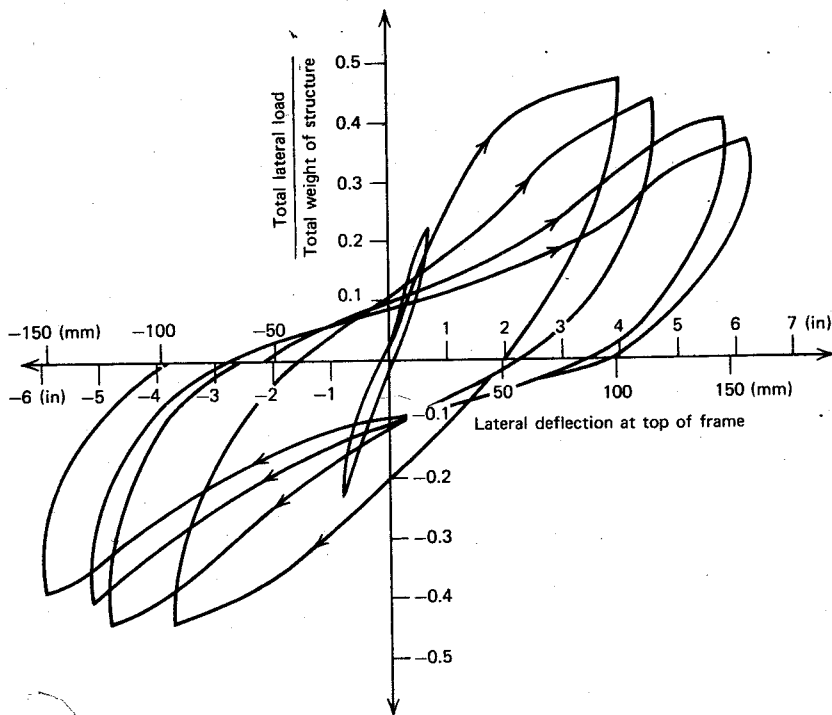


Fig. 11.45. Lateral load-deflection curves for model reinforced concrete building structure.^{11.32}

Biaxial Load Effects

Earthquake ground motions occur in random directions, but it has been the practice in seismic design to consider seismic loading to act only in the directions of the principal axes of the structure and only in one direction at a time. In fact, a general angle of seismic loading can produce a very severe condition in a building structure, and it may be extremely difficult to prevent the formation of plastic hinges in columns in the general case of loading. The effects of biaxial loading have been discussed previously by Armstrong,^{11.33} Row,^{11.34} and others.

Consider a symmetrical building structure with plan as in Fig. 11.46a subjected to lateral seismic loading in a general direction. Let a floor of the building deflect in the direction of the loading, as in Fig. 11.46b. It is evident that the angle θ need not be very large before yielding will be enforced in the beams in both directions. For example, if a displacement ductility factor

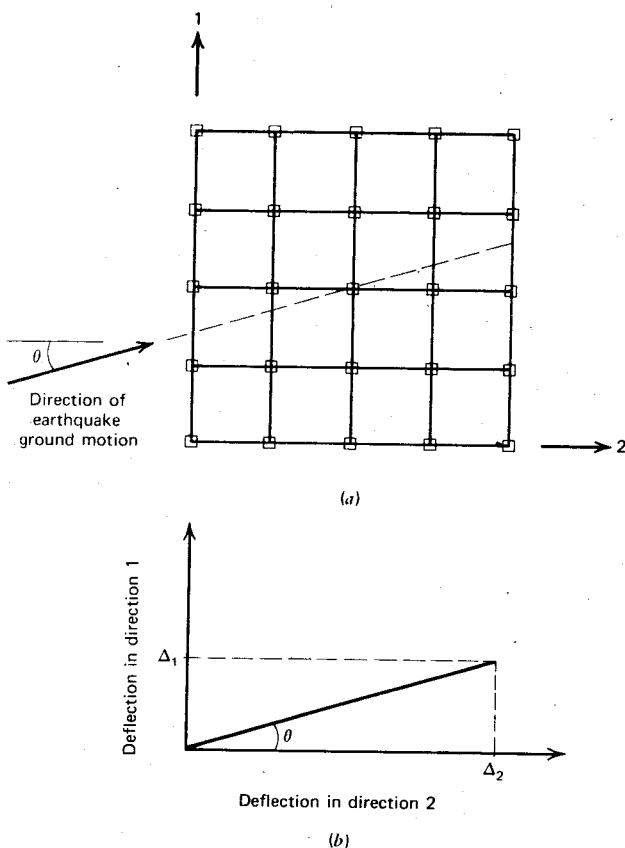


Fig. 11.46. General direction of earthquake loading on building. (a) Plan of building. (b) Horizontal deflection of a floor.

$\mu = \Delta_u/\Delta_y$ of 4 is reached by the symmetrical structure of Fig. 11.46a in direction 2, it only requires $\Delta_1 = \Delta_2/4$ to cause yielding in direction 1 as well. Thus for a displacement ductility factor of 4, the loading need only be inclined at an angle $\theta = \tan^{-1} 0.25 = 14^\circ$ to one principal axis of the building to cause yielding in both directions of a symmetrical building. Thus yielding in both directions may occur simultaneously for much of the loading. The simultaneous loading of the frames in both directions has the following effects.

1. Biaxial bending of the columns reduces the flexural strength of the columns (see Section 5.4), but the resultant moment from the beam system

applied to the column is increased. For example, if the moment applied by the beams in each direction is ΣM_{ub} , the resultant moment applied biaxially to the column will be $\sqrt{2} \Sigma M_{ub}$. This 41% increase in applied moment from the beams, combined with a reduction in the flexural strength of the column due to biaxial bending, may cause the columns to form plastic hinges before the beams, resulting in possible brittle failure and collapse.

2. The shear force acting on the columns will be higher than for yielding of the frames, in one direction only (41% higher if beams of equal strength exist in each direction). This higher shear force is to be resisted by sections loaded along a diagonal.

3. Similarly, joint cores at beam-column intersections will be acted on by higher shear forces. Also, with plastic hinging of members occurring in two directions, the confinement of the joint core provided by the surrounding beams may be less effective.

Definition of Ultimate Deformation

The definition of the ultimate deformation often causes difficulty when the available ductility of a structure or structural component subjected to seismic loading is being calculated or measured. The available ultimate deformation is not necessarily that deformation corresponding to the maximum load carrying capacity; therefore, it is not necessarily that deformation which corresponds to a particular extreme fiber compressive concrete strain or a particular steel strain. It does seem that the definition adopted for the ultimate deformation should depend on how great a reduction in load-carrying capacity can be tolerated and/or the degree of damage to the structure that can be tolerated. If damage cannot be tolerated at all (e.g., in prestigious structures or structures containing dangerous chemicals), it may be that an entirely elastic response needs to be assured and the design strengths need to be correspondingly high. At the other end of the scale, survival without collapse may be the only criterion, in which case very large strains could be tolerated, involving structural damage perhaps beyond repair, during the response. For cases in between, limiting strains or deformations could be set. Many elements and structures have a capacity for deformation beyond the peak of the load-deflection curve. When survival without collapse is the criterion, it is too conservative to define the ultimate deformation as the deformation corresponding to the maximum load-carrying capacity. It would seem reasonable to recognize at least some of this deformation capacity after the maximum load has been reached and to define the available ultimate deformation as that deformation when the load-carrying capacity has reduced by some arbitrary amount after maximum load. For example, a 10 or 20% reduction in maximum load-carrying capacity could be tolerated

in many cases, but the exact amount would depend on the particular case. In important cases a step-by-step dynamic analysis could be used to determine whether a certain load-displacement hysteretic behavior of the structure was adequate to survive the earthquake.

11.6.7 ACI Code Special Provisions for Seismic Design of Ductile Frames

The 1971 ACI code^{11,8} has an appendix containing special provisions for seismic design. According to the Commentary,^{11,10} the provisions "are intended to apply to reinforced concrete structures located in a seismic zone where major damage to construction has a high possibility of occurrence, and designed with a substantial reduction in total lateral seismic forces due to the use of lateral load-resisting systems consisting of ductile moment resisting space frames. . . ." The special provisions are not mandatory if load reduction factors for lateral seismic forces are not utilized. The provisions apply to frames with cast-in-place beam-column connections. The requirements therefore apply to frames that "will be forced into lateral deformations sufficient to create reversible plastic hinges by the action of the most severe earthquake." The provisions are based on 1967 and 1968 editions of the SEAOC code^{11,23} and other information and research results. The provisions for frames are divided into sections on flexural members, columns, and beam-column joints. Some of the important points stated are summarized below.

Flexural Members

An upper limit is placed on the flexural steel ratio ρ . The maximum value of ρ shall not exceed 0.5 of that value producing balanced conditions. Reference to Eq. 4.48 shows that this requirement is

$$\rho \leq 0.5 \left(\frac{0.85f'_c\beta_1}{f_y} \frac{0.003E_s}{0.003E_s + f_y} + \frac{\rho'f'_s}{f_y} \right) \quad (11.54)$$

Provision is also made to ensure that a minimum quantity of top and bottom reinforcement is always present. Both the top and the bottom steel are to have a steel ratio of at least $200/f_y$, with the steel yield strength f_y in psi (1 psi = 0.00689 N/mm²), throughout the length of the member. Recommendations are also made to ensure that sufficient steel is present to allow for unforeseen shifts in the points of contraflexure. At column connections, the positive moment capacity should be at least 50% of the negative moment capacity, and the reinforcement should be continuous through columns where possible. At external columns, beam reinforcement should be terminated in the far face of the column, using a hook plus any additional extension necessary for anchorage.

The design shear force is calculated on the basis of the design gravity loads on the member and from the moment capacities of plastic hinges at the ends of the member produced by lateral displacement. Figure 11.47 illustrates the calculation. The use of the actual ultimate moment capacities means that the moment-induced shears cannot exceed the calculated values. Minimum web reinforcement is provided throughout the length of the member, and spacing should not exceed $d/4$ in plastic hinge zones and $d/2$ elsewhere, where d = effective depth of member. The stirrups should be closed around bars required to act as compression reinforcement and in plastic hinge regions, and the spacing should not exceed specified values.

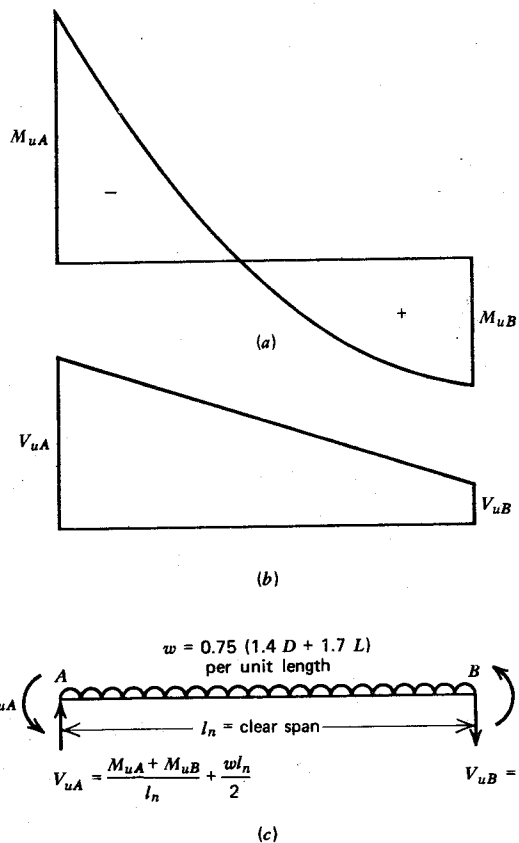


Fig. 11.47. Calculation of shear force with seismic loading. (a) Bending moment diagram. (b) Shear force diagram. (c) Actions on member.

Tension steel should not be spliced by lapping in regions of tension or reversing stress unless a specified quantity of closed stirrups are present.

Columns

The vertical reinforcement ratio is limited to the range 0.01 to 0.06. Normally, at any beam-column connection the sum of the moment strengths of the column shall be greater than the sum of the moment strengths of the beam along each principal plane at the connection. Exceptions to this requirement are found when the sum of the moment strengths of the confined core sections of the column is sufficient to resist the design loads or when the remaining columns and flexural members can resist the applied loads at that level by themselves. The requirement is intended to ensure that plastic hinges form in the beams rather than the columns.

Columns shall be designed as flexural members if the maximum design axial load of the column P_e is less than or equal to 0.4 of the balanced failure axial load capacity P_b (i.e., $P_e \leq 0.4P_b$).

If $P_e > 0.4P_b$, the core of the column shall be confined by special transverse reinforcement consisting of hoops or spirals over the end regions of the columns. Each end region is at least equal to the overall column depth, or 18 in (457 mm), or one-sixth of the clear height of the column. This special transverse steel ensures ductility, should plastic hinges form at the column ends. Where a spiral is used, the volumetric ratio of spiral steel should be at least that given by Eq. 5.6, namely,

$$\rho_s = 0.45 \frac{f'_c}{f_y} \left(\frac{A_g}{A_c} - 1 \right) \quad (11.55)$$

but not less than $0.12f'_c/f_y$. Where rectangular hoop reinforcement is used, the required area of bar is calculated from

$$A_{sh} = \frac{l_h \rho_s s_h}{2} \quad (11.56)$$

where A_{sh} = area of one leg of transverse bar, l_h = maximum unsupported length of hoop side measured between legs or supplementary crossties, s_h = center-to-center spacing of hoops [not to exceed 4 in (182 mm)], and ρ_s = volumetric ratio given by Eq. 11.55, substituting area of rectangular core to the outside of hoops for A_c , and f_y = hoop bar yield strength. Supplementary crossties, if used, shall be of the same diameter as the hoop bar and shall engage the hoop with a hook. Special transverse confining steel is required for the full height of columns that support discontinuous shear walls. The shear strength of a column should at least equal the applied shears at the formation of plastic hinges in the frame found from the sum of

the moments at the ends of the column divided by the column height. Shear reinforcement in columns should be at a spacing not exceeding $d/2$. Splices in vertical reinforcement shall preferably be made in the midheight regions of columns.

Beam-Column Connections

Special transverse reinforcement through the connection should satisfy Eqs. 11.55 or 11.56. Also the connection should have sufficient shear strength to at least equal the shear forces induced on the joint core by the yield forces of the beam reinforcement and the column shears. A free body of a typical interior connection appears in Fig. 11.48. The shear force to be resisted is the

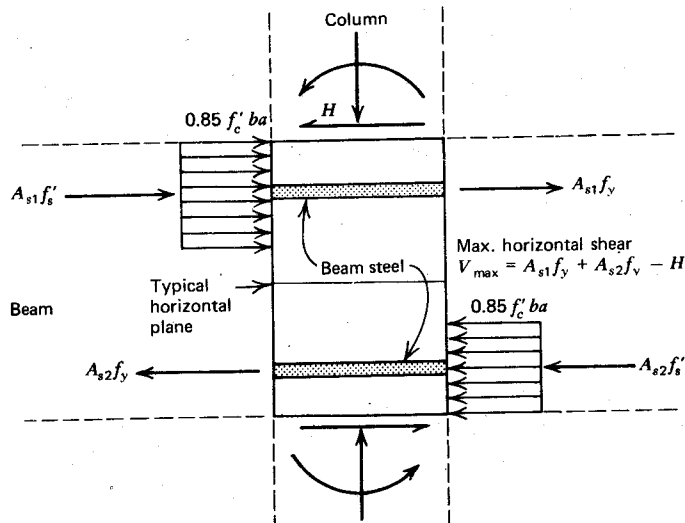


Fig. 11.48. Horizontal shear forces acting on joint core during seismic loading.

total shear force acting on each horizontal section of the joint core. Similar shear strength equations for the concrete shear-resisting mechanism and for the transverse reinforcement as used for columns are recommended by the code. Where connections have beams framing in on four sides of the column which cover a substantial proportion of the column face, the code allows the required shear reinforcement to be reduced by one-half.

11.6.8 Discussion of ACI Code Special Provisions for Seismic Design of Ductile Frames

Flexural Members

CURVATURE DUCTILITY

The curvature ductility factor of flexural members ensured by Eq. 11.54 has already been briefly discussed in Section 6.3.2. Figures 6.9 and 6.10 give φ_u/φ_y values for rectangular sections having different steel and concrete strengths and steel contents. It is evident that at the negative moment, plastic hinge in a beam at a column face ρ' will be approximately one-half of ρ or more, because the section is required to have a positive moment capacity that is at least one-half the negative moment capacity. As is indicated in Section 6.3.2, if the compression steel is yielding and $\rho' = 0.5\rho$, Eq. 11.54 will ensure $\varphi_u/\varphi_y > 6$ for $\varepsilon_c = 0.004$. Reference to Corley's equation 6.46 for ε_c indicates that given typical b/z values and the presence of a moderate amount of closed stirrups, ε_c values greater than 0.006 can be achieved. Hence $\varphi_u/\varphi_y > 10$ should be ensured by Eq. 11.54 at negative moment hinges, and greater values will be reached with some reduction in moment capacity at very high strains. A positive moment hinges, there will be significant amounts of compression steel available, and a wider flange reducing the ρ value; hence the available φ_u/φ_y value should be at least that at a negative moment hinge. Figures 6.9 and 6.10 also indicate that sections reinforced with Grade 40 ($f_y = 276 \text{ N/mm}^2$) steel according to Eq. 11.54 will be more ductile than sections reinforced with Grade 60 ($f_y = 414 \text{ N/mm}^2$) steel. Concrete crushing commences when the extreme fiber concrete strain exceeds approximately 0.004, and hence some member damage can be expected if concrete strains greater than 0.004 are to be reached.

In Section 11.6.4 it was suggested that beams of well-designed frames should be capable of achieving φ_u/φ_y values of at least 4μ , where μ is the displacement ductility factor. The displacement ductility factor is related to the reduction factor R by Eq. 11.38 or 11.39, where R is the ratio of static lateral design load to elastic response inertia load. On this basis, Eq. 11.54 may not always be stringent enough, and it would be better to use curvature ductility diagrams such as Figs. 6.9 and 6.10 to ascertain whether a given section is sufficiently ductile.

BUCKLING OF REINFORCEMENT

In plastic hinge regions at large deformations there is a danger of reduction in ductility due to buckling of compression reinforcement. The provisions require closed stirrups spaced not further apart than 16 bar diameters or 12 in (305 mm) in regions where bars act as compression reinforcement. Cyclic

(reversed) loading of steel causes a reduction in the tangent modulus of elasticity of the steel at low levels of stress (see Figs. 2.27 to 2.29), owing to the Bauschinger effect, and this could lead to buckling of reinforcing bars in compression at lower levels of load than expected. It is recommended that in plastic hinge zones the spacing of closed stirrups surrounding the compression steel not exceed 6 compression steel bar diameters. This matter is further discussed in Chapter 13.

SHEAR STRENGTH

The ACI provisions recommend the design of shear reinforcement by normal procedures that do not take into account the possible deterioration of the shear carried by the concrete during high-intensity reversed loading. Reversal of moment in plastic hinge regions causes a reduction in the shear force carried by the concrete across the compression zone and in the shear force carried by aggregate interlock and dowel action (see Section 7.9). This is because at some stages full-depth open flexural cracks will exist in the member in such regions, with moment carried only by a steel couple, and there will be alternating opening and closing of diagonal tension cracks. This points to the need for ignoring the concrete shear-resisting mechanism and for providing web reinforcement to resist the total shear force over regions in beams where yielding of the flexural reinforcement under cyclic loading is a possibility. This amounts to assuming that $v_c = 0$ in those regions.

Columns

AVOIDANCE OF PLASTIC HINGES

The code aims at having plastic hinges form in the beams rather than the columns by requiring that the sum of the moment strengths of the columns exceed the sum of the beam strengths at a connection in each principal plane, except where special provisions are made. This requirement unfortunately will not prevent column hinging for two reasons, as discussed below.

We know from Section 11.6.5 that nonlinear dynamic analyses have shown that at various stages during an earthquake points of contraflexure may occur well away from the midheights of columns. Columns can even be in single curvature at times. Thus bending moment distributions such as in Fig. 11.49 are possible (see also Fig. 11.35). At a typical joint, the total beam input is resisted by the sum of the column moments; therefore, we have

$$\Sigma M_b = M_{b1} + M_{b2} = M_{c1} + M_{c2}$$

The greatest column moment is given by

$$M_{c1} = \Sigma M_b - M_{c2} \quad (11.57)$$

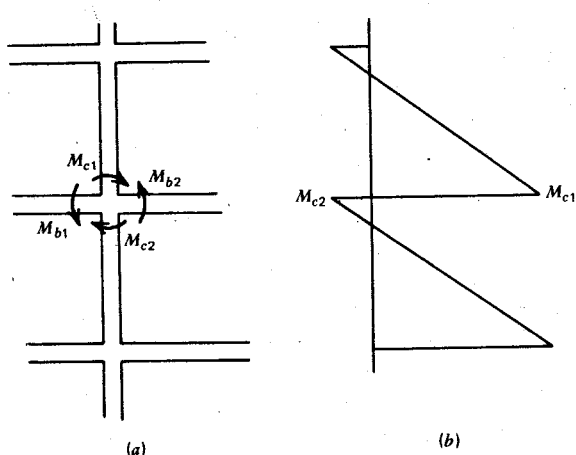


Fig. 11.49. Moments at beam-column joint. (a) Part of frame. (b) Column bending moment.

Now if ΣM_{ub} is the total input when the beams are at ultimate moment capacity, and M_{uc1} is the ultimate moment capacity of column 1, and we wish to prevent the formation of a plastic hinge in column 1, the requirement is

$$M_{uc1} > \Sigma M_{ub} - M_{c2} \quad (11.58)$$

If the column remains in double curvature, the limiting case occurs when $M_{c2} \rightarrow 0$, and Eq. 11.58 requires that $M_{uc1} > \Sigma M_{ub}$. If the columns are in single curvature, Eq. 11.58 requires that $M_{uc1} > \Sigma M_{ub} + M_{c2}$. Thus the ACI requirement that the sum of the column strengths shall exceed the sum of the beam strengths at a joint will not prevent column hinging. To make certain that plastic hinges do not form in columns, we would have to demand that the flexural strength of each column section at least equal the sum of the flexural strengths of the beam sections in the plane of bending, if the point of contraflexure can be anywhere within the story height. If the point of contraflexure lies outside the story height, an even greater column capacity would be required. This point is further discussed in Section 11.6.11.

In Section 11.6.6 the effect of earthquake loading in a general horizontal direction acting on the structure was discussed. It was evident that such loading, if not acting in one of the principal directions of the building, reduced the flexural strength of the columns because of biaxial bending and increased the beam moment input to the columns because of the components of moment strength received from the beams. For example, if biaxial bending reduces the column flexural strength by 30% and increases the beam moment

input by 40%, the columns need to be twice as strong as for the uniaxial bending case. The situation can be particularly serious at corner columns, where in addition to biaxial bending effects, the earthquake-induced axial load input from two beams at right angles can be additive.

It is apparent that the simple ACI provision will not prevent the formation of plastic hinges in columns. In the general case, shifts of points of contraflexure away from midheights of columns, and loading not applied along a principal axis, will necessitate column strengths considerably greater than the ACI requirement if plastic hinges in columns are to be avoided. The difficulty of preventing plastic hinges from forming in columns is such that some column hinging must be considered to be inevitable. Note that the formation of plastic hinges at only one end of the columns in a story will not lead to a column sidesway mechanism unless plastic hinges due to bending moments of the opposite sign form in the columns of another story.

DUCTILITY

The provisions require the end regions of columns to be confined by special transverse steel in the form of spirals or rectangular hoops if the maximum design axial load exceeds 0.4 of the balanced failure load. The quantity of special transverse steel is given by Eqs. 11.55 or 11.56.

Equation 11.55 for spiral steel was derived in Section 5.2 and is based on the requirement that the axial load strength of a spiral column after the concrete cover has spalled off should at least equal the axial load strength of the column before spalling. Equation 11.56 for rectangular hoops was devised to provide in a rectangular core the same confinement that would exist in the core of an equivalent spiral column, assuming that the efficiency of rectangular hoops as confining reinforcement is 50% that of spirals. Figure 11.50 illustrates the derivation of Eq. 11.56.^{11,10} For the free body of Fig. 11.50a and

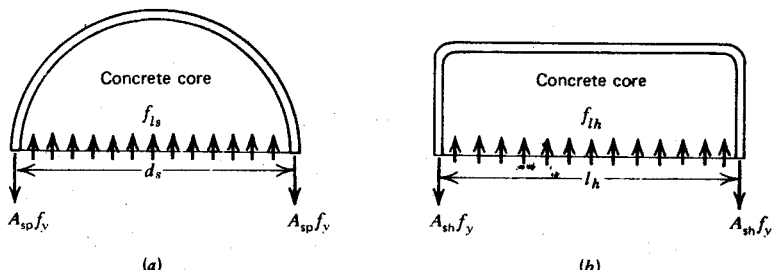


Fig. 11.50. Concrete confining pressure on columns. (a) From a spiral column. (b) From a hoop column.

the notation given there, we have

$$f_{ls} s d_s = 2 f_y A_{sp}$$

$$\therefore f_{ls} = \frac{2 f_y A_{sp}}{s d_s}$$

where s = spacing of spiral.

For the free body in Fig. 11.50b, we write

$$f_{lh} s_h l_h = 2 f_y A_{sh}$$

$$\therefore f_{lh} = \frac{2 f_y A_{sh}}{s_h l_h}$$

where s_h = spacing of hoops.

For equal confinement, it is assumed that $f_{lh} = 2 f_{ls}$ is required.

$$\therefore \frac{2 f_y A_{sh}}{s_h l_h} = 2 \frac{2 f_y A_{sp}}{s d_s}$$

$$\therefore A_{sh} = \frac{2 s_h l_h A_{sp}}{s d_s}$$

Now for the spiral column we have

$$\rho_s = \frac{A_{sp} \pi d_s}{s \pi d_s^2 / 4} = \frac{4 A_{sp}}{s d_s} \quad \text{or} \quad A_{sp} = \frac{\rho_s s d_s}{4}$$

$$\therefore A_{sh} = \frac{2 s_h l_h \rho_s s d_s}{s d_s} = \frac{l_h \rho_s s_h}{2}$$

which is Eq. 11.56. When supplementary crossties are present, the ACI provisions allow the substitution of the unsupported length of hoop side for l_h in the foregoing equation. This results in a reduction in the total area of transverse steel through the section. For example, the introduction of two supplementary crossties into the section of Fig. 11.51 would reduce l_h by two-thirds; therefore, according to Eq. 11.56, it would reduce A_{sh} by two-thirds, resulting in the total area of transverse steel across section XX being reduced by 33%. This is to give some recognition to the more favorable confinement obtained from the reduced unsupported length of hoop side.

It should be pointed out that Eqs. 11.55 and 11.56 will not necessarily result in adequate curvature ductility. These two equations are based on a philosophy of preserving the ultimate strength of axially loaded columns after spalling of the concrete cover, rather than emphasizing the ultimate deformation of eccentrically loaded columns. Since the ductility of the concrete will be increased by the presence of the confining steel, these equations

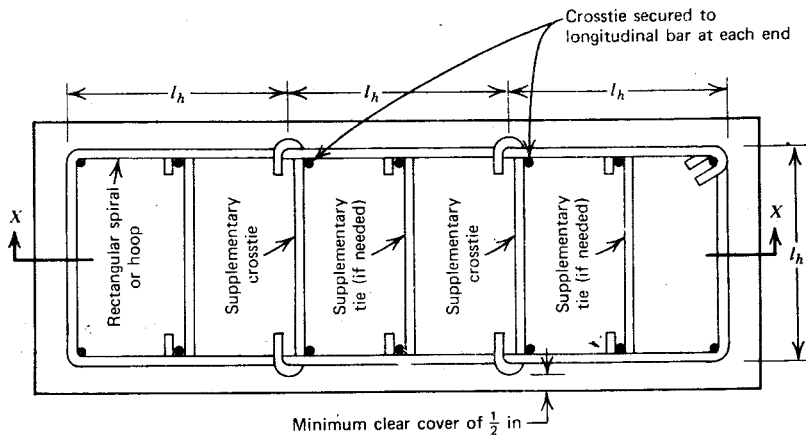


Fig. 11.51. Section of column with hoops and supplementary crossties.^{11,10}

will result in improved column behavior. However, a better attempt could be made at determining the amount of confining steel actually necessary to achieve the required ultimate curvatures for the usual case of eccentric loading. It is not even certain that the axial load will not be reduced after spalling. The uniform distribution of lateral stress in the concrete due to rectangular hoops (Fig. 11.50b) is certainly not factual, since the hoops will be capable of applying only a confining pressure near the corner regions, because of the small flexural stiffness of the hoop bar. Also, there is no guarantee that the hoop steel will reach the yield strength. The behavior of concrete confined by rectangular hoops is discussed in Section 2.1.3, and it is evident that rectangular hoops may cause only a slight strength increase, even though the ductility increases significantly. The equations are also very severe on columns having small cross sections. For example, if $f'_c = 4000$ psi (27.6 N/mm^2), $f_y = 40,000$ psi (276 N/mm^2), and the concrete cover to the hoops is $1\frac{1}{2}$ in (38 mm), the spacing of $\frac{3}{4}$ in (19.1 mm) diameter square hoops indicated by Eq. 11.56 is 3.2 in (80 mm) for 24 in (610 mm) square columns ($\rho_s = 0.0138$) and 3.0 in (77 mm) for 12 in (305 mm) square columns ($\rho_s = 0.0351$). The smaller section is required to have a much larger confining pressure on the concrete because of the large effect of the A_g/A_c ratio in the expression for ρ_s . Hence the equation may be overly conservative for columns having small cross sections. The effect of spalling of the concrete on the content of transverse steel may be overemphasized by these equations.

It is of interest to note that the SEAOC code^{11,23} provisions for special transverse steel for confinement requires only two-thirds of the transverse

steel given by Eq. 11.56 when single rectangular hoops are used without supplementary crossties. The difference between the SEAOC and ACI equations becomes smaller when supplementary crossties are used.

It is apparent that Eqs. 11.55 and 11.56, and the SEAOC requirements, can be regarded only as a crude guide to the amount of steel required for ductile behavior. A more rational approach for determining the quantity of confining steel required for adequate ductility based on moment-curvature relationships is described in Section 11.6.9.

SHEAR STRENGTH

The ACI provisions require the transverse reinforcement to be sufficient to ensure that the shear capacity of the member is at least equal to the shear force at the formation of the plastic hinges in the frame. Transverse reinforcement is assumed to be able to play the roles of shear reinforcement and confining reinforcement simultaneously. Shear is assumed to be carried by the concrete shear-resisting mechanism, as in the normal design procedure; hence the provisions take no account of the possible deterioration of the shear capacity of the concrete under reversed loading. As with beams, it appears that the contribution of the concrete to the shear strength, v_c , in the plastic hinge zones should be taken as zero and the shear force carried entirely by the web reinforcement. Between plastic hinges (i.e., away from the ends of columns) shear can be considered to be carried by the concrete. The requirement that the whole of the shear capacity at the plastic hinges be provided by the web reinforcement may be conservative for high axial compressive loads, and future experimental evidence may reveal that some shear can be carried by the concrete if the axial compressive load is high. It may be reasonable to ignore the shear carried by the concrete when $P_u < P_b$ and to let the concrete carry one-half the normal v_c when $P_u > P_b$.

The provisions also fail to mention the high shear forces that may be induced in a column when earthquake loading acts in a general direction on the structure. The moment input into the column is increased (see Section 11.6.6), resulting in a greater shear force, and this enhanced shear force is to be resisted by a section loaded in the direction of its diagonal. The shear strength of diagonally loaded rectangular sections has not been properly investigated. Nevertheless, the contribution of web reinforcement to the shear strength can be assessed by summing the components of the web bar forces intersected by the diagonal tension crack.

Beam-Column Joints

The provisions indicate that the shear strength of the joint core may be calculated by summing the contribution from the concrete shear-resisting

mechanism v_c and the transverse reinforcement, using the same shear strength equations as for the columns. Recent tests discussed in Chapter 13 have indicated that such a procedure is unsatisfactory when cyclic (reversed) high-intensity loading is applied to the joint, because the concrete in the joint core breaks down. The mechanism of shear resistance of reinforced concrete joint cores is not fully understood at present, but it would appear to be erroneous to base a design procedure for joint cores on test results obtained from members. Recent experimental evidence discussed in Chapter 13 indicates that the critical crack runs from corner to corner of the joint core, not at 45° to the axes of the intersecting members; and a better design procedure would seem to be to provide sufficient transverse reinforcement to resist the total shear force across the corner to corner crack.

Also, the provisions make no mention of the high shear forces that will be induced in a joint core when the earthquake acts in a general direction on the structure, resulting in concurrent loading on both axes of the building. The joint shear force in the general case is greater than for seismic loading along one axis of the building. Also, such general loading, causing yielding of the beam system in two directions simultaneously, may mean that joint confinement from surrounding beams is not as efficient as implied by the provisions.

Recent research and design procedures for joint cores are discussed in detail in Chapter 13.

11.6.9 An Alternative Procedure for Calculating Special Transverse Reinforcement for Confinement in the Plastic Hinge Zones of Columns

The Approach

Previous considerations, discussed in Section 11.6.8, have indicated that some plastic hinging of columns must be accepted as inevitable during a very large earthquake, because seismic loading that acts simultaneously in the directions of both principal axes of the building, and the presence of points of contrabflexure near the ends of columns, will result in high bending moments in columns. To prevent plastic hinges in columns would require columns that are much stronger than the beams. Also, the presence of walls, and unintentional strength variations of members, could lead to column hinging. Thus the potential plastic hinge zones of columns should be capable of ductile behavior.

As stated earlier, the existing code approach for the determination of special transverse steel is based on a philosophy of maintaining the axial

load strength of the column after spalling of the cover concrete. This procedure does not relate detailing requirements to the required plastic rotation capacities of eccentrically loaded column sections.

The moment-curvature relationship provides a measure of the plastic rotation capacity of sections, and an approach based on ensuring a satisfactory moment-curvature relationship could form a rational basis for detailing columns for ductility. A problem in assessing the available curvature ductility factor ϕ_u/ϕ_y from a moment-curvature relationship is the definition of the ultimate curvature ϕ_u . It is evident that many sections maintain considerable capacity for plastic rotation beyond the peak of the moment-curvature curve and, as discussed in Section 11.6.6, it would be reasonable to recognize this and to define ϕ_u as the curvature when the moment capacity of the section had reduced to 80 to 90% of the maximum moment. Also, we know from previous considerations that columns at bases should be capable of reaching ϕ_u/ϕ_y values of up to 4μ , where μ is the displacement ductility factor. A reasonable criterion would be to require the potential plastic hinge zones of columns to be capable of achieving a ϕ_u/ϕ_y value of at least 4μ . This should provide sufficient ductility, unless overstrong or understrong elements enforce column hinging in one story. The derivation of moment-curvature relationships from the stress-strain curves of confined concrete and longitudinal steel allows the application of this criterion and enables the determination of the required amount of transverse reinforcement.

Moment-Curvature Analysis

In deriving the moment-curvature characteristics of eccentrically loaded rectangular reinforced concrete column sections, the following factors are taken into account:

1. Level of axial load on column.
2. Longitudinal steel content.
3. Proportion of column section confined.
4. Material stress-strain characteristics.

Ideally the effects of cyclic loading should also be considered, but the complexity of cyclic load analysis makes it difficult to study a large range of cases. In this study monotonic loading is analyzed, and this should give a reasonable assessment in the first instance.

The assumptions made in theoretical moment-curvature analysis, and the method of analysis, are outlined in Sections 6.2.2 and 6.5.3. The longitudinal steel reinforcement is assumed to have the stress-strain curve defined by Eqs. 6.28 to 6.32. This curve, which includes the effect of strain hardening, is illustrated in Fig. 2.25c. The concrete confined by rectangular

hoops is assumed to have the stress-strain curve in compression defined by Eqs. 2.6 to 2.11 (see Fig. 2.18). The slope of the falling branch of the curve for confined concrete is defined by a parameter Z , given by

$$Z = \frac{0.5}{\frac{\frac{3}{4}\rho_s \sqrt{b''}}{s_h} + \frac{3 + 0.002f'_c}{f'_c - 1000} - 0.002} \quad (11.59)$$

where ρ_s = ratio of volume of transverse hooping reinforcement to volume of concrete core measured to outside of hoops, b'' = width of confined core measured to outside of hoops, s_h = spacing of transverse hoops, and f'_c = compressive cylinder strength of concrete in psi (1 psi = 0.00689 N/mm²). The stress-strain curve for the cover concrete (outside the hoops) in compression is assumed to be identical to that of the confined concrete up to a strain of 0.004. Cover concrete at strains greater than 0.004 is assumed to have spalled and to have zero strength. The tensile strength of concrete is ignored.

In practice, various arrangements of transverse steel involving overlapping hoops, or hoops with supplementary crossties, are needed in all but small column sections, to provide lateral support to the longitudinal bars in the section. The definition of Z for such a case has been discussed in Section 6.5.2, and a column section with one possible steel arrangement appears in Fig. 11.52.

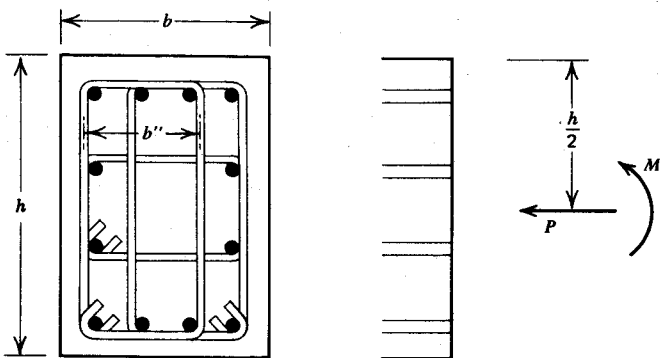


Fig. 11.52. Section of column and external actions.

For this arrangement Z may be calculated assuming b'' = width of side of one hoop, s_h = spacing of sets of overlapping hoops, and ρ_s = ratio of volume of one hoop to volume of concrete core within that hoop. There is a lack of test data on the efficiency of various arrangements of transverse steel. Hence in the meantime it is prudent to adopt conservative definitions.

The procedure for conducting the moment-curvature analysis has been outlined in Section 6.2.2. A convenient approach is to divide the section into a number of discrete laminae having the orientation of the neutral axis, and to replace the longitudinal steel by an equivalent thin tube (illustrated in Fig. 6.19 and described in Example 6.3). The internal actions are determined by summing the lamina contributions and the moment-curvature relationship found by an iterative procedure and by successively incrementing the value of extreme fiber concrete strain.

Figure 6.20 plots moment-curvature curves obtained from a column reinforced with Grade 40 ($f_y = 276 \text{ N/mm}^2$) longitudinal steel. Some of the conclusions reached from an analysis^{11.35, 11.36} of a range of variables are as follows.

1. A large transverse steel content leads to better concrete stress-strain characteristics, enabling the moment capacity to be better maintained at high curvatures.
2. A large longitudinal steel content means that less reliance is placed on the concrete capacity, and therefore the moment capacity can be better maintained at high curvatures.
3. A large axial load means that a large proportion of the load is carried by the concrete; thus the moment capacity may not be well maintained at high curvatures.
4. High-strength longitudinal steel with early strain hardening maintains the moment capacity better than mild steel in which strain hardening does not commence until very high strains.
5. High-strength concrete results in a greater reduction in the moment capacity at the spalling of the cover concrete.
6. A large proportion of cover concrete, as in small sections, results in a greater reduction in moment capacity at the spalling of the cover concrete.

Approach for Determining Transverse Steel Required for Ductility

The transverse steel requirements for columns can be assessed from the moment-curvature curves by establishing the Z values required to achieve adequate ductility. For seismic design, as discussed previously, the requirement could be a curvature ductility factor ϕ_u/ϕ_y of 16 at a moment capacity of not less than 0.85 of the maximum moment capacity, if the displacement ductility factor is 4.

Norton^{11.35} has conducted an analytical investigation of square columns using the approach just summarized. Figures 11.53 to 11.55 show typical moment-curvature curves obtained for bending about a principal axis, holding axial load constant at various levels. On each curve, A denotes the onset of spalling of the cover concrete (extreme fiber concrete strain of 0.004),

and C and T denote the onset of strain hardening of the compression and tension steel, respectively. The curves are drawn from the first yielding of the tension steel. The Grade 60 steel ($f_y = 414 \text{ N/mm}^2$) was assumed to have the following properties (see the notation of Fig. 2.25c): $\epsilon_{sh} = 4\epsilon_y$, $\epsilon_{su} = 0.12$ and $f_{su} = 1.58f_y$. The longitudinal steel was distributed around the section perimeter. The cover to the outside of the hoops was assumed to be $c = 1.5 \text{ in}$ (38 mm). From the moment-curvature ductility curves of Figs. 11.53

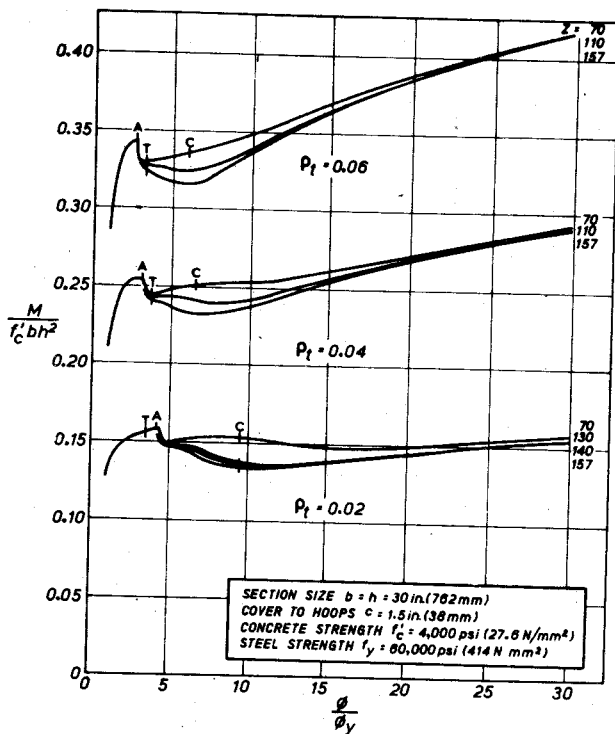


Fig. 11.53. Moment-ductility curves for $P = 0.1f_y'A_g$.

to 11.55, and others for different section sizes, Z values meeting the above-mentioned ultimate curvature requirement have been obtained^{11.35} (see Table 11.3). When the ultimate curvature requirement could not be met with reasonable amounts of transverse steel, no Z value is indicated in the table. The analysis assumes that the compression steel does not buckle. The calculated strain in the compression steel at $\phi_u/\phi_y = 16$ for each case is

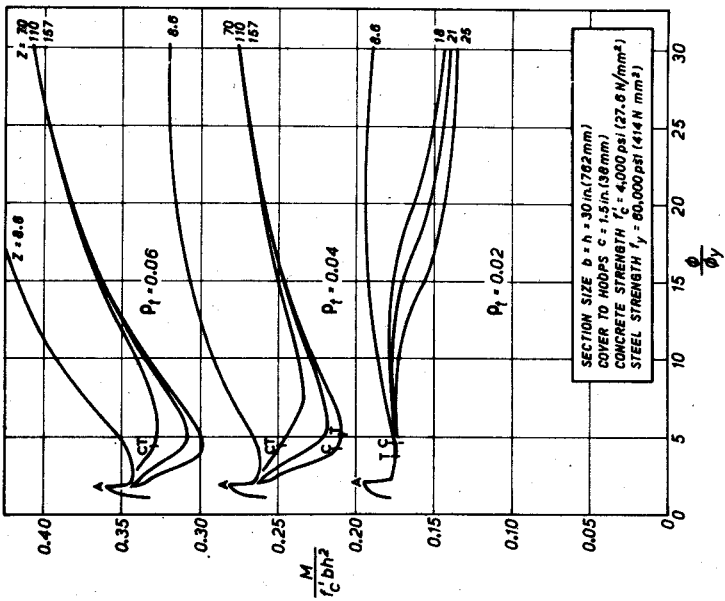
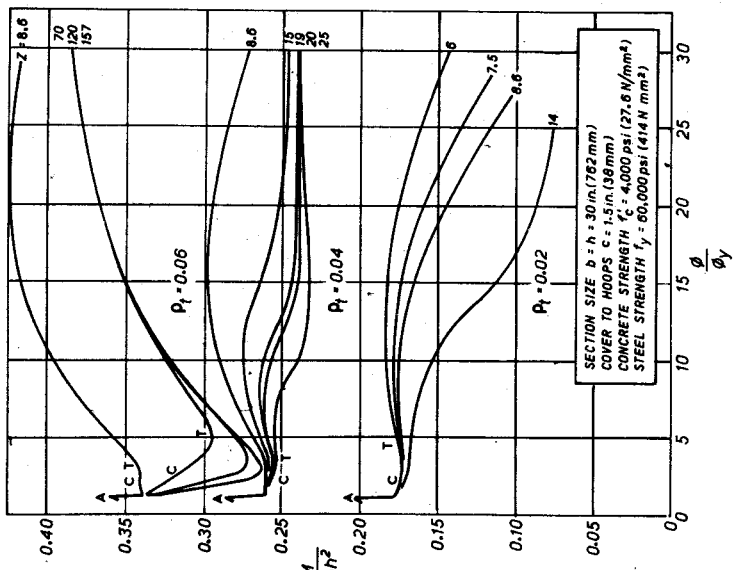


Fig. 11.55. Moment-ductility curves for $P = 0.5f'_c A_g$.

Fig. 11.54. Moment-ductility curves for $P = 0.3f'_c A_g$.

included in parentheses beside the Z values in Table 11.3. The compression steel strains are large; hence the hoops must be closely spaced to avoid buckling.

Table 11.3 Approximate Z Values and Steel Compressive Strain^a Required for a Moment Capacity of 85% of Maximum Moment Capacity at $\phi_u/\phi_y = 16$ for Concrete $f'_c = 4000$ psi (27.6 N/mm²), Longitudinal Steel $f_y = 60,000$ psi (414 N/mm²), uniformly distributed around section perimeter, cover to hoops $c = 1.5$ in (38 mm)

Section Size	Longitudinal Steel Ratio, $\rho_t = A_{st}/A_g$	Axial Load Level, $P/f'_c A_g$			
		0.1	0.2	0.3	0.5
15 in square (381 mm)	0.02	55 (0.019)	16 (0.023)	5 (0.030)	—
	0.04	127 (0.025)	127 (0.033)	25 (0.037)	9 (0.074)
	0.06	127 (0.027)	127 (0.034)	127 (0.040)	127 (0.073)
20 in square (508 mm)	0.02	90 (0.021)	28 (0.025)	14 (0.032)	—
	0.04	140 (0.026)	140 (0.033)	70 (0.041)	13 (0.067)
	0.06	140 (0.027)	140 (0.033)	140 (0.040)	140 (0.068)
30 in square (762 mm)	0.02	157 (0.023)	39 (0.028)	21 (0.034)	7.5 (0.057)
	0.04	157 (0.025)	157 (0.033)	157 (0.042)	19 (0.059)
	0.06	157 (0.027)	157 (0.033)	157 (0.041)	157 (0.061)

^a Steel compressive strain appears in parentheses beside the Z values.

The Z values in Table 11.3 may be used to design the transverse reinforcement for ductile columns with the stated material properties. The Z value corresponding to a given arrangement of hoops may be calculated using Eq. 11.59, as discussed in Section 6.5.2. For example, for the arrangement of three overlapping hoops appearing in the column section of Fig. 11.52, if the hoop diameter is $\frac{1}{2}$ in (12.7 mm), the spacing of each set of hoops is $s_h = 4$ in (102 mm), column dimensions are $b = h = 20$ in (508 mm), cover thickness $c = 1.5$ in (38 mm), concrete strength $f'_c = 4000$ psi (27.6 N/mm²), and assuming that $b'' = \frac{2}{3}(b - 2c)$, Eq. 11.59 gives

$$Z = \frac{0.5}{0.75 \times \frac{2(17 + 11.33)0.2}{17 \times 11.33 \times 4} \sqrt{\frac{11.33}{4}} + \frac{3 + 8}{3000} - 0.002} = 24.8$$

Table 11.4 gives some values of Z calculated thus for the arrangement of three overlapping hoops in Fig. 11.52 for various hoop diameters and spacing of hoop sets. The Z values for other hoop diameters and spacings can also be

Table 11.4 Z Values for Square Sections Having Three Overlapping Rectangular Hoops: Unsupported Length of Hoop Side = $\frac{2}{3} \times$ dimension of confined core, $f'_c = 4000$ psi (27.6 N/mm²) and $c = 1.5$ in (38 mm)^a

Transverse Steel, Diameter at Centers	Section Size		
	15 in (381 mm)	20 in (508 mm)	30 in (762 mm)
$\frac{3}{8}$ in (9.5 mm) at 12 in (305 mm)	125	138	155
$\frac{3}{8}$ in (9.5 mm) at 4 in (102 mm)	36	42	51
$\frac{1}{2}$ in (12.7 mm) at 4 in (102 mm)	21	25	31
$\frac{5}{8}$ in (15.9 mm) at 4 in (102 mm)	14	16	20
$\frac{3}{4}$ in (19.1 mm) at 4 in (102 mm)	9.9	12	15

^a ACI 318-71 requires for $P > 0.4P_b$ $\frac{5}{8}$ in (15.9 mm) diameter hoops with $f_y = 40,000$ psi (276 N/mm²) spaced as follows:

for 15 in (381 mm) section, spacing = 3.1 in (79 mm), giving $Z = 9.6$

for 20 in (508 mm) section, spacing = 3.2 in (81 mm), giving $Z = 12$

for 30 in (762 mm) section, spacing = 2.9 in (74 mm), giving $Z = 13$

found. Tables similar to Table 11.4 can be compiled for other hoop arrangements and concrete strengths. Tables 11.3 and 11.4 can be used to design the transverse steel of columns with the material properties and hoop arrangement of those tables. For example, a 15 in (381 mm) square column with $A_{st}/A_g = 0.04$ and $P = 0.3f'_c A_g$ would require $Z = 25$ according to Table 11.3, and $\frac{1}{2}$ in (12.7 mm) diameter hoops at 4 in (102 mm) centers would satisfy this requirement according to Table 11.4.

The Z values required for other strengths of steel and concrete can be determined. Other results are reported by Norton^{11.35} and also by Park and Sampson.^{11.36}

ACI 318-71 requires special transverse steel in columns when the axial load level exceeds $0.4P_b$, where P_b is the axial load at the simultaneous attainment of an extreme fiber concrete compressive strain of 0.003 and of yielding of the tension steel. A $0.4P_b$ axial load corresponds to load intensities varying from $0.12f'_c A_g$ for a 10 in (254 mm) square section with $f'_c = 6$ ksi (41.4 N/mm²) and $f_y = 60$ ksi (414 N/mm²) to $0.18f'_c A_g$ for a 30 in (762 mm) square section with $f'_c = 4$ ksi (27.6 N/mm²) and $f_y = 40$ ksi (276 N/mm²). The Z values corresponding to the ACI 318-71 special transverse steel requirements for the arrangement of three overlapping hoops are shown appended to Table 11.4. Comparison with the Z values indicated in Table 11.3 for axial load in the range $0.2f'_c A_g$ to $0.5f'_c A_g$ shows the ACI provisions to be conservative except for heavily loaded columns having small

cross sections and small longitudinal steel contents. Results obtained previously^{11,36} for a section with mild steel ($f_y = 40,000$ psi (276 N/mm 2)) longitudinal reinforcement indicated a greater transverse steel demand than Table 11.3.

Comments on the Approach

The approach just given depends very much on the ultimate curvature demand and the definition of ultimate curvature, and also on the assumed stress-strain curves for confined concrete and for steel.

The assumed stress-strain curve for Grade 60 ($f_y = 414$ N/mm 2) steel used to obtain the tabulated and plotted results of Table 11.3 and Figs. 11.53 to 11.55 includes the effect of strain hardening. Strain hardening was assumed to commence at 4 times the yield strain. The early onset of strain hardening of the longitudinal steel allows the moment capacity of the section to be maintained better than for steel without early strain hardening. Reliance on strain hardening may be regarded as unwise, since the stage at which strain hardening commences is not covered by steel specifications. Nevertheless it is realistic to include its effect.

In addition, the transverse steel simultaneously acts as shear reinforcement and provides restraint against lateral buckling of the longitudinal reinforcement. Always verify that sufficient transverse steel is present to act as shear reinforcement. To control buckling of longitudinal bars, the spacing of hoops should not exceed 4 in (102 mm) and should not be greater than 6 longitudinal bar diameters.

11.6.10 Earthquake Energy Dissipation by Special Devices

The conventional approach to seismic-resistant design—namely, relying on ductile behavior of the structural members for energy dissipation—has the obvious disadvantage that the structure will be damaged during a major earthquake and will need to be repaired. The damage may even be so serious that the structure must be demolished. An alternative approach is to separate the load-carrying function of the structure from the energy-dissipating function. This can be achieved by incorporating into the structure special devices for dissipating the energy generated in the structure by the earthquake motions. These devices would protect the structures from damage.

Examples of mechanisms of energy dissipation incorporating devices of mild steel which could be used in structures are the rolling (bending) of U-shaped strips, the torsion of short bars, and the flexure of short beams. Devices based on these mechanisms can be incorporated between moving surfaces or in diagonal bracing in frames. Results of investigations in New Zealand of the behavior of these devices has recently been reported by Kelly et al.^{11,37} The tests revealed that the plastic torsion of mild steel is an ex-

tremely efficient mechanism for the dissipation of energy. At plastic strains in range 3 to 12% it was found to be possible to dissipate energy of the order of 2000 to 7500 lb · in/in³ per cycle (14 to 50 × 10⁶ J/m³ per cycle) with lifetimes in the range of 100 to 1000 cycles. It is evident that the use of such devices in structures has potential, and further research to produce commercially available items should be encouraged.

One method suggested for limiting the maximum dynamic forces to which a multistory structure is subjected to during an earthquake is the "soft story" approach. The columns of a lower story, typically the first story of the structure, are designed to yield at a predetermined lateral load. After yielding commences, all the inelastic deformations will occur in those columns, and the structure above will be protected from higher lateral forces. Possible methods of design of the soft story have been proposed by Fintel and Khan.^{11,38} However, a designer should approach such a solution with caution. The columns of the soft story must be accurately designed—that is, neither over strength nor understrength is permissible. Fluctuations of column loads during the earthquake, caused by reversal of overturning moment and vertical accelerations, make such a strength analysis for the columns difficult. Also, the ductility demands on the columns of that story will be considerable. The lateral displacements in the soft story would be large, and provision needs to be made to accommodate them. Straightening of columns after the earthquake will also present difficulties.

Other possible methods for isolating parts of structures from earthquakes are discussed by Newmark and Rosenblueth.^{11,22}

11.6.11 Capacity Design for Seismic Loading of Frames

Since it is impossible to accurately predict the characteristics of the ground motions that may occur at any given site, it is impossible to evaluate the complete behavior of a reinforced concrete multistory frame when subjected to very large seismic disturbances. However, it is possible to impart to the structure features that will ensure the most desirable behavior. In terms of damage, ductility, energy dissipation, or failure, this means a desirable sequence in the breakdown of the complex chain of resistance in a frame. It implies a desirable hierarchy in the failure mode of the structure. To establish any sequence in the failure mechanism of a complex chain, it is necessary to know the strength of each link. This knowledge must not be based on safe assumptions or dependable capacities but realistically on the most probable strengths of the structural components, which will be subjected to very large deformations during a catastrophic earthquake. The definitions of various strengths and the relationship between them were discussed in Chapter 1.

In spite of the probabilistic nature of the design load or displacement pattern to be applied to the structure, in the light of present knowledge, a

deterministic allocation of strength and ductility properties holds the best promise for a successful response and the prevention of collapse during a catastrophic earthquake. This philosophy may be incorporated in a rational capacity design process. In the capacity design of earthquake-resistant structures, energy-dissipating elements of mechanisms are chosen and suitably detailed, and other structural elements are provided with sufficient reserve strength capacity, to ensure that the chosen energy-dissipating mechanisms are maintained at near their full strength throughout the deformations that may occur. To illustrate the capacity design approach, let us briefly discuss the derivation of the design shear force for beams and design loads on columns of frames.

Capacity Design for Shear in Beams

If a nonductile shear failure is to be suppressed, it is necessary to ensure that the dependable shear strength of the beam V_d is equal to or larger than the shear force associated with the flexural overstrength M_o of the beam, which cannot be exceeded during the seismic excitation. In addition to earthquake moment-induced shear, provision needs to be made for shear forces resulting from gravity load and vertical accelerations. Hence with reference to Fig. 11.47, at the left-hand support we have

$$V_{dA} \geq \frac{M_{oA} + M_{oB}}{l_n} + \lambda_a \frac{wl_n}{2} \quad (11.60)$$

where V_{dA} = dependable shear strength of beam at A

M_{oA} , M_{oB} = flexural overstrength capacities at potential plastic hinges at A and B

λ_a = factor allowing for vertical acceleration

l_n = clear span of beam

w = design uniform dead and live load factored as in Fig. 11.47

For routine design it is more convenient to express this relationship in terms of ideal strengths and the appropriate strength factors as set out in Eqs. 1.5 and 1.7. Accordingly, Eq. 11.60 becomes

$$V_{iA} = \frac{1}{\varphi} \left(\varphi_o \frac{M_{iA} + M_{iB}}{l_n} + \lambda_a \frac{wl_n}{2} \right) \quad (11.61)$$

where V_{iA} = ideal shear strength of the beam at A, to be supplied entirely by reinforcement

M_{iA} , M_{iB} = ideal flexural strength of the support sections (i.e., $M_{iA} = A_s f_y j d$ at support A)

φ = capacity reduction factor for shear (i.e., 0.85)

φ_o = flexural overstrength factor (e.g., 1.3)

A typical allowance for vertical acceleration due to seismic motions would be $0.25g$, resulting in $\lambda_a = 1.25$. With the chosen numerical values for all factors, Eq. 11.61 becomes

$$V_{iA} = 1.53 \frac{M_{iA} + M_{iB}}{l_n} + 1.47 \frac{wl_n}{2} \quad (11.62)$$

It is evident that the degree of protection against a possible shear failure in seismic design needs to be considerably greater than for gravity or wind load design.

Capacity Design of Columns

The estimation of column moments and concurrent axial loads in earthquake resistant frames is much more difficult. Before outlining the capacity design procedure relevant to columns, we must restate the design criteria that are to be met.

In the previous discussion it was repeatedly emphasized that the formation of plastic hinges in columns should be avoided if possible. Apart from the very large curvature ductility demand associated with column sidesway mechanisms, which was illustrated in several examples, there are other reasons for avoiding or at least delaying column plastic hinges. A column failure has much more serious consequences than a beam failure. Column yielding in all columns of a story will lead to permanent misalignment of the building. Compression load, most commonly present in columns, reduces the available curvature ductility. Column hinging, associated with large interstory sway, introduces problems of instability, which in turn may jeopardize the gravity load-carrying capacity of the structure.

The question that arises is: How can a reasonable degree of protection be provided by the designer if he accepts that during a large random dynamic excitation, column hinging is to be prevented or delayed, except at a few unavoidable localities.

In accordance with the capacity design philosophy, it would be necessary to ensure that the dependable flexural capacity of a critical column section, adjacent to a column-beam joint, is at least equal to the worst probable flexural demand that may occur concurrently with a probable axial load. It should be noted that the relationship between moment input and flexural strength in columns need not be as stringent as was the case for shear in beams, because the column section will have been designed for ductility.

FLEXURAL DEMAND FOR COLUMN SECTIONS

Because of the disproportionate distribution of moments around column-beam joints during the higher modes of response of a multistory frame, bending moments at the critical sections considerably larger than those

derived from static analysis could result. This was pointed out previously with reference to Fig. 11.35 and in Section 11.6.8. To minimize the likelihood of column yielding, the dependable column strength at a critical section (e.g., above the floor level in Fig. 11.49), must be made larger than the probable moment input from the adjoining beams. That is, we need

$$M_{dc1} \geq \lambda_{c1} \Sigma M_{pb} \quad (11.63)$$

where M_{dc1} = dependable flexural capacity of column section in presence of appropriate axial load

ΣM_{pb} = sum of probable beam flexural capacities when plastic hinges form in the beams

λ_{c1} = moment distribution factor, depending on inelastic dynamic response of frame when subjected to earthquake ground motions.

Case studies^{11.29} have indicated that for regular frames the value for λ_{c1} could be between 0.8 to 1.3, the higher value being observed for a rather flexible frame and the smaller value being representative of a relatively rigid frame that would respond predominantly in its first mode of vibration.

Again Eq. 11.63 is more conveniently expressed in terms of ideal strengths as defined in Chapter 1; thus we have

$$M_{ic1} \geq \frac{\lambda_{c1}}{\varphi_c} \Sigma \varphi_{pb} M_{ib} \quad (11.64)$$

where M_{ic1} = ideal flexural strength of column section in presence of design axial load

M_{ib} = ideal flexural strength of beams

φ_{pb} = probable strength factor for beams as defined in Section 1.4.4

φ_c = capacity reduction factor for columns

To illustrate the implications of this relationship, Eq. 11.64 is compared with current requirements of the ACI^{11.8} and SEAOC^{11.23} codes, using typical values for the various factors.

According to these two codes, it is found that with $\varphi_c = 0.7$ and $\varphi_b = 0.9$

$$M_{ic1} \geq \frac{0.5}{\varphi_c} \Sigma \varphi_b M_{ib} = 0.64 \Sigma M_{ib} \quad (11.65)$$

The SEAOC code^{11.23} stipulates that the beam overstrengths, with $M_{ob} = 1.25 M_{ib}$, must be considered when determining the shear forces acting on beams; but surprisingly, the code does not require this for column bending moment design.

The 0.5 factor in Eq. 11.65 results from the assumption that the total beam moment input, ΣM_{ib} , is distributed in equal proportions between the column sections above and below the floor.

For the extreme case of disproportionate distribution of column moments, a column capacity reduction factor of $\varphi_c = 0.9$ may be considered to be adequate. Hence by assuming that $\varphi_{pb} = 1.1$, Eq. 11.64 becomes

$$M_{ic1} \geq 0.98 \sum M_{ib} \quad \text{when } \lambda_{c1} = 0.8 \quad (11.66a)$$

$$M_{ic1} \geq 1.58 \sum M_{ib} \quad \text{when } \lambda_{c1} = 1.3 \quad (11.66b)$$

In this case no allowance has been made for the possible development of beam overstrength. It is seen that in comparison with the ACI and SEAOC code requirements, the proposed capacity design procedure gives considerably greater protection against column yielding, the required ideal column strengths of Eqs. 11.66a and 11.66b being 1.53 and 2.47 times that of the code equation 11.65. In fact, it could be inferred from the Commentary to the SEAOC code that $\varphi_b = \varphi_c = 1$ may be assumed in Eq. 11.65, making the required ideal column strength according to that code even smaller.

AXIAL LOAD DETERMINATION FOR COLUMNS

In seismic design it is important to determine accurately the probable earthquake-induced axial loads on the columns. These loads are particularly critical in the case of exterior columns. When frames are designed for equivalent static lateral loads, the corresponding axial loads are readily derived. However, these forces are representative of only the first mode response of the structure; they do not reflect the true column loads that can develop in a frame. An approach to determine column loads used in New Zealand assumes, in accordance with capacity design philosophy, that all beams framing into a column develop their flexural overstrengths simultaneously over the full height of the structure. This implies that the column load input at each floor is given by summing the input shear forces from the beams, using shear force equations similar to the right-hand side of Eq. 11.60, taking the first term as positive or negative depending on the side of the column. The column loads so obtained are then used to design the column sections; a column capacity reduction factor, $\varphi_c = 0.7$, is used in the section design. This procedure appears to be unnecessarily severe, particularly for tall frames. It was pointed out earlier that during the inelastic dynamic response of a frame, beam plastic hinges form in groups, typically over two to five floors at a time, and travel up the full height of the frame. When calculating the earthquake-induced column loads, therefore, it would be more rational to make some allowance for the fact that not all possible beam plastic hinges are present simultaneously.

Such an approach is illustrated for a 20-story example structure in Fig. 11.56. For the purpose of deriving the critical lateral load induced column loads for the sixth-story columns, it may be assumed that the overstrengths M_{ob} of all the beams at six floors immediately above the sixth story are

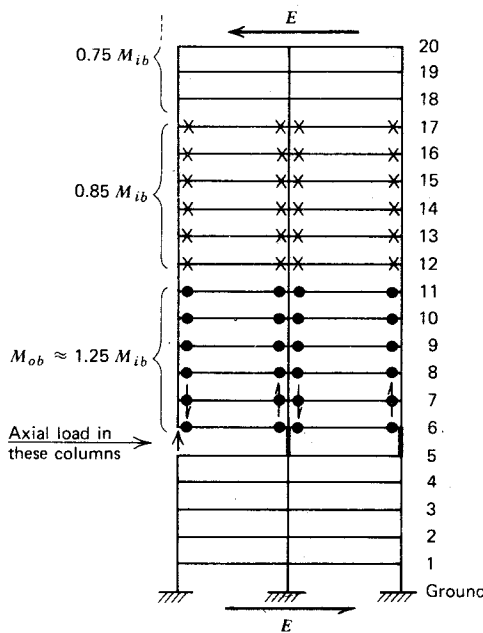


Fig. 11.56. Beam moment and plastic hinge pattern for evaluating earthquake-induced axial loads in columns.

developed. Typically these may be 125% of the ideal beam strength, M_{ib} , so that $M_{ob} = 1.25M_{ib}$. It is unlikely that plastic hinges have formed in the beams of the next six floors above, but it may be assumed that, say, 85% of the ideal strength of each of the beams at these floors will be developed. For the next six floors above, a further reduction to, say, 75% of the ideal beam strengths may be assumed, as illustrated in Fig. 11.56.

The column loads so derived would then have to be combined with the appropriate factored gravity loads and vertical acceleration components to give upper-bound and lower-bound values for the column loads. Since these axial loads are based on extreme and transient capacity conditions of behavior, there appears to be no need to introduce a further capacity reduction factor φ_c . An ideal section strength equal to the axial load so derived may be sufficient. Some reserve strength will be available in any case, because the probable strength of the column section will be in excess of the ideal strength, as shown in Chapter 1, particularly when large axial compression makes the contribution of the concrete compression strength significant. It is to be remembered that the probable strength of the concrete in place is likely to be well in excess of the ideal strength f'_c .

SHEAR FORCE ON COLUMNS

From the foregoing it is evident that a somewhat larger degree of protection against shear failure in columns must be provided, simply because column shear failures are brittle. To be consistent with the capacity design philosophy, one would tend to consider the simultaneous development of plastic hinges at the top and bottom of a column. However, these sections have already been designed separately for the maximum likely moment inputs. As Fig. 11.57 reveals, column bending moments corresponding with two plastic hinges could not occur. Figure 11.57a shows the moment pattern for column

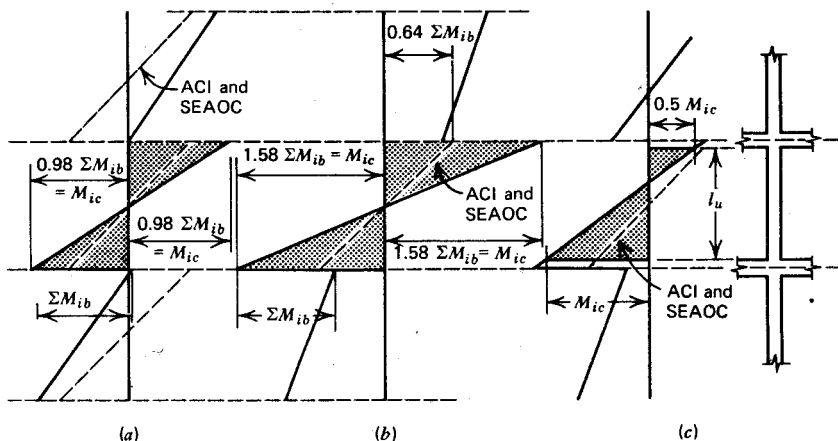


Fig. 11.57. Moment patterns to determine column shear forces.

sections that could develop 98% of the total beam moment input at the top and at the bottom of the story, Fig. 11.57b shows the same for 158% beam moment input, in accordance with Eqs. 11.66a and 11.66b. The broken line indicates the moment pattern that would result from the current ACI^{11.8} and SEAOC^{11.23} code requirements.

It would be unreasonable to determine the design column shear force from the full M_{ic} moment at each of the columns, since normally the moment at one end is considerably less than M_{ic} . A reasonable moment pattern from which the maximum likely column shear forces could be derived is suggested in Fig. 11.57c, so that

$$V_{ic} \geq \frac{1.5M_{ic}}{\varphi l_u} \quad (11.67)$$

where V_{ic} = ideal shear strength of column

M_{ic} = ideal flexural strength of column section in presence of that axial load which results in a maximum column flexural strength

l_u = clear height of column

φ = capacity reduction factor for shear (i.e., 0.85)

Conclusions

A rational capacity design procedure is likely to give a large degree of protection against brittle failures and column yielding. In cases of unusual behavior, caused by extreme ground motions, column yielding may occur. However, the suggested procedure is likely to ensure a small ductility demand on columns. Further work is required to establish reliable numerical values for the various strength parameters. It is particularly important to evaluate from case studies, or otherwise, the likely range of the values of the moment distribution factor λ_c , which depend on the moment patterns up the height of columns at instants of the dynamic response of a frame. To sustain the principal energy-dissipating system (i.e., beam yielding) under concurrent seismic excitation along both principal axes of a building even larger reserve strengths must be allocated to the columns. It is evident that many design problems in reinforced concrete space frames, such as column yielding, beam-column joint detailing, and instability due to drift, can be avoided if an independent lateral load resisting system, consisting of reinforced concrete shear walls, is provided in both principal directions. These ideas are examined in the next chapter.

11.7 REFERENCES

- 11.1 W. H. Glanville and F. G. Thomas, "The Redistribution of Moments in Reinforced Concrete Beams and Frames," *Journal of the Institution of Civil Engineers*, Vol. 3, Paper No. 5061, 1935-1936.
- 11.2 A. L. Lazaro and R. Richards, "Full-Range Analysis of Concrete Frames," *Journal of the Structural Division, ASCE*, Vol. 99, ST8, August 1973, pp. 1761-1783.
- 11.3 W. B. Cranston, "Tests on Reinforced Concrete Frames, 1: Pinned Portal Frames," Technical Report TRA 392, Cement and Concrete Association, London, August 1965.
- 11.4 W. B. Cranston, "A Computer Method for Inelastic Analysis of Frames," Technical Report TRA 386, Cement and Concrete Association, London, March 1965.
- 11.5 J. M. Becker, "Inelastic Analysis of Reinforced Concrete Frames." Master of Science thesis, Cornell University, Ithaca, N.Y., 1967.
- 11.6 J. Blaauwendaard, "Realistic Analysis of Reinforced Concrete Framed Structures," *Heron*, Vol. 18, No. 4, Delft, 1972, 31 pp.
- 11.7 M. Menegotto and P. E. Pinto, "Method of Analysis for Cyclically Loaded R.C. Plane Frames Including Changes in Geometry and Non-Elastic Behaviour of Elements Under

- Combined Normal Force and Bending," Symposium on the Resistance and Ultimate Deformability of Structures Acted on by Well Defined Repeated Loads, International Association for Bridge and Structural Engineering, *Preliminary Report*, Vol. 13, Lisbon, 1973, pp. 15-22.
- 11.8 ACI Committee 318, "Building Code Requirements for Reinforced Concrete (ACI 318-71)," American Concrete Institute, Detroit, 1971, 78 pp.
- 11.9 H. Okamura, S. N. Pagay, J. E. Breen, and P. M. Ferguson, "Elastic Frame Analysis—Corrections Necessary for Design of Short Columns in Braced Frames," *Journal ACI*, Vol. 67, No. 11, November 1970, pp. 894-897.
- 11.10 ACI Committee 318, "Commentary on Building Code Requirements for Reinforced Concrete (ACI 318-71)," American Concrete Institute, Detroit, 1971, 96 pp.
- 11.11 M. Z. Cohn, "Rotational Compatibility in the Limit Design of Reinforced Concrete Continuous Beams," *Proceedings of the International Symposium on the Flexural Mechanics of Reinforced Concrete, ASCE-ACI*, Miami, November 1964, pp. 359-382.
- 11.12 A. H. Mattock, "Redistribution of Design Bending Moments in Reinforced Concrete Continuous Beams," *Proceedings of the Institution of Civil Engineers*, Vol. 13, 1959, pp. 35-46.
- 11.13 BSI, "Code of Practice for the Structural Use of Concrete," CP110: Part 1: 1972, British Standards Institution, London, 1972, 154 pp.
- 11.14 ICE Research Committee, "Ultimate Load Design of Concrete Structures," *Proceedings of Institution of Civil Engineers*, Vol. 21, February 1962, pp. 399-442. (Discussion in *Proceedings*, October and November, 1962, and June 1963).
- 11.15 ACI-ASCE Committee 428, "Progress Report on Code Clauses for Limit Design," *Journal ACI*, Vol. 65, No. 9, September 1968, pp. 713-720.
- 11.16 A. L. L. Baker, *Ultimate Load Theory Applied to the Design of Reinforced and Prestressed Concrete Frames*, Concrete Publications Ltd, London, 1956, 91 pp.
- 11.17 A. L. L. Baker and A. M. N. Amarakone, "Inelastic Hyperstatic Frames Analysis," *Proceedings of International Symposium on the Flexural Mechanics of Reinforced Concrete, ASCE-ACI*, Miami, November 1964, pp. 85-136.
- 11.18 M. Z. Cohn, "Limit Design of Reinforced Concrete Frames," *Journal of the Structural Division, ASCE*, Vol. 94, ST10, October 1968, pp. 2467-2483.
- 11.19 H. A. Sawyer, "Design of Concrete Frames for Two Failure Stages," *Proceedings of International Symposium on the Flexural Mechanics of Reinforced Concrete, ASCE-ACI*, Miami, November 1964, pp. 405-431.
- 11.20 R. W. Furlong, "Design of Concrete Frames by Assigned Limit Moments," *Journal ACI*, Vol. 67, No. 4, April 1970, pp. 341-353.
- 11.21 R. L. Wiegel, editor, *Earthquake Engineering*, Prentice-Hall, Englewood Cliffs, N.J., 1970, 518 pp.
- 11.22 N. M. Newmark and E. Rosenblueth, *Fundamentals of Earthquake Engineering*, Prentice-Hall, Englewood Cliffs, N.J., 1971, 640 pp.
- 11.23 SEAOC, "Recommended Lateral Force Requirements and Commentary," Seismology Committee, Structural Engineers' Association of California, San Francisco, 1973, 146 pp.
- 11.24 ICBO, *Uniform Building Code*, International Conference of Building Officials, Pasadena, Calif., Vol. 1, 1970, 651 pp.
- 11.25 J. A. Blume, N. M. Newmark, and L. H. Corning, *Design of Multistory Reinforced Concrete Buildings for Earthquake Motions*, Portland Cement Association, Skokie, Ill., 1961, 318 pp.

- 11.26 R. W. Clough, "Effect of Stiffness Degradation on Earthquake Ductility Requirements," Report No. 66-16, Structural Engineering Laboratory, Berkeley, University of California, October 1966.
- 11.27 R. Park, "Ductility of Reinforced Concrete Frames Under Seismic Loading," *New Zealand Engineering*, Vol. 23, No. 11, November 1968, pp. 427-435.
- 11.28 R. W. Clough, K. L. Benuska, and E. L. Wilson, "Inelastic Earthquake Response of Tall Buildings," *Proceedings Third World Conference on Earthquake Engineering*, New Zealand, 1965, pp. 2.68-2.89.
- 11.29 T. E. Kelly, "Some Seismic Design Aspects of Multistorey Concrete Frames," Master of Engineering Report, University of Canterbury, New Zealand, 1974, 163 pp.
- 11.30 ACI Committee 439, "Effect of Steel Strength and Reinforcement Ratio on the Mode of Failure and Strain Energy Capacity of Reinforced Concrete Beams," *Journal ACI*, Vol. 66, No. 3, March 1969, pp. 165-173.
- 11.31 P. C. Jennings, "Response of Simple Yielding Structures to Earthquake Excitation." Ph.D. thesis, California Institute of Technology, Pasadena, 1963.
- 11.32 G. K. Wilby, "Response of Reinforced Concrete Structures to Seismic Motions." Ph.D. thesis in preparation, University of Canterbury, New Zealand, 1974.
- 11.33 I. C. Armstrong, "Capacity Design of Reinforced Concrete Frames for Ductile Earthquake Performance," *Bulletin of New Zealand Society for Earthquake Engineering*, Vol. 5, No. 4, December 1972, pp. 133-142.
- 11.34 D. G. Row, "The Effects of Skew Seismic Response on Reinforced Concrete Frames," Master of Engineering report, University of Canterbury, New Zealand, 1973, 101 pp.
- 11.35 J. A. Norton, "Ductility of Rectangular Reinforced Concrete Columns," Master of Engineering report, University of Canterbury, New Zealand, 1972, 110 pp. plus appendices.
- 11.36 R. Park and R. A. Sampson, "Ductility of Reinforced Concrete Column Sections in Seismic Design," *Journal ACI*, Vol. 69, No. 9, September 1972, pp. 543-551. (Erratum: the figure captions for Figs. 3 and 4 should be transposed.)
- 11.37 J. M. Kelly, R. I. Skinner, and A. J. Heine, "Mechanisms of Energy Absorption in Special Devices for Use in Earthquake Resistant Structures," *Bulletin of New Zealand Society for Earthquake Engineering*, Vol. 5, No. 3, September 1972, pp. 63-88.
- 11.38 M. Fintel and F. R. Khan, "Shock-Absorbing Soft Story Concept for Multistory Earthquake Structures," *Journal ACI*, Vol. 66, No. 5, May 1969, pp. 381-390.

Shear Walls of Multistory Buildings

12.1 INTRODUCTION

The usefulness of walls in the structural planning of multistory buildings has long been recognized. When walls are situated in advantageous positions in a building, they can be very efficient in resisting lateral loads originating from wind or earthquakes. Because a large portion of the lateral load on a building, if not the whole amount, and the horizontal shear force resulting from the load, are often assigned to such structural elements, they have been called shear walls. The name is unfortunate, for only rarely is the critical mode of resistance associated with shear. Multistory buildings have become taller and more slender, and with this trend the analysis of shear walls may emerge as a critical design item. More often than not, shear walls are pierced by numerous openings. The structural engineer is fortunate if these are arranged in a systematic pattern.

In a number of papers, published mainly in the last decade, the elastic behavior of various shear walls has been examined. The proceedings of a symposium sponsored by the University of Southampton^{12.1} represents a good summary of the present state of knowledge of shear wall structures. Some of the conclusions of these studies are considered in the following.

Code recommendations used in the past 10 years have been largely based on the pioneering work of Benjamin and Williams^{12.2, 12.3} on low-rise shear walls. Also, the findings of de Paiva and Siess^{12.4} and the early works of Slater, Lord, and Zippordt^{12.5} on deep beams were interpreted to apply to low-rise shear walls. The work of Cardenas et al.^{12.6, 12.7} and Barda^{12.8} at the Portland Cement Association Research and Development Laboratories in Skokie, Illinois, has contributed much toward the present understanding of shear wall components. Certain aspects arising from the seismic resistance and elastoplastic response of coupled shear walls and their components have been studied at the University of Canterbury, and the more important conclusions of these are incorporated in this chapter.

The emphasis has been placed on behavior as witnessed from tests. Much

work is still to be done before we can predict reliably the elastoplastic response of shear wall structures. No attempt is made here to trace the origin and evaluation of the loadings such as may arise from wind or seismic effect, but as in previous chapters, attention is focused on ductility and energy absorption aspects dictated by the nature of earthquake response.

The use of shear walls or their equivalent becomes imperative in certain high-rise buildings if interstory deflections, caused by lateral loading, are to be controlled. Well-designed shear walls in seismic areas have a very good record. Not only can they provide adequate structural safety, but they also give a great measure of protection against costly nonstructural damage during moderate seismic disturbances.

12.2 THE BEHAVIOR OF CANTILEVER WALLS

12.2.1 Tall Walls Having Rectangular Cross Sections

A single cantilever shear wall, like that in Fig. 12.1 can be expected to behave essentially in the same way as a reinforced concrete beam. The narrow cross section (i.e., small width) suggests that the problem of instability of the compression edge may arise (see Section 4.5). Normally the floor slabs of a multi-story building, indicated in Fig. 12.1, act as horizontal diaphragms and will provide lateral support; thus the critical length, with respect to buckling, may be taken as being equal to the floor height.

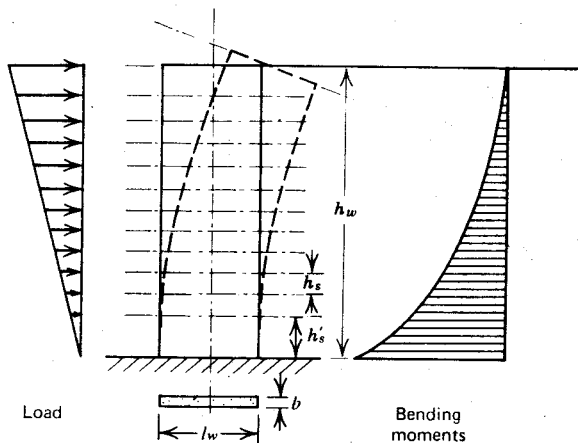


Fig. 12.1. A cantilever shear wall.

The shear wall, as a large cantilever, will be subjected to bending moments and shear forces originating largely from lateral loads, and to axial compression caused by gravity. Accordingly, the strength of the critical section across the wall can be evaluated from the moment-axial force interaction relationship, presented in Chapter 5. The vertical or flexural reinforcement in the web portion of a shear wall, which can be considerable, should be taken into account when assessing the flexural capacity.

Essential prerequisites are adequate foundations giving full base fixity, and sufficient connection of the shear walls to each floor to transmit the horizontal load.

The Flexural Strength of Tall Shear Walls

In many shear walls, particularly in areas not affected by earthquakes, the strength requirement for flexural steel is not great. In such walls it has been a traditional practice to provide about 0.25% reinforcement in both directions. Thus in walls subjected to small bending, 0.25% or slightly more reinforcement has been placed uniformly over the entire depth. Naturally such an arrangement does not efficiently utilize the steel at the ultimate moment because many bars operate on a relatively small internal lever arm. Moreover, the ultimate curvature, hence the curvature ductility, is considerably reduced when a large amount of flexural steel is used in this form. Cordenas and Magura^{12,7} have shown this for a typical wall section with a depth to width ratio of 25. Their example is reproduced in Fig. 12.2, where the moments and curvatures are expressed as percentages of the corresponding ultimate quantities for a section with the minimum ($\rho_v = 0.25\%$) steel content. Clearly uniform steel distribution across the section is not only uneconomical but highly undesirable for larger steel contents whenever energy absorption in the postelastic range is wanted.

In an efficient shear wall section, subjected to considerable moments, the bulk of the flexural reinforcement will be placed close to the tensile edge. Because of moment reversals originating from lateral loads, equal amounts of reinforcement are normally required at both extremities. Thus if necessary, a considerable part of the bending moment can be resisted by the internal "steel couple," and this will result in improved ductility properties. In the section with the nonuniform steel distribution in Fig. 12.2, minimum vertical reinforcement (0.25%) has been placed over the inner 80% of the depth. The remainder of the steel has been allocated to the outer (10%) zones of the section. The increased strengths and ductility due to this arrangement are evident from the diagram.

Because of the large cross-sectional area, the axial compressive load on shear walls is often considerably smaller than that which would cause a

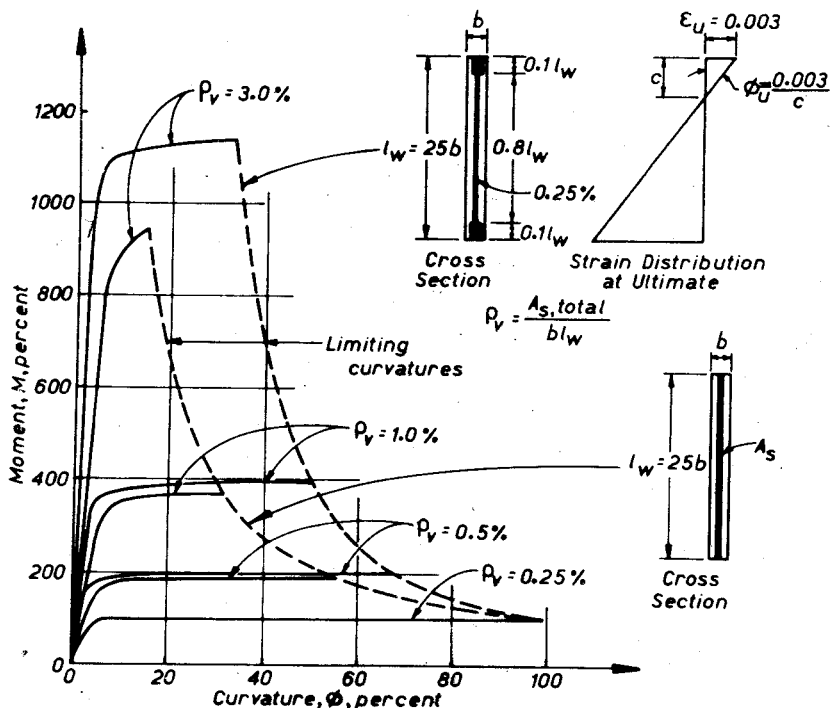


Fig. 12.2. Effect of amount and distribution of vertical reinforcement on ultimate curvature.^{12.7}

balanced failure condition (P_b). As a result, the moment capacity is usually increased by gravity forces in shear walls. However, it must be remembered that axial compression will reduce ductility.

When it is desirable to increase the ductility of a cantilever shear wall—normally at its base, where overturning moments and axial compression are the largest—the concrete in the compression zone must be confined. It is suggested that the confining steel be provided in the same way as in tied columns (see Chapters 11 and 13) and be extended at least over that part of the depth l_w where concrete strains in excess of 0.003 are required when the desired ductility is attained. At any rate, transverse ties around the flexural bars, which may be subjected to compression yield, should be provided at least in the same way as in axially loaded columns, to prevent buckling of these bars (see Section 13.5). This is particularly important over the region of a possible plastic hinge, which may extend over a full story height or more. Over this distance, nominal ties at code-specified maximum spacing are not

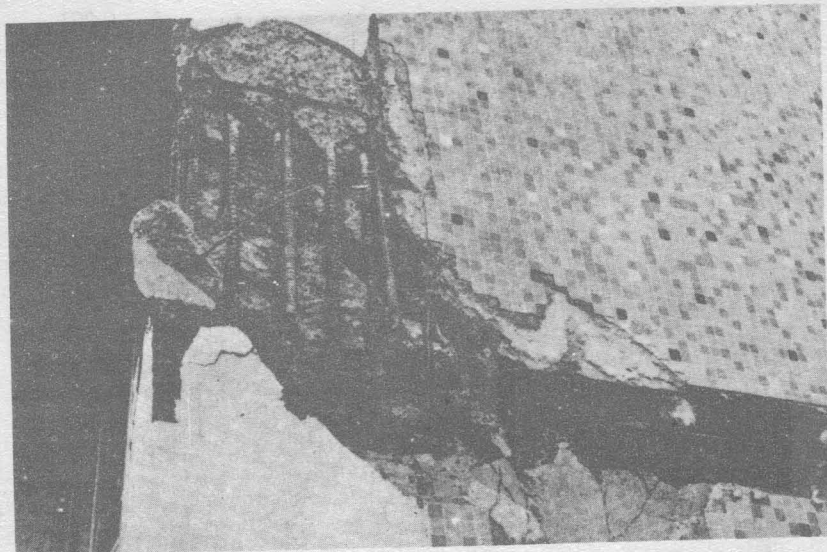


Fig. 12.3. Failure along a construction joint exposing edge bars at a lap. Holy Cross Hospital after the San Fernando Earthquake.^{12,13}

likely to be sufficient when yielding at both extremities of the shear wall section can be caused by several seismic shocks. Only closely spaced ties can retain the cracked concrete core within the vertical flexural bars at the extremities of the section (see Fig. 12.3) and prevent buckling of the longitudinal bars.

The flexural strength of a rectangular shear wall containing uniformly distributed vertical reinforcement and subjected to axial load can be derived from first principles (see Chapter 5). Considerable simplifications result, however, if the contribution of the reinforcement in the elastic core is neglected.^{12,6} From first principles, the corresponding conservative approximation gives

$$M_u = 0.5 A_s f_y l_w \left(1 + \frac{N_u}{A_s f_y}\right) \left(1 - \frac{c}{l_w}\right) \quad (12.1)$$

where N_u , the axial load, is taken as positive for compression and A_s is the total uniformly distributed wall steel. The other terms are evident from Fig. 12.2.

The instability of thin shear walls needs to be considered. Conservatively, the extreme fibers of the wall section can be treated as an isolated column subjected to axial compression only and liable to buckle about the weak axis

of the section. If necessary, the flexural rigidity of the wall section in the transverse direction can be increased by a return, as in Fig. 12.4. This may be necessary between the ground and first floors of a building, where maximum actions occur often over maximum unsupported lengths.

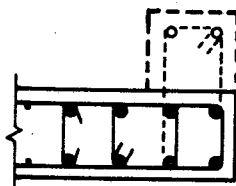


Fig. 12.4. Wall return to increase stability.

The Shear Strength of Tall Shear Walls

The shear strength of tall shear walls can be assessed the same way as in beams. Due allowance can be made for the contribution of the axial compression in boosting the share of the concrete shear resisting mechanism, as measured by the nominal shear stress v_c (see Section 7.6.1). In doing so, the adverse effect of vertical accelerations induced by earthquakes should also be considered. At the base of the wall, where yielding of the flexural steel in both faces is possible, the contribution of the concrete toward the shear strength should be neglected when the axial compressive stress on the gross wall area, P_u/A_g , is less than $0.2f'_c$, since this small compression might possibly be offset by vertical acceleration causing tension. Aspects relating to this principle are also discussed in Chapters 7 and 13. This implies that when $P_u/A_g < 0.2f'_c$, shear reinforcement in the form of horizontal stirrups should be provided at least over the possible length of the plastic hinge at the base of the wall to carry all the shear force. The effect of the aspect ratio of the wall on shear strength was thought to be important in short shear walls, and the subject is discussed in Section 12.2.2.

The minimum reinforcement of 0.25% in the horizontal direction, when appropriately anchored, will resist an equivalent nominal shear stress of approximately $2\sqrt{f'_c}$ psi ($0.166\sqrt{f'_c}$ N/mm²) (see Eq. 7.23a). At least the same amount will be supplied by the concrete when the flexural steel is in the elastic range. Consequently, in the nominally reinforced upper parts of rectangular cantilever shear walls, a shear strength equivalent of $4\sqrt{f'_c}$ psi ($0.333\sqrt{f'_c}$ N/mm²) is available,^{12,6} and this is often more than adequate.

The effective depth of a rectangular shear wall section is affected by the arrangement of the vertical steel. In applying the appropriate equations for

nominal shear stress, Eq. 7.5, and stirrup reinforcement, Eq. 7.23a, the effective depth d need not be taken as less than $0.8l_w$. This is a good approximation for the common cases. Moreover, some allowance has been made for this^{12,6} in the relevant equation of the ACI code. The Portland Cement Association tests on high-rise shear wall models have demonstrated that the present ACI approach gives a conservative estimate of the shear strength for monotonic loading.^{12,6}

The effect of diagonal cracking on the distribution of flexural steel stresses should be considered the same way as in beams. For cutting off the vertical reinforcement in the outer parts of the wall section, the appropriate displacement of the bending moment diagram, shown in Chapter 7, should be used. Again it may be noted that the effective depth of the wall could be more than one story height.

Construction Joints Across Shear Walls

Earthquake damage in shear walls has been often observed at construction joints along which sliding movement occurred. These are more common in low shear walls, which carry small gravity loads. However, such damage has been evident in high-rise shear walls as well (see Figs. 12.3 and 12.22). It is therefore necessary to ensure that sufficient vertical reinforcement is provided in the web of the shear wall to suppress a sliding shear failure.

In Chapter 7 the mechanism of aggregate interlock or shear friction was outlined, with particular reference to construction joints. It was shown that the average shear stress that can be safely transferred across a well-prepared rough horizontal joint is at least

$$v_{uf} = \frac{N + A_{vf} f_y}{A_g} \quad (12.2)$$

where N = axial force on section, taken as positive when producing compression

A_{vf} = total (vertical) steel to be utilized for required clamping force

A_g = gross sectional area of wall

v_{uf} = nominal shear stress transmitted across construction joint

In a shear wall subjected to seismic load, the beneficial effect of the axial compression must not be overestimated. Only the real gravity load, with appropriate reduction (say 20%) for negative vertical acceleration, should be taken into account. Hence by assuming the effective depth of the shear wall to be $0.8l_w$, we have as the dependable nominal shear strength

$$v_{uf} = \varphi \frac{0.80N + A_{vf} f_y}{0.8bl_w} \quad (12.2a)$$

where the capacity reduction factor φ may be taken as 0.85.

The strength of the construction joint must be equal to but preferably greater than the shear strength v_u , required at that particular level. In this context, shear strength, $v_u = V_u/0.8bl_w$, refers to the diagonal tension strength of the wall. According to Eq. 12.2a, then, when $v_{uf} \geq v_u$, the required steel content $\rho_{vf} = A_{vf}/A_g$ across the construction joint becomes

$$\rho_{vf} \geq \left(v_u - 0.85 \frac{N}{A_g} \right) \frac{0.94}{f_y} \geq 0.0025 = \rho_{vf, \min} \quad (12.3)$$

With a small amount of axial compression, it will not be difficult to satisfy Eq. 12.3. In the absence of axial compression, however, the minimum vertical reinforcing content of 0.25% in the core of the wall is not likely to be adequate unless the ultimate shear stress than is to be developed is very small. Figure 12.5 shows the amount of vertical reinforcement (Eq. 12.3)

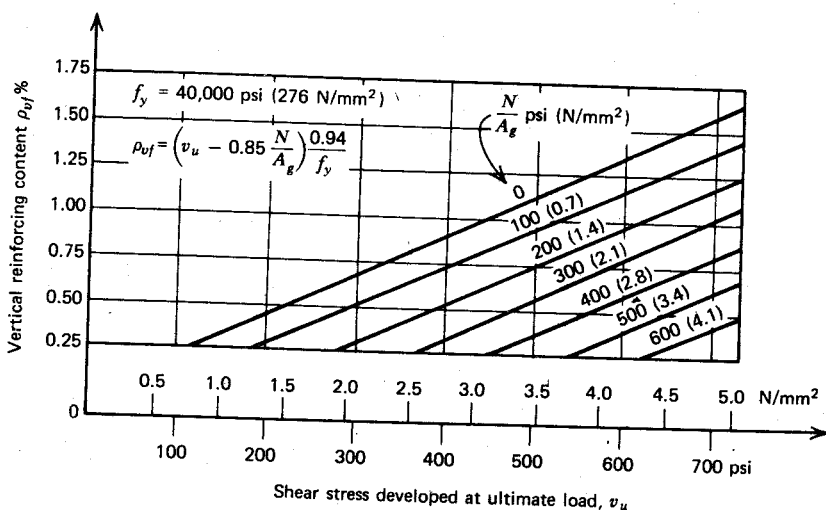


Fig. 12.5. Vertical reinforcement requirements across a construction joint of a shear wall.

to be provided across a horizontal construction joint. This is a function of the nominal shear stress v_u to be resisted at that level of the joint, together 40,000 psi (276 N/mm²). It is important that this amount of vertical reinforcement be provided over each foot length of the wall section. The clamping force of one bar is effective only in the immediate vicinity of that bar, with different intensities of axial compression stresses for a yield strength of. Consequently, heavy reinforcement situated near the extreme vertical edges of the wall sections should not be included in the evaluation of the clamping force across the core of the section.

12.2.2 Squat Shear Walls Having Rectangular Cross Sections

In many low-rise buildings, the height of the cantilever shear walls is less than their length (i.e., their structural depth). Clearly, in such situations, the assessment of the flexural and shear strength and appropriate reinforcement cannot be based on the conventional techniques applicable to taller walls. Rather, the principles established in connection with the behavior of deep beams are relevant. It is no longer possible to discuss separately flexure and shear, since the two are more intimately interrelated in squat shear walls.

Low-rise shear walls normally carry only very small gravity loads, and for this reason their beneficial effect, derived at least for shear strength, is best ignored. The flexural steel demand will also be small in most cases because of the relatively large available internal lever arm. It will be more practical, therefore, to distribute the vertical (i.e., flexural) reinforcement uniformly over the full length of the wall, allowing only a nominal increase at the vertical edges.

For seismic loading the corresponding loss of ductility is not likely to be of great importance for two reasons. First, the low steel requirement is often satisfied by near-minimum steel content (i.e., 0.25%), which provides sufficient energy absorption in the postelastic range (see Fig. 12.2). Second, properly detailed squat shear walls can be made to absorb all or most of the seismic shock in the elastic range without demand for great reinforcement contents.

For want of other and better information, it has been the practice to attempt to predict the likely behavior of low-rise shear walls from tests carried out on deep beams. Geometric similarities suggest such a procedure. Most tests on deep beams have a common feature—the load is directly applied to the top and bottom faces of the simply supported specimens in the span and at the supports, respectively. It was pointed out in Section 7.3.3 that this form of load application considerably enhances the effectiveness of arch action. Stirrups crossing the main diagonal crack, forming between load point and support, are not engaged in efficient shear resistance because no compression struts can form between stirrup anchorages. The arch disposes of the shear along the shortest possible route, and this is associated with smaller deformations. It is not surprising, therefore, to find from experiments that additional stirrups did not improve shear strength.^{12,4}

For the common shear wall of a building, the load is introduced along the joint between floor slabs and walls as a line load. Clearly no effective arch action can develop with this type of loading. Leonhardt and Walther^{13,21} demonstrated this behavior convincingly in a test of a deep beam, shown in

Fig. 13.47 and discussed in Section 13.7.4. The crack pattern reveals the formation of diagonal struts, hence the engagement of stirrups. A similar crack pattern, likely to occur in a low-rise shear wall, is sketched in Fig. 12.6. From considerations of equilibrium of the triangular free body, marked 1, it is evident that horizontal stirrups are required to resist the shearing stress applied along the top edge. The diagonal compression forces set up in the

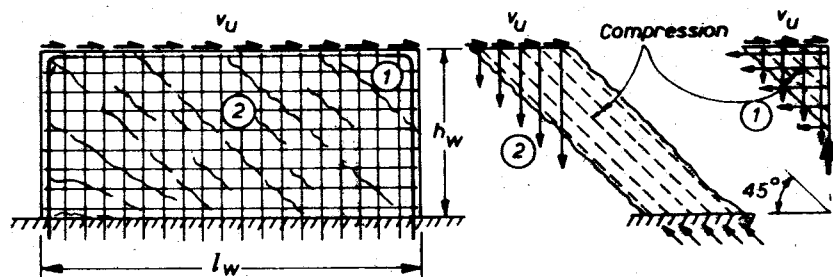


Fig. 12.6. The shear resistance of low-rise shear walls.

free body also require vertical reinforcement. In the absence of external vertical compression, the horizontal and vertical steel must be equal, to enable 45° compression diagonals to be generated. In the free body bound by two diagonal cracks and marked 2, on the other hand, only vertical forces, equal to the shear intensity, need be generated to develop the necessary diagonal compression. This steel is often referred to as shear reinforcement, even though its principal role is to resist the moment that tends to overturn free body 2. Figure 12.6 thus illustrates the role of vertical and horizontal bars in resisting shear forces in low-rise shear walls.

In early systematic studies of squat shear walls, Benjamin and Williams applied a concentrated lateral load to the tension side of short cantilevers.^{12.2, 12.3} Some of the design recommendations in the 1960s were based on these findings and on the early deep-beam tests of the U.S. Bureau of Standards.^{12.5} The linear arch, whose inclination is indicated by the h_w/l_w ratio, was significant in carrying the shear in all these tests. The use of this ratio in relation to the shear strength of shear walls, has recently been abandoned.^{12.9}

To study the behavior of squat shear walls and the effects of both the flexural (vertical) and shear (horizontal) reinforcement on the failure mode and on ductility, tests have been carried out at the University of Canterbury^{12.11} on square 6 in (150 mm) thick cantilever shear walls. The walls

were subjected to a load in such a way that the shear force was distributed along the top edge (see Fig. 12.7). For convenience, the applied load is expressed in terms of the nominal shear stress v and the theoretical ultimate capacity P_u^* . The failure mode of each of the test walls is evident from Fig. 12.7.

1. Wall A was deliberately underdesigned for shear. Stirrups were expected to resist only 50% of the load, which would have been developed if flexure governed the strength. Figure 12.7a shows the development of diagonal cracks during 12 cycles of the loading. Considerable strain hardening occurred in the reinforcement because 123% of the theoretical shear capacity and 108% of the flexural capacity could be developed. At failure, one stirrup fractured, demonstrating the effectiveness of stirrups in such squat shear walls.

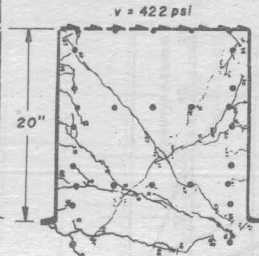
2. Wall B was identical to wall A except that shear reinforcement was provided in excess of the flexural capacity. The theoretical flexural strength was associated with moderate nominal shear stresses [i.e., $5.6\sqrt{f'_c}$ psi ($0.47\sqrt{f'_c}$ N/mm²)]. The specimen exceeded its ultimate design capacity in each of the "plastic" cycles and could not be destroyed as contemplated because the loading frame was unable to match the specimen's ductility. Figure 12.7b shows Wall B at various stages of the loading.

3. By providing more vertical reinforcement in wall C, the flexural capacity was made approximately twice that of wall B. This flexural strength required the development of large shear stresses [i.e., approximately $10\sqrt{f'_c}$ psi ($0.83\sqrt{f'_c}$ N/mm²)]. The design shear strength of the wall was in excess of its flexural capacity; hence a flexural failure could be expected. As Fig. 12.7c shows, a sliding shear failure occurred in the twelfth cycle of loading at 39% of the theoretical shear capacity of the specimen. This type of failure, typical of deep members when high-intensity cyclic (reversed) shear is applied, cannot be prevented by additional stirrup reinforcement. A sliding shear failure would not normally be found in tests with monotonic loading because up to crushing, the compression zone remains relatively intact. This type of failure is discussed in greater detail in Section 12.5.3 when the behavior of deep spandrel beams is reviewed.

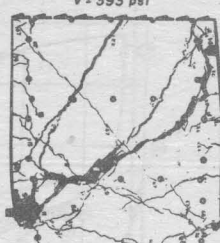
Figure 12.8 gives the load-rotation relationship for all three walls: where "rotation" is defined as the lateral deflection of wall divided by its height. Cycles 1 to 4 show the initial elastic response and cycles 7 to 8 indicate the elastic response after one moderate excursion beyond the yield range in each direction was made. The plastic response of each wall can be conveniently expressed by the cumulative ductility factor, where "ductility factor" is defined as the ratio of the maximum wall rotation attained in a load cycle to the wall rotation at the first yielding, obtained in the fifth load



(a) 1ST CYCLE .75 P_u^*



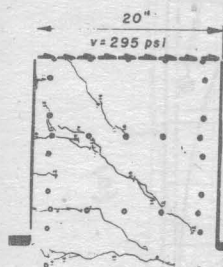
5TH CYCLE 1.06 P_u^*



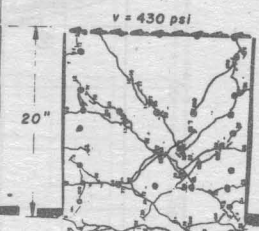
12TH CYCLE - .99 P_u^*

1 psi = 0.00689 N/mm²

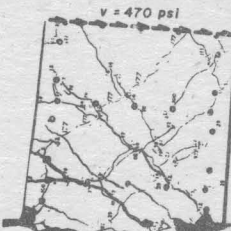
1 in = 25.4 mm



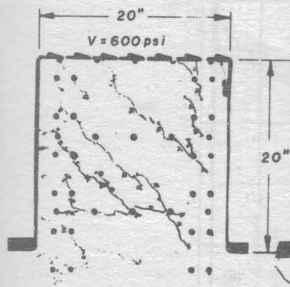
(b) 1ST CYCLE .75 P_u^*



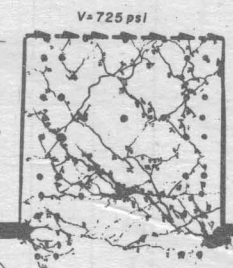
6TH CYCLE - 1.08 P_u^*



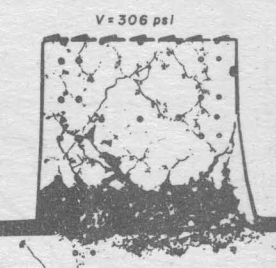
13TH CYCLE 1.16 P_u^*



(c) 1ST CYCLE .76 P_u^*

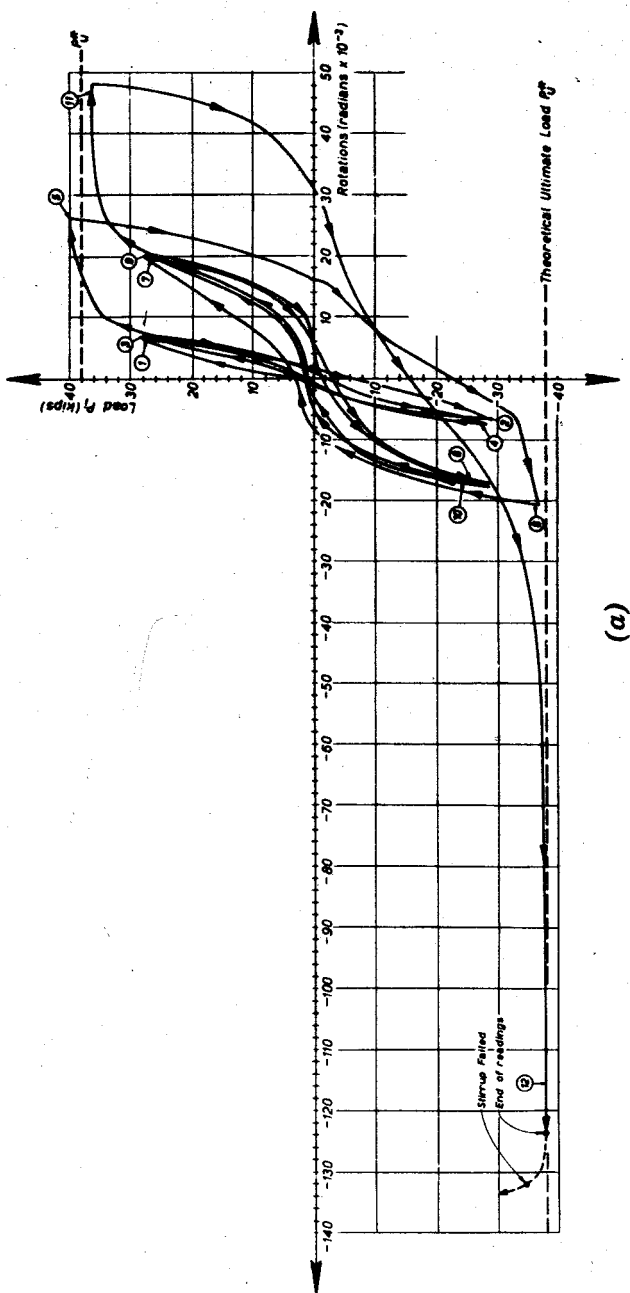


11TH CYCLE .92 P_u^*



12TH CYCLE - .39 P_u^*

Fig. 12.7. The failure modes of three squat shear wall models.^{12,11} (a) Wall A. (b) Wall B. (c) Wall C.



(a)

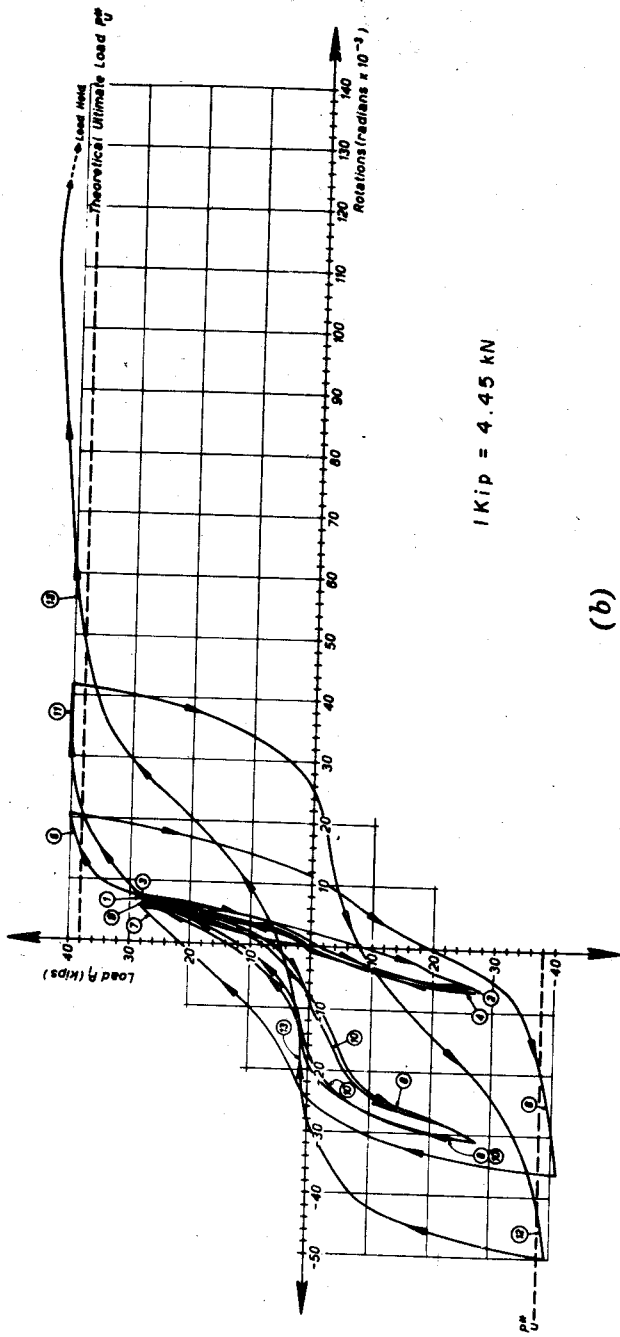
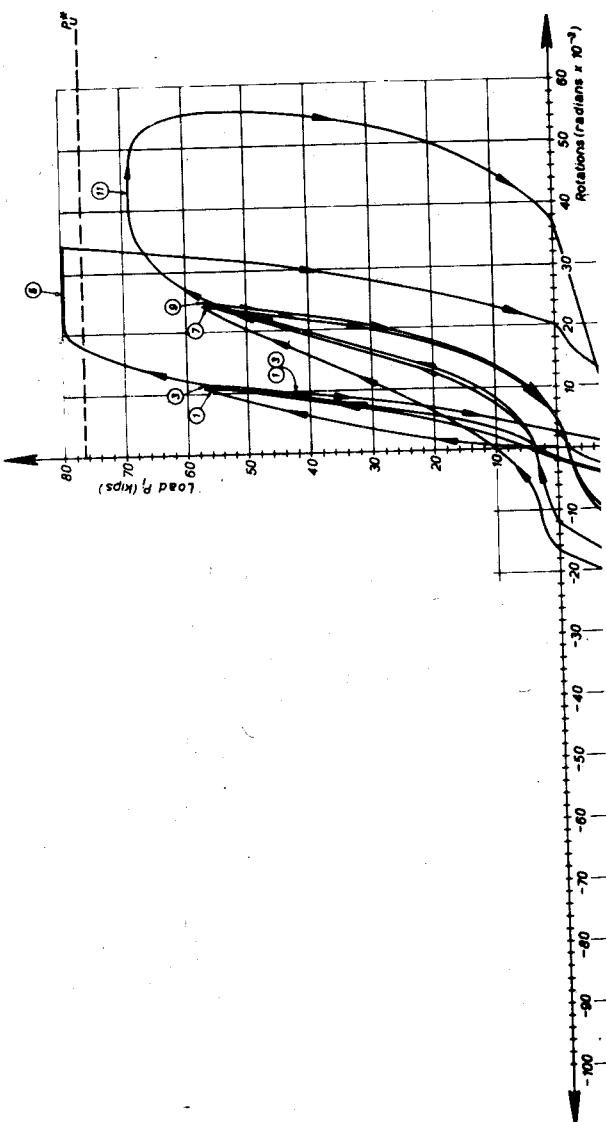


Fig. 12.8. Load-rotation relationships for squat shear walls subjected to cyclic loading. (a) Wall A. (b) Wall B. (c) Wall C.
(See also pages 624-5)



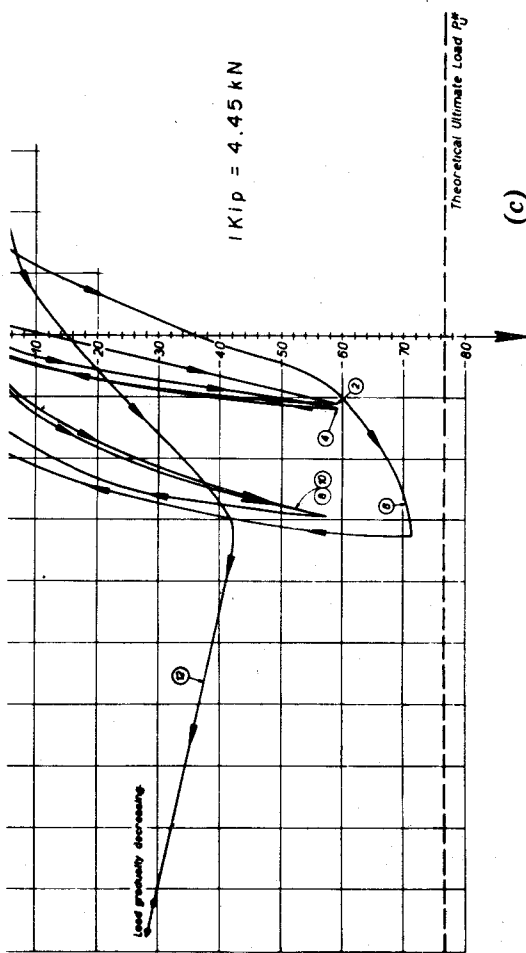


Fig. 12.8. (continued)

cycle. This cumulative ductility factor was 46, 56 and 30 for walls A, B and C respectively. Not only was wall C the least ductile one, but it also showed a distinct loss of strength during testing. The superior performance of wall B suggests two important conclusions for design:

(a) If a ductile (i.e., a flexural) failure mechanism is desired in a low-rise shear wall, the nominal shear stresses associated with the flexural overcapacity of the wall must be moderate, say, $v_s \leq 6\sqrt{f'_c}$ psi ($0.5\sqrt{f'_c}$ N/mm²). This is normally not difficult to achieve. If necessary, the wall thickness should be increased.

(b) Because the flexural failure mechanism is associated with large cracks, no reliance should be placed on the contribution of concrete toward shear strength. Consequently, the whole of the shear force should be resisted by web reinforcement.

It is to be noted that the possible effect of axial compression was not considered in these tests.

The ACI code^{12.10} provisions for the shear strength of walls were outlined in Chapter 7. The only difference between the shear provisions for walls and beams is in the assessment of v_c , the contribution of the concrete, taking into account the presence of axial load. The background to these provisions has been discussed by Cardenas, Hanson, Corley, and Hognestad,^{12.6} who have shown with their tests and those of many others, that the present ACI code^{12.10} recommendations for walls are conservative and satisfactory.

The minimum shear reinforcement should not be less than 0.25% of the concrete area. It was mentioned earlier that in long, and low shear walls, as in Fig. 12.6., the vertical web reinforcement will be more effective in enabling diagonal compression struts to form. Therefore, in walls with h_w/l_w less than 0.5, the ACI code^{12.10} requires vertical web steel ρ_n equal to the amount of horizontal shear reinforcement. For shear walls having height/length ratios between 0.5 and 2.5, a linear interpolation is suggested between this steel and the minimum of 0.25%, giving

$$\rho_n = 0.0025 + 0.5 \left(2.5 - \frac{h_w}{l_w} \right) (\rho_h - 0.0025) \quad (12.4a)$$

$$\rho_n \geq 0.0025 \quad (12.4b)$$

$$\rho_n \leq \rho_h = \frac{v_u - v_c}{f_y} \quad (12.4c)$$

where ρ_n and ρ_h = vertical and horizontal steel content per unit wall area.

Shear walls are sometimes surrounded by a peripheral frame that may contain substantial reinforcement. The behavior of these walls, also containing openings, was studied experimentally by Umemura^{12.12} and others.

Some researchers have attempted to evaluate the behavior of such walls from the superposition of the frame action and diaphragm action of the wall infill. The approach is justified when no homogeneous connection exists between the two, which is the case for steel or reinforced concrete frames with masonry infill panels. However, a monolithically cast, reinforced concrete shear wall with boundary elements will tend to act as one unit, and every effort should be made in the process of designing and detailing to encourage this most efficient behavior.

12.2.3 Flanged Cantilever Shear Walls

There is no reason to expect tall flanged shear walls, such as that in Fig. 12.9, to behave differently from those having rectangular cross sections. When the axial force is small, we can anticipate that these walls too will utilize the internal "steel couple" in the postelastic range, since the reinforcing content in both flanges is normally the same. Hence ample ductility should be available if required during an earthquake of catastrophic magnitude provided that restraint against steel buckling is adequate.

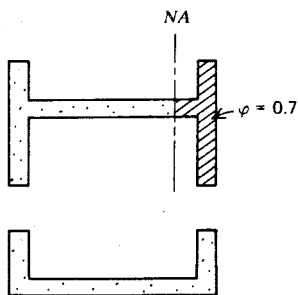


Fig. 12.9. Flanged cross sections.

When the axial compression is significant, the whole of one flange and part of the web may be in compression. In such cases it appears advisable to consider the flanges as axially loaded, tied columns. Accordingly, a lower capacity reduction factor (i.e., $\varphi = 0.7$) would be more appropriate when assessing ultimate capacity in this situation. For intermediate positions of the neutral axis, the value of φ can be suitably interpolated between 0.7 and 0.9. The importance of providing sufficient transverse reinforcement around the main vertical steel in the flanges is evident.

Flanges will considerably boost the moment of resistance of tall cantilever shear walls. Hence the resistance of shear forces in the web may be more critical than in walls having rectangular cross sections. Particular attention must

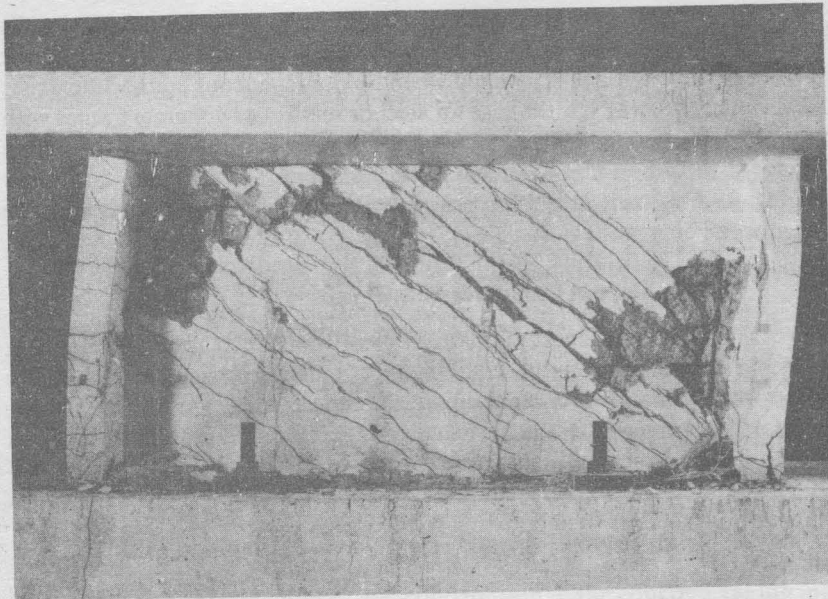


Fig. 12.10. Shear failure of low-rise flanged shear wall.^{12.8} (Courtesy Portland Cement Association.)

be given to horizontal construction joints, which may be more severely loaded, as well. In a well-designed shear wall, the shear reinforcement is not expected to yield at any stage of the loading.

The behavior of short flanged shear walls is more complex. Even a small amount of vertical reinforcement in wide flanges can provide a flexural capacity that is associated with excessive shear load on the web. Barda studied experimentally such walls^{12.8} and confirmed the effectiveness of vertical shear reinforcement in shear walls with h_w/l_w ratio of 0.5. These one-third scale wall specimens (see Fig. 12.10), were deliberately reinforced to encourage a shear failure to occur. Under a nominal shear stress of 800 psi (5.5 N/mm²), the vertical web reinforcement yielded, but no yielding was observed in the vertical flange steel. The elongation of the vertical shear reinforcement caused a hogging curvature of the slab, and the cracks that resulted in the slab are visible in Fig. 12.10. Mesh reinforcement was found to be effective in distributing uniformly the diagonal cracks and in controlling their width. In low-rise flanged shear walls, construction joints may become the critical failure plane.

Barda^{12.8} determined the internal tension force resultants from strain measurements. Combining this information with the external load, the inter-

nal compression resultants for similar specimens could also be found. This study shows (see Fig. 12.11) that the compression flange is not effective in squat shear walls, since the ideal large internal lever arm necessary for "beam" behavior cannot be developed.

12.2.4 Moment-Axial Load Interaction for Shear Wall Sections

Cross sections of flanged, angle, or channel shapes often appear in shear walls, forming the core of multistory buildings. These may be subjected to axial loads of varying intensity, including net tension, together with bending moments about one or both principal axes. For practical reasons the cross sections remain reasonably constant over the full height of the structure. It is possible, and it may be advantageous, to evaluate the interaction relationship between flexure and axial force for such cantilever shear walls. It can be rather cumbersome to work out the required reinforcement for a particular load interaction, but it is relatively easy to determine the possible load combinations for given arrangements and amounts of reinforcement, particularly with the aid of a computer. The results can then be used to allocate the required reinforcement at any level along the full height of the structure.

When a channel-shaped cross section is subjected to axial load and flexure about its weak principal axis, interaction curves of the type illustrated in Fig. 12.12 result. In this particular section the reinforcement was assumed to be uniformly distributed along the center of the wall thickness. The load eccentricity is with reference to the plastic centroid of the section. A positive moment is considered to cause compression at the tips of the flanges and tension in the web of the channel. For pure flexure, this would be an over-reinforced section with about 3% total steel content. For a reversed (negative)

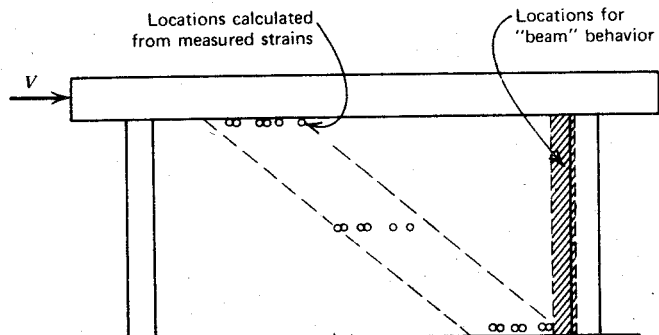


Fig. 12.11. Location of internal compression resultant in flanged low-rise shear walls.^{12.8}

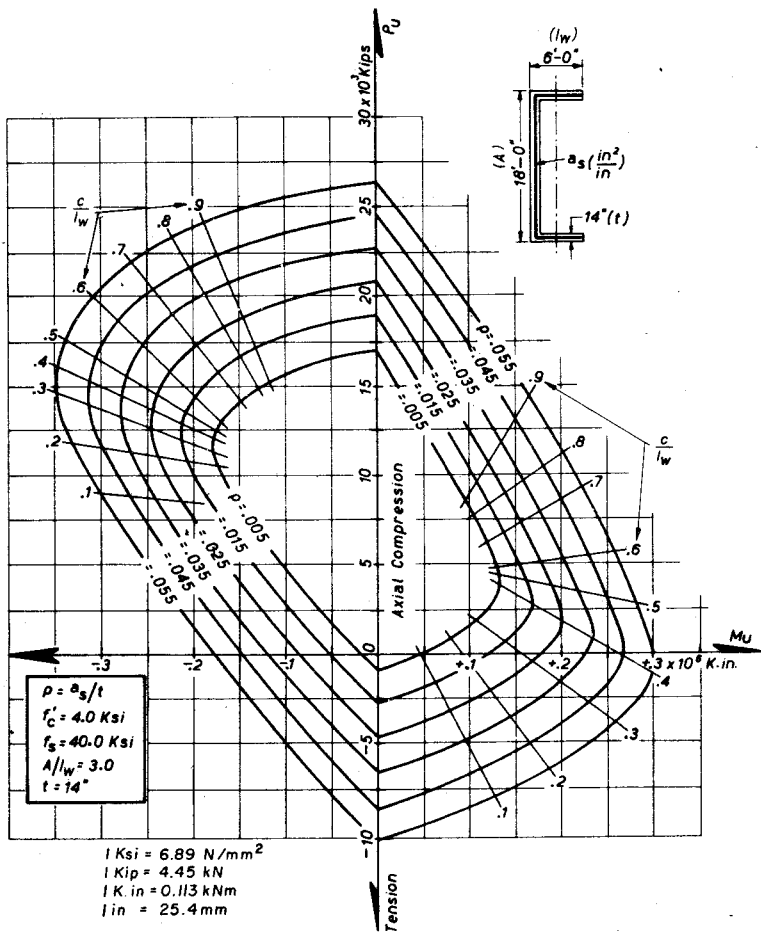


Fig. 12.12. Typical moment-axial force interaction relationships for a channel-shaped shear wall.

moment, causing compression in the web of the section, a marked increase in moment capacity follows the application of compression forces. The computations were carried out^{12,14} for positions of the neutral axis when the same swept throughout the section, the concrete compression strain being kept constant ($\varepsilon_c = 0.003$) at the extreme compression fiber for a particular sense of the bending moment as outlined in Section 5.3.4. The wall section in Fig. 12.12 is suitable to resist moderate axial tension in combination with positive moments, and considerable axial compression with negative moments. These are typical load combinations occurring in coupled shear wall structures.

To be able to assess the extension of the compression zone over the shear wall section, the designer can also determine the neutral axis position with respect to the primary compression edge. These positions are shown in Fig. 12.12 in terms of the ratio of the neutral axis depth to the overall depth, c/l_w . Thus an appropriate value for the undercapacity factor φ can be estimated for any load situation. In the example section of Fig. 12.12, for a negative bending moment with moderate axial compression, c/l_w could be 0.1; thus $0.1 \times 6 \times 12 = 7.2$ in (i.e., about half the web thickness) would be under compression. For this case, $\varphi = 0.9$ would be appropriate. On the other hand, for a positive moment with only a small compression force, $0.5 \times 6 \times 12 = 36$ in of the flange could be under compression. Because the section is only 14 in wide, $\varphi = 0.7$ would be a more suitable value.

12.2.5 Interaction of Cantilever Shear Walls With Each Other

In certain multistory buildings, such as apartment houses, the gravity load as well as the lateral wind or seismic load is carried by shear walls. A typical floor plan of such a building is given in Fig. 12.13. The floor slab may be considered to be very flexible compared with the flexural stiffness of the walls, with respect to their major axis; thus in most cases the flexural resistance of the slab during lateral loading need not be taken into account. The slabs act as horizontal diaphragms, extending between cantilever walls, and they are expected to ensure that the positions of the walls, relative to each other, do not change during lateral displacement of the floors. The flexural resistance of rectangular walls with respect to their weak axis may also be neglected in a lateral load analysis.

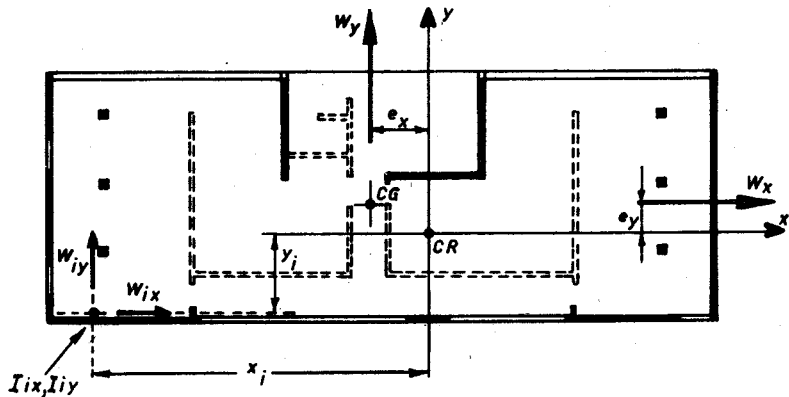


Fig. 12.13. Shear walls of an apartment building.

The elastic analysis of a set of interconnected cantilevers, modeled in Fig. 12.14, can be rather complex if we allow for shear deformations, and torsion with restrained warping in the individual wall units. Rigorous solutions have been proposed by Stiller,^{12.15} Beck,^{12.16} Rosman,^{12.17} and others, and all assume perfectly elastic behavior of the homogeneous isotropic

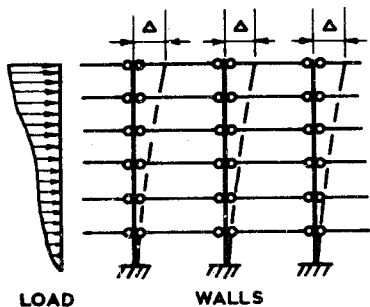


Fig. 12.14. Mathematical model of interacting cantilever shear walls.

structure. However, with certain simplification, the total lateral load can be easily distributed among all cantilever walls. This approximation implies that only flexural deformations occur, which means that the load pattern over the height of each wall is similar. With reference to Fig. 12.13, the distribution of the total lateral seismic load, W_x or W_y , among all cantilever walls, may then be approximated by the following expressions:

$$W_{ix} = W'_{ix} + W''_{ix} \quad (12.5a)$$

$$W_{iy} = W'_{iy} + W''_{iy} \quad (12.5b)$$

where

$$W'_{ix} = \frac{I_{iy}}{\sum I_{iy}} W_x \quad (12.6a)$$

$$W'_{iy} = \frac{I_{ix}}{\sum I_{ix}} W_y \quad (12.6b)$$

$$W''_{ix} = \frac{y_i I_{iy}}{\sum (x_i^2 I_{ix} + y_i^2 I_{iy})} e_y W_x \quad (12.7a)$$

$$W''_{iy} = \frac{x_i I_{ix}}{\sum (x_i^2 I_{ix} + y_i^2 I_{iy})} e_x W_y \quad (12.7b)$$

where W_{ix} , W_{iy} = share of wall i in resisting total external lateral load in x and y directions, respectively

W'_{ix}, W'_{iy} = load induced in wall by interstory translations only

W''_{ix}, W''_{iy} = load induced in wall by interstory torsion only

W_x, W_y = total external load to be resisted by all walls

I_{ix}, I_{iy} = appropriate second moment of area of a wall section about its x and y axes

x_i, y_i = coordinates of wall with respect to center of rigidity CR of load-resisting system

e_x, e_y = eccentricities resulting from noncoincidence of center of gravity CG (mass), and center of rigidity

If W_x and W_y are caused by wind loads, the center of mass should be replaced by the position of the resultant wind force.

Equations 12.5 to 12.7 are analogous to those used in the analysis of rivet groups and are considered to yield sufficiently accurate results when seismic loading is being studied. The errors, which may result from neglecting the shear deformations and the torsional resistance of the walls with open sections, are likely to be smaller than those due to ignoring the effect of cracking on stiffness. The onset of cracking and the consequent loss of stiffness is also affected by the gravity load intensity on each wall.

The foregoing approach should be adequate for an ultimate load analysis, for it represents a statically admissible situation. This approximate elastic analysis is likely to assure that the ultimate resisting capacity of all cantilever walls would be attained at about the same time. With the shapes used for cantilever shear walls of high-rise apartment buildings, there is no reason to expect a deficiency of ductility as long as premature secondary failures (bond, shear, instability, etc.) are not permitted to occur.

For shear walls with a height/depth ratio of less than 3 ($h_w/l_w < 3$), the shear deformations may become predominant enough to be considered in stiffness or deflection computations. Shear distortions are more significant in flanged walls.

In estimating the deflections of solid cantilever shear walls for the purpose of assessing the period of vibration of the structure, the principles of elastic behavior may be used, but Young's modulus E_c and the modulus of rigidity G could be reduced to allow for loss of stiffness caused by flexural and diagonal cracking^{12.18} (see also Section 7.7).

12.3 INTERACTION OF SHEAR WALLS AND RIGID JOINTED FRAMES

It is beyond the scope of this book to discuss techniques for assessing the interaction of shear walls and moment-resisting frames. Several methods of structural analysis are available to cope with this problem.^{12.19, 12.20}

However, certain problems arise from the distinctly different behaviors of walls and frames.

Figure 12.15a illustrates a cantilever shear wall and a frame, both carrying the same load at a certain height. This causes the shear wall to suffer bending distortions and to assume a constant slope above the loaded level. The originally horizontal sections at each floor tilt. The frame experiences mainly translatory displacements and tends to become vertical above the load level.

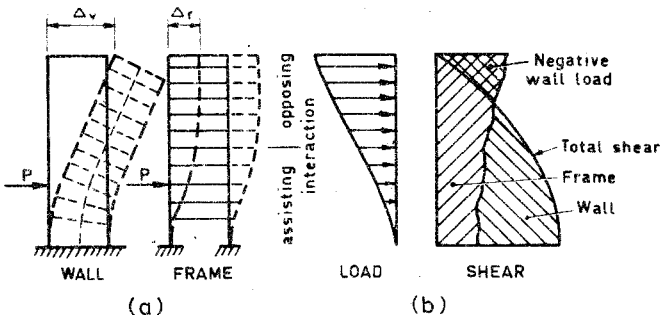


Fig. 12.15. Interaction of shear walls and rigid jointed frames.

When column shortenings are neglected, which is justified for buildings of moderate height, the floors remain horizontal. Because of the incompatibility of the deformations, a shear wall can oppose a moment-resisting frame at the upper floors. Only at the lower floors do the two structures assist each other in carrying the external load. The typical distribution of the lateral load between a tall and a relatively slender shear wall and a frame is illustrated, in terms of the shear forces, in Fig. 12.15b.

Other examples of the use of shear walls in combination with frames, and methods of analysis, are given in a report on the response of buildings to lateral forces, by ACI Committee 442,^{12,21} together with an extensive bibliography.

12.4 SHEAR WALLS WITH OPENINGS

Windows, doors, and service ducts require that exterior or interior shear walls be provided with openings. To ensure a rational structure, it is important that sensible decisions be made at the early stages of the planning, with respect to the positioning of openings throughout the building. (A

"rational shear wall structure" is one whose essential behavior can be assessed by bare inspection.)

Irrational shear wall structures usually defy solution by normal structural analysis. In such cases model investigations or finite element studies can assist in evaluating the internal forces. Only special experimental studies can disclose the important aspects of ultimate strength, energy absorption, and ductility demand in irrational reinforced concrete shear walls. It is not uncommon for the results of such research to become available when the construction of the shear wall structure is completed.

It is imperative that the openings interfere as little as possible with the moment and the shear-carrying capacity of the structure. A good example of an irrational shear wall appears in Fig. 12.16a. The flexural resistance of the

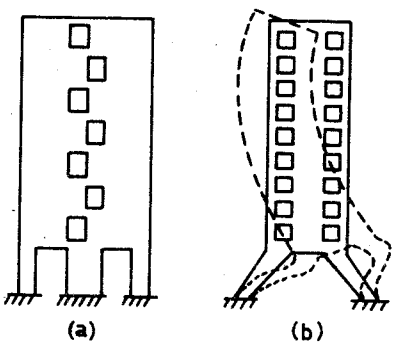


Fig. 12.16. Irrational shear walls. (a) Interference with flexural and shear strength. (b) Undesirable deformations due to sloping legs.

cantilever structure at the critical base section is drastically reduced by the sudden change from a wall section into columns. The staggered arrangement of openings seriously reduces the contact area between the two walls, where the shearing forces should be transmitted. The legs of the wall illustrated in Fig. 12.16b could lead to an undesirable situation in which the sway mechanism of the legs tilts the wall in a direction opposite to the direction of the sway.

Observations made on the probable behavior of shear walls during seismic disturbances strongly indicate the undesirability of replacing massive walls near their base with lighter column members. Figure 12.17, taken from a theoretical study of pierced shear walls, presents wall types that are satisfactory for wind load resistance but are likely to invite disaster in a major earthquake. For these walls, the energy absorption in the postelastic range may be concentrated in a few relatively light legs, and it may be associated with ductility demands that cannot be met in reinforced concrete.

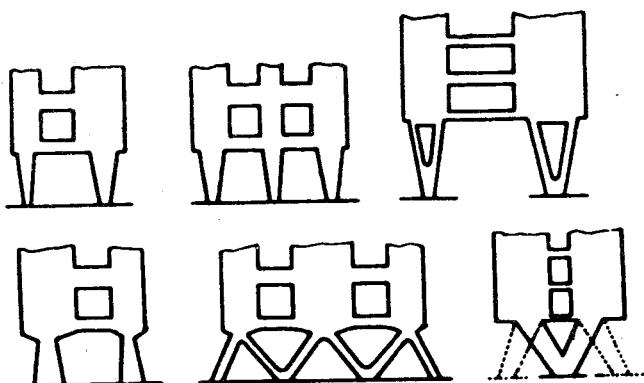


Fig. 12.17. Undesirable forms for earthquake-resistant shear walls.

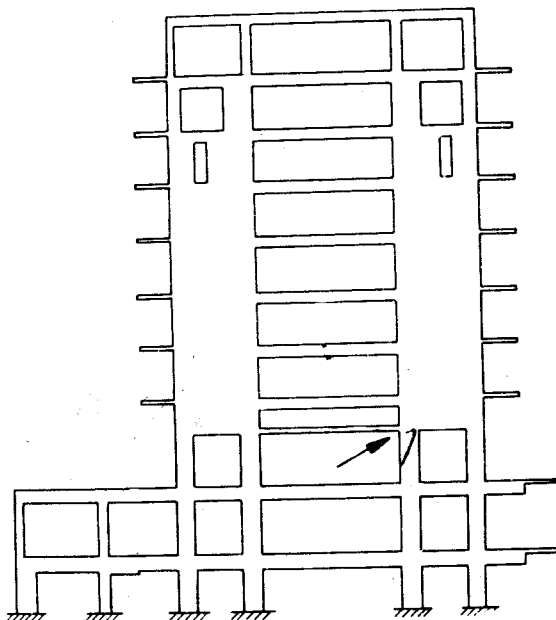


Fig. 12.18. The framing of the Macuto-Sheraton Hotel in Venezuela.

An example of unsatisfactory structural behavior was observed in the Macuto-Sheraton hotel in Venezuela. In this building, 18 in (455 mm) thick shear walls transmitted the seismic load to 43 in (1090 mm) diameter round columns at the fourth floor.^{12,22} During the July 29, 1967, Caracas earthquake, a row of the third floor columns failed in shear and compression. The location is indicated by an arrow in Fig. 12.18. The overturning moments from the shear walls induced large axial forces on the columns, and these reduced their flexural ductility. A closeup view of a failed column appears in Fig. 7.21.

12.5 COUPLED SHEAR WALLS

12.5.1 Introduction

Many shear walls contain one or more vertical rows of openings. A particularly common example of such a structure is the "shear core" of a tall building, which accommodates elevator shafts, stairwells, and service ducts. Access doors to these shafts pierce the walls. Thus the walls on each side of openings may be interconnected by short, often deep, beams. It is customary to refer to such walls as being "coupled" by beams. A typical structure is illustrated in Fig. 12.19a.

Frequently it is difficult to classify a coupled shear wall structure. On one hand the structure may be considered to be a wall containing openings; on the other, it may be more appropriate to speak of a rigid jointed frame consisting of deep members. Both definitions indicate that the conventional manual techniques of structural analysis may not be adequate.

Before the behavior of a coupled shear wall can be assessed with confidence, we must examine two types of deformation normally neglected in frame analysis.

The coupling system, consisting of a number of short coupling beams, transmits shearing forces from one wall to another (see Fig. 12.19a), subjecting coupling beams to flexure and shear. Because of the small span/depth ratios of these beams, shear deformations may become very significant.

Owing to their large stiffnesses, the coupling beams are sensitive to relative movements of their built-in supports. For this reason the axial deformations of the coupled walls, which are responsible for such movements, may have a considerable effect on the overall behavior. The small span/depth ratios of the members, and the required consideration of axial deformations, means that manual techniques of frame analysis cannot be readily applied. Therefore, an alternative method, which permits the required information for design to be obtained with relative ease, particularly when a

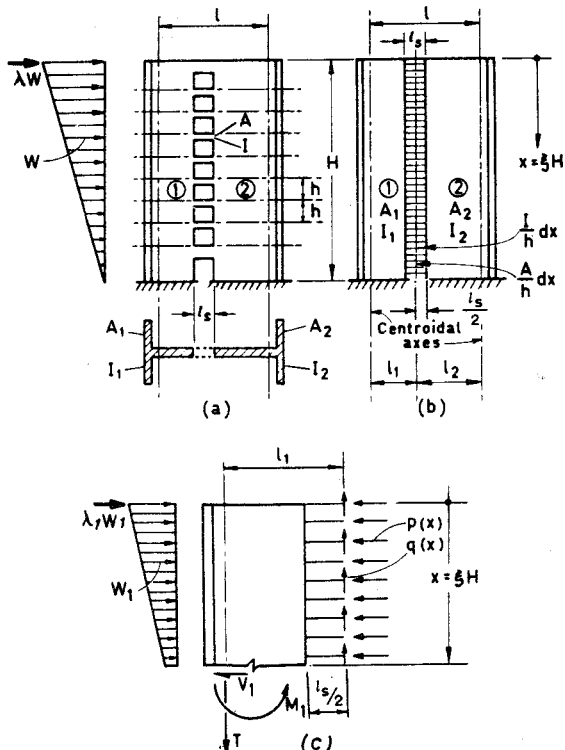


Fig. 12.19. Coupled shear walls and their mathematical model. (a) Prototype structure. (b) Mathematical model. (c) Internal and external actions.

small computer is available, has become popular. The method is referred to as the "laminar analysis" or "continuum" approach.

12.5.2 The Laminar Analysis Used to Predict Linear Elastic Response

To evaluate various aspects of behavior of coupled shear walls, the concepts of the Beck-Rosman laminar analysis have been used in several studies.^{12.23-12.25} The idea of simulation originated with Chitty.^{12.26} The approach employs a mathematical model in which the discrete connecting beams are replaced by an equivalent continuous elastic medium (i.e., infinitesimal elastic laminae). This enables a highly statically indeterminate problem to be reduced to a relatively simple one in which the indeterminate

shearing forces across the connecting beams are obtained from a continuous function. The prototype structure and its mathematical model are illustrated in Fig. 12.19. The approximations involved in the use of this elastic laminar coupling are usually well within the acceptable limits of structural design, particularly for tall buildings. Photoelastic studies, and other model studies, have verified that the method results in a satisfactory degree of accuracy. It is not the purpose of this chapter to elaborate on this technique, which has been refined and extended for various situations in a number of research papers.^{12.27}

The most important action of an external lateral load, the bending or overturning moment, must be resisted at any horizontal section across the shear wall structure (see Fig. 12.19c). The corresponding equilibrium statement is

$$M_0 = M_1 + M_2 + lT \quad (12.8)$$

where M_0 = total external moment

M_1, M_2 = internal moments generated in wall 1 or wall 2

T = axial force induced in the walls, tension in wall 1, and compression in wall 2 of Fig. 12.19b

l = distance between centroids of the two walls

All these actions are considered at level x .

The aim of the laminar analysis is to determine the internal actions just defined. An isolated free body, consisting of a part of wall 1 and laminae, cut through their midspan point of contraflexure, is shown in Fig. 12.19c. The laminae are subjected only to shearing forces $q(x)$ and axial forces, $p(x)$ at the midspan points. The share of the total external load resisted by wall 1 is W_1 and $\lambda_1 W_1$. By considering the conditions of compatible deformations, a second-order differential equation can be established which usually yields the laminar shear forces $q(x)$ over the full height of the coupled shear wall structure.

The axial force in the walls results from the accumulation of the shearing forces across the coupling system of beams or laminae. The larger the stiffness of the coupling system relative to the walls, the more efficient the coupling, the larger the induced vertical shearing forces in the beams, and the larger the consequent axial force in the walls. The interplay between the modes of internal moment resistance, as shown by Eq. 12.8, depends on the strength and stiffness of the coupling between the two walls. Clearly it is more efficient to resist the external moment predominantly by internal forces T , which operate with a large lever arm l , than by component internal moments M_1 and M_2 .

The relative proportions of the contributions of the internal couple, lT , in resisting the external moments M_0 , at various levels of an elastic 20-story

shear core are presented in Fig. 12.20. It is seen that the coupling is efficient for the top half of the structure for all but the shallowest beams. At the base, little difference in behavior is indicated for 24 in (610 mm) deep or infinitely stiff beams. The latter represents the case when no distortions occur in the process of shear transfer from one wall to another; that is, a continuous linear strain distribution occurs across the entire shear wall structure. The low efficiency of 6 in (150 mm) deep coupling beams shows the approach to the other limiting situation when $lT = 0$; that is, when the entire external moment is resisted by flexure in the component cantilever walls M_1 and M_2 .

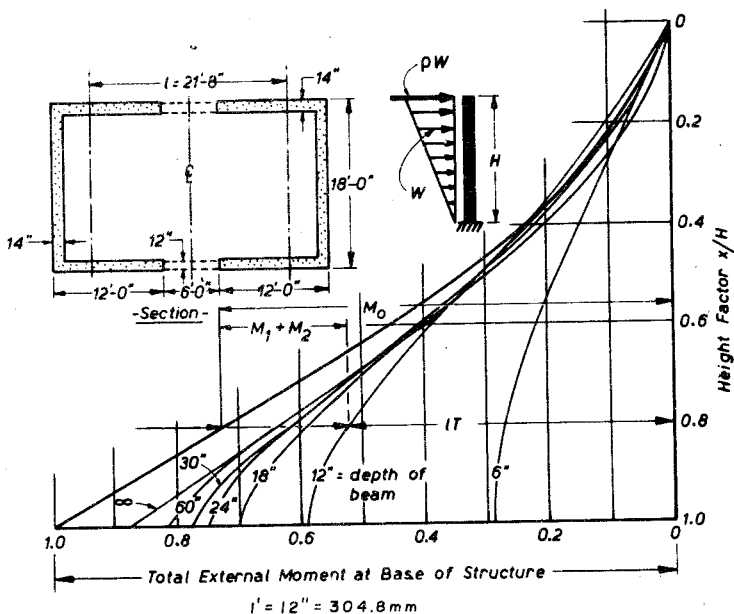


Fig. 12.20. The mode of internal moment resistance in a coupled shear wall structure.

The role of cracking in the elastic behavior of shear walls has been examined theoretically and experimentally.^{12,28, 12,29} Because of the very large differences between the stiffnesses of the components, and the drastic loss of stiffness in the coupling system after diagonal cracking, a 75 to 100% increase in both the deflection and the wall moments has been obtained in case studies in which allowance was made for cracking. It is best to make a number of assumptions with regard to loss of stiffness caused by cracking in the walls and the coupling system and to carry out an analysis for each. The results,

given by continuous functions, can then be conveniently transformed into discrete actions at each floor, and these are subsequently used in the design of the structure.

Figure 12.19 illustrates the most common type of regular coupled shear wall structure. The laminar analysis can deal also with other boundary conditions, such as infinitely rigid coupling at the top and hinged or elastically restrained wall bases. Rosman has developed solutions for many different boundary conditions.^{12.30} One of the shortcomings of this technique is its inability to deal readily with walls having variable sectional properties. For such structures, standard computer programs applicable to frames will be more useful, or tables can be used, such as prepared by Burns.^{12.31} It is also possible to cater for variable sectional properties if the techniques of finite difference analysis are applied to the standard laminar analysis.^{12.37}

12.5.3 Elastoplastic Behavior of Coupled Shear Walls

Problems of Elastoplastic Behavior

The strength of two coupled shear walls, subject to seismic-type lateral loading, is reached when a collapse mechanism is formed. Two plastic hinges in each coupling beam are required to terminate its ability to accept additional shear. In addition, one plastic hinge needs to be developed in each of the cantilever walls, normally at their base, to complete the collapse mechanism. The sequence of hinge formation for a given loading will depend on the relative strength and stiffness of the components. The mechanism is similar to that shown for a multistory frame in Fig. 11.31.

The behavior of some coupled shear walls that were exposed to severe earthquakes, indicated that all or most coupling beams failed before the ultimate strength of the coupled walls was attained. Classic examples are some of the end shear wall frames of two 14-story buildings, severely damaged during the 1964 Alaska earthquake^{12.32} (see Figs. 12.21 and 12.22). It is possible, however, that in some structures the ultimate strength of the walls will be exhausted before plastic hinges form in the coupling beams.

Relatively few analytical studies on the plastic behavior of shear walls have been reported. Winokur and Gluck^{12.33} proposed an analysis based on a uniform distribution of flexural strength up the coupling system. These coupling beams, often short and relatively deep, may be subjected to high shearing stresses when the ultimate flexural strength is to be developed. In deep spandrel beams, these shear forces not only inhibit the full development of the flexural capacity, they also restrict the ductility obtainable.^{12.29} It is therefore important to assess the ductility demand on the coupling system when the overall ultimate strength of the coupled shear wall structure



Fig. 12.21. The Mount McKinley Building in Anchorage, Alaska, damaged during the earthquake of March 27, 1964. (Courtesy American Iron and Steel Institute.)



Fig. 12.22. Closeup of coupling beams in the Mount McKinley building in Anchorage. (Courtesy American Iron and Steel Institute.)

is being determined. Theoretical studies have indicated that for the critical coupling beams, the required ductilities may be in excess of those experimentally obtained for similar members.^{12,34} Figure 12.23 plots the results of such an analysis, carried out for a 20-story shear core with the same dimensions given in Fig. 12.20. On the right-hand side the load-roof displacement relationship is given with numbers indicating the following distinct stages of the analysis.

1. Fully elastic response under a code-specified equivalent lateral static load of the form shown in Fig. 12.20.
2. The critically situated laminae, about one-third up the building, commence yielding. The dotted curve in the central insert shows the distribution of laminar shear forces q at this stage of the loading. The yield rotation is θ_y .
3. With further increase of loading, more than 90% of the laminae have yielded, thus have developed their uniform ultimate strength q_u . The accumulation of these forces will result in the maximum axial force on the

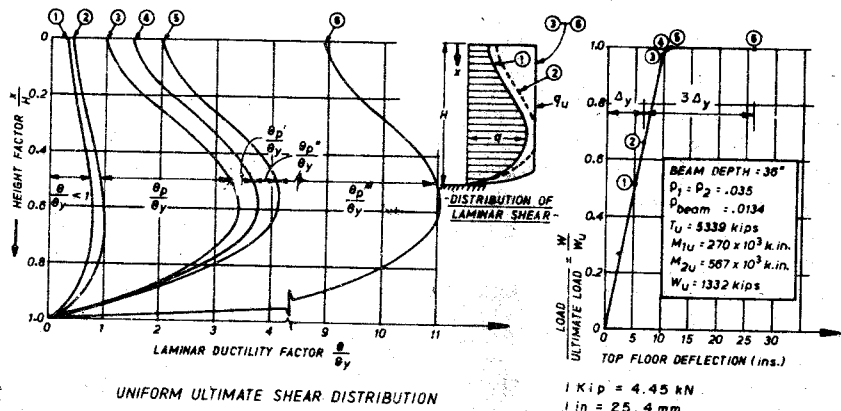


Fig. 12.23. Laminar shear force distribution, ductility demand, and top floor deflections for a 20-story coupled shear wall structure having coupling beams of uniform strength.

coupled walls. Further loading is assumed to generate no further shear in the coupling system, hence no further axial load on the walls. Until this stage, both walls are assumed to remain elastic.

4. The flexural strength, in the presence of the axial tension, of wall 1, is developed at this stage of loading. Each wall has a reinforcement content of $\rho = 3.5\%$.

5. After a small increase of lateral load, the flexural strength is also reached at the base of wall 2 (subjected to compression). In a more exact analysis, however, the compatibility of deformations in the two walls indicates, that yielding will occur at the base of both walls at approximately the same load level. The theoretical ultimate load capacity of the coupled shear wall structure is attained at this stage. Although the two walls are geometrically similar (see Fig. 12.20), the structure is not symmetrical because of the different extents of cracking, hence loss of stiffness, in the two walls.

6. To investigate the behavior corresponding with a large overall ductility demand, using a displacement ductility factor of 4, further displacement is imposed on the structure, making the top floor deflection four times as much as that which occurred at the first yielding of the coupling beams or laminae. This deflection is 26 in in the example structure.

The rotations at the boundaries of the coupling beams can be obtained from the wall deformations, and from these the laminar ductility demand may be determined. The results presented on the left-hand side of Fig. 12.23, show the plastic rotations θ_p in terms of the yield rotation θ_y for each of the six stages of behavior. It is evident that if the coupling system is to follow the

prescribed overall structural deformations, the coupling beams must maintain the full shear q_u , while undergoing plastic rotations corresponding with a laminar ductility factor exceeding 11. This is a large ductility requirement. The definition of laminar rotation appears in the insert of Fig. 12.29b.

In a similar theoretical study the same structure was examined on the assumption that the strength of the coupling system corresponded with the strength demand within the elastic range (see central insert in Fig. 12.24).

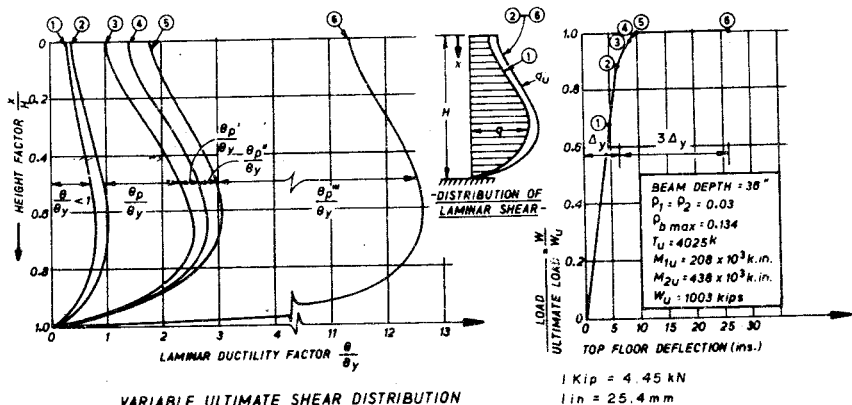


Fig. 12.24. Laminar shear force distribution, ductility demand, and top floor deflections for a 20-story coupled shear wall structure having variable strength coupling beams.

The shear strength of the critically situated lamina is the same as the strength of all laminae in the previous example. Both walls were reinforced vertically with $\rho = 3.0\%$. Plastic hinges formed at the base of the wall at loads a little larger than the load at which the simultaneous yielding of all laminae set in. Naturally, the ultimate strength of the structure (1003 kips) is less than that of the previous example (1332 kips) (see Fig. 12.24).

Apart from the strengths of the coupled walls at foundation level, and the issues discussed in Section 12.2.1, three critical areas of behavior require the designer's attention. These are illustrated in Fig. 12.25 and the features numbered are described below.

1. The previous theoretical study indicated that to ensure a displacement ductility factor of 4, the ductility demand on the coupling beams may have to be very large. It is therefore necessary to examine available experimental evidence, to determine whether such ductility demands can be met. This is carried out in the next section of this chapter.

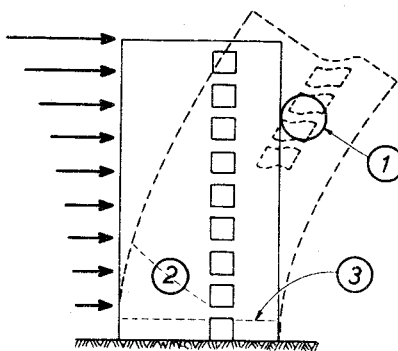


Fig. 12.25. Critical areas of behavior in coupled shear walls.

2. One of the walls is subjected to considerable tension in addition to flexure and shear. This load may adversely affect the diagonal tension capacity of a shear wall. From experimental work with beams (discussed in Section 7.6.2) and tests of small-scale reinforced concrete coupled shear walls, (Fig. 12.35), the current ACI code^{12.10} provisions appear to be adequate. The angle of the potential diagonal tension crack in Fig. 12.25 does not seem to be affected by axial tension in the wall. After reversed cyclic loading, however, the potential diagonal failure crack associated with axial tension may link up with flexural cracks that formed during previous loading in the opposite direction. Diagonal cracks so formed may encounter a lesser number of stirrups than intended. Fortunately the two walls are interconnected and thus a redistribution of shear forces to the other wall, the shear capacity of which is greatly boosted by axial compression, can take place.

3. The total horizontal shear also must be transferred across horizontal construction joints. The mechanism of interface shear transfer and the reinforcing of construction joints have been examined in Section 12.2.1. Large axial tension may exist across such a joint (see Fig. 12.25), and particular attention needs to be paid to this contingency.

Strength and Behavior of Coupling Beams

Observations of earthquake damage have repeatedly indicated the failure by diagonal tension of coupling or spandrel beams containing insufficient web reinforcement (see Fig. 12.22). Clearly such failures, usually brittle, which result in a high rate of strength degradation under cyclic loading,^{12.35} must be suppressed if satisfactory seismic resistance is to be provided. Irrespective of the design loads, the shear strength of a coupling beam must be equal to or larger than its flexural capacity. This requirement may impose

an upper limit on the flexural steel content in such beams, particularly when they are deep relative to their span.

The currently accepted upper limit for the nominal shear stress across a beam is at least $v_u = 10\phi_v \sqrt{f'_c}$ (psi), as was shown in Section 7.4.2; thus the maximum shear force to which a coupling beam can be subjected is

$$V_u \leq 10\phi_v bd\sqrt{f'_c} \quad (12.9)$$

With reference to Figs. 12.19 and 12.26, a good approximation for the

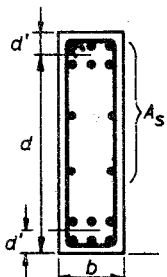


Fig. 12.26. Sectional properties of a typical coupling beam.

shearing force corresponding to the dependable flexural capacity of a typical beam is

$$V_u = \frac{2M_u}{l_s} = \frac{2}{l_s} \phi_m (d - d') A_s f_y \quad (12.10)$$

where ϕ_v = capacity reduction factor in shear = 0.85

ϕ_m = capacity reduction factor in flexure = 0.90
in accordance with ACI code^{12.10}

l_s = clear span of coupling beam

By equating the shear capacities (i.e., Eqs. 12.9 and 12.10), it is found that

$$\frac{A_s}{bd} = \frac{4.7l_s\sqrt{f'_c}}{(d - d')f_y} < \rho_{\max} \quad (12.11a)$$

It may be noted that all reinforcement in the tension zone of the beam section should be included in the flexural strength evaluation (see Fig. 12.26).

One might be led to believe that because of the equal amount of top and bottom reinforcement, such beams would possess very large flexural ductility (see Chapter 6).

For beams with a span/depth ratio of less than 2, the shearing forces and consequent diagonal cracking cause a radical redistribution of the tensile

forces along the flexural reinforcement. For small span/depth ratios, tensile stress will exist in the reinforcement at locations in which conventional flexural theory indicates that compression stresses should be present. Theoretical considerations similar to those discussed in Section 7.5.1, based on the behavior of diagonally cracked deep reinforced concrete beams, have confirmed this redistribution of forces in the flexural steel; experiments have also verified the phenomenon.^{12,29} Figure 12.27 represents a typical spandrel beam that has been subjected to equal moments at both ends, causing a point of zero bending moment to exist at midspan. Since the two support sections are relatively near each other, the redistribution of forces in the top or bottom reinforcement is no longer a local effect. For convenience, the tension in the top reinforcement is shown above and that of the bottom bars is recorded below the horizontal axis of the diagram at four load increments. Shear and consequent diagonal cracking have the following results.

1. Tension in the flexural reinforcement in areas in which, according to the bending moment patterns, compression should prevail.
2. A spread of tension over the entire length of the beam if the span/depth ratio is small enough ($l_s/h < 1.5$).
3. Invalidations of the design concepts of doubly reinforced beams since both the top and bottom reinforcement can be in tension at the critical sections. The compression in the concrete is not relieved by the reinforcement, and an increase in ductility due to the reinforcement cannot be expected, either. In fact, because the top and bottom reinforcement is in tension at the critical section, the concrete has to carry a larger internal compression force than if the beam were singly reinforced. Thus the interaction between flexure and shear in deep coupling beams causes a reduction in the flexural capacity.

In the final stages of loading, irrespective of the amount of web reinforcement used, the bulk of the shearing force in the beams must be transferred across the concrete compression zone into the shear walls. This is because only a small amount of the total shear can be transmitted by dowel action of the flexural reinforcement. However, the concrete in the compression zone areas would have been cracked during preceding load cycles, the cracks being opened and closed several times; therefore; its capacity to transfer shear would have been drastically reduced. Indeed, deep beams, fully reinforced against a possible diagonal tension failure, have been observed to fail in direct sliding shear along the critical support section.^{12,35} In Fig. 12.28, a beam having an aspect ratio l_s/h of 1.29, illustrates this type of failure after cyclic loading, which is associated with the breakdown of the aggregate interlock mechanism. The gauge locations at which the

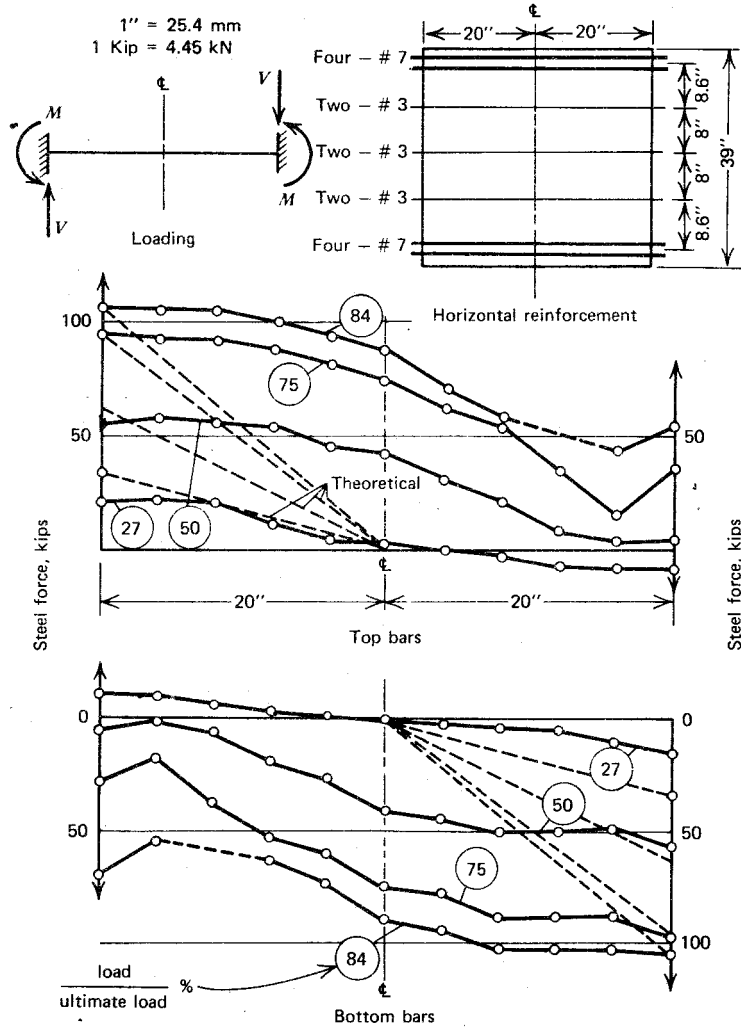


Fig. 12.27. The tension force distribution along the flexural reinforcement of a deep coupling beam.

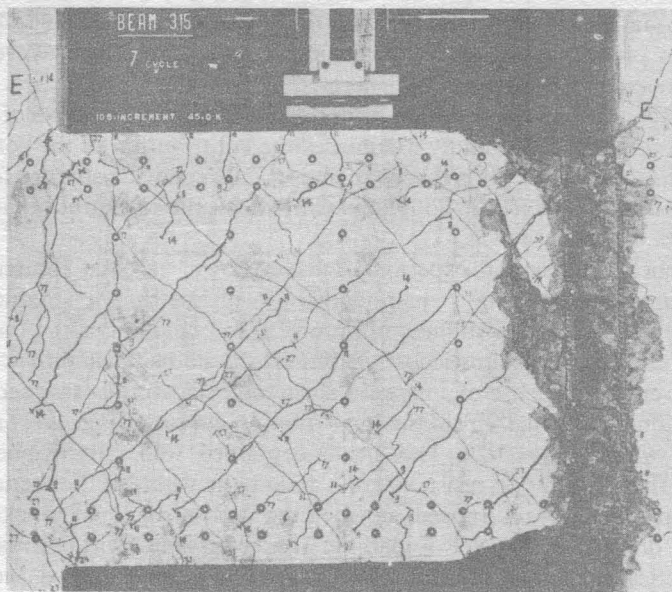


Fig. 12.28. Sliding shear failure in coupling beams.

flexural steel strains used in Fig. 12.27 were obtained can also be seen in this photograph.

Once an excursion in the postelastic range has been made during seismic-type alternating load cycles, the plastic rotational capacity of conventionally reinforced coupling beams is restricted by the ineffectiveness of the compression reinforcement and by the possibility of a sliding shear failure. A conventional coupling beam will contain equal top and bottom reinforcement extending without reduction along the full span, with smaller size horizontal intermediate bars and stirrups as illustrated in Fig. 12.26. To ensure some measure of ductility during cyclic reversed loading of earthquake-resistant shear walls, it is suggested that the shear force be limited by restricting the flexural steel content to

$$\rho_{\max} = 3 \frac{l_s \sqrt{f'_c}}{h f_y} \quad (12.11b)$$

where the stresses are in psi units. This will ensure that the nominal shear stress in the coupling beams will not rise above 60% of the maximum value recommended by the ACI code.^{12.10}

Occasionally it will be found that this limitation does not permit efficient utilization of coupled shear walls because it limits the magnitude of the maximum axial force that can be generated in the walls.

The diagonal cracking resulting from the alternating application of shear forces, as in Fig. 12.28, rapidly diminishes the contribution of the concrete toward shear resistance. It is therefore important to provide stirrups for the full shear force, generated in coupling beams when their flexural capacity is developed.

Theoretical studies and experiments have shown^{12,29} that the stiffness of coupling beams having a span/depth ratio of less than 1.5 reduces to less than one-fifth of the stiffness of an uncracked beam after the onset of diagonal cracking. This drastic loss of stiffness should be taken into account when the elastic response of a coupled shear wall structure is assessed. The loss of stiffness is evident from the load-rotation curves of Fig. 12.29a for a beam in which $l_s/h = 1.29$. This beam contained web reinforcement in excess of that required to resist, by truss action, the whole of the theoretical maximum flexure load. Indeed, no yielding across diagonal cracks was observed during the 7 cycles of loading. The beam failed without reaching its theoretical maximum flexural capacity, 184.0 kips, after limited ductility, by sliding shear, as in Fig. 12.28.

When insufficient web reinforcement is provided, the stirrups will yield, and a much greater degree of stiffness degradation ensues. This is particularly noticeable when small loads are applied in a new load cycle. Large rotations occur before the previously opened diagonal cracks close, permitting the newly formed diagonal compression to be transmitted. Figure 12.29b illustrates this behavior.

Because the top and bottom reinforcement is in tension over the full clear span of a coupling beam when $l_s/h \leq 1.5$, the beam becomes longer during inelastic loading cycles.^{12,28} All intermediate bars, distributed over the depth of the beam, are thus strained, and they contribute toward the strength of the beam. Figure 12.27 shows that the total tension force generated in all the horizontal reinforcement is approximately constant over the span, and the internal compression must therefore act along a diagonal. If elongation of the steel occurs, the two coupled walls in a multistory structure are pushed apart. Floor slabs are likely to restrain this movement to some extent, and such restrained coupling beams would probably exhibit a larger strength than laboratory specimens tested without floor slabs present.

Recent experiments at the University of Canterbury revealed^{12,35, 12,36} that the ductility and useful strength of coupling beams can be considerably improved if instead of the previously described conventional steel arrangement, the principal reinforcement is placed diagonally in the beam. The design of such a beam can be based on the premise that the shearing force resolves

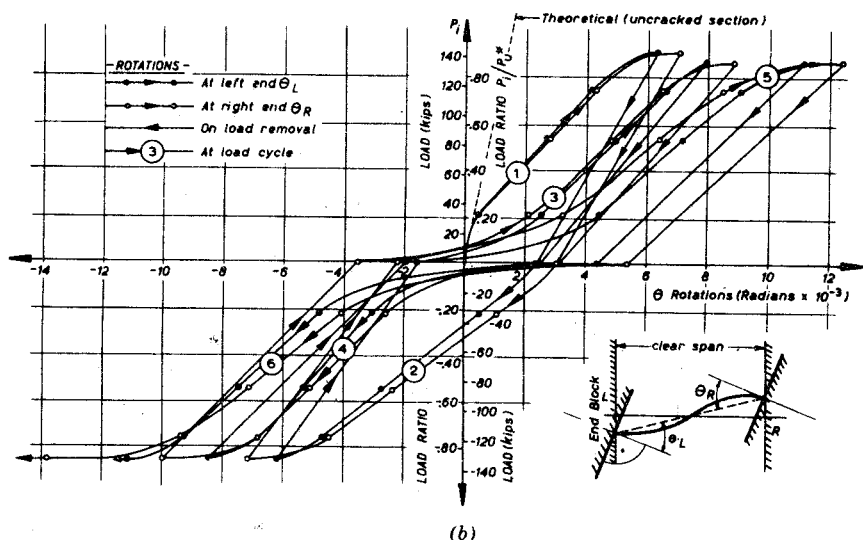
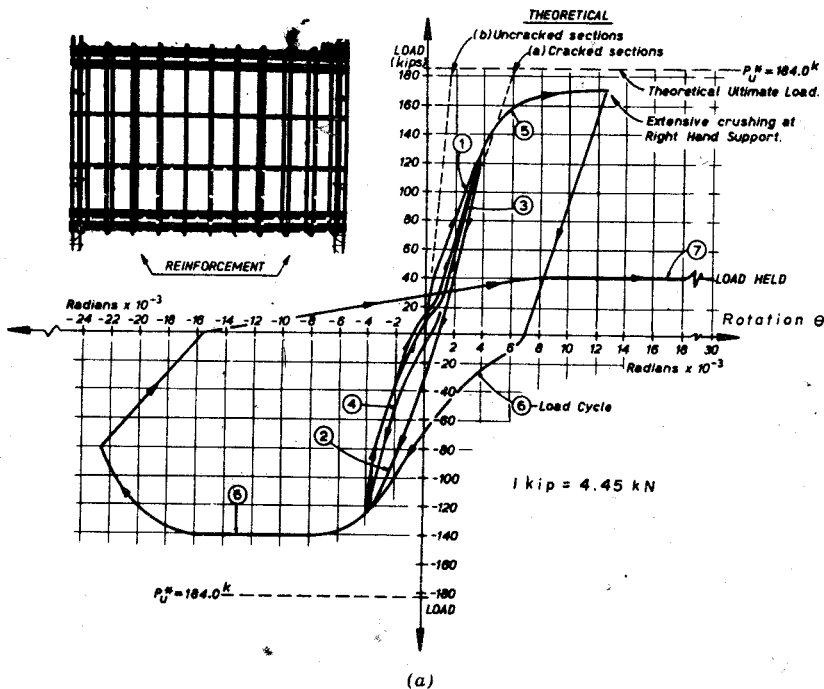


Fig. 12.29. Load-rotation relationship for coupling beams containing web reinforcement that is (a) sufficient, (b) insufficient.

itself into diagonal compression and tension forces, intersecting each other at midspan where no moment is to be resisted, as in Fig. 12.30. Initially the diagonal compression is transmitted by the concrete, and the compression steel makes an insignificant contribution. After the first excursion of the diagonal tension bars into the yield range, however, large cracks form and remain open when the load is removed. When the reversed load is applied,

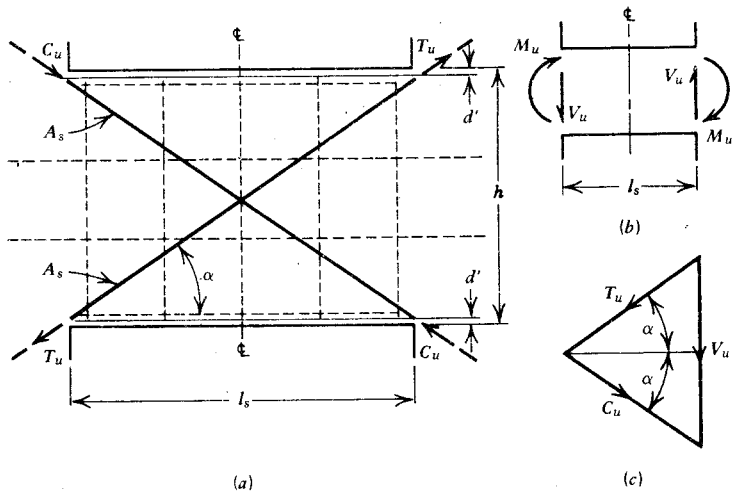


Fig. 12.30. Model of diagonally reinforced coupling beam. (a) Geometry of the reinforcement. (b) External actions. (c) Internal forces.

as during an earthquake, these bars are subjected to large compression stresses, perhaps yielding, before the previously formed cracks close. Accordingly, at the development of the yield strength, Figs. 12.30a and 12.30c give

$$T_u = C_u = A_s f_y \quad \text{and} \quad V_u = 2T_u \sin \alpha$$

hence

$$A_s = \frac{V_u}{2f_y \sin \alpha} \quad (12.12)$$

where $\tan \alpha = \frac{h - 2d'}{l_s}$

The resisting moment at the supports of the beam (Fig. 12.30b), may be found if desired, either from the shear force, that is,

$$M_u = \frac{V_u l_s}{2} = l_s T_u \sin \alpha \quad (12.13a)$$

or from the horizontal components of the diagonal forces, that is,

$$M_u = (h - 2d')T_u \cos \alpha \quad (12.13b)$$

Since equal amounts of steel are to be provided in both diagonal bands, the loss of the contribution of the concrete is without consequence, provided the diagonal compression bars do not become unstable. For seismic-type loading it is therefore important to have ample ties around the diagonal compression bars, to retain the concrete around the bars. The main purpose of the retained concrete is to furnish some lateral flexural rigidity to the diagonal strut, thus to enable compression yielding of the main diagonal bars to take place. At the University of Canterbury where beams only 6 in (150 mm) thick were studied, buckling failures were clearly identified.^{12.36} A suggested arrangement of reinforcement is presented in Fig. 12.31.

Because the concrete, apart from stabilizing the compression bars, has no influence on the behavior of diagonally reinforced coupling beams, no degradation in strength or stiffness is to be expected during alternating cyclic loading that imposes moderate ductility. Figure 12.32 gives the load-rotation relationship for a beam having the same overall dimensions as

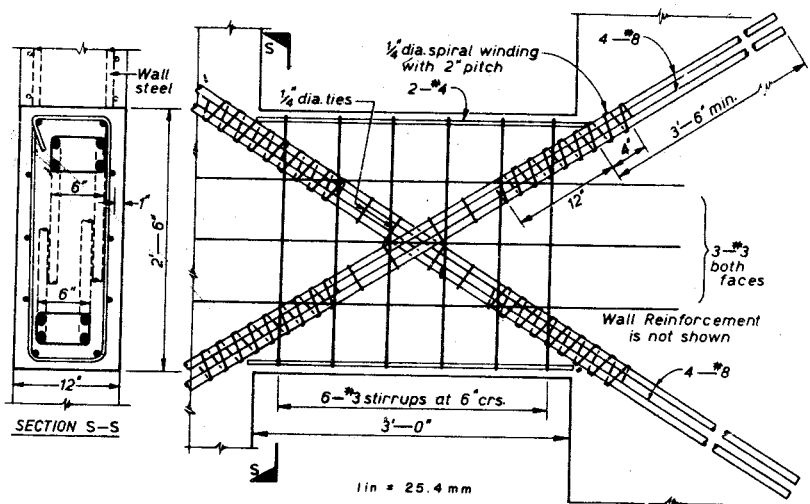


Fig. 12.31. Suggested steel arrangement in a diagonally reinforced coupling beam.

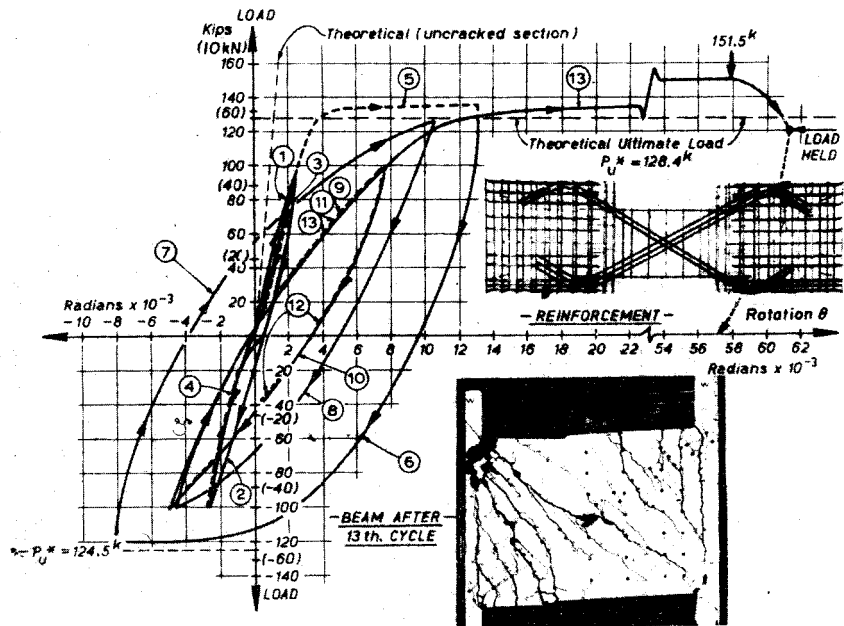


Fig. 12.32. Load-rotation relationship for a diagonally reinforced coupling beam.

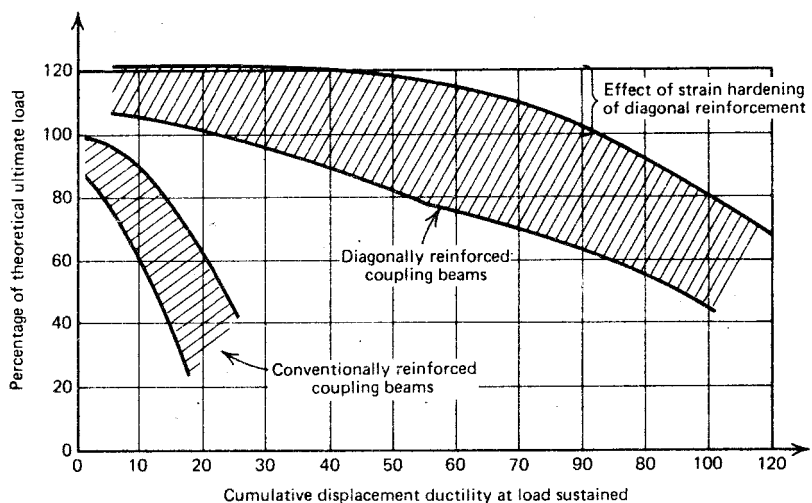


Fig. 12.33. Cumulative ductilities imposed on conventionally and diagonally reinforced coupling beams.

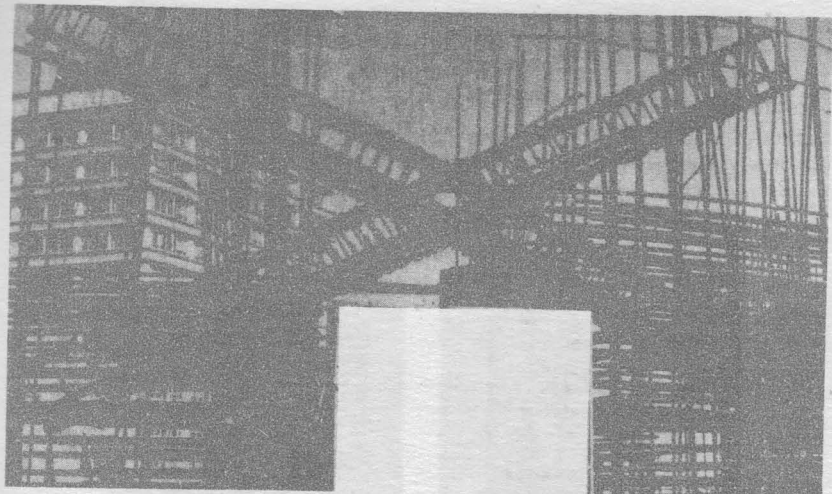


Fig. 12.34. Diagonal reinforcement for a coupling beam of a shear wall. (Courtesy New Zealand Ministry of Works.)

that in Fig. 12.28. The hysteresis loops for this beam have the characteristics of a steel member. Strength degradation occurs only when the buckling of the compression bars commences. When load reversals occur, however, these bars can take up tension and straighten themselves. The process leads eventually to the complete breaking up of the concrete around the compression bars, hence to further loss of restraint against buckling and consequent loss of strength.

The superior response of these diagonally reinforced beams under high-intensity alternating loading can be seen in a comparison of the reduction in strength with the cumulative ductility imposed during cyclic loading on beams tested at the University of Canterbury^{12,36} (Fig. 12.33). The span depth ratio l_s/h of these beams varied between 1.03 and 1.29. Figure 12.34 illustrates the reinforcement for such a beam in the new New Zealand parliament building in Wellington.

Strength of Coupled Walls

Once the bending moments and the shear and axial forces generated in a coupled shear wall structure by lateral load have been derived, from a laminar analysis or otherwise, they can be combined with the gravity actions. Each of the walls may now be considered as a cantilever, and its flexural and shear strength can be determined in accordance with the principles outlined in

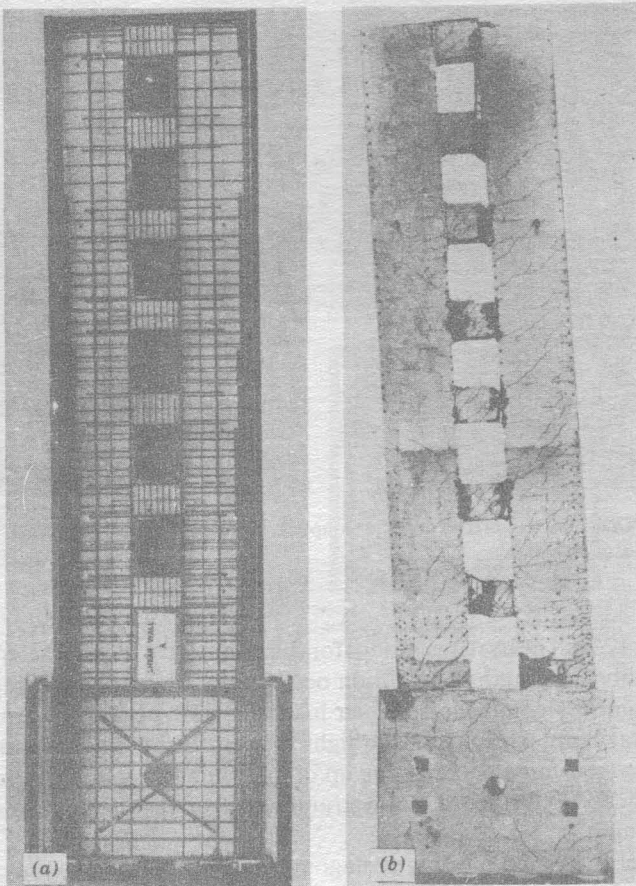


Fig. 12.35. Arrangement of reinforcement and crack patterns of two coupled shear wall specimens.^{12,37} (a, b) Shear wall A. (c, d) Shear wall B.

Section 12.2. Normally two possibly critical situations must be examined—one when the lateral load induces a compressive axial force in the wall, and the other when this force is tensile. The latter, when combined with gravity-induced compression, often results in a net tension in the wall, with a consequent increase in the flexural steel demand. In these cases, interaction curves such as those in Fig. 12.12, can be used conveniently.

The shear strength of walls in the presence of axial compression or tension can be determined as discussed in Chapter 7. It is emphasized once more that the full horizontal shear reinforcement must be provided near the bases of these walls where yielding of the vertical flexural reinforcement could be extensive.

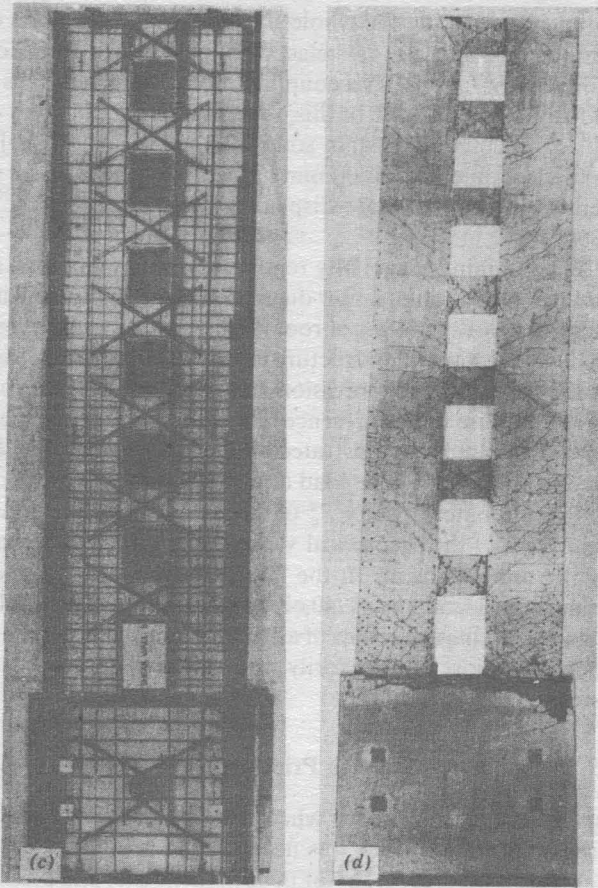


Fig. 12.35. (continued)

12.5.4 Experiments with Coupled Shear Walls

To verify the elastoplastic behavior of components in the whole structure, two quarter-scale seven-story reinforced concrete coupled shear walls were tested at the University of Canterbury.^{12,37} To simulate a triangular distribution of lateral static load, point loads of equal intensity were applied at the seventh, fifth, and third floors. The loading direction was cycled during the test. To compensate for gravity effects at the critical base sections of the cantilever walls, a uniform compression of 250 psi (1.72 N/mm^2) was applied to each wall by means of a single, centrally positioned, ungrouted prestressed cable. Both structures were designed for the same ultimate load capacity. The reinforcing cages and the specimens after failure are shown in Fig. 12.35. In wall A, conventional beam reinforcement was provided with

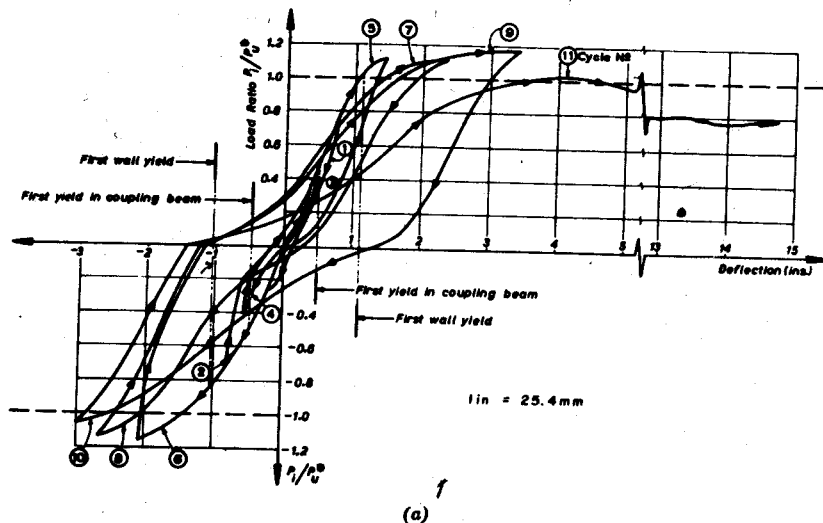
stirrups theoretically resisting the whole shear by truss action. As expected, after three excursions into the postelastic range in each direction of the loading, a sliding shear failure of all coupling beams occurred. This is clearly evident from Fig. 12.35b. In spite of this, remarkable ductility was exhibited by shear wall A, which could sustain some 80% of the theoretical ultimate load at a roof deflection of 5 ft (1500 mm), in terms of the full-size structure. This is evident from the load-roof displacement relationship for this wall (see Fig. 12.36a).

Shear wall B, containing diagonally reinforced coupling beams, sustained much less damage, even though larger ductilities, corresponding with overall ductility factors of 4 to 12 in terms of roof level displacements, were imposed on the model during testing. The structure failed eventually because of lateral instability at the base of the compression wall. In a prototype structure this would not occur because of the presence of a slab diaphragm. The excellent response of this structure is demonstrated by the load-displacement relationship, presented in Fig. 12.36b. The load at any stage P_i is expressed in terms of the theoretical ultimate capacity P_u^* of the structure. A maximum load of up to 20% in excess of the theoretical value was attained because of strain hardening of the reinforcement. In the fifteenth cycle of load, the average imposed interstory deflection was 1/40 of the story height. The stable hysteresis curves, having the characteristics of a steel member, suggest that this type of structure meets most satisfactorily the requirements of earthquake-resistant design.

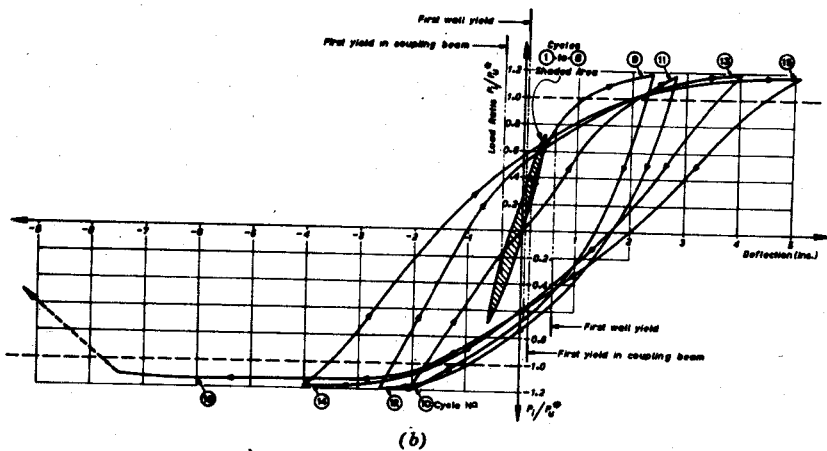
12.5.5 Summary of Design Principles

To ensure satisfactory performance when coupled shear wall structures are exposed to severe seismic shocks, it is necessary to be able to assess at least approximately the structures' behavior in both the elastic and plastic range of loading. Desirable behavior can be expected only if the structure is made capable of following a preferred sequence of yielding. From the point of view of damage control, and possible repair, it is desirable that the wall components be the last ones to suffer during the process of imposing incremental ultimate conditions.

Considerations of the strength of conventionally reinforced coupling beams indicate that full protection against diagonal tension failure during cyclic loading is required, and the flexural steel content in both faces should be moderate to ensure maximum ductility and to avoid early failure by sliding shear. Deep coupling beams subjected to large shearing forces cannot be expected to be ductile enough to sustain plastic deformations associated with an overall ductility factor of 4 for the entire structure. If conventionally reinforced beams are to be used for seismic-resistant design, the ductility



(a)



(b)

Fig. 12.36. Load-roof displacement relationship for shear walls with: (a) conventionally reinforced and (b) diagonally reinforced coupling beams.^{12.37}

demand on them must be limited. This can be achieved only by designing the coupled shear wall structure for a greater strength, permitting a large proportion of the energy to be absorbed in the elastic range.

When diagonal reinforcement is used in coupling beams and adequate ties are provided to enable the compression struts to sustain yield load without buckling, satisfactory performance can be expected: these beams have been found to meet successfully ductility demands comparable to those shown in the previous example structure. Additional light secondary or basketing reinforcement, consisting of a mesh in both faces of a coupling beam, will also be required to hold the broken concrete particles in place when large plastic displacements occur during a catastrophic earthquake (see Fig. 12.31).

The study of two coupled shear walls, for which the laminar analysis was found to be a convenient analytical tool, illustrates the interplay of wall and beam components during the inelastic response of the structure to a static lateral load. When the strength of the coupling beams is large so that the major component of the internal moment of resistance, Eq. 12.8, results from the relatively large axial loads in the walls rather than from wall moments, as in Fig. 12.20, the major part of the total energy will be dissipated by the coupling system. It is important to note that in a shear wall structure designed according to these propositions, a substantial part of the energy during severe seismic excitation will be dissipated by the ductile coupling system before the walls become inelastic. This means that during a disturbance imposing moderate overall ductility demands on the structure, the walls could escape permanent structural damage and the coupling beams could be replaced or repaired with relative ease, if necessary. These features will undoubtedly also be evident in seismic-resistant structures in which more than two walls are coupled. An analytical assessment, however, is beyond the scope of this text.

12.6 REFERENCES

- 12.1 *Symposium on Tall Buildings With Particular Reference to Shear Wall Structures*. University of Southampton, April 1966, Oxford, Pergamon Press, 1967.
- 12.2 J. R. Benjamin and H. Williams, "The Behaviour of One-Storey Reinforced Concrete Shear Walls," *Journal of the Structural Division, ASCE*, Vol. 83, ST3, May 1957, pp. 1-49.
- 12.3 J. R. Benjamin and H. A. Williams, "Behaviour of One-Storey Reinforced Concrete Shear Walls Containing Openings," *Journal ACI*, Vol. 55, No. 11, November 1958, pp. 605-618.
- 12.4 R. H. A. de Paiva and C. P. Siess, "Strength and Behaviour of Deep Beams in Shear," *Journal of the Structural Division, ASCE*, Vol. 91, ST5, October 1965, pp. 19-41.
- 12.5 A. W. Slater, A. R. Lord, and R. R. Zippoldt, "Shear Tests on Reinforced Concrete Beams," Department of Commerce, Bureau of Standards, Technologic Paper No. 314, 1926, pp. 387-495.

- 12.6 A. E. Cardenas, J. M. Hanson, W. G. Corley, and E. Hognestad, "Design Provisions for Shear Walls," *Journal ACI*, Vol. 70, No. 3, March 1973, pp. 221-230.
- 12.7 A. E. Cardenas and D. D. Magura, "Strength of High-Rise Shear Walls—Rectangular Cross Sections," *ACI Special Publication 36, Response of Multistorey Concrete Structures to Lateral Forces*, 1973, pp. 119-150.
- 12.8 F. Barda, "Shear Strength of Low-Rise Walls with Boundary Elements," Ph.D. dissertation, Lehigh University, Bethlehem, Pa., 1972, 278 pp.
- 12.9 P. F. Fratessa and T. Zsutty, "Strength and Performance of Concrete Shear Walls," A report to the Structural Engineers' Association of Northern California Seismology Subcommittee on Shear Walls, San Francisco, 1970, 49 pp.
- 12.10 "Building Code Requirements for Reinforced Concrete (ACI 318-71)," American Concrete Institute, Detroit, 1971, 78 pp.
- 12.11 W. J. Beekhuis, "An Experimental Study of Squat Shear Walls," Master of Engineering Report, Department of Civil Engineering, University of Canterbury, Christchurch, New Zealand, 1971, 132 pp.
- 12.12 H. Umemura, H. Aoyama, and H. M. Liao, "Studies of Reinforced Concrete Wall and Framed Masonry Shear Walls," Report, University of Tokyo, 1964, 89 pp.
- 12.13 P. C. Jennings, "Engineering Features of the San Fernando Earthquake, February 9, 1971," California Institute of Technology, Report EERL 71-02, Pasadena, June 1971, 512 pp.
- 12.14 T. Paulay, "Some Aspects of Shear Wall Design," *Bulletin of the New Zealand Society for Earthquake Engineering*, Vol. 5, No. 3, September 1972, pp. 89-105.
- 12.15 M. Stiller, "Verteilung der Horizontalkräfte auf die aussteifenden Scheibensysteme von Hochhäusern," *Beton- und Stahlbetonbau*, Vol. 60, No. 2, 1965, pp. 42-45.
- 12.16 H. Beck and H. Schaefer, "Die Berechnung von Hochhäusern durch Zusammenfassung aller aussteifenden Bauteile zu einem Balken," *Der Bauingenieur*, Vol. 44, No. 3, 1969, pp. 80-87.
- 12.17 R. Rosman, "Analysis of Special Concrete Shear Wall Systems," *Proceedings of the Institution of Civil Engineers*, 1970, Supplement (VI) Paper 72665, pp. 131-152.
- 12.18 N. B. Green, "Factors in the Aseismic Design of Reinforced Concrete Shear Walls Without Openings," *Journal ACI*, Vol. 65, August 1968, pp. 629-633.
- 12.19 F. R. Khan and J. A. Sbarounis, "Interaction of Shear Walls and Frames," *Journal of the Structural Division, ASCE*, Vol. 90, ST3, June 1964, pp. 285-335.
- 12.20 "Design of Combined Frames and Shear Walls," Advanced Engineering Bulletin No. 14, Portland Cement Association, Skokie, Ill., 1965, 36 pp.
- 12.21 ACI Committee 442, "Response of Buildings to Lateral Forces," *Journal ACI*, Vol. 68, No. 2, February 1971, pp. 81-106.
- 12.22 M. E. Sozen, "The Caracas Earthquake of July 29, 1967," *Journal ACI*, Vol. 65, May 1968, pp. 394-401.
- 12.23 H. Beck, "Contribution to the Analysis of Coupled Shear Walls," *Journal ACI*, Vol. 59, August 1962, pp. 1055-1070.
- 12.24 R. Rosman, "Approximate Analysis of Shear Walls Subject to Lateral Loads," *Journal ACI*, Vol. 61, June 1964, pp. 717-733.
- 12.25 R. Rosman, "An Approximate Method of Analysis of Walls of Multistorey Buildings," *Civil Engineering and Public Works Review*, Vol. 59, January 1964, pp. 67-69.
- 12.26 L. Chitty, "On the Cantilever Composed of a Number of Parallel Beams Interconnected by Cross Bars," London, Edinburgh, and Dublin, *Philosophical Magazine and Journal of Science*, Vol. 38, October 1947, pp. 685-699.

- 12.27 A. Coull and B. Stafford Smith, "Analysis of Shear Wall Structures" (a review of previous research). In Ref. 12.1, pp. 139-155.
- 12.28 T. Paulay, "The Coupling of Reinforced Concrete Shear Walls," *Proceedings, Fourth World Conference on Earthquake Engineering*, January 1969, Santiago, Chile, Vol. B-2, pp. 75-90.
- 12.29 T. Paulay, "Coupling Beams of Reinforced Concrete Shear Walls," *Journal of the Structural Division, ASCE*, Vol. 97, ST3, March 1971, pp. 843-862.
- 12.30 R. Rosman, *Statik und Dynamik der Scheibensisteme des Hochbaues*, Springer, Berlin, 1968, 317 pp.
- 12.31 R. J. Burns, "An Approximate Method of Analysing Coupled Shear Walls Subject to Triangular Loading," *Proceedings, Third World Conference on Earthquake Engineering*, 1965, New Zealand, Vol. III, pp. IV-123-140.
- 12.32 V. B. Berg and J. L. Stratta, *Anchorage and the Alaska Earthquake of March 27, 1964*, American Iron and Steel Institute, New York, 1964, 63 pp.
- 12.33 A. Winokur and J. Gluck, "Ultimate Strength Analysis of Coupled Shear Walls," *Journal ACI*, Vol. 65, No. 12, December 1968, pp. 1029-1035.
- 12.34 T. Paulay, "An Elasto-Plastic Analysis of Coupled Shear Walls," *Journal ACI*, Vol. 67, No. 11, November 1970, pp. 915-22.
- 12.35 T. Paulay, "Simulated Seismic Loading of Spandrel Beams," *Journal of the Structural Division, ASCE*, Vol. 97, ST9, September 1971, pp. 2407-2419.
- 12.36 T. Paulay and J. R. Binney, "Diagonally Reinforced Coupling Beams of Shear Walls," *ACI Special Publication 42*, Detroit, 1974, Vol. 2, pp. 579-598.
- 12.37 A. R. Santhakumar, "The Ductility of Coupled Shear Walls," Ph.D. thesis, 1974, University of Canterbury, Christchurch, New Zealand, 412 pp.

The Art of Detailing

13.1 INTRODUCTION

Recent advances in the understanding of the behavior of concrete structures have resulted in more sophisticated methods of analysis and design. Computer-oriented techniques enable the elastic or inelastic analyses of highly indeterminate structures to be carried out speedily. One might think that this development alone would account for more functional and economical structures.

Every good designer knows, however, that there is more to design than proportioning a structural section or obtaining safe stresses. Overall economy, and the feasibility and ease of construction, are some of the equally important aspects of a successful design. In fact, an elaborate analysis becomes worthless if the computations are not translated into successful structures. Such may be the case when a structure is represented by a set of poorly detailed drawings. Structural analysis is no more than one of the many tools used by the skillful engineer in the broad process of design. It is a necessary but insufficient prerequisite of a good design.^{13.1}

Detailing consists of the preparation of placing drawings, reinforcing bar details, and bar lists that are used for the fabrication and placement of reinforcement in the structures.^{13.2} But detailing also incorporates the whole thought process by which the designer enables each part of his structure to perform safely under service conditions and efficiently when subject to ultimate load or deformations.

To reinforce a concrete structure correctly, the designer must possess a penetrating understanding of its behavior—an understanding beyond the establishment of the equations of equilibrium and strain compatibility. This understanding must be based on a thorough knowledge of the properties of materials and structural behavior as evidenced by tests, rather than on the results obtained from mathematical models. Design based on the concept of strength and collapse behavior reflects this philosophy to a great extent.

It is also to be realized that if the vast amount of construction work that is waiting to be done is to proceed rapidly and efficiently, there must be some standardization and simplification of the detailing of reinforced concrete. This is essential if we are to take advantage of the potentiality of computers in detailing, scheduling, and data processing of the reinforcement, and presenting the results in such a way that the contractor can translate the information into completed work without delay or difficulty.^{13.3}

Seismic aspects of detailing were studied and reported by ACI Committee 315.^{13.4} However, considerably more experimental study, simulating seismic conditions, is required before satisfactory conclusion with respect to detailing will be obtained. A number of suggestions related to seismic performance and based on recent research findings are made in subsequent sections.

Detailing based on an understanding of and feeling for the structural behavior of reinforced concrete in an increasing range of situations, on the knowledge of the changing demands of economy, and on the limitations of construction practices, is likely to require as much creative power as the derivation of structural actions by mathematical analysis.

In compiling this chapter, necessarily limited to a few specific situations most frequently encountered in building frames, much inspiration was gained from the work of Leonhardt, who did a great deal to draw attention to this neglected aspect of the design process.

13.2 THE PURPOSE OF REINFORCEMENT

Before the detailing of reinforcement is examined, it is helpful to have its purpose clearly defined. Reinforcing steel in concrete may be provided to accomplish the following:

1. Resist the internal tensile forces as derived from analysis, which assumes that the surrounding concrete does not develop any tension. The reinforcement thus must ensure that a serviceable structure possesses adequate strength.
2. Ensure that crack widths under service conditions do not exceed the recommended values as set out in Chapter 10. It is to be remembered that reinforcement, within practical and economical limits, cannot prevent cracking.
3. Prevent excessive cracking that may result from shrinkage or temperature changes when structural elements are restrained.
4. Supply compressive forces when the concrete alone, which is more suitable to fulfill this function, is not capable of resisting the internal pressure.
5. Restrain compression bars against lateral movement, prevent buckling,

and provide confinement in highly stressed areas of compression zones of columns, beams, and joints.

6. Provide protection against spalling of the fire protective cover over rolled steel members, also giving temporary support to the reinforcing system during construction.

Recommendations for detailing for some of these purposes, particularly crack control, have been made in previous chapters. Some of the most important guiding principles in the art of detailing are those associated with bond and anchorage (see Chapter 9).

13.3 DIRECTIONAL CHANGES OF INTERNAL FORCES

Whenever a loaded concrete structural member is not straight, or its dimensions are abruptly changed, internal forces are generated. The existence of these forces is sometimes overlooked, yet they must be considered when the members are being detailed.

The two tensile forces T_1 and T_2 generated at the kink of the reinforcing bars (see Fig. 13.1a) are not unidirectional; hence a third force R results. This would tend to cause a splitting crack along the bar if the tensile strength of the concrete is overcome. Where the angular change is small ($\alpha < 15^\circ$), stirrups at and in the immediate vicinity of the kink can be used to transfer the force back into the compression zone of the member. To prevent premature cracking, it is advisable to proportion conservatively the stirrup

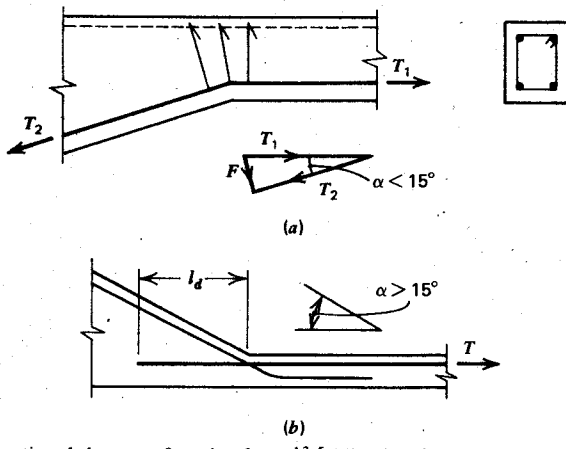


Fig. 13.1. Directional changes of tension force.^{13.5} (a) Using ties when angular change is small
(b) Main bars overlapping when inclination is large.

reinforcement (i.e., say, for $1.5F$). For larger angular changes the reinforcement should be anchored by means of a straight extension so that no transverse force is generated at the kink (see Fig. 13.1b).

The same principle applies when the internal compression force changes its direction abruptly or continuously. Figure 13.2 shows the outward pointing resultant generated in a small flanged *T* beam. Closely spaced

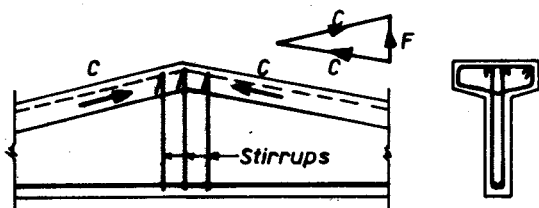
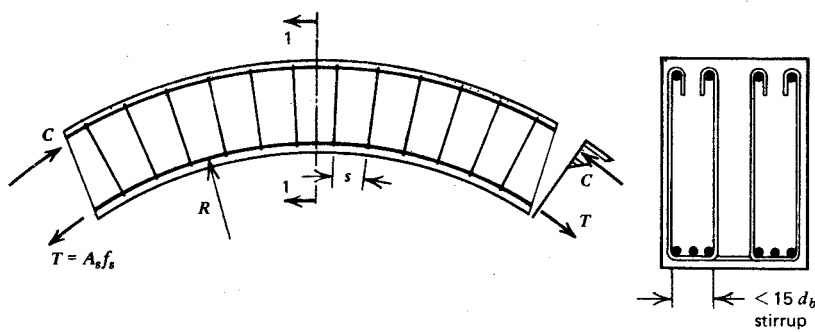


Fig. 13.2. Directional change of compression force in *T* beam.^{13.5}

stirrups and transverse reinforcement in the flange must be provided to prevent a breaking away of the flange.

Large transverse forces are generated at joints, such as the eaves and the apex of a portal frame. These are considered separately in Section 13.8.

In curved members, such as that appearing in Fig. 13.3, equal and opposite radial forces induced by bending moments can cause internal transverse tension. Hence stirrups at regular spacing are required to enable these forces to balance each other. Considering the tensile force in the flexural reinforcement, it follows from first principles and from Fig. 13.3 that the radial



Section 1-1

Fig. 13.3. Stirrups resist radial forces in curved members.^{13.5}

transverse load per unit length p_r , is

$$p_r = \frac{T}{R} = \frac{A_s f_s}{R} \quad (13.1)$$

hence stirrups at spacing s will be required so that the stirrup area is

$$A_{sr} = \frac{p_r s}{f_{sr}} \quad (13.2)$$

where f_{sr} is the design stress in the stirrups and R is the radius of the circle. It may be assumed^{13.5} that a two-legged stirrup can effectively resist the force generated by all curved flexural bars within a distance of 15 stirrup diameters between the two legs (see Fig. 13.3). The stirrup spacing s must be so selected that the cover will not break away between two stirrups when the curved bar tends to straighten. The affected area (cross-hatched in Fig. 13.4) is described below.

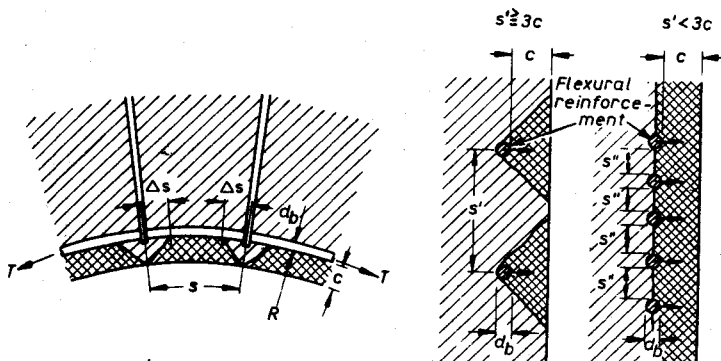


Fig. 13.4. Assumed failure modes associated with radial forces induced in curved members.^{13.5}

Leonhardt^{13.5} has suggested that by considering the approximate flexural stiffness of the curved bars and by limiting the tensile stress in the cover concrete to one-sixth of the tensile strength f'_t of the concrete (to allow for microcracking and shrinkage), the stirrup spacing should not exceed the following values:

$$s \leq \frac{2\Delta s}{1 - \frac{f'_t c R}{420 d_b^2}} \quad \text{when } s' \geq 3c \quad (13.3a)$$

or

$$s \leq \frac{2\Delta s}{1 - \frac{f'_t s'' R}{840 d_b^2}} \quad \text{when } s' < 3c \quad (13.3b)$$

where $\Delta s \leq 3d_b$ or $\Delta s < c$, whichever is smaller. All dimensions appearing in Eqs. 13.3 are shown in Fig. 13.4. The tensile strength of the concrete f'_c is to be expressed in psi units. The equations are based on the assumption that the working stress f_s in the curved main bars does not exceed 34,000 psi (234 N/mm²).

When the radius of curvature R is large enough, the cover concrete will be sufficient to supply the radial tensile forces to balance those generated by the curved main bars. With the same assumption with regard to strength properties, stirrups can be omitted when

$$R \geq \frac{300d_b^2}{c} \quad \text{for } f'_c = 3000 \text{ psi (21 N/mm}^2\text{)} \quad (13.4a)$$

$$R \geq \frac{240d_b^2}{c} \quad \text{for } f'_c = 4000 \text{ psi (28 N/mm}^2\text{)} \quad (13.4b)$$

when $s' \geq 3c$ and

$$R \geq \frac{600d_b^2}{s''} \quad \text{for } f'_c = 3000 \text{ psi (21 N/mm}^2\text{)} \quad (13.4c)$$

$$R \geq \frac{400d_b^2}{s''} \quad \text{for } f'_c \geq 4000 \text{ psi (28 N/mm}^2\text{)} \quad (13.4d)$$

when $s' < 3c$.

When two layers of bars occur at right angles to each other and the curved bars are highly stressed, it is preferable to place them in the second layer, to increase the cover c .

Curved bars may cause splitting and consequent spalling of the cover in structures such as circular plates. Fig. 13.5 presents the plan of a circular bar

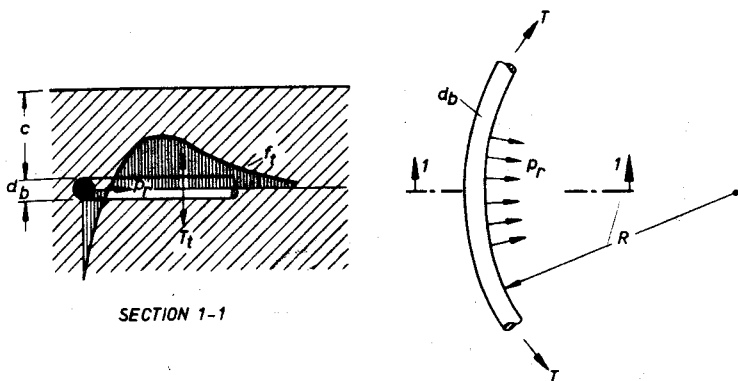


Fig. 13.5. Circular tensile bars cause transverse splitting stresses.^{13.5}

and the distribution of transverse tensile stresses that may be responsible for splitting in the plane of the bar. Leonhardt^{13,5} proposed that with the previously made assumptions, the cover should be selected so that

$$R \geq \frac{144d_b^2}{c} \quad \text{for } f'_c = 3000 \text{ psi (21 N/mm}^2\text{)} \quad (13.5a)$$

$$R \geq \frac{92d_b^2}{c} \quad \text{for } f'_c \geq 4000 \text{ psi (28 N/mm}^2\text{)} \quad (13.5b)$$

unless transverse reinforcement is provided. The circumferential bars in plates should be inside the radial bars and the latter may be tied together if the radius of the circular bars is smaller than that given by Eq. 13.5.

Codes specify the shape of sharp bends, such as occur in hooks, in a way that will limit the resulting bearing pressures and splitting stresses. It is assumed in codes that sufficient transverse reinforcement is present to resist the transverse tensile forces, should a splitting crack occur. If bent-up bars in beams are to be used, they should be kept away from the side of the beam, where the danger of the spalling of the side cover is the greatest.

13.4 THE DETAILING OF BEAMS

In several chapters we have discussed in some detail the flexural behavior and strength of reinforced concrete members. It must be evident that satisfactory behavior and adequate strength can be attained only by the efficient interaction of concrete and steel. Skillful detailing will assure this goal. The aim of this section is to illustrate, by examining a few typical situations, that good practice in detailing is likely to lead to improved structural behavior. Some of these suggestions have already been adopted by many designers of concrete structures, perhaps by intuition; others have been derived from recent research work.

13.4.1 Localities for Anchorage

From previous discussion of the bond performance it is apparent that the considerable effect on the quality of bond. It has been generally accepted practice to have bars terminated in compression zones. It is questionable whether much benefit would result from such an arrangement in all cases. Compression stresses acting parallel to a bar are unlikely to minimize the danger of splitting, which arises from tensile stresses acting at right angles to stress conditions of the concrete surrounding an anchored bar must have a the bar. Admittedly, a compression zone is free of transverse cracks, which are

known to be the origin of splitting cracks. Bottom bars in the end span of continuous beams show better anchorage at the simply supported end than in the vicinity of the point of contraflexure where they enter a compression zone. This indicates that compression stresses acting transversely to an anchored bar are more beneficial. Such is the situation when the reaction is applied to the tension face of a beam, as in Fig. 13.6. Similarly, when the concrete is subject to transverse tensile stress, the bond conditions can only

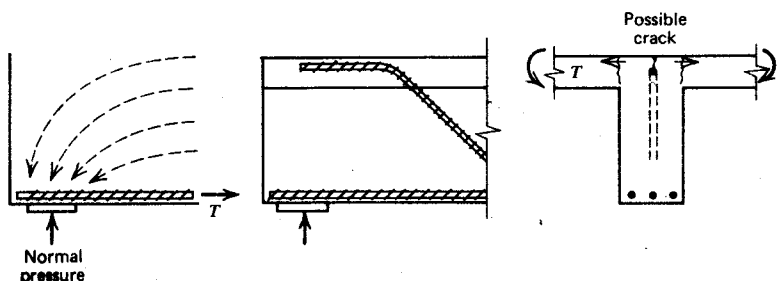


Fig. 13.6. Transverse pressure or tension at anchorage of beam reinforcement.^{13.1}

deteriorate. This may be the case for the top bars in T beams which lie in the negative moment zone of the supported slab (see Fig. 13.6). Untrauer and Henry have shown^{13.6} that the bond strength increases appreciably when normal pressure is present. The increase is more pronounced at ultimate load and for larger bars. This suggests that it may be better to seek areas of normal pressure in preference to compression zones for the anchorage of flexural reinforcement.

When bars are terminated in the tension zone of a beam, which contains sufficient transverse web reinforcement, considerable benefit may be derived from the compression that exists in the web as a result of truss action. For

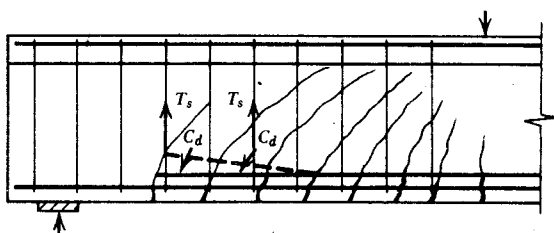


Fig. 13.7. Anchorage of flexural bars in diagonal compression zone.^{13.1}

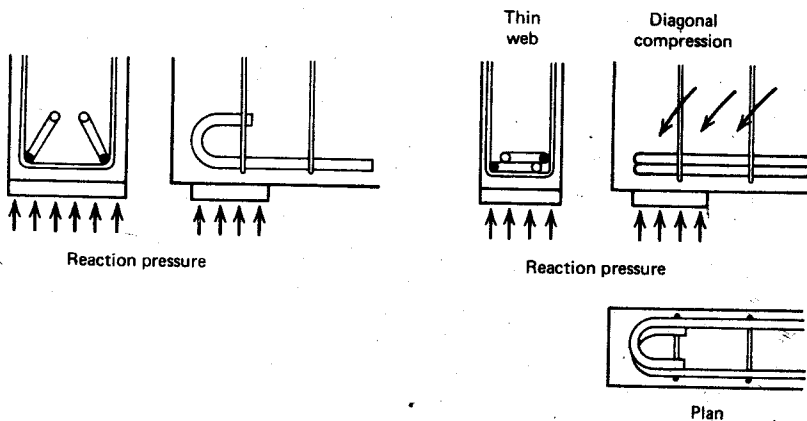


Fig. 13.8. Utilization of transverse compression at hooked anchorages.^{13.5}

this reason horizontal bars can be bent into the web to expose them to the diagonal pressure, as in Fig. 13.7 (see also Fig. 7.14). For similar reasons the hooked anchorage at the simply supported end of a beam can be much improved if the hooks are tilted or, preferably, if they lie in a near-horizontal position. Splitting effects are thus largely counteracted by the normal pressure originating from the reaction (see Fig. 13.8).

In precast concrete beams the length available for end anchorage may be so short that only special devices, such as those illustrated in Fig. 13.9, can

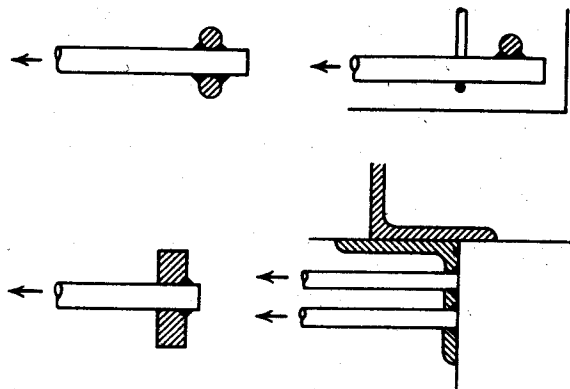


Fig. 13.9. Special anchorage devices employed when sufficient anchorage length is not available.^{13.5}

ensure the development of the required bar strength. In many situations, such as corbels or deep beams, crossbars welded on to the flexural reinforcement may be used (see Fig. 13.9). Because the support point is very often close to the free end of the beam, failure along a steep diagonal crack is a distinct possibility (see Fig. 13.10). Additional inclined small-diameter bars can be provided to ensure that no sliding failure can occur. The bars can be sized using the shear friction concept of load transfer discussed in Section 7.8. It should be remembered that the anchorage conditions for top bars are always inferior to those of bottom bars because of increased sedimentation and because the surrounding concrete may be in a state of transverse tensile

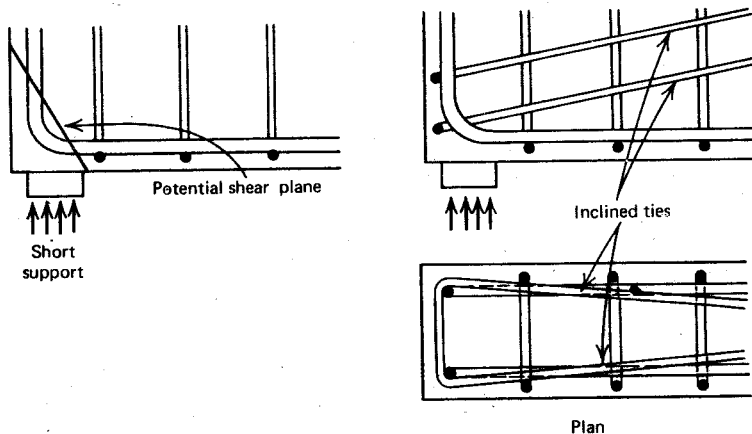
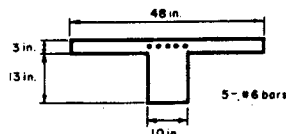
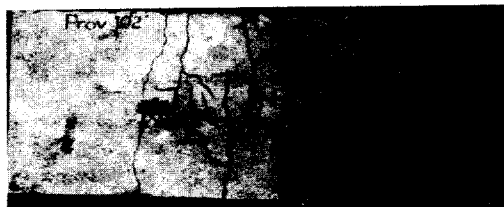


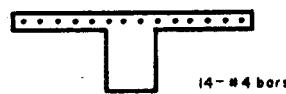
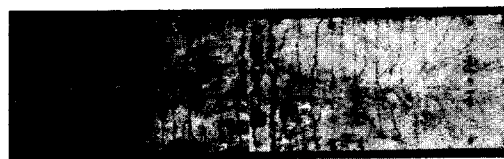
Fig. 13.10. Reinforcement to prevent sliding shear failure when reaction is applied close to free end of beam.^{13.5}

stress or, more often than not, is cracked. This is particularly true at interior columns of floors where beams intersect. Even under working load, such areas of a beam will shed some load to positive moment zones because of loss of stiffness. This effect will not be detrimental in any way as long as proportioning and careful anchorage detailing of the positive reinforcement enables it to accept the redistributed load.

Concentration and multilayered arrangement of negative reinforcement represents another source of deterioration of bond. It may result in an increase of crack widths. The crack pattern in the flange of two *T* beams tested by Waestlund and Jonsson^{13.7} shows to some extent this phenomenon. The maximum crack widths in these beams (Fig. 13.11a and b) were 0.046 in (1.17 mm) and 0.0046 in (0.117 mm), respectively, when the steel stress was 22,700 psi (157 N/mm²) in both cases. The measured largest crack widths



(a)



(b)

Fig. 13.11. Crack formation in T beams under 22,700 psi (157 N/mm²) steel stress.^{13.7} (a) Maximum crack width 0.046 in (1.17 mm). (b) Maximum crack width 0.0046 (0.117 mm).

over the interior supports of two identical beams tested by Leonhardt, Walther, and Dilger^{13.1} are compared at various load increments in Fig. 13.12.

The spreading of the negative steel into the adjoining slab, preferably using smaller diameter bars, has the added advantage of giving a slightly larger internal lever arm and providing better access for vibrators in a usually

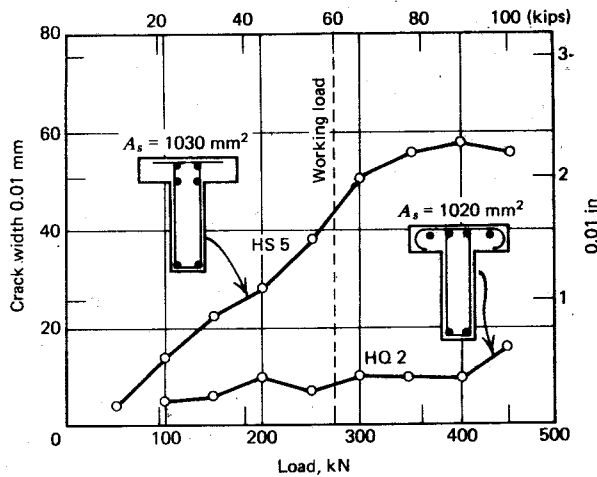


Fig. 13.12. A comparison of crack width in identical T beams.^{13.1}

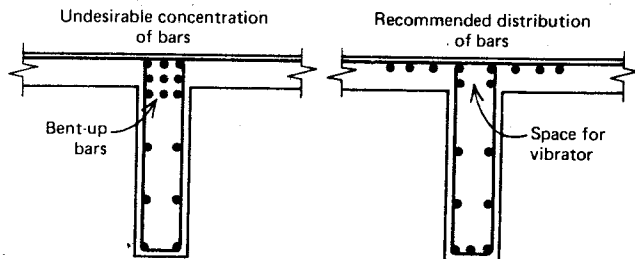


Fig. 13.13. Suggested improvement in the detailing of top reinforcement of beams.^{13.5}

overcrowded beam-column joint (see Fig. 13.13). This procedure should be applied with discretion when heavy web reinforcement is present. For an efficient truss action to develop, it is desirable to place the major part of the flexural reinforcement within the multilegged cage of the stirrups.

In beams with a small shear span/depth ratio a/d , arch action is the predominant mode of shear resistance after the onset of diagonal cracking. Accordingly, the flexural reinforcement is required to function as the tie of this arch (see Fig. 7.10). Any arrangement that reduces the amount of flexural steel, such as the bending up of bars (see Fig. 13.14a), is likely to reduce the ultimate shear strength. In such situations it is better to carry the whole of the

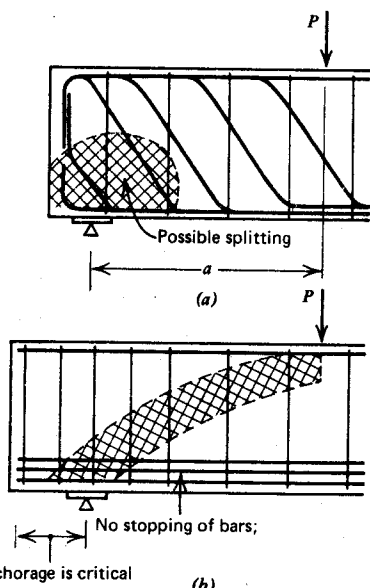


Fig. 13.14. Anchorage in short beams affect arch action.^{13.1}

flexural reinforcement to the support, as in Fig. 13.14b. To enable the concentrated bond forces to be transmitted to these bars over a very short length, closely spaced stirrups or binding should not be omitted.^{13.1}

13.4.2 Interaction of Flexural and Shear Reinforcement

In Chapter 7 the shear resistance of web reinforcement was examined with the aid of the "truss analogy." From the study of a joint of this truss (Fig. 7.14), it is apparent that diagonal compression can be resisted only at the intersection of the horizontal and vertical reinforcements, the hypothetical "pin joint" of the analogous truss. For this reason, the stirrup, which is the tension member in the web, must be able to develop its full strength over its entire height between the top and bottom "pin joints" along the shear span. Stirrups are not meant to develop bond between the "chords" and must be anchored accordingly. Figure 13.15 presents some undesirable stirrup forms and some others that would meet the anchorage requirements given.

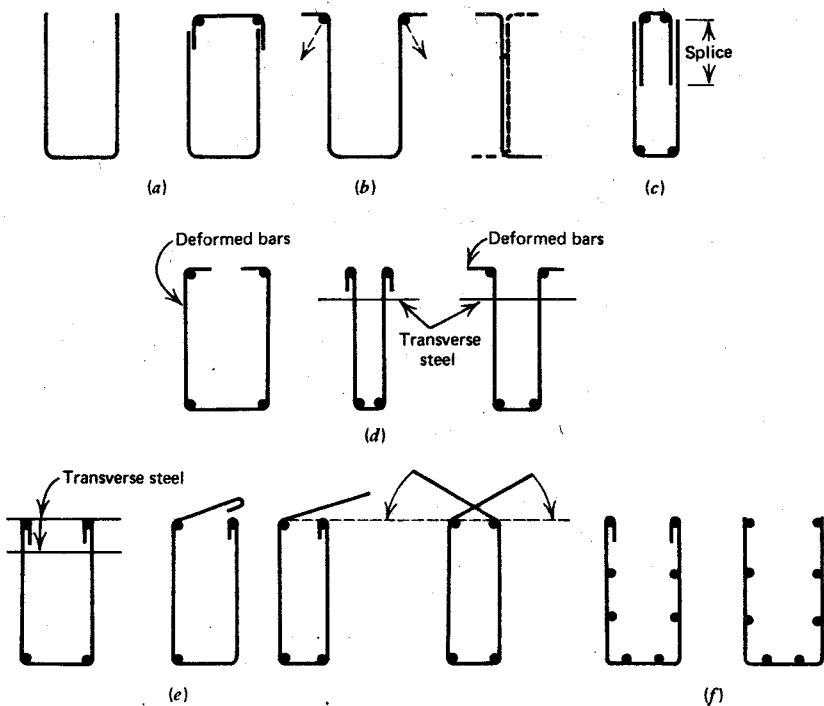


Fig. 13.15. Different stirrup forms. (a) Incorrect. (b) Insufficient. (c) Undesirable. (d) Limited applicability. (e) Satisfactory shapes. (f) Made of welded wire mesh.

Larger longitudinal bars passing through the hooks of the stirrups are essential because they must distribute the concentrated bearing received from the stirrups. It may be optimistic to assume that the end of the stirrup, not bent around a longitudinal bar in the compression zone of the beam, is well anchored. At ultimate load, particularly when diagonal cracks have developed, the neutral axis may move very close to the compression edge. Since stirrups depend greatly on this concentrated form of anchorage, it is desirable to have them fit tightly and be in contact with the longitudinal bars they surround. The sensitivity of hooks with respect to slip and the consequent effect on enlarged crack widths was pointed out in Section 9.4.2.

The normal practice is to bend stirrups around longitudinal bars with an angle of 135° . Some codes permit a 90° turn for stirrups and ties. At plastic hinges where the cover may spall off, a 90° turn will be unsatisfactory. This arrangement may also lead to the unsatisfactory behavior^{13.8} of closed stirrups illustrated in Fig. 13.16.

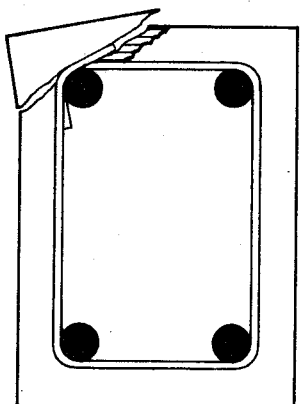


Fig. 13.16. Possible failure caused by insufficient anchorage of stirrups.

When large shearing forces are present and more than two bars are used to resist flexure, it is more desirable to form a "truss joint" at each of the longitudinal bars. Therefore multileg stirrups should be used. This will ensure that the bond forces will develop at the "right" places (i.e., at each longitudinal bar). The undesirable concentration of diagonal compression in wide beams is represented in Fig. 13.17. In the absence of vertical stirrup legs, the center bars are incapable of resisting vertical forces, thus are inefficient in receiving bond forces. A secondary purpose of stirrups in surrounding the flexural tension reinforcement—namely, the prevention of the opening of

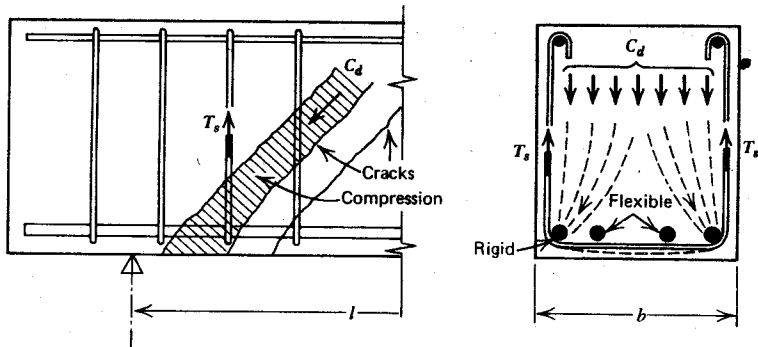


Fig. 13.17. Undesirable distribution of diagonal compression because of wide stirrups.^{13.1}

bond-generated longitudinal splitting cracks in the shear span—should also be kept in mind.

The extensive shear investigations of Leonhardt and Walther^{13.9} have indicated that bent-up bars from the flexural reinforcement are often responsible for inferior performance. The following reasons may be given for the undesirability of bent-up diagonal bars as shear reinforcement.

1. When widely spaced, bent-up bars cause large stress concentration in the bends. These may lead to splitting, particularly when the arrangement is unsymmetrical (see Fig. 13.18).
2. When closely spaced—which would eliminate the undesirable effects—bent-up bars deprive the flexural reinforcement of too many bars.

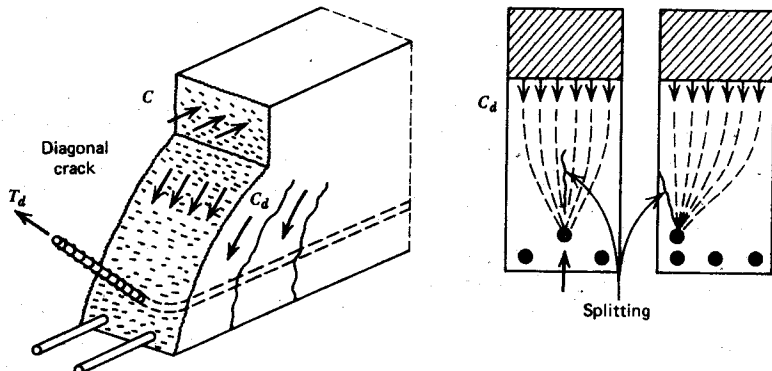


Fig. 13.18. Isolated bent-up bars do not support compression forces satisfactorily.^{13.1}

3. When compared with stirrups, they do not provide confinement for the concrete in compression.
4. They generally lead to larger crack widths.
5. They are more difficult to manufacture and to handle on the site, and are therefore relatively expensive.

The crack widths at various load increments, measured by Leonhardt and Walther^{13,9} on four beams of identical dimensions and steel contents, are given in Fig. 13.19. The beneficial effect of closely spaced stirrups, particu-

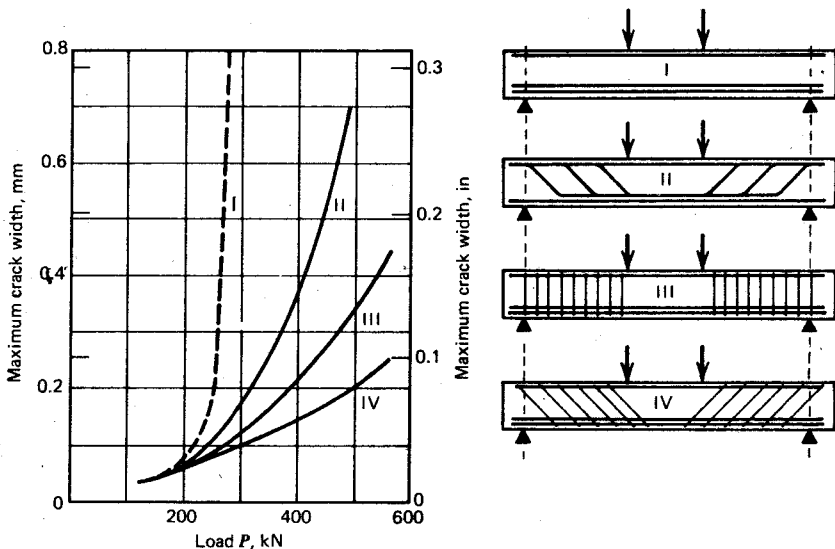


Fig. 13.19. Maximum width of shear cracks for different types of web reinforcement.^{13,9}

larly diagonal ones, is quite apparent. Diagonal stirrups are usually impractical, but they can be used effectively in foundation beams and walls where no reversal of stresses occur. Such walls have often been made unnecessarily thick to reduce high nominal shear stresses.

Short diagonal bars adjacent to supports have not proved very efficient. As Fig. 13.20 indicates, the lower portion of these bars may be "pushed down" by diagonal compression, consequently, diagonal cracks penetrate the compression zone. Bent-up bars may be used with full anchorage length, but closely spaced stirrups perform better.

Some schools of thought maintain that diagonal tension can be resisted

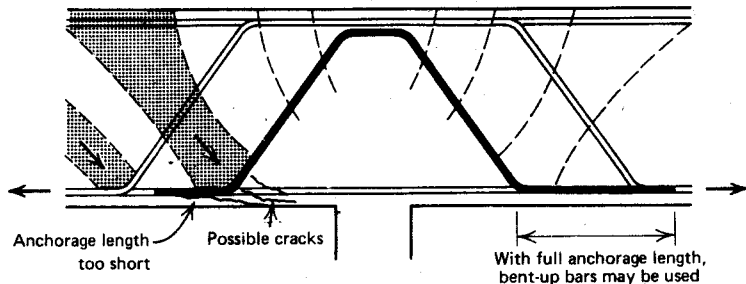


Fig. 13.20. Additional diagonal bars at supports perform poorly.^{13.1}

only by diagonal bars or mesh reinforcement; for this reason, it has been sometimes suggested that horizontal bars within the web should also be provided. Tests have indicated^{13.9} that up till failure only small strains occur in intermediate horizontal bars placed in beams of usual proportions. However, their beneficial effect on crack control, particularly in deeper beams, is very marked (see Fig. 13.13). In such situations, welded meshes can be used to advantage for the web reinforcement. When the applied load occurs close to the support, producing a low shear-span/depth ratio, arch action becomes predominant after diagonal cracking. Consequently, horizontal bars over the short shear span, as in Fig. 13.21, will improve conditions around the reaction and will increase the shear friction strength along a potential diagonal crack between the load and reaction points.

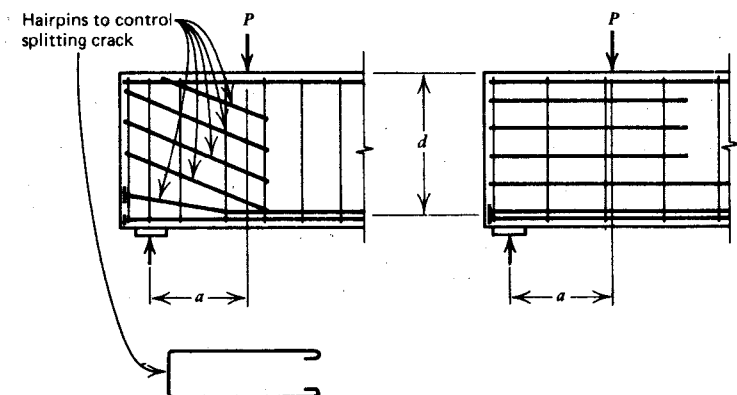


Fig. 13.21. Secondary inclined or horizontal reinforcement when load is applied near the support.

13.4.3 The Detailing of Support and Load Points

In most experiments the external load is applied directly to the compression zone of the test beam. This creates a biaxial state of stress that improves the behavior at ultimate load. Reactions for the same beams normally act against the flexural reinforcement, as shown in Figs. 13.14 and 13.21, thus greatly improving anchorage conditions. In actual structures these favorable conditions often do not exist.

When the reaction is applied to the soffit of a beam, as in Fig. 13.22a, the critical section for shear is approximately at a distance d from the support. However, when the reaction is applied from above (see Fig. 13.22b), the critical section is clearly at the face of the support. In the second case further

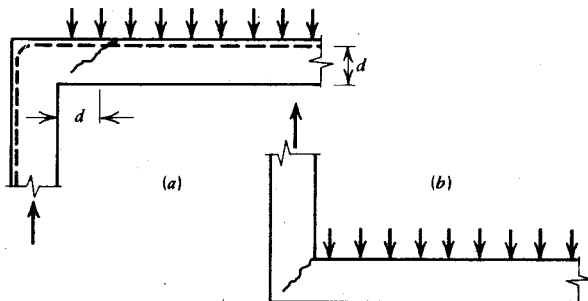


Fig. 13.22. Formation of diagonal crack indicates critical section when reaction is applied (a) from below or (b) from above a beam.

precautions must be taken by the detailer to ensure that the reaction is "guided" into the correct area of the supported beams or slab, which must be suspended.

It is essential that the reaction for gravity loads always develop at the bottom of a beam, regardless of whether it is simply supported or continuous. For example, the diagonal compression resulting from truss or arch action in a suspended beam or slab (see Fig. 13.23) should find an effective support. Thus the bottom reinforcement in the slab should pass above the transverse bars situated in the corners of closely spaced suspender loops. The mat so formed at the bottom of the wall-slab junction is well suited to receive the vertical component of the diagonal compression.

Often little thought is given to the development of the necessary reaction at the point at which a secondary beam is supported by a primary girder. It is customary to assume that by means of truss action approximately one-half

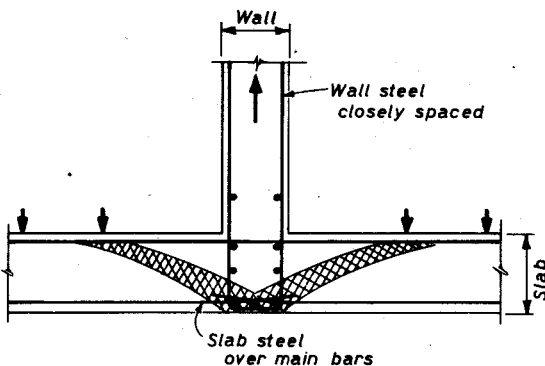


Fig. 13.23. Closely spaced wall reinforcement outside the horizontal steel effectively supports a suspended slab.^{13.1}

the reaction is transferred to the top and the other half to the bottom regions of the supporting girder. The shear force distribution corresponding with this assumption is represented in Fig. 13.24a. The actual behavior of the beam, as indicated by tests,^{13.1} is different. A portion of the shear is always resisted by the concrete mechanisms (discussed in Chapter 7), and because flexural cracks are absent, the diagonal crack does not necessarily form at the support. Both these aspects suggest that the shear is predominantly sustained by diagonal compression (see Fig. 13.24b). The lack of sufficient support for diagonal compression in the vicinity of the main girder led to the failure in one of the beams of the torsion tests at the University of Toronto^{13.10} (see Fig. 13.25).

Stirrups in the secondary beam *B*, and particularly in the girder *A* in Fig. 13.24b, are better suited to receive the diagonal compression force. The stirrups in the girder *A* should transmit the reaction *V* to the girder's compression zone, where it can resolve itself into diagonal compression forces. The

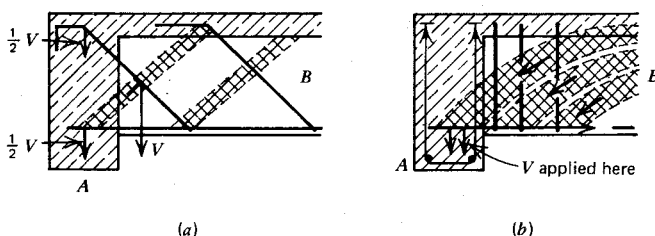


Fig. 13.24. Main girder supporting secondary beam.^{13.1} (a) With bent-up flexural bars; (b) With stirrups.

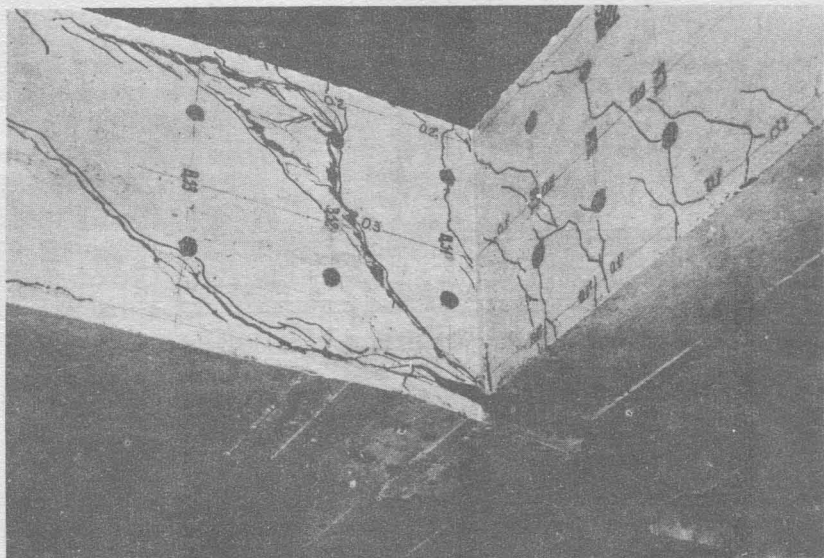


Fig. 13.25. Lack of support for diagonal compression in secondary beam.^{13.10}

suggested arrangement of stirrups is shown in greater detail in Fig. 13.26. The importance of "holding down" the compression zone of girders at point loads not directly applied to the top surface of the beam, to ensure efficient arch action, was pointed out in Chapter 7.

Leonhardt recommends^{13.1} that the "suspender" stirrups to be placed in the main girder *A*, in addition to those required for shear resistance, be capable of resisting a force

$$V_s^* = \frac{h_b}{h_a} V$$

where V = load received from beam *B*

h_a, h_b = depth of beams, as in Fig. 13.26

Baumann and Rüsch, on the other hand, suggest^{13.11} that suspender stirrup reinforcement be provided for the whole shear or reaction force, because large strains in these stirrups can lead to horizontal splitting cracks along the flexural reinforcement of the supporting girder. The cost of the additional steel is usually negligible.

When beams of equal depth meet, the bottom steel of the secondary beam should lie above the bottom reinforcement of the supporting girder.

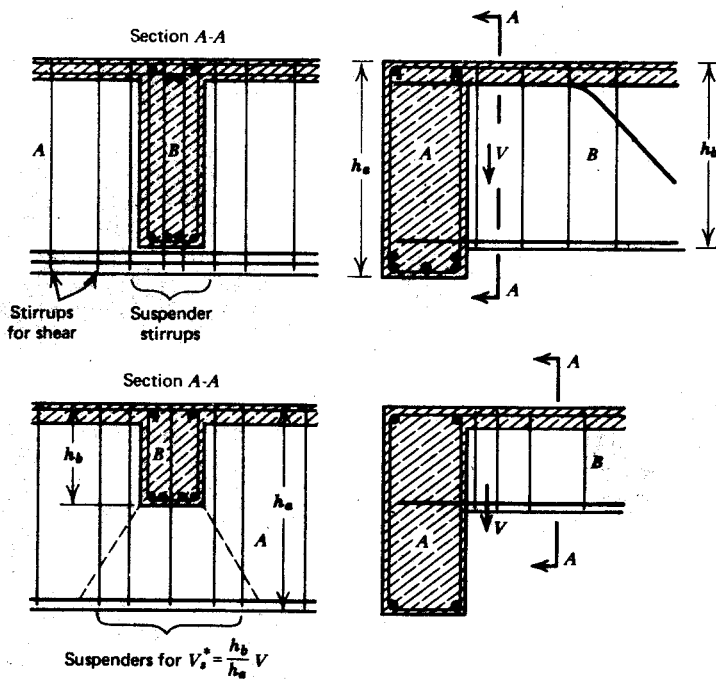


Fig. 13.26. Suspender stirrups receive reactions from secondary beam.^{13.1}

This way the maximum benefit will be derived for the anchorage as a result of normal pressure induced by diagonal compression in the secondary *B* beams. An example is given in Fig. 13.27. The suspender stirrups should be provided for the total reaction required from beam *I* at the sides of the girder in accordance with equilibrium requirements.

In beams symmetrically loaded with two point loads, a constant moment zone exists between these loads across which no shear is transferred. When these loads originate from secondary beams, as in the bottom example in Fig. 13.26, the required suspender stirrups should be spread toward the shear span side of the supporting girder, since stirrups in a constant moment zone will be ineffective.

The cantilever slab (Fig. 13.28) is another example that is encountered when the diagonal compression is directed toward the bottom edge of the supporting beam. Thus it is important to carry the reaction from this area toward the top of the beam. The individual bars shown in the diagram suggest one solution to this problem.

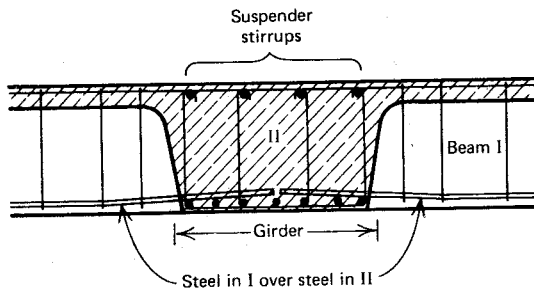


Fig. 13.27. Beam supporting beam of equal depth.^{13.1}

In precast concrete construction, an intermediate hinge is often required along a span; careful detailing is mandatory in such cases, since only about half the effective beam depth is available. Figure 13.29a indicates the flow of the internal compression forces. Suspender stirrups must be provided to carry the full reaction to the top edge of both beams. From the ends of these stirrups, a diagonal strut can then develop in the direction of the bearing plate. Leonhardt suggested^{13.5} special stirrups for 1.2 times the shear force R . The anchorage length of the bottom reinforcement, assumed to extend over distance $1.2h_2$, as in Fig. 13.29b, should be sufficient to develop a horizontal force equal to $1.2R$. Sufficient (hairpin) reinforcement must extend horizontally past the reentrant corners where a potential diagonal crack can develop.

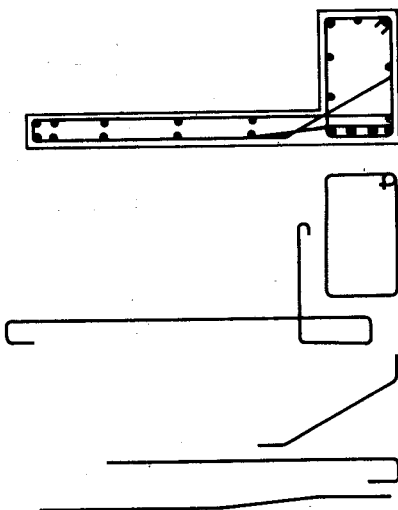


Fig. 13.28. Beam supporting cantilever slab.^{13.5}

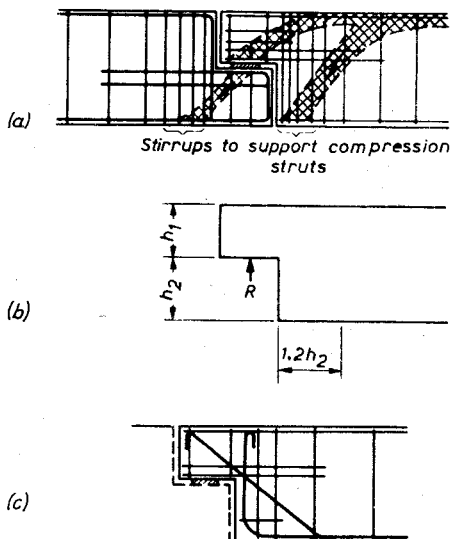


Fig. 13.29. Short cantilevers form hinge in span of beam.^{13.5} (a) Using orthogonal reinforcement. (b) Using bent-up bars.

The reinforcement of the short cantilevers is similar to that of corbels, discussed in Section 13.6.

When the beam is deep, some of the flexural bars may be bent up diagonally, in accordance with Fig. 13.29c. Often it is difficult to provide sufficient anchorage for them in the smaller cantilever part of the articulation.

When point loads along a reinforced concrete girder are to be applied to its underside, a device that transfers these forces to the top of the beam must be used. Figure 13.30 shows some solutions.^{13.5} Since there is no intention to transfer this load anywhere but to the top of the girder, plain round bars can be used, and the bond can be destroyed along their length. When crane girders are supported, it is preferable to post-tension these high-strength hanger bars or bolts, assuming that enough compression force remains between the bottom bearing plate and the concrete after vertical load application, shrinkage, and creep, to transfer horizontal forces resulting from the operation of a crane.

13.4.4 Cutting Off the Flexural Reinforcement

Wherever a bar is terminated in the tension zone of a beam, a discontinuity is created. The sudden reduction in the tension **steel area** results in a sudden increase in steel strain. This in turn causes the **cracks** that are initiated by the

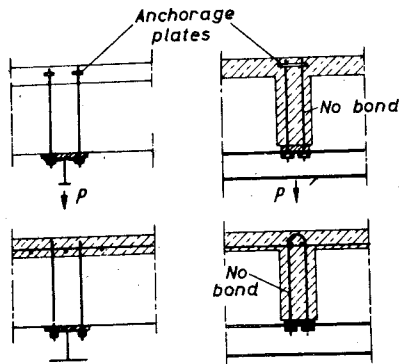


Fig. 13.30. Means by which force applied at soffit of beam can be transferred to its top.^{13.5}

cutoff bars to become wider. Whenever shear forces can assume a critical magnitude, these initiated cracks become inclined. Probably because of reduction in aggregate interlock strength, such cracks often lead to a premature shear failure. It is essential, therefore, that the shear strength of such areas of a beam be supplemented by web reinforcement. Codes^{13.12} require additional stirrups in the vicinity of cutoff points of the flexural reinforcement in the tension zone.

Ferguson and Husain^{13.13} found that apart from carrying the entire flexural reinforcement through the tension zone, the best way of avoiding the initiation of a shear failure at a load less than that which corresponds with the flexural capacity, is to bend the tension bars up into the web of the beam (see Fig. 13.7). In the detailing of the flexural reinforcement in the tension zone, it is essential to avoid points of abrupt changes. To demonstrate this effect, an investigator placed an additional short bar in an otherwise adequately reinforced beam. The beam showed a lower shear strength than a companion, which did not contain an extra bar.

The effect of shear and consequent diagonal cracking on the curtailment of flexural reinforcement, as expressed by the "Tjd diagram," was discussed in Section 7.5.1.

13.5 THE DETAILING OF COMPRESSION MEMBERS

Bond and anchorage conditions are more favorable in compression members. Consequently fewer difficulties arise with respect to detailing main column bars. A few points related to the splicing of column bars deserve attention.

A considerable fraction of the compression force in a bar is transferred by end bearing, but this action is generally overlooked since no allowance is

made for it in the design of a column splice. The concrete in the immediate vicinity of the bar end may not be capable of absorbing the stresses. In numerous columns tested at the University of Stuttgart,^{13,14} the concrete under each of the spliced bars burst laterally before the member could attain its ultimate strength. It appears that the slip required to mobilize bond stresses cannot take place before the end-bearing resistance at the bars is overcome. Figure 9.23 shows a splice failure in a column.^{13,14}

Additional transverse reinforcement at and near the ends of spliced bars is imperative, to give confinement to the highly stressed concrete (shaded areas in Fig. 13.31a). An arrangement of additional ties at compression splices suggested by Leonhardt and Teichen^{13,14} appears in Fig. 13.32.

This weakness of a compression splice suggests that it might be better to place the splice in a low-stress area (e.g., midheight of a column), if such a place exists. In earthquake-resistant structures, a column may be subjected to very large bending moments, therefore possibly to plastic hinging at the top and bottom ends. For this reason, splicing should be near midheight.

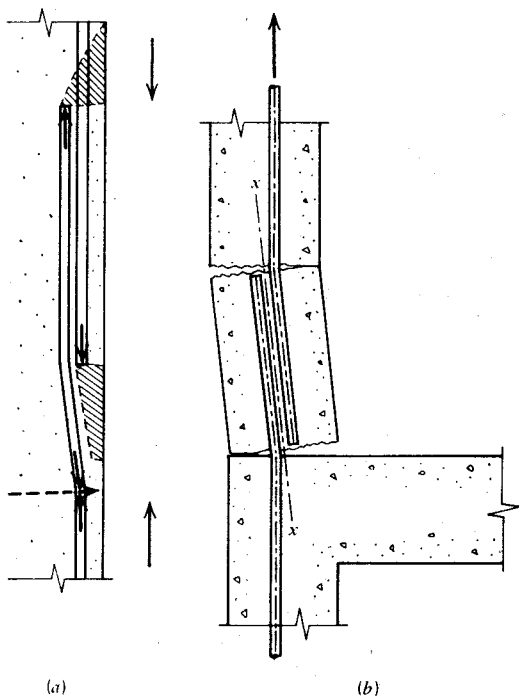


Fig. 13.31. Transverse forces introduced when bar offsets occur. (a) In column splices. (b) In eccentric tension splices.

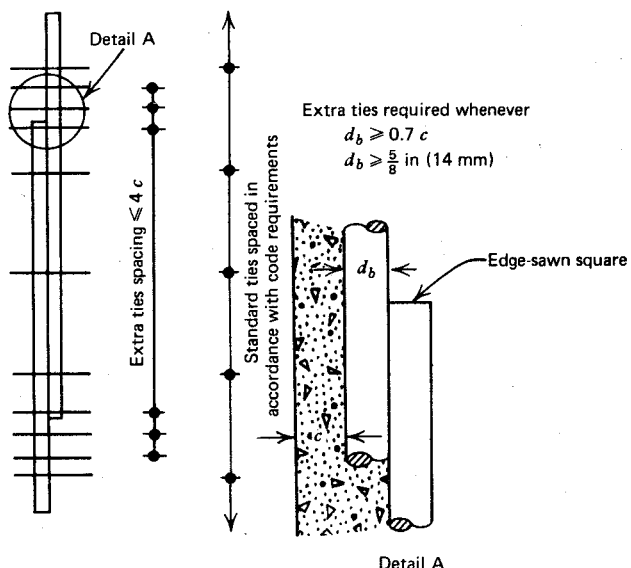


Fig. 13.32. Additional ties required at ends of compression splices.^{13.14}

Wherever the steel force changes its direction (i.e., at cranks), transverse forces are generated. Additional ties placed at such points should have a strength in excess—(say, by 50%)—of the transverse force (broken line arrow in Fig. 13.31a), generated when the column bar yields. Similar considerations will require transverse reinforcement at the upper crank (Fig. 13.31a) when the column bar is in tension.

When single layered reinforcement is used in thin walls, a transverse offset should be avoided. Tension, induced by a seismic disturbance, may lead to the situation illustrated in Fig. 13.31b.

The purpose of transverse reinforcement in columns is threefold. Each of these requires considerations to ensure that the particular purpose is fulfilled.

1. Column bars carrying compression loads are liable to buckle. Under large strains, when yielding in the steel is approached, the lateral restraint provided by the cover concrete can not be relied on. Therefore, transverse ties must provide adequate lateral support to each column bar, to prevent instability due to outward buckling. The present ACI code^{13.12} specifies a maximum tie spacing of 16 times the diameter of the column bar. From a theoretical consideration of the problem, Bresler and Gilbert^{13.15} have shown that the critical unsupported length of compression bars is in excess of this, hence the present provision is adequate. When alternating plasticity occurs,

however, the tangent modulus of elasticity of the compression reinforcement is greatly reduced because of Bauschinger effect. Thus the critical buckling load in earthquake-affected column bars is substantially diminished. To sustain the full yield capacity of compression bars, the unsupported length must be considerably reduced. Bresler recommends, therefore, that within a length equal to one-sixth of the column height, at each end of the column, the tie spacing should not exceed $6d_b$. This requirement is normally met when confining reinforcement is used.

It is not the strength but rather the stiffness of the ties that matters. Ties must be large enough to prevent lateral displacement of the column bars at yield. For this reason, codes^{13,12} stipulate minimum tie sizes.

2. Columns of buildings subjected to seismic loading often carry large flexural and shear loads. When diagonal tension cracks are possible, shear reinforcement will be required. Therefore, the anchorage and the shape of the ties must be such that tensile forces resulting from truss action can be transferred from one face of the column to the other. This is particularly important in possible plastic hinge regions, where the contribution of the concrete to shear resistance is diminished or becomes negligible.

3. The third purpose of ties is to provide confinement to the concrete core. An analytical evaluation of confining steel was given in Chapter 2. It is to be noted that the effectiveness of confinement by ties comes from the locations at which the longitudinal steel is held rigidly in position, not from the straight

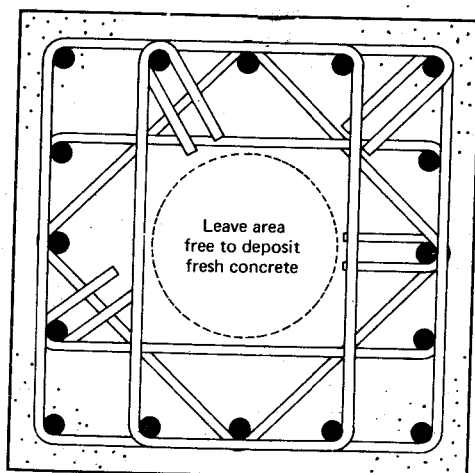


Fig. 13.33. Confining steel in columns subjected to heavy seismic forces.

portion of ties extending horizontally between points of directional changes (see Fig. 2.14) unless supplementary cross ties connect the sides.

Figure 13.33 illustrates a situation that may be encountered in columns affected by seismic loading. When heavy ties [i.e., larger than $\frac{5}{8}$ in (16 mm)] are used, the hooks may interfere with the placing of vertical bars and the concrete; here butt or lap welded ties, as shown in Fig. 13.76, may be more expedient.

13.6 BRACKETS AND CORBELS

13.6.1 Behavior

Point loads originating from gantry girders or precast concrete beams must often be sustained by brackets or corbels very near the face of a supporting column. It is difficult to assess explicitly the elastic behavior of such short and relatively deep cantilevers. Finite element analyses or photoelastic model studies, however, can furnish the required stress trajectories, which describe best the mechanism of load disposal. When the load intensity is sufficiently large, cracks will form approximately at right angles to these principal tension trajectories. After cracking of the concrete, the reinforcement will operate most efficiently if it is located at least approximately along such tension trajectories, and if it can generate its resisting moment with the maximum internal lever arm.

The distribution of principal stresses in a trapezoidal corbel and its supporting column, obtained by Franz and Niedenhoff^{13,16} from photoelastic models, is represented in Fig. 13.34. The load received from a gantry girder is simulated. An evaluation of such a study reveals the existence of four conditions.

1. The tensile stresses along the top edge are almost constant between the load point and the column face. Since the spacing of the trajectories does not vary greatly, the total tensile force is also nearly constant.
2. The compression force along the sloping edge of the corbel is also approximately constant, indicating that a diagonal compression strut develops.
3. The inclined tensile stresses arising from the change of direction of the compression force are very small.
4. The shape of the bracket has little effect on the state of the stresses. In a rectangular bracket, as in Fig. 13.35, the outer corner, opposite the load point, is virtually stress free.

These observations indicate that in spite of the complexity of the stress pattern, a simple design procedure, based on an internal linear arch

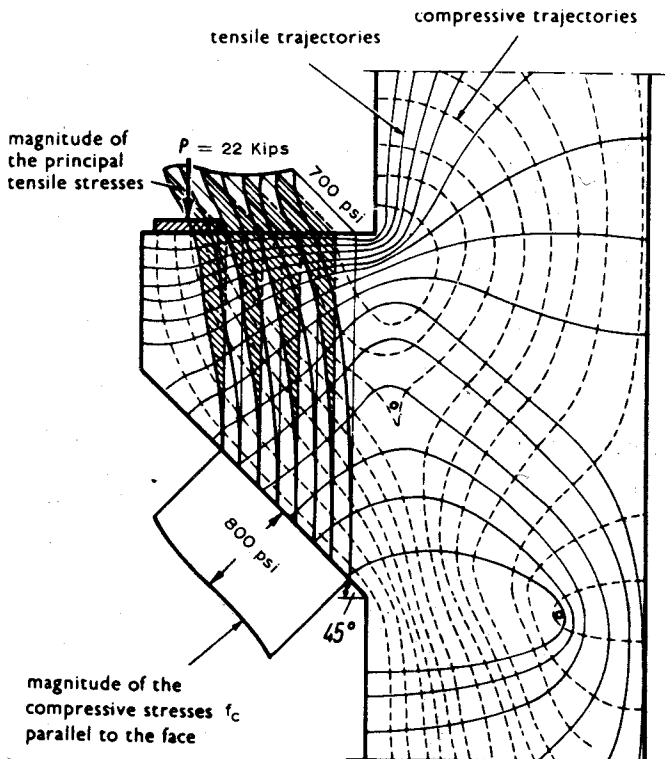


Fig. 13.34. Stress trajectories in a homogeneous elastic bracket.^{13.16}

mechanism, could be followed. The crack pattern in test specimens verifies this. The shearing force is resisted by the vertical component of the inclined compression rather than by shear stresses along the critical section. In very lightly reinforced corbels, the critical flexural crack at the face of the supporting column may propagate near the compression edge, because of the small depth of compression zone; thus a sliding shear failure could occur. The resisting mechanisms of dowel and aggregate interlock action or crack friction would need to be mobilized in this situation.

In the traditional approach to the problem, one would have relied on the consideration of shear stresses. Indeed, corbels have often been reinforced with diagonals, as in Fig. 13.35, to take a substantial part or the whole of the shearing force. The investigations of Franz and Niedenhoff^{13.16} have conclusively proved the inefficiency of this approach. The displacements across cracks correspond with a rigid body rotation of the bracket about a

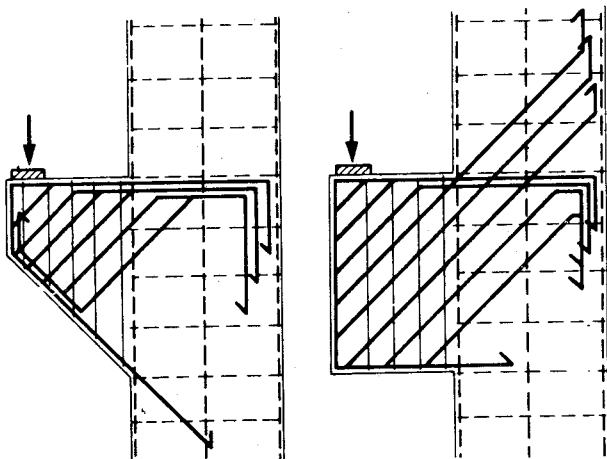


Fig. 13.35. Traditional diagonally reinforced corbels.^{13.16}

center, located very near the compression root (see Fig. 13.37). Thus the displacements near the top edge are almost horizontal, and diagonal bars, therefore, would be subjected to considerable dowel forces. Moreover, bent-up bars do not provide sufficient horizontal steel area in the immediate vicinity of the applied load; consequently, anchorage failures were observed.

13.6.2 Failure Mechanisms

Kriz and Raths carried out an extensive test program,^{13.17} and the current recommendations of the ACI code^{13.12} are based on their findings. From their studies the following failure mechanisms can be identified.

1. Flexural tension failure occurs when excessive yielding of the flexural reinforcement causes the concrete to crush at the sloping end of the corbel. The flexural cracks become extremely wide (see Fig. 13.36a).
2. Diagonal splitting develops along the diagonal compression strut after the formation of flexural cracks. The failure ultimately is due to shear compression (see Fig. 13.36b).
3. A series of short and steep diagonal cracks may lead to a sliding shear failure as these cracks interconnect, when the corbel separates itself from the column face (see Fig. 13.36c).
4. When the load is applied too near the free end of a short cantilever, a splitting failure along poorly anchored flexural reinforcement can occur (see Fig. 13.36d). The rotating end of a freely supported beam may place the

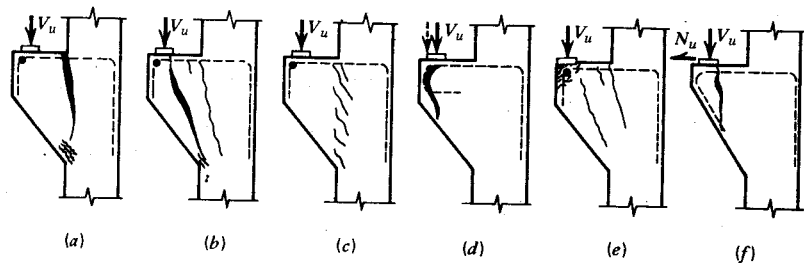


Fig. 13.36. Failure mechanisms in corbels. (a) Flexural tension. (b) Diagonal splitting (c) Sliding shear. (d) Anchorage splitting. (e) Crushing due to bearing. (f) Horizontal tension.

reaction near the edge of the bearing plate, and the unintended eccentricity can bring about this type of failure.

5. With too small or very flexible bearing plates, or when the corbel is too narrow, the concrete may crush underneath, leading to a bearing failure (see Fig. 13.36e).

6. Several of these mechanisms are accentuated when a horizontal force N_u is present in addition to the gravity load V_u . This may result from dynamic effects on crane girders, or it may be induced by shrinkage, creep, or temperature shortening of restrained precast concrete beams attached to the corbel.

A potential failure situation can arise when the outer face of the corbel is too shallow and an adverse horizontal load is also introduced, as in Fig. 13.36f.

7. The linear arch mechanism implies that the capacity of the flexural reinforcement has to be developed in the immediate vicinity of the bearing plate. This leads to a major failure mechanism in corbels—the breakdown of anchorage. Clearly, the diagonal compression strut cannot develop unless its horizontal component is transmitted to the main reinforcement near the free end of the corbel.

The detailing requirements of corbels follow directly from the seven failure mechanisms just listed. It is evident that vertical stirrups, intended for shear resistance, would be ineffective in all these situations.

It appears that the design may be based on any statically admissible resisting mechanism^{13.18} that recognizes relative stiffness, where applicable, and the principal displacements within the corbel near failure. Comparative tests indicate that some diagonal reinforcement can be used to advantage and that an optimum combination of horizontal and diagonal steel may result in a minimum steel demand.^{13.19} Such an economic advantage, however, may be offset by the increased labor involved in the making of bent-up bars.

13.6.3 Proportioning and Detailing of Corbels

The choice of the flexural reinforcement can be based on conservative assumptions to ensure that a corbel supporting a primary structural member does not yield before the ultimate capacity of the primary member is attained. This can be achieved if the flexural steel, to be determined from first principles, is supplemented by horizontal bars in the upper two-thirds of the corbel. For most cases the internal lever arm may be estimated at $z = 0.85d$. Alternatively, the concepts of the flexural resistance at ultimate may be applied, as in Fig. 13.37a. The compression force inclined at an angle α is

$$C = 0.85abf'_c = \frac{T}{\cos \alpha} = \frac{A_s f_y}{\cos \alpha} = \frac{V}{\sin \alpha}$$

where b is the width of the corbel and the other variables may be identified from Fig. 13.37a. Hence we have

$$a = \frac{A_s}{0.85b \cos \alpha} \frac{f_y}{f'_c} \quad (13.6)$$

and

$$z = d - \frac{a}{2 \cos \alpha} \quad (13.7)$$

where

$$\tan \alpha = \frac{z}{l}$$

Thus

$$A_s = \frac{Vl}{zf_y} \quad (13.8)$$

It is best to solve these equations by trial and error. It is suggested^{13.16} that additional horizontal steel, $A_h \geq 0.25A_s$, should be provided over the depth of the corbel.

The design procedure of the ACI code^{13.12} is entirely empirical. It is a simplified version of the propositions of Kriz and Raths^{13.17} and is based on more than 200 tests. In this approach the nominal shear stress across the deepest section of the corbel has been related to the load, N_u and V_u , steel content $\rho = A_s/bd$, concrete strength, and shear-span/depth ratio l/d . The simplified form of this empirical relationship is

$$v_u = \left(6.5 - 5.1 \sqrt{\frac{N_u}{V_u}} \right) \left(1 - \frac{l}{2d} \right) \left\{ 1 + \left[64 + 160 \sqrt{\left(\frac{N_u}{V_u} \right)^3} \right] \rho \right\} \sqrt{f'_c} \text{ (psi)} \quad (13.9)$$

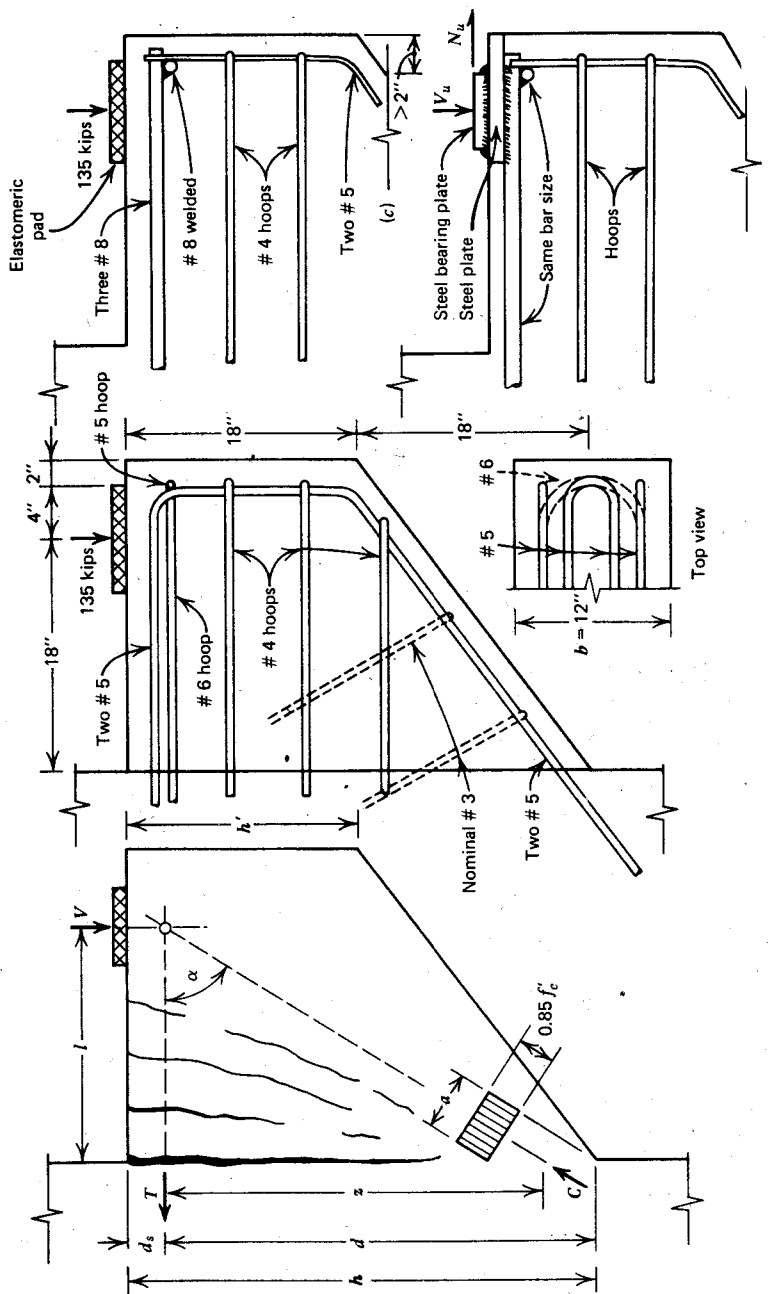


Fig. 13.37. Internal forces and alternative details of a corbel. (a) Basic dimensions. (b) Typical details using small bars. (c) The anchorage of large bars. (d) Welded connection for horizontal tension.

It is to be used with the following restrictions (see also Figs. 13.37a and 13.36f):

1. $l/d \leq 1$
2. $d \leq 2h'$
3. $0.04 \leq \rho(f_y/f'_c) \leq 0.13$
4. $N_u/V_u \geq 0.20$
5. N_u to be treated as live load (see Fig. 13.37d).
6. $0.5 \leq A_h/A_s \leq 1.0$, where A_h is the horizontal web reinforcement parallel to the main tension steel A_s .

When sliding supports are provided, so that no horizontal tension N_u can be introduced, as in Fig. 13.37c, Eq. 13.9 reduces to

$$v_u = 6.5 \left(1 - \frac{l}{2d}\right) (1 + 64\rho_v) \sqrt{f'_c} \text{ (psi)} \quad (13.10)$$

where

$$\rho_v = \frac{A_s + A_h}{bd} \leq 0.20 \frac{f'_c}{f_y} \quad (13.11)$$

When the corbel is very short (i.e., $l/d < 0.5$), the sliding shear along the face of the column may become critical (Fig. 13.36c). For this situation, the shear friction concept of load resistance might be more applicable (see Section 7.8).

By considering the limits given by Eq. 13.10 and Section 7.8.2, and the appropriate restrictions listed earlier, it may be shown that the maximum acceptable shear stresses will be between the limits of

$$3.25\sqrt{f'_c} \leq v_u \leq \left\{ \begin{array}{l} 17.2\sqrt{f'_c} \\ 0.2f'_c \\ 800 \text{ psi} \end{array} \right\} \text{ whichever is smaller}$$

$$(1\sqrt{f'_c} \text{ psi} = 0.083\sqrt{f'_c} \text{ N/mm}^2)$$

For most cases, $v_u = 10\sqrt{f'_c}$ psi will give a good first approximation for the smallest practical size of a corbel.

A trial-and-error application of these design propositions is presented in Example 13.1.

Effective anchorage for the horizontal reinforcement at the free end of the corbel is essential. When the flexural bars consist of small diameter bars, a horizontal loop (see Fig. 13.37b) can be used. For larger bars, mechanical anchorages will be necessary. A large diameter crossbar or a structural angle welded to the ends of the flexural bars can provide this anchorage

(Fig. 13.37c). To avoid the type of failure shown in Fig. 13.36d, the end of the bearing plate should not extend beyond the anchorage [i.e., it should be no closer than 2 in (50 mm) to the free end: see Fig. 13.37b].

When a horizontal tension is to be resisted, this force should be directly transferred to the flexural steel by welding the same on to the base plate (see Fig. 13.37d).

13.6.4 Other Types of Bracket

The principles of load disposal discussed in the foregoing sections can also be applied to double brackets. Two types of reinforcing, crack patterns, and behavior for typical double brackets are compared in Fig. 13.38. The specimen with horizontal bars carried 23% larger ultimate load. When inverted, these brackets may be considered as simply supported deep beams; the design of these is treated in Section 13.7. The center of rotation near failure (Fig. 13.38c) indicates the direction of displacement at the level of the reinforcement and once again points to the inefficiency of bent-up bars.

Occasionally the point load is introduced at or near the bottom edge of the bracket. The natural (i.e., shortest) path for the tension forces will now be the diagonal. The appropriate arrangement of reinforcement is shown for a typical case^{13.16} in Fig. 13.39a. The introduction of the load near the lower edge of the corbel may originate from a double bracket, as in Fig. 13.39b, or from a continuous crane girder. In both cases the reactive forces (shear) required for the member supported by the corbel are largely transmitted by internal diagonal compression forces that intersect the corbel near its bottom edge. From this zone the load has to be transmitted by diagonal tension and horizontal compression (Fig. 13.39a).

Almost invariably, distress of corbels in the field can be traced to poor detailing.^{13.17}

Example 13.1

Corbel design

A bracket, illustrated in Fig. 13.37b, is to carry a combined dead and live load of 135 kips (600 kN) at ultimate load at 18 in (457 mm) from the face of a column 16 in (406 mm) wide. An elastomeric pad will ensure that horizontal forces are not introduced to the corbel. The amount and arrangement of the reinforcement are to be determined using $f_y = 60,000$ psi (414 N/mm²), $f'_c = 3000$ psi (20.7 N/mm²), and $\phi = 0.85$.

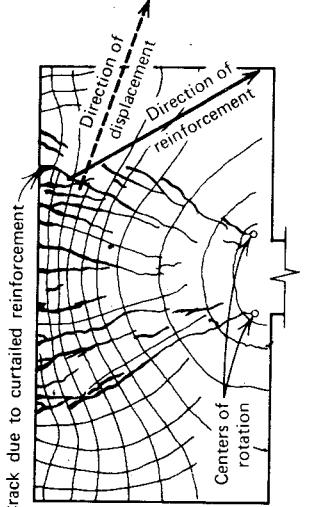
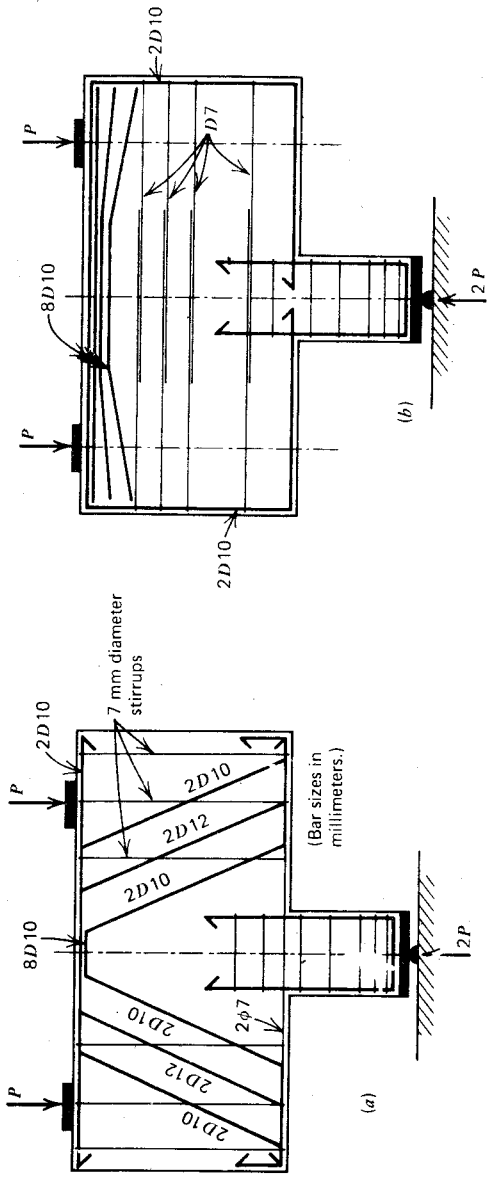


Fig. 13.38. Double brackets. 13.16

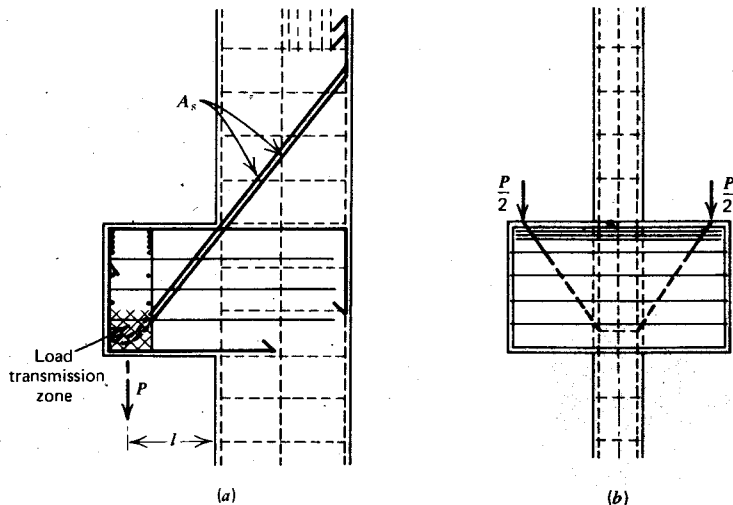


Fig. 13.39. Introduction of load at bottom of corbel by means of double bracket.^{13.16} (a) Side view. (b) Front view.

Design shear:

$$V_u = \frac{135}{0.85} = 159 \text{ Kips}$$

Assume $l/d = 0.67$,

$$\text{hence } d = \frac{18}{0.67} = 27 \text{ in,} \quad \text{try } h = 30 \text{ in}$$

Assume $v_u = 10\sqrt{f'_c} = 550 \text{ psi}$, hence

$$b = \frac{V_u}{dv_u} = \frac{159,000}{550 \times 27} = 10.7 \text{ in}$$

Assume therefore $b = 12 \text{ in}$ and $z = 0.85d = 23 \text{ in}$.

From Eq. 13.8, write

$$A_s = \frac{M}{zf_y} = \frac{18 \times 159}{23 \times 60} = 2.07 \text{ in}^2$$

and take

$$A_h = 0.5 A_s = 1.03 \text{ in}^2$$

Check these quantities using ACI^{13.12} requirements.

Equation 13.11 gives

$$\rho_v = \frac{A_s + A_h}{bd} = \frac{2.07 + 1.03}{12 \times 27} = 0.0096 < 0.20 \frac{f'_c}{f_y} = \frac{0.2 \times 3}{60} = 0.01$$

Equation 13.10 gives

$$v_u = 6.5 \left(1 - \frac{l}{2d}\right) (1 + 64\rho_v) \sqrt{f'_c}$$

$$= 6.5 \left(1 - \frac{18}{2 \times 27}\right) (1 + 64 \times 0.0096) \sqrt{3000} = 383 \text{ psi}$$

Compare $v = 159,000/(12 \times 27) = 491 > 383 \text{ psi}$. Not satisfactory.

For a second trial, increase d to approximately $491/383 \times 27 = 34 \text{ in.}$
Hence assume $h = 36$, $d = 33$, $b = 12 \text{ in.}$

For flexural steel try two No. 6 and four No. 5; thus $A_s = 2.08 \text{ in}^2$.

For horizontal stirrups try three No. 4 hoops; thus $A_h = 1.18 \text{ in}^2$.

Check again:

$$\rho_v = \frac{2.08 + 1.18}{12 \times 33} = 0.0082 < 0.01 \quad (\text{Eq. 13.11})$$

$$v_u = 6.5 \left(1 - \frac{18}{2 \times 33}\right) (1 + 64 \times 0.0082) \sqrt{3000} = 395 \text{ psi}$$

(Eq. 13.10)

Compare $v = 159,000/(12 \times 33) = 402 \approx 395 \text{ psi}$. Satisfactory.

Details of this reinforcement appear in Fig. 13.37b.

As an alternative, three No. 8 bars may be used for the top bars, with a welded crossbar at the end affording the required anchorage. This is illustrated in Fig. 13.37c.

13.7 DEEP BEAMS

13.7.1 Introduction

When the span/depth ratio of simply supported beams is less than 2, or less than 2.5 for any span of a continuous beam, it is customary to define these beams as deep. As with brackets, the traditional principles of stress analysis are neither suitable nor adequate to determine the strength of reinforced concrete deep beams. Most commonly, these structures are encountered in

rectangular suspended containers, such as silos and bunkers with pyramidal hoppers, in foundation walls supporting strip footings or raft slabs, in parapet walls, and in shear wall structures that resist lateral forces in buildings.

The stresses in isotropic homogeneous deep beams before cracking can be determined using finite element analyses or photoelastic model studies. It is found that the smaller the span/depth ratio (i.e., less than 2.5), the more pronounced the deviation of the stress pattern from that of Bernoulli and Navier. As an example, Fig. 13.40 shows the distribution of horizontal flexural stresses at the midspan of simply supported beams having different span/depth (l/h) ratios, when carrying a uniformly distributed load of intensity w per unit length.^{13.20} The midspan moment being $wl^2/8$, the usual extreme fiber stress at midspan of a square panel ($l/d = 1.0$) would be $f_t = f_c = 6M/bh^2 = 0.75w/b$. Figure 13.40 indicates that the tensile stresses at the bottom fiber are more than twice this intensity. Similar deviations occur for the distribution of shear stresses. For the determination of principal tensile stresses, the vertical stresses, particularly at the support points of the wall-beam panel, are of great importance.

This type of structure is rather sensitive with respect to the loading at the boundaries. The length of the bearings of the beam in Fig. 13.40 would affect the principal stresses, which can be very critical in the immediate vicinity of these supports. Similarly, stiffening ribs, cross walls, or extended columns at the supports would markedly influence the stress patterns. One of the most significant aspects of stress analysis would be the manner of application of the load, which is uniformly distributed in the case depicted in Fig. 13.40. The gravity load could be in form of bearing pressure applied to the top-surface of the wall-beam panel, causing vertical compressive stresses, which the concrete usually can resist without difficulty. In other cases the weight to be supported may have to be suspended from the bottom edge, creating a more adverse stress pattern in a deep reinforced concrete beam. This is the case when the sloping walls of a hopper or the flat bottom of a rectangular tank must be suspended from deep beams that form the structure's side walls. Clearly extra reinforcement is required for such situations. Numerous studies have traced the stress distribution for these variables. The results can be used by placing reinforcement to resist the tensile stresses in the homogeneous body. The concrete compression stresses are seldom critical. Such solutions, however, fail to take into account the anchorage requirements for the reinforcement, perhaps the most important aspect of deep beam design, and the considerable increase of diagonal compression stresses near supports after the onset of cracking.

The steel demand is seldom large for these structures, and a high degree of accuracy for its determination is not warranted. For this reason, approximate design techniques have been developed that cover most load and

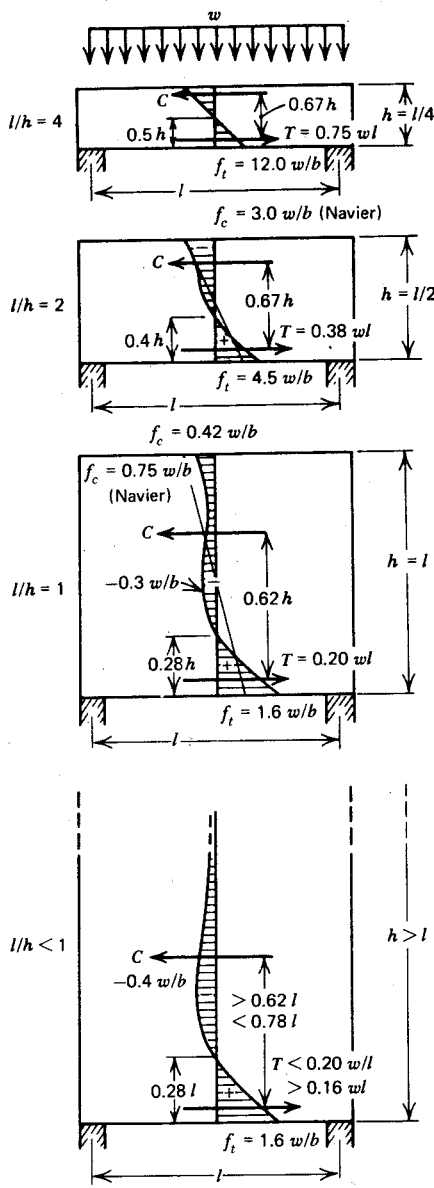


Fig. 13.40. Distribution of flexural stresses in homogeneous simply supported beams.^{13.21}

boundary conditions, take into account the fact that the concrete cracks in the tension zones, and suit better the construction requirements.

The background to the propositions that follow is largely the experimental investigation of Leonhardt and Walther^{13.21} at the University of Stuttgart. Recommendations based mainly on their findings have also been formulated by the European Concrete Committee.^{13.22} The experiments were designed to explore the detailing requirements and other aspects of deep beams. Only the effects of gravity loads are examined in this section. Seismic features, which may be relevant to deep beams, were discussed in greater detail in Chapter 12.

The ACI code^{13.12} also makes some special provisions for deep beams loaded at the top or compression face only. Only the effects on the web, in terms of nominal shear stresses and shear reinforcement are considered by the ACI code. The recommendations refer to beams with a clear span/depth ratio (l/h) of up to 5. For a higher ratio of l/h , the shear strength design principles of ordinary beams apply (see also Section 7.10).

13.7.2 Simply Supported Beams

Considering a square beam ($l/h = 1.0$), two observations may be made from Fig. 13.40. First, the total internal tensile force for the homogeneous simply supported deep beam could be computed by using the internal lever arm, which is $z = 0.62h$. It is interesting that this is approximately the same for all beams in Fig. 13.40; that is, it is not affected greatly by the span/depth ratio, l/h . For a slender beam, $z = \frac{2}{3}h$. Second, the tension zone in the bottom of the beam is relatively small (approximately $0.25l$), and this suggests that the principal flexural reinforcement should be placed in this area.

The internal lever arm for very deep beams does not appear to increase greatly after cracking.^{13.21} For design purposes the following approximation for the internal lever arm z may be made.^{13.22}

$$z = 0.2(l + 2h) \quad \text{when } 1 \leq \frac{l}{h} \leq 2 \quad (13.12a)$$

or

$$z = 0.6l \quad \text{where } \frac{l}{h} < 1 \quad (13.12b)$$

For convenience, the curves in Fig. 13.41 may be used. Obviously the steel area so computed must not be less than what one would obtain from ordinary flexural analysis, as explained in Chapter 4.

In these equations, the center-to-center distance between supports, or 1.15 times the clear span, whichever is smaller, should be taken for the span l .

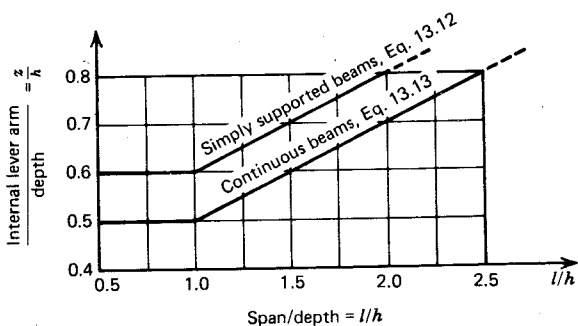


Fig. 13.41. Internal lever arm of deep beams.

The flexural reinforcement so computed should be distributed, using relatively small size bars, over a vertical distance equal to $0.25h - 0.05l$, where $h \leq l$. This is to be measured from the lower face of the beam, as indicated in Fig. 13.42.

From the study of corbels in Section 13.6, it is also evident that a centrally applied point load is disposed of primarily by arch action. This necessitates very good anchorages and the extension of the entire flexural reinforcement to the supports. It is suggested^{13.22} that at the inner face of the supports, the anchorage should develop at least 80% of the maximum calculated steel force. The prevention of anchorage failure before the attainment of the required strength of the flexural reinforcement can be achieved only if small

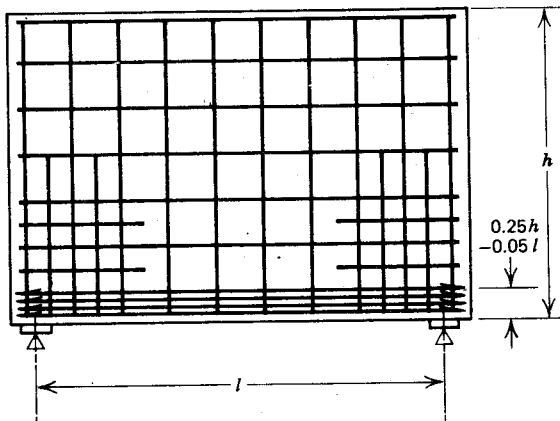


Fig. 13.42. Reinforcing of a simply supported deep beam.^{13.22}

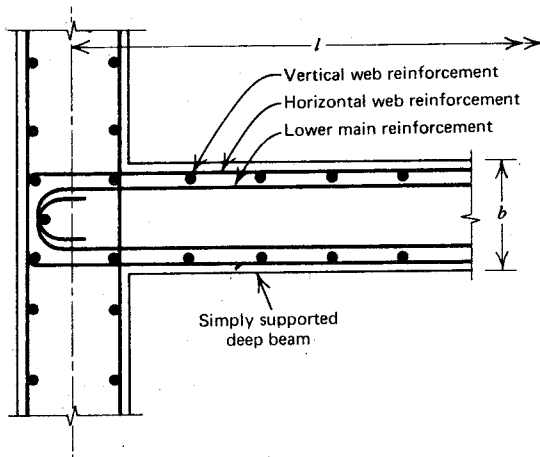


Fig. 13.43. Plan view of reinforcement at support of simply supported deep beam.^{13.22}

diameter bars or mechanical anchorages are used. Early test beams employing plain bars or bent-up bars (which drastically reduced the amount of reinforcement at the supports) normally failed at the anchorages at a relatively low load. Horizontal hooks, subject to transverse compression at the supports, are to be preferred to upstanding hooks. A typical plan of the flexural and web reinforcement at the support of a simply supported deep beam is shown in Fig. 13.43.

13.7.3 Continuous Deep Beams

The deviation from the linear pattern of the stress profiles across the midspan and support sections of a continuous homogeneous deep beam is even greater than in the case of simply supported beams. The internal lever arm of the stress resultants decreases rapidly as the span/depth ratio of the beams approaches unity.^{13.23} In particular, the tension force over the support (i.e., negative moment) region can be closer to the compression edge than to the tension edge of the beams. This feature of deep beams will have to be considered, even though the internal lever arms will increase in both the negative and positive moment zones after cracking, and especially when yielding of the flexural steel has set in.

The shear stresses, when combined with the vertical compression stresses originating from bearing at the supports, will generate steeply inclined principal compressive stresses. This suggests that shear is transferred mainly by arch action.

To simplify the flexural steel computations, the CEB suggests^{13.22} that the internal lever arm z be computed for both the negative and positive moments, from the following equations:

$$z = 0.2(l + 1.5h) \quad \text{when } 1 \leq \frac{l}{h} \leq 2.5 \quad (13.13a)$$

or

$$z = 0.5l \quad \text{when } \frac{l}{h} < 1 \quad (13.13b)$$

Again, for convenience, refer to the graph of Fig. 13.41.

The bending moments may be computed as for slender beams—that is, $wl^2/12$ and $wl^2/24$ for the support and midspan moments, respectively, of the continuous spans. In a cracked beam, too, the internal lever arm is likely to be smaller over the support than it is at midspan. Equation 13.13 does not show this, but the apparent discrepancy is compensated for because the actual moments at the supports are smaller than those predicted by the customary analysis. Correspondingly, the midspan moment for a cracked beam, is larger than $wl^2/24$. This was also observed in tests.^{13.21}

The midspan (positive) reinforcement should be arranged exactly the same as for simply supported beams, all bars being anchored at or passing through the supports. Half the negative reinforcement over the supports should extend over the full length of the adjacent spans. The other half can be stopped at a distance of $0.4l$ or $0.4h$, whichever is smaller, from the edge of the support. The support (negative) reinforcement should be uniformly distributed into two bands, as in Fig. 13.44.

1. In the upper band, with a depth of $0.2h$, the distributed steel should be

$$A_{s1} = 0.5 \left(\frac{l}{h} - 1 \right) A_s \quad (13.14)$$

2. The remainder of the steel, $A_{s2} = A_s - A_{s1}$, should be placed in the lower band with a depth of $0.6h$.

The depth to be considered need not be larger than the span. In wall beams whose depth is larger than the span, only nominal horizontal steel need be placed in the upper parts of the beam.

The compression forces due to flexure are rarely critical in deep beams, but the possibility of lateral buckling of the compression zone in thin wall beams may need to be examined. It is more important to protect the compression zone over the support where diagonal compression due to shear concentration may be critical. A shear stress intensity, computed as for normal beams, has no physical meaning; but satisfactory behavior can be expected

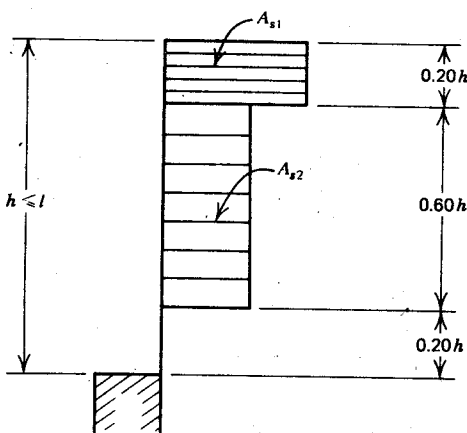


Fig. 13.44. Suggested distribution of negative flexural reinforcement at support of continuous deep beams.^{13.22}

if the maximum shear force is limited to

$$V_{\max} \leq 0.08\phi b_w h f'_c \quad (13.15)$$

where $h \leq l$ and $\phi = 0.85$.

Several CEB recommendations^{13.22} relating to deep beams originate from consideration of crack width control rather than ultimate strength.

In normal (slender) beams, the diagonal cracking load sets the limit to the usable shear strength in the absence of web reinforcement. When suitably introduced in a deep beam, a load considerably in excess of the diagonal cracking load can be carried because of the great stiffness and strength of the arch mechanism. Eventually, however, crack widths become excessive, and nominal shear stresses therefore must be limited (Eq. 13.15).

13.7.4 Web Reinforcement in Deep Beams

Gravity load, introduced along the top edge of a wall beam, is disposed of mainly by arch action. The flexural steel failed in the test beam shown in Fig. 13.45a, revealing that stirrups are not crossed by cracks. The load will naturally choose to dispose of itself through the stiffer of two possible resisting systems, and in deep beams the arch is always stiffer than the truss mechanism. Normally, therefore, stirrups are not necessary. A minimum reinforcement of 0.2%, in the form of small-diameter deformed bars placed in both directions, as in reinforced concrete walls, is adequate. In continuous beams, half the horizontal (negative) flexural reinforcement may be

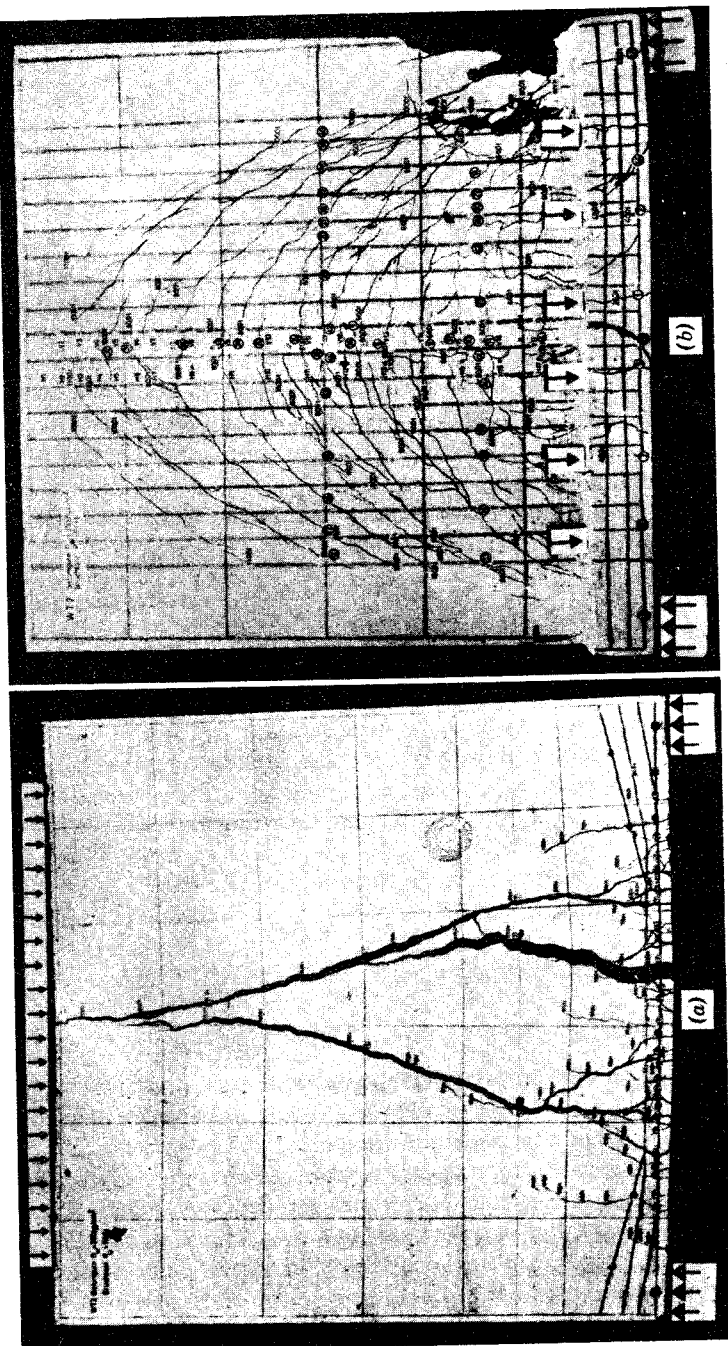


Fig. 13.45. Failure of simply supported deep beam. ^{13.21} Load introduced at (a) top edge, (b) bottom edge.

part of this (see Section 13.7.3). Near the supports, however, additional bars of the same size used for the mesh reinforcement should be introduced, as indicated in Fig. 13.46a.

The 1971 ACI code^{13,12} for the first time has provisions for the assessment of the shear strength of deep beams. The recommendations are restricted to simply supported beams with a clear span (l_n) to effective depth (d) ratio of less than 5, if the beams are loaded on the top face and supported on the bottom face. The background of the design approach, similar to that used for normal beams, was outlined by Joint ASCE-ACI Task Committee 426 in 1973.^{13,24} It is postulated that the shear capacity of a member is obtained by superposition of the capacity of the concrete and that of the web reinforcement. Recognition of the reserve shear capacity of a deep beam without web reinforcement led to the development of the semiempirical expression

$$v_c = \left(3.5 - 2.5 \frac{M_u}{V_u d} \right) \left(1.9 \sqrt{f'_c} + 2500 \rho_w \frac{V_u d}{M_u} \right) \leq 6 \sqrt{f'_c} \text{ (psi)} \quad (13.16)$$

The second term gives the inclined cracking shear for normal beams (see Eq. 7.15), and the first term represents the increase in the shear over that causing cracking. The value of the first term shall not exceed 2.5. The equation is intended to apply at the critical sections located at distance $0.15l_n$ from the face of the support for uniformly loaded beams, or one-half shear span, but not more than the effective depth d from the support for beams subjected to concentrated loads.

In the ACI approach, the derivation of the web reinforcement's contribution toward shear resistance is based on the shear friction concept, discussed in Section 7.8. It is assumed that when there develops a steep diagonal crack, such as in Fig. 13.45a, shear displacements will occur. The resulting increase in crack width will then fully mobilize all reinforcement crossing such a crack. The component of the yield force, acting at right angles to the inclined crack, can then be assumed to supply the required clamping force for the shear friction mechanism to operate. This way horizontal web reinforcement can substantially contribute toward the shear strength of the web if the bending moment at the section considered is small. From an experimental derivation of the relationship between the inclination of the diagonal crack and the span/depth ratio l_n/d , and the acceptance of an apparent coefficient of friction of 1.0 along the potential diagonal failure crack, it was shown^{13,24} that

$$v_s = v_u - v_c = \left[\frac{A_v}{12s} \left(1 + \frac{l_n}{d} \right) + \frac{A_{vh}}{12s_h} \left(11 - \frac{l_n}{d} \right) \right] \frac{f_y}{b_w} \quad (13.17)$$

where $v_u = V_u/b_w d$.

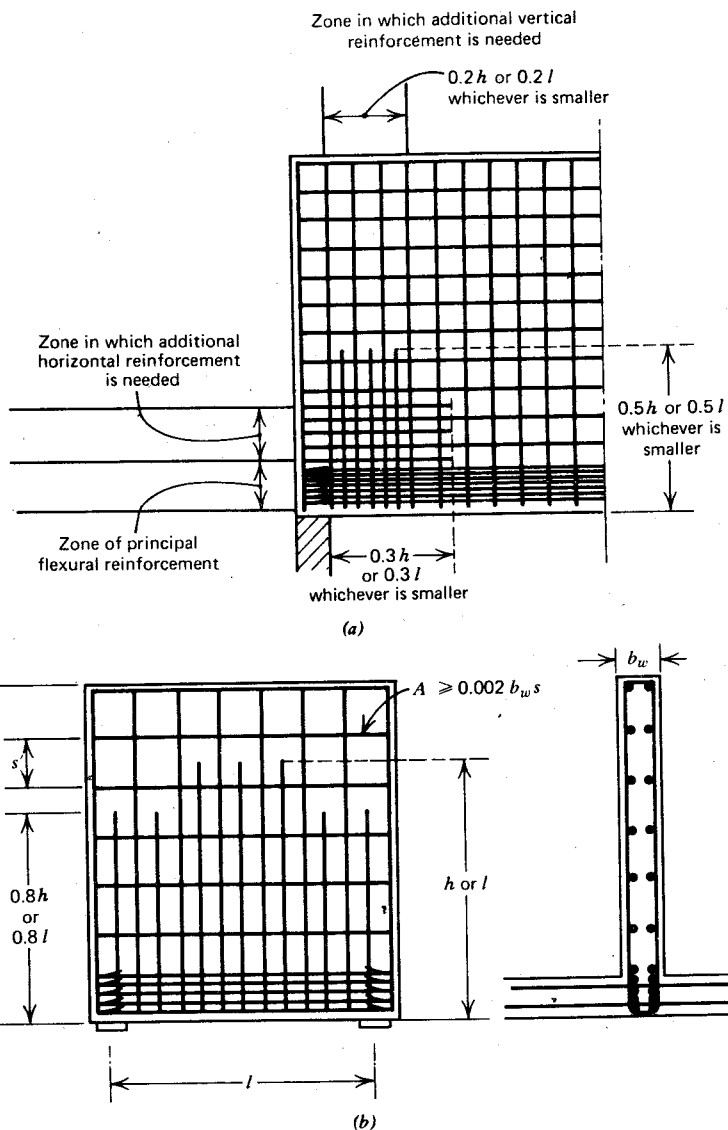


Fig. 13.46. Additional reinforcement required in simply supported deep beams for (a) shear near the supports, (b) loads applied near bottom edge.^{13.22}

The web reinforcement can thus be determined. The following limitations apply:

1. The area of the shear reinforcement A_v , perpendicular to the main reinforcement, shall not be less than $0.0015b_w s$, where b_w is the width of the web.
2. The spacing of these stirrups s shall not exceed $d/5$.
3. The area of the shear reinforcement A_{vh} , parallel to the main reinforcement, shall not be less than $0.0025b_w s$.
4. The spacing of these bars s_h shall not exceed $d/3$ or 18 in (450 mm).
5. When $l_n/d \leq 2$,

$$v_u \leq 8\sqrt{f'_c} \text{ (psi)} \quad (13.18a)$$

6. When $2 \leq l_n/d \leq 5$,

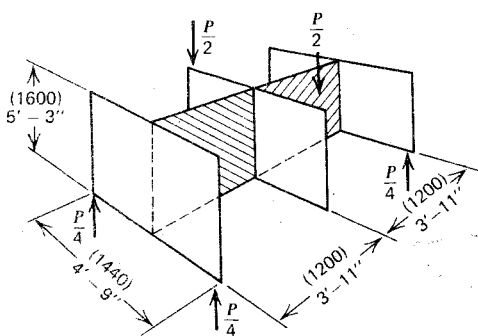
$$v_u \leq \frac{2}{3} \left(10 + \frac{l_n}{d} \right) \sqrt{f'_c} \text{ (psi)} \quad (13.18b)$$

The equivalent CEB^{13.22} value, given by Eq. 13.15 is only about half as much as that obtained from Eq. 13.18.

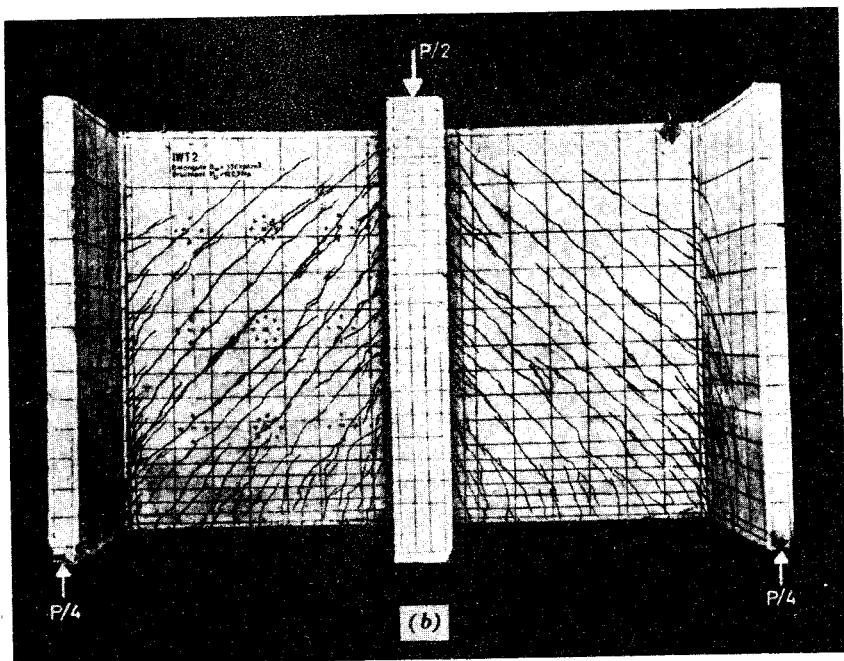
When the load is suspended from near the bottom edge of a deep beam, it must be carried mainly by vertical or inclined tension toward the supports. To enable the compression arch to develop, the whole of the suspended load must be transferred by means of vertical reinforcement into the compression zone of the beam. This should be achieved without exceeding the yield strength of the stirrups (suspension reinforcement), to protect the flexural reinforcement against possible horizontal splitting and to ensure satisfactory crack control in the web during service load [i.e., for $f_s < 30,000$ psi (200 N/mm²)]. The behavior of such a beam is vividly demonstrated by a test specimen reproduced in Fig. 13.45b. Diagonal compression at the right-hand abutment of the arch was the cause of the failure in this beam.

Suspender stirrups should completely surround the bottom flexural reinforcement and extend into the compression zone of the wall beam, as in Fig. 13.46b. The spacing of the vertical bars should not exceed 6 in (150 mm).

Special provision is also needed when loads or reactions are introduced along the full depth of a beam—for example, when deep wall beams support each other, as illustrated in Fig. 13.47. This specimen^{13.21} is used in the discussion that follows. The load from the central cross beam is transmitted, mainly via diagonal compression, into the bottom part of the long wall beam. From there the load must be taken up into the top of the main wall beam, permitting a linear arch to dispose of it toward the bottom of the supporting cross beams. Hence at the central junction, vertical suspension reinforcement is to be provided for the whole force P , and this should surround the



(a)



(b)

Fig. 13.47. Deep beam supported by deep beams.^{13,21} (a) Overall dimensions. (b) Crack pattern.

bottom flexural bars in the main wall beam. The bars must extend vertically to a height of h or l , whichever is smaller—4 ft 9 in (1.44 m), in the case of the example structure of Fig. 13.47. Similarly, at the supporting end beams half the load must be received by suspension reinforcement, a typical arrangement is shown in Fig. 13.48a. Tests have demonstrated that diagonal bars bent to a large radius at the beam-to-beam junction are also effective, but their allocated load contribution should not exceed 60% of the total load. A typical arrangement appears in Fig. 13.48b.

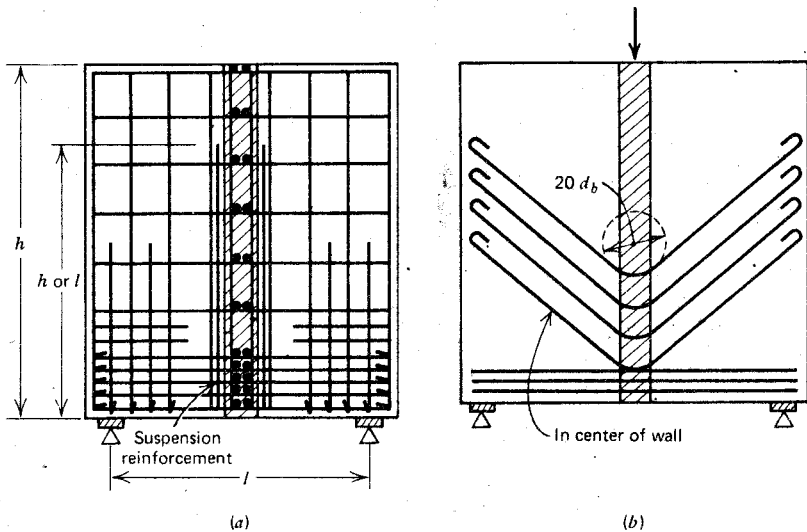


Fig. 13.48. Suspension reinforcement to be provided where deep beam supports another deep beam^{13.22} using (a) orthogonal arrangement or (b) bent-up bars.

The diagonal cracks formed in the main wall beam in Fig. 13.47b clearly show the inclination of the diagonal compression struts. To enable these forces to resolve themselves into vertical and horizontal components, well-anchored horizontal steel is required at the abutment of the struts. The CEB^{13.22} recommends that mesh reinforcement be provided in the support area, as in Fig. 13.46a to resist the entire vertical reaction force. The horizontal bars of this mesh, that must extend by a distance $0.3l$ or $0.3h$ from the face of the support together with those which run right through the span of the wall beam, should be capable of resisting at least 80% of the reaction (maximum shear) force. The short vertical bars of the mesh must extend by $0.5l$ or $0.5h$, whichever is less, above the soffit of the beam.

13.7.5 Introduction of Concentrated Loads

The bearing stresses in areas where point loads are introduced need to be examined because deep beams can sustain very large forces with relatively small demand for reinforcement. The support points are such localities. Reactive forces can be computed as for normal (slender) beams. However, it should be borne in mind that at the interior supports of continuous deep beams, a moment smaller than that predicted by the customary elastic analysis is resisted (see Section 13.7.3). Consequently, the conventionally computed reaction at the exterior supports of continuous deep beams should be increased by 10% for bearing design purposes.

Where the beam is provided with a stiffening rib or column, which enlarges the beam at its supports over a substantial portion of its height h , the bearing stresses are normally not critical. In the absence of ribs or columns, the magnitude of the reaction at the ultimate load should not exceed

$$0.60b(t + h_0)f'_c \quad (13.19a)$$

at exterior supports and

$$0.90b(t + 2h_0)f'_c \quad (13.19b)$$

at interior supports,

where b = width of beam

h_0 = depth of a rib or flange that may stiffen lower portion of beam

t = length of support under consideration, which should not exceed one-fifth of the smaller of the adjacent spans

These dimensions are also illustrated in Fig. 13.49.

Because of their very large stiffness deep beams are extremely sensitive to imposed deformations. Hence care should be taken to ensure that displacements of the supports of continuous deep beams do not occur.

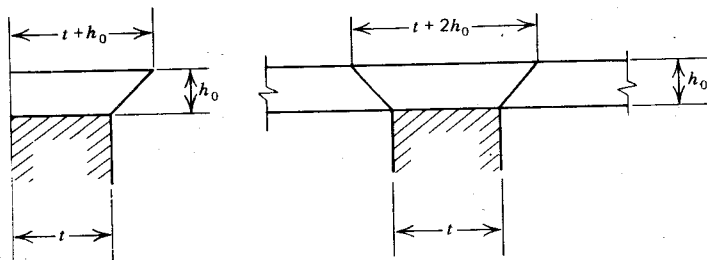


Fig. 13.49. Assumed spreading of bearing stresses at supports of deep beams.^{13.22}

Alternatively, additional reinforcement should be provided to allow for substantial changes in moments due to possible support settlement.

It is not uncommon that heavy, concentrated loads are introduced directly above the support points of deep beams. This situation, illustrated in Fig. 13.50, is similar to that which arises at the anchorage point of a prestressing cable. The concentrated forces are dispersed in the web of the beam, and unless a continuous vertical stiffening rib is extended between load point and support this dispersal should be considered. Consequently, the CEB^{13.22} suggests

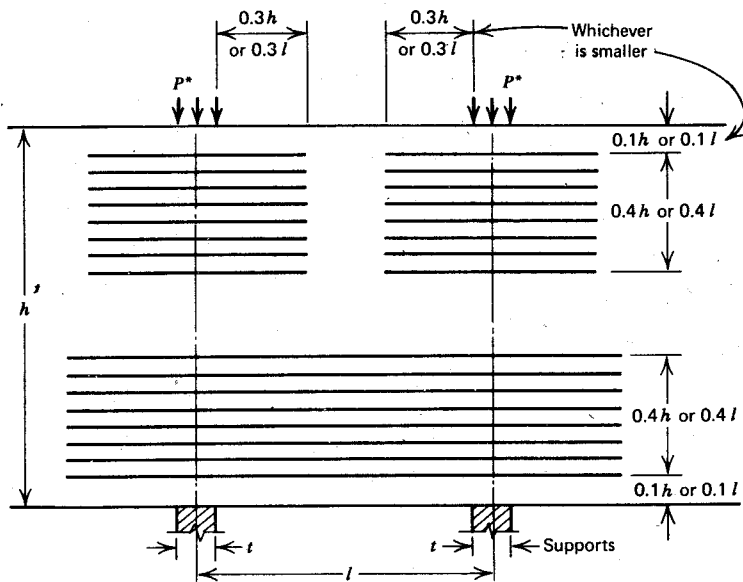


Fig. 13.50. Arrangement of reinforcement required for transmission of concentrated forces across continuous deep beams.^{13.22}

horizontal supplementary reinforcement in two bands, each capable of resisting a tensile force equal to one-quarter of the applied load.

In the assessment of the shear or diagonal compression capacity of the web, in accordance with Eq. 13.15 the CEB recommends that an additional design shear force of

$$\frac{P^*}{2} \left(\frac{l - 2t}{l} \right) \quad \text{or} \quad \frac{P^*}{2} \left(\frac{h - 2t}{h} \right) \quad (13.20a)$$

be allowed for at interior supports and

$$P^* \left(\frac{l-t}{l} \right) \quad \text{or} \quad P^* \left(\frac{h-t}{h} \right) \quad (13.20b)$$

at the exterior supports, to compensate for the effects of P^* introduced as indicated in Fig. 13.50. In each case, only the lesser of the two expressions need be considered.

13.8 BEAM-COLUMN JOINTS

13.8.1 Introduction

It is surprising that until recently little attention has been given to the design of joints in reinforced concrete structures. It appears that after the evaluation of working stresses in adjacent members, most designers normally assumed that conditions within the joint, which often had somewhat larger dimensions than the members it joined, were not critical. The gradual adoption of the philosophy of limit state design has exposed the weakness of this assumption. Joints are often the weakest links in a structural system. Much valuable work has been done in this area very recently. However, our understanding of joint behavior and of existing detailing practice is still in need of much improvement.

The following section attempts to identify the major problems in joint behavior, illustrating these when possible with the limited amount of experimental evidence that was available at the time of writing. Of the vast number of possible ways of joining concrete structural members to meet many load types and combinations, only a few can be examined within the scope of this book. However, the examples presented should help in the study of many other situations. Correct identification of the problem is the key to successful detailing.

The essential requirements for the satisfactory performance of a joint in a reinforced concrete structure can be summed up as follows:

1. A joint should exhibit a service load performance equal in quality to that of the members it joins.
2. A joint should possess a strength that corresponds at least with the most adverse load combinations that the adjoining members could possibly sustain, several times if necessary.
3. The strength of the joint should not normally govern the strength of the structure, and its behavior should not impede the development of the full strength of the adjoining member.

4. Ease of construction and access for depositing and compacting concrete are other prominent issues of joint design.

The structural demand on joints is greatly affected by the type of loading; therefore, it may be appropriate to use design procedures in which the severity of each type of loading is recognized. In certain joints—for example, continuous reinforced concrete structures subjected to gravity loading only—strength under monotonic loading without stress reversals will be the design criterion. In other cases, not only strength but ductility of the adjoining members under reversed loading will govern the design of joints: a rigid jointed multistory frame under seismic load conditions would represent these conditions. A large amount of joint reinforcement can be expected for the second case because strength degradation of the concrete under repeated reversed loading will occur.

13.8.2 Knee Joints

In numerous structures, continuity between two adjacent members is necessary even though the members meet at an angle. The corner joint of a portal frame is the most common example. The internal forces generated at such a knee joint may cause failure within the joint before the strength of the beam or column, whichever is weaker, is attained.

The relative size of the members and the magnitude of the actions will affect not only behavior but also the practical limits of detailing. In a slab-to-wall connection it will be desirable to omit all secondary reinforcement. In a substantial column-beam joint, on the other hand, suitable ties and stirrups, similar to those used in the adjacent members, will be quite in order. Considerable lateral restraint exists in a joint that is long in the transverse direction (e.g., between a bridge slab and its supporting abutment wall). Such restraint can effectively suppress splitting cracks, which can develop at anchorages within the joint. In a portal frame, however, little lateral confinement will be available when members in the joint region, at right angles to the frame, are absent. The three-dimensionality of the resisting mechanism in joints should not be overlooked.

The behavior of the right angle corner joint is fundamentally affected by the sense of the loading. For this reason, such a knee will be examined separately for a moment that tends to close the right angle and for another that tends to open it.

Corner Joints Under Closing Loads

A typical knee joint, subjected to a "closing" bending moment and corresponding actions, appears in Fig. 13.51. The outer bars, being continuous, have sufficient anchorage, and provided a splitting failure does not occur

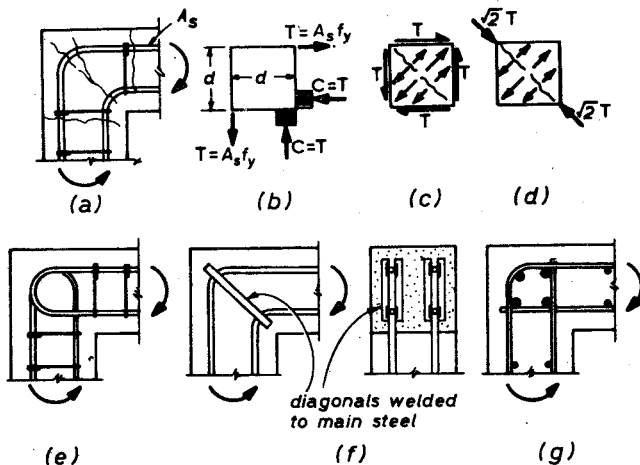


Fig. 13.51. Actions and details of knee joints subjected to closing moments. (a) Typical cracks. (b) Internal forces. (c) Crack due to shear. (d) Splitting crack. (e) Overlapping hoops. (f) Diagonal stiffeners. (g) Transverse bearing bars.

because of high bearing within the bend, the full strength of these bars can normally be developed. Because of the biaxial state of stress at the inner corner, compression strains considerably in excess of 0.003 can be sustained. When, for the purpose of strength, no reliance is placed on the compression steel, it does not seem to matter how the inner bars are anchored.^{13.25}

The forces generated by flexure and acting against an idealized free body, representing a square corner joint, are shown in Fig. 13.51b. It is assumed that these forces are introduced into the joint core in the form of uniform shear stresses resulting from anchorage bond, as in Fig. 13.51c; then a diagonal crack can be expected when the diagonal tension stress approaches the tensile strength f'_t of the concrete

$$f'_t = \frac{T}{bd} = \frac{A_s f_y}{bd} = \rho f_y \approx 6\sqrt{f'_c} \text{ (psi)}$$

This condition would limit the flexural steel content to

$$\rho \leq \frac{f'_t}{f_y} \quad (13.21a)$$

The second alternative of load introduction into the joint core (Fig. 13.51d) corresponds better with the conditions at ultimate load. Here the steel and concrete forces combine to produce a single diagonal compression resultant, because of the bond deterioration along the outer bars. Kemp and

Mukherjee^{13,26} have shown that by considering the splitting tensile strength of the concrete f'_t , the limiting steel content in this case becomes, approximately

$$\rho \leq 1.2 \frac{f'_t}{f_y} \quad (13.21b)$$

Indeed, in their tests^{13,26} the full flexural capacity of the adjoining members at the face of the joint was attained when the steel content was slightly below this limit. For higher values of ρ , a brittle splitting failure occurred at less than the full strength of adjoining members. In tests at the University of Nottingham,^{13,25} the full moment capacity was attained for a variety of steel arrangements, with $\rho = 0.75\%$. On the other hand, joints studied by Swann,^{13,27} with $\rho = 3.0\%$, failed at a load less than 80% of the theoretical ultimate values, derived from the flexural capacity of the adjoining section.

Because of the small size of the members, no attempt was made in these tests to control the development of the critical diagonal crack (see Fig. 13.51a) by reinforcement, and two notable exceptions were observed. Lapped flexural bars forming hoops, as in Fig. 13.51e, did not perform well,^{13,25} even though low steel content was used. However, when the diagonal compression was resisted by reinforcement, in a similar way to the action of a diagonal stiffener plate in a steel joint (see Fig. 13.51f), the flexural capacity of the adjoining section could be developed even with a high ($\rho = 3.0\%$) steel content.^{13,27} The behavior in both cases would be expected intuitively.

From the foregoing it may be concluded that for knee joints of small members, slabs and walls in particular, adequate strength can be expected only under the following conditions:

1. The tension steel is continuous around the corner (i.e., it is not lapped within the joint).
2. The tension bars are bent to a sufficient radius to prevent bearing or splitting failure under the bars. Nominal transverse bars placed under the bent bars, as in Fig. 13.51g, will be beneficial in this respect.
3. The amount of tension reinforcement is (conservatively) limited to $\rho \leq 6\sqrt{f'_c/f_y}$, where stresses are in psi units.

When using larger structural members having substantial reinforcing content, secondary reinforcement is required to preserve the integrity of the concrete within the joint. Figure 13.52 illustrates the threefold purpose of steel with respect to the following points.

1. Bars at right angles to the potential diagonal crack should prevent the growth and the widening of the cracks, thus enabling the compression force to be developed between the inner corner and the bend of the main tension steel.

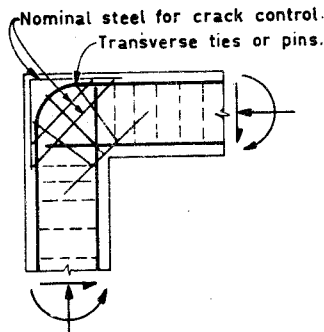


Fig. 13.52. Secondary reinforcement at knee of portal frame.

2. Rectangular ties should surround the tension steel also within the joint and should prevent the widening of splitting cracks, if they occur, in the plane of the bent flexural tension bars.

3. The transverse legs of the same ties can be utilized to provide confinement for the inner corner, which is subjected to concentrated compression.

Corner Joints Under Opening Loads

The previously discussed right angle corner joint is more severely affected when the applied moments tend to open this angle. The resulting forces are represented in Fig. 13.53 for a commonly used joint detail. As Fig. 13.53c indicates, the compression forces near the outer corner give rise to a resultant that tends to push off the triangular portion of the joint. Only an internal tension force ($\sqrt{2}T$) would be capable of resisting this diagonal force. The

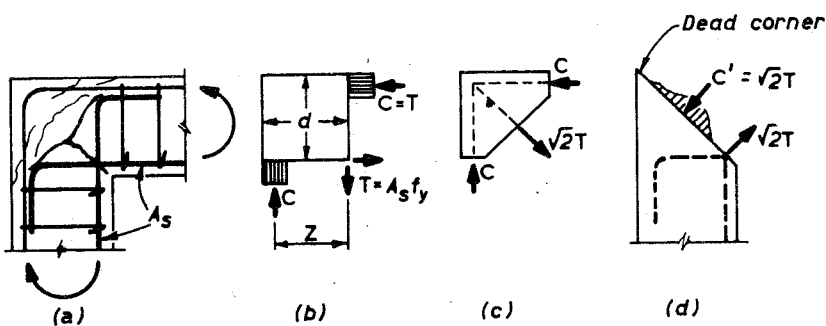


Fig. 13.53. Actions on opening right angle joints. (a) Typical cracks. (b) Internal forces. (c) Forces pushing off corner of joint. (d) Forces along joint diagonal.

crack patterns in test specimens, such as shown in Fig. 13.53a, uniquely verify this behavior.

For continuous long joints, which occur in structures illustrated in Fig. 13.54, a relatively small amount of flexural steel is likely to be required, and for these secondary reinforcement is seldom used.

In the University of Nottingham tests,^{13.25} members approximately 8 in (203 mm) deep were joined and eight different detailing arrangements having a flexural steel content $\rho = 0.75\%$ were compared; not one specimen attained more than 50% of the flexural capacity of the members joined. In most of these tests, arrangements similar to that in Fig. 13.51a were used. As expected, the interior bars will tend to straighten. The detail is an example of an entirely unsatisfactory solution, unfortunately often used, when loads open a joint.

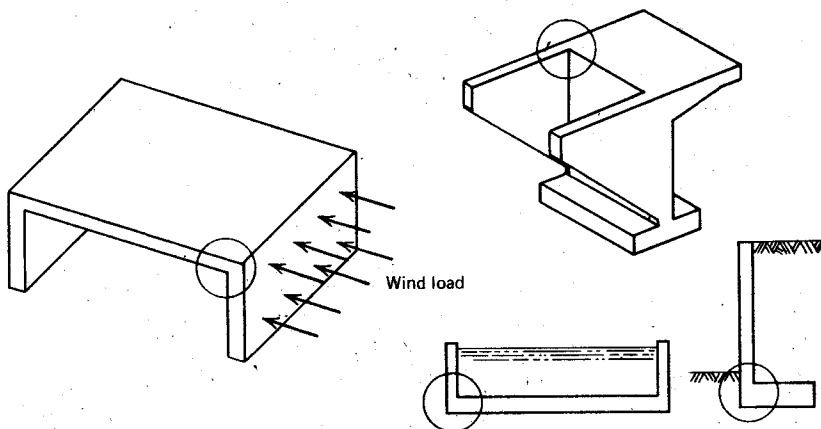


Fig. 13.54. Examples of continuous corners that may be subjected to opening loads.

Diagonal stirrups in these^{13.25} small members increased the joint capacity by a mere 10 to 20%. The contribution of short stirrups is very sensitive to the quality of anchorage. Only when tightly bent around the main reinforcement can they immediately respond to load, thus controlling the growth of cracks.

Swann^{13.27} compared several joint steel arrangements in 6 in (152 mm) deep members, some of them in common usage. He also found that the member capacities could not be approached. Some of his specimens, together with the measured joint capacities, as a percentage of the computed strength of the member, are presented in Fig. 13.55. Cases (a) and (b) are examples of extremely poor detailing. The disappointing performance of detail (c), commonly used, should be noted. Specimens (f) and (g) represent

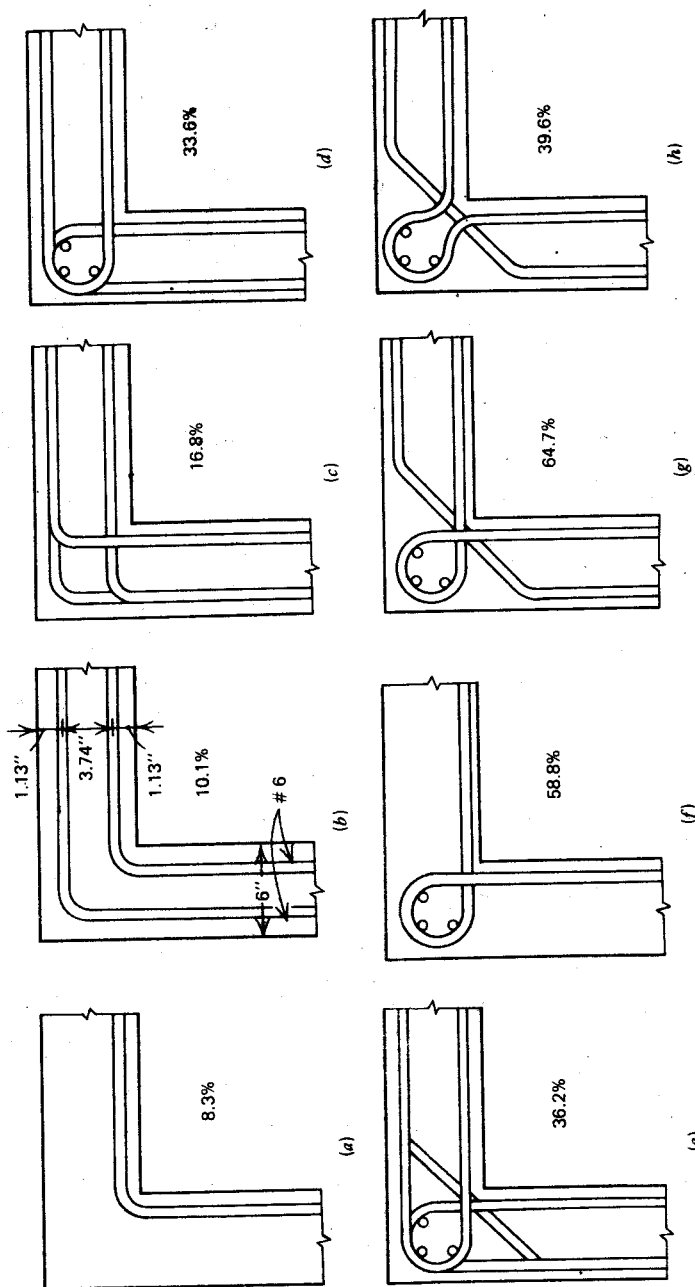


Fig. 13.55. Corner joints studied by Swann.^{13,27} Percentages indicate $M_{test}/M_{calculated}$. (a-b) Unsatisfactory joints. (c-e) Commonly used details. (f-h) Arrangements using hoops.

the best solution that can be provided in small members without secondary reinforcement. Swann's specimens had a flexural steel content of 3 %, and a better performance would have been obtained if a smaller reinforcing content had been used. This is evident from Nilsson's work,^{13.28} which indicated that even with as little as 0.5 to 0.8% flexural steel content and an anchorage similar to that in Fig. 13.55f, only about 80% of the flexural capacity is attained. The investigation was prompted by observed failures and excessive cracking at the junction of wing walls of bridge abutments in Sweden (see Fig. 13.54).

Clearly the use of secondary reinforcement to resist diagonal tension cannot be avoided in structural members of major frames. In the absence of secondary reinforcement, failure of the joint after the early onset of cracking, as in Figs. 13.53a and 13.53c, will be imminent. Even in small joints marked improvement was observed^{13.27, 13.29} when tight fitting stirrups, similar to the diagonals in Fig. 13.51f, were used.

A suggested solution for a large joint appears in Fig. 13.56. Until experimental studies produce a more precise design technique, it is suggested that

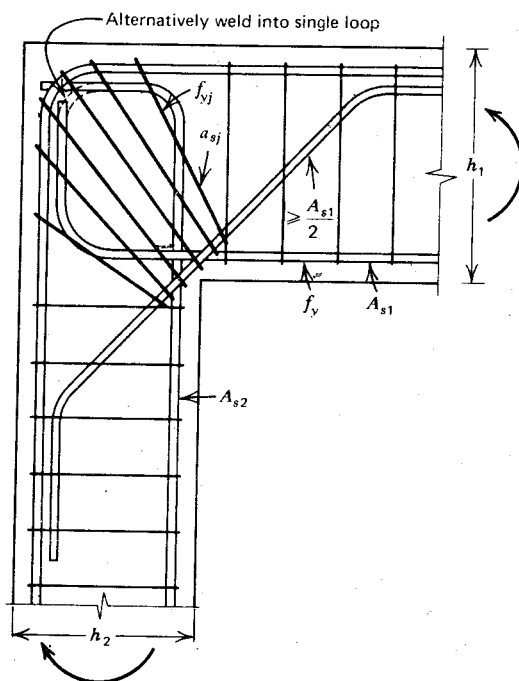


Fig. 13.56. Suggested details for large opening knee joint.

radial hoops be provided to resist the whole of the diagonal tension across the corner. This force can be approximated from the model of Fig. 13.53c. Accordingly, using the notation of Fig. 13.56, the area of one radial hoop is approximately

$$a_{sj} = \left[\frac{f_y}{f_{yj}} \sqrt{1 + \left(\frac{h_1}{h_2} \right)^2} \right] \frac{A_{s1}}{n} \quad (13.22a)$$

assuming that the bottom beam steel A_{s1} limits the magnitude of the moment that can be applied to the joint, and that f_{yj} is the yield strength of the radial hoops of which n legs are provided.

Diagonal principal reinforcement across the interior tension corner, equal to or larger than one-half^{13.30} the governing flexural steel A_{s1} , will prevent deep yield penetration into the joint area along the flexural steel and will also provide suitable anchorage for the radial hoops (see Fig. 13.56).

When the tension bars are formed into a continuous loop by welding or bending, as indicated by the broken lines in Fig. 13.56, the amount of radial hoops could be reduced. Nilsson's research^{13.31} suggests that the single continuous loop of the main flexural steel with some large diagonal bars across the inner corner, as in Fig. 13.56, provides sufficient resistance against diagonal tension failure when the flexural steel content is not excessive. Thus it is proposed that radial hoops be provided when the flexural steel content exceeds 0.5 %. Accordingly, the area of one radial hoop is

$$a_{sj}^* = \left(\frac{\rho - 0.005}{\rho} \right) \left\{ \left[\frac{f_y}{f_{yj}} \sqrt{1 + \left(\frac{h_1}{h_2} \right)^2} \right] \frac{A_{s1}}{n} \right\} \quad (13.22b)$$

where $\rho = A_{s1}/bd_1$ in the critical member and the second term in the right-hand side is Eq. 13.22a.

A haunch at the reentrant corner, accommodating substantial diagonal flexural bars, will force the plastic hinge away from the face of the joint. This shift is likely to improve the precarious anchorage of the main tension reinforcement, where the same enters the joint. The increased internal lever arm within the joint will reduce the internal force, thus the joint may become a noncritical link in the structural system. Connor and Kaar demonstrated this behavior with haunched corner joints of precast concrete frames.^{13.32}

When a large number of bars are involved in the type of joint suggested in Fig. 13.56, problems of construction may arise because of congestion at the reentrant corner. In this situation an orthogonal reinforcement arrangement may be more practical, as discussed in the next section.

Alternating Repeated Loading of Knee Joints

The previous discussion on knee joints pointed to the nature of concrete stresses within a joint. With high-intensity alternating loading, this concrete

may crack in two principal directions, and the flexural bars have to be anchored in this region. Generally the bars at the inside of the joint must be bent through 90°, to achieve the required development lengths. Repeated yielding of the flexural bars at and near the inner faces of a knee joint will progressively destroy the bond over the straight portion of these bars. This was found in the experiments of Bertero and McClure,^{13,33} who subjected small-scale single bay portal frames to alternating lateral loading. Very large anchorage losses in the joint region were observed after 10 cycles of loading to 78% of theoretical ultimate capacity. The strengths of their joints could be maintained only by mechanical anchorages. Other small-scale tests have shown that poorly detailed joints (see, e.g., Fig. 13.55b), do not even allow the ultimate capacity to be approached in the first cycle of loading.^{13,34} Knee joints subjected to alternating reversed loading require great care in detailing. Since the joint has to cope with loads that tend to alternately close or open the angle, both systems of diagonal reinforcement (Figs. 13.52 and 13.56) are required. For such a situation, an orthogonal mesh of reinforcement would be better suited. In the absence of experimental information, it is suggested that joint hoops be provided to resist separately the horizontal and the vertical components of the principal diagonal tension force that acts across the potential failure crack and tends to separate the joint area into two triangles. The derivation of the secondary joint steel may be followed using the models given for an opening knee joint in Fig. 13.57a and for a closing joint in Fig. 13.57b. Because the concrete is thoroughly cracked in both directions after high-intensity cyclic loading, and because benefit from any axial compression in the members of closing joints is very doubtful, no reliance should be placed on the concrete to resist internal shearing or tensile forces. Similar solution, suggested by Hanson,^{13,35} is illustrated in Fig. 13.57c.

It might be optimistic to expect that all ties, especially those within the compression zone of the joint, will function with equal efficiency. It would be prudent to rely only on ties that are situated within, say, two-thirds of the depth and are nearer to the forces to be resisted in tension. With this modification, it follows from Fig. 13.57 that the area of one joint stirrup is

$$a_{s1} = 15 \frac{s_1}{d_1} A_{s1} \quad (13.23a)$$

$$a_{s2} = 1.5 \frac{s_2 d_1}{d_2^2} A_{s1} \quad (13.23b)$$

assuming that $A_{s1} \leq (d_2/d_1)A_{s2}$ and that the yield strength of all reinforcement is the same, where A_{s1} and A_{s2} are the steel areas required to develop the flexural tensions T_1 and T_2 in Fig. 13.57.

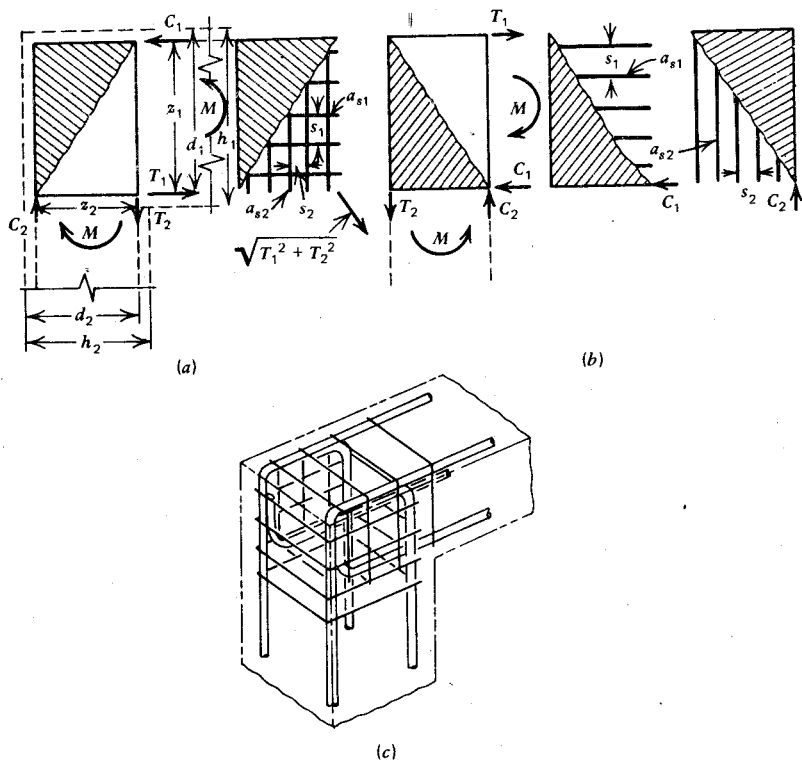


Fig. 13.57. Orthogonal reinforcement in knee joints subjected to alternating loading. (a) Actions on opening joint. (b) Actions on closing joint. (c) Orthogonal stirrups.

13.8.3 Exterior Joints of Multistory Plane Frames

Critical Aspects of Joint Behavior

A particularly critical situation can arise in certain exterior column-beam joints of plane multistory frames when these are subjected to seismic loading. The external action and the corresponding internal forces generated around such a joint are indicated in Fig. 13.58a. The following notation refers to the stress resultants:

C_c = compression in concrete

C_s = compression in reinforcement

T = tension force in reinforcement

V = sum of shearing stresses

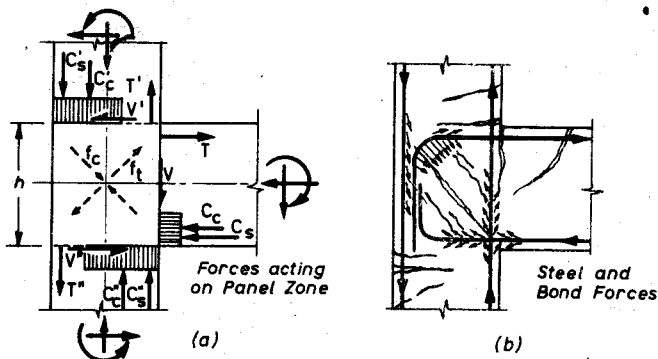


Fig. 13.58. Actions at exterior column-beam joint of a multistory frame. (a) stress resultants. (b) Crack pattern and bond forces.

From the position of the stress resultants it is apparent that diagonal tension and compression stresses (f_c and f_t) are induced in the panel zone of the joint. The diagonal tension may be high when the ultimate capacity of the adjoining members is developed, and this can lead to extensive diagonal cracking. The severity of diagonal tension is influenced by flexural steel content and the magnitude of the axial compression load on the column.

Two questions of joint behavior deserve careful study. First, how is the bond performance of the bars affected by the state of the surrounding concrete? If any deterioration of bond occurs, how can full anchorage within the joint be developed to enable the adjoining members to sustain their full flexural capacities during several reversals of moment, if necessary?

Second, if the concrete in the joint core suffers cross cracking, as in Fig. 13.59, thus loses its tensile strength, how can it transfer the required compression and shearing forces?

The bond conditions for various locations of the bars within a joint can be examined from Fig. 13.58b. For the load pattern in Fig. 13.58a, assuming that the axial compression on the column is small, the following observations may be made.

1. The anchorage conditions for the top beam bars are extremely unfavorable where they enter the joint. The surrounding concrete is subject to sedimentation, and it is exposed to transverse tension. Usually a splitting crack forms along these bars at a relatively early stage of the loading. Repeated loading will aggravate the situation, and a complete loss of bond up to the beginning of the bent portion of the bar may occur. Consequently, high bearing stresses may be generated in the bend which can be sustained

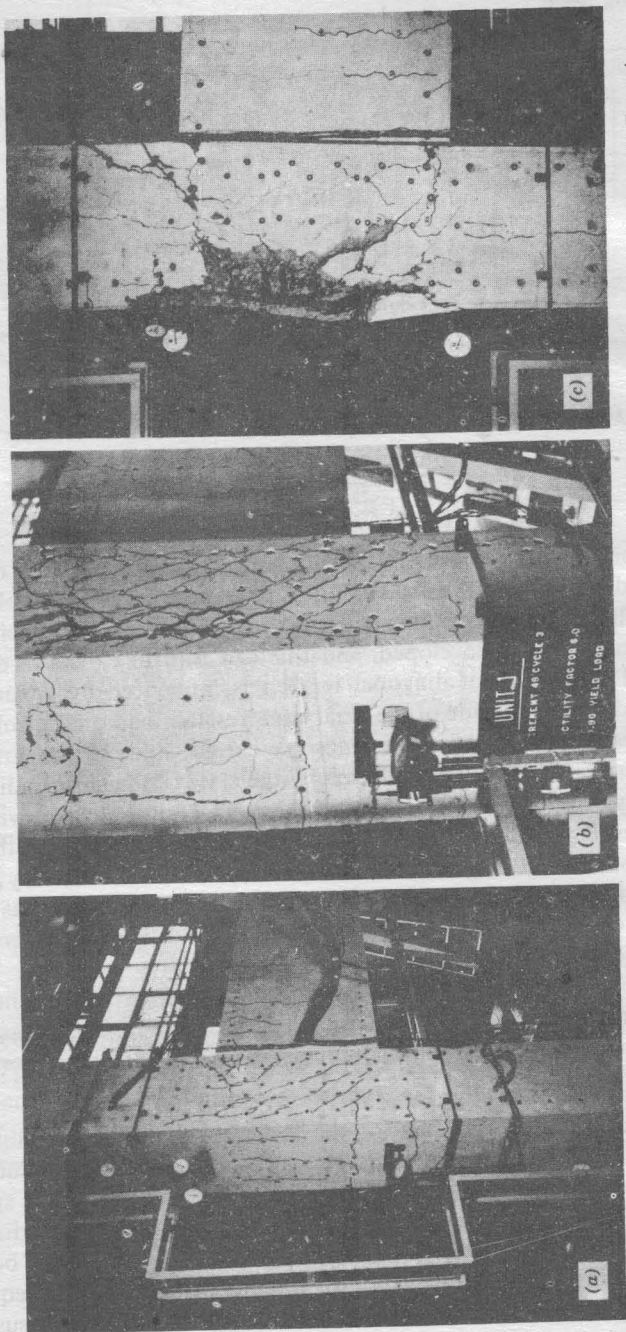


Fig. 13.59. Exterior column-beam joint.^{13,36} (a) Diagonal cracking across joint core and splitting cracks along outer column bars. (b) Extensive cracking after cyclic loading, affecting anchorage of column bars. (c) Separation of cover concrete.

only if the surrounding concrete is in sound condition. The straight vertical portion following the bend must be sufficiently long if the full strength of the top bar is to be developed.

It may be noted that bending the top steel into the joint induces concrete hoop forces along the "right" direction. (The forces transmitted from the bars to the concrete by bearing or bond are indicated by the small arrows in Fig. 13.58b). A top bar bent upward, a tempting proposition from a construction point of view, is likely to be very much less effective.

2. The bottom beam bars, in compression, enter the joint in a region of ideal bond conditions, since the surrounding concrete is also in compression transversely to the bars. Because of reversed loading and subsequent possible tensile yielding of these bars, however, serious bond deterioration can occur here too, as outlined in item 1. The straight portion of the bars beyond the bend remains largely ineffective for compression loads. Therefore, after a few cycles of reversed seismic loading, serious anchorage losses can occur, particularly when the beam frames into a shallow column.

3. The outer column bars are subjected to perhaps the most severe bond conditions. Over the depth h of the beam, a total bond force of

$$C'_s + T'' \leq 2A_s f_y$$

where A_s = area of the outer column bars, needs to be transferred to the concrete in the joint, if the internal forces at the critical sections across the column (Fig. 13.58a) are to be sustained. If code recommendations are to be adhered to, the available anchorage length h is grossly inadequate. Moreover, the entire bond force is to be transferred into the panel zone of the joint and not, as one might be tempted to assume, partly into the cover and partly into the core of the joint. The extremely high bond stresses along the outer column bars can be the cause of vertical splitting cracks (see Fig. 13.59a). These might interconnect and in turn cause the cover to separate itself (see Fig. 13.59c). Unfortunately, the failure planes along splitting cracks around these bars coincide during reversed loading.

Figure 13.58b suggests that the shearing and compression forces resulting from the particular load pattern are largely transmitted by a diagonal strut across the joint. As Fig. 13.59a reveals, there are in fact several struts separated from one another by diagonal cracks. It would be extremely optimistic to assume that the full compression strength f'_c could be approached in these struts. Not only are they subjected to indeterminable eccentricities, they are also exposed to transverse tensile strains. In this biaxial state of stress, a considerable reduction of compressive strength ensues.

Cyclic loading in cross-cracked concrete causes a repeated opening and closure of cracks. Because of the dominance of shearing action across the joint, movements parallel to open cracks will also occur. When the cracks

become large, because the transverse reinforcement has yielded, the process of grinding and progressive splitting due to uneven concrete bearing begins. A complete disintegration of the concrete within the body of the joint can result. This is associated with drastic volumetric increase of the core unless containment is provided.

Observed Behavior of Exterior Joints

A study of exterior isolated column-beam joints was undertaken by Hanson and Connor.^{13,37} They demonstrated that a joint without transverse reinforcement could not sustain much load after the third moderate cycle of reversed loading. The concrete burst and the column bars buckled. In joints that contained hoop reinforcement equal to that required for confinement in the column above and below, the hoop steel stresses increased during cyclic alternating loading till yielding occurred. This clearly showed the important role of transverse joint reinforcement for seismic-type loadings. Under the most severe load conditions, a rotational ductility factor of ± 5 was imposed on the beam's plastic hinge. This is considerably less than could be expected at the same place during a major earthquake shock, which would impose lateral displacements on the building corresponding with a displacement ductility factor of 4. To test the suitability of the joint for sustaining the imposed column load after high-intensity cyclic loading, a relatively large compression was applied to the columns of these PCA specimens. However, only about one-third the flexural capacity of the columns was utilized when the beam of the specimens reached yield; consequently, small bond forces were generated in the column bars. Therefore, the observations made could be optimistic when applied to other situations in which the rotational ductility demand is higher, the columns are less strong, and the beneficial compression across the joint is absent.

The current recommendation of the ACI code^{13,12} with respect to joints is based on these PCA tests.^{13,37} It rests on the contentious premises that the joint behavior is governed by shear and that the accepted parameters of shear resistance in beams are applicable. Joint actions must not reduce the column's compression capacity, hence the transverse reinforcement within the joint must not be less than that required for the column it supports.

Accordingly, the required shear reinforcement in the column is arrived at by first considering the horizontal shear across the joint from Fig. 13.58a.

$$V_j = T - V' = A_s f_y - V' \quad (13.24)$$

This shear is assumed to be resisted by the mechanisms other than the web reinforcement V_c and by the web reinforcement V_s . Both shear-resisting

components were studied in Chapter 7. On the basis of the 45° truss analogy, we have

$$A_v = \frac{sV_s}{f_y d} = v_s \frac{sb_w}{f_y} \quad (7.23a)$$

The contribution of the concrete (i.e., other mechanisms V_c) is assessed by Eqs. 7.34b and 7.35 with allowance for the beneficial effect of the axial compression. The upper limit of the computed nominal shear stress within the joint is not explicitly restricted by the code. Often this nominal shear stress, $v_j = V_j/bd$, is well in excess of $10\sqrt{f'_c}$ to $11.5\sqrt{f'_c}$ (psi), the maximum value recommended for beams.

The 1971 version of the SEAOC code^{13,38} recommends that when the axial compression stress computed on the gross concrete section is less than $0.12f'_c$, its beneficial effect on shear resistance in the joint be neglected; that is, the whole joint shear V_j be allocated to stirrups ($V_s = V_j$).

According to the code^{13,12} when beams of approximately equal depth and a width of not less than one-half the column width frame from four directions into the column, the transverse reinforcement need be only one-half that required by Eq. 7.23a. This provision allows for a considerable reduction in transverse steel due to the assumed increased confinement of the concrete within the joint due to the surrounding beams.

Tests in progress at the University of Canterbury^{13,36, 13,39, 13,40-13,42} furnish less favorable results than the PCA tests.^{13,37} The Canterbury specimens were subjected to small or no column loads, and the imposed rotational ductility factors were progressively increased from 5 to 10 and 15, or greater, to be more consistent with typical requirements when a displacement ductility factor of 4 is to be attained. A number of observations, relevant to detailing, from the Canterbury tests, are recorded next.

1. The failure of 13 exterior column-beam joint specimens occurred in the joint rather than in one of the adjoining members. Even in the more heavily reinforced assemblies, the flexural capacity of the critical member could not be sustained after a few substantial excursions into the postelastic range, because of joint deterioration.

2. Joint reinforcement provided in accordance with the current ACI code recommendations, including an allowance for the contribution of mechanisms other than stirrups (V_c), proved to be inadequate.^{13,39} In the absence of substantial axial compression on the columns, it appears that no reliance can be placed on the thoroughly cross-cracked concrete (see Fig. 13.59) to resist shearing forces.

3. Joint failure ensued also in all specimens in which full or excess shear reinforcement was provided in accordance with the 45° truss analogy, to resist the whole of the theoretical maximum joint shear.^{13,40} This suggests

that the traditional truss model, which has proved so useful for beams and columns, is perhaps not applicable to this situation. Indeed, it was found that transverse shear reinforcement placed in the joint in level with the compression zone of the beam was not yielding.^{13.36}

The conventional truss analogy is associated with 45° cracks, most commonly observed in the shear span of beams. Only in a square-shaped joint will the critical diagonal crack develop along this angle. In other cases, a failure crack will tend to bisect the joint along one of its diagonals (see Fig. 13.62).

4. When the transverse shear reinforcement across diagonal cracks of joints commences to yield, disintegration of the concrete begins, because of the repeated opening and closing of cracks along which shear displacements also occur. The anchorage of beam or column bars cannot be maintained under such conditions (see Fig. 13.59b).

5. The continuous hoop form of beam bar anchorage, shown in Fig. 13.60 for specimens R1, R2, and R3, proved to be considerably inferior in comparison with separate anchorages of the top and bottom reinforcement. However, this may not be the case if the column has a considerable depth.

6. In the small columns used in the Canterbury tests, the anchorage lengths, computed from the inner face of the columns, were not always adequate. Splitting cracks along and diagonal cracks above the straight horizontal portion of the beam bars suggest that it would be prudent to ignore or reduce this length in the determination of the development length (see Fig. 13.59c).

7. Confinement of the joint region is imperative. Ties used for shear reinforcement are ineffective for confinement except in the four corners of the column, where they are bent around column bars. All tests showed considerable bowing of the ties in all three free sides of the joint. This allowed a volumetric increase of the concrete in the core of the joint, hence the loss of diagonal compression capacity. Attempts to introduce additional confining steel brought promising results (see Figs. 13.60 and 13.63).

It was pointed out earlier that the most precarious bond conditions in a joint prevail for the outer column bars. In their immediate vicinity are located the beam bars, bent over 90°, which need to exchange bond forces with the column bars. As a result, the surrounding concrete is subjected to high shear forces which may have to be transferred across cracks by means of aggregate interlock (shear-friction mechanism) (see Figs. 13.59 and 13.61). Adequate reinforcement crossing these cracks and placed between the perimeter ties could ensure that the cracks remain small, thus enabling the transfer of shearing forces.

8. The geometry of the joint may have a profound effect on its behavior. Figure 13.59 shows one specimen of a series^{13.36} in which the disadvantage

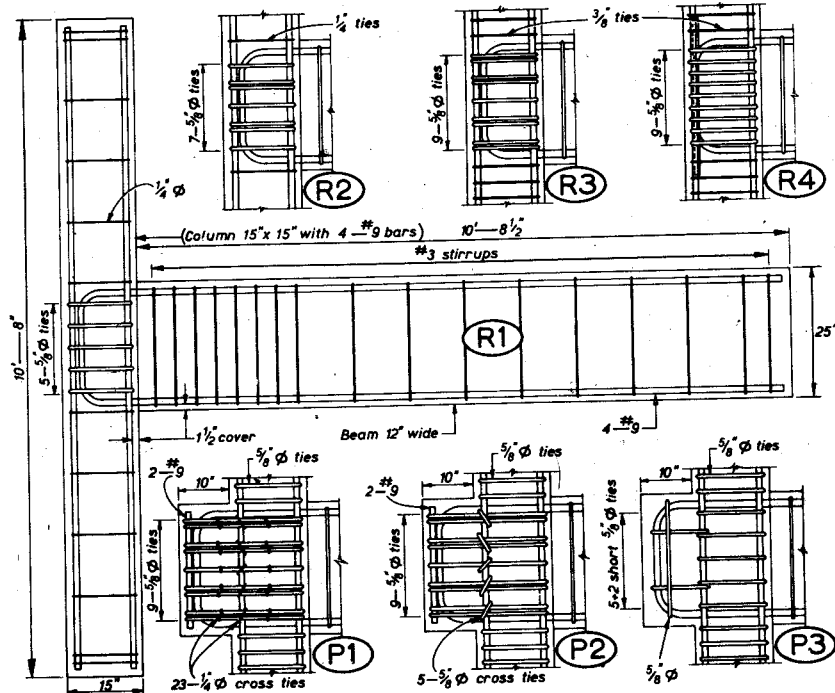


Fig. 13.60. Deep beam-shallow column joint specimens tested at the University of Canterbury.^{13.42}

of having a deeper beam framing into a shallow column, not unfrequently encountered in two- to four-story buildings, became evident. Successive attempts to boost the capacity of the joint by providing more shear reinforcement, as documented by the series R tests in Figs. 13.60 and 13.63, failed to produce satisfactory performance.

Figure 13.63 shows the load sustained, in terms of the computed strength of the specimens, as a function of the imposed cumulative displacement ductility factor, measured by the tip deflection of the beams. This is by no means a unique measure of the deformation capacity of the structure with respect to repeated loading into the postelastic range. A single loading imposing very large plastic deformation has more detrimental effects on subsequent behavior under reversed loading than a number of loads corresponding with cumulative ductility factors equal to that associated with the single loading. The seven specimens recorded in Figs. 13.60 and 13.63 have all been subjected to approximately the same reversed cyclic load pattern; therefore,

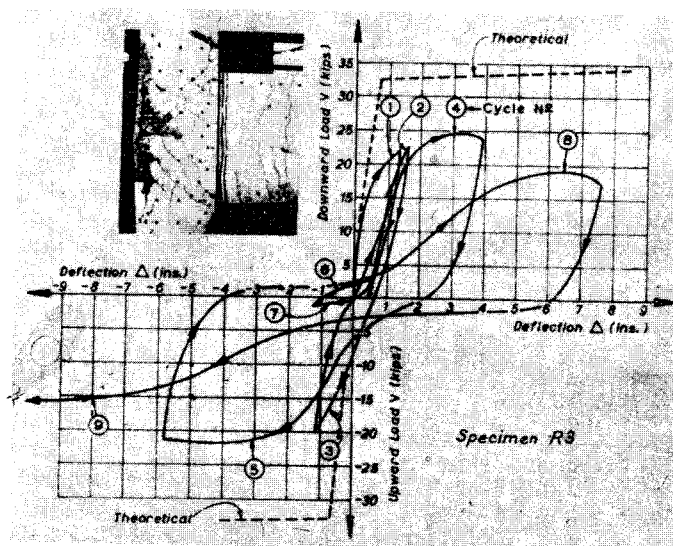


Fig. 13.61. Load-deflection relationship for a beam-column joint specimen.^{13.36}

the cumulative ductility was chosen as a means of comparing their performance. The four lower curves (R1 to R4) represent specimens identical to that in Fig. 13.59 except for the joint tie content and form of anchorage of the beam reinforcement. Demonstrably, not one specimen attained the theoretical flexural capacity; the degradation of strength should also be noted. The performance of a heavily reinforced joint area (specimen R3) during cyclic loading is presented in Fig. 13.61. It became evident that additional shear reinforcement would serve no useful purpose and that only a radical change in the geometry of the joint could hold some promise of improvement.

The arrangement in Fig. 13.60 shows how, with the addition of a stub beam in the series P tests, the effective anchorage of the flexural reinforcement has been relocated from the shear affected core of the joint to a relatively undisturbed zone.^{13.41} Indeed, the crack pattern appearing in Fig. 13.62, which developed during several cycles of reversed loading, suggests that satisfactory bond conditions must exist in the stub beam. The superior performance of specimens P1 to P3 is evidenced by the top curves in Fig. 13.63. In the three tests the full theoretical strength of the critical members was attained in both directions of the loading, and considerably larger cumulative ductilities were obtained. The beneficial effect of only a small amount of confining reinforcement across the core of the joint of specimen P1, as in

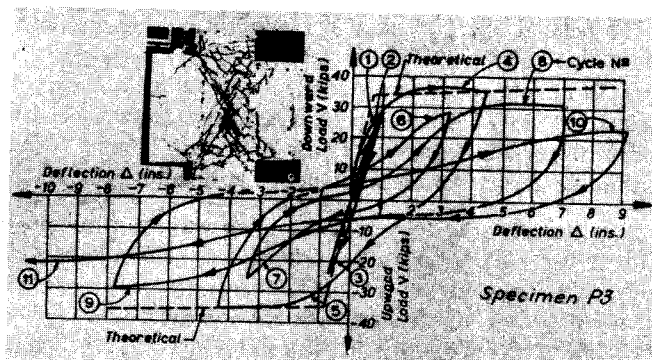


Fig. 13.62. Load-deflection relationship for beam-column joint specimen with beam stub.^{13.41}

Fig. 13.60, indicates that the weakness of an adequately shear reinforced joint under reversed loading is the transverse expansion of the deteriorating concrete.

9. The absolute size of a joint has a bearing on its performance. Ideal bond and anchorage conditions are much more difficult to attain in small joints. The conflicting interests of structural performance (i.e., the use of small diameter bars to improve bond) and that of construction (i.e., the use of fewer large bars to avoid congestion), are nowhere more evident than in the detailing of joints.

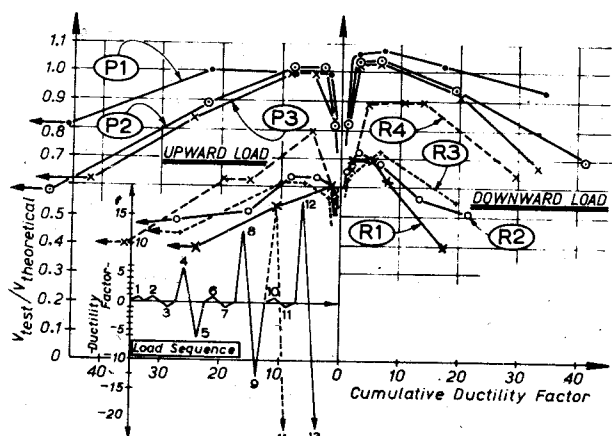


Fig. 13.63. Strength degradation of exterior beam-column joint specimens with cumulative imposed ductility.^{13.42}

10. The beneficial effect of axial compression on the column on joint performance has been convincingly demonstrated by the PCA tests.^{13,37} That this benefit could be reliably predicted with the use of the existing shear strength equation (Eq. 7.35), developed for slender beams subjected to flexure, shear, and compression, would be a suspicious coincidence. The issue will have to await the accumulation of further experimental evidence.

Joint distortion after the development of two-way cracking, normally not allowed for in the evaluation of the response of the whole building frame, can considerably contribute toward the lateral displacement of the structure. The loss of stiffness in the hysteresis loops for the beam end deflections (Figs. 13.61 and 13.62) is mainly due to joint distortions. A comparison of the computed (with allowance for cracking in the members) and observed deformations of a test assembly^{13,36} is presented in Fig. 13.64. The discrepancy is due to joint distortions.

13.8.4 Interior Joints of Multistory Plane Frames

Some observations must be added to those of the previous section when an interior joint of a plane frame is examined. The configuration of a typical interior column-beam joint is given in Fig. 13.65. Important new features of this joint are the anchorage of the beam flexural reinforcement and the increase of the shear force across the joint. From Fig. 13.65 it is evident that the total horizontal shear force is now

$$V_j = (f_s A_s)_1 + C_2 - V' = (f_s A_s)_1 + (f_s A_s)_2 - V' \quad (13.25)$$

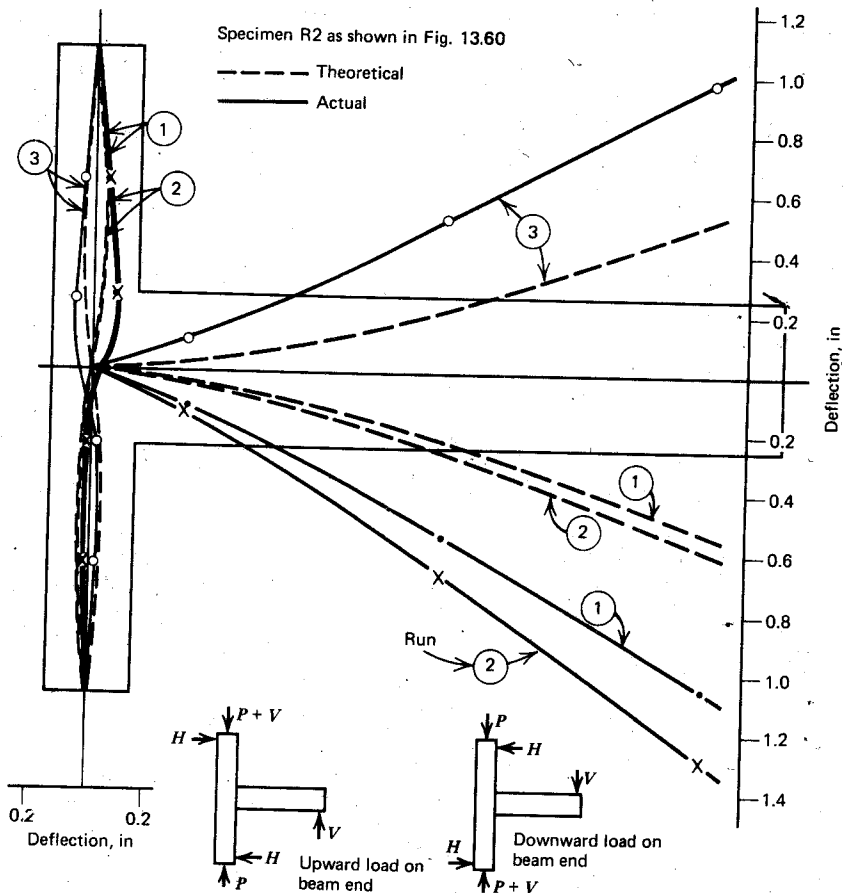
Figure 13.65 illustrates a beam in which the bottom reinforcement area is approximately one-half that of the top steel. For this case, at ultimate load, we have

$$V_j \approx \frac{3}{2} f_y A_s - V'$$

In spandrel beams carrying only small gravity loads, equal amounts of top and bottom steel are usually provided for lateral load resistance. In this case $V_j \leq 2f_y A_s - V'$. Hence the joint shear could be approximately twice as great as that encountered in an exterior joint that connects only one beam.

The bond force to be disposed of by one of the top beam bars in Fig. 13.65 results from the net force acting on the bar at the column faces

$$\text{bond force} = \frac{\pi d_b^2}{4} (f_y + f'_s)$$



where f'_s is the compression steel stress at the far face of the joint. After repeated alternating loading in spandrels (with equal top and bottom steel) compression yielding can also occur; thus the bond force can approach $2A_s f_y$ in magnitude. Therefore, the desired yield strength of the reinforcement can be developed only if this bond force can be disposed of within the joint. Note that as opposed to exterior joints in Fig. 13.60, the bond force in interior joints must be developed entirely by bond stresses. When computed, these stresses are usually found to be well in excess of magnitudes recommended by codes.

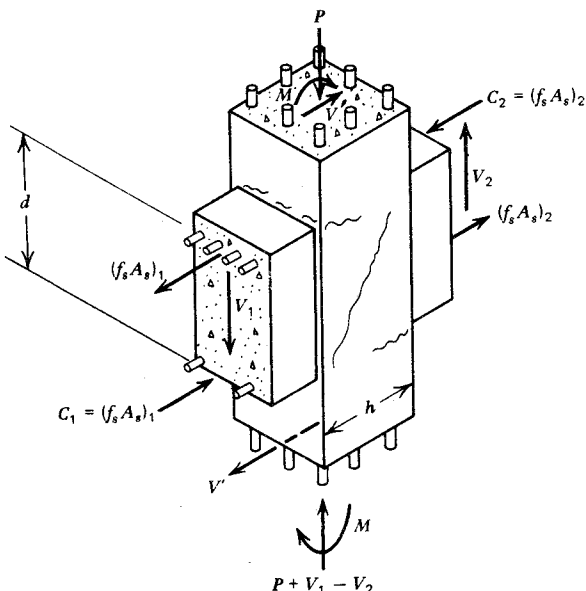


Fig. 13.65. Actions on interior joint of multistory plane frame.

Interplay of Forces in Interior Joints Subjected to Moments and Shear

The interplay of joint forces associated with a desired joint behavior is illustrated in a series of idealized diagrams in Fig. 13.66. The forces exerted by the four members of a plane frame against the joint appear in Fig. 13.66a. For the sake of simplicity it is assumed that the bending moments introduced are the same at all four sides of the joint. The joint shear V_j , obtained from Eq. 13.25, can be the cause of extensive diagonal cracking in the joint core.

Two mechanisms capable of transmitting shearing forces from one face of a joint to the other can be identified in this model. It is assumed that the strength of these two systems, to be examined later, is additive.

Figure 13.66b suggests that all the compressive forces carried by the concrete could combine by equilibrating each other through a single, broad diagonal strut across the joint. When yielding in the flexural reinforcement occurs, it is appropriate to assume that the whole shear force in each of the adjoining members is introduced to the joint core through the concrete compression zones in the beams and columns, respectively. The compression forces C_c and C'_c and the shearing forces V and V' could balance each other

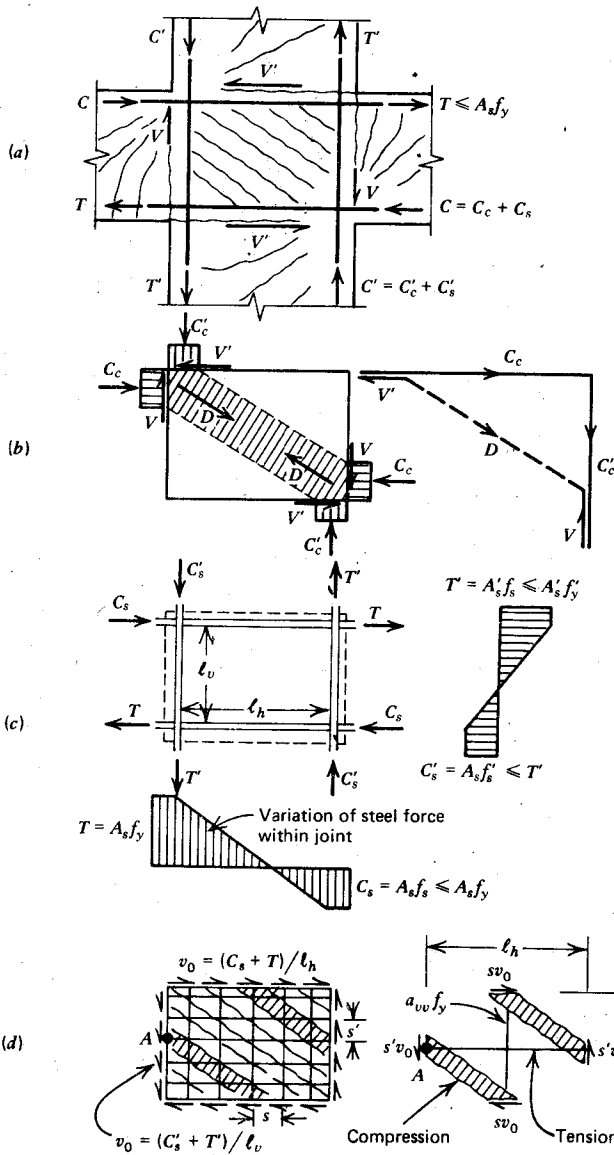


Fig. 13.66. Idealized behavior of interior beam-column joints. (a) Internal actions and crack pattern. (b) Shear transfer by compression mechanism. (c) Forces in the reinforcement only. (d) Shear transfer by truss mechanism.

by means of a diagonal compression force D , without the aid of any reinforcement. In terms of nominal shear stresses and the dimensions given in Fig. 13.65, the shear capacity of this mechanism can be expressed by

$$v_c = \frac{C_c - V}{bd} \quad (13.26)$$

The disposition of the steel forces within the joint now has to be evaluated. The relevant forces applied to the ends of the reinforcing bars, embedded in the concrete of the joint core, are represented in Fig. 13.66c. If it is assumed that the bond force in each bar is absorbed by bond stresses of uniform intensity, the bar forces will change linearly from tension at one end to compression at the other, as illustrated by two diagrams in Fig. 13.66c. The bond force per unit length will be accordingly $v_0 = (C_s + T)/\ell_h$ and $v_0 = (C_s' + T')/\ell_v$ along the beam and column reinforcement, respectively. In terms of nominal shear stresses, the shear flow v_0 becomes approximately

$$v_s = \frac{v_0}{b} \approx \frac{C_s + T}{bd} \quad (13.27)$$

where b is the width of the column.

Figure 13.66d suggests how each bond force component acting over a small length needs to resolve itself into a diagonal compression force and a vertical or horizontal tension force, if this mechanism is to be sustained. The whole panel zone may be thought of as being made up of self-equilibrated elements, illustrated in Fig. 13.66d. The diagonal compression forces could be supplied by concrete struts, formed between diagonal cracks. The tensile forces would require a mesh or well-anchored horizontal and vertical bars, where the bond forces are introduced. It is thus evident that to sustain the desired bond forces v_0 , the amount of horizontal and vertical "shear reinforcement" required will be

$$a_{vh} = \frac{(C_s + T)s'}{\ell_v f_y} \quad (13.28a)$$

$$a_{vv} = \frac{s}{s'} a_{vh} \quad (13.28b)$$

at yield strength, where a_{vh} = area of each horizontal stirrup and a_{vv} = area of each vertical stirrup. These two equations may be derived from first principles and consideration of the equilibrium of a point in the panel zone, such as point A in Fig. 13.66d.

By similarity to the design procedure used for shear in beams, the combined action of the two mechanisms just described may be expressed thus:

$$v_j = v_c + v_s \quad (13.29)$$

where the second term, Eq. 13.27, represents the joint shear sustained by the mesh reinforcement.

It is hoped that experimental studies will disclose in the near future the extent to which these two mechanisms will remain effective during high-intensity reversed cyclic loading. It was pointed out repeatedly in previous chapters that the concrete in the compression zone of a beam will withdraw from participation if permanent elongations are caused in the reinforcement by tensile yielding during previous reversed loadings. In spandrel beams having equal top and bottom steel, the compression in the concrete may diminish so greatly that the contribution of the joint mechanism given in Fig. 13.66b (i.e., v_c) may become insignificant. The entire joint shear would then need to be carried by joint shear reinforcement. On this ground, the contribution of the concrete toward shear resistance in the joint core of earthquake-resistant structures should be ignored in the design.

The effectiveness of the joint shear reinforcement, as modeled in Fig. 13.66d, depends on the ability of the flexural reinforcement and the surrounding concrete to interchange high-intensity bond forces throughout the loading procedure. When severe reversed loading produces bond deterioration, the desirable distribution of steel forces (see Fig. 13.66c), changes radically. There is no alternative means of anchoring the bars, as there was in the case of exterior joints, where bars are bent over. Hanson identified this loss of bond in his experiments^{13,43} using Grade 60 ($f_y = 414 \text{ N/mm}^2$) steel. In spite of this, full strength capacity was sustained in Hanson's tests because the tension steel entering the joint found anchorage in the beam at the far side of the joint. This implies that after a few reversals the top and the bottom beam steel can be in tension on both sides of the column. In underreinforced beams this phenomenon may not have further consequences. In more heavily reinforced members, however, the complete loss of compression steel may seriously impair their ductility. Not only is any relief in the compression load-carrying capacity of the concrete absent, but larger compression forces are imposed on the critical section in the beam's endeavor to balance the increased internal tensile forces. The phenomenon may reduce the ductility of the section adjacent to the column. The limited experimental work conducted so far has not clarified this aspect, nor does it suggest remedial measures. Because of the critical nature of bond stresses it is likely that small diameter bars passing through the joint will perform better than large bars. The foregoing observations are also intended to draw attention once more to the intimate relationship between joint core behavior and the expected performance of the adjoining members.

In most columns of seismic-resistant frames, the principal reinforcement—particularly vertical bars not situated near the extreme fibers of the moment-affected section—will remain well below yield level when plastic hinges in

adjoining beams are expected to develop. For this reason one may expect intermediate column bars, passing through a joint core, to replace the function of vertical joint shear reinforcement in Fig. 13.66d. However, the vertical shear reinforcement may become necessary when the column reinforcement is placed only at the four corners or across the moment-affected faces only.

The orthogonal shear reinforcement in the core may well be replaced by diagonal steel. In most cases this would be entirely impractical. When the joint geometry permits it, however, all or part of the flexural reinforcement from the top of one beam may be bent down across an interior joint into the bottom of the other beam. This would greatly relieve the concrete in the joint core and would eliminate most of the bond forces. In the absence of experimental evidence, design propositions are not offered here.

Effect of Axial Compression on Joint Behavior

Axial compression can be expected to improve joint behavior and reduce the demand for joint shear reinforcement. The simplified model, (Fig. 13.67) suggests that a steeper diagonal compression strut may form as a result of an enlarged compression block across the column section. The horizontal component of the diagonal force, sustained by this strut, could consist of the beam compression force C , less the column shear V' , and a fraction of the beam tensile force T . It is evident that the horizontal bond force along the beam bars can now be disposed of more easily within the wider diagonal compression strut. Web steel reinforcement, according to this model,

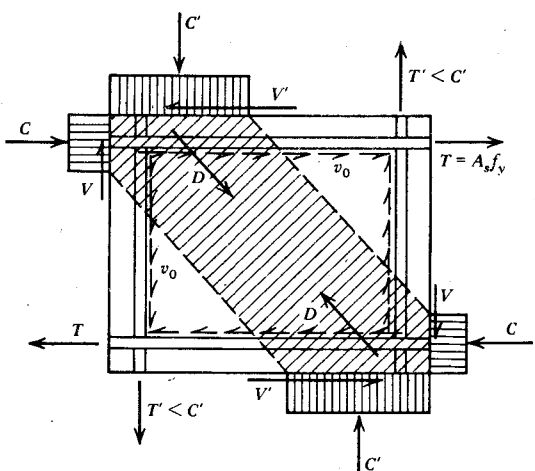


Fig. 13.67. Idealized disposition of forces in joint core with compression load on column.

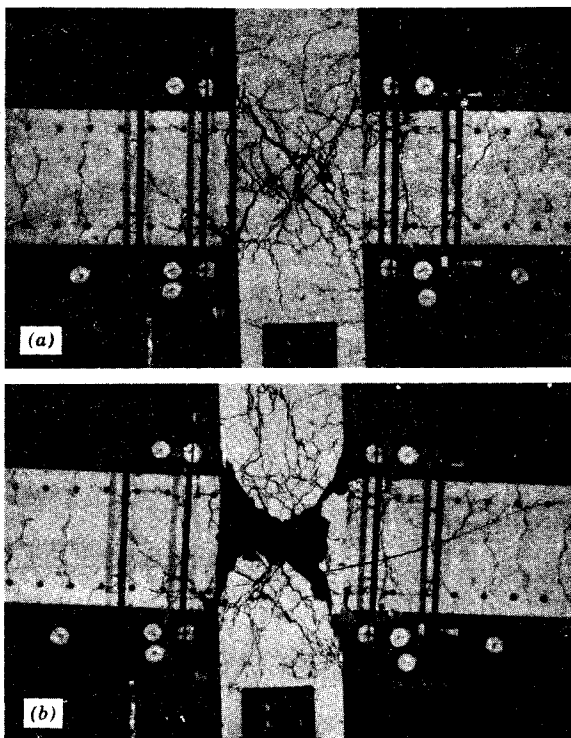


Fig. 13.68. Crack patterns of interior beam-column joint.^{13,44} (a) At application of maximum bending moment. (b) At end of twelfth load run.

would be required only to enable bond forces v_0 to be introduced into the core zone outside the shaded area in Fig. 13.67. The apparent contribution of the concrete toward the shear strength of the joint core v_c is thus enhanced, and the demand for shear reinforcement v_s according to Eq. 13.29 is reduced. A quantitative evaluation of the joint shear reinforcement in the presence of compression in the column has yet to be developed.

Effect of Joint Core Failure on Frame Deformations

The unsatisfactory behavior of a typical interior joint of a plane frame^{13,44} can be seen in Fig. 13.68, which shows an assembly in which failure has occurred mainly in the joint. The loading system and details of the assembly appear in Fig. 13.69. The assembly had been designed according to the 1971 ACI code^{13,12} requirements for ductile frames in seismic zones. The

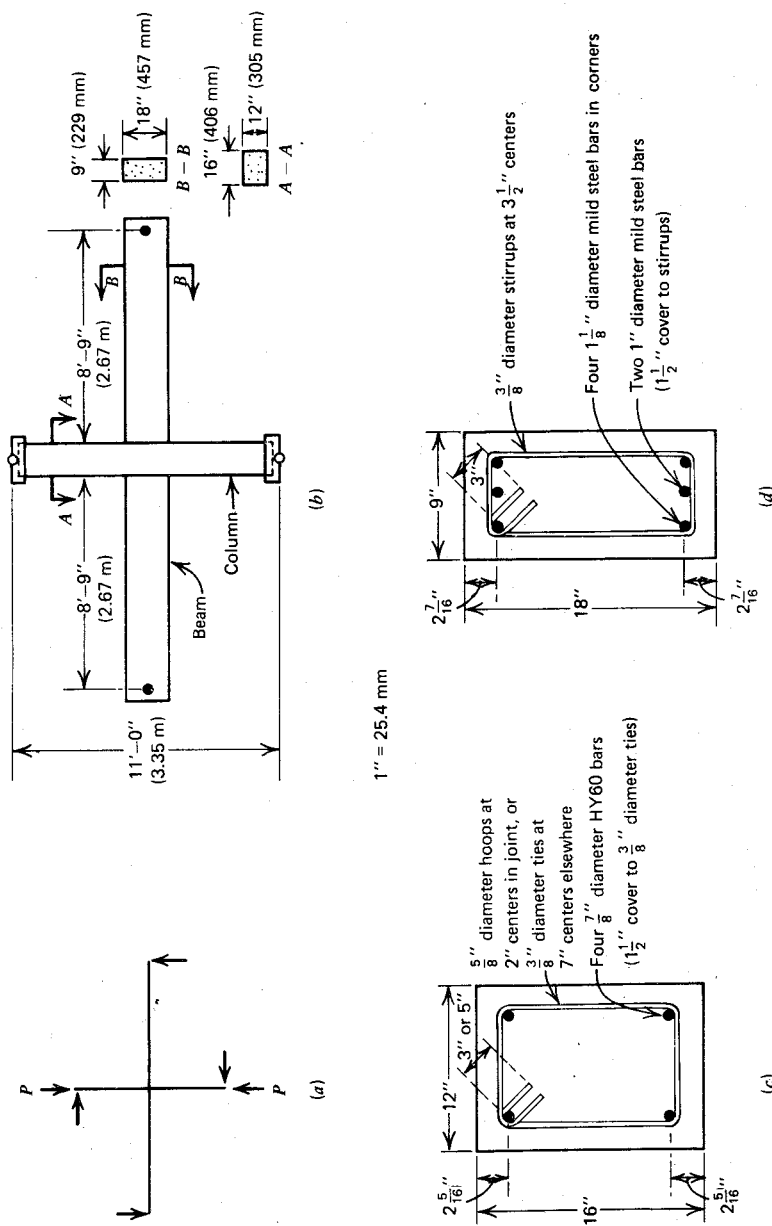


Fig. 13.69. Details of beam-column test specimen.^{13.44} (a) Loading system. (b) Dimensions of test assembly. (c) Column section. (d) Beam section.

columns, which were stronger than the beams, were subjected during the test to a constant axial load of $0.22f'_c A_g$, while the members were subjected to static reversed lateral loading, as shown in Fig. 13.69a. The beam and column details are given in Figs. 13.69b to 13.69d. Note that the transverse steel in the joint consisted of No. 5 (16 mm diameter) hoops at 2 in (51 mm) centers. Figure 13.70 shows the measured moment-curvature behavior of the beam

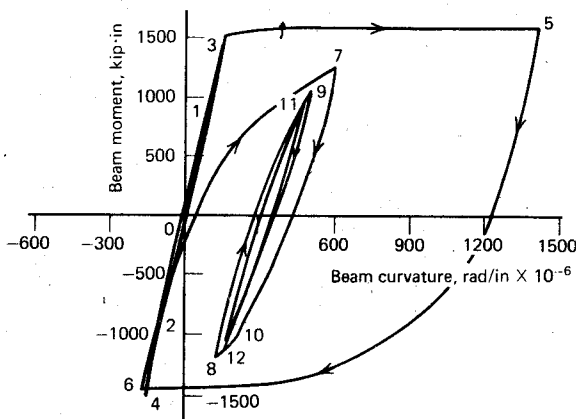


Fig. 13.70. Measured moment-average curvature relationship for plastic hinge in beam.^{13.44}

at the plastic hinge position adjacent to the column face. It is evident that relatively little subsequent plastic deformation occurred in the beam after the first two large yield rotations. Following the development of the full plastic moments in the beam hinges, the beam bars began to slip within the joint and large diagonal cracks developed (see Fig. 13.68a). From the measured beam moment at the column-face-beam-end deflection relationship (Fig. 13.71), it is seen that beam deflections equal to or larger than those which occurred at the development of maximum strength in each direction, were imposed in subsequent load cycles. The capacity as well as the stiffness of the assembly deteriorated gradually during the testing. A comparison of Figs. 13.70 and 13.71 reveals that the large plastic deformations are mainly due to joint panel zone deformations. The joint was reinforced for a shear force corresponding to 106% of the capacity of the assembly, using the ACI code procedure.^{13.12} The shear reinforcement in the joint panel zone commenced to yield when the full theoretical capacity was attained in the fifth load run (Fig. 13.70). Park and Thompson^{13.44} observed satisfactory joint

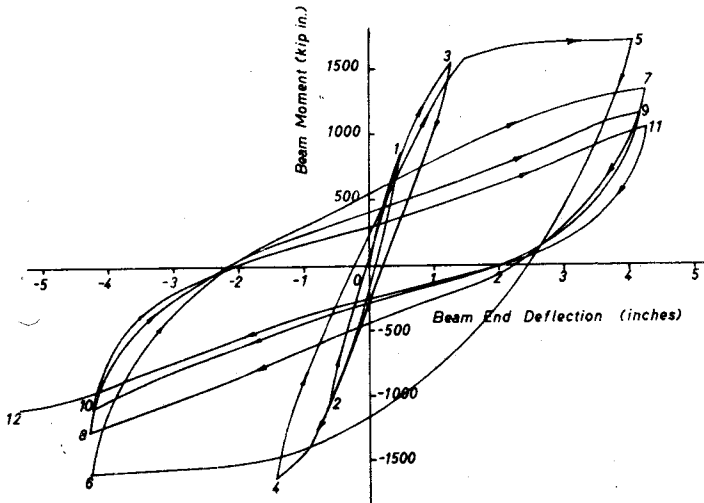


Fig. 13.71. Measured beam end deflection-beam moment at column face relationship.^{13.44}

behavior in an assembly having the same load capacity, in which the beam was fully prestressed. A prestressing tendon at mid depth across the joint core kept the width of the diagonal cracks small.

Because of the high shear, hence diagonal compression stress, intensity, the use of closely spaced transverse confining reinforcement in joints is unavoidable. The critical nature of the joints for seismic loading, quite overlooked until recently, has also been observed by Ohsaki in tests with full size specimens.^{13.45}

13.8.5 Suggestions for the Detailing of Joints

The following recommendations are made in connection with the requirements of anchorage, shear, and confinement within a joint core of earthquake resistant structures.

Anchorage

Because of the inevitable loss of bond at the inner face of an exterior joint, development length of the beam reinforcement should be computed from the beginning of the 90° bend, rather than from the face of the column (see Fig. 13.72a). In wide columns, any portion of the beam bars within the outer third of the column (Fig. 13.72b) could be considered for computing develop-

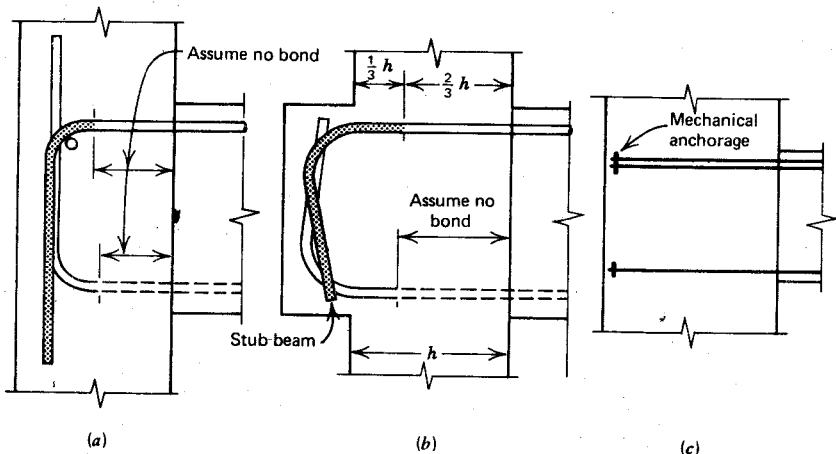


Fig. 13.72. Anchorage of beam bars in columns using (a) bent-up bars; (b) bent-up bars in stub beam; (c) mechanical anchorages.

ment length. For shallow columns, the use of stub beams, as in Fig. 13.72b, will be imperative. A large diameter bearing bar fitted along the 90° bend of the beam bars should be beneficial in distributing bearing stresses (see Figs. 13.72a and 13.75c).

In deep columns and whenever straight beam bars are preferred, mechanical anchorages, as in Fig. 13.72c, could be advantageous. The top bars in a beam passing through holes in a bearing plate may be welded to a steel plate as in Fig. 13.73.

Joint ties should be so arranged that the critical outer column bars and the bent-down portions of the beam bars are held against the core of the joint.

Shear Strength

When the computed axial compression on the column is small (i.e., when the average stress on the gross concrete area is less than, say, $0.12f'_c$, including allowance for vertical acceleration generated by earthquakes), the contribution of the concrete shear resistance should be ignored, and shear reinforcement for the entire joint shearing force should be provided,^{13.38} $V_s = V_j$. In exterior joints only the ties that are situated in the outer two-thirds of length of the potential diagonal failure crack, which runs from corner to corner of the joint, should be considered to be effective (see Fig.

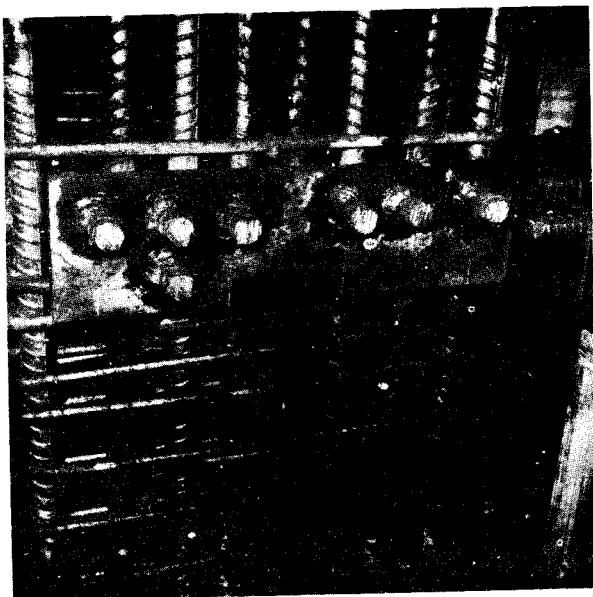


Fig. 13.73. Anchorage plate for beam bars at outer face of an exterior column. (Courtesy Lewis & Williamson, Consulting Engineers, Auckland, New Zealand.)

13.74). Accordingly, from Fig. 13.74 we have if V_s is the joint shear to be carried by the ties

$$A_v = \frac{1.5V_s s}{df_y} \quad (13.30)$$

where A_v = total area of tie legs in a set making up one layer of shear reinforcement, and d = effective depth of the beam. To allow for reversed loading, the corresponding equation will determine the joint shear reinforcement in the lower two-thirds of the joint. This proposition is more severe than any code requirement existing, at the time of writing this book, for joints in which the beam depth to column depth ratio is less than approximately 1.5. In accordance with the design philosophy outlined in Chapter 11 for multistory buildings, the joint should be considered as part of the column; hence allowance should be made for the possible overstrength of the beam when computing the value of the joint shear V_j to determine $V_s = V_j - V_c$.

Because the major part of the shear force is introduced to an interior joint by bond forces along the top and bottom reinforcement, as illustrated in Figure 13.66c, rather than by bearing stresses as in Fig. 13.58b, it is likely

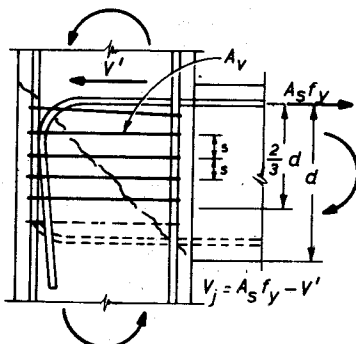


Fig. 13.74. Effective ties resisting shear in an exterior beam-column joint.

that all ties in the joint core will participate in the shear resistance. Consequently Eq. 13.30 may be modified as follows

$$A_v = \frac{V_s s}{(d - d')f_y} \quad (13.31)$$

where $(d - d')$ is the distance between the centroids of the top and bottom beam reinforcement.

To protect the core concrete against excessive diagonal compression, an upper limit must be set for the joint shear, normally expressed in terms of a nominal shearing stress. Further research is required to establish this value, which may be well in excess of the corresponding value suggested for beams [i.e., $10\sqrt{f'_c}$ to $11.5\sqrt{f'_c}$ (psi)] because of confinement.

Confinement

It was pointed out earlier that the nominal shearing stresses, hence the diagonal compression stresses within the joint, may become large. These compression stresses are responsible for the eventual destruction of the concrete core when high-intensity cyclic loading is applied, particularly if the shear reinforcement is permitted to yield. Effective confinement is therefore imperative in any joint. There is insufficient experimental evidence at hand to allow us to determine the amount of confining reinforcement required in a joint, but it is suggested that not less than that used in columns (Eqs. 11.55 and 11.56) should be provided, irrespective of the intensity of the axial load on the columns.

Shear reinforcement confines only the corner zones of the joint, and horizontal tie legs are quite ineffective in furnishing restraint against the volumetric increase of the core concrete. Hence additional confining bars must be provided at right angles to the shear reinforcement. These bars should

not be placed further than 6 in (150 mm) apart. Suggested arrangements for horizontal joint reinforcement for an exterior beam-column joint appear in Fig. 13.75. Particular attention must be paid to the confinement of the outside face of the joint, opposite the beam, where very high bond forces must be developed. Here the roles of ties and confining steel can be combined. Only with the effective confinement can the shear capacity of a joint be developed.

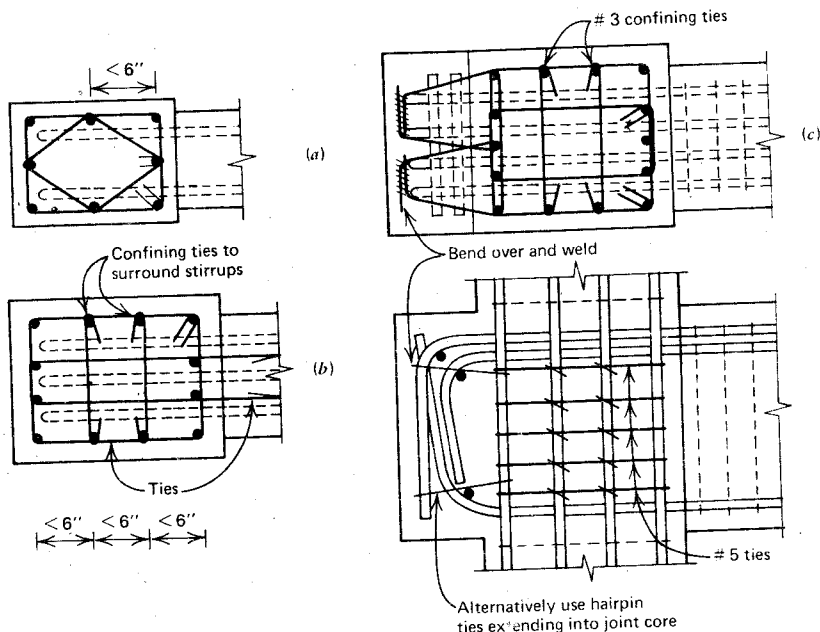


Fig. 13.75. Suggested arrangement of joint stirrups and ties for exterior beam-column joint in a (a) small column; (b) medium size column; (c) column with stub beam.

13.8.6 Joints of Multistory Space Frames

The most common joint occurs at the interior of a multistory frame system in which four beams, generally at right angles to each other, meet at a continuous column. When a major seismic disturbance imposes alternating yield conditions along one of the major axes of the building, thereby generating critical shear stresses across the core of the joint as outlined in Section 13.8.4, confinement against lateral expansion of the joint will be provided by the

beams at right angles to the plane of the earthquake-affected frames. Considerable restraint can be offered by the nonyielding flexural steel in these beams which cross the joint transversely.

Hanson^{13,43} and Connor,^{13,37} who simulated this situation with stub beams cast at right angles to the column-beam specimens, found a marked improvement in joint behavior over that of frames having beams only in one plane. The present ACI recommendations^{13,12} are based on their evidence. Accordingly, only one-half the shear reinforcement, computed from Eqs. 13.25 and 7.23a, need to be provided if beams not less than half as wide as the column and not less than three-fourths as deep as the deepest beam, are provided on all four sides of the column.

Problems not yet visualized might be disclosed by further research on joints having beams on four sides, where the ductility demands imposed are more severe than those applied in the PCA^{13,37, 13,43} tests.

When the axes of the beams and the columns do not coincide, secondary actions, such as torsion, will be generated. The behavior of the joint becomes more complex, and in the absence of experimental studies only crude provisions can be made for these load conditions. In structures affected by seismicity, such joints should be avoided. Torsion so introduced caused heavy damage in buildings during the 1968 Tokachioki earthquake.^{13,46}

For convenience, wind or seismic actions are generally considered to be acting independently along one of the two principal axes of a rectangular building frame. It was pointed out earlier that the maximum amplitude of ground accelerations, velocities, and displacements might occur at an angle to both principal axes, producing an overall skew bending effect. This occurrence might mobilize the full strength of all four beams framing into a column, thus imposing extreme load conditions on the joint. Figure 13.76 illustrates the construction difficulties involved in providing joint reinforcement in a column where the concurrent hinging of three beams entering the joint was considered. The situation can be particularly critical at corner columns where the axial forces induced in the columns by lateral skew loads are additive.

Even under unidirectional load application, coincident with one of the principal axes of a multistory, rectilinear, rigid jointed space frame, there may occur secondary effects in beams at right angles that could cause considerable structural damage. Large joint rotations in a plane frame may introduce torsion into beams that enter such joints at right angles to the plane of action, owing to the presence of the floor slab, monolithically cast with the beams. The imposed twist may cause excessive diagonal cracking in beams not subjected to flexure, and this may affect their performance when lateral load along the other principal direction of the building is to be resisted. Figure 13.77 shows different views of a corner joint in a small-scale six-story

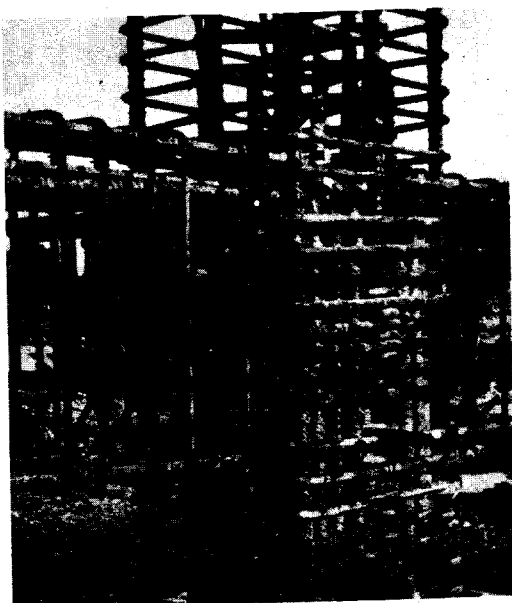


Fig. 13.76. Joint reinforcement in an exterior column where concurrent hinging of three beams was considered. (Courtesy New Zealand Ministry of Works.)

reinforced concrete frame that was subjected to simulated unidirectional seismic loading.^{13.47} (Details of the frame are given in Figs. 11.42 to 11.45.) The torsional effects at the corner of the slab and in the beam framing at right angles to the plane of loading, indicated by arrows, are evident.

The use of steel fiber reinforcement in the joint areas holds promise of improving performance by virtue of the increased tensile strength of the concrete core.^{13.48}

Example 13.2

A 24 in \times 18 in (610 mm \times 457 mm) beam frames into an exterior 20 in (508 mm) square column. Three No. 10 (32 mm) top bars and three No. 8 (25 mm) bottom bars enter the joint from the beam. The column is reinforced by No. 8 (25 mm) bars. The yield strength of the beam reinforcement is 40,000 psi (276 N/mm²) and that of the column steel is 60,000 psi (414 N/mm²). The concrete cylinder strength is 3600 psi (17.9 N/mm²), and 2 in (50 mm) cover exists to all main bars. The capacity reduction factor is $\phi = 0.85$.

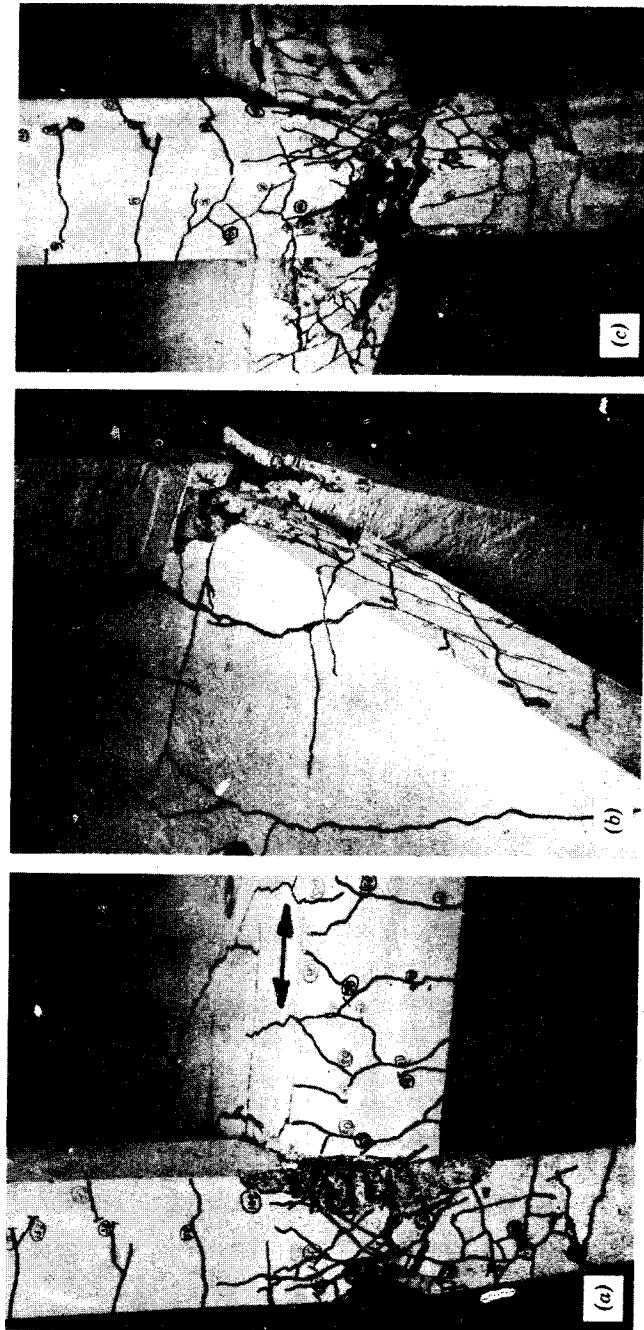


Fig. 13.77. Corner joint at first floor of laterally loaded reinforced concrete model frame.^{13,47} (a) Plastic hinge in beam and column and extensive cracking of joint core. (b) Diagonal cracking across corner of floor slab. (c) Diagonal cracking caused by twisting in beam at right angles to that shown in (a), and spalling at the back of joint.

The column carries an axial compression of 360 kips (1600 kN) when the top steel of the beam is in tension and 180 kips (800 kN) when the bottom steel is in tension. The column may be assumed to have a point of contraflexure 5 ft (1524 mm) above and below the beam axis during sidesway.

The required confining reinforcement in the column consists of No. 4 (12.7 mm) rectangular hoops with one central supplementary No. 4 crosstie in both directions, all spaced at 4 in (102 mm) centers. Determine the joint reinforcement for shear in accordance with (1) ACI 318-71 requirements, (2) the recommendations contained in Section 13.8.5.

Solution

1. ACI 318-71 requirements^{13.12}

tension in top bars

$$A_s f_y = 3 \times 1.23 \times 40 = 147.6 \text{ kips}$$

depth of compression block in beam if compression steel is neglected

$$a = \frac{147.6}{0.85 \times 3.6 \times 18} = 2.68 \text{ in}$$

effective depth for top steel

$$d = 24 - 2 - 0.5 \times 1.25 = 21.4 \text{ in}$$

for concrete compressive force

$$j = 1 - \frac{a}{2d} = 1 - \frac{2.68}{2 \times 21.4} = 0.94$$

effective depth for bottom steel

$$d = 24 - 2 - 0.5 \times 1 = 21.5 \text{ in}$$

for compression steel

$$j = \frac{d - d'}{d} = \frac{21.4 - 2.5}{21.4} = 0.883 < 0.94$$

Ideal moment from the beam is approximately $0.883 \times 21.4 \times 147.6 = 2790$ kip·in. Assuming this moment to be resisted in equal proportions below and above the joint, the column shear is approximately

$$V_{col} = \frac{0.5 \times 2790}{5 \times 12} = 23.2 \approx 23 \text{ kips}$$

From Eq. 13.24 we have $V_j = 147.6 - 23 = 124.6$ kips

$$\therefore v_u = \frac{V_j}{\varphi b d} = \frac{124,600}{0.85 \times 20 \times 17.5} = 419 \text{ psi (2.89 N/mm}^2\text{)}$$

From Eq. 7.35b, we have

$$v_c = 3.5 \sqrt{3600} \sqrt{1 + 0.002 \times 360,000/400} = 351 \text{ psi}$$

$$\therefore v_s = 419 - 351 = 68 \text{ psi}$$

Equation 7.23a, with $s = 4$ in, gives $A_v = 68 \times 4 \times 20/60,000 = 0.091$ in 2 . This value is less than the confining steel required, and it does not govern the design. Note that following the ACI recommendations, some 84% of the total shear was allocated to the concrete, v_c .

for reversed moment

$$A_s f_y = 3 \times 0.785 \times 40 = 94.2 \text{ kips}$$

flexural capacity of beam

$$\approx 0.883 \times 21.5 \times 94.2 = 1790 \text{ kip} \cdot \text{in}$$

column shear is approximately

$$V_{col} = 0.5 \times \frac{1790}{60} = 14.9 \text{ kips}$$

joint shear

$$V_j = 94.2 - 14.9 = 79.3 \text{ kips}$$

$$\therefore v_u = \frac{79,300}{0.85 \times 20 \times 17.5} = 267 \text{ psi}$$

Equation 7.35b gives

$$v_c = 3.5 \sqrt{3600} \sqrt{1 + 0.002 \times 180,000/400} = 289 \text{ psi}$$

Hence no joint shear reinforcement is required for this case.

2. Recommendations contained in Section 13.8.5

In assessing the beam's flexural capacity, allow for 25% overstrength, giving

$$A_s f_y = 1.25 \times 147.6 = 184.5 \text{ kips}$$

column shear from Section 1

$$V_{col} = 1.25 \times 23.2 = 29.0 \text{ kips}$$

joint shear

$$V_j = 184.5 - 29.0 = 155.5 \text{ kips}$$

$$v_u = \frac{155,500}{0.85 \times 20 \times 17.5} = 521 \text{ psi (3.59 N/mm}^2)$$

When $v_c = 0$, $v_s = 521$ psi, and $s = 4$ in.

Equation 13.30 gives

$$A_v = \frac{1.5 \times 155.5 \times 4}{0.85 \times 21.5 \times 60} = 0.871 \text{ in}^2$$

A No. 5 (16 mm) rectangular tie and a single No. 5 central supplementary leg would provide 0.915 in^2 every 4 in. This is more than the confining steel requirements.

It is evident that the amount of joint shear reinforcement depends largely on the extent by which the shear strength of the core is effected by the axial compression in the columns.

For example, if it is assumed that the shear strength benefits from the axial compression stress that is in excess of $0.12f'_c$, as is implied by the SEAOC recommendations,^{13.38} the joint shear reinforcement is reduced as follows.

axial compression on the column

$$360,000/4000 = 900 \text{ psi} = 0.25f'_c \text{ (psi)}$$

for assessing shear strength consider only

$$(0.25 - 0.12)f'_c = 0.13 \times 3600 = 468 \text{ psi compression}$$

Equation 7.35b gives

$$v_c = 3.5 \sqrt{3600} \sqrt{1 + 0.002 \times 468} = 292 \text{ psi}$$

Hence the area of stirrups placed at 4 in centres is by proportion

$$\frac{521 - 292}{521} \times 0.871 = 0.383 \text{ in}^2$$

The confining steel provided is more than this.

Example 13.3

A 22 in \times 16 in (559 \times 406 mm) spandrel beam passes continuously through the same 20 in (508 mm) square column, described in

Example 13.2. This beam, situated at right angles to the beam of Example 13.2, is reinforced with three No. 10 (32 mm) bars at the top, having $3\frac{1}{4}$ in (83 mm) cover, and three No. 8 (25 mm) bars at the bottom, having 2 in (50 mm) cover. For lateral load induced shears in this direction, the minimum axial load on the column to be considered is 270 kips (1200 kN).

The strength properties are as in the previous example.

Determine the joint shear reinforcement in accordance with (1) ACI 318-71^{13.12} requirements, (2) the recommendations of Section 13.8.5.

Solution

1. ACI 318-71 requirements

We have an interior joint similar to that in Fig. 13.65. The tension force in the top steel is $3.69 \times 40 = 147.6$ kips, and in the bottom steel the force is $2.36 \times 40 = 94.4$ kips. The approximate flexural capacity of the top steel is Tjd , where

$$jd \approx 22 - 3.25 - 0.5 \times 1.25 - 2 - 0.5 \times 1 = 15.6 \text{ in} = d - d'$$

$$\text{hence } M_{u,\text{top}} \approx 147.6 \times 15.6 \approx 2300 \text{ kip} \cdot \text{in}$$

For the bottom steel the same internal lever arm may be assumed; giving

$$M_{u,\text{bottom}} = 94.4 \times 15.6 = 1470 \text{ kip} \cdot \text{in}$$

Hence the column shear is approximately

$$V_{\text{col}} = \frac{0.5(2300 + 1470)}{5 \times 12} = 31.4 \text{ kips}$$

From Eq. 13.25 we have $V_j = 147.6 + 94.4 - 31.4 = 210.6$ kips

$$\therefore v_u = \frac{210,600}{0.85 \times 20 \times 17.5} = 708 \text{ psi (4.88 N/mm}^2\text{)}$$

From Eq. 7.35b we have

$$v_c = 3.5\sqrt{3600} \sqrt{1 + 0.002 \times 270,000/400} = 322 \text{ psi}$$

$$\therefore v_s = 708 - 322 = 386 \text{ psi}$$

Equation 7.23a, with $s = 4$ in, gives

$$A_v = 386 \times 4 \times 20/60,000 = 0.515 \text{ in}^2$$

From Example 13.2, three No. 4 (12 mm) legs, giving 0.588 in^2 , were required for confinement. This is adequate for the joint shear.

2. Recommendation contained in Section 13.8.5

In assessing the beam's flexural capacity, 25% overstrength is considered. Thus we have

$$V_j = 1.25 \times 210.6 = 263.3 \text{ kips}$$

$$\therefore v_u = \frac{263,300}{0.85 \times 20 \times 17.5} = 884 \text{ psi (6.1 N/mm}^2)$$

Note that this is $14.73\sqrt{f'_c}$ (psi). Assume $v_c = 0$; hence stirrups must resist the whole shear in accordance with Eq. 13.31.

$$A_v = \frac{263.3 \times 4}{0.85 \times 15.6 \times 60} = 1.33 \text{ in}^2$$

If No. 6 (18.8 mm) peripheral hoops and one No. 5 (16 mm) inner leg are used, the stirrup spacing would have to be

$$(2 \times 0.44 + 0.305) \times 4/1.33 = 3.56 \approx 3\frac{1}{2} \text{ in (90 mm)}$$

13.9 CONCLUSION

The previous discussions attempted to illustrate through a few examples that thorough understanding of structural behavior should express itself in thoughtful detailing. Only a well-detailed structure can attain the desired quality of performance, whose prediction is the purpose of this book. The importance of efficient detailing cannot be overemphasized, especially for structures in a country that is subject to earthquakes. The extensive damage and the failures of buildings in cities experiencing severe earthquakes can be directly attributed to substandard or negligent detailing, and such destruction should serve as a reminder that sound detailing is paramount in the broad process of structural design.

13.10 REFERENCES

- 13.1 F. Leonhardt, "Über die Kunst des Bewehrens von Stahlbetontragwerken," *Beton- und Stahlbetonbau*, Vol. 60, 1965, No. 8, pp. 181-192; No. 9, pp. 212-220.
- 13.2 *Manual of Standard Practice for Detailing Reinforced Concrete Structures*, proposed revision of ACI 315-65, American Concrete Institute, 5th ed., 1970.
- 13.3 "The Detailing of Reinforced Concrete," A technical report of the Joint Committee of the Concrete Society and the Institution of Structural Engineers, London, 1968.
- 13.4 ACI Committee 315, "Seismic Details for Special Ductile Frames," *Journal ACI*, Vol. 67, No. 5, May 1970, pp. 374-379.

- 13.5 F. Leonhardt, "Das Bewehren von Stahlbetontragwerken," *Beton- Kalender 1971*, Wilhelm Ernst & Sohn, Berlin, Part II, pp. 303-398.
- 13.6 R. E. Untrauer and R. L. Henry, "Influence of Normal Pressure on Bond Strength," *Journal ACI*, Vol. 62, No. 5, May 1965, pp. 577-586.
- 13.7 G. Waestlund, "Use of High-Strength Steel in Reinforced Concrete," *Journal ACI*, Vol. 30, No. 12, June 1959, pp. 1237-1250.
- 13.8 P. E. Regan, "Behaviour of Reinforced and Prestressed Concrete Subjected to Shear Forces," *Proceedings of the Institution of Civil Engineers*, Supplement XVII, 1971, Paper 744IS, pp. 337-364.
- 13.9 F. Leonhardt, "Reducing the Shear Reinforcement in Reinforced Concrete Beams and Slabs," *Magazine of Concrete Research*, Vol. 17, No. 53, December 1965, pp. 187-198.
- 13.10 M. P. Collins and P. Lampert, "Redistribution of Moments at Cracking—The Key to Simpler Torsion Design," Publication 71-21, Department of Civil Engineering, University of Toronto, 1971, 51 pp.
- 13.11 T. Baumann and H. Rüsch, "Schubversuche mit indirekter Krafteinleitung," Deutscher Ausschuss für Stahlbeton, Bulletin No. 210, Wilhelm Ernst & Sohn, Berlin, 1970, pp. 1-41.
- 13.12 "Building Code Requirements for Reinforced Concrete ACI 318-71," American Concrete Institute, Detroit, 1971, pp. 78.
- 13.13 P. M. Ferguson and S. I. Husain, "Strength Effect of Cutting Off Tension Bars in Concrete Beams," Research Report, 80-IF, University of Texas, Austin, 1967.
- 13.14 F. Leonhardt and K.-T. Teichen, "Druck-Stöße von Bewehrungsstäben," Deutscher Ausschuss für Stahlbeton, Bulletin No. 222, Wilhelm Ernst & Sohn, Berlin, 1972, pp. 1-53.
- 13.15 B. Bresler and P. H. Gilbert, "Tie Requirements for Reinforced Concrete Columns," *Journal ACI*, Vol. 58, No. 5, November 1961, pp. 555-570.
- 13.16 G. Franz and H. Niedenhoff, *The Reinforcement of Brackets and Short Deep Beams*, Cement and Concrete Association, Library Translation No. 114, London, 1963.
- 13.17 L. B. Kriz and C. H. Raths, "Connections in Precast Concrete Structures—Strength of Corbels," *Journal of the Prestressed Concrete Institute*, Vol. 10, No. 1, February 1965, pp. 16-61.
- 13.18 "Neubearbeitung von DIN 4224, Bemessung im Beton- und Stahlbetonbau," Deutscher Ausschuss für Stahlbeton, 1968.
- 13.19 A. Mehmel and W. Freitag, "Trafähigkeitsversuche an Stahlbetonkonsolen," *Der Bauingenieur*, Vol. 42, No. 10, October 1967, pp. 362-369.
- 13.20 F. Dischinger, *Beitrag zur Theorie der Halbscheibe und des Wandartigen Balkens*, Vol. 1, International Association for Bridge and Structural Engineering, Zurich, 1932.
- 13.21 F. Leonhardt and R. Walther, "Wandartiger Träger," Deutscher Ausschuss für Stahlbeton, Bulletin No. 178, Wilhelm Ernst & Sohn, Berlin, 1966, 159 pp.
- 13.22 Comité Européen du Béton-Fédération Internationale de la Précontrainte, *International Recommendations for the Design and Construction of Concrete Structures*, Appendix 3, 1st ed., June 1970. Published by the Cement and Concrete Association, London.
- 13.23 R. Thon, "Beitrag zur Berechnung und Bemessung durchlaufender Wandartiger Träger," *Beton- und Stahlbetonbau*, Vol. 53, No. 12, December 1958, pp. 297-306.
- 13.24 Joint ASCE-ACI Task Committee 426, "The Shear Strength of Reinforced Concrete Members," *Journal of the Structural Division, ASCE*, Vol. 99, ST6, June 1973, pp. 1091-1187.
- 13.25 B. Mayfield, F. K. Kong, A. Bennison, and J. C. D. T. Davies, "Corner Joint Details in Structural Lightweight Concrete," *Journal ACI*, Vol. 68, No. 5, May 1971, pp. 366-372.

- 13.26 E. L. Kemp and P. R. Mukherjee, "Inelastic Behaviour of Concrete Knee Joints," *The Consulting Engineer*, October 1968, pp. 44-48.
- 13.27 R. A. Swann, "Flexural Strength of Corners of Reinforced Concrete Portal Frames," Technical Report, TRA 434, Cement and Concrete Association, London, November 1969, 14 pp.
- 13.28 I. H. E. Nilsson, "Ramhorn av Armerad Betong med Positivt Moment," Forsokrapporter 1-4, Chalmers University of Technology, Göteborg, 1968.
- 13.29 G. Somerville and H. P. J. Taylor, "The Influence of Reinforcement Detailing on the Strength of Concrete Structures," *The Structural Engineer*, Vol. 50, No. 1, January 1972, pp. 7-19.
- 13.30 I. H. E. Nilsson, and A. Losberg, A discussion of the paper "Opportunities in Bond Research" by ACI Committee 408, *Proceedings, ACI Journal*, Vol. 68, No. 5, May 1971, pp. 393-396.
- 13.31 I. H. E. Nilsson, "Ramhorn av Armerad Betong med Positivt Moment. Konstruktiv utformning av ramhorn med dragen insida," Report 68:2, Chalmers University of Technology, Göteborg, 1968, 39 pp.
- 13.32 H. W. Conner and P. H. Kaar, "Precast Rigid Frame Buildings—Component Tests," Bulletin D123, Portland Cement Association, Development Department, 1967, 12 pp.
- 13.33 V. V. Bertero and G. McClure, "Behaviour of Reinforced Concrete Frames Subjected to Repeated Reversible Loads," *Journal ACI*, Vol. 61, No. 10, October 1964, pp. 1305-1330.
- 13.34 F. Beaufait and R. R. Williams, "Experimental Study of Reinforced Concrete Frames Subjected to Alternating Sway Forces," *Journal ACI*, Vol. 65, No. 11, November 1968, pp. 980-984.
- 13.35 N. W. Hanson, Discussion of Ref. 13.34, *Journal ACI*, Vol. 66, No. 5, May 1969, pp. 442-443.
- 13.36 G. W. Renton, "The Behaviour of Reinforced Concrete Beam-Column Joints Under Cyclic Loading," Master of Engineering thesis, University of Canterbury, Christchurch, New Zealand, 1972, 181 pp.
- 13.37 N. W. Hanson and H. W. Conner, "Seismic Resistance of Reinforced Concrete Beam-Column Joints," *Proceedings Structural Division ASCE*, Vol. 93, ST5, October 1967, pp. 533-560.
- 13.38 "Recommended Lateral Force Requirements and Commentary," Seismology Committee, Structural Engineers Association of California, 1969, 1970, and 1971 revisions.
- 13.39 L. M. Megget, "Anchorage of Beam Reinforcement in Seismic Resistant Reinforced Concrete Frames," Master of Engineering report, University of Canterbury, Christchurch, New Zealand, 1971, 85 pp.
- 13.40 B. J. Smith, "Exterior Reinforced Concrete Joints With Low Axial Load Under Seismic Loading," Master of Engineering report, University of Canterbury, Christchurch, New Zealand, 1972, 103 pp.
- 13.41 R. N. Patton, "Behaviour Under Seismic Loading of Reinforced Concrete Beam-Column Joints With Anchorage Blocks," Master of Engineering report, University of Canterbury, Christchurch, New Zealand, 1972, 103 pp.
- 13.42 R. Park and T. Paulay, "Behaviour of Reinforced Concrete External Beam-Column Joints Under Cyclic Loading," Vol. I., Paper 88, *Proceedings, Fifth World Conference on Earthquake Engineering*, Rome, 1973, 10 pp.
- 13.43 N. W. Hanson, "Seismic Resistance of Concrete Frames With Grade 60 Reinforcement," *Journal of the Structural Division ASCE*, Vol. 93, ST5, October 1971, pp. 533-560.

References

- 13.44 R. Park and K. J. Thompson, "Behaviour of Prestressed, Partially Prestressed and Reinforced Concrete Interior Beam-Column Assemblies under Cyclic Loading: Test Results of Units 1 to 7," Research Report 74-9, Department of Civil Engineering, University of Canterbury, 1974, 42 pp.
- 13.45 Y. Ohsaki, M. Watabe, and Y. Matsushima, "Experimental Study on Five-Storey Full Size Apartment House of Reinforced Concrete Walled Frames," *Proceedings of the U.S.-Japan Seminar on Earthquake Engineering With Emphasis on the Safety of School Buildings*, September 1970, pp. 240-266.
- 13.46 K. Ogura, "Outline of Damage to Reinforced Concrete Structures," Ref. 13.45, pp. 38-48.
- 13.47 G. K. Wilby, "Response of Reinforced Concrete Structures to Earthquake Motions." Ph.D. thesis in preparation, 1974, University of Canterbury, New Zealand.
- 13.48 C. H. Henager, "A Steel Fibrous, Ductile Concrete Joint for Seismic-Resistant Structures," Symposium on Reinforced Concrete Structures in Seismic Zones, ACI Annual Convention, San Francisco, 1974, 23 pp.

Index

- Additional moments in columns, 172
Aggregate interlock, *see* Interface shear
Aims of detailing, 663
Alignment, charts for effective length, 187
Allowable stress, 2, 441
Alternative design method:
 doubly reinforced rectangular beam sections, 446
 general, 1, 4, 441
 singly reinforced rectangular beam sections, 442
T-beam sections, 448
see also Elastic theory for flexural stresses
 in beams; Working stress design method
Anchorage bond, 393, 669, 746
Arch action, 285
Axially loaded columns:
 analysis and design, 118, 452
 axial load combined with bending, 123, 452
Balanced flexural failure conditions:
 rectangular beam sections, 65, 86
 rectangular column sections, 127
T-beam sections, 96
Bars, *see* Reinforcement
Beams:
 anchorage, 669
 buckling of compression bars, 581, 584, 688
 coupling beams of shear walls, 645
 curvature ductility of sections, 203, 221, 554, 563, 584
 cutting off flexural reinforcement, 685
 deep beams:
 continuous, 700, 705
 introduction of concentrated loads, 714
 simply supported, 700, 703
 web reinforcement, 707
elastic theory for flexural stresses:
 assumption, 428
 design, 441, 442, 448
 internal couple method, 429
 shrinkage stresses, 457
 transformed section method, 436
flexural strength of sections:
 assumptions of theory, 48
 balanced failure, 65, 86, 96
 biaxial bending, 106
 compression failure, 64, 81
 design charts and tables, 71, 72, 73, 74
 rectangular sections singly reinforced:
 analysis, 61
 design, 69
 rectangular sections doubly reinforced:
 analysis, 79
 design, 83
 sections with bars at various levels or
 steel lacking a well-defined yield
 strength, 101
T and I sections:
 analysis, 92
 design, 95
 tension failure, 62, 81
interaction of flexural and shear reinforcement, 675
lateral instability, 113
maximum reinforcement content, 69, 87, 96, 580, 584
minimum reinforcement content, 75, 580
shear strength:
 without web reinforcement, 291
 with web reinforcement, 299, 581, 585
splices, 419, 421
support and load points, 680
Beam action, 279

- Beam-column joints (connections) of multistorey frames:**
 axial compression, 742
 core deformation, 743
 design:
 anchorage, 746
 confinement, 749
 shear, 583, 590, 747
 exterior, 583, 590, 726, 746
 interior, 583, 590, 736, 774
 space frames, 583, 590, 750
- Beam-column knee joints (connections):**
 closing, 717
 opening, 720
 repeated loading, 724
- Bending combined with axial load, 123, 452**
- Bending moments:**
 complete analysis, 502
 elastic theory, 505, 507
 limit design, 512, 515
- Bent up bars for shear reinforcement, *see* Web reinforcement**
- Biaxial bending:**
 beams, 106
 columns, 154, 158, 162, 577
- Bond (anchorage):**
 anchorage or development bond, 393, 669
 cyclic and repeated loading, 404, 576
 flexural bond, 394, 417
 hooks, 411
 nature of bond resistance, 394
 splices:
 compression, 421, 686
 mechanical or contact, 423
 tension, 419
 splitting failure, 403
 straight anchorage:
 in compression, 416, 746
 in tension, 410, 746
 usable strength, 407.
- Brackets and corbels:**
 behavior, 690
 failure mechanisms, 692
 proportioning, 694
- Buckling effect in slender columns, 181**
- Capacity design, 600**
- Cantilever walls, *see* Shear walls**
- Capacity reduction factor, 5**
- Circular column sections, 148**
- Columns:**
 axially loaded, 118, 450
 biaxial flexural strength of sections:
 general theory, 154
 approximate methods, 158
 design charts, 162
 curvature ductility of sections, 217, 221, 232, 592
 eccentrically loaded, 123, 452
 elastic theory for direct and flexural stresses, 450, 452
 hoop, 582, 587, 591, 688
 maximum reinforcement content, 143
 minimum reinforcement content, 143
 plastic centroid, 127
 short, 118, 123, 154, 450
 slender, *see* Slender columns
 spiral, 119, 582, 688
 splices, 419, 421, 423, 686
 shear strength, 293, 310, 582, 590
 tied, 119, 688
- Uniaxial flexural strength of sections:**
 assumptions of theory, 48
 balanced failure, 127
 circular column sections, 148
 compression failure, 126, 129, 138, 149, 150
- Design charts, 153**
- Rectangular sections with bars at one or two faces:**
 analysis, 125
 design, 135
- Rectangular sections with bars at four faces, 143**
- Sections with bars in circular array, 148**
- Tension failure, 128, 137, 149**
- Combined stress behaviour of concrete, 17**
- Complete moment analysis, 502**
- Compression failure (flexure):**
 beam sections, 64, 81
 column sections, 126, 129, 138, 149, 150
- Compressive stress block of concrete, 52, 56, 58, 224**
- Compressive strength of concrete, 11**
- Compression steel in beams, 79, 83, 429, 438, 444, 581, 584**
- Concrete:**
 combined stress behaviour, 17
 compressive strength, 11
 compressive stress block, 52, 56, 58, 224

Index

- confinement by rectangular hoops, 21, 26, 221, 224, 229, 582, 587, 591, 688
 confinement by spirals, 21, 25, 221, 582, 587
 creep, 30, 474
 cyclic stress-strain behaviour, 14
 maximum strain, at flexural strength, 54, 221, 224, 248, 249
 at ultimate curvature, 56, 205, 221, 224, 248, 249, 516
 modulus of elasticity, 12, 427
 modulus of rupture, 15
 monotonic stress-strain behavior, 11
 Poisson's ratio, 17
 shrinkage, 33, 457
 tensile strength, 15
- Confinement of concrete:**
 by rectangular hoops, 21, 26, 221, 224, 229, 582, 587, 591, 688
 by spirals, 21, 25, 221, 582, 587
- Connections, see Beam-column connections**
- Construction Joints, 325, 616**
- Control of deflections, 463**
- Control of flexural crack widths, 490**
- Corbels, see Brackets**
- Coupled shear walls:**
 design principles, 658
 diagonal reinforcement, 652
 elastoplastic analysis, 641
 flexural strength, 655
 laminar elastic theory analysis, 638
 shear strength, 655
 strength of coupling beams, 645
- Cover, protective, 476**
- Cracking moment, 467**
- Cracking of concrete:**
 allowable widths, 476, 490
 causes, 477
 control of flexural crack widths, 490
 long-term effects, 489
 mechanism of flexural cracking:
 classical theory, 479
 general approach, 484
 non-slip theory, 482
 statistical approach, 483
- Creep of concrete, 30, 474**
- Curvature of a member, 196, 467**
- Curvature ductility:**
 available, 203, 217, 221, 232
 calculation of required, 496, 518, 521, 552
 554, 563, 584, 591
- Cyclic load behaviour of members:**
 bond, 404, 570
 flexure, 254, 570
 shear, 332, 570
- Cyclic stress-strain behaviour:**
 concrete, 14
 steel, 40
- Deep beams:**
 continuous, 700, 705
 introduction of concentrated loads, 714
 simply supported, 700, 703
 web reinforcement, 707
- Deformed bar reinforcement, 36**
- Deflections:**
 at first yield load, 552, 555
 at service load:
 allowable, 461, 464
 calculation, 465, 470
 control of, 463
 due to concrete creep, 468, 474
 due to concrete shrinkage, 468, 472
 due to shear, 315, 316
 more accurate calculations, 470
 theory, 236, 237, 315, 467, 472, 474
 at ultimate load:
 cyclic loading, 254
 plastic hinge rotation, 245
 summation of discrete rotations at cracks, 250
 theory, 236, 237, 242, 250, 552, 557
- Deformations, see Deflections**
- Design charts and tables:**
 beams, 71, 72, 73, 74
 columns, 153, 162
- Design for flexure, see Flexural strength of sections; Alternative design method**
- Design for shear, see Shear strength**
- Detailing:**
 aims, 663
 beams:
 anchorage, 669
 cutting off flexural reinforcement, 685
 interaction of flexural and shear reinforcement, 675
 support and load points, 680
 beam-column joints (connections) of multi-storey frames:

- anchorage, 746
 axial compression, 742
 confinement, 749
 core deformation, 743
 exterior, 583, 590, 726, 746
 interior, 583, 590, 736, 774
 shear, 583, 590, 747
 space frames, 583, 590, 750
- beam-column knee joints (connections):
 closing, 717
 opening, 720
 repeated loading, 724
- brackets and corbels:
 behavior, 690
 failure mechanisms, 692
 proportioning, 694
- columns:
 splices, 686
 transverse reinforcement, 688
- deep beams:
 continuous, 700, 705
 introduction of concentrated load, 714
 simply supported, 700, 703
 web reinforcement, 707
- direction changes of forces, 664
 purpose of reinforcement, 664
- Dependable strength, 5, 8, 601, 603
- Design methods, 1
- Design strength, 3
- Development bond, 393
- Development length, 410, 416
- Diagonal reinforcement for shear, 652
- Direction changes of forces, 665
- Displacement ductility factor, 547
- Doubly reinforced beam sections, 79, 83, 106, 429, 436, 446, 580, 645
- Ductile design for seismic loading:
 frames, 554, 563, 569, 577, 580, 584, 591, 600
 shear walls, 611, 618, 627, 641, 658
- Ductility:
 curvature ductility factor, 206
 charts for curvature ductility factor of beams, 208, 209, 210, 211
 displacement ductility factor, 547
 provisions, 7, 216
 unconfined beam sections, 203
 unconfined column sections, 217
 sections with confined concrete, 221
- Dynamic analysis, 547, 563
- Earthquake resistant design, *see* Seismic design
- Eccentrically loaded columns, 123, 452
- Effective flexural rigidity, 239, 467
- Effective length of columns, 183
- Effective modulus of columns, 183
- Effective modulus of elasticity of concrete, 427
- Effective width of T sections, 99
- Elastic theory bending moments, 505
- Elastic theory for flexural stresses in beams:
 assumptions, 428
 design, 1, 4, 441, 442, 448
 internal couple method, 429
 shrinkage stresses, 457
 transformed section method, 436
- Elastic theory for direct and flexural stresses in columns, 450, 452
- Energy dissipation by special devices, 599
- Equivalent rectangular stress block, 52, 56, 58, 226
- Flanged shear walls, 627
- Flexural bond, 394, 417
- Flexural members, *see* Beams
- Flexural rigidity:
 cracked sections, 437, 466
 effective, 239, 467
 general, 183, 198, 242, 437, 466
 uncracked sections, 437, 466
- Flexural strength of sections:
 assumptions of theory, 48
 biaxial bending, 106, 154
 rectangular beam sections, 61, 69, 79, 83, 645
 rectangular column sections, 125, 135, 143, 612
 sections having bars at various levels or steel lacking a well-defined yield strength, 101, 143, 148
- T and I beam sections, 92, 95
- Flexure-shear interaction, 301
- Flexure-torsion interaction, 357, 377
- Frames:
 complete moment analysis, 502
 ductile design for seismic loading, 554, 563, 569, 577, 580, 584, 591, 600
 elastic theory bending moments, 505

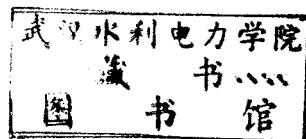
Index

- limit design, 512, 515
- moment redistribution, 496, 507
- see also* Beams; Beam-column joints; and Columns
- Hooks for anchorage, 411
- Hoop columns, 582, 587, 591
- Ideal strength, 5, 8, 601, 603
- Interaction of shear walls with frames, 633
- Interaction of shear walls with other shear walls, 631
- Interface shear:
 - construction joints, 325, 616
 - precracked concrete interfaces, 321
 - uncracked concrete interfaces, 320
- Joints, construction, 325, 616
- Lap splices:
 - compression, 421, 686
 - tension, 419, 582
- Lateral instability of beams, 113
- Length effects of columns, *see* Slender columns
- Limit design:
 - bending moment distribution, 512, 515
 - calculation, of required plastic hinge rotations, 496, 516, 521
 - of service load stresses and deflections, 517, 529
 - comments, 544
 - methods, 515, 518
- Load factors, 4
- Long columns, *see* Slender columns
- Maximum reinforcement content:
 - beams, 69, 87, 96, 580, 584
 - columns, 143, 582
- Maximum strain in concrete:
 - at flexural strength, 54, 221, 224, 248, 249
 - at ultimate curvature, 56, 205, 221, 224, 248, 249, 516, 579
- Mechanism of formation of flexural cracks, 479
- Members with flexure, *see* Beams
- Members with flexure and axial load, *see* Columns
- Minimum reinforcement content:
 - beams, 75, 580
 - columns, 143, 582
- Modulus of elasticity:
 - concrete, 12, 427
 - steel, 37
- Modulus of rupture of concrete, 15
- Moment-axial load interaction:
 - columns, 123, 152
 - shear walls, 629
- Moment-curvature relationships, 196, 199, 203, 217, 221, 254, 592
- Moment of inertia, 198, 239, 242, 438, 467
- Moment magnifier method for columns, 180
- Moment redistribution, 496, 507
- Monotonic stress-strain behaviour:
 - concrete, 11
 - steel, 37
- Nonrectangular compressed areas, 56
- Overstrength, 9, 601
- Openings in shear walls, 634
- Plastic centroid of columns, 127
- Plastic hinge length, 244, 248, 249, 250
- Plastic hinge rotation:
 - available, 245, 307
 - calculation of required, 496, 521, 552, 557, 563
- Poisson's ratio of concrete, 17
- Probable strength, 8, 603
- Primary torsion, 346
- Principal stresses, 272
- Rate of loading effects, 568
- Rectangular beam sections:
 - doubly reinforced, 79, 83, 106, 429, 436, 446, 580, 645
 - singly reinforced, 61, 69, 429, 436, 442
- Rectangular column sections, 125, 135, 143, 148, 154, 450, 452
- Redistribution of moments, 496, 507
- Reinforcement (steel):
 - anchorage, *see* Bond
 - cyclic stress-strain behaviour, 40
 - deformed, 36
 - modulus of elasticity, 37
 - monotonic stress-strain behaviour, 37
 - weights and dimensions of deformed bars, 37

- Repeated load behaviour, *see* Cyclic load behaviour
 Reversed load effects, *see* Cyclic load behaviour
- Secondary moments in columns, 173
 Secondary torsion, 346
 Seismic design:
 ACI 318-71 special provisions, 580
 basic concepts, 545
 beams:
 buckling of reinforcement, 581, 584
 curvature ductility, 580, 584
 shear strength, 581, 585, 658
 beam-column connections, 583, 590, 746
 biaxial load effects, 577
 capacity design:
 axial load determination for columns, 604
 flexural strength of columns, 602
 shear strength of beams, 601
 shear strength of columns, 606
 columns:
 avoidance of plastic hinges, 582, 585
 ductility, 582, 587, 591
 shear strength, 582, 590
 curvature ductility requirements, 552, 554, 563
 cyclic load effects, 569
 displacement ductility requirements, 547
 dynamic analyses, 547, 563
 energy dissipation by special devices, 599
 loading, 545
 rate of loading effects, 568
 reversed load effects, *see* Cyclic load effects
 shear walls, 611, 618, 627, 641, 658
 special transverse steel, 582, 587, 688
 static collapse mechanisms:
 beam sidesway, 559
 column sidesway, 557
 Service load behaviour, 426
 Serviceability, 6; *see also* Cracking; Deflections
 Shear-flexure-axial force interaction, 310
 Shear friction, 320, 321, 325
 Shear stiffness, 315, 316
 Shear strength:
 arch action, 285
 beam action, 279
 construction joints, 325, 616
- cyclic and repeated loading, 332, 581, 582, 585, 590
 design, 291, 299, 310, 581, 582, 585, 590, 615, 618, 655
 diagonal reinforcement, 652
 effect on flexural steel requirements, 304
 effect on plastic hinges, 307
 flexure-shear interaction, 301
 interface shear:
 construction joints, 325, 616
 precracked concrete interfaces, 321
 uncracked concrete interfaces, 320
 mechanism of resistance:
 beams without web reinforcement, 276
 beams with web reinforcement, 293
 columns, 310
 principal stresses, 272
 shear-flexure-axial force interaction, 310
 size effects, 287
 truss mechanism, 294
 variable depth of member, 274
 web reinforcement, 293, 581, 582, 585, 590
 Shear-torsion interaction, 359, 370
 Shear walls:
 cantilever walls, 611
 coupled walls:
 design principles, 658
 diagonal reinforcement, 652
 elastoplastic analysis, 641
 flexural strength, 655
 laminar elastic theory analysis, 638
 shear strength, 655
 strength of coupling beams, 645
 ductile design for seismic loading, 611, 618, 627, 641, 658
 flanged walls, 627
 interaction with frames, 633
 interaction with other walls, 631
 moment-axial load interaction, 629
 openings, 634
 squat walls with rectangular sections, 618
 tall walls with rectangular sections:
 construction joints, 616
 flexural strength, 612
 shear strength, 615
 Short columns, 118, 123, 154, 450
 Shrinkage of concrete, 33, 457
 Shrinkage stresses:
 symmetrical sections, 457
 unsymmetrical sections, 459

- Singly reinforced beam sections, 61, 69, 429, 436, 442
- Size effects on shear strength, 287
- Slender columns:
- additional moments, 172
 - alignment charts for effective length, 187
 - approximate design by moment magnifier method, 180
 - behaviour, 172
 - definition, 172
 - effective length, 183
 - "exact" design, 179
 - flexural rigidity, 183
 - secondary moments, 173
- Special transverse steel, 582, 587, 688
- Spiral columns, 119, 582, 587
- Splices:
- compression, 421, 686
 - mechanical or contact, 423
 - tension, 419, 582
- Splitting failure, 403
- Squat shear walls with rectangular sections, 618
- Static collapse mechanisms, 496, 512, 515, 557, 559
- Steel, *see* Reinforcement
- Stirrups, *see* Web reinforcement
- Straight anchorages, in compression, 416
- in tension, 410
- Strain in concrete:
- at flexural strength, 54, 221, 224, 248, 249
 - at ultimate curvature, 56, 205, 221, 224, 248, 249, 516, 579
- Strength:
- design, 3
 - dependable, 5, 8, 601, 603
 - ideal, 5, 8, 601, 603
 - overstrength, 9, 601
 - probable, 8, 603
- Strength and serviceability design, 3
- Stress-strain behaviour:
- concrete, 11, 14
 - steel, 37, 40
- Tall shear walls with rectangular sections, 611
- T-beam sections:
- analysis for flexure, 92, 432
 - design for flexure, 95, 448
 - effective width, 99, 357
- Tensile strength of concrete, 15
- Tension failure (flexure):
- beam sections, 62, 81
 - column sections, 128, 137, 149
- Tied columns, 119
- Torsional strength:
- flexure-torsion interaction, 357, 377
 - plain concrete:
 - elastic behaviour, 348
 - plastic behaviour, 351
 - tubular sections, 354 - primary torsion, 346
 - secondary torsion, 346
 - torsion-shear interaction, 359, 370
 - web reinforcement, 361, 370
- Torsion in statically indeterminate structures, 389
- Torsion-shear interaction, 359, 370
- Torsional stiffness, 383
- Transformed section, 436, 452
- Truss mechanism, 294
- Tubular sections, 354
- Variable depth of member, 274
- Walls, *see* Shear walls
- Web reinforcement:
- shear, 293, 581, 582, 585, 590, 615, 645
 - torsion, 361, 370
- Working stress design method, 1, 441
- Yield point, 37
- Yield strength, 37

050776



内 部 交 流

F147/60 (英 3-3/739)

钢筋混凝土结构

B000460